



Jerome J. Connor · Susan Faraji

Fundamentals of Structural Engineering

Second Edition

 Springer

Fundamentals of Structural Engineering

Jerome J. Connor • Susan Faraji

Fundamentals of Structural Engineering

Second Edition

 Springer

Jerome J. Connor
Department of Civil & Environmental
Engineering
Massachusetts Institute of Technology
Cambridge, MA, USA

Susan Faraji
Department of Civil & Environmental Engineering
University of Massachusetts-Lowell
Lowell, MA, USA

ISBN 978-3-319-24329-0 ISBN 978-3-319-24331-3 (eBook)
DOI 10.1007/978-3-319-24331-3

Library of Congress Control Number: 2015958840

Springer Cham Heidelberg New York Dordrecht London

© Springer International Publishing Switzerland 2013, 2016

This work is subject to copyright. All rights are reserved by the Publisher, whether the whole or part of the material is concerned, specifically the rights of translation, reprinting, reuse of illustrations, recitation, broadcasting, reproduction on microfilms or in any other physical way, and transmission or information storage and retrieval, electronic adaptation, computer software, or by similar or dissimilar methodology now known or hereafter developed.

The use of general descriptive names, registered names, trademarks, service marks, etc. in this publication does not imply, even in the absence of a specific statement, that such names are exempt from the relevant protective laws and regulations and therefore free for general use.

The publisher, the authors and the editors are safe to assume that the advice and information in this book are believed to be true and accurate at the date of publication. Neither the publisher nor the authors or the editors give a warranty, express or implied, with respect to the material contained herein or for any errors or omissions that may have been made.

Printed on acid-free paper

Springer International Publishing AG Switzerland is part of Springer Science+Business Media
(www.springer.com)

Preface

The first edition considered only linear elastic behavior of structures. This assumption is reasonable for assessing the structural response in the early stage of design where one is attempting to estimate design details. As a design progresses, other critical behavioral issues need to be addressed.

The first issue concerns geometric nonlinearity which results when a flexible member is subjected to axial compression loading as well as transverse loading. This combination causes a loss in axial stiffness for the member, which may result in a loss in stability for the structural system. Euler buckling is an example of this type of nonlinear behavior.

The second issue is related to the behavior of the material used to fabricate structural members. Steel and concrete are the most popular materials for structural applications. These materials have a finite elastic range, i.e., they behave elastically up to a certain stress level. Beyond this level, their stiffness decreases dramatically and they experience significant deformation that remains when the specimen is unloaded. This deformation is referred to as “inelastic deformation.” The result of this type of member behavior is the fact that the member has a finite load carrying capacity. From a structural system perspective, it follows that the structure has a finite load capacity. Given the experience with recent structural failures, structural engineers are now being required to estimate the “limit” capacity of their design using inelastic analysis procedures. Computer-based analysis is essential for this task.

We have addressed both issues in this edition. Geometric nonlinearity is basically a displacement issue, so it is incorporated in Chap. 10. We derive the nonlinear equations for a member; develop the general solution, specialize the solutions for various boundary conditions; and finally present the generalized nonlinear “member” equations which are used in computer-based analysis methods. Examples illustrating the effect of coupling between compressive axial load and lateral displacement (P-delta effect) are included. This treatment provides sufficient exposure to geometric nonlinearity that we feel is necessary to prepare the student for professional practice.

Inelastic analysis is included in Part III which deals with professional practice; we have added an additional chapter focused exclusively on inelastic analysis. We start by reviewing the basic properties of structural steel and concrete and then establish the expressions for the moment capacity of beams. We use these results together with some simple analytical methods

to establish the limit loading for some simple beam and frames. For complex structures, one needs to resort to computer-based procedures. We describe a finite element-based method that allows one to treat the nonlinear load displacement behavior and to estimate the limiting load. This approach is referred to as a “pushover” analysis. Examples illustrating pushover analyses of frames subjected to combined gravity and seismic loadings are included. Just as for the geometric nonlinear case, our objective is to provide sufficient exposure to the material so that the student is “informed” about the nonlinear issues. One can gain a deeper background from more advanced specialized references.

Aside from these two major additions, the overall organization of the second edition is similar to the first edition. Some material that we feel is obsolete has been deleted (e.g., conjugate beam), and other materials such as force envelopes have been expanded. In general, we have tried to place more emphasis on computer base approaches since professional practice is moving in that direction. However, we still place the primary emphasis on developing a fundamental understanding of structural behavior through analytical solutions and computer-based computations.

Audience

The intended audience of this book is that of students majoring in civil engineering or architecture who have been exposed to the basic concepts of engineering mechanics and mechanics of materials. The book is sufficiently comprehensive to be used for both undergraduate and higher level structures subjects. In addition, it can serve students as a valuable resource as they study for the engineering certification examination and as a reference later in their careers. Practicing professionals will also find the book useful for self-study, for review for the professional registration examination, and as a reference book.

Motivation

The availability of inexpensive digital computers and user-friendly structural engineering software has revolutionized the practice of structural engineering. Engineers now routinely employ computer-based procedures throughout the various phases of the analysis and design detailing processes. As a result, with these tools engineers can now deal with more complex structures than in the past. Given that these tools are now essential in engineering practice, the critical question facing faculty involved in the teaching of structural engineering is “How the traditional teaching paradigm should be modified for the computer age?” We believe that more exposure to computer-based analysis is needed at an early stage in the course development. However, since the phrase “garbage in garbage out” is especially relevant for computer-based analysis, we also believe that the student needs to develop, through formal

training in analysis methodology, the ability to estimate qualitatively the behavior of a structure subjected to a given loading and to confirm qualitative estimates with some simple manual computations.

Based on a review of the current structural engineering academic literature, it appears that the current set of undergraduate textbooks are focused mainly on either (1) teaching manual analysis methods and applying them to simple idealized structures or (2) reformulating structural analysis methods in terms of matrix notation. The first approach is based on the premise that intuition about structural behavior is developed as one works through the manual computations, which, at times, may seem exhaustive. The second approach provides the basis for developing and understanding computer software codes but does not contribute toward developing intuition about structural behavior.

Clearly there is a need for a text that provides a balanced treatment of both classical and modern computer-based analysis methods in a seamless way and also stresses the development of an intuitive understanding of structural behavior. Engineers reason about behavior using simple models and intuition that they have acquired through problem-solving experience. The approach adopted in this text is to develop this type of intuition through computer simulation which allows one to rapidly explore how the structure responds to changes in geometry and physical parameters. We believe this approach better prepares the reader for the practice of structural engineering.

Objectives

Structural engineers have two major responsibilities during the design process. First, they must synthesize the structural system, i.e., select the geometry and the type of structural members that make up the structure. Second, they must size the members such that the structure can comfortably support the design loading. Creating a structural concept requires a deep knowledge of structural behavior. Sizing the members requires information about the internal forces resulting from the loading. These data are acquired through intelligent application of analysis methods, mainly computer-based methods. With these responsibilities in mind, we have selected the following objectives for this book:

- *Develop the reader's ability to analyze structures using manual computational procedures.*
- *Educate the reader about structural behavior.* We believe that a strong analytical background based on classical analysis methodology combined with computer simulation facilitates the development of an understanding of structural behavior.
- *Provide the reader with an in-depth exposure to computer-based analysis methods.* Show how computer-based methods can be used to determine, with minimal effort, how structures respond to loads and also how to establish the extreme values of design variables required for design detailing.

- *Develop the reader's ability to validate computer-based predictions of structural response.*
- *Provide the reader with idealization strategies for reducing complex structures to simple structural models.*
- *Develop an appreciation for and an awareness of the limitations of using simple structural models to predict structural behavior through examples which illustrate behavioral trends as structures become more complex.*

Organization

We have organized this text into three parts. Parts I and II are intended to provide the student with the necessary computational tools and also to develop an understanding of structural behavior by covering analysis methodologies, ranging from traditional classical methods through computer-based methods, for skeletal-type structures, i.e., structures composed of one-dimensional slender members. Part I deals with statically determinate structures; statically indeterminate structures are covered in Part II. Certain classical methods which we consider redundant have been omitted. Some approximate methods which are useful for estimating the response using hand computations have been included. Part III is devoted to structural engineering issues for a range of structures frequently encountered in practice. Emphasis is placed on structural idealization, how one identifies critical loading patterns, and how one generates the extreme values of design variables corresponding to a combination of gravity, live, wind, earthquake loading, and support settlement using computer software systems.

Brief descriptions of the subject content for each part are presented below.

Part I discusses statically determinate structures. We start with an introduction to structural engineering. Statically determinate structures are introduced next. The treatment is limited to linear elastic behavior and static loading. Separate chapters are devoted to different skeletal structural types such as trusses, beams, frames, cables, curved members, footings, and retaining walls. Each chapter is self-contained in that all the related analysis issues for the particular structural type are discussed and illustrated. For example, the chapter on beams deals with constructing shear and moment diagrams, methods for computing the deflection due to bending, influence lines, force envelopes, and symmetry properties. We find it convenient from a pedagogical perspective to concentrate the related material in one location. It is also convenient for the reader since now there is a single source point for knowledge about each structural type rather than having the knowledge distributed throughout the text. We start with trusses since they involve the least amount of theory. The material on frames is based on beam theory, so it is logical to present it directly after beam theory. Cables and curved members are special structural types that generally receive a lower priority, due to time constraints, when selecting a syllabus. We have included these topics here, as

well as a treatment of footings and retaining walls, because they are statically determinate structures. We revisit these structures later in Part III.

Part II presents methods for analyzing statically indeterminate structures and applies these methods to a broad range of structural types. Two classical analysis methods are described, namely, the force (also referred to as the flexibility) method and the displacement (or stiffness) method. We also present some approximate analysis methods that are based on various types of force and stiffness assumptions. These methods are useful for estimating the structural response due to lateral loads using simple hand computations. Lastly, we reformulate the traditional displacement method as a finite element method using matrix notation. The finite element formulation (FEM) is the basis of most existing structural analysis software packages. Our objectives here are twofold: first, we want to enable the reader to be able to use FEM methods in an *intelligent* way, and second, we want the reader to develop an understanding of structural behavior by applying analysis methods to a broad range of determinate and indeterminate skeletal structures. *We believe that using computer analysis software as a simulation tool to explore structural behavior is a very effective way of building up a knowledge base of behavioral modes, especially for the types of structures commonly employed in practice.*

Part III discusses typical structural engineering problems. Our objective here is to expose the reader to a select set of activities that are now routinely carried out by structural engineers using structural engineering software. These activities are related to the approach followed to establish the “values” for the design variables. Defining these values is the key step in the engineering design process; once they are known, one can proceed to the design detailing phase. Specific chapters deal with horizontal structures such as multi-span girder, arch, and cable-stayed bridge systems, modeling of three-dimensional vertical structures subjected to lateral loading, and vertical structures such as low- and high-rise buildings subjected to gravity loading. The topics cover constructing idealized structural models, establishing the critical design loading patterns for a combination of gravity and live loading, using analysis software to compute the corresponding design values for the idealized structures, defining the lateral loading due to wind and earthquake excitation for buildings, and estimating the three-dimensional response of low-rise buildings subjected to seismic and wind loadings.

Course Suggestions

The following suggestions apply for students majoring in either civil engineering or architecture. Depending on the time available, we suggest organizing the material into either a two-semester or a three-semester sequence of subjects.

Our recommendations for the three-semester sequence are as follows:

Structures I

The goal of this subject is to provide the skills for the analysis of statically determinate trusses, beams, frames, and cables and to introduce some computer-based analysis methods.

Chapters 1, 2, part of 3, part of 4, and the first part of 5

Structures II

The objectives of this subject are to present both classical and computer-based analysis methods for statically indeterminate structures such as multi-span beams, gable frames, arches, and cable-stayed structures subjected to various loadings. The emphasis is on using analysis methods to develop an understanding of the behavior of structures.

Chapters 9, 10, 11, 12, 6, and the last part of 5

Structures III

This subject is intended to serve as an introduction to the practice of structural engineering. The material is presented as case studies for the two most common types of structures, bridges, and buildings. Issues such as geometrical configurations, idealized structural models, types and distribution of loadings, determination of the values of the design variables such as the peak moment in a beam, force envelopes, and inelastic behavior are discussed. Both the superstructure and the substructure components are considered. Extensive use of computer software is made throughout the subject. Recitation classes dealing with the design detailing of steel and concrete elements can be taught in parallel with the lectures.

Chapters 13, 14, 15, 16, 7, and 8

The makeup of the two-semester sequence depends on how much background in mechanics and elementary structures the typical student has and the goal of the undergraduate program. One possibility is to teach Structures I and II described above. Another possible option is to combine Structures I and II into a single subject offering together with Structures III. A suggested combined subject is listed below.

Structures (Combined I + II)

Chapters 3, 4 (partial), 9 (partial), 10, 11, and 12

Features of the Text

Organization by Structural Type

The chapters are organized such that an individual chapter contains all the information pertaining to a particular structural type. We believe this organization facilitates access to information. Since the basic principles are generic, it also reinforces these principles throughout the development of successive chapters.

Classical Analysis Methods

In-depth coverage of classical analysis methods with numerous examples helps students learn fundamental concepts and develop a “feel” and context for structural behavior.

Analysis by Hand Computation

The book helps teach students to do simple hand computing, so that as they move into doing more complex computational analysis, they can quickly check that their computer-generated results make sense.

Gradual Introduction of Computer Analysis

The text provides students with a gradual transition from classical methods to computational methods, with examples and homework problems designed to bring students along by incorporating computational methods when most appropriate to in-depth coverage of finite element methods for skeletal structures.

Example Problems

Example problems in each chapter illustrate solutions to structural analysis problems, including some problems illustrating computer analysis. Most of the example problems are based on real scenarios that students will encounter in professional practice.

Units

Both SI and customary US units are used in the examples and homework problems.

Homework Problems that Build Students’ Skills

An extensive set of homework problems for each chapter provides students with more exposure to the concepts and skills developed in the chapters. The

difficulty level is varied so that students can build confidence by starting with simple problems and advancing toward more complex problems.

Comprehensive Breadth and Depth, Practical Topics

The comprehensive breadth and depth of this text means it may be used for two or more courses, so it is useful to students for their courses and as a professional reference. Special topics such as the simplifications associated with symmetry and antisymmetry, arch-type structures, and cable-stayed structures are topics that a practicing structural engineer needs to be familiar with.

Cambridge, MA
Lowell, MA

Jerome J. Connor
Susan Faraji

Acknowledgments

We would like to thank our spouses Barbara Connor and Richard Hennessey for their patience and moral support over the seemingly endless time required to complete this text. We are most appreciative. We would also like to thank our colleagues and students who provided us with many valuable suggestions concerning the content and organization of the text. We are especially indebted to Dr. Moneer Tewfik and Dr. Carlos Brebbia for their constructive criticisms and enthusiastic support as the text was evolving into its final form.

Contents

Part I Statically Determinate Structures

1	Introduction to Structural Engineering	3
1.1	Types of Structures and Structural Components	4
1.1.1	Structural Components	4
1.1.2	Types of Structures	4
1.2	Critical Concerns of Structural Engineering	4
1.2.1	Reactions	5
1.2.2	Initial Stability	7
1.2.3	Loss of Stability Due to Material Failure	11
1.2.4	Buckling Failure Mode	12
1.2.5	Priorities for Stability	12
1.3	Types of Loads	12
1.3.1	Source of Loads	13
1.3.2	Properties of Loadings	15
1.3.3	Gravity Live Loads	16
1.3.4	Wind Loading	17
1.3.5	Snow Loading	22
1.3.6	Earthquake Loading	23
1.4	Structural Design Philosophy	26
1.5	Basic Analytical Tools of Structural Analysis	27
1.5.1	Concept of Equilibrium: Concurrent Force System	27
1.5.2	Concept of Equilibrium: Nonconcurrent Force System	28
1.5.3	Idealized Structure: Free Body Diagrams	30
1.5.4	Internal Forces	30
1.5.5	Deformations and Displacements	33
1.5.6	Structural Behavior: Structural Analysis	35
1.5.7	The Importance of Displacements	40
1.6	Summary	42
1.6.1	Objectives of the Chapter	42
1.6.2	Key Issues and Concepts Introduced	42

2	Statically Determinate Truss Structures	47
2.1	Introduction: Types of Truss Structures	47
2.1.1	Structural Idealization	48
2.1.2	Historical Background	50
2.2	Analysis of Planar Trusses	55
2.2.1	Equilibrium Considerations	56
2.2.2	Statically Determinate Planar Trusses	57
2.2.3	Stability Criterion	58
2.2.4	Method of Joints: Planar Trusses	61
2.2.5	Method of Sections	77
2.2.6	Complex Trusses	86
2.3	Computation of Deflections	90
2.3.1	Introduction	90
2.3.2	Force–Deformation Relationship	90
2.3.3	Deformation–Displacement Relations	91
2.3.4	Method of Virtual Forces	93
2.4	Influence Lines	105
2.5	Analysis of Three-Dimensional Trusses	114
2.5.1	Introduction	114
2.5.2	Restraining Rigid Body Motion	114
2.5.3	Static Determinacy	118
2.5.4	Method of Joints for 3-D Trusses	120
2.6	Matrix Formulation: Equilibrium Analysis of Statically Determinate 3-D Trusses	131
2.6.1	Notation	131
2.6.2	Member–Node Incidence	133
2.6.3	Force Equilibrium Equations	133
2.6.4	Stability	135
2.6.5	Matrix Formulation: Computation of Displacements	135
2.7	Summary	141
2.7.1	Objectives of the Chapter	141
2.7.2	Key Facts and Concepts	142
2.8	Problems	142
3	Statically Determinate Beams	163
3.1	Definition of a Prismatic Beam	163
3.2	Stability and Determinacy of Beams: Planar Bending	165
3.2.1	Fixed Support: Planar Loading	168
3.2.2	Hinged Support: Planar Loading	168
3.2.3	Roller Support: Planar Loading	169
3.2.4	3-D Fixed Support	170
3.2.5	3-D Hinged Support	170
3.2.6	3-D Roller Support: Z Direction	170
3.2.7	Static Determinacy: Planar Beam Systems	171

3.2.8	Unstable Support Arrangements	171
3.2.9	Beam with Multiple Supports	171
3.2.10	Beam with a Moment Release	172
3.3	Reactions: Planar Loading	173
3.4	Internal Forces: Planar Loading	182
3.5	Differential Equations of Equilibrium: Planar Loading	190
3.6	Displacement and Deformation of Slender Beams: Planar Loading	210
3.6.1	Moment: Curvature Relationship	212
3.6.2	Qualitative Reasoning About Deflected Shapes	213
3.6.3	Moment Area Theorems	218
3.6.4	Computing Displacements with the Method of Virtual Forces	231
3.6.5	Computing Displacements for Non-prismatic Members	241
3.7	Deformation–Displacement Relations for Deep Beams: Planar Loading	244
3.8	Torsion of Prismatic Members	247
3.9	Symmetry and Anti-symmetry	250
3.9.1	Symmetry and Anti-symmetry: Shear and Moment Diagrams	250
3.9.2	Symmetry and Anti-symmetry: Deflected Shapes	254
3.10	Influence Lines and Force Envelopes for Statically Determinate Beams	258
3.10.1	The Engineering Process	258
3.10.2	Influence Lines and Force Envelopes	259
3.11	Summary	285
3.11.1	Objectives of the Chapter	285
3.11.2	Key Facts and Concepts	285
3.12	Problems	286
4	Statically Determinate Plane Frames	305
4.1	Definition of Plane Frames	305
4.2	Statical Determinacy: Planar Loading	306
4.3	Analysis of Statically Determinate Frames	310
4.3.1	Behavior of Portal Frames: Analytical Solution	323
4.4	Pitched Roof Frames	326
4.4.1	Member Loads	326
4.4.2	Analytical Solutions for Pitched Roof Frames	330
4.5	A-Frames	341
4.6	Deflection of Frames Using the Principle of Virtual Forces	344
4.7	Deflection Profiles: Plane Frame Structures	356

4.8	Computer-Based Analysis: Plane Frames	358
4.9	Plane Frames: Out of Plane Loading	359
4.10	Summary	363
	4.10.1 Objectives	363
	4.10.2 Key Concepts	363
4.11	Problems	363
5	Cable Structures	383
5.1	Introduction	383
5.2	Cables Subjected to Concentrated Loads	386
	5.2.1 Horizontal Cables	386
	5.2.2 Inclined Cables	393
5.3	Cables Subjected to Distributed Loading	397
	5.3.1 Horizontal Cable: Uniform Loading per Horizontal Projection	397
	5.3.2 Inclined Cables	399
5.4	Advanced Topics	403
	5.4.1 Arc Length	403
	5.4.2 Equivalent Axial Stiffness	407
	5.4.3 Equivalent Axial Stiffness for an Inclined Cable	409
	5.4.4 Cable Shape Under Self Weight: Catenary	412
5.5	Summary	415
	5.5.1 Objectives	415
	5.5.2 Key Concepts	416
5.6	Problems	416
6	Statically Determinate Curved Members	423
6.1	A Brief History of Arch-Type Structures	423
6.2	Modeling of Arch Structures	429
6.3	Internal Forces in Curved Members	431
6.4	Parabolic Geometry	435
6.5	Method of Virtual Forces for Curved Members	442
	6.5.1 Non-shallow Slender Curved Members	443
	6.5.2 Shallow Slender Curved Members	443
	6.5.3 Circular Curved Member	447
6.6	Analysis of Three-Hinged Arches	450
6.7	Summary	463
	6.7.1 Objectives	463
	6.7.2 Key Factors and Concepts	463
6.8	Problems	464
7	Shallow Foundations	475
7.1	Introduction	475
	7.1.1 Types of Foundations	475
	7.1.2 Types of Shallow Foundations	476
	7.1.3 Soil Pressure Distribution	477

7.2	An Analytical Method for Evaluating the Soil Pressure Distribution Under a Footing	479
7.3	Dimensioning a Single Rectangular Footing	483
7.4	Dimensioning Combined Footings	493
7.5	Dimensioning Strap Footings	502
7.6	Summary	514
	7.6.1 Objectives of the Chapter	514
7.7	Problems	515
8	Vertical Retaining Wall Structures	525
8.1	Introduction	525
	8.1.1 Types of Retaining Walls	525
	8.1.2 Gravity Walls	526
	8.1.3 Cantilever Walls	527
8.2	Force Due to the Backfill Material	528
	8.2.1 Different Types of Materials	528
	8.2.2 Rankine Theory: Active Soil Pressure	530
8.3	Stability Analysis of Retaining Walls	531
8.4	Pressure Distribution Under the Wall Footing	533
8.5	Critical Sections for Design of Cantilever Walls	548
8.6	Summary	552
	8.6.1 Objectives of the Chapter	552
	8.6.2 Key Concepts and Facts	552
8.7	Problems	552

Part II Statically Indeterminate Structures

9	The Force Method	561
9.1	Introduction	561
9.2	Maxwell’s Law of Reciprocal Displacements	569
9.3	Application of the Force Method to Beam-Type Structures	571
	9.3.1 Beam with Yielding Supports	577
	9.3.2 Fixed-Ended Beams	588
	9.3.3 Analytical Solutions for Multi-Span Beams	596
9.4	Application to Arch-Type Structures	603
9.5	Application to Frame-Type Structures	612
	9.5.1 General Approach	612
	9.5.2 Portal Frames	613
	9.5.3 Pitched Roof Frames	625
9.6	Indeterminate Trusses	629
9.7	Summary	636
	9.7.1 Objectives	636
	9.7.2 Key Factors and Concepts	637
9.8	Problems	637
10	The Displacement Method	649
10.1	Introduction	649
10.2	Displacement Method Applied to a Plane Truss	651

10.3	Member Equations for Frame-Type Structures	653
10.4	The Displacement Method Applied to Beam Structures	658
10.4.1	Two-Span Beams	658
10.4.2	Multi-Span Beams	672
10.5	The Displacement Method Applied to Rigid Frames	685
10.5.1	Portal Frames: Symmetrical Loading	689
10.5.2	Portal Frames: Anti-symmetrical Loading	690
10.6	The Moment Distribution Solution Procedure for Multi-span Beams	697
10.6.1	Introduction	697
10.6.2	Incorporation of Moment Releases at Supports	701
10.6.3	Moment Distribution for Multiple Free Nodes	703
10.7	Moment Distribution: Frame Structures	709
10.7.1	Frames: No Sideway	709
10.7.2	Frames with Sideway	718
10.8	Plane Frames: Out of Plane Loading	729
10.8.1	Slope-Deflection Equations: Out of Plane Loading	729
10.9	Nonlinear Member Equations for Frame-Type Structures	734
10.9.1	Geometric Nonlinearity	734
10.9.2	Geometric Equations Accounting for Geometric Nonlinearity	737
10.9.3	Solution for Compressive Axial Load	741
10.9.4	Nonlinear Member End Actions–End Displacement Equations	744
10.10	Summary	751
10.10.1	Objectives	751
10.10.2	Key Factors and Concepts	751
10.11	Problems	752
11	Approximate Methods for Estimating Forces in Statically Indeterminate Structures	767
11.1	Introduction	767
11.2	Multi-span Beams: Gravity Loading	768
11.2.1	Basic Data-Moment Diagrams	768
11.2.2	Quantitative Reasoning Based on Relative Stiffness	769
11.3	Multistory Rigid Frames: Gravity Loading	770
11.4	Multistory Rigid Frames: Lateral Loading	771
11.4.1	Portal Method	772
11.4.2	Shear Stiffness Method: Low-Rise Rigid Frames	779
11.4.3	Low-Rise Rigid Frames with Bracing	785

11.5	High-Rise Rigid Frames: The Cantilever Method	790
11.6	Summary	796
	11.6.1 Objectives of the Chapter	796
	11.6.2 Key Concepts	796
11.7	Problems	797
12	Finite Element Displacement Method for Framed Structures	805
12.1	Introduction	805
12.2	Key Steps of the Finite Element Displacement Method for Member Systems	805
12.3	Matrix Formulation of the Member Equations: Planar Behavior	807
12.4	Local and Global Reference Frames	809
12.5	Nodal Force Equilibrium Equations	812
12.6	Introduction of Nodal Supports	818
	12.6.1 Systematic Approach	819
12.7	Specialized Formulation for Beam and Truss Structures	834
	12.7.1 The Steps Involved for Plane Truss Structures	834
	12.7.2 The Steps Involved for Beam Structures with Transverse Loading—Planar Behavior	839
12.8	Three-Dimensional Formulation	850
12.9	Summary	860
	12.9.1 Objectives	860
12.10	Problems	860
 Part III Practice of Structural Engineering		
13	Multi-span Horizontal Structures	873
13.1	The Engineering Process for Girders	873
13.2	Influence Lines for Indeterminate Beams Using Müller-Breslau’s Principle	875
13.3	Engineering Issues for Multi-span Girder Bridges	880
	13.3.1 Geometric Configurations	880
	13.3.2 Choice of Span Lengths	882
	13.3.3 Live Loads for Multi-span Highway Bridge Girders: Moment Envelopes	885
	13.3.4 Loading Due to Support Settlements	890
13.4	Case Studies	893
	13.4.1 Case Study I: A Three-Span Continuous Girder Bridge	893
	13.4.2 Case Study II: Two-Hinged Parabolic Arch Response—Truck Loading	899

13.4.3	Case Study III: Three-Span Parabolic Arch Response—Truck Loading	902
13.4.4	Case Study IV: Cable-Stayed Bridge	903
13.5	Summary	907
13.5.1	Objectives	907
13.5.2	Key Facts and Concepts	907
13.6	Problems	908
14	Lateral Load Issues for Buildings	915
14.1	Types of Multistory Building Systems	915
14.2	Treatment of Lateral Loading	917
14.2.1	Wind Loading	918
14.2.2	Earthquake Loading	920
14.3	Building Response Under Lateral Loads	925
14.3.1	Center of Twist: One-Story Frame	926
14.3.2	Center of Mass: One-Story Frame	937
14.3.3	One-Story Frame: General Response	940
14.3.4	Multistory Response	943
14.3.5	Matrix Formulation: Shear Beam Model	946
14.4	Response of Symmetrical Buildings	949
14.5	Summary	964
14.5.1	Objectives	964
14.5.2	Key Facts and Concepts	965
14.6	Problems	965
15	Vertical Loads on Multistory Buildings	975
15.1	Loads on Frames	975
15.2	Treatment of Gravity Floor Loads	977
15.3	Live Load Patterns for Frame Structures	980
15.4	A Case Study: Four-Story Building	989
15.4.1	Building Details and Objectives	989
15.4.2	Case (1) Frames Are Braced in Both N–S and E–W Directions: Computation Details	991
15.4.3	Case (2) Frames Are Rigid in the N–S Direction But Remain Braced in the E–W Direction	997
15.4.4	Discussion	1005
15.5	Summary	1006
15.5.1	Objectives	1006
15.5.2	Key Concepts	1006
15.6	Problems	1006
16	Inelastic Response of Structures	1013
16.1	Stress–Strain Behavior of Structural Steels	1013
16.2	Inelastic Moment–Curvature Relationships	1015
16.3	Limit Analysis: A Simplified Approach	1018

16.4	Nonlinear Analysis Scheme	1026
16.5	Summary	1031
	16.5.1 Objectives	1031
16.6	Problems	1032
	Index	1035

Photo Credits

Chapter 1

Fig. 1.1c Offshore Platform, Brazil. This image was produced by Agência Brasil, a public Brazilian news agency and published under a Creative Commons Attribution License. It was accessed in February 2012 from [http://en.wikipedia.org/wiki/File:Oil_platform_P-51_\(Brazil\).jpg](http://en.wikipedia.org/wiki/File:Oil_platform_P-51_(Brazil).jpg)

Fig. 1.1a Skyscraper under construction in Kutuzovsky Prospekt, Moscow, Russia. This image, created by Denghu, is licensed under a Creative Commons Attribution 3.0 Unported License. The image was accessed in April 2012 from http://commons.wikimedia.org/wiki/File:Skyscraper_Kutuzovsky_Prospekt_Moscow.jpg

Fig. 1.8 Millau Viaduct, Author: Delphine DE ANDRIA Date: 18.11.2007, from FreeMages. Accessed May 2012 from <http://www.freemages.co.uk/browse/photo-916-millau-viaduct.html>. This work is licensed under a Creative Commons Attribution 3.0 Unported License.

Chapter 2

Fig. 2.13 Three-dimensional truss of roof system. This image of the lead shot tower in Melbourne, Australia, created by freeaussiestock.com, is licensed under a Creative Commons Attribution 3.0 Unported License. The image was accessed in February 2012 from http://freeaussiestock.com/free/Victoria/Melbourne/slides/shot_tower.htm

Chapter 5

Fig. 5.1 Clifton Suspension bridge, England. Picture taken by Adrian Pingstone in October 2003 and placed in the public domain. Accessed in February 2012 from <http://commons.wikimedia.org/wiki/File:Clifton.bridge arp.750pix.jpg>

Fig. 5.5 Munich Olympic stadium, view from Olympic Tower. Picture taken by Arad Mojtahedi in July 2008 and placed in the public domain. Accessed in May 2012 from http://commons.wikimedia.org/wiki/File:Olympiastadion_Muenchen.jpg

Fig. 5.21 Millau Viaduct, Author: Delphine DE ANDRIA, Date: 18.11.2007, from FreeMages. Accessed in May 2012 from <http://www.freemages.co.uk/browse/photo-916-millau-viaduct.html>. This work is licensed under a Creative Commons Attribution 3.0 Unported License.

Chapter 6

Fig. 6.5 Alcantara Toledo Bridge, Puente de Alcántara, Toledo, Spain. This image was originally posted to Flickr on December 19, 2006 and published under a Creative Commons Attribution License. It was accessed in February 2012 from http://commons.wikimedia.org/wiki/File:Puente_Alcantara_toledo.jpg

Fig. 6.7 Eads Bridge, USA. This image was originally posted to Flickr by Kopper at <http://flickr.com/photos/94086509@N00/2745897992>. It was reviewed on January 18, 2011 (2011-01-18) by the FlickreviewR robot and confirmed to be licensed under the terms of the cc-by-2.0 (Creative Commons Attribution 2.0). It was accessed in February 2012 from http://commons.wikimedia.org/wiki/File:Eads_Bridge-1.jpg

Fig. 6.8 Salginatobel Bridge, Switzerland. Bild (Figure) 1.4-45 Ansicht der Salginatobelbrücke. P. 81 in Mehlhorn, G. et al. "Brückenbau auf dem Weg vom Altertum zum modernen Brückenbau," in Handbuch Brücken. Gerhard Mehlhorn (Ed). Berlin, Heidelberg. Springer-Verlag (2010)

Fig. 6.9a New Gorge Arch, West Virginia. This image was originally posted to Flickr by nukeit1 at <http://flickr.com/photos/88893304@N00/244750516>. It was reviewed on November 14, 2007 (2007-11-14) by the FlickreviewR robot and confirmed to be licensed under the terms of the cc-by-2.0 (Creative Commons Attribution 2.0). It was accessed in February 2012 from http://commons.wikimedia.org/wiki/File:New_River_Gorge_Bridge_West_Virginia_244750516.jpg

Chapter 8

Fig. 8.4 Gravity retaining wall. Courtesy of HNTB Corporation, 31 St. James Avenue, Suite 300 Boston, MA 02116, USA

Chapter 13

Fig. 13.1a Multi-span curved steel box girder bridge. Courtesy of HNTB Corporation, 31 St. James Avenue, Suite 300, Boston, MA 02116, USA

Fig. 13.1c The John James Audubon Bridge crossing the Mississippi River. This image is credited to the Louisiana TIMED Managers and was accessed in April 2012 from http://commons.wikimedia.org/wiki/File:Audubon_Bridge2.jpg

Fig. 13.34 Typical cable-stayed scheme. This work has been released into the public domain by its author, Kelly C. Cook. This applies worldwide. The image was accessed in February 2012 from http://commons.wikimedia.org/wiki/File:Sunshine_Skyway_from_Tampa_Bay.jpeg

Problem 13.9 Puente del Alamillo in Seville, Spain. This work has been released into the public domain by its author, Consorcio Turismo Sevilla. This applies worldwide. The image was accessed in March 2012 from http://en.wikipedia.org/wiki/File:Puente_del_Alamillo.jpg

Statically Determinate Structures

A structure is an assemblage of components which are connected in such a way that the structure can withstand the action of loads that are applied to it. These loads may be due to gravity, wind, ground shaking, impact, temperature, or other environmental sources. Structures are everywhere in the built environment. Buildings, bridges, tunnels, storage tanks, and transmission lines are examples of a “structure.” Structural engineering is the discipline which is concerned with identifying the loads that a structure may experience over its expected life, determining a suitable arrangement of structural members, selecting the material and dimensions of the members, defining the assembly process, and lastly monitoring the structure as it is being assembled and possibly also over its life.

In Part I, we first present an overview of structural engineering so that the reader can develop an appreciation for the broad range of tasks that structural engineers carry out and the challenges that they face in creating structures which perform satisfactorily under the loadings that they are subjected to. We then discuss a particular subgroup of structures called statically determinate structures. This subgroup is relatively easy to deal with analytically since only equilibrium concepts are involved. Also, most structures belong to this category. Trusses, beams, frames, cables, curved members, shallow foundations, and vertical retaining walls are described in separate chapters. The last two topics are not normally covered in elementary texts, but we have included them here for completeness.

In general, all structures can be classified as either statically determinate or statically indeterminate. Part II describes techniques for dealing with statically indeterminate structures.

Part III describes how the methodologies presented in Parts I and II are applied to “engineer” various types of bridges and buildings. This section is intended to identify the key issues involved in structural engineering practice.

Abstract

A structure is an assemblage of components which are connected in such a way that the structure can withstand the action of loads that are applied to it. These loads may be due to gravity, wind, ground shaking, impact, temperature, or other environmental sources. Examples of structures employed in civil infrastructure are buildings, bridges, dams, tunnels, storage tanks, and transmission line towers. Non-civil applications include aerospace structures such as airplane fuselages, missiles; naval structures such as ships, offshore platforms; and automotive structures such as cars and trucks. Structural engineering is the discipline which is concerned with identifying the loads that a structure may experience over its expected life, determining a suitable arrangement of structural members, selecting the material and dimensions of the members, defining the assembly process, and lastly monitoring the structure as it is being assembled and possibly also over its life.

In this chapter, we describe first the various types of structures. Each structure is categorized according to its particular function and the configuration of its components. We then discuss the critical issues that a structural engineer needs to address when designing or assessing the adequacy of a structure. The most important issue is preventing failure, especially a sudden catastrophic failure. We describe various failure modes: initial instability, material failure, and buckling of individual structural components. In order to carry out a structural design, one needs to specify the loading which is also a critical concern. Fortunately, the technical literature contains considerable information about loadings. We present here an overview of the nature of the different loads and establish their relative importance for the most common civil structures. Conventional structural design philosophy and the different approaches for implementing this design strategy are described next. Lastly, we briefly discuss some basic analytical methods of structural engineering and describe how they are applied to analyze structures.

1.1 Types of Structures and Structural Components

Structures are everywhere in the built environment. Buildings, bridges, tunnels, storage tanks, and transmission lines are examples of a “structure.” Structures differ in their *makeup*, i.e., the type and configuration of the components, and also in their *function*. Our approach to describing a structure is based on identifying a set of attributes which relate to these properties.

1.1.1 Structural Components

The components are the basic building blocks of a structure. We refer to them as structural elements. Elements are classified into two categories according to their geometry [1]:

1. *Line Elements*—The geometry is essentially one-dimensional, i.e., one dimension is large with respect to the other two dimensions. Examples are cables, beams, columns, and arches. Another term for a line element is member.
2. *Surface Elements*—One dimension is small in comparison to the other two dimensions. The elements are plate-like. Examples are flat plates, curved plates, and shells such as spherical, cylindrical, and hyperbolic paraboloids.

1.1.2 Types of Structures

A structure is classified according to its function and the type of elements used to make up the structure. Typical structures and their corresponding functions are listed in Table 1.1 and illustrated in Fig. 1.1. A classification according to makeup is listed in Table 1.2 and illustrated in Fig. 1.2.

1.2 Critical Concerns of Structural Engineering

Of primary concern to a structural engineer is ensuring that the structure *will not collapse* when subjected to its design loading. This requires firstly that the engineer properly identify the extreme loading that the structure may experience over its design life and secondly, ensure that the forces generated internally within the structure due to external loading *satisfy the conditions for force equilibrium*. In general, a structure will deform, i.e., change its shape, when loaded. It may also

Table 1.1 Structures classified by function

Structural type	Function
Building	Provide shelter above ground
Bridge	Provide means of traversing above ground over a site
Tunnel	Provide means of traversing underground through a site
Tower	Support transmission lines and broadcasting devices
Retaining walls	Retain earth or other material
Containments	Provide means of storage of materials, also enclose dangerous devices such as nuclear reactors
Platforms	Provide a platform for storage of materials and machinery either onshore or offshore

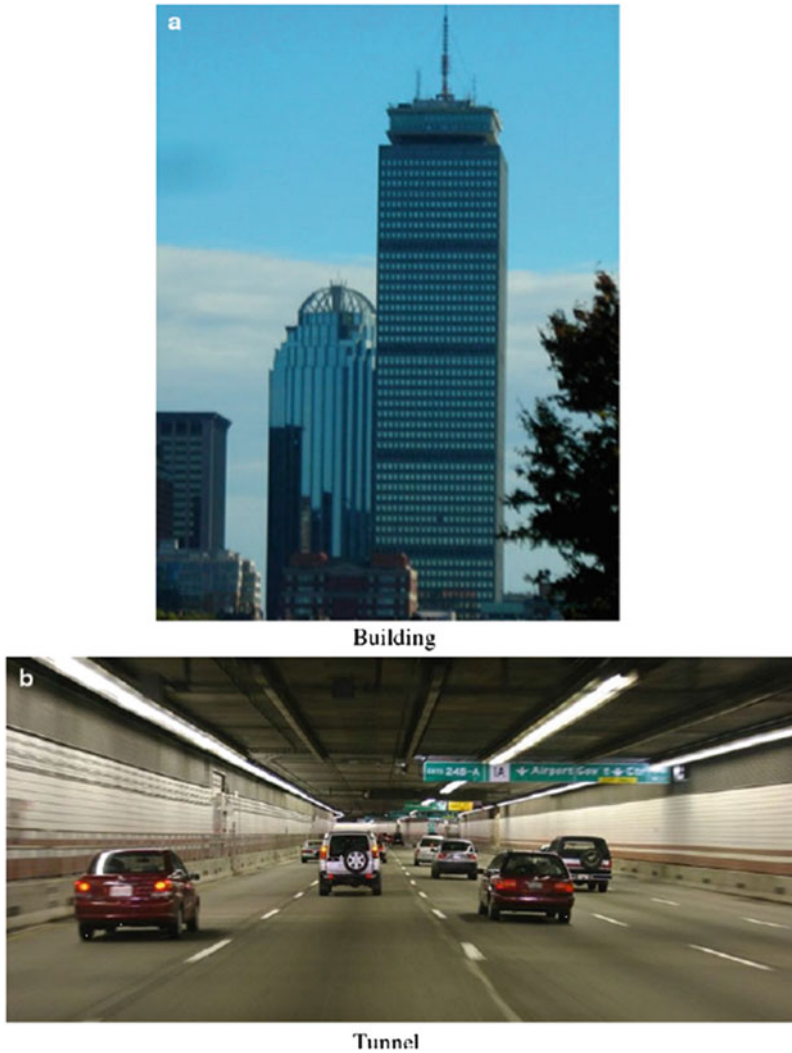


Fig. 1.1 Examples of typical structures classified by function

move as a rigid body if not properly restrained. Certain structures such as airplanes and automobiles are designed to move. However, civil structures are generally limited to small motion due to deformation, and *rigid* body motion is prohibited. Identifying the design loads is discussed later in this chapter. We focus here on the force equilibrium requirement for civil structures.

1.2.1 Reactions

Civil structures are connected to the ground at certain points called supports. When the external loading is applied to the structure, the supports develop forces which oppose the tendency of the



Offshore platforms



Bridge

Fig. 1.1 (continued)

structure to move. These forces are called reactions [2]. The nature and number of reactions depends on the type of support. Figure 1.3 shows the most common types of idealized structural supports for any planar structure. A roller support allows motion in the longitudinal direction but not in the transverse direction. A hinge prevents motion in both the longitudinal and transverse directions but allows rotation about the pin connection. Lastly, the clamped (fixed) support restrains rotation as well

Table 1.2 Structures classified by makeup

Structural type	Composition
Frame	<ul style="list-style-type: none"> Composed of members rigidly or semirigidly connected in rectangular or triangular patterns May be contained in a single plane (plane frame, plane grid), or in a 3D configuration (space frame)
Truss	<ul style="list-style-type: none"> A type of framed structure where the members are connected together at their ends with frictionless pins (plane or space truss)
Girder/beam	<ul style="list-style-type: none"> Composed of straight members connected sequentially (end to end) An additional descriptor related to the type of member cross section is used <p>Examples are plate girders, box girders, and tub girders</p>
Arch	<ul style="list-style-type: none"> Curved beams (usually in one plane)
Cable	<ul style="list-style-type: none"> Composed of cables and possibly other types of elements such as girders <p>Examples are cable-stayed bridges and tensioned grids</p>
Shell	<ul style="list-style-type: none"> Composed of surface elements and possibly also line elements such as beams <p>The elements may be flat (plate structures) or curved (spherical or cylindrical roof structures)</p>

as translation with two reaction forces and one moment. Three-dimensional supports are similar in nature. There is an increase from 2 to 3 and from 3 to 6 in the number of reactions for the 3D hinge and a clamped support.

1.2.2 Initial Stability

If either the number or nature of the reactions is insufficient to satisfy the equilibrium conditions, the structure is said to be initially unstable. Figure 1.4a illustrates this case. The structure consists of a triangular arrangement of members that are pinned at their ends. This combination of members forms a rigid body. However, the arrangement is supported on two roller supports which offer no resistance to horizontal motion, and consequently the structure is initially unstable. This situation can be corrected by changing one of the roller supports to a hinge support, as shown in Fig. 1.4b. In general, a rigid body is initially stable when translational and rotational motions are prevented in three mutually orthogonal directions.

Even when the structure is adequately supported, it still may be initially unstable if the members are not properly connected together to provide sufficient internal forces to resist the applied external forces. Consider the four member pin-connected planar structure shown in Fig. 1.5a. The horizontal force, P , cannot be transmitted to the support since the force in member 1-2 is vertical and therefore cannot have a horizontal component. Adding a diagonal member, either 1-3 or 2-4, would make the structure stable.

In summary, initial instability can occur either due to a *lack of appropriate supports* or to an *inadequate arrangement of members*. The test for initial instability is whether there are sufficient reactions and internal member forces to equilibrate the applied external loads. Assuming the structure is initially stable, there still may be a problem if certain structural components fail under the action of the extreme loading and cause the structure to *lose* its ability to carry load. In what follows, we discuss various failure scenarios for structures which are loaded.



Frame

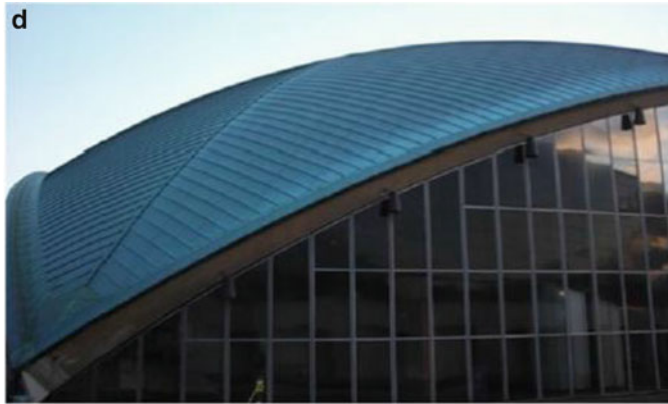


Bridge girder



Space Truss

Fig. 1.2 Structures classified by makeups



Shell



Arch bridge



Cable-girder system (suspension bridge)

Fig. 1.2 (continued)

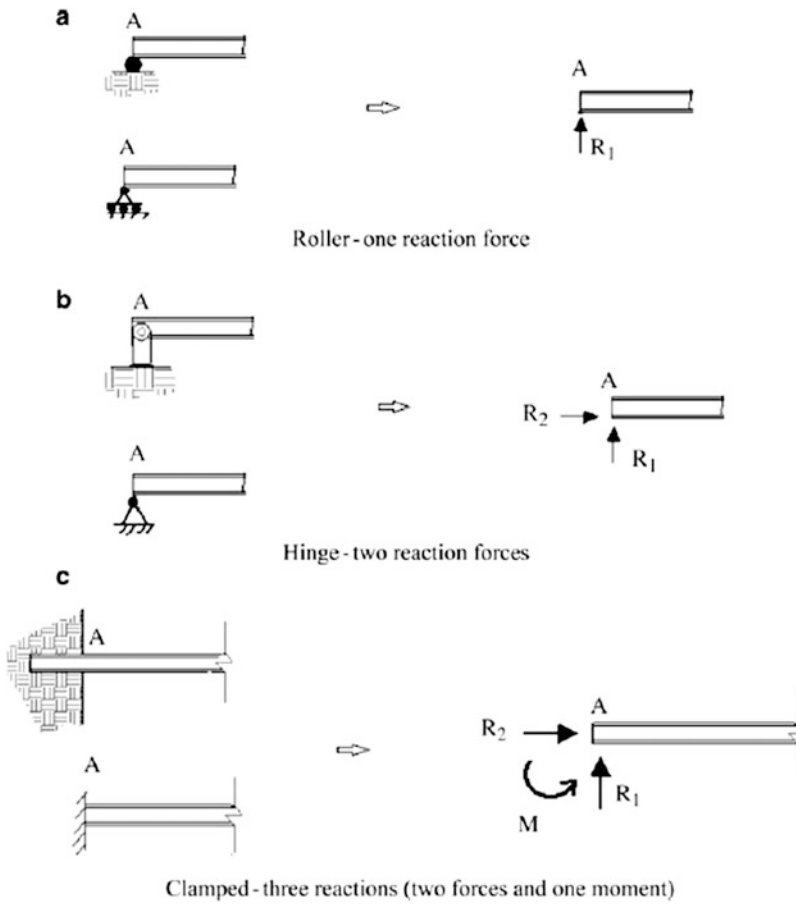


Fig. 1.3 Typical supports for planar structures

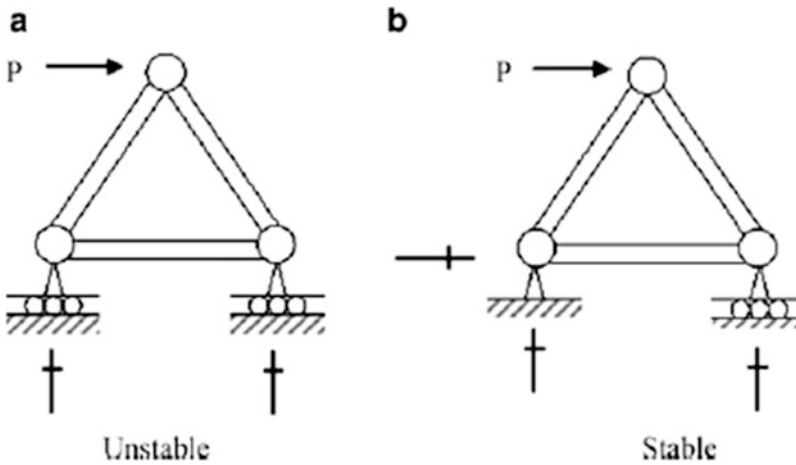


Fig. 1.4 Examples of unstable and stable support conditions—planar structure

Fig. 1.5 Stabilizing an initially unstable planar structure

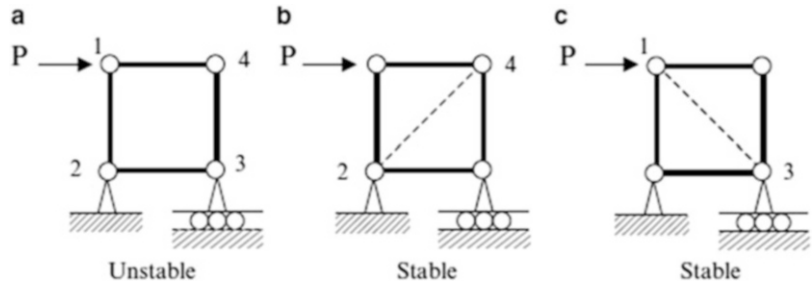
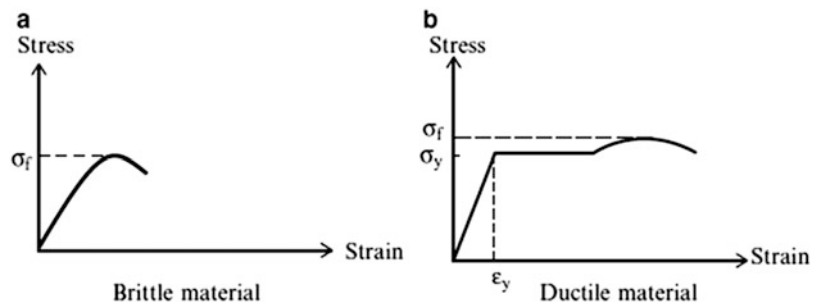


Fig. 1.6 Stress–strain behavior of brittle and ductile materials



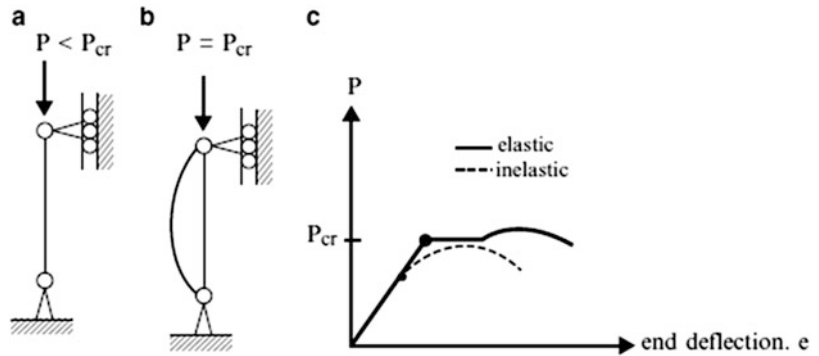
1.2.3 Loss of Stability Due to Material Failure

In the first scenario, the level of stress in a component reaches the ultimate stress for the material, causing a material failure, which, in turn, triggers a failure of the component. This type of failure depends on the stress–strain relationship for the material. Figure 1.6 illustrates the tensile stress–extensional strain response of tension specimens fabricated from two different types of materials [3, 4]. The behavior of the first material is essentially linear up to a peak stress, σ_f , at which point the material fractures and loses its ability to carry any load. This behavior is referred to as *brittle behavior* and obviously is not desirable from a structural behavior perspective.

The second response is completely different. The initial behavior is linear up to a certain stress value defined as the yield stress, σ_y . For further straining, the stress remains essentially constant. Eventually, the material stiffens and ultimately fails at a level of strain which is considerably greater than the yield strain, ϵ_y . This behavior is typical for *ductile* materials such as the steels used in civil structures. In practice, the maximum allowable strain is limited to a multiple of the yield strain. This factor is called the ductility ratio (μ) and is on the order of 5. Ductile behavior is obviously more desirable since a member fabricated out of a ductile material does not lose its load capacity when yielding occurs. However, it cannot carry additional loading after yielding since the resistance remains constant.

From a design perspective, the structural engineer must *avoid* brittle behavior since it can result in *sudden* catastrophic failure. Ductile behavior and the associated inelastic deformation are acceptable provided that the ductility demand is within the design limit. Limit state design is a paradigm for dimensioning structural components that assumes the component is at its limit deformation state and calculates the force capacity based on the yield stress [5]. This topic is dealt with in Chap. 16.

Fig. 1.7 Behavior of a flexible member



1.2.4 Buckling Failure Mode

Another possible failure scenario for a structural component is buckling. Buckling is a phenomenon associated with long slender members subjected to compressive loading [3, 4]. We illustrate this behavior using the member shown in Fig. 1.7a. As the axial loading is increased, the member remains straight until a critical load value is reached. At this point, the member adopts a deflected configuration (Fig. 1.7b) with the load remaining constant. The member force remains essentially constant as the end deflection, e , is increased (Fig. 1.7c). This load deflection behavior is similar to inelastic action in the sense that the member experiences a large deflection with essentially no increase in load. For flexible members, the critical load for buckling (P_{cr}) is generally less than the axial compressive strength based on yielding, *therefore buckling usually controls the design*.

1.2.5 Priorities for Stability

Finally, summarizing and prioritizing the different concerns discussed in the previous sections, the highest priority is ensuring the structure is initially stable. If not stable, the structure will fail under an infinitesimal load. The second priority is avoiding buckling of the members. Buckling can result in large deformation and significant loss in load capacity for a member, which could cause the structure to lose its ability to support the applied loading. The third priority is limiting inelastic deformation of members under the extreme design loading. Although there is no loss in load capacity, the member cannot provide any additional load capacity, and therefore the deformation will increase significantly when the external loading is increased. We discuss this topic further in Sect. 1.4 where we present design philosophies.

1.3 Types of Loads

As described above, structures must be proportioned so that they will not fail or deform excessively under the loads they may be subjected to over their expected life. Therefore, it is critical that the nature and magnitude of the loads they may experience be accurately defined. Usually, there are a number of different loads, and the question as to which loads may occur simultaneously needs to be addressed when specifying the design loading. In general, the structural engineer works with codes, which specify design loadings for various types of structures. General building codes such as the “International Building Code” [6] specify the requirements of governmental agencies for minimum

design loads for structures and minimum standards for construction. Professional technical societies such as the American Society of Civil Engineers (ASCE) [7], the American Concrete Institute (ACI) [8], the American Institute of Steel Construction (AISC) [9], and the British Standards Institute (BSI) [10] publish detailed technical standards that are also used to establish design loads and structural performance requirements. In what follows, we present an overview of the nature of the different loads and provide a sense of their relative importance for the most common civil structures.

1.3.1 Source of Loads

Loads are caused by various actions: the interaction of the structure with the natural environment; carrying out the function they are expected to perform; construction of the structure; and terrorist activities.

1.3.1.1 Interaction with the Environment

Interaction with the natural environment generates the following types of loads:

- Gravity—gravitational force associated with mass
- Snow—gravity-type loading
- Wind—steady flow, gusts
- Earthquake—ground shaking resulting from a seismic event
- Water—scour, hydrostatic pressure, wave impact
- Ice—scour, impact
- Earth pressure—soil–structure interaction for foundations and underground structures
- Thermal—seasonal temperature variations

The relative importance of these sources depends on the nature of the structure and the geographical location of the site. For example, building design is generally governed by gravity, snow, wind, and possibly earthquake loads. Low-rise buildings in arctic regions tend to be governed by snow loading. Underground basement structures and tunnels are designed for earth pressure, hydrostatic pressure, and possibly earthquake loads. Gravity is the dominant source of load for bridge structures. Wave and ice action control the design of offshore platforms in coastal arctic waters such as the coasts of Alaska and Newfoundland. Structures located in California need to be designed for high seismic load. Structures located in Florida need to be designed for high wind load due to hurricanes. Thermal loads occur when structural elements are exposed to temperature change and are not allowed to expand or contract.

1.3.1.2 Function

Function-related loads are structure specific. For bridges, vehicular traffic consisting of cars, trucks, and trains generates gravity-type load, in addition to the self-weight load. Office buildings are intended to provide shelter for people and office equipment. A uniformly distributed gravity floor load is specified according to the nature of the occupancy of the building. Legal offices and libraries tend to have a larger design floor loading since they normally have more storage files than a normal office. Containment structures usually store materials such as liquids and granular solids. The associated loading is a distributed internal pressure which may vary over the height of the structure.

1.3.1.3 Construction

Construction loading depends on the process followed to assemble the structure. Detailed force analyses at various stages of the construction are required for complex structures such as segmented long-span bridges for which the erection loading dominates the design. The structural engineer is responsible for approving the construction loads when separate firms carry out engineering and construction. A present trend is for a single organization to carry out both the engineering design and construction (the design-build paradigm where engineering companies and construction companies form a joint venture for the specific project). In this case, a team consisting of structural engineers and construction engineers jointly carries out the design. An example of this type of partnering is the construction of the Millau Viaduct in southwestern France, shown in Fig. 1.8. The spans were constructed by cantilevering segments out from existing piers, a technically challenging operation that required constant monitoring. The bridge piers are the highest in the world: the central pier is 280 m high.

1.3.1.4 Terrorist Loads

Terrorist loads are a new problem for structural engineers, driven primarily by the need to protect essential facilities from terrorist groups. Design criteria are continuously evolving, and tend to be directed more at providing multilevel defense barriers to prevent incidents, rather than to design for a specific incident. Clearly, there are certain incidents that a structure cannot be designed to safely handle, such as the plane impacts that destroyed the World Trade Center Towers. Examining progressive collapse mechanisms is now required for significant buildings and is the responsibility of the structural engineer.



Fig. 1.8 Millau Viaduct

1.3.2 Properties of Loadings

The previous discussion was focused on the source of loadings, i.e., environmental, functional, construction, and terrorist activity. Loadings are also characterized by attributes, which relate to properties of the loads. Table 1.3 lists the most relevant attributes and their possible values.

Duration relates to the time period over which the loading is applied. Long-term loads, such as self-weight are referred to as dead loads. Loads whose magnitude or location changes are called temporary loads. Examples of temporary loads are the weight of vehicles crossing a bridge, stored items in buildings, wind and seismic loads, and construction loads.

Most loads are represented as being applied over a finite area. For example, a line of trucks is represented with an equivalent uniformly distributed load. However, there are cases where the loaded area is small, and it is more convenient to treat the load as being concentrated at a particular point. A member partially supported by cables such as a cable-stayed girder is an example of concentrated loading.

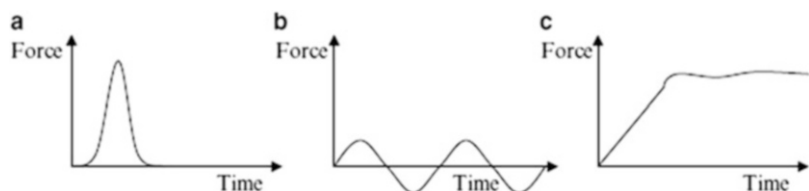
Temporal distribution refers to the rate of change of the magnitude of the temporary loading with time. An impulsive load is characterized by a rapid increase over a very short duration and then a drop off. Figure 1.9 illustrates this case. Examples are forces due to collisions, dropped masses, brittle fracture material failures, and slamming action due to waves breaking on a structure. Cyclic loading alternates in direction (+ and -) and the period may change for successive cycles. The limiting case of cyclic loading is harmonic excitation where the amplitude and period are constant. Seismic excitation is cyclic. Rotating machinery such as printing presses, electric generators, and turbines produce harmonic excitation on their supports when they are not properly balanced. Quasi-static loading is characterized by a relatively slow build up of magnitude, reaching essentially a steady state. Because they are applied slowly, there is no appreciable dynamic amplification and the structure responds as if the load was a *static* load. Steady winds are treated as quasi-static; wind gusts are impulsive. Wind may also produce a periodic loading resulting from vortex shedding. We discuss this phenomenon later in this section.

The design life of a structure is that time period over which the structure is expected to function without any loss in operational capacity. Civil structures have long design lives vs. other structures such as motorcars, airplanes, and computers. A typical building structure can last several centuries. Bridges are exposed to more severe environmental actions, and tend to last a shorter period, say 50–75 years. The current design philosophy is to extend the useful life of bridges to at least 100 years.

Table 1.3 Loading attributes

Attribute	Value
Duration	Temporary or permanent
Spatial distribution	Concentrated or distributed
Temporal distribution	Impulsive; cyclic; quasi-static
Degree of certainty	Return period; probability of occurrence

Fig. 1.9 Temporal variation of loading. (a) Impulsive. (b) Cyclic. (c) Quasi-static



The Millau viaduct shown in Fig. 1.8 is intended to function at its full design capacity for at least 125 years.

Given that the natural environment varies continuously, the structural engineer is faced with a difficult problem: the most critical natural event, such as a windstorm or an earthquake that is likely to occur during the design life of the structure located at a particular site needs to be identified. To handle this problem, natural events are modeled as stochastic processes. The data for a particular event, say wind velocity at location x , is arranged according to return period which can be interpreted as the average time interval between occurrences of the event. One speaks of the 10-year wind, the 50-year wind, the 100-year wind, etc. Government agencies have compiled this data, which is incorporated in design codes. Given the design life and the value of return period chosen for the structure, the probability of the structure experiencing the chosen event is estimated as the ratio of the design life to the return period. For example, a building with a 50-year design life has a 50 % chance of experiencing the 100-year event during its lifetime. Typical design return periods are ≈ 50 years for wind loads and between 500 and 2500 years for severe seismic loads.

Specifying a loading having a higher return period reduces the probability of occurrence of that load intensity over the design life. Another strategy for establishing design loads associated with uncertain natural events is to increase the load magnitude according to the importance of the structure. Importance is related to the nature of occupancy of the structure. In ASCE Standards 7-05 [7], four occupancy categories are defined using the *potential hazard to human life in the event of a failure* as a basis. They are listed in Table 1.4 for reference.

The factor used to increase the loading is called the importance factor, and denoted by I . Table 1.5 lists the values of I recommended by ASCE 7-05 [7] for each category and type of loading.

For example, one increases the earthquake loading by 50 % for an essential structure (category 4).

1.3.3 Gravity Live Loads

Gravitational loads are the dominant loads for bridges and low-rise buildings located in areas, where the seismic activity is moderate. They act in the downward vertical direction and are generally a combination of fixed (dead) and temporary (live) loads. The dead load is due to the weight of the construction materials and permanently fixed equipment incorporated into the structure. As

Table 1.4 Occupancy categories

Category	Description
I	Structures that represent a low hazard to human life in the event of a failure
II	All structures outside of categories I, III, and IV
III	Structures that represent a substantial hazard to human life in the event of failure
IV	Essential structures. Failure not allowed

Table 1.5 Values of I

Category	Wind		Snow	Earthquake
	Non-horizontal	Horizontal		
I	0.87	0.77	0.80	1.00
II	1.00	1.00	1.00	1.00
III	1.15	1.15	1.10	1.25
IV	1.15	1.15	1.20	1.50

Table 1.6 Uniformly distributed live loads (ASCE 7-05)

Occupancy	Magnitude lbs/ft ² (kN/m ²)
Computer equipment	150 (7.18)
Dormitories	80 (3.83)
File room	125 (6.00)
Court rooms	50–100 (2.4–4.79)
Scientific laboratories	100 (4.79)
Public rooms	100 (4.79)
Rest rooms	60 (2.87)
Laundries	150 (7.18)
Foundries	600 (28.73)
Ice manufacturing	300 (14.36)
Transformer rooms	200 (9.58)
Storage, hay, or grain	300 (14.36)

mentioned earlier, temporary live loads depend on the function of the structure. Typical values of live loads for buildings are listed in Table 1.6. A reasonable estimate of live load for office/residential facilities is ≈ 100 lbs/ft² (4.8 kN/m²). Industrial facilities have higher live loadings, ranging up to 600 lbs/ft² for foundries.

Live loading for bridges is specified in terms of standard truck loads. In the USA, bridge loads are defined by the American Association of State Highway and Transportation Officials (AASHTO) [11]. They consist of a combination of the Design truck or tandem, and Design lane load.

The design truck loading has a total weight of 72 kip (323 kN), with a variable axle spacing is shown in Fig. 1.10. The design tandem shall consist of a pair of 25 kip (112 kN) axles spaced 4 ft (1.2 m) apart. The transverse spacing of wheels shall be taken as 6 ft (1.83 m). The design lane load shall consist of a load of 0.64 kip/ft² (30.64 kN/m²) uniformly distributed in the longitudinal direction and uniformly distributed over a 10 ft (3 m) width in the transverse direction.

1.3.4 Wind Loading

1.3.4.1 Wind Pressure Distribution

The effect of wind acting on a building is represented by a pressure loading distributed over the exterior surface. This pressure loading depends on the geometry of the structure and the geographic location of the site. Figure 1.11 illustrates the flow past a low-rise, single story, flat roof structure. The sharp corners such as at point A causes flow separation, resulting in eddies forming and turbulence zones on the flat roof, side faces, and leeward face. The sense of the pressure is positive (inward) on the incident face and negative (outward) in the turbulence zones.

In general, the magnitude of the pressure varies over the faces, and depends on both the shape of the structure and the design wind velocity at the site. The influence of shape is illustrated by Fig. 1.12, which shows the effect of roof angle on the pressure distribution. When $\theta > 45^\circ$, there is a transition from negative to positive pressure on face AB of the inclined roof. This shift is due to the flow separation point moving from A to B for steeply inclined roofs.

1.3.4.2 Wind Velocity

The effect of the site is characterized firstly by the topography at the site, and secondly by the regional wind environment. Exposure categories are defined to describe the local topography and to establish the level of exposure to wind. ASCE 7-05 adopts the following definitions of exposure categories.

Fig. 1.10 Characteristics of the AASHTO design truck

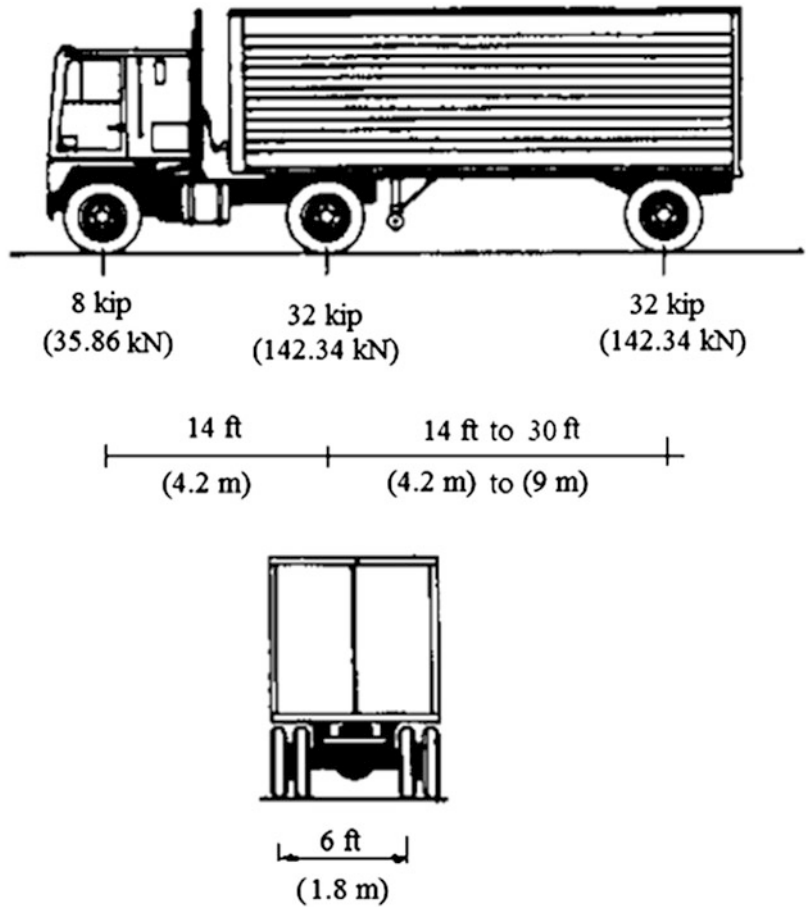


Fig. 1.11 Flow lines and pressure distributions due to wind

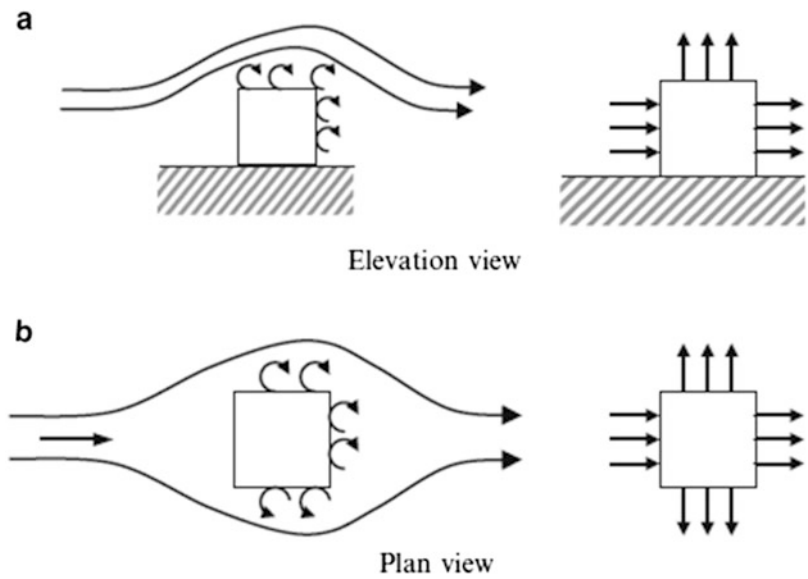
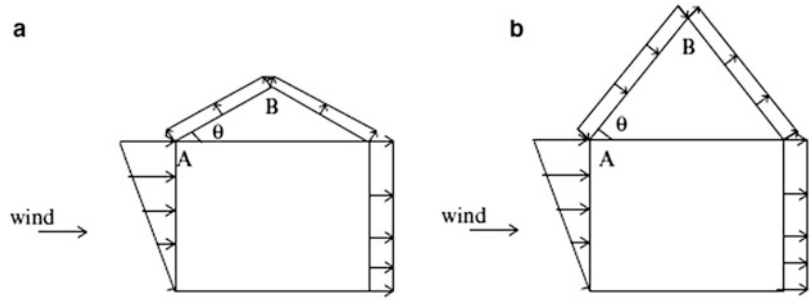


Fig. 1.12 Wind pressure profiles for a gable roof. (a) $\theta < 45^\circ$. (b) $\theta > 45^\circ$



- Category B:* Site located within an urban or suburban area having numerous closely spaced obstructions similar in size to a single family dwelling, and extending at least 2600 ft from the site.
- Category D:* Site located in a flat unobstructed area or on a water surface outside hurricane prone regions, and extending at least 5000 ft from the site.
- Category C:* All cases where exposure categories B and D do not apply.

Regional wind environments are represented by maps containing wind speed data for a specified return period and exposure category. Figure 1.13 shows US data for the 50-year wind speed observed at 10 m elevation corresponding to Exposure C. The higher wind speeds along the East and Gulf Coasts reflects the occurrence of hurricanes in these regions. Typical 50-year wind speeds are on the order of 100 miles per hour (45 m/s).

Given a site, one can establish the 50-year wind speed at 10 m elevation using Fig. 1.13. In general, the wind velocity increases with distance from the ground. A typical approximation is a power law:

$$V(z) = \bar{V} \left(\frac{z}{\bar{z}} \right)^{1/\alpha} \tag{1.1}$$

where z is the elevation above the ground, \bar{V} is the velocity measured at elevation \bar{z} , and $\alpha \approx 7$. For US data, one takes $\bar{z} = 10\text{m}$ and \bar{V} given by Fig. 1.13.

1.3.4.3 Pressure Profiles

The next step is to establish the vertical pressure distribution associated with this velocity distribution, and then modify it to account for the shape of the building. Pressure and velocity are related by Bernoulli's Equation, which is a statement of conservation of energy. Specialized for steady irrotational inviscid flow of a weightless fluid, the Law states that [12]

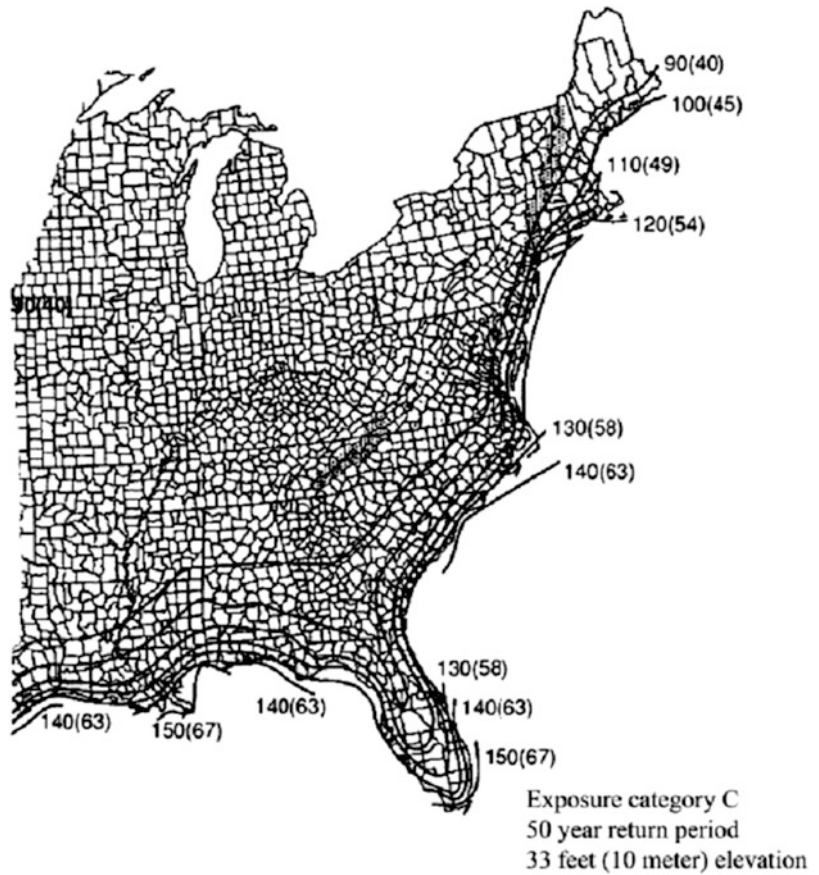
$$E = \text{Energy per unit volume} = p + \frac{1}{2}\rho V^2 \tag{1.2}$$

is constant along a streamline. Here, p is the pressure energy, ρ is the mass density, and $1/2\rho V^2$ is the kinetic energy per unit volume. Assuming the pressure is zero in the free stream flow regime away from the structure, and taking point (1) in the free stream and point (2) at the structure, one obtains

$$p_2 = \frac{1}{2}\rho(V_1^2 - V_2^2) \tag{1.3}$$

The free stream velocity, V_1 , is defined by (1.1). Considering the flow to be stopped by the structure, ($V_2 \approx 0$), it follows that the maximum pressure energy associated with the free stream velocity is estimated as

Fig. 1.13 Basic wind speed miles per hour (meter per second) for the East coast of the USA



$$(p_2)_{\max} = \frac{1}{2} \rho V_1^2 = p_{\text{stag}} \quad (1.4)$$

This pressure is called the stagnation pressure and is generally expressed in terms of the reference velocity, \bar{V} , at $z = 10$ m and a function $k(z)$ which defines the vertical distribution.

$$p_{\text{stag}} = \frac{1}{2} \rho \bar{V}^2 k(z) \quad (1.5)$$

ASCE 7-05 tabulates values of $k(z)$ vs. z .

The actual pressure distribution is influenced by the geometric shape which tends to change both the magnitude and sense of the pressure. Figures 1.11 and 1.12 illustrate this effect for flat and gable roof structures. Design codes handle this aspect by introducing “shape” factors for different regions of the structural surface. They also include a gust factor for “dynamic” loading, and an importance factor for the structure. The final expression for the design pressure has the following general form:

$$P_{\text{design}} = IGC_p(z)p_{\text{stag}} \quad (1.6)$$

where $C_p(z)$ is the pressure coefficient that accounts for the shape, G is the gust factor, and I is the importance factor corresponding to the occupancy category. Values for these parameters are code dependent. The determination of the design pressure can be labor intensive if one wants to account

fully for the spatial distribution of design pressure. A reasonable estimate can be obtained using the simplified procedure illustrated in the following example which is appropriate for low-rise buildings.

Example 1.1 Wind Pressure Distribution on a Low-Rise Gable Roof Structure

Given: The structure shown in Fig. E1.1a. There are four surface areas included in the sketch. Zone (1) is the windward face, zone (2) is the leeward face, and zones (3) and (4) are on the gable roof.

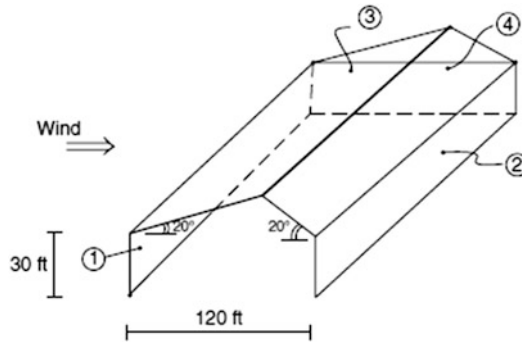


Fig. E1.1a

Determine: The wind pressure distribution on the interior zone away from the ends. Assume

$$\bar{V} = 100 \text{ mph and exposure } C$$

Solution: Applying (1.5) leads to

$$p_{\text{stag}} = (0.00256)(10^4)k(z) = 25.6k(z) \text{ (lb/ft}^2\text{)}$$

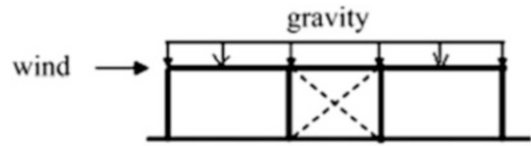
Values of $k(z)$ and the corresponding p_{stag} are listed below

z (ft)	$k(z)$	p_{stag} (lb/ft ²)
15	0.85	21.8
20	0.90	23.0
25	0.94	24.1
30	0.98	25.1

We assume the structure is Category III and use $I = 1.15$. For low-rise buildings with $h < 60$ ft, the factors G and C_p are combined and specified as constant for each zone. Using data from ASCE 7-05, the values are

Zone	GC_p	IGC_p
1	0.53	0.609
2	-0.43	-0.495
3	-0.69	-0.794
4	-0.48	-0.552

Fig. 1.14 Lateral bracing system



Lastly, we compute the design pressure using (1.6). The ASCE 7-05 code assumes that p_{design} varies on the windward force (zone 1), but specifies constant distributions for the other zones. The details are listed below.

Zone 1	$p_{\text{design}} = 0.609 (25.6) k(z) = 15.59 k(z)$
Zone 2	$p_{\text{design}} = -0.495 (25.6) k(30) = -12.42 \text{ psf}$
Zone 3	$p_{\text{design}} = -0.791 (25.6) k(30) = -19.92 \text{ psf}$
Zone 4	$p_{\text{design}} = -0.552 (25.6) k(30) = -13.85 \text{ psf}$

Pressure distributions generated with (1.6) define the quasi-static wind load, which acts predominantly in the horizontal (lateral) direction. For low-rise buildings, gravity loads are the dominant loads and generally control the structural dimensioning process for vertical members. Since the wind loads are horizontal, whereas the gravity loads are vertical, lateral structural bracing systems such as shown in Fig. 1.14 need to be incorporated in certain types of structures such as a braced frames. This topic is addressed further in Chaps. 11, 14, and 15.

1.3.4.4 Vortex Shedding Pressure

The action of a steady wind on a structure is represented by quasi-static forces. However, a steady wind also creates periodic forces due to the shedding of vortices from the turbulence zones at the leeward face [12]. Consider the rectangular cross-section plan view shown in Fig. 1.15. As the incident flow velocity increases, eddies are created at the upper and lower surfaces and exit downstream. This shedding pattern develops a cyclic mode, shedding alternately between the upper and lower surfaces, which result in an antisymmetric pressure distribution. The net effect is a periodic force, F_t , acting in the transverse direction with frequency, f_s . An estimate for the shedding frequency is

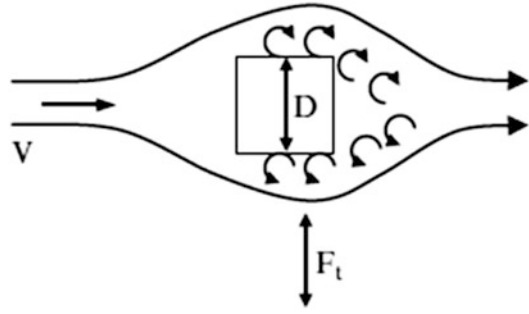
$$f_s (\text{cycles per second}) \approx \frac{0.2V}{D} \quad (1.7)$$

where D is a representative dimension in the transverse direction, and V is the free stream velocity. Vortex shedding is a major concern for tall buildings and slender long-span horizontal structures since these structures are flexible and consequently more susceptible to transverse periodic excitation with a frequency close to f_s . Low-rise buildings are stiffer and relatively insensitive to vortex shedding-induced transverse motion.

1.3.5 Snow Loading

Design snow loads for a structure are based on ground snow load data for the region, where the structure is located. Snow loads act on the roof zones of structures. For a flat roof, defined as a roof with a slope angle less than 5° , the snow load is represented as a uniform downward pressure, p_f . The

Fig. 1.15 Vortex shedding patterns—plan view



magnitude of p_f depends on the exposure category and regional environment at the site, as well as the importance of the structure. We express p_f as

$$p_f = Cp_g \quad (1.8)$$

where p_g is the ground snow pressure given by Fig. 1.16a and C is a factor that incorporates the exposure and importance parameters. A typical value of C is ≈ 1 . The ground snow pressure varies from 0 in the southeastern zone of the USA up to ≈ 100 psf in northern New England.

A sloped roof is defined as a roof with a slope angle greater than 5° . The snow load on a sloped roof is expressed in terms of the *horizontal projected area* rather than the actual surface area. Figure 1.16b illustrates this definition.

The sloped roof pressure depends on the slope angle as well as the other parameters mentioned earlier.

$$p_s = C_s p_f \quad (1.9)$$

where C_s is a slope coefficient. In general, $C_s \leq 1$. For $\theta \lesssim 30^\circ$, one usually assumes $C_s \approx 1$ and takes $p_s \approx p_f$.

When the roof has projections as illustrated in Fig. 1.17, a nonuniform snow loading can result due to the drifting on both the windward and leeward faces produced by wind. Drifts are modeled as triangular surcharge loadings. The details are code dependent.

1.3.6 Earthquake Loading

The structural engineer's task is to design structures such that they can resist the ground shaking associated with an earthquake without collapsing. Since an earthquake may occur anytime during the design life, the first task is to identify the magnitude of peak ground acceleration (ρga) that has a specified probability of occurrence during the design life. A common value is 2 % probability of occurrence in 50 years, which corresponds to a return period of 2500 years. Earthquake ground motion is site specific in that it depends on the location and soil conditions for the site. Sites near known faults and sites on soft soils such as soft clay experience more intense ground motion. Factors such as the importance of the building, the geographic location of the site, and the type of soil must be taken into account when specifying the design magnitude for ρga .

In order to understand how buildings respond to ground motion, one needs to examine the dynamic response. Consider the three-story frame shown in Fig. 1.18a. We approximate it with the simple beam/mass system defined in Fig. 1.18b. This approximation, known as a single degree-of-freedom

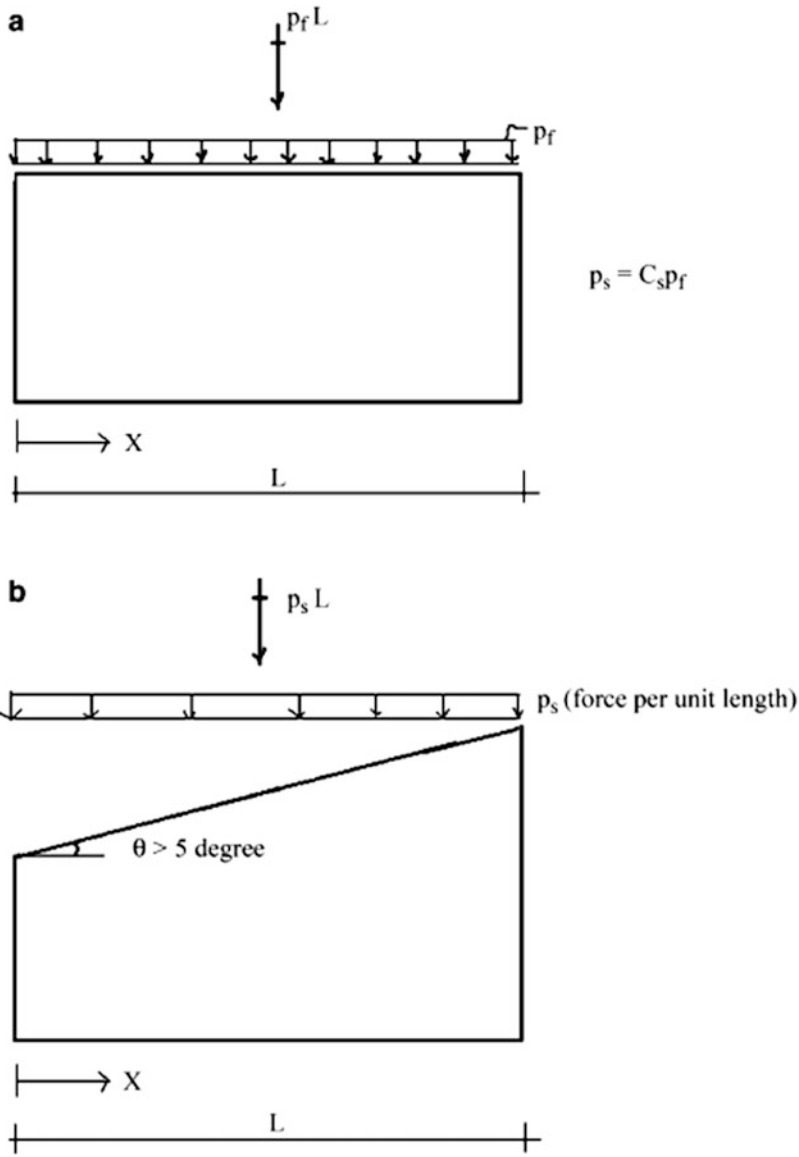


Fig. 1.16 Snow loadings on sloped and flat roofs. (a) Flat roof. (b) Sloped roof

Fig. 1.17 Snow drift profiles

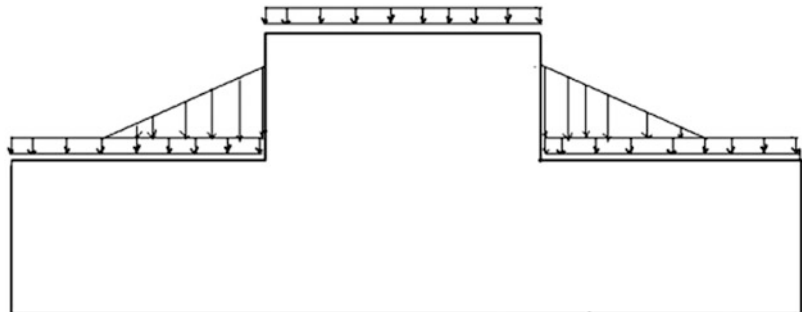


Fig. 1.18 A typical three-story frame and the corresponding one degree-of-freedom model

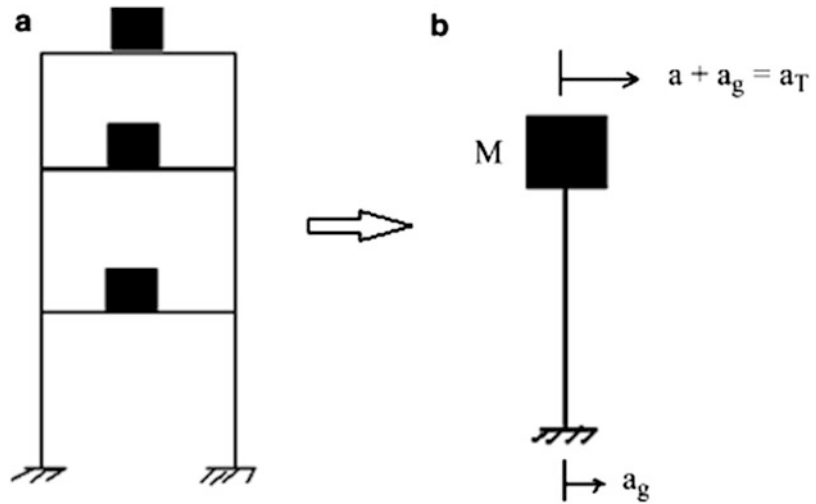
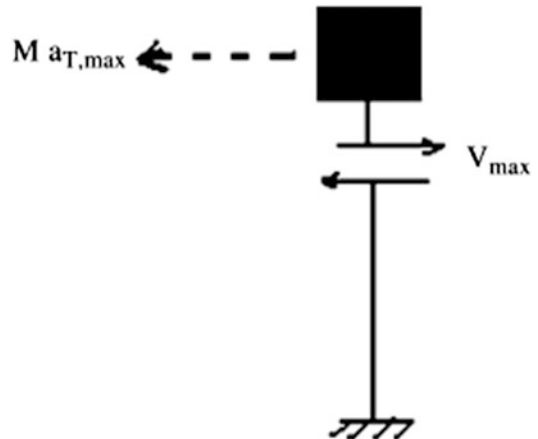


Fig. 1.19 Peak lateral inertia force

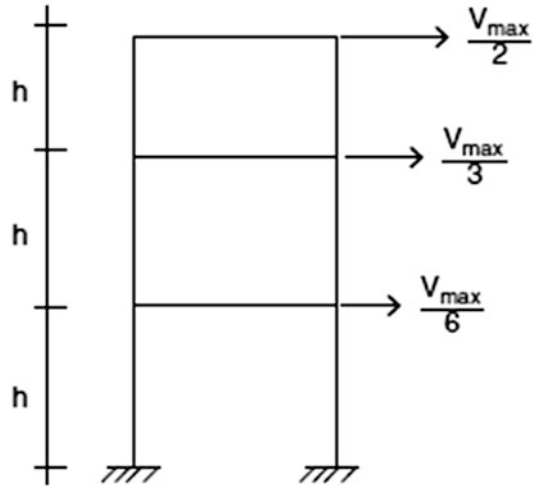


model, provides useful information concerning the influence of certain structural properties on the response.

The ground acceleration is defined as a_g . This motion causes the mass to vibrate. We define $a_{T,max}$ as the peak total acceleration of the mass (Fig. 1.19). If the frame is very stiff, $a_{T,max}$ is essentially equal to $a_{g,max}$, the peak ground acceleration. When the frame is very flexible, $a_{T,max}$ is *small in comparison to* $a_{g,max}$. It follows that the *stiffness* of the structure has a *significant influence* on the peak total acceleration response. The peak acceleration also depends on the geographic location and the soil conditions at the site. Data concerning earthquake accelerations is published by the US Geological Survey on their Web site [13]. This site contains an extensive set of earthquake ground motion records for the USA and other major seismically active regions throughout the world.

The motion of the mass generates an inertia force which is resisted by the lateral shear force in the system. The maximum value of the lateral shear force is denoted as V_{max} .

Fig. 1.20 Seismic lateral load profile



$$V_{\max} = Ma_{T,\max} = W \left(\frac{a_{T,\max}}{g} \right) \quad (1.10)$$

Given the structural weight, W , and the peak total acceleration, one can estimate the peak total lateral load that the structure will experience due to seismic excitation. This load is assumed to be distributed linearly throughout the height of the structure, as indicated in Fig. 1.20, and used to generate an initial structural design. The final design is checked with a more refined dynamic analysis. Seismic design is an advanced topic within the field of structural engineering. We discuss this topic in more detail in Chap. 14.

1.4 Structural Design Philosophy

Conventional structural design philosophy is based on satisfying two requirements, namely safety and serviceability [7]. Safety relates to extreme loadings, which have a very low probability of occurrence, on the order of 2 %, during a structure's life, and is concerned with the collapse of the structure, major damage to the structure and its contents, and loss of life. The most important priority is ensuring sufficient structural integrity so that sudden collapse is avoided. Serviceability pertains to medium to large loadings, which are likely to occur during the structure's lifetime. For service loadings, the structure should remain operational. It should suffer minimal damage, and furthermore, the motion experienced by the structure should not exceed specified comfort levels for humans and motion-sensitive equipment mounted on the structure. Typical occurrence probabilities for service loads range from 10 to 50 %.

Safety concerns are satisfied by requiring the resistance, i.e., the strength of the individual structural elements to be greater than the demand associated with the extreme loading. Once the structure is dimensioned, the stiffness properties are derived and used to check the various serviceability constraints such as elastic behavior. Iteration is usually necessary for convergence to an acceptable structural design. This approach is referred to as strength-based design since the elements are dimensioned initially according to strength requirements.

Applying a strength-based approach for preliminary design is appropriate when strength is the dominant design requirement. In the past, most structural design problems have fallen in this

category. However, the following developments have occurred recently that limit the effectiveness of the strength-based approach. Firstly, the trend toward more flexible structures such as tall buildings and long-span horizontal structures has resulted in more structural motion under service loading, thus shifting the emphasis toward serviceability. Secondly, some new types of facilities such as micro device manufacturing centers and hospital operating centers have more severe design constraints on motion than the typical civil structure. For example, the environment for micro device manufacturing must be essentially motion free. Thirdly, recent advances in material science and engineering have resulted in significant increases in the strength of traditional civil engineering materials. However, the material stiffness has not increased at the same rate. The lag in material stiffness vs. material strength has led to a problem with satisfying the requirements on the various motion parameters. Indeed, for very high strength materials, the motion requirements control the design. Fourthly, experience with recent earthquakes has shown that the cost of repairing structural damage due to inelastic deformation is considerably greater than anticipated. This finding has resulted in a trend toward decreasing the reliance on inelastic deformation to dissipate energy and shifting to other type of energy dissipating and energy absorption mechanisms.

Performance-based design [14] is an alternate design paradigm that addresses these issues. The approach takes as its primary objective the satisfaction of motion-related design requirements such as restrictions on displacement and acceleration and seeks the optimal deployment of material stiffness and motion control devices to achieve these design targets as well as satisfy the constraints on strength. Limit state design can be interpreted as a form of performance-based design, where the structure is allowed to experience a specific amount of inelastic deformation under the extreme loading.

1.5 Basic Analytical Tools of Structural Analysis

Engineering a structure involves not only dimensioning the structure but also evaluating whether the structure's response under the construction and design loadings satisfy the specified design criteria. Response evaluation is commonly referred to as structural analysis and is carried out with certain analytical methods developed in the field of Engineering Mechanics and adopted for structural systems. In this section, we review these methods and illustrate their application to some simple structures. Most of this material is covered in textbooks dealing with Statics and Mechanics of Materials [2–4] and Structural Analysis [15–17]. Heyman's text [18] contains an excellent description of the "underlying science of Structural Engineering."

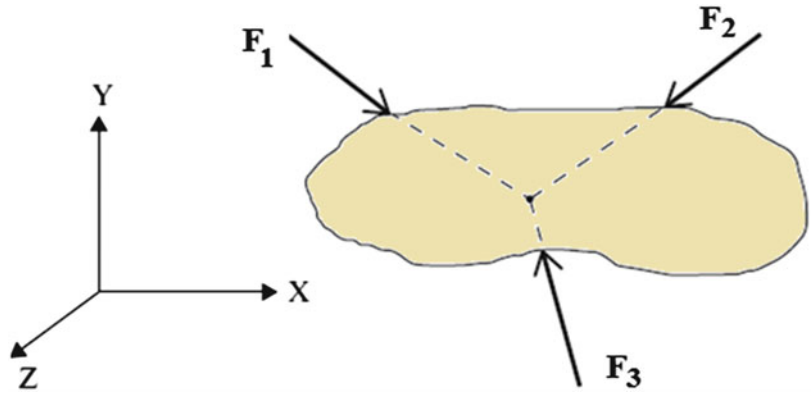
1.5.1 Concept of Equilibrium: Concurrent Force System

We begin with a discussion of static equilibrium conditions for solid bodies. This topic is relevant to structural engineering since structures are solid bodies subjected to loads, and we need to ensure that a structure remain at rest, i.e., that it is in a state of equilibrium.

The simplest case is a body subjected to a set of concurrent forces. By definition, the lines of action of the forces comprising a concurrent force system intersect at a common point. Figure 1.21 illustrates this case. For static equilibrium, the resultant of the force system must be a null vector.

$$\mathbf{R} = \mathbf{F}_1 + \mathbf{F}_2 + \mathbf{F}_3 = \mathbf{0} \quad (1.11)$$

Fig. 1.21 Concurrent force system



We convert the vector equilibrium over to a set of algebraic equations by resolving the force vectors into their components with respect to an arbitrary set of orthogonal directions (X, Y, Z). This operation leads to

$$\begin{aligned}\sum_{i=1}^3 F_{i,x} &= F_{1,x} + F_{2,x} + F_{3,x} = 0 \\ \sum_{i=1}^3 F_{i,y} &= F_{1,y} + F_{2,y} + F_{3,y} = 0 \\ \sum_{i=1}^3 F_{i,z} &= F_{1,z} + F_{2,z} + F_{3,z} = 0\end{aligned}\quad (1.12)$$

We find it more convenient to work with (1.12) rather than (1.11).

When all the force vectors are in one plane, say the $X - Y$ plane, the force system is called a planar force system and (1.12) reduces to two equations. Most of the force systems that we deal with will be planar systems.

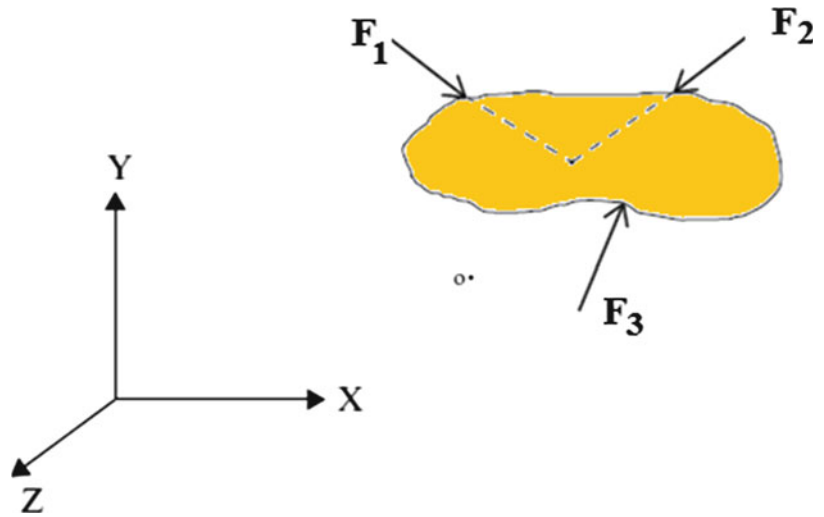
1.5.2 Concept of Equilibrium: Nonconcurrent Force System

The next level of complexity is a body subjected to a nonconcurrent planar force system. Referring to Fig. 1.22, the forces tend to rotate the body as well as translate it. Static equilibrium requires the resultant force vector to vanish and, in addition, the resultant moment vector about an arbitrary point to vanish.

$$\begin{aligned}\mathbf{R} &= \mathbf{F}_1 + \mathbf{F}_2 + \mathbf{F}_3 = \mathbf{0} \\ \mathbf{M}_o &= \mathbf{0}\end{aligned}\quad (1.13)$$

Resolving the force and moment vectors into their X, Y, Z components leads to six scalar equations, three for force and three for moment. When the force system is planar, say in the $X - Y$ plane, (1.13) reduce to three scalar equations

Fig. 1.22 Nonconcurrent force system



$$\begin{aligned} \sum_{i=1}^3 F_{i,x} &= 0 \\ \sum_{i=1}^3 F_{i,y} &= 0 \\ \sum M_o &= 0 \end{aligned} \tag{1.14}$$

where o is an arbitrary point in the $x - y$ plane. Note that now for a planar system there are three equilibrium conditions vs. two for a concurrent system. Note also that since there are three equilibrium equations, one needs to apply three restraints to prevent planar rigid body motion.

Example 1.2 Equilibrium Equations

Given: The rigid body and force system shown in Fig. E1.2a. Forces A_x , A_y , and B_y are unknown.

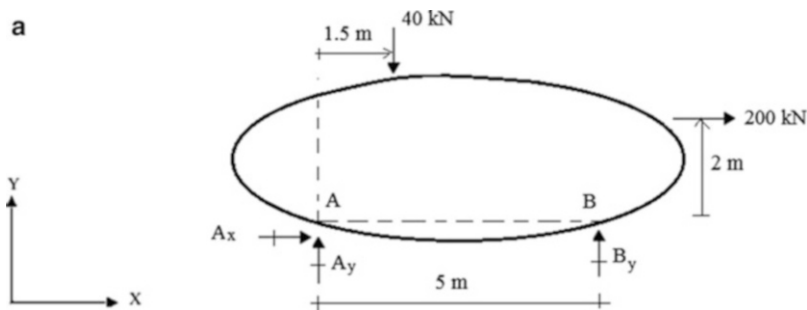


Fig. E1.2a

Determine: The forces A_x , A_y , and B_y

Solution: We sum moments about A, and solve for B_Y

$$\begin{aligned}\sum M_A &= -40(1.5) - 200(2) + B_Y(5) = 0 \\ B_Y &= +92 \Rightarrow B_Y = 92 \text{ kN } \uparrow\end{aligned}$$

Next, summing forces in the X and Y directions leads to (Fig. E1.2b)

$$\begin{aligned}\sum F_x \rightarrow^+ &= A_x + 200 = 0 \Rightarrow A_x = -200 \Rightarrow A_x = 200 \text{ kN } \leftarrow \\ \sum F_y \uparrow^+ &= A_y + 92 - 40 = 0 \Rightarrow A_y = -52 \Rightarrow A_y = 52 \text{ kN } \downarrow\end{aligned}$$

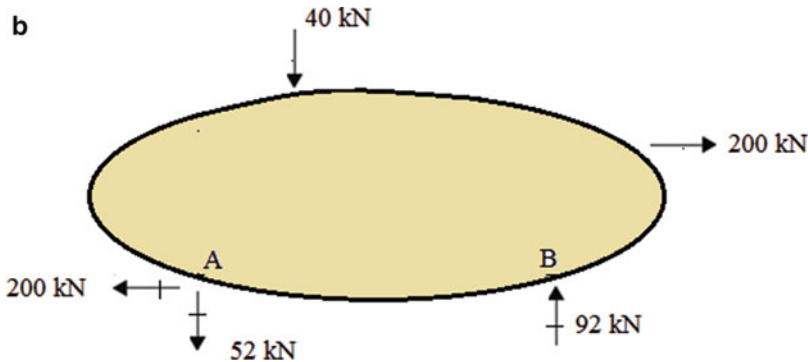


Fig. E1.2b

1.5.3 Idealized Structure: Free Body Diagrams

Generating an idealization of an actual structure is the key step in applying the equilibrium equations. Given a structure acted upon by external loads and constrained against motion by supports, one idealizes the structure by identifying the external loads and supports, and replacing the supports with their corresponding unknown reaction forces. This process is called constructing the free body diagram (FBD). Figure 1.23a, b illustrates the details involved.

One applies the equilibrium equations to the FBD. Note that this diagram has four unknown reaction forces. Since there are only three equilibrium equations, one cannot determine all the reaction forces using only the equilibrium conditions. In this case, we say that the structure is *statically indeterminate*.

Constructing an FBD is *an essential step* in applying the equilibrium equations. The process is particularly useful when the structure is actually a collection of interconnected structural components such as a framed structure. One first generates an FBD for the entire structure and then works with separate FBDs for the individual members. We illustrate this approach throughout the text.

1.5.4 Internal Forces

Consider the body shown in Fig. 1.24a. Suppose we pass a cutting plane as indicated and separate the two segments. We represent the action of body “n” on body “m” by a force \vec{F} and moment \vec{M} . From Newton’s third law, the action of body m on body n is opposite in sense.

Once the reaction forces are known, we can determine \vec{F} and \vec{M} by applying the equilibrium conditions to either segment. These force quantities are called “*internal forces*” in contrast to the

Fig. 1.23 Constructing the free body diagram (FBD)

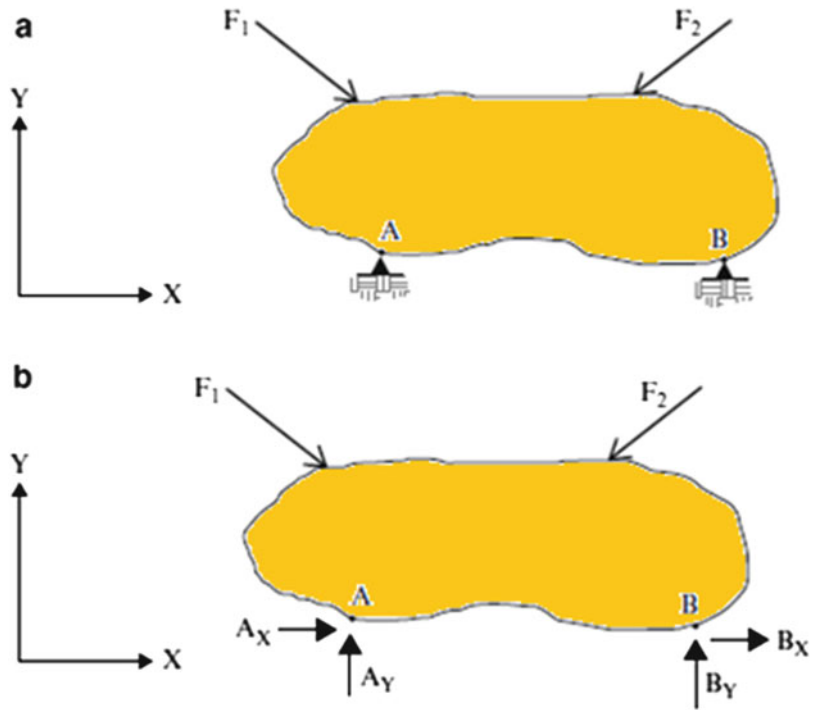
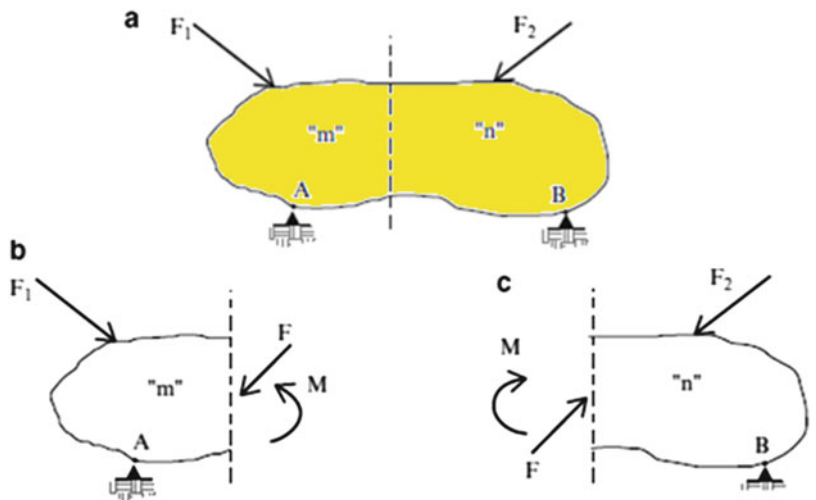


Fig. 1.24 Definition of internal forces



reactions which are “*external forces*.” Note that the magnitude of the internal forces varies with the location of the cutting plane. The following example illustrates the process of computing internal forces.

Example 1.3

Given: The body and loading shown in Fig. E1.3a.

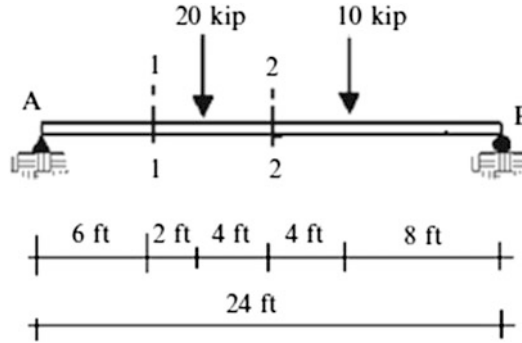


Fig. E1.3a

Determine: The internal forces at Sects. 1-1 and 2-2

Solution: First, we determine the reactions at A and B by applying the equilibrium conditions to entire body AB (Fig. E1.3b).

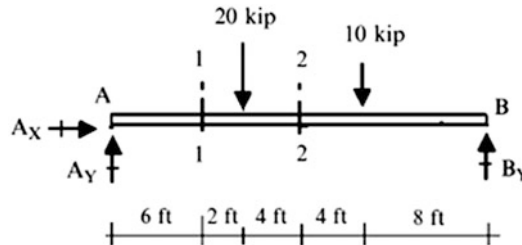


Fig. E1.3b

The static equilibrium equations are

$$\begin{aligned}\sum F_x &= 0 & A_x &= 0 \\ \sum F_y &= 0 & A_y + B_y &= 30 \\ \sum M_{\text{about } A} &= 0 & 8(20) + 16(10) - 24B_y &= 0\end{aligned}$$

We solve for B_y , $B_y = \frac{20}{3} + \frac{2}{3}(10) = 13.3 \text{ kip } \uparrow$
and then A_y $A_y = 16.7 \text{ kip } \uparrow$

Next, we work with the FBDs shown below. We replace the internal force vector with its normal and tangential components, F and V (Figs. E1.3c and E1.3d).

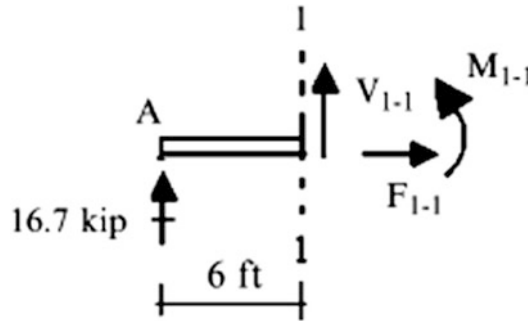


Fig. E1.3c Left segment-cutting plane 1-1

Applying the equilibrium conditions to the above segment leads to

$$\sum F_{x \rightarrow +} F_{1-1} = 0$$

$$\sum F_{y \uparrow +} = 0 \quad V_{1-1} + 16.7 = 0 \Rightarrow V_{1-1} = 16.7 \text{ kip } \downarrow$$

$$\sum M_{\text{about } 1-1} = 0 \quad M_{1-1} - 16.7(6) = 0 \Rightarrow M_{1-1} = 100.2 \text{ kip ft counterclockwise}$$

Applying the equilibrium conditions to the segment shown below leads to

$$\sum F_{x \rightarrow +} F_{2-2} = 0$$

$$\sum F_{y \uparrow +} = 0 \quad V_{2-2} - 20 + 16.7 = 0 \Rightarrow V_{2-2} = 3.3 \text{ kip } \downarrow$$

$$\sum M_{\text{about } 2-2} = 0 \quad M_{2-2} - 12(16.7) + 4(20) = 0 \Rightarrow M_{2-2} = 120.4 \text{ kip ft counterclockwise}$$

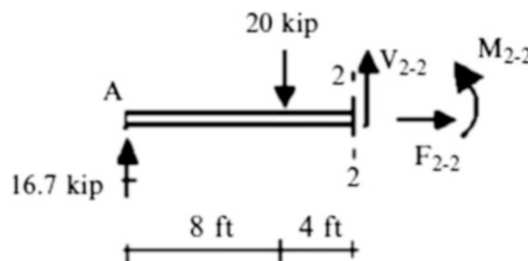


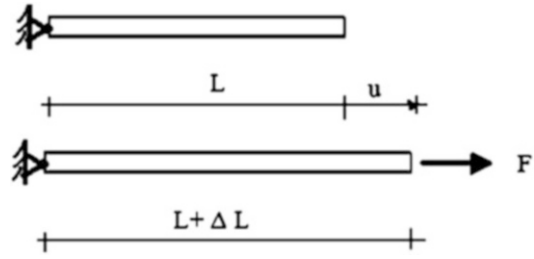
Fig. E1.3d Left segment-cutting plane 2-2

Note that the sense of V_{1-1} and V_{2-2} are opposite to the directions we chose initially.

1.5.5 Deformations and Displacements

When a body is subjected to external loads, internal forces are developed in order to maintain equilibrium between the internal segments. These forces produce stresses which in turn produce strains that cause the body to change its shape and displace from its unloaded position.

Fig. 1.25 Unreformed and deformed states



Consider the member shown in Fig. 1.25. We apply an axial force which generates the axial stress, σ , equal to

$$\sigma = \frac{F}{A} \quad (1.15)$$

where A is the cross-sectional area. The resulting strain depends on E , the modulus of elasticity for the material [3, 4].

$$\varepsilon = \frac{\sigma}{E} \quad (1.16)$$

By definition, the extensional strain is the relative change in length.

$$\varepsilon = \frac{\Delta L}{L} \quad (1.17)$$

Then,

$$\Delta L = L\varepsilon = \left(\frac{L}{AE}\right)F \quad (1.18)$$

We refer to the movement due to strain as the displacement and denote it by u . It follows that ΔL is equal to u . Finally, we write (1.18) as

$$u = \left(\frac{L}{AE}\right)F \quad (1.19)$$

Strains are generally referred to as deformations since they relate to a change in shape. This example illustrates that displacements are a consequence of deformations which are due to forces. Note that deformations are dimensionless quantities whereas displacements have geometric units such as either length (translation) or angle (rotation). The coefficient of F in (1.19) has units of displacement/force. We interpret this coefficient as a measure of the flexibility of the member. Here, we are defining flexibility as displacement per unit force. The inverse of flexibility is called stiffness. Stiffness relates the force required to introduce a unit displacement. Inverting (1.19) leads to

$$F = \left(\frac{AE}{L}\right)u \quad (1.20)$$

It follows that the stiffness of an axial loaded member is equal to $\frac{AE}{L}$.

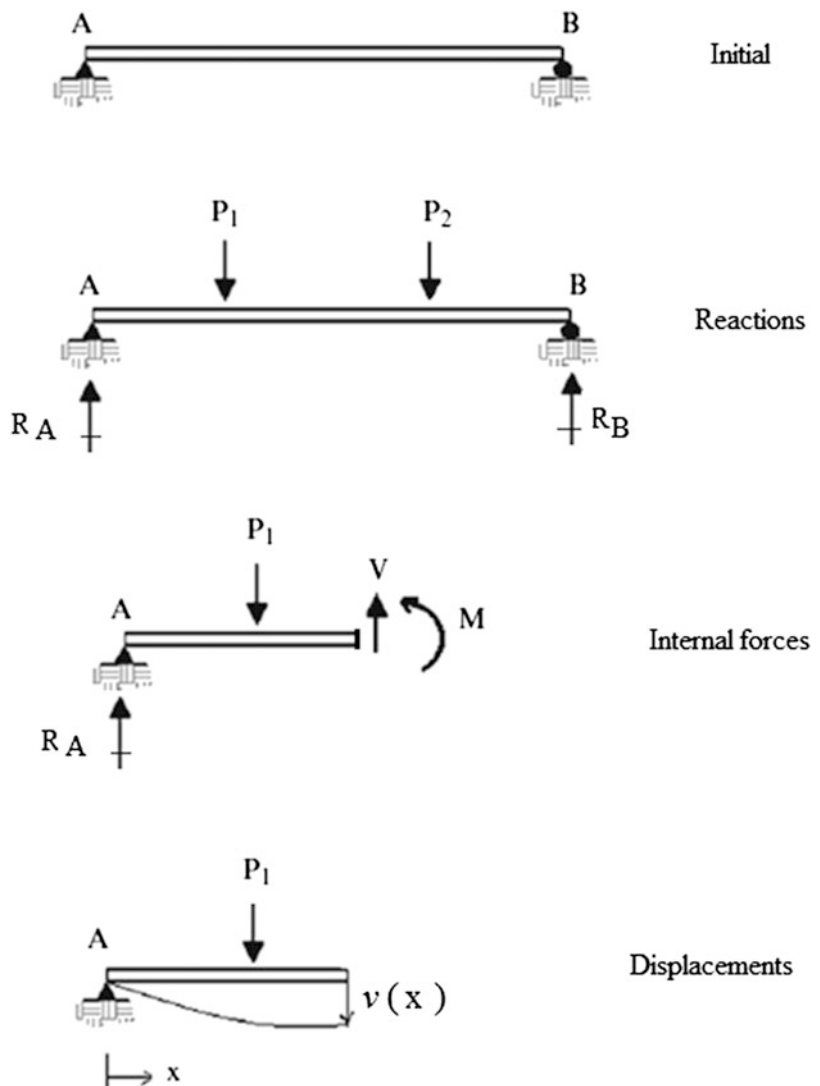
Stiffness and flexibility are important concepts in structural engineering. We use them to reason qualitatively about the change in behavior of a structure when we introduce modifications to the geometry and structural members. Obviously, to reduce displacements, one makes the structure stiffer. How this is achieved is one of the themes of this text.

1.5.6 Structural Behavior: Structural Analysis

When a structure is subjected to an external loading, it responds by developing internal forces which lead to internal stresses. The stresses generate strains, resulting in displacements from the initial unloaded position. Figure 1.26 illustrates the displacement process for a beam-type member subjected to a transverse loading. This process continues until the internal stresses reach a level at which the external loading is equilibrated by the internal forces. The final displacement profile corresponds to this equilibrium state.

Structural analysis is concerned with quantifying the response of structures subjected to external loading. The scope includes determining the magnitude of the reactions, internal forces, and displacements. The analysis is generally carried out in the order shown in Fig. 1.26.

Fig. 1.26 Simple beam response



1.5.6.1 Study Forces

In the study of forces, we apply the equilibrium equations to various FBDs. We work initially with the FBD for the structure treated as a single body and determine the reactions. Once the reactions are known, we select various cutting planes and determine the corresponding internal forces. This phase involves some heuristic knowledge as to “the best” choice of cutting planes.

1.5.6.2 Study Displacements

Displacements are the geometric measures that define the position of the structure under the applied external loading. Displacements are a consequence of internal stresses and are usually expressed in terms of the internal forces. The form of the “force-displacement” relations depends on the type of structural member, e.g., a truss member and a beam. We discuss this topic in more detail in Chaps. 2 and 3. In what follows, we illustrate these computations for some fairly simple structures.

Example 1.4

Given: The structure defined in Fig. E1.4a. Member AB is a rigid member. It is connected to a hinge support at A, and supported at B by a cable, BC.

Determine: The reactions, cable tension, and vertical displacement at B. Assume $E_C = 200$ Gpa, $A_C = 600$ mm², $h = 4$ m, $L = 10$ m, and $P = 80$ kN

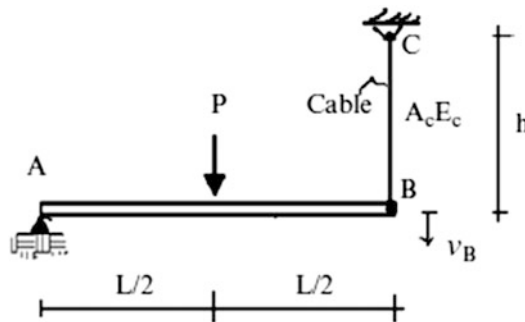


Fig. E1.4a

Solution: We start with the FBD of the entire structure shown in Fig. E1.4b. We note that the cable force is tension. Requiring the sum of the moments of the forces with respect to point A to vanish leads to the T_C

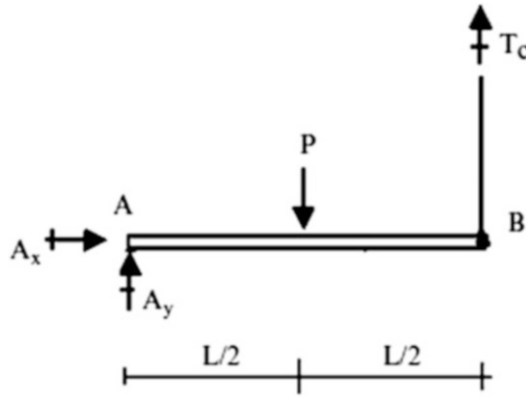


Fig. E1.4b

$$\begin{aligned}\sum M_{\text{about A}} &= \frac{L}{2}P - LT_C = 0 \\ &\Downarrow \\ T_C &= \frac{P}{2}\end{aligned}$$

Next, we determine the reactions at A using force summations.

$$\begin{aligned}\sum F_Y = 0 \quad A_y + T_C - P = 0 &\Rightarrow A_y = \frac{P}{2} \\ \sum F_x = 0 \quad A_x = 0\end{aligned}$$

The vertical displacement of B is equal to the extension of the cable. Noting (1.19), the expression for v_B is

$$v_B = \left(\frac{h}{A_c E_c}\right) T_C = \frac{h}{A_c E_c} \left(\frac{P}{2}\right) = \frac{4,000}{(600)(200)} \left(\frac{80}{2}\right) = 1.33 \text{ mm} \downarrow$$

In what follows, we illustrate the application of the general analysis procedure to the idealized structure defined in Fig. 1.27. Member ABCD is considered to be rigid. It is supported by a hinge at A and springs at C and D. The force, P , is constant. Replacing the hinge support and springs with their corresponding forces results in the FBD shown in Fig. 1.27b. There are four unknown forces; A_x , A_y , F_c , and F_d . Setting the resultant force equal to zero leads to

$$\begin{aligned}A_x &= 0 \\ A_y + F_c + F_d &= P\end{aligned}\tag{1.21}$$

Next, we require that the moment vanish at A.

$$\frac{l}{4}P = \frac{l}{2}F_c + lF_d\tag{1.22}$$

Since there are more force unknowns than force equilibrium equations, the structure is statically indeterminate.

Fig. 1.27 Rigid member on springs

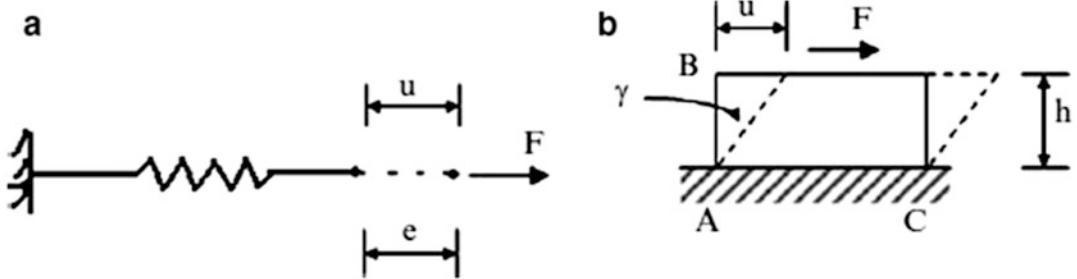
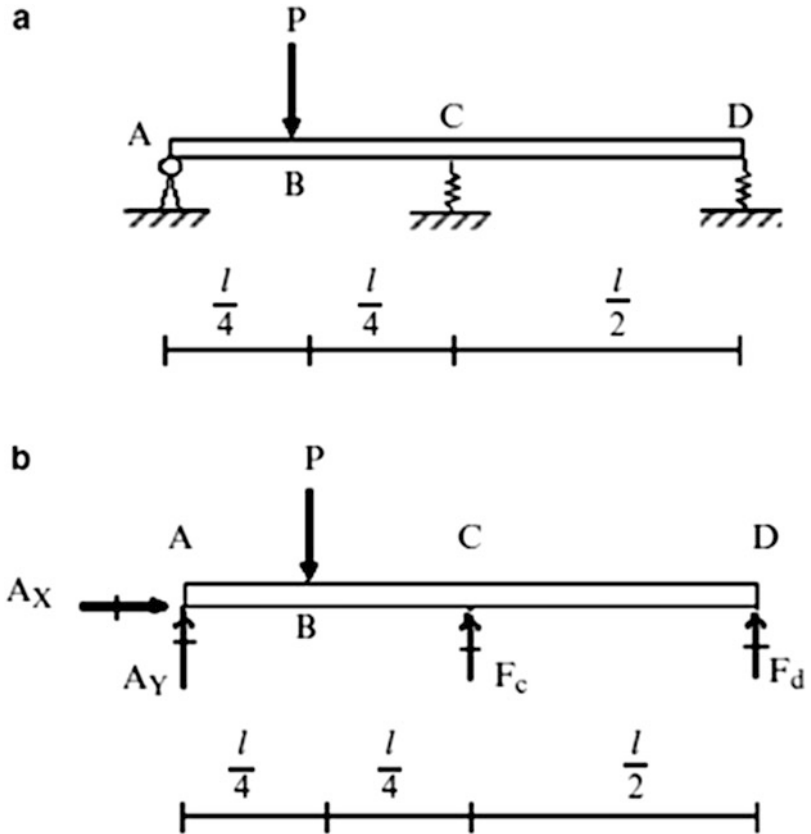
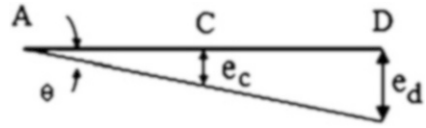


Fig. 1.28 Deformation modes. (a) Extension. (b) Shear

We generate additional equations by examining how the structure deforms. Deformation is a consequence of applying a force to a material. Deformation is associated with a change in shape. Figure 1.28 illustrates various deformation modes: the first is extension of a spring; the second is shear. A rigid body is an idealized case: the deformations are considered to be negligible.

An important phase in the analysis of a deformable body is the study of deformations. One first identifies the displacement variables that define the “deformed” position and then, using geometric analysis, establishes the expressions relating the deformations of the deformable structural elements with the displacements. We illustrate this process for the structure defined in Fig. 1.29.

Fig. 1.29 Deformation–displacement relations



Member ABCD is assumed to be rigid and therefore remains straight when the load is applied. Deformation occurs in the springs at C and D, causing ABCD to rotate about the hinge at A. There is only one independent displacement variable. We take it to be the rotation angle θ shown in Fig. 1.29. With this choice of sense, the springs compress. When θ is small, the spring deformations can be approximated as linear functions of θ . This approximation is valid for most cases.

$$\begin{aligned} e_c &= \left(\frac{l}{2}\right)\theta \\ e_d &= l\theta \end{aligned} \quad (1.23)$$

The last step in the analysis involves relating the deformations and the corresponding internal forces. For this example structure, the internal forces are the spring forces, F_c and F_d . In general, the relationship between the force and deformation of a component is a function of the makeup of the component (i.e., the material used and the geometry of the component). Here, we assume the behavior is linear and write

$$\begin{aligned} F_c &= k_c e_c \\ F_d &= k_d e_d \end{aligned} \quad (1.24)$$

where k_c and k_d are the spring stiffness factors. Note that the units of k are force/length since e has units of length.

At this point, we have completed the formulation phase. There are seven equations, (1.21)–(1.23), relating the seven variables consisting of the four forces, one displacement, and two deformations. Therefore, the problem is solvable. How one proceeds through the solution phase depends on what variables one wants to determine first.

Starting with (1.23), we observe that the reaction A_v can be determined once the spring forces are known. Therefore, we hold this equation in reserve, and focus on the remaining equations. We can combine (1.23) and (1.24) by substituting for the deformations. The resulting equations together with (1.24) are

$$F_c = \left(k_c \frac{l}{2}\right)\theta, \quad F_d = (k_d l)\theta \quad (1.25a)$$

$$\frac{l}{4}P = \frac{l}{2}F_c + lF_d \quad (1.25b)$$

The most convenient strategy is to substitute for F_c, F_d in the second equation. Then,

$$\frac{l}{4}P = l\left(\frac{l}{4}k_c + k_d\right)\theta$$

and

$$\theta = \frac{P}{(4k_d + k_c)l} \quad (1.26)$$

Finally, the spring forces corresponding to this value of θ are

$$F_c = \frac{k_c}{2(4k_d + k_c)} P$$

$$F_d = \frac{k_d}{(4k_d + k_c)} P \quad (1.27)$$

An alternate strategy is to solve first for one of the spring forces. Suppose we take F_c as the primary force variable. Using (1.25b), we solve for F_c .

$$F_c = \frac{1}{2}P - 2F_d \quad (1.28)$$

Another equation relating F_c and F_d is obtained by eliminating θ in (1.25a). The steps are

$$\theta = \frac{1}{k_c(l/2)} F_c \quad (1.29)$$

and

$$F_d = \frac{2k_d}{k_c} F_c \quad (1.30)$$

Equation (1.30) represents a constraint on the spring forces. The deformations of the springs are not arbitrary; they must satisfy (1.23), which can be written as:

$$e_d = 2e_c \quad (1.31)$$

Finally, substituting for F_d in (1.28) and solving for F_c leads to

$$F_c = \left(\frac{1/2}{1 + 4k_d/k_c} \right) P \quad (1.32)$$

The rotation angle is determined with (1.29) and F_c with (1.30).

We refer to the first solution procedure as the *displacement or stiffness method*. It is relatively simple to execute since it involves only substitution. Most of the structural analysis computer programs are based on this method. The second procedure is called the *force or flexibility method*. Some manipulation of the equations is required when the structure is statically indeterminate and consequently the method is somewhat more difficult to apply in this case. However, the Force Method is more convenient to apply than the displacement method when the structure is statically determinate, since the forces can be determined using only the equilibrium equations. The approach in part I of the text is based on the Force Method. Later in part II, we discuss the Force and Displacement methods in more detail.

1.5.7 The Importance of Displacements

Displacements are important for two reasons. Firstly, the serviceability requirement for structures is usually specified as a limit on the magnitude of certain displacements. Secondly, for indeterminate structures, one cannot determine the internal forces using only the equations of static equilibrium.

One needs to consider the displacements and internal forces simultaneously. This topic is addressed in part II of the text. The following example illustrates one of the strategies employed for a statically indeterminate beam.

Example 1.5: A Statically Indeterminate Beam

Given: The beam shown in Fig. E1.5a.

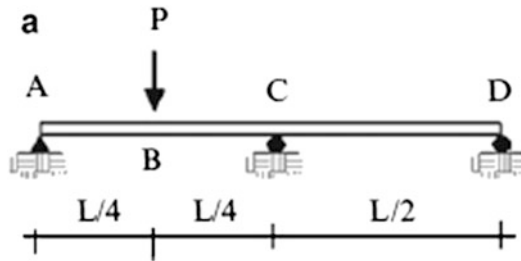


Fig. E1.5a

Determine: The reactions.

Solution: First, we construct the FBD for the beam (Figs. E1.5b and E1.5c).

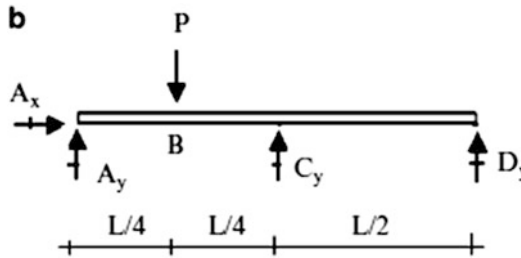


Fig. E1.5b

Considering summation of forces in the X and Y directions and summation of moments about A, we obtain the following three equations.

$$\begin{aligned}\sum F_{x \rightarrow +} &= 0 \quad \Rightarrow \quad A_x = 0 \\ \sum F_{y \uparrow +} &= 0 \quad \Rightarrow \quad A_y + C_y + D_y = P \\ \sum M_{\text{about A}} &= 0 \quad \Rightarrow \quad \frac{L}{4}P = \frac{L}{2}C_y + LD_y\end{aligned}$$

We have only two equations for the three vertical reactions, A_y , C_y , and D_y . Therefore, we *cannot* determine their magnitude using only the force equilibrium equations.

The Force (or Flexibility) method for this problem is based on releasing one of the roller supports, say support C, replacing it with an unknown force, C_y , and allowing point C to move vertically under the action of the applied loads. First, we take $C_y = 0$ and apply P . Point C moves an amount $\Delta_c|_p$ shown in the figure below. Then, we take $P = 0$, $C_y = 1$, and determine $\Delta_c|_1$ the corresponding

movement at C due to a unit upward force at C. Assuming the support at C is unyielding, the net movement must be zero. Therefore, we increase the force C_y until this condition is satisfied. Once C_y is known, we can find the remaining forces using the equations of static equilibrium. In order to carry out this solution procedure, one needs to have a method for computing displacements of beams. These methods are described in Chap. 3.

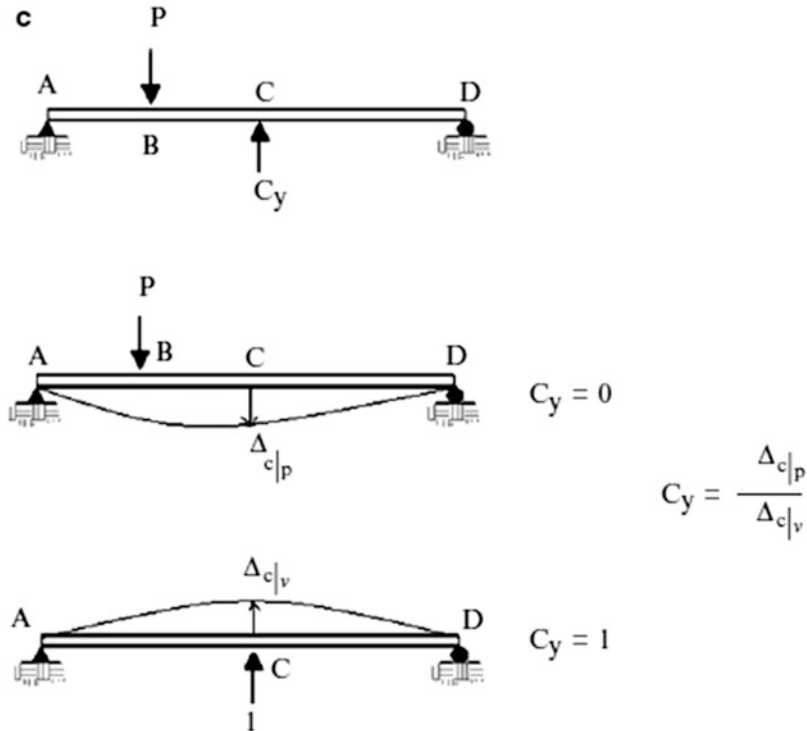


Fig. E1.5c

1.6 Summary

1.6.1 Objectives of the Chapter

- Provide an overview of the set of issues that a structural engineer needs to address as a practicing professional engineer.
- Introduce the basic analytical methods of structural analysis and describe how they are applied to determine the response of a structure.

1.6.2 Key Issues and Concepts Introduced

- A structure is an assemblage of structural components which are arranged in such a way that the structure can withstand the action of the loads that are applied to it. Structures are classified according to their makeup such as trusses, frames, and their functions such as bridges, office buildings.

- The primary concern of a structural engineer is to ensure that the structure *will not collapse* during its expected lifetime. This requires firstly that the engineer properly identify the extreme loading that the structure is likely to experience over its design life, and secondly, that the structure is dimensioned so that it has adequate capacity to resist the extreme loading.
- Structures are restrained against rigid body motion by supports. When the structure is loaded, reaction forces are developed by the supports. A minimum of three nonconcurrent reaction forces are necessary to prevent rigid body motion for a planar structure.
- Initial instability occurs when the reactions are insufficient or the members are not properly arranged to resist applied external forces. In this case, the structure will fail under an infinitesimal load. This condition can be corrected by modifying the supports or including additional members.
- Loss of stability under loading can occur when a primary structural member loses its capacity to carry load due to either elastic buckling or failure of the material. There are two modes of material failure: “brittle” and “ductile.” Brittle failure occurs suddenly with a complete loss in load capacity. One should avoid this mechanism. Ductile failure is evidenced by substantial inelastic deformation and loss in stiffness. The limit state design procedure allows for a limited amount of inelastic deformation.
- Loads applied to civil structures are categorized according to direction. Vertical loads are due to gravitational forces and are defined in terms of the weight of objects. Lateral loads are produced by natural events such as wind and earthquake. The relative importance of these loads depends on the nature of the structure and the geographical location of the site.
- Loads are also generated during the construction of the structure. The design loading for certain types of structures such as segmented concrete girders is controlled by the construction process. Most structural failures occur during the construction process.
- Loads are also classified according to the time period over which the loads are applied. Long-term loads, such as self-weight, are called “dead” loads. Loads whose magnitude or location changes are called “live” loads. Typical live loads are produced by vehicles crossing bridges, and people occupying buildings.
- Extreme loads such as wind and earthquakes are defined in terms of their return period, which is interpreted as the average time interval between occurrences of the event. One speaks of the 50-year wind, the 50-year earthquake, etc. The magnitude of the load increases with increasing return period.
- The design life of a structure is the time period over which the structure is expected to function without any loss in functionality. Bridges are designed to last at least 100 years. Industrial buildings are expected to have design lives usually greater than 100 years. The probability that a structure will experience an extreme event over its design life is approximately equal to the ratio of the design life to the return period.
- The effect of wind acting on a building is represented by a pressure loading distributed over the external surfaces. The magnitude and spatial variation of the pressure depends on the shape of the building and the local wind environment. Positive pressure is generated on windward vertical forces and steeply inclined roofs. Turbulence zones occur on flat roof and leeward faces and result in negative pressure.
- Design codes specify procedures for computing the spatial distribution of wind pressure given the expected extreme wind velocity at the geographic location. The wind velocity tends to be larger in coastal regions. A typical wind velocity for coastal regions of the USA is 100 miles per hour. The corresponding wind pressure is approximately 20 psf.
- Snow loading is represented as a uniform download pressure acting on the roof zones of a structure. Design snow pressure is based on ground snow data for the region where the structure

is located. Snow is an important loading for the northern part of the USA, Canada, and Eastern Europe.

- Earthquakes produce sudden intense short-term ground motion which causes structures to vibrate. The lateral floor loading is due to the inertia forces associated with the acceleration generated by the ground shaking and is generally expressed as $(W_f/g)a_{\max}$, where W_f is the floor weight, and a_{\max} is the peak value of floor acceleration. Seismic engineering is specialized technical area which is beyond the scope of this textbook. However, the reader should be knowledgeable of the general seismic design strategy.
- Conventional structural design philosophy is based on satisfying two requirements: safety and serviceability. Safety relates to extreme loading and is concerned with preventing collapse and loss of life. Safety is achieved by providing more resistance than is required for the extreme loading. Serviceability relates to loading which occurs during the structure's lifetime. One needs to ensure that the structure remains operational and has no damage.
- Motion-Based Design, also called performance-based design, is an alternate design methodology that takes as its primary objective the satisfaction of motion-related design requirements such as displacement and acceleration. The goal here is to provide sufficient stiffness and energy dissipation mechanisms to limit the motion under extreme loading.
- Structural analysis is concerned with quantifying the response of a structure subjected to external loading. This effort involves determining the reactions, internal forces, and displacement profiles. One generally carries out the analysis in two steps: study of forces and study of displacements. In the study of forces, one applies the force equilibrium equations to isolated segments of the structure called FBDs. Selecting appropriate FBDs is a skill acquired through practice. In the study of displacements, one first uses a geometric-based approach to express the deformation measures in terms of displacement measures. The displacement measures are then related to the internal forces by introducing certain material properties such as the elastic modulus. These relations allow one to determine the displacements, given the internal forces. We apply this approach throughout part II of the text. It provides the basis for the analysis of statically indeterminate structures.

References

1. Schodek DL, Bechthold M. Structures. Englewood Cliffs: Pearson/Prentice Hall; 2008.
2. Hibbeler RC. Engineering mechanics statics and dynamics. 11th ed. Englewood Cliffs: Pearson/Prentice Hall; 2007.
3. Hibbeler RC. Mechanics of materials. Upper Saddle River: Prentice Hall; 2008.
4. Gere JM. Mechanics of materials. 6th ed. Belmont: Brooks/Coll; 2004.
5. Segui WT. Steel design. 4th ed. Toronto: Thomson; 2007.
6. International Code Council (ICC). International building code. Washington: ICC; 2009.
7. Structural Engineering Institute (ASCE). ASCE/SEI 7-05. Minimum design loads for buildings and other structures. New York: ASCE; 2006.
8. American Concrete Institute (ACI). Building code requirements for structural concrete (ACI 318-14). Farmington Hills, MI: ACI; 2014.
9. American Institute of Steel Construction (AISC). AISC-ASD/LRFD steel construction manual. 14th ed. Chicago: AISC; 2011.
10. Eurocode (1-9). British Standards Institute. London, UK; 2009.
11. American Association of State Highway and Transportation Officials (AASHTO). AASHTO LRFD bridge design specifications. 7th ed. Washington, DC: AASHTO; 2015.
12. Streeter VL. Fluid mechanics. New York: McGraw-Hill; 1966.

-
13. United States Geological Survey (USGS). National Earthquake Information Center (NEIC), Denver, Colorado.
 14. Federal Emergency Management Agency FEMA445. Next generation performance-based design guidelines. Washington; 2006.
 15. Hibbeler RC. Structural analysis. 7th ed. Upper Saddle River: Pearson/Prentice Hall; 2009.
 16. Leet KM, Uang CM. Fundamentals of structural analysis. 2nd ed. New York: McGraw-Hill; 2005.
 17. McCormac JC. Structural analysis using classical and matrix methods. Hoboken: Wiley; 2007.
 18. Heyman J. The science of structural engineering. London: Imperial College; 1999.

Abstract

We begin this chapter by reviewing the historical development of truss structures. Trusses have played a key role in the expansion of the highway and railroad systems during the past two centuries. From a mechanics perspective, they are ideal structures for introducing the concepts of equilibrium and displacement. We deal first with the issues of stability and static determinacy, and then move on to describe manual and computer-based techniques for determining the internal forces generated by external loads. A computational scheme for determining the displacements of truss structures is presented next. Given a structure, one needs information concerning how the internal forces vary as the external live load is repositioned on the structure for the design phase. This type of information is provided by an influence line. We introduce influence lines in the last section of this chapter and illustrate how they are constructed for typical trusses. This chapter focuses on linear elastic structural analysis. Nonlinear structural analysis is playing an increasingly more important role in structural design. However, we believe an understanding of linear analysis is essential before discussing the topic of nonlinear analysis.

2.1 Introduction: Types of Truss Structures

Simple two-dimensional (2-D) truss structures are formed by combining one-dimensional linear members to create a triangular pattern. One starts with a triangular unit, and then adds a pair of members to form an additional triangular unit. This process is repeated until the complete structure is assembled. Figure 2.1 illustrates this process for the case where all the members are contained in a single plane. Such structures are called *plane* trusses; the nodes are also called “*Joints*.”

Three members connected at their ends form a rigid structure in the sense that, when loaded, the change in shape of the structure is due only to the deformation of the members. It follows that a

Fig. 2.1 Simple planar truss construction

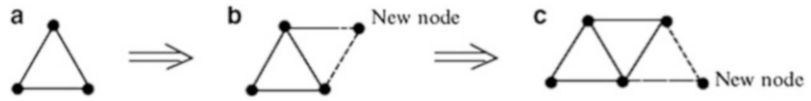


Fig. 2.2 Simple space truss construction

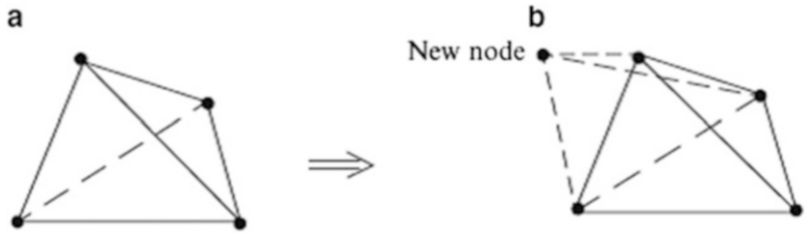
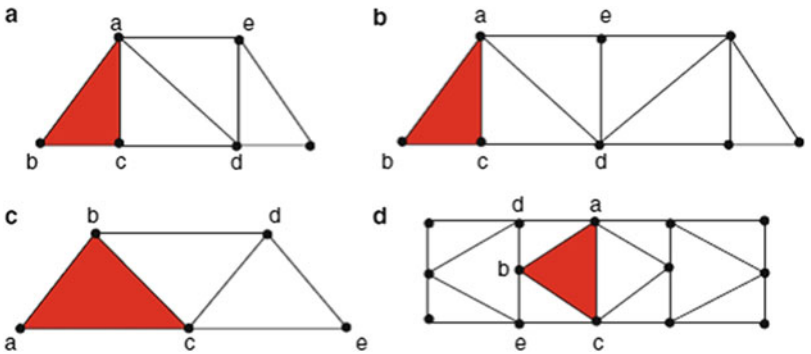


Fig. 2.3 Simple planar trusses



structure constructed in the manner described above is also rigid provided that the structure is suitably supported.

Simple three-dimensional (3-D) space trusses are composed of tetrahedral units. Starting with a tetrahedral unit, one forms an additional tetrahedral unit by adding three linear elements, as illustrated in Fig. 2.2. When the structure is suitably supported to prevent rigid body motion, the assemblage is rigid. The question of suitable supports is addressed later in the chapter.

Examples of simple planar trusses are shown in Fig. 2.3. Starting with the initial triangle abc, one adds the nodes d, e, etc.

Trusses may also be constructed by using simple trusses as the “members,” connected together by additional members or joints. These structures are called *compound trusses*. Figure 2.4 shows several examples of compound trusses, where the simple trusses are shown as shaded areas.

A truss geometry that does not fall in either the simple or compound category is called a complex truss [1]. Examples are shown in Fig. 2.5. This type of truss is not used as frequently as either simple or compound trusses.

2.1.1 Structural Idealization

Trusses are components of larger structural systems, such as buildings, bridges, and towers. In order to evaluate the behavior under loading, one needs to identify the main structural components of

Fig. 2.4 Compound planar trusses

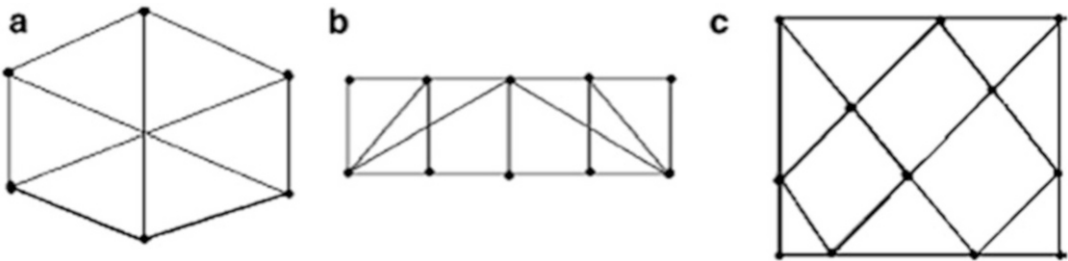
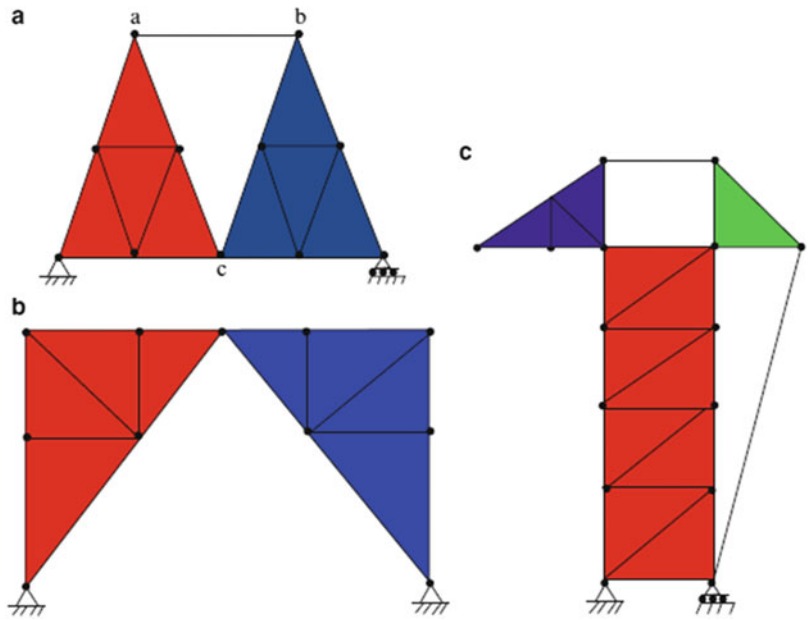


Fig. 2.5 Complex planar trusses

the system and determine how the external load is transmitted from one component to another. This process is called “structural idealization;” it is a key step in the analysis process. In what follows, we illustrate idealization strategies for typical bridges and roof systems.

Figure 2.6 shows a typical single span truss bridge system. The key components are the two simple planar trusses, the lateral bracing systems at the top, sides, and bottom levels and the flooring system consisting of floor stringers/beams and deck slab. Loading applied to the deck slab is transmitted through the stringer/beam system to the bottom nodes of the two planar trusses. The major percentage of the analysis effort is concerned with analyzing a simple truss for dead weight, wind, and traffic loading.

Roofing system for buildings such as warehouses, shopping centers, and sports facilities employ trusses to support the roof envelope. Figure 2.7 illustrates a scheme for a typical roofing system for a single-story industrial building. The roof system consists of steel decking attached to purlins which, in turn, are supported at the top nodes of the planar trusses. Loading applied to the roof area in a bay is transmitted through the purlins to the trusses adjacent to the bay, and eventually to the supports. Bracing is incorporated to carry the lateral loading which may act either in the longitudinal or

Fig. 2.6 Single span truss bridge system

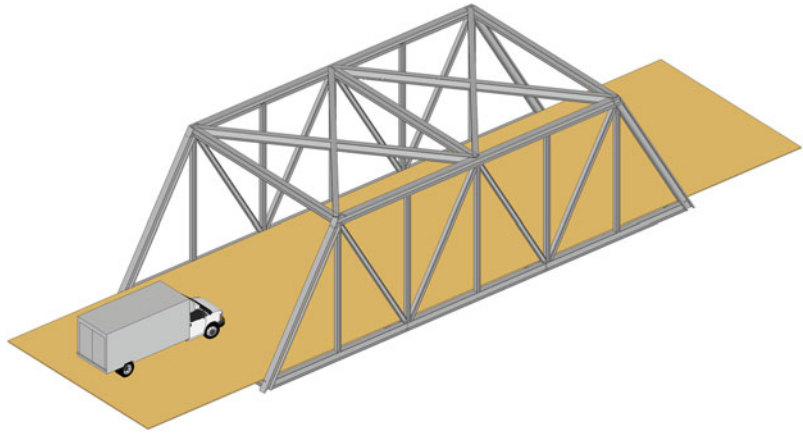
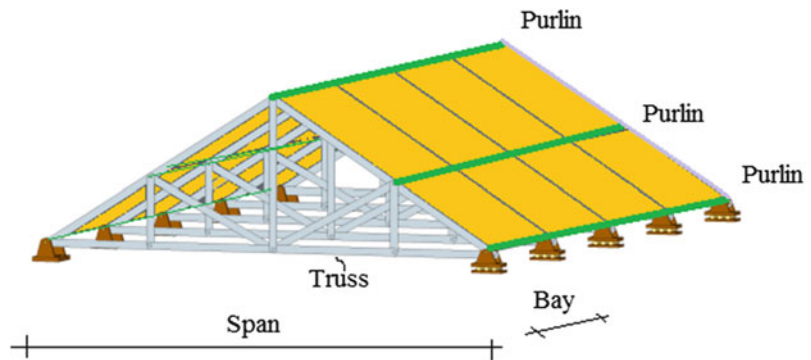


Fig. 2.7 Typical industrial building roofing system



transverse direction. The primary effort for this structural system is concerned with analyzing a single planar roof truss for the tributary area loading applied at the top chord nodes.

2.1.2 Historical Background

The first application of truss type structures is believed to be in Egyptian boats built between 3100 and 2700 BC. Egyptian boat builders used trusses constructed by tying the members together with vines to form the sides and attached the outer hull to these structures. The Romans used wood trusses for bridges and roofs. Examples are a bridge over the Danube (circa 106 AD) and the entrance to the Pantheon (circa 120 AD). The next time frame is that of the Middle Ages. Examples of trusses are found in English cathedrals (Salisbury Cathedral, circa 1258 AD) and great halls (Westminster Palace, circa 1400). Deployment of wooden trusses continued through the Gothic and Renaissance periods, mainly to support roofs. The Engineers of these time periods intuitively understood the rigidity provided by the triangular form, but lacked a theory that they could apply to evaluate the response for a given load.

A major contribution to the theory is the work of Leonardo da Vinci (1452–1519), who formulated the concepts of force and moment as vectors and showed that forces can be combined using a graphical construction that is now called the force parallelogram. From the early 1600s to the

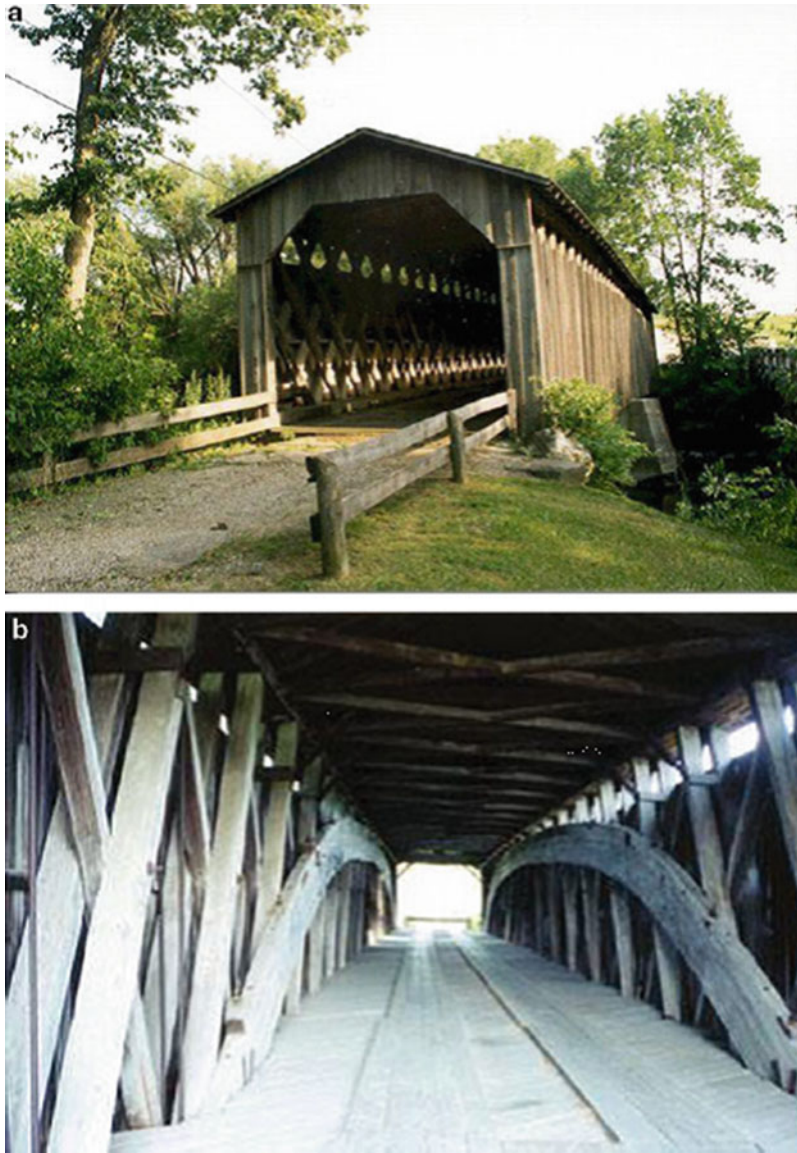
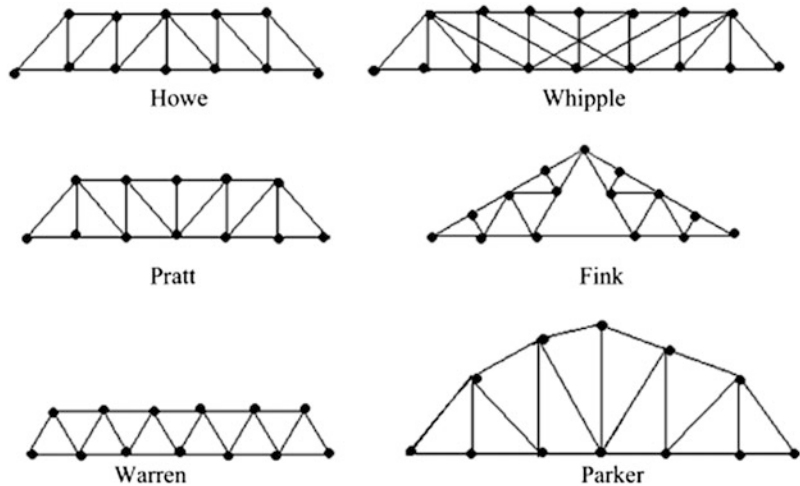


Fig. 2.8 Covered wood bridges

mid-1800s, many advances in the development of a scientific basis for a theory of structures were made. Key contributors were Newton (1642–1729), Hooke (1635–1703), Galileo Galilei (first useable formula for strength of a cantilever beam-1638), Euler (theory of buckling of columns-1757), Bernoulli (bending deformation of a beam-1741), Navier (produced an integrated theory of Structural Mechanics—1826), and Mobius (published the *Textbook of Statics*—1837).

Wooden bridge truss structures were popular in the early 1800s, especially in the USA. There are many examples of covered wooden bridges in Vermont and New Hampshire. Figure 2.8 illustrates some typical structural schemes.

Fig. 2.9 Examples of named trusses



There was a flourishing industry in New England producing wooden bridge trusses, many of which were exported to Europe. As with many emerging technologies, competition from other emerging technologies occurred and eventually took over the market for the product. The first impetus for change was the Industrial Revolution which occurred in the early 1800s. The concept of the railroad was invented during this period. This invention created a demand for more robust and more durable bridges to carry the heavier moving loads over longer spans. Cost also became an issue. Up to this time, wooden bridges were designed to carry light pedestrian and horse and carriage traffic over relatively short spans. Their expected life was short, but since they used local materials and local labor, they were not expensive and durability was not an issue. However, they were not adequate for the railroad traffic and other solutions were needed.

Another technology that was evolving in the late 1700s was iron making. Processes for making cast and wrought iron cheaper than existing methods were developed in the 1780s. Methods for shaping wrought iron into shapes that could be used as truss members were also invented simultaneously. These inventions set the stage for the use of iron members in trusses during the early 1800s. Initially, wrought iron was used for tension elements and wood for compression elements. Gradually, cast iron replaced wood for compression elements. The first all iron truss bridge in the USA was built in 1840 by Squire Whipple, a leading bridge designer in the USA at that time. He is also known for his book *Essay on Bridge Building*, published in 1847, the first publication on Structural Theory by a US author. Some other designers active in the 1840s were W. Howe, T. Pratt, A. Fink in North America, and J. Warren in the UK. Trusses of this era were given the name of the individual who designed or constructed them. Examples are shown in Fig. 2.9.

Starting around 1850, iron trusses were used not only for bridges but also for other long-span structures such as market halls, exhibition buildings, and railway stations. Notable examples are the Crystal Palace, the Eiffel tower, and the Saint Pancras station (Fig. 2.10).

During the period from 1850 to 1870, an improved version of iron called steel was invented. This material was much stronger than cast iron; more ductile than wrought iron, and quickly displaced iron as the material of choice. The first all steel truss bridge in the USA was built for the Chicago and Alton Railroad in 1879. The structure consisted of a series of Whipple trusses with a total length of 1500 ft spanning over the Mississippi River at Glasgow, Missouri. The first major long-span steel bridge was the Firth of Forth Bridge built in Scotland in 1890. Another similar

Fig. 2.10 Examples of structures made of iron trusses. (a) Crystal Palace. (b) Eiffel Tower. (c) Saint Pancras station



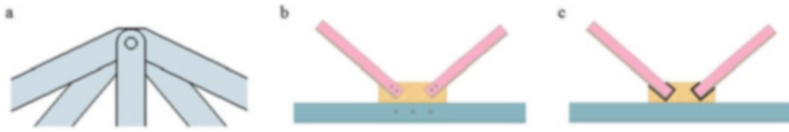


Fig. 2.11 Typical pin joint connections. (a) Frictionless pin. (b) Bolted connection. (c) Welded connection



Fig. 2.12 Example of early steel bridges—Firth of Forth Bridge, Scotland

cantilever style truss bridge was built over the St. Lawrence River in Quebec, Canada in 1919. The initial steel structures used eyebars and pins. Rivets replaced pins as connectors in the late 1800s.

High-strength bolts and welding are now used to connect the structural members in today's modern steel constructions. Figure 2.11 illustrates typical bolted and welded connections. Connection details are usually designed by the steel fabricator and checked by the structural engineer. The goal in connection design is to minimize steel erection time.

Steel truss bridges were the dominant choice for long-span crossings until the mid-1900s when another structural form, the cable-stayed bridge, emerged as a competitor. Cable-stayed bridges have essentially captured the market for spans up to about 900 m. Segmented concrete girder construction has also emerged as a major competitor for somewhat shorter spans. Plane trusses now are used mainly for prefabricated joists, for gable roof systems, and for spanning long interior distances in buildings and sporting facilities such as convention halls and stadiums. Three-dimensional space trusses are used in dome type structures such as shown in Fig. 2.13, and also for towers. One of the most notable examples of the space truss concept is the Eiffel Tower in Paris, France.



Fig. 2.13 Three-dimensional truss roof system

2.2 Analysis of Planar Trusses

In this section, we focus on introducing analysis and behavior issues for planar trusses. The discussion is extended in the next section to deal with three-dimensional space structures.

The analysis of trusses is based on the following idealizations that ensure that the forces in the members are purely axial:

1. The loads and displacement restraints are applied only at the nodes.
2. The members are connected with frictionless pins so that the members can rotate freely and no moment exists at the ends.
3. The stress due to the weight of the members is small in comparison to the stress due to the applied loads.
4. Each member is straight and is arranged such that its centroidal axis coincides with the line connecting the nodal points.

With these restrictions, it follows that a member is subjected only to an axial force at each end. These forces are equal in magnitude and their line of action coincides with the centroidal axis of the member. There is only one unknown per member, the magnitude of the force. The resulting state is uniform axial stress throughout the member. Depending on the loading, the member force may be either tension or compression. Figure 2.14 illustrates free body diagrams for a truss member and its associated nodes.

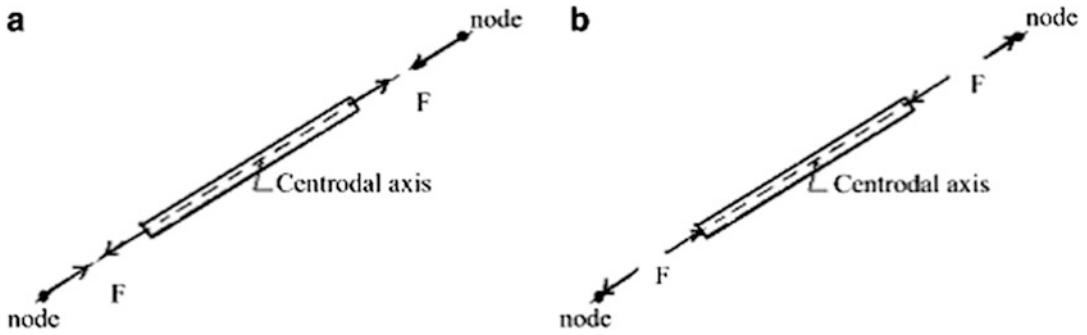
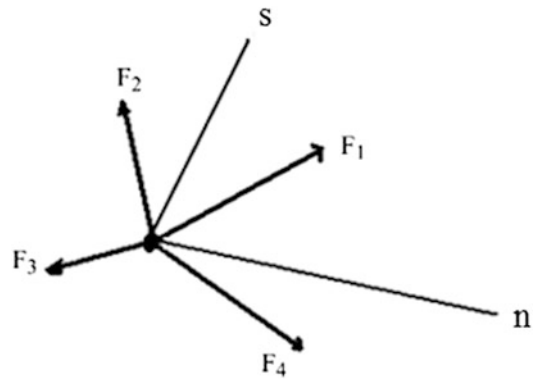


Fig. 2.14 Free body diagram of a truss member and its associated nodes. (a) Tension. (b) Compression

Fig. 2.15 Concurrent force system at a node



2.2.1 Equilibrium Considerations

The equilibrium requirements for a body subjected to a non-concurrent force system are specified in Sect. 1.5.2. In general, the resultant force vector and the resultant moment vector with respect to an arbitrary moment center must vanish. One can apply these requirements either to the complete truss or to the individual nodes.

Each node of a plane truss is acted upon by a set of coplanar concurrent forces. There are no moments since the pins are frictionless and the lines of action of the forces intersect at the node. For equilibrium of a node, the resultant force vector must vanish. In Squire Whipple's time (1840s), equilibrium was enforced using Leonardo da Vinci's graphical method based on the force polygon. Now, one applies an analytical approach based on resolving the force vectors into components and summing the components. The corresponding scalar equilibrium equations are

$$\sum F_n = 0 \quad \sum F_s = 0 \quad (2.1)$$

where n and s are two arbitrary nonparallel directions in the plane. Figure 2.15 illustrates this notation.

2.2.2 Statically Determinate Planar Trusses

In general, three motion restraints are required to prevent rigid body motion of a planar truss. Two of these restraints may be parallel. However, the third restraint cannot be parallel to the other two restraints since, in this case, the truss could translate in the direction normal to the parallel restraint direction. Each restraint generates an unknown force, called a reaction. Therefore, the minimum number of reactions is 3.

Examples of typical support motion restraints and the corresponding reactions are shown in Fig. 2.16.

There are two scalar equilibrium equations per node for a plane truss. Assuming that there are j nodes, it follows that there are a total of $2j$ equilibrium equations available to determine the force unknowns. We suppose there are m members and r reactions. Then, since each member and each reaction involves only one unknown force magnitude, the total number of force unknowns is equal to $m + r$.

When the number of force unknowns is equal to the number of equilibrium equations, the structure is said to be *statically determinate*. If $m + r < 2j$, the truss is unstable since there are an insufficient number of either member forces or reactions or possibly both to equilibrate the applied loads. It follows that a plane truss is statically determinate, unstable, or indeterminate when

$$\begin{aligned}
 m + r &= 2j && \text{Statically determinate} \\
 m + r &< 2j && \text{Unstable} \\
 m + r &> 2j && \text{Statically indeterminate}
 \end{aligned}
 \tag{2.2}$$

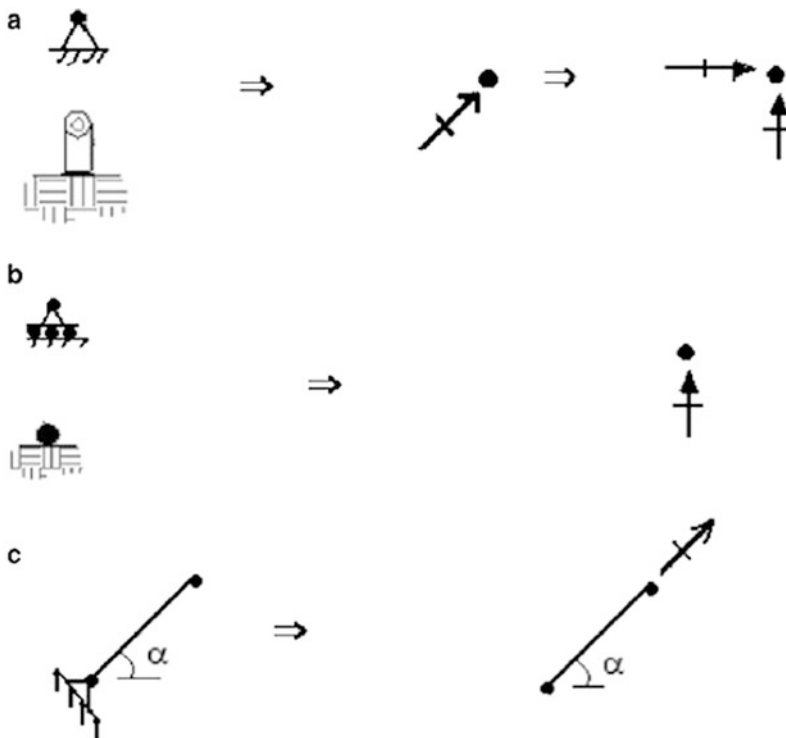


Fig. 2.16 Types of supports for planar trusses. (a) Hinge support (two restraints \Rightarrow two reactions). (b) Roller Support (one restraint \Rightarrow one reaction). (c) Rigid link

A word of caution: a statically determinate truss may also be unstable if the reactions are not properly aligned so as to prevent rigid body motion of the truss. We discuss this point in more detail in the following section.

2.2.3 Stability Criterion

In this section, we examine in more detail the question of whether a planar truss structure is initially stable. Assuming a plane truss has m members, r reactions, and j joints, there are $2j$ force equilibrium equations that relate the known (given) joint loads and the $(m + r)$ unknown forces. If $m + r < 2j$, the number of force unknowns is less than the number of equilibrium equations that the forces must satisfy. Mathematically, the problem is said to be underdetermined or inconsistent. One cannot find the exact solution for an arbitrary loading, except in the trivial case where the magnitude of all the loads is zero, and consequently the forces are zero. Once a nontrivial load is applied, the structure cannot resist it, and motion ensues. The descriptor “initial instability” is used to denote this condition.

Even when $m + r = 2j$, a truss may still be unstable if the motion. restraints are not properly arranged to prevent rigid body motion of the structure. There may be an insufficient number of restraints or the restraints may be aligned in such a way that rotation of a segment is possible. The stability of a complex truss depends on the geometrical arrangements of the members. Even though the truss satisfies the condition, $m + r = 2j$, and has sufficient restraints, it still may be unstable. The instability condition becomes evident when one attempts to determine the member forces using the $2j$ force equilibrium equations. The solution is not unique when the structure is unstable.

When $m + r > 2j$ and the structure is suitably restrained against rigid body motion, the structure is said to be statically indeterminate. This terminology follows from the fact that now there are more force unknowns than equilibrium equations, and not all the forces can be determined with only equilibrium considerations. One needs some additional equations. We address this type of problem in Part II.

In what follows, we illustrate the initial stability criteria with typical examples. Stability can be defined in a more rigorous way using certain concepts of linear algebra, a branch of mathematics that deals with linear algebraic equations. This approach is discussed in Sect. 2.6

Example 2.1 Simple Trusses

Given: The structures shown in Fig. E2.1a–d

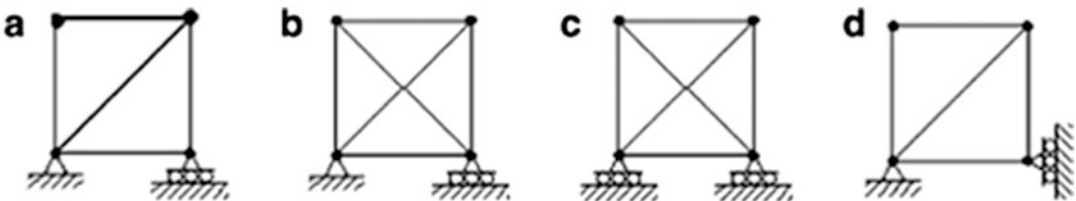


Fig. E2.1

Determine: Whether the structures are initially stable, determinate, or indeterminate.

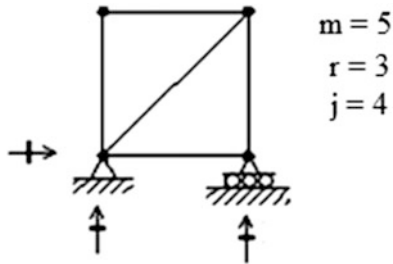
Solutions:

Case (a): There are five members, three reactions, and four nodes. Then applying (2.2)

$$m + r = 8$$

$$2j = 8$$

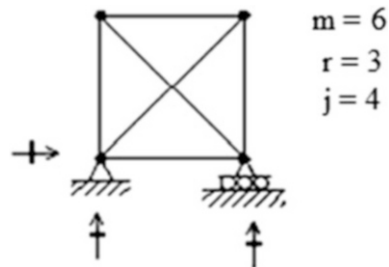
The structure is determinate and initially stable.



Case (b):

$$m + r = 9$$

$$2j = 8$$

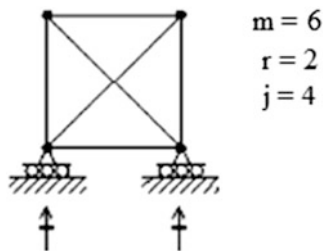


There is one extra force and therefore the structure is initially stable and indeterminate to the first degree.

Case(c): The stability criterion appears to be satisfied.

$$m + r = 8$$

$$2j = 8$$

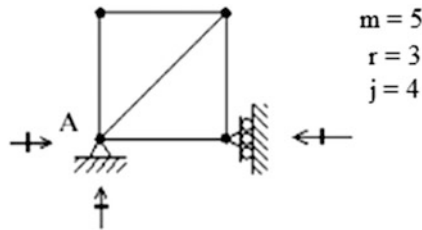


However, the number of supports is insufficient to prevent rigid body motion in the horizontal direction. Therefore, the structure is initially unstable.

Case (d): The stability criterion appears to be satisfied.

$$m + r = 8$$

$$2j = 8$$



However, the three displacement restraints are concurrent (point A), and therefore the structure can rotate at point A. It follows that the structure is initially unstable.

Example 2.2 A Compound Truss

Given: The structure shown in Fig. E2.2a. This compound truss is actually a combination of two simple trusses.

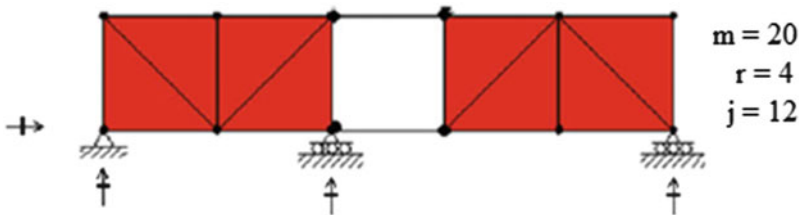


Fig. E2.2a

Determine: Is the structure statically determinate?

Solution: The structure is statically determinate and stable.

$$m + r = 24$$

$$2j = 24$$

Example 2.3 A Complex Truss

Given: The complex truss defined in Fig. E2.3a.

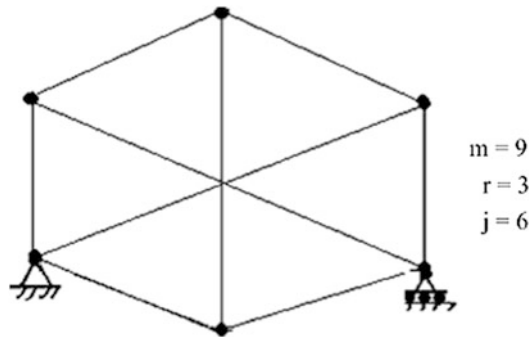


Fig. E2.3a

Determine: Is the truss statically determinate?

Solution: There are three restraints, six joints, and nine members.

$$\begin{aligned}m + r &= 12 \\2j &= 12\end{aligned}$$

The truss appears to be stable. Note that the condition, $m + r = 2j$ is *necessary* but not *sufficient* to ensure stability of this truss. Sufficient conditions are discussed further in Sect. 2.6.

In what follows, we describe two classical hand computation-based procedures for finding the member forces in *simple* and *compound trusses* due to an applied loading. These approaches are useful for gaining insight as to how loads are carried by structures. That is the most important aspect of structural engineering that one needs to master in order to be a successful practitioner. Also, although most current structural analysis is computer based, one still needs to be able to assess the computer-generated results with a simple independent hand computation.

2.2.4 Method of Joints: Planar Trusses

Each joint of a plane truss is subjected to a concurrent force system. Since there are two equilibrium equations for a 2-D concurrent force system, one can solve for at most two force unknowns at a particular joint. The strategy for the method of joints is to proceed from joint to joint, starting with the free body diagram of a joint that has only two unknowns, solving for these unknowns, and then using this newly acquired force information to identify another eligible joint. One continues until equilibrium has been enforced at all the joints. When all the joints are in equilibrium, the total structure will be in equilibrium. This analysis procedure was first described in Squire Whipple's 1840 Essay on Bridge Building.

Enforcing the equilibrium conditions is simplified if one works with the force components referred to a common reference frame. Once one component is known, it is a simple step to determine the magnitude of the other component and the force. As an illustration, we consider the member shown in Fig. 2.17. The ratio of force components is equal to the ratio of the projected lengths. This equality follows from the fact that the direction of the force is the same as the direction of the line. Here, we are taking the horizontal and vertical directions as the common reference frame.

Fig. 2.17 Force components

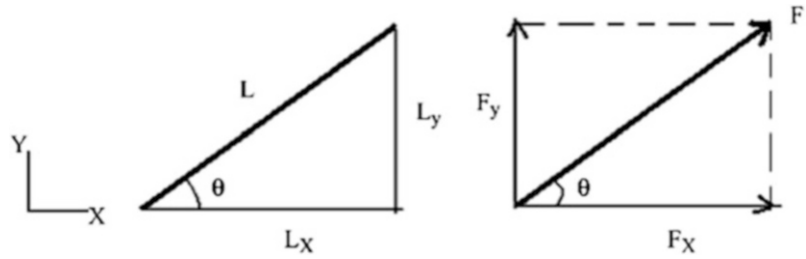
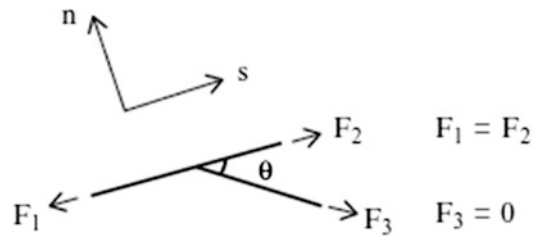


Fig. 2.18 Zero force member



$$\frac{F_y}{F_x} = \frac{L_y}{L_x} = \tan \theta$$

Similarly, the force is determined using

$$F = \frac{F_x}{\cos \theta} = \frac{F_y}{\sin \theta}$$

Another simplification is possible when the joint has only three members, two of which are colinear, and there is *no* applied load at the joint. Figure 2.18 illustrates this case. There is only one force acting at an angle to the direction of the two common members, and equilibrium in the normal direction (n) requires the magnitude of this force to be zero. The other two forces must have the same magnitude.

When applying the method of joints, it is convenient to first determine the reactions by enforcing global equilibrium on the total structure. With the reactions known, it may be easier to locate a joint having only two unknown member forces.

In what follows, we present a set of examples that illustrate how the method of joints is efficiently applied.

Example 2.4 Three-Member Truss Analyzed by the Methods of Joints

Given: The truss and loading defined by Fig. E2.4a.

Determine: The reactions and member forces.

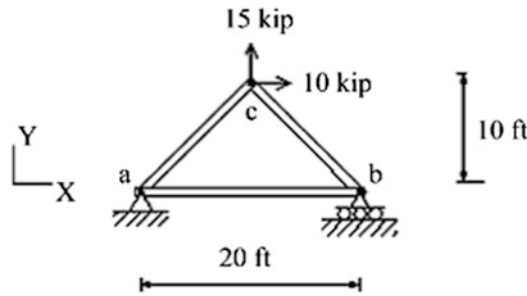


Fig. E2.4a

Solution: We first find the reactions at joints a and b. Moment summation about joint a leads to the y reaction at b. Force summations provide the remaining two reaction forces. The results are shown in Fig. E2.4b.

$$\sum M_a = 0 \quad \curvearrowright \quad 10(10) - 15(10) - R_b(20) = 0 \quad \Rightarrow \quad R_b = -2.5 \quad \therefore R_b = 2.5 \text{ kip } \downarrow$$

$$\sum F_x = 0 \rightarrow + \quad R_{ax} + 10 = 0 \quad \Rightarrow \quad R_{ax} = -10 \quad \therefore R_{ax} = 10 \text{ kip } \leftarrow$$

$$\sum F_y = 0 \uparrow + \quad R_{ay} + 15 - 2.5 = 0 \quad \Rightarrow \quad R_{ay} = -12.5 \quad \therefore R_{ay} = 12.5 \text{ kip } \downarrow$$

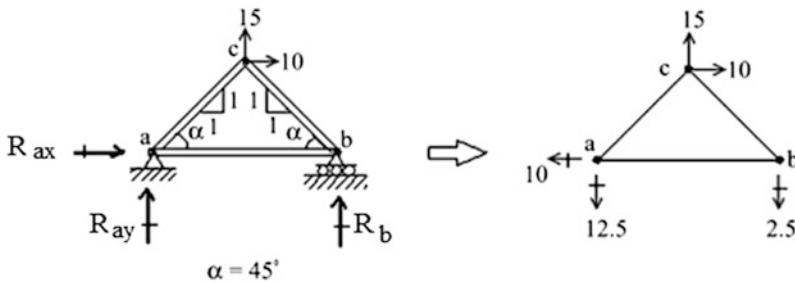


Fig. E2.4b Reactions

One can start at any joint since they all have just two unknown member forces. We pick joint b (Fig. E2.4c). Summation of forces in the y direction gives $F_{bc,y} = 2.5$ kip. Then, summing forces in the x direction requires F_{ba} being compressive and equal to 2.5 kip. We indicate a tensile member force with an arrow pointing away from the joint. The opposite sense is used for compression. One converts the force components to the force magnitude using the Pythagorean Theorem,

$$F = \sqrt{F_x^2 + F_y^2}.$$

$$\sum F_y = 0 \quad F_{bc,y} = 2.5 \uparrow \quad \text{Then } F_{bc,x} = 2.5 \leftarrow \quad \therefore F_{bc} = 2.5\sqrt{2} \text{ kip (tension)}$$

$$\sum F_x = 0 \quad F_{ba} = 2.5 \text{ kip (compression)}$$

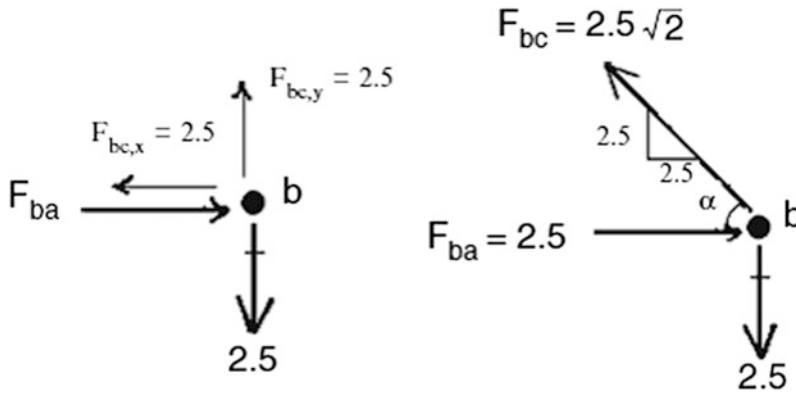


Fig. E2.4c Joint b

There is only one unknown member force left, F_{ca} . One can work with either joint a or joint c. We pick joint c. The free body diagram for joint c is shown in Fig. E2.4d. Equilibrium in the x direction requires $F_{ca,x} = 12.5$ kip.

$$\sum F_x = 0 \quad F_{ca,x} = 12.5 \leftarrow \quad \therefore F_{ca} = 12.5\sqrt{2} \text{ kip (tension)}$$

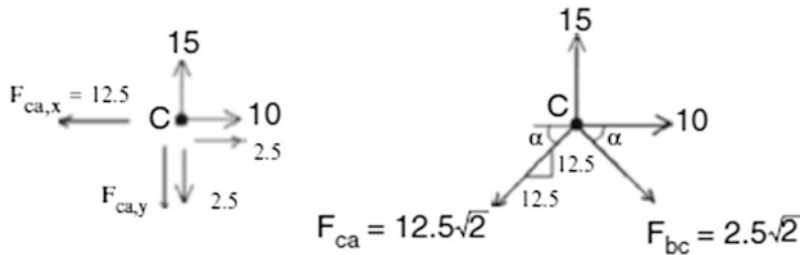


Fig. E2.4d Joint C

Note that in this example we do not need to use the remaining equilibrium equations (one for joint c and two for joint a) since we used instead three global equilibrium equations to calculate the reactions. The total number of joint equilibrium equations is equal to six (two per joint \times three joints). If we use three equations for global equilibrium, there are only three independent equations left to apply to the joints. The final results are shown on the sketch below. Tensile forces are denoted with a + sign, and compressive forces with a - sign.

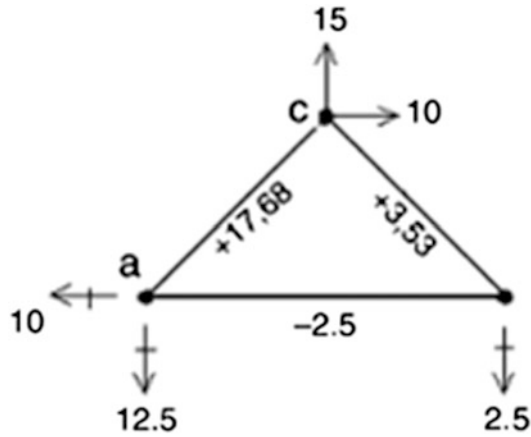


Fig. E2.4e

Example 2.5 Five-Member Truss Analyzed by the Methods of Joints

Given: The truss defined in Fig. E2.5a.

Determine: The reactions and member forces for the loading shown.

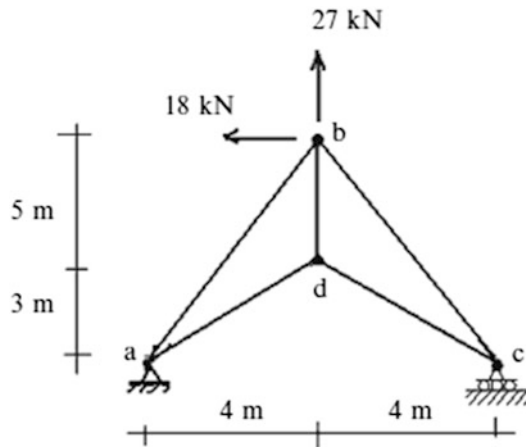


Fig. E2.5a

Solution: We first find the reactions and then proceed starting with joint a, and then moving to joints c and d.

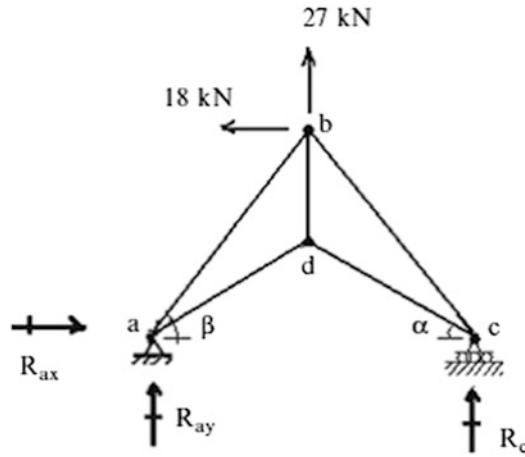


Fig. E2.5b

$$\Sigma M_a = 0 \quad +\curvearrowright \quad -27(4) - 18(8) - R_c(8) = 0 \Rightarrow R_c = -31.5 \quad \therefore R_c = 31.5 \text{ kip } \downarrow$$

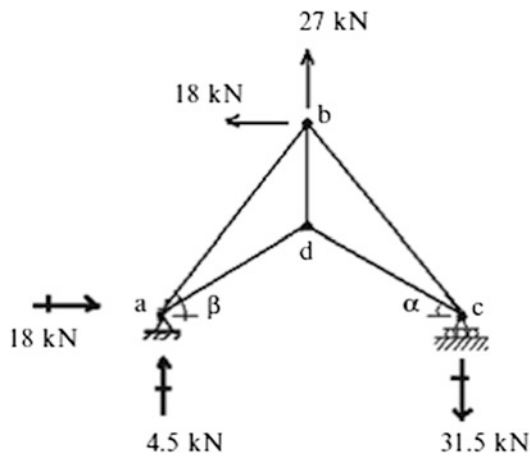


Fig. E2.5c

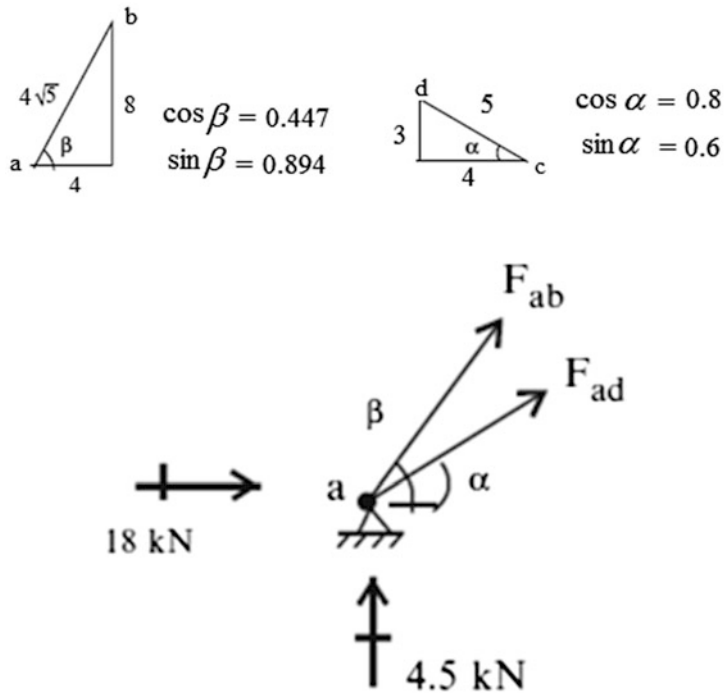


Fig. E2.5d Joint a

$$\begin{cases} \sum F_x = 0 & F_{ad} \cos \alpha + F_{ab} \cos \beta + 18 = 0 \\ \sum F_y = 0 & F_{ad} \sin \alpha + F_{ab} \sin \beta + 4.5 = 0 \end{cases} \Rightarrow \begin{cases} F_{ad} = -31.5 \text{ kN} \\ F_{ab} = 16.1 \text{ kN} \end{cases}$$

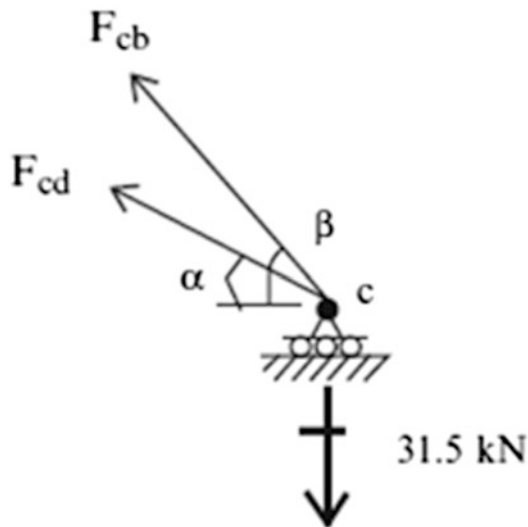


Fig. E2.5e Joint c

$$\begin{cases} \sum F_x = 0 & F_{cd} \cos \alpha + F_{cb} \cos \beta = 0 \\ \sum F_y = 0 & F_{cd} \sin \alpha + F_{cb} \sin \beta - 31.5 = 0 \end{cases} \Rightarrow \begin{cases} F_{cd} = -31.5 \text{ kN} \\ F_{cb} = 56.35 \text{ kN} \end{cases}$$

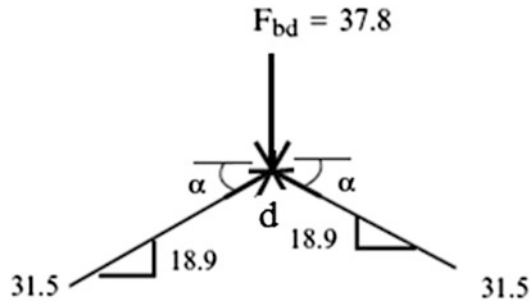
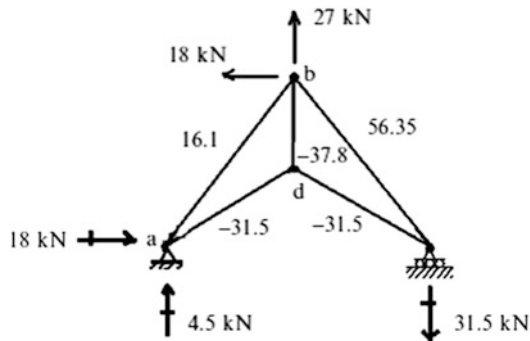


Fig. E2.5f Joint d

$$\sum F_y = 0 \quad F_{bd} = 37.8 \text{ kN (compression)}$$

The final forces are listed below.



Example 2.6 Five-Member Truss Analyzed by the Methods of Joints

Given: The truss defined in Fig. E2.6a.

Determine: The reactions and member forces for the loading shown.

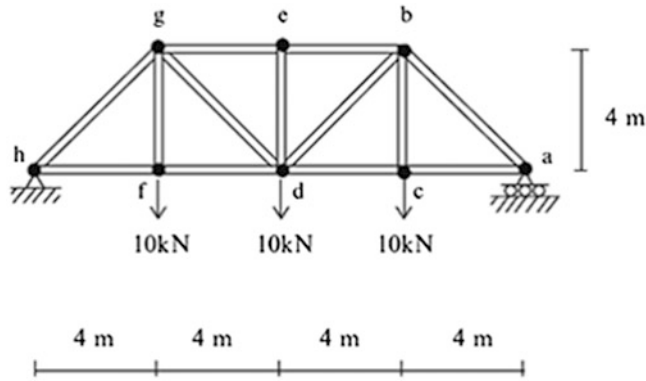


Fig. E2.6a Bridge truss

Solution: We note that the structure and loading are symmetrical with respect to a vertical axis through points e and d. It follows that the forces in symmetrically located members are equal, and therefore we need to find the forces in only 1/2 of the structure. Joints c, e, and f are special in the sense that two incident members are colinear. Then, noting Fig. 2.18,

$$F_{cb} = 10 \text{ kN (tension)} \quad F_{ed} = 0 \quad F_{fg} = 10 \text{ kN (tension)}$$

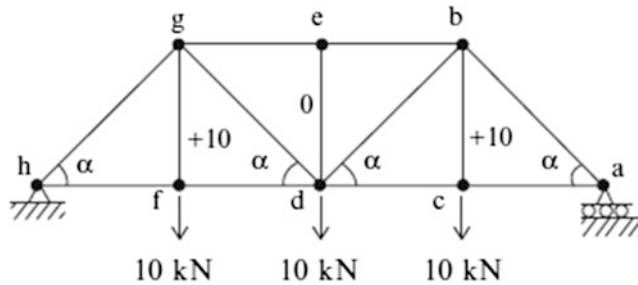


Fig. E2.6b

There are multiple options. We can first find the reactions and then proceed inward, starting with joint a, and then moving to joints c and b. An alternate approach would be to start at joint d, find the y component of F_{bd} , and then move to joint b.

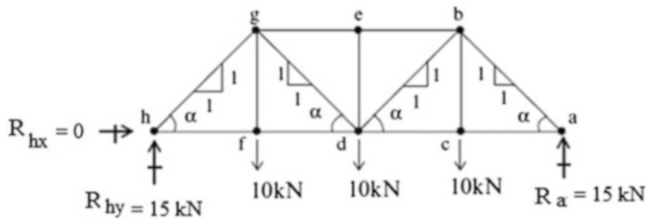


Fig. E2.6c Reactions

We list the results for the first approach below. We first find $F_{ba,y}$ with the vertical equilibrium condition at joint a. Then, we find F_{ac} from the horizontal component of F_{ba} .

$$\begin{aligned}\sum F_y = 0 \quad F_{ba,y} = 15 \text{ kN} \downarrow \quad \text{Then } F_{ba,x} = 15 \text{ kN} \rightarrow \\ \therefore F_{ba} = 15\sqrt{2} \text{ kN (compression)} \\ \sum F_x = 0 \quad F_{ac} = 15 \text{ kN (tension)}\end{aligned}$$

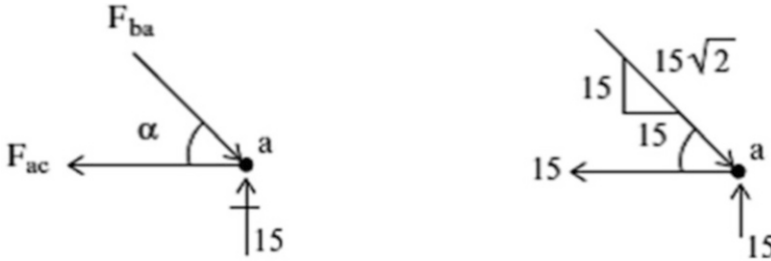


Fig. E2.6d Joint a

At joint c, we note from the sketch that $F_{dc} = 15 \text{ kN}$ (tension).

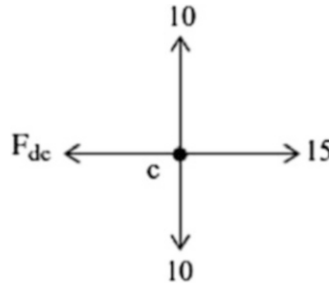


Fig. E2.6e Joint c

At joint b, we note from the sketch that F_{db} must be in tension and F_{be} must be in compression.

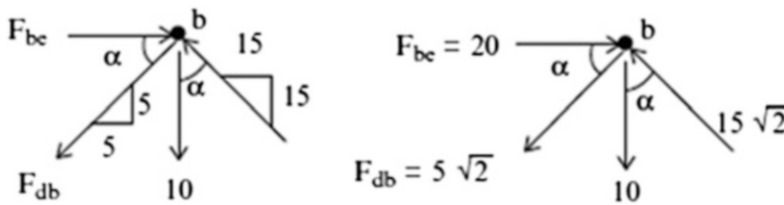


Fig. E2.6f Joint b

We first find $F_{db,y}$ with the vertical equilibrium condition at joint b.

$$\sum F_y = 0 \quad F_{db,y} = 5 \downarrow$$

Then, $F_{db,x} = 5 \leftarrow \therefore F_{db} = 5\sqrt{2} \text{ kN (tension)}$.

Then, we apply the horizontal equilibrium equation at joint b.

$$\sum F_x = 0 \quad F_{be} = 20 \text{ kN (compression)}$$

The resultant member forces are shown below. Note that, for this loading, the members in the top zone (the top chord) are in compression and the bottom chord members are in tension. The interior vertical and diagonal members are in tension. When iron was used as a structural material, cast iron, which is relatively weak in tension, was employed for the top chord members and wrought iron, which is relatively strong in tension, for the verticals, diagonals, and bottom chord members.

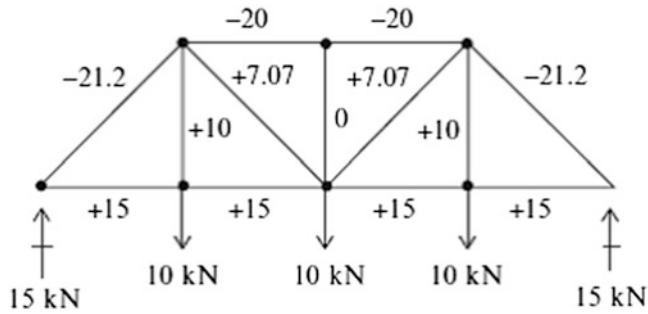


Fig. E2.6g

If the truss structure is inverted as shown below, the sense of the member forces is also reversed. This geometric arrangement is preferred for bridge crossings when the clearance below the structure is not a problem.

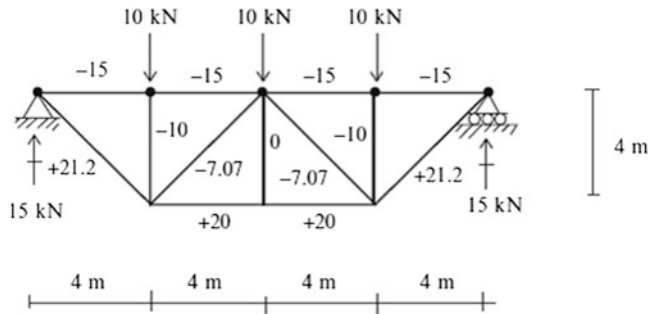


Fig. E2.6h

Example 2.7 A Cantilever Truss Analyzed by Methods of Joints

Given: The truss and loading defined by Fig. E2.7a.

Determine: The member forces for the loading shown.

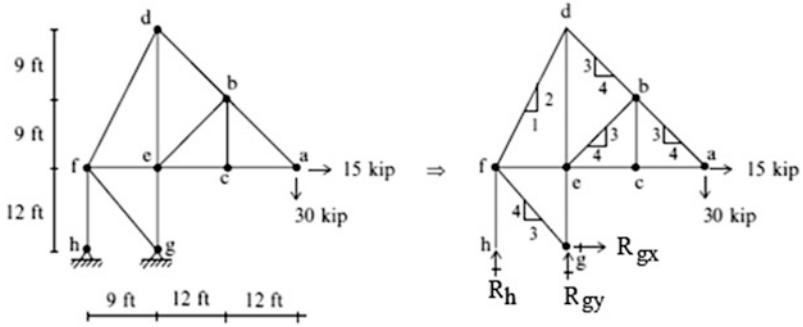


Fig. E2.7a

Solution: First, we determine the zero force members. Starting at joint c, we observe that $F_{cb} = 0$. Then, moving to joint b, it follows that $F_{be} = 0$.

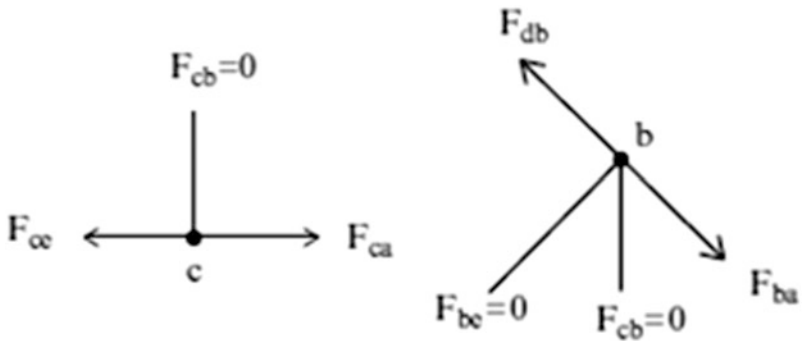


Fig. E2.7b Zero force members

In this case, we do not need to first find the reactions. We can start at joint a.

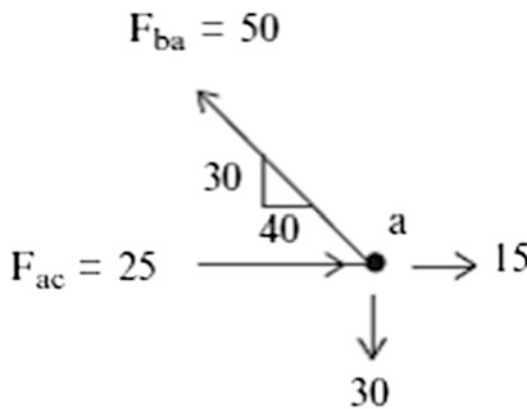


Fig. E2.7c Joint a

$$\sum F_y = 0 \quad F_{ba,y} = 30 \rightarrow F_{ba,x} = 40 \quad \therefore F_{ba} = 50 \text{ kip (tension)}$$

Given F_{ba} , we determine F_{ac}

$$\sum F_x = 0 \quad F_{ac} = 25 \text{ kip (compression)}$$

Next, we move to joint d and determine F_{df}

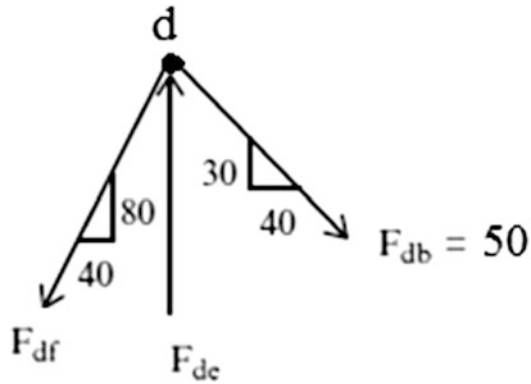


Fig. E2.7d Joint d

$$\sum F_x = 0 \quad F_{df,x} = 40 \quad \therefore F_{df,y} = 80 \quad F_{df} = 40\sqrt{5} \text{ kip (tension)}$$

With F_{df} known, we can determine F_{de}

$$\sum F_y = 0 \quad F_{de} = 110 \text{ kip (compression)}$$

At joint e, we determine F_{ef} and F_{eg} .

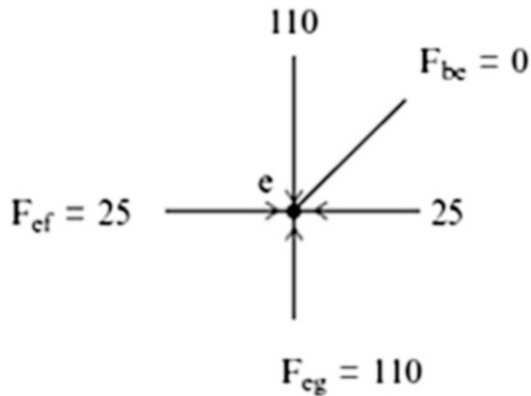


Fig. E2.7e Joint e

The last joint is joint f. We first determine $F_{fg,x}$

$$\sum F_x = 0 \quad F_{fg,x} = 15 \quad \therefore F_{fg,y} = 20 \quad F_{fg} = 25 \text{ kip (compression)}$$

Then, $\sum F_y = 0 \quad F_{fh} = 100 \text{ kip (tension)}$

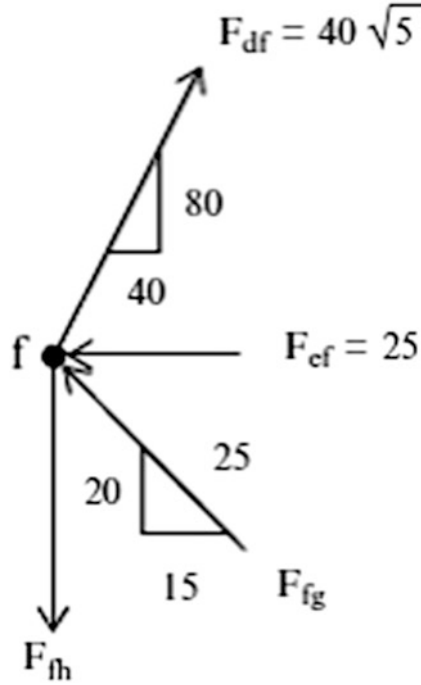


Fig. E2.7f Joint f

The final forces are listed below.

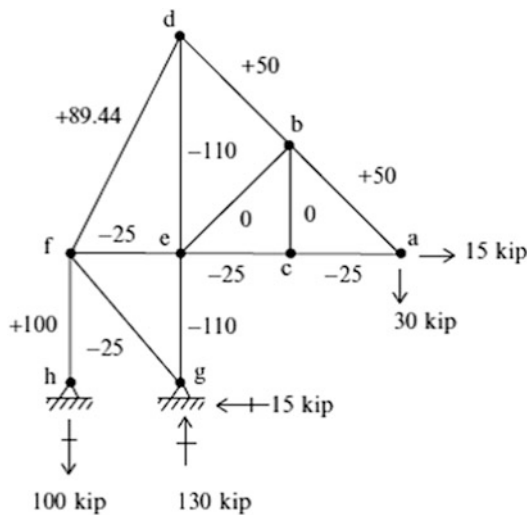


Fig. E2.7g

Example 2.8 Gable Roof Truss Analyzed by the Method of Joints

Given: The truss and loading defined by Fig. E2.8a.

Determine: The member forces.

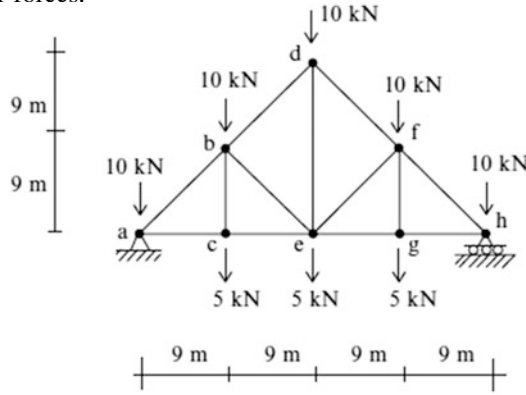


Fig. E2.8a

Solution: Fig. E2.8a shows a typical truss structure for supporting roof (top joints) and ceiling (bottom joints) loads. Members cb and gf function to transfer loads to the top joints (b and f). Their force magnitudes are

$$F_{bc} = 5 \text{ kN (tension)} \quad F_{gf} = 5 \text{ kN (tension)}$$

All the remaining joints have at least three unknown member forces and reactions. Therefore, we start the analysis by first finding the reactions.

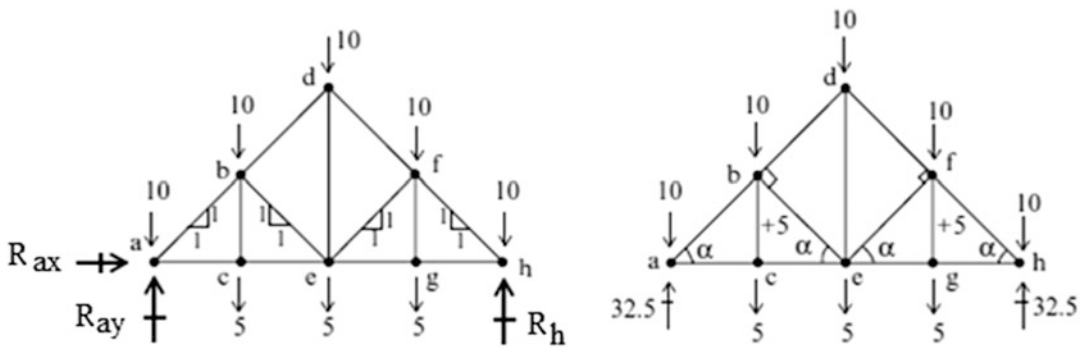


Fig. E2.8b Reactions

Given the reactions, we start at joint a. Force F_{ba} must be compression and $F_{ba,y} = 22.5 \downarrow$. Then, $F_{ba,x} = 22.5 \leftarrow$ and $F_{ba} = 22.5\sqrt{2} \text{ kN (compression)}$. It follows that, F_{ac} is in tension and equal to 22.5 kN.

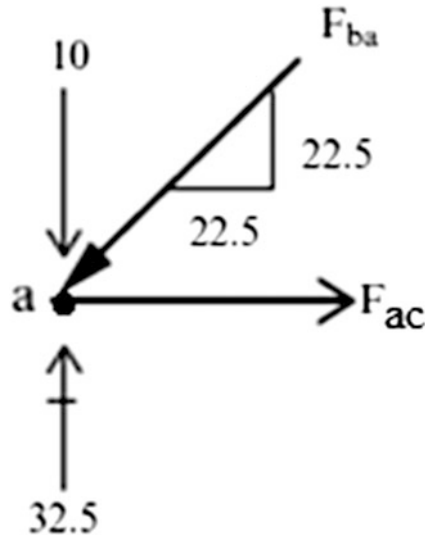


Fig. E2.8c Joint a

We then move on to joint b. Members ab and bd are colinear, and member be is normal to this common direction. Summing forces in the normal direction results in

$$\sum F_n = 0 \quad F_{be} = (10 + 5) \cos \alpha = 15 \frac{\sqrt{2}}{2} \text{ kN (compression)}$$

Next, summing forces in the tangential direction leads to F_{bd} .

$$\sum F_t = 0 \quad F_{bd} = 22.5\sqrt{2} - (10 + 5) \cos \alpha = 15\sqrt{2} \text{ kN (compression)}$$

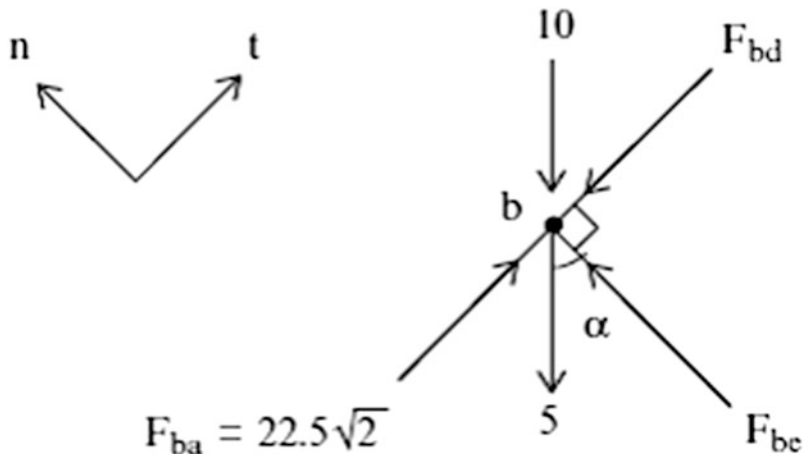


Fig. E2.8d Joint b

The last force is F_{de} . We use joint d shown in Fig. E2.8e. Summing forces in the y direction leads to $F_{de} = 20 \text{ kN (tension)}$

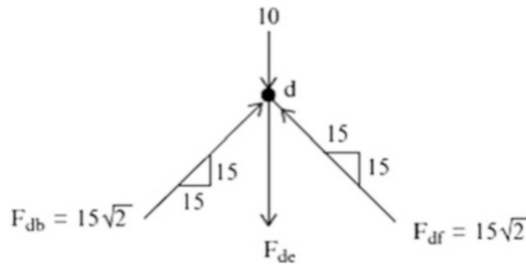


Fig. E2.8e Joint d

The final forces are listed below.

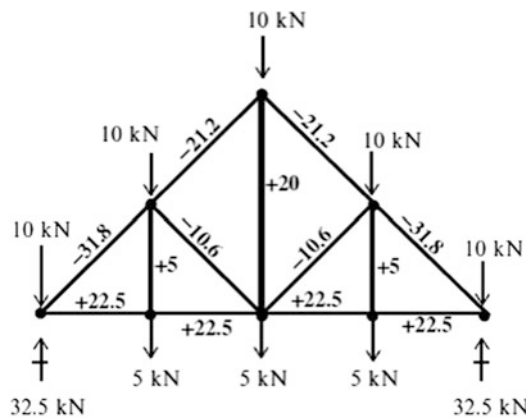


Fig. E2.8f

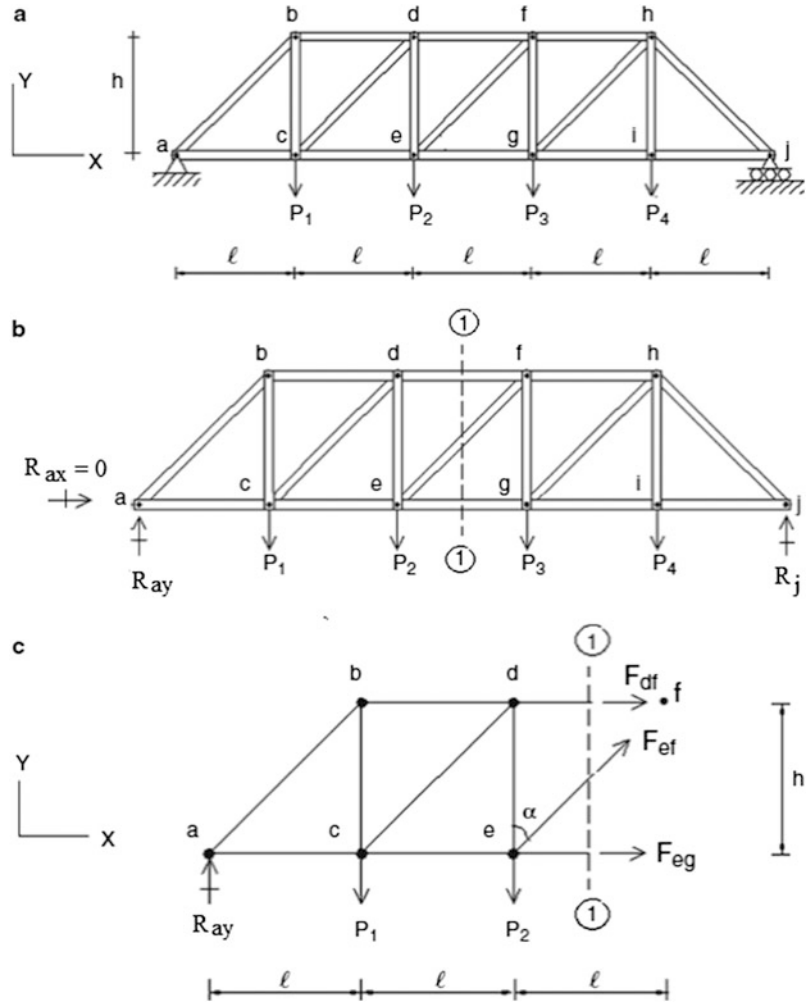
2.2.5 Method of Sections

If one wants to determine only the force in a particular member, applying the method of joints might not be convenient since in general it involves first finding the force in other members. For example, consider the truss shown in Fig. 2.19a. Suppose the force in member ef is desired. One possible strategy is to first determine the reactions at joint a , then proceed to joints b , c , d , and lastly e , where the Y component of F_{ef} can be determined once F_{ed} is known. Another possible strategy is to start at joint j , and then precede to joints i , h , g , and f . Either approach requires some preliminary computation that provides information on forces that may or may not be of interest.

The method of sections is an analysis procedure that avoids this preliminary computation. One passes a cutting plane through the truss, isolates either the left or right segment, and applies the equilibrium equations for a rigid body to the segment. The choice of cutting plane is critical. It must cut the particular member whose force is desired, and other members that are concurrent. This restriction is necessary since there are only three equilibrium equations for planar loading, and therefore, one can only determine three unknowns.

We illustrate this method for the truss defined in Fig. 2.19a. We start by determining the reaction at a . To determine F_{ef} , we use the vertical cutting plane 1-1 and consider the left segment shown in Fig. 2.19c. Summing forces in the Y direction leads to:

Fig. 2.19 (a) An example of a truss. (b) Cutting vertical plane. (c) Truss segment for method of sections



$$\sum F_y = 0 \quad \uparrow^+ \quad F_{ef} \cos \alpha = P_1 + P_2 - R_{ay} \quad (2.3)$$

We point out here that the function of the diagonal members is to equilibrate the unbalanced vertical forces at the sections along the longitudinal axis. These forces are called “shear” forces.

If the force in member df is desired, one can use the moment equilibrium condition with respect to joint e which is the point of concurrency for members ef and eg .

$$\sum M_{\text{about } e} = 0 \quad hF_{df} = lP_1 - 2lR_{ay} \quad (2.4)$$

Similarly, for member eg , we use moment equilibrium about joint f :

$$\sum M_{\text{about } f} = 0 \quad hF_{eg} = 3lR_{ay} - 2lP_1 - lP_2 \quad (2.5)$$

For parallel chord trusses (top and bottom chords are parallel), the function of the chords is to equilibrate the unbalanced moments at the various sections. One chord force is compressive, the other force is tensile. For downward vertical loading, the top chord is generally in compression, and the bottom is in tension. The method of section is convenient in the sense that it allows one to easily identify the sense of a particular member force.

Example 2.9 Application of the Method of Sections to a Parallel Chord Truss

Given: The structure and loading shown in Fig. E2.9a

Determine: The force in members F_{gd} , F_{gf} , and F_{dc} .

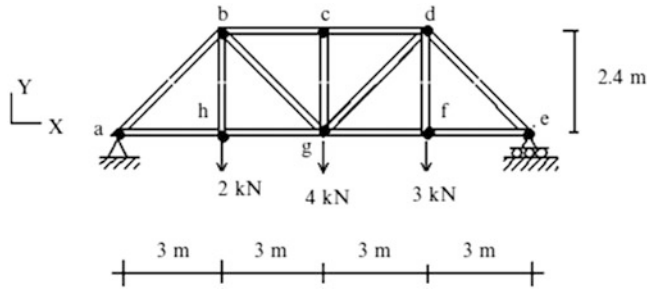


Fig. E2.9a

Solution: We start by determining the reactions.

$$\sum M_a = 0 \quad \curvearrowright \quad 2(3) + 4(6) + 3(9) - R_e(12) = 0 \quad \Rightarrow \quad R_e = 4.75 \text{ kN } \uparrow$$

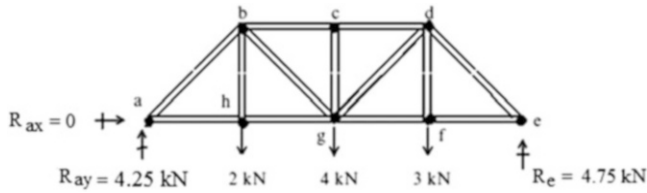


Fig. E2.9b

Then, we pass a vertical cutting plane through the panel between joints d and c and consider the left segment. Enforcing equilibrium leads to:

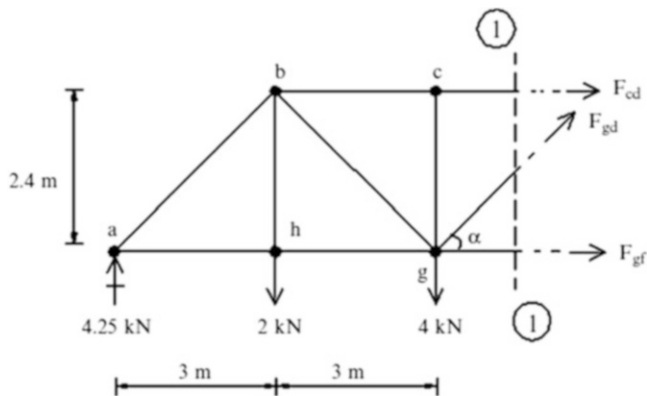


Fig. E2.9c

$$\sum F_y = 0 \quad F_{gd,y} = 1.75 \uparrow$$

Therefore, $F_{gd,x} = 2.1875$ and $F_{gd} = 2.8$ kN (tension)

$$\sum M_{atg} = 0 \quad F_{cd}(2.4) - 2(3) + 4.25(6) = 0 \quad F_{cd} = -8.125$$

Therefore, $F_{cd} = 8.125$ kN (compression)

$$\sum F_x = 0 \quad F_{gf} - 8.125 + 2.1875 = 0 \quad F_{gf} = +5.9375$$

Therefore, $F_{gf} = 5.9375$ kN (tension).

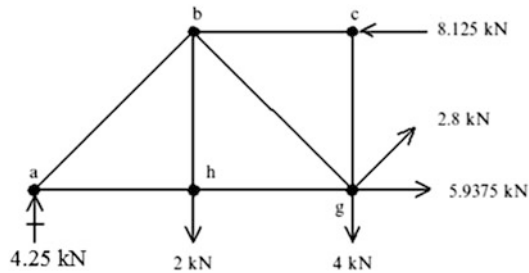


Fig. E2.9d

Example 2.10 The Method of Sections Applied to a Roof Truss

Given: The structure shown in Fig. E2.10a.

Determine: The member forces F_{db} , F_{be} , and F_{ce} .

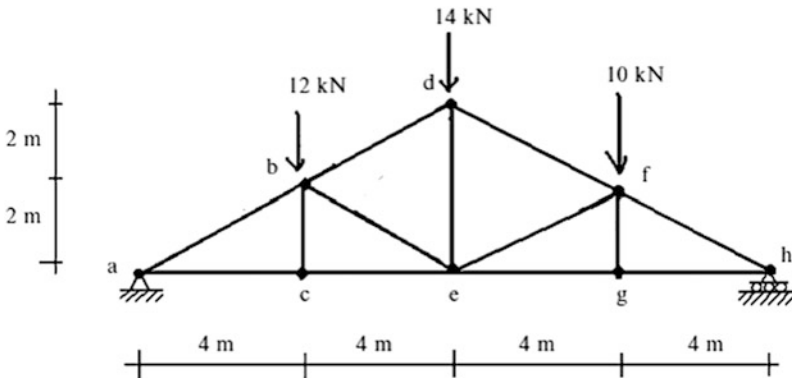


Fig. E2.10a

Solution: We determine the reactions first.

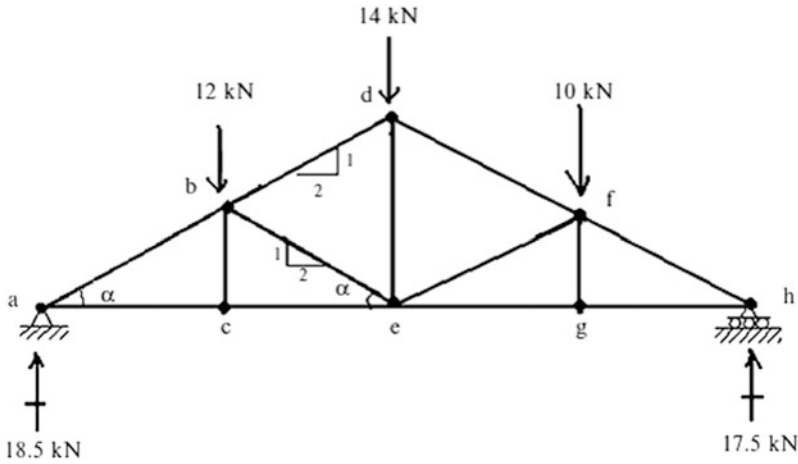


Fig. E2.10b

To determine the member forces F_{db} , F_{be} , and F_{ce} , we use a vertical cutting plane. The appropriate segment is shown in Fig. E2.10c. Various options are possible. We choose first to determine F_{db} by summing moments about e. Then, summing moments about b leads to F_{ce} . Lastly, we can find F_{be} by summing either X or Y forces.

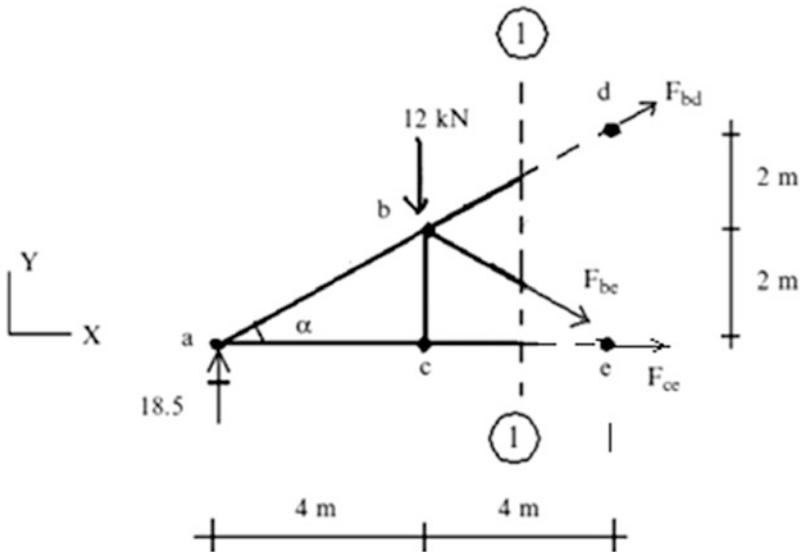


Fig. E2.10c

The calculations for this analysis procedure are listed below:

$$\sum M_e = 0 \quad \curvearrowright \quad 4 F_{bd,x} + (18.5) 8 - (12) 4 = 0$$

$$F_{bd,x} = -25 \quad F_{bd} = \frac{F_{bd,x}}{\cos \alpha} = 27.95 \text{ kN (Compression)}$$

$$\begin{aligned}\sum M_b = 0 \quad \curvearrowright \quad & -2F_{ce} + (18.5)4 = 0 \\ & F_{ce} = 37 \text{ kN (Tension)}\end{aligned}$$

$$\begin{aligned}\sum F_Y = 0 \uparrow + \quad & -F_{be,y} - 12 - 12.5 + 18.5 = 0 \\ F_{be,y} = -6 \quad & \Rightarrow F_{be} = \frac{F_{be,y}}{\sin \alpha} = 13.41 \text{ kN (compression)}\end{aligned}$$

Example 2.11 Analysis of K-Type Trusses with the Method of Sections

Given: The truss defined in Fig. E2.11a.

Determine: The member forces F_{ab} , F_{be} , F_{cd} , and F_{ce} .

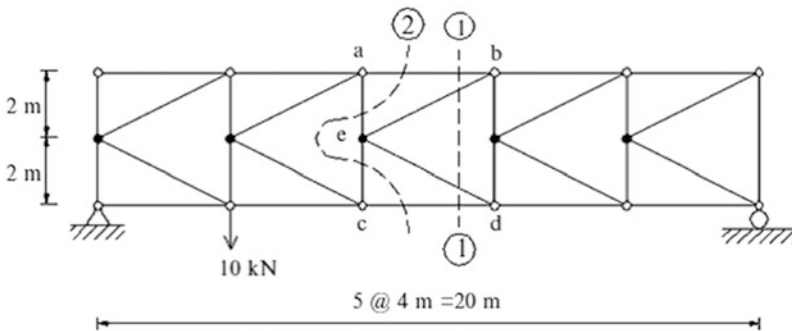


Fig. E2.11a

Solution: We determine reactions first.

A vertical section such as ①—① cuts four unknown forces and does not lead to a solution. There are no vertical cutting planes that involve only three unknown forces. Therefore, one has to be more creative with the choice of planes. For this type of truss, plane ②—② is the appropriate choice. Isolating the left segment and summing moments about joint c results in F_{ab} :

$$\sum M_c = 0 \quad \curvearrowright \quad 4F_{ab} - 10(4) + 8(8) = 0 \rightarrow F_{ab} = -6 \quad \therefore F_{ab} = 6 \text{ kN (Compression)}$$

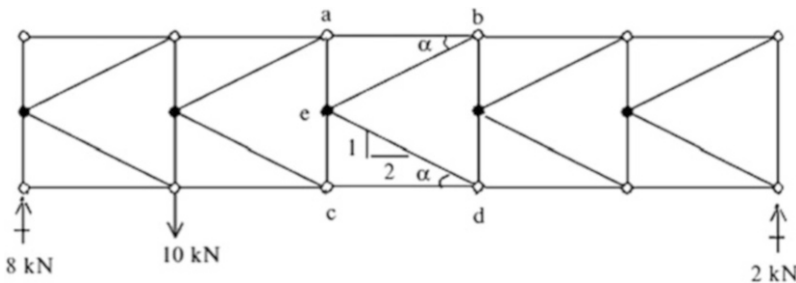


Fig. E2.11b

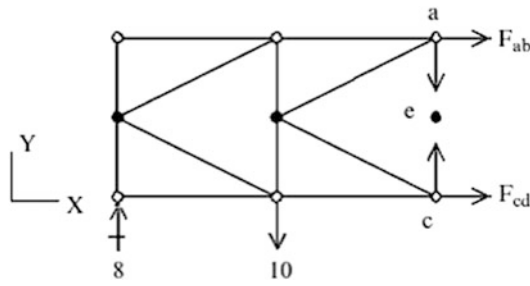


Fig. E2.11c

Then summing X forces,

$$\sum F_x = 0 \quad F_{cd} = -F_{ab} = +6 \quad \therefore F_{cd} = 6 \text{ kN (tension)}$$

The diagonal forces F_{eb} and F_{cd} are found using section ①—①. Summing moments about joint d leads to F_{eb} :

$$\sum M_d = 0 \quad \curvearrowright \quad 4(F_{ab} + F_{eb,x}) - 10(8) + 8(12) = 0 \quad 4(-6 + F_{eb,x}) + 16 = 0$$

$$F_{eb,x} = +2 \quad \therefore F_{eb} = \frac{F_{eb,x}}{\cos \alpha} = 2.24 \text{ kN (tension)}$$

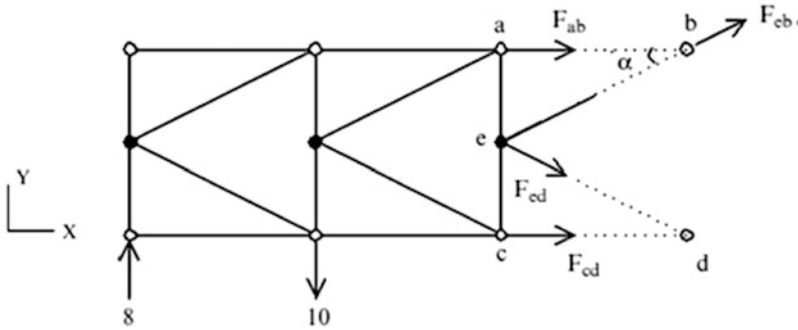


Fig. E2.11d

We find F_{cd} by summing x forces, and noting that the horizontal components of the chord forces must cancel.

$$\sum F_x = 0 \quad F_{ed,x} = -F_{cd,x} \quad \therefore F_{ed} = 2.24 \text{ kN (compression)}$$

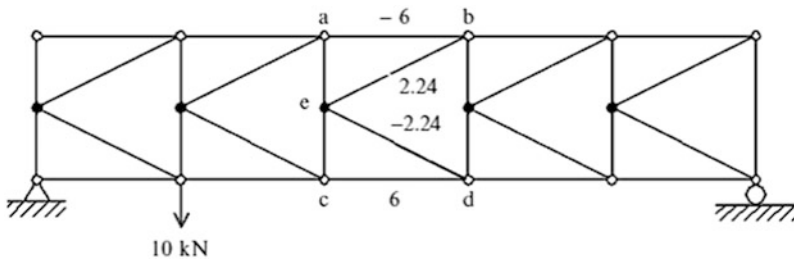


Fig. E2.11e

If one wants all the member forces, one can apply multiple cutting planes or combinations of the method of joints and method of sections. How one proceeds is a matter of personal preference.

Example 2.12: A Hybrid Analysis Strategy

Given: The truss defined in Fig. E2.12a

Determine: All the member forces using a combination of the method of joints and the method of sections.

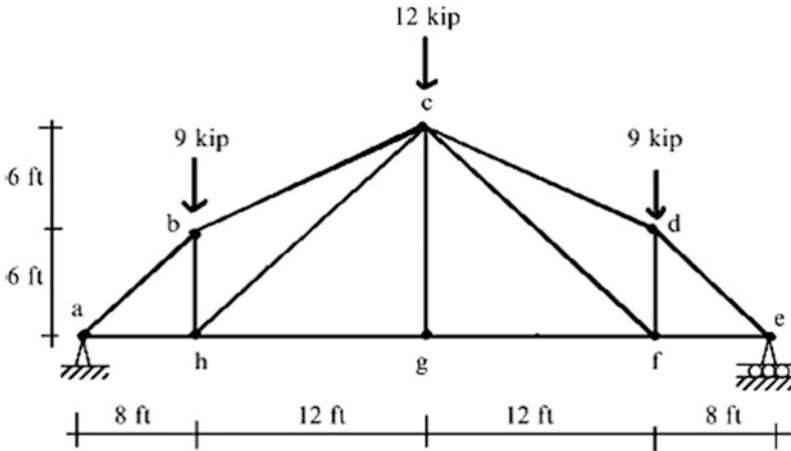


Fig. E2.12a

Solution: We note that the structure and loading are symmetrical with respect to a vertical axis through points c and g . It follows that the forces in symmetrically located members are equal, and therefore we need to find the forces in only $\frac{1}{2}$ of the structure. We start by determining the reactions. The member forces F_{bc} , F_{hc} , and F_{hg} can be determined by passing vertical cutting plane 1-1 and enforcing the equilibrium equations.

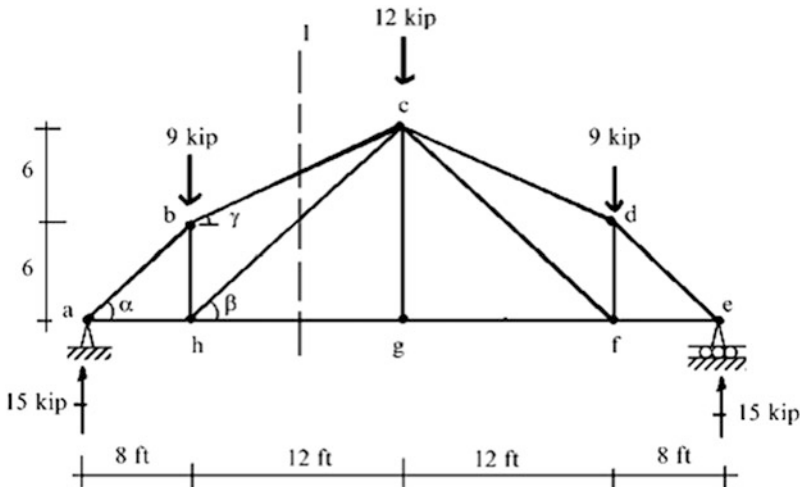


Fig. E2.12b

Considering the left segment and enforcing equilibrium leads to:

Section I-I:

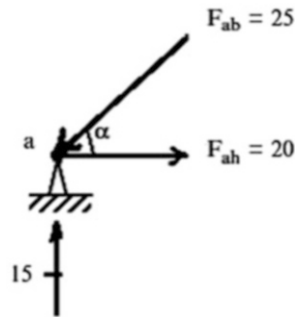
$$\sum M_{ath} = 0 \quad (F_{bc} \cos \gamma)(6) + 15(8) = 0 \quad F_{bc} = 10\sqrt{5} \text{ kip (compression)}$$

$$\sum F_y = 0 \quad F_{hc} = 4\sqrt{2} \text{ kip (tension)}$$

$$\sum F_x = 0 \quad F_{hg} = 16 \text{ kip (tension)}$$

We then enforce equilibrium at joints a and h.

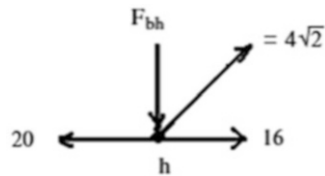
Equilibrium at joint a:



$$\sum F_y = 0 \quad F_{ab,y} = 15 \downarrow \quad \therefore F_{ab} = 25 \text{ kip (compression)}$$

$$\sum F_x = 0 \quad F_{ah} = -F_{ab,x} = 20 \text{ kip (tension)}$$

Equilibrium at joint h:



$$\sum F_y = 0 \quad F_{bh} = -F_{ch,y} = 4 \text{ kip (compression)}$$

The final member forces are listed below.

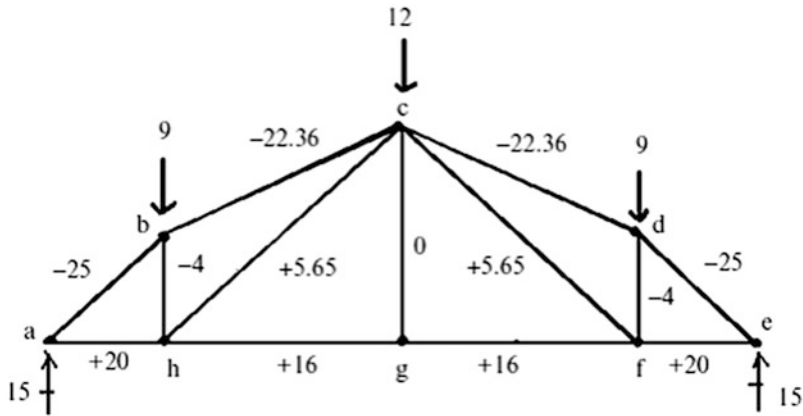


Fig. E2.12c

2.2.6 Complex Trusses

Complex trusses are defined as truss structures that cannot be classified as either simple or compound trusses. In order to determine the member forces, one has to establish the complete set of nodal force equilibrium equations expressed in terms of the member forces. If the truss is statically determinate, the number of equations will be equal to the number of force unknowns, and theoretically one can solve these equations for the force unknowns. However, if one cannot determine the member forces, the statically determinate truss is said to be geometrically unstable. In what follows, we expand on this point.

Consider the planar truss shown in Fig. 2.20a. There are nine members, three reactions, and six nodes. Then,

$$2j = 12$$

$$m + r = 9 + 3 = 12$$

and the truss is statically determinate. It also has a sufficient number of reactions to prevent rigid body motions.

We use 3 of the 12 equilibrium equations to determine the reactions, leaving 9 equations available to solve for the 9 member forces.

$$\sum F_x = 0 \quad R_{1x} = P \leftarrow$$

$$\sum M_{at 1} = 0 \quad R_5 = \frac{P}{2} \uparrow$$

$$\sum F_y = 0 \quad R_{1y} = \frac{P}{2} \downarrow$$

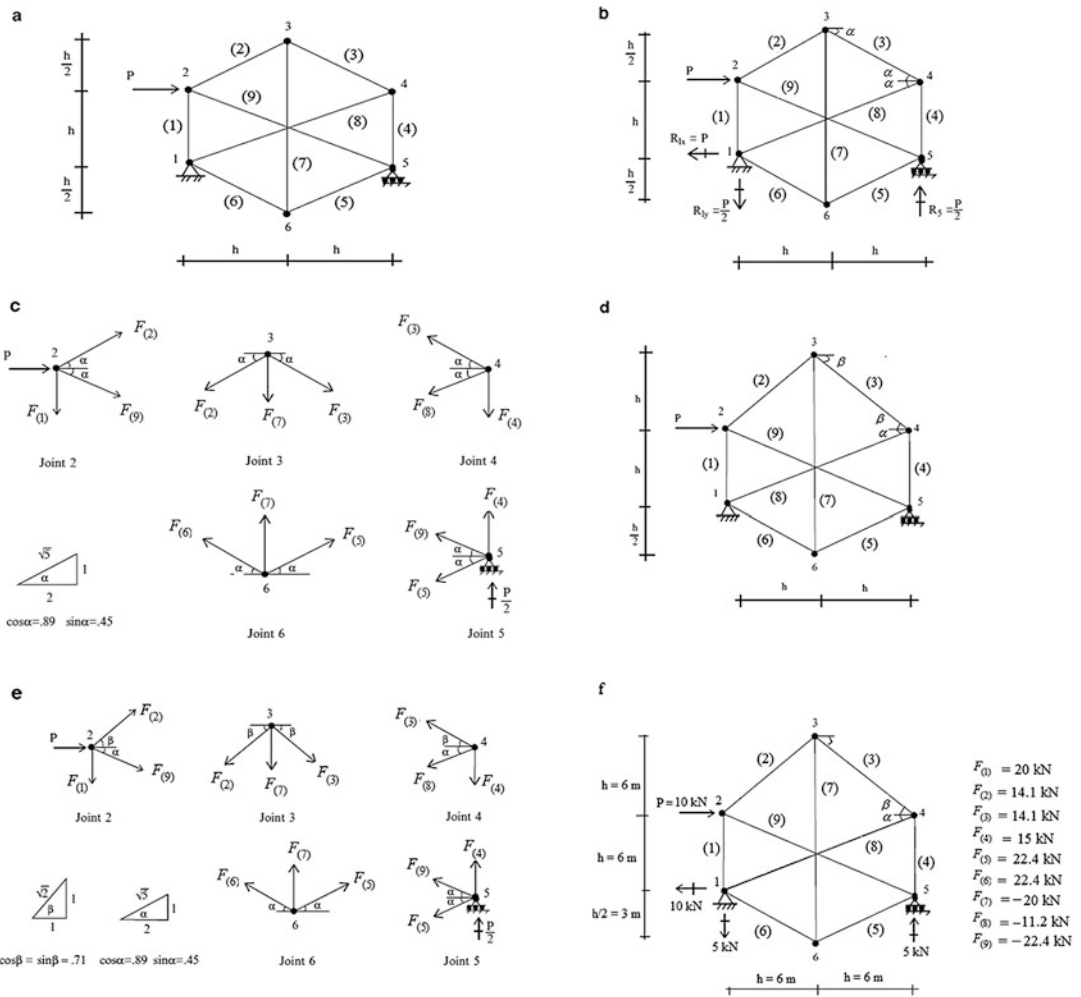


Fig. 2.20 (a) Planar truss geometry. (b) Reactions. (c) Joint equilibrium. (d) Modified geometry. (e) Joint equilibrium. (f) Member forces

Enforcing equilibrium at joints 2–6 results in the following nine equations:

$$\begin{aligned}
 \text{Joint 2} & \begin{cases} \sum F_x = 0 & (\cos \alpha)F_{(2)} + (\cos \alpha)F_{(9)} = -P \\ \sum F_y = 0 & -F_{(1)} + (\sin \alpha)F_{(2)} - (\sin \alpha)F_{(9)} = 0 \end{cases} \\
 \text{Joint 3} & \begin{cases} \sum F_x = 0 & (\cos \alpha)F_{(2)} - (\cos \alpha)F_{(3)} = 0 \\ \sum F_y = 0 & (\sin \alpha)F_{(2)} + (\sin \alpha)F_{(3)} + F_{(7)} = 0 \end{cases} \\
 \text{Joint 4} & \begin{cases} \sum F_x = 0 & (\cos \alpha)F_{(3)} + (\cos \alpha)F_{(8)} = 0 \\ \sum F_y = 0 & (\sin \alpha)F_{(3)} - F_{(4)} - (\sin \alpha)F_{(8)} = 0 \end{cases} \\
 \text{Joint 5} & \begin{cases} \sum F_x = 0 & (\cos \alpha)F_{(5)} + (\cos \alpha)F_{(9)} = 0 \\ \sum F_y = 0 & F_{(4)} - (\sin \alpha)F_{(5)} + (\sin \alpha)F_{(9)} = -\frac{P}{2} \end{cases} \\
 \text{Joint 6} & \begin{cases} \sum F_x = 0 & (\cos \alpha)F_{(5)} - (\cos \alpha)F_{(6)} = 0 \end{cases}
 \end{aligned} \tag{2.6}$$

We express (2.6) in matrix form

$$\mathbf{BF} = \mathbf{C} \quad (2.7)$$

where

$$\mathbf{F} = \begin{Bmatrix} F_{(1)} \\ F_{(2)} \\ F_{(3)} \\ F_{(4)} \\ F_{(5)} \\ F_{(6)} \\ F_{(7)} \\ F_{(8)} \\ F_{(9)} \end{Bmatrix} \quad \mathbf{C} = \begin{Bmatrix} -P \\ 0 \\ 0 \\ 0 \\ 0 \\ 0 \\ 0 \\ \frac{P}{2} \\ 0 \end{Bmatrix}$$

$$\mathbf{B} = \begin{bmatrix} 0 & \cos \alpha & 0 & 0 & 0 & 0 & 0 & 0 & \cos \alpha \\ -1 & \sin \alpha & 0 & 0 & 0 & 0 & 0 & 0 & -\sin \alpha \\ 0 & -\cos \alpha & \cos \alpha & 0 & 0 & 0 & 0 & 0 & 0 \\ 0 & \sin \alpha & \sin \alpha & 0 & 0 & 0 & 1 & 0 & 0 \\ 0 & 0 & \cos \alpha & 0 & 0 & 0 & 0 & \cos \alpha & 0 \\ 0 & 0 & \sin \alpha & -1 & 0 & 0 & 0 & -\sin \alpha & 0 \\ 0 & 0 & 0 & 0 & \cos \alpha & 0 & 0 & 0 & \cos \alpha \\ 0 & 0 & 0 & 1 & -\sin \alpha & 0 & 0 & 0 & \sin \alpha \\ 0 & 0 & 0 & 0 & \cos \alpha & -\cos \alpha & 0 & 0 & 0 \end{bmatrix}$$

The coefficient matrix, \mathbf{B} is singular (the determinate of \mathbf{B} equals 0). Therefore, a unique solution for the unknown forces does not exist for an arbitrary nodal load. The truss is said to be geometrically unstable since the elements of \mathbf{B} depend only on the geometric pattern.

In order to eliminate the instability, one needs to change the geometry. We modify the truss by changing the vertical position of node 3 as shown in Fig. 2.20d. The individual nodal force systems are defined in Fig. 2.20e and the corresponding nodal force equilibrium equations are listed in (2.8). Note the change in the coefficients.

$$\begin{aligned}
 \text{Joint 2} & \begin{cases} \sum F_x = 0 & (\cos \beta)F_{(2)} + (\cos \alpha)F_{(9)} = -P \\ \sum F_y = 0 & -F_{(1)} + (\sin \beta)F_{(2)} - (\sin \alpha)F_{(9)} = 0 \end{cases} \\
 \text{Joint 3} & \begin{cases} \sum F_x = 0 & -(\cos \beta)F_{(2)} + (\cos \beta)F_{(3)} = 0 \\ \sum F_y = 0 & (\sin \beta)F_{(2)} + (\sin \beta)F_{(3)} + F_{(7)} = 0 \end{cases} \\
 \text{Joint 4} & \begin{cases} \sum F_x = 0 & (\cos \beta)F_{(3)} + (\cos \alpha)F_{(8)} = 0 \\ \sum F_y = 0 & (\sin \beta)F_{(3)} - F_{(4)} - (\sin \alpha)F_{(8)} = 0 \end{cases} \\
 \text{Joint 5} & \begin{cases} \sum F_x = 0 & (\cos \alpha)F_{(5)} + (\cos \alpha)F_{(9)} = 0 \\ \sum F_y = 0 & F_{(4)} - (\sin \alpha)F_{(5)} + (\sin \alpha)F_{(9)} = -\frac{P}{2} \end{cases} \\
 \text{Joint 6} & \begin{cases} \sum F_x = 0 & (\cos \alpha)F_{(5)} - (\cos \alpha)F_{(6)} = 0 \end{cases}
 \end{aligned} \tag{2.8}$$

In this case, the coefficient matrix \mathbf{B} is nonsingular ($\det \mathbf{B} \neq 0$), and it follows that the structure is geometrically stable:

$$\mathbf{B} = \begin{bmatrix} 0 & \cos \beta & 0 & 0 & 0 & 0 & 0 & 0 & \cos \alpha \\ -1 & \sin \beta & 0 & 0 & 0 & 0 & 0 & 0 & -\sin \alpha \\ 0 & -\cos \beta & \cos \beta & 0 & 0 & 0 & 0 & 0 & 0 \\ 0 & \sin \beta & \sin \beta & 0 & 0 & 0 & 1 & 0 & 0 \\ 0 & 0 & \cos \beta & 0 & 0 & 0 & 0 & \cos \alpha & 0 \\ 0 & 0 & \sin \beta & -1 & 0 & 0 & 0 & -\sin \alpha & 0 \\ 0 & 0 & 0 & 0 & \cos \alpha & 0 & 0 & 0 & \cos \alpha \\ 0 & 0 & 0 & 1 & -\sin \alpha & 0 & 0 & 0 & \sin \alpha \\ 0 & 0 & 0 & 0 & \cos \alpha & -\cos \alpha & 0 & 0 & 0 \end{bmatrix}$$

Solving (2.8) using a computer software system [2] leads to the member forces listed below.

$$\mathbf{F} = \mathbf{B}^{-1}\mathbf{C} = \begin{Bmatrix} 2P \\ 1.41P \\ 1.41P \\ 1.5P \\ 2.24P \\ 2.24P \\ -2P \\ -1.12P \\ -2.24P \end{Bmatrix} \Rightarrow \begin{Bmatrix} F_{(1)} \\ F_{(2)} \\ F_{(3)} \\ F_{(4)} \\ F_{(5)} \\ F_{(6)} \\ F_{(7)} \\ F_{(8)} \\ F_{(9)} \end{Bmatrix} = \begin{Bmatrix} 2P \\ 1.41P \\ 1.41P \\ 1.5P \\ 2.24P \\ 2.24P \\ -2P \\ -1.12P \\ -2.24P \end{Bmatrix}$$

For $P = 10$ kN and $h = 6$ m, the member forces are listed in Fig. 2.20f.

Assembling the nodal force equilibrium equations usually is a tedious operation, especially for three-dimensional space structures. The process can be automated by using matrix operations. We will describe one approach later in Sect. 2.6.

2.3 Computation of Deflections

2.3.1 Introduction

The deflections of the joints are due to the change in length of the members that make up the truss. Each member is subjected to an axial force which produces, depending on the sense, either an extension or a contraction along the member. We call these movements “axial deformation.” The study of deflection involves two steps. Firstly, we determine the axial deformation due to the applied loading. This step involves introducing the material properties for the members. Secondly, we need to relate the deflections to the axial deformations. This step is purely geometric. In what follows, we develop procedures for determining the axial deformation due to an axial force, and the joint deflections resulting from a set of axial deformations. The latter procedure is carried out here using a manual computation scheme. A computer-based scheme is described in the next section.

2.3.2 Force–Deformation Relationship

Consider the axially loaded member shown in Fig. 2.21. We suppose an axial force, F , is applied, and the member extends an amount e . Assuming the material is linear elastic, e is a linear function of F . We estimate the proportionality factor by first determining the stress, then the strain, and lastly the extension. We discussed this approach in Chap. 1. The steps are briefly reviewed here.

1. Stress

$$\sigma = \frac{F}{A}$$

where A is the cross-sectional area

2. Strain

$$\varepsilon = \frac{\sigma}{E} = \frac{F}{AE}$$

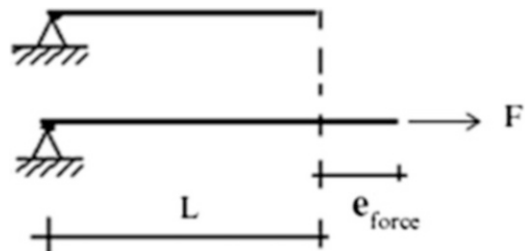
where E is young’s modulus

3. Extension

$$e_{\text{force}} = L\varepsilon = \frac{FL}{AE}$$

where L is the member length

Fig. 2.21 Axially loaded member



The member may also experience an extension due to a temperature change or a fabrication error. Introducing these additional terms, the total extension is expressed as

$$e = e_{\text{force}} + e_{\text{temperature}} + e_{\text{fabrication error}} \quad (2.9)$$

where

$$e_{\text{force}} = \frac{FL}{AE}$$

$$e_{\text{temperature}} = \alpha \Delta TL$$

$$e_{\text{fabrication error}} = e_0$$

α is the coefficient of thermal expansion, ΔT is the temperature change, and e_0 represents the fabrication error. The *total extension*, e , is the quantity that produces the displacement of the node.

2.3.3 Deformation–Displacement Relations

Consider the planar truss structure shown in Fig. 2.22. Suppose the members experience deformation and one wants to determine the final position of node B. Our approach is based on first temporarily disconnecting the members at B, allowing the member deformations to occur, and then rotating the members such that they are reconnected. The movements of the nodes from the original configuration to the new configuration are defined as the displacements. These quantities are usually referred to a global reference frame having axes X and Y and corresponding displacement components u and v .

For structural materials such as steel, the extensions are small in comparison to the original length. Then, the member rotations will also be small. Noting Fig. 2.22b, and the above assumptions, it follows that the displacements are related to the deformations by

$$u \approx e_{AB}$$

$$v \approx e_{BC} \quad (2.10)$$

The simplicity of this results is due to the fact that the structure's geometry is simple (the members are orthogonal to the coordinate axes).

We consider the single member AB defined in Fig. 2.23. Our strategy is to track the motion of the end B as it experiences an extension, e . The final length is $(L + e)$ where e is the extension. We assume $\Delta\theta$ is small and project the final length onto the original direction. This step provides a first-order estimate for the extension in terms of the nodal displacements.

Fig. 2.22 Initial and deformed geometries. (a) Initial geometry. (b) Deformed configuration

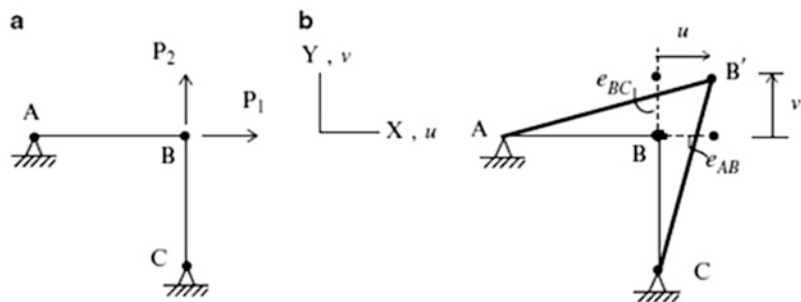


Fig. 2.23 Extension displacement relationships

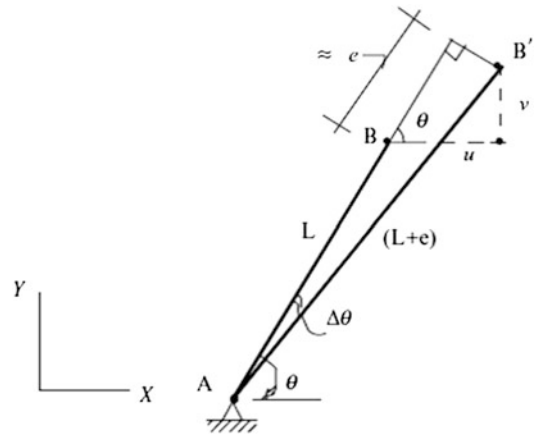
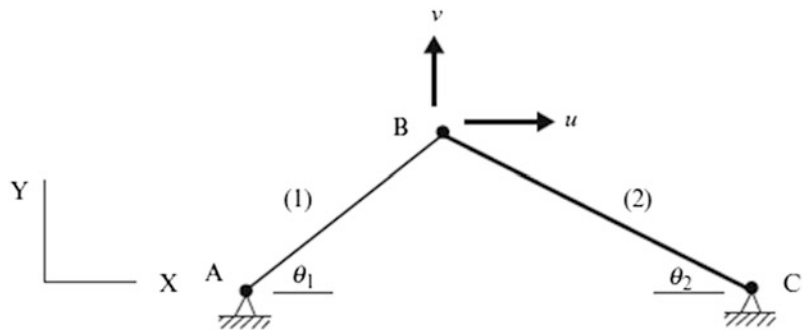


Fig. 2.24 Geometry—two-member truss



$$e \approx u \cos \theta + v \sin \theta \quad (2.11)$$

We consider next a two-member planar truss shown in Fig. 2.24. Since the member orientations are arbitrary, the deformation–displacement relations will involve all the displacement components. Applying (2.11) to the above structure leads to

$$\begin{aligned} e_1 &= u \cos \theta_1 + v \sin \theta_1 \\ e_2 &= -u \cos \theta_2 + v \sin \theta_2 \end{aligned} \quad (2.12)$$

Given the member forces, one computes the extensions e_1 and e_2 and finally determines the displacements by solving (2.12).

$$\begin{aligned} u &= e_1 \frac{\sin \theta_2}{\sin \theta_1 \cos \theta_2 + \cos \theta_1 \sin \theta_2} - e_2 \frac{\sin \theta_1}{\sin \theta_1 \cos \theta_2 + \cos \theta_1 \sin \theta_2} \\ v &= e_1 \frac{\cos \theta_2}{\sin \theta_1 \cos \theta_2 + \cos \theta_1 \sin \theta_2} + e_2 \frac{\cos \theta_1}{\sin \theta_1 \cos \theta_2 + \cos \theta_1 \sin \theta_2} \end{aligned}$$

2.3.4 Method of Virtual Forces

The formulation described in the previous section is not convenient for manual computation, even for fairly simple trusses. However, there is an alternative procedure called the Virtual Force Method, which avoids the need to solve simultaneous equations. Engineers prefer this approach since it is based on executing a set of force equilibrium analyses, a task that they are more familiar with.

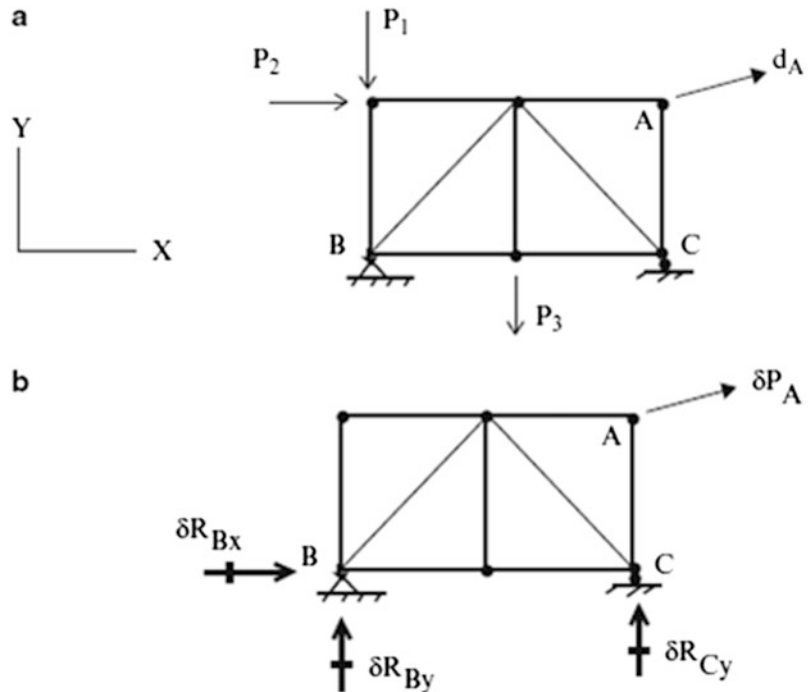
The Method of Virtual Forces is a procedure for determining the deflection at a particular point in a structure given that the member forces are known. A general proof of the method can be found in [3]. We apply the method here for truss type structures. Later in the following chapters, we apply the procedure to beam and frame type structures. The method is restricted to static loading and geometrically linear behavior, i.e., where the displacements are small. This is not a serious restriction for civil structures such as building and bridges.

Consider a typical truss shown in Fig. 2.25a. Suppose the deflection, d_A , in a specified direction at point A is desired. One applies a virtual force, δP_A , at A in the specified desired direction and computes the corresponding member forces, δF , and reactions, δR , using only the static equilibrium equations. Usually, one takes δP_A to be a unit load. Note that this virtual force system is “specialized” for the particular displacement that one is seeking. The displacement is determined using the following expression:

$$d_A \delta P_A = \sum_{\text{members}} e \delta F - \sum_{\text{reactions}} \bar{d} \delta R \tag{2.13}$$

where e is the total extension defined by (2.9), \bar{d} is the support movement, and δR the corresponding reaction. When the supports are unyielding, $\bar{d} = 0$, and the statement simplifies to

Fig. 2.25 (a) Desired deflection—actual force system F . (b) Virtual force system δF



$$d_A \delta P_A = \sum_{\text{members}} e \delta F \quad (2.14)$$

Given the actual forces, one evaluates e with (2.9), then determines the product, $e \delta F$, and lastly sums over the members. Applying (2.13) is equivalent to solving the set of simultaneous equations relating the deformations and the displacements. The following example illustrates this point.

Example 2.13 Computation of Deflection—Virtual Force Method

Given: The plane truss shown in Fig. E2.13a. Assume $A = 1300 \text{ mm}^2$ and $E = 200 \text{ GPa}$ for all members.

Determine: The horizontal displacement at c (u_c).

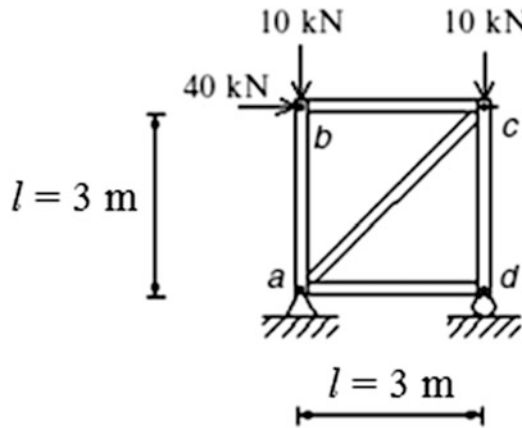


Fig. E2.13a Geometry and loading

Solution: Applying (2.14), the horizontal displacement at node c (u_c) is determined with

$$u_c \delta P = \sum e_{\text{force}} \delta F_u = \sum \left(\frac{FL}{AE} \right) \delta F_u$$

The actual and virtual forces are listed below.

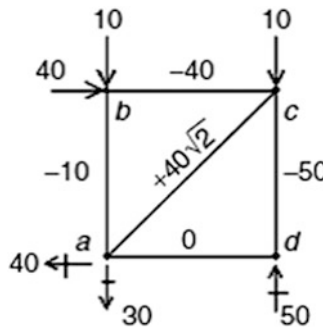


Fig. E2.13b Actual forces, F

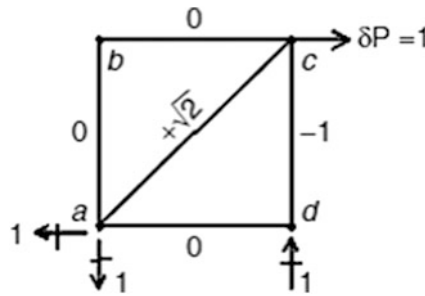


Fig. E2.13c Virtual forces, δF

Using this data, and assuming AE is constant, the computation proceeds as follows:

Member	L	F	δF_u	$e_{\text{force}} = \frac{FL}{AE}$	$e \delta F_u$
ab	l	-10	0	$-10 \frac{l}{AE}$	0
bc	l	-40	0	$-40 \frac{l}{AE}$	0
cd	l	-50	-1	$-50 \frac{l}{AE}$	$50 \frac{l}{AE}$
da	l	0	0	0	0
ac	$l\sqrt{2}$	$40\sqrt{2}$	$\sqrt{2}$	$80 \frac{l}{AE}$	$80\sqrt{2} \frac{l}{AE}$

$$u_c = \sum e_{\text{force}} \delta F_u = \frac{l}{AE} (80\sqrt{2} + 50)$$

The plus sign indicates the deflection is in the direction of the unit load. For $A = 1300 \text{ mm}^2$, $E = 200 \text{ GPa}$, and $l = 3 \text{ m}$, the displacement is

$$u_c = \frac{3(10^3)}{1300(200)} (80\sqrt{2} + 50) = 1.88 \text{ mm} \rightarrow$$

We point out that the virtual force (δF) results identify which member deformations contribute to the corresponding deflection. In this case, only two-member deformations contribute to the horizontal displacement.

Example 2.14 Computation of Deflection—Virtual Force Method

Given: The plane truss shown in Fig. E2.14a. Assume $E = 200 \text{ GPa}$.

Determine: The value of A required to limit the vertical displacement at e (v_e) to be equal to 10 mm. Assume AE is constant for all members.

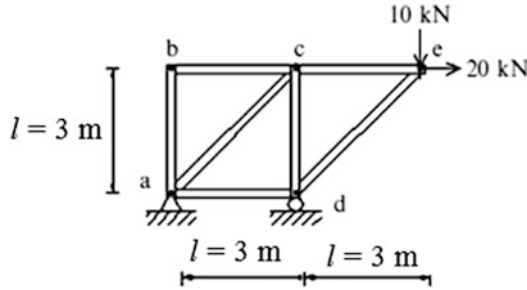


Fig. E2.14a Geometry and loading

Solution: Using (2.14) the vertical displacement at node e (v_e) is determined with

$$v_e \delta P = \sum e_{\text{force}} \delta F_v = \sum \left(\frac{FL}{AE} \right) \delta F_v$$

The actual and virtual forces are listed below.

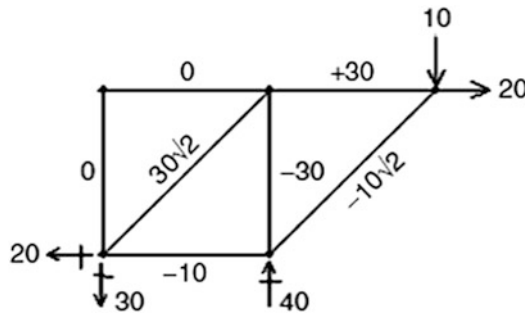


Fig. E2.14b Actual forces, F

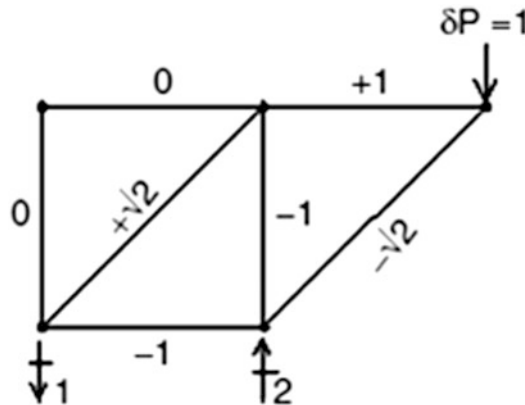


Fig. E2.14c Virtual forces, δF

Using this data, and assuming AE is constant, the following computations are carried out:

Member	L	F	δF_v	$e_{\text{force}} = \frac{F L}{AE}$	$e_{\text{force}} \delta F_v$
ab	l	0	0	0	0
bc	l	0	0	0	0
cd	l	-30	-1	$-30 \frac{l}{AE}$	$30 \frac{l}{AE}$
da	l	-10	-1	$-10 \frac{l}{AE}$	$10 \frac{l}{AE}$
ac	$l\sqrt{2}$	$30\sqrt{2}$	$\sqrt{2}$	$60 \frac{l}{AE}$	$60\sqrt{2} \frac{l}{AE}$
ce	l	30	1	$30 \frac{l}{AE}$	$30 \frac{l}{AE}$
ed	$l\sqrt{2}$	$-10\sqrt{2}$	$-\sqrt{2}$	$-20 \frac{l}{AE}$	$20\sqrt{2} \frac{l}{AE}$
					$\sum e_{\text{force}} \delta F_v = \frac{l}{AE}(80\sqrt{2} + 70)$

$$v_c = \sum e_{\text{force}} \delta F_v = \frac{l}{AE} (80\sqrt{2} + 70)$$

The plus sign indicates the deflection is in the direction of the unit load. For $E = 200$ GPa, and $l = 3000$ mm, the required area is

$$A_{\text{required}} = \frac{l}{v_c E} (80\sqrt{2} + 70) = \frac{(3000)}{10(200)} (80\sqrt{2} + 70) = 275 \text{ mm}^2$$

Example 2.15 Computation of Deflection—Virtual Force Method

Given: The plane truss shown in Fig. E2.15a. Assume $A = 3000 \text{ mm}^2$ and $E = 200$ GPa for all members.

Determine: The vertical displacement at c (v_c) due to the loading shown and a settlement of 10 mm at support a .

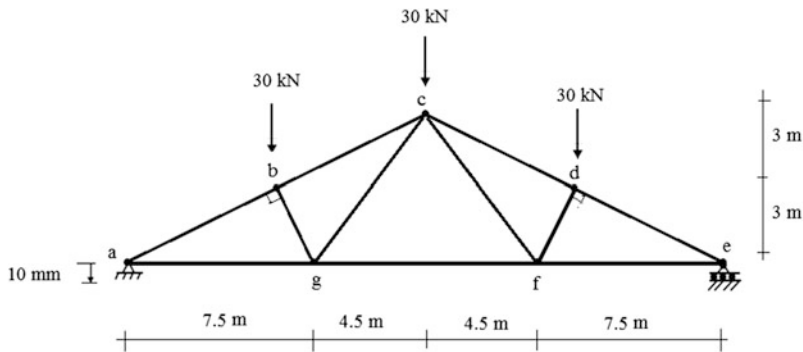


Fig. E2.15a

Solution: Using (2.13), the vertical displacement at c (v_c) is determined with v_c

$$v_c = \sum_{\text{members}} e \delta F_v - \sum_{\text{reactions}} \bar{d} \delta R$$

The actual and virtual forces are listed below.

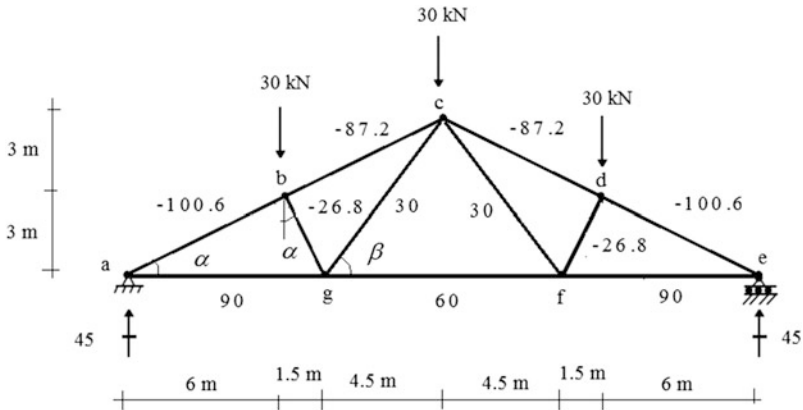


Fig. E2.15b Actual forces, F

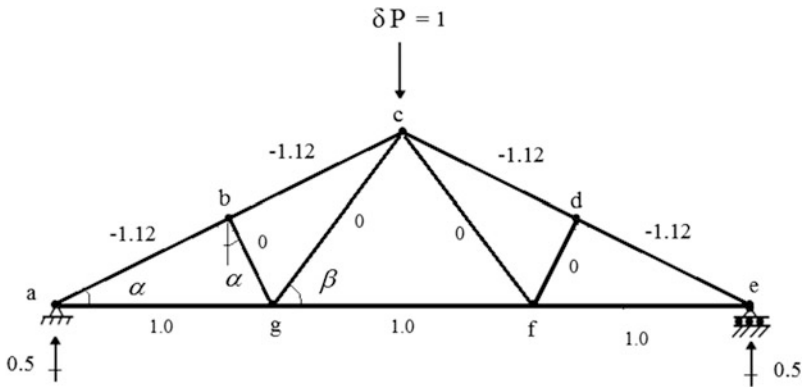


Fig. E2.15c Virtual forces, δF

Using this data, and assuming AE is constant, the computation proceeds as follows:

Member	L (mm)	F	δF_v	$L F \delta F_v$
ab	6708	-100.6	-1.12	$756(10)^3$
bc	6708	-87.2	-1.12	$655(10)^3$
cd	6708	-87.2	-1.12	$655(10)^3$
de	6708	-100.6	-1.12	$756(10)^3$
ef	7500	90	1.0	$675(10)^3$
fg	9000	60	1.0	$540(10)^3$
ga	7500	90	1.0	$675(10)^3$
bg	3354	-26.8	0	0
gc	7500	30	0	0
cf	7500	30	0	0
fd	3354	-26.8	0	0

$$\sum LF \delta F_v = 4712(10)^3$$

$$v_c = \frac{1}{AE} \left(\sum LF \delta F_v \right) - \delta R_a(v_a) = \frac{1}{3000(200)} (4,712,000) - (0.5)(-10) = +12.85 \text{ mm}$$

$\therefore v_c = 12.85 \text{ mm} \downarrow$

Example 2.16 Computation of Deflection—Virtual Force Method

Given: The plane truss shown in Fig. E2.16a. Member bc and cf also have a fabrication error of +0.5 in.

Determine: The vertical component of the displacement at joint g (v_g). Take $A = 2 \text{ in.}^2$ and $E = 29,000 \text{ ksi}$ for all the members.

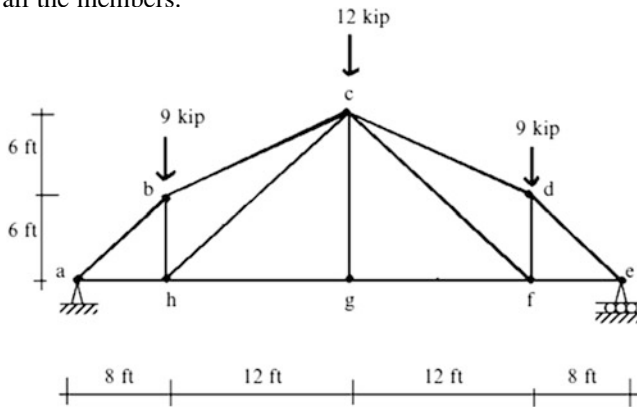


Fig. E2.16a

Solution: The actual and virtual forces are listed below.

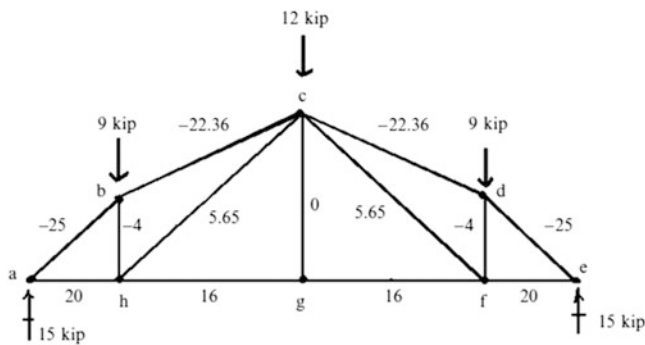


Fig. E2.16b Actual forces, F

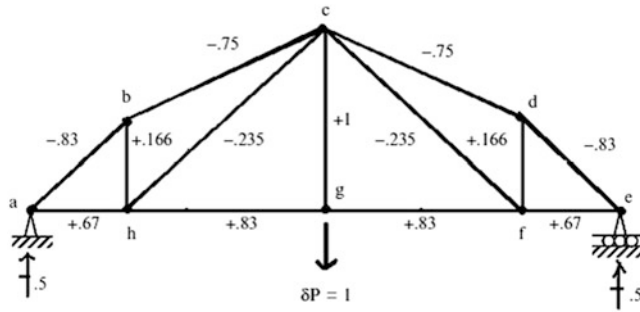


Fig. E2.16c Virtual forces, δF

Using this data, the following computations are carried out:

Member	L (in.)	L/A	F	δF_v	$\frac{L}{A} \delta F_v$	e_0 in.	$e_0 \delta F_v$
ab	120	60	-25	-0.83	1245	0	0
bc	161	80.5	-22.36	-0.75	1350	+0.5	-0.375
cd	161	80.5	-22.36	-0.75	1350	0	0
de	120	60	-25	-0.83	1245	0	0
ef	96	48	20	0.67	643	0	0
fg	144	72	16	0.83	960	0	0
gh	144	72	16	0.83	960	0	0
ha	96	48	20	0.67	643	0	0
bh	72	36	-4	0.166	-24	0	0
cg	144	72	0	1	0	0	0
df	72	36	-4	0.166	-24	0	0
ch	203.6	101.8	5.65	-0.235	-135.7	0	0
cf	203.6	101.8	5.65	-0.235	-135.7	+0.5	-0.1175
					$\sum \frac{L}{A} \delta F_v = 8077$		$\sum e_0 \delta F_v = -0.49$

$$v_{g_{\text{load}}} = \sum e_{\text{force}} \delta F_v = \sum \left(\frac{L}{AE} F \right) \delta F_v = \frac{8077}{29,000} = +0.278 \text{ in.} \Rightarrow v_{g_{\text{load}}} = 0.28 \text{ in.} \downarrow$$

$$v_{g_{\text{fabrication error}}} = \sum e_0 \delta F_v = -0.49 \text{ in.} \Rightarrow v_{g_{\text{fabrication error}}} = 0.49 \text{ in.} \uparrow$$

$$v_{g_{\text{(load+fabrication)}}} = +0.278 - 0.49 = -0.21 \text{ in.} \Rightarrow v_{g_{\text{(load+fabrication)}}} = 0.21 \text{ in.} \uparrow$$

Example 2.17 Deflection of a Gable Truss

Given: The plane truss shown in Fig. E2.17a. The truss has variable cross sections, such that $A = 6500 \text{ mm}^2$ for top chord members, $A = 3900 \text{ mm}^2$ for bottom chord members, $A = 1300 \text{ mm}^2$ for diagonal members, and $A = 650 \text{ mm}^2$ for vertical members, $l = 3 \text{ m}$, $P = 10 \text{ kN}$, and $E = 200 \text{ GPa}$.

Determine: The vertical displacement of node j (v_j) and the horizontal displacement of node g (u_g).

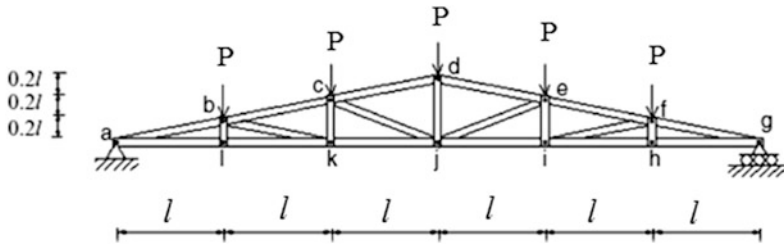


Fig. E2.17a Geometry and loading

Solution: The actual and virtual forces are listed below.

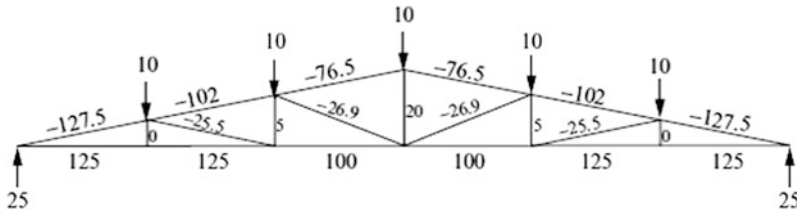


Fig. E2.17b Actual forces F

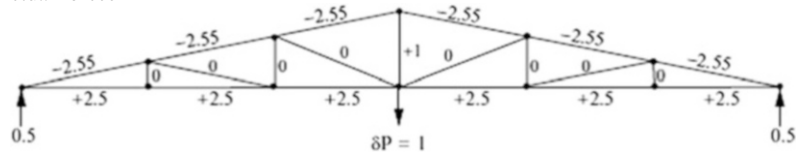


Fig. E2.17c Virtual forces δF_v

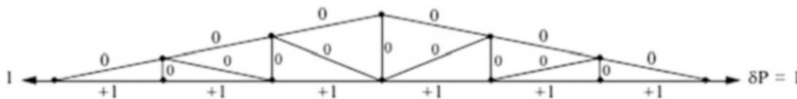


Fig. E2.17d Virtual forces δF_u

The computations are organized using the spreadsheet format listed below. Note that the upper and lower chords and only the central member contribute to the central vertical deflection. And only the lower chord contributes to the horizontal support deflection. The plus sign indicates the deflection is in the direction of the unit load.

Member	L (mm)	A (mm ²)	L/A	F (kN)	δF_u	δF_v	$(L/A)F \delta F_u$	$(L/A)F \delta F_v$
ab	3059	6500	0.47	-127.5	0.0	-2.55	0	152.8
bc	3059	6500	0.47	-102.0	0.0	-2.55	0	122.2
cd	3059	6500	0.47	-76.5	0.0	-2.55	0	91.7
de	3059	6500	0.47	-76.5	0.0	-2.55	0	91.7
ef	3059	6500	0.47	-102.0	0.0	-2.55	0	122.2
fg	3059	6500	0.47	-127.5	0.0	-2.55	0	152.8
gh	3000	3900	0.77	125.0	1.0	2.5	96.2	240.6
hi	3000	3900	0.77	125.0	1.0	2.5	96.2	240.6
ij	3000	3900	0.77	100.0	1.0	2.5	77	192.5
jk	3000	3900	0.77	100.0	1.0	2.5	77	192.5
kl	3000	3900	0.77	125.0	1.0	2.5	96.2	240.6

Member	L (mm)	A (mm ²)	L/A	F (kN)	δF_u	δF_v	$(L/A)F \delta F_u$	$(L/A)F \delta F_v$
la	3000	3900	0.77	125.0	1.0	2.5	96.2	240.6
bl	600	650	0.92	0.0	0.0	0.0	0	0
ck	1200	650	1.85	5.0	0.0	0.0	0	0
dj	1800	650	2.77	20.0	0.0	1.0	0	55.4
ei	1200	650	1.85	5.0	0.0	0.0	0	0
fh	600	650	0.92	0.0	0.0	0.0	0	0
bk	3059	1300	2.35	-25.5	0.0	0.0	0	0
cj	3231	1300	2.48	-26.9	0.0	0.0	0	0
ej	3231	1300	2.48	-26.9	0.0	0.0	0	0
fi	3059	1300	4.71	-25.5	0.0	0.0	0	0

The remaining computations involve dividing by E .

$$\sum \left(\left(\frac{L}{A} \right) F \delta F_u \right) = 538.8 \text{ kN/mm}$$

$$\therefore u_g = \sum \sum e_{\text{force}} \delta F_u = \frac{1}{E} \sum \sum \left(\left(\frac{L}{A} \right) F \delta F_u \right) = 538.8/200 = 2.69 \text{ mm} \rightarrow$$

$$\sum \left(\left(\frac{L}{A} \right) F \delta F_v \right) = 2136.2 \text{ kN/mm}$$

$$\therefore v_j = \sum \sum e_{\text{force}} \delta F_v = \frac{1}{E} \sum \sum \left(\left(\frac{L}{A} \right) F \delta F_v \right) = 2136.2/200 = 10.7 \text{ mm} \downarrow$$

We pointed out earlier that the distribution of member forces depends on the orientation of the diagonal members. We illustrate this behavior by reversing the diagonal pattern for the truss defined in Fig. E2.17a. The member forces corresponding to the same loading are listed in Fig. E2.17e. Suppose the vertical deflection at mid-span is desired. The corresponding virtual force system is shown in Fig. E2.17f.

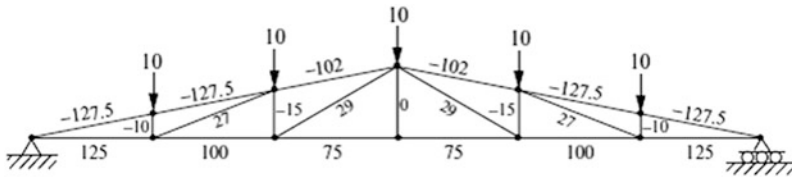


Fig. E2.17e Diagonal pattern reversed—actual forces F

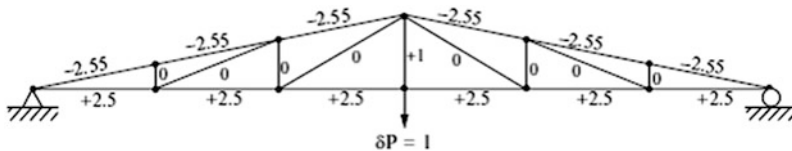


Fig. E2.17f Diagonal pattern reversed—virtual forces δF_v

Member	L (mm)	A (mm ²)	L/A	F	δF_v	$(L/A)F \delta F_v$
ab	3059	6500	0.47	-127.5	-2.55	153
bc	3059	6500	0.47	-127.5	-2.55	153
cd	3059	6500	0.47	-102	-2.55	122.2

Member	L (mm)	A (mm ²)	L/A	F	δF_v	$(L/A)F \delta F_v$
de	3059	6500	0.47	-102	-2.55	122.2
ef	3059	6500	0.47	-127.5	-2.55	153
fg	3059	6500	0.47	-127.5	-2.55	153
gh	3000	3900	0.77	125.0	2.5	240.6
hi	3000	3900	0.77	100	2.5	192.5
ij	3000	3900	0.77	75	2.5	144.4
jk	3000	3900	0.77	75	2.5	144.4
kl	3000	3900	0.77	100	2.5	192.5
la	3000	3900	0.77	125	2.5	240.6
bl	600	650	0.92	-10	0.0	0
ck	1200	650	1.85	-15	0.0	0
dj	1800	650	2.77	0	1.0	0
ei	1200	650	1.85	-15	0.0	0
fh	600	650	0.92	-10	0.0	0
bk	3059	1300	2.35	27	0.0	0
dk	3498	1300	2.69	29	0.0	0
di	3498	1300	2.69	29	0.0	0
fi	3059	1300	2.35	27	0.0	0

Using the data listed above, the mid-span deflection calculations are

$$\sum \left(\left(\frac{L}{A} \right) F \delta F_v \right) = 2011 \text{ kN/mm}$$

$$\therefore v_j = \sum \Sigma e_{\text{force}} \delta F_v = \frac{1}{E} \sum \Sigma \left(\left(\frac{L}{A} \right) F \delta F_v \right) = 2011/200 = 10 \text{ mm} \downarrow$$

The examples presented to this point have been concerned with loads. Structures are also subjected to seasonal (and daily) temperature changes and it is of interest to determine the corresponding nodal displacements. A unique feature of statically determinate structures is their ability to accommodate temperature changes without experiencing member forces. When subjected to a temperature change, a statically determinate structure adjusts its geometry in such a way that there are *no forces introduced in the members*. From a design perspective, this behavior is very desirable since member forces, i.e., stresses, are due only to the loads. However, one may need to compute the deflected shape due to temperature change from some initial state. The effect of temperature change is to produce an additional extension in a truss member given by:

$$e_{\text{temperature}} = \alpha \Delta T L$$

where α is a material property, defined as the coefficient of thermal expansion, and ΔT is the temperature change from the initial state. Then, the form of the Principle of Virtual force specialized for only temperature and unyielding supports reduces to

$$d\delta P = \sum (e_{\text{temperature}})(\delta F) \quad (2.15)$$

The computational procedure is similar to the approach discussed earlier. We evaluate $(\alpha \Delta T L)$ for the members. Then, given a desired deflection, we apply the appropriate virtual loading and compute δF for the members. Lastly, we evaluate the summation. The following example illustrates the details. This discussion applies only for statically determinate trusses. A temperature change introduces internal forces in statically indeterminate trusses. Analysis procedures for this case are discussed in Chaps. 9 and 10.

Example 2.18 Computation of Deflection Due to Temperature

Given: The plane truss shown in Fig. E2.18a.

Determine: The vertical displacement at joint d due to temperature increase of $\Delta T = 65^\circ\text{F}$ for all members. Assume $A = 2 \text{ in.}^2$, $E = 29,000 \text{ ksi}$, and $\alpha = 6.5 (10^{-6})/^\circ\text{F}$.

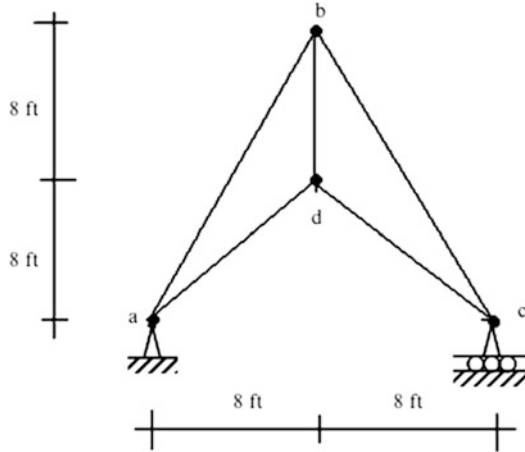


Fig. E2.18a

Solution: The corresponding virtual force system is listed below.

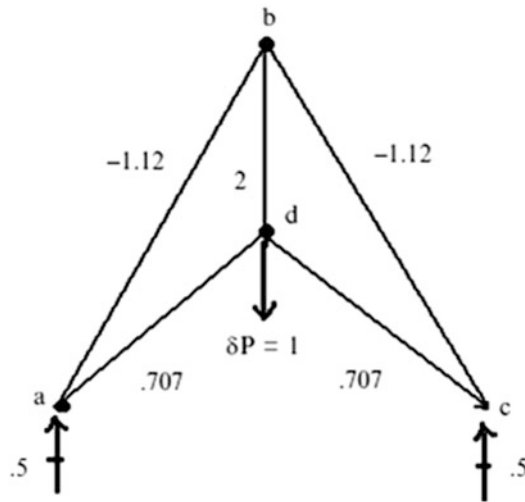


Fig. E2.18b Virtual forces δF

Member	$L \text{ (in.)}$	$e = \alpha\Delta TL$	δF_v	$e \delta F_v$
ab	214.7	0.091	-1.12	-0.102
bc	214.7	0.091	-1.12	-0.102
cd	135.7	0.057	0.707	0.04

Member	L (in.)	$e = \alpha\Delta TL$	δF_v	$e \delta F_v$
da	135.7	0.057	0.707	0.04
bd	96	0.041	2	0.082
				$\sum e \delta F = -0.042$

$$v_d = \sum e_{\text{temperature}} \delta F_v = (\alpha \Delta T L) \delta F_v = -0.042 \Rightarrow v_d = 0.042 \text{ in. } \uparrow$$

2.4 Influence Lines

Consider the plane bridge truss shown in Fig. 2.26a. To design a particular member, one needs to know the maximum force in the member due to the design loading. The dead loading generally acts over the entire structure, i.e., on all the nodes. For this loading component, one places all the dead load on the structure and carries out a single analysis for the member forces. The live loading, by definition, can act anywhere on the structure and therefore one needs to determine the location of the live loading that produces the maximum force in the member that is being designed. A systematic approach to locating the critical position of the live loading is based on first constructing an influence line for the member force. This construction involves a series of analyses, one for each possible location of live loading. The live load is usually taken as a single force, of unit magnitude, which is moved from node to node across the structure. The resulting influence line is a plot of the member force as a function of the location of the applied load. Figure 2.26b illustrates the possible nodal positions of a vertical load applied to the bottom chord, and the corresponding member forces. Given this data, one can construct an influence line for any of the member forces.

The process described above assumes the loading is a concentrated load applied at the nodes. For bridge structures, the live loading is actually applied to the deck which transmits the load to the transverse beams, and finally to the nodes. The deck is usually simply supported on the transverse beams, so the complete deck-beam system is statically determinate and one can determine the reactions at the nodes using only the equations of statics. We illustrate this computation using the structure shown in Fig. 2.27a. We suppose a truck loading is passing over the span.

Consider the position shown in Fig. 2.27b. The wheel loads act on the deck segments gf and fe . The live load vehicle analysis reduces to just applying loads to the nodes adjacent to the vehicle since the deck segments (gf and fe) are simply supported. Noting Fig. 2.27c, the equivalent nodal loads are

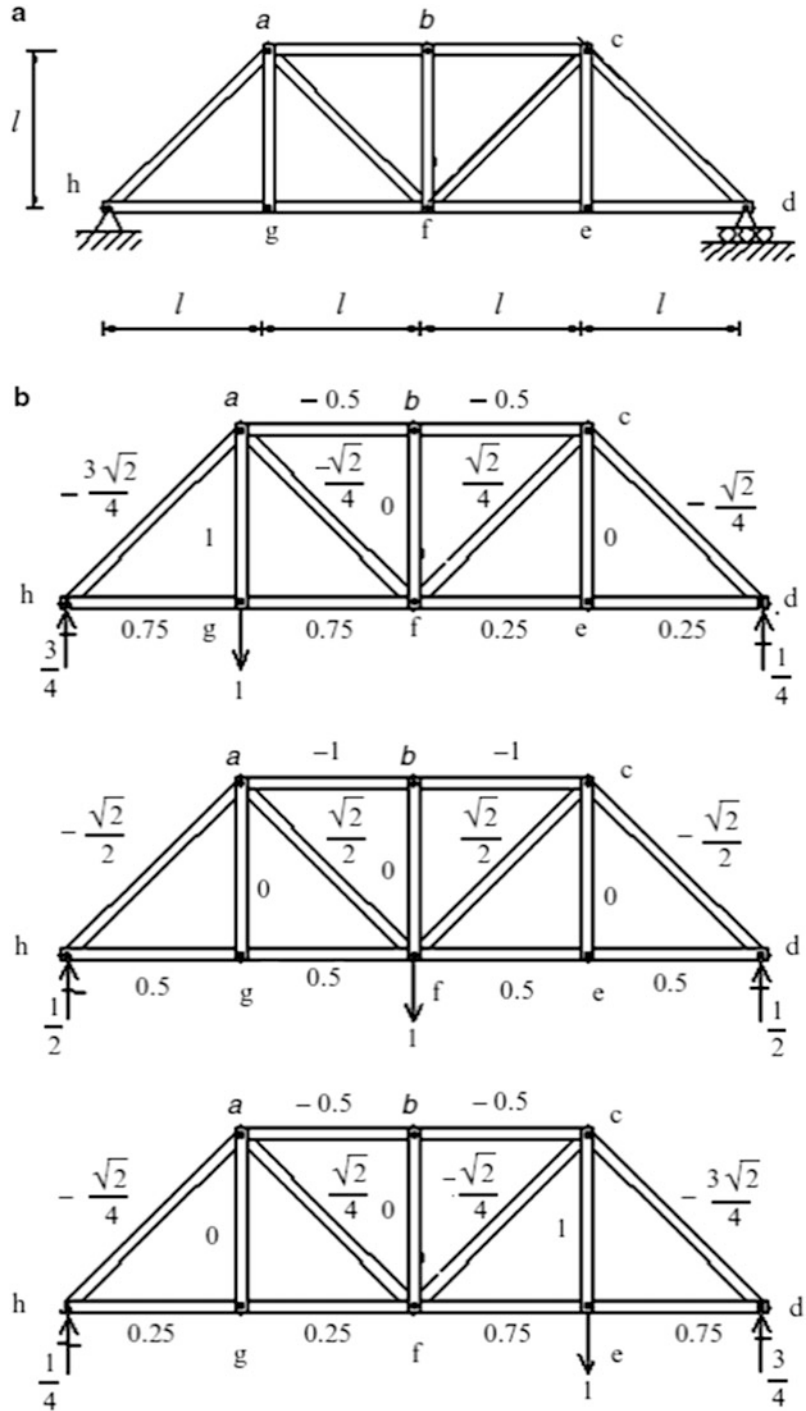
$$\begin{aligned} R_1 &= \left(1 - \frac{x}{l}\right) P_1 \\ R_2 &= \left(\frac{x}{l}\right) P_1 + \left(2 - \frac{x}{l} - \frac{h}{l}\right) P_2 \\ R_3 &= \left(\frac{x}{l} + \frac{h}{l} - 1\right) P_2 \end{aligned}$$

Note that the reactions are linear functions of x , the position coordinate for the truck.

We define F_j as the force in member j . Applying separate unit loads at nodes g and f leads to $F_j|_g$ and $F_j|_f$. Then, according to the equations listed above, the force due to a unit load at x is

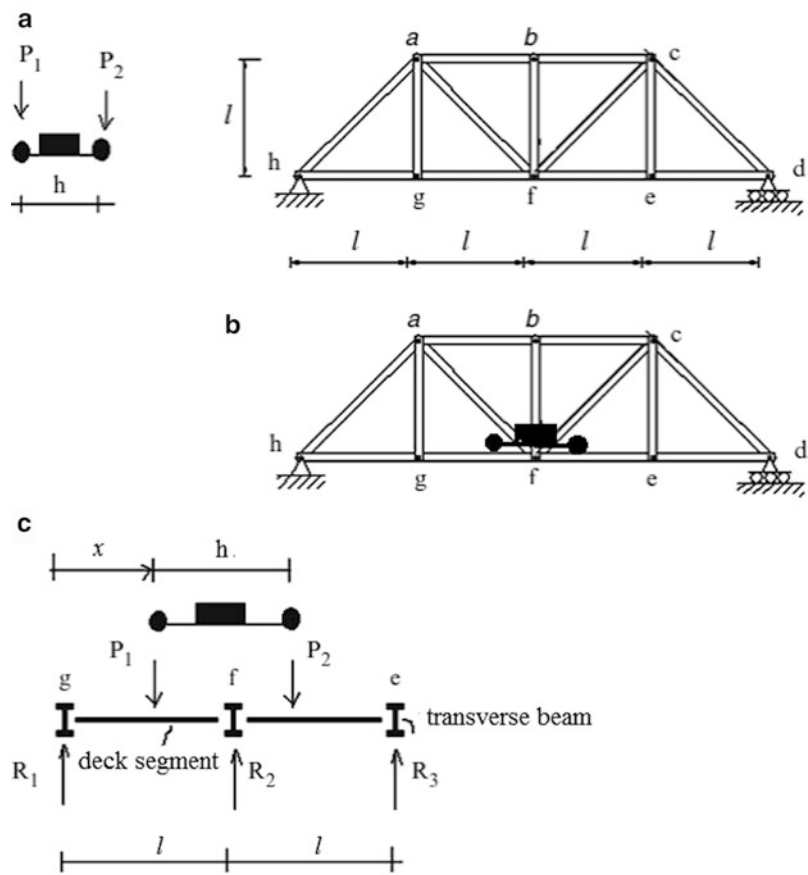
$$F_j|_x = \left(1 - \frac{x}{l}\right) F_j|_g + \left(\frac{x}{l}\right) F_j|_f$$

Fig. 2.26 (a) Truss geometry. (b) Load positions and corresponding member forces



The most convenient way to present these results is to construct a plot of F_j vs. x , where F_j is the force in member j due to a unit load at x , and x is taken to range over the nodes on the bottom chord. We need to apply these loads *only at the nodes* since the plot is *linear* between adjacent nodes. Plots of this type are called influence lines. Figure 2.28a shows the influence line for chord member ab . This

Fig. 2.27 (a) Truss geometry. (b). Loaded position. (c) Free body diagram-transverse beam



visual representation is convenient since one can immediately identify the critical location of the load. For the chord member, ab, the maximum magnitude occurs when the load is applied at mid-span. Also, we note that the force is compression for all locations.

Given an actual loading distribution, one evaluates the contribution of each load, and then sums the contributions. If the actual live load consisted of a uniform loading, then it follows that one would load the entire span. The maximum force due to the truck loading is determined by positioning the truck loads as indicated in Fig. 2.28b. In general, one positions the vehicle such that the maximum vehicle load acts on node f.

The influence line for member fg is plotted in Fig. 2.28c. In this case, the member force is always tension.

The function of the diagonal members is to transmit the vertical forces from node to node along the span. This action is called “shear.” The influence line for a diagonal is different than the influence lines for upper and lower chord members, in that it has both positive and negative values. Figure 2.28d shows the result for diagonal af. A load applied at node g generates compression, whereas loads at nodes f and e produce tension. Lastly, a symmetrically located diagonal with opposite orientation, such as cf vs. af, has an influence line that is a rotated version of its corresponding member (see Fig. 2.28d vs. Fig. 2.28e).

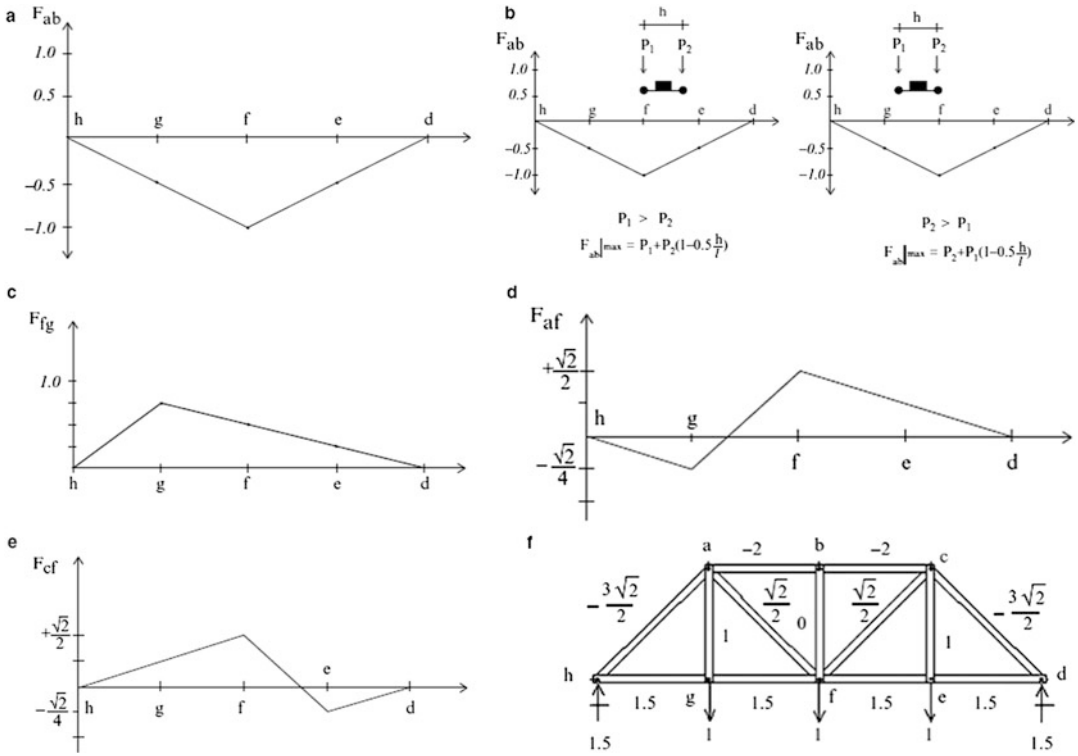


Fig. 2.28 (a) Influence line for cord member ab. (b) Vehicle positioning for $F_{ab}|_{\max}$. (c) Influence line for chord member fg. (d) Influence line for diagonal member af. (e) Influence line for diagonal member cf. (f) Uniform unit load

Because the influence lines for diagonals have both positive and negative values, one needs to consider two patterns of live load in order to establish the peak value of the member force.

For member af, the extreme values are

Load at node f $F = \sqrt{2}/2$

Load at node g $F = \sqrt{2}/4$

For member cf, the extreme values are

Loads at node e $F = \sqrt{2}/4$

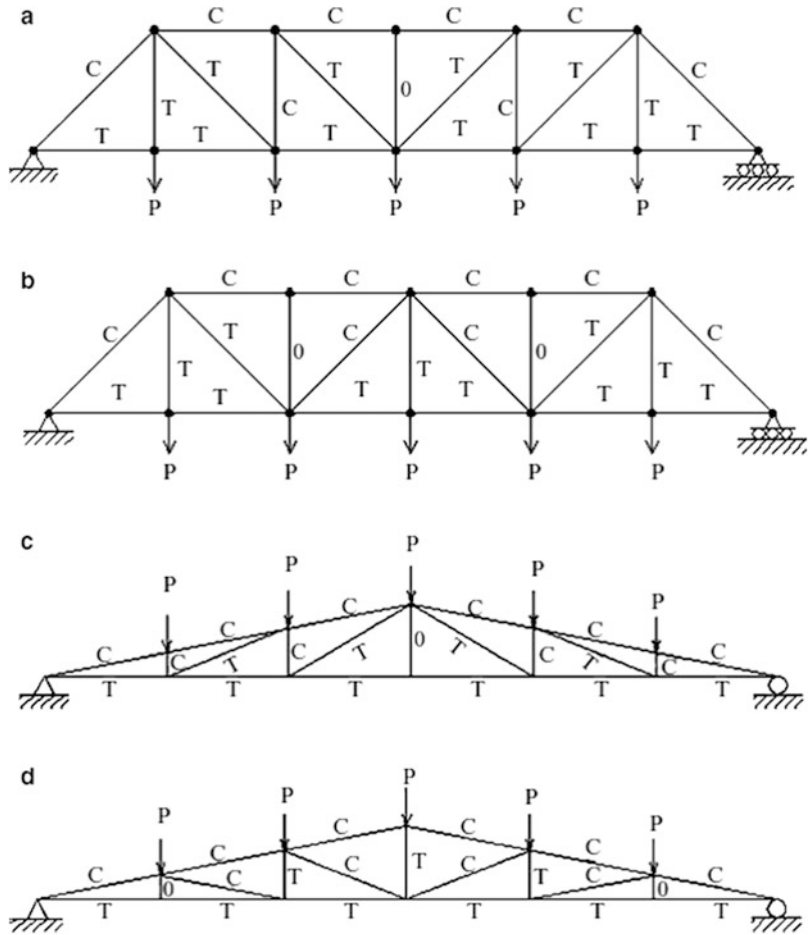
Loads at node f $F = \sqrt{2}/2$

If a uniform load is applied (see Fig. 2.28f), the peak force values for both members will be:

$$F_{\max} = +\sqrt{2}/2$$

As mentioned earlier, diagonal members function to transmit vertical loads to the end supports. We showed above that the sense of the diagonal force depends on the orientation of the member. The sense of the diagonal force is important since slender members behave differently under compression vs. tension. A slender member subjected to compressive load will fail by buckling rather than by yielding since the buckling load is considerably less than the yield force. Therefore, from a design perspective one should avoid using slender compression members. For truss type structures, this problem can be avoided by selecting an appropriate diagonal orientation pattern.

Fig. 2.29 Force pattern for various truss geometries. (a) Pratt truss. (b) Warren truss. (c) Pratt truss. (d) Howe truss



As an example, consider the two diagonal patterns shown in Fig. 2.29a, b. The sense of the member forces due to a uniform live load is indicated by C (compression) and T (tension).

Pattern (a) is more desirable since all the interior diagonals are in tension. However, some of the vertical members are in compression. Pattern (b) has alternating sense for the diagonals; the vertical hangers are all in tension. In general, for both truss types the top chord forces are compression and the bottom chord forces are tension. Figure 2.29c, d show similar results for inclined chord trusses. The designators “Pratt,” “Warren,” and “Howe” refer to the individuals who invented these geometrical forms.

Example 2.19

Given: The structure and truck loading shown in Fig. E2.19a.

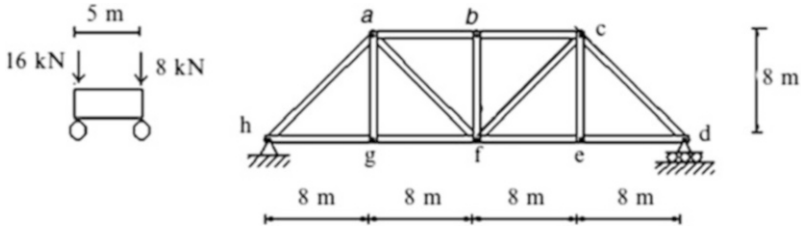


Fig. E2.19a

Determine: The maximum force in members ab and fg due to the truck loading.

Solution: We first determine the influence lines for a unit vertical force applied along the bottom nodes.

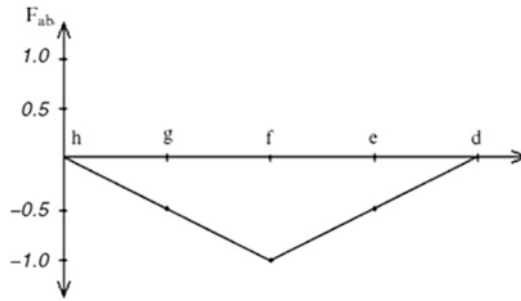


Fig. E2.19b Influence line for member ab

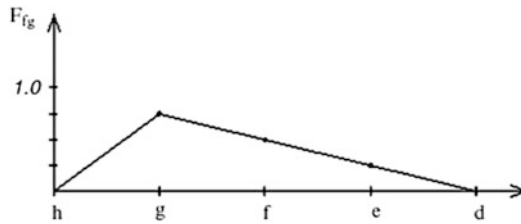


Fig. E2.19c Influence line for member fg

Then, we position the truck loading as indicated in Figs. E2.19d and E2.19e

$$F_{ab_{\max}} = 16(-1) + 8(-0.69) = -21.52 \quad \therefore F_{ab_{\max}} = 21.52 \text{ kN compression}$$

$$F_{fg_{\max}} = 16(0.75) + 8(0.59) = +16.72 \quad \therefore F_{fg_{\max}} = 16.72 \text{ kN tension}$$

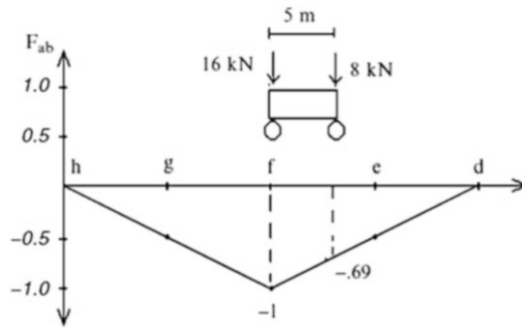


Fig. E2.19d

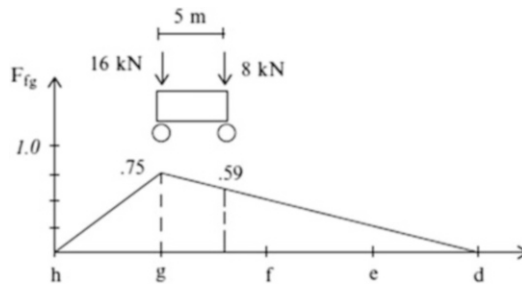


Fig. E2.19e

Example 2.20 Live Load Analysis for a Gable Roof Structure

Given: The gable roof structure shown in Fig. E2.20a.

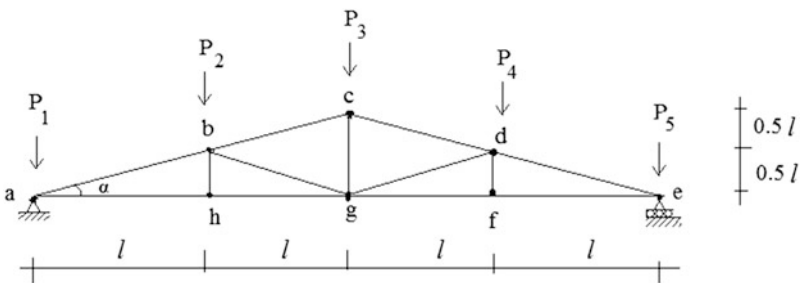


Fig. E2.20a Structural geometry and nodal loads

Determine:

- (i) Tabulate all the member forces due to the individual unit nodal forces applied to the top chord. We refer to this type of table as a force influence table.
- (ii) Use the force influence table to draw the influence lines for member cd and fg.
- (iii) Calculate the reactions and member forces for members cd and fg for $P_1 = P_5 = 7.5\text{ kN}$, and $P_2 = P_3 = P_4 = 15\text{ kN}$.

Solution:

Part (i) the member forces due to the individual unit nodal loads are listed in Fig. E2.20b.

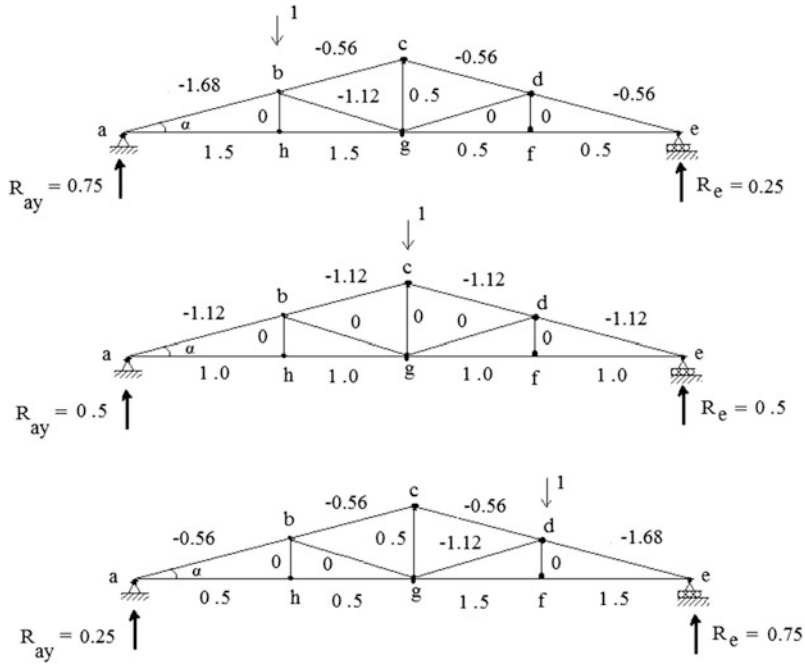


Fig. E2.20b Force results for different unit load positions

The complete set of member force results are listed in the following Table. One uses this table in two ways. Firstly, scanning down a column shows the member which is most highly stressed by the loading acting at the position corresponding to the column. Scanning across a row identifies the loading which has the maximum contribution to the member force.

Force influence table			
Member	$P_2 = 1$	$P_3 = 1$	$P_4 = 1$
ab	-1.68	-1.12	-0.56
bc	-0.56	-1.12	-0.56
cd	-0.56	-1.12	-0.56
de	-0.56	-1.12	-1.68
ef	0.5	1.0	1.5
fg	0.5	1.0	1.5
gh	1.5	1.0	0.5
ha	1.5	1.0	0.5
bh	0	0	0
cg	0.5	0	0.5
df	0	0	0
bg	-1.12	0	0
gd	0	0	-1.12
R_{ay}	0.25	0.5	0.75
R_e	0.75	0.5	0.25

Part (ii) One can interpret the force influence table as representing the complete set of influence lines for the individual members. We use this data to draw influence line for member cd and fg.

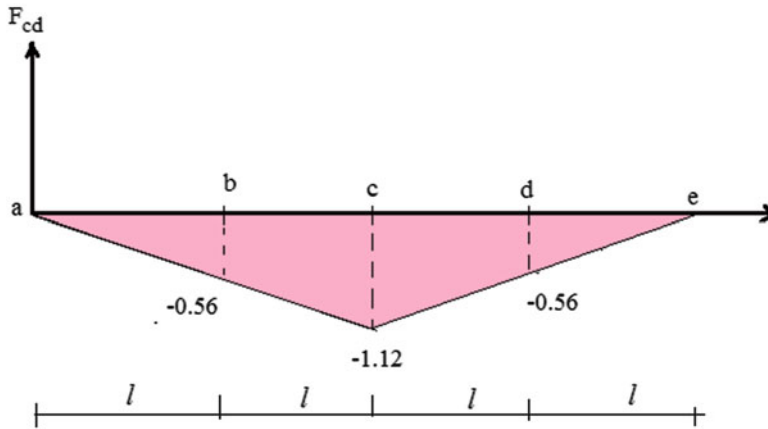


Fig. E2.20c Influence line for member cd

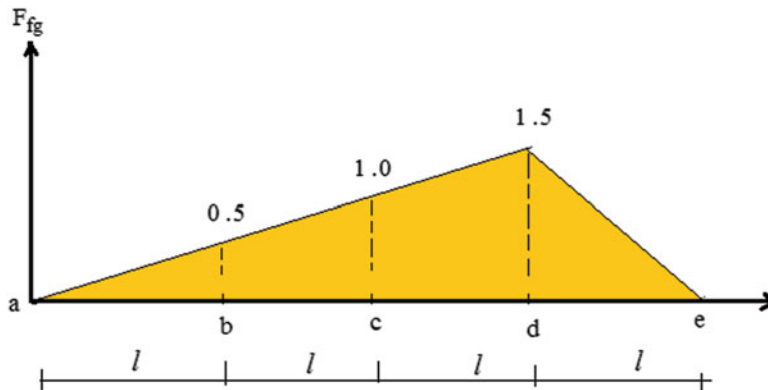


Fig. E2.20d Influence line for member fg

Part (iii) By using the force influence table, the corresponding forces in members cd and fg and reactions are determined as follows:

$$F_{cd} = 15(-0.56) + 15(-1.12) + 15(-0.56) = -33.6 \quad \therefore F_{cd} = 33.6 \text{ kN compression}$$

$$F_{fg} = 15(0.5) + 15(1.0) + 15(1.5) = 45 \quad \therefore F_{fg} = 45 \text{ kN tension}$$

$$R_{ay} = 7.5 + 15(0.25) + 15(0.5) + 15(0.75) = 30 \quad \therefore R_{ay} = 30 \text{ kN } \uparrow$$

$$R_e = 7.5 + 15(0.75) + 15(0.5) + 15(0.25) = 30 \quad \therefore R_e = 30 \text{ kN } \uparrow$$

2.5 Analysis of Three-Dimensional Trusses

2.5.1 Introduction

Most structural systems such as highway bridges and roof systems can be considered to be composed of a set of planar trusses. However, there are exceptions, such as towers and domed structures, which cannot be decomposed into planar components and consequently one needs to deal with three-dimensional combinations of members. These structural types are called space structures.

The basic unit for a 3-D space truss is the tetrahedron, a geometrical object composed of six members that form four triangular faces. Figure 2.30 illustrates this object. We form a 3-D structure by attaching members to existing nodes. Each new node requires three members. Provided that the structure is suitably supported with respect to rigid body motion, the displacements that the structure experiences when loaded are due only to deformation of the members.

Space truss structures are used for vertical structures such as towers and long-span horizontal structures covering areas such as exhibition halls and covered stadiums. They usually are much more complex than simple plane trusses, and therefore more difficult to analyze.

The equilibrium analysis for three-dimensional trusses is similar to that for planar structures except that now there are three force equilibrium equations per node instead of two equations. One can apply either the method of joints or the method of sections. Manual analysis techniques are difficult to apply for large-scale space structures, and one usually resorts to computer-based analysis procedures. Our immediate objectives in this section are to discuss how a space structure needs to be restrained in order to prevent rigid body motion and to illustrate some manual calculations using the methods of joints. We present a computer-based method in the next section.

2.5.2 Restraining Rigid Body Motion

A rigid three-dimensional body requires six motion constraints to be fully constrained; three with respect to translation, and three with respect to rotation. We select an orthogonal reference frame having directions X , Y , and Z . Preventing translation is achieved by constraining motion in the X , Y , and Z directions as illustrated in Fig. 2.31. Even when suitably restrained against translation, the body

Fig. 2.30 Tetrahedron units for 3-D trusses

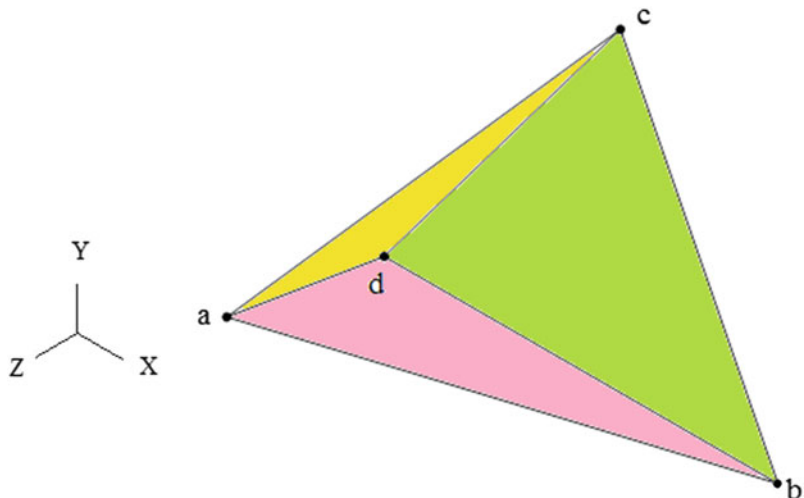


Fig. 2.31 Restraints for a 3-D rigid object

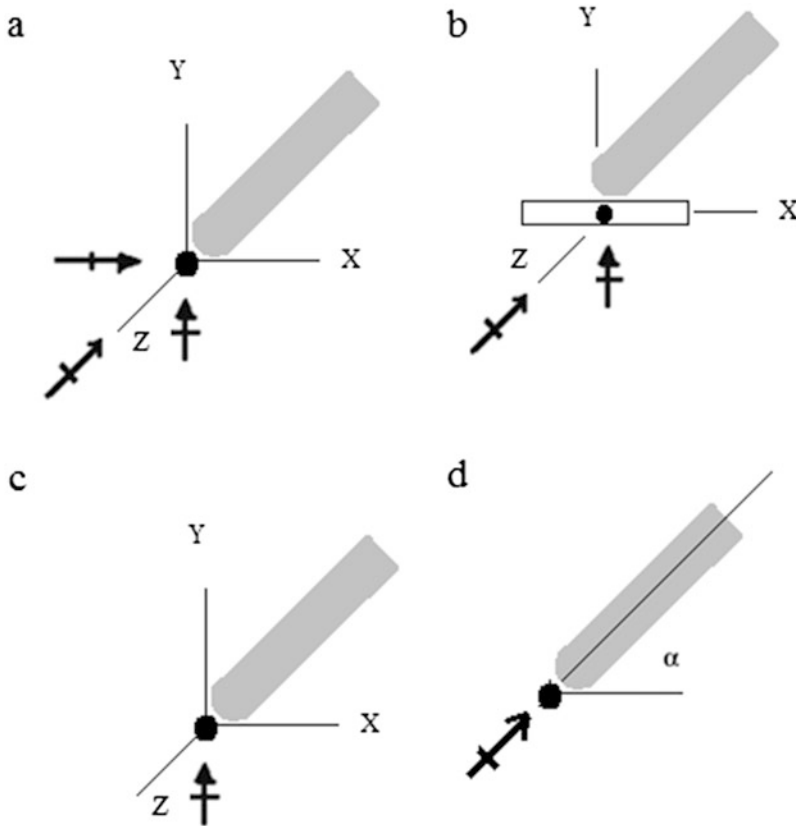
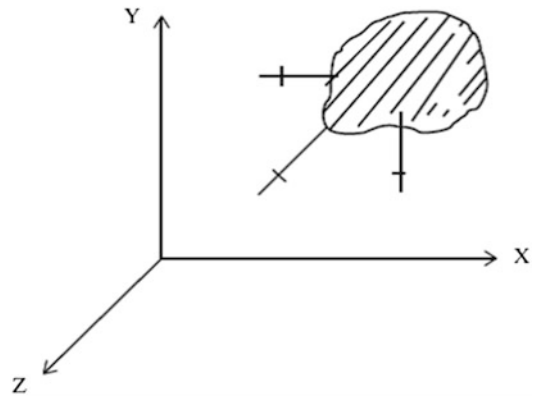


Fig. 2.32 Types of supports for space trusses. (a) Hinge joint. (b) Slotted roller. (c) Roller. (d) Rigid link

can rotate and we need to provide additional constraints which eliminate rotation about the X, Y, and Z axes. To prevent rotation about an axis, say the X axis, one applies a translational constraint in a direction which does not pass through X. This rule is used to select three additional constraint directions, making a total of six restraints. If one introduces more than six restraints, the structure is said to be statically indeterminate with respect to the reactions. Various examples illustrating the selection of restraints are listed below (Fig. 2.32).

Example 2.21 Various Restraint Schemes

Given: The 3-D truss shown in Fig. E2.21a, b.

Determine: Possible restraint schemes.

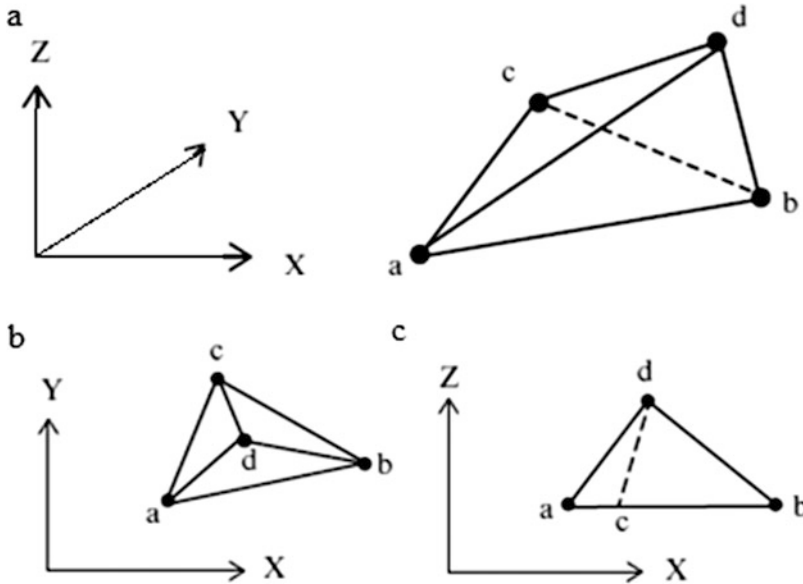


Fig. E2.21 (a) 3-D truss. (b) $x - y$ plan view. (c) $x - z$ plan view

Solution: The preferred way of displaying 3-D objects is to work with projections on the $X - Y$ and $X - Z$ planes, referred to as the “plan” and “elevation” views. The projections corresponding to the object defined in Fig. E2.21a are shown in Fig. E2.21b, c.

The choice of restraints is not unique. One can employ a 3-D hinge which provides full restraint against translation, or roller type supports which provide restraint against motion in a particular direction. Suppose we place a 3-D hinge at joint a. Then, a is “fixed” with respect to translation in the X , Y , and Z directions.

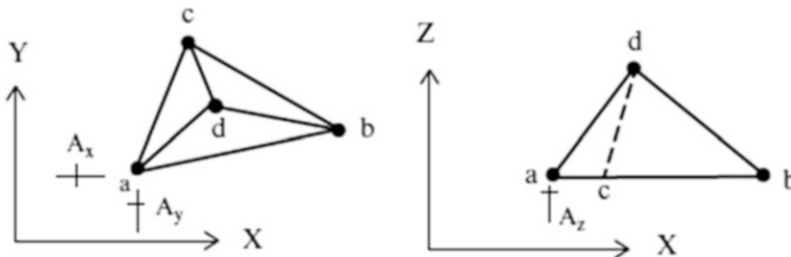


Fig. E2.21d 3-D hinge at a

With these restraints, the body can still rotate about either line a-b or line a-c, or a line parallel to the Z axis through a. The first two modes are controlled with Z restraints applied at b and c. The third

mode is controlled with either an X or Y restraint applied at either b or c. Figure E2.21e shows the complete set of displacement restraints chosen.

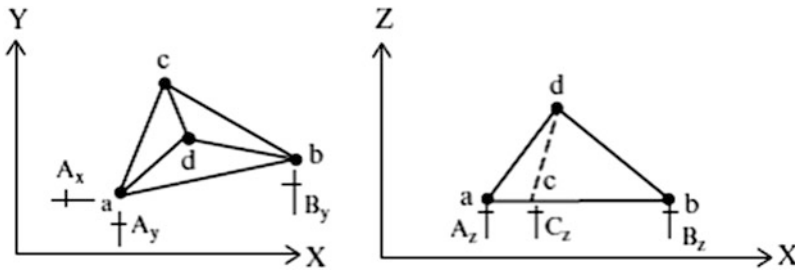


Fig. E2.21e Complete set of restraints

Other possible restraint schemes are shown in Figs. E2.21f, E2.21g, and E2.21h. Our strategy is to first restrain translation and then deal with the rotation modes.

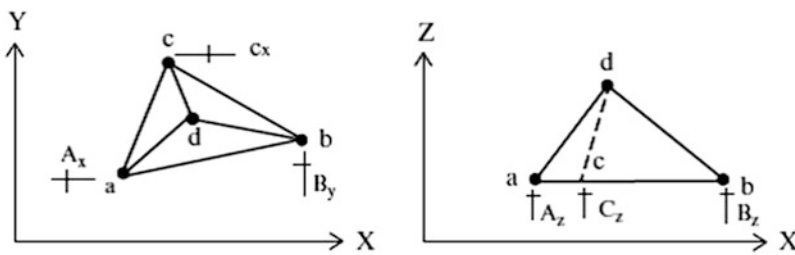


Fig. E2.21f Alternative restraint scheme #1

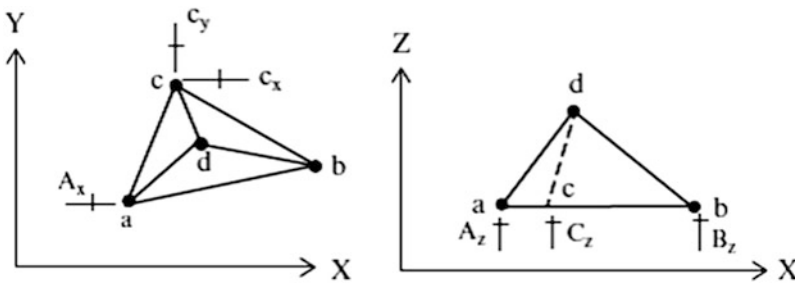


Fig. E2.21g Alternative restraint scheme #2

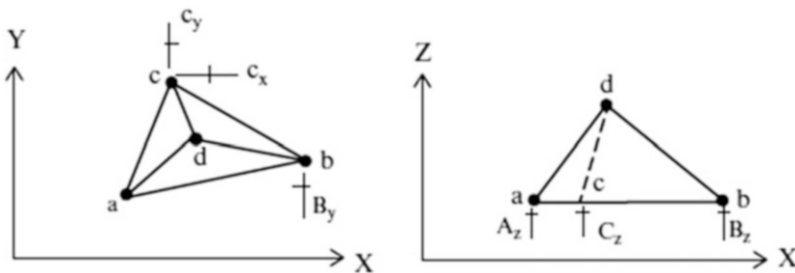


Fig. E2.21h Alternative restraint scheme #3

2.5.3 Static Determinacy

The approach we followed in Sect. 2.2.2 for 2-D Plane trusses is also applicable for 3-D trusses. One just has to include the additional variables associated with shifting from two to three dimensions. Each member of a truss structure has a single force measure, the magnitude of the axial force. However, for 3-D trusses, there are three equilibrium equations per node instead of two for a plane truss. Defining m as the number of members, r as the number of reactions, and j as the number of nodes, it follows that the number of force unknowns and the number of force equilibrium equations available are

$$\text{Force unknowns} = m + r$$

$$\text{Force equilibrium equations} = 3j$$

The structure is statically determinate when $m + r = 3j$. If $m + r > 3j$, there are more force unknowns than available equilibrium equations and the structure is designated as statically indeterminate. Lastly, if $m + r < 3j$, there are less force unknowns than required to withstand an arbitrary nodal loading, and the structure is unstable, i.e., it is incapable of supporting an arbitrarily small loading.

$$m + r \begin{cases} < 3J & \text{unstable} \\ = 3J & \text{determinate} \\ > 3J & \text{indeterminate} \end{cases}$$

In addition to these criteria, the structure must be suitably restrained against rigid body motion.

Example 2.22 A Stable Determinate Truss

Given: The truss defined in Fig. E2.22a, b.

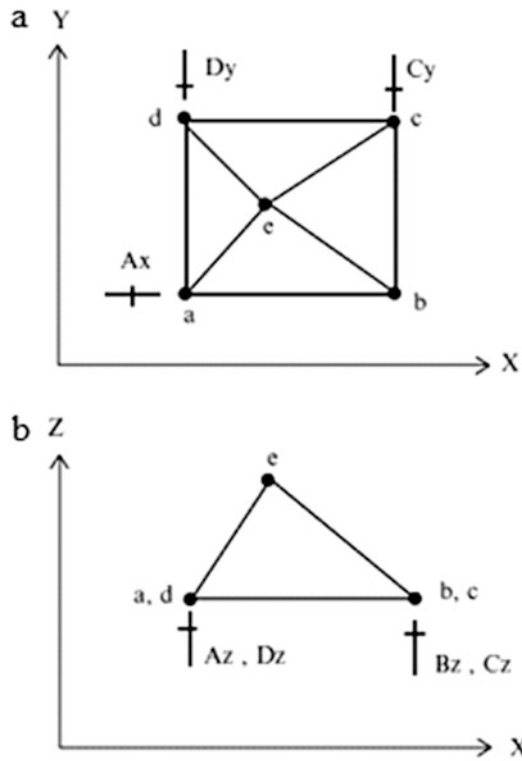


Fig. E2.22 3-D truss. (a) $x - y$ plan view. (b) $x - z$ plan view

Determine: The stability

Solution: For the structure shown above, there are eight members, seven reactions, and five joints.

$$m = 8 \quad r = 7 \quad j = 5$$

$$m + r = 3j$$

The structure is initially stable.

Example 2.23 An Unstable Structure

Given: The truss defined in Figs. E2.23a and E2.23b

Determine: The stability

Solution: The number of force unknowns is equal to the number of available force equilibrium equations but the structure has a fundamental flaw. The translation restraints in the $X - Y$ plane are concurrent, i.e., they intersect at a common point, c' , shown in Fig. E2.23a. As a result, the structure cannot resist rotation about a Z axis through c' .

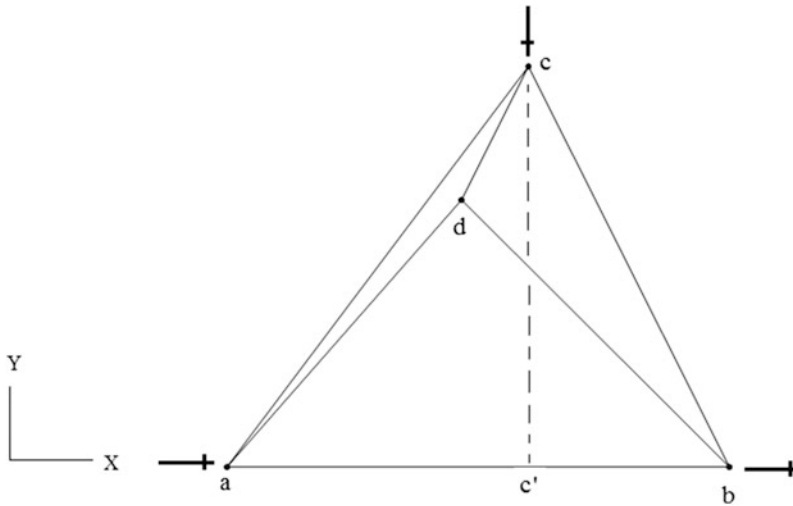


Fig. E2.23a $x - y$ plan view

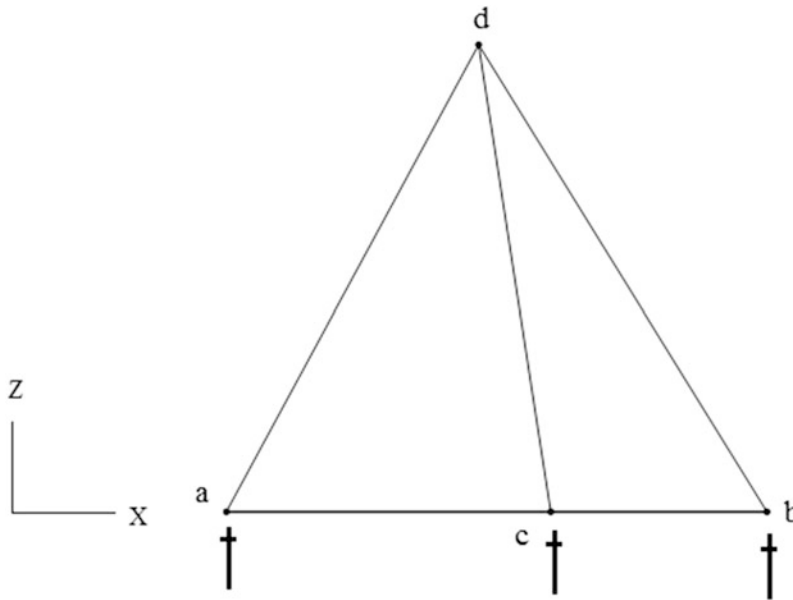
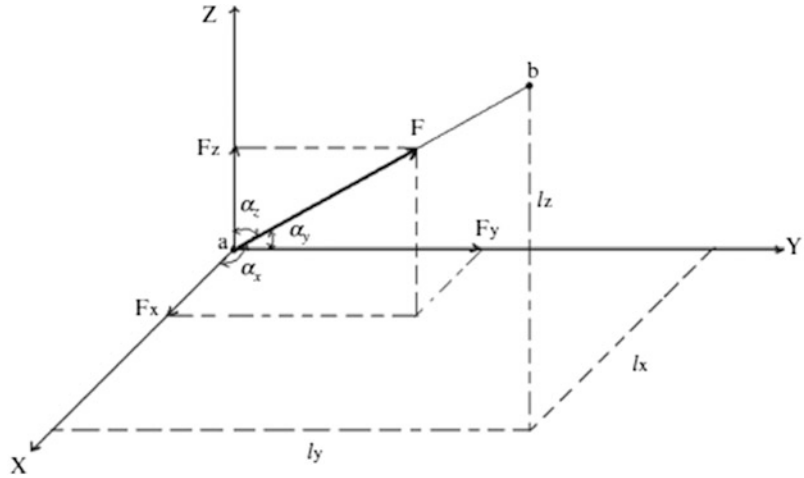


Fig. E2.23b $x - z$ plan view

2.5.4 Method of Joints for 3-D Trusses

Each member of a space truss is assumed to be pinned at its ends to nodes in such a way that there is no bending in the member, only an axial force whose direction coincides with the centroidal axis. The direction of the force is determined by the geometry of the member, so one needs only to determine the magnitude. We find these quantities using force equilibrium equations. Our overall strategy is to first determine the reactions with the global equilibrium conditions. Once the reactions are known, we

Fig. 2.33 Resolution of a force into its components



range over the nodes and establish the nodal force equilibrium equations for each node. This process is similar to the method of joints for Planar Trusses except that now there are three equilibrium equations per node. The member forces are computed by solving the set of nodal force equilibrium equations.

Consider the force vector shown in Fig. 2.33. Since the force vector orientation coincides with the direction of the centroidal axis for member ab , the force components are related to the geometric projections of the member length. We resolve the force vector into X , Y , and Z components, and label the components as F_x , F_y , and F_z . Noting the commonality of directions, the force components are related to the force magnitude and geometric projections by

$$\begin{aligned}\frac{F_x}{F} &= \frac{\ell_x}{\ell} = \cos \alpha_x = \beta_x \\ \frac{F_y}{F} &= \frac{\ell_y}{\ell} = \cos \alpha_y = \beta_y \\ \frac{F_z}{F} &= \frac{\ell_z}{\ell} = \cos \alpha_z = \beta_z\end{aligned}\quad (2.16)$$

The coefficients, β_x , β_y , and β_z , are called direction cosines. Given the coordinates of the nodes at each end (a , b), one determines the projection and length using

$$\begin{aligned}l_x &= x_b - x_a \\ l_y &= y_b - y_a \\ l_z &= z_b - z_a \\ l &= \sqrt{l_x^2 + l_y^2 + l_z^2}\end{aligned}\quad (2.17)$$

We are assuming the positive sense of the member is from node a toward node b . These relationships allow one to carry out the equilibrium analysis working initially with the components and then evaluate the force magnitude.

$$F = \sqrt{F_x^2 + F_y^2 + F_z^2}\quad (2.18)$$

We illustrate the analysis process with the following examples. There are many ways to carry out the analysis. Our approach here is based primarily on trying to avoid solving sets of simultaneous equations relating the force magnitudes. However, there are cases where this strategy is not possible.

Example 2.24 Analysis of a Tripod Structure

Given: The tripod structure shown in Fig. E2.24a, b. The supports at a, b, and c are fully restrained against translation with 3-D hinges.

Determine: The force in each member.

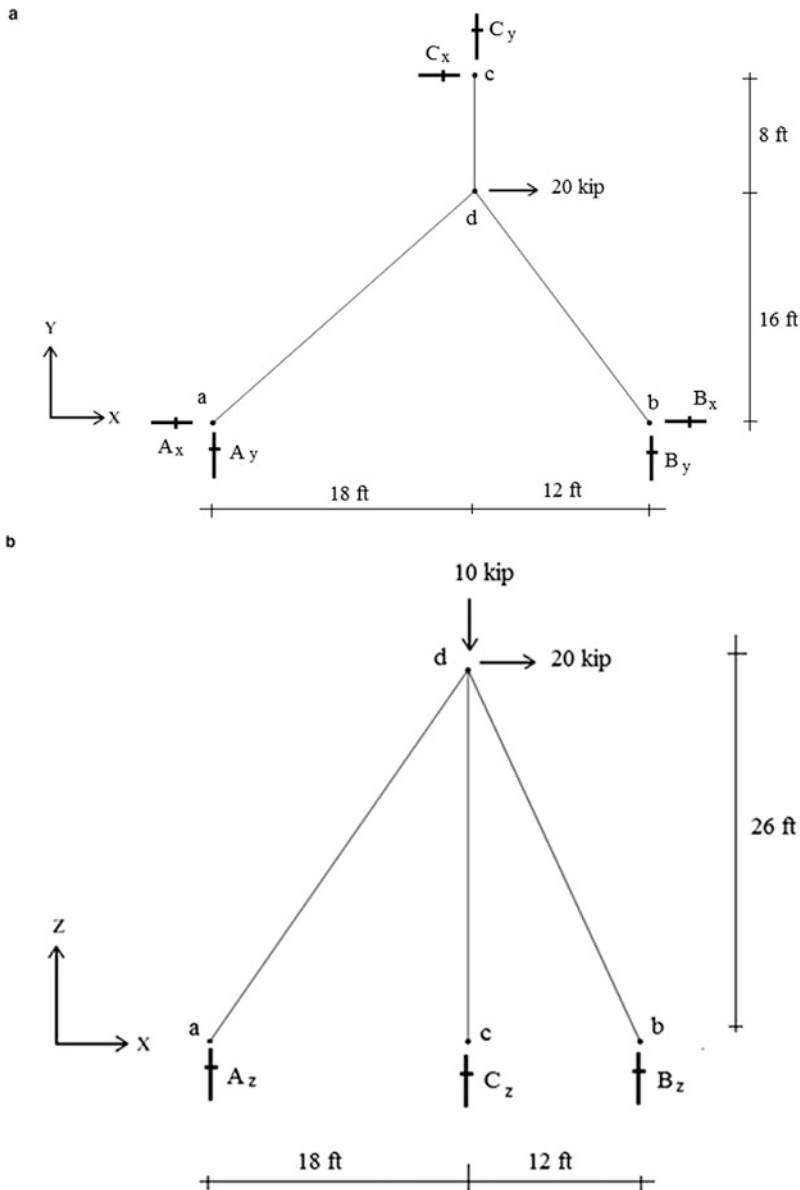


Fig. E2.24 Tripod geometry and supports. (a) *x* - *y* plan view. (b) *x* - *z* plan view

Solution: There are three reactions per support, making a total of nine reaction unknowns. Adding the three unknown member forces raises the total number of force unknowns to 12. Each joint has three force equilibrium equations and there are four joints, so the structure is statically determinate.

The first step is to determine the direction cosines for the members. This data is listed in Table E2.24.1 below.

Table E2.24.1

Member	l_x	l_y	l_z	l	β_x	β_y	β_z
ad	18	16	26	35.4	0.508	0.452	0.734
bd	12	16	26	32.8	0.366	0.488	0.793
cd	0	8	26	27.2	0.000	0.294	0.956

We first determine the Z reaction at c by enforcing moment equilibrium about an X axis through a - b .

$$10(16) - C_z(24) = 0$$

$$C_z = 6.67 \text{ kip } \uparrow$$

The reaction force at c is equal to the z component of the force in member cd . Therefore,

$$F_{cd,z} = -C_z = -6.67 \quad \Rightarrow \quad F_{cd} = \frac{6.67}{0.956} = 6.98 \text{ (compression)}$$

Then,

$$C_x = F_{cd,x} = 0$$

and

$$C_y = -F_{cd,y} = -6.67(0.294) = 2.05 \text{ kip } \downarrow$$

We determine the Y reaction at b by summing moments about the Z axis through a .

$$20(16) + 2.05(18) = 30B_y$$

$$B_y = 11.90 \text{ kip } \uparrow$$

Then,

$$F_{bd,y} = -B_y = -11.90 \quad \Rightarrow \quad F_{bd} = \frac{11.9}{0.488} = 24.39 \text{ (compression)}$$

Therefore,

$$B_x = -F_{bd,x} = 8.92 \leftarrow$$

and

$$F_{bd,z} = 0.793(24.39) = 19.33$$

$$B_z = -F_{bd,z} = 19.33 \uparrow$$

Lastly, we sum forces in the Z direction and determine the reaction at A.

$$B_z + C_z + A_z = 10$$

$$A_z = 10 - 6.67 - 19.33 = -16$$

$$A_z = 16 \text{ kip } \downarrow$$

Then,

$$F_{ad,z} = -A_z = 16 \quad \Rightarrow \quad F_{ad} = \frac{16}{0.734} = 21.8 \text{ (tension)}$$

and

$$A_x = -F_{ad,x} = 0.508(21.8) = 11.07 \text{ kip } \leftarrow$$

$$A_y = -F_{ad,y} = 0.452(21.8) = 9.85 \text{ kip } \downarrow$$

We were able to find the member forces working at any time with no more than a single unknown. A more direct but also more computationally intensive approach would be to work with joint d and generate the three force equilibrium equations expressed in terms of the magnitudes of the three-member forces. In this approach, we use the direction cosine information listed in Table E2.24.1 and assume all the member forces are tension. Noting (2.16), the corresponding force equilibrium equations are

$$\text{Joint d} \begin{cases} \sum F_x = 0 & 20 + 0.366F_{bd} - 0.508F_{ad} = 0 \\ \sum F_y = 0 & 0.294F_{cd} - 0.452F_{ad} - 0.488F_{bd} = 0 \\ \sum F_z = 0 & 10 + 0.734F_{ad} + 0.793F_{bd} + 0.956F_{cd} = 0 \end{cases} \Rightarrow \begin{cases} F_{ad} = 21.81 \text{ kip} \\ F_{bd} = -24.39 \text{ kip} \\ F_{cd} = -6.97 \text{ kip} \end{cases}$$

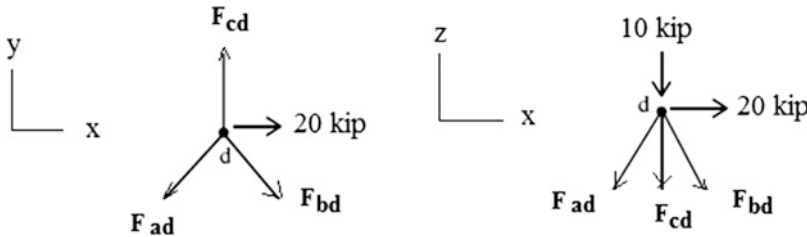


Fig. E2.24c Joint d

Table E2.24.2

Member	Force	Force _x	Force _y	Force _z
ad	21.81(tension)	11.07	9.85	16.00
bd	24.39 (compression)	8.93	11.90	19.33
cd	6.97(compression)	0.00	2.05	6.67

Example 2.25 Analysis of a Tetrahedron

Given: The tetrahedron structure defined in Fig. E2.25a, b.

Determine: The member forces.

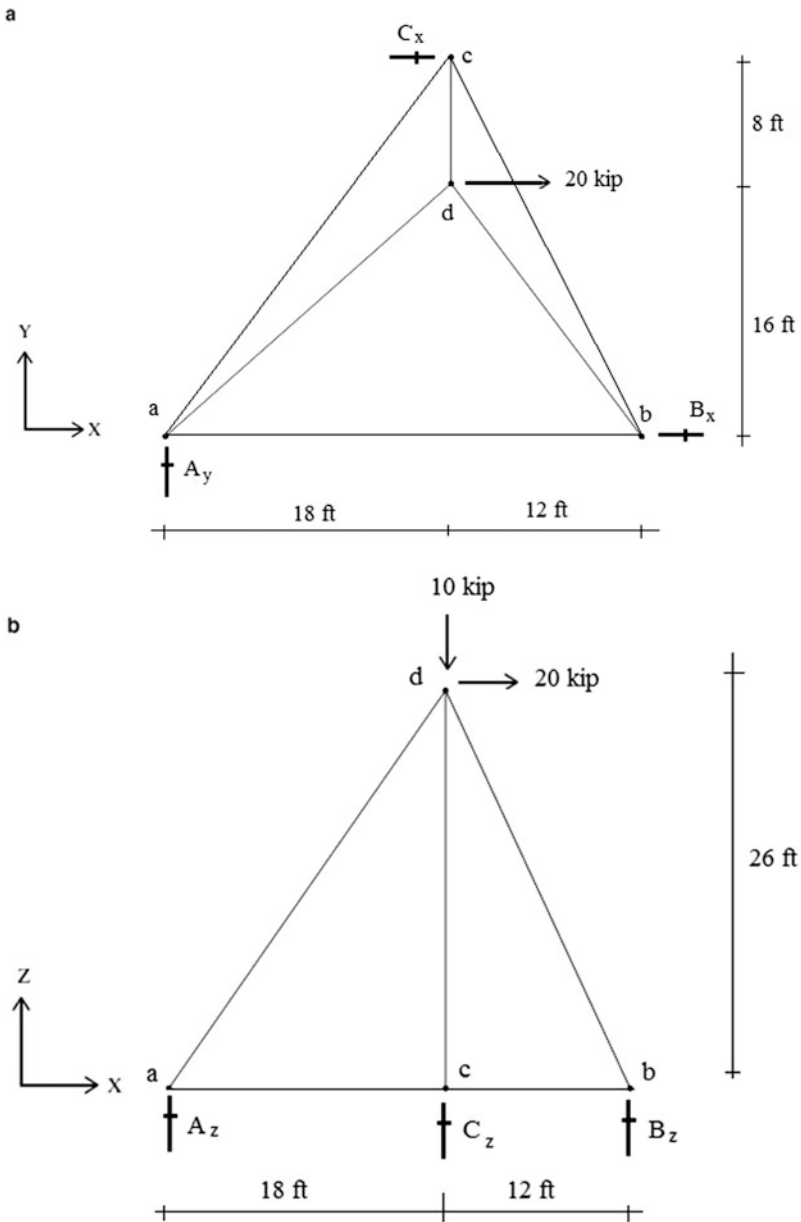


Fig. E2.25 Tetrahedron geometry and support. (a) $x - y$ plan view. (b) $x - z$ plan view

Solution: There are six reactions (three Z forces, two X forces, and one Y force), six members, and four joints. The determinacy criteria,

$$3j = m + r \rightarrow 3(4) = 6 + 6$$

is satisfied, so the structure is statically determinate.

We first determine the direction cosines for the members listed in Table E2.25.1

Table E2.25.1

Member	l_x	l_y	l_z	l	β_x	β_y	β_z
ac	18	24	0	30.0	0.600	0.800	0.000
ab	30	0	0	30.0	1.000	0.000	0.000
bc	12	24	0	26.8	0.447	0.895	0.000
ad	18	16	26	25.4	0.508	0.452	0.734
cd	0	8	26	27.2	0.000	0.290	0.960
bd	12	16	26	32.8	0.366	0.488	0.793

Next, we determine the Z reactions at a, b, and c.

$$\begin{aligned} \sum M_x \quad \text{at } a &= 0 \\ 10(16) &= 24C_z \\ C_z &= 6.67 \uparrow \end{aligned}$$

$$\begin{aligned} \sum M_y \quad \text{at } a &= 0 \\ 20(26) + 10(18) &= 6.67(18) + 30B_z \\ B_z &= 19.33 \uparrow \end{aligned}$$

$$\begin{aligned} \sum F_z &= 0 \uparrow^+ \\ 19.33 + 6.67 + A_z &= 10 \\ A_z &= 16 \downarrow \end{aligned}$$

The Y component at a is determined with: $\Sigma F_y = 0 \therefore A_y = 0$. Then, we enforce $\Sigma M_z = 0$ with respect to a Z axis through a.

$$\begin{aligned} 24C_x &= 20(16) \\ C_x &= 13.34 \leftarrow \end{aligned}$$

Lastly, we evaluate B_x

$$\begin{aligned} \sum F_x &= 0 \quad C_x + B_x = 20 \\ B_x &= 6.66 \leftarrow \end{aligned}$$

With the reactions known, each of the joints involves only three unknowns, and we can start with any joint. It is most convenient to start with joint b and enforce Z equilibrium.

$$\sum F_z = 0 \quad F_{bd,z} = B_z = 19.33$$

Then,

$$F_{bd} = -24.4 \text{ (compression)}$$

We find F_{cb} by summing Y forces at b.

$$\begin{aligned}\sum F_y &= 0 + F_{cb,y} + F_{bd,y} = 0 \\ F_{cb,y} &= 11.91 \\ F_{cb} &= +13.3 \text{ (tension)}\end{aligned}$$

Then, we find F_{ab} by summing X forces at b.

$$\begin{aligned}F_{ab} + F_{cb,x} + B_x - F_{bd,x} &= 0 \\ F_{ab} &= -3.69 \text{ (compression)}\end{aligned}$$

We move on to joint c. Summing Z forces yields F_{cd}

$$\begin{aligned}\sum F_z &= 0 \quad C_z + F_{cd,z} = 0 \\ F_{cd,z} &= -6.67 \\ F_{cd} &= -6.95 \text{ (compression)}\end{aligned}$$

Summing X (or Y) forces leads to F_{ab}

$$\begin{aligned}\sum F_x &= 0 \quad B_x + F_{ab,x} - F_{cb,x} = 0 \\ F_{ab,x} &= -13.34 + 5.94 = -7.40 \\ F_{ab} &= -12.33 \text{ (compression)}\end{aligned}$$

The last step is to determine F_{ad} by enforcing Z force equilibrium at a.

$$\begin{aligned}\sum F_z &= 0 \quad F_{ad,z} + A_z = 0 \\ F_{ad,z} &= 16 \\ F_{ad} &= +21.8 \text{ (tension)}\end{aligned}$$

We could have solved this problem by establishing the three force equilibrium equations for joint d, and finding F_{ad} , F_{cd} , F_{bd} . Once the reactions are known, we could set up the equations for joints c and b, and solve for the member forces F_{ac} , F_{bc} , and F_{ab} . We followed a different approach to illustrate how one applies the method of joints in a selective manner to a 3-D space truss.

Example 2.26 Displacement Computation—3-D Truss

Given: The tripod structure defined in Fig. E2.26a, b.

Determine: The displacements at joint d due to loading shown and a temperature increase of $\Delta T = 80^\circ\text{F}$ for all the members. Assume $A = 2.0 \text{ in.}^2$, $E = 29 \times 10^3 \text{ ksi}$, and $\alpha = 6.6 \times 10^{-6}/^\circ\text{F}$.

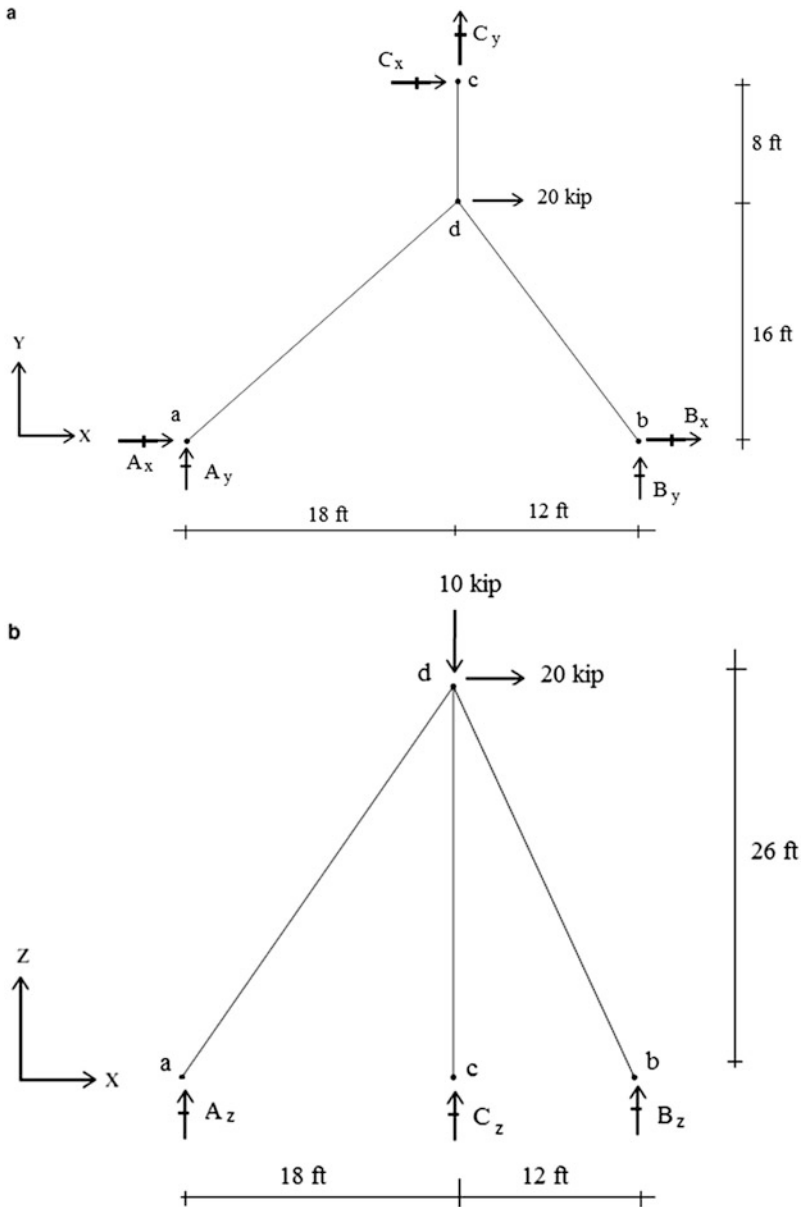


Fig. E2.26 Tripod geometry and supports. (a) $x - y$ plan view. (b) $x - z$ plan view

Solution: We apply the virtual loads δP_x , δP_y , and δP_z , (see Fig. E2.26c, d) at joint d and determine the corresponding virtual member forces, δF_u , δF_v , and δF_w . The individual displacement components due to loading are determined with:

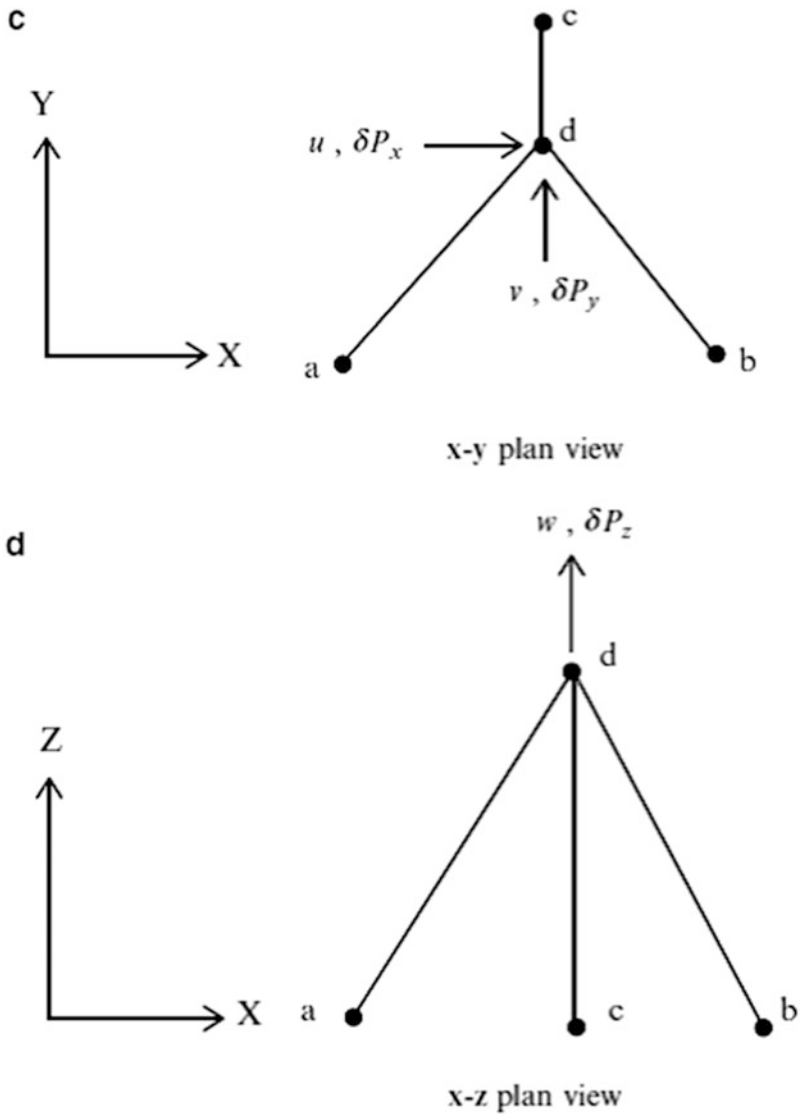


Fig. E2.26c Virtual forces

$$u \delta P_x = \sum \left(\frac{FL}{AE} \right) \delta F_u$$

$$v \delta P_y = \sum \left(\frac{FL}{AE} \right) \delta F_v$$

$$w \delta P_z = \sum \left(\frac{FL}{AE} \right) \delta F_w$$

For temperature change, we use

$$\begin{aligned}u \delta P_x &= \sum (\alpha \Delta T L) \delta F_u \\v \delta P_y &= \sum (\alpha \Delta T L) \delta F_v \\w \delta P_z &= \sum (\alpha \Delta T L) \delta F_w\end{aligned}$$

The relevant data needed to evaluate displacements is listed in Table E2.26.1. Note that we need to shift length units over to inches when computing $(\frac{FL}{AE})$ and $(\alpha \Delta T L)$.

We use the member forces determined in Example 2.24.

$$\text{Joint d} \begin{cases} \sum F_x = 0 & 20 + 0.366F_{bd} - 0.508F_{ad} = 0 \\ \sum F_y = 0 & 0.294F_{cd} - 0.452F_{ad} - 0.488F_{bd} = 0 \\ \sum F_z = 0 & 10 + 0.734F_{ad} + 0.793F_{bd} + 0.956F_{cd} = 0 \end{cases} \Rightarrow \begin{cases} F_{ad} = 21.81 \text{ kip} \\ F_{bd} = -24.39 \text{ kip} \\ F_{cd} = -6.97 \text{ kip} \end{cases}$$

For $\delta P_u = 1$:

$$\text{Joint d} \begin{cases} \sum F_x = 0 & 0.366\delta F_{ubd} - 0.508\delta F_{uad} = -1 \\ \sum F_y = 0 & 0.294\delta F_{ucd} - 0.452\delta F_{uad} - 0.488\delta F_{ubd} = 0 \\ \sum F_z = 0 & 0.734\delta F_{uad} + 0.793\delta F_{ubd} + 0.956\delta F_{ucd} = 0 \end{cases} \Rightarrow \begin{cases} \delta F_{uad} = 1.18 \\ \delta F_{ubd} = -1.09 \\ \delta F_{ucd} = 0 \end{cases}$$

For $\delta P_v = 1$

$$\text{Joint d} \begin{cases} \sum F_x = 0 & 0.366\delta F_{vbd} - 0.508\delta F_{vad} = 0 \\ \sum F_y = 0 & 0.294\delta F_{vcd} - 0.452\delta F_{vad} - 0.488\delta F_{vbd} = -1 \\ \sum F_z = 0 & 0.734\delta F_{vad} + 0.793\delta F_{vbd} + 0.956\delta F_{vcd} = 0 \end{cases} \Rightarrow \begin{cases} \delta F_{vad} = 0.59 \\ \delta F_{vbd} = 0.82 \\ \delta F_{vcd} = -1.13 \end{cases}$$

For $\delta P_w = 1$:

$$\text{Joint d} \begin{cases} \sum F_x = 0 & 0.366\delta F_{wbd} - 0.508\delta F_{wad} = 0 \\ \sum F_y = 0 & 0.294\delta F_{wcd} - 0.452\delta F_{wad} - 0.488\delta F_{wbd} = 0 \\ \sum F_z = 0 & 0.734\delta F_{wad} + 0.793\delta F_{wbd} + 0.956\delta F_{wcd} = -1.0 \end{cases} \Rightarrow \begin{cases} \delta F_{wad} = 0.18 \\ \delta F_{wbd} = 0.25 \\ \delta F_{wcd} = 0.70 \end{cases}$$

The relevant data needed to evaluate displacements is listed in Table E2.26.1.

Table E2.26.1

Member	l (ft)	A (in. ²)	F	For $\delta P = 1.0$			$\frac{FL}{AE}$ (in.)	$\alpha L \Delta T$ (in)
				δF_u	δF_v	δF_w		
ad	35.4	2.0	21.81	1.18	0.59	0.18	0.160	0.224
bd	32.8	2.0	-24.39	-1.09	0.82	0.25	-0.165	0.208
cd	27.2	2.0	-6.97	0.00	-1.13	0.70	-0.039	0.172

The displacements due to loads are

$$u_{\text{load}} = \sum \left(\frac{FL}{AE} \right) \delta F_u = (0.160)(1.18) + (-0.165)(-1.09) = 0.369 \text{ in.}$$

$$v_{\text{load}} = \sum \left(\frac{FL}{AE} \right) \delta F_v = (0.160)(0.59) + (-0.165)(0.82) + (-0.039)(-1.13) = 0.003 \text{ in.}$$

$$w_{\text{load}} = \sum \left(\frac{FL}{AE} \right) \delta F_w = (0.160)(0.18) + (-0.165)(0.25) + (-0.039)(0.70) = -0.039 \text{ in.}$$

A 80 °F temperature increase produces the following displacements:

$$u_{\text{temp}} = \sum (\alpha \Delta T L) \delta F_u = (0.224)(1.18) + (0.208)(-1.09) = 0.038 \text{ in.}$$

$$v_{\text{temp}} = \sum (\alpha \Delta T L) \delta F_v = (0.224)(0.59) + (0.208)(0.82) + (0.172)(-1.13) = 0.108 \text{ in.}$$

$$w_{\text{temp}} = \sum (\alpha \Delta T L) \delta F_w = (0.224)(0.18) + (0.208)(0.25) + (0.172)(0.70) = 0.213 \text{ in.}$$

The total displacements are

$$u_{(\text{load}+\text{temp})} = 0.369 + 0.038 = 0.407 \text{ in.}$$

$$v_{(\text{load}+\text{temp})} = 0.003 + 0.108 = 0.111 \text{ in.}$$

$$w_{(\text{load}+\text{temp})} = -0.039 + 0.213 = 0.174 \text{ in.}$$

2.6 Matrix Formulation: Equilibrium Analysis of Statically Determinate 3-D Trusses

Manual techniques are easy to apply for simple geometries, but become more difficult with increasing geometric complexity. The equilibrium analysis approaches described in the previous sections can be formulated as a sequence of matrix operations which can be readily automated for computer-based analysis. In what follows, we describe one approach for the equilibrium analysis of statically determinate 3-D trusses. We present a more general matrix formulation later in Chap. 12.

2.6.1 Notation

A truss is an assembly of nodes that are interconnected with members. It is convenient to define the geometry with respect to a global Cartesian coordinate system, XYZ , and number the nodes and members sequentially. Figure 2.34 illustrates this scheme. The structure has four nodes and six members.

We assume a positive sense for each member and define the direction cosines consistent with the assumed sense. The positive and negative nodes for member n are denoted as n_+ and n_- . Noting (2.16) and (2.17), the direction cosines for member n are determined using

Fig. 2.34 Numbering scheme

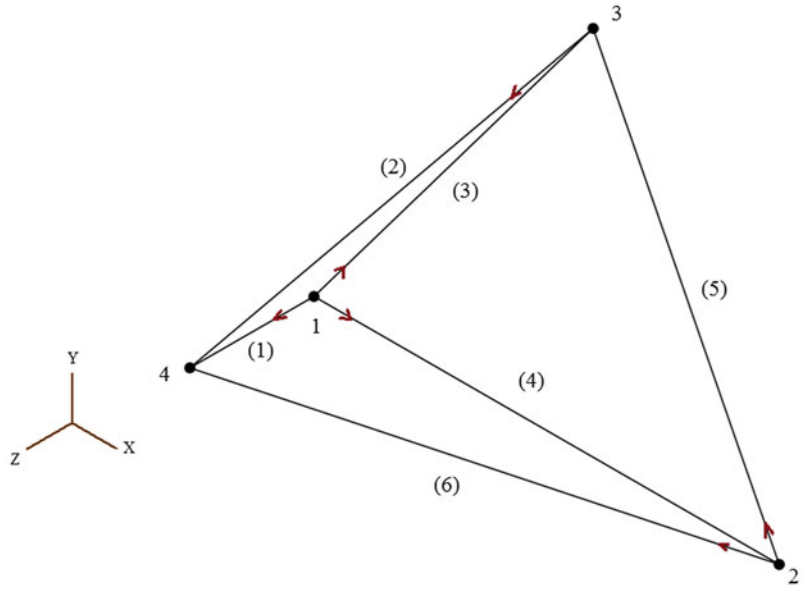
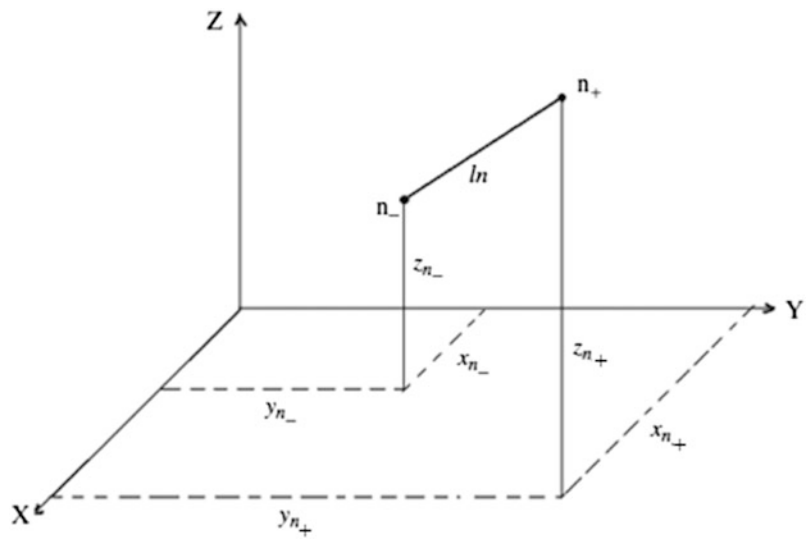


Fig. 2.35 Geometry-member n



$$\begin{aligned} \frac{x_{n_+} - x_{n_-}}{l_n} &= \beta_{n_x} \\ \frac{y_{n_+} - y_{n_-}}{l_n} &= \beta_{n_y} \\ \frac{z_{n_+} - z_{n_-}}{l_n} &= \beta_{n_z} \end{aligned} \tag{2.19}$$

It is convenient to introduce matrix notation at this point (Fig. 2.35). We define the nodal coordinate matrix for node j as

$$\mathbf{x}_j = \begin{Bmatrix} x_j \\ y_j \\ z_j \end{Bmatrix} \quad (2.20)$$

and the direction cosine matrix for member n as

$$\boldsymbol{\beta}_n = \begin{Bmatrix} \beta_{nx} \\ \beta_{ny} \\ \beta_{nz} \end{Bmatrix} \quad (2.21)$$

With this notation, the matrix form of (2.19) is

$$\boldsymbol{\beta}_n = \frac{1}{l_n} (\mathbf{x}_{n_+} - \mathbf{x}_{n_-}) \quad (2.22)$$

where

$$l_n^2 = (\mathbf{x}_{n_+} - \mathbf{x}_{n_-})^T (\mathbf{x}_{n_+} - \mathbf{x}_{n_-})$$

2.6.2 Member–Node Incidence

The computation of the direction cosines can be automated using the topological data for the members and nodes. This data is represented in tabular form. One lists, for each member, the node numbers for the positive and negative ends of the member. It is commonly referred to as the member–node incidence table. The table corresponding to the structure defined in Fig. 2.34 is listed below. One loops over the members, extracts the nodal coordinates from the global coordinate vector, executes the operation defined by (2.22), and obtains the member direction cosine matrix, $\boldsymbol{\beta}$.

Member	Negative node	Positive node
(1)	1	4
(2)	3	4
(3)	1	3
(4)	1	2
(5)	2	3
(6)	2	4

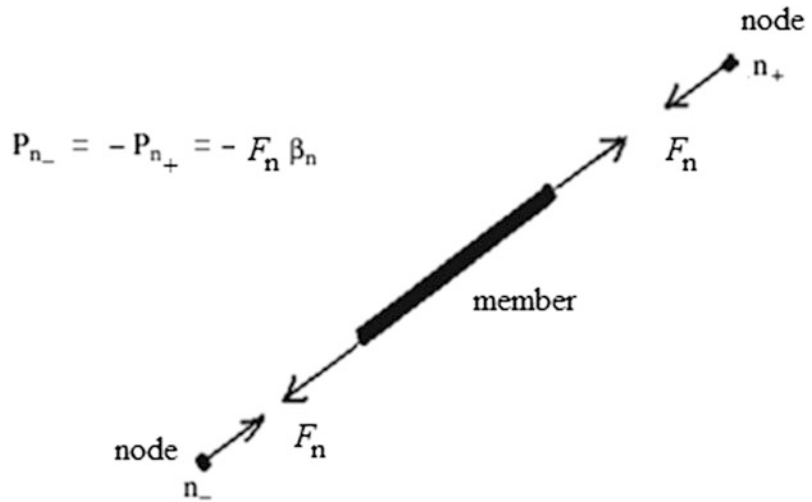
2.6.3 Force Equilibrium Equations

The force vector for a member points in the positive direction of the member, i.e., from the negative end toward the positive end. Noting (2.16), the set of Cartesian components for member n are listed in the matrix, \mathbf{P}_n , which is related to $\boldsymbol{\beta}_n$ by

$$\mathbf{P}_n = \begin{Bmatrix} F_x \\ F_y \\ F_z \end{Bmatrix} = F_n \boldsymbol{\beta}_n \quad (2.23)$$

The force components acting on the nodes at the ends of the member are equal to $\pm \mathbf{P}_n$. Figure 2.36 illustrates this distribution.

Fig. 2.36 Member end forces



We generate the set of force equilibrium equations for a node by summing the force matrices acting on the node. Consider node l . Let \mathbf{P}_l be the external force matrix for node l . The matrix equation for node l involves the member force matrices for those members which are positive incident and negative incident on node l .

$$\mathbf{P}_l = \sum_{n_+} (F_n \beta_n) + \sum_{n_-} (-F_n \beta_n) \quad (2.24)$$

This step is carried out for each node. Equation (2.24) represents i scalar equations, where $i = 2$ for a plane truss and $i = 3$ for a space truss. We assemble the complete set of equations in partitioned form, taking blocks of i rows. Assuming j nodes and m members, the equations are written as.

$$\mathbf{P}' = \mathbf{B}' \mathbf{F} \quad (2.25)$$

where the dimensions of the global matrices are

$$\mathbf{B}' = (i \text{ times } j) \times m, \quad \mathbf{F} = m \times 1, \quad \mathbf{P}' = (i \text{ times } j) \times 1$$

The algorithms for generating \mathbf{P}' and \mathbf{B}' are

$$\left. \begin{array}{l} \text{For member } n \quad (n = 1, 2, \dots, m) \\ \left. \begin{array}{l} +\beta_n \text{ in partitioned row } n_+, \text{ column } n \\ -\beta_n \text{ in partitioned row } n_-, \text{ column } n \end{array} \right\} \text{ of } \mathbf{B}' \end{array} \right\} \quad (2.26)$$

For node $l \quad (l = 1, 2, \dots, j)$
External load \mathbf{P}_l in partitioned row l of \mathbf{P}'

These operations can be easily implemented using spreadsheet software. The required size of the spreadsheet is i times j rows and $m + 1$ columns, (m columns for the member forces and one column for the external nodal loads). Applying (2.26) to the structure shown in Fig. 2.34 and noting the incidence table leads to the following form of \mathbf{B}' .

	F_1	F_2	F_3	F_4	F_5	F_6
Node 1	$-\beta_1$		$-\beta_3$	$-\beta_4$		
Node 2				$+\beta_4$	$-\beta_5$	$-\beta_6$
Node 3		$-\beta_2$	$+\beta_3$		$+\beta_5$	
Node 4	$+\beta_1$	$+\beta_2$				$+\beta_6$

↑
i row

Certain joint loads correspond to the r reactions which are not initially known. We separate out the rows in \mathbf{B}' and \mathbf{P}' corresponding to the r reactions, resulting in i times $(j - r)$ rows relating the m force unknowns. The reduced set of equations is expressed as (we drop the prime superscript on \mathbf{B} and \mathbf{P} to simplify the equation)

$$\mathbf{P} = \mathbf{B}\mathbf{F} \quad (2.27)$$

When the structure is statically determinate, $m = i$ times $(j - r)$, and since the coefficient matrix \mathbf{B} is now square, one can solve for \mathbf{F} . We used a similar approach when discussing complex planar trusses in Sect. 2.2.6.

2.6.4 Stability

A structure is said to be stable when a unique solution for the member forces exists for a given set of external loads. The relationship between the loading and the resulting member forces is defined by the linear matrix equation, (2.27). Noting Cramer's rule [4], the stability requirement can be expressed as

$$\text{determinant}(\mathbf{B}) \neq 0 \quad (2.28)$$

which is equivalent to requiring \mathbf{B} to be nonsingular. Singularity can be due to an insufficient number or improper orientation of the restraints. It may also arise due to the geometrical pattern of the members. Complex trusses, such as the example discussed in Sect. 2.2, may exhibit this deficiency even though they appear to be stable.

2.6.5 Matrix Formulation: Computation of Displacements

The manual process described in the previous section for computing displacements is not suited for large-scale structures. We faced a similar problem with the analysis of space trusses, and in that case, we resorted to a computer-based scheme. We follow a similar strategy here. We utilize the matrix notation introduced earlier, and just have to define some additional terms related to deformation and nodal displacement.

Noting (2.11), we see that e involves the direction cosines for the member, and the nodal displacements. Using the notation for the direction cosine matrix defined by (2.15) and also defining \mathbf{u} as the nodal displacement matrix,

$$\begin{aligned}\boldsymbol{\beta} &= \{\beta_x, \beta_y, \beta_z\} \\ \mathbf{u} &= \{u, v, w\}\end{aligned}\quad (2.29)$$

we express the extension e as a matrix product.

$$e = \boldsymbol{\beta}^T \mathbf{u} \quad (2.30)$$

We generalize (2.30) for a member n connected to nodes n_+ and n_-

$$e_n = \boldsymbol{\beta}_n^T (\mathbf{u}_{n_+} - \mathbf{u}_{n_-}) \quad (2.31)$$

Note that this matrix expression applies to both 2-D and 3-D structures.

Following the strategy used to assemble the matrix force equilibrium equations, we assemble the complete set of deformation–displacement relations for the structure. They have the following form

$$\mathbf{e} = (\mathbf{B}')^T \mathbf{U}' \quad (2.32)$$

where

$$\mathbf{U}' = \{u_1, u_2, \dots, u_j\}, \quad \mathbf{e} = \{e_1, e_2, \dots, e_m\}$$

and \mathbf{B}' is defined by (2.20). Note that \mathbf{B}' is the matrix associated with the matrix force equilibrium equations (2.19). Some of the nodal displacements correspond to locations, where constraints are applied and their magnitudes are known. When the structure is statically determinate, support movement introduces no deformation, and we can delete these terms from \mathbf{U}' . We also delete the corresponding rows of \mathbf{B}' . These operations lead to the modified equation

$$\mathbf{e} = \mathbf{B}^T \mathbf{U} \quad (2.33)$$

Note that the corresponding modified equilibrium equations have the form $\mathbf{P} = \mathbf{B}\mathbf{F}$.

The duality between these equations is called the “Static-Geometric” analogy.

Once \mathbf{F} is known, one determines the extension of a member using

$$e = \left(\frac{L}{AE}\right)F + e_1$$

where e_1 contains terms due to temperature and fabrication error. We express the set of deformations in matrix form

$$\mathbf{e} = \mathbf{f}\mathbf{F} + \mathbf{e}_1 \quad (2.34)$$

where \mathbf{f} is a diagonal matrix containing the flexibility coefficients for the members,

$$\mathbf{f} = \begin{bmatrix} \left(\frac{L}{AE}\right)_1 & & & \\ & \left(\frac{L}{AE}\right)_2 & & \\ & & \ddots & \\ & & & \left(\frac{L}{AE}\right)_m \end{bmatrix} \quad (2.35)$$

Given \mathbf{P} , one generates \mathbf{B} and, solves for \mathbf{F} ,

$$\mathbf{F} = \mathbf{B}^{-1}\mathbf{P} \quad (2.36)$$

Then, we compute \mathbf{e} with (2.34) and lastly solve for \mathbf{U} using.

$$\mathbf{U} = (\mathbf{B}^{-1})^T \mathbf{e} \quad (2.37)$$

This approach can be represented as a series of computer operations. The major computational effort is in assembling and inverting \mathbf{B} . The deflection computation requires minimal additional effort since one needs to compute \mathbf{B}^{-1} in order to determine the member forces.

Using matrix notation, it is relatively straightforward to prove the validity of the Method of Virtual Forces. We apply a virtual force $\delta\mathbf{P}'$ and find the corresponding virtual forces using the matrix equilibrium equations.

$$\delta\mathbf{P}' = \mathbf{B}' \delta\mathbf{F} \quad (2.38)$$

Member forces which satisfy the force equilibrium equations are said to be statically permissible. Note that $\delta\mathbf{P}'$ includes both the external nodal loads and the reactions. The extensions are related to the nodal displacements by (2.32)

$$\mathbf{e} = (\mathbf{B}')^T \mathbf{U}' \quad (2.38a)$$

where \mathbf{U}' contains both the nodal displacements and support movements. We multiply (2.38a) by $\delta\mathbf{F}^T$,

$$\delta\mathbf{F}^T \mathbf{e} = \delta\mathbf{F}^T \left[(\mathbf{B}')^T \mathbf{U}' \right] \quad (2.38b)$$

and note the identity,

$$\delta\mathbf{F}^T (\mathbf{B}')^T \equiv [\mathbf{B}' \delta\mathbf{F}]^T \equiv (\delta\mathbf{P}')^T \quad (2.39)$$

Then, (2.38b) takes the form

$$\delta\mathbf{F}^T \mathbf{e} = (\delta\mathbf{P}')^T \mathbf{U}' \quad (2.40)$$

Separating out the prescribed support displacements and reactions, and expanding the matrix products leads to the scalar equation

$$\sum \delta F \cdot e = \sum \delta P \cdot u + \sum \delta R \cdot \bar{u} \quad (2.41)$$

The final form follows when δP is specialized as a single force.

Example 2.27 Planar Complex Truss

Given: The planar structure shown in Fig. E2.27. Assume equal cross-sectional areas.

Determine:

- The displacements at the nodes. Take $A = 10 \text{ in.}^2$ and $E = 29,000 \text{ ksi}$.
- The value of A required to limiting the horizontal displacement to 1.5 in.

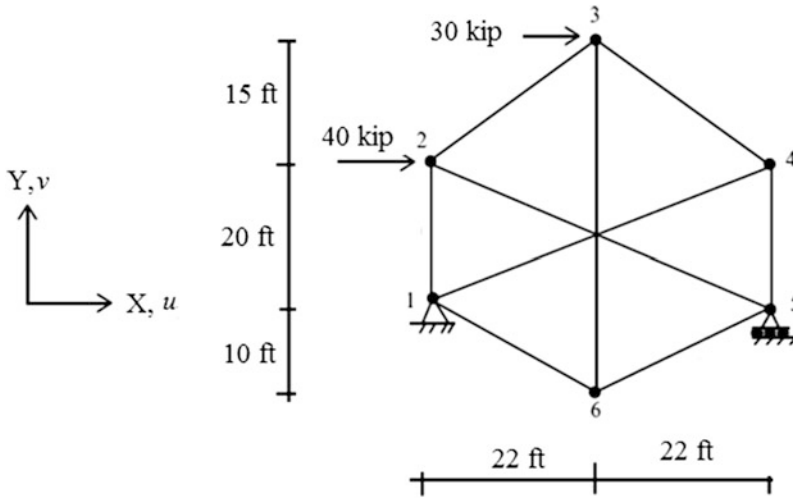


Fig. E2.27

Solution: This truss is a complex truss similar to example discussed in Sect. 2.2.5. One needs to solve the complete set of force equilibrium equations to find the member forces. Therefore, applying the Method of Virtual Forces is not computationally advantageous in this case, so we use a computer-based scheme. The computer method presented above is applicable for both planar and 3-D trusses. We just need to take $i = 2$ for the planar case. The results for the nodal displacements are listed below.

$$\begin{cases} u_1 = 0 \\ v_1 = 0 \end{cases}$$

$$\begin{cases} u_2 = 4.88 \text{ in.} \\ v_2 = 0.13 \text{ in.} \end{cases}$$

$$\begin{cases} u_3 = 2.34 \text{ in.} \\ v_3 = 4.15 \text{ in.} \end{cases}$$

$$\begin{cases} u_4 = -0.27 \text{ in.} \\ v_4 = 0.09 \text{ in.} \end{cases}$$

$$\begin{cases} u_5 = 4.42 \text{ in.} \\ v_5 = 0 \end{cases}$$

$$\begin{cases} u_6 = 2.2 \text{ in.} \\ v_6 = 4.43 \text{ in.} \end{cases}$$

The area required to limit the horizontal displacement to 1.5 in. is

$$A_{\text{required}} = (10) \frac{4.88}{1.5} = 32.53 \text{ in.}^2$$

The revised nodal displacements for $A = 32.53 \text{ in.}^2$ will be

$$\begin{cases} u_1 = 0 \\ v_1 = 0 \end{cases}$$

$$\begin{cases} u_2 = 1.5 \text{ in.} \\ v_2 = 0.04 \text{ in.} \end{cases}$$

$$\begin{cases} u_3 = 0.72 \text{ in.} \\ v_3 = 1.27 \text{ in.} \end{cases}$$

$$\begin{cases} u_4 = -0.08 \text{ in.} \\ v_4 = 0.03 \text{ in.} \end{cases}$$

$$\begin{cases} u_5 = 1.36 \text{ in.} \\ v_5 = 0 \end{cases}$$

$$\begin{cases} u_6 = 0.68 \text{ in.} \\ v_6 = 1.36 \text{ in.} \end{cases}$$

Example 2.28 Space Truss

Given: The space structure shown in Fig. E2.28. Assume equal cross-sectional areas. Take $A = 1300 \text{ mm}^2$ and $E = 200 \text{ GPa}$.

Determine: The member forces, the reactions, and the nodal displacements. Use computer-based scheme.

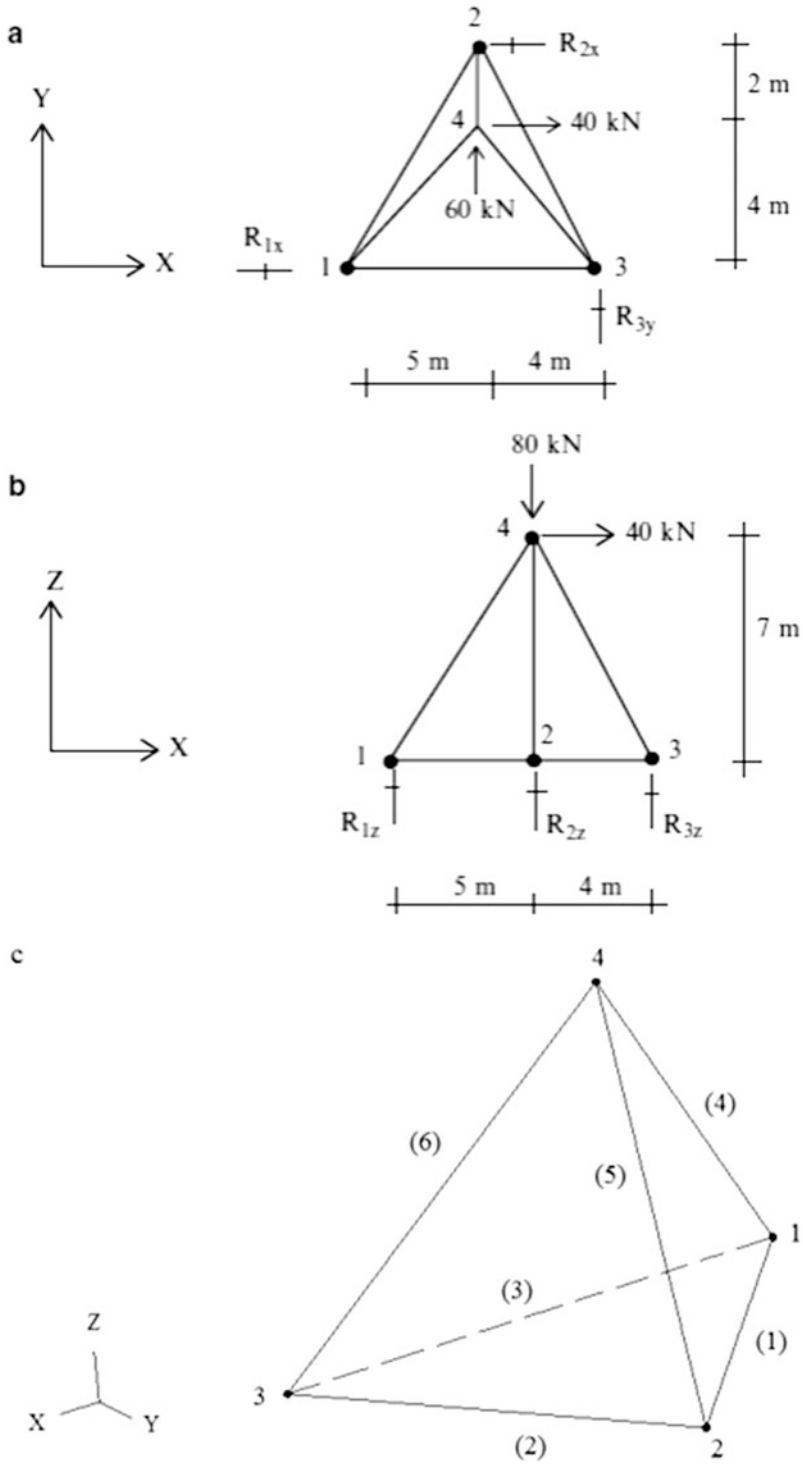


Fig. E2.28 3-D Truss. (a) $x-y$ plan view. (b) $x-z$ plan view. (c) Isometric view

Solution: The joint displacements, the member forces, and the reactions are listed below.

Joint displacements:

$$\text{Joint 1} \begin{cases} u_1 = 0 \\ v_1 = 4.9 \text{ mm} \\ w_1 = 0 \end{cases}$$

$$\text{Joint 2} \begin{cases} u_2 = 0 \\ v_2 = 3.5 \text{ mm} \\ w_2 = 0 \end{cases}$$

$$\text{Joint 3} \begin{cases} u_3 = -1.3 \text{ mm} \\ v_3 = 0 \\ w_3 = 0 \end{cases}$$

$$\text{Joint 4} \begin{cases} u_4 = 4.5 \text{ mm} \\ v_4 = 8.9 \text{ mm} \\ w_4 = -2.2 \text{ mm} \end{cases}$$

Member forces and reactions:

$$\begin{cases} F_{(1)} = -37.47 \text{ kN} \\ F_{(2)} = 76.94 \text{ kN} \\ F_{(3)} = -38.66 \text{ kN} \\ F_{(4)} = 68.26 \text{ kN} \\ F_{(5)} = -128.27 \text{ kN} \\ F_{(6)} = -9.05 \text{ kN} \end{cases} \quad \begin{cases} R_{1x} = 26.67 \text{ kN} \\ R_{1z} = -50.37 \text{ kN} \\ R_{2x} = -66.67 \text{ kN} \\ R_{2z} = 123.33 \text{ kN} \\ R_{3y} = -60.00 \text{ kN} \\ R_{3z} = 7.04 \text{ kN} \end{cases}$$

2.7 Summary**2.7.1 Objectives of the Chapter**

- To develop a criteria for assessing the initial stability of truss type structures
- To present methods for determining the axial forces in the members of statically determinate trusses
- To present a matrix-based formulation for the analyses of arbitrary statically determinate trusses
- To present methods for computing the displaced configuration of a truss
- To introduce the concept of an influence line and illustrate its application to trusses

2.7.2 Key Facts and Concepts

- The statical determinacy of a plane truss is determined by comparing the number of unknown forces vs. the number of available force equilibrium equations.
- The forces in the members of a statically determinate truss are independent of the member properties such as area and material modulus and support movements.
- The two force analysis procedures are the method of joints and the method of sections. The method of joints strategy proceeds from joint to joint, always working with a joint having a statically determinate force system. This approach generates all the member forces. The method of sections is designed to allow one to determine the force in a particular member. One passes a cutting plane through the structure, selects either segment, and applies the equilibrium conditions. This method requires less computation and generally is easier to apply.
- Given the external loads, one can determine the internal member forces using force equilibrium equations when the truss is statically determinate. The displacements due to the loading can be computed manually using the method of virtual forces. To determine the displacement at a point A in a particular direction, d_a , one applies a virtual force δP_a at point A in the same direction as the desired displacement and computes, using static equilibrium equations, the internal forces δF , and reactions, δR , due to δP_a . The displacement is given by

$$d_a \delta P_a = \sum_{\text{members}} e \delta F - \sum_{\text{reactions}} \bar{d} \delta R$$

where \bar{d} is the prescribed support movement and e is the elongation of the member due to force, temperature change, and initial fabrication error.

$$e = \left(\frac{FL}{AE} \right) + (\alpha \Delta T L) + e_0$$

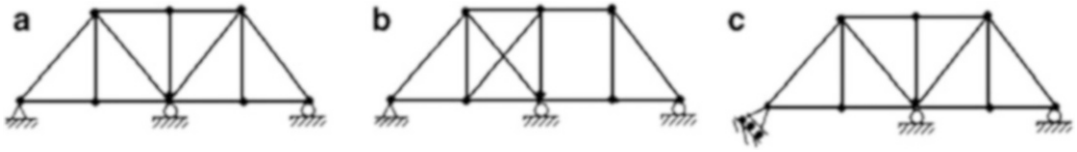
This method is restricted to static loading and small displacements. It is also applicable for statically indeterminate trusses when the member forces are known.

- The concept of influence lines is very useful for dealing with the live loading which can act anywhere on the structure. Given a particular member force and a particular type of live loading, usually a unit vertical loading, the influence line displays graphically the magnitude of the force for various locations of the load. By viewing the plot, one can immediately determine the position of the load that produces the peak magnitude of the member force.

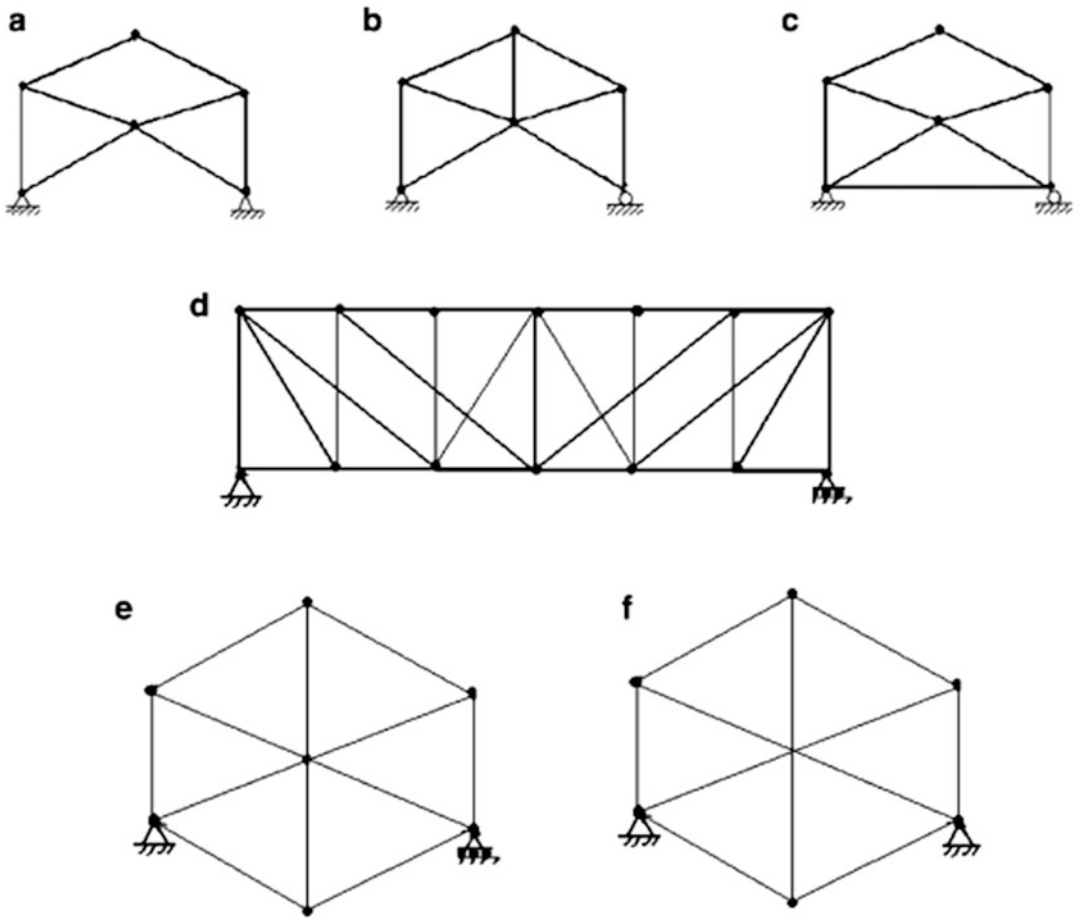
2.8 Problems

Classify each of the following plane trusses defined in Problems 2.1–2.4 as initially stable or unstable. If stable, then classify them as statically determinate or indeterminate. For indeterminate trusses, determine the degree of static indeterminacy.

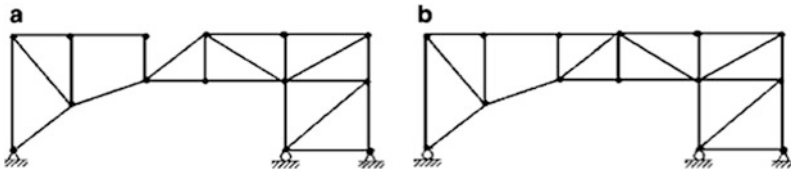
Problem 2.1



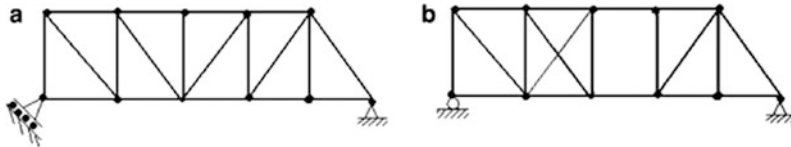
Problem 2.2



Problem 2.3

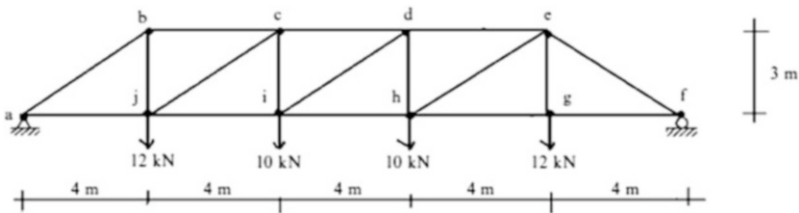


Problem 2.4

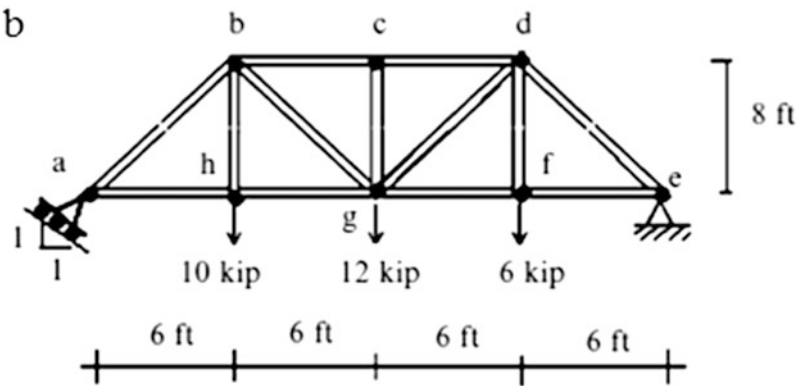
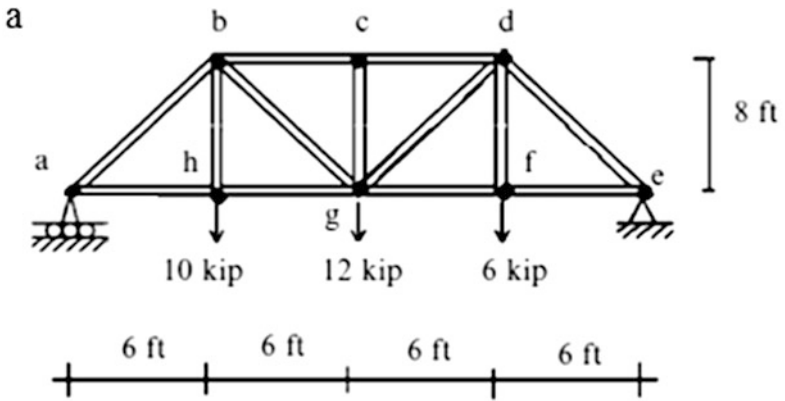


Determine all the member forces for the plane trusses defined in Problems 2.5–2.12 using the method of joints.

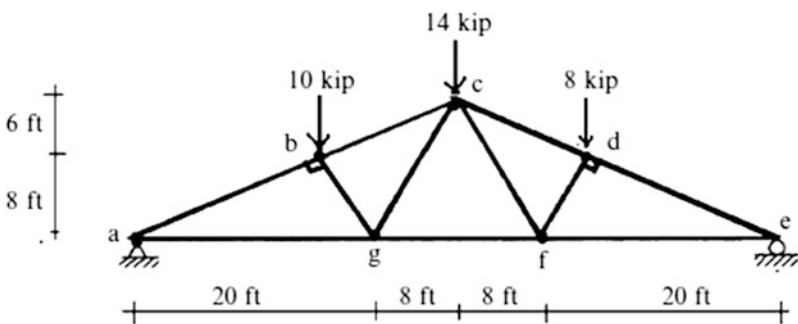
Problem 2.5



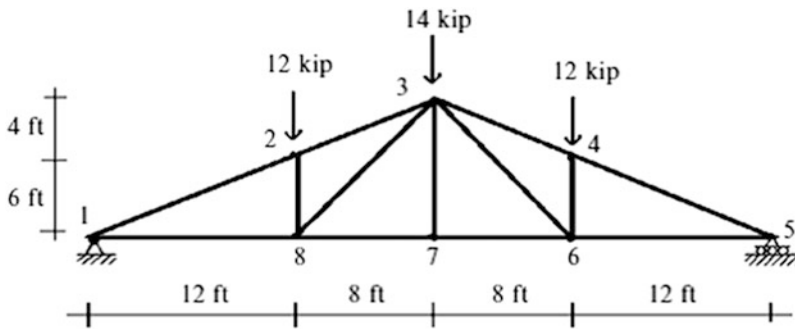
Problem 2.6



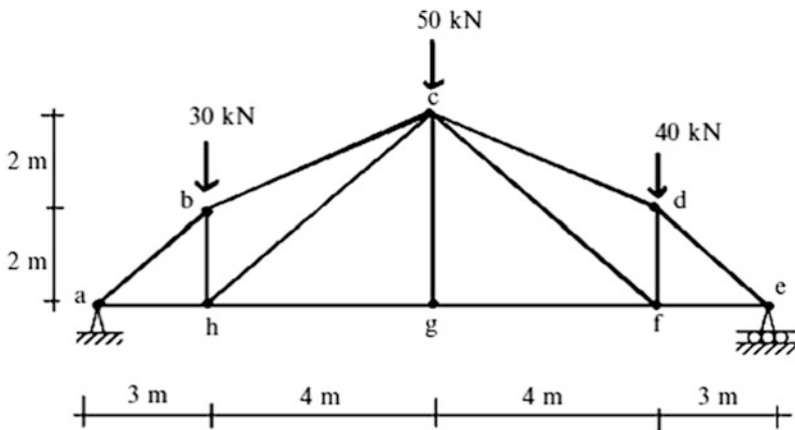
Problem 2.7



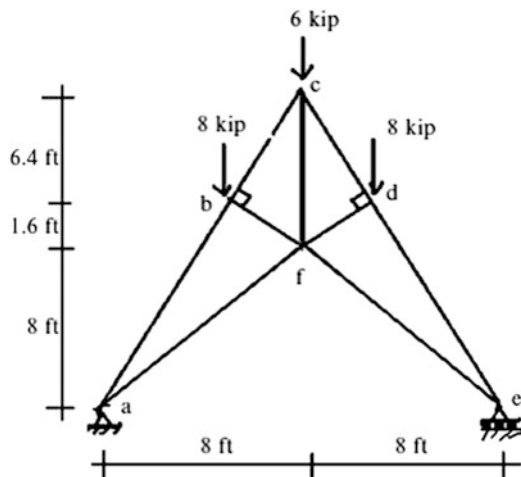
Problem 2.8



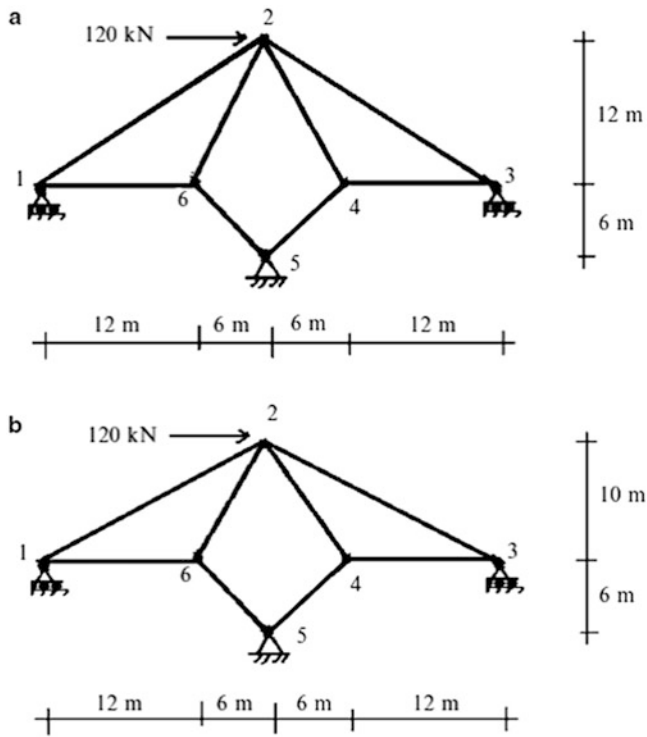
Problem 2.9



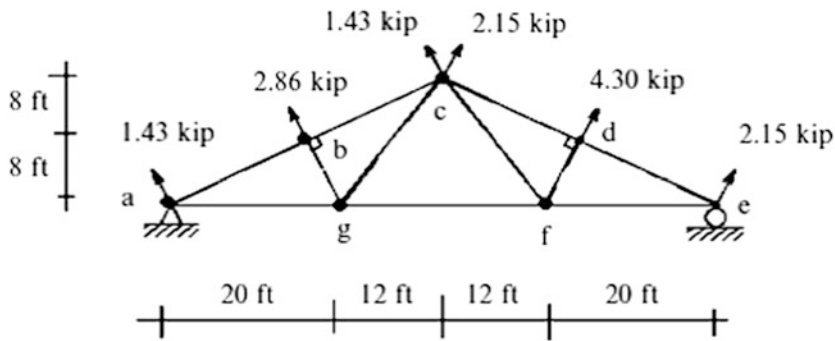
Problem 2.10



Problem 2.11

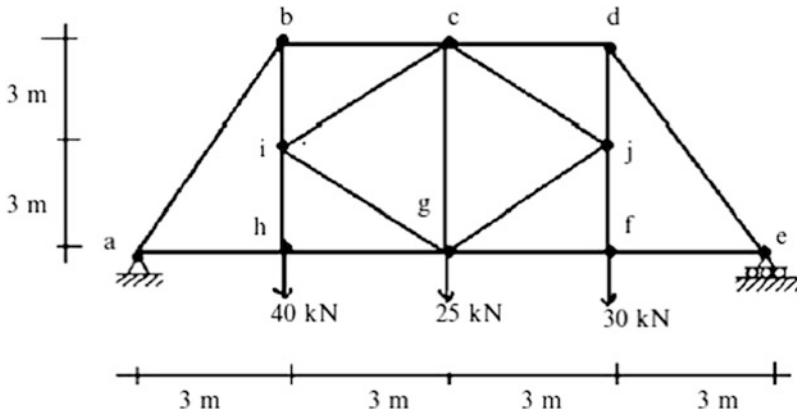


Problem 2.12

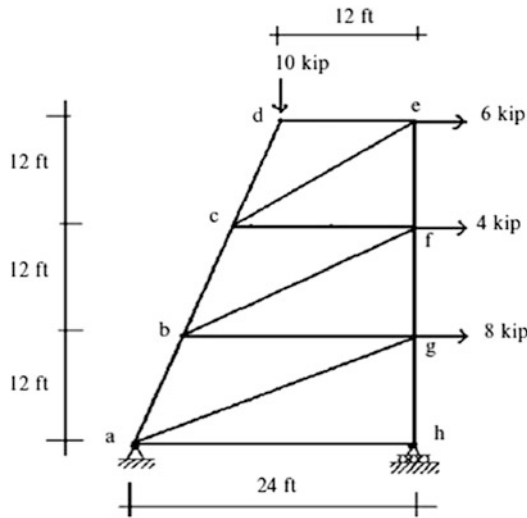


Determine all the member forces for the plane trusses defined in Problems 2.13–2.18 using a combination of the method of joints and the method of sections.

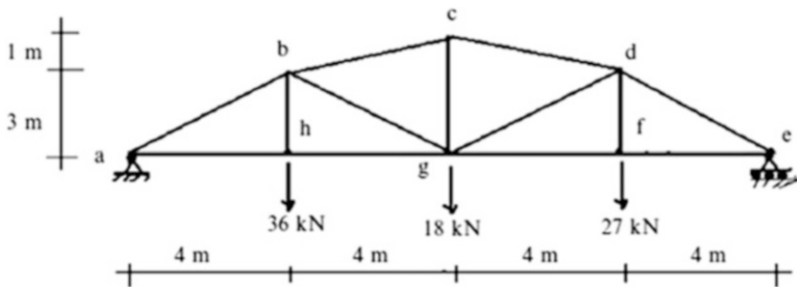
Problem 2.13



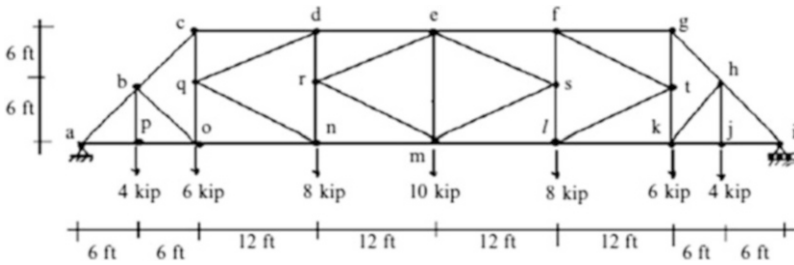
Problem 2.14



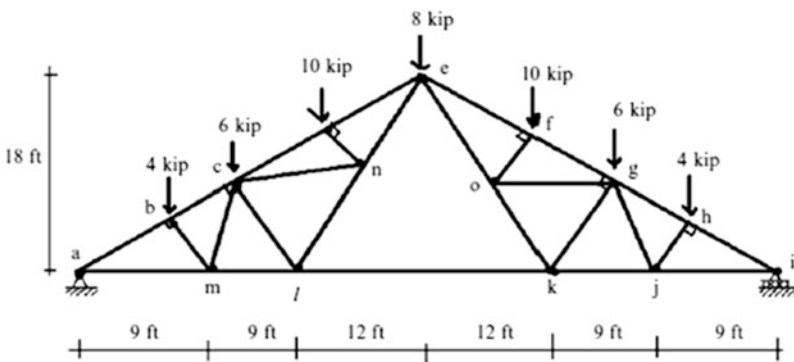
Problem 2.15



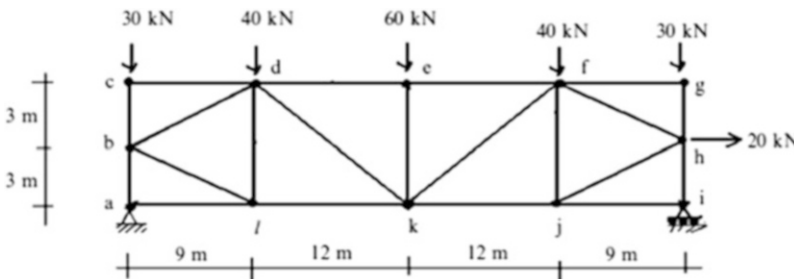
Problem 2.16



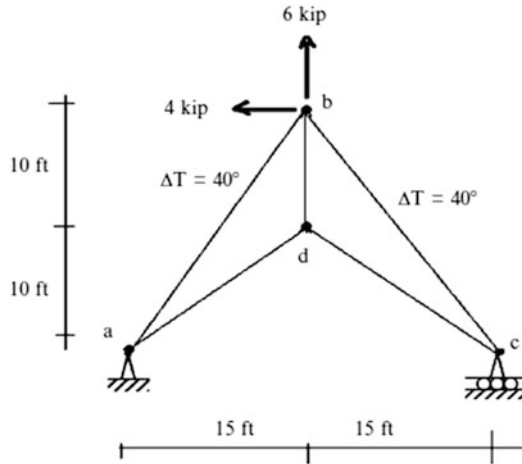
Problem 2.17



Problem 2.18



Problem 2.19 Use the principle of virtual forces to determine the horizontal and vertical displacement at joint b due to loading shown and temperature increase of $\Delta T = 40^\circ\text{F}$ for members ab and bc. Assume $A = 1.4 \text{ in.}^2$, $E = 29,000 \text{ ksi}$, and $\alpha = 6.5 (10^{-6})/^\circ\text{F}$



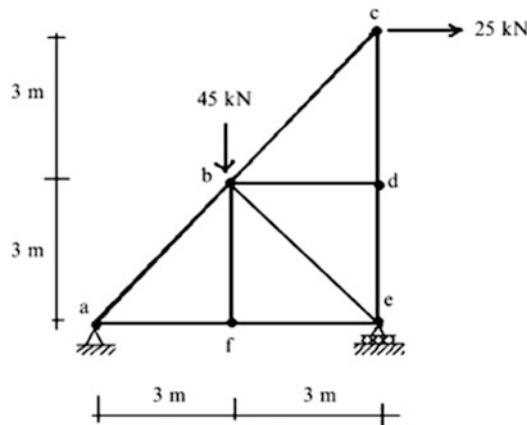
Problem 2.20 For the plane truss shown, use the principle of virtual forces to determine the vertical displacement at joint b and the horizontal displacement at joint c. $E = 200 \text{ GPa}$. The areas of the members are as follow:

$$A_{ab} = A_{bc} = A_{be} = 1290 \text{ mm}^2$$

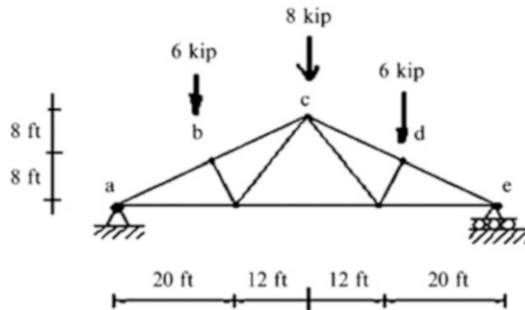
$$A_{bf} = A_{bd} = 645 \text{ mm}^2$$

$$A_{cd} = A_{de} = 1935 \text{ mm}^2$$

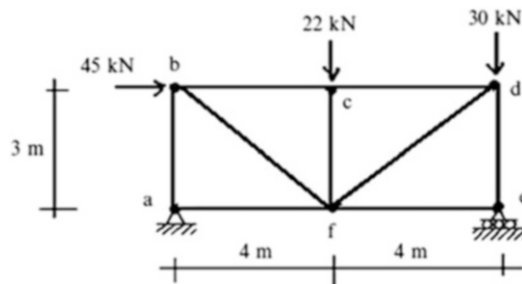
$$A_{af} = A_{fe} = 2580 \text{ mm}^2$$



Problem 2.21 For the plane truss shown, use the principle of virtual forces to determine the vertical displacement at joint C due to the loading shown and a settlement of 0.5 inch at support a. Assume $A = 2 \text{ in.}^2$ and $E = 29,000 \text{ ksi}$.



Problem 2.22 For the plane truss shown, use the principle of virtual forces to determine the vertical and horizontal displacement at joint d.



$$A = 1300 \text{ mm}^2$$

$$E = 200 \text{ GPa}$$

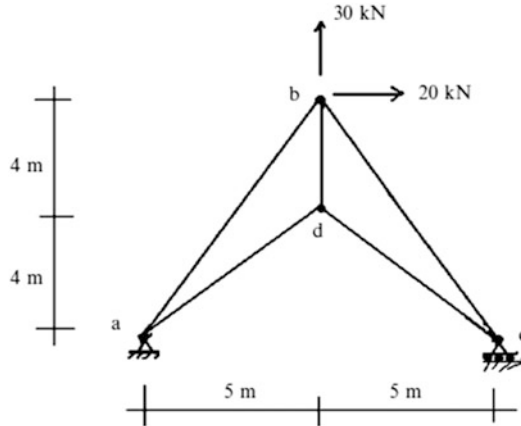
Problem 2.23 Use the principle of virtual forces to determine the horizontal and vertical displacement at joint b due to:

- Loading shown.
- Temperature increase of $\Delta T = 16 \text{ }^\circ\text{C}$ for members ab and bc.

$$A = 900 \text{ mm}^2$$

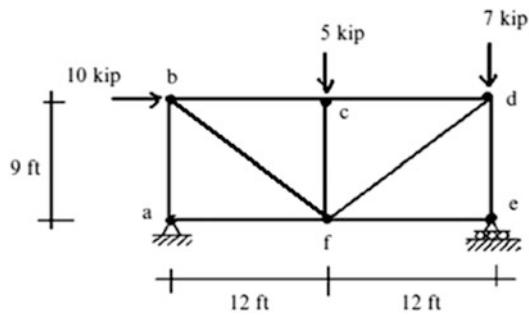
$$E = 200 \text{ GPa}$$

$$\alpha = 12 \times 10^{-6} / ^\circ\text{C}$$



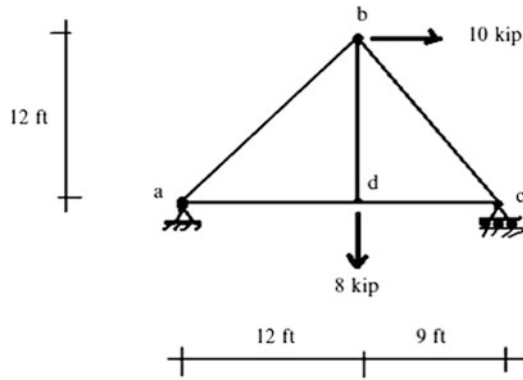
Problem 2.24 Use the principle of virtual force method to determine the horizontal component of the displacement at joint d. Assume $A = 0.5 \text{ in.}^2$ and $E = 29,000 \text{ ksi}$.

- (i) For the loading shown
- (ii) For a fabrication error of -0.25 in. for members ac and df
- (iii) For the summation of Case (i) and Case (ii) loadings.



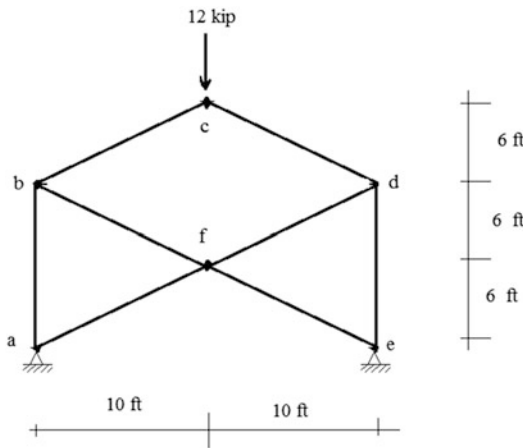
Problem 2.25 Use the principle of virtual forces method to determine the horizontal component of the displacement at joint b. Assume $A = 0.5 \text{ in.}^2$, $E = 30,000 \text{ ksi}$, $\alpha = 6.5 \times 10^{-6}/^\circ\text{F}$

- (i) For the loading shown
- (ii) For a temperature increase of $\Delta T = 60 \text{ }^\circ\text{F}$ for all members
- (iii) For the summation of Case (i) and Case (ii) loadings.

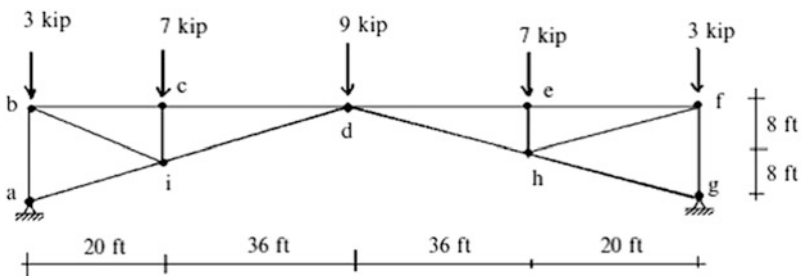


Problem 2.26 For the plane truss shown below, use the principle of virtual forces to determine the vertical displacement at joint f.

$A = 2 \text{ in.}^2$
 $E = 29,000 \text{ ksi}$

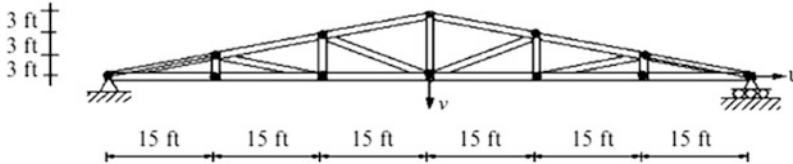


Problem 2.27 For the plane truss shown below, determine the required cross-sectional area for the truss members to limit the vertical deflection at d to 0.56 in. Assume equal cross-sectional areas. $E = 29,000 \text{ ksi}$.



Problem 2.28 For the plane truss shown in Problem 2.12, use the principle of virtual forces to determine the vertical displacement at joint g. The areas are 4 in.^2 for top chord members, 3 in.^2 for bottom chord members, and 2 in.^2 for other members. $E = 29,000 \text{ ksi}$.

Problem 2.29



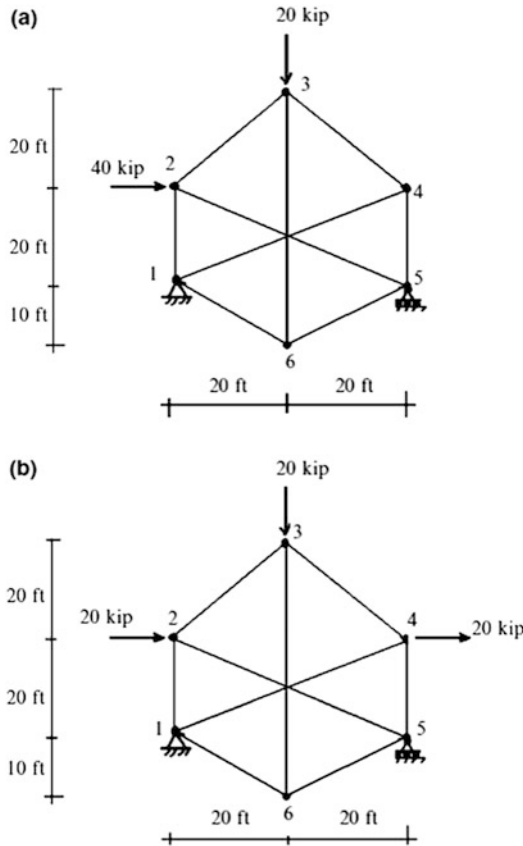
Suppose the top chord members in the truss defined above experience a temperature decrease of $60 \text{ }^\circ\text{F}$. Determine the resulting displacements, u and v . $A = 2 \text{ in.}^2$, $E = 29,000 \text{ ksi}$ and $\alpha = 6.5 \times 10^{-6}/^\circ\text{F}$.

Problem 2.30 Solve Problem 2.15 using computer software. Assume the cross-sectional areas are equal to A .

- Demonstrate that the member forces are independent of A by generating solutions for different values of A .
- Determine the value of A required to limit the vertical displacement to 50 mm.

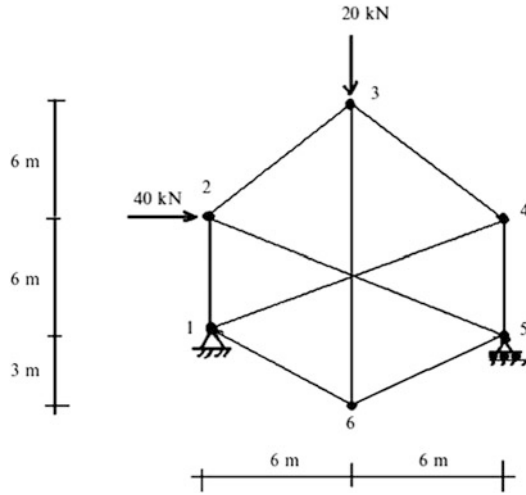
Problem 2.31 Consider the complex truss defined below in Figure (a). Use computer software to determine the member forces for the loading shown in Figure (a).

- Assume equal areas
- Take an arbitrary set of areas
- Determine the member forces corresponding to the loading shown in Figure (b). Are the forces similar to the results of part (a). Discuss.

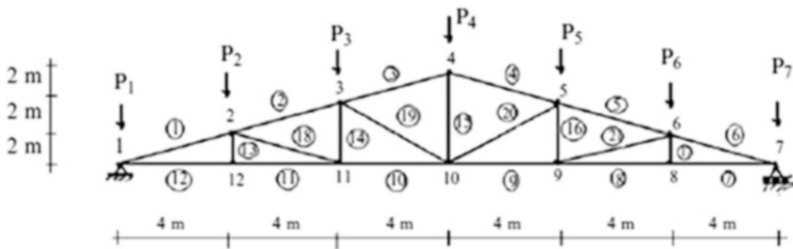


Problem 2.32 Solve Problem 2.11(a) using computer software. Assuming the cross-sectional areas are equal to A . Demonstrate that the member forces are independent of A by generating solution of different values of A .

Problem 2.33 Consider the complex truss defined below. Assume equal areas. Use computer software to determine the member forces and joint displacements. Determine the area for which the maximum displacement equals 30 mm. $E = 200$ GPa.

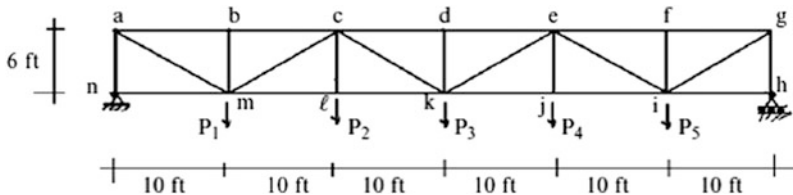


Problem 2.34 For the truss and the loading shown:



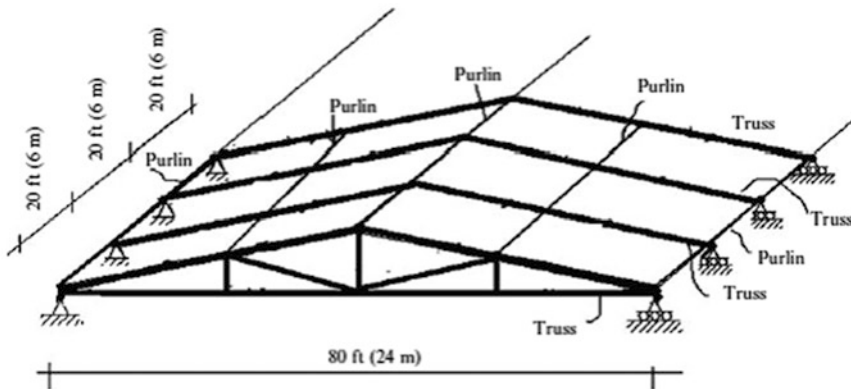
- (a) Tabulate all the member forces due to the individual unit vertical nodal forces applied to the top chord (force influence table). Use computer software.
- (b) Use the force influence table in part (a) to
 - (i) Draw influence lines for members 15, 4, and 20.
 - (ii) Calculate the member forces in members 3, 19, 10, and 14 for the following loading: $P_2 = 10 \text{ kN}$, $P_4 = 6 \text{ kN}$, and $P_6 = 8 \text{ kN}$.

Problem 2.35 For the truss and the loading shown:

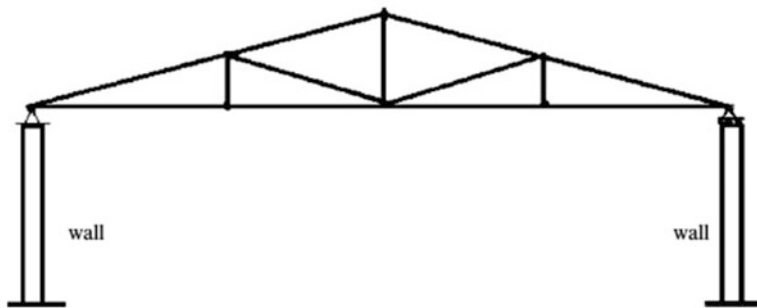


- (a) Tabulate all the member forces due to the individual unit vertical nodal forces applied to the bottom chord (force influence table). Use computer software.
- (b) Use the force influence table in part (a) to
 - (i) Draw influence lines for members bc, cm, and ji.
 - (ii) Calculate the member forces in members ke, de, kl, and ei for the loading $P_1 = 8$ kip, $P_3 = 10$ kip, and $P_4 = 4$ kip.

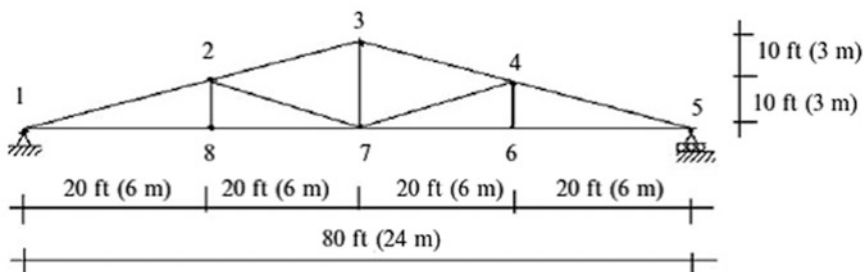
Problem 2.36 The roof structure shown below consists of trusses spaced uniformly, 20 ft (6 m) on center, along the length of the building and tied together by purlins and x-bracing. The roofing materials are supported by the purlins which span between trusses at the truss joints.



(a) Roof structural make-up



(b) Elevation-typical truss



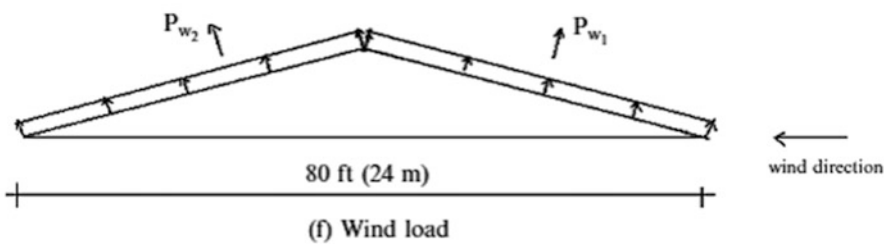
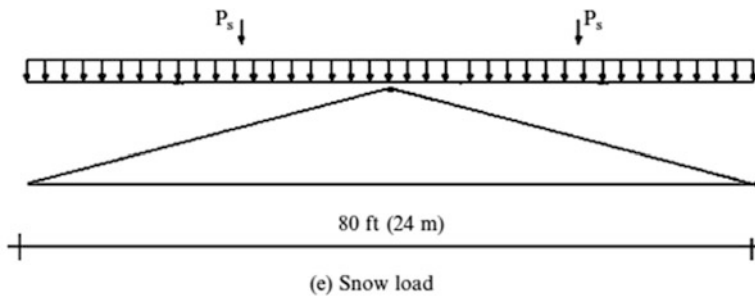
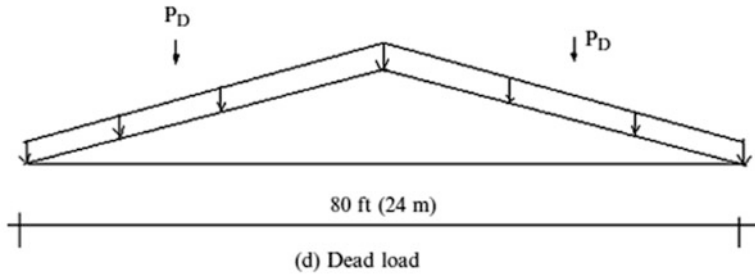
(c) Truss geometry

Consider the following loadings:

Dead load: roof material, purlins, truss members, estimated at 15 psf (720 Pa) of roof surface

Snow load: 20 psf (960 Pa) of horizontal projection of the roof surface

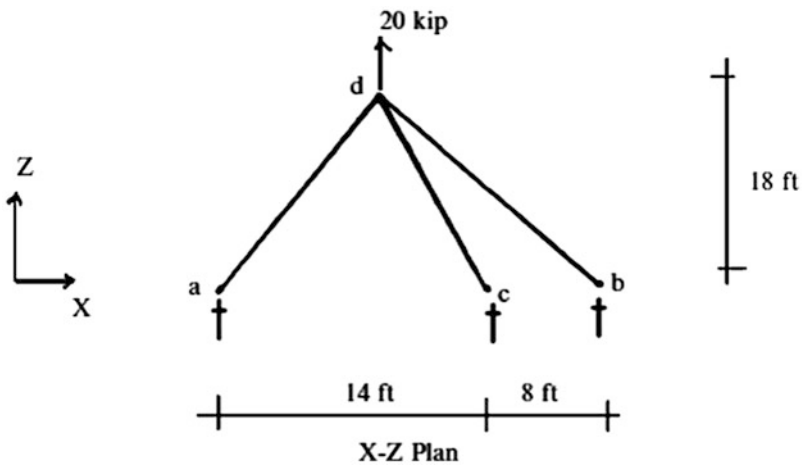
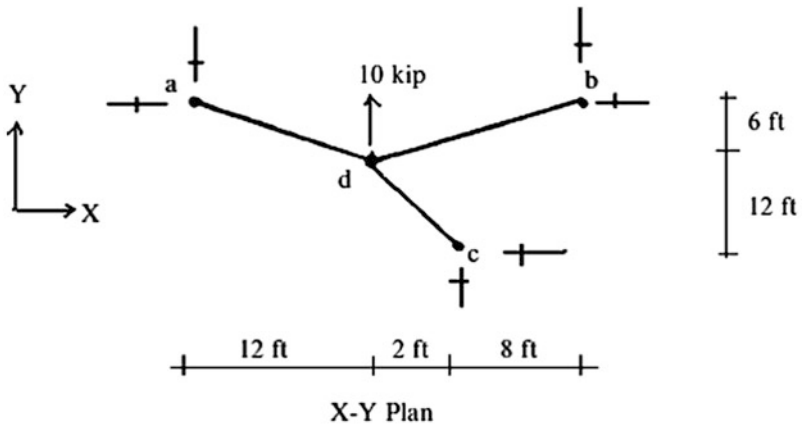
Wind load: windward face 12 psf (575 Pa), leeward face 8 psf (385 Pa) normal to roof surface



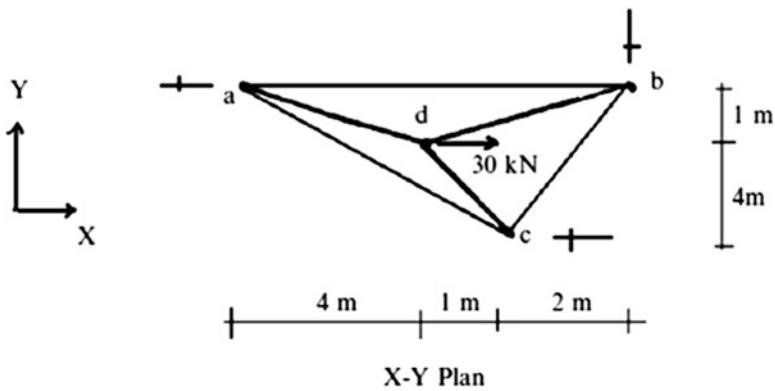
Determine the following quantities for the typical interior truss:

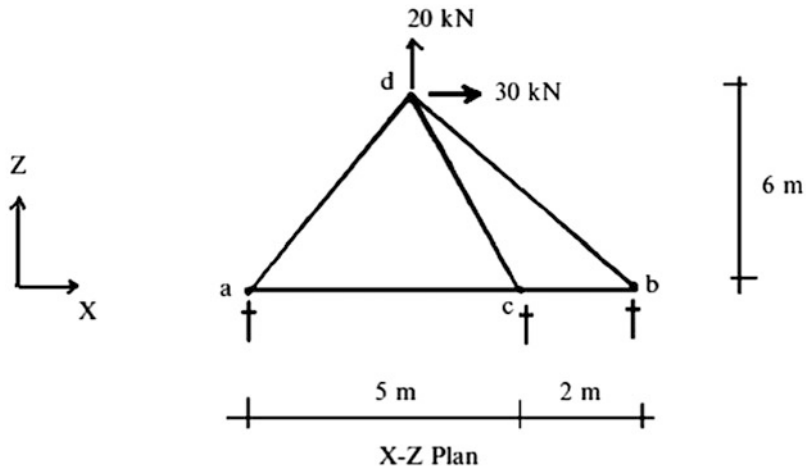
- Compute the truss nodal loads associated with gravity, snow, and wind.
- Use computer software to determine the member forces due to dead load, snow load, and wind. Tabulate the member force results.

Problem 2.37 Determine the member forces for the space truss shown.

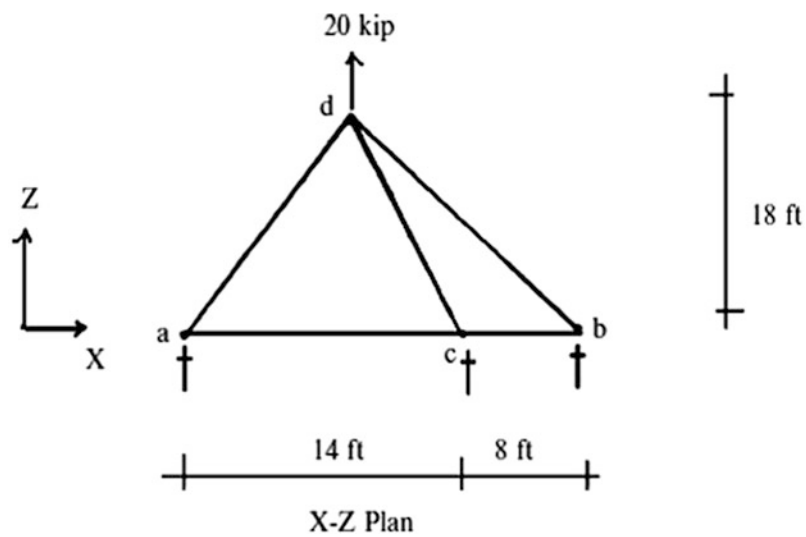
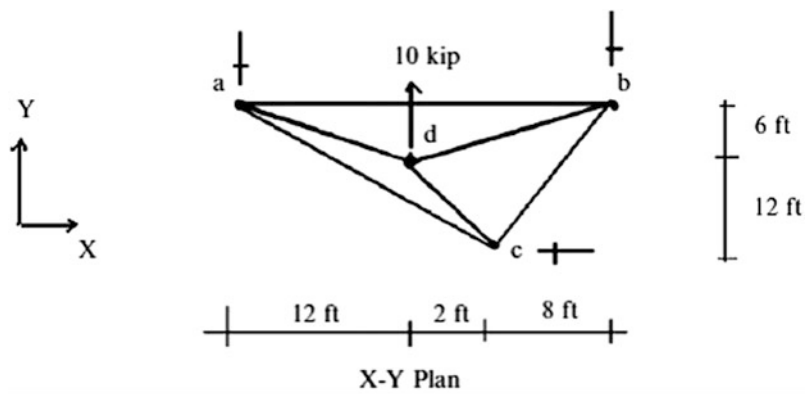


Problem 2.38 Determine the member forces for the space truss shown.

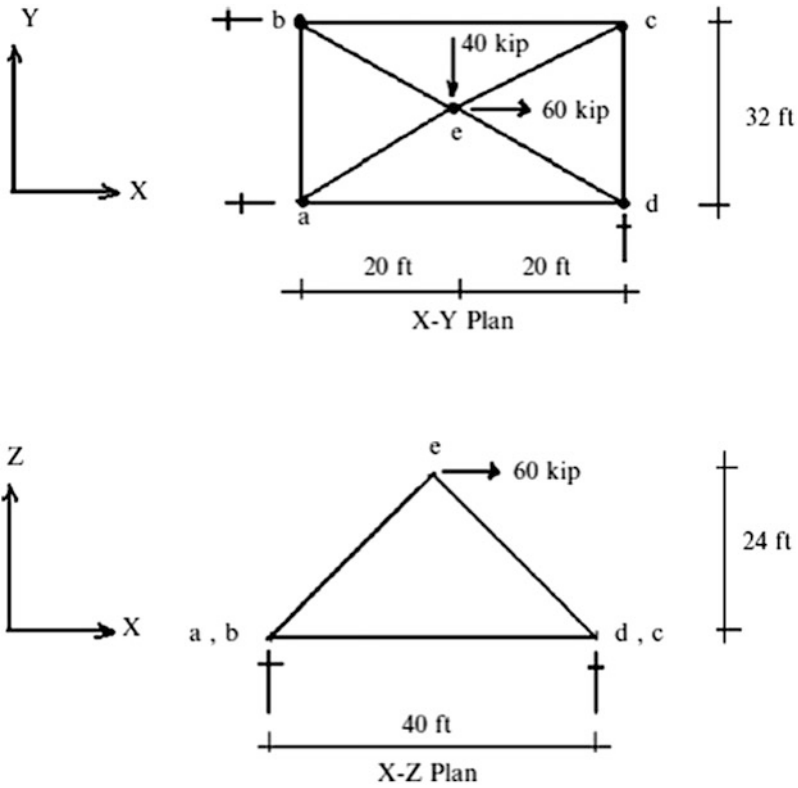




Problem 2.39 Determine the member forces for the space truss shown.



Problem 2.40 Determine the member forces for the space truss shown.



Problem 2.41 For the space truss shown in Problem 2.37, use the principle of virtual forces to determine the displacements u , v , and w at joint d . $E = 29,000$ ksi and $A = 3.0$ in.²

References

1. Faraji S, Ting J, Crovo DS, Ernst H. Nonlinear analysis of integral bridges: finite element model. *ASCE J Geotech Geoenviron Eng.* 2001;127(5):454–61.
2. Mathcad 14.0, Engineering calculations software.
3. Tauchert TR. *Energy principles in structural mechanics.* New York: McGraw-Hill; 1974.
4. Connor JJ. *Introduction to structural motion control.* Upper Saddle River: Prentice Hall; 2003.

Abstract

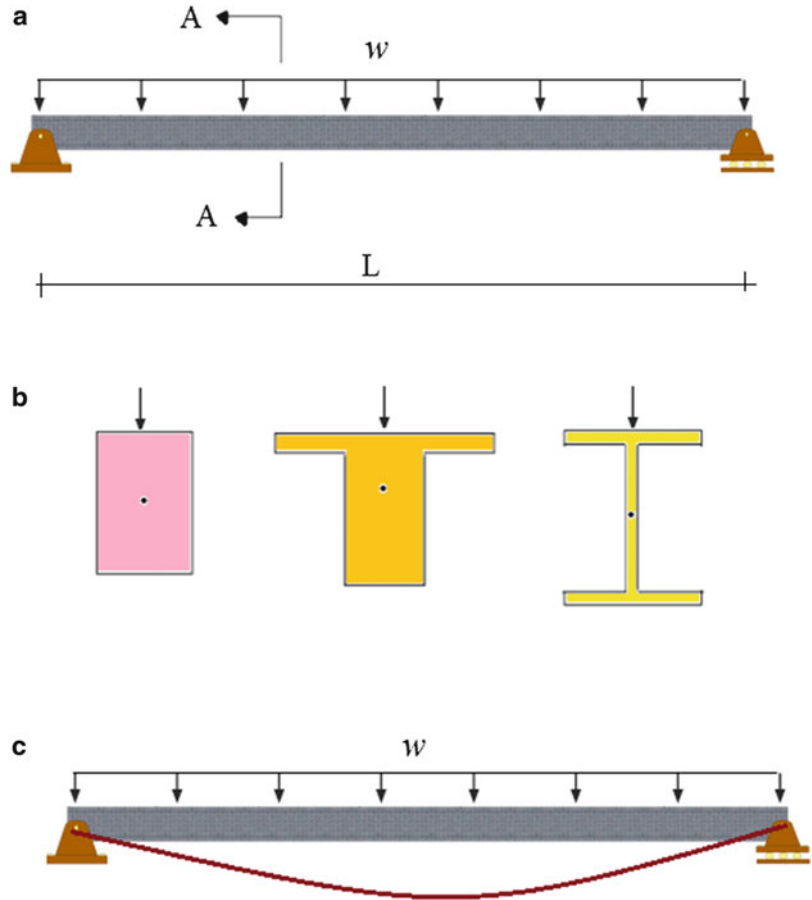
Our focus in this chapter is on describing how beams behave under transverse loading, i.e., when the loading acts normal to the longitudinal axes. This problem is called the “beam bending” problem. The first step in the analysis of a statically determinate beam is the determination of the reactions. Given the reactions, one can establish the internal forces using equilibrium-based procedures. These forces generate deformations that cause the beam to displace. We discuss in detail the relationship between the internal forces and the corresponding displacements and describe two quantitative analysis procedures for establishing the displacements due to a particular loading. The last section of the chapter presents some basic analysis strategies employed in the design of beams such as influence lines and global envelopes.

3.1 Definition of a Prismatic Beam

Beams are used extensively in structures, primarily in flooring systems for buildings and bridges. They belong to the line element category, i.e., their longitudinal dimension is large in comparison to their cross-sectional dimensions. Whereas truss members are loaded axially, beams are loaded normal to the longitudinal direction, and carry the loading by bending and twisting action. This mode is illustrated in Fig. 3.1. The transverse loading produces transverse deflection, which results in a nonuniform distribution of stress throughout the body.

Most of the applications of beams in building structures involve straight beams with constant cross-section. We refer to this subgroup as prismatic beams. Figure 3.2 defines the geometrical parameters and notation used for prismatic beams. The longitudinal axis- X passes through the centroid of the cross-section, and the Y , Z axes are taken as the principal inertia directions. The relevant definition equations are

Fig. 3.1 Beam cross-sections and bending mode. (a) Simply supported beam. (b) Section A-A—cross-section examples. Rectangular, T shape, I shape. (c) Bending mode



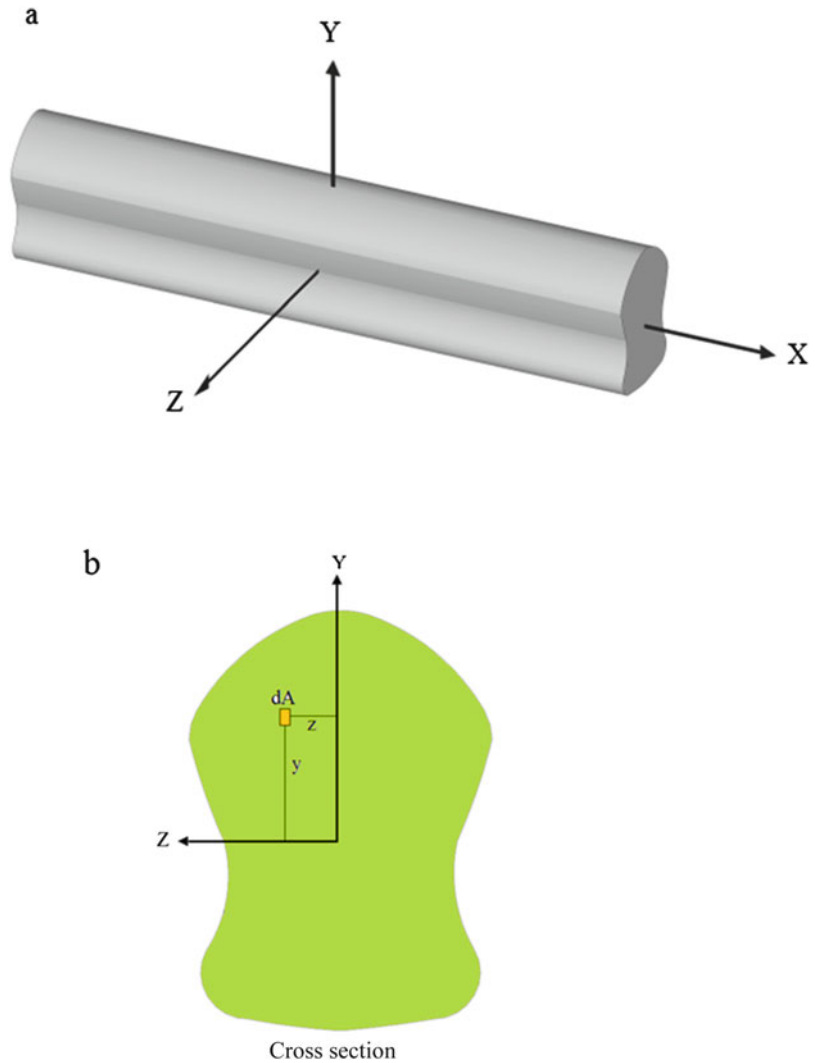
$$\begin{aligned}
 \int_A y dA &= \int_A z dA = \int_A yz dA = 0 \\
 I_z &= \int_A y^2 dA \\
 I_y &= \int_A z^2 dA
 \end{aligned} \tag{3.1}$$

These conditions ensure that when the applied loads are in the $X - Y$ plane, points on the longitudinal axis will not displace in the Z direction. Figure 3.3 illustrates this mode of behavior, the longitudinal axis- X becomes a curve $\nu(x)$ contained in the $X - Y$ plane. This type of behavior is Stabilitycalled *planar bending*.

There are cases where the line of action of the loading does not pass through the X -axis, such as illustrated in Fig. 3.4. The eccentricity produces a torsional moment about the X -axis, and the cross-section will rotate as well as deflect. This behavior is called “combined bending and torsion.” A prismatic member acted upon by just a torsional moment will experience only torsional behavior, i.e., the cross-section will just twist.

Mechanics of Solids texts deal with stresses and strains in beams. *Our objective here is not to redevelop this material but rather to utilize it and formulate a structural theory for beams that will provide the basis for analyzing the behavior of structures composed of beam elements.* Since structural theory is founded on Engineering Mechanics Theory, at least one subject dealing with

Fig. 3.2 Notations for prismatic beam—symmetrical cross-section



Engineering Mechanics is usually required before studying Structural Theory. We assume that the reader has this level of exposure to Engineering Mechanics.

3.2 Stability and Determinacy of Beams: Planar Bending

We presented the general concept of stability of a rigid body in Chap. 1 and used the general concept to develop stability criteria for truss-type structures in Chap. 2. In what follows, we examine the stability question for beam-type structures and develop similar criteria. For completeness, we first briefly review the basis for stability discussed in Chap. 1.

Consider the rigid body shown in Fig. 3.5. Assume the body can move only in the $X - Y$ plane. There are three types of planar motion for a rigid body: translation in the x direction, u_A , translation in the y direction, v_A , and rotation about an axis normal to the $X - Y$ plane, ω_A . A body is said to be stable when rigid body motion is prevented. Therefore, it follows that one must provide three motion constraints to restrain motion in the $X - Y$ plane.

Fig. 3.3 Planar bending mode

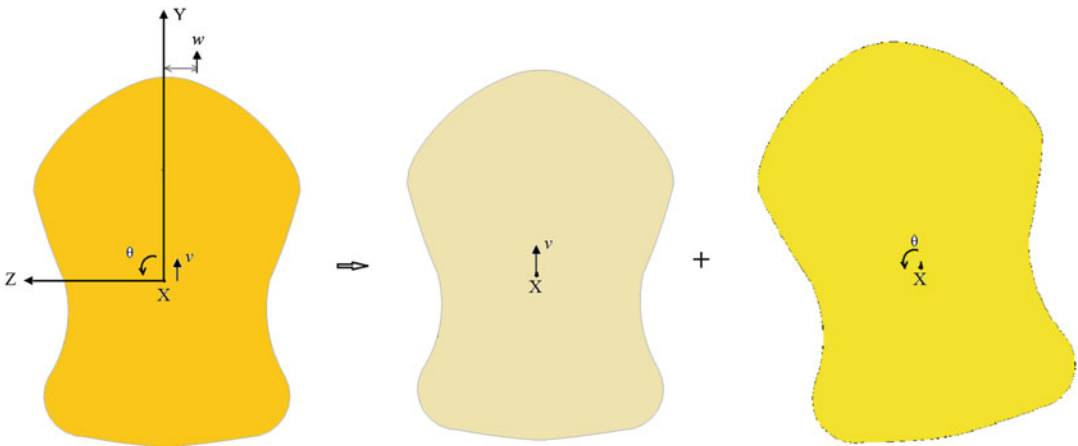
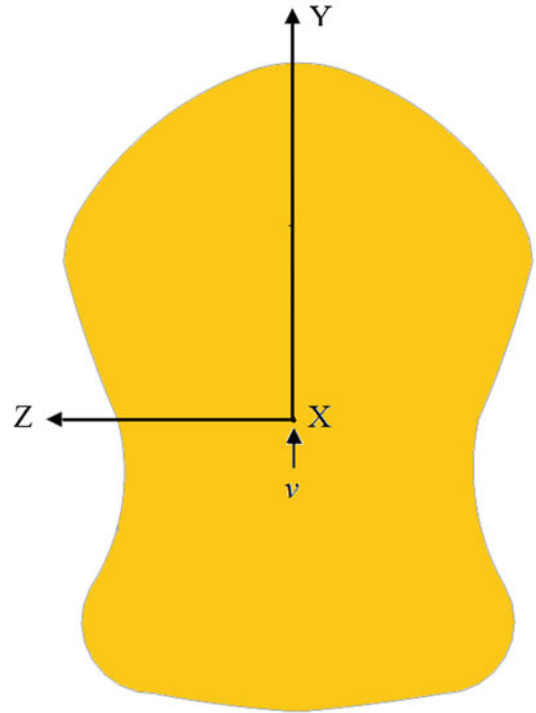


Fig. 3.4 Combined bending and torsion

One needs to be careful in selecting the orientation of the three translation constraints. Consider Fig. 3.6. We first choose two directions, “*a*” and “*b*” in the $X - Y$ plane. They intersect at point o . With these two constraints, the only possible rigid body motion is rotation about point o . If we take the third direction as “*c*,” this rotation is not prevented. *Therefore, it follows that the three directions must be nonconcurrent as well as coplanar, i.e., they cannot intersect at a common point.* This implies that they must not be parallel. Any other direction, such as “*d*” is permissible.

Fig. 3.5 Planar rigid body motions

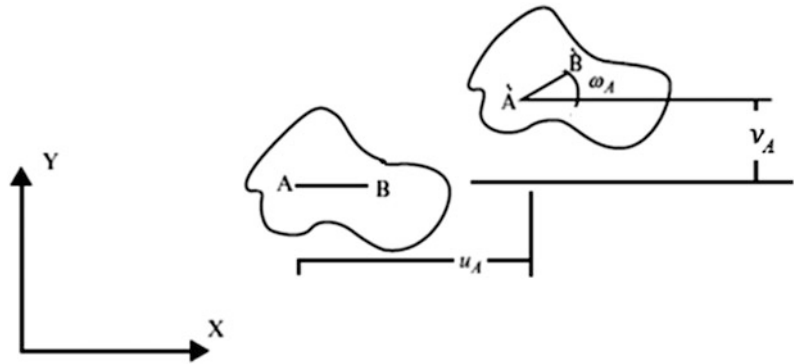
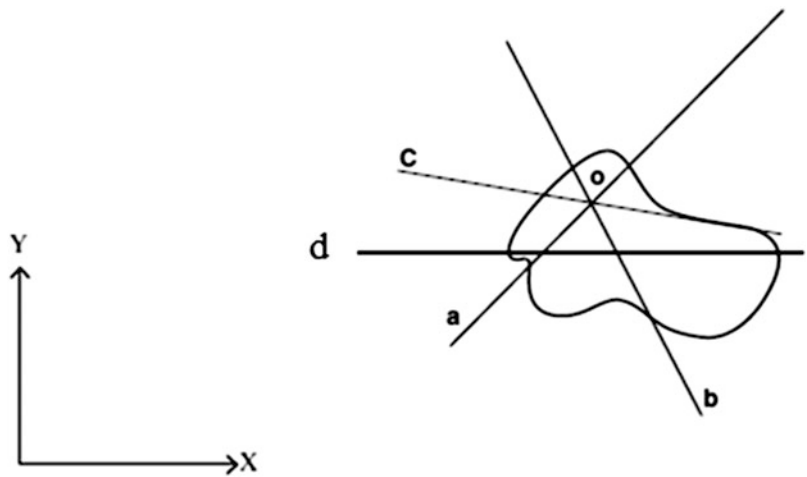
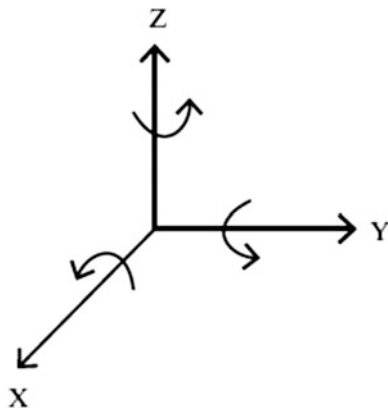


Fig. 3.6 Concurrent displacement constraints



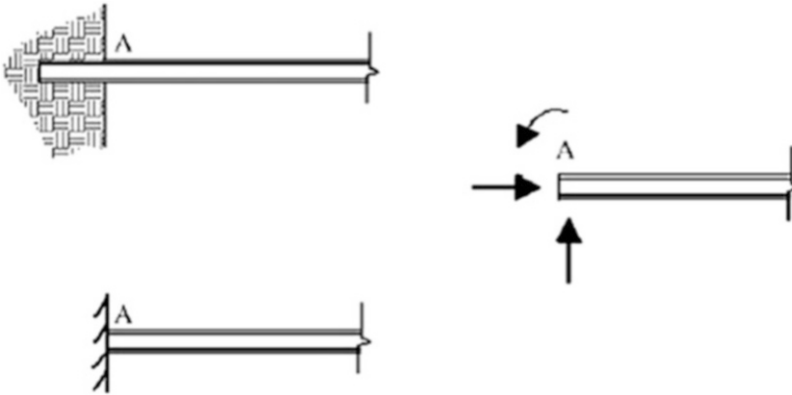
When the loading is arbitrary, the body needs to be constrained against motion in any plane. This requires six constraints, three with respect to translation and three with respect to rotation about the X, Y, and Z direction. The strategy for selecting restraints is similar to the treatment of 3-D truss structures. We point out that for pure rotational loading only one rotational restraint is required.



Motion constraints produce reaction forces when the body is loaded. The nature of the reaction forces depends on the constraints. Various types of supports for beams subjected to planar bending are illustrated below.

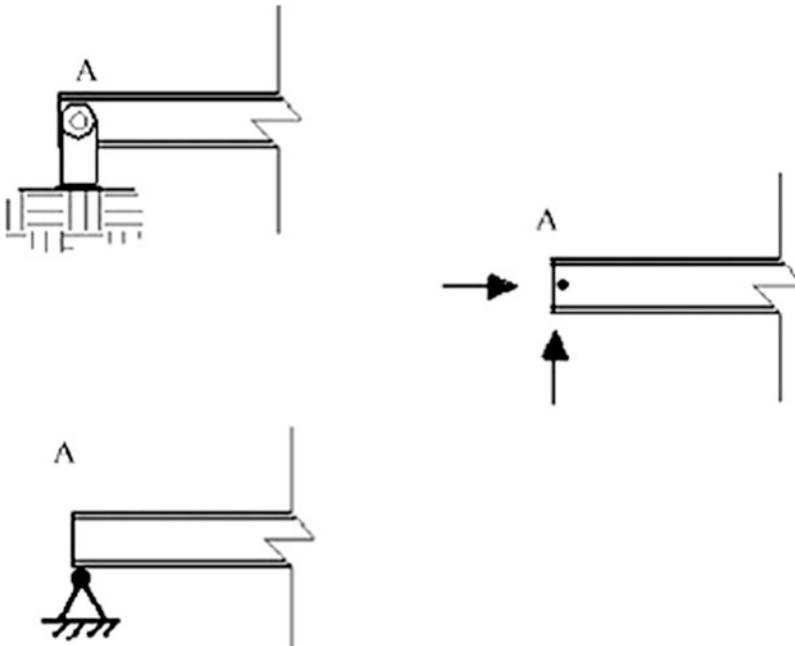
3.2.1 Fixed Support: Planar Loading

The beam is embedded at point A in such a way that the end is prevented from translating or rotating. We say the member is “fixed” at A. The reactions consist of two forces and one moment.



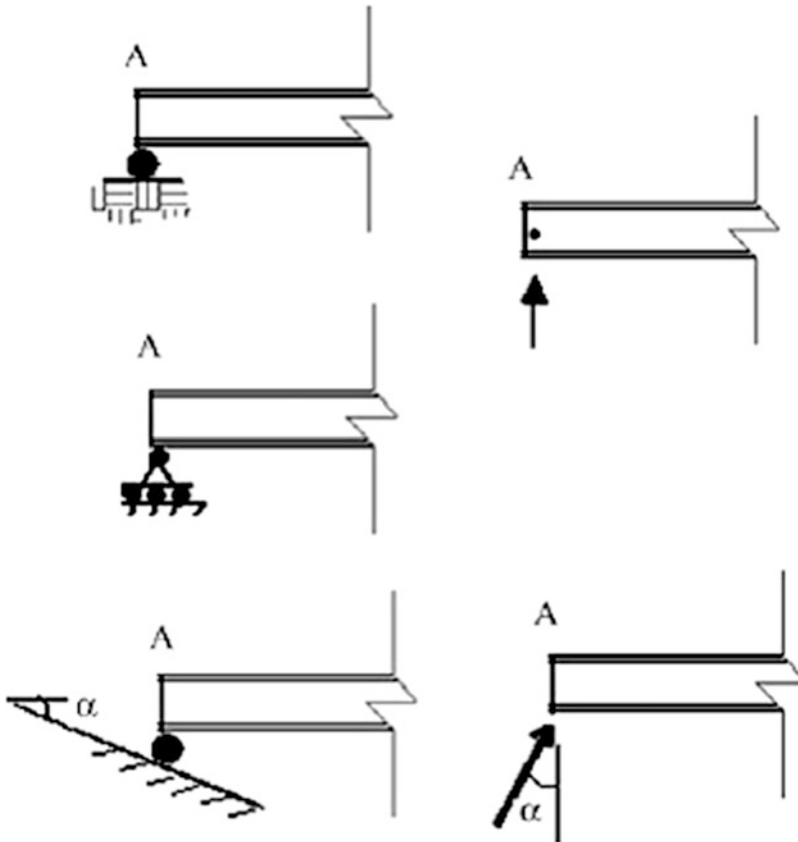
3.2.2 Hinged Support: Planar Loading

Suppose A is to be fully restrained against translation. This can be achieved by pinning the member. Horizontal and vertical reactions are produced.



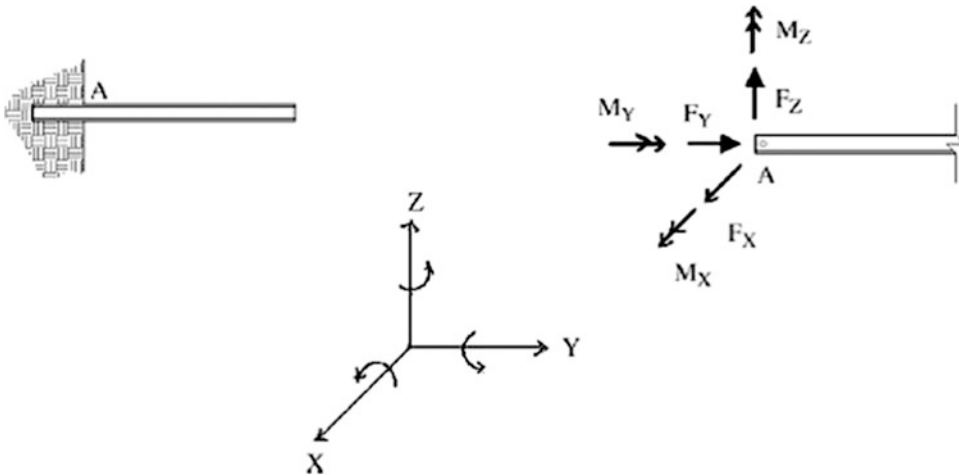
3.2.3 Roller Support: Planar Loading

Suppose A is to be restrained against motion perpendicular to the surface of contact. We add a restraint to A by inserting a device that allows motion parallel to the surface of contact but fully restrains motion in the direction perpendicular to the surface. We refer to this device as a roller. This restraint produces a reaction force perpendicular to the surface of contact.

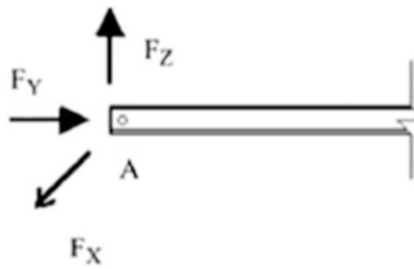


When the loading is three dimensional, additional restraints are required. The supports described above needs to be modified to deal with these additional restraints. Typical schemes are shown below.

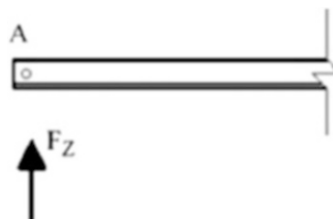
3.2.4 3-D Fixed Support



3.2.5 3-D Hinged Support



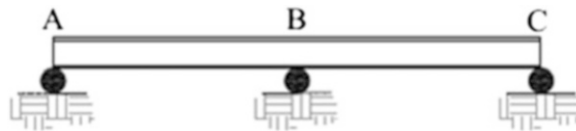
3.2.6 3-D Roller Support: Z Direction



3.2.7 Static Determinacy: Planar Beam Systems

In general, a body restrained with three *nonconcurrent* coplanar displacement constraints is stable for planar loading. When loading is applied, the only motion that occurs is due to deformation of the body resulting from the stresses introduced in the body by the loading. The motion restraints introduce reaction forces. Since there are three equations of force equilibrium for a body, and only three unknown forces, one can determine these force unknowns using only the force equilibrium equations. *In this case, we say that the structure is stable and statically determinate. If a body is over restrained, i.e., if there are more than three nonconcurrent displacement restraints, we say that the structure is statically indeterminate.* This terminology follows from the fact that now there are more than three force unknowns and consequently one cannot uniquely determine these unknowns with only the three available force equilibrium equations. Statically indeterminate structures require a more rigorous structural theory and therefore we postpone their treatment to part II of the text. In what follows, we present some examples of statically determinate and statically indeterminate planar beams.

3.2.8 Unstable Support Arrangements



The beam shown above has the proper number of constraints, but they are all vertical. There is no constraint against horizontal motion, and therefore the beam is unstable.



The beam shown above is unstable. The roller support at B constrains motion in the horizontal direction but does not prevent rigid body motion about point A.

3.2.9 Beam with Multiple Supports

There are three vertical restraints and one horizontal restraint. These restraints produce the four reaction forces shown below.

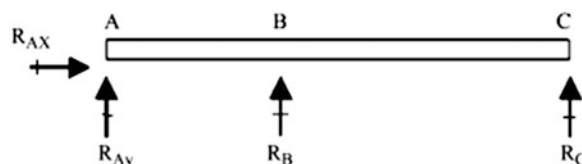


Fig. 3.7 Two-span beam

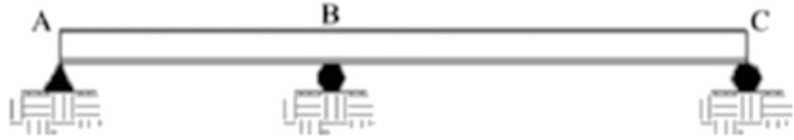


Fig. 3.8 Beam with moment release

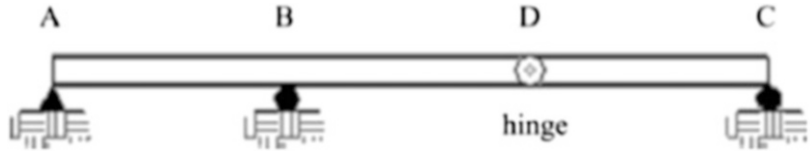
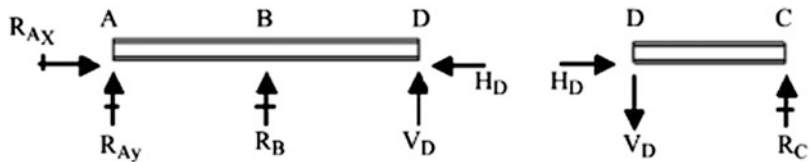
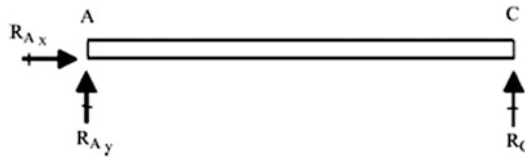


Fig. 3.9 Free body diagram for beam with moment release



One of the vertical restraints is redundant, i.e., is not needed for stability and therefore can be deleted. Deleting the support at B results in the structure shown below.



A beam supported only at its ends in a minimal way is referred to as a simple supported beam.



The beam depicted in Fig. 3.7 is called a two-span continuous beam. This beam is statically indeterminate to the first degree. We will show later that multi-span continuous beams are more structurally efficient than simply supported beams in the sense that they deflect less for a given design loading.

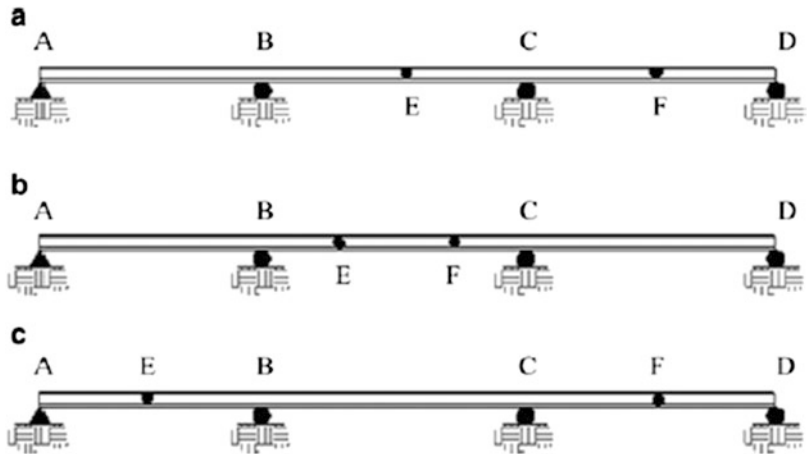
3.2.10 Beam with a Moment Release

Suppose we cut the beam shown in Fig. 3.8 at point D and insert a frictionless hinge. We refer to the hinge as a moment release since the moment is zero. The hinge does not restrain rotation at D, and member DC is free to rotate about D. The beam is now statically determinate. The corresponding reaction forces are listed below on the free body diagrams (Fig. 3.9).

Fig. 3.10 Three-span beam



Fig. 3.11 Statically determinate versions of three-span beam with moment releases



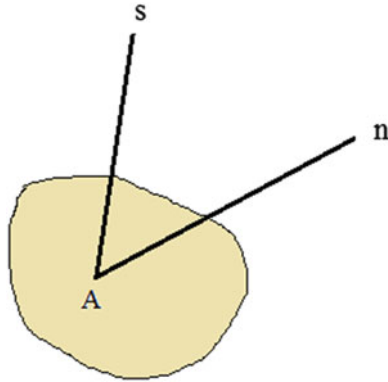
Member DC is statically determinate since there are only three reaction forces. Once the forces at D are known, the remaining reactions for member ABD can be determined. Therefore, it follows that inserting a hinge at D reduces the static indeterminacy by 1°.

We consider next the three-span continuous beam shown in Fig. 3.10. This structure is indeterminate to the second degree since there are two extra vertical supports. One can reduce the structure to a statically determinate structure by inserting two moment releases. Various possibilities are listed in Fig. 3.11. The optimal location of moment releases is illustrated in Examples 3.33 and 3.34.

3.3 Reactions: Planar Loading

When a structure is subjected to external loads, the displacement restraints develop reaction forces to resist the tendency for motion. If the structure is statically determinate, we can determine these forces using the three global force equilibrium equations for planar loading applied to a body. One selects a set of directions $n-n$ and $s-s$, where $s-s$ is not parallel to $n-n$. The steps are

- (i) Summation of forces in direction $n - n = 0$
 - (ii) Summation of forces in direction $s - s = 0$
 where direction $s - s$ is not parallel to direction $n - n$
 - (iii) Summation of moments about an arbitrary point, $A = 0$
- (3.2)



One constructs a free body diagram of the structure and applies these equations in such a way as to obtain a set of uncoupled equations, which can be easily solved.

When a statically indeterminate structure has a sufficient number of releases such that it is reduced to being statically determinate, we proceed in a similar way except that now we need to consider more than one free body. The following series of examples illustrate the strategy for computing the reactions.

Example 3.1 Beam with Two Over Hangs

Given: The beam shown in Fig. E3.1a.

Determine: The reactions.

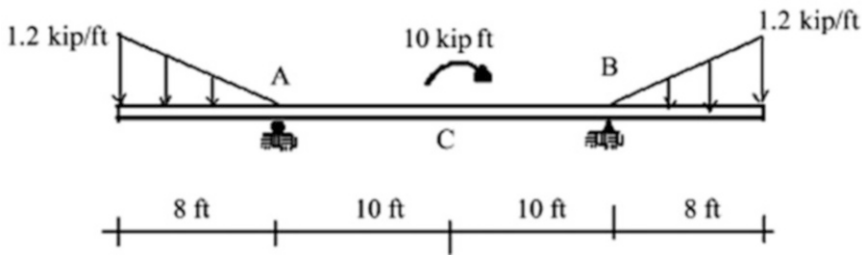


Fig. E3.1a

Solution: Summing moments about B leads to the vertical reaction at A.

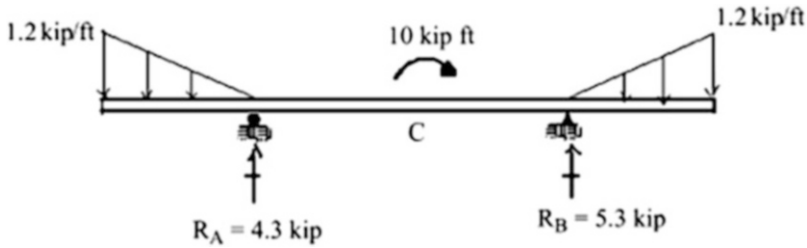
$$\begin{aligned}\sum M_B &= 0 \\ R_A(20) + 10 + \frac{1}{2}(1.2)(8)\frac{2}{3}(8) - 1.2\left(\frac{8}{2}\right)\left(20 + \frac{2}{3}8\right) &= 0 \\ \therefore R_A &= 4.3 \uparrow\end{aligned}$$

Summing the vertical forces,

$$\sum F_Y = 0 \quad R_B + 4.3 - 1.2 \left(\frac{8}{2} \right) (2) = 0$$

$$\therefore R_B = 5.3 \uparrow$$

The reactions are listed below.



Example 3.2 Simply Supported Beam

Given: The beam shown in Fig. E3.2a.

Determine: The reactions.

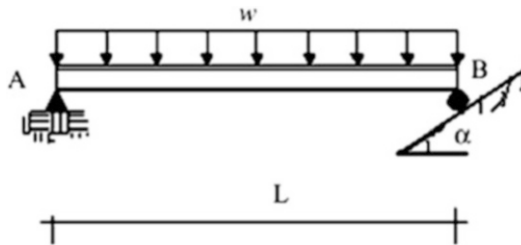


Fig. E3.2a

Solution: As a first step, we construct the free body diagram for the beam. The reaction at B is normal to the inclined surface. We resolve it into horizontal and vertical components using (Fig. E3.2b)

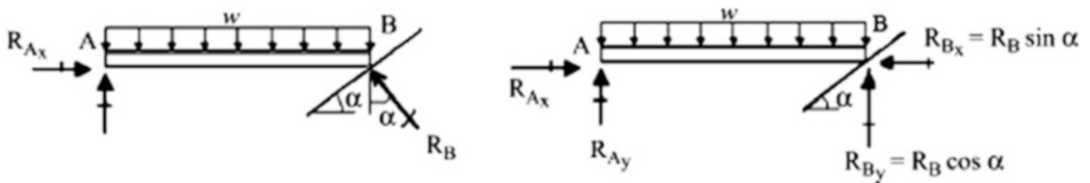


Fig. E3.2b

$$R_{By} = R_B \cos \alpha \quad R_{Bx} = R_B \sin \alpha$$

Summing moments about A leads to the vertical reaction at B.

$$\begin{aligned}\sum M_A &= 0 \\ wL\left(\frac{L}{2}\right) - LR_{By} &= 0 \\ \therefore R_{By} &= \frac{wL}{2} \uparrow\end{aligned}$$

Given R_{By} , we find the reaction R_B

$$R_B = \frac{R_{By}}{\cos \alpha} = \frac{wL}{2 \cos \alpha}$$

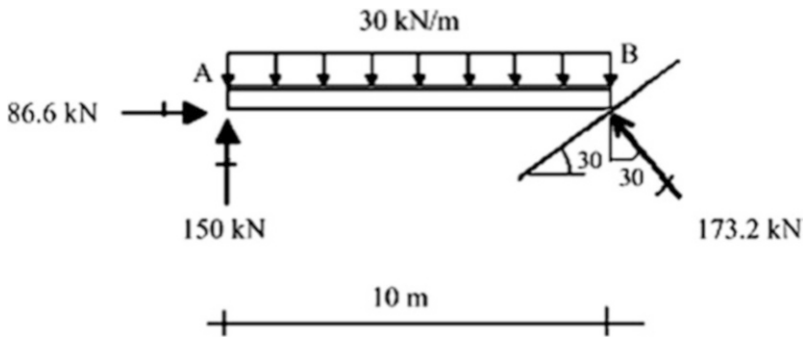
The corresponding horizontal component is

$$R_{Bx} = R_B \sin \alpha = \frac{wL}{2} \tan \alpha \leftarrow$$

We determine the reactions at A using force summations.

$$\begin{aligned}\sum F_x = 0 \quad R_{Ax} &= -R_{Bx} = \frac{wL}{2} \tan \alpha \rightarrow \\ \sum F_y = 0 \uparrow^+ \quad R_{Ay} + R_{By} - wL &= 0 \quad R_{Ay} = \frac{wL}{2} \uparrow\end{aligned}$$

Suppose $w = 30 \text{ kN/m}$, $\alpha = 30^\circ$ and $L = 10 \text{ m}$. The reactions are listed below.



Example 3.3 Two-Span Beam with a Moment Release

Given: The beam shown in Fig. E3.3a. There is a moment release at D.

Determine: The reactions.

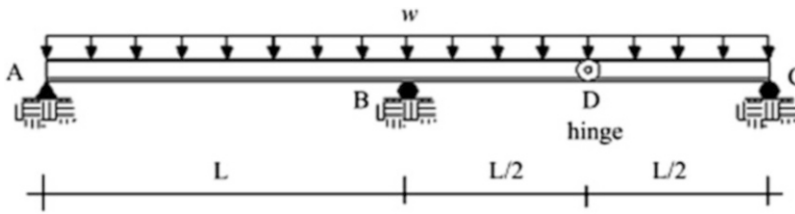
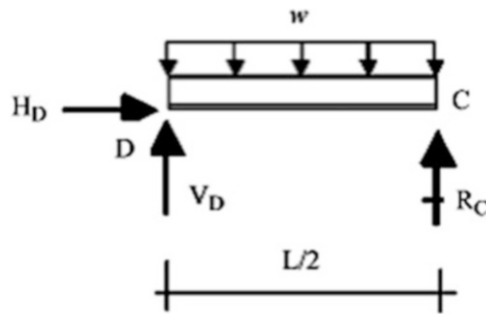


Fig. E3.3a

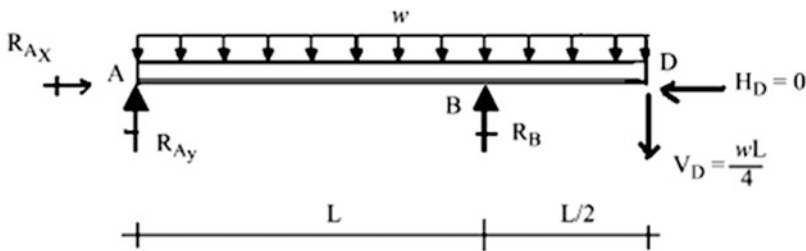
Solution: The most direct way of analyzing this structure is to first work with a free body diagram of beam segment DC.



Applying the equilibrium conditions to this segment results in

$$\begin{aligned} \sum M_D = 0 \quad R_C &= \frac{wL}{4} \uparrow \\ \sum F_Y = 0 \quad V_D &= \frac{wL}{4} \uparrow \\ \sum F_x = 0 \quad H_D &= 0 \end{aligned}$$

With the internal forces at D known, we can now proceed with the analysis of segment ABD.



Summing moments about A leads to R_B

$$\sum M_A = 0 \quad (0.75L)(1.5wL) + (1.5L)(0.25wL) - LR_B = 0$$

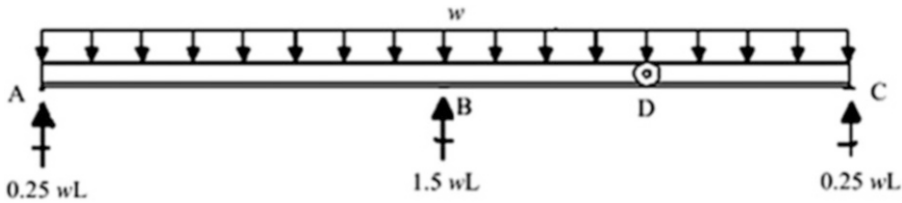
$$R_B = 1.5wL \uparrow$$

Summing the vertical and horizontal forces,

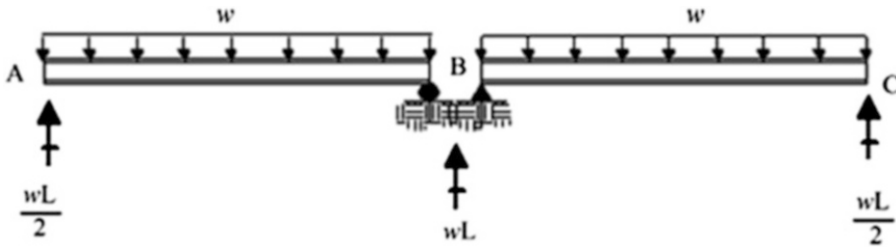
$$\sum F_Y = 0 \quad R_{Ay} = 1.75wL - R_B = 0.25wL \uparrow$$

$$\sum F_x = 0 \quad R_{Ax} = 0$$

The reactions are listed below.



If the hinge was placed at point B, the structure would act as two simply supported beams, and the reactions would be as shown below.



Example 3.4

Given: The beam shown in Fig. E3.4a.

Determine: The reactions.

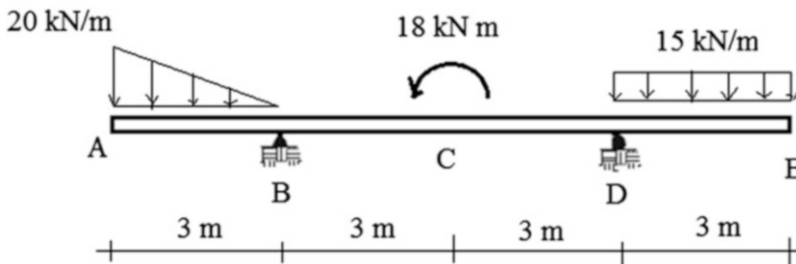


Fig. E3.4a

Solution: Summing moments about B leads to the vertical reaction at D.

$$\sum M_B = 0$$

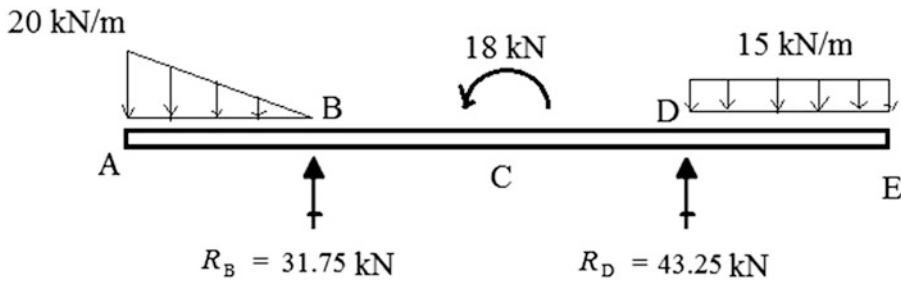
$$R_D(6) + 20\left(\frac{3}{2}\right)(2) + 18 - 15(3)(7.5) = 0 \quad \therefore R_D = 43.25 \uparrow$$

Summing the vertical forces,

$$\sum F_Y = 0 \quad R_B + 43.25 - 15(3) - 20\left(\frac{3}{2}\right) = 0$$

$$\therefore R_B = 31.75 \uparrow$$

The reactions are listed below.



Example 3.5 Three-Span Beam with Two Moment Releases

Given: The beam shown in Fig. E3.5a.

Determine: The reactions.

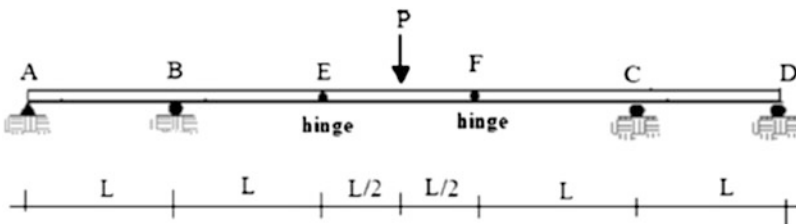
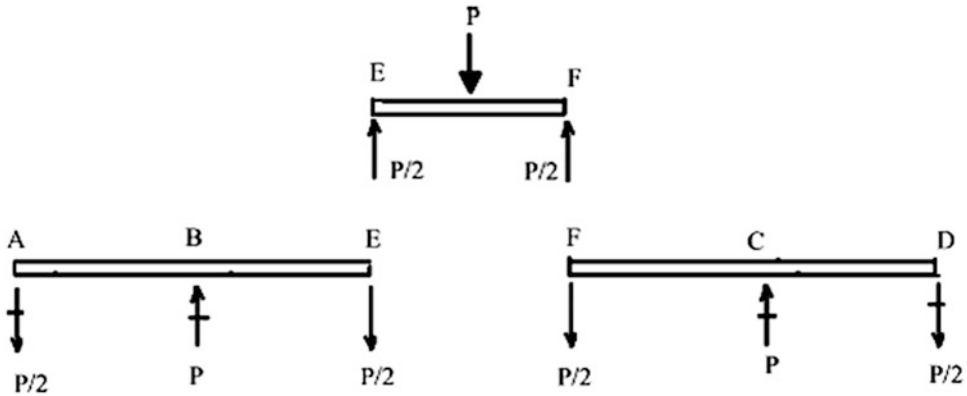
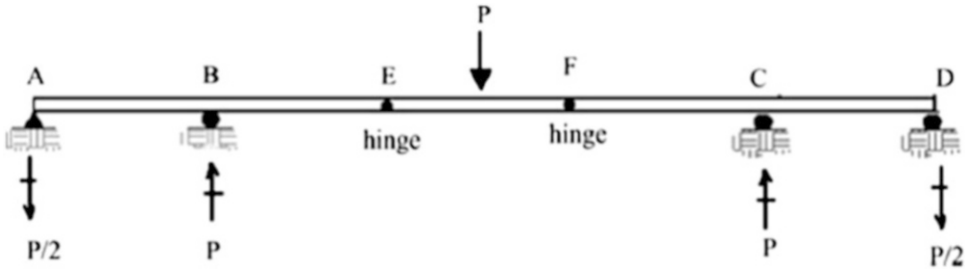


Fig. E3.5a

Solution: We first work with a free body diagram of beam segment EF. Then, with the internal forces at E and F known, we proceed with the analysis of segment ABE and FCD.



The reactions are listed below.



Example 3.6 Horizontal Beam Supporting a Vertical Sign

Given: The structure defined in Fig. E3.6a. Member BED is rigidly attached to the beam, ABC. Member FG is simply supported on member BED. Assume member FG has some self-weight, W and is acted upon by a uniform horizontal wind load p . This structure is an idealization of a highway sign supported on a beam.

Determine: The reactions.

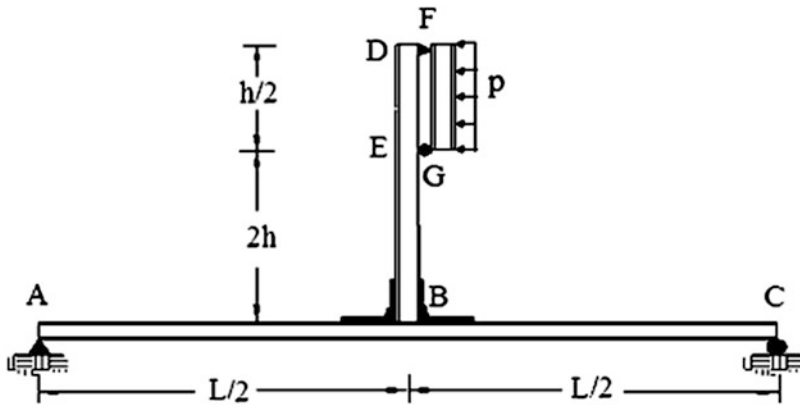
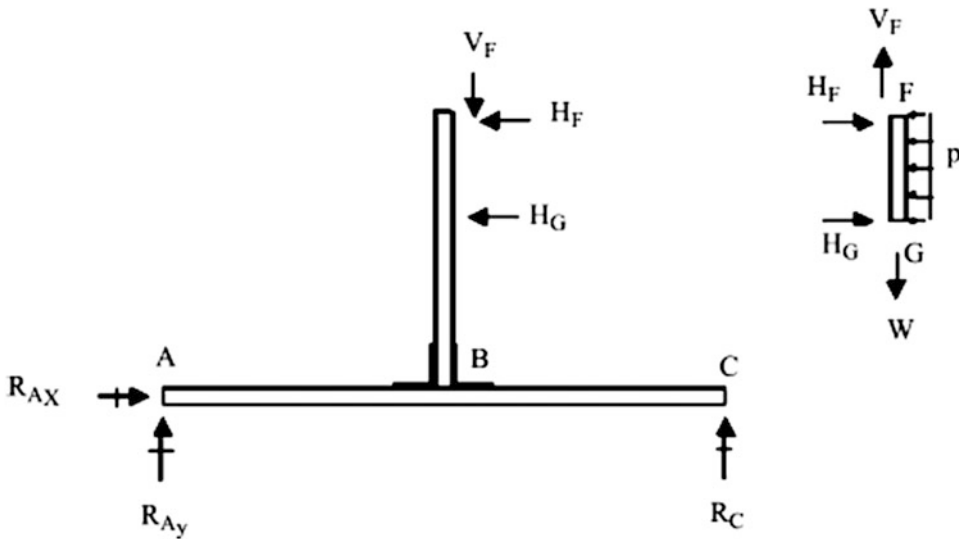


Fig. E3.6a

Solution: We work with two free body diagrams, one for member FG and the other for the remaining part of the structure.

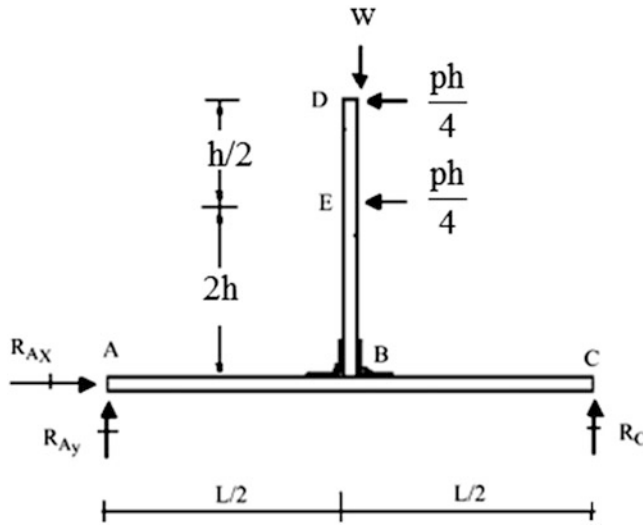


Consider first member FG. Enforcing equilibrium leads to:

$$V_F = W$$

$$H_F = H_G = \frac{ph}{4}$$

Next, we apply these forces to the structure composed of member ABC and member BED. The free body diagram is shown below.



Summing moments about A leads to R_C

$$\begin{aligned}\sum M_A &= 0 \\ W\frac{L}{2} &= \frac{ph}{4}(2h) + \frac{ph}{4}(2.5h) + R_C L \\ \therefore R_C &= \frac{W}{2} - ph\left(1.125\frac{h}{L}\right)\end{aligned}$$

The horizontal and vertical reactions at A are

$$\begin{aligned}R_{Ax} &= \frac{ph}{2} \\ R_{Ay} &= \frac{W}{2} + ph\left(1.125\frac{h}{L}\right)\end{aligned}$$

Note that the vertical reaction at C may become negative if ph is large with respect to W and h is of the order of L .

3.4 Internal Forces: Planar Loading

We have shown that external loads produce reaction forces. The next question we need to address is: What is the effect of this combination of external loads and reaction forces on the body? We answer this question by examining the equilibrium of an arbitrary segment of the body.

Consider the uniformly loaded, simply supported beam shown in Fig. 3.12a. We pass a cutting plane a distance x from the left end and consider either the left or right segment.

The external loads create a force unbalance. To maintain equilibrium, a vertical force, $V(x)$, and a moment, $M(x)$, are required at the section. We refer to these quantities as the *internal shear force and bending moment*. The magnitudes of $V(x)$ and $M(x)$ for this section are

Fig. 3.12 Internal shear and moment. (a) beam. (b) Segmented beam

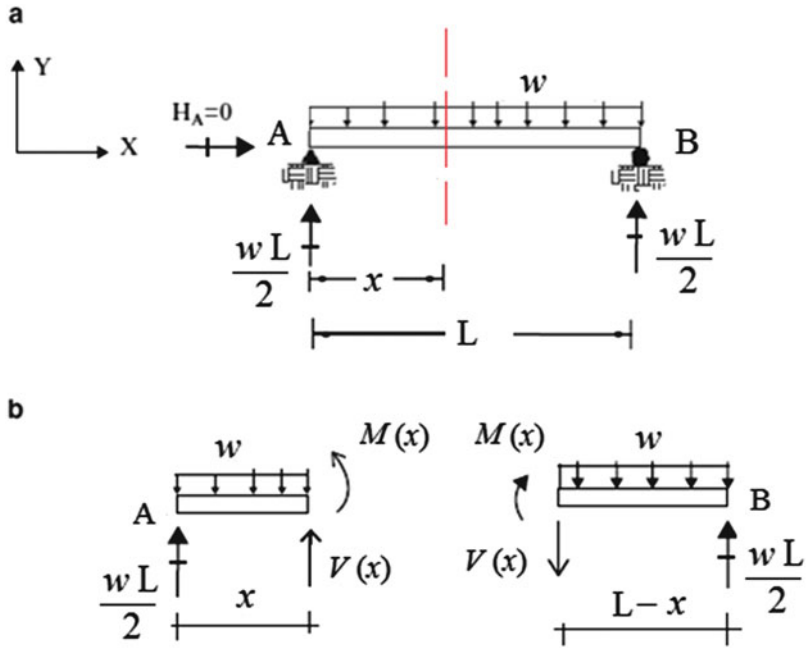
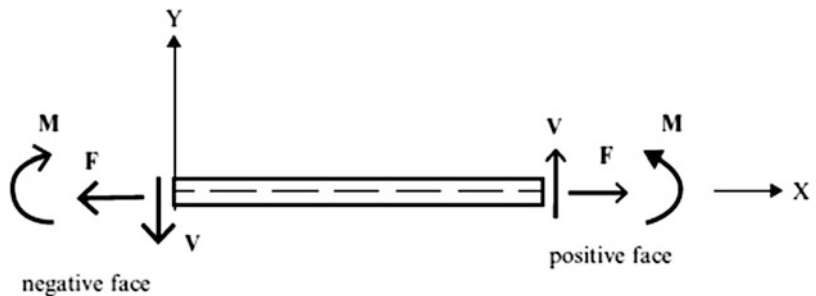


Fig. 3.13 Sign convention for internal forces



$$\begin{aligned}
 V(x) &= -\frac{wL}{2} + wx \\
 M(x) &= \frac{wL}{2}x - \frac{wx^2}{2}
 \end{aligned}
 \tag{3.3}$$

We need to first define a sign convention for the positive directions of the internal force quantities. This notation is shown in Fig. 3.13 for a positive face, i.e., a face whose outward normal points in the $+X$ direction. The shear force is positive when it points in the $+Y$ direction, and the positive sense for moment is from X to Y . Depending on the external loading, there may also be an axial force. The positive sense for the axial force is taken as the $+X$ direction. These directions are reversed for a negative face.

This sign convention is also used in the matrix formulation of the beam bending problem which is the basis for computer-based analysis software. Historically, some authors use a sign convention for shear which is opposite to this choice. We prefer to employ the above convention since it is consistent with the output of structural software systems and therefore allows the reader to transition easily from analytical to digital computation schemes.

Fig. 3.14 Shear and moment diagrams

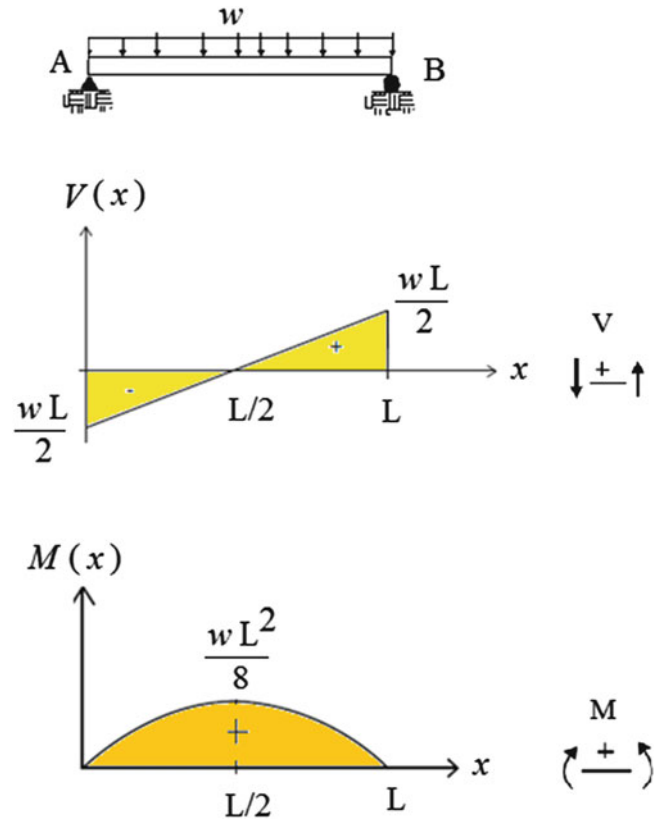


Figure 3.14 shows the variation of these quantities for the beam defined in Fig. 3.12. The shear varies linearly, with maximum values at the supports. The moment varies parabolically, and the maximum value occurs at mid-span. These plots are called “shear” and “moment” diagrams. Positive moment is plotted on the top face in the USA. In the UK, positive moment is plotted on the bottom face. Again, it is a question of what convention one is most comfortable with.

The maximum bending moment and shear force are used to determine the dimensions of the cross-section. The specific design procedure depends on the material selected, such as wood, steel, or concrete, and the design code adopted.

One constructs the internal force distributions by selecting various cutting planes, evaluating the corresponding values, and then extrapolating between the sections. With some experience, one can become very proficient at this operation. We illustrate the process with the following examples.

Example 3.7 Cantilever Beam with Multiple Concentrated Loads

Given: The cantilever beam with two concentrated loads shown in Fig. E3.7a.

Determine: The shear and moment diagrams.

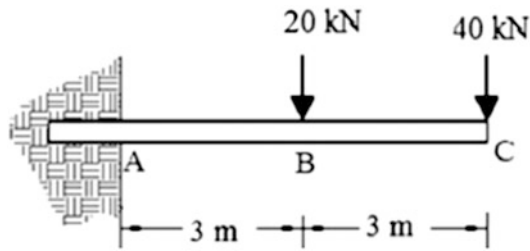
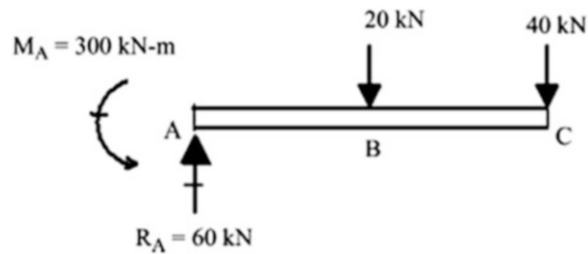


Fig. E3.7a

Solution: We first determine the reactions at A by enforcing the equilibrium equations.

$$\sum F_y = 0 \quad R_A - 20 - 40 = 0 \Rightarrow R_A = 60 \text{ kN}$$

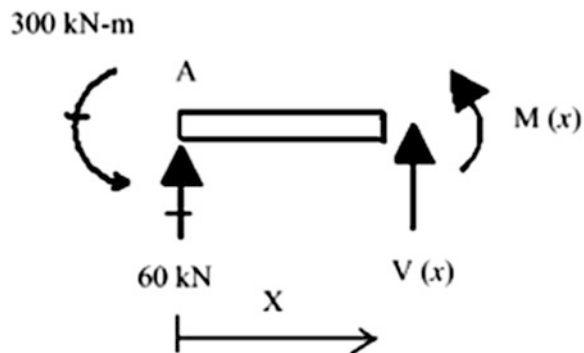
$$\sum M_A = 0 \quad M_A - 20(3) - 40(6) = 0 \Rightarrow M_A = 300 \text{ kN}\cdot\text{m}$$



Then, we pass a cutting plane between points A and B

$$0 \leq x < 3 \quad V(x) = -60$$

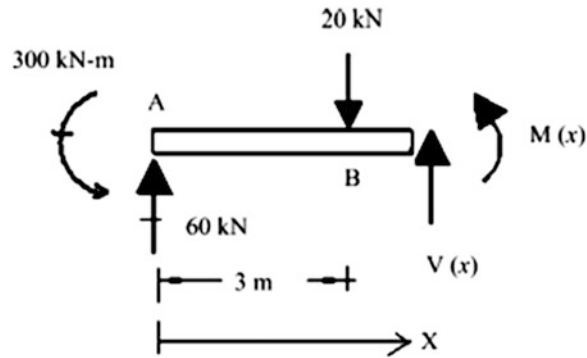
$$M(x) = -300 + 60x$$



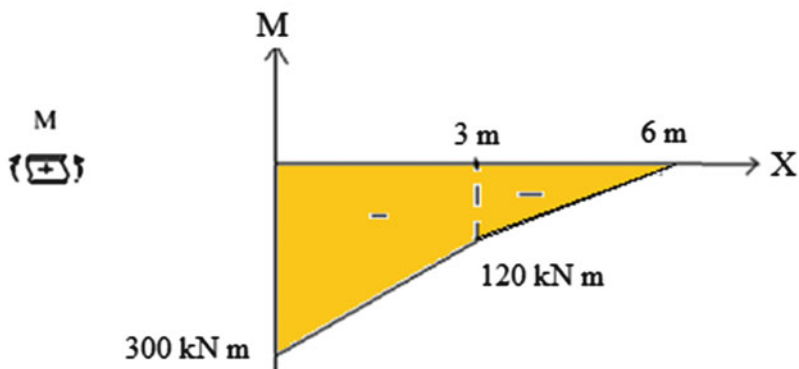
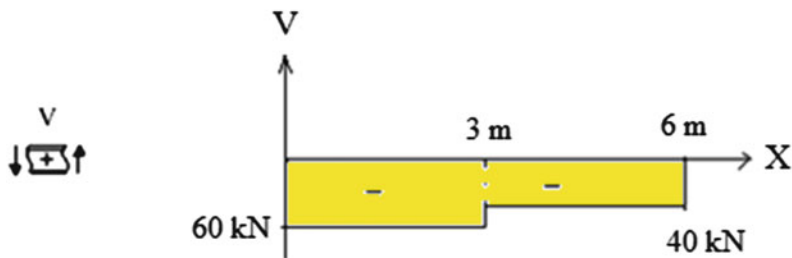
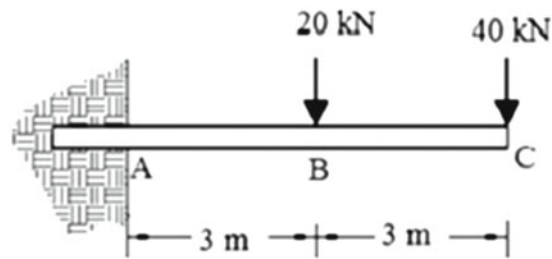
Lastly, we cut between B and C.

$$3 < x \leq 6 \quad V(x) = -40$$

$$M(x) = -300 + 60x - 20(x - 3) = 40x - 240$$



The distributions are plotted below.



There are some features that we want to point out. Firstly, a concentrated load produces a discontinuity in the form of a “jump” in the shear force, such as at points B and C. Secondly, when the loading consists only of concentrated loads, the shear diagram consists of segments having constant values, and the moment diagram is composed of a set of straight-line segments. We have demonstrated these features here. Later in the next section, we will establish a proof based on equilibrium considerations. A thought question: When would the moment diagram have a jump in the moment value? Hint: Consider Example 3.15.

Example 3.8 Cantilever Beam with Uniform Loading

Given: The uniformly loaded cantilever beam shown in Fig. E3.8a.

Determine: The shear and moment distributions.

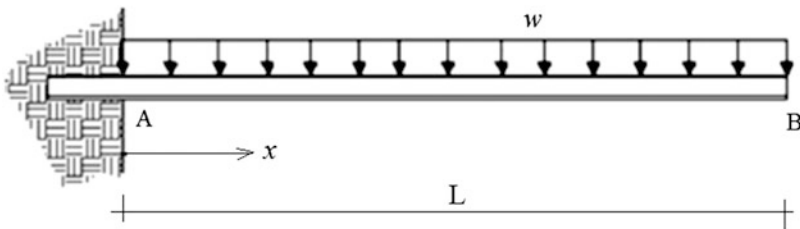
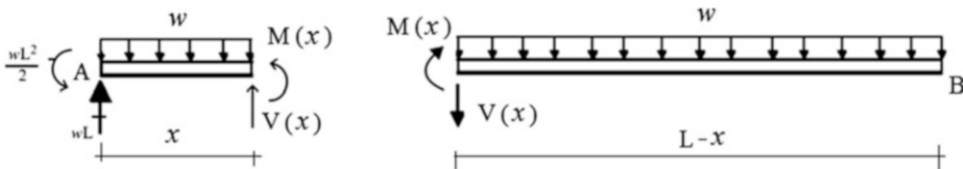


Fig. E3.8a

Solution: We pass a cutting plane between points A and B. Then, we can consider either segment shown below.

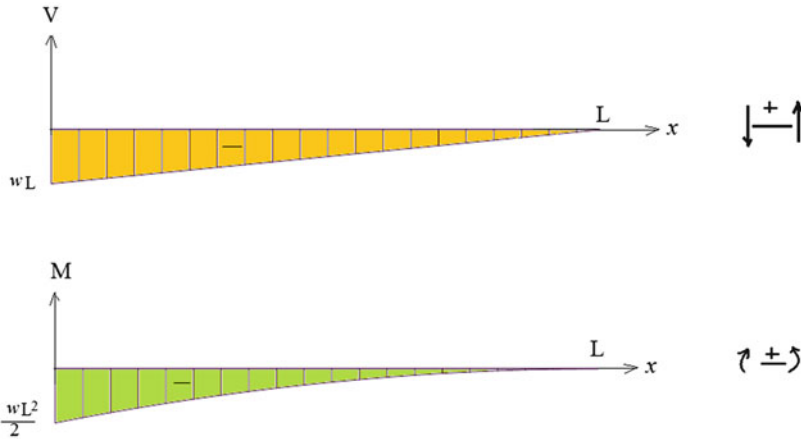


The shear and moment required for equilibrium are

$$0 \leq x \leq L \quad V(x) = -w(L-x)$$

$$M(x) = -\frac{w}{2}(L-x)^2$$

These functions are plotted below. Note that the maximum moment varies as L^2 .



Example 3.9 Beam with an Eccentric Lateral Load

Given: The structure defined in Fig. E3.9a. Member BC is rigidly attached to member AB at B.

Determine: The axial, shear, and moment diagrams.

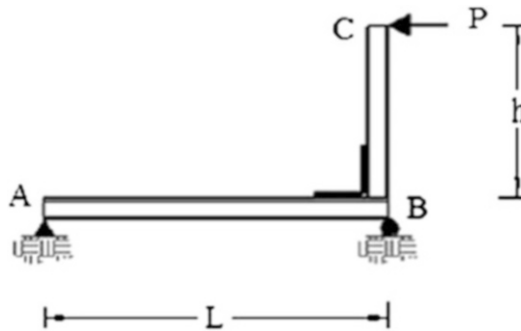


Fig. E3.9a

Solution: Member BC is rigidly attached to the beam, AB, and has a horizontal load applied at its end. The effect of this force is to apply a bending moment at B, which causes beam AB to bend. Figure E3.9b illustrates the deflected shape.

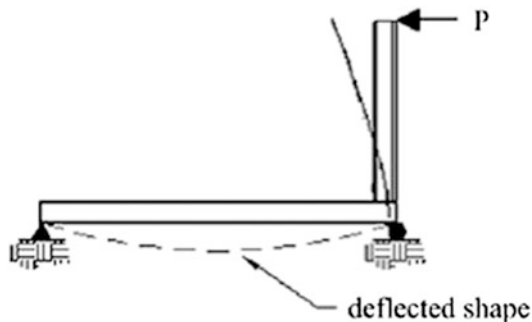
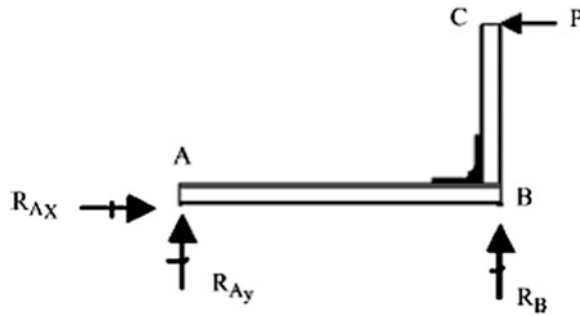


Fig. E3.9b

We determine the reactions first. The free body diagram is shown below.



Moment summation about A leads to

$$\sum M_A = 0$$

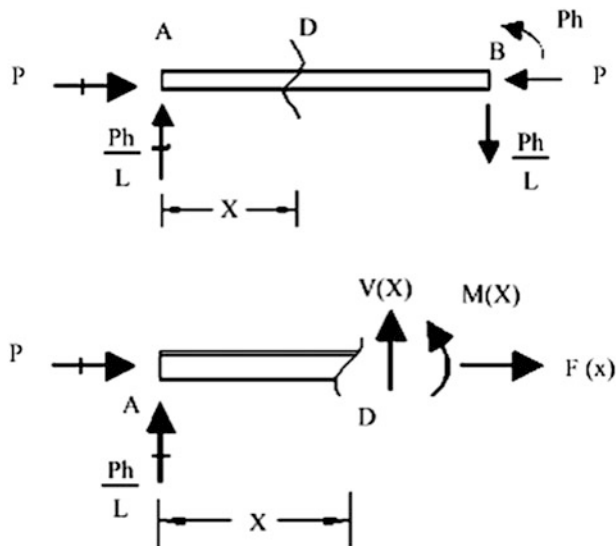
$$R_B L + Ph = 0 \Rightarrow R_B = -\frac{h}{L}P \Rightarrow R_B = \frac{h}{L}P \downarrow$$

The reactions at A required for equilibrium are

$$\sum F_y = 0 \Rightarrow R_{Ay} = -V_B = \frac{h}{L}P \Rightarrow R_{Ay} = \frac{h}{L}P \uparrow$$

$$\sum F_x = 0 \Rightarrow R_{Ax} = P \rightarrow$$

Next, we pass a cutting plane at D, isolate the left segment, and enforce equilibrium.



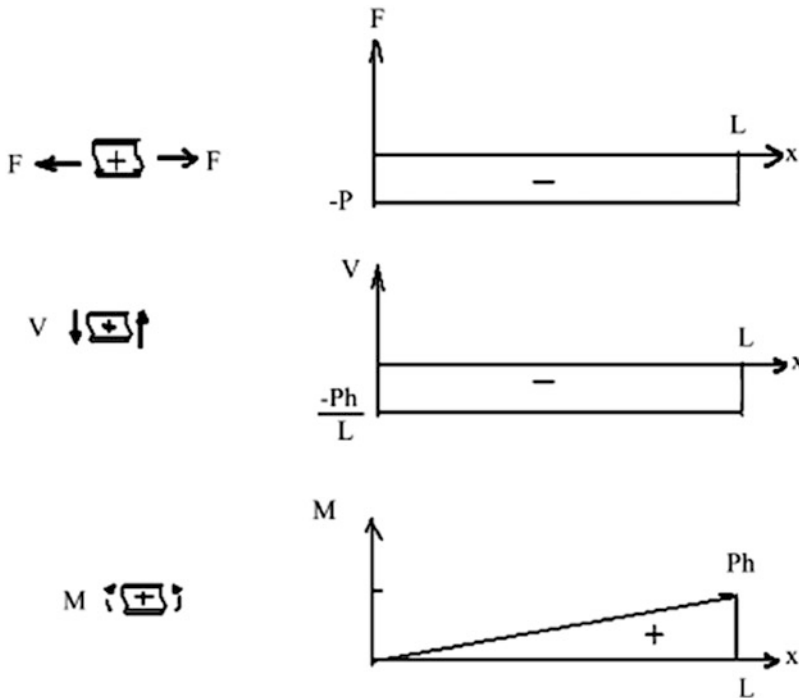
The results are

$$V(x) = -Ph/L$$

$$M(x) = (Ph/L)x$$

$$F(x) = -P$$

The beam is subjected to combined compression and bending: The maximum moment is equal to Ph and occurs at B. This is the critical section for design. Plots of F , V , and M for member AB are shown below.



3.5 Differential Equations of Equilibrium: Planar Loading

The strategy described in the previous section was based on working with a free body diagram of a large segment of the beam and determining the shear and moment by applying the equilibrium equations. We generate the distributions of these quantities by selecting various free body diagrams. This approach is convenient when the loading is fairly simple, i.e., it consists of a combination of concentrated forces and uniformly distributed loadings. For complex distributed loadings expressed as analytic functions, one needs a more systematic approach for enforcing the equilibrium conditions. In what follows, we describe an approach based on applying the equilibrium conditions to a differential element of the beam, resulting in a set of differential equations relating the shear force and moment to the applied distributed loading.

Consider the beam and the differential element shown in Fig. 3.15. We use the same sign convention for V and M as defined in Sect. 3.4. We take the positive sense of the distributed loading to be “downward” since these loadings are generally associated with gravity. Considering V and M to be functions of x , expanding these variables in terms of their differentials, and retaining up to first-order terms results in the forces shown in Fig. 3.15b.

Summing forces in the Y direction,

$$V + \frac{dV}{dx} \frac{dx}{2} - \left(V - \frac{dV}{dx} \frac{dx}{2} \right) - w dx = 0$$

and combining terms leads to

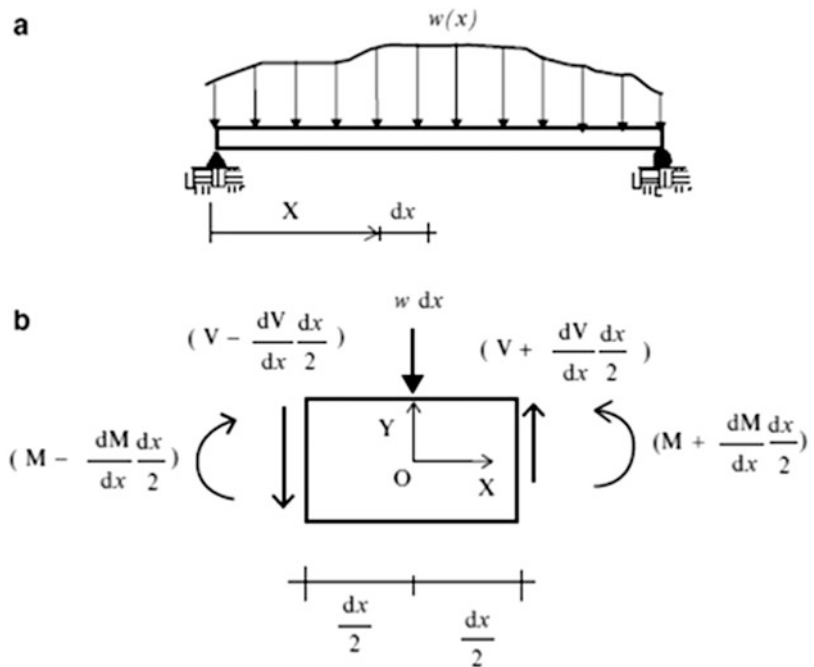
$$\left(\frac{dV}{dx} - w \right) dx = 0$$

Lastly, since this equation must be satisfied for arbitrary dx , it follows that

$$\frac{dV}{dx} = w \tag{3.4}$$

In words, “the rate of change of the shear force is equal to the applied distributed loading.” Repeating this analysis for moment summation about point o , the steps are

Fig. 3.15 Beam with arbitrary distributed loading. (a) Beam. (b) Differential beam element



$$\begin{aligned}
 M + \frac{dM}{dx} \frac{dx}{2} - \left(M - \frac{dM}{dx} \frac{dx}{2} \right) + \left(V + \frac{dV}{dx} \frac{dx}{2} \right) \frac{dx}{2} + \left(V - \frac{dV}{dx} \frac{dx}{2} \right) \frac{dx}{2} &= 0 \\
 \Downarrow \\
 \left(\frac{dM}{dx} + V \right) dx &= 0 \\
 \Downarrow \\
 \frac{dM}{dx} + V &= 0 \\
 \Downarrow \\
 \frac{dM}{dx} &= -V
 \end{aligned} \tag{3.5}$$

Equation (3.5) states that “the rate of change of the bending moment is equal to minus the shear force.”

These two relations are very useful for checking the consistency of the shear and moment diagrams. One can reason qualitatively about the shape of these diagrams using only information about the loading on a segment of the beam. For example, if $w = 0$, the shear is constant and the moment varies linearly. If $w = \text{constant}$, the shear varies linearly and the moment varies quadratically.

One can establish a set of integral equations by integrating the derivative terms. Consider two points, x_1 and x_2 , on the longitudinal X -axis. Integrating (3.4) and (3.5) between these points leads to

$$V_2 - V_1 = \int_{x_1}^{x_2} w \, dx \tag{3.6}$$

$$M_2 - M_1 = - \int_{x_1}^{x_2} V \, dx \tag{3.7}$$

Equation (3.6) can be interpreted as: “The difference in shear between two points is equal to the area under the distributed loading diagram included between these points.” Equation (3.7) relates the change in moment to the area under the shear diagram between these points. Figure 3.16 illustrates these interpretations.

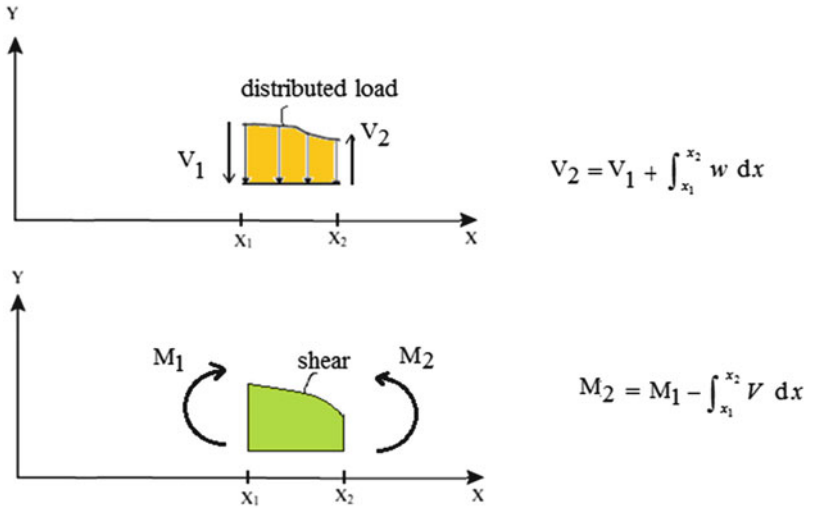
The integral forms are useful if one wants to either compute values at discrete points or determine analytical solutions. The differential forms are more convenient for qualitatively reasoning about the shape of the diagrams. We generally use both approaches to construct shear and moment diagrams.

Another useful property that can be established from (3.5) relates to the maximum values of the moment. We know from calculus that extreme values of a continuous function are located at points where the first derivative is zero. Applying this theorem to the moment function, $M(x)$, the location x^* , of an extreme value (either maximum or minimum) of moment is found by solving:

$$\left. \frac{dM}{dx} \right|_{x=x^*} = 0 \tag{3.8}$$

Noting (3.5), it follows that *extreme values of moment occur at points where the shear force is zero*. One first generates the shear diagrams from the applied loading. This process identifies the points of zero shear. If only peak values of moment are of interest, one selects free body diagrams by passing cutting planes through these locations and applies the equilibrium conditions. This approach is the most direct procedure.

Fig. 3.16 Interpretation of shear and moment in terms of segmental loadings



When the loading consists of concentrated forces, the shear diagram has a discontinuity at the point of application of each concentrated force. By considering the equilibrium of a differential element at the point (see Fig. 3.17), one can establish that the “jump” in shear is equal to the applied load. Similarly, the jump in moment is equal to the applied external moment, M .

$$V_{+face} - V_{-face} = P \tag{3.9}$$

$$M_{+face} - M_{-face} = -M \tag{3.10}$$

One applies (3.6) and (3.7) to generate solutions for the segments adjacent to the discontinuities and uses (3.9) and (3.10) to connect the solutions.

In what follows, we illustrate the application of the differential/integral equation representation to generate shear and moment diagrams. This material overlaps slightly with the material presented in the previous section. Some repetition is useful for reinforcing basic concepts.

Example 3.10 Cantilever Beam—Triangular Loading

Given: A cantilever beam with a triangular distributed loading (Fig. E3.10a).

Determine: $V(x)$ and $M(x)$.

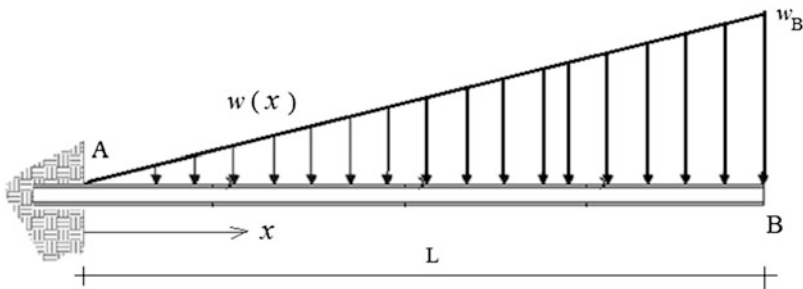
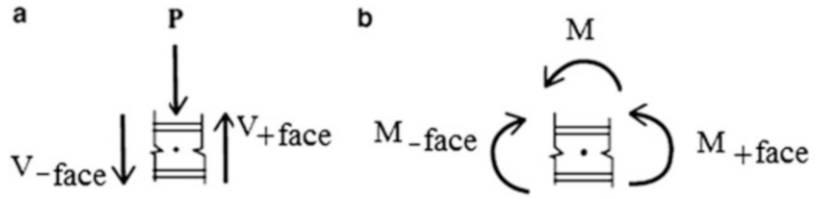


Fig. E3.10a

Fig. 3.17 Jump conditions. (a) Shear. (b) Moment



Solution: First, we determine the reactions at A (Fig. E3.10b)

$$\sum F_Y = 0 \quad R_A = \frac{w_B L}{2} \uparrow$$

$$\sum M_A = 0 \quad M_A = \frac{w_B L^2}{3}$$

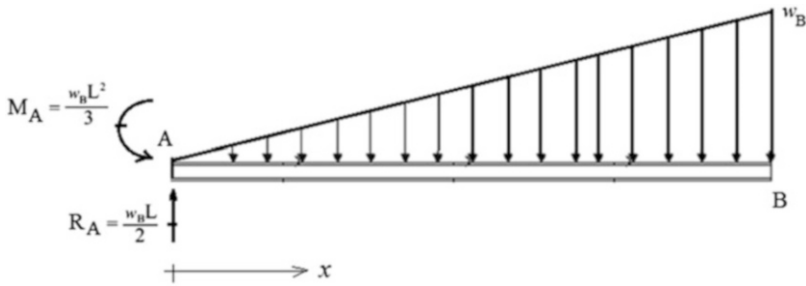


Fig. E3.10b Reactions

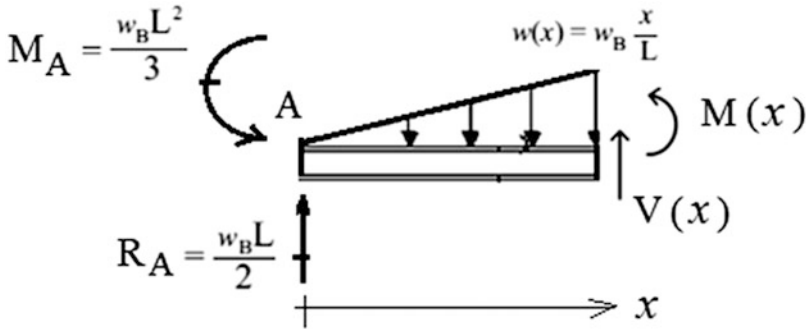


Fig. E3.10c Internal shear and moment

Next, we determine the shear, $V(x)$, with (3.6) (Fig. E3.10c). Integrating between points A and x

$$V(x) - V_A = \int_0^x w(x) dx = \int_0^x \frac{w_B x}{L} dx = \frac{w_B x^2}{2L} \Big|_0^x = \frac{w_B x^2}{2L}$$

Noting that $V_A = -R_A = -\frac{w_B L}{2}$, the solution for $V(x)$ reduces to

$$V(x) = \frac{w_B}{2} \left(-L + \frac{x^2}{L} \right)$$

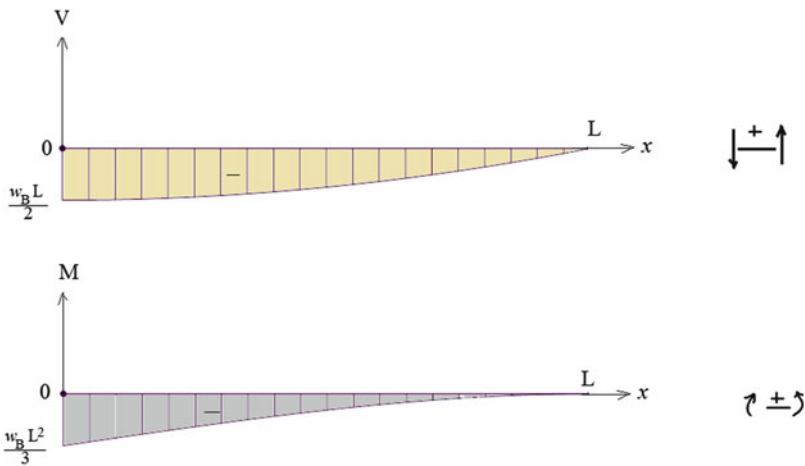
We determine the moment, $M(x)$, with (3.7)

$$M(x) - M_A = - \int_0^x V(x) dx = \int_0^x \frac{w_B}{2} \left(L - \frac{x^2}{L} \right) dx = \frac{w_B}{2} \left(Lx - \frac{x^3}{3L} \right)$$

Noting that $M_A = -\frac{w_B L^2}{3}$, one obtains

$$M(x) = w_B \left(-\frac{x^3}{6L} + \frac{Lx}{2} - \frac{L^2}{3} \right)$$

The shear and moment distribution are plotted below. Note that the peak values of shear and moment occur at $x = 0$. Also note that the boundary conditions at B are $V_B = M_B = 0$ since this cross-section is free, i.e., unrestrained and unloaded.



Example 3.11 Distributed and Concentrated Loads

Given: The beam and loading defined in Fig. E3.11a.

Determine: $V(x)$ and $M(x)$.

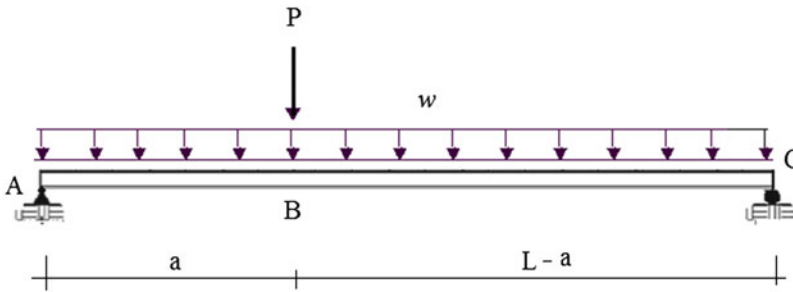


Fig. E3.11a

Solution: This example illustrates how to deal with a combination of distributed and concentrated loads. We separate the distributed and the concentrated loads and then superimpose the results (Fig. E3.11b).

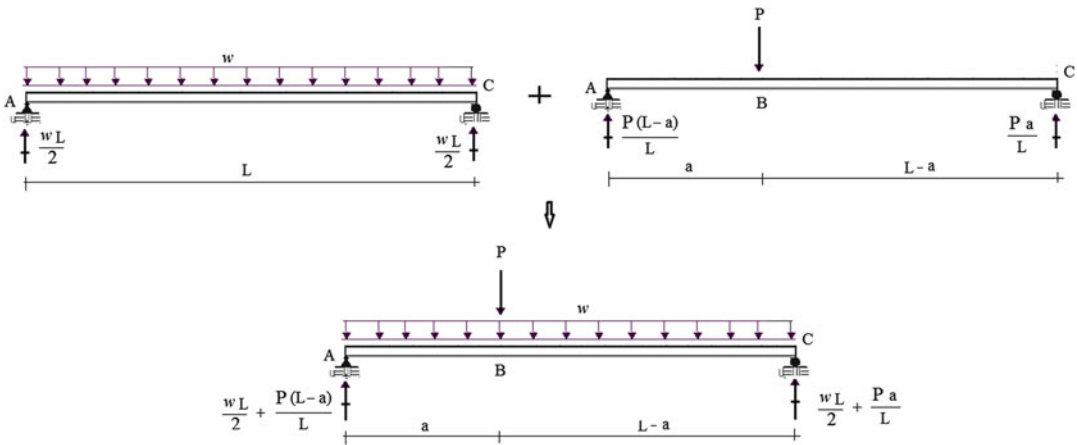


Fig. E3.11b Reactions

We consider first the segment AB. Applying (3.6) and (3.7), and noting the boundary conditions at $x = 0$, the distributions for $0 \leq x < a$ are

$$V(x) = -\frac{wL}{2} - \frac{(L-a)P}{L} + wx$$

$$M(x) = \frac{wL}{2}x + \frac{P(L-a)}{L}x - \frac{1}{2}wx^2$$

The values of V and M just to the left of point B are

$$V_{B-} = -\frac{wL}{2} + wa - \frac{P(L-a)}{L}$$

$$M_{B-} = \frac{wL}{2}a - \frac{1}{2}wa^2 + \frac{P(L-a)}{L}a$$

Applying (3.9) and (3.10) for the jump conditions at B, and noting signs, the quantities just to the right of B are

$$V_{B+} = P + V_{B-} = -\frac{wL}{2} + wa - \frac{Pa}{L}$$

$$M_{B+} = M_{B-} = \frac{wL}{2}a - \frac{1}{2}wa^2 + \frac{P(L-a)}{L}a$$

Note that there is no jump in moment for this example. Applying (3.6) and (3.7), these expressions for $a < x \leq L$ expand to

$$V(x) = \frac{Pa}{L} - \frac{wL}{2} + wx$$

$$M(x) = Pa - \frac{Pax}{L} + \frac{wLx}{2} - \frac{wx^2}{2}$$

The approach we followed here is general and applies for all loadings. It is fairly straightforward to establish the expressions for the regions $0 \leq x < a$ and $a < x \leq L$. An easier way to obtain the shear and moment diagrams for this example would be to generate separate diagrams for the two types of loadings and then superimpose the results. The individual shear and moment diagrams are plotted below (Figs. E3.11c and E3.11d).

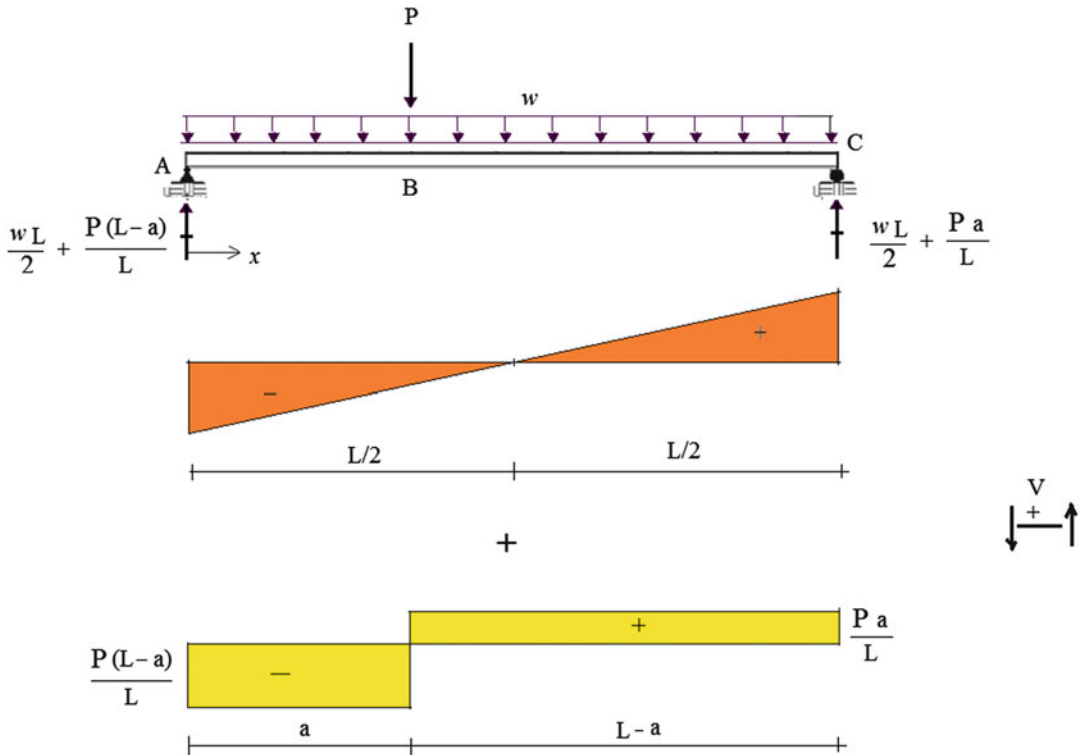


Fig. E3.11c Shear diagrams

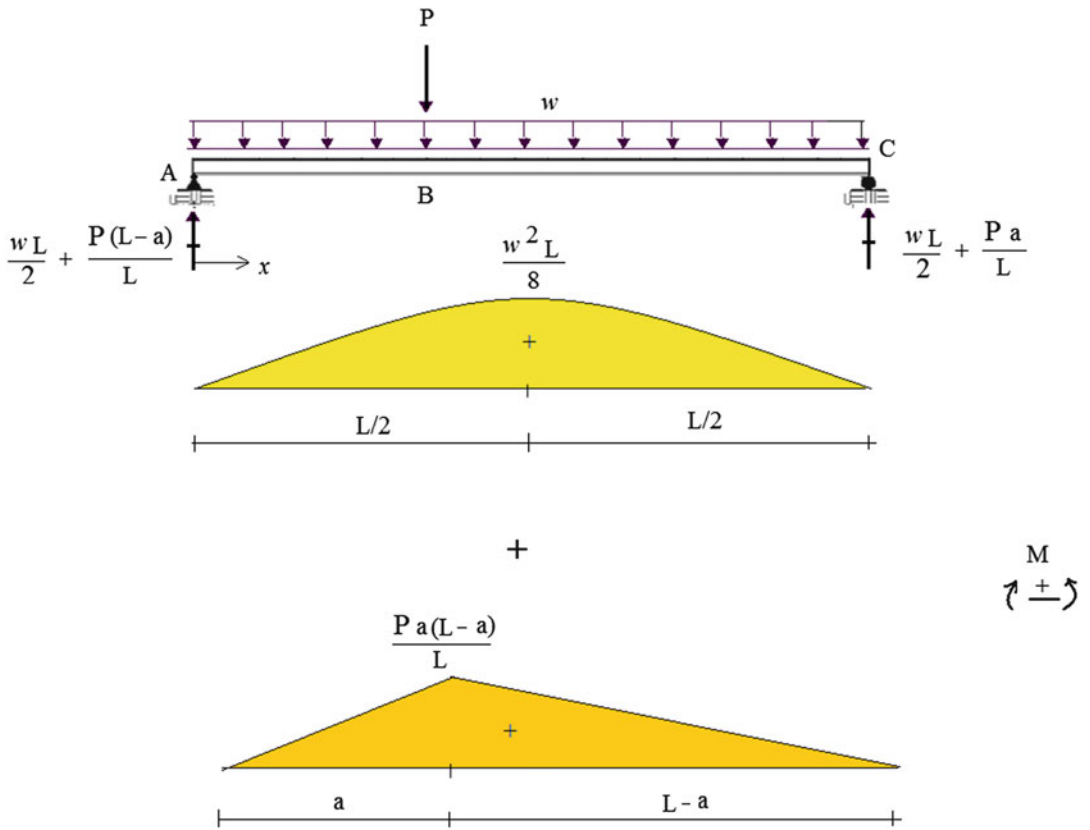
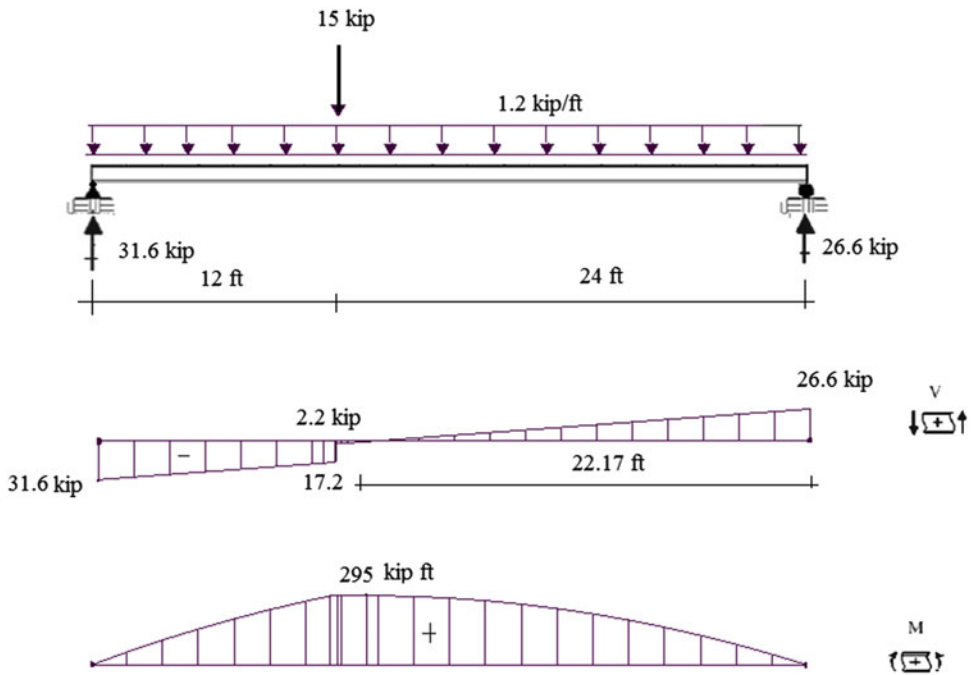


Fig. E3.11d Moment diagrams Suppose $P = 15$ kip, $a = 12$ ft, $L = 36$ ft, and $w = 1.2$ kip/ft. The combined shear and moment diagrams are plotted below.



Example 3.12 Uniform Loading Combined with End Moments

Given: A simply supported beam subjected to a uniform loading and bending moments at the ends. This is a typical case for a floor beam in a rigid building frame, i.e., where the beam-column connections apply moment to the ends of the beam (Fig. E3.12a).

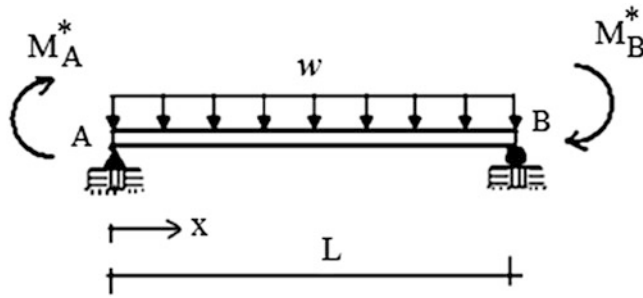


Fig. E3.12a

Determine: The location and magnitude of the maximum moment.

Solution: We consider separate loadings and then superimpose the results. The solution due to the end moment is (Fig. E3.12b)

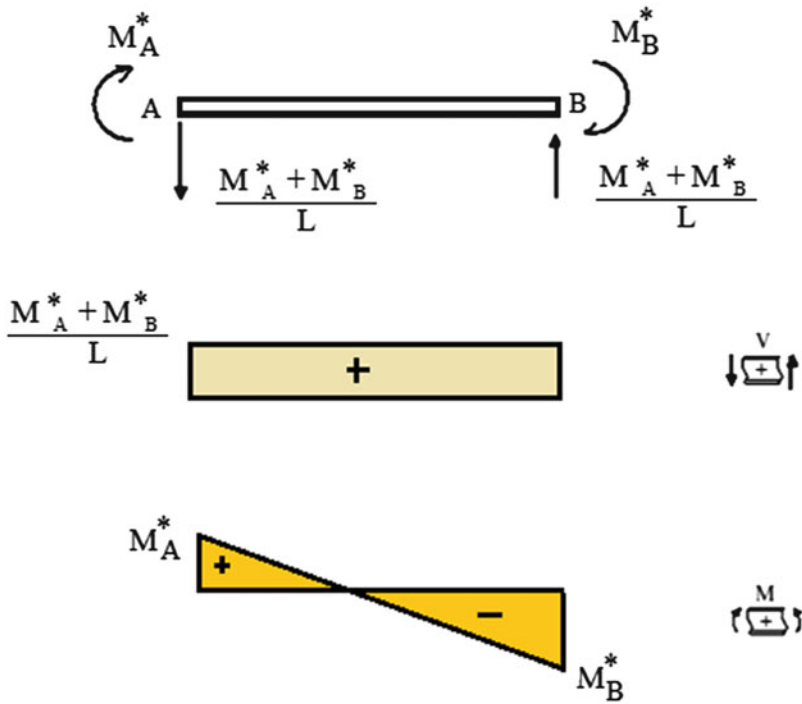


Fig. E3.12b

The uniform loading provides the following distribution (Fig. E3.12c):

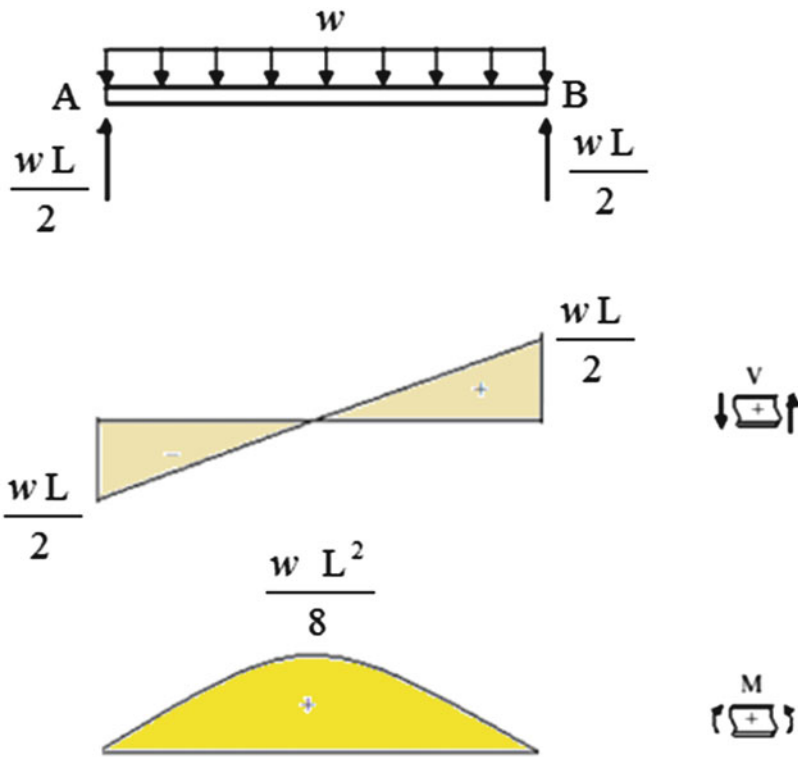


Fig. E3.12c

Combining these solutions leads to the analytical solution

$$V(x) = -\frac{wL}{2} + wx + \frac{M_A^* + M_B^*}{L}$$

$$M(x) = M_A^* - \frac{M_A^* + M_B^*}{L}x + \frac{wL}{2}x - \frac{wx^2}{2}$$

These functions are plotted below (Figs. E3.12d and E3.12e).

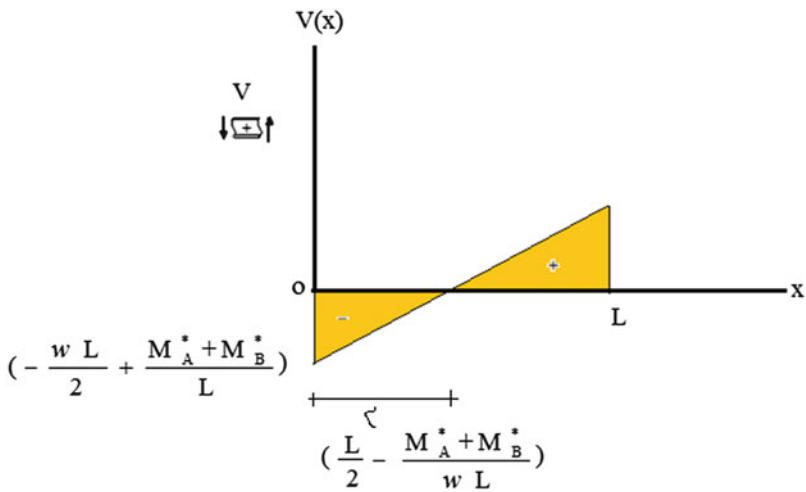


Fig. E3.12d

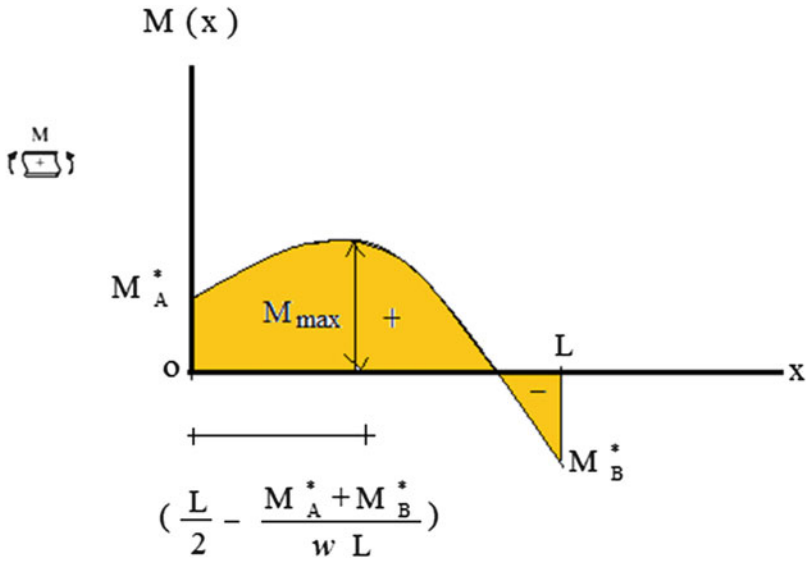


Fig. E3.12e

The peak moment occurs where the shear is zero. Noting the plot of $V(x)$, the shear is zero at x_{\max} .

$$\begin{aligned}
 V &= 0 \\
 &\downarrow \\
 x_{\max} &= \frac{L}{2} - \frac{M_A^* + M_B^*}{wL}
 \end{aligned}$$

The form of the solution suggests that we express the sum of the end moments as

$$M_A^* + M_B^* = \frac{\alpha}{2} wL^2$$

where α is a dimensionless parameter. Substituting for this term, the equation simplifies to

$$x_{\max} = \frac{L}{2}(1 - \alpha)$$

Lastly, we determine M_{\max} using this value for x .

$$M_{\max} = M_A^* + \frac{wL^2}{8}(1 - \alpha)^2$$

Given w and the end moments, one evaluates α ,

$$\alpha = \frac{M_A^* + M_B^*}{\frac{wL^2}{2}}$$

and then M_{\max} . When $\alpha = \pm 1$, the peak moment occurs at an end point and equals the applied end moment.

The case where the end moments are equal in magnitude but opposite in sense is of considerable interest. One sets $M_A^* = -M_B^* = -M^*$, and it follows that $\alpha = 0$. The moment diagram is symmetrical with respect to the centerline. The peak negative values of moment occur at the end points; the peak positive moment occurs at the center point of the span (Fig. E3.12f).

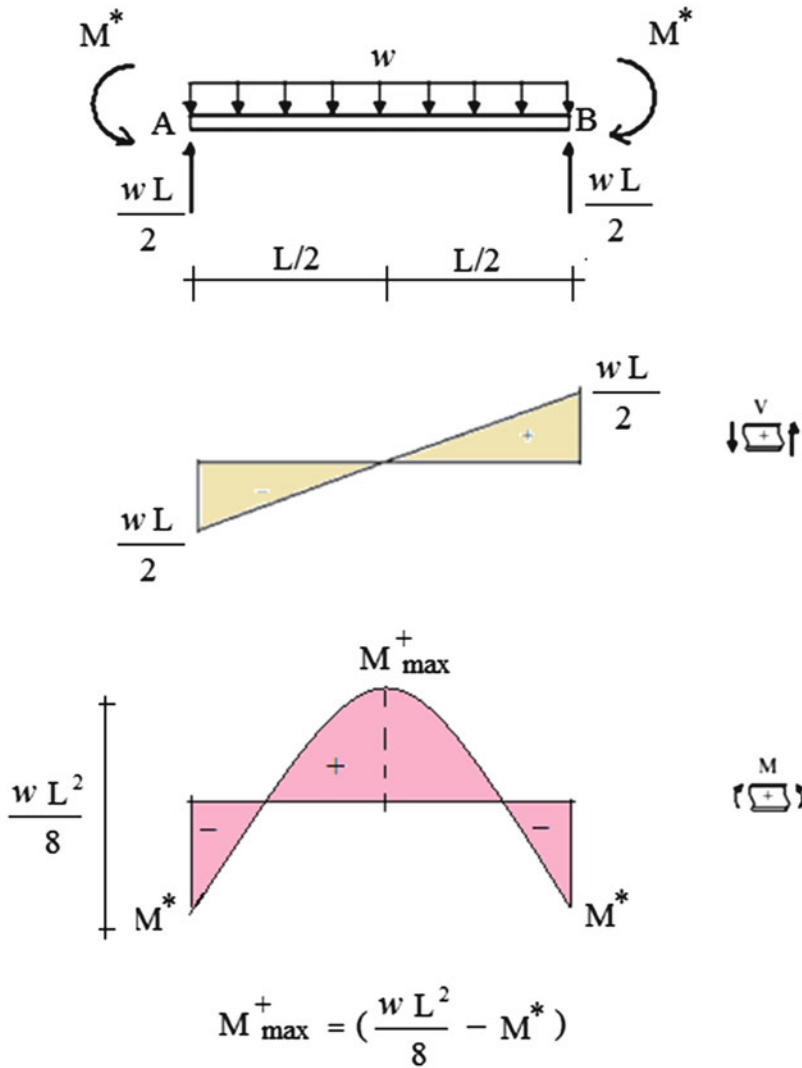


Fig. E3.12f

When there is no end restraint, $M^* = 0$. Then, $M_{\max}^+ = wL^2/8$. The effect of end restraint is to *reduce* the positive moment and introduce a negative moment at the ends. This behavior is typical for rigid frames such as building frames subjected to gravity loading. We examine this behavior in more detail in Chap. 15.

Example 3.13

Given: The beam shown in Fig. E3.13a

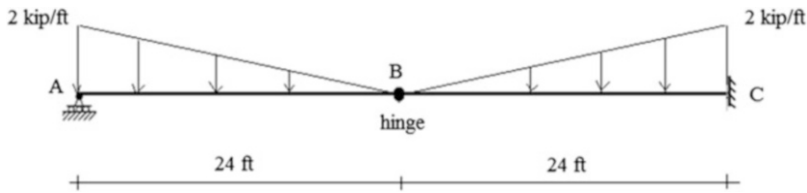


Fig. E3.13a

Determine: The reactions, shear, and bending moment distributions.

Solution: We draw the free body diagram of beam segment AB. Applying the equilibrium conditions to this segment results in (Fig. E3.13b)

$$\begin{aligned}\sum M_A = 0 \quad V_B(24) - (2)\frac{(24)(24)}{2} \cdot \frac{24}{3} &= 0 \quad V_B = 8 \text{ kip} \\ \sum F_y = 0 \quad R_A - (2)\frac{(24)}{2} + 8 &= 0 \quad R_A = 16 \text{ kip}\end{aligned}$$

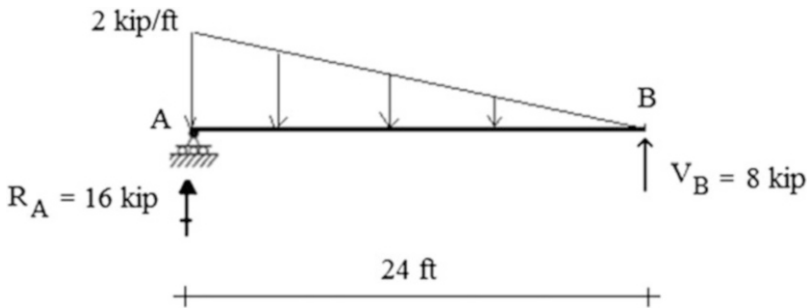


Fig. E3.13b Segment AB

With the internal force at B known, one can now proceed with the analysis of segment BC (Fig. E3.13c).

$$\begin{aligned}\sum F_y = 0 \quad - (2)\frac{(24)}{2} - 8 + R_C &= 0 \quad \Rightarrow \quad R_C = 32 \text{ kip} \uparrow \\ \sum M_C = 0 \quad - M_C + 8(24) + (2)\frac{(24)(24)}{2} \cdot \frac{24}{3} &= 0 \quad \Rightarrow \quad M_C = 384 \text{ kip ft clockwise}\end{aligned}$$

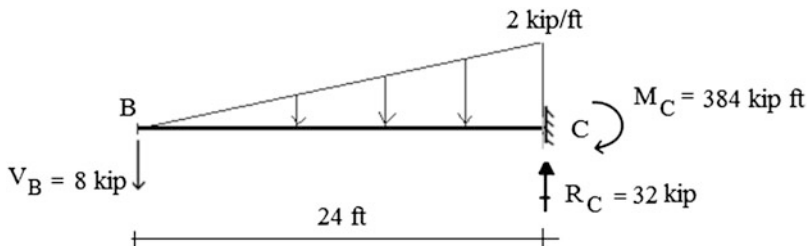
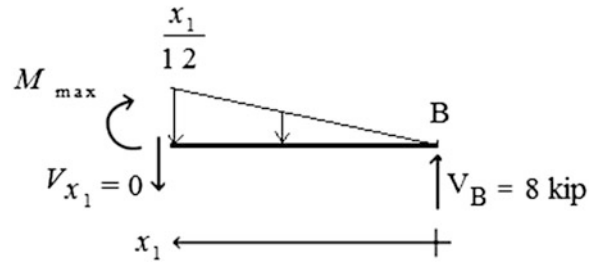


Fig. E3.13c Segment BC

The peak moment occurs where the shear is zero.

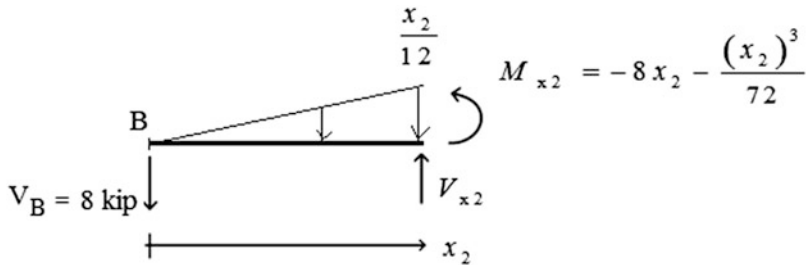
Segment AB:



$$\sum F_y = 0 \quad 8 - \frac{1}{2} \left(\frac{x_1}{12} \right) x_1 = 0 \quad \rightarrow \quad x_1 = 13.85 \text{ ft}$$

$$\therefore M_{\max} = 8(13.85) - (13.85) \left(\frac{13.85}{12} \right) \frac{1}{2} \left(\frac{13.85}{3} \right) = +73.9 \text{ kip ft}$$

Segment BC:



$$\sum F_y = 0 \quad V_{x_2} = 8 + \frac{1}{2} \left(\frac{x_2}{12} \right) x_2 \neq 0$$

Therefore, there is no peak moment between B and C.

The shear and bending moment diagrams are listed below (Fig. E3.13d).

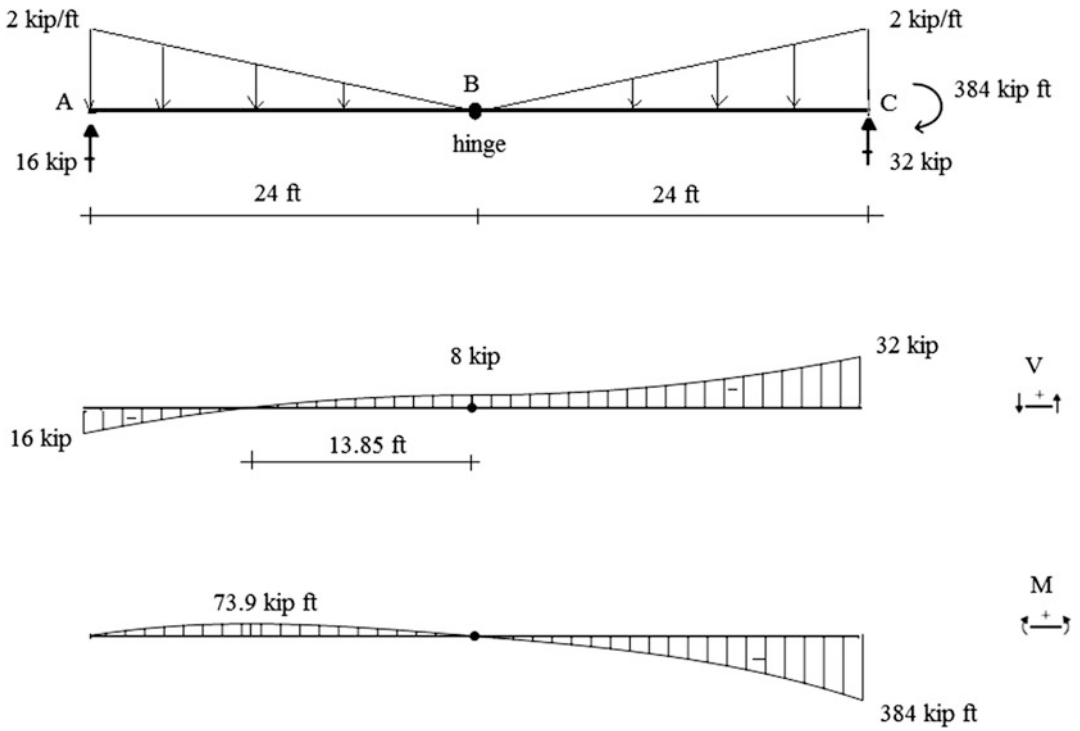


Fig. E3.13d

Example 3.14

Given: The beam shown in Fig. E3.14a

Determine: The reactions, and the shear and bending moment distributions.

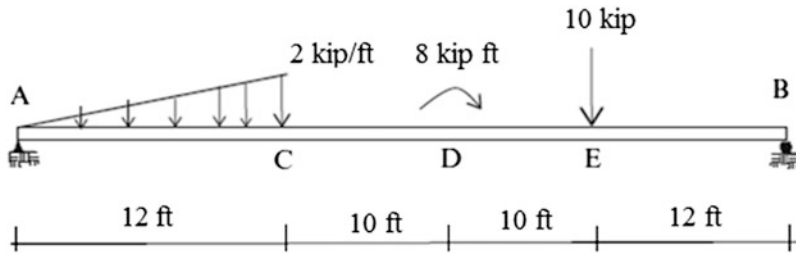


Fig. E3.14a

Solution: We first determine the reaction at B using $\sum M_A = 0$. We then compute the reaction at A by summing forces in the Y direction (Fig. E3.14b).

$$\sum M_A = 0 \quad -R_B(44) + (2)\left(\frac{12}{2}\right)\frac{2}{3}(12) + 8 + 10(32) = 0 \quad R_B = 9.64 \uparrow$$

$$\sum F_Y = 0 \quad R_A - 2\left(\frac{12}{2}\right) - 10 + 9.64 = 0 \quad R_A = 12.36 \uparrow$$

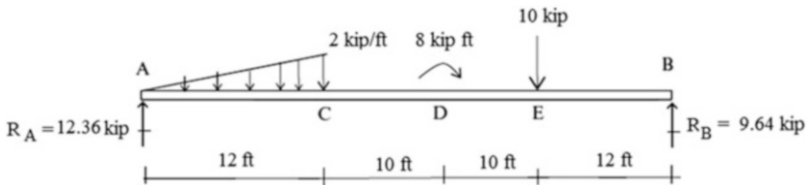


Fig. E3.14b

We determine the shear, $V(x)$, with (3.6) (Fig. E3.14c). Integrating between points A and x

$$V(x) - V_A = \int_0^x w(x)dx = \int_0^x \frac{x}{6}dx = \frac{x^2}{12} \Big|_0^x = \frac{x^2}{12} \quad 0 \leq x \leq 12$$

Noting that $V_A = -12.36$, the solution for $V(x)$ reduces to

$$V(x) = \frac{x^2}{12} - 12.36$$

We determine the *moment* $M(x)$, with (3.7) (Fig. E3.14c). Integrating between points A and x

$$M(x) - M_A = -\int_0^x V(x)dx = -\int_0^x \left(\frac{x^2}{12} - 12.36\right)dx = -\frac{x^3}{36} + 12.36x \quad 0 \leq x \leq 12$$

Noting that $M_A = 0$, one obtains

$$M(x) = -\frac{x^3}{36} + 12.36x$$

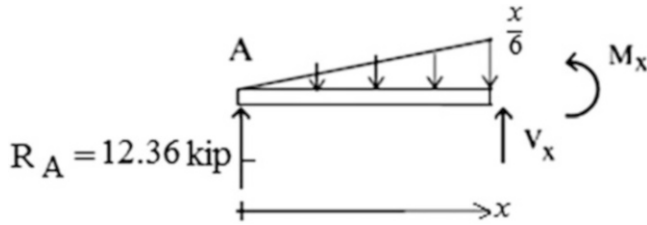
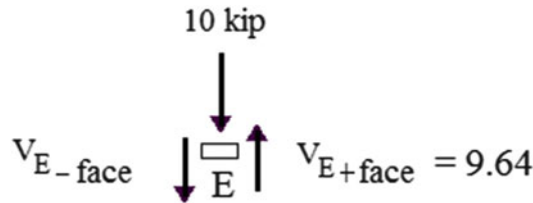


Fig. E3.14c

Note that there is a jump in the shear at E.



$$\sum F_y = 0 \quad V_{E\text{-face}} - 9.64 + 10 = 0 \quad V_{E\text{-face}} = -0.36 \quad V_{E\text{-face}} = 0.36 \uparrow \text{kip}$$

Applying (3.7) to the different segments results in:

Segment EB

$$M_B - M_E = -\int_{E \rightarrow B} V dx = -9.64(12) = -115.68$$

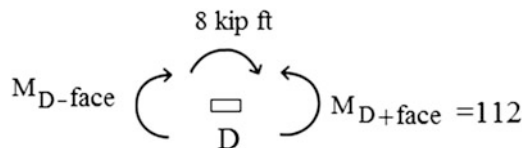
$$M_B = 0 \quad \therefore M_E = 115.68 \text{ kip ft}$$

Segment DE

$$M_E - M_D = -\int_{E \rightarrow B} V dx = -(-0.36)(10) = 3.6$$

$$M_E = 115.68 \quad \therefore M_D = 112 \text{ kip ft}$$

Note that there is a jump in the bending moment at D.



$$\sum M = 0 \quad M_{D\text{-face}} + 8 - 112 = 0 \quad M_{D\text{-face}} = 104 \text{ kip ft}$$

Segment CD

$$M_D - M_C = - \int_{E \rightarrow B} V dx = -(-0.36)(10) = 3.6$$

$$M_D = 104. \quad \therefore M_C = 100.4 \text{ kip ft}$$

The reactions, shear, and bending moment distributions are listed below (Fig. E3.14d).

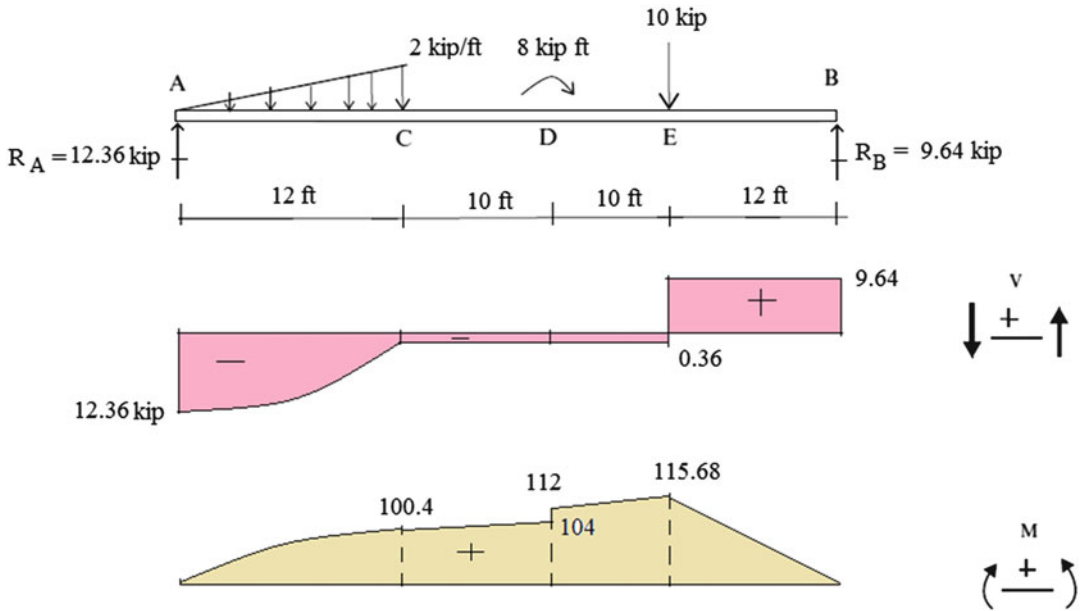


Fig. E3.14d

3.6 Displacement and Deformation of Slender Beams: Planar Loading

Fig. 3.18 Slender beam. (a) Initial. (b) Deformed

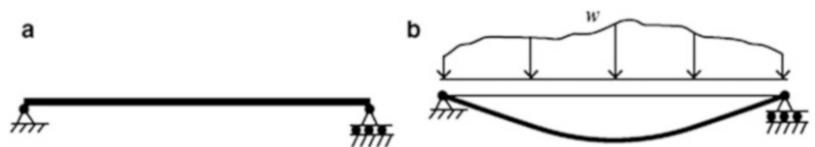


Fig. 3.19 Definition of displacement components

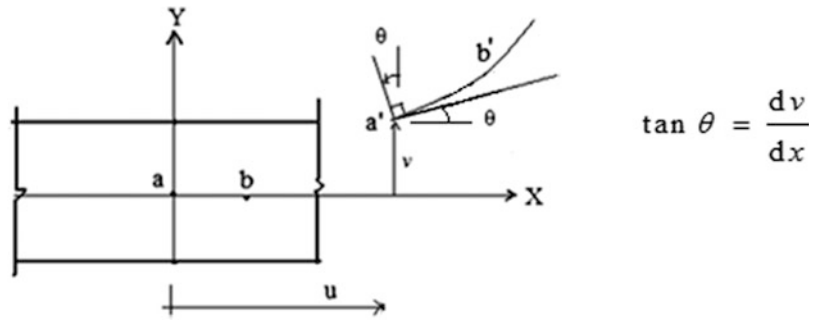


Figure 3.18 shows how a slender beam responds to a transverse planar loading. The geometric quantities that define the movement of the beam from its unloaded position due to an applied loading are defined as the displacements. Displacements are also referred to as deflections. Consider the segment of a homogeneous beam shown in Fig. 3.19. We take the X -axis to coincide with the initial position of the centroidal axis and the Y -axis to be 90° counterclockwise from the X -axis. When the loading is applied in the $X - Y$ plane, points on the centroidal axis move horizontally and vertically. We assume the cross-section, which is initially normal to the centroidal axis, remains normal to the curve connecting the displaced points. This is a standard assumption for beams known as “Kirchoff’s” hypothesis and implies that the cross-section rotates through the same angle as the tangent to the centroidal axis. Kirchoff’s hypothesis is valid for slender beams, i.e., beams having a depth to span ratio less than about 0.1. With this assumption, the independent geometric measures are the two displacement components, $u(x)$ and $v(x)$, which are functions of x for static loading. Given $v(x)$, we find the cross-sectional rotation, $\theta(x)$, with the geometric relation.

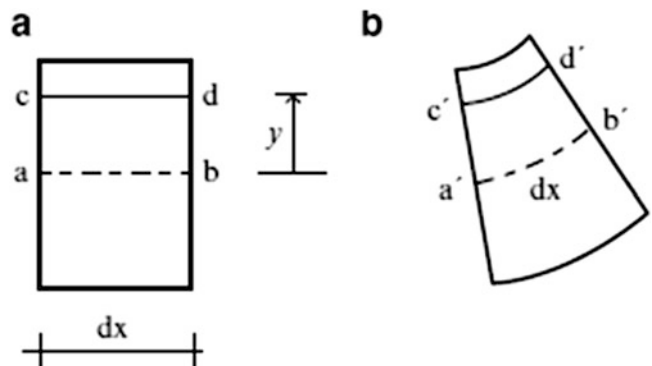
The next assumption that we introduce concerns the magnitude of θ . We assume here that θ^2 is small in comparison to unity, which implies that the tangent is essentially equal to the angle in radians:

$$\tan \theta \approx \theta \tag{3.11}$$

Then, the expression for θ reduces to

$$\theta \approx + \frac{dv}{dx} \tag{3.12}$$

Fig. 3.20 Differential beam elements. (a) Initial. (b) Deformed



Deformations are dimensionless strain measures resulting from displacements. Consider the differential elements shown in Fig. 3.20. The initial rectangular shape is transformed to a quadrilateral shape with curved upper and lower edges. Adjacent cross-sections experience a relative rotation equal to $(d\theta/dx)dx$, which causes line elements parallel to the centroidal axis to either elongate or contract. These changes in length produce extensional strains. A line element located y units above the centroidal axis experiences a strain $\epsilon(y)$ equal to

$$\epsilon(y) = -y \frac{d\theta}{dx} \quad (3.13)$$

According to this model, the strain varies linearly over the cross-section and the peak strain values occur at the upper and lower surfaces; the centroidal axis is not strained.

At this point, we introduce some standard notation for the derivative of the cross-section rotation angle, θ .

$$\begin{aligned} \chi &= \text{curvature} \equiv \frac{d\theta}{dx} \approx \frac{d^2v}{dx^2} \text{ (units of radians/length)} \\ \rho &= \text{radius of curvature} = \frac{1}{\chi} \text{ (units of length)} \end{aligned} \quad (3.14)$$

We prefer to work with the curvature and express the extensional strain as

$$\epsilon = -y\chi \quad (3.15)$$

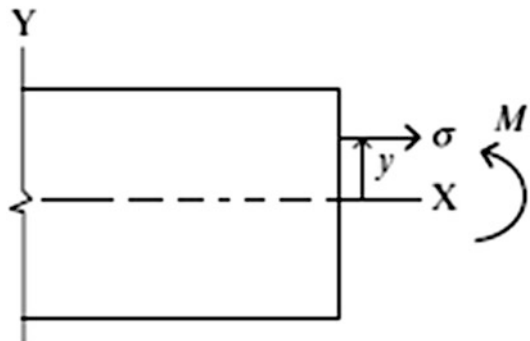
Given χ , one can establish qualitatively the shape of the curve defining the displaced centroidal axis. An analytical solution for the displacement, v , can also be determined by integrating (3.14). We will illustrate both procedures in later sections.

3.6.1 Moment: Curvature Relationship

We have demonstrated how to establish the bending moment distribution corresponding to a given loading. We have also showed how the displacement field can be generated once the curvature is known. To find the displacements due to a given loading, we need to relate the moment and the corresponding curvature along the centroidal axis. Given this relationship, it is a fairly straightforward process to move from prescribed loading to the resulting displacement.

The positive sense of the bending moment on a positive cross-section is defined as counterclockwise. Then noting Fig. 3.21, the moment and normal stress are related by

Fig. 3.21 Definition of normal stress and moment



$$M = \int_A -y\sigma \, dA \quad (3.16)$$

We determine the stress using the stress–strain relation. In what follows, we assume the material behavior is linear elastic. The stress is a linear function of the strain in this case.

$$\sigma = E\varepsilon = -yE\chi \quad (3.17)$$

where E is Young's modulus for the material. Substituting for σ in (3.16) leads to

$$M = EI\chi \quad (3.18)$$

where $I = \int y^2 dA$. Given M and EI , one finds the curvature (χ) with

$$\chi = \frac{M}{EI} \quad (3.19)$$

and then the displacement v by integrating

$$\frac{d^2v}{dx^2} = \chi = \frac{M}{EI} \quad (3.20)$$

The complete solution of (3.20) consists of a homogeneous term and a particular term,

$$v = c_0 + c_1x + v_p \quad (3.21)$$

where v_p is the particular solution corresponding to the function, M/EI , and c_0, c_1 are constants. Two boundary conditions on v are required to determine c_0 and c_1 .

3.6.2 Qualitative Reasoning About Deflected Shapes

Noting (3.18) and the fact that EI is always positive, it follows that the sense of curvature χ is the same as the sense of M . The deflected shapes corresponding to positive and negative curvature are shown in Fig. 3.22. It is more convenient to interpret these deflected shapes as the result of applying positive and negative moments. Figure 3.23 illustrates this interpretation.

We divide the moment diagrams into positive and negative moment zones and identify, using Fig. 3.23, the appropriate shape for each zone. Points where the moment changes sign are called inflection points. The curvature is zero at an inflection point, which implies that the curve is locally straight. We deal with inflection points by adjusting the orientation of adjoint shapes such that their tangents coincide at the inflection point. Figure 3.24 illustrates this process.

Fig. 3.22 Deflected shapes for positive and negative curvature

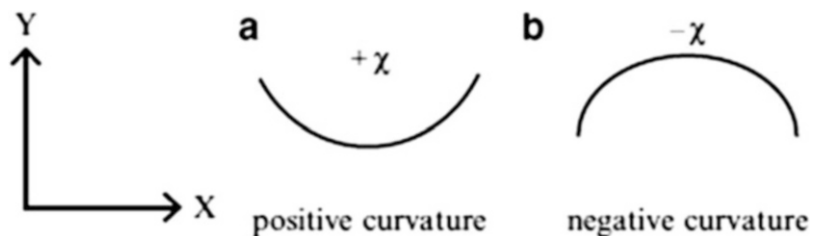


Fig. 3.23 Deflected shape for positive and negative moments

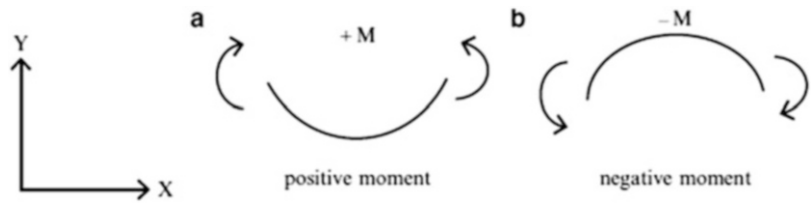
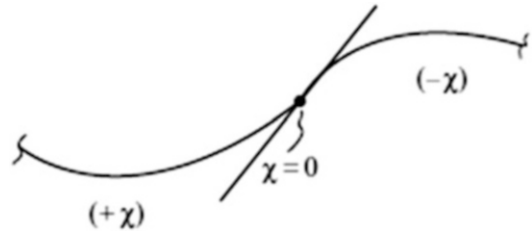


Fig. 3.24 Shape transition at an inflection point



The last step involves enforcing the displacement boundary conditions associated with end conditions. Figure 3.25 shows four types of end conditions (full fixity, hinge, roller, and free) with their corresponding displacement measures that are constrained by these conditions.

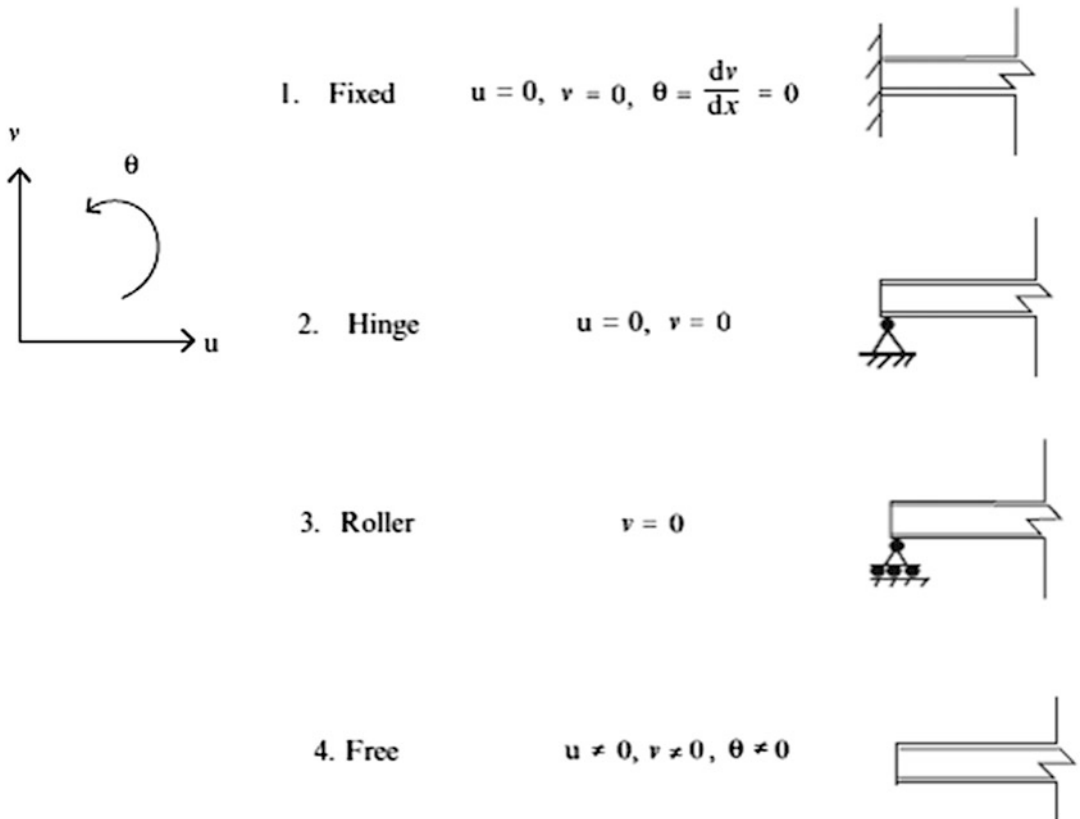


Fig. 3.25 Types of end conditions—displacement measures

The deflected shape must pass through a support. If an end is fixed, the cross-section cannot rotate at that point. We need to orient the deflected shape such that the tangent coincides with the initial centroidal axis. In what follows, we present a series of examples which illustrate the process of developing qualitative estimates of deflected shapes given the bending moment distribution.

Example 3.15 Deflected Shape—Uniformly Loaded, Simply Supported Beam

Given: The uniformly loaded, simply supported beam shown in Fig. E3.15a.

Determine: The deflected shape.

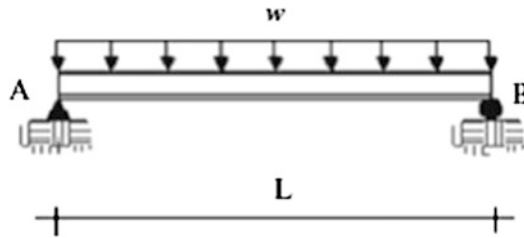


Fig. E3.15a

Solution: The moment is positive throughout the span so Fig. 3.23a applies. The displacement boundary conditions require

$$v(0) = v(L) = 0$$

One starts at the left end, sketches a curve with increasing positive curvature up to mid-span and then reverses the process. The deflected shape is symmetrical with respect to mid-span since the moment diagrams and support locations are symmetrical (Figs. E3.15b and E3.15c).

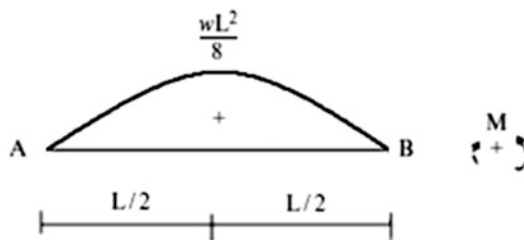


Fig. E3.15b Moment diagram

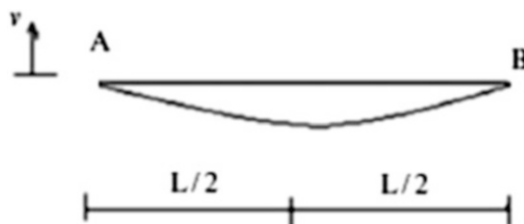


Fig. E3.15c Deflected shape

Example 3.16 Deflected Shape—Cantilever Beam

Given: The cantilever beam defined in Fig. E3.16a.

Determine: The deflected shape.

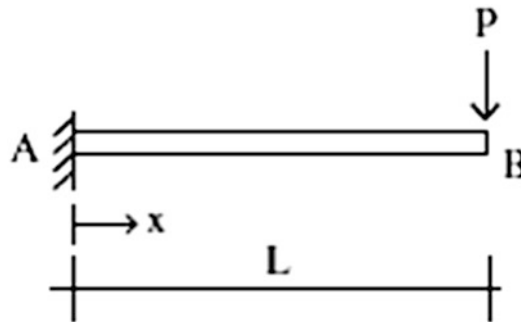


Fig. E3.16a

Solution: We note that the moment is negative throughout the span. Point A is fixed and therefore the tangent must be horizontal at this point. The displacement boundary conditions require

$$v(0) = \theta(0) = 0$$

We start at point A and sketch a curve with decreasing negative curvature up to $x = L$ (Figs. E3.16b and E3.16c).



Fig. E3.16b Moment diagram



Fig. E3.16c Deflected shape

Example 3.17 Deflected Shape of a Beam with an Overhang

Given: The beam with overhang shown in Fig. E3.17a.

Determine: The deflected shape.

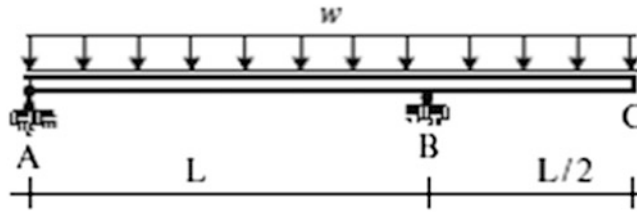


Fig. E3.17a

Solution: We note that Fig. E3.17b shows that the moment diagram has both positive and negative regions with an inflection point at $x = 0.75L$. Therefore, it follows that the left segment has positive curvature and the right segment has negative curvature. We need to join these shapes such that the tangent is continuous at point D and the deflections are zero at points A and B (Fig. E3.17c).

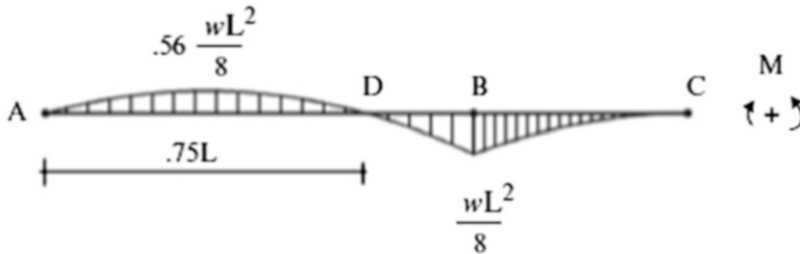


Fig. E3.17b Moment diagram

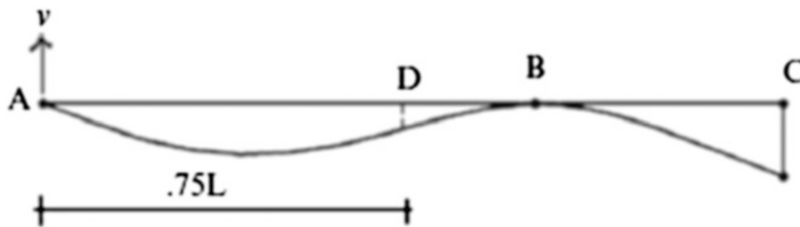


Fig. E3.17c Deflected shape

Example 3.18 Deflected Shape—Beam with a Moment Release

Given: The beam shown in Fig. E3.18a.

Determine: The deflected shape.

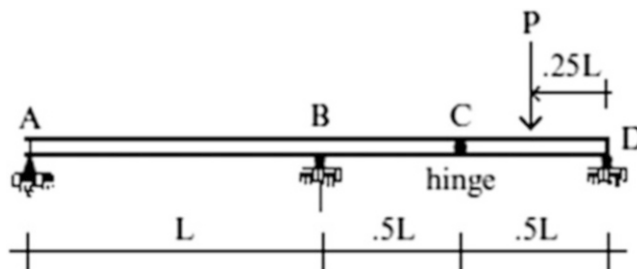


Fig. E3.18a

Solution: Member CD is connected to member ABC with a hinge at point C. A hinge is a physical artifact that allows the members connected to it to rotate freely, i.e., no moment is introduced. A hinge point is different from an inflection point. Although the moment is zero for both hinge and inflection points, the cross-sectional rotation is discontinuous at a hinge, whereas it is continuous at an inflection point. This feature is illustrated in the displacement sketch shown below. The left segment (ABC) has negative curvature. The right segment (CD) has positive curvature (Figs. E3.18b and E3.18c).

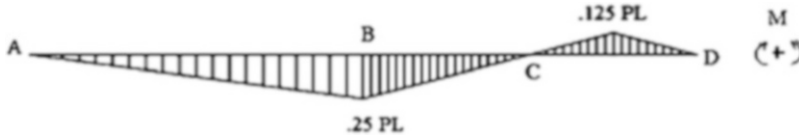


Fig. E3.18b Moment diagram

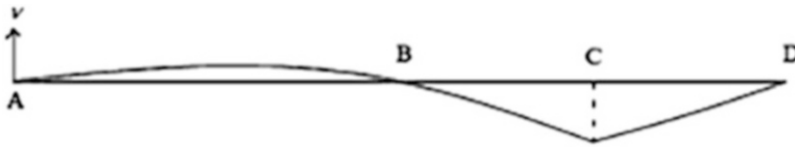


Fig. E3.18c Deflected shape

3.6.3 Moment Area Theorems

The starting point for quantitative analysis is the set of differential equations relating the moment, the cross-sectional rotation, and the deflection.

$$\begin{aligned}\frac{d\theta}{dx} &= \frac{M(x)}{EI} \\ \frac{dv}{dx} &= \theta(x)\end{aligned}\quad (3.22)$$

Given $M(x)/EI$, we integrate $d\theta/dx$ between two points x_1 and x_2 on the x -axis and write the result as

$$\theta(x_2) - \theta(x_1) = \int_{x_1}^{x_2} \frac{M(x)}{EI} dx \quad (3.23)$$

We interpret (3.23) as “The difference in rotation between 2 points is equal to the area of the M/EI diagram included between these points.” This statement is referred to as the “First Moment Area” theorem. Taking x_2 as x in (3.23), we can express $\theta(x)$ as

$$\theta(x) = \theta(x_1) + \int_{x_1}^x \frac{M(x)}{EI} dx \quad (3.24)$$

Given $\theta(x)$, we solve for $v(x_2)$.

$$v(x_2) = v(x_1) + \int_{x_1}^{x_2} \theta(x) dx \quad (3.25)$$

Evaluating (3.24) first, and then substituting for $\theta(x)$ in (3.25) leads to

$$v(x_2) - v(x_1) = (x_2 - x_1)\theta(x_1) + \int_{x_1}^{x_2} \left\{ \int_{x_1}^x \frac{M(x)}{EI} dx \right\} dx \quad (3.26)$$

The double integral in (3.26) can be evaluated using integration by parts. First, we note the following identity,

$$d(uv) = u dv + v du \quad (3.27)$$

Integrating between x_1 and x_2 ,

$$\int_{x_1}^{x_2} d(uv) = \int_{x_1}^{x_2} (u dv + v du) \quad (3.28)$$

and rearranging terms leads to

$$\int_{x_1}^{x_2} u dv = uv \Big|_{x_1}^{x_2} - \int_{x_1}^{x_2} v du \quad (3.29)$$

We take

$$\begin{aligned} u &= \int_{x_1}^x \frac{M}{EI} dx \\ dv &= dx \end{aligned} \quad (3.30)$$

in (3.26). Using (3.29), the double integral can be expressed as

$$\begin{aligned} \int_{x_1}^{x_2} \left\{ \int_{x_1}^x \frac{M(x)}{EI} dx \right\} dx &= \left[x \int_{x_1}^x \frac{M(x)}{EI} dx \right]_{x_1}^{x_2} - \int_{x_1}^{x_2} x \frac{M(x)}{EI} dx \\ &= \int_{x_1}^{x_2} (x_2 - x) \frac{M(x)}{EI} dx \end{aligned} \quad (3.31)$$

Finally, an alternate form of (3.26) is

$$v(x_2) - v(x_1) = (x_2 - x_1)\theta(x_1) + \int_{x_1}^{x_2} (x_2 - x) \frac{M(x)}{EI} dx \quad (3.32)$$

This form is referred to as the “Second Moment Area Theorem.” Figure 3.26 shows that the last term can be interpreted as the moment of the M/EI diagram with respect to x_2 . It represents the deflection from the tangent at point 1, as indicated in Fig. 3.27.

Fig. 3.26 Area and moment of area

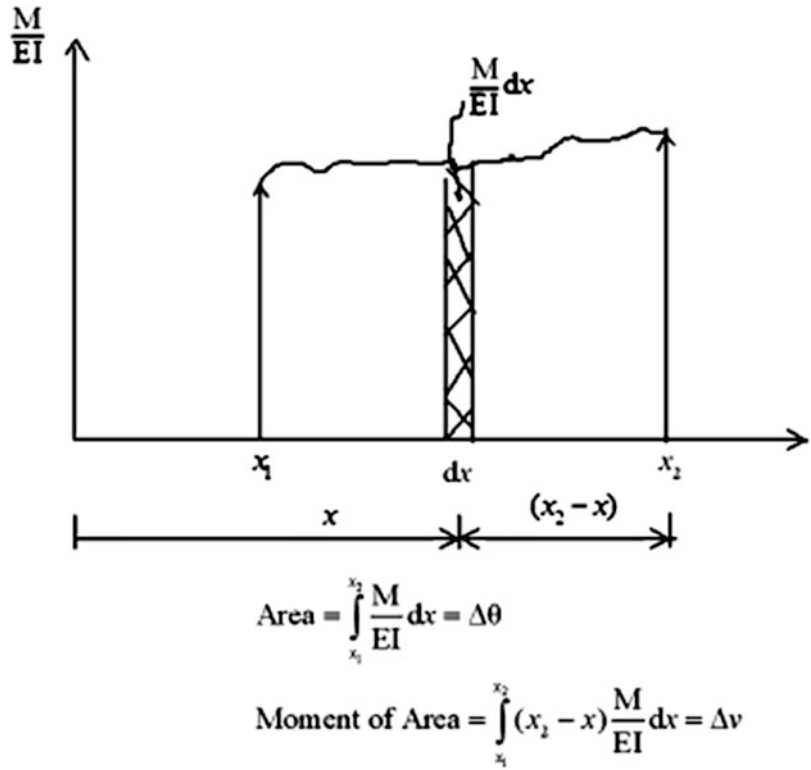
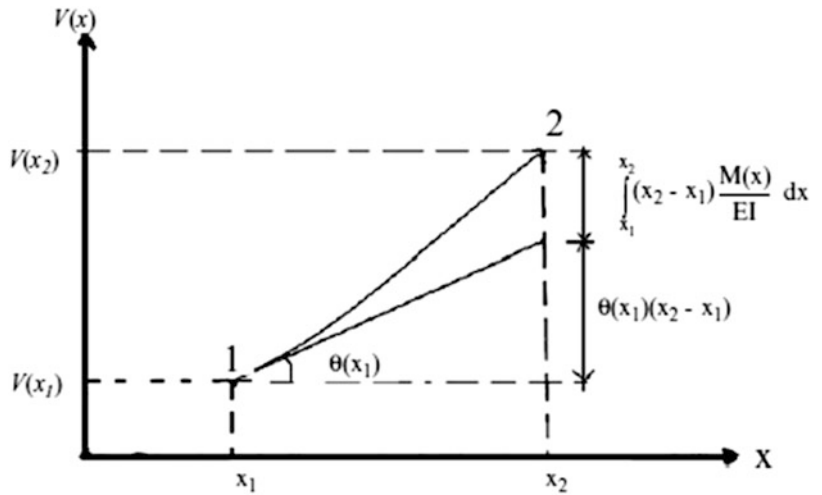


Fig. 3.27 Graphic interpolation of (3.26)



Using the Moment Area theorems, one has to evaluate only two integrals,

$$J(x) = \int_{x_1}^x \frac{M(x)}{EI} dx$$

$$H(x) = \int_{x_1}^x x \frac{M(x)}{EI} dx$$
(3.33)

When I is a complicated function of x , these integrals can be evaluated using a symbolic integration scheme or the numerical integration scheme described in Sect. 3.6.5. The final expressions for $\nu(x)$ and $\theta(x)$ in terms of $\nu(x_1)$, $\theta(x_1)$ and these integrals are (we take $x_2 = x$ in (3.23) and (3.32))

$$\begin{aligned}\theta(x) &= \theta(x_1) + J(x) \\ v(x) &= v(x_1) + (x - x_1)\theta(x_1) + xJ(x) - H(x)\end{aligned}\quad (3.34)$$

Example 3.19 Deflected Shape—Cantilever Beam

Given: The cantilever beam shown in Fig. E3.19a. Consider EI is constant.

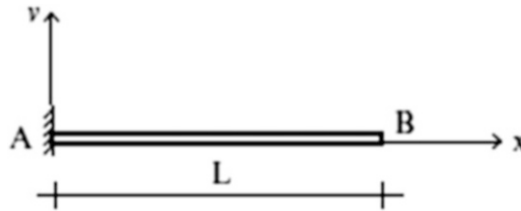


Fig. E3.19a

Determine: The deflected shapes for various loadings: concentrated moment, concentrated force, and uniform load.

Solution: We measure x from the left support. The displacement boundary conditions are

$$v_A = v(0) = 0$$

$$\theta_A = \theta(0) = 0$$

Taking $x_1 = 0$ and noting the boundary conditions at $x = 0$, (3.34) reduces to

$$0 \leq x \leq L$$

$$\theta(x) = \int_0^x \frac{M(x)}{EI} dx$$

$$v(x) = x \int_0^x \frac{M(x)}{EI} dx - \int_0^x x \frac{M(x)}{EI} dx$$

Solutions for various loadings are listed below.

1. *Concentrated moment* (Fig. E3.19b)

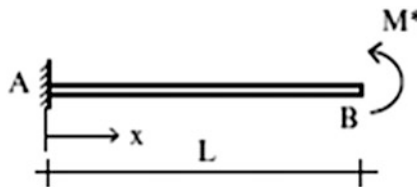
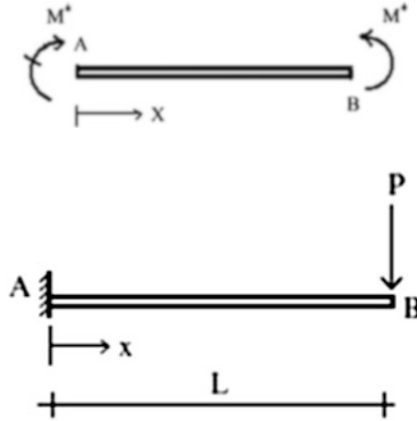


Fig. E3.19b

The expressions for $M(x)$, $\theta(x)$, and $v(x)$ for a concentrated moment are as follows:



$$M(x) = M^* \quad 0 \leq x \leq L$$

$$\theta(x) = \frac{1}{EI} \int_0^x M(x) dx = \frac{M^*}{EI} x$$

$$v(x) = \frac{x}{EI} \int_0^x M(x) dx - \frac{1}{EI} \int_0^x x M(x) dx = \frac{M^* x^2}{EI} - \frac{M^* x^2}{2EI} = + \frac{M^* x^2}{2EI}$$

Specific values are

$$\theta_B = \frac{M^* L}{EI}$$

$$v_B = \frac{M^* L^2}{2EI}$$

2. Concentrated Force (Fig. E3.19c)

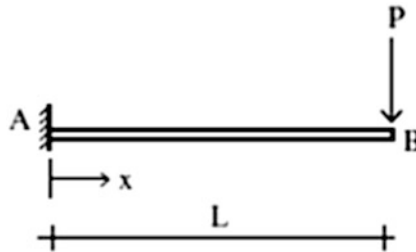
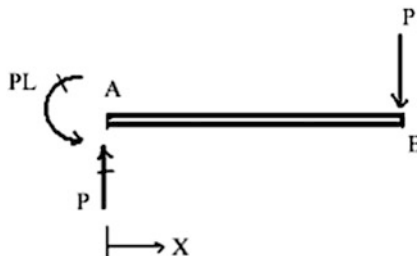


Fig. E3.19c

The expressions for $M(x)$, $\theta(x)$, and $v(x)$ for a concentrated load are as follows:



$$M(x) = +P(x - L) \quad 0 \leq x \leq L$$

$$\theta(x) = \frac{1}{EI} \int_0^x M(x) dx = \frac{P}{EI} \left(\frac{x^2}{2} - Lx \right)$$

$$v(x) = \frac{x}{EI} \int_0^x M(x) dx - \frac{1}{EI} \int_0^x xM(x) dx = \frac{P}{EI} \left(\frac{x^3}{6} - \frac{Lx^2}{2} \right)$$

Specific values are

$$\theta_B = -\frac{PL^2}{2EI}$$

$$v_B = -\frac{PL^3}{3EI}$$

3. Uniform Loading (Fig. E3.19d)

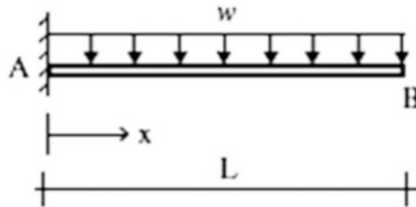
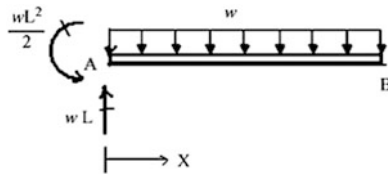


Fig. E3.19d

The expressions for $M(x)$, $\theta(x)$, and $v(x)$ for a uniform load are as follows:



$$M(x) = -\frac{wx^2}{2} + wLx - \frac{wL^2}{2} \quad 0 \leq x \leq L$$

$$\theta(x) = \frac{1}{EI} \int_0^x M(x) dx = \frac{w}{6EI} (-x^3 + 3Lx^2 - 3L^2x)$$

$$v(x) = \frac{x}{EI} \int_0^x M(x) dx - \frac{1}{EI} \int_0^x xM(x) dx = \frac{w}{24EI} (-x^4 + 4Lx^3 - 6L^2x^2)$$

Specific values are

$$\theta_B = -\frac{wL^3}{6EI}$$

$$v_B = -\frac{wL^4}{8EI}$$

Example 3.20 Deflected Shape—Simply Supported Beam

Given: The simply supported beam shown in Fig. E3.20a. Consider EI is constant.

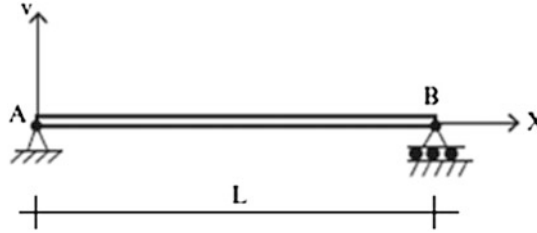


Fig. E3.20a

Determine: The deflected shape under different load conditions.

Solution: We measure x from the left support. The displacement boundary conditions are

$$v_A = v(0) = 0$$

$$v_B = v(L) = 0$$

$$\theta_A = \theta(0) \neq 0$$

$$\theta_B = \theta(L) \neq 0$$

Noting the boundary conditions at $x = 0$, the general solution (3.34) for constant EI is given by

$$0 \leq x \leq L$$

$$\theta(x) = \theta(0) + \int_0^x \frac{M(x)}{EI} dx$$

$$v(x) = x\theta(0) + x \int_0^x \frac{M(x)}{EI} dx - \int_0^x x \frac{M(x)}{EI} dx$$

We determine $\theta(0)$ using the remaining boundary condition, $v(L) = 0$. Evaluating $v(x)$ at $x = L$ and equating the result to 0 leads to

$$\theta(0) = - \int_0^L \frac{M(x)}{EI} dx + \frac{1}{L} \int_0^L x \frac{M(x)}{EI} dx$$

Various loading cases are considered below. We omit the integral details and just present the final solutions.

1. Concentrated Moment (Fig. E3.20b)

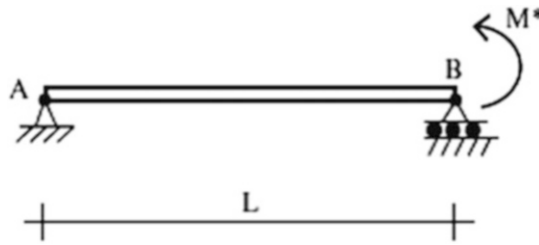
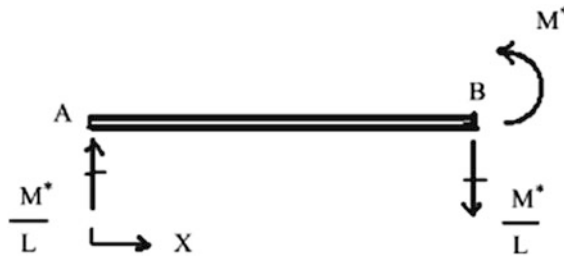


Fig. E3.20b

The expressions for $M(x)$, $\theta(x)$, and $v(x)$ for a concentrated moment are as follows:



$$M(x) = \frac{M^*}{L}x \quad 0 \leq x \leq L$$

$$\begin{aligned} \theta(x) &= -\int_0^L \frac{M(x)}{EI} dx + \frac{1}{L} \int_0^L x \frac{M(x)}{EI} dx + \int_0^x \frac{M(x)}{EI} dx \\ &= \frac{M^*L}{EI} \left(\frac{x^2}{2L^2} - \frac{1}{6} \right) \end{aligned}$$

$$\begin{aligned} v(x) &= -x \int_0^L \frac{M(x)}{EI} dx + \frac{x}{L} \int_0^L x \frac{M(x)}{EI} dx + x \int_0^x \frac{M(x)}{EI} dx - \int_0^x x \frac{M(x)}{EI} dx \\ &= \frac{M^*L^2}{6EI} \left(\frac{x^3}{L^3} - \frac{x}{L} \right) \end{aligned}$$

Specific values are

$$\begin{aligned} \theta_A &= -\frac{M^*L}{6EI} \\ \theta_B &= \frac{M^*L}{3EI} - \frac{M^*L^2}{EI} \quad \text{at } x = \frac{L}{\sqrt{3}} \approx 0.58L \\ v_{\max} &= -\frac{\sqrt{3}}{27} \end{aligned}$$

2. Concentrated Force (Fig. E3.20c)

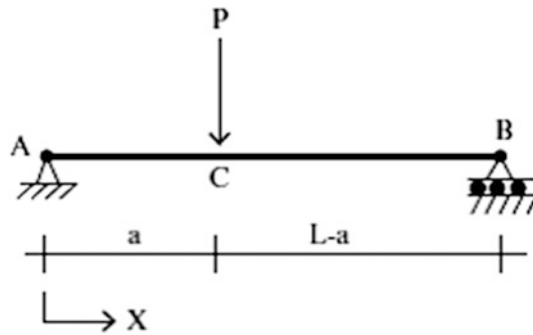
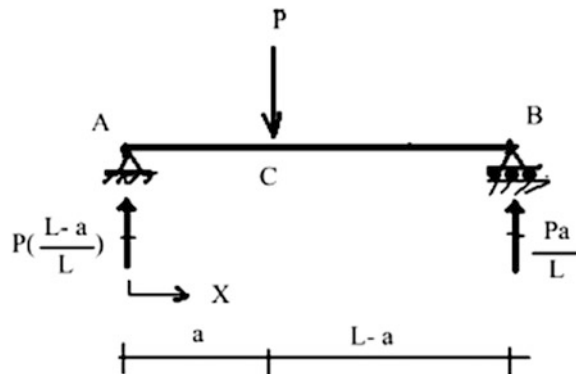


Fig. E3.20c

The expressions for $M(x)$, $\theta(x)$, and $v(x)$ for a concentrated load are as follows:



$$M(x) = P\left(\frac{L-a}{L}\right)x \quad 0 \leq x \leq a$$

$$M(x) = \frac{Pa}{L}(L-x) \quad a \leq x \leq L$$

Segment AC $0 \leq x \leq a$

$$\begin{aligned} \theta(x) &= -\int_0^L \frac{M(x)}{EI} dx + \frac{1}{L} \int_0^L x \frac{M(x)}{EI} dx + \int_0^x \frac{M(x)}{EI} dx \\ &= -\frac{PL^2}{EI} \left(1 - \frac{a}{L}\right) \left[-\frac{1}{2} \left(\frac{x}{L}\right)^2 + \frac{1a}{6L} \left(2 - \frac{a}{L}\right) \right] \end{aligned}$$

$$\begin{aligned}
 v(x) &= -x \int_0^L \frac{M(x)}{EI} dx + \frac{x}{L} \int_0^L x \frac{M(x)}{EI} dx + x \int_0^x \frac{M(x)}{EI} dx - \int_0^x x \frac{M(x)}{EI} dx \\
 &= -\frac{PL^3}{EI} \left(1 - \frac{a}{L}\right) \left[-\frac{1}{6} \left(\frac{x}{L}\right)^3 + \frac{1ax}{6LL} \left(2 - \frac{a}{L}\right) \right]
 \end{aligned}$$

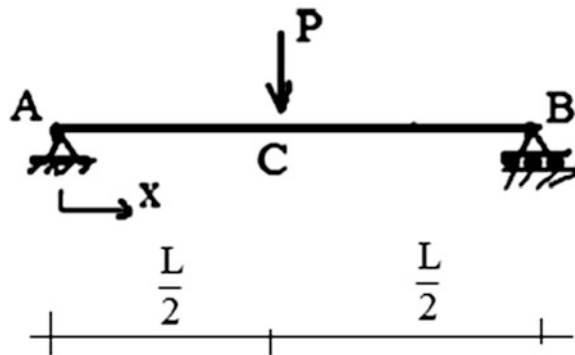
Segment CB $a \leq x \leq L$

$$\begin{aligned}
 \theta(x) &= -\frac{PL^2}{EI} \left(\frac{1}{3} + \frac{1}{6} \left(\frac{a}{L}\right)^2 - \frac{x}{L} + \frac{1}{2} \left(\frac{x}{L}\right)^2 \right) \left(\frac{a}{L}\right) \\
 v(x) &= -\frac{PL^3}{EI} \left(\frac{1a}{6L}\right) \left[-\left(\frac{a}{L}\right)^2 + \frac{x}{L} \left(2 + \left(\frac{a}{L}\right)^2\right) - 3\left(\frac{x}{L}\right)^2 + \left(\frac{x}{L}\right)^3 \right]
 \end{aligned}$$

Specific values are

$$\begin{aligned}
 \theta_A &= -\frac{Pa(2L^2 - 3aL + a^2)}{6EIL} \\
 \theta_B &= \frac{Pa}{6EIL}(L^2 - a^2) \\
 v_C &= -\frac{Pa^2(L - a)^2}{3EIL}
 \end{aligned}$$

The maximum deflection occurs at the point, where $\theta(x) = 0$. This location depends on a . When $a < L/2$ the peak displacement occurs in segment CB. The location reverses when $a > L/2$.
Special case: $a = L/2$



$$\begin{aligned}
 \theta_{\max} = \theta_B = -\theta_A &= \frac{PL^2}{16EI} \\
 \theta_C &= 0 \\
 v_{\max} &= -\frac{PL^3}{48EI} \quad \text{at } x = \frac{L}{2}
 \end{aligned}$$

3. Uniform Loading (Fig. E3.20d)

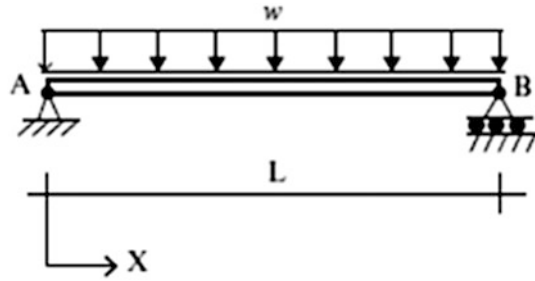
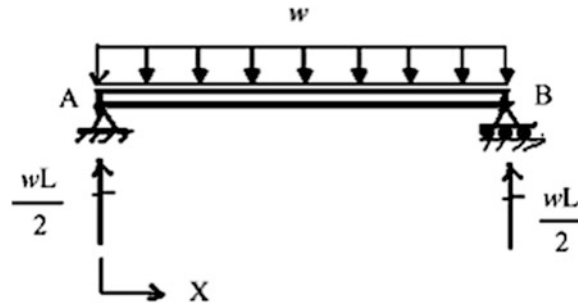


Fig. E3.20d

The expressions for $M(x)$, $\theta(x)$, and $v(x)$ for a uniform load are as follows:



$$M(x) = -\frac{wx^2}{2} + \frac{wL}{2}x \quad 0 \leq x \leq L$$

$$\theta(x) = -\int_0^L \frac{M(x)}{EI} dx + \frac{1}{L} \int_0^L x \frac{M(x)}{EI} dx + \int_0^x \frac{M(x)}{EI} dx$$

$$= \frac{wL^3}{24EI} \left(-4\frac{x^3}{L^3} + 6\frac{x^2}{L^2} - 1 \right)$$

$$v(x) = -x \int_0^L \frac{M(x)}{EI} dx + \frac{x}{L} \int_0^L x \frac{M(x)}{EI} dx + x \int_0^x \frac{M(x)}{EI} dx - \int_0^x x \frac{M(x)}{EI} dx$$

$$= \frac{wL^4}{24EI} \left(-\frac{x^4}{L^4} + 2\frac{x^3}{L^3} - \frac{x}{L} \right)$$

Specific values are

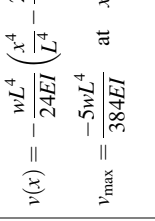
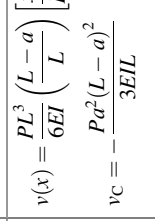
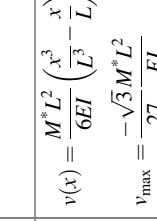
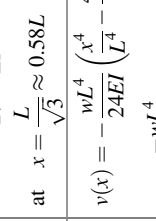
$$\theta_A = -\theta_B = -\frac{wL^3}{24EI}$$

$$v_{\max} = -\frac{5wL^4}{384EI} \quad \text{at } x = \frac{L}{2}$$

Note that the rotation is zero at mid-span since the loading and the structure are symmetrical.

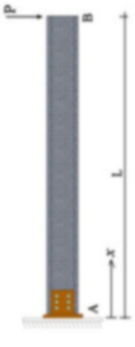
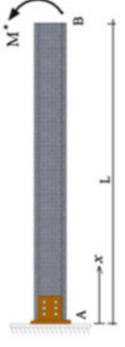
For future reference, the end displacements corresponding to typical loading condition are summarized in Table 3.1. We utilize these results in formulating the Force method to be presented in Chap. 9.

Table 3.1 Catalogue of displacements for various loading condition cases

Loading	Rotation θ^+ counter clockwise	Translation v^+ \uparrow
	$\theta(x) = -\frac{wL^3}{24EI} \left(\frac{4x^3}{L^3} - \frac{6x^2}{L^2} + 1 \right)$ $\theta_B = -\theta_A = \frac{wL^3}{24EI}$	$v(x) = -\frac{wL^4}{24EI} \left(\frac{x^4}{L^4} - \frac{2x^3}{L^3} + \frac{x}{L} \right)$ $v_{\max} = \frac{-5wL^4}{384EI} \quad \text{at } x = \frac{L}{2}$
	$\theta(x) = \frac{PL^2}{6EI} \left(1 - \frac{a}{L} \right) \left[3 \left(\frac{x}{L} \right)^2 - \frac{2a}{L} + \frac{a^2}{L^2} \right] \quad 0 \leq x \leq a$ $\theta_A = -\frac{Pa(2L^2 - 3aL + a^2)}{6EIL}$ $\theta_B = \frac{Pa(L^2 - a^2)}{6EIL}$	$v(x) = \frac{PL^3(L-a)}{6EI} \left(\frac{x}{L} \right) \left[\frac{x^3}{L^3} - \frac{2ax}{L^2} + \frac{a^2x}{L^3} \right] \quad 0 \leq x \leq a$ $v_C = -\frac{Pa^2(L-a)^2}{3EIL}$
	$\theta(x) = \frac{M^*L}{EI} \left(\frac{x^2}{2L^2} - \frac{1}{6} \right)$ $\theta_A = \frac{-M^*L}{6EI}$ $\theta_B = \frac{M^*L}{3EI}$	$v(x) = \frac{M^*L^2}{6EI} \left(\frac{x^3}{L^3} - \frac{x}{L} \right)$ $v_{\max} = \frac{-\sqrt{3}M^*L^2}{27EI}$ $\text{at } x = \frac{L}{\sqrt{3}} \approx 0.58L$
	$\theta(x) = -\frac{wL^3}{6EI} \left(\frac{x^3}{L^3} - \frac{3x^2}{L^2} + \frac{3x}{L} \right)$ $\theta_B = \frac{-wL^3}{6EI}$	$v(x) = -\frac{wL^4}{24EI} \left(\frac{x^4}{L^4} - \frac{4x^3}{L^3} + \frac{6x^2}{L^2} \right)$ $v_B = \frac{-wL^4}{8EI}$

(continued)

Table 3.1 (continued)

Loading	Rotation θ^+ counter clockwise	Translation v^+ \uparrow
	$\theta(x) = \frac{P}{EI} \left(\frac{x^2}{2} - Lx \right)$ $\theta_B = \frac{-PL^2}{2EI}$	$v(x) = \frac{P}{6EI} (x^3 - 3Lx^2)$ $v_B = \frac{-PL^3}{3EI}$
	$\theta(x) = \frac{M^*}{EI} x \theta_B = \frac{M^* L}{EI}$	$v(x) = \frac{M^* x^2}{2EI}$ $v_B = \frac{M^* L^2}{2EI}$

3.6.4 Computing Displacements with the Method of Virtual Forces

The procedures described in the previous section are intended to generate analytical solutions for the displacement and rotation. In many cases, one is interested only in the motion measures for a particular point. Rather than generate the complete analytical solution and then evaluate it at the point of interest, one can apply the Method of Virtual Forces. The Method of Virtual Forces specialized for bending of slender beams is defined in [1]. We express the principle as

$$d \cdot \delta P = \int_L (\text{bending deformation})(\delta M(x))dx \tag{3.35}$$

where d is the desired displacement measure, δP is the virtual force in the direction of d , and $\delta M(x)$ is the virtual moment due to δP . The deformation due to transverse shear is not included since it is negligible for slender beams. When the behavior is linear elastic, the bending deformation is related to the moment by

$$\text{bending deformation} \equiv \frac{d\theta}{dx} = \frac{M(x)}{EI}$$

and (3.35) takes the form

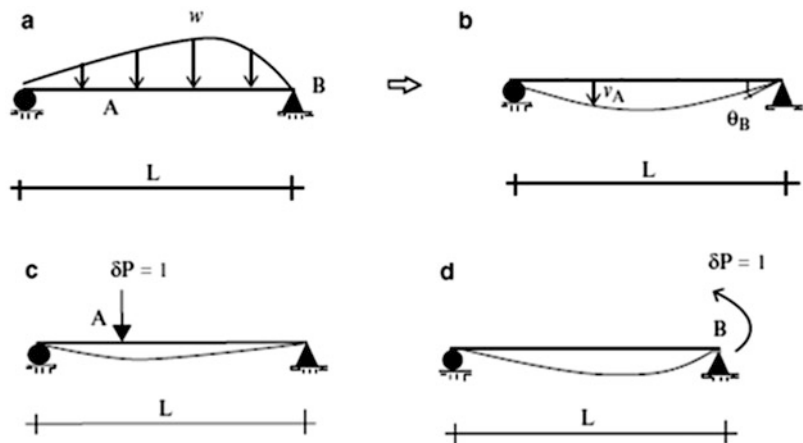
$$d \cdot \delta P = \int_L \frac{M(x)}{EI} \delta M(x)dx \tag{3.36}$$

The steps involved in applying the principle are as follows. We use as an example, the beam shown in Fig. 3.28. To determine a desired vertical displacement or rotation such as v_A or θ_B , one applies the corresponding virtual force or virtual moment in the direction of the desired displacement or rotation, determines the virtual moment $\delta M_v(x)$ or $\delta M_\theta(x)$, and then evaluates the following integrals.

$$v_A = \int_L \frac{M(x)}{EI} \delta M_v(x)dx$$

$$\theta_B = \int_L \frac{M(x)}{EI} \delta M_\theta(x)dx$$

Fig. 3.28 Actual and virtual loads moments. (a) Actual load $M(x)$. (b) Deflected shape. (c) Virtual load δM_v for v_A . (d) Virtual load $\delta M_\theta(x)$ for θ_B



Just as we did for truss structures in Chap. 2, one takes δP to be a unit value. We illustrate the application of this procedure with the following examples.

Example 3.21 Deflection Computation—Method of Virtual Forces

Given: A uniformly loaded cantilever beam shown in Fig. E3.21a.

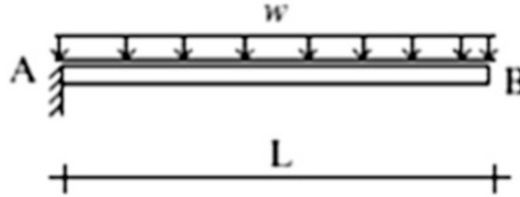


Fig. E3.21a

Determine: The vertical displacement and rotation at B. Take EI as constant.

Solution: We start by evaluating the moment distribution corresponding to the applied loading. This is defined in Fig. E3.21b. The virtual moment distributions corresponding to v_B , θ_B are defined in Figs. E3.21c and E3.21d. Note that we take δP to be either a unit force (for displacement) or a unit moment (for rotation).

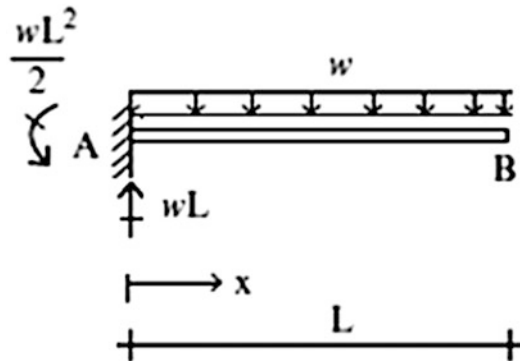


Fig. E3.21b $M(x)$

The actual moment $M(x)$ is

$$0 \leq x \leq L \quad M(x) = wLx - w\frac{x^2}{2} - \frac{wL^2}{2} = -\frac{w}{2}(x-L)^2$$

Vertical deflection at B: We apply the virtual vertical force, $\delta P = 1$ at point B and compute the corresponding virtual moment.

$$0 \leq x \leq L \quad \delta M_{v_B}(x) = x - L$$

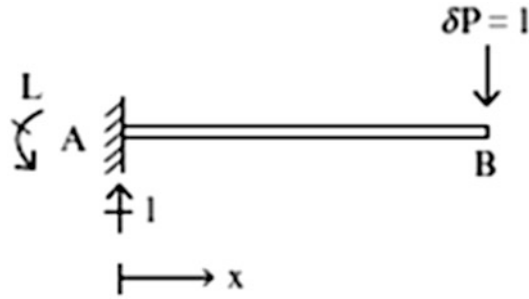


Fig. E3.21c $\delta M_{v_B}(x)$

Then, noting (3.36)

$$\begin{aligned} v_B &= \int_L \frac{M(x)}{EI} \delta M_{v_B}(x) dx = \frac{1}{EI} \int_0^L -\frac{w}{2}(x-L)^2(x-L) dx \\ &= \frac{1}{EI} \int_0^L -\frac{w}{2}(x-L)^3 dx \end{aligned}$$

Integrating leads to

$$v_B = \frac{wL^4}{8EI} \downarrow$$

Rotation at B: We apply the virtual moment, $\delta P = 1$ at point B and determine $\delta M(x)$.

This loading produces a constant bending moment,

$$0 \leq x \leq L \quad \delta M_{\theta_B}(x) = -1$$

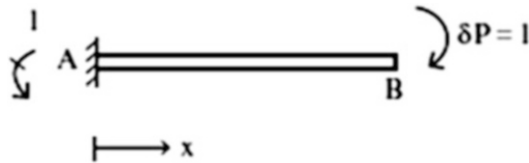


Fig. E3.21d $\delta M_{\theta_B}(x)$

Then, noting (3.36)

$$\theta_B = \int_L \frac{M(x)}{EI} \delta M_{\theta_B}(x) dx = \frac{1}{EI} \int_0^L -\frac{w}{2}(x-L)^2(-1) dx$$

Finally, one obtains

$$\theta_B = \frac{wL^3}{6EI} \text{ clockwise}$$

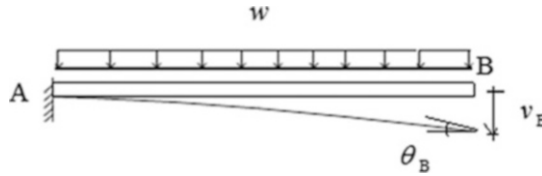


Fig. E3.21e Deflected shape

Example 3.22 Deflection Computation—Method of Virtual Forces

Given: The simply supported beam shown in Fig. E3.22a.

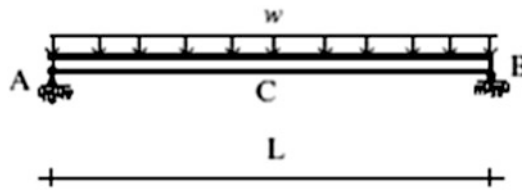


Fig. E3.22a

Determine: The vertical deflection and rotation at point C located at mid-span. Take EI is constant.

Solution: We start by evaluating the moment distribution corresponding to the applied loading. This is defined in Fig. E3.22b. The virtual moment distributions corresponding to v_C , θ_C are defined in Figs. E3.22c and E3.22d. Note that we take δP to be either a unit force (for displacement) or a unit moment (for rotation).

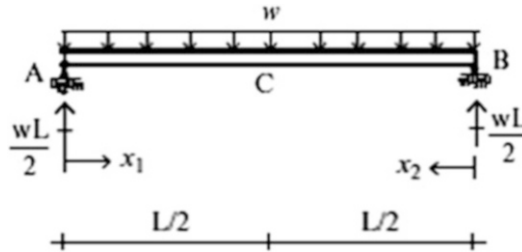


Fig. E3.22b $M(x)$

The actual moment is

$$0 < x_1 < L \quad M(x_1) = \frac{wL}{2}x_1 - \frac{wx_1^2}{2}$$

$$0 < x_2 < L \quad M(x_2) = \frac{wL}{2}x_2 - \frac{wx_2^2}{2}$$

Vertical displacement at C: We apply a unit virtual load at point C and determine $\delta M(x)$.

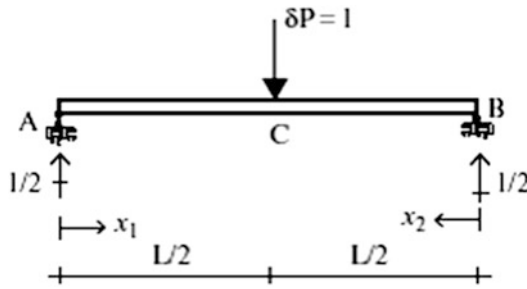


Fig. E3.22c $\delta M_{\nu C}(x)$

$$0 < x_1 < \frac{L}{2} \quad \delta M_{\nu C}(x_1) = \frac{1}{2}x_1$$

$$0 < x_2 < \frac{L}{2} \quad \delta M_{\nu C}(x_2) = \frac{1}{2}x_2$$

Then, evaluating the integral in (3.36), we obtain

$$v_C = \int_{AC} \left(\frac{M(x_1)}{EI} \delta M_{\nu C}(x_1) \right) dx_1 + \int_{BC} \left(\frac{M(x_2)}{EI} \delta M_{\nu C}(x_2) \right) dx_2$$

$$= \frac{1}{EI} \left[\int_0^{L/2} \left(\frac{1}{2}x_1 \right) \left(\frac{wLx_1}{2} - \frac{wx_1^2}{2} \right) dx_1 + \int_0^{L/2} \left(\frac{1}{2}x_2 \right) \left(\frac{wLx_2}{2} - \frac{wx_2^2}{2} \right) dx_2 \right]$$

$$= \frac{5wL^4}{384EI} \downarrow$$

Rotation at C: We apply a unit virtual moment at point C and determine $\delta M(x)$.

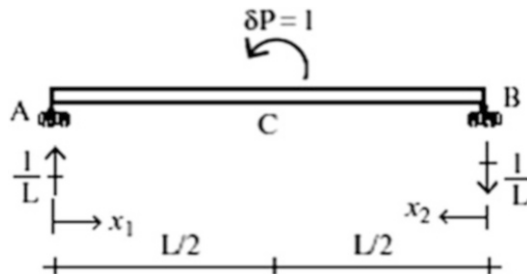


Fig. E3.22d $\delta M_{\theta C}(x)$

$$0 < x_1 < \frac{L}{2} \quad \delta M_{\theta C}(x_1) = \frac{x_1}{L}$$

$$0 < x_2 < \frac{L}{2} \quad \delta M_{\theta C}(x_2) = -\frac{x_2}{L}$$

Then, evaluating the integral in (3.36), we obtain

$$\begin{aligned}\theta_C &= \int_{AC} \left(\frac{M(x_1)}{EI} \delta M_{\theta_C}(x_1) \right) dx_1 + \int_{BC} \left(\frac{M(x_2)}{EI} \delta M_{\theta_C}(x_2) \right) dx_2 \\ &= \frac{1}{EI} \left\{ \int_0^{L/2} \left(\frac{x_1}{L} \right) \left(\frac{wLx_1}{2} - \frac{wx_1^2}{2} \right) dx_1 + \int_0^{L/2} \left(\frac{-x_2}{L} \right) \left(\frac{wLx_2}{2} - \frac{wx_2^2}{2} \right) dx_2 \right\} = 0\end{aligned}$$

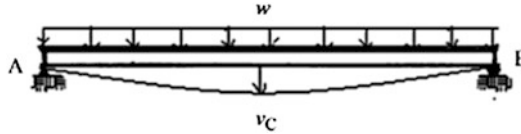


Fig. E3.22e Deflected shape

Example 3.23 Deflection Computation—Method of Virtual Forces

Given: The beam shown in Fig. E3.23a.

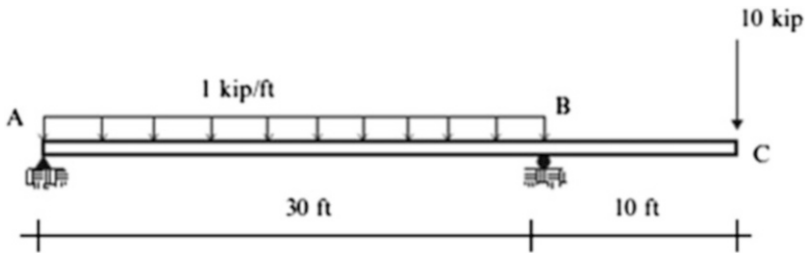


Fig. E3.23a

Determine: Use the virtual force method to determine the vertical deflection and rotation at C. $E = 29,000$ ksi and $I = 300$ in.⁴

Solution: We start by evaluating the moment distribution corresponding to the applied loading. We divide up the structure into two segments AB and CB.

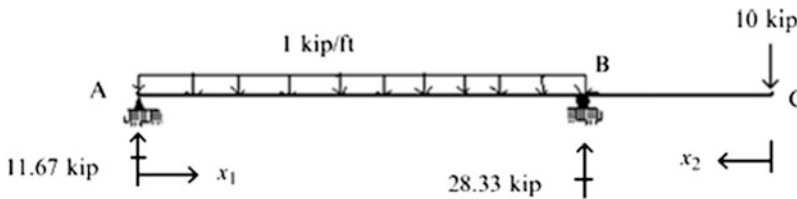


Fig. E3.23b $M(x)$

$$\begin{aligned}0 < x_1 < 30 & M(x_1) = 11.67x_1 - \frac{x_1^2}{2} \\ 0 < x_2 < 10 & M(x_2) = -10x_2\end{aligned}$$

Vertical deflection at C: We apply a unit virtual load at point C and determine $\delta M(x)$.

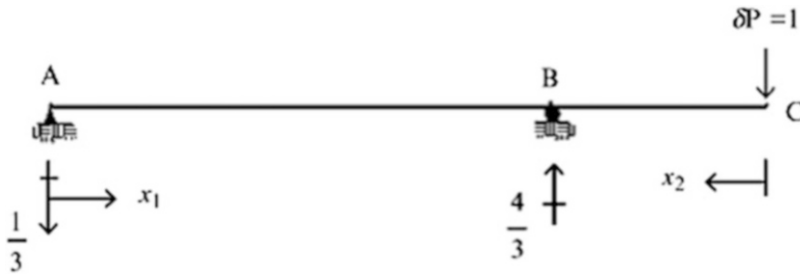


Fig. E3.23c $\delta M_{vC}(x)$

$$0 < x_1 < 30 \quad \delta M_{vC}(x_1) = -\frac{x_1}{3}$$

$$0 < x_2 < 10 \quad \delta M_{vC}(x_2) = -x_2$$

Then, noting (3.36), we divide up the structure into two segments AB and CB and integrate over each segment. The total integral is given by

$$\begin{aligned} v_C &= \int_{AB} \left(\frac{M(x_1)}{EI} \delta M_{vC}(x_1) \right) dx_1 + \int_{CB} \left(\frac{M(x_2)}{EI} \delta M_{vC}(x_2) \right) dx_2 \\ &= \frac{1}{EI} \int_0^{30} \left(11.67x_1 - \frac{x_1^2}{2} \right) \left(-\frac{x_1}{3} \right) dx_1 + \frac{1}{EI} \int_0^{10} (-10x_2)(-x_2) dx_2 \\ &= + \frac{2073.33 \text{ kip ft}^3}{EI} = \frac{2073.33(12)^3}{29,000(300)} = +0.41 \text{ in.} \end{aligned}$$

The positive sign indicates that the vertical displacement is in the direction of the unit load.

$$\therefore v_C = 0.41 \text{ in. } \downarrow$$

Rotation at C: We apply a unit virtual moment at point C and determine $\delta M(x)$.

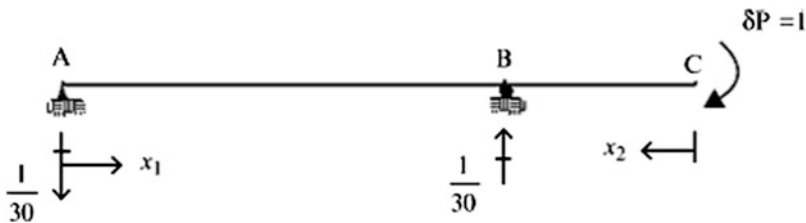


Fig. E3.23d $\delta M_{\theta C}(x)$

$$0 < x_1 < 30 \quad \delta M_{\theta C}(x) = -\frac{x_1}{30}$$

$$0 < x_2 < 10 \quad \delta M_{\theta C}(x) = -1$$

Then, noting (3.36)

$$\begin{aligned} \theta_C &= \int_{AB} \left(\frac{M(x)}{EI} \delta M_{\theta_C}(x) \right) dx_1 + \int_{CB} \left(\frac{M(x)}{EI} \delta M_{\theta_C}(x) \right) dx_2 \\ &= \frac{1}{EI} \int_0^{30} \left(11.67x_1 - \frac{x_1^2}{2} \right) \left(-\frac{x_1}{30} \right) dx_1 + \frac{1}{EI} \int_0^{10} (-10x_2)(-1) dx_2 \\ &= \frac{374 \text{ kip ft}^2}{EI} = \frac{374(12)^2}{29,000(300)} = +0.0063 \text{ rad} \end{aligned}$$

The positive sign indicates that the rotation is in the direction of the unit moment.

$$\therefore \theta_C = 0.0063 \text{ rad clockwise}$$

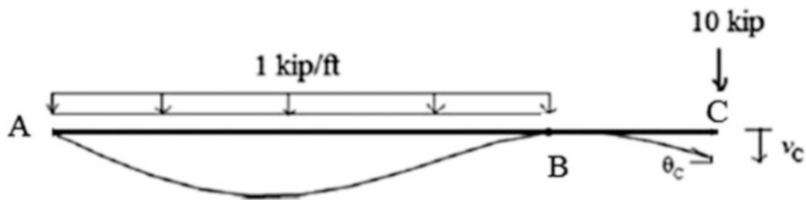


Fig. E3.23e Deflected shape

Example 3.24 Deflection Computation—Method of Virtual Forces

Given: The beam shown in Fig. E3.24a.

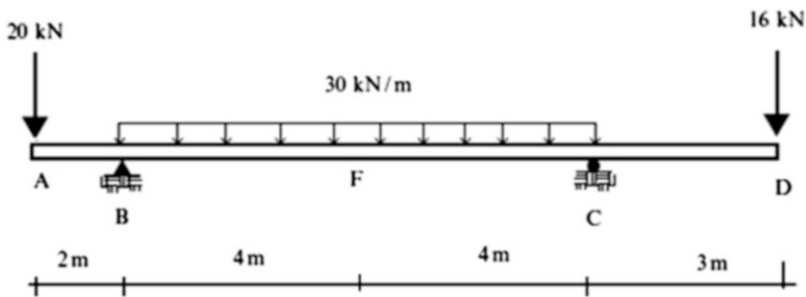


Fig. E3.24a

Determine: Use the virtual force method to determine the vertical deflection at F, rotation at B, and rotation at D. Assume $E = 200 \text{ GPa}$ and $I = 120(10)^6 \text{ mm}^4$.

Solution: We start by evaluating the moment distribution corresponding to the applied loading.

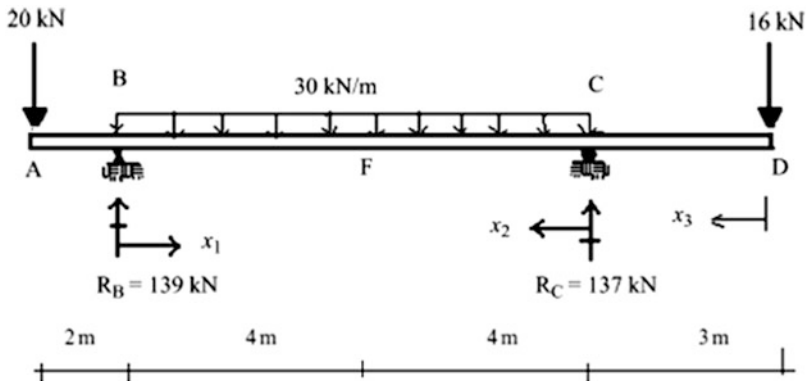


Fig. E3.24b $M(x)$

$$\begin{aligned}
 0 < x_1 < 8 \quad M(x_1) &= -15x_1^2 + 139x_1 - 20(x_1 + 2) = -15x_1^2 + 119x_1 - 40 \\
 0 < x_2 < 8 \quad M(x_2) &= -15x_2^2 + 137x_2 - 16(x_2 + 3) = -15x_2^2 + 121x_2 - 48 \\
 0 < x_3 < 3 \quad M(x_3) &= -16x_3
 \end{aligned}$$

Vertical deflection at F: We apply a unit virtual load at point F and determine δM .

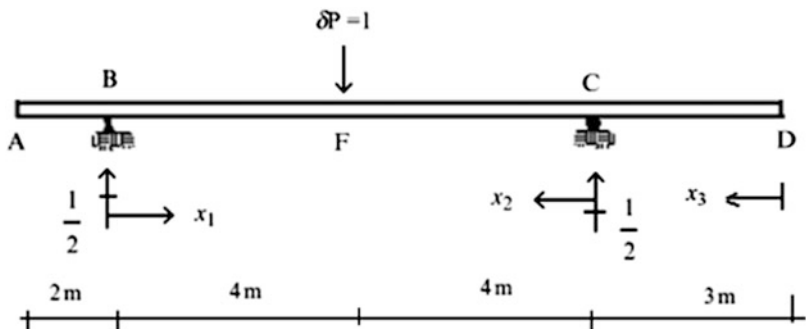


Fig. E3.24c $\delta M_{v_F}(x)$

$$\begin{aligned}
 0 < x_1 < 4 \quad \delta M_{v_F}(x_1) &= \frac{1}{2}x_1 \\
 0 < x_2 < 4 \quad \delta M_{v_F}(x_2) &= \frac{1}{2}x_2
 \end{aligned}$$

Then, noting (3.36)

$$\begin{aligned}
 v_F &= \int_{BF} \left(\frac{M(x_1)}{EI} \delta M_{v_F}(x_1) \right) dx_1 + \int_{CF} \left(\frac{M(x_2)}{EI} \delta M_{v_F}(x_2) \right) dx_2 \\
 &= \frac{1}{EI} \left\{ \int_0^4 (-15x_1^2 + 119x_1 - 40) \left(\frac{x_1}{2} \right) dx_1 + \int_0^4 (-15x_2^2 + 121x_2 - 48) \left(\frac{x_2}{2} \right) dx_2 \right\} \\
 &= \frac{1248 \text{ kNm}^3}{EI} = \frac{1248(10)^9}{200(120)(10)^6} = 52 \text{ mm}
 \end{aligned}$$

The positive sign indicates that the vertical displacement is in the direction of the unit load.

$$\therefore v_F = 52 \text{ mm } \downarrow$$

Rotation at B: We apply a unit moment at point B and determine $\delta M(x)$.

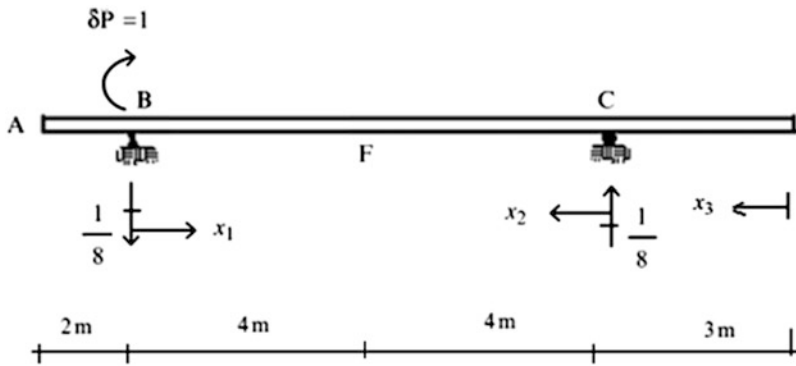


Fig. E3.24d $\delta M_{\theta_B}(x)$

$$0 < x_2 < 8 \quad \delta M_{\theta_B}(x_2) = \frac{1}{8}x_2$$

Then, noting (3.36)

$$\begin{aligned} \theta_B &= \int_{CB} \frac{M(x_2)}{EI} \delta M_{\theta_B}(x_2) dx_2 = \frac{1}{EI} \int_0^8 (-15x_2^2 + 121x_2 - 48) \left(\frac{x_2}{8}\right) dx_2 \\ &= \frac{469.3 \text{ kNm}^2}{EI} = \frac{469.3(10)^6}{200(120)(10)^6} = +0.0195 \text{ rad} \end{aligned}$$

The positive sign indicates that the rotation is in the direction of the unit moment.

$$\therefore \theta_B = 0.0195 \text{ rad clockwise}$$

Rotation at D: We apply a unit moment at point D and determine $\delta M(x)$.

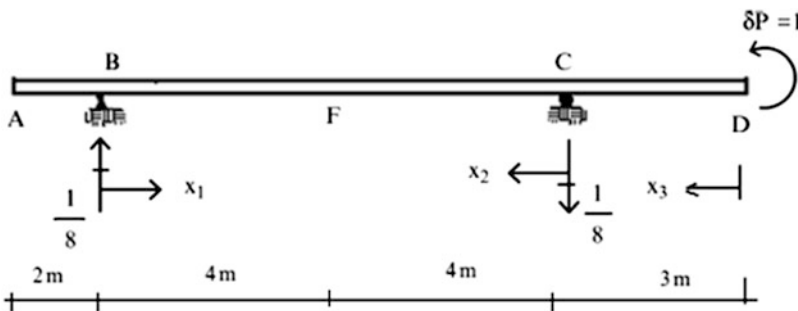


Fig. E3.24e $\delta M_{\theta_D}(x)$

$$0 < x_1 < 8 \quad \delta M_{\theta_D}(x_1) = \frac{1}{8}x_1$$

$$0 < x_3 < 3 \quad \delta M_{\theta_D}(x_3) = 1$$

Then, noting (3.36)

$$\begin{aligned}\theta_D &= \int_{BC} \frac{M(x_1)}{EI} \delta M_{\theta_D}(x_1) dx_1 + \int_{DC} \frac{M(x_3)}{EI} \delta M_{\theta_D}(x_3) dx_3 \\ &= \frac{1}{EI} \int_0^8 (-15x_1^2 + 119x_1 - 40) \left(\frac{x_1}{8}\right) dx_1 + \frac{1}{EI} \int_0^3 (-16x_3)(1) dx_3 \\ &= + \frac{386.7 \text{ kNm}^2}{EI} = \frac{386.7(10)^6}{200(120)(10)^6} = 0.016 \text{ rad}\end{aligned}$$

The positive sign indicates that the rotation is in the direction of the unit moment.

$$\therefore \theta_D = 0.016 \text{ rad counterclockwise}$$

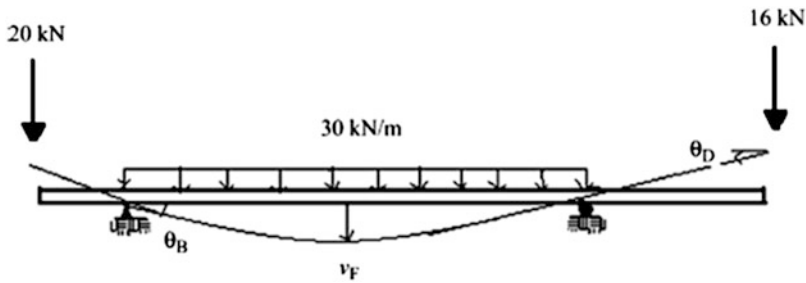


Fig. E3.24f Deflected shape

3.6.5 Computing Displacements for Non-prismatic Members

When the member is non-prismatic, I is a function of x and it may be difficult to obtain a closed form solution for the integral involving $1/I$. In this case, one can employ a numerical integration scheme. In what follows, we describe a numerical integration procedure which can be easily programmed.

Consider the problem of evaluating the following integral

$$J = \int_{x_A}^{x_B} f(x) dx \quad (3.37)$$

We divide the total interval into n equal segments of length h

$$h = \frac{x_B - x_A}{n} \quad (3.38)$$

and denote the values of x and f at the equally spaced points as

$$\begin{aligned}x_1, x_2, x_3, \dots, x_{n+1} \\ f_1, f_2, f_3, \dots, f_{n+1}\end{aligned}$$

This notation is illustrated in Fig. 3.29.

Fig. 3.29 Piecewise function approximation

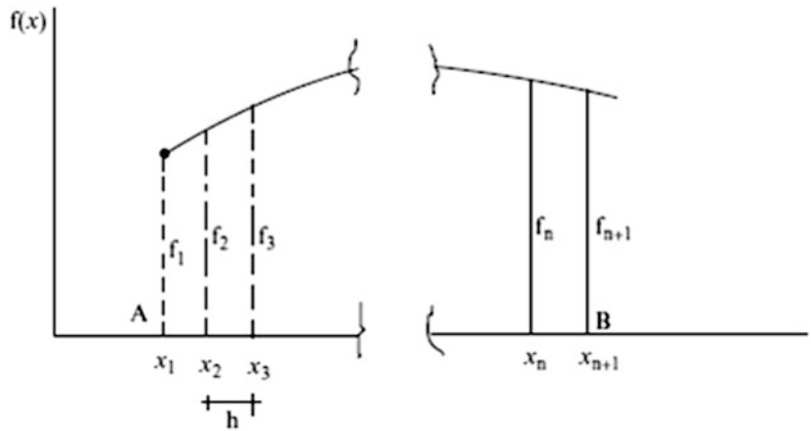
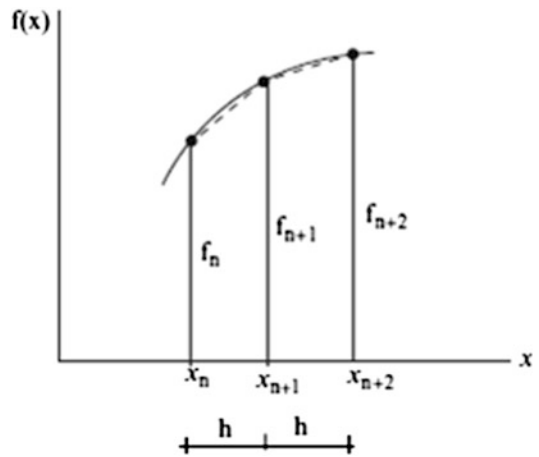


Fig. 3.30 Notation



The simplest approach is based on approximating the actual curve of $f(x)$ with a set of straight lines connecting (f_n, f_{n+1}) , (f_{n+1}, f_{n+2}) , etc. as shown in Fig. 3.30.

The incremental area between x_n and x_{n+1} is approximated as

$$\Delta J_{n,n+1} = \int_{x_n}^{x_{n+1}} f(x)dx \approx \frac{h}{2}(f_n + f_{n+1}) \tag{3.39}$$

Also, the area between x_1 and x_n is expressed as

$$J_n = \int_{x_1}^{x_n} f(x)dx \tag{3.40}$$

Starting with $J_1 = 0$, one generates successive areas with

$$\begin{aligned} J_2 &= J_1 + \Delta J_{1,2} = \Delta J_{1,2} \\ J_3 &= J_2 + \Delta J_{2,3} \\ &\vdots \\ J_n &= J_{n-1} + \Delta J_{n-1,n} \\ J_{n+1} &= J_n + \Delta J_{n,n+1} \end{aligned} \tag{3.41}$$

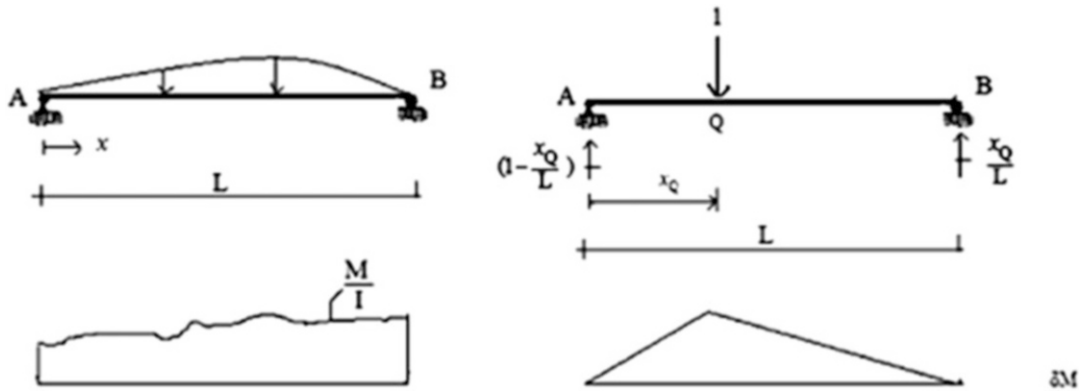


Fig. 3.31 Moment distribution

The total integral, J_{n+1} expands to

$$J_{n+1} = \int_{x_1}^{x_{n+1}} f(x)dx \approx h \left\{ \frac{1}{2}(f_1 + f_{n+1}) + \sum_{j=2}^n f_j \right\} \tag{3.42}$$

Equation (3.42) is known as the ‘‘Trapezoidal’’ Rule. One uses (3.41) to evaluate the intermediate integrals when applying the Moment Area Theorems such as (3.33) and (3.34). Equation (3.42) is also used with the Virtual Force Method.

We illustrate the application of this approach defined by (3.36) to the beam defined in Fig. 3.31. Suppose the vertical displacement at point Q is desired. Given $M(x)$ and $I(x)$, we subdivide the X -axis into n equal intervals and evaluate M/I and $\delta M(x)$ at each point.

$$h = \frac{L}{n}$$

$$x_k = (k - 1)h \quad k = 1, 2, \dots, n + 1$$

$$\delta M(x_k) = \left(1 - \frac{x_Q}{L}\right)x_k \quad x < x_Q$$

$$\delta M(x_k) = (L - x_k)\frac{x_Q}{L} \quad x > x_Q$$

Lastly, we take $f = \left(\frac{M}{I}\right)\delta M$ in (3.42) and evaluate the summation. The choice of h depends on the ‘‘smoothness’’ of the function M/I ; a typical value is $L/20$. One can assess the accuracy by refining the initial choice for h and comparing the corresponding values of the integral.

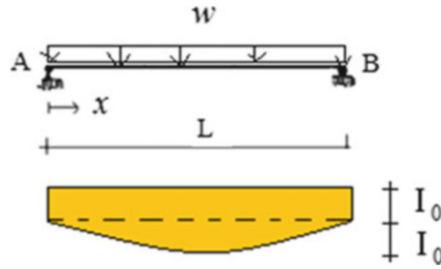
Suppose the deflection at $x = L/2$ is desired. The virtual moment for this case is

$$\begin{cases} \delta M(x) = \left(1 - \frac{1}{2}\right)x_k = \frac{1}{2}x_k & \text{for } x_k < \frac{L}{2} \\ \delta M(x) = (L - x_k)\frac{1}{2} & \text{for } x_k > \frac{L}{2}. \end{cases}$$

We also suppose the loading is uniform and the variation of I is given by

$$I = I_0 \left\{ 1 + 4 \left[\frac{x}{L} - \left(\frac{x}{L} \right)^2 \right] \right\}$$

where I_0 is constant.



The corresponding moment is

$$M = \frac{wL}{2}x - \frac{wx^2}{2} = \frac{wL^2}{8} \left\{ 4 \left[\frac{x}{L} - \left(\frac{x}{L} \right)^2 \right] \right\}$$

Substituting for M , δM , and I , the virtual force expression for the displacement takes the form

$$v \left(x = \frac{L}{2} \right) = \frac{wL^4}{8EI_0} \int_0^1 \left\{ \frac{4 \left[\frac{x}{L} - \left(\frac{x}{L} \right)^2 \right] \frac{\delta M}{L}}{1 + 4 \left[\frac{x}{L} - \left(\frac{x}{L} \right)^2 \right]} \right\} d \left(\frac{x}{L} \right) = \frac{wL^4}{8EI_0} \alpha$$

where α is a dimensionless coefficient that depends on the interval size.

We subdivide the interval 0–1 into n such intervals. Applying Equation (3.42) and taking a range of values for n leads to

$$\begin{aligned} n = 10 & \quad \alpha = 0.065 \\ n = 20 & \quad \alpha = 0.0559 \\ n = 30 & \quad \alpha = 0.0559 \end{aligned}$$

We note that taking $n = 20$ is sufficiently accurate. We used MATLAB [2] to program the computation associated with Equation (3.42).

3.7 Deformation–Displacement Relations for Deep Beams: Planar Loading

When the depth to span ratio is greater than 0.1, the theory presented in Sect. 3.6, which is based on Kirchhoff’s hypothesis, needs to be modified to include the transverse shear deformation. Figure 3.32 illustrates this case: the cross-section remains a plane but is no longer normal to the centroidal axis. Defining β as the rotation of the cross-section, and γ as the transverse shear strain, it follows that

$$\gamma = \theta - \beta \approx \frac{dv}{dx} - \beta \quad (3.43)$$

The extensional strain now involves β rather than θ .

$$\varepsilon(y) = -y \frac{d\beta}{dx} \quad (3.44)$$

Expressions for the internal force variables, V and M , in terms of the deformation measures are derived in a similar way as followed in Sect. 3.6.1. We express them as:

Fig. 3.32 Deformation with transverse shear deformation

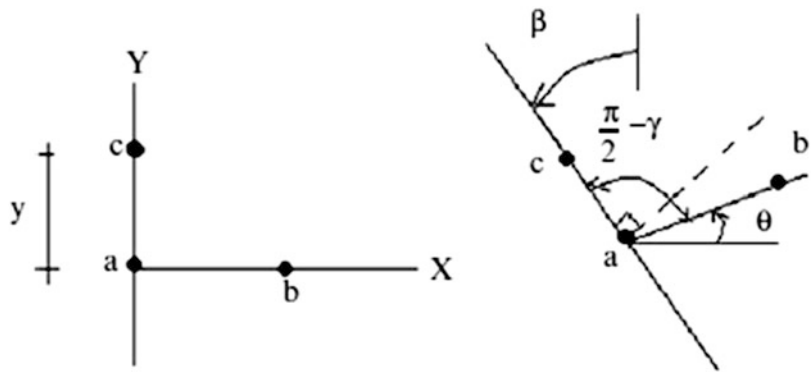
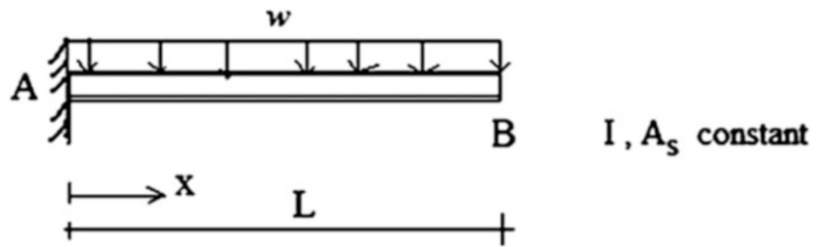


Fig. 3.33 Cantilever beam



$$\begin{aligned} M &= EI \frac{d\beta}{dx} \\ V &= GA_s \gamma \end{aligned} \tag{3.45}$$

where G is the material shear modulus and A_s is the effective shear area, i.e., the cross-sectional area over which the shear stress is essentially uniformly distributed. For an I shape steel section, A_s is taken as the web area.

Given M and V , one first determines β by integrating between two points, x_A and x

$$\beta(x) - \beta(x_A) = \int_{x_A}^x \frac{M}{EI} dx \tag{3.46}$$

If A is a fixed support, $\beta(x_A) = 0$. Once β is known, we find v by integrating

$$\frac{dv}{dx} = \beta + \frac{V}{GA_s}$$

This leads to

$$v(x) - v(x_A) = \int_{x_A}^x \left(\beta + \frac{V}{GA_s} \right) dx \tag{3.47}$$

In general, two boundary conditions are required to specify the two integration constants.

For example, consider the structure and loading defined in Fig. 3.33.

The transverse shear force and moment expressions are

$$V(x) = -w(L - x)$$

$$M(x) = -\frac{w}{2}(L - x)^2$$

Point A is a fixed support. Then, $\beta(x_A) = v(x_A) = 0$. Noting (3.46),

$$\begin{aligned} \beta &= \int_0^x -\frac{w}{2EI}(L - x)^2 dx \\ &\quad \downarrow \\ \beta &= \frac{w}{6EI}(L - x)^3 - \frac{w}{6EI}L^3 \end{aligned}$$

Substituting for β in (3.47) leads to

$$\begin{aligned} v(x) &= \left[\frac{w}{2GA_s}(L - x)^2 \right]_0^x + \left[-\frac{w}{24EI}(L - x)^4 - \frac{w}{6EI}L^3x \right]_0^x \\ &= \frac{w}{2GA_s} \left((L - x)^2 - L^2 \right) + \frac{w}{6EI} \left(-\frac{1}{4}(L - x)^4 - L^3x + \frac{L^4}{4} \right) \end{aligned} \quad (3.48)$$

Specializing for $x = L$, the end displacement is equal to

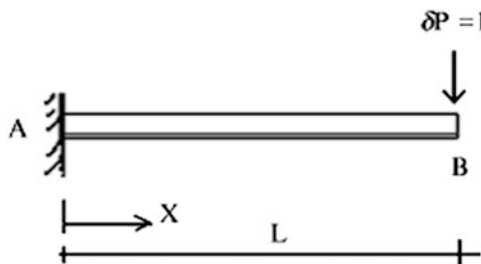
$$+ \uparrow v(L) = -\frac{wL^4}{8EI} \left(1 + \frac{4EI}{GA_sL^2} \right)$$

The effect of shear deformation is to “increase” the displacement by a dimensionless factor which is proportioned to the ratio EI/GA_sL^2 . This factor is usually small with respect to 1 for a homogeneous cross-section. It may be large for composite beams that have a “soft” core, i.e., where $G \ll E$.

Rather than work with the deformation–displacement results, one can apply an extended form of the Principle of Virtual Forces. We add the shear deformation term to the integral and also introduce the virtual shear force δV . Then, (3.36) expands to

$$d \cdot \delta P = \int_L \left(\frac{M(x)}{EI} \delta M(x) + \frac{V(x)}{GA_s} \delta V(x) \right) dx \quad (3.49)$$

The steps involved are the same as for slender beams. One now has to determine δV as well as δM for a given δP . Revisiting the previous example defined in Fig. 3.33, we compute $v(L)$. The details are as follows.



$$\begin{aligned} \delta V(x) &= -1 \\ \delta M(x) &= -(L - x) \end{aligned}$$

$$\begin{aligned}
 + \downarrow v(L) &= \int_0^L \frac{w}{2EI}(L-x)^2(L-x)dx + \int_0^L \frac{-w}{GA_s}(L-x)(-1)dx \\
 &= \left[\frac{-w}{8EI}(L-x)^4 \right]_0^L + \left[-\frac{w}{2GA_s}(L-x)^2 \right]_0^L \\
 &= \frac{w}{8EI}L^4 + \frac{w}{2GA_s}L^2
 \end{aligned}$$

Applying the Principle of Virtual Forces for this example involves less algebra than required for integration.

3.8 Torsion of Prismatic Members

Consider the prismatic member shown in Fig. 3.34. Up to this point, we have assumed the line of action of the external loading passes through the centroidal axis, and consequently the member just bends in the $X - Y$ plane. This assumption is not always true, and there are cases where the loading may have some eccentricity with respect to the X -axis. When this occurs, the member twists about the X -axis as well as bends in the $X - Y$ plane.

We deal with an eccentric load by translating its line of action to pass through the X -axis. This process produces a torsional moment about X as illustrated in Fig. 3.34.

The torsional moment is resisted by shearing stresses acting in the plane of the cross-section, resulting in shear strain and ultimately rotation of the cross-section about the X -axis. Mechanics of Solids texts such as [1] present a detailed theory of torsion of prismatic members so we just list the resultant equations here. First, we introduce the following notation listed in Fig. 3.35

Fig. 3.34 Prismatic member—eccentric load

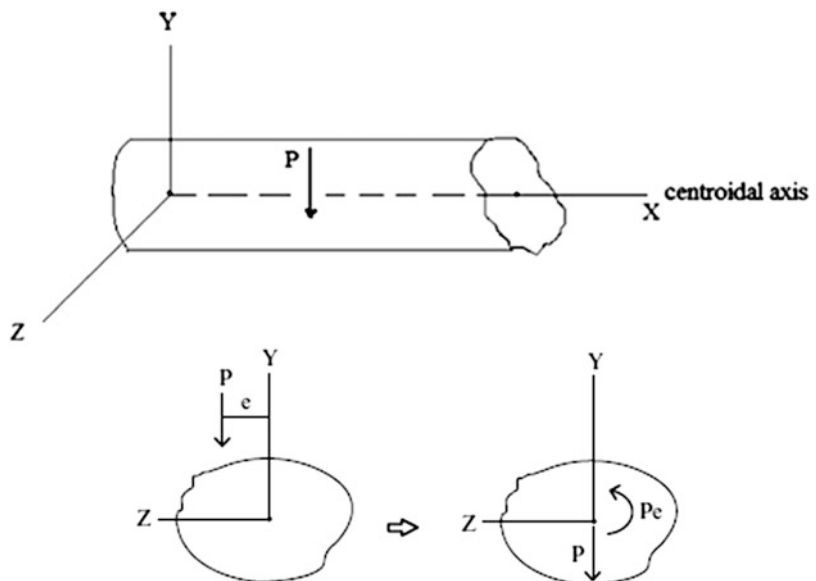
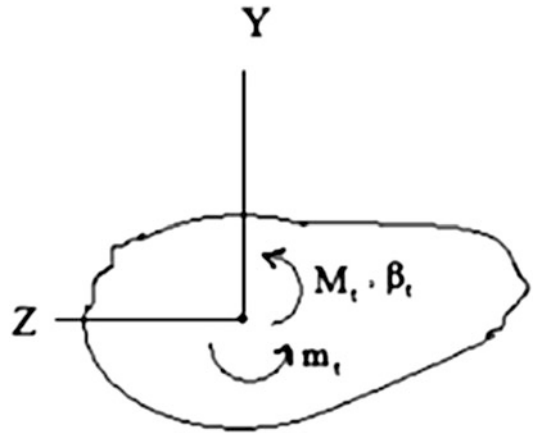


Fig. 3.35 Notation



M_t = moment vector about the X -axis (positive sense from Y toward Z)

β_t = rotational vector about the X -axis

m_t = distributed external torsional moment loading

J = torsional cross-sectional property (similar to I for plane bending)

The differential equation of equilibrium for torsion has the form

$$\frac{dM_t}{dx} + m_t = 0 \quad (3.50)$$

One needs to restrain the member at one point for stability. A free end has $M_t = 0$. Given M_t , one determines the rotation with

$$M_t = GJ \frac{d\beta_t}{dx} \quad (3.51)$$

Note the similarity between the expression for bending and twisting. We find β_t by integrating (3.51).

$$\beta_t(x) - \beta_t(x_A) = \int_{x_A}^x \frac{M_t}{GJ} dx \quad (3.52)$$

A boundary condition on β_t is required to determine $\beta_t(x)$. Typical boundary conditions are illustrated below.



The principle of Virtual Forces can be extended to deal with combined bending and twisting by adding the twist deformation term to the integration. The general expression which includes all deformation terms is

$$d\delta P_A = \int_L \left(\frac{M}{EI} \delta M + \frac{V}{GA_s} \delta V + \frac{M_t}{GJ} \delta M_t \right) dx \quad (3.53)$$

where δM_t is the virtual torsional moment.

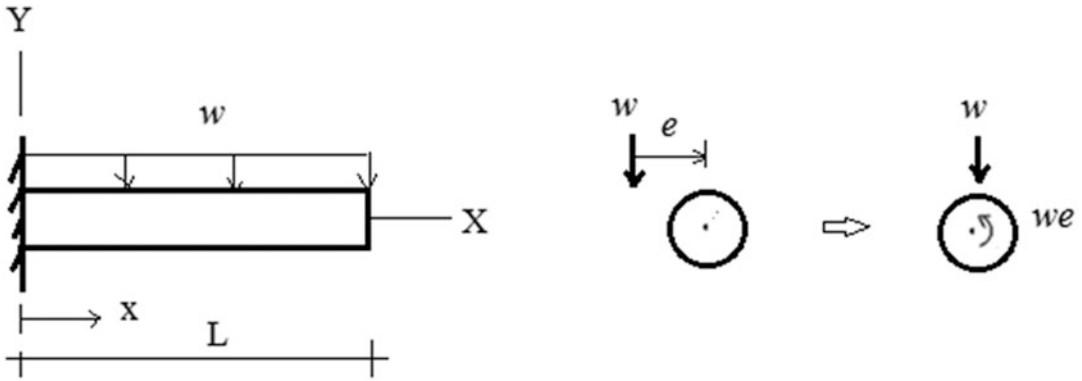


Fig. 3.36 Eccentrically loaded member

When bending and twisting are coupled because of eccentric loading, it is convenient to solve the bending and twisting problems separately, and then combine the solutions.

In what follows, we illustrate this approach.

The eccentric load shown in Fig. 3.36 produces the distributed torsional loading equal to we , and the planar loading w . Noting (3.50), the torsional moment is

$$M_t = we(L - x)$$

We determine the twist with (3.52). The left end is fixed, so $\beta_t(0) = 0$. Then,

$$\begin{aligned}\beta_t(x) &= \int_0^x \frac{1}{GJ} [we(L - x)] = -\frac{we}{2GJ} (L - x)^2 \Big|_0^x \\ \beta_t(x) &= \frac{we}{2GJ} (2Lx - x^2)\end{aligned}$$

The solution for plane bending is generated with (3.22)

$$\begin{aligned}\frac{d\theta}{dx} &= -\frac{w}{2EI} (L - x)^2 \\ \theta(x) &= \left[\frac{w}{6EI} (L - x)^3 \right]_0^x = \frac{w}{6EI} (L - x)^3 - \frac{wL^3}{6EI} \\ v(x) &= \left[-\frac{w}{24EI} (L - x)^4 - \frac{wL^3x}{6EI} \right]_0^x = \frac{w}{6EI} \left\{ -\frac{1}{4} (L - x)^4 - L^3x + \frac{L^4}{4} \right\}\end{aligned}$$

The solution for a cantilever beam subjected to a concentrated torsional moment at the free end is needed later when we deal with plane grids.

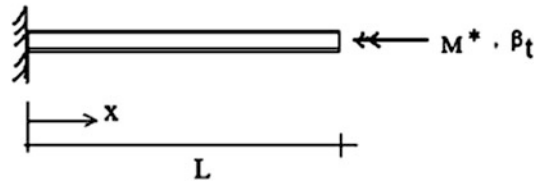
Noting Fig. 3.37, the torsional moment is constant,

$$M_t = M^*$$

and the twist angle varies linearly with x

$$\beta_t = \frac{M^*}{GJ} x \quad (3.54)$$

Fig. 3.37 Pure torsion



3.9 Symmetry and Anti-symmetry

3.9.1 Symmetry and Anti-symmetry: Shear and Moment Diagrams

This section discusses the relationship between certain properties of the shear and moment diagrams and the nature of the loading distribution and support locations. We first introduce some background material on symmetrical and anti-symmetrical functions.

Consider the function $f(x)$ shown in Fig. 3.38. We say the function is symmetrical with respect to $x = 0$ when $f(-x) = f(x)$ and anti-symmetrical when $f(-x) = -f(x)$. Symmetrical functions have $df/dx = 0$ at $x = 0$. Anti-symmetrical functions have $f = 0$ at $x = 0$. One can establish that the derivative of a symmetrical function is an anti-symmetrical function. Similarly, the derivative of an anti-symmetrical function is a symmetrical function. If we know that a function is either symmetrical or anti-symmetrical, then we have to generate only one-half the distribution. The shape of the other half follows by definition of the symmetry properties.

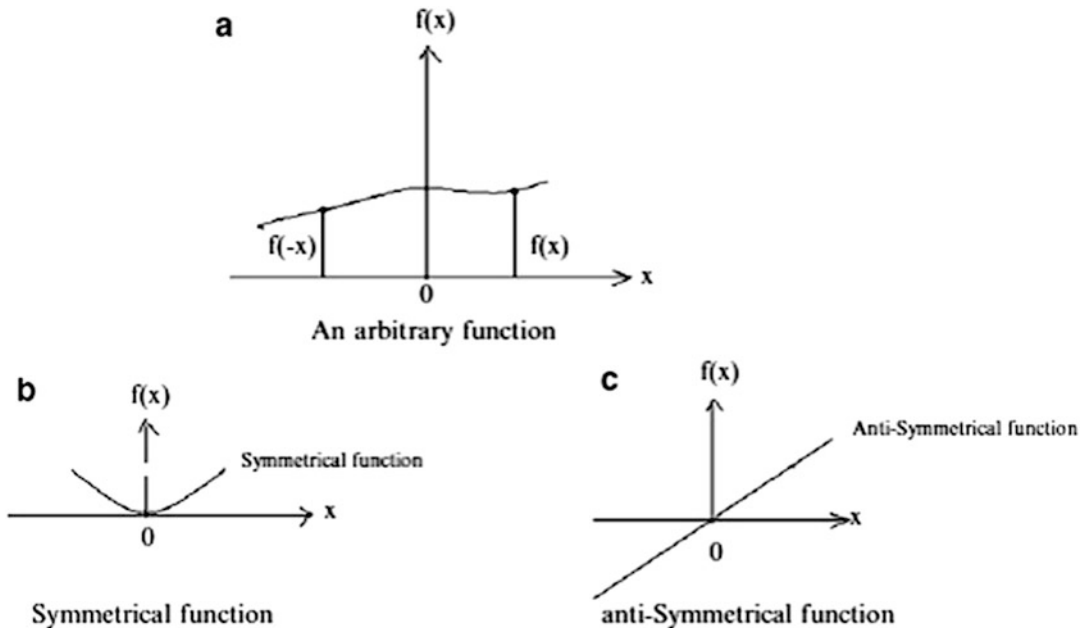


Fig. 3.38 Symmetry and anti-symmetry properties

Starting with the basic differential equations relating the shear, moment, and applied distributed loadings:

$$\begin{aligned}\frac{dV}{dx} &= w \\ \frac{dM}{dx} &= -V \\ \frac{dM_t}{dx} + m_t &= 0\end{aligned}$$

we can deduce the following properties for V , M , and M_t , given the nature of the loading

1. w is a symmetrical function
 - V is anti-symmetrical
 - M is symmetrical
2. w is an anti-symmetrical function
 - V is symmetrical
 - M is anti-symmetrical
3. m_t is a symmetrical function
 - M_t is anti-symmetrical
4. m_t is an anti-symmetrical function
 - M_t is symmetrical

The following cases illustrate these rules.

Symmetrical—planar loading:

Case (a) (Fig. 3.39):

Case (b) (Fig. 3.40):

Note that the center section is in pure bending, i.e., the shear force is zero. This loading scheme is used to test beams in bending

Anti-symmetry—planar loading:

Case (a) (Fig. 3.41):

Case (b) (Fig. 3.42):

We use the concept of symmetry to represent an arbitrary loading as a superposition of symmetrical and anti-symmetrical loadings. Then, we generate the individual shear and moment diagrams and combine them. As an illustration, consider a simply supported beam with a single concentrated force shown in Fig. 3.43a. We replace it with two sets of forces, one symmetrical and the other anti-symmetrical, as shown in Fig. 3.43b. Then, we use the results shown in Figs. 3.40 and 3.42 to construct the shear and moment diagrams.

Fig. 3.39 Symmetrical uniform loading

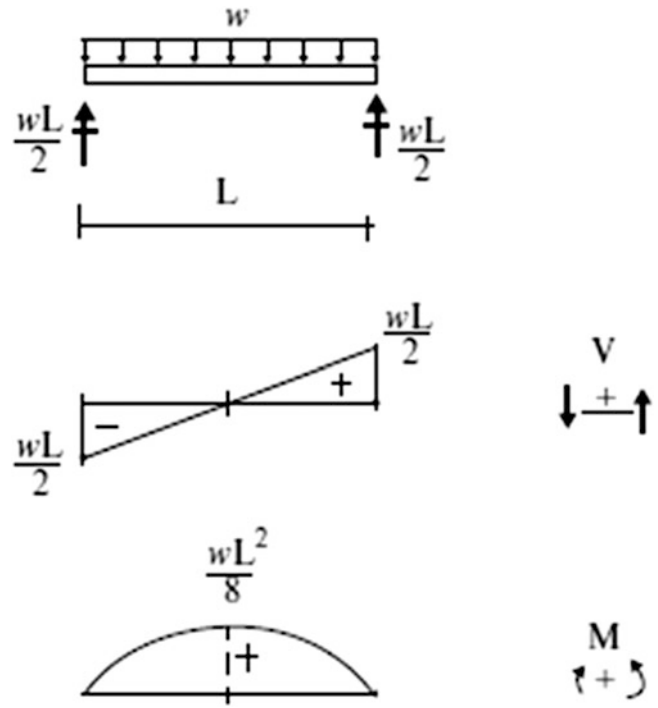


Fig. 3.40 Symmetrical 2-point loading

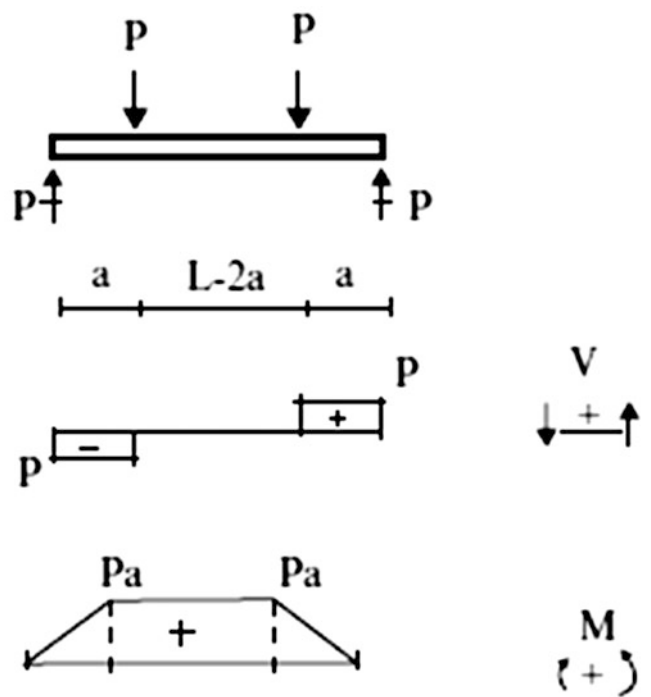


Fig. 3.41 Anti-symmetrical uniform loading

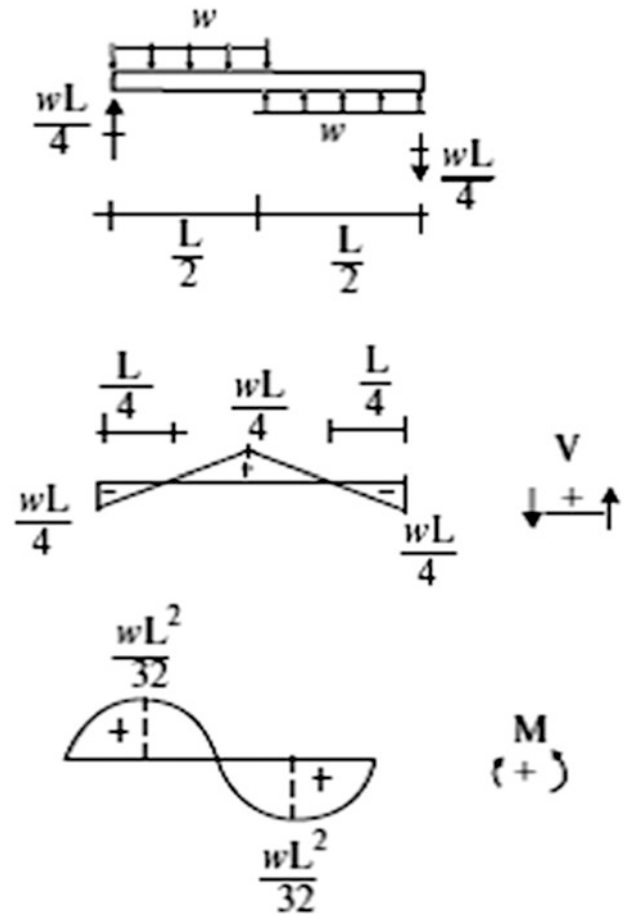


Fig. 3.42 Anti-symmetrical 2-point loading

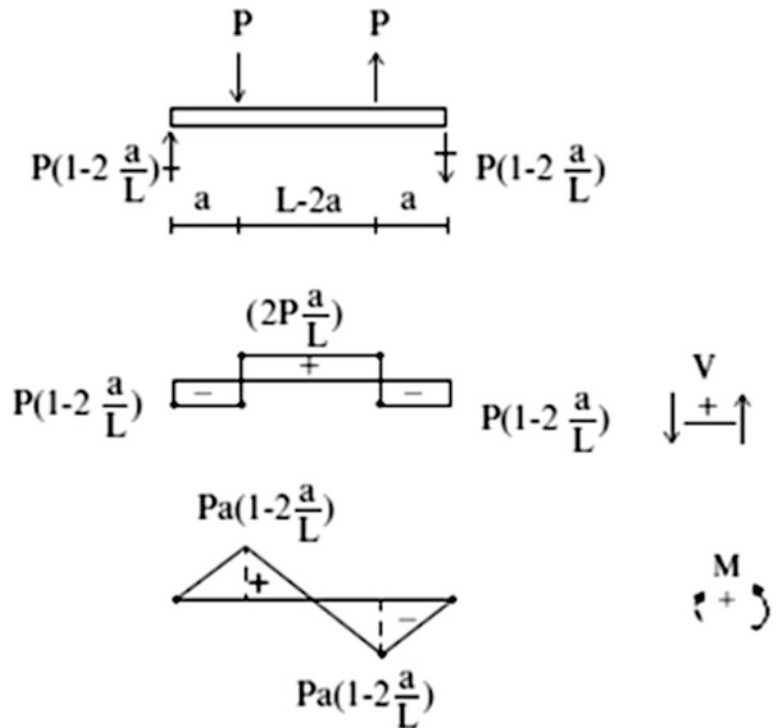
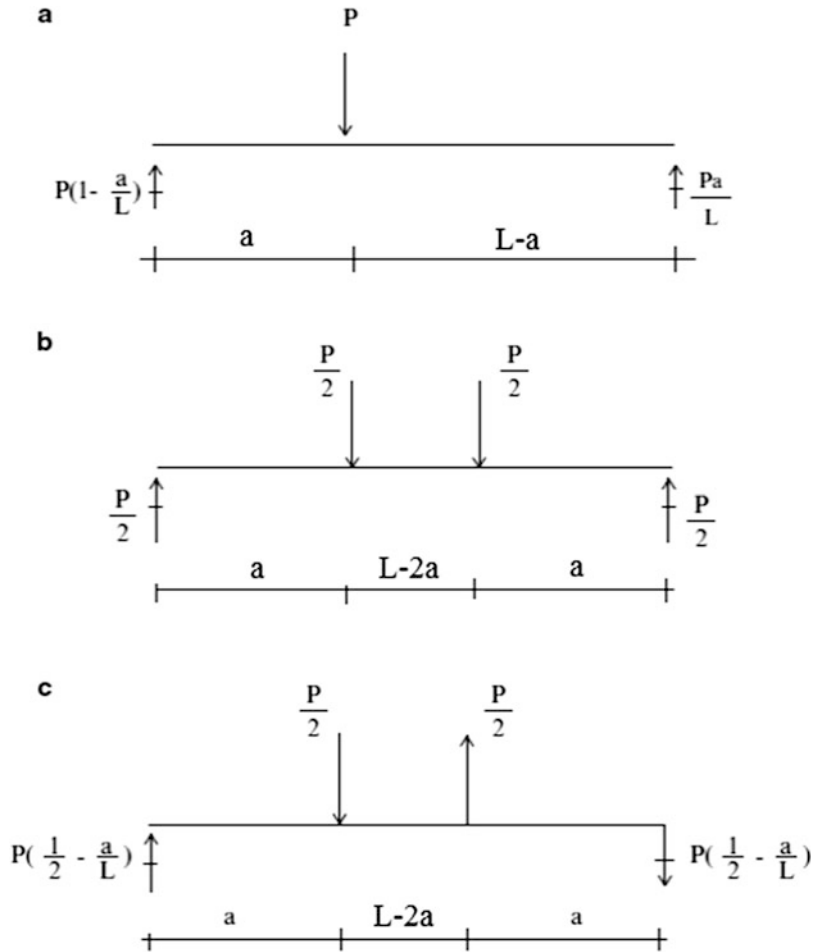


Fig. 3.43 Representation of an arbitrary loading by superposition. (a) Single concentrated load. (b) Set of symmetrical loads. (c) Set of anti-symmetrical loads



3.9.2 Symmetry and Anti-symmetry: Deflected Shapes

A structure is said to be geometrically symmetrical with respect to a particular axis when, if one rotates the portion either to the right or to the left of the axis through 180° , it coincides identically with the other portion. Figure 3.44 illustrates this definition. If we rotate A-B about axis 1-1, it ends up exactly on A-C. A mathematical definition of geometric symmetry can be stated as follows: for every point having coordinates X, Y , there exists a corresponding point with coordinates $-X, Y$.

In addition to geometric symmetry, we also introduce the concept of support symmetry. The supports must be located symmetrically with respect to the axis of geometric symmetry and be of the same nature, e.g., vertical, horizontal, and rotational constraints. Consider Fig. 3.45. There are four vertical restraints at points A, B, C, and D. The geometric symmetry axis, 1-1, passes through mid-span. For complete symmetry, the pin support at point D needs to be shifted to the end of the span. Another example is shown in Fig. 3.46.

Fig. 3.44 Geometric symmetry

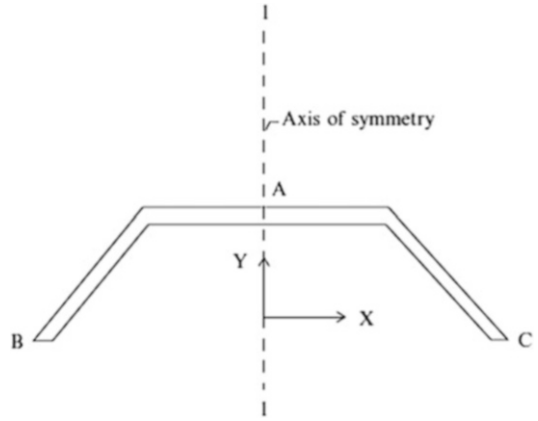


Fig. 3.45 Unsymmetrical support

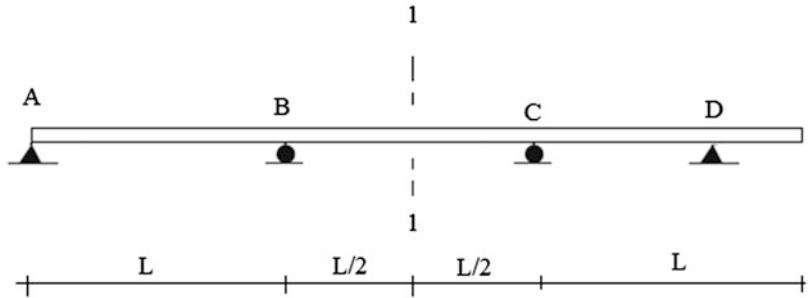
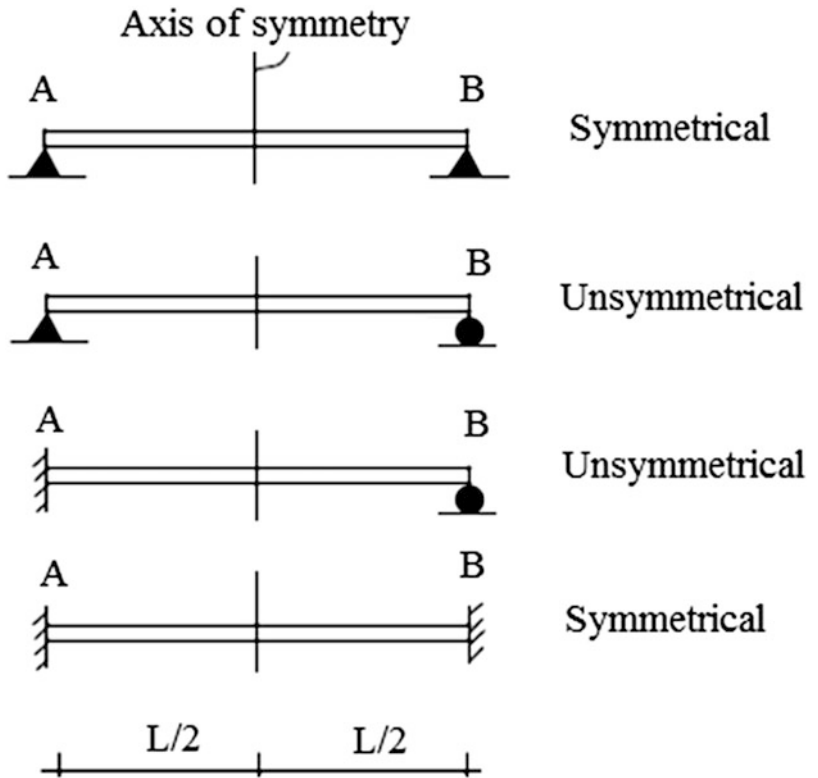


Fig. 3.46 Support symmetry examples



We say a structure is symmetrical when it has both geometric and support symmetry. The symmetry property is very useful since it leads to the following conclusions:

When a symmetrical structure is loaded symmetrically, the resulting deflected shape is also symmetrical. Similarly, a symmetrical structure loaded anti-symmetrically has an anti-symmetric deflected shape.

These conclusions follow from the differential equations listed below and the properties of symmetrical and anti-symmetrical functions:

$$\begin{aligned}
 \frac{dV}{dx} &= w \\
 \frac{dM}{dx} &= -V \\
 \frac{dM_t}{dx} + m_t &= 0 \\
 \frac{d\beta}{dx} &= \frac{M}{EI} \\
 \frac{dV}{dx} &= \beta + \frac{V}{GJ} \\
 \frac{d\beta_t}{dx} &= \frac{M_t}{GJ}
 \end{aligned}
 \tag{3.56}$$

If $f(x)$ is symmetrical, df/dx is anti-symmetrical; if $f(x)$ is anti-symmetrical, df/dx is symmetrical.

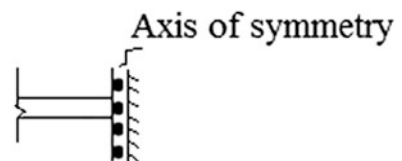
Using these properties, we construct the following table relating the response variables to the loading for a symmetrical structure (Table 3.2).

Table 3.2 Loading response relationships—symmetrical structure

Loading	Response variables
w symmetrical	V anti-symmetrical
	M symmetrical
	β anti-symmetrical
	v symmetrical
w anti-symmetrical	V symmetric
	M anti-symmetrical
	β symmetrical
	v anti-symmetrical
m_t symmetrical	M_t anti-symmetrical
	β_t symmetrical
m_t anti-symmetrical	M_t symmetrical
	β_t anti-symmetrical

We have placed a lot of emphasis here on symmetry because it is useful for qualitative reasoning. It also allows us to work with only one-half the structure provided that we introduce appropriate boundary conditions on the axis of symmetry. The boundary conditions for the symmetrical case follow from the fact that V , β , and M_t are anti-symmetric functions and therefore vanish at the

Fig. 3.47 Symmetrical boundary conditions on a symmetry axis



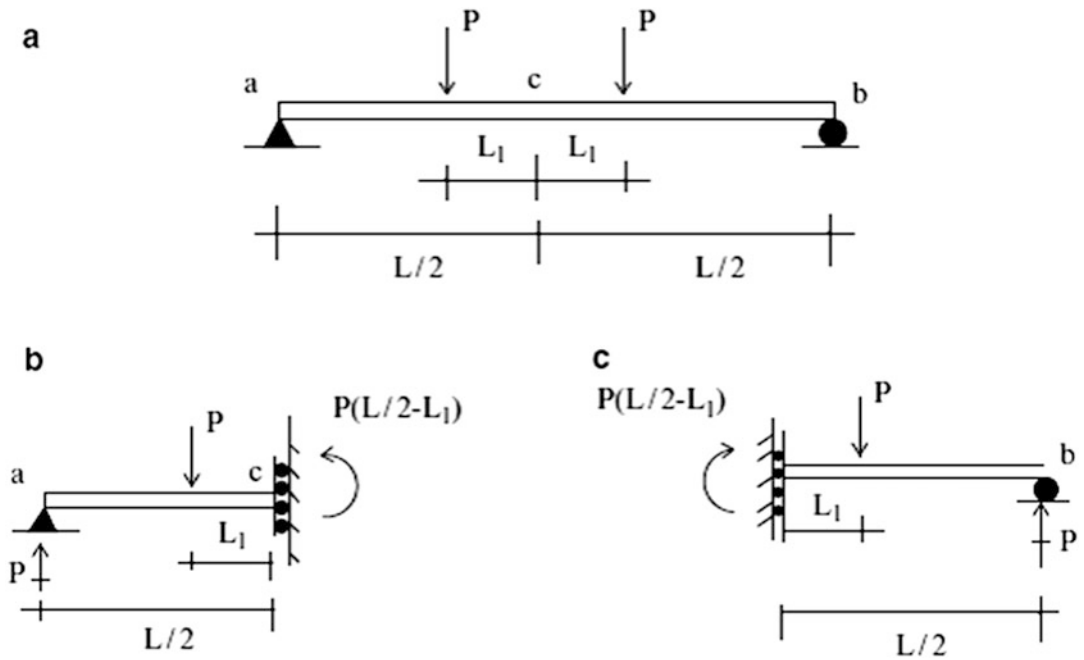


Fig. 3.48 Boundary conditions on symmetry axis—symmetrical planar loading. (a) Symmetrical load. (b) Left segment. (c) Right segment

symmetry axis. We introduce a new support symbol shown in Fig. 3.47, which represents these conditions. The roller support releases V and M ; the rigid end plate eliminates β .

For example, consider the symmetrically loaded simply supported beam shown in Fig. 3.48a. We can work with either the left or right segment. We choose to work with the left segment, with an appropriate support at c on the axis of symmetry. The displacement boundary conditions for this segment are

$$\begin{aligned} v_a &= 0, & \theta_a &\neq 0 \\ v_c &\neq 0, & \theta_c &= 0 \end{aligned}$$

The solution generated with this segment also applies for the other segment (the right portion).

When the loading is anti-symmetric, the bending moment and displacement are also anti-symmetric functions which vanish at the symmetry axis. For this case, the appropriate support on the axis of symmetry is a roller support. We replace the full beam with the segments shown in Fig. 3.49b, c. We analyze the left segment, and then reverse the sense of the response variables for the other segment.

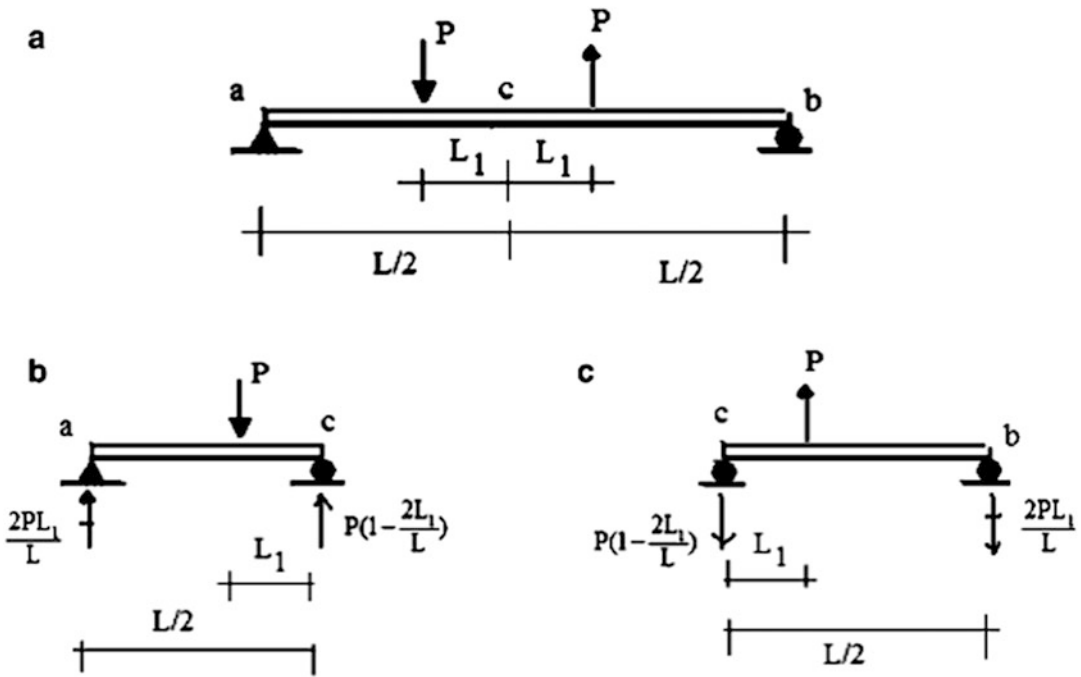


Fig. 3.49 Bending conditions on symmetry axis—anti-symmetrical planar loading. (a) Anti-symmetrical planar load. (b) Left segment. (c) Right segment

3.10 Influence Lines and Force Envelopes for Statically Determinate Beams

3.10.1 The Engineering Process

The Force envelopesInfluence linesobjective of the engineering process is to define the physical makeup of the beam, i.e., the material, the shape of the cross-section, and special cross-section features such as steel reinforcement in the case of a reinforced concrete beam. Cross-sectional properties are governed by the strength of the material and constraints associated with the specific design codes recommended for the different structural materials such as concrete, steel, and wood. Given the maximum values of shear and moment at a particular location, the choice of material, and the general shape of the cross-section, the determination of the specific cross-sectional dimensions at that location involves applying numerical procedures specific to the associated design code. This computational aspect of the engineering process is called design detailing. There are an extensive set of computer-aided design tools available for design detailing. *Therefore, we focus here mainly on that aspect of the engineering process associated with the determination of the “maximum” values of shear and moment for statically determinate beams.* Parts II and III extend the discussion to statically indeterminate structures.

Shear and bending moment result when an external loading is applied to a beam. We described in Sect. 3.4 how one can establish the shear and moment distributions corresponding to a given loading. *For statically determinate beams, the internal forces depend only on the external loading and geometry; they are independent of the cross-sectional properties.* Now, the loading consists of two contributions: dead and live. The dead loading is fixed, i.e., its magnitude and spatial distribution are

constant over time. Live loading is, by definition, time varying over the life of the structure. This variability creates a problem when one is trying to establish the maximum values of shear and moment needed to dimension the cross-section. If the cross-section is allowed to vary, one needs the absolute maximum positive and negative values at discrete points along the axis. This information is essential for reinforced concrete beams in order to specify the steel reinforcement.

3.10.2 Influence Lines and Force Envelopes

In what follows, we describe two approaches for treating live loadings. In the first approach, we select a particular location on the longitudinal axis, and determine analytically how the internal forces (shear and moment) vary as the live load is positioned at different points along the span. The analysis is usually carried out for a single concentrated load, and the force magnitude is plotted vs. the load location along the span. This plot is referred to as an influence line, and allows one to easily identify the position of the live load which produces the maximum value of the force quantity at the particular section on the span. By scanning the influence line plot, one can establish the absolute maximum and minimum value for this particular section. This information is sufficient for detailed design of the cross-section at that location.

However, in order to dimension the complete beam, one also needs similar information at other locations along the beam. This data is generated by repeating the influence line process at discrete points along the span, and determining the absolute max/min values from the corresponding influence lines. The results (positive and negative values) are plotted at each discrete point. Plots of this type are called force envelopes. Given the force envelope, one can readily establish the design force requirement at an arbitrary discrete point.

It is important to distinguish between influence lines and force envelopes. An influence line provides information about forces at a particular section due to live loading passing along the span. A force envelope presents information about the extreme force values at discrete points along the span due to live loading passing along the span. Constructing a force envelope based on n discrete points along the span requires n separate analyses. Most commercial civil structural software has the ability to generate force envelope for various live load configurations.

Consider the simply supported beam shown in Fig. 3.50a. Suppose the influence line for the positive moment at A is desired. We apply force P at location x , and evaluate the moment at A. This quantity is a function of x .

$$\begin{aligned} M_A &= PL \left(1 - \frac{x_A}{L}\right) \frac{x}{L} \quad \text{for } x < x_A \\ M_A &= PL \left(1 - \frac{x}{L}\right) \frac{x_A}{L} \quad \text{for } x > x_A \end{aligned} \quad (3.57)$$

Letting x range from 0 to L leads to the plot shown in Fig. 3.50c. The maximum value of M_A occurs when the load is acting at point A.

$$\left. \frac{M_A}{PL} \right|_{\max} = \left(1 - \frac{x_A}{L}\right) \frac{x_A}{L}$$

This value provides input for the moment envelope. We repeat the computation taking different points such as x_A , x_B , and x_C . The conventional way of representing this data is to show the discrete points along the span and list the corresponding absolute values at each point. Figure 3.50d illustrates this approach.

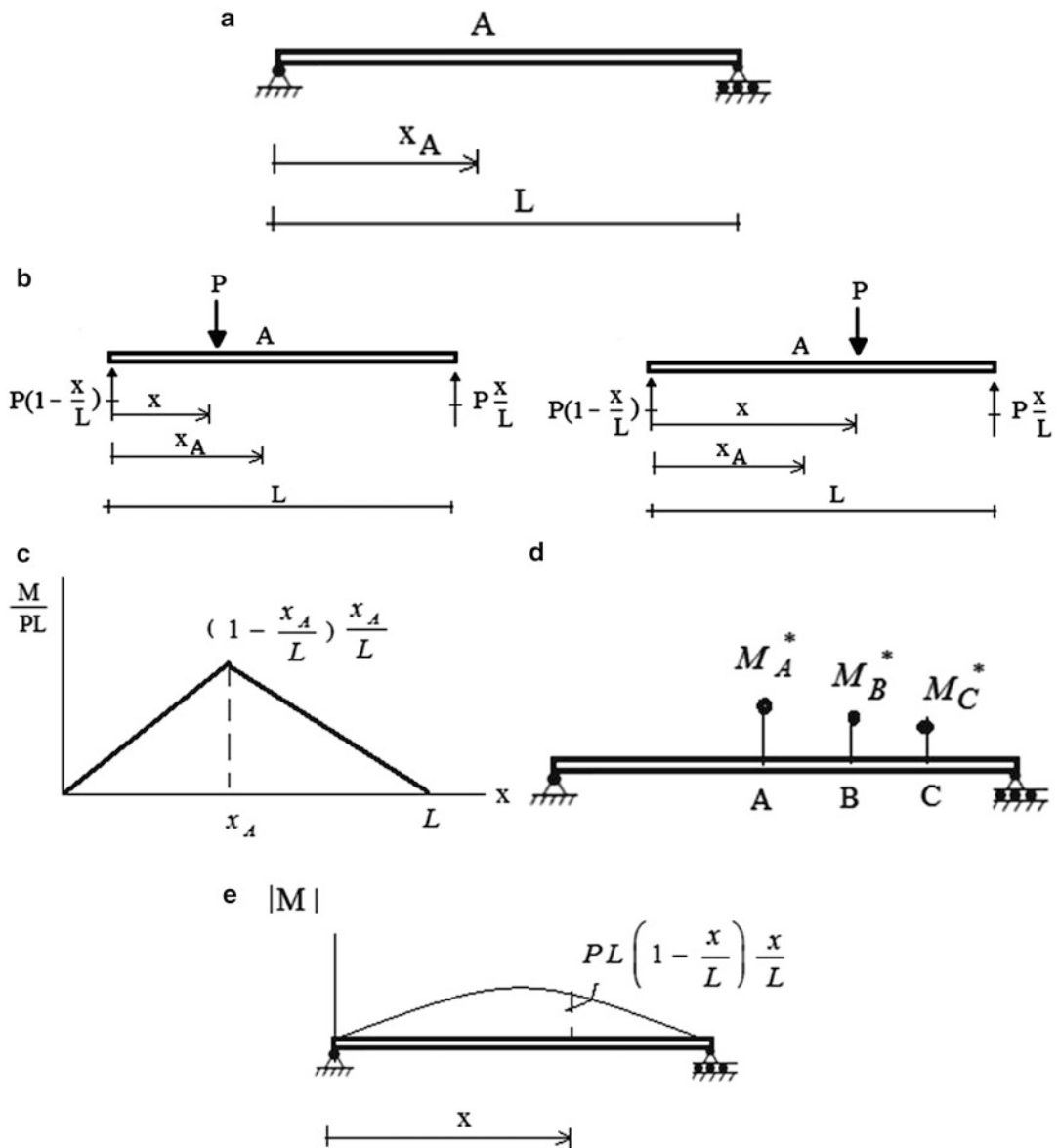


Fig. 3.50 (a) Beam. (b) Loading patterns – Concentrated load P at $x < x_A$ and $x > x_A$. (c) Moment diagram. (d) Different load patterns. (e) Moment diagram. (f) Shear diagrams for concentrated load P at $x < x_A$ and $x > x_A$. (g) Influence line for shear at location x_A . (h) Maximum and minimum shear. (i) Shear force envelope

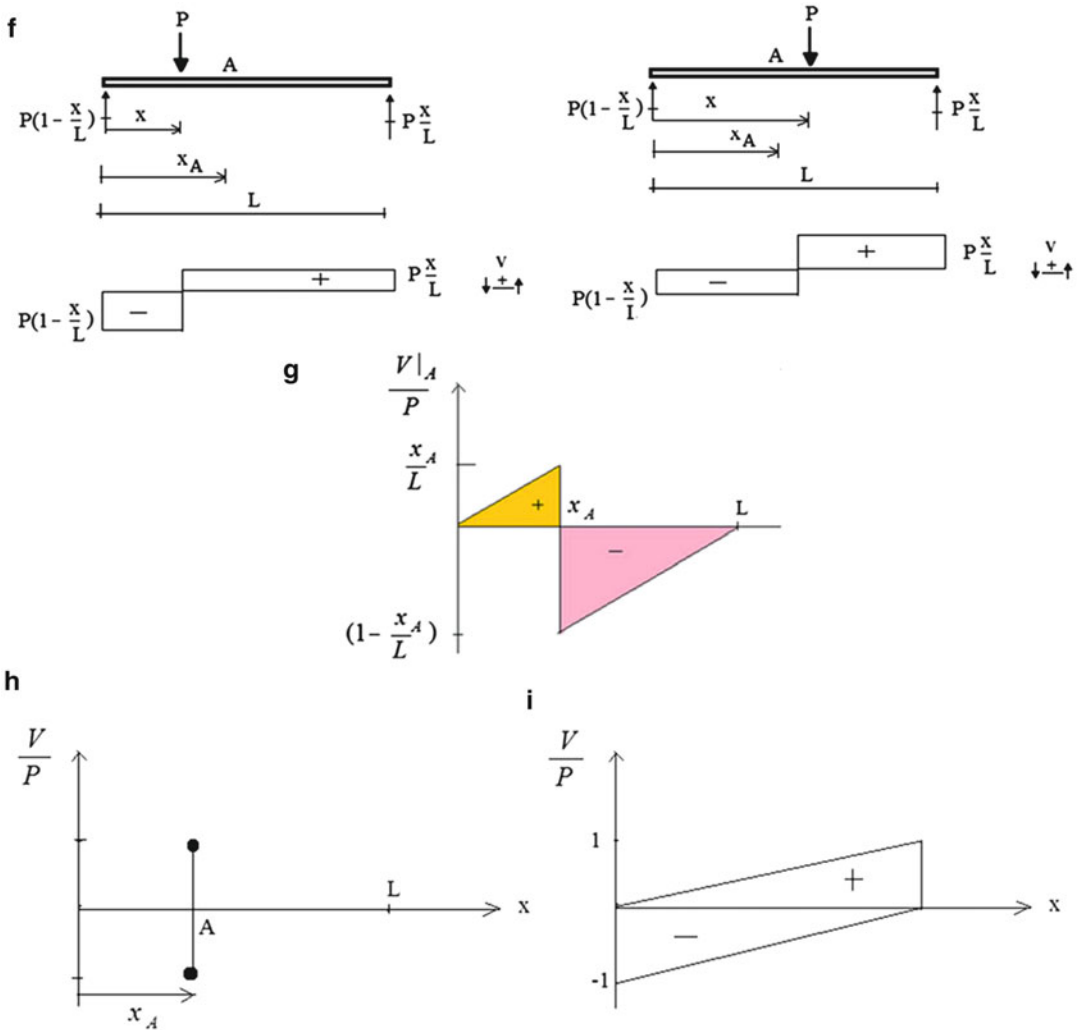


Fig. 3.50 (continued)

Location	Maximum positive moment
x_A	$PL(1 - \frac{x_A}{L})\frac{x_A}{L} = M_A^*$
:	:
x_B	$PL(1 - \frac{x_B}{L})\frac{x_B}{L} = M_B^*$
:	:
x_C	$PL(1 - \frac{x_C}{L})\frac{x_C}{L} = M_C^*$

One selects a sufficient number of points so that the local extremities are identified. The limiting form of the force envelope based on many points is a parabola.

We proceed in a similar manner to establish the influence line and force envelope for the shear force. The shear diagram for a single concentrated force applied at x is shown in Fig. 3.50f.

Suppose we want the influence line for the shear at location x_A . Noting Fig. 3.50f, the shear force at x_A for the different positions of the load is

$$\begin{aligned} x < x_A \quad V|_A &= +\frac{Px}{L} \\ x > x_A \quad V|_A &= -P\left(1 - \frac{x}{L}\right) \end{aligned} \quad (3.58)$$

These functions are plotted in Fig. 3.50g. At point x_A , there is a discontinuity in the magnitude of V equal to P and a reversal in the sense. This behavior is characteristic of concentrated forces.

To construct the force envelope, we note that maximum and minimum values of shear at point A are

$$\begin{aligned} \left(\frac{V}{P}\right)_{\max} &= +\frac{x_A}{L} \\ \left(\frac{V}{P}\right)_{\min} &= -\left(1 - \frac{x_A}{L}\right) \end{aligned}$$

These values are plotted on the span at point A (Fig. 3.50h).

Repeating the process for different points, one obtains the force envelope shown in Fig. 3.50i.

Example 3.25 Construction of Influence Lines

Given: The beam shown in Fig. E3.25a.

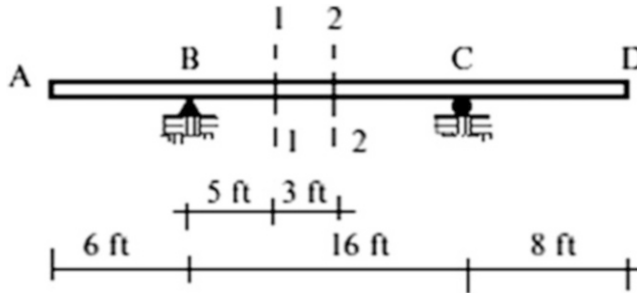
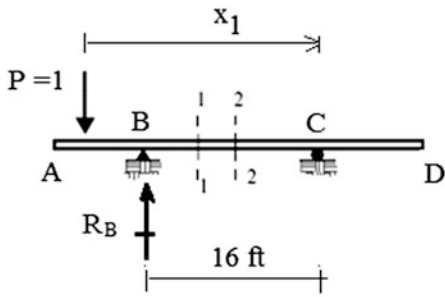


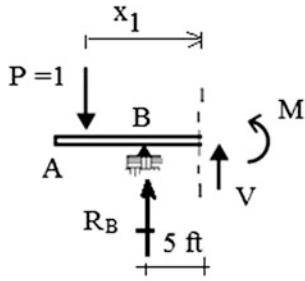
Fig. E3.25a

Determine: The influence lines for the vertical reactions at B and C, moment at section 2-2, and the moment and shear forces at section 1-1. Suppose a uniformly distributed live load of $w_L = 1.2$ kip/ft and uniformly distributed dead load of $w_D = 0.75$ kip/ft are placed on the beam. Using these results, determine the maximum value of the vertical reaction at B and the maximum and minimum values of moment at section 2-2.

Solution: Note that the influence lines are linear because the equilibrium equations are linear in the position variable (see Fig. E3.25b).

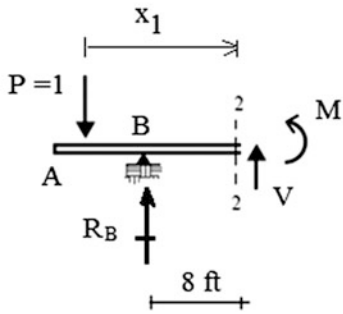


$$R_B = \frac{x_1}{16} P$$



$$M = 5R_B - x_1 P$$

$$V = -R_B + P$$



$$M = 8R_B - x_1 P$$

$$V = -R_B + P$$

Fig. E3.25b

The influence lines corresponding to the force quantities of interest are plotted in Fig. E3.25c.

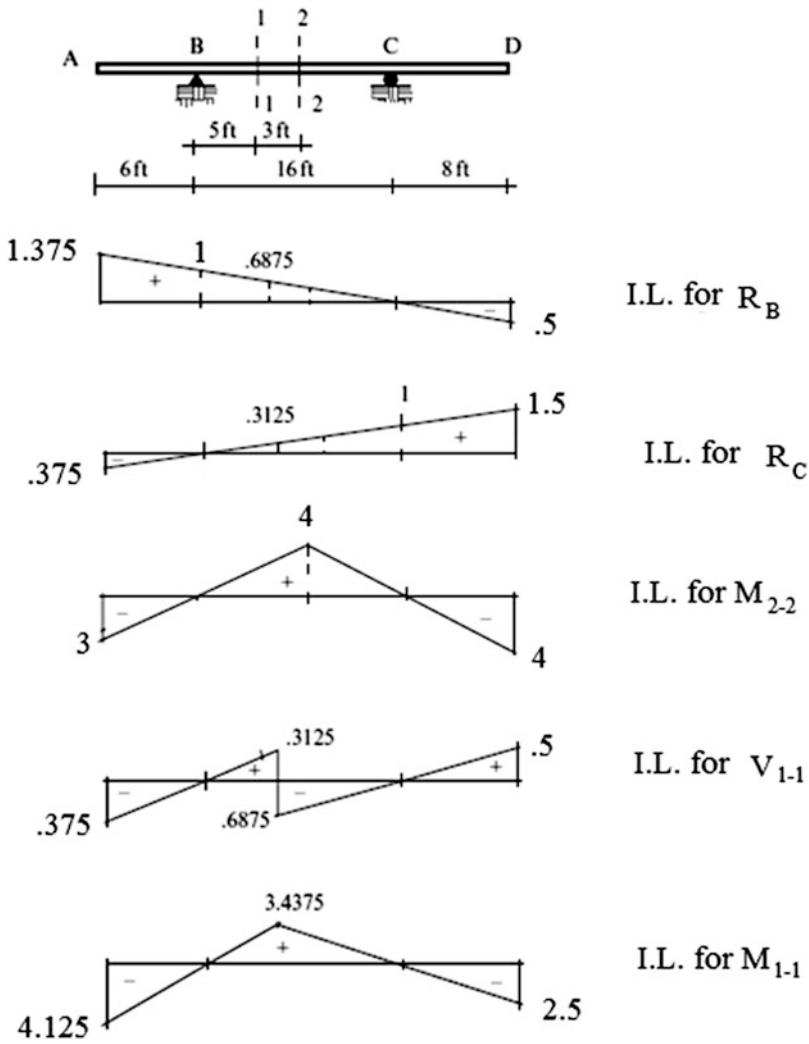


Fig. E3.25c Influence lines for R_B , R_C , V_{1-1} , M_{2-2} , and M_{1-1}

Then, the peak value of R_B is determined using data shown in Fig. E3.25d.

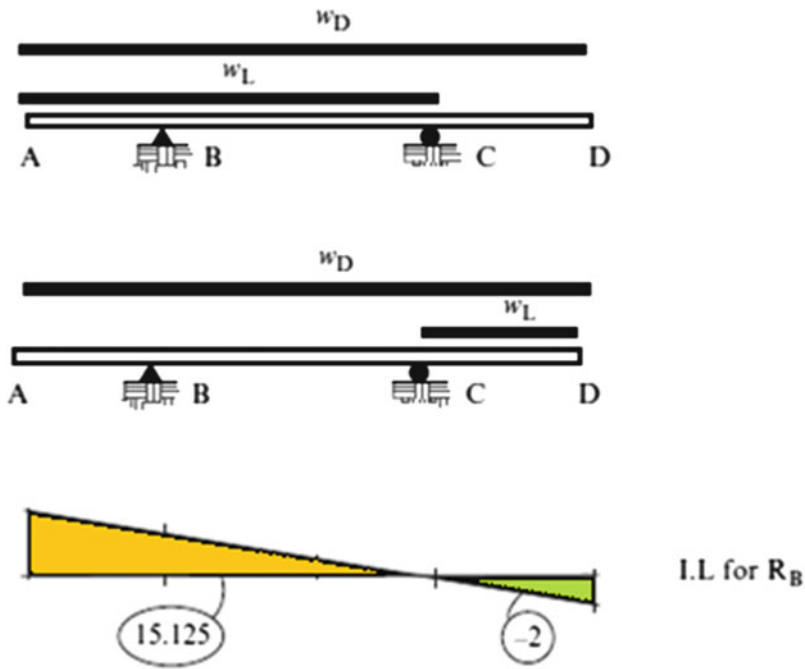


Fig. E3.25d Maximum and minimum values of R_B

$$R_{B_{max}} = 1.2(15.125) + 0.75(15.125 - 2) = 28 \text{ kip}$$

Similarly, the peak values of moment at section 2-2 are generated using the data shown in Fig. E3.25e.

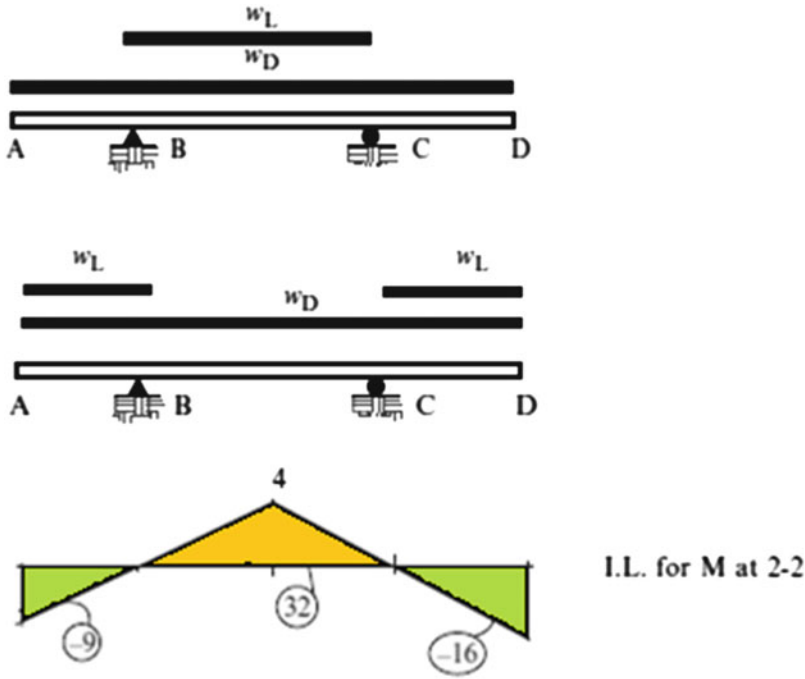


Fig. E3.25e

$$\begin{cases} M_{\max} \text{ at } 2-2 = 1.2(32) + 0.75(32 - 9 - 16) = 43.65 \text{ kip ft} \\ M_{\min} \text{ at } 2-2 = 1.2(-9 - 16) + 0.75(32 - 9 - 16) = -24.75 \text{ kip ft} \end{cases}$$

Example 3.26

Given: The two-span beam shown in Fig. E3.26a. There is a hinge (moment release) at the midpoint of the second span.

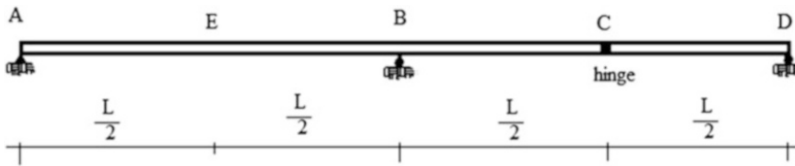


Fig. E3.26a

Determine: The influence line for the bending moment at E and the moment force envelope.

Solution: We consider a unit vertical load moving across the span and use the free body diagrams to determine the moment diagrams. Figure E3.26b shows that the reaction at D equals zero when the load is acting on member ABC.

$$\begin{aligned} R_B &= \frac{x}{L} \\ R_A &= 1 - \frac{x}{L} \quad \text{for } 0 < x < 1.5L \end{aligned}$$

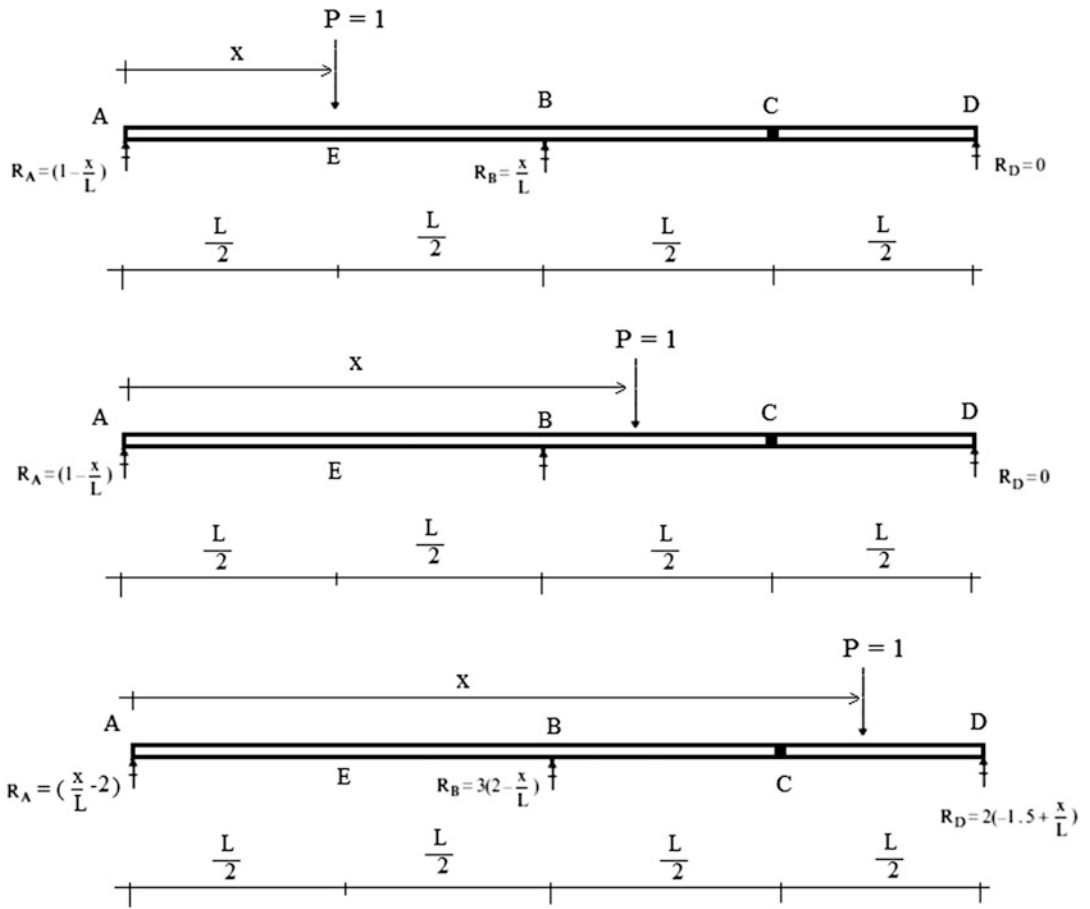


Fig. E3.26b

The behavior changes when the loading passes to member CD. Now there is a reaction at D which releases some of the load on member ABC.

$$\begin{aligned}
 R_D &= 2\left(-1.5 + \frac{x}{L}\right) \\
 R_B &= 3\left(2 - \frac{x}{L}\right) \quad \text{for } 1.5L < x < 2L \\
 R_A &= \left(\frac{x}{L} - 2\right)
 \end{aligned}$$

The moment distribution corresponding to these loading cases are plotted in Fig. E3.26c.

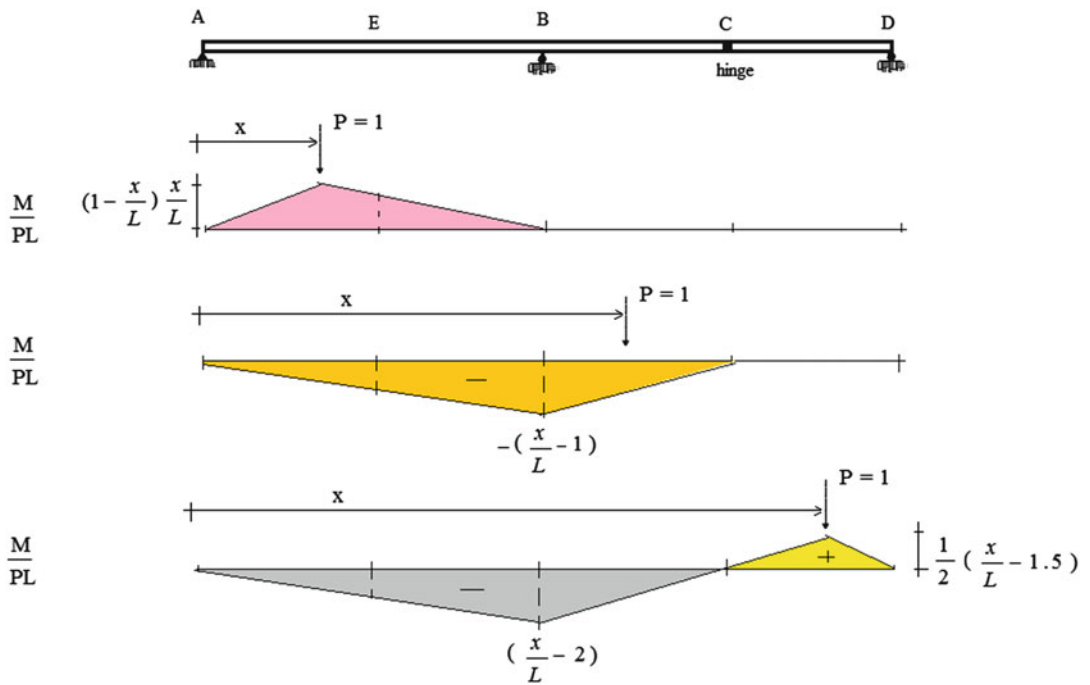


Fig. E3.26c

We note that the moment at E is positive when the load is on span AB, and switches to a negative value when the load moves on to span BCD. The influence line for the bending moment at E is plotted in Fig. E3.26d.

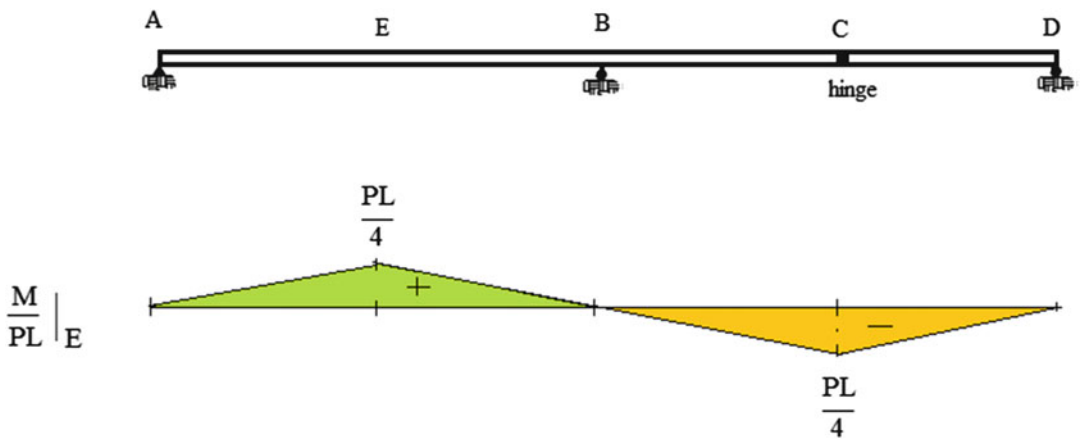


Fig. E3.26d

The moment force envelope is constructed using Fig. E3.26c. Span AB has both positive and negative components; span BC has a negative component; and span CD has a positive component. These segments are plotted in Fig. E3.26e.

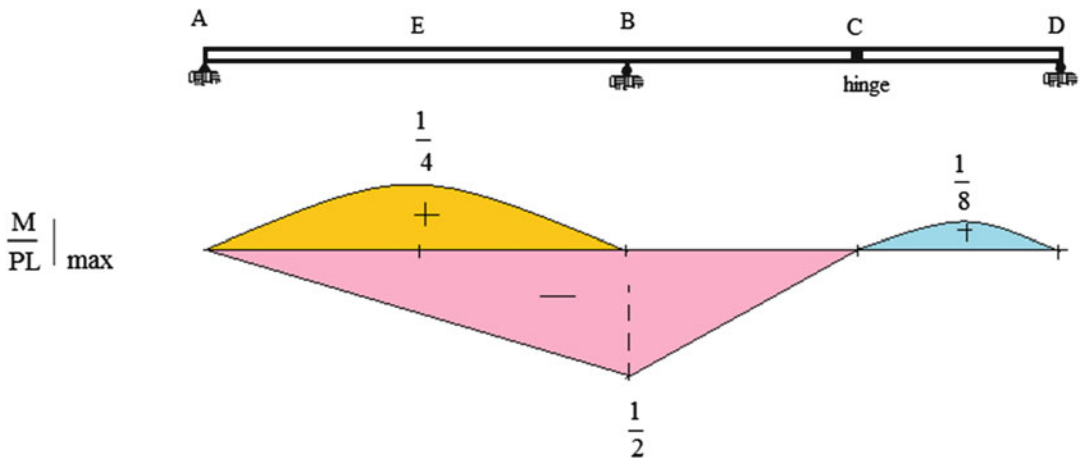


Fig. E3.26e

Example 3.27 Cantilever Construction-Concentrated Loading

Given: The three-span symmetrical scheme shown in Fig. E3.27a. There are two moment releases located symmetrically with respect to the centerline of the center span. This structure is statically determinate: Member cd functions as a simply supported member; segments bc and de act as cantilevers in providing support for member cd. The structural arrangement is called cantilever construction and is used for spanning distances which are too large for a single span or a combination of two spans.

Determine: A method for selecting L_1 and the location of the moment releases corresponding to a concentrated live loading P for a given length, given L_T .

Solution: The optimal geometric arrangement is determined by equating the maximum moments in the different spans. Given the total crossing length, L_T , one generates a conceptual design by selecting L_1 , and α which defines the location of the hinges. The remaining steps are straightforward. One applies the design loading, determines the maximum moments for each beam segment, and designs the corresponding cross-sections. The local topography may control where the interior supports may be located. We assume here that we are not constrained in choosing L_1 and describe below how one can utilize moment diagrams to arrive at an optimal choice for L_1 and α .

We consider the design load to be a single concentrated force that can act on any span. The approach that we follow is to move the load across the total span and generate a sequence of moment diagrams. This calculation provides information on the location of the load that generates the maximum moment for each span.

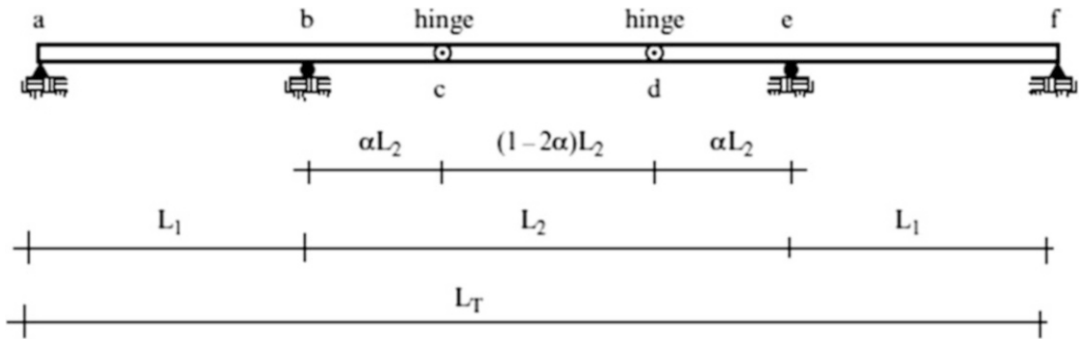


Fig. E3.27a

When the load is on ab, member ab functions as a simply supported beam, and we know from the previous example that the critical location is at mid-span. As the load moves from b to c, bc acts like a cantilever, and the critical location is point c. Lastly, applying the load at the midpoint of c, d produces the maximum moment for cd. Since the structure is symmetrical, we need to move the load over only one-half the span. Moment diagrams for these cases are shown in Figs. E3.327b, E3.327c, and E3.327d.

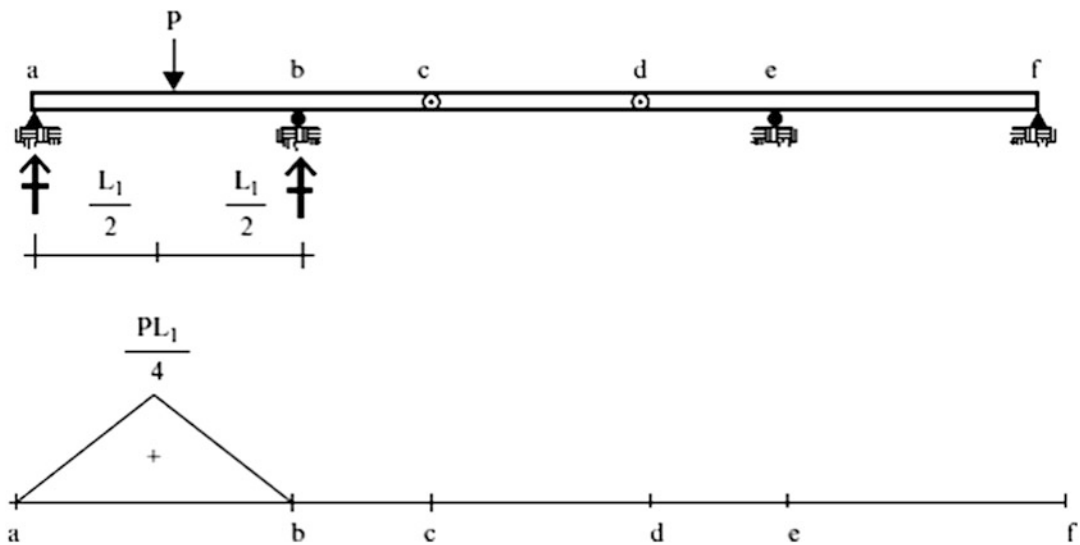


Fig. E3.27b Moment diagram—load on member AB

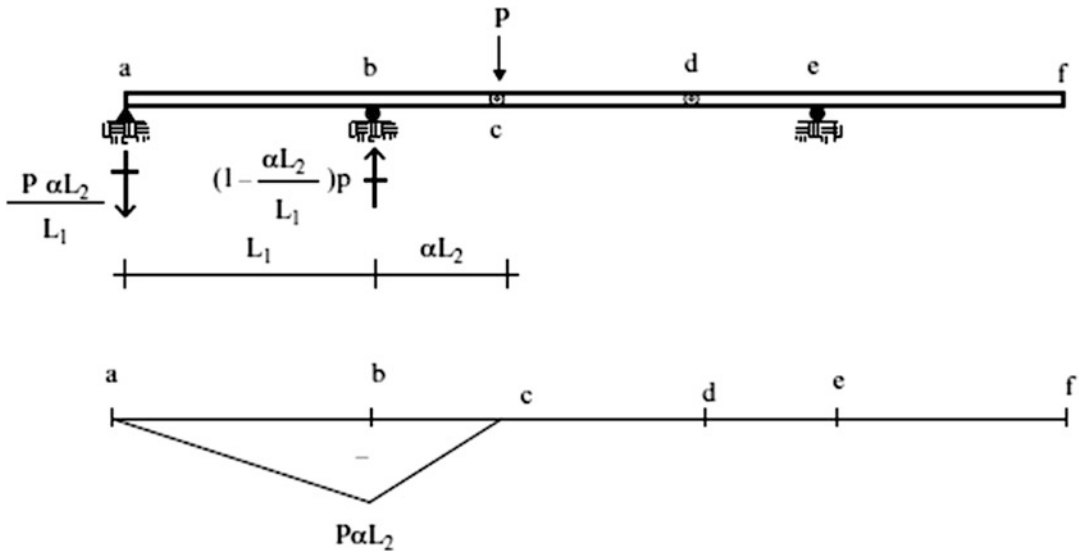


Fig. E3.27c Moment diagram—load on member BC

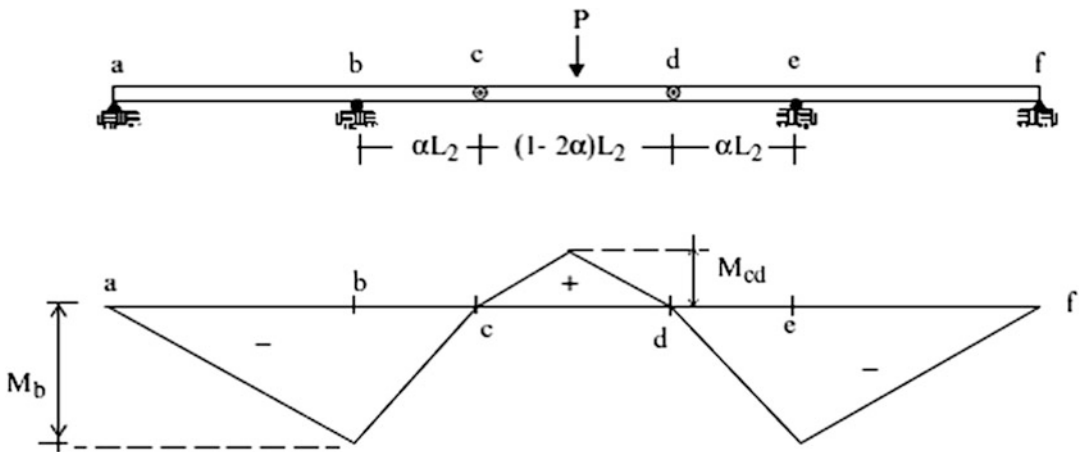


Fig. E3.27d Moment diagram—load on member CD Based on these analyses, the design moments for the individual spans are

$$M_{|_{ab}} = \frac{PL_1}{4} \quad M_{|_{fe}} = M_{|_{ab}}$$

$$M_{|_{bc}} = P\alpha L_2 \quad M_{|_{ed}} = M_{|_{bc}}$$

$$M_{|_{cd}} = \frac{PL_2(1 - 2\alpha)}{4}$$

$$M_b = \frac{P}{2}\alpha L_2 \quad M_e = M_b$$

From a constructability perspective, a constant cross-section throughout the total span is desirable. This goal is achieved by equating the design moments and leads to values for L₁ and α. Starting with M_{bc} = M_{cd}, one obtains

$$P\alpha L_2 = \frac{PL_2(1-2\alpha)}{4}$$

$$\alpha = \frac{(1-2\alpha)}{4} \quad \Downarrow \quad \alpha = \frac{1}{6}$$

Next, we equate M_{ab} and M_{bc} , resulting in

$$\frac{PL_1}{4} = P\alpha L_2$$

$$\Downarrow$$

$$L_1 = \frac{2}{3}L_2$$

The “optimal” center span is

$$2L_1 + L_2 = L_T$$

$$\Downarrow$$

$$L_2 = \frac{3}{7}L_T = 0.429L_T$$

If the interior supports can be located such that these span lengths can be realized, the design is *optimal for this particular design loading*. We want to emphasize here that analysis is useful for gaining insight about behavior, which provides the basis for rational design. One could have solved this problem by iterating through various geometries, i.e., assuming values for α and L_1 , but the strategy described above is a better structural engineering approach.

Example 3.28 Cantilever Construction—Uniform Design Loading

Given: The three-span symmetrical structure shown in Fig. E3.28a.

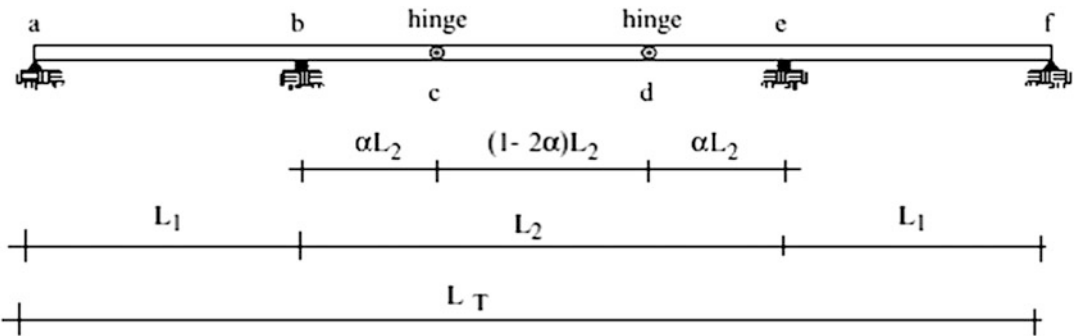


Fig. E3.28a

Determine: The optimal values of L_1 and α corresponding to a uniform live loading w .

Solution: Using the results of the previous example, first, we establish the influence lines for the moment at mid-span of ab (M_{1-1}), at point b (M_b), and at mid-span of member cd (M_{2-2}). They are plotted in Fig. E3.28b.

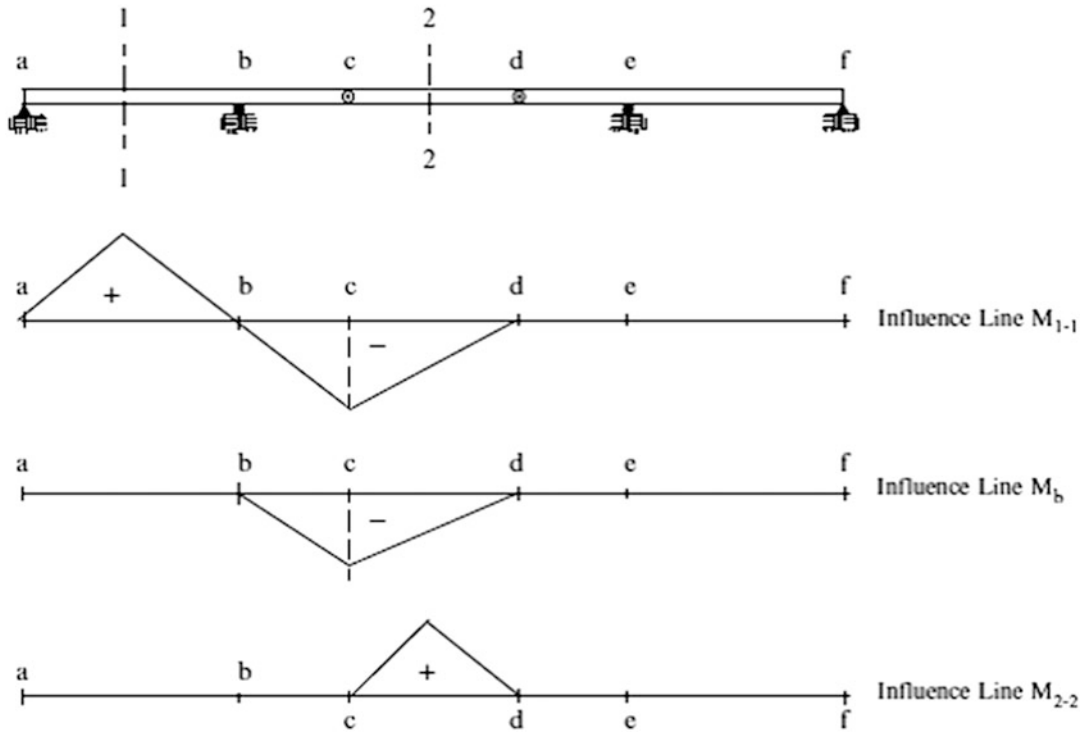


Fig. E3.28b Influence lines

We suppose that the uniformly distributed loading can be applied on an arbitrary segment of a span. We start with the side span, ab . Based on the influence line, we load span ab (Fig. E3.28c).

Next, we load the center span. Loading the segment bcd produces the maximum values for M_b and M_{cd} (Fig. E3.28d). The third option is to load the center span (Fig. E3.28e).

The peak values for these loading schemes are

$$M_{ab} = \frac{wL_1^2}{8}$$

$$M_{cd} = \frac{wL_2^2}{8}(1 - 2\alpha)^2$$

$$M_{bc} = \frac{wL_2^2}{2}[\alpha^2 + \alpha(1 - 2\alpha)]$$

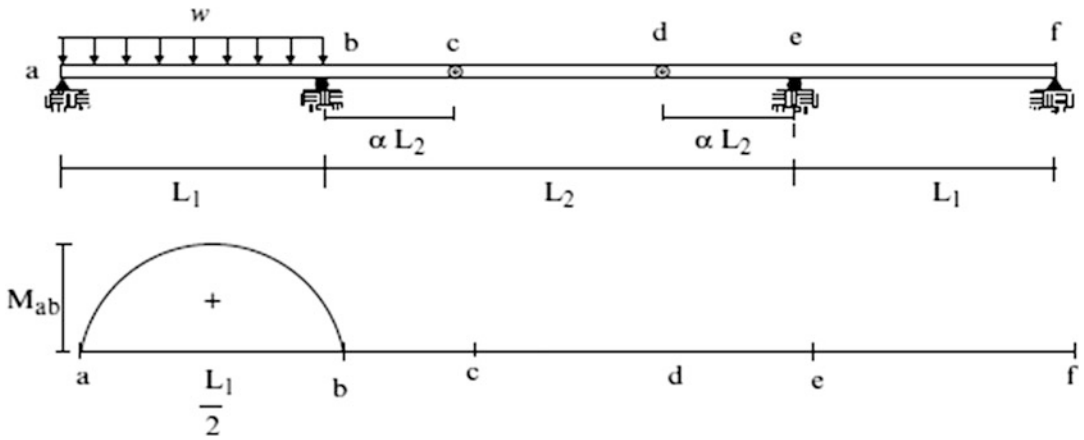


Fig. E3.28c Moment diagram

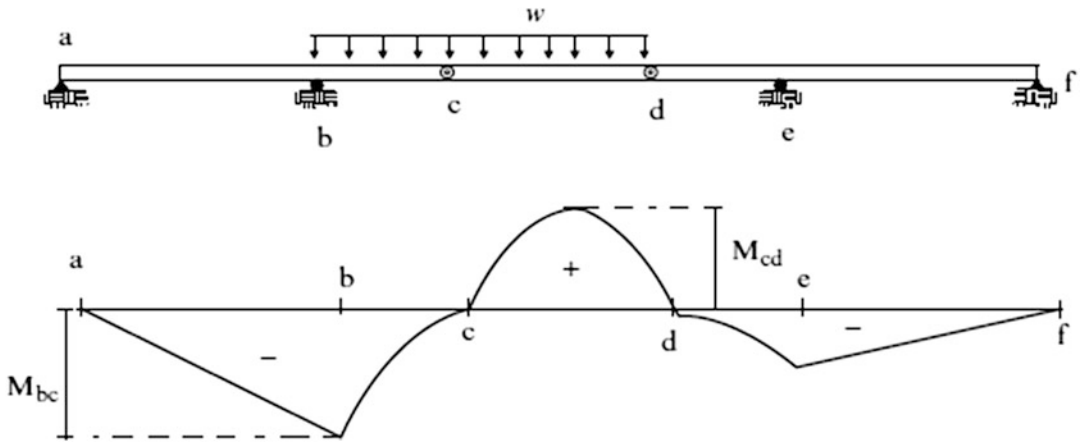


Fig. E3.28d Moment diagram

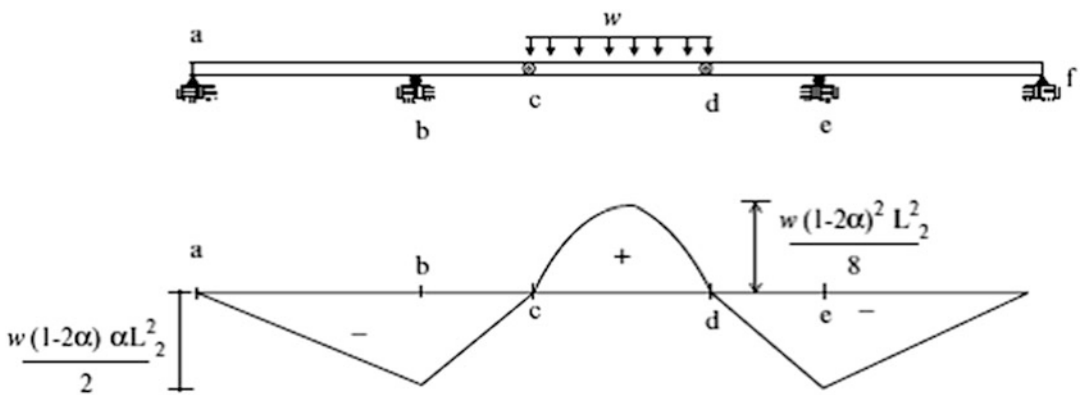


Fig. E3.28e Moment diagram

The remaining steps are the same as for the previous example. We want to use a constant cross-section for the total span and therefore equate the design moments. This step results in values for α and L_1 .

Setting $M_{bc} = M_{cd}$ results in

$$\frac{1}{8}(1 - 2\alpha)^2 = [\alpha^2 + \alpha(1 - 2\alpha)]8\alpha^2 - 8\alpha + 1 = 0 \Downarrow \alpha = \frac{1}{2}\left(1 - \frac{\sqrt{2}}{2}\right) = 0.147$$

Setting $M_{ab} = M_{cd}$ leads to

$$\begin{aligned} \frac{wL_1^2}{8} &= \frac{wL_2^2}{8}(1 - 2\alpha)^2 = \frac{wL_2^2}{8}\left(\frac{\sqrt{2}}{2}\right)^2 & L_2 &= 0.707L_1 \\ \therefore L_1 &= \frac{\sqrt{2}}{2} \end{aligned}$$

Lastly, L_2 is related to the total span by

$$\begin{aligned} 2L_1 + L_2 &= L_T \\ \Downarrow \\ (1 + \sqrt{2})L_2 &= L_T \\ \Downarrow \\ L_2 &= 0.414L_T \end{aligned}$$

These results are close to the values based on using a single concentrated load.

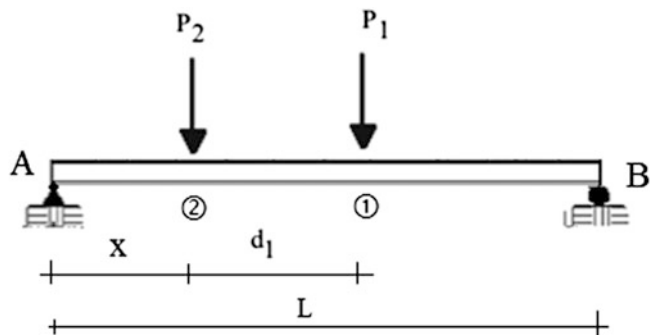
Examples 3.27 and 3.28 illustrate an extremely important feature of statically determinate structures. The reactions and internal forces produced by a specific loading depend only on the *geometry* of the structure. They are independent of the properties of the components that comprise the structure. This fact allows one to obtain a more favorable internal force distribution by adjusting the geometry as we did here.

These examples also illustrate the use of cantilever construction combined with internal moment releases. In Part II of the text, we rework those problems using beams which are continuous over all three spans, i.e., we remove the moment releases. The resulting structures are statically indeterminate.

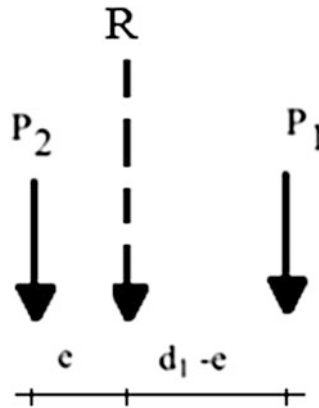
3.10.2.1 Multiple Concentrated Loads

We consider next the case where there are two concentrated forces. This loading can simulate the load corresponding to a two axle vehicle. The notation is defined in Fig. 3.51.

Fig. 3.51 Two concentrated forces



The resultant force $R = P_1 + P_2$ is located e units from the line of action of P_2 .



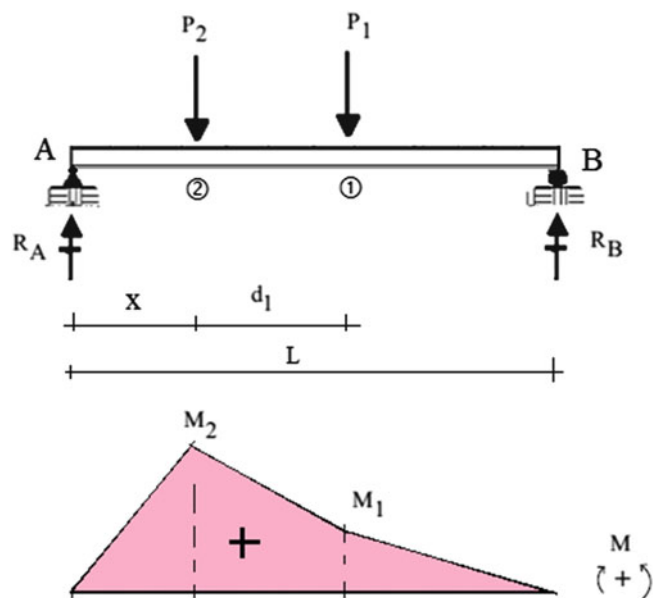
where

$$e = \frac{P_1}{P_1 + P_2} d_1$$

The moment diagram for a set of concentrated forces is piecewise linear with peak values at the points of application of the forces. Figure 3.52 shows the result for this loading case. Analytical expressions for the reactions and the moments at points ② and ① are

$$\begin{aligned} R_A &= (P_1 + P_2) \frac{1}{L} (L - x) - P_1 \frac{d_1}{L} \\ R_B &= (P_1 + P_2) \frac{x}{L} + P_1 \frac{d_1}{L} \\ M_1 &= (P_1 + P_2) \frac{x}{L} (L - x - d_1) + P_1 \frac{d_1}{L} (L - x - d_1) \\ M_2 &= (P_1 + P_2) \frac{x}{L} (L - x) - P_1 \frac{d_1}{L} x \end{aligned} \tag{3.59}$$

Fig. 3.52 Moment diagram—arbitrary position of loading



These moments are quadratic functions of x . One can compute M_1 and M_2 for a range of x values and determine the values of x corresponding to the peak values. Alternatively, one can determine the value of x corresponding to a maximum value of a particular moment by differentiating the corresponding moment expression with respect to x and setting the result equal to zero.

Maximum value of M_2

$$\begin{aligned}\frac{\partial M_2}{\partial x} &= 0 \\ (P_1 + P_2)\left(1 - 2\frac{x}{L}\right) - P_1\frac{d_1}{L} &= 0 \\ x|_{M_{2\max}} &= \frac{L}{2} - \frac{d_1}{2}\left(\frac{P_1}{P_1 + P_2}\right) = \frac{L}{2} - \frac{e}{2}\end{aligned}\quad (3.60)$$

Maximum value of M_1

$$\begin{aligned}\frac{\partial M_1}{\partial x} &= 0 \\ (P_1 + P_2)(L - 2x - d_1) - P_1d_1 &= 0 \\ x|_{M_{1\max}} &= \frac{L}{2} - \frac{d_1}{2} - \frac{e}{2}\end{aligned}\quad (3.61)$$

We can interpret the critical location for the maximum value of M_2 from the sketch shown in Fig. 3.53a. The force P_2 is located $e/2$ units to the left of mid-span and the line of action of the resultant is $e/2$ units to the right of mid-span. A similar result applies for M_1 . P_1 is positioned such that P_1 and R are equidistant from mid-span as shown in Fig. 3.53b.

The absolute maximum live load moment is found by evaluating M_1 and M_2 using the corresponding values of $x|_{M_{1\max}}$ and $x|_{M_{2\max}}$. In most cases, the absolute maximum moment occurs at the point of application of the *largest force* positioned according to (3.60) and (3.61).

Example 3.29 Illustration of Computation of Maximum Moments for Two-Force Loading

Given: The beam shown in Fig. E3.29a and the following data

$$R = W \quad P_1 = 0.2W \quad P_2 = 0.8W \quad d_1 = 14 \text{ ft} \quad L = 40 \text{ ft}$$

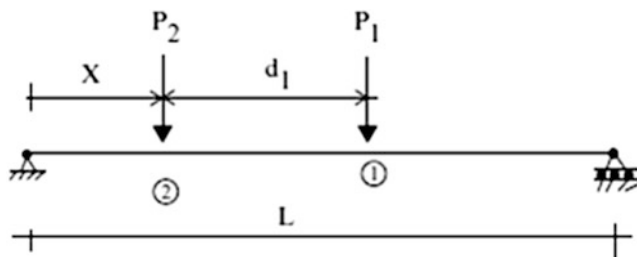
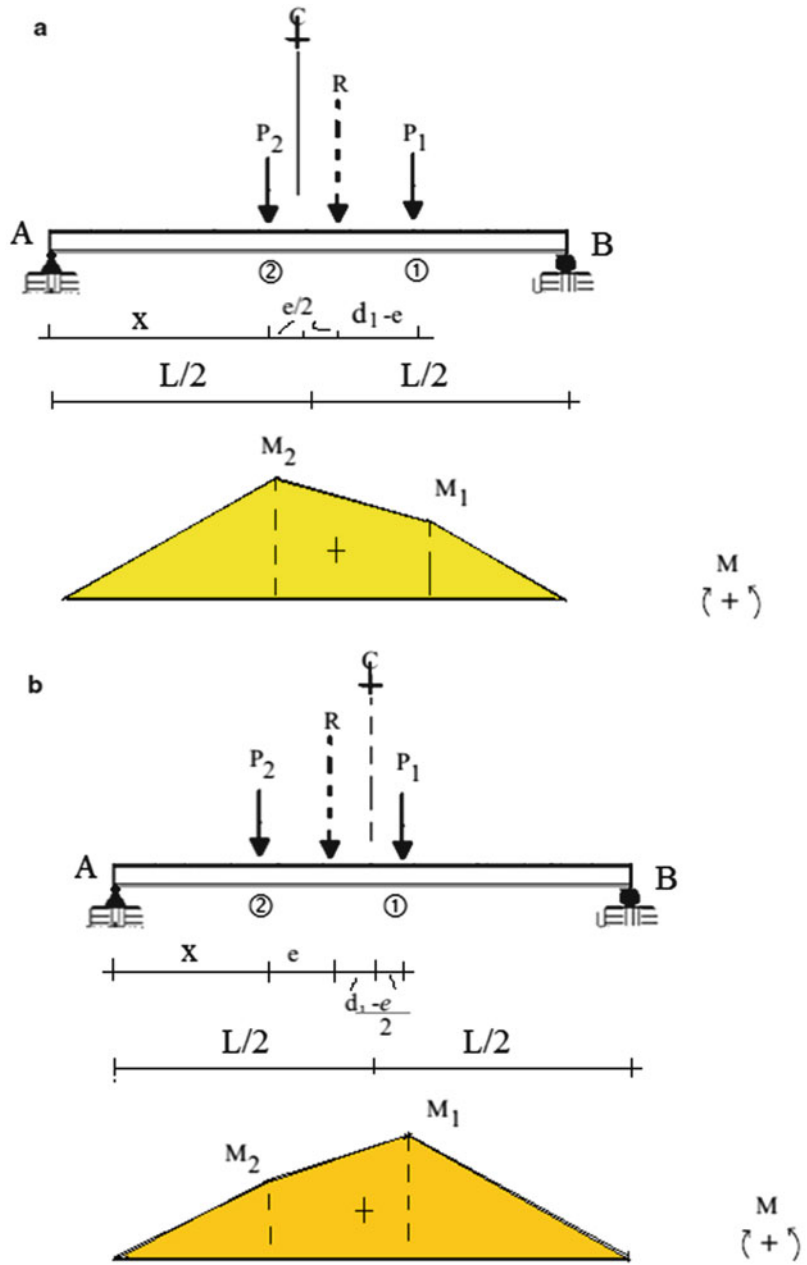


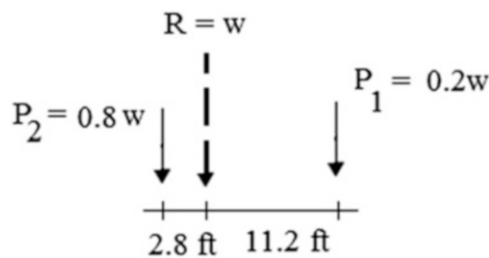
Fig. E3.29a

Determine: The maximum possible moment in the beam as the two-force loading system moves across the span.

Fig. 3.53 Critical location of loading for maximum bending moments. (a) $x|_{M_{2max}}$, (b) $x|_{M_{1max}}$



Solution: The resultant is located $e = \frac{0.2W}{W}(14) = 2.8$ ft from P_2 .



Using (3.60)

$$x|_{M_{2\max}} = \frac{L}{2} - \frac{e}{2} = 20 - 1.4 = 18.6 \text{ ft}$$

Using (3.59) and the above value for x , the reactions and bending moments are

$$R_A = 0.465W$$

$$R_B = 0.535W$$

$$M_1 = 3.96W$$

$$M_2 = 8.69W$$

The critical loading position for M_2 is shown in Fig. E3.29b.

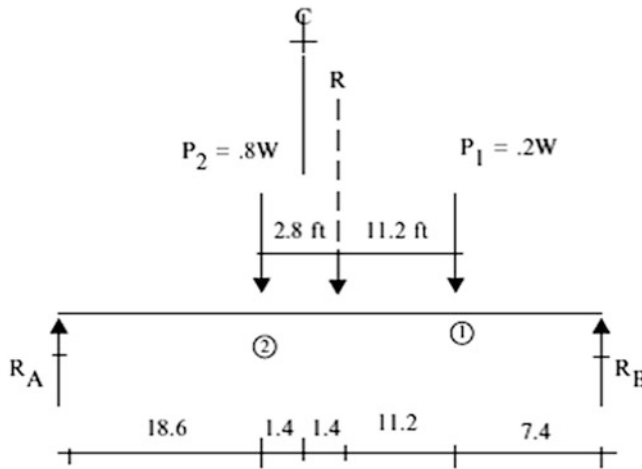


Fig. E3.29b

We compute M_1 in a similar way. The critical location is found using (3.61).

$$x|_{M_{1\max}} = \frac{L}{2} - \frac{d_1}{2} - \frac{e}{2} = 20 - 7 - 1.4 = 11.6 \text{ ft}$$

Next, we apply (3.59).

$$R_A = 0.64W$$

$$R_B = 0.36W$$

$$M_1 = 5.184W$$

$$M_2 = 7.424W$$

The critical loading position for M_1 is shown in Fig. E3.29c.

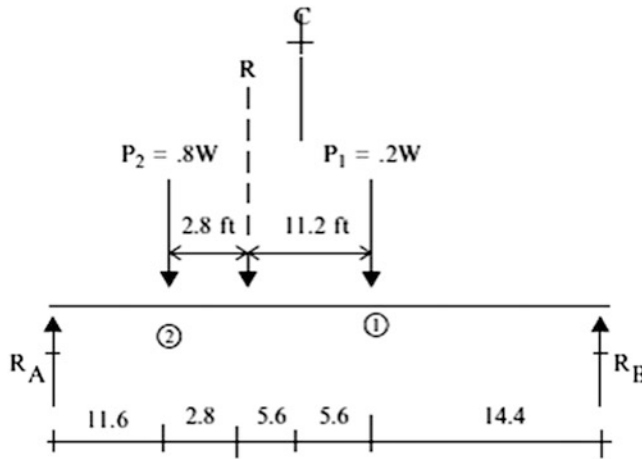


Fig. E3.29c

It follows that the absolute maximum live load moment occurs when P_2 is positioned 18.6 ft from the left support. This point is close to mid-span (Fig. E3.29d).

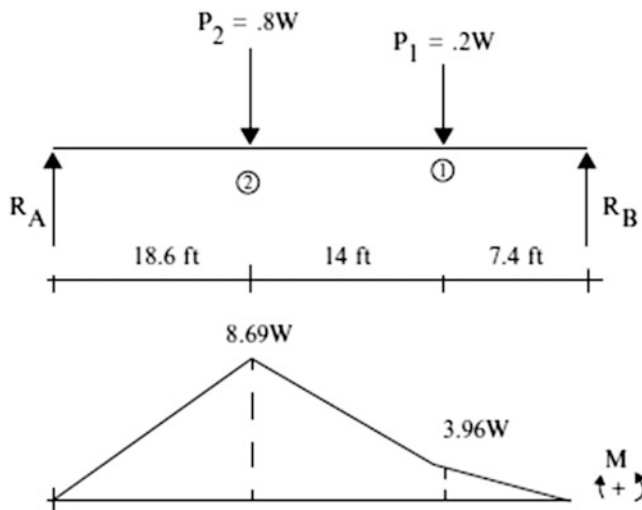


Fig. E3.29d

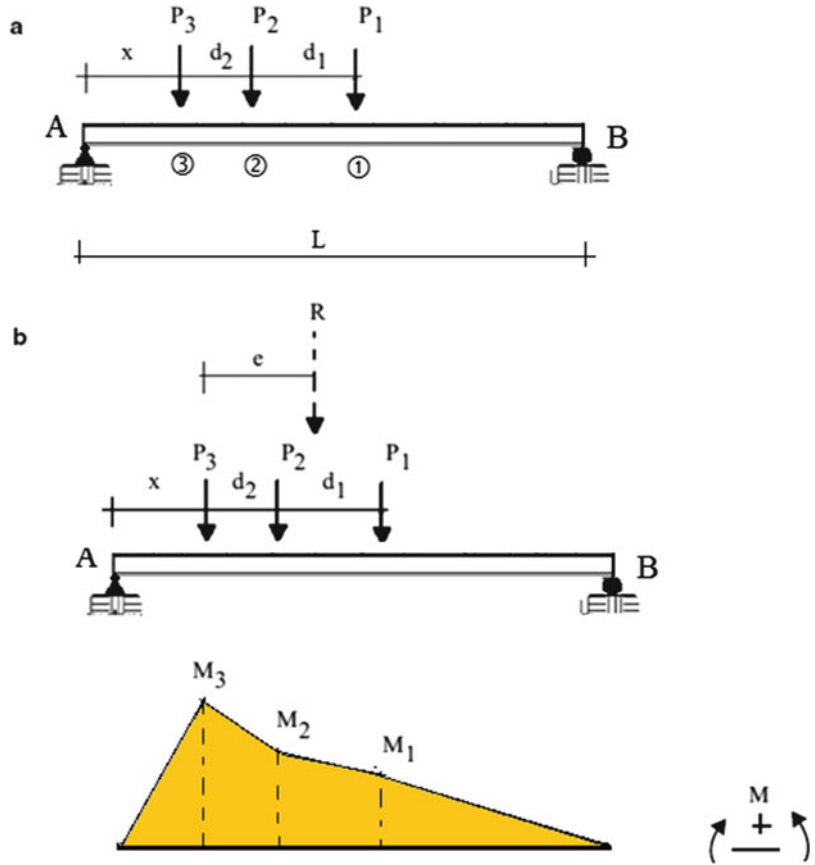
The analysis for the case of three concentrated loads proceeds in a similar way. Figure 3.54 shows the notation used to define the loading and the location of the resultant force. The moment diagram is piecewise linear with peaks at the point of application of the concentrated loads.

We generate expressions for the bending moments at points ①, ①, and ① for an arbitrary position of the loading defined by x and then determine the locations of maximum moment by differentiating these expressions. First, we locate the resultant force

$$R = P_1 + P_2 + P_3$$

$$e = \frac{d_2 P_2 + (d_1 + d_2) P_1}{R} \tag{3.62}$$

Fig. 3.54 Notation and moment diagram—three concentrated loads



The moments at locations 1, 2, and 3 are functions of x .

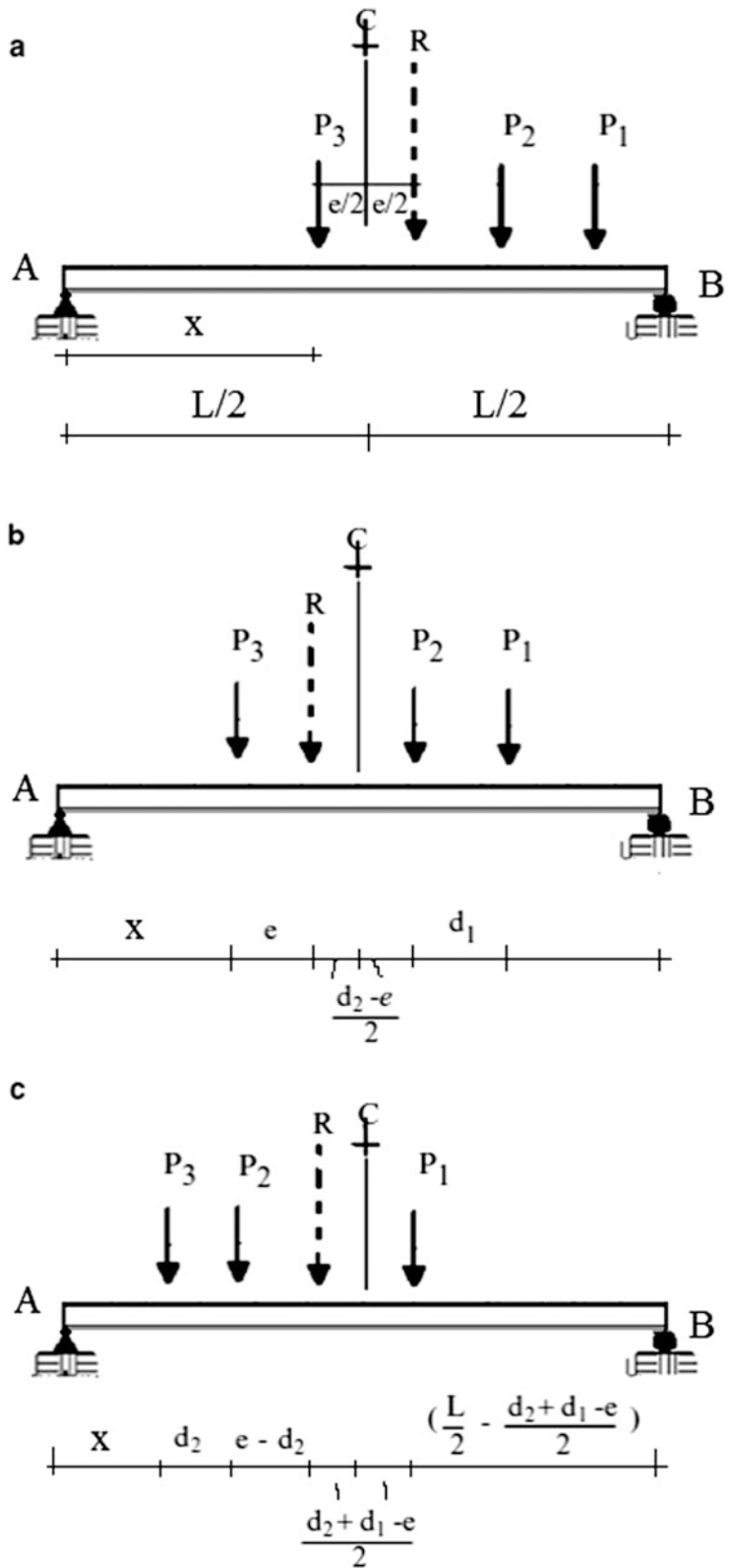
$$\begin{aligned}
 M_3 &= \frac{R}{L}(L - x - e)x \\
 M_2 &= \frac{R}{L}(L - x - e)(x + d_2) - P_3d_2 \\
 M_1 &= \frac{R}{L}(L - x - d_2 - d_1)(x + e)
 \end{aligned}
 \tag{3.63}$$

Differentiating each expression with respect to x and equating the result to zero leads to the equations for the critical values of x that correspond to relative maximum values of the moments.

$$\begin{aligned}
 \text{For } M_3|_{\max} \quad x &= \frac{1}{2}(L - e) \\
 \text{For } M_2|_{\max} \quad x &= \frac{1}{2}(L - e - d_2) \\
 \text{For } M_1|_{\max} \quad x &= \frac{1}{2}(L - d_2 - d_1 - e)
 \end{aligned}
 \tag{3.64}$$

The positions of the loading corresponding to these three values of x are plotted in Fig. 3.55. Note that the results are similar to the two concentrated load case. We need to evaluate (3.63) for each value of x in order to establish the absolute maximum value of the bending moment.

Fig. 3.55 Possible locations of loading for maximum moment



Example 3.30

Given: The beam shown in Fig. E3.30a.

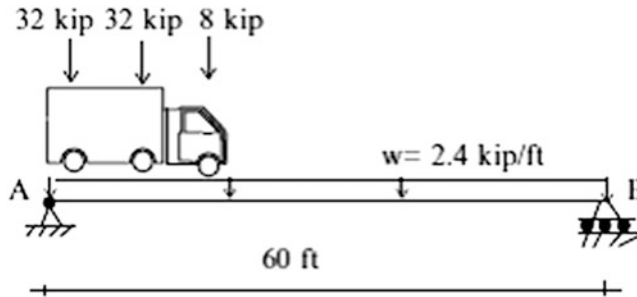


Fig. E3.30a

Determine: The maximum possible moment in the beam caused by

1. A truck moving across the span (Fig. E3.30b).

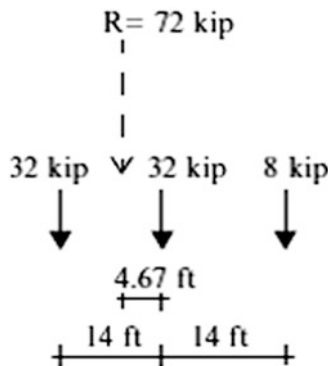


Fig. E3.30b

2. A uniformly distributed dead load of $w = 2.4$ kip/ft in addition to the truck loading.

Solution:

Part (1): The critical truck loading position is defined by Fig. E3.30c. The corresponding bending moment diagram is plotted below; the maximum moment occurs 2.3 ft from the center of the span.

$$M_{\max} = 806.7 \text{ kip ft.}$$

Part (2): The bending moment diagram for uniform loading is parabolic, with a maximum value at mid-span.

$$M_{\text{dead}}(x) = 72x - 1.2x^2 \quad 0 \leq x \leq 60$$

We estimate the peak moment due to the combined loading by adding corresponding moment values from Figs. E3.30c and E3.30d.

$$\begin{aligned}
 M_{\text{combined}} &= (M_{\text{dead}} + M_{\text{truck}})_{\text{at } x=32.33 \text{ ft}} = 1073.5 + 806.7 \approx 1880 \text{ kip ft} \\
 M_{\text{combined}} &= (M_{\text{dead}} + M_{\text{truck}})_{\text{at } x=30 \text{ ft}} = 1080 + 791 \approx 1871 \text{ kip ft}
 \end{aligned}
 \left. \vphantom{\begin{aligned} M_{\text{combined}} \\ M_{\text{combined}} \end{aligned}} \right\} M_{\text{max}} = 1880 \text{ kip ft}$$

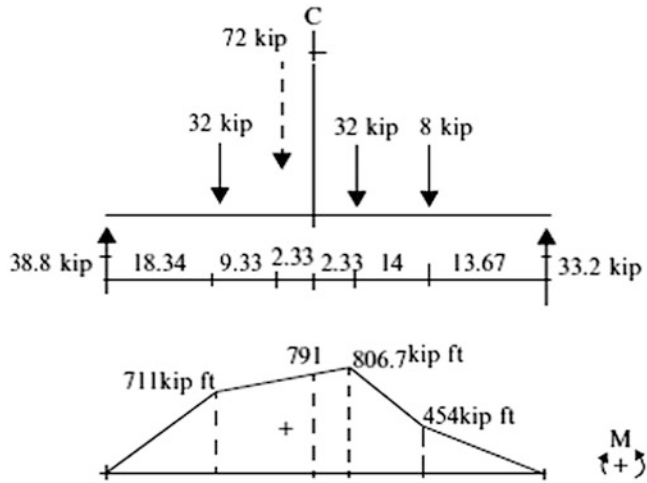


Fig. E3.30c Moment distribution for moving truck load

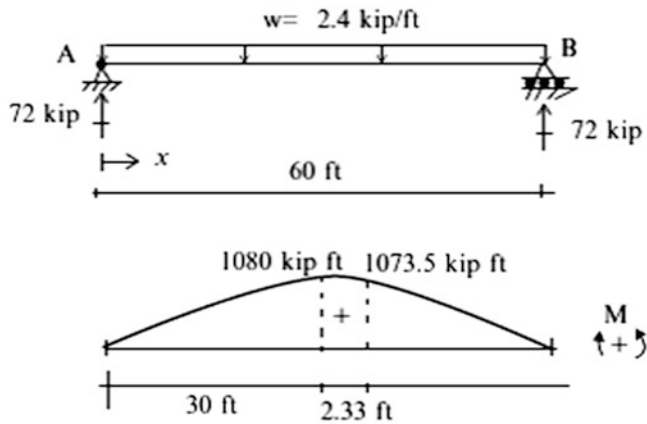


Fig. E3.30d Moment distribution for dead load When there are multiple loadings, it is more convenient to generate discrete moment envelope using a computer-based analysis system. The discrete moment envelope for the combined (dead + truck) loading is plotted below (Fig. E3.30e). Scanning the envelope shows that the maximum moment occurs at $x = 30.9 \text{ ft}$ and $M_{\text{max}} = 1882.6 \text{ kip ft}$. This result shows that it was reasonable to superimpose the moment diagrams in this example.

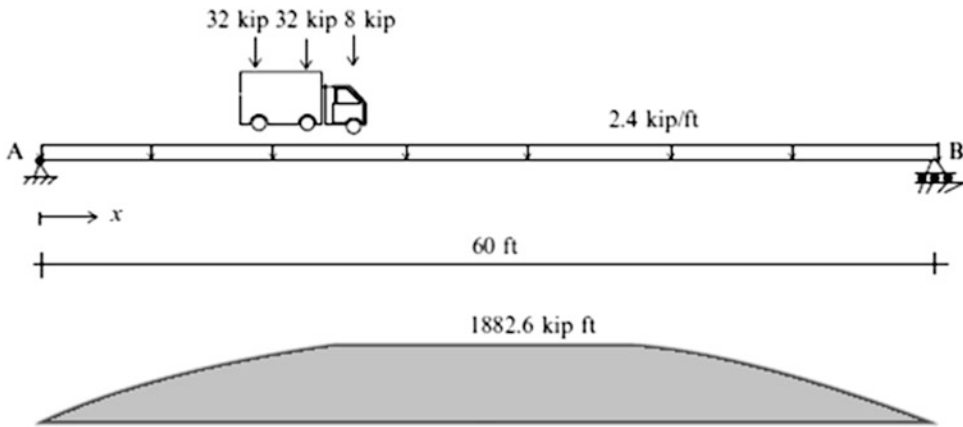


Fig. E3.30e Discrete moment envelope for the combined (dead + truck) loading

3.11 Summary

3.11.1 Objectives of the Chapter

- To develop analytical and computational methods for quantifying the behavior of beams subjected to transverse loading. Of particular interest are the reactions, the internal forces (shear, bending, and twisting moments), and the displacements.
- To introduce the concepts of influence lines and force envelopes which are needed to establish design values for beam cross-sections.

3.11.2 Key Facts and Concepts

- A stable statically determinate beam requires three nonconcurrent displacement restraints. There are three reaction forces which are determined using the static equilibrium equations.
- External loads are resisted by internal forces acting on a cross-section. For planar loading, these quantities consist of an axial force, F , a transverse shear force, V , and a bending moment, M . One can establish the magnitude of these variables using the static equilibrium equations. Alternatively, one can start with the following differential equilibrium equations,

$$\frac{dV}{dx} = w$$

$$\frac{dM}{dx} = -V$$

Integrating between points 1 and 2 leads to

$$V_2 - V_1 = \int_{x_1}^{x_2} w \, dx$$

$$M_2 - M_1 = - \int_{x_1}^{x_2} V \, dx$$

The first equation states that the difference in shear is equal to the area under the loading diagram. The second equation states that the change in moment is equal to minus the area under the shear diagram.

- Planar bending results in a transverse displacement, $v(x)$. When the beam is slender, these variables are related by

$$\frac{d^2v}{dx^2} = \frac{M}{EI}$$

where I is the second moment of area for the section. Given $M(x)$, one determines $v(x)$ by integrating this expression and noting the two boundary conditions on v .

- The transverse displacement at a particular point can also be determined using the Principle of Virtual Forces specialized for planar bending of slender beams.

$$d \delta P = \int_L \frac{M}{EI} \delta M \, dx$$

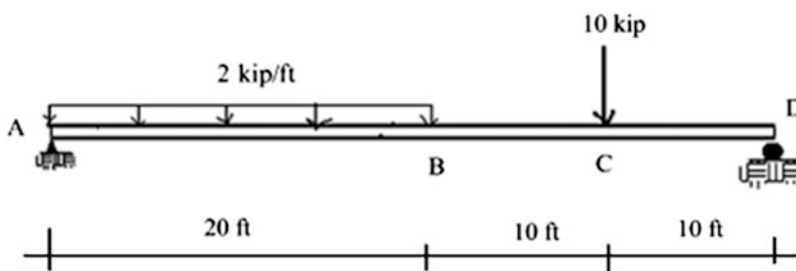
Here, d is the desired displacement, δP is a virtual force in the direction of d , and δM is the virtual moment corresponding to δP . One usually employs numerical integration when the integral is complex.

- An influence line is a plot of the magnitude of a particular internal force quantity, say the bending moment at a specific location, vs. the position of a unit concentrated load as it moves across the span. It is useful for establishing the peak magnitude of the force quantity at that location.
- A force envelope is a plot of the maximum positive and negative values of a force quantity, say the bending moment, at different sections along the beam. This data is used to determine cross-sectional properties.

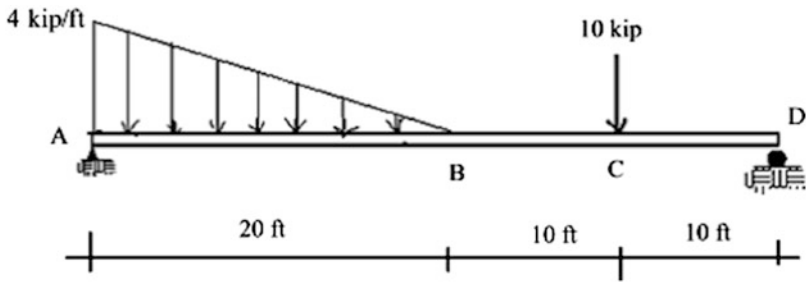
3.12 Problems

For the beams defined in Problems 3.1–3.20, compute the reactions and draw the shear and moment diagrams.

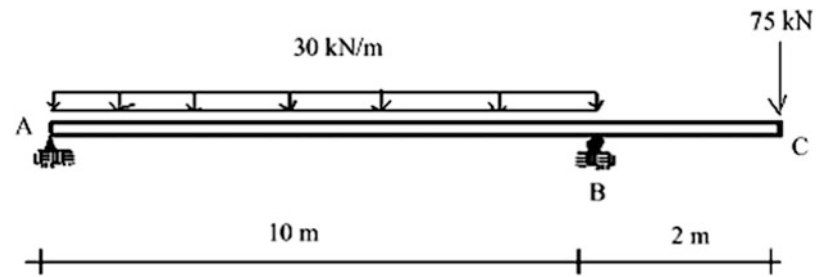
Problem 3.1



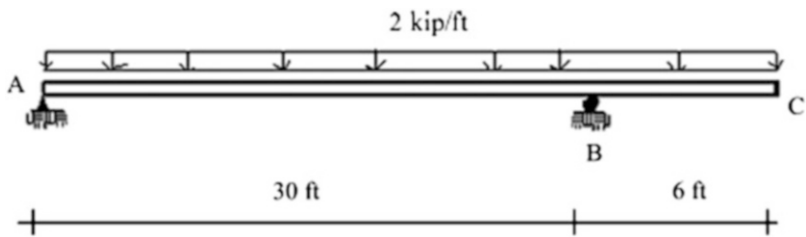
Problem 3.2



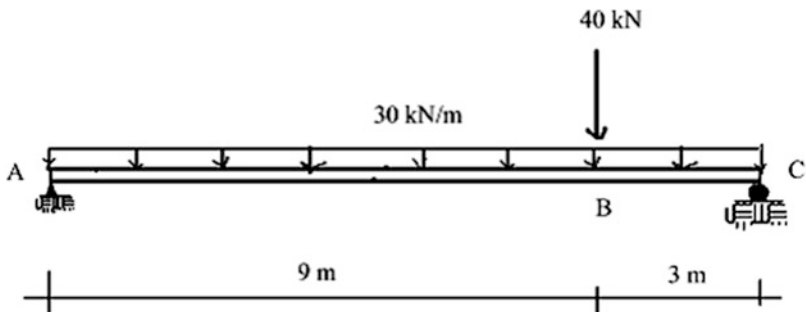
Problem 3.3



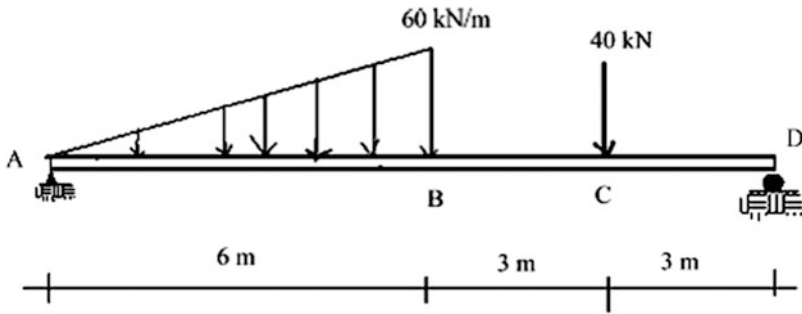
Problem 3.4



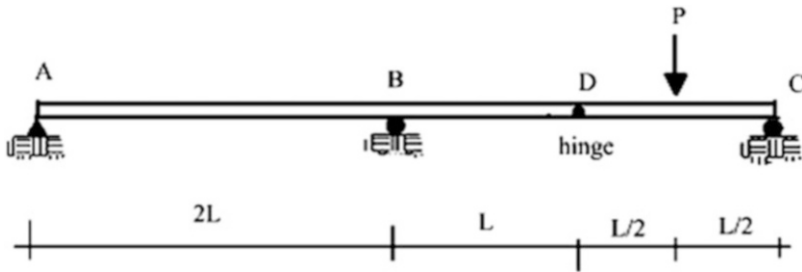
Problem 3.5



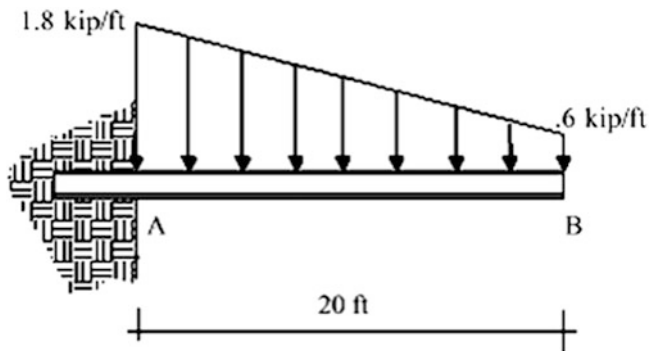
Problem 3.6



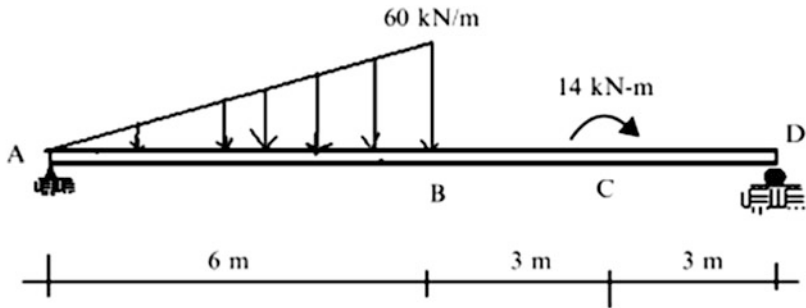
Problem 3.7



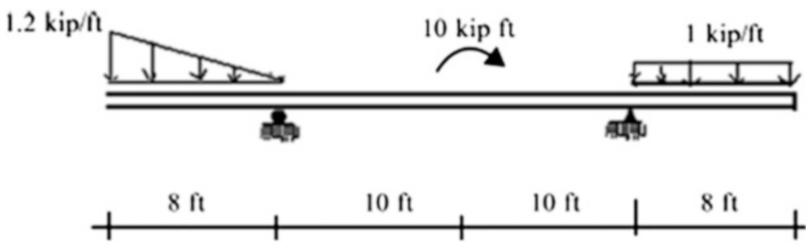
Problem 3.8



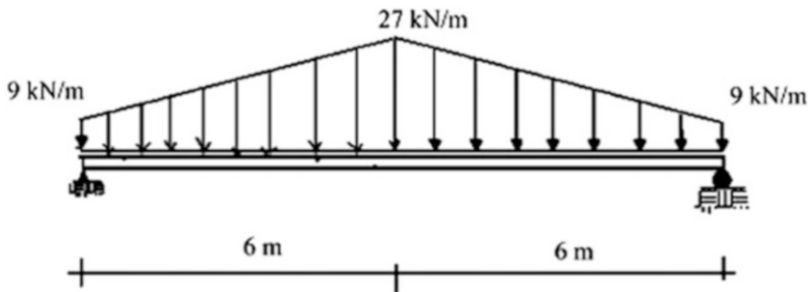
Problem 3.9



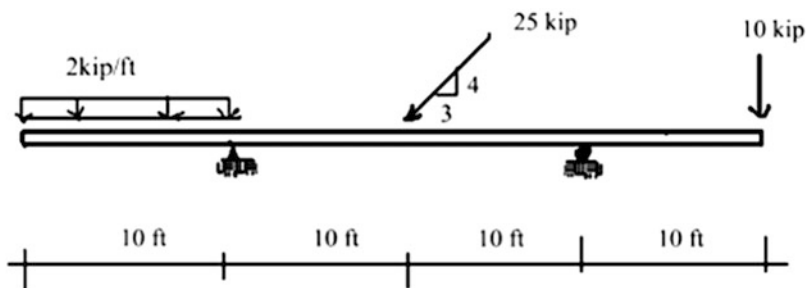
Problem 3.10



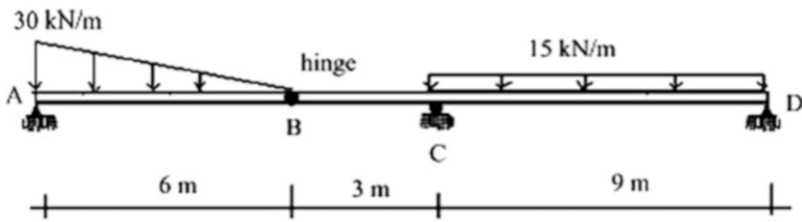
Problem 3.11



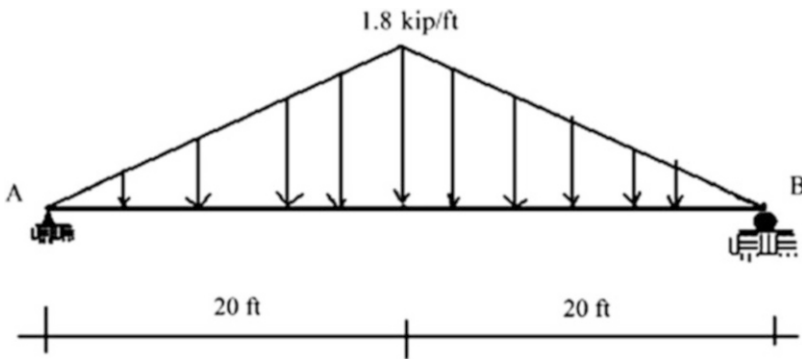
Problem 3.12



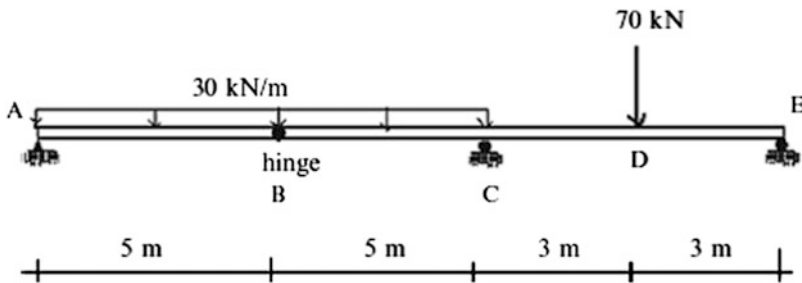
Problem 3.13



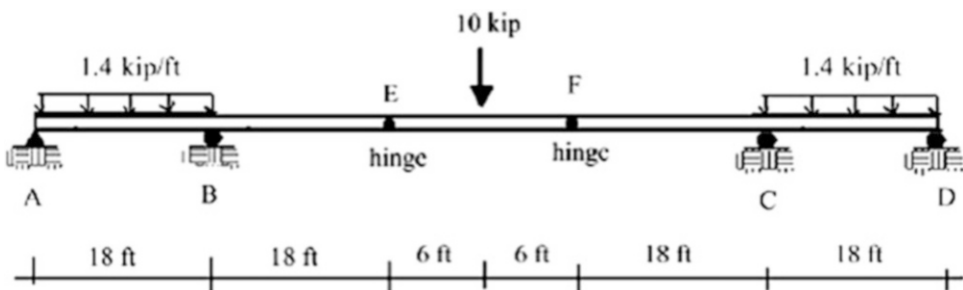
Problem 3.14



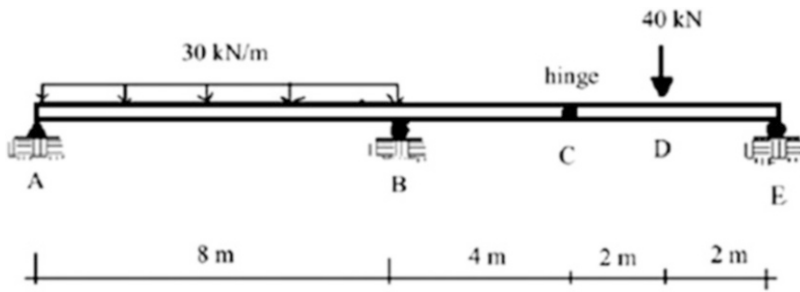
Problem 3.15



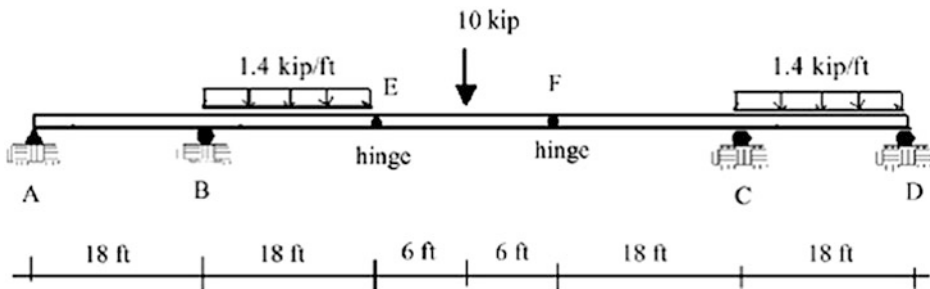
Problem 3.16



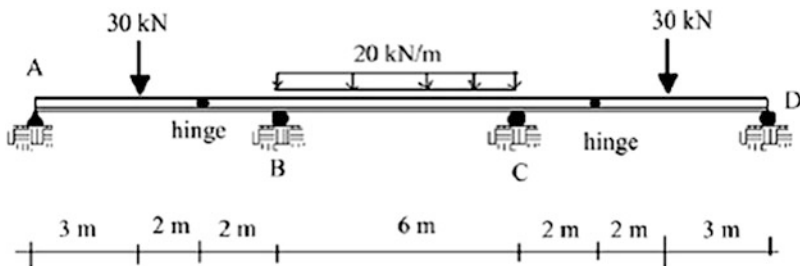
Problem 3.17



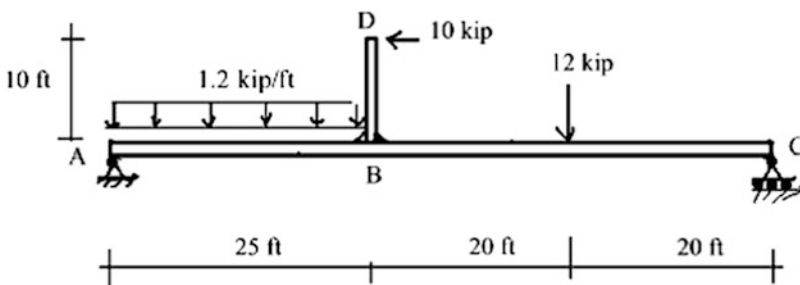
Problem 3.18



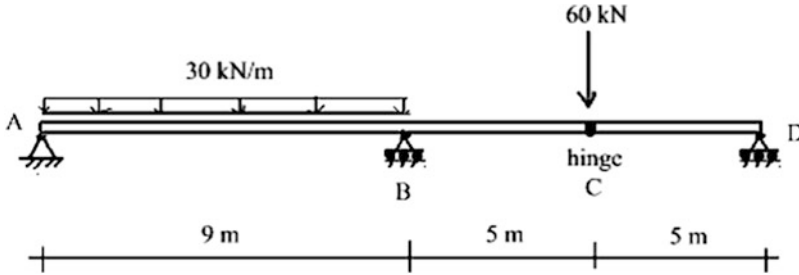
Problem 3.19



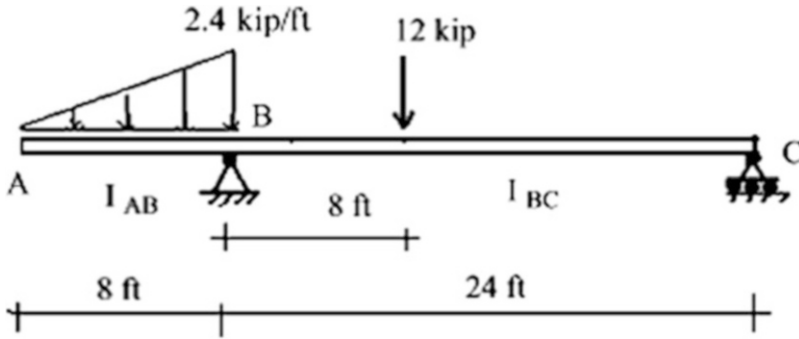
Problem 3.20 Member BD is rigidly attached to the beam at B.



Problem 3.21 Determine the maximum bending moment. Assume EI is constant.



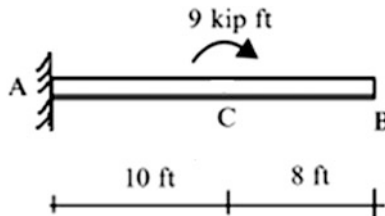
Problem 3.22 Determine the maximum bending moment. Does the bending moment distribution depend on either E or I ? Justify your response.



For the beams defined in Problems 3.23–3.26, use the Table 3.1 to determine the vertical deflection and rotation measures indicated. Assume EI is constant.

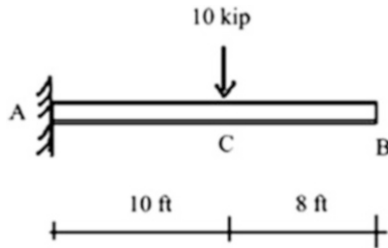
Problem 3.23

$$\theta_B, v_B I = 200 \text{ in.}^4, \quad E = 29,000 \text{ kip/in}^2$$



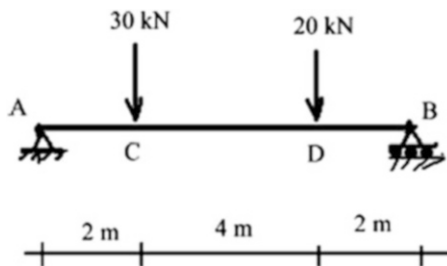
Problem 3.24

$$\theta_B, v_B I = 200 \text{ in.}^4, \quad E = 29,000 \text{ ksi}$$



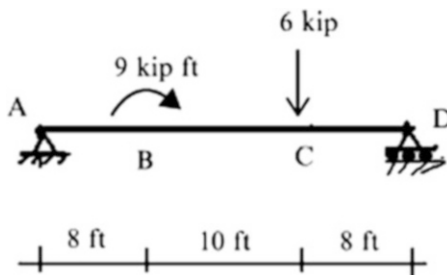
Problem 3.25

$$\theta_A, v_C I = 80(10^6) \text{ mm}^4, \quad E = 200 \text{ GPa}$$



Problem 3.26

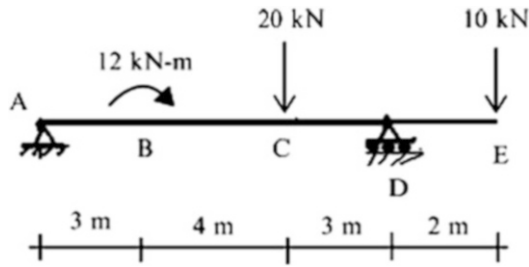
$$\theta_D, v_C I = 200 \text{ in.}^4, \quad E = 29,000 \text{ ksi}$$



For the beams defined in Problems 3.27–3.35, use the virtual force method to determine the vertical deflection and rotation measures indicated.

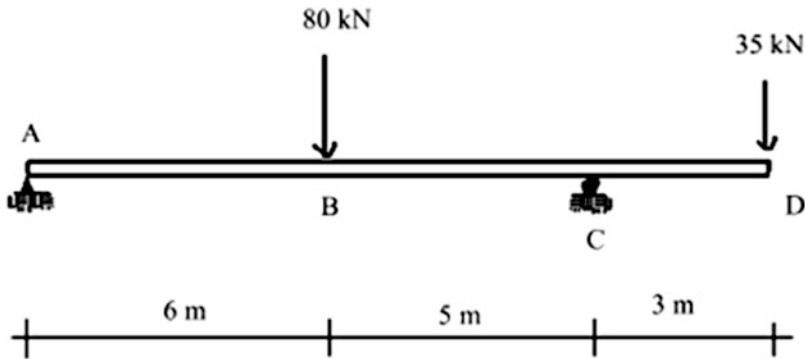
Problem 3.27

$$\theta_D, v_C I = 80(10^6) \text{mm}^4, \quad E = 200 \text{ GPa}$$



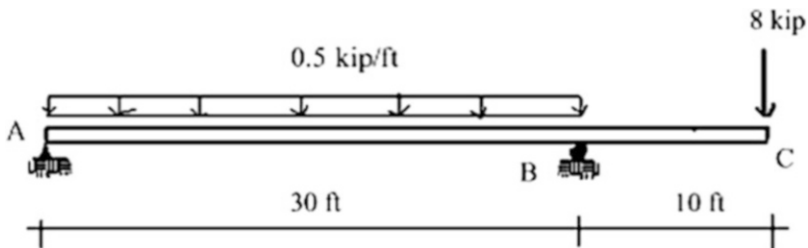
Problem 3.28

$$\theta_B, v_D I = 120(10^6) \text{mm}^4, \quad E = 200 \text{ GPa}$$



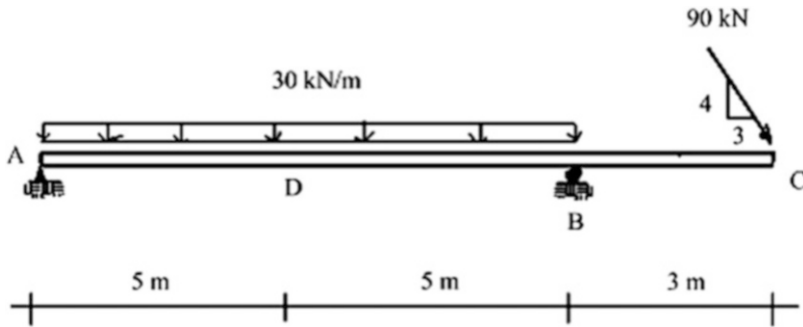
Problem 3.29

$$\theta_A, v_C I = 300 \text{in.}^4, \quad E = 29,000 \text{ ksi}$$



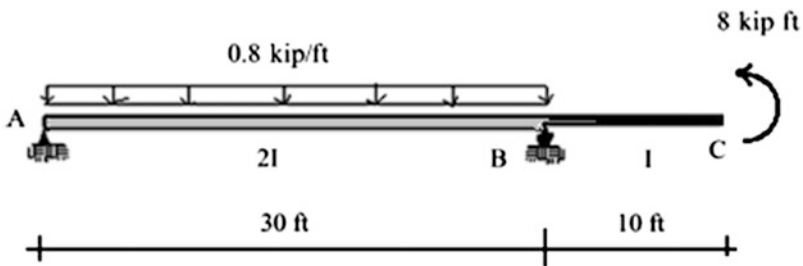
Problem 3.30

$$\theta_C, v_D I = 120(10^6) \text{mm}^4, \quad E = 200 \text{GPa}$$



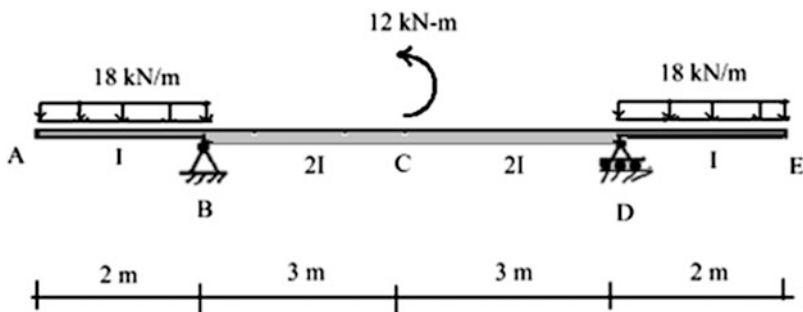
Problem 3.31

$$\theta_C, v_C I = 200 \text{in.}^4, \quad E = 29,000 \text{ksi}$$



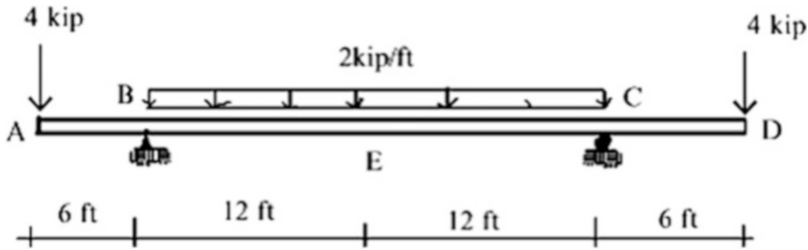
Problem 3.32

$$\theta_C, v_C I = 100(10^6) \text{mm}^4, \quad E = 200 \text{GPa}$$



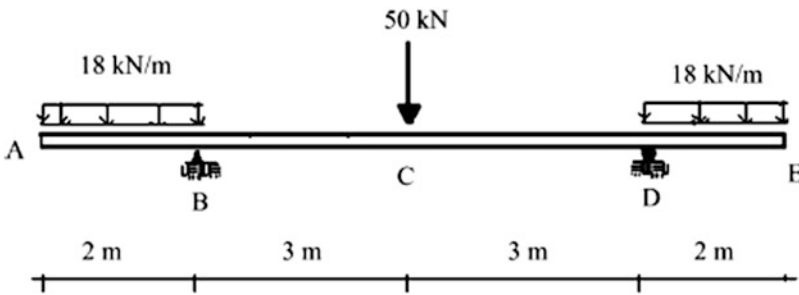
Problem 3.33

$$\theta_B, v_E I = 300 \text{ in.}^4, \quad E = 29,000 \text{ ksi}$$



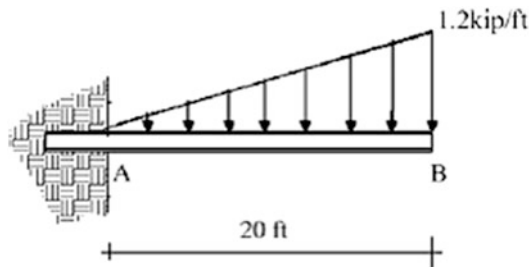
Problem 3.34

$$\theta_C, \theta_E, \text{ and } v_E I = 160(10^6) \text{ mm}^4, \quad E = 200 \text{ GPa}$$



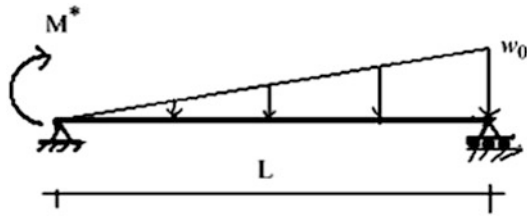
Problem 3.35

$$\theta_B, v_B I = 120 \text{ in.}^4, \quad E = 29,000 \text{ ksi}$$

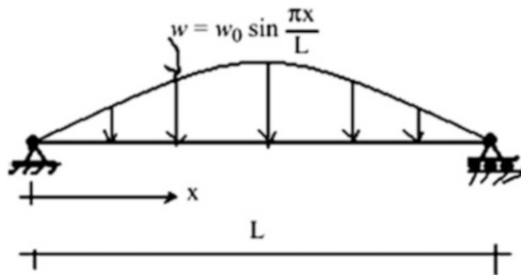


Determine the analytical solutions for the deflected shape for the beams defined in Problems 3.36–3.39. Assume EI is constant.

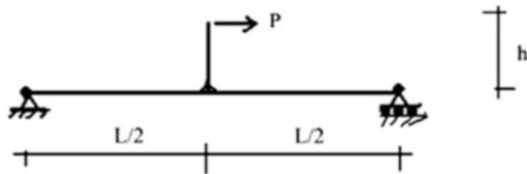
Problem 3.36



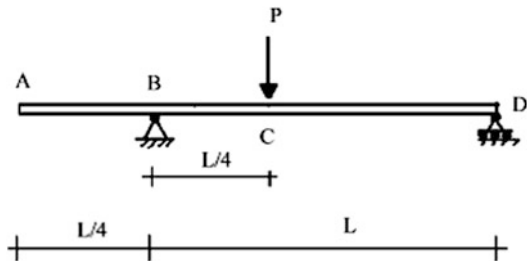
Problem 3.37



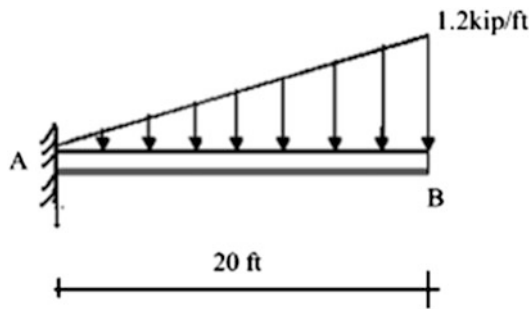
Problem 3.38



Problem 3.39



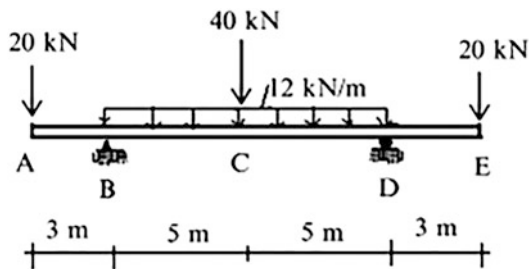
Problem 3.40 Determine the value of I require to limit the vertical deflection at B to $1/2$ in. $E = 29,000$ ksi.



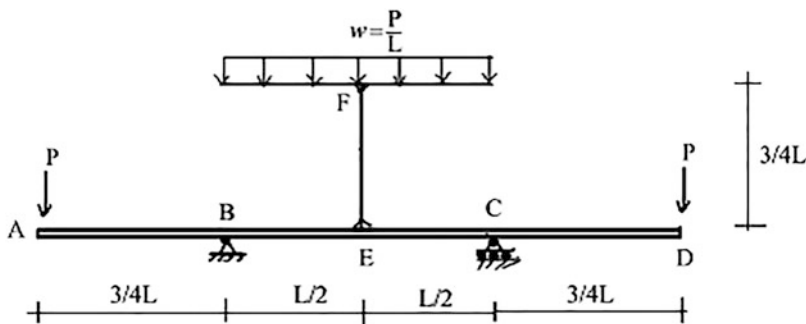
Problem 3.41

- (a) Solve Problem 3.39 using computer software. Consider different sets of values for EI . Show that the magnitude of the deflection varies as $1/EI$. Assume $P = 100$ kN, and $L = 8$ m.
- (b) Suppose the peak deflection is specified. How would you determine the appropriate value of I ?

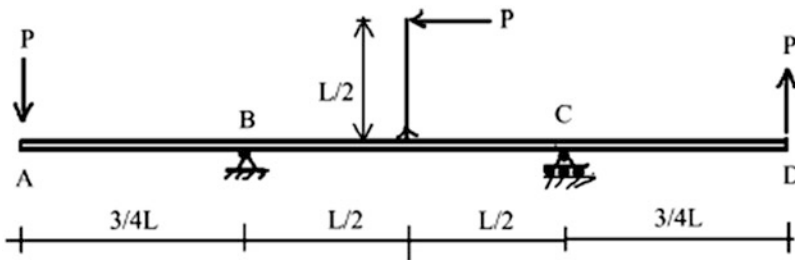
Problem 3.42 Utilize symmetry to sketch the deflected shape. EI is constant. Assume $E = 200$ GPa and $I = 160(10)^6$ mm⁴.



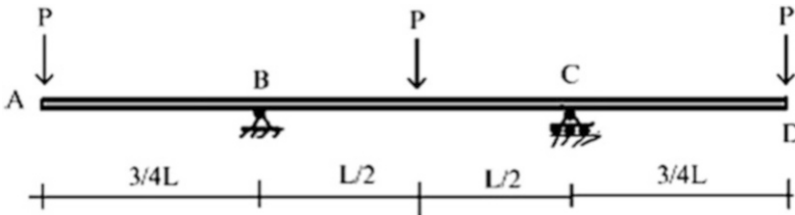
Problem 3.43 Determine the vertical deflection of point A. Sketch the deflected shape of the beam. EI is constant.



Problem 3.44 Determine the vertical deflection of point A. Sketch the deflected shape of the beam. EI is constant.

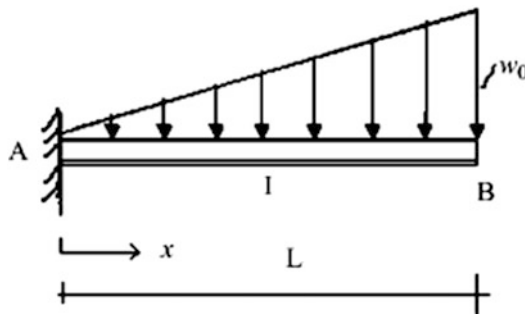


Problem 3.45 Determine the vertical deflection of point A. Sketch the deflected shape. EI is constant.

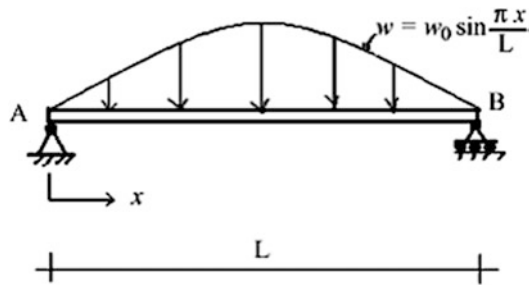


Problem 3.46 Consider the cantilever beam shown below. Determine the displacement at B due to the loading. Use the principle of Virtual Forces and evaluate the corresponding integral with the trapezoidal rule.

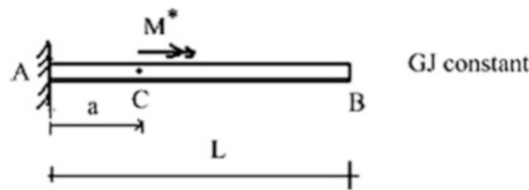
Take $w_0 = 10 \text{ kip/ft}$, $L = 20 \text{ ft}$, $I_0 = 1000 \text{ in.}^4$, $E = 29,000 \text{ ksi}$, $I = I_0 \left(1 + \cos \frac{\pi x}{2L}\right)$.



Problem 3.47 Assume AB is a “deep” beam. I and A are constant. Determine the analytical solution for β (the rotation of the cross-section) and v .



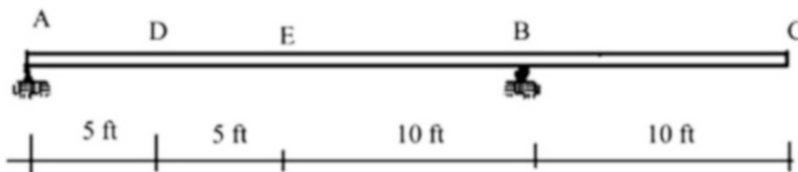
Problem 3.48



1. Determine β_t (the rotation of the cross-section about the longitudinal axis) at B due to the concentrated torque at C.
2. Suppose a distribution torque, m_t , is applied along A–B. Determine $M_t(x)$. Take $m_t = \sin \frac{\pi x}{2L}$
3. Determine β_t at B due to the distributed torsional loading.

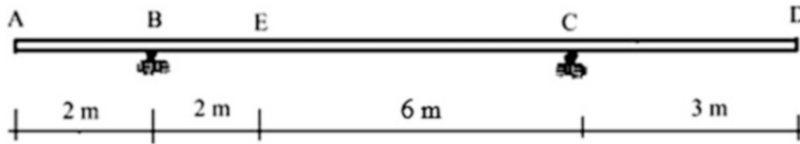
Problem 3.49 Draw the influence lines for:

- (a) Reaction at A
- (b) Moment at E
- (c) Shear at D



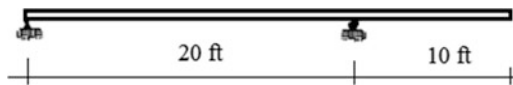
Problem 3.50

Draw the influence lines for the moment and shear at E.



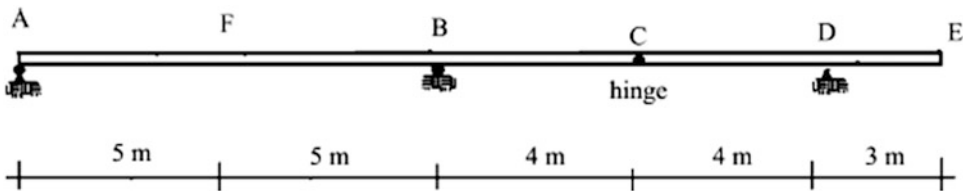
Problem 3.51

For the beams shown, determine the moment envelope corresponding to a single concentrated load moving across the span.



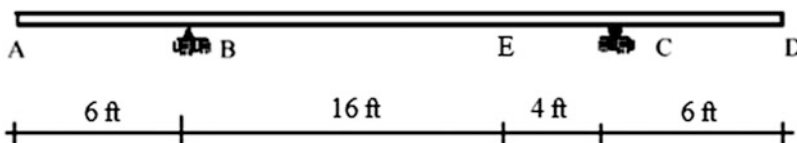
Problem 3.52

- (a) Draw the influence lines for moment at F and moment at B.
- (b) Draw the moment envelope.

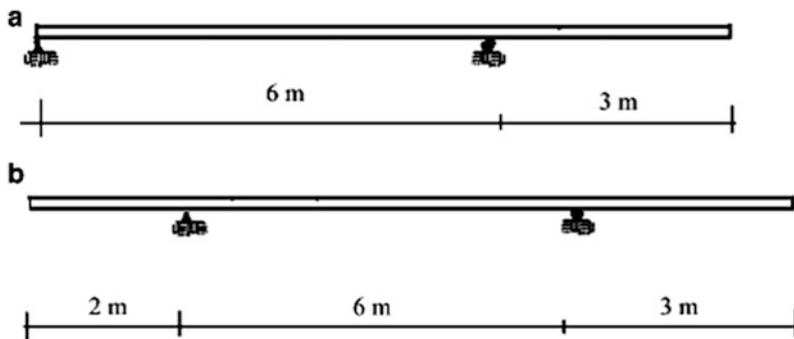


Suppose a uniformly distributed dead load of 18 kN/m and uniformly distributed live load of 30 kN/m are placed on the beam. Use the above results for influence lines to determine the maximum values for the moment at point F and point B. Also show the position of the live load on the beam for these limiting cases.

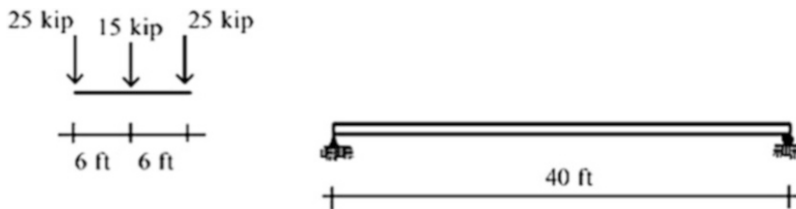
Problem 3.53 Suppose a uniformly distributed live load of 1.2 kip/ft and uniformly distributed dead load of 0.8 kip/ft are placed on the beam. Determine the critical loading pattern that results in the maximum and minimum values of moment at E.



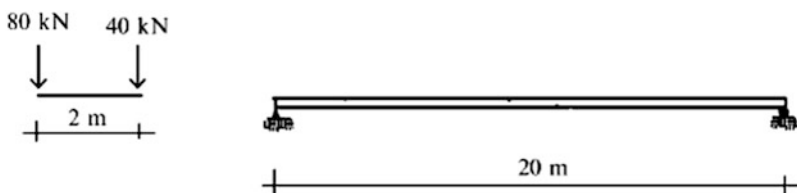
Problem 3.54 For the beams shown, determine the moment envelope corresponding to a single concentrated load moving across the span.



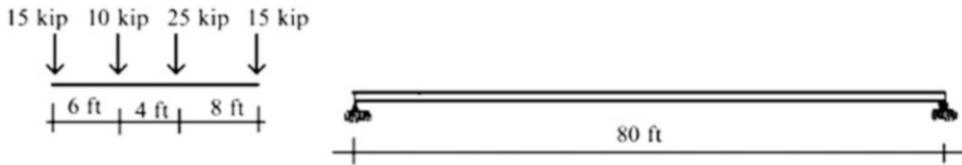
Problem 3.55 Determine the maximum possible moment in the 40 ft span beam as the loading system shown moves across the span. Use either the analytical approach or the moment envelope corresponding to the loading.



Problem 3.56 Determine the location of the maximum possible moment in the 20 m span beam as the loading system shown moves across the span.

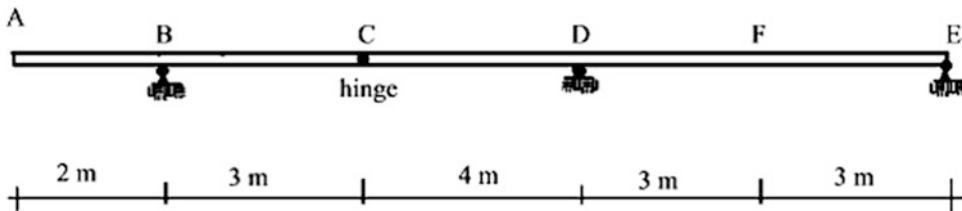


Problem 3.57 Determine the maximum possible moment in a 80 ft span beam as the loading system shown moves across the span. Assume a uniform load of 2 kip/ft also acts on the span. Use computer software.

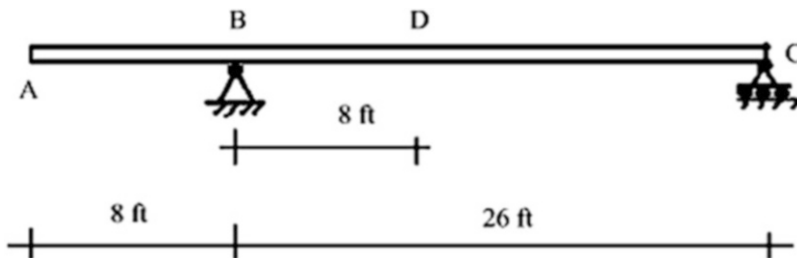


Problem 3.58 For the beam shown:

- (a) Draw the influence lines for the vertical reaction at support D, and the moment at point F.
- (b) For a uniformly distributed live load of 20 kN/m, use the above results to determine the maximum values of the reaction at D, and the moment at F. Also show the position of the live load on the beam.
- (c) Establish the moment envelope corresponding to a single concentrated vertical load.



Problem 3.59 For the beam shown below



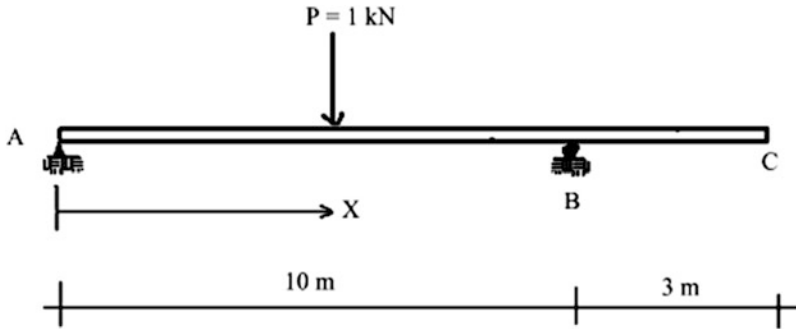
Determine the influence line for:

- (a) The vertical reaction at C
- (b) The moment at D

If a uniformly distributed live load of 1.8 kip/ft and uniformly distributed dead load of 1.4 kip/ft are placed on the beam, use the above results to determine the maximum and minimum values of

- (a) The vertical reaction at C
- (b) The moment at D

Problem 3.60 Using computer software, determine the influence line for the vertical displacement at $x = 5$ m. Assume EI is constant.



Hint: Apply a unit load at $x = 5$ m and determine the deflected shape. This is a scaled version of the influence line. Verify by moving the load and recomputing the displacement at $x = 5$ m.

References

1. Tauchert TR. Energy principles in structural mechanics. New York: McGraw-Hill; 1974.
2. Matlab 7.13, Engineering calculations software.

Abstract

Plane frame structures are composed of structural members which lie in a single plane. When loaded in this plane, they are subjected to both bending and axial action. Of particular interest are the shear and moment distributions for the members due to gravity and lateral loadings. We describe in this chapter analysis strategies for typical statically determinate single-story frames. Numerous examples illustrating the response are presented to provide the reader with insight as to the behavior of these structural types. We also describe how the Method of Virtual Forces can be applied to compute displacements of frames. The theory for frame structures is based on the theory of beams presented in Chap. 3. Later in Chaps. 9, 10, and 15, we extend the discussion to deal with statically indeterminate frames and space frames.

4.1 Definition of Plane Frames

The two dominant planar structural systems are plane trusses and plane frames. Plane trusses were discussed in detail in Chap. 2. Both structural systems are formed by connecting structural members at their ends such that they are in a single plane. The systems differ in the way the individual members are connected and loaded. Loads are applied at nodes (joints) for truss structures. Consequently, the member forces are purely axial. Frame structures behave in a completely different way. The loading is applied directly to the members, resulting in internal shear and moment as well as axial force in the members. Depending on the geometric configuration, a set of members may experience predominately bending action; these members are called “beams.” Another set may experience predominately axial action. They are called “columns.” The typical building frame is composed of a combination of beams and columns.

Frames are categorized partly by their geometry and partly by the nature of the member/member connection, i.e., pinned vs. rigid connection. Figure 4.1 illustrates some typical rigid plane frames used mainly for light manufacturing factories, warehouses, and office buildings. We generate three-dimensional frames by suitably combining plane frames.

Fig. 4.1 Typical plane building frames. (a) Rigid portal frame. (b) Rigid multi-bay portal frame. (c) Multistory rigid frame. (d) Multistory braced frame

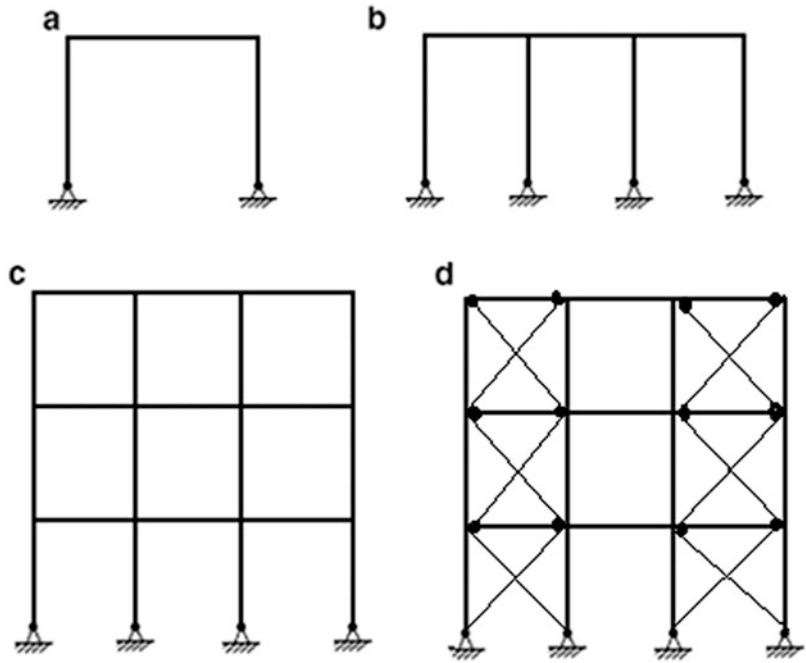


Fig. 4.2 A-frame

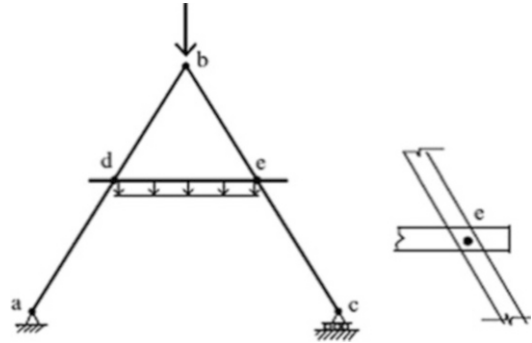


Figure 4.2 shows an A-frame, named obviously for its geometry. This frame has three members ab , bc , and de that are pinned together at points d , b , and e . Loads may be applied at the connection points, such as b , or on a member, such as de . A-frames are typically supported at the base of their legs, such as at a and c . Because of the nature of the loading and restraints, the members in an A-frame generally experience bending as well as axial force.

To provide more vertical clearance in the interior of the portal frame, and also to improve the aesthetics, a more open interior space is created by pitching the top member as illustrated in Fig. 4.3. Pitched roof frames are also referred to as gable frames. Architects tend to prefer them for churches, gymnasias, and exhibition halls.

4.2 Statical Determinacy: Planar Loading

All the plane frames that we have discussed so far can be regarded as rigid bodies in the sense that if they are adequately supported, the only motion they will experience when a planar load is applied will

Fig. 4.3 Gable (pitched roof) frames

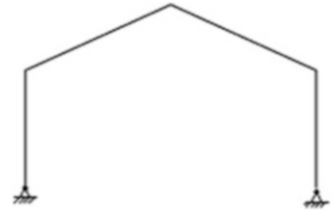


Fig. 4.4 Statically determinate support schemes for planar frames

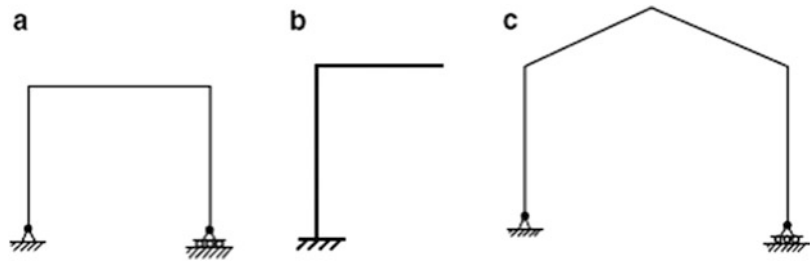
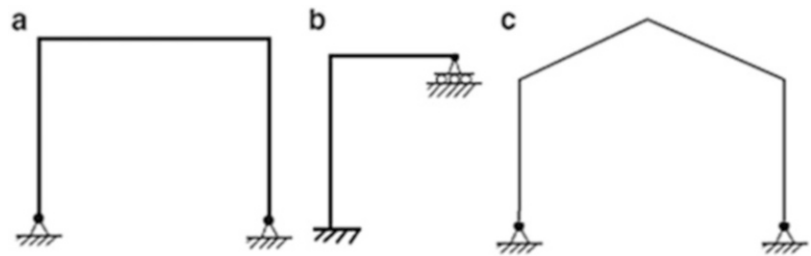


Fig. 4.5 Statically indeterminate support schemes—planar frames



be due to deformation of the members. Therefore, we need to support them with only three nonconcurrent displacement restraints. One can use a single, fully fixed support scheme, or a combination of hinge and roller supports. Examples of “adequate” support schemes are shown in Fig. 4.4. All these schemes are statically determinate. In this case, one first determines the reactions and then analyzes the individual members.

If more than three displacement restraints are used, the plane frames are statically indeterminate. In many cases, two hinge supports are used for portal and gable frames (see Fig. 4.5). We cannot determine the reaction forces in these frame structures using only the three available equilibrium equations since there are now four unknown reaction forces. They are reduced to statically determinate structures by inserting a hinge which acts as a moment release. We refer to these modified structures as 3-hinge frames (see Fig. 4.6).

Statical determinacy is evaluated by comparing the number of unknown forces with the number of equilibrium equations available. For a planar member subjected to planar loading, there are three internal forces: axial, shear, and moment. Once these force quantities are known at a point, the force quantities at any other point in the member can be determined using the equilibrium equations. Figure 4.7 illustrates the use of equilibrium equations for the member segment AB. Therefore, it follows that there are only *three force unknowns for each member* of a rigid planar frame subjected to planar loading.

We define a node (joint) as the intersection of two or more members, or the end of a member connected to a support. A node is acted upon by member forces associated with the members' incident on the node. Figure 4.8 illustrates the forces acting on node B.

Fig. 4.6 3-Hinge plane frames

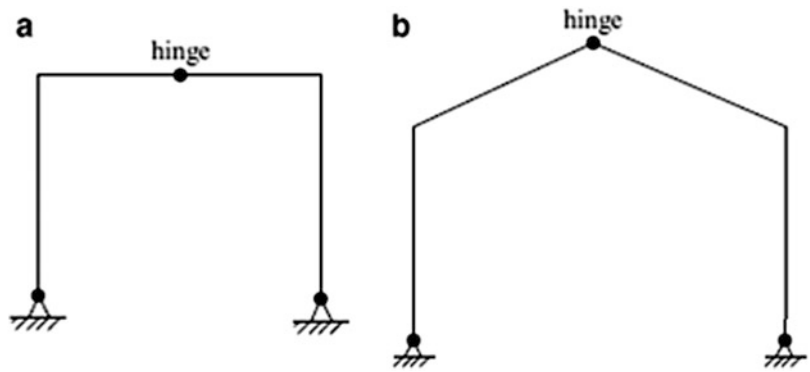


Fig. 4.7 Free body diagram—member forces

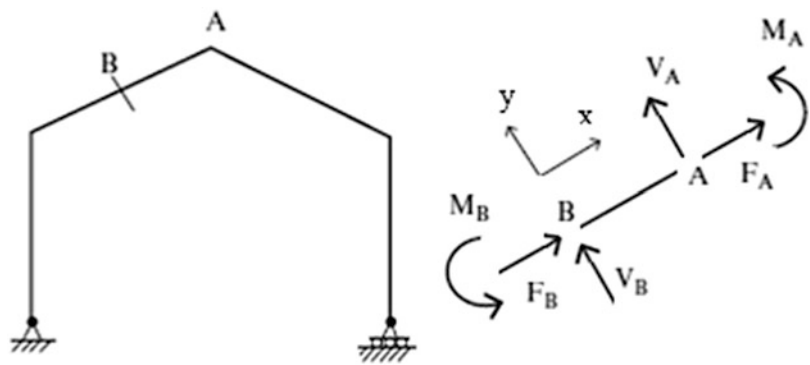
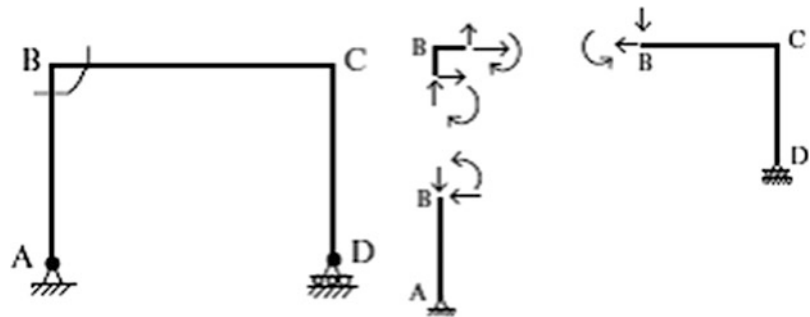
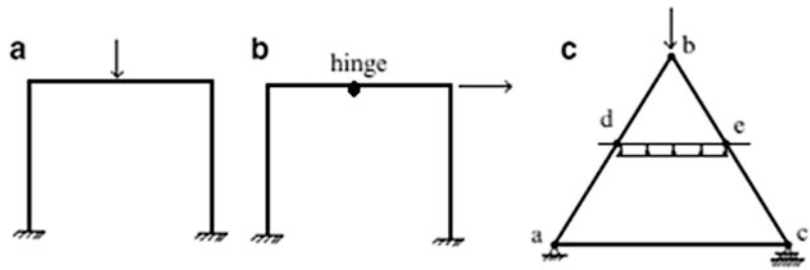


Fig. 4.8 Free body diagram—node B



These nodal forces comprise a general planar force system for which there are three equilibrium equations available; summation of forces in two nonparallel directions and summation of moments. Summing up force unknowns, we have three for each member plus the number of displacement restraints. Summing up equations, there are three for each node plus the number of force releases (e.g., moment releases) introduced. Letting m denote the number of members, r the number of

Fig. 4.9 Indeterminate portal and A-frames



displacement restraints, j the number of nodes, and n the number of releases, the criterion for statical determinacy of *rigid plane frames* can be expressed as

$$3m + r - n = 3j \tag{4.1}$$

We apply this criterion to the portal frames shown in Figs. 4.4a, 4.5a, and 4.6b. For the portal frame in Fig. 4.4a

$$m = 3, \quad r = 3, \quad j = 4$$

For the corresponding frame in Fig. 4.5a

$$m = 3, \quad r = 4, \quad j = 4$$

This structure is indeterminate to the first degree. The 3-hinge frame in Fig. 4.6a has

$$m = 4, \quad r = 4, \quad n = 1, \quad j = 5$$

Inserting the moment release reduces the number of unknowns and now the resulting structure is statically determinate.

Consider the plane frames shown in Fig. 4.9. The frame in Fig. 4.9a is indeterminate to the third degree.

$$m = 3, \quad r = 6, \quad j = 4$$

The frame in Fig. 4.9b is indeterminate to the second degree.

$$m = 4, \quad r = 6, \quad j = 5 \quad n = 1$$

Equation (4.1) applies to rigid plane frames, i.e., where the members are rigidly connected to each other at nodes. The members of an A-frame are connected with pins that allow relative rotation and therefore A-frames are *not* rigid frames. We establish a criterion for A-frame type structures following the same approach described above. Each member has three equilibrium equations. Therefore, the total number of equilibrium equations is equal to $3m$. Each pin introduces two force unknowns. Letting n_p denote the number of pins, the total number of force unknowns is equal to $2n_p$ plus the number of displacement restraints. It follows that

$$2n_p + r = 3m \tag{4.2}$$

for static determinacy of A-frame type structures. Applying this criterion to the structure shown in Fig. 4.2, one has $n_p = 3, r = 3, m = 3$, and the structure is statically determinate. If we add another member at the base, as shown in Fig. 4.9c, $n_p = 5, r = 3, m = 4$, and the structure becomes statically indeterminate to the first degree.

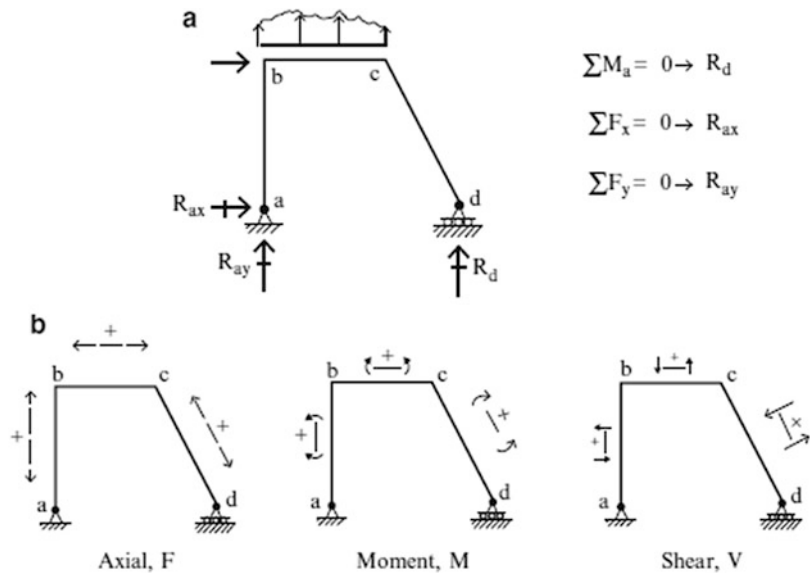
4.3 Analysis of Statically Determinate Frames

In this section, we illustrate with numerous examples the analysis process for statically determinate frames such as shown in Fig. 4.10a. In these examples, our primary focus is on the generation of the internal force distributions. Of particular interest are the location and magnitude of the peak values of moment, shear, and axial force since these quantities are needed for the design of the member cross sections.

The analysis strategy for these structures is as follows. We first find the reactions by enforcing the global equilibrium equations. Once the reactions are known, we draw free body diagrams for the members and determine the force distributions in the members. *We define the positive sense of bending moment according to whether it produces compression on the exterior face.* The sign conventions for bending moment, transverse shear, and axial force are defined in Fig. 4.10b.

The following examples illustrate this analysis strategy. Later, we present analytical solutions which are useful for developing an understanding of the behavior.

Fig. 4.10 (a) Typical frame. (b) Sign convention for the bending moment, transverse shear, and axial force



Example 4.1 Unsymmetrical Cantilever Frame

Given: The structure defined in Fig. E4.1a.

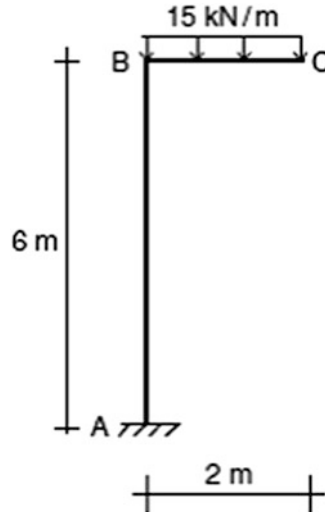


Fig. E4.1a

Determine: The reactions and draw the shear and moment diagrams.

Solution: We first determine the reactions at A, and then the shear and moment at B. These results are listed in Figs. E4.1b and E4.1c. Once these values are known, the shear and moment diagrams for members CB and BA can be constructed. The final results are plotted in Fig. E4.1d.

$$\begin{aligned} \sum F_x &= 0 & R_{Ax} &= 0 \\ \sum F_y &= 0 & R_{Ay} - (15)(2) &= 0 & R_{Ay} &= 30 \text{ kN } \uparrow \\ \sum M_A &= 0 & M_A - (15)(2)(1) &= 0 & M_A &= 30 \text{ kN-m counter clockwise} \end{aligned}$$

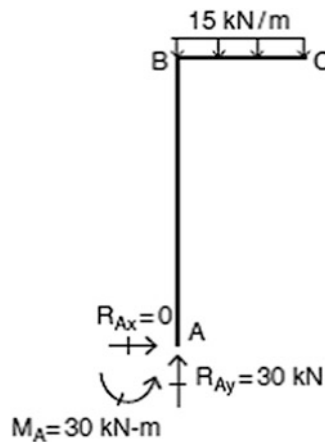


Fig. E4.1b Reactions

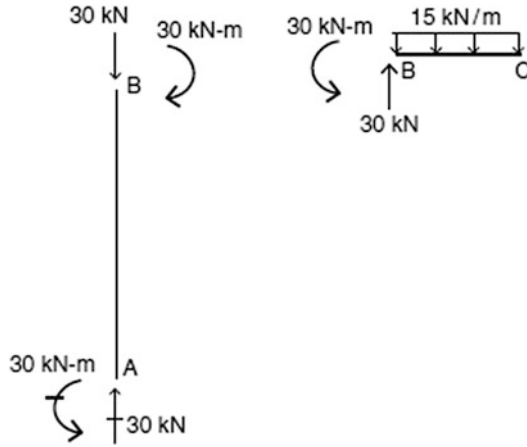


Fig. E4.1c End actions

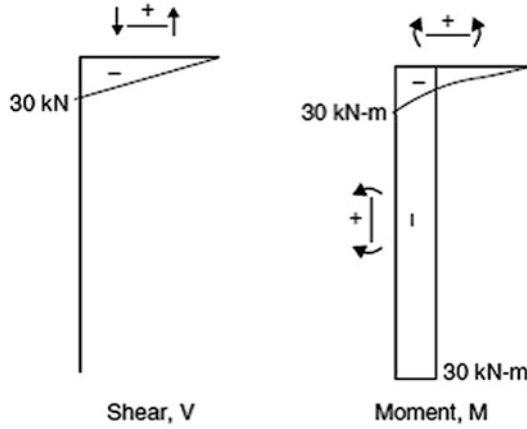


Fig. E4.1d Shear and moment diagrams

Example 4.2 Symmetrical Cantilever Frame

Given: The structure defined in Fig. E4.2a.

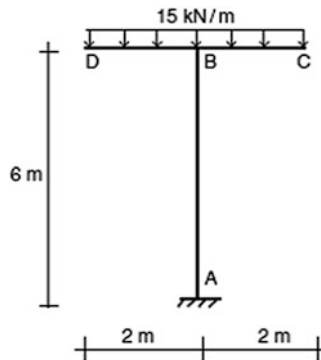


Fig. E4.2a

Determine: The reactions and draw the shear and moment diagrams.

Solution: We determine the reactions at A and shear and moment at B. The results are shown in Figs. E4.2b and E4.2c.

$$\begin{aligned} \sum F_x = 0 & \quad R_{Ax} = 0 \\ \sum F_y = 0 & \quad R_{Ay} - (15)(4) = 0 & \quad R_{Ay} = 60 \text{ kN } \uparrow \\ \sum M_A = 0 & \quad M_A - (15)(2)(1) + (15)(2)(1) = 0 & \quad M_A = 0 \end{aligned}$$

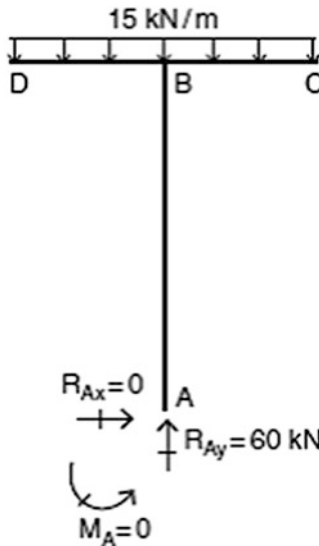


Fig. E4.2b Reactions

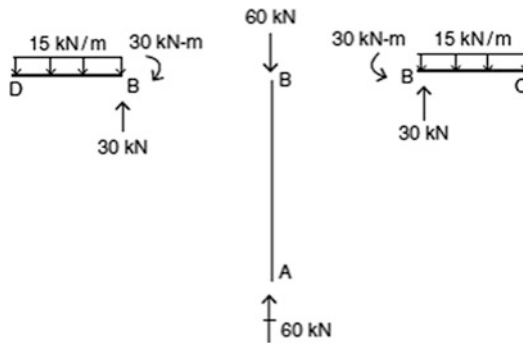


Fig. E4.2c End actions

Finally, the shear and moment diagrams for the structures are plotted in Fig. E4.2d. Note that member AB now has no bending moment, just axial compression of 60 kN.

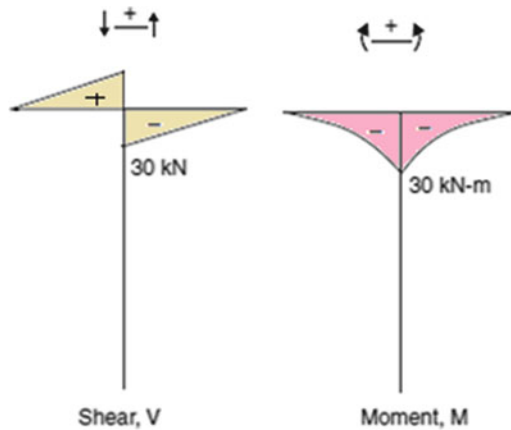


Fig. E4.2d Shear and moment diagrams

Example 4.3 Angle-Type Frame Segment

Given: The frame defined in Fig. E4.3a.

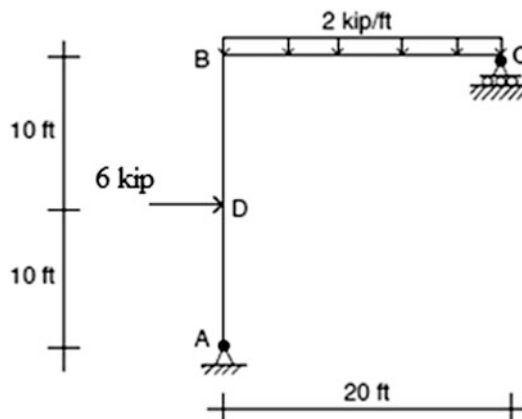


Fig. E4.3a

Determine: The reactions and draw the shear and moment diagrams.

Solution: We determine the vertical reaction at C by summing moments about A. The reactions at A follow from force equilibrium considerations (Fig. E4.3b).

$$\begin{aligned} \sum M_A = 0 & \quad 2(20)(10) + 6(10) - R_C(20) = 0 & \quad R_C = 23 \text{ kip } \uparrow \\ \sum F_x = 0 & \quad R_{Ax} = 6 \text{ kip } \leftarrow \\ \sum F_y = 0 & \quad R_{Ay} - 2(20) + 23 = 0 & \quad R_{Ay} = 17 \text{ kip } \uparrow \end{aligned}$$

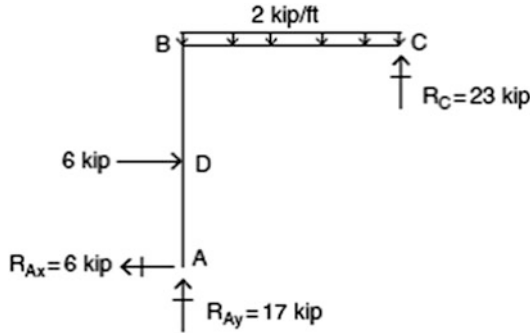


Fig. E4.3b Reactions

Next, we determine the end moments and end shears for segments CB and BA using the equilibrium equations for the members. Figure E4.3c contains these results.

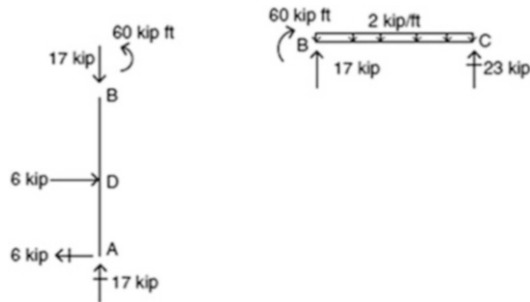
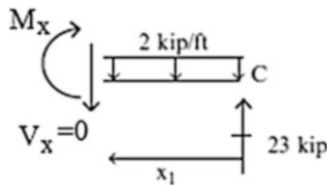


Fig. E4.3c End actions

Lastly, we generate the shear and bending moment diagrams (Fig. E4.3d). The maximum moment occurs in member BC. We determine its location by noting that the moment is maximum when the shear is zero.



$$23 - (2)x_1 = 0 \rightarrow x_1 = 11.5 \text{ ft}$$

Then, $M_{\max} = 23(11.5) - \frac{2(11.5)^2}{2} = 132.25 \text{ kip ft}$

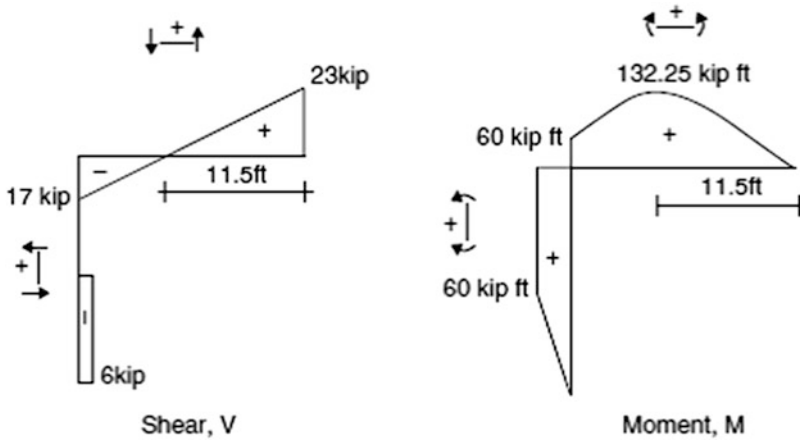


Fig. E4.3d Shear and moment diagrams

Example 4.4 Simply Supported Portal Frame

Given: The portal frame defined in Fig. E4.4a.

Determine: The shear and moment distributions.

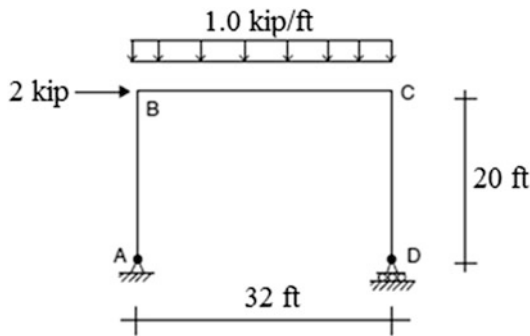


Fig. E4.4a

Solution: The reaction at D is found by summing moments about A. We then determine the reactions at A using force equilibrium considerations. Figure E4.4b shows the result.

$$\begin{aligned} \sum M_A = 0 & \quad 1(32)(16) + 2(20) - R_D(32) = 0 & \quad R_D = 17.25 \uparrow \\ \sum F_x = 0 & \quad R_{Ax} = 2 \leftarrow \\ \sum F_y = 0 & \quad R_{Ay} - 1(32) + 17.25 = 0 & \quad R_{Ay} = 14.75 \uparrow \end{aligned}$$

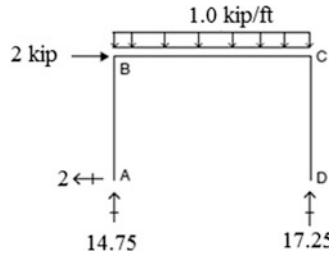


Fig. E4.4b Reactions

Isolating the individual members and enforcing equilibrium leads to the end forces and moments shown in Fig. E4.4c.

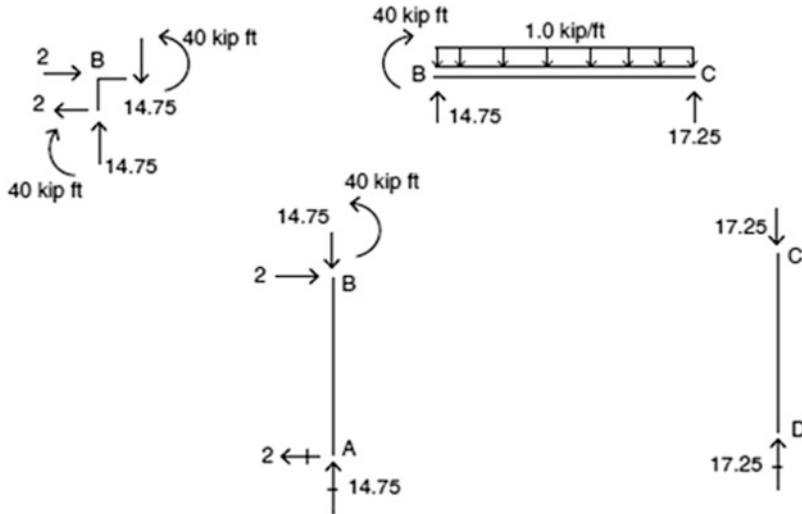
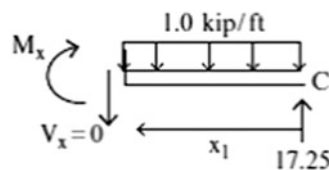


Fig. E4.4c End actions

We locate the maximum moment in member BC. Suppose the moment is a maximum at $x = x_1$. Setting the shear at this point equal to zero leads to



$$17.25 - x_1(1) = 0 \rightarrow x_1 = 17.25 \text{ ft}$$

Then, $M_{\max} = 17.25(17.25) - \frac{(1)(17.25)^2}{2} = 148.78 \text{ kip ft}$

The shear and moment diagrams are plotted in Fig. E4.4d.

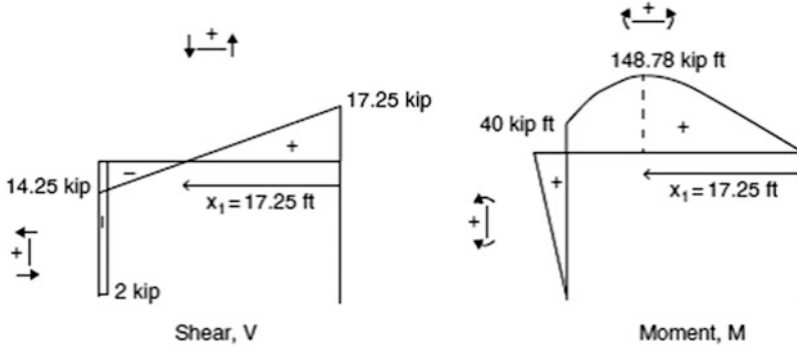


Fig. E4.4d Shear and moment diagrams

Example 4.5 3-Hinge Portal Frame

Given: The 3-hinge frame defined in Fig. E4.5a.

Determine: The shear and moment distributions.

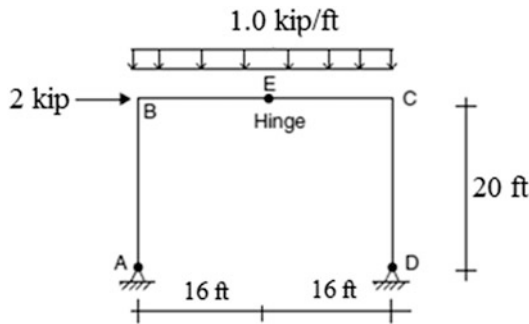


Fig. E4.5a

Solution: Results for the various analysis steps are listed in Figs. E4.5b, E4.5c, E4.5d, E4.5e, E4.5f, and E4.5g.

Step 1: Reactions at D and A

The vertical reaction at D is found by summing moments about A.

$$\sum M_A = 0 \quad R_{Dy}(32) - (1)(32)(16) - 2(20) = 0 \quad R_{Dy} = 17.25 \text{ kip } \uparrow$$

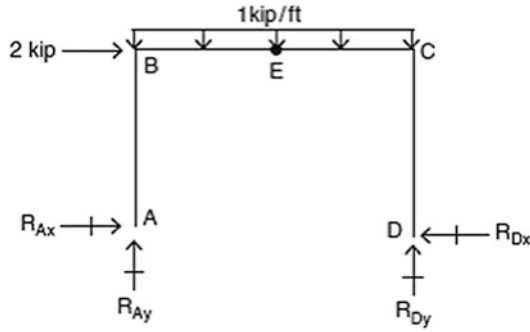


Fig. E4.5b

Next, we work with the free body diagram of segment ECD. Applying the equilibrium conditions to this segment results in

$$\begin{aligned} \sum M_E = 0 \quad & 17.25(16) - (1)(16)(8) - R_{Dx}(20) = 0 \quad R_{Dx} = 7.4 \text{ kip } \leftarrow \\ \sum F_x = 0 \quad & F_E = -R_{Dx} = 7.4 \text{ kip } \rightarrow \\ \sum F_y = 0 \quad & -V_E + 17.25 - (1)(16) = 0 \quad V_E = 1.25 \text{ kip } \downarrow \end{aligned}$$

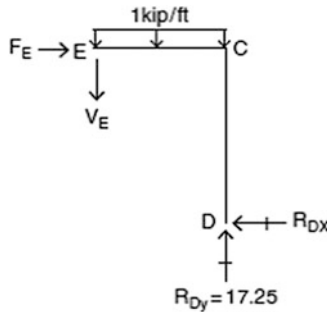


Fig. E4.5c

With the internal forces at E known, we can now proceed with the analysis of segment ABE.

$$\sum F_x = 0 \quad R_{Ax} + 2 - 7.4 = 0 \quad R_{Ax} = 5.4 \text{ kip } \rightarrow$$

$$\sum F_y = 0 \quad R_{Ay} + 17.25 - (1)(32) = 0 \quad R_{Ay} = 14.75 \text{ kip } \uparrow$$

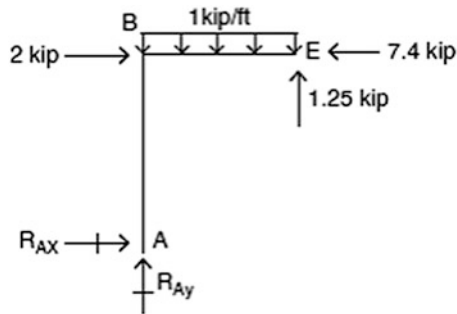


Fig. E4.5d

Reactions are listed below

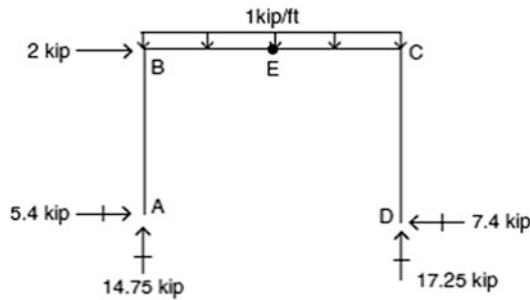


Fig. E4.5e Reactions

Step 2: End actions at B and C

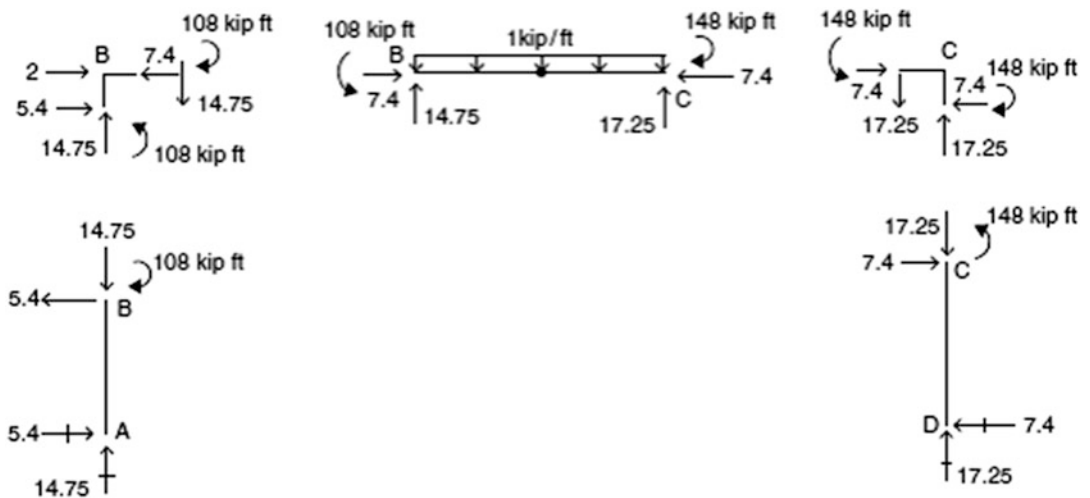
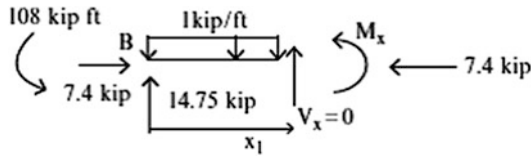


Fig. E4.5f End actions

Step 3: Shear and moment diagrams

First, we locate the maximum moment in member BC.



$$14.75 - (1)x_1 = 0 \rightarrow x_1 = 14.75 \text{ ft}$$

Then, $M_{\max} = 14.75(14.75) - \frac{1(14.75)^2}{2} - 108 = 0.78 \text{ kip ft}$

The corresponding shear and moment diagrams are listed in Fig. E4.5g.

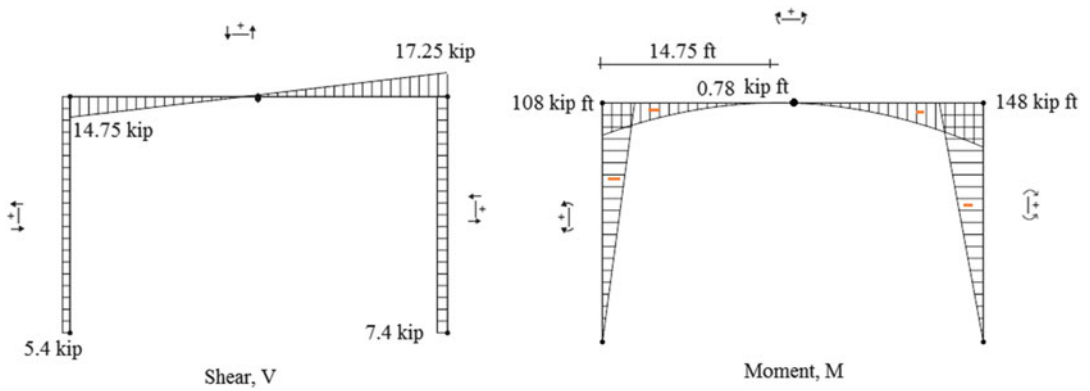


Fig. E4.5g Shear and moment diagrams

Example 4.6 Portal Frame with Overhang

Given: The portal frame defined in Fig. E4.6a.

Determine: The shear and moment diagrams.

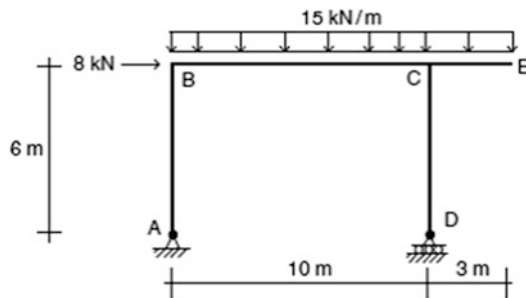


Fig. E4.6a

Solution: Results for the various analysis steps are listed in Figs. E4.6b, E4.6c, and E4.6d.

$$\sum M_A = 0 \quad R_D(10) - 8(6) - (15)(13)(6.5) = 0 \quad R_D = 131.55 \text{ kN } \uparrow$$

$$\sum F_x = 0 \quad R_{Ax} = 8 \text{ kN } \leftarrow$$

$$\sum F_y = 0 \quad R_{Ay} + 131.55 - (15)(13) = 0 \quad R_{Ay} = 63.45 \text{ kN } \uparrow$$

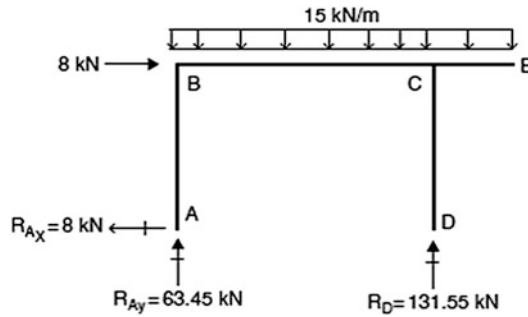


Fig. E4.6b Reactions

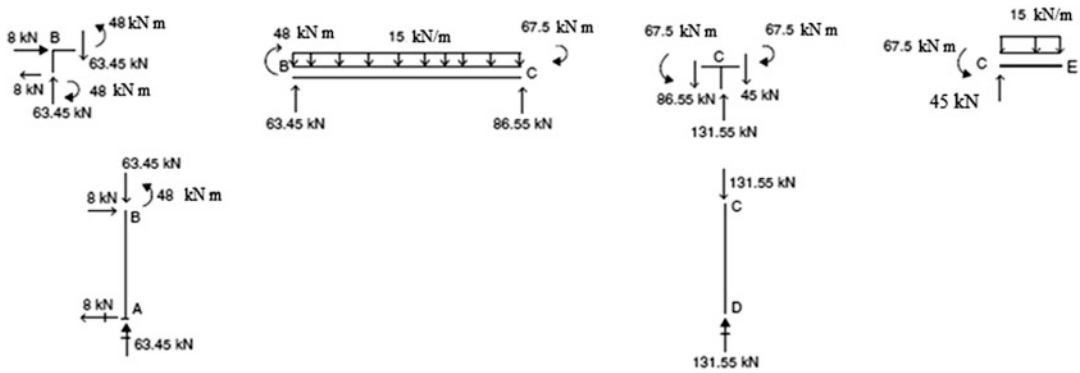
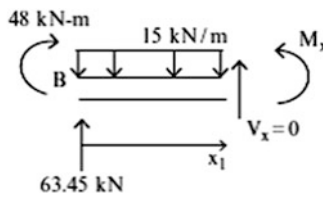


Fig. E4.6c End actions

First, we locate the maximum moment in member BC.



$$63.45 - (15)x_1 = 0 \rightarrow x_1 = 4.23 \text{ m}$$

$$\text{Then, } M_{\max} = 63.45(4.23) - \frac{(15)(4.23)^2}{2} + 48 = 182 \text{ kN m}$$

The corresponding shear and moment diagrams are listed in Fig. E4.6d.

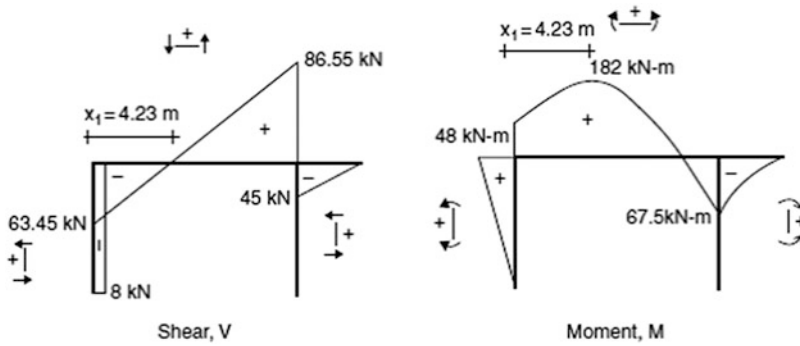


Fig. E4.6d Shear and moment diagrams

4.3.1 Behavior of Portal Frames: Analytical Solution

The previous examples illustrated numerical aspects of the analysis process for single-story statically determinate portal frames. For future reference, we list below the corresponding analytical solutions (Figs. 4.11, 4.12, 4.13, and 4.14). We consider both gravity and lateral loading. These solutions are useful for reasoning about the behavior of this type of frame when the geometric parameters are varied.

Portal frame—Gravity loading: Shown in Fig. 4.11

Portal frame—Lateral loading: Shown in Fig. 4.12

3-hinge portal frame—gravity loading: Shown in Fig. 4.13

3-hinge portal frame—lateral loading: Shown in Fig. 4.14

Fig. 4.11 Statically determinate portal frame under gravity loading. (a) Geometry and loading. (b) Reactions. (c) Shear diagram. (d) Moment diagram

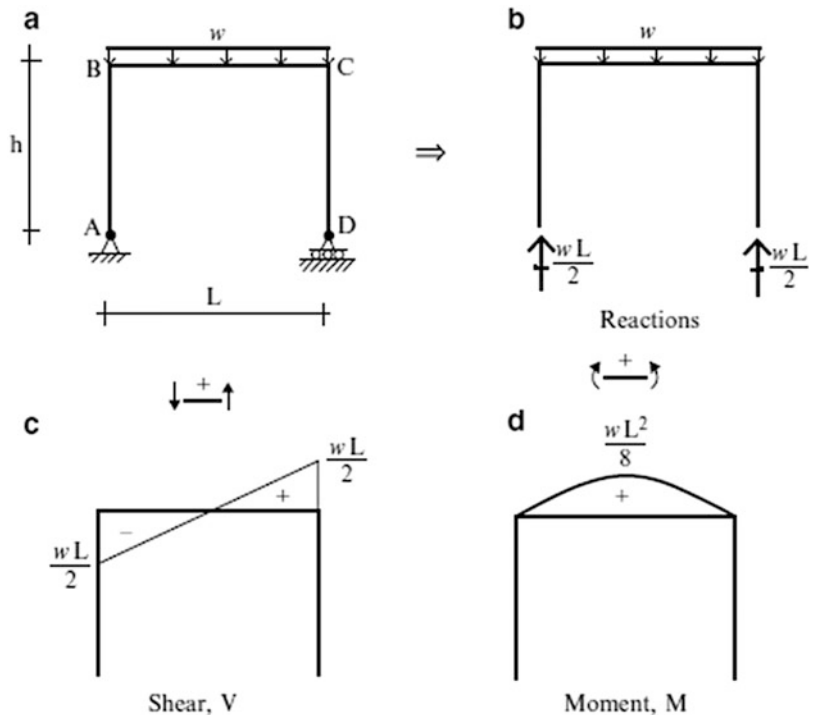


Fig. 4.12 Statically determinate portal frame under lateral loading. (a) Geometry and loading. (b) Reactions. (c) Shear diagram. (d) Moment diagram

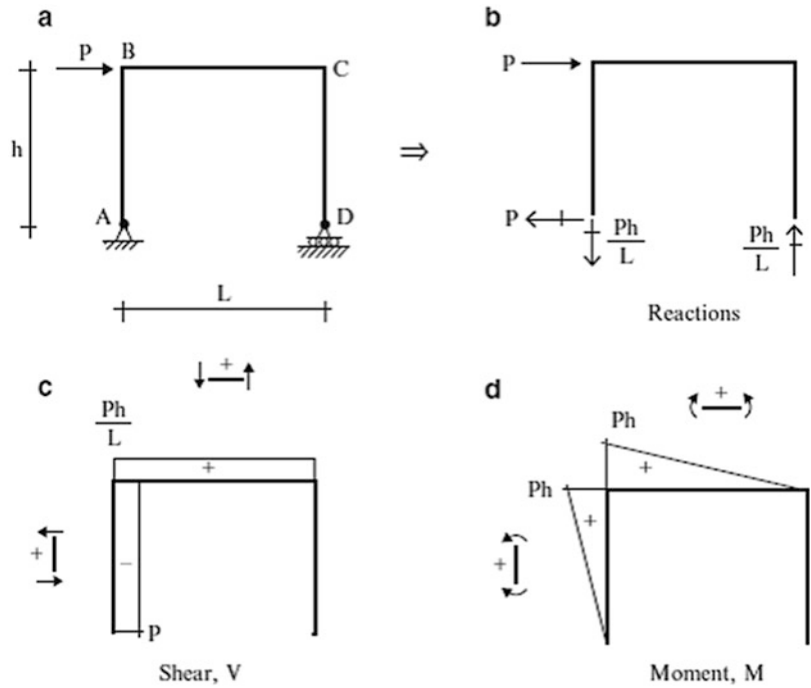


Fig. 4.13 Statically determinate 3-hinge portal frame under gravity loading. (a) Geometry and loading. (b) Reactions. (c) Shear diagram. (d) Moment diagram

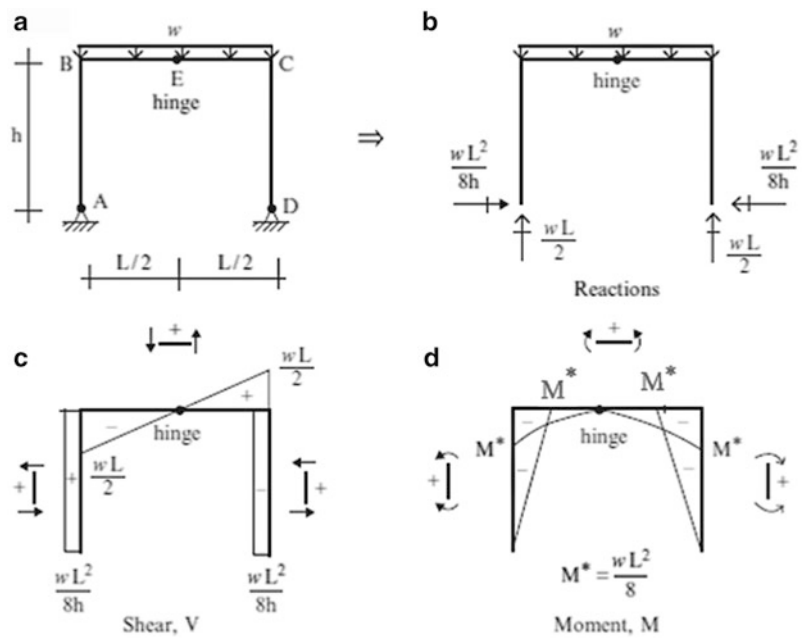


Fig. 4.14 Statically determinate 3-hinge portal frame under lateral loading. (a) Geometry and loading. (b) Reactions. (c) Shear diagram. (d) Moment diagram

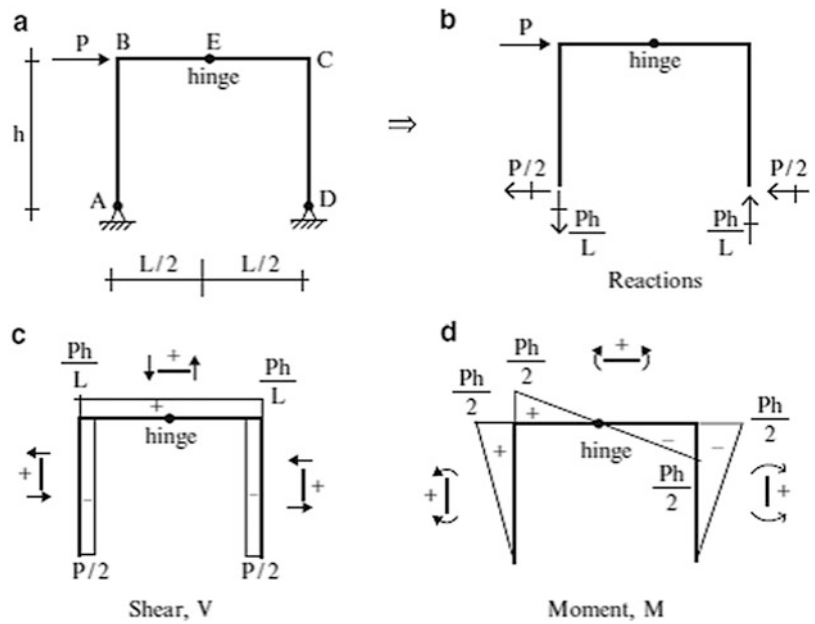
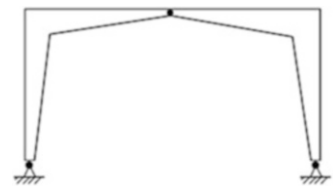


Fig. 4.15 Variable cross-section 3-hinge frame



These results show that the magnitude of the peak moment due to the uniform gravity load is the same for both structures but of opposite sense (Figs. 4.11 and 4.13). The peak moment occurs at the corner points for the 3-hinge frame and at mid-span for the simply supported frame which behaves as a simply supported beam. The response under lateral loading is quite different (Figs. 4.12 and 4.14). There is a 50 % reduction in peak moment for the 3-hinge case due to the inclusion of an additional horizontal restraint at support D.

For the 3-hinge frame, we note that the bending moment diagram due to gravity loading is symmetrical. In general, a symmetrical structure responds symmetrically when the loading is symmetrical. We also note that the bending moment diagram for lateral loading applied to the 3-hinge frame is anti-symmetrical.

Both loadings produce moment distributions having peaks at the corner points. In strength-based design, the cross-sectional dimensions depend on the design moment; the deepest section is required by the peak moment. Applying this design approach to the 3-hinge frame, we can use variable depth members with the depth increased at the corner points and decreased at the supports and mid-span. Figure 4.15 illustrates a typical geometry. Variable depth 3-hinge frames are quite popular. We point out again here that the internal force distribution in statically determinate structures depends only on the loading and geometry and is independent of the cross-sectional properties of the members. Therefore, provided we keep the same geometry (centerline dimensions), we can vary the cross-section properties for a 3-hinge frame without changing the moment distributions.

4.4 Pitched Roof Frames

In this section, we deal with a different type of portal frame structure: the roof members are sloped upward to create a pitched roof. This design creates a more open interior space and avoids the problem of rain water pounding or snow accumulating on flat roofs. Figure 4.16 shows the structures under consideration. The first structure is a rigid frame with a combination of pin and roller supports; the second structure is a 3-hinge frame. Both structures are analyzed by first finding the reactions and then isolating individual members to determine the member end forces, and the internal force distributions.

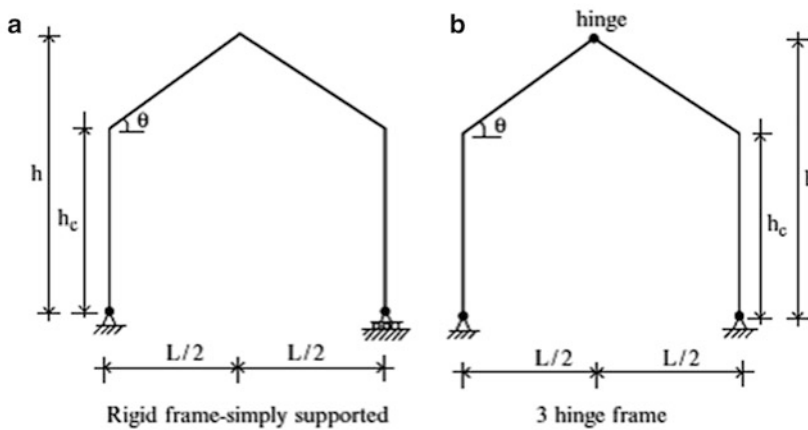
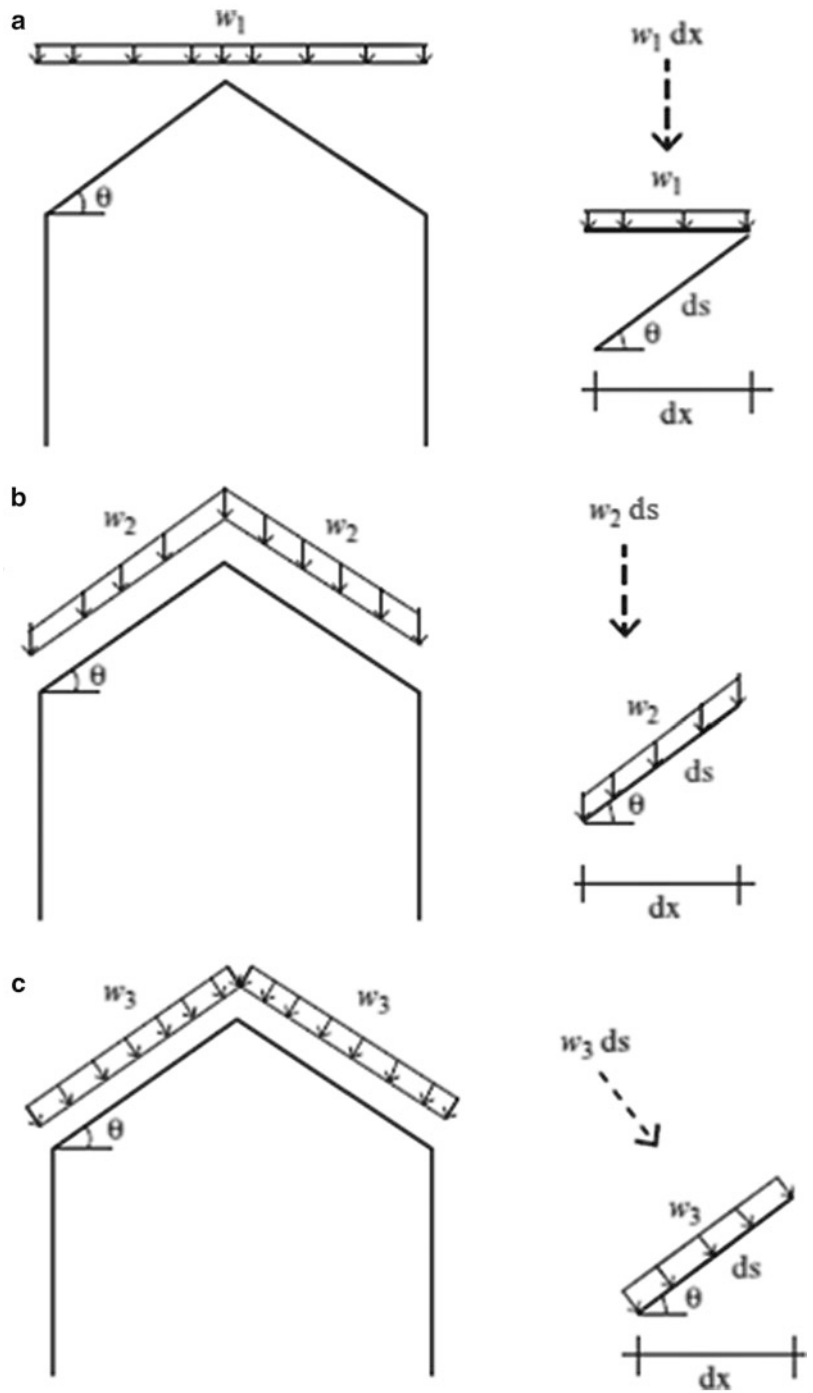


Fig. 4.16 Pitched roof frames

4.4.1 Member Loads

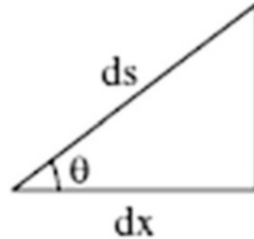
Typical loads that may be applied to an inclined member are illustrated in Fig. 4.17. They may act either in the vertical direction or normal to the member. In the vertical direction, they may be defined either in terms of the horizontal projection of the length of the member or in terms of the length of the member.

Fig. 4.17 Loading on an inclined member. (a) Vertical load per horizontal projection. (b) Vertical load per length. (c) Normal load per length



When computing the reactions, it is convenient to work with loads referred to horizontal and vertical directions and expressed in terms of the horizontal projection. The w_1 loading is already in this form. For the w_2 load, we note that

$$dx = ds \cos \theta$$

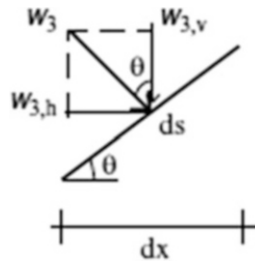


Then,

$$w_2 ds = \frac{w_2 dx}{\cos \theta} \quad (4.3)$$

$$w_{2,v} = \frac{w_2}{\cos \theta}$$

The w_3 load is normal to the member. We project it onto the vertical and horizontal directions and then substitute for ds .



$$(w_3 ds) \cos \theta = w_{3,v} dx$$

$$w_3 ds \sin \theta = w_{3,h} dx$$

$$w_3 \frac{dx}{\cos \theta} \sin \theta = w_{3,h} dx$$

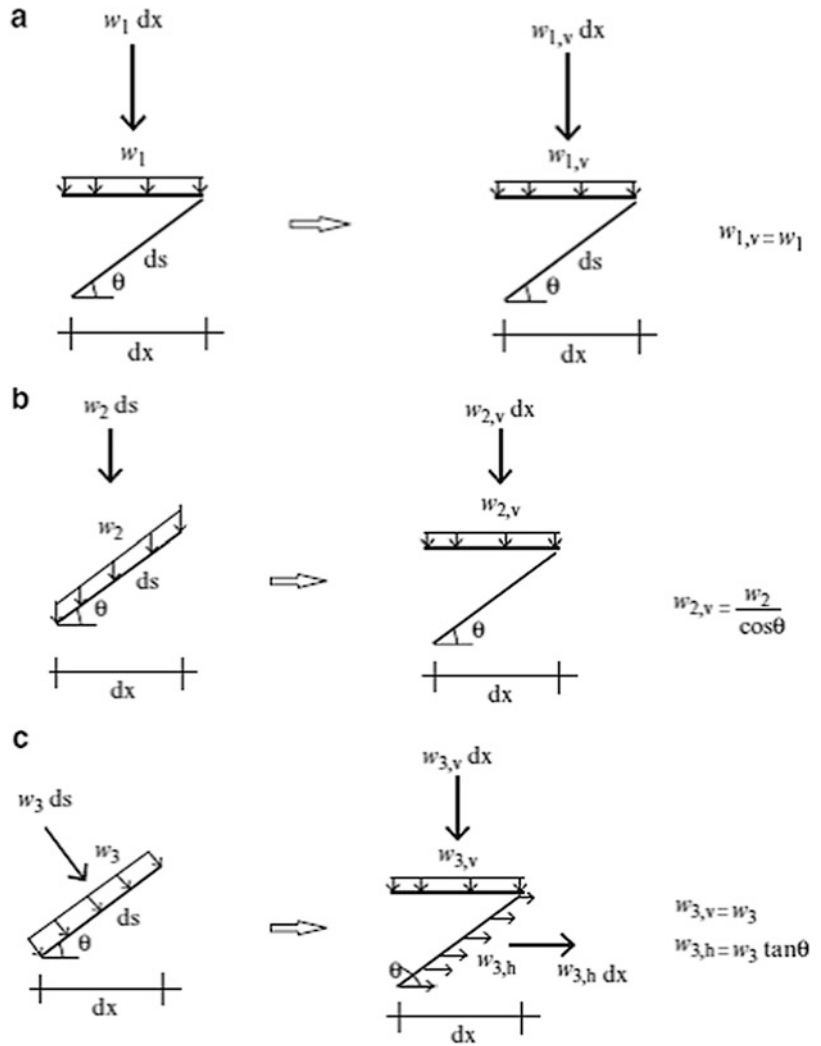
The final result is

$$w_{3,v} = w_3 \quad (4.4)$$

$$w_{3,h} = w_3 \tan \theta$$

It follows that the equivalent vertical loading per horizontal projection is equal to the normal load per unit length. These results are summarized in Fig. 4.18.

Fig. 4.18 Equivalent vertical member loadings. (a) Per horizontal projection. (b) Per length. (c) Normal load



When computing the axial force, shear, and moment distribution along a member, it is more convenient to work with loads referred to the normal and tangential directions of the member and expressed in terms of the member arc length. The approach is similar to the strategy followed above. The results, as summarized, below are (Fig. 4.19):

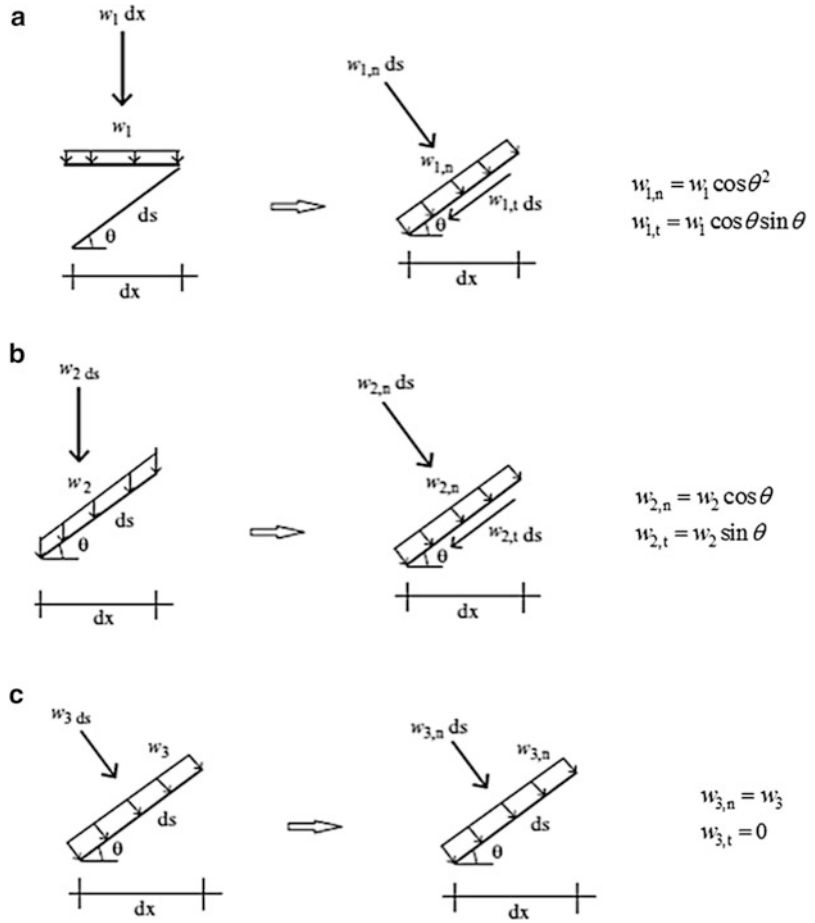
Vertical–horizontal projection loading:

$$\begin{aligned}
 w_{1,n} &= w_1 \cos^2 \theta \\
 w_{1,t} &= w_1 \cos \theta \sin \theta
 \end{aligned}
 \tag{4.5}$$

Member loading:

$$\begin{aligned}
 w_{2,n} &= w_2 \cos \theta \\
 w_{2,t} &= w_2 \sin \theta \\
 w_{3,n} &= w_3 \\
 w_{3,t} &= 0
 \end{aligned}
 \tag{4.6}$$

Fig. 4.19 Equivalent normal and tangential member loadings. (a) Vertical per projected length. (b) Vertical per length. (c) Normal



4.4.2 Analytical Solutions for Pitched Roof Frames

Analytical solutions for the bending moment distribution are tabulated in this section. They are used for assessing the sensitivity of the response to changes in the geometric parameters.

Gravity loading per unit horizontal projection: Results are listed in Figs. 4.20 and 4.21.

Lateral Loading: Results are listed in Figs. 4.22 and 4.23.

Fig. 4.20 Simply supported gable rigid frame. (a) Structure and loading. (b) Moment diagram

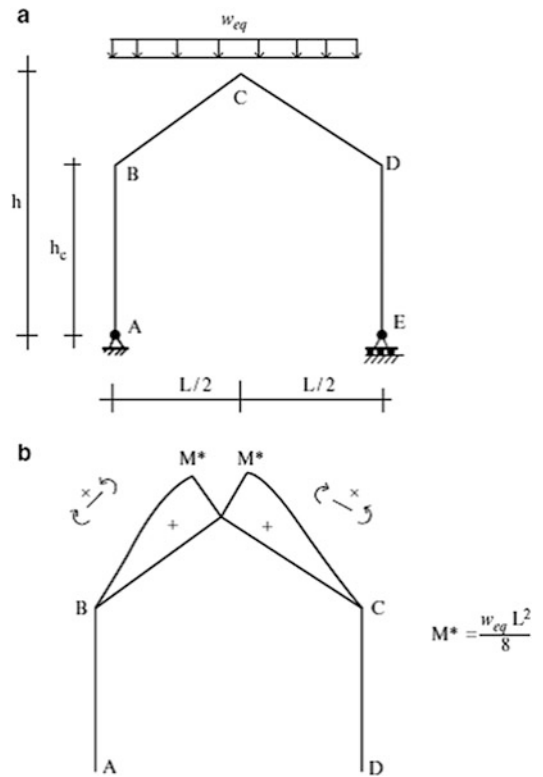


Fig. 4.21 3-Hinge frame under gravity loading. (a) Structure and loading. (b) Moment diagram

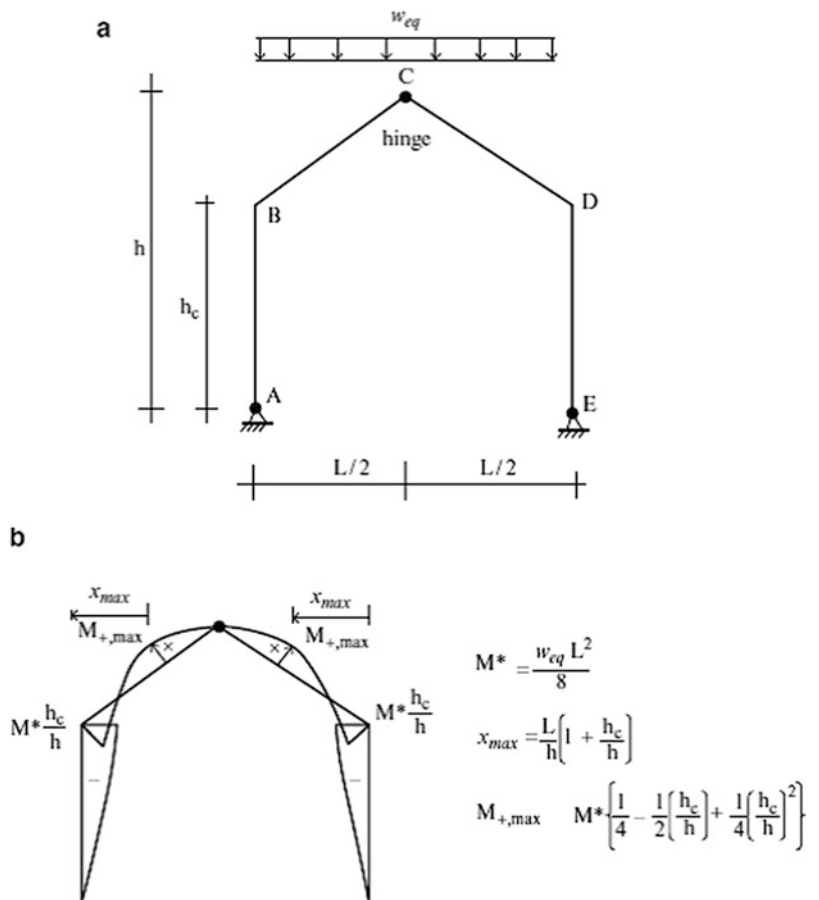


Fig. 4.22 Simply supported rigid frame—lateral loading. (a) Structure and loading. (b) Moment diagram

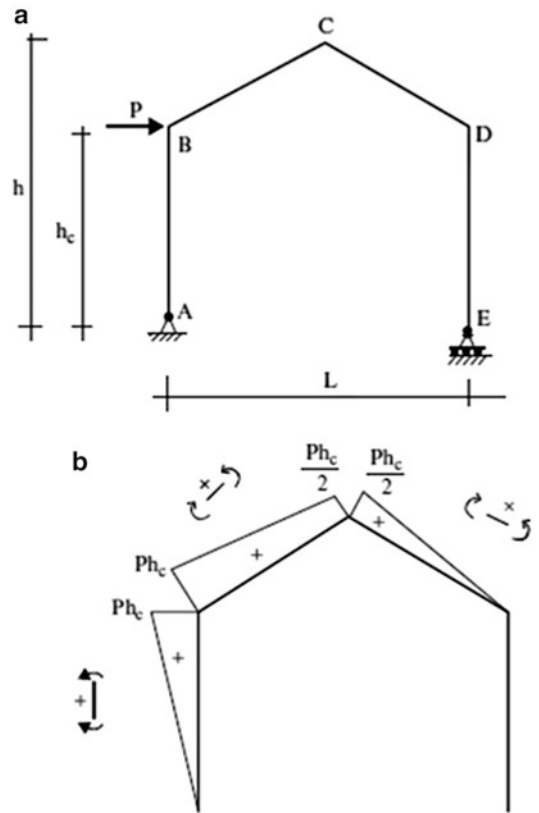
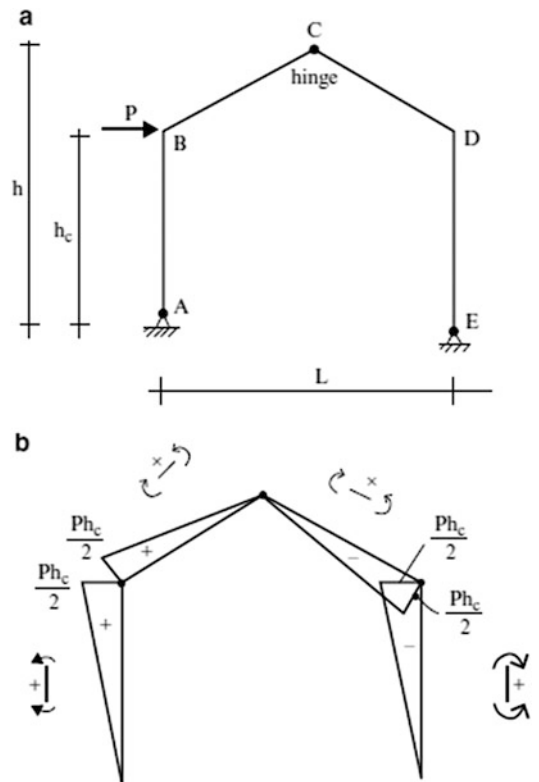


Fig. 4.23 3-Hinge frame—lateral loading. (a) Structure and loading. (b) Moment diagram



Example 4.7 Simply Supported Gable Frame—Lateral Load

Given: The gable frame with the lateral load defined in Fig. E4.7a.

Determine: The shear, moment, and axial force diagrams.

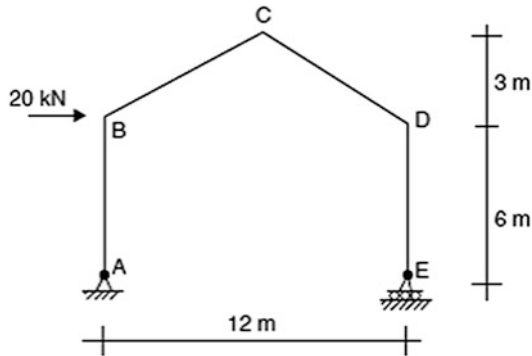


Fig. E4.7a

Solution: Moment summation about A leads to the vertical reaction at E. The reactions at A follow from force equilibrium considerations. Next, we determine the end forces and moments for the individual members. Lastly, we generate the shear and moment diagrams. Results for the various analysis steps are listed in Figs. E4.7b, E4.7c, E4.7d, and E4.7e.

Step 1: Reactions

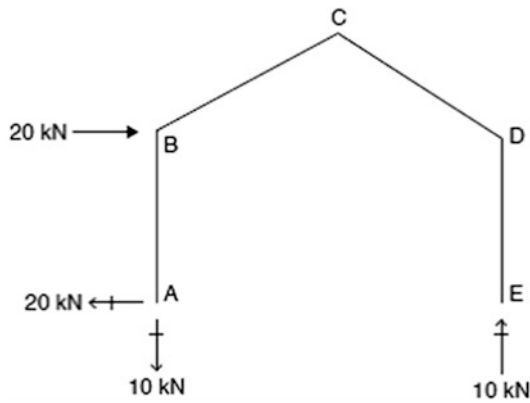


Fig. E4.7b Reactions

Step 2: End forces

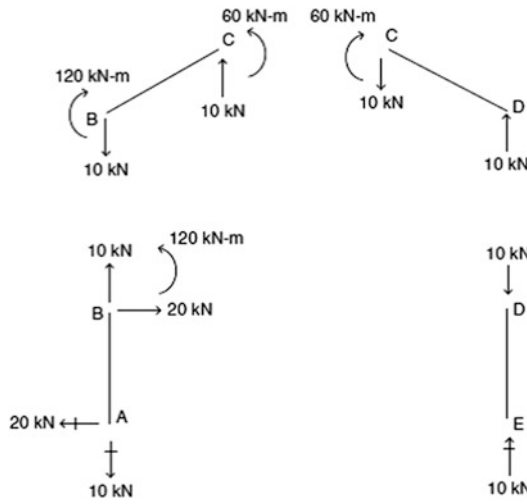


Fig. E4.7c End forces—global frame

Step 3: Member forces—member frames

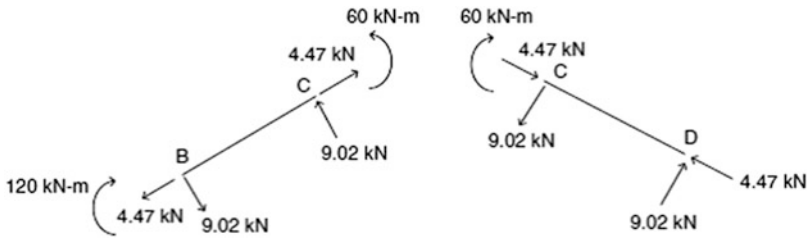


Fig. E4.7d End forces in local member frame

Step 4: Internal force diagrams

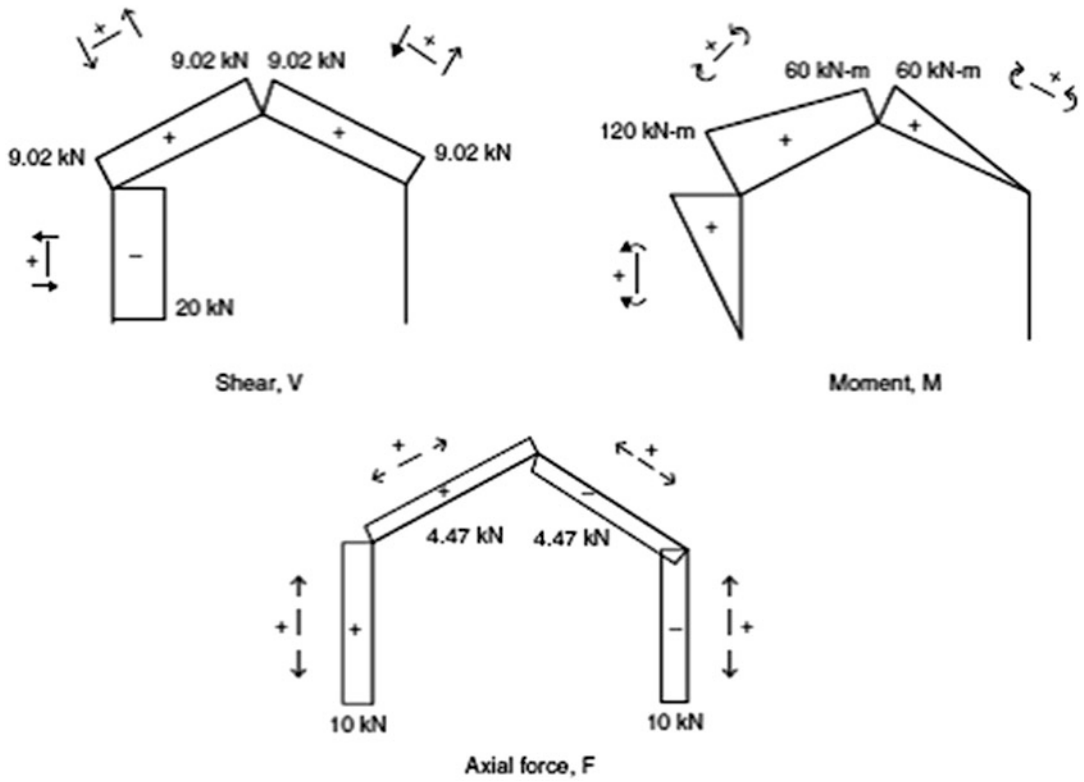


Fig. E4.7e Force distributions

Example 4.8 3-Hinge Gable Frame—Lateral Loading

Given: The 3-hinge gable frame shown in Fig. E4.8a.

Determine: The shear, moment, and axial force diagrams.

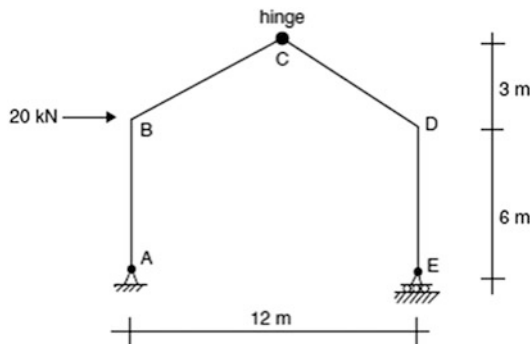


Fig. E4.8a

Solution:

Step 1: Reactions

The reactions (Fig. E4.8b) are determined by summing moments about A and C and applying the force equilibrium conditions.

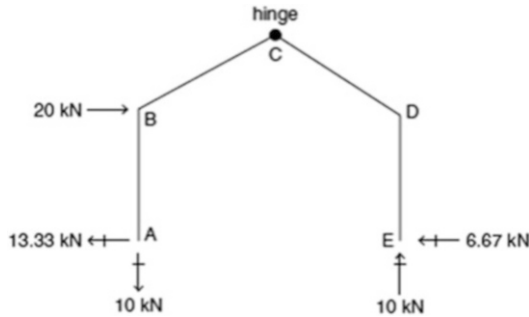


Fig. E4.8b Reactions

Step 2: End forces—global frame (Fig. E4.8c)

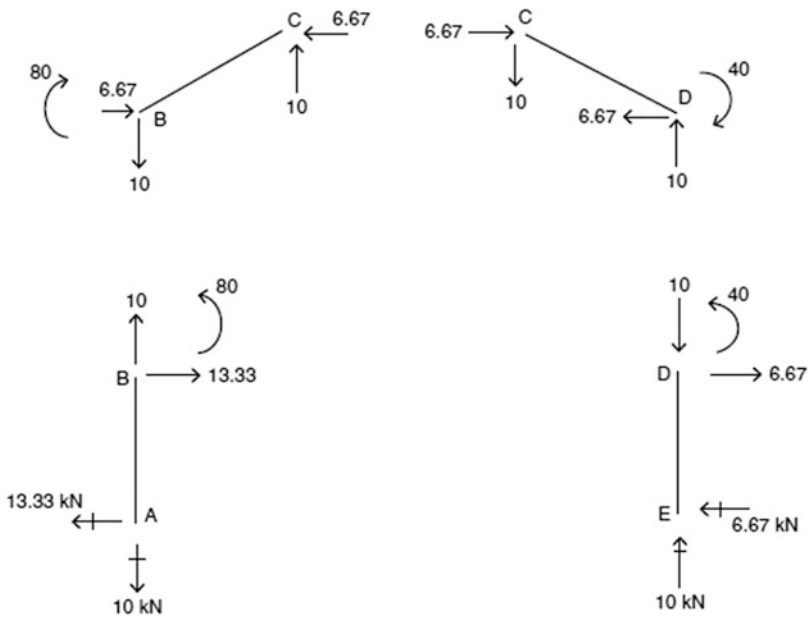


Fig. E4.8c End forces

Step 3: End forces—local member frame

Figure E4.8d shows the end forces and moments resolved into components referred to the local member frame.

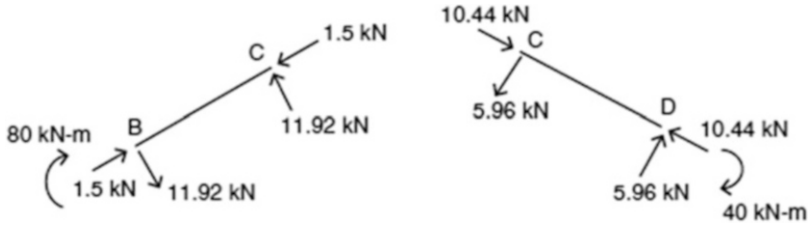


Fig. E4.8d End actions in local member frame

Step 4: Internal force distribution (Fig. E4.8e)

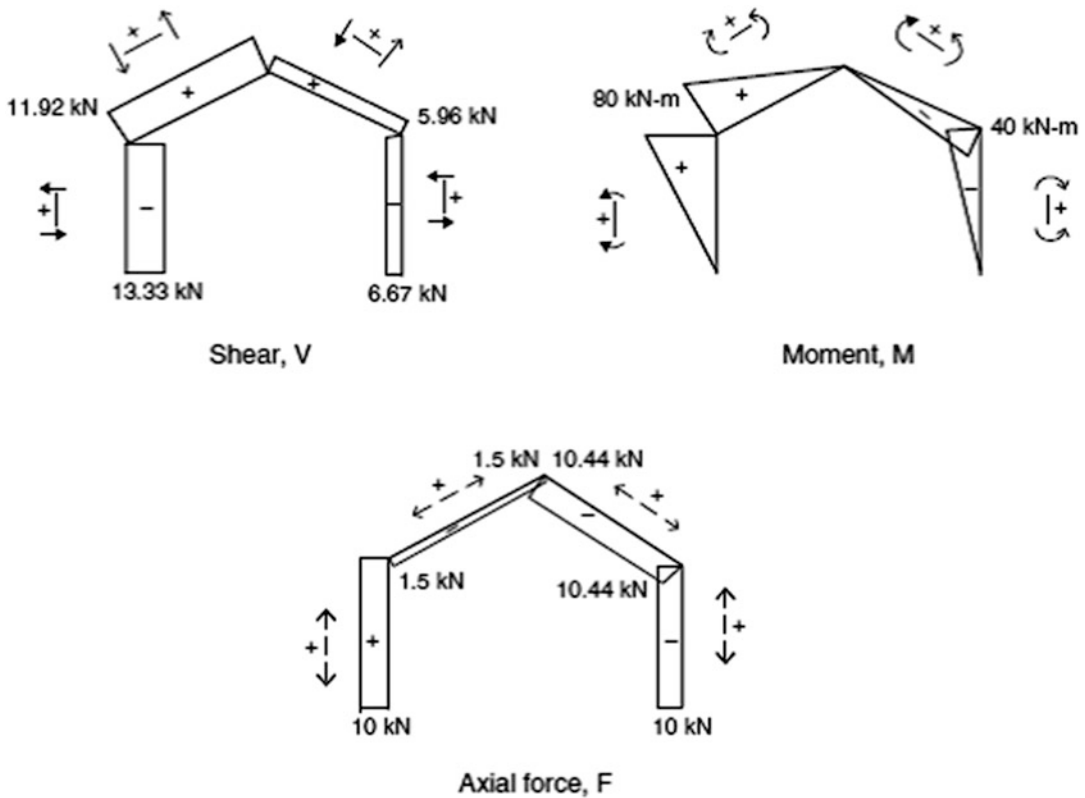


Fig. E4.8e Force distributions

Note that the 3-hinge gable structure has a lower value of peak moment.

Example 4.9 Simply Supported Gable Frame—Unsymmetrical Loading

Given: The frame defined in Fig. E4.9a. The loading consists of a vertical load per horizontal projection applied to member BC.

Determine: The member force diagrams.

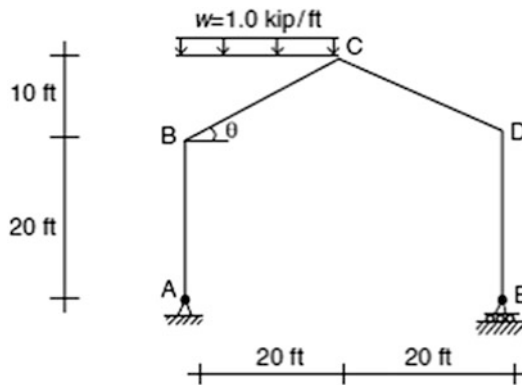


Fig. E4.9a

Solution: The reactions at E and A are determined by summing moments about A and by enforcing vertical equilibrium. Figure E4.9b shows the results.

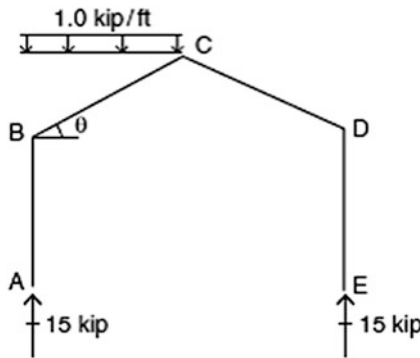


Fig. E4.9b Reactions

Next, we determine the end forces and moments for the individual members. Then, we need to resolve the loading and the end forces for members BC and CD into normal and tangential components. The transformed quantities are listed in Figs. E4.9c and E4.9d.

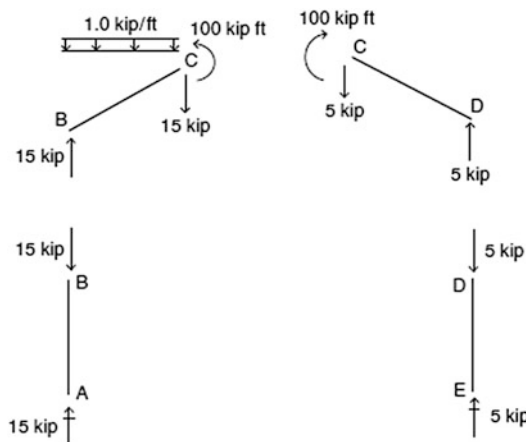


Fig. E4.9c End actions—global frame

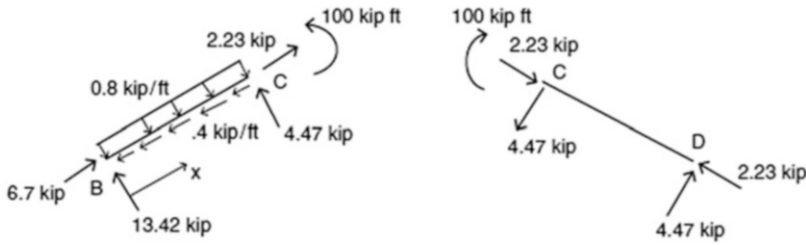


Fig. E4.9d End actions—local frame

The maximum moment in member BC occurs at x_1 . We determine the location by setting the shear equal to zero.

$$13.42 - 0.8x_1 = 0 \Rightarrow x_1 = 16.775$$

Then, $M_{\max} = 13.42(16.775) - 0.8(16.775)^2(\frac{1}{2}) = 112.56 \text{ kip ft}$

Figure E4.9e contains the shear, moment, and axial force diagrams.

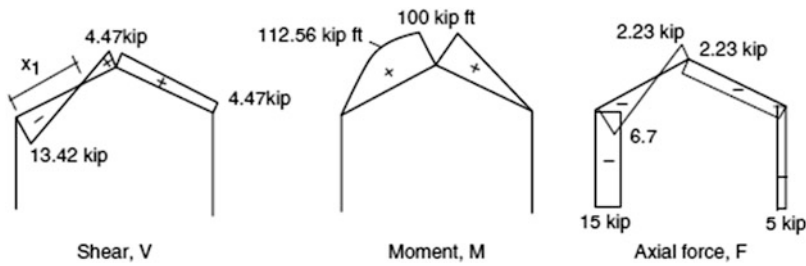


Fig. E4.9e Internal force diagrams

Example 4.10 3-Hinge Gable Frame

Given: The 3-hinge gable frame shown in Fig. E4.10a.

Determine: The shear and moment diagrams.

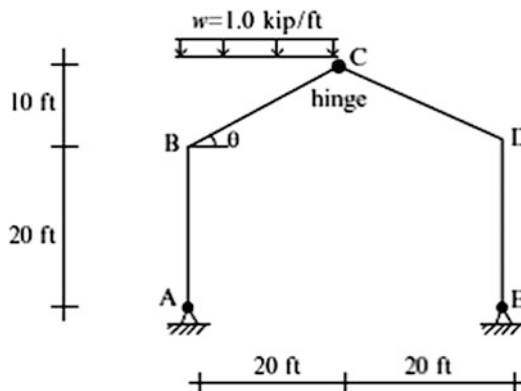


Fig. E4.10a

Solution: We analyzed a similar loading condition in Example 4.9. The results for the different analysis phases are listed in Figs. E4.10b, E4.10c, and E4.10d. Comparing Fig. E4.10e with Fig. E4.9e shows that there is a substantial *reduction* in the magnitude of the maximum moment when the 3-hinged gable frame is used.

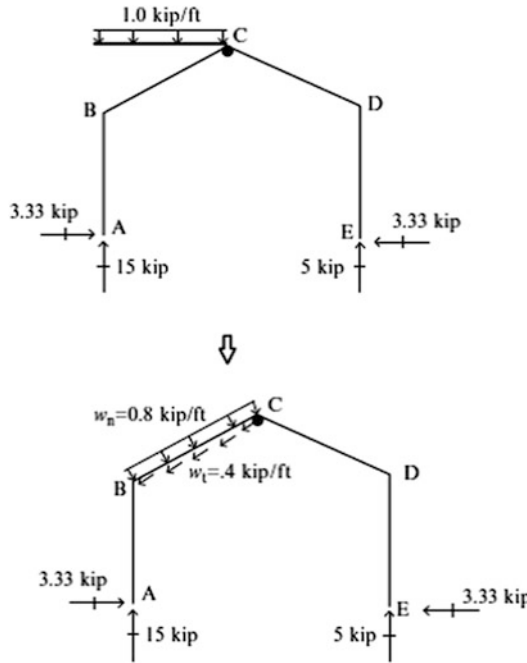


Fig. E4.10b Reactions

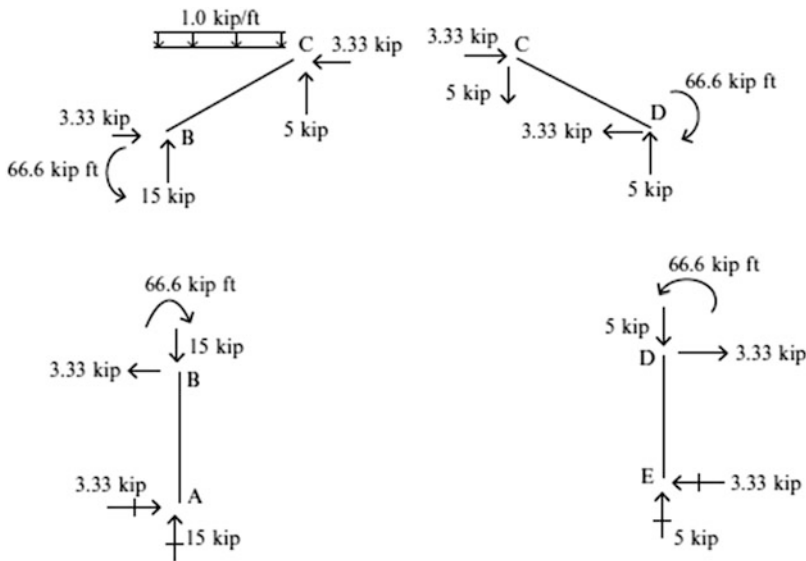


Fig. E4.10c End forces

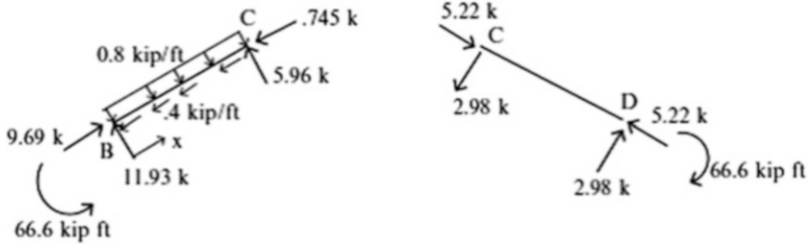


Fig. E4.10d End forces in local frame

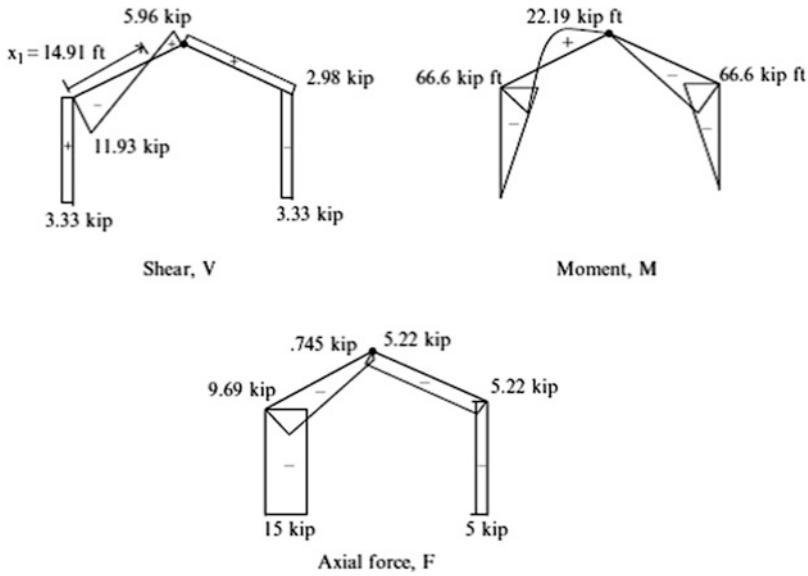


Fig. E4.10e Shear and moment diagrams

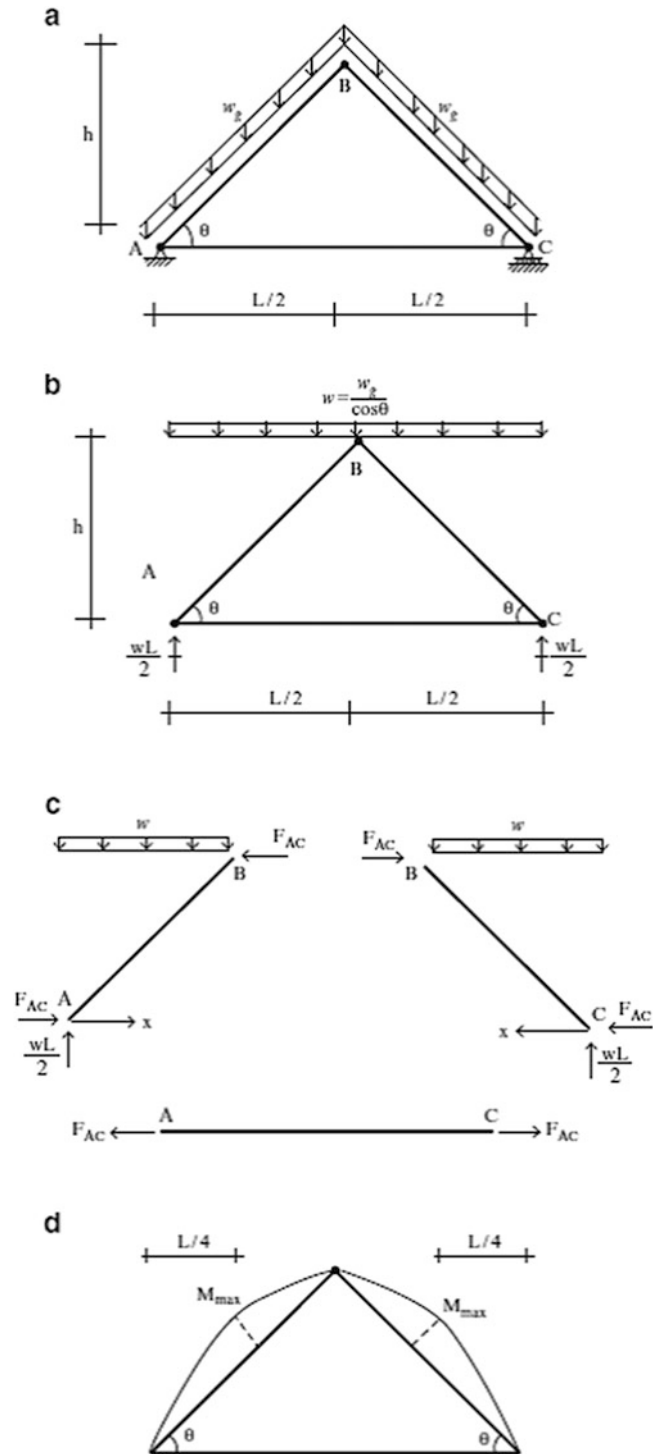
4.5 A-Frames

A-frames are obviously named for their geometry. Loads may be applied at the connection points or on the members. A-frames are typically supported at the base of their legs. Because of the nature of the loading and restraints, the members in an A-frame generally experience bending as well as axial force.

We consider first the triangular frame shown in Fig. 4.24. The inclined members are subjected to a uniform distributed loading per unit length w_g which represents the self-weight of the members and the weight of the roof that is supported by the member.

We convert w_g to an equivalent vertical loading per horizontal projection w using (4.3). We start the analysis process by first finding the reactions at A and C.

Fig. 4.24 (a) Geometry and loading. (b) A-frame loading and reactions. (c) Free body diagrams. (d) Moment diagram



Next, we isolate member BC (see Fig. 4.24c).

$$\sum M_{\text{at B}} = -\frac{w}{2}\left(\frac{L}{2}\right)^2 + \frac{wL}{2}\left(\frac{L}{2}\right) - hF_{\text{AC}} = 0$$

$$\Downarrow$$

$$F_{\text{AC}} = \frac{wL^2}{8h}$$

The horizontal internal force at B must equilibrate F_{AC} . Lastly, we determine the moment distribution in members AB and BC. Noting Fig. 4.24c, the bending moment at location x is given by

$$M(x) = \frac{wL}{2}x - F_{\text{AC}}\left(\frac{2h}{L}\right)x - \frac{wx^2}{2} = \frac{wL}{4}x - \frac{wx^2}{2}$$

The maximum moment occurs at $x = L/4$ and is equal to

$$M_{\text{max}} = \frac{wL^2}{32}$$

Replacing w with w_g , we express M_{max} as

$$M_{\text{max}} = \left(\frac{w_g}{\cos \theta}\right)\frac{L^2}{32}$$

As θ increases, the moment increases even though the projected length of the member remains constant.

We discuss next the frame shown in Fig. 4.25a. There are two loadings: a concentrated force at B and a uniform distributed loading applied to DE.

We first determine the reactions and then isolate member BC.

Summing moments about A leads to

$$P\left(\frac{L}{2}\right) + \frac{wL}{2}\left(\frac{L}{2}\right) = R_C L \quad R_C = \frac{P}{2} + \frac{wL}{4}$$

The results are listed below. Noting Fig. 4.25d, we sum moments about B to determine the horizontal component of the force in member DE.

$$\frac{L}{2}\left(\frac{P}{2} + \frac{wL}{4}\right) = \frac{wLL}{4} + \frac{h}{2}F_{\text{de}}$$

$$F_{\text{de}} = \frac{PL}{2h} + \frac{wL^2}{8h}$$

The bending moment distribution is plotted in Fig. 4.25e. Note that there is bending in the legs even though P is applied at node A. This is due to the location of member DE. If we move member DE down to the supports A and C, the moment in the legs would vanish.

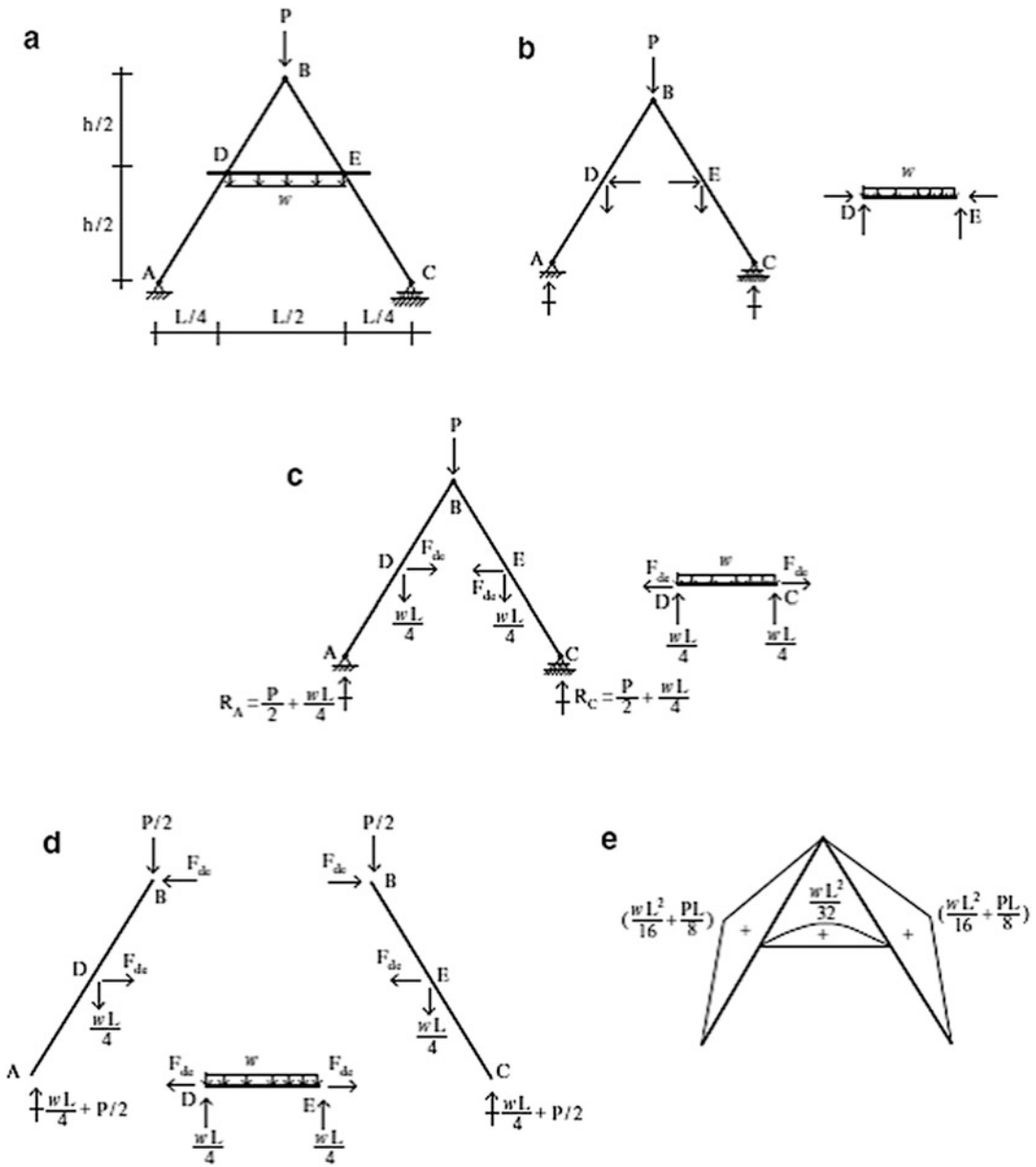


Fig. 4.25 (a) A-frame geometry and loading. (b–d) Free body diagrams. (e) Bending moment distribution

4.6 Deflection of Frames Using the Principle of Virtual Forces

The Principle of Virtual Forces specialized for a planar frame structure subjected to planar loading is derived in [1]. The general form is

$$d\delta P = \sum_{\text{members}} \int_s \left\{ \frac{M}{EI} \delta M + \frac{F}{AE} \delta F + \frac{V}{GA_s} \delta V \right\} ds \quad (4.7)$$

Frames carry loading primarily by bending action. Axial and shear forces are developed as a result of the bending action, but the contribution to the displacement produced by shear deformation is generally small in comparison to the displacement associated with bending deformation and axial deformation. Therefore, we neglect this term and work with a reduced form of the principle of Virtual Forces.

$$d\delta P = \sum_{\text{members}} \int_s \left\{ \frac{M}{EI} \delta M + \frac{F}{AE} \delta F \right\} ds \quad (4.8)$$

where δP is either a unit force (for displacement) or a unit moment (for rotation) in the direction of the desired displacement d ; δM , and δF are the virtual moment and axial force due to δP . The integration is carried out over the length of each member and then summed up.

For low-rise frames, i.e., where the ratio of height to width is on the order of unity, the axial deformation term is also small. In this case, one neglects the axial deformation term in (4.8) and works with the following form

$$d\delta P = \sum_{\text{members}} \int_s \left(\frac{M}{EI} \right) (\delta M) ds \quad (4.9)$$

Axial deformation is significant for tall buildings, and (4.8) is used for this case. In what follows, we illustrate the application of the Principle of Virtual Forces to some typical low-rise structures. We revisit this topic later in Chap. 9, which deals with statically indeterminate frames.

Example 4.11 Computation of Deflections—Cantilever-Type Structure

Given: The structure shown in Fig. E4.11a. Assume EI is constant.

$$E = 29,000 \text{ ksi}, \quad I = 300 \text{ in.}^4$$

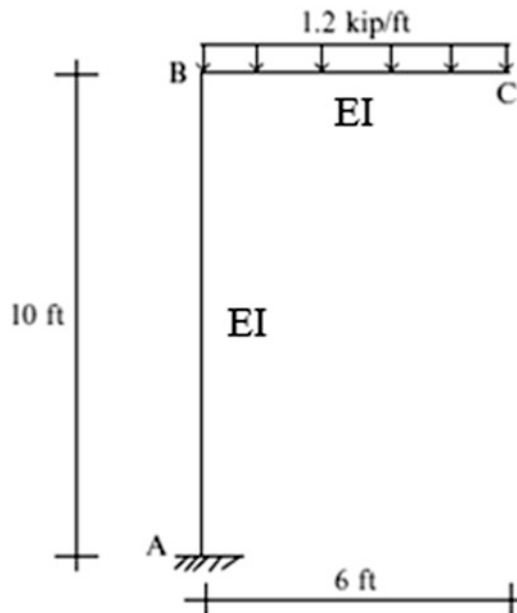


Fig. E4.11a

Determine: The horizontal and vertical deflections and the rotation at point C, the tip of the cantilever segment.

Solution: We start by evaluating the moment distribution corresponding to the applied loading. This is defined in Fig. E4.11b. The virtual moment distributions corresponding to u_c , v_c , and θ_c are defined in Figs. E4.11c, E4.11d, and E4.11e, respectively. Note that we take δP to be either a unit force (for displacement) or a unit moment (for rotation).

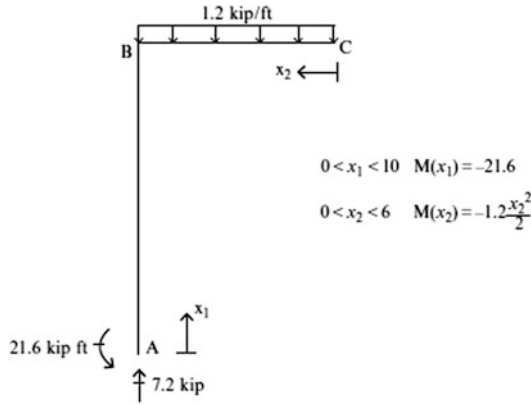


Fig. E4.11b $M(x)$

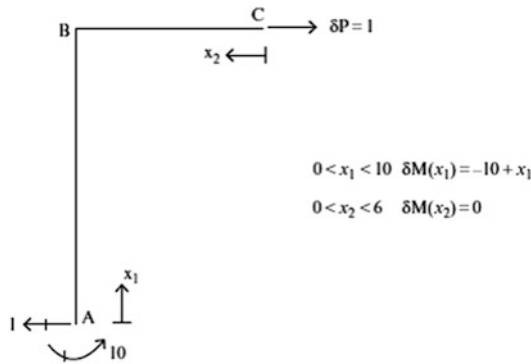


Fig. E4.11c $\delta M(x)$ for u_c

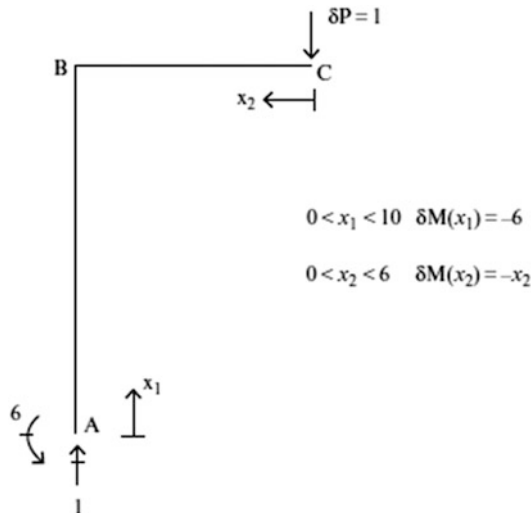


Fig. E4.11d $\delta M(x)$ for v_c

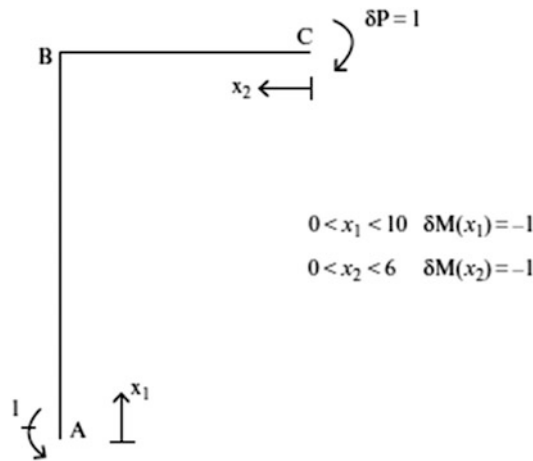


Fig. E4.11e $\delta M(x)$ for θ_c

We divide up the structure into two segments AB and CB and integrate over each segment. The total integral is given by

$$\sum_{\text{members}} \int_s \left(\frac{M}{EI} \delta M \right) ds = \int_{AB} \left(\frac{M}{EI} \delta M \right) dx_1 + \int_{CB} \left(\frac{M}{EI} \delta M \right) dx_2$$

The expressions for u_c , v_c , and θ_c are generated using the moment distributions listed above.

$$EIu_c = \int_0^{10} (-21.6)(-10 + x_1) dx_1 = 1080 \text{ kip ft}^3$$

$$u_c = \frac{1080(12)^3}{29,000(300)} = 0.2145 \text{ in.} \rightarrow$$

$$EIv_c = \int_0^{10} (-21.6)(-6) dx_1 + \int_0^6 \left(-\frac{1.2}{2} x_2^2 \right) (-x_2) dx_2 = 1490 \text{ kip ft}^3$$

$$v_c = \frac{1490(12)^3}{29,000(300)} = 0.296 \text{ in.} \downarrow$$

$$EI\theta_c = \int_0^{10} (-21.6)(-1) dx_1 + \int_0^6 \left(-\frac{1.2}{2} x_2^2 \right) (-1) dx_2 = 259 \text{ kip ft}^2$$

$$\theta_c = \frac{259(12)^2}{29,000(300)} = 0.0043 \text{ rad clockwise}$$

Example 4.12 Computation of Deflections

Given: The structure shown in Fig. E4.12a. $E = 29,000 \text{ ksi}$, $I = 900 \text{ in.}^4$

Determine: The horizontal displacements at points C and D and the rotation at B.

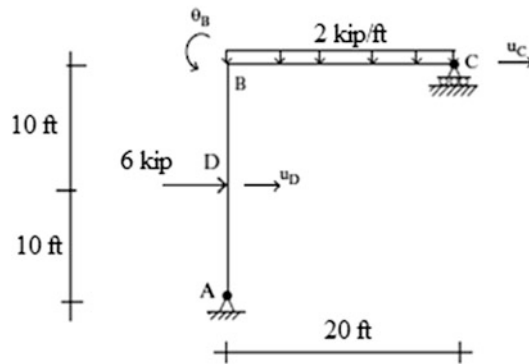


Fig. E4.12a

Solution: We start by evaluating the moment distribution corresponding to the applied loading. This is defined in Fig. E4.12b.

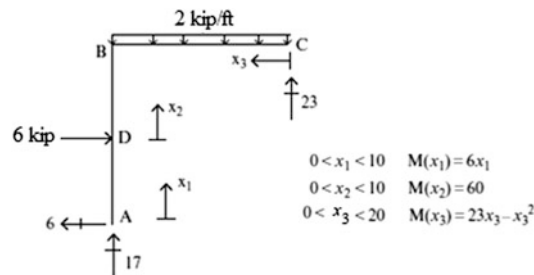


Fig. E4.12b $M(x)$

The virtual moment distributions corresponding to u_C and u_D are listed in Figs. E4.12c and E4.12d.

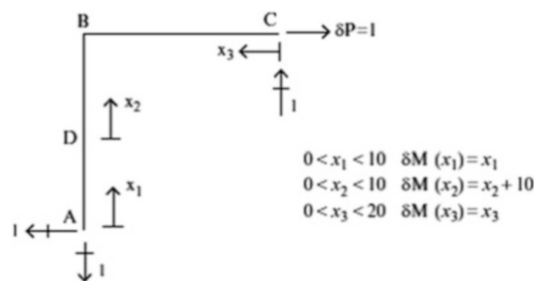


Fig. E4.12c δM for u_C

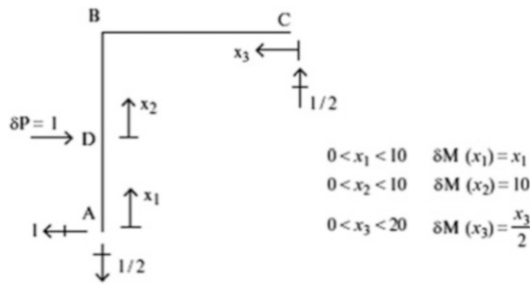


Fig. E4.12d δM for u_D

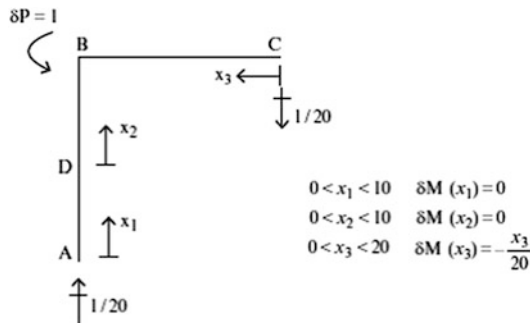


Fig. E4.12e δM for θ_B

We express the total integral as the sum of three integrals.

$$\sum_{\text{members}} \int_s \left(\frac{M}{EI} \delta M \right) ds = \int_{AD} \left(\frac{M}{EI} \delta M \right) dx_1 + \int_{DB} \left(\frac{M}{EI} \delta M \right) dx_2 + \int_{CB} \left(\frac{M}{EI} \delta M \right) dx_3$$

The corresponding form for u_c is

$$EIu_C = \int_0^{10} 6x_1(x_1)dx_1 + \int_0^{10} (x_2 + 10)(60)dx_2 + \int_0^{20} (23x_3 - x_3^2)(x_3)dx_3$$

$$dx_3 = \left| 2x_1^3 \right|_0^{10} + \left| 30x_2^2 + 600x_2 \right|_0^{10} + \left| \frac{23x_3^3}{3} - \frac{x_3^4}{4} \right|_0^{20} = 32,333 \text{ kip ft}^3$$

$$u_C = \frac{32,333 \times (12)^3}{(29,000)(900)} = 2.14 \text{ in.} \rightarrow$$

Following a similar procedure, we determine u_D

$$\begin{aligned} EIu_D &= \int_0^{10} 6x_1(x_1)dx_1 + \int_0^{10} 60(10)dx_2 + \int_0^{20} (23x_3 - x_3^2) \left(\frac{x_2}{3}\right) dx_3 \\ &= \left| 2x_1^3 \right|_0^{10} + \left| 600x_2 \right|_0^{10} + \left| \frac{23x_3^3}{6} - \frac{1}{8}x_3^4 \right|_0^{20} = 18,667 \text{ kip ft}^3 \\ u_D &= \frac{18,667(12)^3}{(29,000)(900)} = 1.23 \text{ in.} \rightarrow \end{aligned}$$

Lastly, we determine θ_B (Fig. E4.12e)

$$\begin{aligned} EI\theta_B &= \int_0^{20} (23x_3 - x_3^2) \left(-\frac{x_3}{20}\right) dx_3 \\ &= \left| -\frac{23x_3^3}{60} + \frac{x_3^4}{80} \right|_0^{20} = -106,667 \text{ kip ft}^2 \\ \theta_B &= -\frac{106,667(12)^2}{(29,000)(900)} = -0.0059 \end{aligned}$$

The minus sign indicates the sense of the rotation is opposite to the initial assumed sense.

$$\theta_B = 0.0059 \text{ rad clockwise}$$

Example 4.13 Computation of Deflection

Given: The steel structure shown in Figs. E4.13a, E4.13b, and E4.13c. Take $I_b = \frac{4}{3}I_c$, $h_C = 4 \text{ m}$, $L_b = 3 \text{ m}$, $P = 40 \text{ kN}$, and $E = 200 \text{ GPa}$.

Determine: The value of I_C required to limit the horizontal displacement at C to be equal to 40 mm.

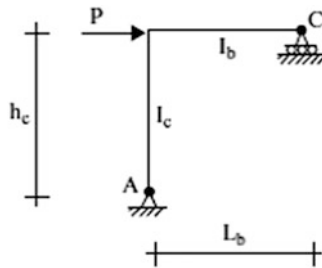


Fig. E4.13a

Solution: We divide up the structure into two segments and express the moments in terms of the local coordinates x_1 and x_2 .

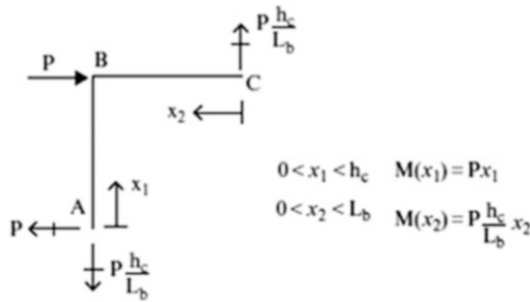


Fig. E4.13b $M(x)$

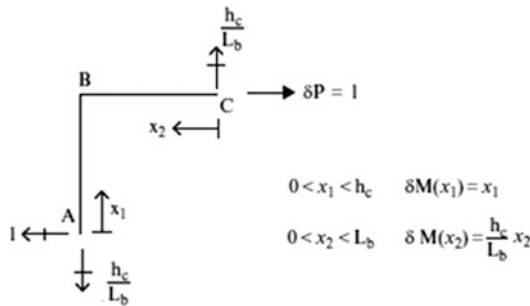


Fig. E4.13c δM for u_C

We express the total integral as the sum of two integrals.

$$\sum_{\text{members}} \int_s \left(\frac{M}{EI} \delta M \right) ds = \int_{AB} \left(\frac{M}{EI} \delta M \right) dx_1 + \int_{CB} \left(\frac{M}{EI} \delta M \right) dx_2$$

The corresponding expression for u_C is

$$\begin{aligned} u_C &= \frac{1}{EI_c} \int_0^{h_c} (Px_1)(x_1) dx_1 + \frac{1}{EI_b} \int_0^{L_b} \left(P \frac{h_c}{L_b} x_2 \right) \left(\frac{h_c}{L_b} x_2 \right) dx_2 \\ &\Downarrow \\ u_C &= \frac{P}{EI_c} \int_0^{h_c} (x_1)^2 dx_1 + \frac{P}{EI_b} \left(\frac{h_c}{L_b} \right)^2 \int_0^{L_b} (x_2)^2 dx_2 \\ &\Downarrow \\ u_C &= \frac{Ph_c^3}{3EI_c} + \frac{PL_b^3}{3EI_b} \left(\frac{h_c}{L_b} \right)^2 = \frac{Ph_c^2}{3E} \left(\frac{h_c}{I_c} + \frac{L_b}{I_b} \right) \end{aligned}$$

Then, for $I_b = \frac{4}{3}I_c$, the I_c required is determined with

$$u_C = \frac{Ph_c^2}{3E} \left(\frac{h_c}{I_c} + \frac{L_b}{I_b} \right) = \frac{40(4000)^2}{3(200)} \left(\frac{4000}{I_c} + \frac{3000}{(4/3)I_c} \right) = 40$$

$$\therefore I_c = 167(10)^6 \text{ mm}^4$$

Example 4.14 Computation of Deflection—Non-prismatic Member

Given: The non-prismatic concrete frame shown in Figs. E4.14a and E4.14b.

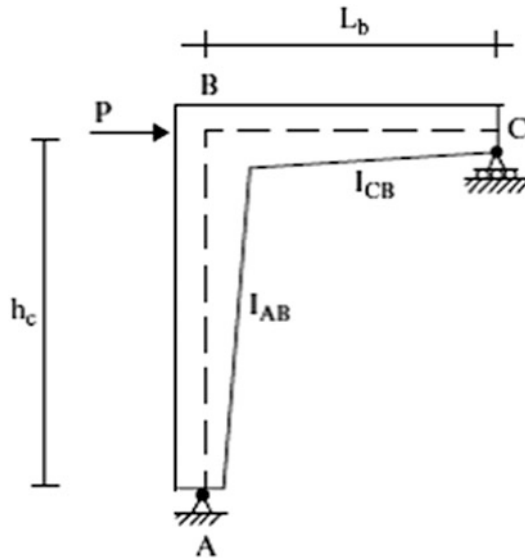


Fig. E4.14a Non-prismatic frame

Assume $h_c = 12$ ft, $L_b = 10$ ft, $P = 10$ kip, and $E = 4000$ ksi. Consider the member depths (d) to vary linearly and the member widths (b) to be constant. Assume the following geometric ratios:

$$d_{AB,1} = 2d_{AB,0}$$

$$d_{CB,1} = 1.5d_{CB,0}$$

$$b = \frac{d_{AB,0}}{2}$$

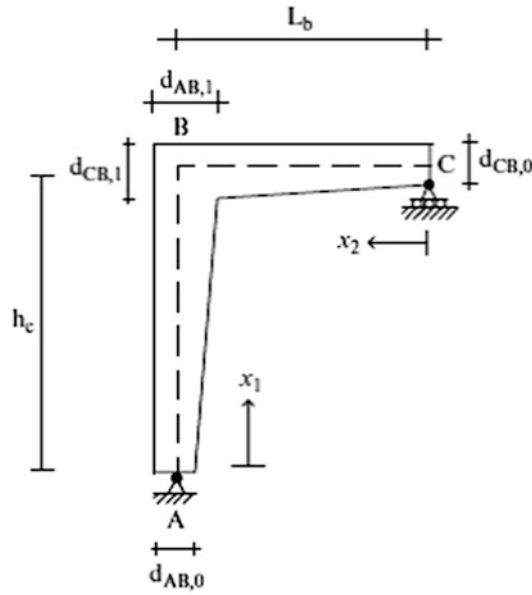


Fig. E4.14b Cross section depths

Determine:

- A general expression for the horizontal displacement at C (u_C).
- Use numerical integration to evaluate u_C as a function of $d_{AB,0}$.
- The value of $d_{AB,0}$ for which $u_C = 1.86$ in.

Solution:

Part (a): The member depth varies linearly. For member AB,

$$\begin{aligned} d(x_1) &= d_{AB,0} \left(1 - \frac{x_1}{h_c} \right) + d_{AB,1} \left(\frac{x_1}{h_c} \right) = d_{AB,0} \left\{ 1 + \frac{x_1}{h_c} \left(\frac{d_{AB,1}}{d_{AB,0}} - 1 \right) \right\} \\ &= d_{AB,0} g_{AB} \left(\frac{x_1}{h_c} \right) \end{aligned}$$

Then,

$$I_{AB} = I_{AB,0} (g_{AB})^3$$

Similarly, for member BC

$$\begin{aligned} d(x_2) &= d_{CB,0} \left\{ 1 + \frac{x_2}{L_b} \left(\frac{d_{CB,1}}{d_{CB,0}} - 1 \right) \right\} = d_{CB,0} g_{CB} \left(\frac{x_2}{L_b} \right) \\ I_{CB} &= I_{CB,0} (g_{CB})^3 \end{aligned}$$

We express the moments in terms of the local coordinates x_1 and x_2 .

$$M(x_1) = Px_1 \quad 0 < x_1 < h_c$$

$$M(x_2) = P \frac{h_c}{L_b} x_2 \quad 0 < x_2 < L_b$$

$$\delta M(x_1) = x_1 \quad 0 < x_1 < h_c$$

$$\delta M(x_2) = \frac{h_c}{L_b} x_2 \quad 0 < x_2 < L_b$$

The moment distributions are listed below.

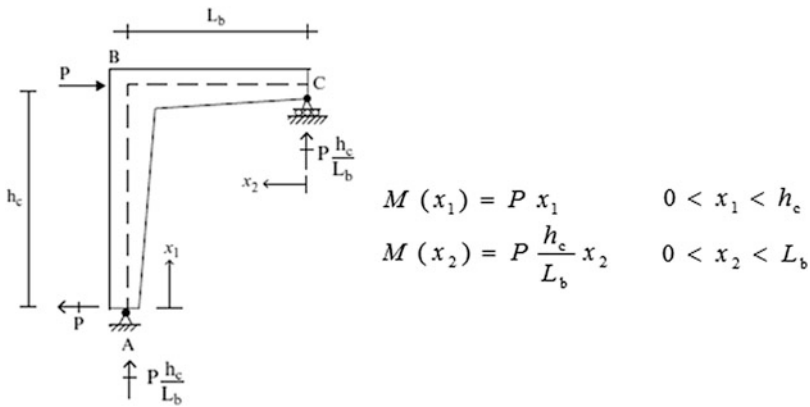


Fig. E4.14c $M(x)$

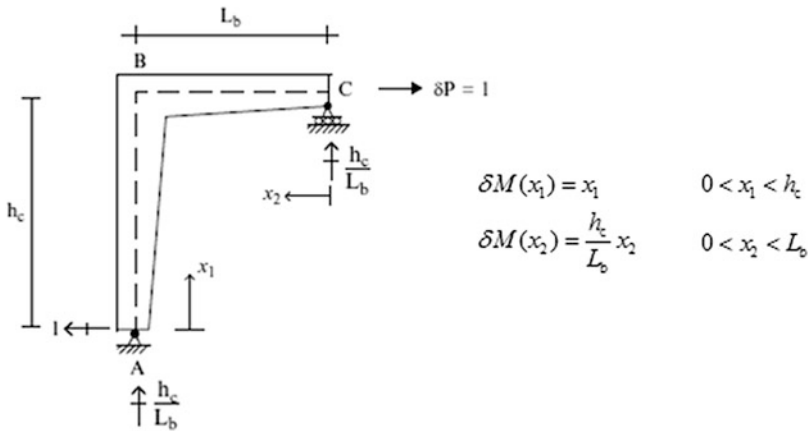


Fig. E4.14d δM for u_C

$$u_C = \frac{1}{E} \int_0^{h_c} \frac{1}{I_{AB}} (Px_1)(x_1) dx_1 + \frac{1}{E} \int_0^{L_b} \frac{1}{I_{CB}} \left(P \frac{h_c}{L_b} x_2 \right) \left(\frac{h_c}{L_b} x_2 \right) dx_2$$

Substituting for I_{AB} and I_{CB} and expressing the integral in terms of the dimensionless values $x_1/h = \bar{x}_1$ and $x_2/L_b = \bar{x}_2$, the expression for u_C reduces to

$$u_C = \frac{P(h_c)^3}{EI_{AB,0}} \int_0^1 \frac{(\bar{x}_1^2) d\bar{x}_1}{(g_{AB})^3} + \frac{P(h_c/L_b)^2(L_b)^3}{EI_{CB,0}} \int_0^1 \frac{(\bar{x}_2^2) d\bar{x}_2}{(g_{CB})^3}$$

Taking $g_{AB} = g_{CB} = 1$ leads to the values for the integrals obtained in Example 3.13, i.e., $1/3$.

Part (b): Using the specified sections, the g functions take the form

$$g_{AB} = 1 + \frac{x_1}{h} = 1 + \bar{x}_1$$

$$g_{CB} = 1 + \frac{1x_2}{2L_b} = 1 + \frac{1}{2}\bar{x}_2$$

Then, the problem reduces to evaluating the following integrals:

$$J_1 = \int_0^1 \frac{(\bar{x}_1^2) d\bar{x}_1}{(1 + \bar{x}_1)^3} \quad \text{and} \quad J_2 = \int_0^1 \frac{(\bar{x}_2^2) d\bar{x}_2}{(1 + (1/2)\bar{x}_2)^3}$$

We compute these values using the trapezoidal rule. Results for different interval sizes are listed below.

N	J_1	J_2
10	0.0682	0.1329
20	0.0682	0.1329
25	0.0682	0.1329
30	0.0682	0.1329

Next, we specify the inertia terms

$$I_{AB,0} = \frac{b(d_{AB,0})^3}{12}$$

$$I_{BC,0} = \frac{b(d_{CB,0})^3}{12}$$

For $I_{AB,0} = (3/4)I_{CB,0}$, the expression for u_C reduces to

$$u_C = \frac{P}{EI_{AB,0}} \left\{ h_c^3 J_1 + \left(\frac{h_c}{L_b} \right)^2 (L_b)^3 \left(\frac{3}{4} \right) (J_2) \right\}$$

Part(c): Setting $u_C = 1.86$ and solving for $I_{AB,0}$ leads to

$$I_{AB,0} = \frac{P}{Eu_C} \left\{ h_c^3 J_1 + \left(\frac{h_c}{L_b} \right)^2 (L_b)^3 \left(\frac{3}{4} \right) (J_2) \right\} = 607 \text{ in.}^2$$

Finally,

$$d_{AB,0} = \{24I_{AB,0}\}^{1/4} = 10.98 \text{ in.}$$

$$d_{CB,0} = \left\{ \frac{4}{3} \right\}^{1/3} d_{AB,0} = 12.1 \text{ in.}$$

4.7 Deflection Profiles: Plane Frame Structures

Applying the principle of Virtual Forces leads to specific displacement measures. If one is more interested in the overall displacement response, then it is necessary to generate the displacement profile for the frame. We dealt with a similar problem in Chap. 3, where we showed how to sketch the deflected shapes of beams given the bending moment distributions. We follow essentially the same approach in this section. Once the bending moment is known, one can determine the curvature, as shown in Fig. 4.26.

In order to establish the deflection profile for the entire frame, one needs to construct the profile for each member, and then join up the individual shapes such as that the displacement restraints are satisfied. We followed a similar strategy for planar beam-type structures; however, the process is somewhat more involved for plane frames.

Consider the portal frame shown in Fig. 4.27. Bending does not occur in AB and CD since the moment is zero. Therefore, these members must remain straight. However, BC bends into a concave shape. The profile consistent with these constraints is plotted below. Note that B, C, and D move laterally under the vertical loading.

Suppose we convert the structure into the 3-hinge frame defined in (Fig. 4.28). Now, the moment diagram is negative for all members. In this case, the profile is symmetrical. There is a discontinuity in the slope at E because of the moment release.

Fig. 4.26 Moment-curvature relationship

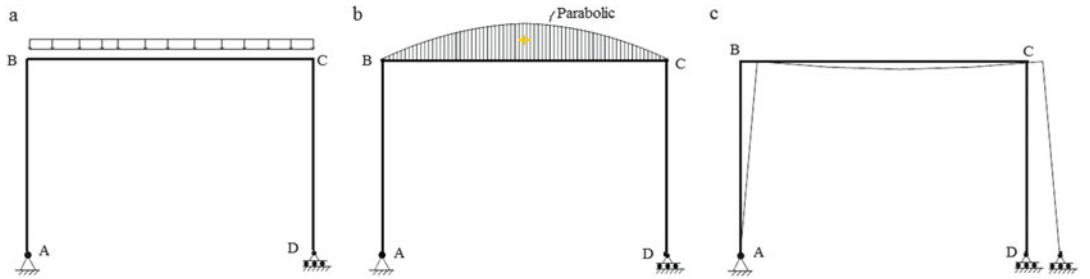


Fig. 4.27 Portal frame. (a) Loading. (b) Bending moment. (c) Deflection profile

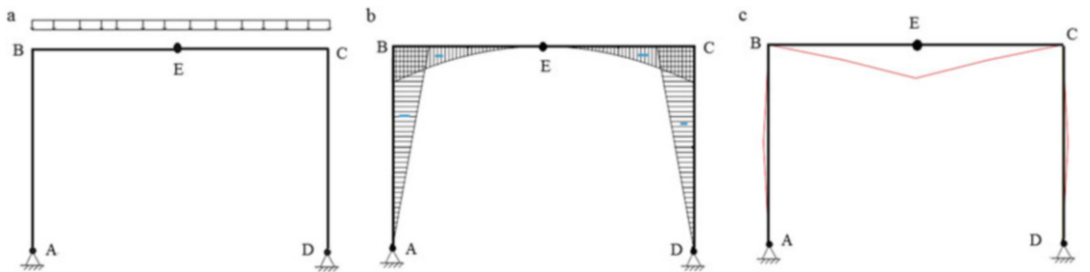


Fig. 4.28 3-Hinge frame. (a) Loading. (b) Bending moment. (c) Deflection profile

Gable frames are treated in a similar manner. The deflection profiles for simply supported and 3-hinge gable frames acted upon by gravity loading are plotted below (Figs. 4.29 and 4.30).

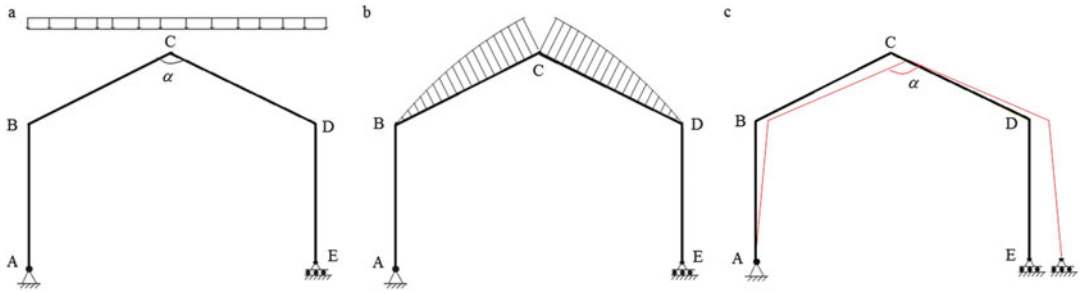


Fig. 4.29 Simply supported gable frame. (a) Loading. (b) Bending moment. (c) Deflection profile

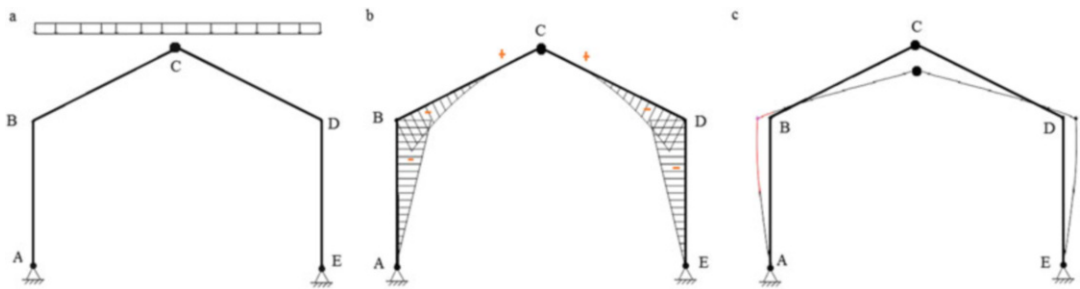


Fig. 4.30 3-Hinge gable frame. (a) Loading. (b) Bending moment. (c) Deflection profile

The examples presented so far have involved gravity loading. Lateral loading is treated in a similar way. One first determines the moment diagrams, and then establishes the curvature patterns for each member. Lateral loading generally produces lateral displacements as well as vertical displacements. Typical examples are listed below (Figs. 4.31, 4.32, and 4.33).

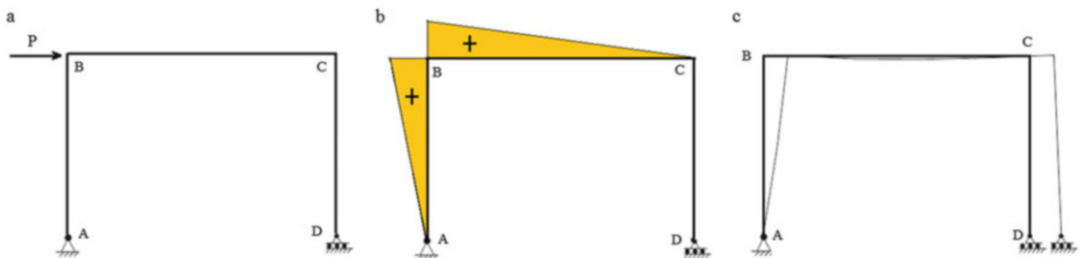


Fig. 4.31 Portal frame. (a) Loading. (b) Bending moment. (c) Deflection profile

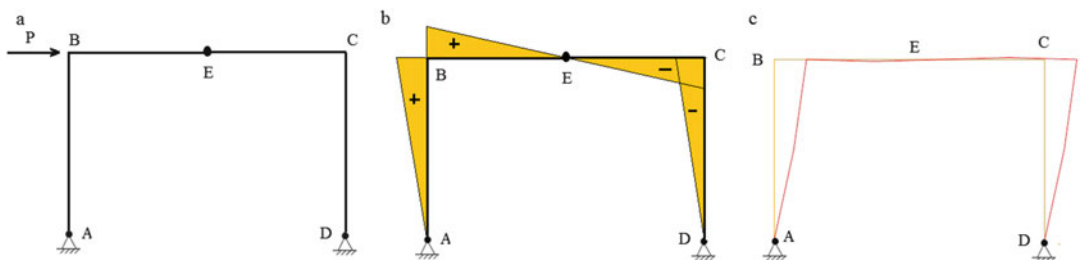


Fig. 4.32 3-Hinge frame. (a) Loading. (b) Bending moment. (c) Deflection profile

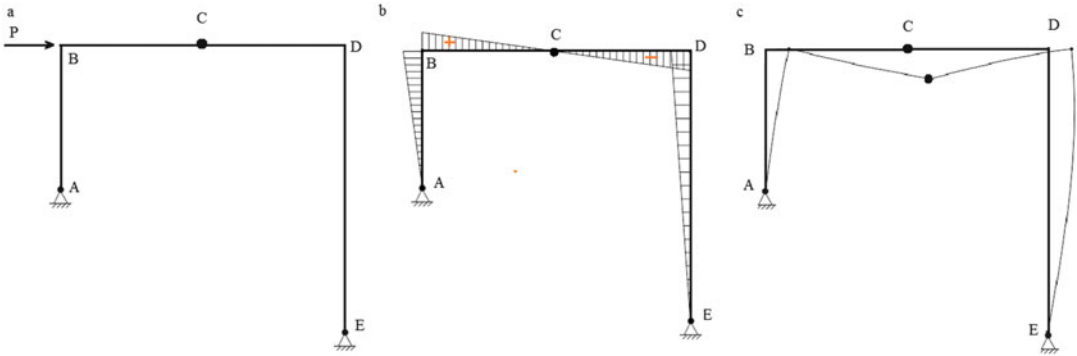


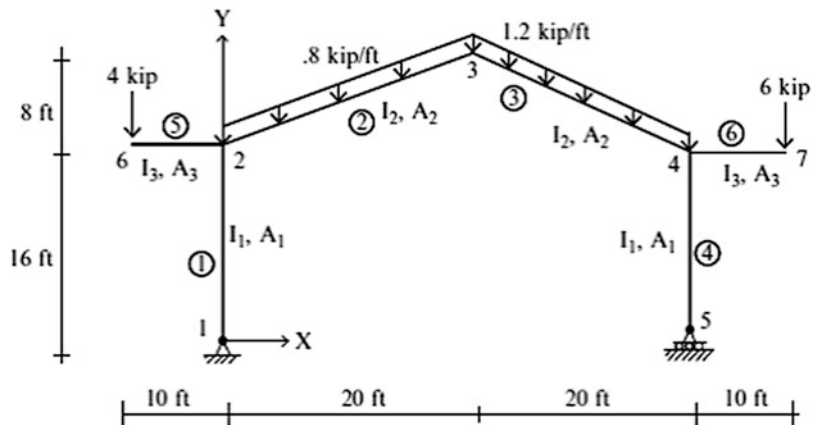
Fig. 4.33 3-Hinge frame. (a) Loading. (b) Bending moment. (c) Deflection profile

4.8 Computer-Based Analysis: Plane Frames

When there are multiple loading conditions, constructing the internal force diagrams and displacement profiles is difficult to execute manually. One generally resorts to computer-based analysis methods specialized for frame structures. The topic is discussed in Chap. 12. The discussion here is intended to be just an introduction.

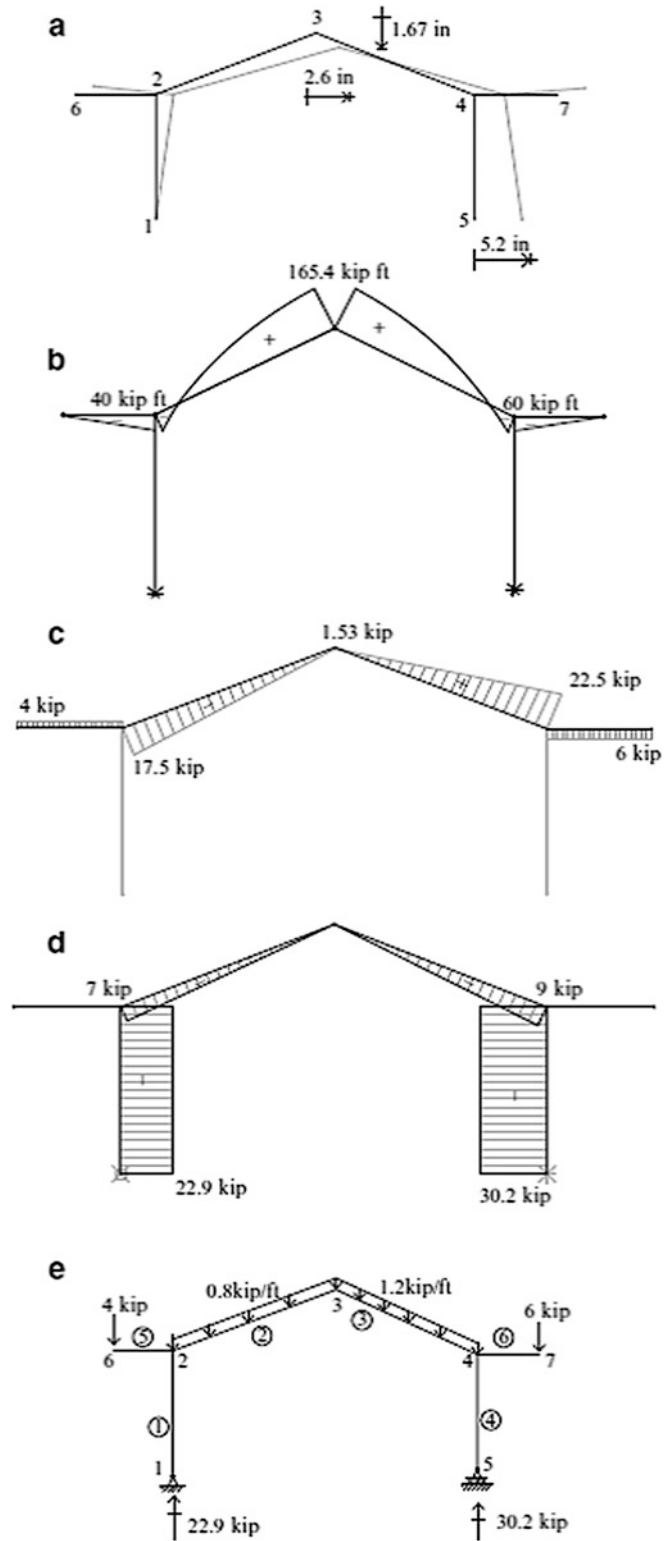
Consider the gable plane frame shown in Fig. 4.34. One starts by numbering the nodes and members, and defines the nodal coordinates and member incidences. Next, one specifies the nodal constraints. For plane frames, there are two coordinates and three displacement variables for each node (two translations and one rotation). Therefore, there are three possible displacement restraints at a node. For this structure, there are two support nodes, nodes 1 and 5. At node 1, the X and Y translations are fully restrained, i.e., they are set to zero. At node 5, the Y translation is fully restrained.

Fig. 4.34 Geometry and loading



Next, information related to the members, such as the cross-sectional properties (A , I), loading applied to the member, and releases such as internal moment releases are specified. Finally, one specifies the desired output. Usually, one is interested in shear and moment diagrams, nodal reactions and displacements, and the deflected shape. Graphical output is most convenient for visualizing the structural response. Typical output plots for the following cross-sectional properties $I_1 = 100 \text{ in.}^4$, $I_2 = 1000 \text{ in.}^4$, $I_3 = 300 \text{ in.}^4$, $E = 29,000 \text{ ksi}$, $A_1 = 14 \text{ in.}^2$, $A_2 = 88 \text{ in.}^2$, and $A_3 = 22 \text{ in.}^2$ are listed in Fig. 4.35.

Fig. 4.35 Graphical output for structure defined in Fig. 4.34. (a) Displacement profile. (b) Bending moment, M . (c) Shear, V . (d) Axial force, F . (e) Reactions



4.9 Plane Frames: Out of Plane Loading

Plane frames are generally used to construct three-dimensional building systems. One arranges the frames in orthogonal patterns to form a stable system. Figure 4.36 illustrates this scheme. Gravity load is applied to the floor slabs. They transfer the load to the individual frames resulting in each frame being subjected to a planar loading. This mechanism is discussed in detail in Chap. 15.

Our interest here is the case where the loading acts normal to the plane frame. One example is the typical highway signpost shown in Fig. 4.37. The sign and the supporting member lie in a single plane. Gravity load acts in this plane. However, the wind load is normal to the plane and produces a combination of bending and twisting for the vertical support. One deals separately with the bending and torsion responses and then superimposes the results.

The typical signpost shown in Fig. 4.37 is statically determinate. We consider the free body diagram shown in Fig. 4.38. The wind load acting on the sign produces bending and twisting moment in the column. We use a double-headed arrow to denote the torsional moment.

Suppose the Y displacement at C is desired. This motion results from the following actions:

Member BC bends in the $X - Y$ plane

$$v_C = \frac{P_w \left(\frac{b}{2}\right)^3}{3EI_2}$$

Member AB bends in the $Y - Z$ plane and twists about the Z axis

$$v_B = \frac{P_w h^3}{3EI_1} \quad \theta_{Bz} = \frac{P_w \left(\frac{b}{2}\right) h}{GJ}$$

where GJ is the torsional rigidity for the cross section.

Fig. 4.36 A typical 3-D system of plane frames

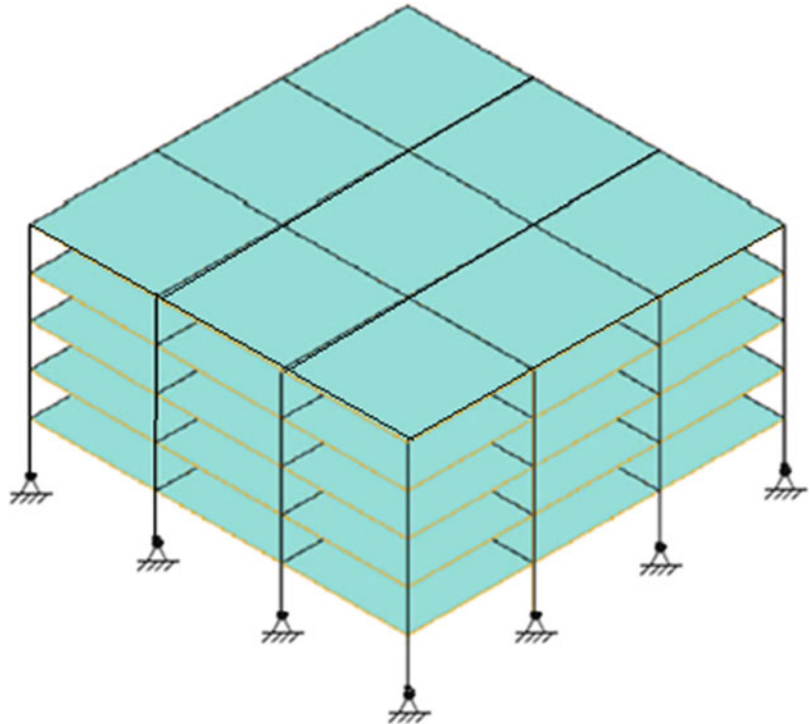


Fig. 4.37 Signpost structure

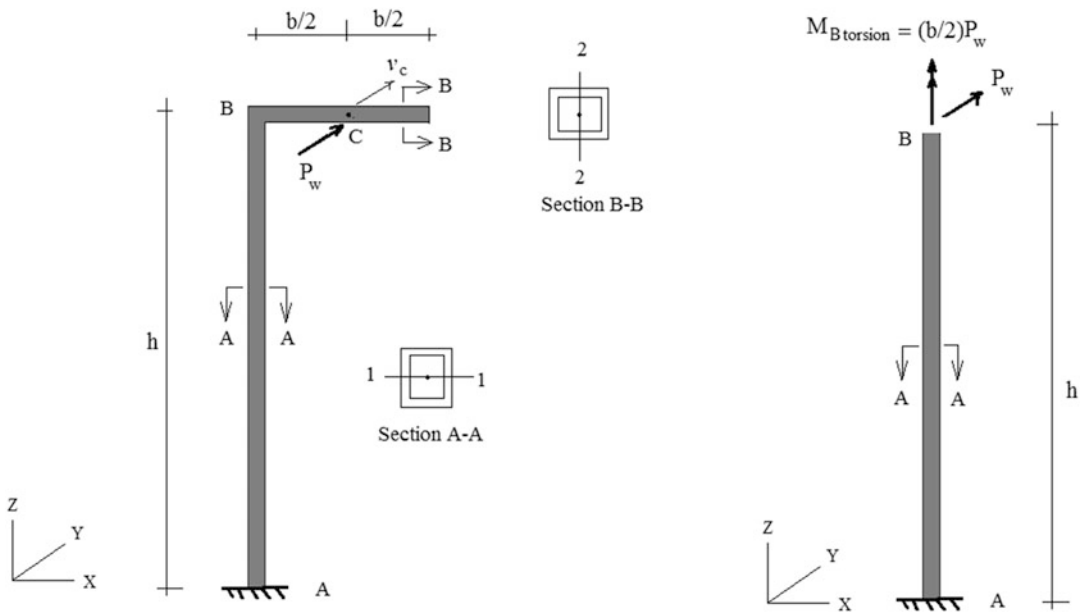
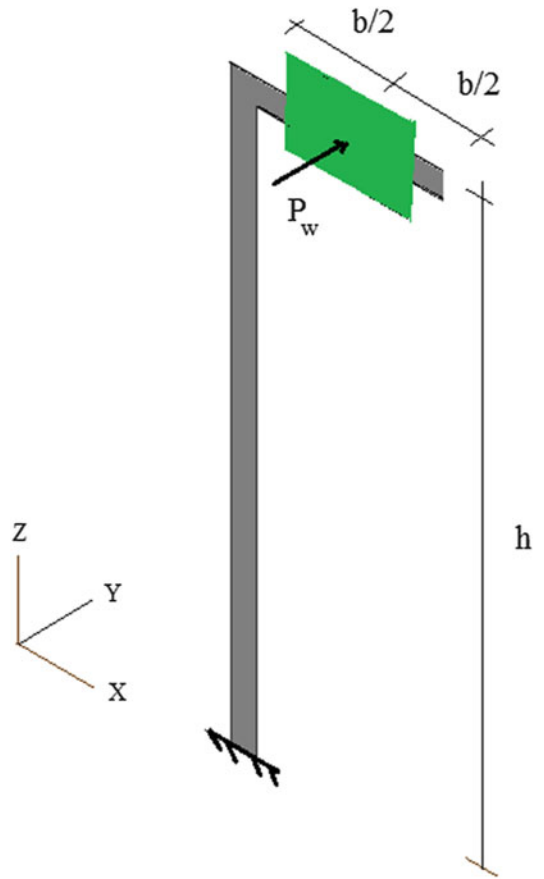
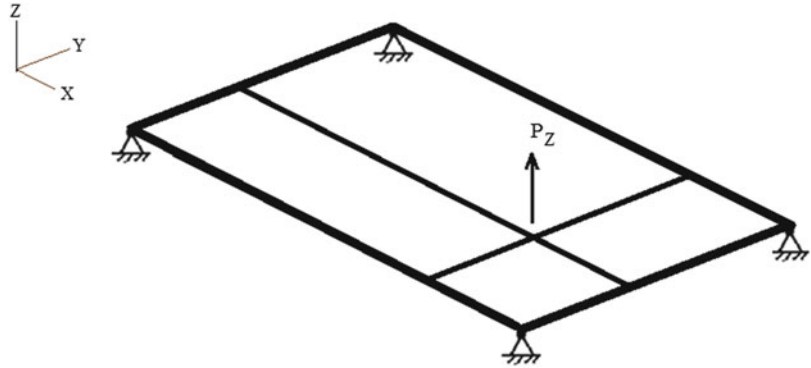


Fig. 4.38 Free body diagrams

Fig. 4.39 Plane grid structure



Node C displaces due to the rotation at B

$$v_C = \left(\frac{b}{2}\right)\theta_{Bz} = \left(\frac{b}{2}\right)^2 \left(P_w \frac{h}{GJ}\right)$$

Summing the individual contributions leads to

$$v_{C \text{ total}} = P_w \left(\frac{b^3}{24EI_2} + \frac{h^3}{3EI_1} + \frac{b^2h}{4GJ} \right)$$

Another example of out-of-plane bending is the transversely loaded grid structure shown in Fig. 4.39. The members are rigidly connected at their ends and experience, depending on their orientation, bending in either the $X - Z$ plane or the $Y - Z$ plane, as well as twist deformation. Plane grids are usually supported at their corners. Sometimes, they are cantilevered out from one edge. Their role is to function as plate-type structures under transverse loading.

Plane grids are *statically indeterminate* systems. Manual calculations are not easily carried out for typical grids so one uses a computer analysis program. This approach is illustrated in Chap. 10.

4.10 Summary

4.10.1 Objectives

- To develop criteria for static determinacy of planar rigid frame structures.
- To develop criteria for static determinacy of planar A-frame structures.
- To present an analysis procedure for statically determinate portal and pitched roof plane frame structures subjected to vertical and lateral loads.
- To compare the bending moment distributions for simple vs. 3-hinged portal frames under vertical and lateral loading.
- To describe how the Principle of Virtual Forces is applied to compute the displacements of frame structures.
- To illustrate a computer-based analysis procedure for plane frames.
- To introduce the analysis procedure for out-of-plane loading applied to plane frames.

4.10.2 Key Concepts

- A planar rigid frame is statically determinate when $3m + r - n = 3j$, where m is the number of members, r is the number of displacement restraints, j is the number of nodes, and n the number of releases.
- A planar A-frame is statically determinate when $3m = r + 2n_p$, where n_p is the number of pins, m is the number of members, and r is the number of displacement restraints.
- The Principle of Virtual Forces specialized for frame structures has the general form

$$d\delta P = \sum_{\text{members}} \int_s \left\{ \frac{M}{EI} \delta M + \frac{F}{AE} \delta F \right\} ds$$

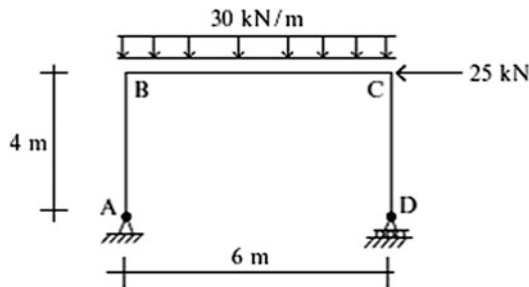
For low-rise frames, the axial deformation term is negligible.

- The peak bending moments in 3-hinged frames generated by lateral loading are generally less than for simple portal frames.

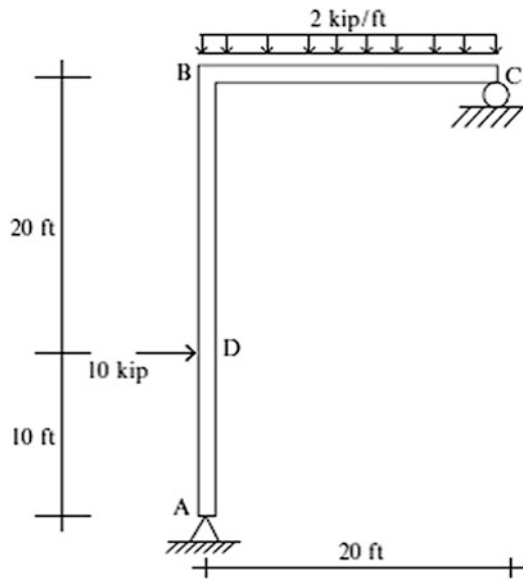
4.11 Problems

For the plane frames defined in Problems 4.1–4.18, determine the reactions, and shear and moment distributions.

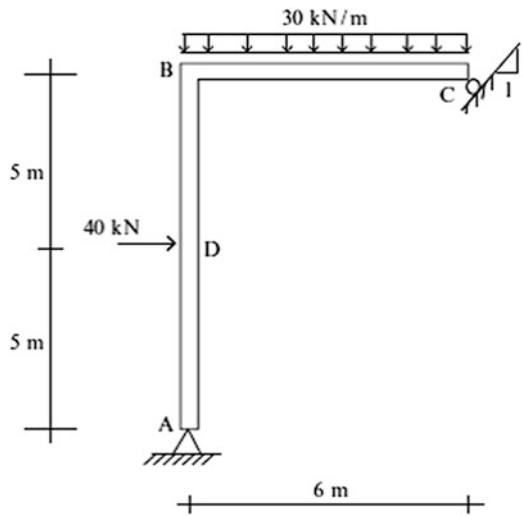
Problem 4.1



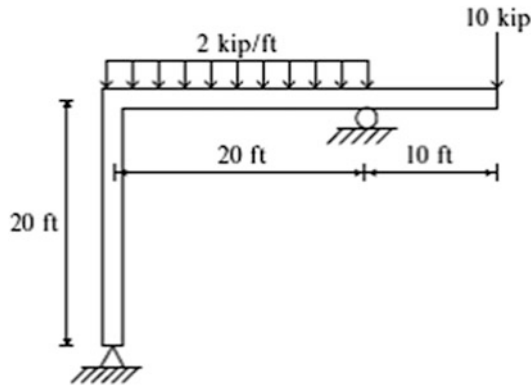
Problem 4.2



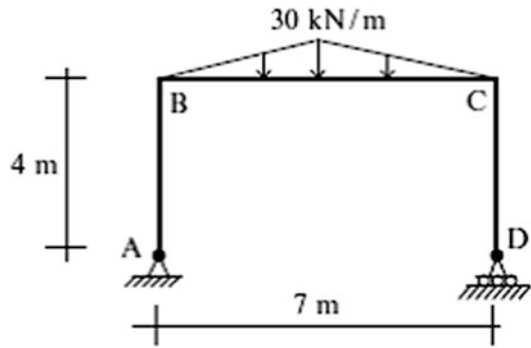
Problem 4.3



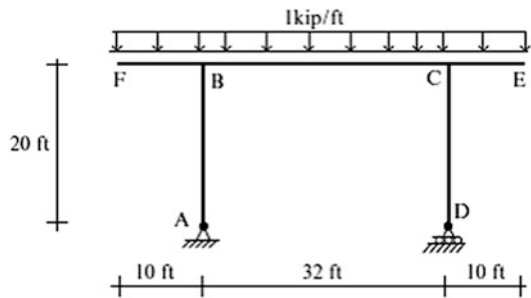
Problem 4.4



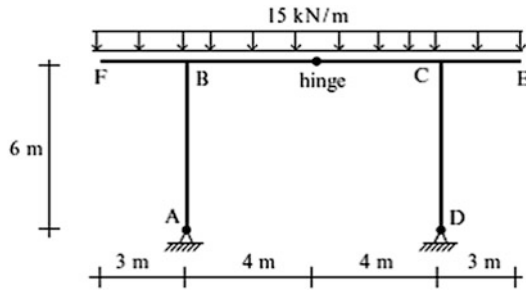
Problem 4.5



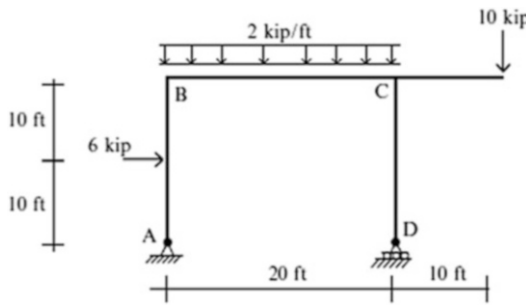
Problem 4.6



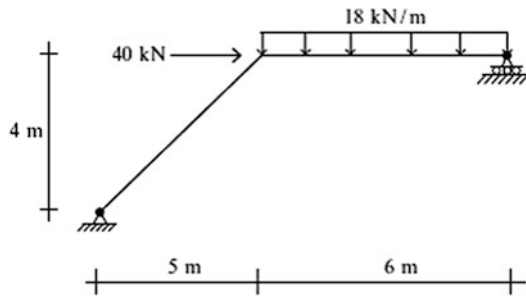
Problem 4.7



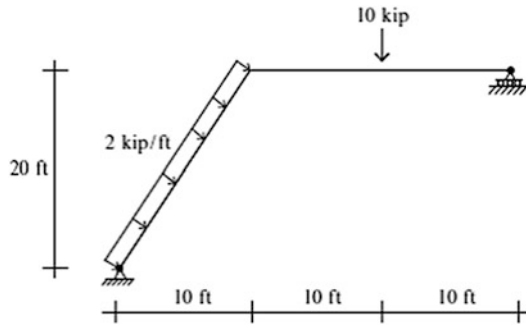
Problem 4.8



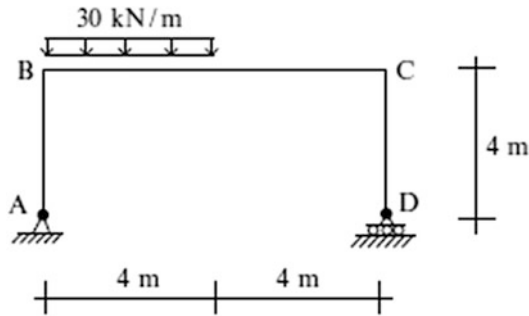
Problem 4.9



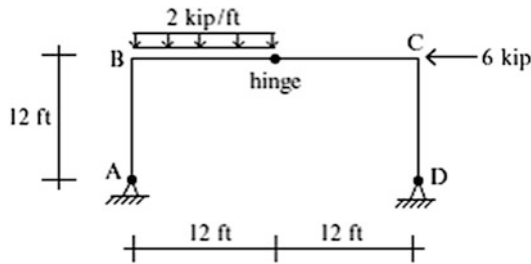
Problem 4.10



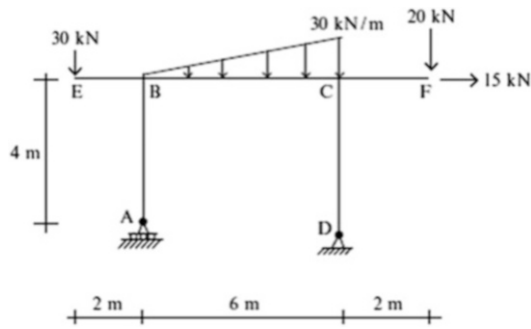
Problem 4.11



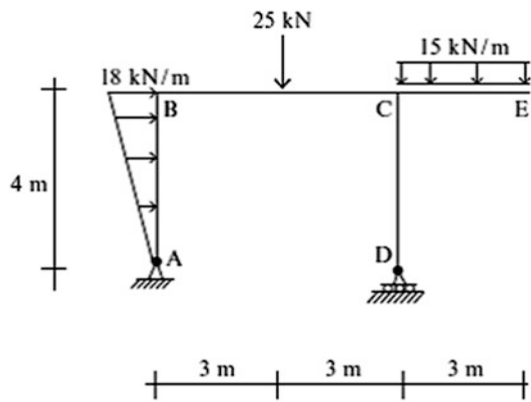
Problem 4.12



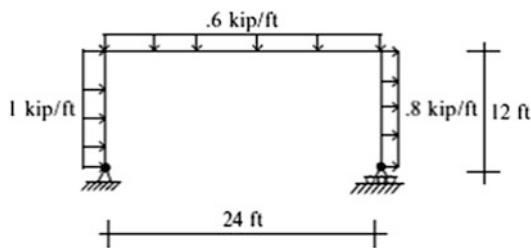
Problem 4.13



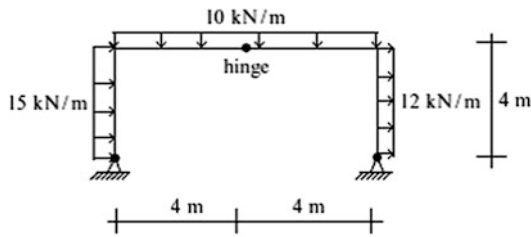
Problem 4.14



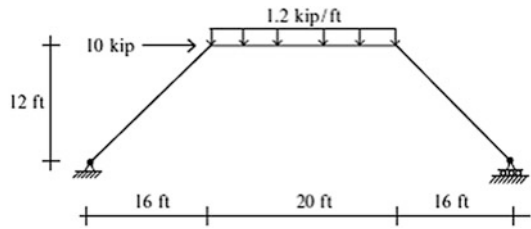
Problem 4.15



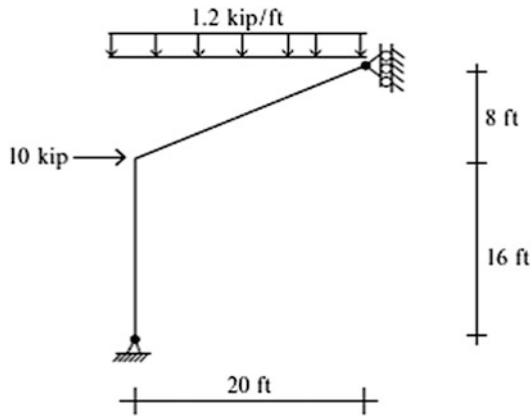
Problem 4.16



Problem 4.17

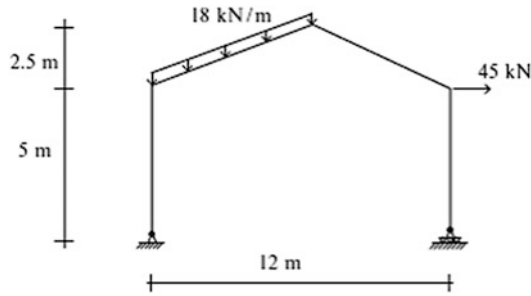


Problem 4.18

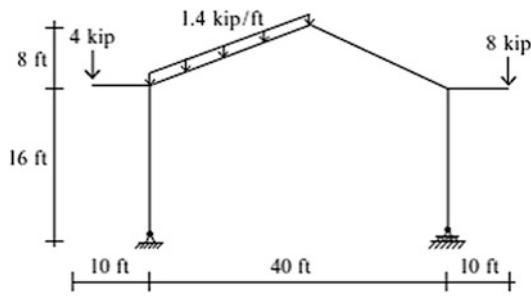


For the gable frames defined in Problems 4.19–4.26, determine the bending moment distributions.

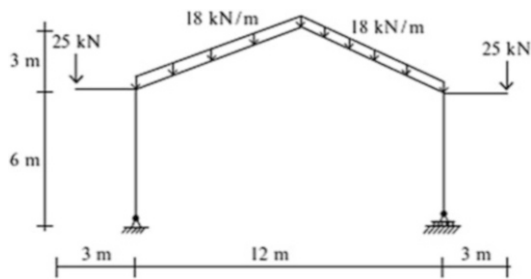
Problem 4.19



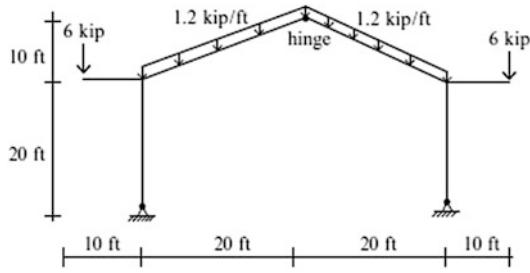
Problem 4.20



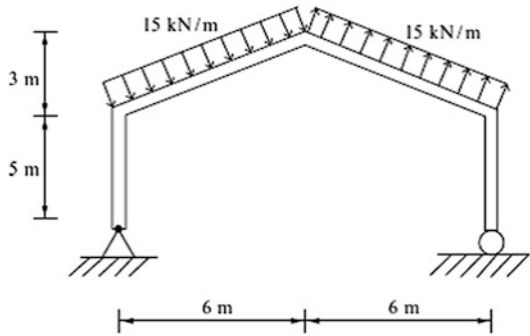
Problem 4.21



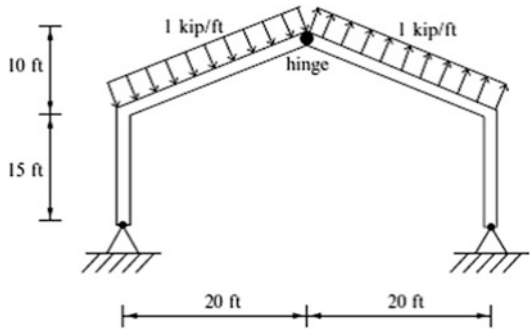
Problem 4.22



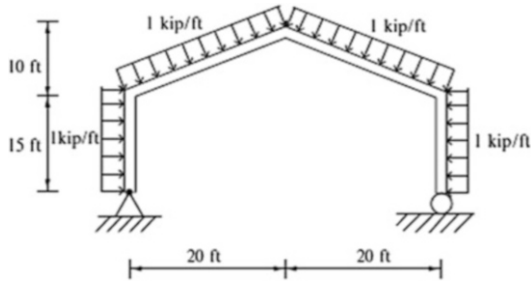
Problem 4.23



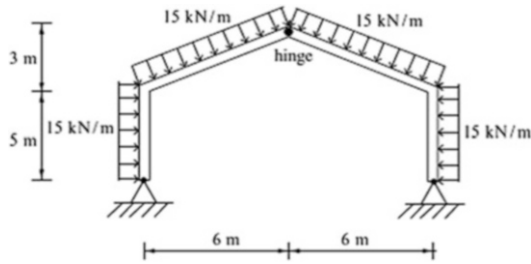
Problem 4.24



Problem 4.25

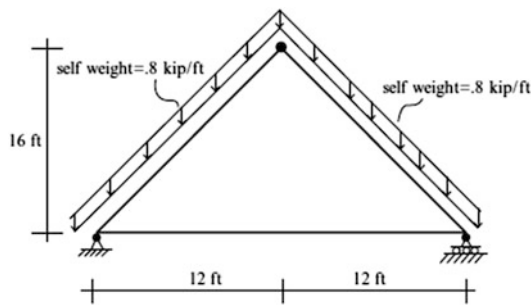


Problem 4.26

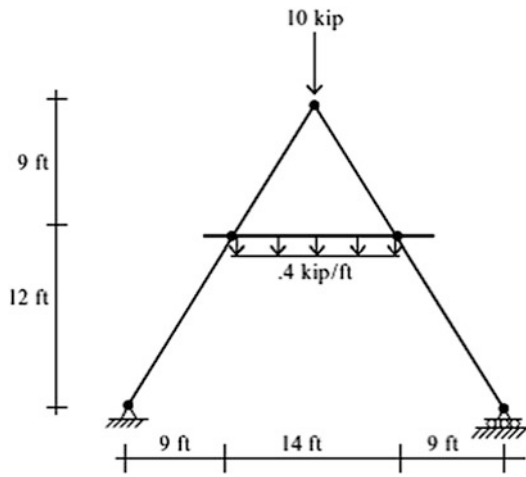


For the A-frames defined in Problems 4.27–4.29, determine the reactions and bending moment distribution.

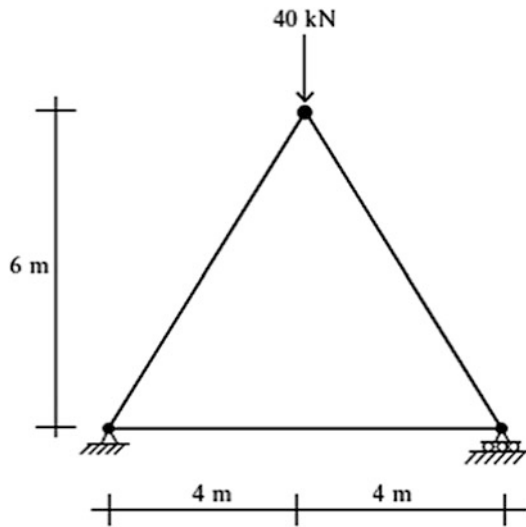
Problem 4.27



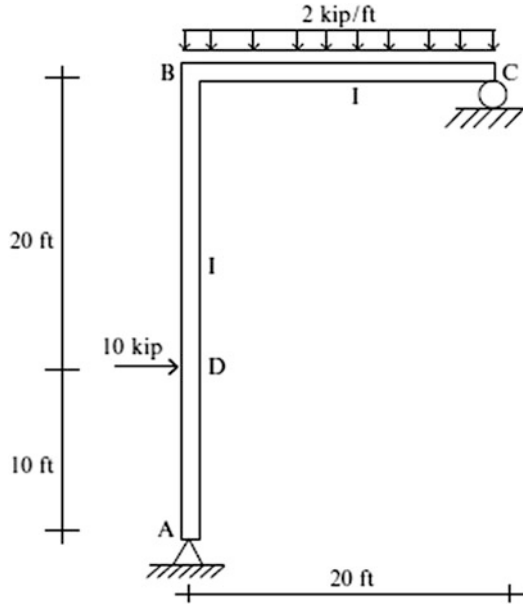
Problem 4.28



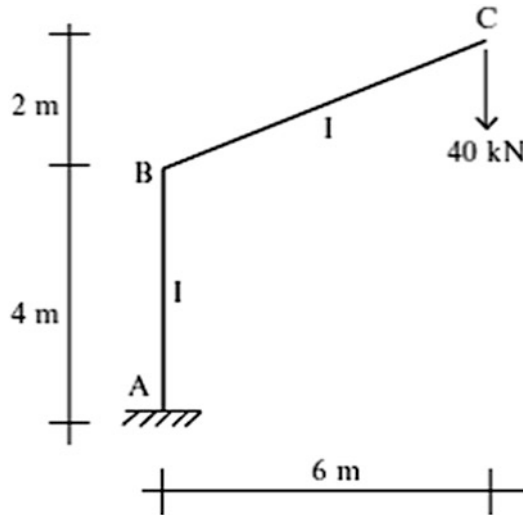
Problem 4.29



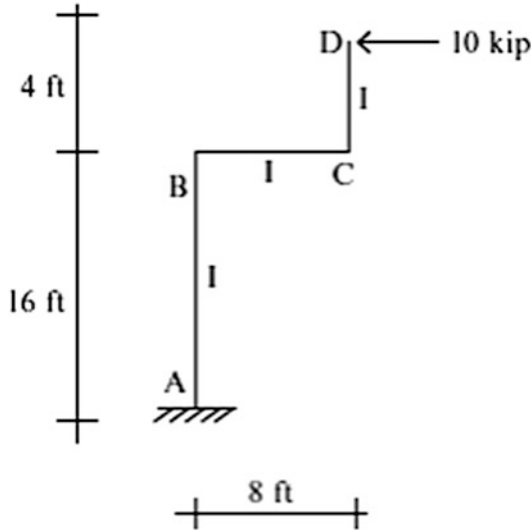
Problem 4.30 Determine the horizontal deflection at D and the clockwise rotation at joint B. Take $E = 29,000$ ksi. Determine the I required to limit the horizontal displacement at D to 2 in. Use the Virtual Force method.



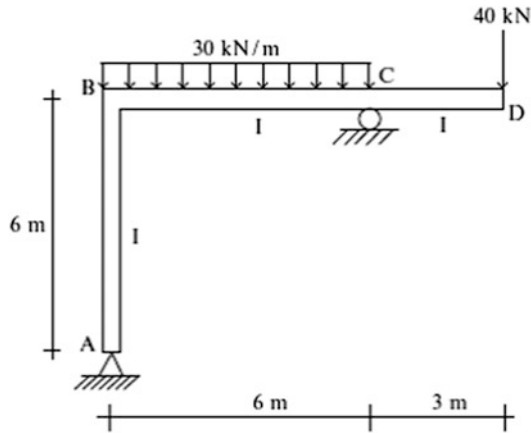
Problem 4.31 Determine the value of I to limit the vertical deflection at C to 30 mm. Take $E = 200$ GPa. Use the Virtual Force method.



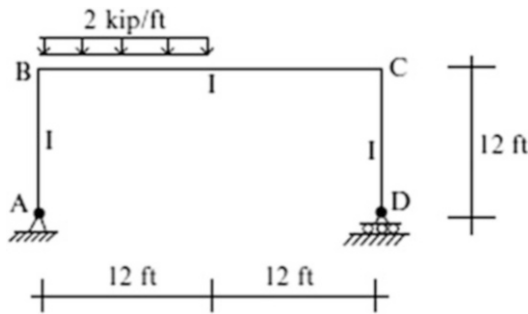
Problem 4.32 Determine the value of I required limiting the horizontal deflection at D to $\frac{1}{2}$ in. Take $E = 29,000$ ksi. Use the Virtual Force method.



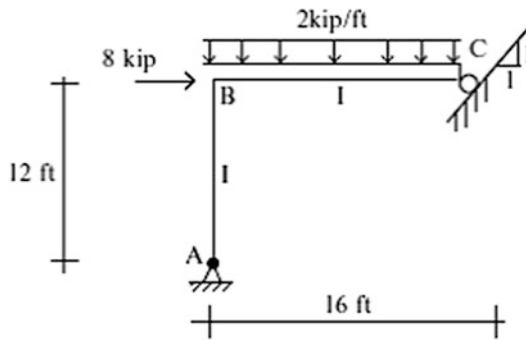
Problem 4.33 Determine the vertical deflection at D and the rotation at joint B. Take $E = 200$ GPa and $I = 60(10)^6$ mm⁴. Use the Virtual Force method.



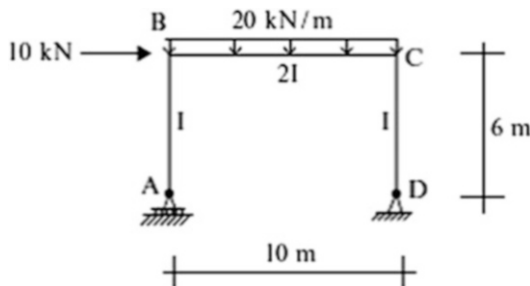
Problem 4.34 Determine the horizontal displacement at joint B. Take $E = 29,000$ ksi and $I = 200$ in.⁴ Use the Virtual Force method.



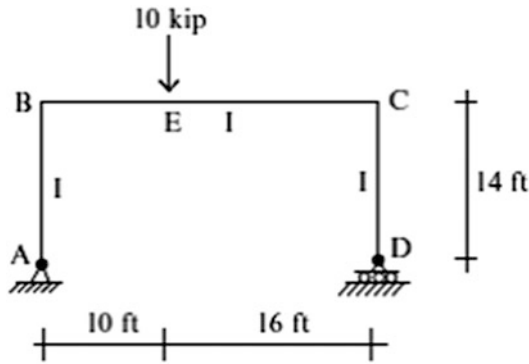
Problem 4.35 Determine the displacement at the roller support C. Take $E = 29,000$ ksi and $I = 100$ in.⁴ Use the Virtual Force method.



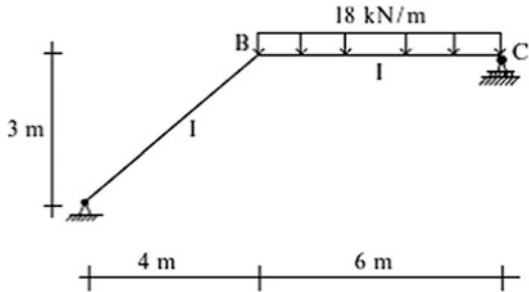
Problem 4.36 Determine the horizontal deflection at C and the rotation at joint B. Take $E = 200$ GPa and $I = 60(10)^6$ mm⁴. Use the Virtual Force method.



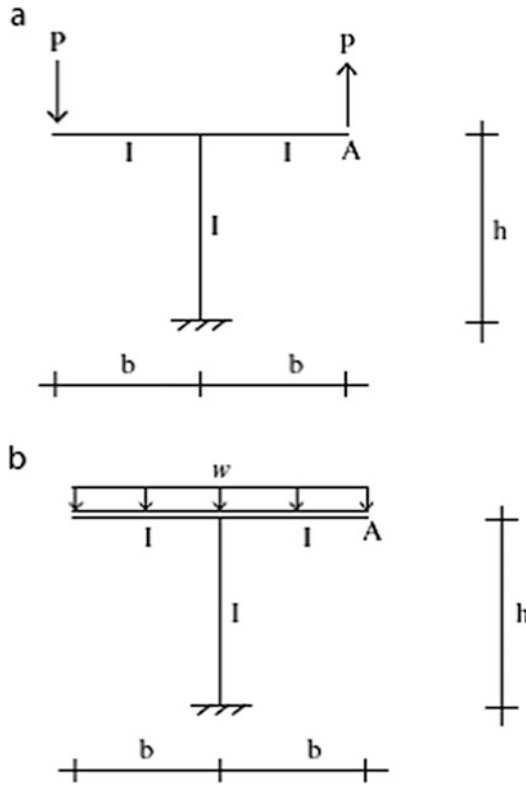
Problem 4.37 Determine the horizontal deflection at C and the vertical deflection at E. Take $E = 29,000$ ksi and $I = 160$ in.⁴ Use the Virtual Force method.



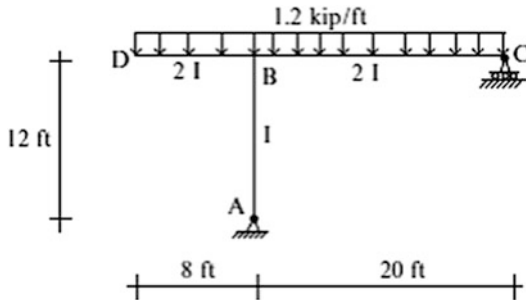
Problem 4.38 Determine the horizontal deflection at C. $I = 100(10)^6$ mm⁴ and $E = 200$ GPa. Sketch the deflected shape. Use the Virtual Force method.



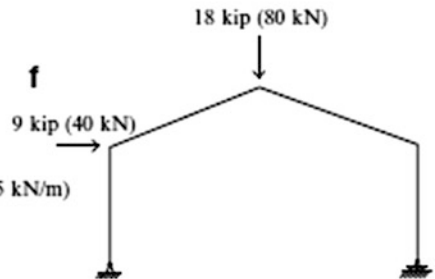
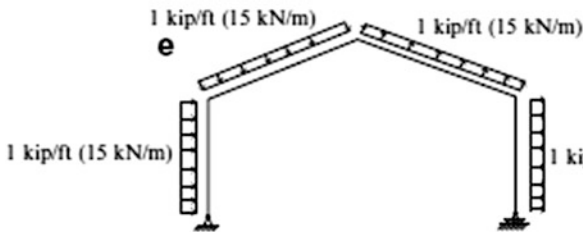
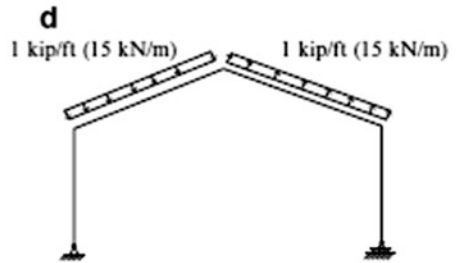
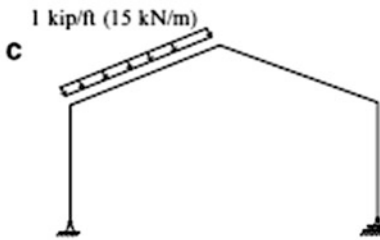
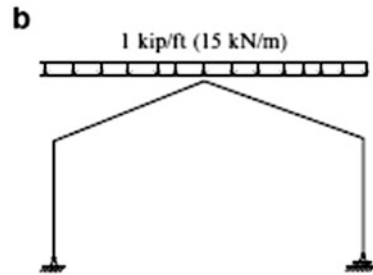
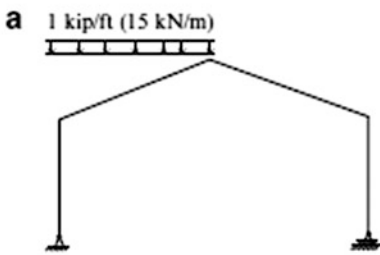
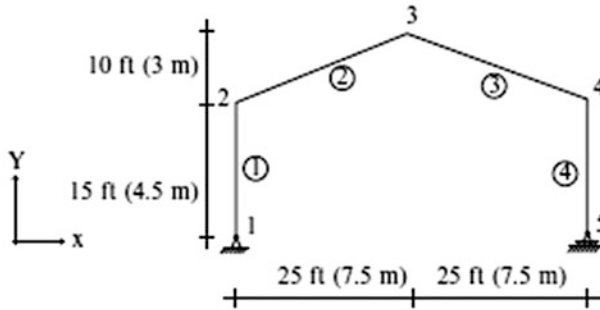
Problem 4.39 Sketch the deflected shapes. Determine the vertical deflection at A. Take $I = 240 \text{ in.}^4$, $E = 29,000 \text{ ksi}$, and $h = 2b = 10 \text{ ft}$.



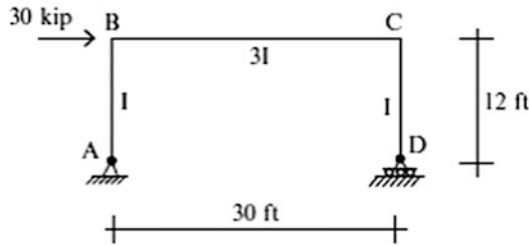
Problem 4.40 Determine the deflection profile for member DBC. Estimate the peak deflection. Use computer software. Note that the deflection is proportional to $1/EI$.



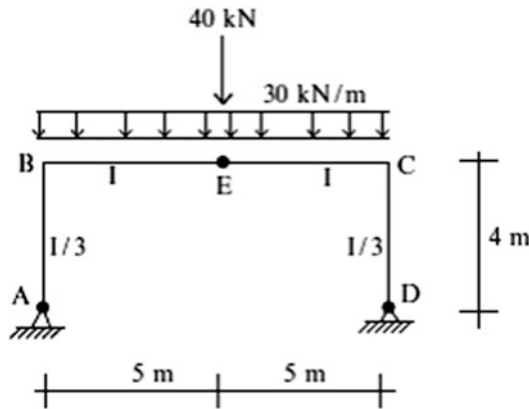
Problem 4.41 Consider the pitched roof frame shown below and the loadings defined in cases (a)–(f). Determine the displacement profiles and shear and moment diagrams. EI is constant. Use a computer software system. Take $I = 10,000 \text{ in.}^4$ ($4160(10)^6 \text{ mm}^4$), $E = 30,000 \text{ ksi}$ (200 GPa).



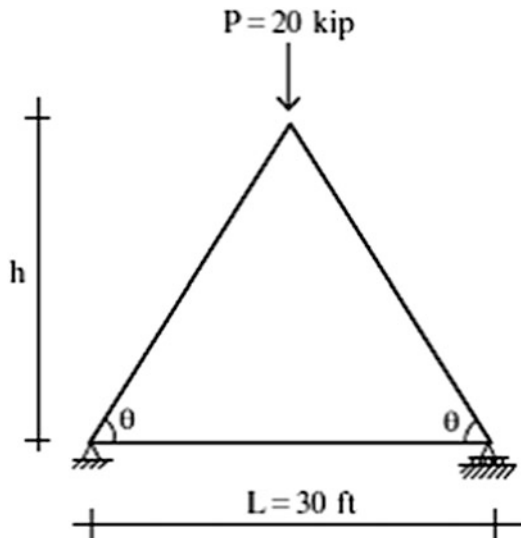
Problem 4.42 Consider the frame shown below. Determine the required minimum I for the frame to limit the horizontal deflection at C to 0.5 in. The material is steel. Use computer software.



Problem 4.43 Consider the frame shown below. Determine the required minimum I for the frame to limit the vertical deflection at E to 15 mm. The material is steel. Use computer software.

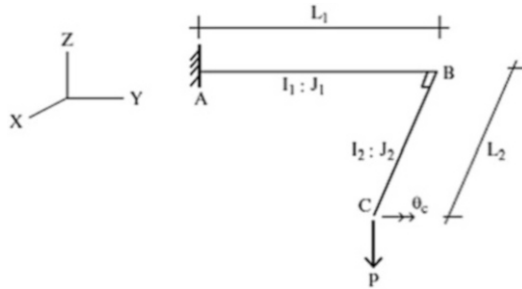


Problem 4.44 Consider the triangular rigid frame shown below. Assume the member properties are constant. $I = 240 \text{ in.}^4$, $A = 24 \text{ in.}^2$ and $E = 29,000 \text{ ksi}$. Use computer software to determine the axial forces and end moments for the following range of values of $\tan \theta = 2h/L = 0.1, 0.2, 0.3, 0.4, 0.5$

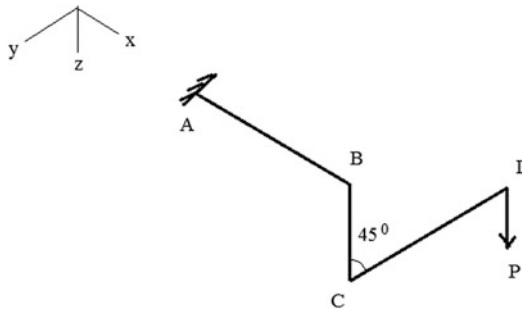


Compare this solution with the solution based on assuming the structure is an ideal truss.

Problem 4.45 Consider the structure consisting of two members rigidly connected at B. The load P is applied perpendicular to the plane ABC. Assume the members are prismatic. Determine θ_y at point C (labeled as θ_c on the figure).



Problem 4.46 Members AB, BC, and CD lie in the $X - Y$ plane. Force P acts in the Z direction. Consider the cross-sectional properties to be constant. Determine the z displacement at B and D. Take $L_{AB} = L, L_{BC} = \frac{L}{2}, L_{CD} = L\sqrt{2}$.



Reference

1. Tauchert TR. Energy principles in structural mechanics. New York: McGraw-Hill; 1974.

Abstract

Historically, cables have been used as structural components in bridge structures. In this chapter, we first examine how the geometry of a cable is related to the loading that is applied to it. We treat concentrated loadings first and then incorporate distributed loadings leading up to a theory for continuously loaded inclined cables. We also analyze the effect of temperature on the cable geometry. Lastly, we develop an approximate formula for estimating the stiffness of a cable modeled as an equivalent straight member. This modeling strategy is used when analyzing cable-stayed structures.

5.1 Introduction

A cable is a flexible structural component that offers no resistance when compressed or bent into a curved shape. Technically, we say a cable has zero bending rigidity. It can support only tensile loading. The first cables were made by twisting vines to form a rope-like member. There are many examples of early cable suspension bridges dating back several thousand years. With the introduction of iron as a structural material, cables were fabricated by connecting wrought iron links. Figure 5.1 shows an example of an iron link suspension bridge, the Clifton Suspension Bridge near Bristol, England built in 1836–1864 and designed by Isambard Brunel.

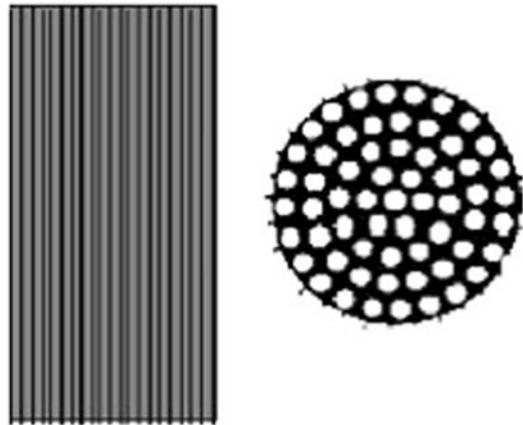
When high-strength steel wires became available, steel replaced wrought iron as the material of choice for cables. Modern cables are composed of multiple wires (up to 150 wires) clustered in a circular cross-section and arranged in a parallel pattern, as illustrated in Fig. 5.2. This arrangement is used for cable-stayed bridges and suspension bridges. The cable is normally coated with a protective substance such as grease and wrapped or inserted in a plastic sheathing.

One of the most notable early applications of steel cables was the Brooklyn Bridge built in 1870–1883 and designed by John Roebling and Wilhelm Hildebrandt. John Roebling also invented and perfected the manufacture of steel wire cable which was used for the bridge. At the time of completion, the total length of the Brooklyn Bridge was 50 % greater than any existing suspension bridge, an extraordinary advancement in bridge engineering (Fig. 5.3).



Fig. 5.1 Clifton Suspension Bridge, England

Fig. 5.2 Cable-strand arrangements



Cable nets are also used as the primary structural elements for long-span horizontal roof structures. Figure 5.4 shows a single-layer cable net structure with a double-curved saddle-shaped surface designed by Schlaich Bergermann and partners for a stadium in Kuwait.

Cable-stayed structures employ cables fabricated from ultra high-strength steel to allow for the high level of tension required for stiffness. The cable-stayed bridge concept has emerged as the predominant choice for main spans up to about 1000 m, replacing the conventional truss structural system. Figure 5.5 shows the Normandy Bridge, with a main span of 856 m. Built in 1995, it held the record for the largest main span until 1999, when it was exceeded by the Tatara Bridge in Japan.



Fig. 5.3 Brooklyn Bridge, USA



Fig. 5.4 Doubly curved single-layer cable net, Kuwait



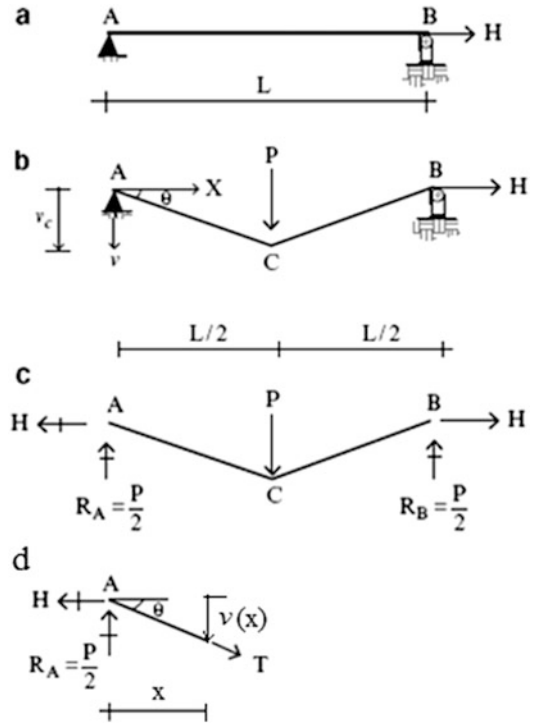
Fig. 5.5 Normandy Bridge, France

5.2 Cables Subjected to Concentrated Loads

5.2.1 Horizontal Cables

Suppose we conduct the following experiment shown in Fig. 5.6. We start with a horizontally aligned cable that is pin connected at A, supported with a roller support at B, and tensioned with a force H . We then apply a concentrated load, P , at mid-span. The cable adopts the triangular shape shown under the action of P . Two questions are of interest. Firstly, why a triangular shape? Secondly, how is the

Fig. 5.6 Transverse loading on pretensioned cable. (a) Axial load. (b) Transverse load added. (c) Free body diagram. (d) Free body diagram of cable segment



downward vertical displacement at mid-span related to P and H ? Historically, the term “sag” is used to describe the vertical motion of a cable.

We answer these questions by noting that the magnitude of the moment at any section along the length of the cable must be zero since a cable has no resistance to bending. Summing moments about B

$$\sum_{\text{at B}} M = R_A L - P \frac{L}{2} = 0 \Rightarrow R_A = \frac{P}{2} \uparrow$$

Next, we consider the free body diagram for the arbitrary segment shown in Fig. 5.6d. Setting the moment at x equal to zero leads to an expression for the sag, $v(x)$.

$$\sum M_{\text{at } x} = \frac{P}{2}x - Hv(x) = 0 \tag{5.1}$$

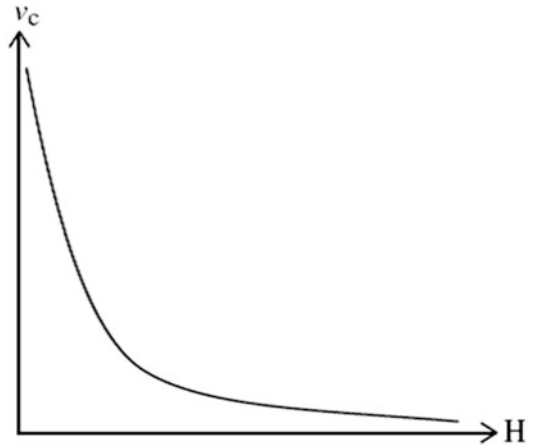
$$v(x) = \frac{P}{2H}x \tag{5.2}$$

Finally, evaluating $v(x)$ at $x = L/2$ results in an equation relating v_C and P .

$$v_C = \frac{PL}{4H} \tag{5.3}$$

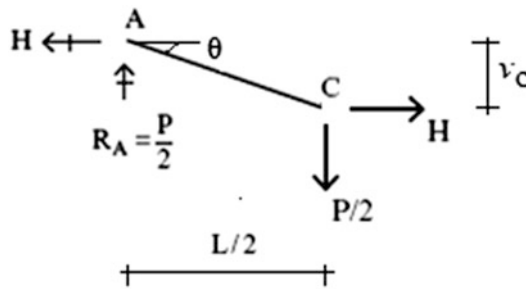
The relationship between v_C and H is plotted below in Fig. 5.7. Usually, one specifies H and determines v_C . However, there are cases where one specifies v_C and determines the required value of H . In general for cable systems, one needs to specify either a force or a sag in order to define the solution.

Fig. 5.7 Relationship between v_c and H



The tension in the cable is given by

$$T = \sqrt{H^2 + \left(\frac{P}{2}\right)^2} = H \sqrt{1 + \left(\frac{P}{2H}\right)^2} \quad (5.4)$$

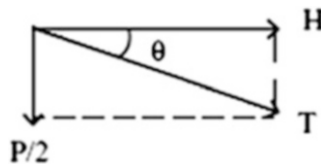


Noting that the angle of inclination of the cable is related to the sag by

$$\tan \theta = \frac{v_c}{L/2} = \frac{P/2}{H} \quad (5.5)$$

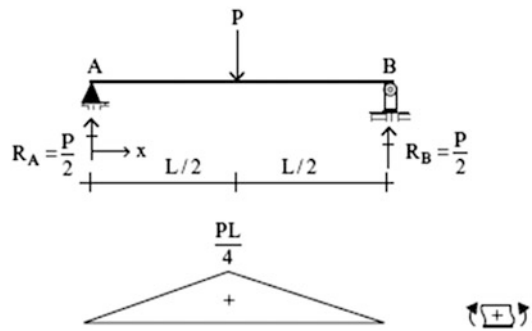
leads to an alternative expression for the tension,

$$T = H \sqrt{1 + \left(\frac{P}{2H}\right)^2} = H \sqrt{1 + \tan^2 \theta} = \frac{H}{\cos \theta} \quad (5.6)$$



When θ is small, T is approximately equal to H .

Fig. 5.8 Moment distribution for simply supported beam $M_0(x)$



Equation (5.1) combines two moment distributions, one due to the transverse loading P and the other due to H . The moment due to P can be interpreted as the moment in a simply supported beam spanning between points A and B , the support points for the cable. Figure 5.8 shows this distribution.

We express (5.1) as

$$M_0(x) - v(x)H = 0 \tag{5.7}$$

where $M_0(x)$ is the moment due to the transverse loading acting on the simply supported beam spanning between A and B . Then, the expression for the sag can be written as

$$v(x) = \frac{M_0(x)}{H} \tag{5.8}$$

We interpret this result as follows. *The shape of the vertical sag of the cable from the horizontal chord is a scaled version of the moment diagram for the transverse loading acting on a simply supported beam spanning between the cable supports.*

We extend this reasoning to a cable subjected to multiple concentrated loads. Figure 5.9a illustrates this case. The moment diagram for a set of concentrated loads is piecewise linear, with peak values at the points of application of the concentrated loads. It follows from (5.8) that the shape of the cable is also piecewise linear. One generates $M_0(x)$, the corresponding shear $V_0(x)$, the displacement v , and the tension T . Details are listed in Fig. 5.9b–d. Note that one has to specify either H or one of the vertical coordinates (v_C or v_D) in order to compute the shape.

$$T = \sqrt{V_0^2 + H^2} = \frac{H}{\cos \theta}$$

Example 5.1 Cable with Multiple Concentrated Loads

Given: The cable and loading shown in Fig. E5.1a.

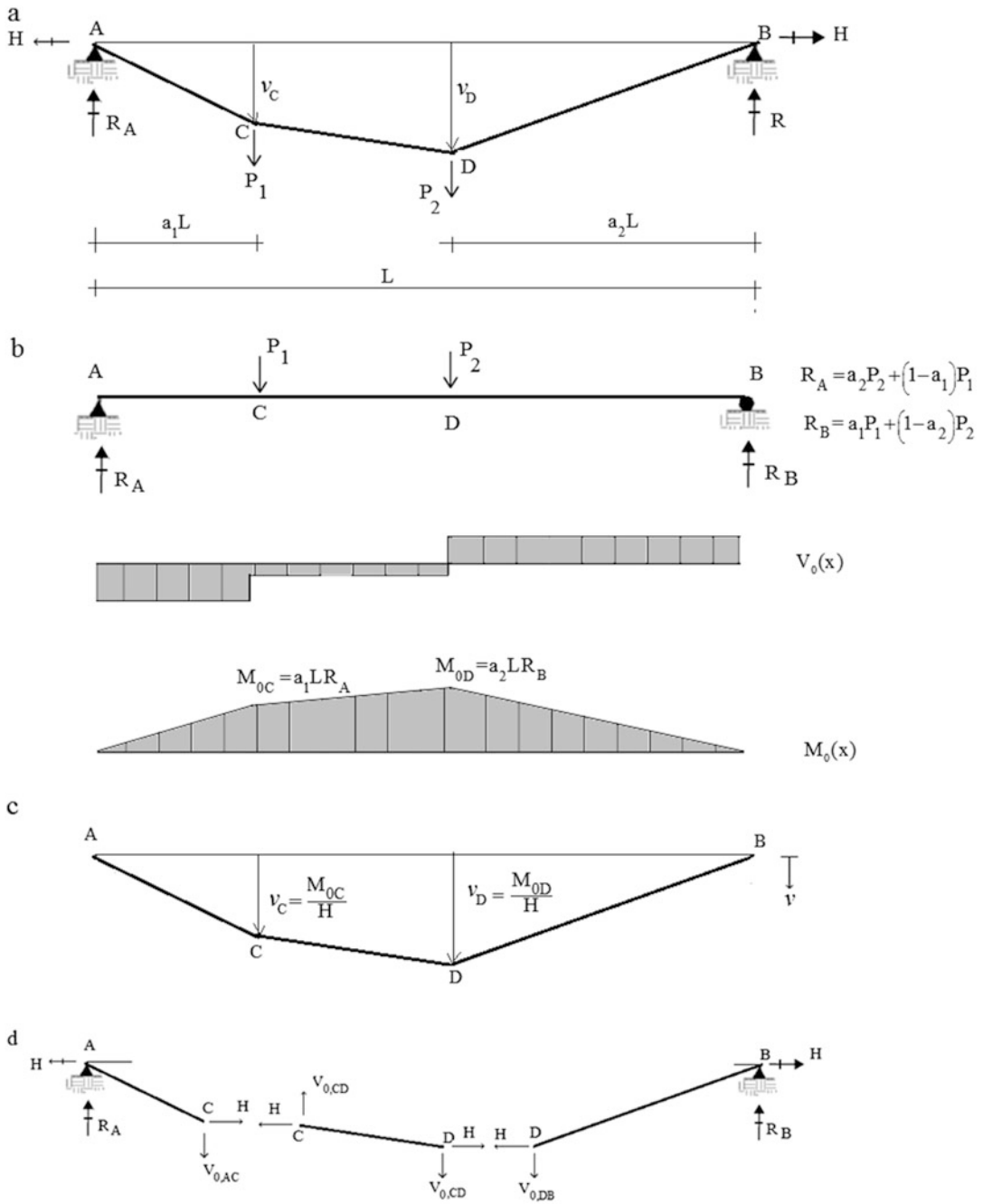


Fig. 5.9 Cable with two concentrated loads. (a) Loading. (b) $V_0(x)$, $M_0(x)$ diagrams. (c) Cable sag profile. (d) Cable tension computation

Determine: The shape corresponding to this loading. Assume (a) $v_D = 6$ ft (b) $v_D = 12$ ft.

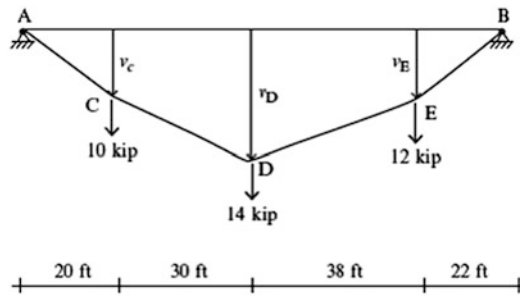


Fig. E5.1a Cable geometry and loading

Solution: First, we find the vertical reactions and generate the shear diagram $V_0(x)$ and moment diagram, $M_0(x)$, treating chord AB as a simply supported beam acted upon by the three vertical forces (Fig. E5.1b).

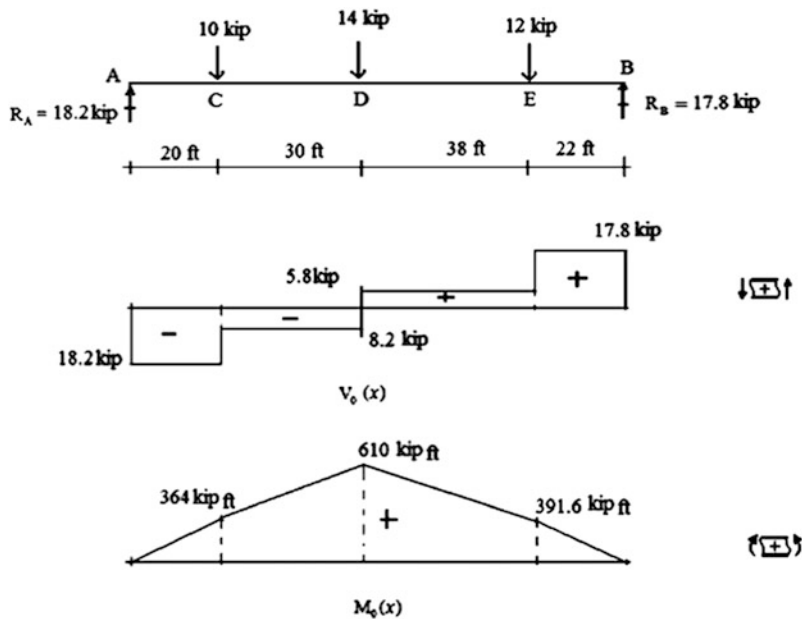


Fig. E5.1b Simply supported beam results

The downward vertical sag from the chord AB is determined with (5.8).

$$+ \downarrow v(x) = \frac{M_0(x)}{H}$$

In order to compute $v(x)$, we need the horizontal force, H .

(a) Taking $v_D = 6$ ft results in

$$6 = \frac{610}{H} \Rightarrow H = 101.67 \text{ kip}$$

The remaining sags are

$$v_C = \frac{364}{101.67} = 3.58 \text{ ft}$$

$$v_E = \frac{391.6}{101.67} = 3.85 \text{ ft}$$

The final results for the shape are plotted below (Fig. E5.1c).

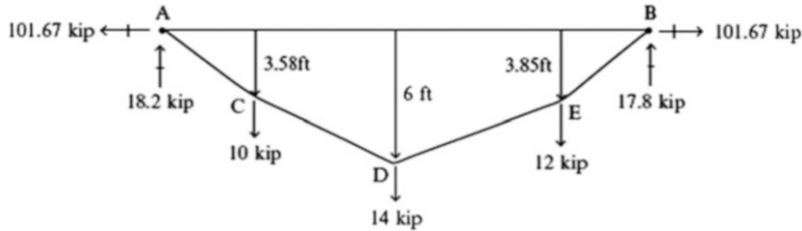


Fig. E5.1c Sag profile for $v_D = 6$ ft

Once the shape is known, one can find the tension in the various segments using (Fig. E5.1d)

$$T = \sqrt{V_o^2 + H^2} = \frac{H}{\cos\theta}$$

Fig. E5.1d Force decomposition

$$T_{AC} = \sqrt{18.2^2 + 101.67^2} = 103.3 \text{ kip}$$

$$T_{CD} = \sqrt{8.2^2 + 101.67^2} = 102 \text{ kip}$$

$$T_{DE} = \sqrt{5.8^2 + 101.67^2} = 101.8 \text{ kip}$$

$$T_{EA} = \sqrt{17.8^2 + 101.67^2} = 103.2 \text{ kip}$$

(b) Taking $v_D = 12$ ft results in

$$H = \frac{610}{12} = 50.83 \text{ kip}$$

$$v_C = \frac{364}{50.83} = 7.16 \text{ ft}$$

$$v_E = \frac{391.6}{50.83} = 7.7 \text{ ft}$$

and

$$T_{AC} = 54 \text{ kip}$$

$$T_{CD} = 51.5 \text{ kip}$$

$$T_{DE} = 51.16 \text{ kip}$$

$$T_{EB} = 53.85 \text{ kip}$$

The sag profile is plotted below (Fig. E5.1e)

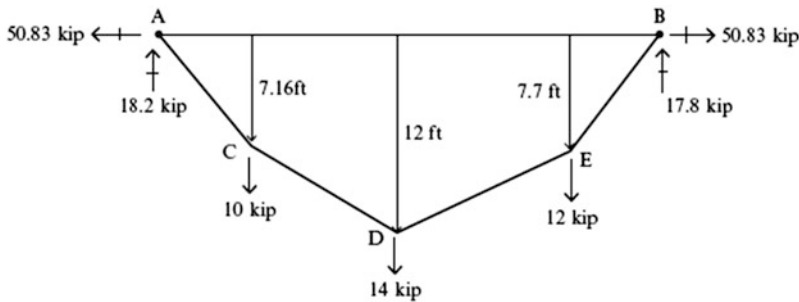
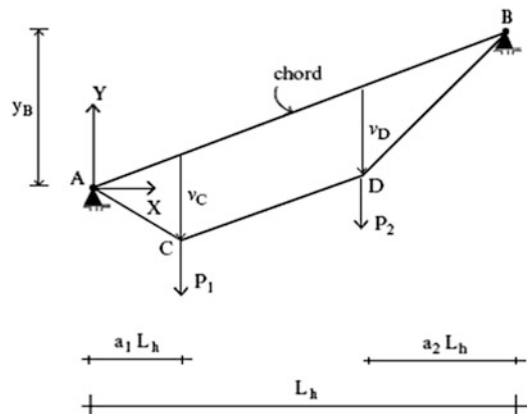


Fig. E5.1e Sag profile for $v_D = 12$ ft

Note that increasing the prescribed value of v_D decreases the cable forces.

5.2.2 Inclined Cables

Fig. 5.10 Inclined cable with concentrated loads



When the cable is inclined, we follow the same approach except that now we measure the *cable sag with respect to the inclined chord*. Consider the cable defined in Fig. 5.10. This example differs from the previous examples only with respect to the inclination of the chord AB.

The reactions and corresponding bending moment distribution generated by the vertical loads are shown in Fig. 5.11. Note that these moment results are identical to the results for the case of a horizontal chord orientation. The reactions generated by the horizontal cable force, H are defined in Fig. 5.12.

Setting the total moment equal to zero leads to

$$\begin{aligned}
 M_0(x) - H \frac{y_B}{L_h} x + H y(x) &= 0 \\
 \Downarrow \\
 M_0(x) &= H \left(\frac{y_B}{L_h} x - y(x) \right) \equiv H v(x) \\
 \Downarrow \\
 v(x) &= \frac{M_0(x)}{H}
 \end{aligned}$$

Note that the solution for $v(x)$ is identical to the results for the horizontal cable except that *now one measures the sag from the inclined chord*.

Fig. 5.11 Simply supported beam results. (a) Vertical loading. (b) $V_0(x)$ diagram. (c) $M_0(x)$ diagram

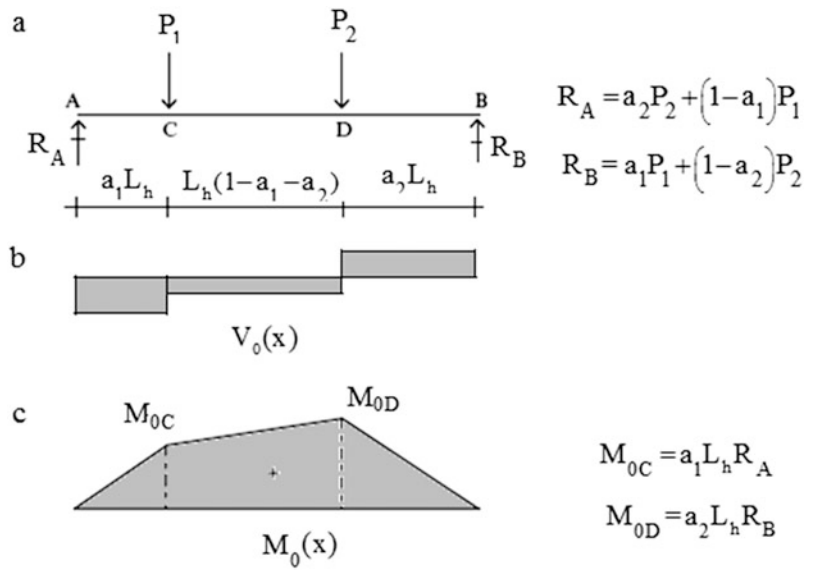
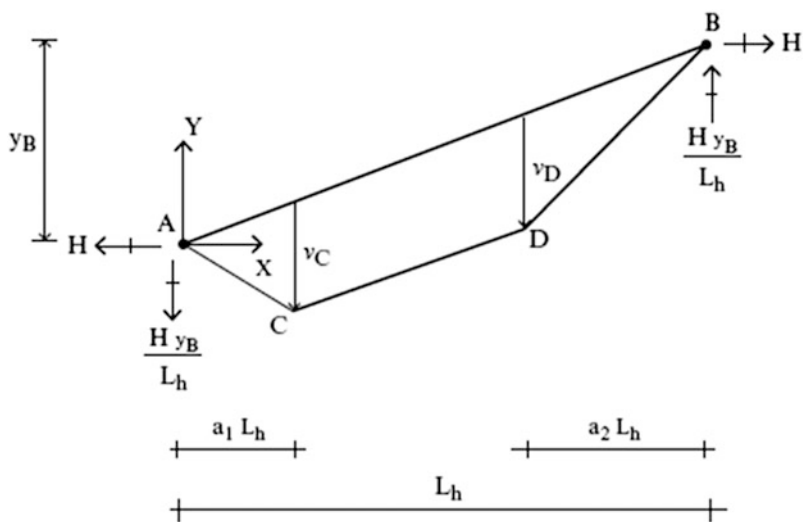


Fig. 5.12 Reactions due to horizontal force, H



Example 5.2 Analysis of an Inclined Cable

Given: The inclined cable and loading shown in Fig. E5.2a.

Determine: The sag of the cable. Assume $v_D = 6$ ft.

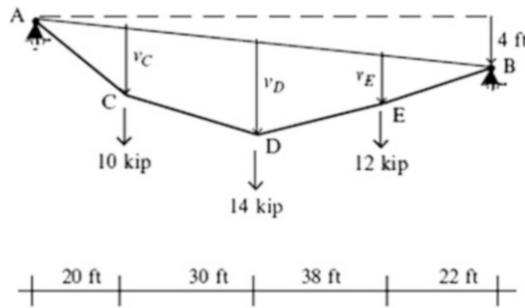


Fig. E5.2a Inclined geometry

Solution: According to the theory presented above, the sag with respect to the inclined chord is given by

$$+ \downarrow v(x) = \frac{M_0(x)}{H}$$

where $M_0(x)$ is the simply supported beam moment (Fig. E5.2b).

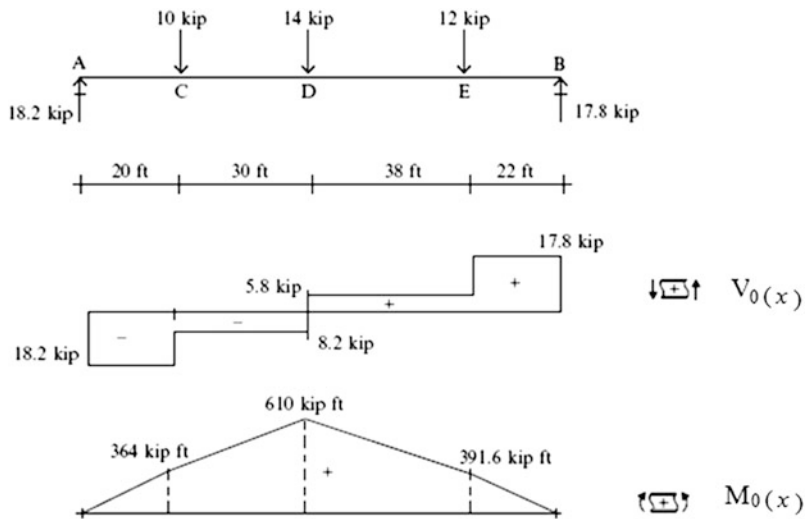


Fig. E5.2b Simply supported beam results

Then,

$$v_C = \frac{364}{H} \quad v_D = \frac{610}{H} \quad v_E = \frac{391.6}{H}$$

For $v_D = 6$ ft, the value of H follows from

$$H = \frac{M_{0D}}{v_D} = \frac{610}{6} = 101.67 \text{ kip}$$

Finally, the values of sag at C and E are

$$v_C = \frac{364}{101.67} = 3.58 \text{ ft}$$

$$v_E = \frac{391.6}{101.67} = 3.85 \text{ ft}$$

To determine the tension, we need to compute the vertical shear in each panel. The vertical reactions due to H (Fig. E5.2c) are

$$\frac{Hy_B}{L} = \frac{101.67(4)}{110} = 3.7 \text{ kip}$$

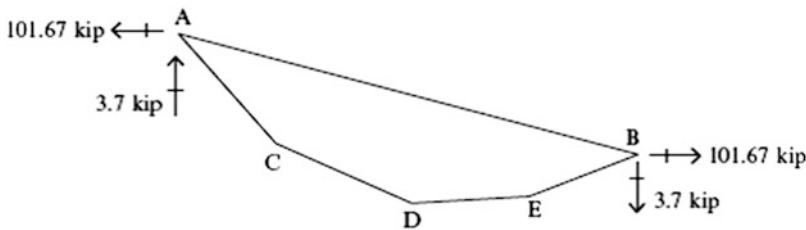


Fig. E5.2c Vertical reactions due to H

The net results for vertical shear are shown in Fig. E5.2d.

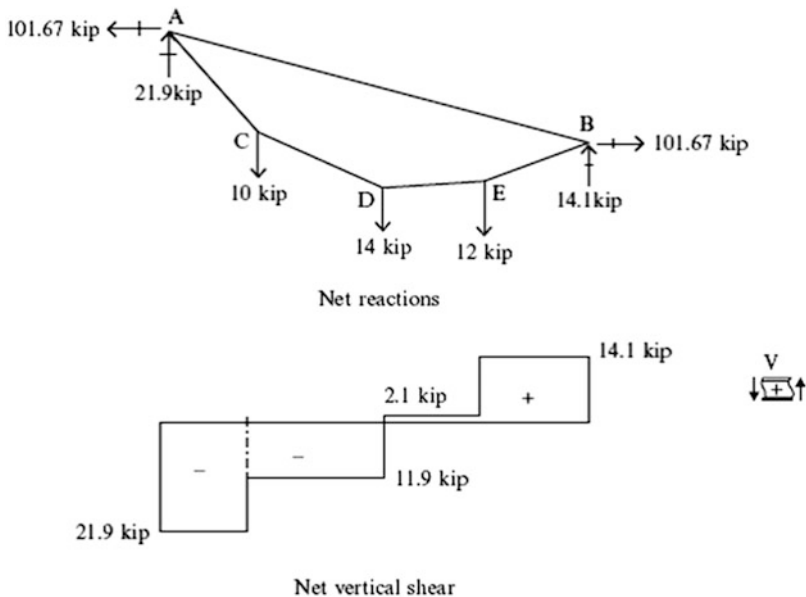


Fig. E5.2d Vertical shear

Lastly, the tension in each segment is computed using these values for V and H . The maximum tension is in segment AC.

$$T_{AC} = \sqrt{21.9^2 + 101.67^2} = 104 \text{ kip}$$

$$T_{CD} = \sqrt{11.9^2 + 101.67^2} = 102.4 \text{ kip}$$

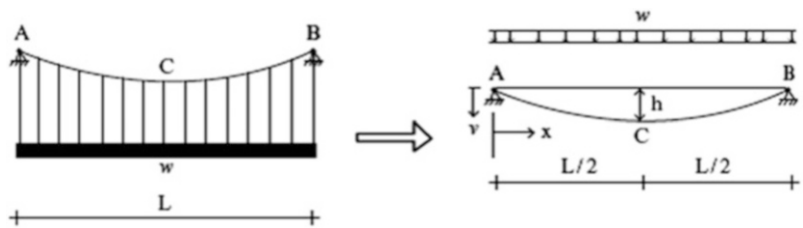
$$T_{DE} = \sqrt{2.1^2 + 101.67^2} = 101.7 \text{ kip}$$

$$T_{EA} = \sqrt{14.09^2 + 101.67^2} = 102.6 \text{ kip}$$

5.3 Cables Subjected to Distributed Loading

5.3.1 Horizontal Cable: Uniform Loading per Horizontal Projection

Fig. 5.13 Cable with a uniformly distributed loading



We consider next the cable system shown in Fig. 5.13. The cable supports a horizontal platform, which in turn, supports a uniform vertical loading. We represent the action of the closely spaced vertical hangers on the cable as a uniform downward loading per unit horizontal projection. The self weight of the cable, which is usually small in comparison to the applied loading, is neglected. Following the procedure described in the previous section, we determine the moment diagram for a simply supported beam spanning between the end supports. *The sag of the cable with respect to the horizontal chord AB is an inverted scaled version of the moment diagram.* The details are shown in Fig. 5.14.

The sag, $\tan \theta$, and T are given by

$$v(x) = \frac{M_0(x)}{H} = \frac{(wL/2)x - (wx^2/2)}{H} = \frac{w}{2H}(Lx - x^2)$$

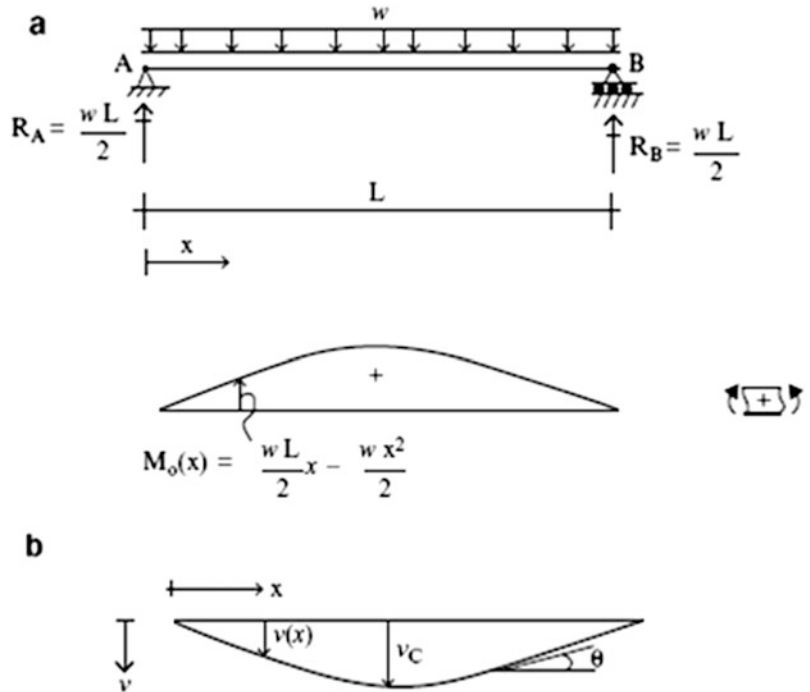
$$\tan \theta = \frac{dv}{dx} = \frac{1}{H} \frac{dM_0(x)}{dx} = \frac{w}{2H}(L - 2x) \quad (5.9)$$

$$T = \frac{H}{\cos \theta}$$

It follows that the shape due to a uniform load is parabolic and the maximum sag occurs at mid-span, point c.

$$v_C = h = \frac{w}{2H}(L^2/2 - L^2/4) = \frac{wL^2}{8H} \quad (5.10)$$

Fig. 5.14 Horizontal cable. (a) Simply supported beam results. (b) Cable sag



Example 5.3

Given: The cable shown in Fig. E5.3a. The loading and desired cable geometry is specified.
Determine: The value of the horizontal tension force, H and the peak value of cable tension, which produces this geometry under the given loading.

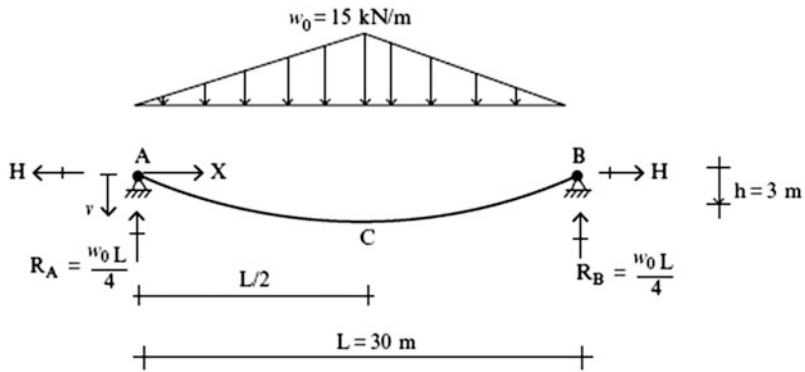
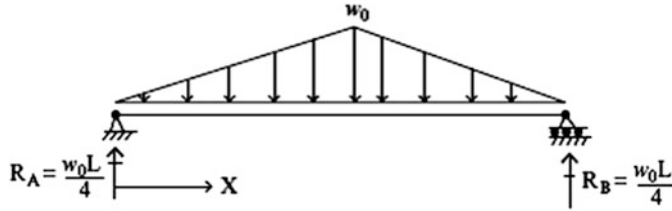


Fig. E5.3a

Solution: We note that the maximum value of ν occurs at $x = L/2$. Then, specializing (5.9) for this value of x leads to the value of H :



$$M_0(x) = \frac{w_0 L}{4} x - \frac{w_0}{3L} x^3 \quad 0 \leq x \leq \frac{L}{2}$$

$$\tan \theta = \frac{1}{H} \frac{dM_0(x)}{dx} = \frac{1}{H} \left(\frac{w_0 L}{4} - \frac{w_0}{L} x^2 \right)$$

$$H = \frac{M_0(x=L/2)}{v_C} = \frac{w_0 L^2}{12} \frac{1}{v_C} = \frac{(15)(30)^2}{12(3)} = 375 \text{ kN}$$

The tension is related to H by:

$$T = \frac{H}{\cos \theta}$$

The peak values of θ occur at $x = 0$ and $x = L$.

$$\tan \theta_{\text{at } x=0} = \frac{1}{H} \left(\frac{w_0 L}{4} \right) = \frac{(15)(30)}{(375)(4)} = 0.3$$

$$\theta_{\text{at } x=0} = 16.7^\circ$$

It follows that

$$\theta_{\text{max}} = \pm 16.7^\circ$$

$$T_{\text{max}} = \frac{H}{\cos \theta} = 391.5 \text{ kN}$$

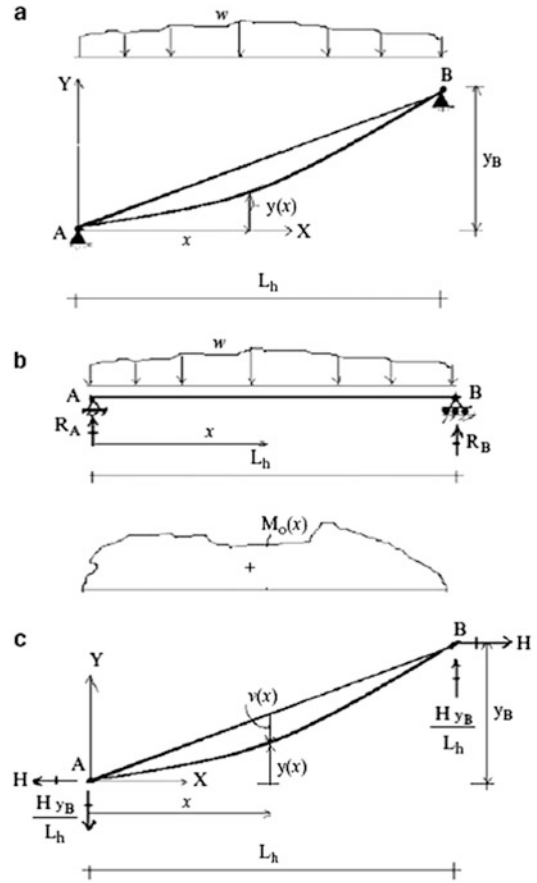
5.3.2 Inclined Cables

Suppose the cable is inclined and subjected to an arbitrary loading. We define the shape by the function $y(x)$. Figure 5.15 defines this notation.

Since the cable has no bending rigidity, the shape of the cable must adjust itself so that the resultant moment due to the vertical load and H vanishes at all points along the cable. Then, setting the total moment at x equal to zero leads to

$$\begin{aligned} \sum M_{\text{at } x} &= M_0(x) + Hy(x) - \frac{Hy_B}{L_h} x = 0 \\ &\Downarrow \\ y(x) &= \frac{y_B}{L_h} x - \frac{M_0(x)}{H} \end{aligned} \quad (5.11)$$

Fig. 5.15 Inclined cable geometry—arbitrary loading. (a) Geometry—arbitrary loading. (b) Simply supported beam results. (c) Reactions due to horizontal force, H



We note from Fig. 5.15 that

$$\frac{y(x) + v(x)}{x} = \frac{y_B}{L_h} \quad (5.12)$$

$$\Downarrow$$

$$y(x) = \frac{y_B}{L_h}x - v(x)$$

Finally, equating (5.11) and (5.12) leads to the expression for the sag,

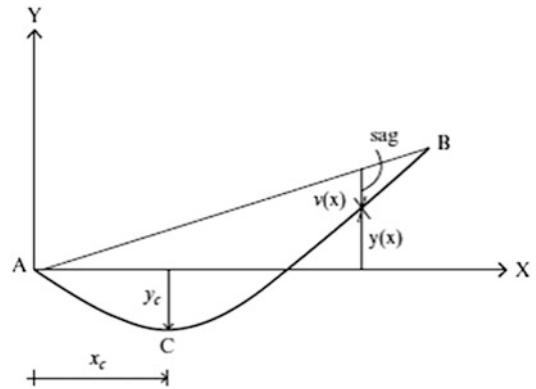
$$v(x) = \frac{M_0(x)}{H} \quad (5.13)$$

We observe that the solution for the sag is identical to the result that we obtained for the horizontal chord orientation *except now one measures the sag from the inclined chord*. The solution is also similar to the case of a set of concentrated loads.

The lowest point on the cable (point C in Fig. 5.16) is determined by setting the slope equal to zero.

$$\left. \frac{dy}{dx} \right|_{x_c} = 0 \quad (5.14)$$

Fig. 5.16 Cable geometry—lowest point



Noting (5.11),

$$\frac{y_B}{L_h} - \frac{1}{H} \frac{dM_0(x)}{dx} = 0 \quad (5.15)$$

For the case where the distributed load is uniform, $M_0(x)$ is parabolic, and (5.15) expands to

$$\frac{y_B}{L_h} - \frac{1}{H} \left(-wx_c + \frac{wL_h}{2} \right) = 0 \quad (5.16)$$

Solving for x leads to

$$x_c = \frac{L_h}{2} - \frac{y_B H}{L_h w} \quad (5.17)$$

For an arbitrary loading, we need to use (5.15).

Example 5.4

Given: The inclined cable is defined in Fig. E5.4a. Point C is the lowest point of the cable.

Determine: The coordinates of point C and the peak values of cable tension.

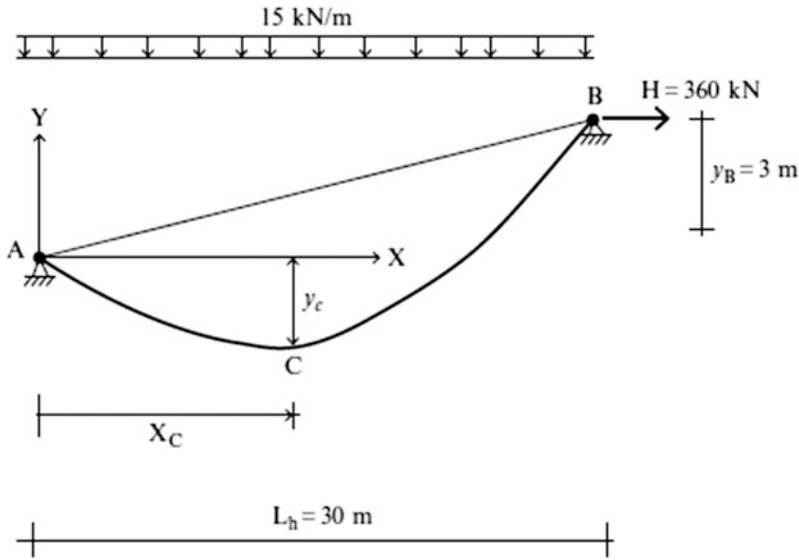


Fig. E5.4a

Solution: Noting (5.17),

$$x_C = \frac{L_h}{2} - \frac{y_B H}{L_h w} = \frac{30}{2} - \frac{3}{30} \left(\frac{360}{15} \right) = 12.6 \text{ m}$$

Applying (5.11) for point C,

$$\begin{aligned} y_C &= x_C \frac{y_B}{L_h} - \frac{w}{2H} \left\{ L_h x_C - (x_C)^2 \right\} = 12.6 \left(\frac{3}{30} \right) - \frac{15}{2(360)} \left(30(12.6) - (12.6)^2 \right) \\ &= -3.3 \text{ m} \end{aligned}$$

Given H , we can find the cable tension at any point with:

$$T = \frac{H}{\cos \theta}$$

where

$$\tan \theta = \frac{dy}{dx} = \frac{y_B}{L_h} - \frac{wL_h}{2H} + \frac{wx}{H}$$

The critical locations are at the support points A and B.

$$\begin{aligned} \tan \theta_A &= \frac{3}{30} - \frac{15(30)}{2(360)} = -0.525 \quad \theta_A = -27.7^\circ \\ \tan \theta_B &= \frac{3}{30} - \frac{15(30)}{2(360)} + \frac{15(30)}{360} = +0.725 \quad \theta_B = +35.9^\circ \\ T_A &= \frac{H}{\cos \theta_A} = 406.6 \text{ kN} \\ T_{\max} = T_B &= \frac{H}{\cos \theta_B} = 444.6 \text{ kN} \end{aligned}$$

5.4 Advanced Topics

This section deals with the calculation of arch length, the axial stiffness, and the effect of temperature. We also discuss a modeling strategy for cable-stayed structures such as guyed towers and cable-stayed bridges.

5.4.1 Arc Length

We consider first the uniformly loaded horizontal cable shown in Fig. 5.17. We have shown that the sag profile due to a uniform load is parabolic,

$$v(x) = \frac{wL}{2H}x - \frac{wx^2}{2H}$$

and the maximum sag occurs at mid-span,

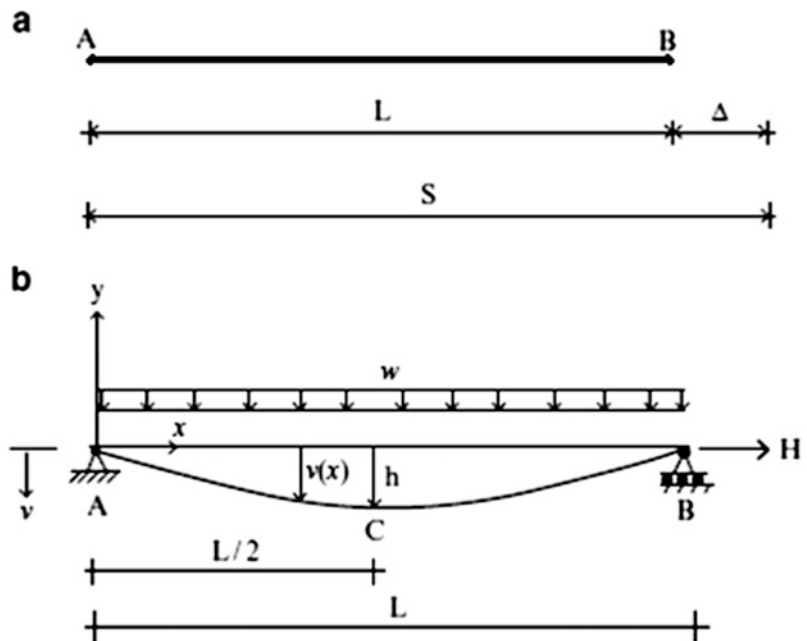
$$v_{\max} \equiv h = \frac{wL^2}{8H}$$

Given H and L , of interest is the total arc length of the cable. We need this quantity in order to determine the effect on the cable geometry of a temperature increase in the cable. Figure 5.17 shows the initial and loaded shapes of the cable. Note that the deformed length is greater than L . We denote this quantity as $L + \Delta$.

The differential arc length, ds , is related to its horizontal and vertical projections by

$$ds = \sqrt{dx^2 + dy^2} = dx\sqrt{1 + \left(\frac{dy}{dx}\right)^2} \tag{5.18}$$

Fig. 5.17 Cable geometry. (a) Initial unloaded. (b) Loaded shape



Integrating between 0 and L leads to an expression for the total arc length

$$S = \int_0^L \left\{ 1 + \left(\frac{dy}{dx} \right)^2 \right\}^{\frac{1}{2}} dx \quad (5.19)$$

Given $y(x)$, one evaluates the integral using either symbolic or numerical integration. When the cable is horizontal, $y(x) = -v(x)$.

$$y(x) = \frac{wL}{2H} \left(-x + \frac{x^2}{L} \right) = \frac{4h}{L} \left(-x + \frac{x^2}{L} \right)$$

When the maximum sag h is small with respect to L , we can assume that dy/dx is small with respect to 1 and simplify the integral in (5.19) using the following binominal series expression,

$$(1 + f)^{\frac{1}{2}} = 1 + \frac{1}{2}f - \frac{1}{8}f^2 + \dots \quad (5.20)$$

$$|f| < 1$$

Taking $f = (dy/dx)^2$ and retaining only the first three terms, we obtain the following approximation for S :

$$S \approx \int_0^L \left\{ 1 + \frac{1}{2} \left(\frac{dy}{dx} \right)^2 - \frac{1}{8} \left(\frac{dy}{dx} \right)^4 \right\} dx \quad (5.21)$$

Noting Fig. 5.17a, we see that $\Delta \approx \frac{1}{2} \int_0^L \left(\frac{dy}{dx} \right)^2 dx$ for a small sag ratio.

Lastly, we evaluate S for the case when the loading is uniform. Retaining the first three terms in (5.21) leads to

$$S \approx L \left\{ 1 + \frac{8}{3} \left(\frac{h}{L} \right)^2 - \frac{32}{5} \left(\frac{h}{L} \right)^4 \right\} \quad (5.22)$$

We refer to h/L as the sag ratio. Equation (5.22) shows that the effect of decreasing the sag ratio is to transform the “curved” cable to essentially a straight segment connecting the two end points. *The cables used for guyed towers and cable-stayed bridges have small sag ratios and are approximated as equivalent straight axial elements. We will discuss this topic in a later section.*

Example 5.5

Given: The cable defined in Fig. E5.5a.

Determine: The length of the cable corresponding to this geometry. Also determine the change in geometry due to a temperature increase of 150 °F. Take $\alpha = 6.6 \times 10^{-6}/^\circ\text{F}$.

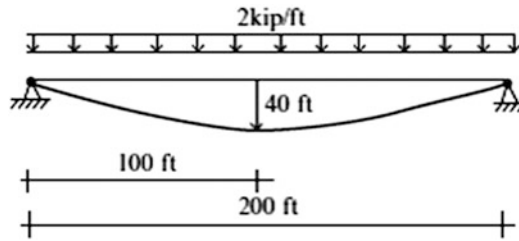


Fig. E5.5a

Solution: The horizontal reaction due to the loading shown is

$$H = \frac{wL^2}{8h} = 250 \text{ kip}$$

We evaluate S using (5.22),

$$S = 200 \left\{ 1 + \frac{8}{3} \left(\frac{40}{200} \right)^2 - \frac{32}{5} \left(\frac{40}{200} \right)^4 \right\} = 200 \{ 1 + 0.107 - 0.01 \}$$

$$S = 219.4 \text{ ft}$$

The change in cable length due to a temperature increase is

$$\Delta S = S(\alpha \Delta T) \approx 219.4(6.6 \times 10^{-6})(150) \approx 0.217 \text{ ft}$$

This length change produces a change in the sag. We differentiate (5.22) with respect to h ,

$$\frac{dS}{dh} \approx \frac{16h}{3L} - \frac{128}{5} \left(\frac{h}{L} \right)^3$$

and solve for dh .

$$dh \approx \frac{dS}{(16/3)(h/L) \left\{ 1 - 4.8(h/L)^2 \right\}}$$

Substituting for dS leads to

$$dh \approx \frac{0.217}{(16/3)(40/200) \left\{ 1 - 4.8(40/200)^2 \right\}} = 0.25 \text{ ft}$$

Finally, we update H using the new values for $h = 40 + 0.25 = 40.25$ ft

$$H = \frac{wL^2}{8h} = \frac{2(200)^2}{8(40.25)} = 248.5 \text{ kip}$$

The effect of temperature increase on H is small for this geometry.

Example 5.6

Given: The uniformly loaded inclined cable is shown in Fig. E5.6a.

Determine: The sag profile and total arc length.

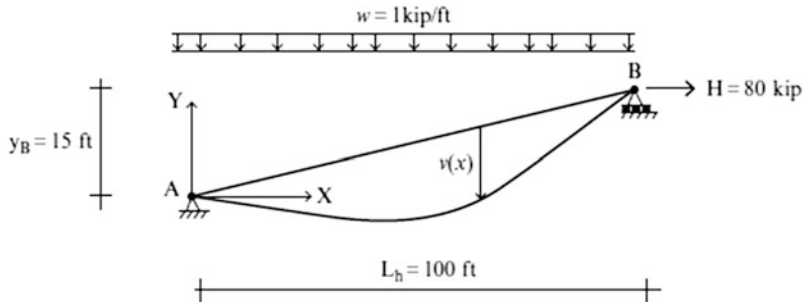


Fig. E5.6a

Solution: The profile defined in terms of $y(x)$ is given by (5.11). For the given dimensions, it expands to

$$\begin{aligned} y(x) &= \frac{y_B}{L_h}x - \frac{M_0(x)}{H} \\ &= \frac{15}{100}x - \left(50x - \frac{x^2}{2}\right)\frac{1}{80} \end{aligned}$$

Then, the sag profile is given by

$$v(x) = +\left(50x - \frac{x^2}{2}\right)\frac{1}{80} = \frac{5}{8}x - \frac{x^2}{160}$$

We determine the total arc length using (5.19).

$$S = \int_0^{L_h} \left\{ 1 + \left(\frac{dy}{dx}\right)^2 \right\}^{1/2} dx$$

Substituting for $y(x)$, S expands to

$$S = \int_0^{100} \left\{ 1 + \left[\frac{15}{100} - \frac{1}{80}(50 - x) \right]^2 \right\}^{1/2} dx$$

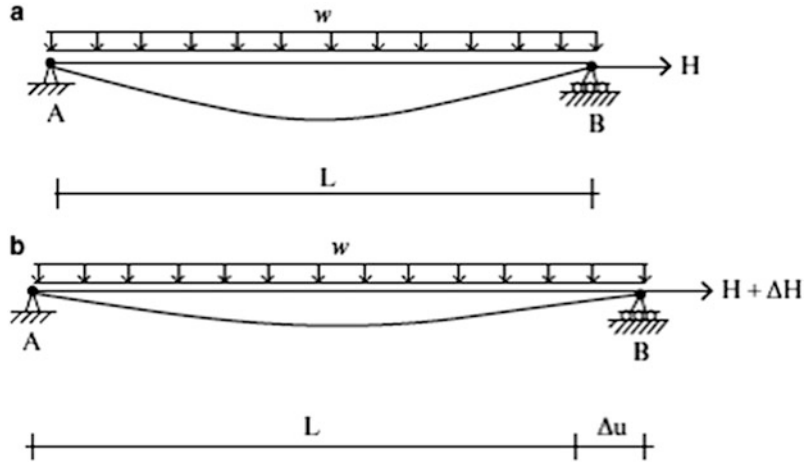
We evaluate the integral using numerical integration. The result is

$$S = 107.16 \text{ ft}$$

5.4.2 Equivalent Axial Stiffness

In what follows, we establish a procedure for modeling a shallow horizontal cable as an equivalent straight axial member. Consider the cable shown in Fig. 5.18. Suppose the horizontal force, H , is increased by a small amount, say ΔH . This action causes the support at B to displace horizontally, an amount Δu . The ratio $\Delta H/\Delta u$ is a measure of the axial stiffness for the cable. We interpret it as the tangent stiffness since we perturbed the system from a “loaded” state.

Fig. 5.18 Actual and perturbed configurations



We generate an expression for the tangent stiffness in the following way. We start with the straight unloaded cable shown in Fig. 5.19 and apply a horizontal force. The cable stretches an amount u_1 . Next, we apply the uniform downward load, holding H constant. Point B moves to the left, an amount u_2 . We estimate u_2 using (5.21) specified for a parabolic shape and *small* sag ratio,

$$u_2 \approx \int_0^L \frac{1}{2} \left(\frac{dy}{dx} \right)^2 dx = \frac{w^2 L^3}{24H^2}$$

The net motion of B is u_B .

$$u_B = u_1 - u_2 = \frac{HL}{AE} - \frac{w^2 L^3}{24H^2} \tag{5.23}$$

Equation (5.23) is plotted in Fig. 5.20. For large H , the first term dominates and the behavior approaches the behavior of an axial member. We want to determine dH/du . Since u_B is a nonlinear function of H , we first find the derivative du/dH , and then invert.

$$\begin{aligned} \frac{du_B}{dH} &= \frac{L}{AE} + \frac{w^2 L^3}{12H^3} = \frac{L}{AE} \left\{ 1 + \frac{1}{12} \frac{AE}{H} \left(\frac{wL}{H} \right)^2 \right\} \\ &\quad \downarrow \\ \frac{dH}{du_B} &= k_t = \left(\frac{1}{1 + (1/12)(AE/H)(wL/H)^2} \right) \frac{AE}{L} \end{aligned} \tag{5.24}$$

Fig. 5.19 Deflection patterns

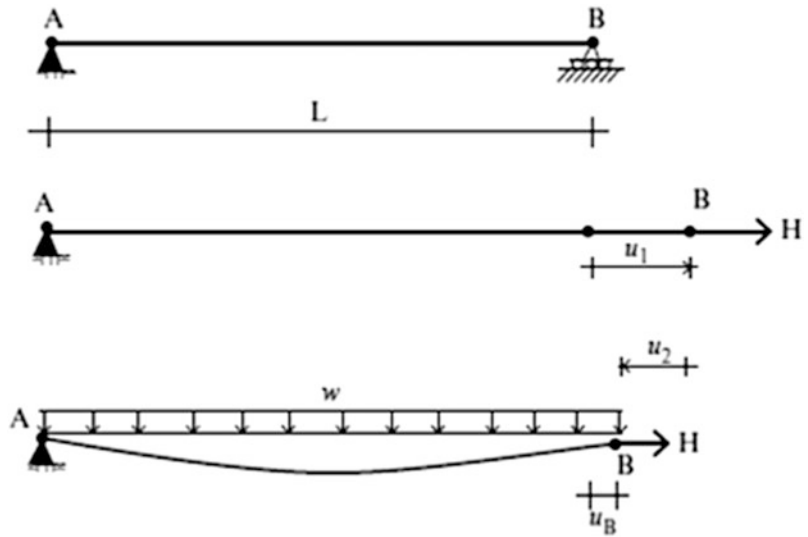
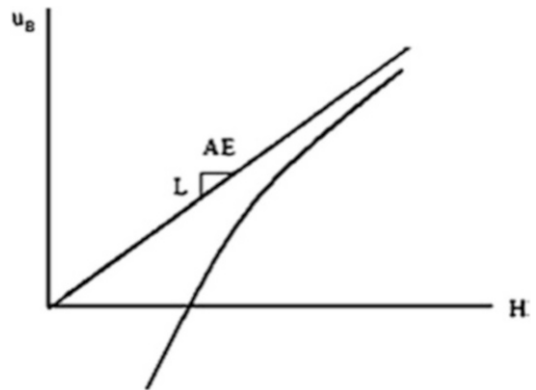


Fig. 5.20 u_B vs. H relationship



Note that AE/L is the axial stiffness of a straight member. Equation (5.24) shows that the tangent stiffness for the horizontal cable approaches AE/L as the tension H is increased.

The tangent stiffness k_t can also be expressed in terms of a modified elastic modulus E_{eq} .

We write (5.24) as $k_t = (A/L)E_{eq}$. Then, the definition equation for E_{eq} follows:

$$E_{eq} = \frac{E}{1 + (1/12)(AE/H)(wL/H)^2} \tag{5.25}$$

In general, $E_{eq} < E$. Substituting the terms,

$$\frac{A}{H} = \frac{1}{\sigma}$$

$$\frac{wL}{H} = 8 \left(\frac{h}{L} \right)$$

transforms (5.25) to

$$E_{eq} = \frac{E}{1 + (16/3)(E/\sigma)(h/L)^2} \tag{5.26}$$

where σ is the stress in the cable. It follows that the equivalent modulus depends on the initial stress in the cable and the sag ratio. A typical value of initial stress is on the order of 50–100 ksi (344,700–1,034,100 kN/m²). Values of sag ratio range from 0.005 to 0.02. The corresponding variation in E_{eq} for a steel cable with $\sigma = 50$ ksi (344,700 kN/m²) is tabulated below.

E/σ	h/L	E_{eq}/E
580	0.005	0.928
	0.01	0.764
	0.02	0.447

Note that a typical sag ratio of 0.01 results in a 25 % reduction in E . One uses high-strength steel strands, on the order of 150 ksi (1,034,100 kN/m²) yield stress, for cable-stayed structures in order to minimize their loss of stiffness due to cable sag.

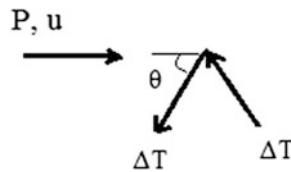
5.4.3 Equivalent Axial Stiffness for an Inclined Cable

In this section, we extend the modeling strategy to deal with shallow inclined cables. Inclined cables with *small sag* ratios are used in cable-stayed bridges and also as supports for guyed towers. Figure 5.21 shows the Millau Viaduct Bridge in France. Figure 5.22 illustrates a two-cable scheme for a guyed tower subjected to wind loading.

We model each cable as a straight axial member with a modulus of elasticity, E_{eq} which depends on the initial tension and geometry of the cable. This approach is reasonable when the changes in geometry and tension due to the applied load are small in comparison to the initial properties.

Equilibrium of the tower requires

$$2\Delta T \cos \theta = P \quad (5.27)$$



The corresponding extension of the “equivalent” straight member due to ΔT is:

$$\Delta e = \frac{\Delta T L}{AE_{\text{eq}}} \quad (5.28)$$

Lastly, we relate Δe to the horizontal displacement u .

$$\Delta e = u \cos \theta$$

Combining these equations leads to an expression relating P and u .

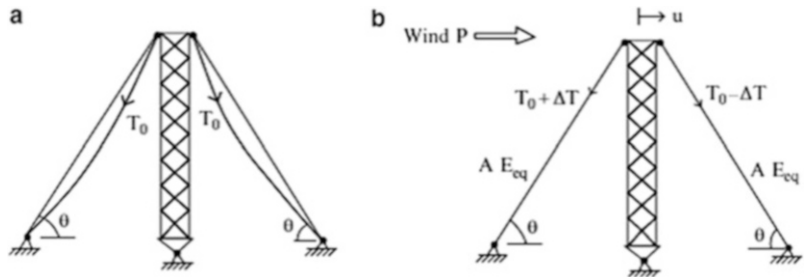
$$P = \left[\frac{2AE_{\text{eq}}}{L} (\cos \theta)^2 \right] u \quad (5.29)$$

The bracketed term represents the lateral stiffness of the tower for a lateral load applied at the top of the tower. Given E_{eq} , one can evaluate the lateral response of the tower with (5.29).



Fig. 5.21 Millau Viaduct Bridge in France

Fig. 5.22 Guyed tower modeling scheme.
 (a) Initial position.
 (b) Loaded position



We develop an expression for E_{cq} by modifying (5.25). Figure 5.23 shows a typical inclined cable and the notation introduced here. The loading acting on the cable is assumed to be the self weight, w_g . Also when the cable is rotated from the horizontal position up to the inclined position, H is now the cable tension, T ; the normal distributed load w becomes $w_g \cos \theta$; and the loading term becomes

$$wL = (w_g \cos \theta)L = w_g L_h \tag{5.30}$$

Substituting for these terms in (5.25) leads to

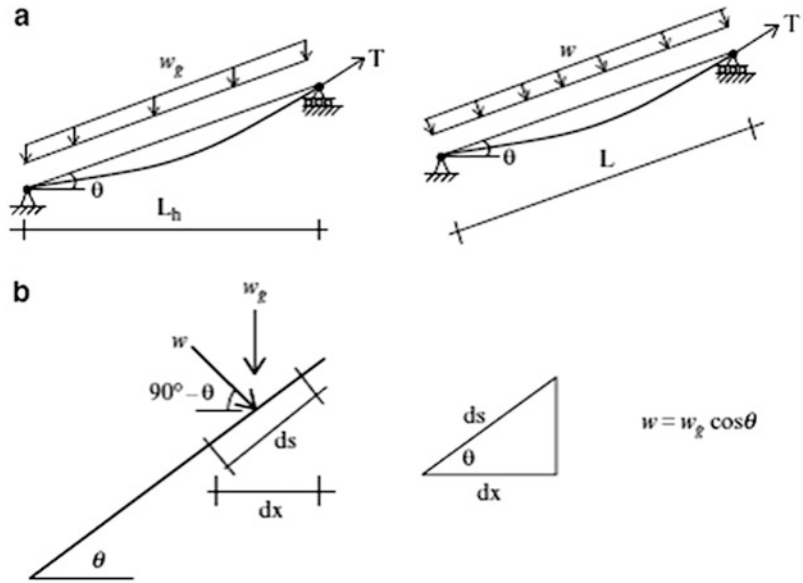
$$E_{cq} \approx \frac{E}{1 + (1/12)(AE/T)(w_g L_h/T)^2} \tag{5.31}$$

Lastly, we introduce the following definitions involving the initial stress and weight density,

$$\frac{A}{T} = \frac{1}{\sigma} \tag{5.32}$$

$$w_g = \gamma_g A$$

Fig. 5.23 Inclined cable geometry. (a) Vertical versus normal loading. (b) Loading components



The final form of (5.31) for an individual cable is

$$E_{eq} = \frac{E}{1 + (1/12)(E/\sigma)(\gamma_g L_h/\sigma)^2} \tag{5.33}$$

Equation (5.33) is known as Ernst’s Formula. This expression is used when modeling the cables in a cable-stayed scheme with equivalent axial member properties.

Example 5.7

Given: The steel cable shown in Fig. E5.7a. Take the initial stress as 700 MPa.

Determine: The equivalent modulus, E_{eq} .

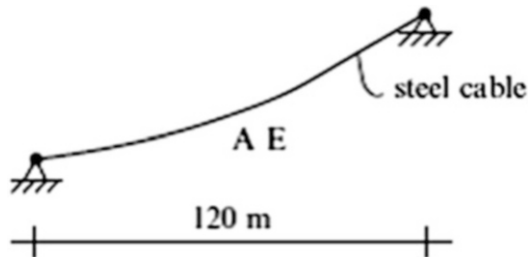
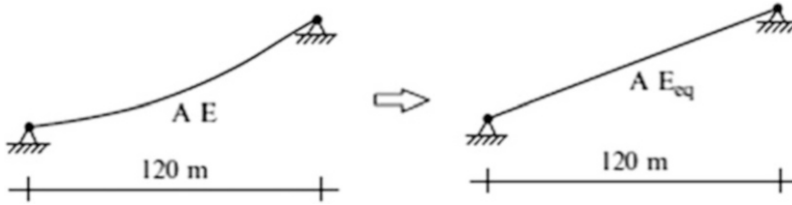


Fig. E5.7a

Solution: The properties of steel are $E = 200$ GPa and $\gamma_g = 77$ kN/m³. Substituting these values in (5.33) leads to

$$\frac{E_{eq}}{E} = \frac{1}{1 + (1/12)(200(10^3)/700)(77(120)/700,000)^2} = 0.996$$

One uses E_{eq} when specifying the properties of the “equivalent” straight axial member.



5.4.4 Cable Shape Under Self Weight: Catenary

There are cases where the loading on a cable is due only to self weight. Electrical transmission lines are one example. The previous analyses have assumed the loading is defined in terms of the horizontal projection (dx). This assumption is reasonable when the slope of the cable is small. In order to investigate the case when the slope is not small, we need to work with the exact equilibrium equation.

Consider the segment shown in Fig. 5.24b. Enforcing equilibrium and noting that the loading is vertical leads to following equations:

$$\begin{aligned}\sum F_y = 0 \quad \frac{d}{dx}(T \sin \theta) dx &= w_g ds \\ \sum F_x = 0 \quad \frac{d}{dx}(T \cos \theta) &= 0 \Rightarrow T \cos \theta = \text{Constant} = H\end{aligned}\quad (5.34)$$

Substituting for T

$$T = \frac{H}{\cos \theta} \Rightarrow T \sin \theta = H \tan \theta = H \frac{dy}{dx}$$

in the first equation in (5.34) leads to

$$H \frac{d^2 y}{dx^2} = w_g \frac{ds}{dx} = w_g \left\{ 1 + \left(\frac{dy}{dx} \right)^2 \right\}^{\frac{1}{2}} \quad (5.35)$$

The general solution of (5.35) is

$$y = \frac{H}{w_g} \cosh\left(\frac{w_g}{H}x + c_1\right) + c_2 \quad (5.36)$$

where c_1 and c_2 are integration constants which are determined using the coordinates of the support points. For the unsymmetrical case, we locate the origin at the left support (Fig. 5.24a). When the cable is symmetrical, it is more convenient to locate the origin at the lowest point.

We consider the symmetrical case shown in Fig. 5.25. We locate the origin at the lowest point. Then for this choice,

$$\begin{aligned}c_1 &= 0 \\ c_2 &= -\frac{H}{w_g}\end{aligned}$$

Fig. 5.24 (a) Cable shape under self weight—catenary. (b) Differential segment

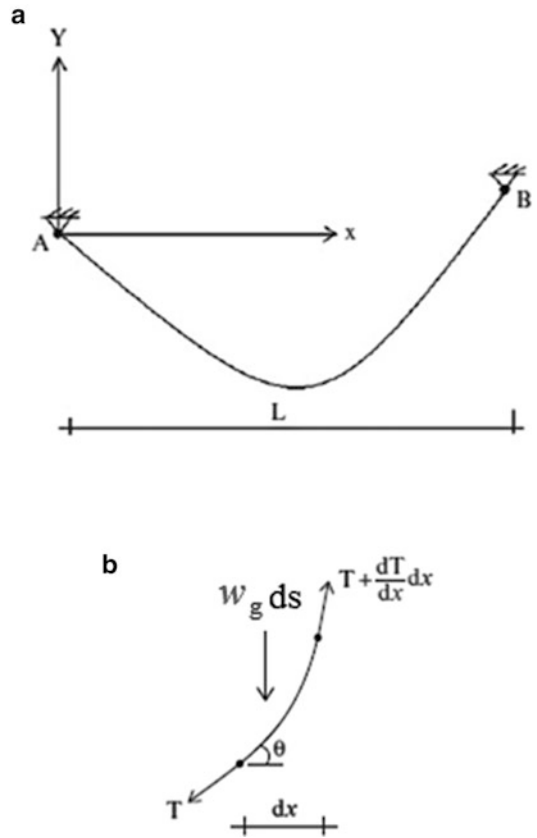
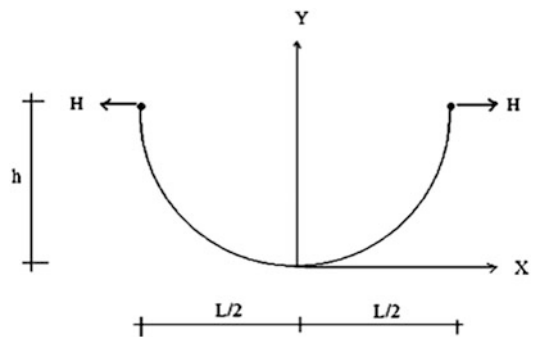


Fig. 5.25 Catenary—symmetrical



and

$$y = \frac{H}{w_g} \left\{ \cosh\left(\frac{w_g x}{H}\right) - 1 \right\}$$

The force H is determined from the condition $y(L/2) = h$

$$h = \frac{H}{w_g} \left\{ \cosh\left(\frac{w_g L}{2H}\right) - 1 \right\} \tag{5.37}$$

We need to solve (5.37) using iteration since it is a transcendental equation.

Expanding the cosh term,

$$\begin{aligned}\cosh x &= 1 + \frac{x^2}{2} + \frac{x^4}{24} + \cdots + \frac{x^n}{n!} \\ &= 1 + \frac{x^2}{2} \left\{ 1 + \frac{x^2}{12} + \cdots + 2 \frac{x^{(n-2)}}{n!} \right\}\end{aligned}\quad (5.38)$$

and noticing that when x^2 is small with respect to 1, the expression can be approximated as

$$\cosh x \approx 1 + \frac{x^2}{2} \left\{ 1 + \frac{x^2}{12} \right\}$$

and taking $x = \frac{w_g L}{2H}$ leads to

$$h \approx \frac{w_g L^2}{8H} \left\{ 1 + \frac{1}{12} \left(\frac{w_g L}{2H} \right)^2 \right\} \quad (5.39)$$

When the loading is assumed to be per unit projected length, the corresponding expression for h is $h = wL^2/8H$. For a given H , h is larger for the self weight case. Also for a given h , H is larger for the self weight case. The difference increases with the sag ratio, h/L .

We find the arc length using (5.35).

$$H \frac{d^2 y}{dx^2} dx = w_g ds$$

Integrating,

$$\begin{aligned}S &= 2 \int_0^{\frac{L}{2}} \left(\frac{1}{w_g} \right) H \frac{d^2 y}{dx^2} dx = \frac{2}{w_g} H \frac{dy}{dx} \Big|_0^{\frac{L}{2}} \\ S &= \frac{2H}{w_g} \sinh \left(\frac{w_g L}{2H} \right)\end{aligned}\quad (5.40)$$

The maximum tension, which occurs at $x = \pm (L/2)$, is determined using

$$T_{\max} = H \cosh \left(\frac{w_g L}{2H} \right) \quad (5.41)$$

Example 5.8

Given: The cable shown in Fig. E5.8a has a self weight of 1.2 kip/ft.

Determine: The arc length, h the maximum tension in the cable using the catenary equations, and the percent of error in the maximum tension value when using parabolic equations. Consider the following values for H : $H = 75, 100, \text{ and } 250$ kip.

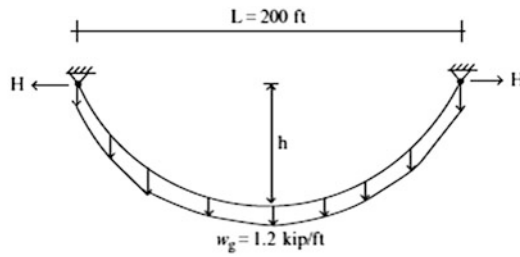


Fig. E5.8a

Solution: The relevant equations are listed below.

$$h = \frac{H}{w_g} \left\{ \cosh \left(\frac{w_g L}{2H} \right) - 1 \right\}$$

$$h_{ap} \approx \frac{w_g L^2}{8H} \left\{ 1 + \frac{1}{12} \left(\frac{w_g L}{2H} \right)^2 \right\}$$

$$S = \frac{2H}{w_g} \sinh \left(\frac{w_g L}{2H} \right)$$

$$T_{max} = H \cosh \left(\frac{w_g L}{2H} \right)$$

These equations are evaluated using a digital computer. The results are summarized in the table below. Note that when h/L is large, the error introduced by the parabolic approximation is significant.

H	Catenary				Parabola		
	S	h	h_{ap}	T_{max}	h	T_{max}	% difference T_{max}
75	296.9	98.6	97	193	80	141.5	27 %
100	251.6	67.5	67.2	181	60	156.2	14 %
250	207.7	24.5	24.5	279	24	277.3	1 %

5.5 Summary

5.5.1 Objectives

- To describe how a cable adjusts its geometry when subjected to a single vertical concentrated load.
- To extend the analysis to a cable subjected to multi-concentrated vertical loads.
- To derive an expression for the deflected shape of the cable when subjected to an arbitrary vertical loading.
- To present a series of examples which illustrate the computational procedure for finding the deflected shape of a cable.
- To derive an approximate expression for the equivalent axial stiffness of a cable modeled as a straight member.

5.5.2 Key Concepts

- Given a cable supported at two points, A and B, and subjected to a vertical loading. The vertical deflection from the chord connecting points A and B is proportional to the bending moment M in a simply supported beam spanning between A and B. One finds the bending moment diagram using a simple equilibrium analysis. The deflection of the cable with respect to the chord AB is an inverted scaled version of the moment diagram.
- Under vertical loading, the horizontal component of the cable force is constant.
- The length of the cable is determined by integrating

$$S = \int_0^L ds = \int_0^L \sqrt{1 + \left(\frac{dy}{dx}\right)^2} dx$$

where

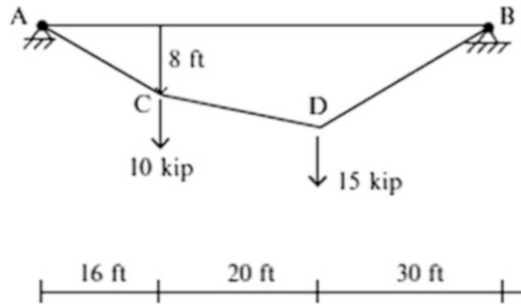
$$y = -\frac{M_0(x)}{H} + \frac{y_B}{L_h}x$$

One usually approximates the integrand with $ds \approx 1 + (1/2) (dy/dx)^2$ when $(dy/dx)^2$ is small in comparison to 1.

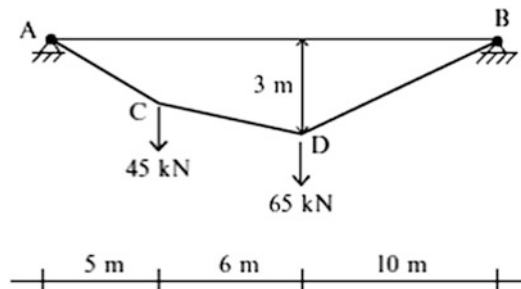
5.6 Problems

For Problems 5.1–5.8, determine the reactions at the supports, and the tension in each segment of the cable.

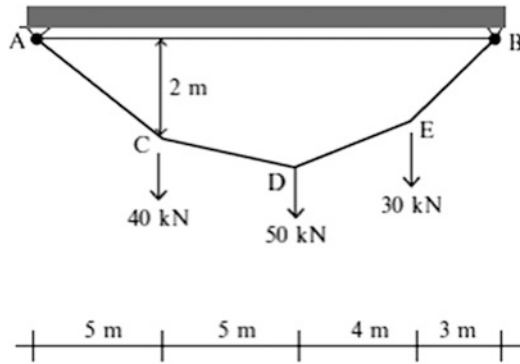
Problem 5.1



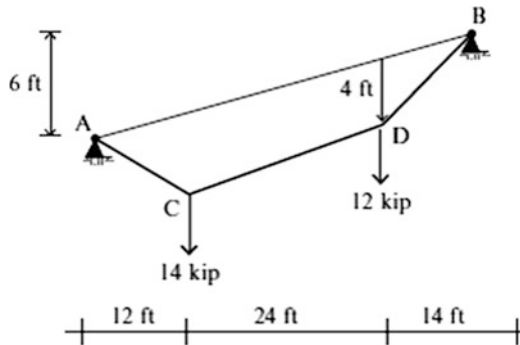
Problem 5.2



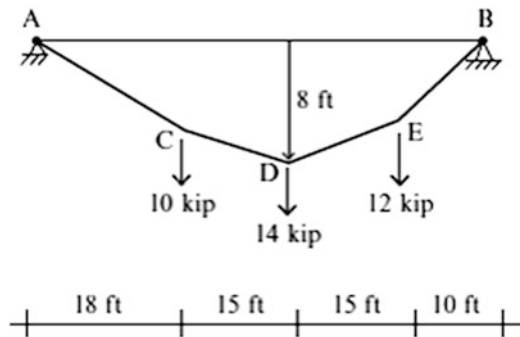
Problem 5.3



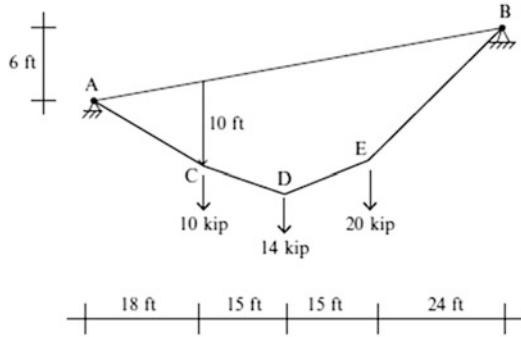
Problem 5.4



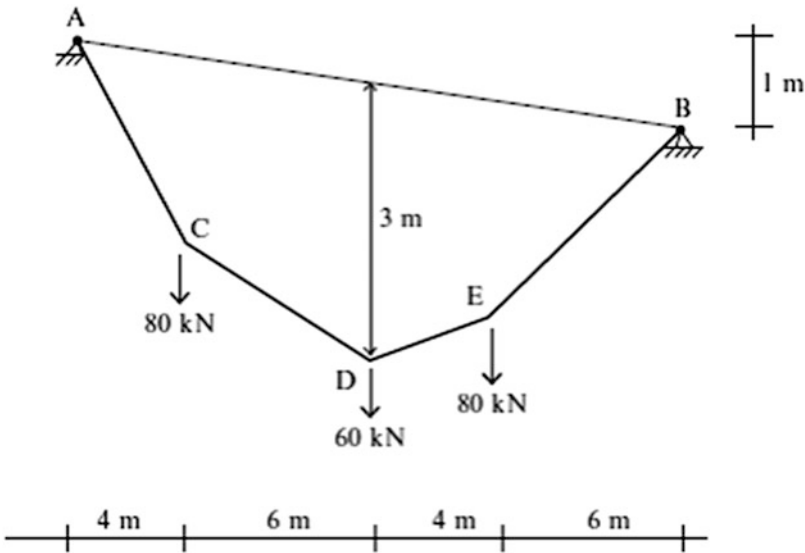
Problem 5.5



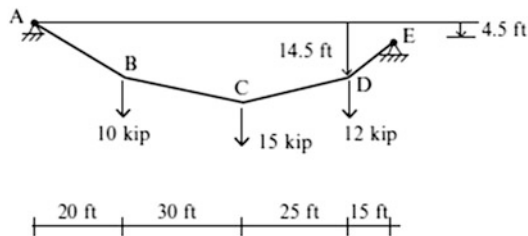
Problem 5.6



Problem 5.7

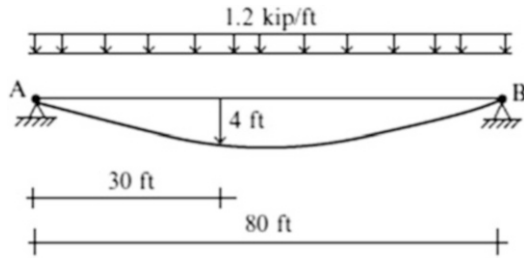


Problem 5.8

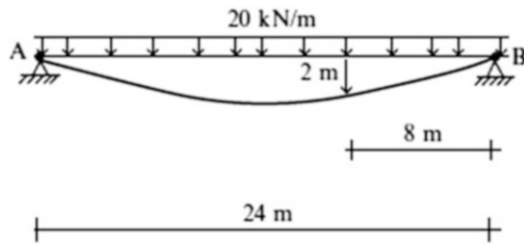


For Problems 5.9–5.14, determine the maximum tension.

Problem 5.9

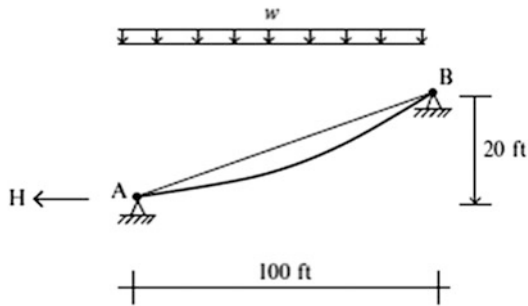


Problem 5.10

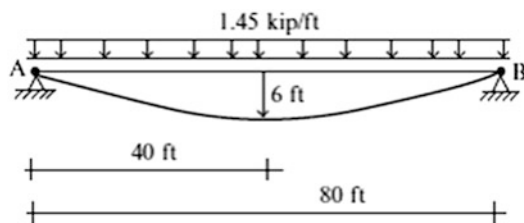


Problem 5.11

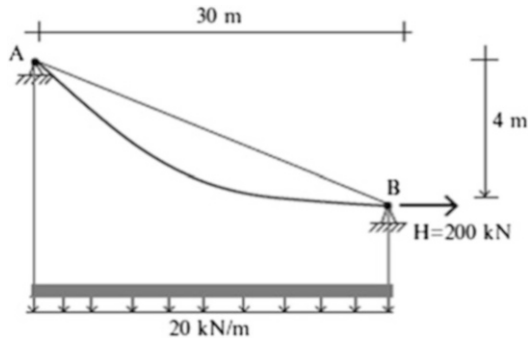
Assume $w = 1.7$ kip/ft and $H = 40$ kip.



Problem 5.12

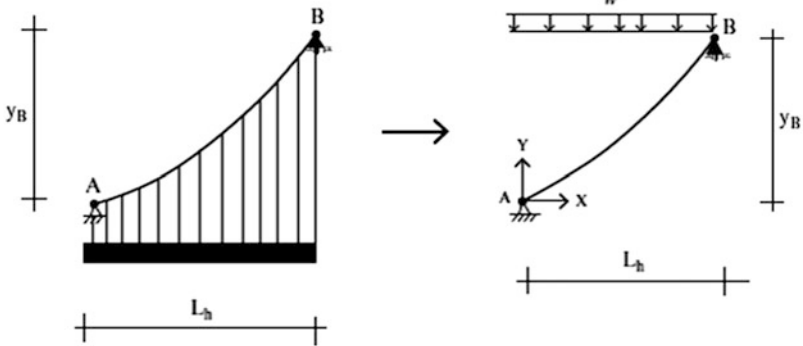


Problem 5.13



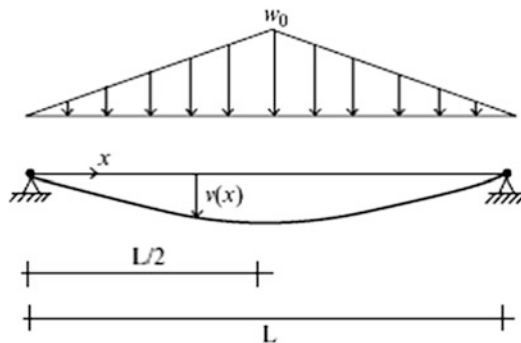
Problem 5.14

Assume $w = 1.4$ kip/ft, $y_B = 10$ ft, $H = 100$ kip, and $L_h = 40$ ft.



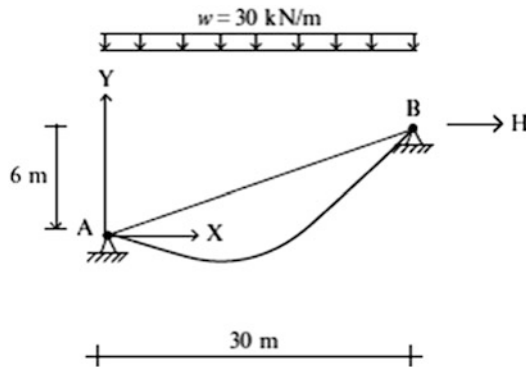
Problem 5.15

Assume $w_0 = 1.8$ kip/ft, $v_{at\ x = 20\ ft} = 2$ ft and $L = 80$ ft. Determine the deflected shape.



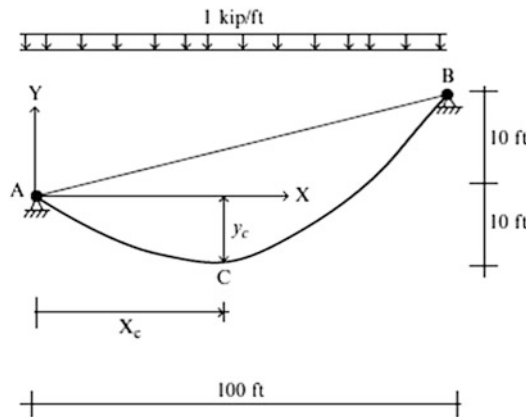
Problem 5.16

Determine the coordinates of the lowest point on the cable for $H = 650 \text{ kN}$



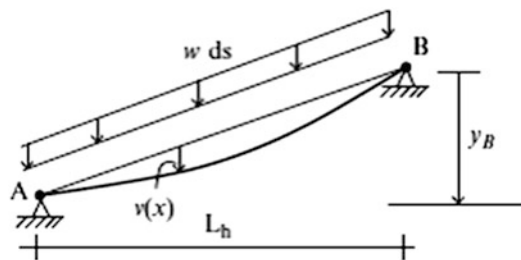
Problem 5.17

Determine the peak values of cable tension.



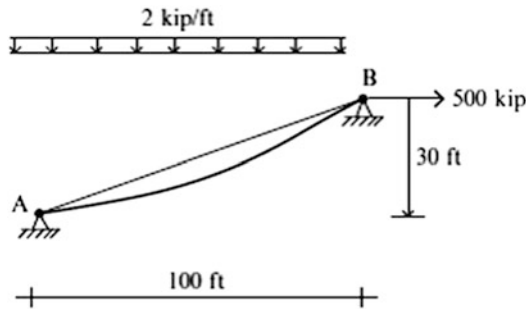
Problem 5.18

Consider the case where the loading is defined in terms of per unit arc length. Derive the expression for the deflected shape, $v(x)$.



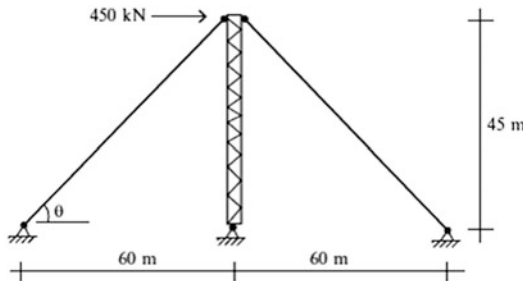
Problem 5.19

- (a) Determine the total arc length for this geometry.
- (b) Determine the effect of a temperature increase of 100 °F. Assume the cable material is steel.



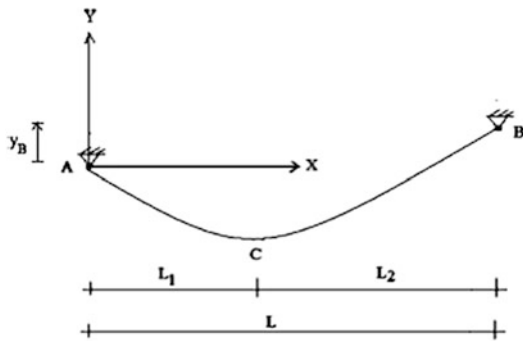
Problem 5.20

Consider the guyed tower scheme shown in the sketch below. Assume the guys are steel cables that are stressed initially to 520 MPa. Determine the cable cross-sectional area required to limit the lateral motion at the top of the tower to 10 mm.



Problem 5.21

The cable shown below carries its own weight. Determine the arc length and y_B . Point C is the lowest point. Assume $w = 0.8$ kip per foot of cable, $L_1 = 60$ ft, $L_2 = 80$ ft, and $H = 150$ kip.



Abstract

Chapter 3 dealt with beams, which are *straight* members subjected to transverse loading. We showed there that transversely loaded beams respond by bending, i.e., they equilibrate the loading by developing internal shear and moment quantities. When the centroidal axis is curved, the behavior of a curved member subjected to transverse loading can undergo a dramatic change from predominately bending action to predominately axial action depending on how the ends are restrained. This characteristic of curved members makes them more efficient than straight members for spanning moderate to large scale openings. A typical application is an arch structure, which is composed of curved members restrained at their ends.

In this chapter, we first develop the general solution for the internal forces existing in a planar curved member and apply it to members having parabolic and circular shapes. Next, we introduce the method of virtual forces specialized for planar curved members and illustrate its application to compute displacements for various geometries. The last section of the chapter deals with the optimal shape for an arch and the analysis of three-hinged arches, a popular form of arch structure. The material presented here also provides the basis for the analysis of statically indeterminate arches treated in Chap. 9.

6.1 A Brief History of Arch-Type Structures

We define an arch as a curved member that spans an opening and is restrained against movement at its ends by abutments. Figure 6.1 illustrates this definition. Arches are designed to carry a vertical loading which, because of the curved nature of the member, is partially resisted by horizontal forces

Fig. 6.1 Definition of an arch

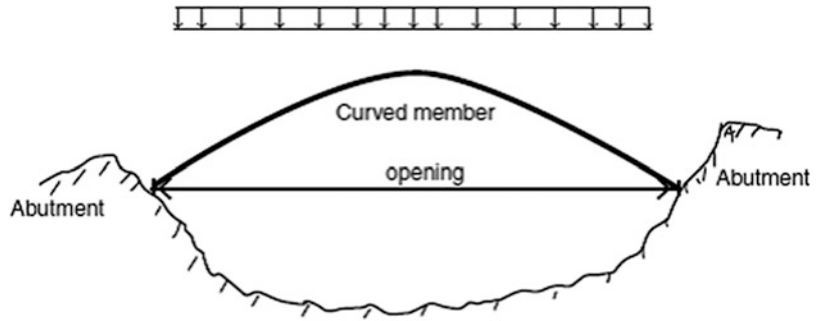
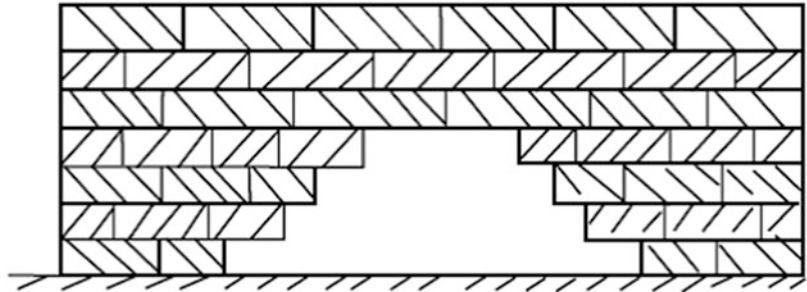


Fig. 6.2 Corbel arch



provided by the abutments. Arches generally are more efficient than straight beam-type structures for spanning an opening since their geometry can be modified so that they carry the transverse loading almost completely by axial action, i.e., by compression. However, abutments are required to develop the compression-type behavior, and this requirement sometimes limits the applicability of the arch for a particular site.

In what follows, we briefly discuss the historical development of arch structures and then present the underlying theory for statically determinate curved members. This theory is similar to the theory for gable roof structures presented in Chap. 4. Later, in Chap. 9, we discuss the theory of statically indeterminate curved members.

Arches have many applications. They are used for openings in walls, for crossing gorges and rivers, and as monumental structures such as the Arc de Triomphe. The first application of arch-type construction in buildings occurred around 4000 BC in Egypt and Greece. Openings in walls were spanned using the scheme shown in Fig. 6.2. Large flat stones were stacked in layers of increasing width until they met at the top layer. Each layer was stabilized by the weight applied above the layer. The concept is called a Corbel arch. No formwork is required to construct the structure. Also, no horizontal thrust and therefore no abutments are needed. The term “false arch” is sometimes used to describe this type of structure. False arches were used almost exclusively in ancient Greece where the techniques of masonry construction were perfected.

The type of arch construction shown in Fig. 6.3 for carrying vertical loading across an opening was introduced by the Egyptians around 3000 BC. It employs tapered stones, called voussoirs, which are arranged around a curved opening in such a manner that each brick is restrained by compressive and frictional forces. The system is unstable until the last stone, called the “keystone,” is placed. Consequently, temporary framework is required during construction.

Starting around 300 BC, the Romans perfected masonry arch construction and built some unique structures, many of which are still functioning after 2000 years. They preferred circular arches and

Fig. 6.3 Keystone arch construction

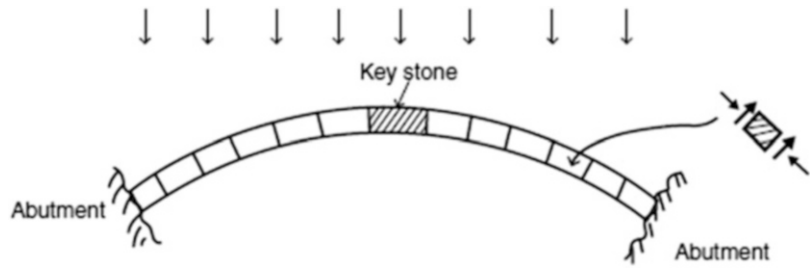


Fig. 6.4 Pont du Gard crossing



included them in buildings, bridges, and aqueducts. One of the most famous examples is the Pont du Gard, shown in Fig. 6.4; a bridge/aqueduct over the river Gard built in 19 BC. Some of the stones weigh up to 6 ton.

Another example of a second-century multiple span Roman arch masonry bridge is shown in Fig. 6.5. The typical span length is 98 ft. This bridge crosses the Tagus River in Spain and was a key element in the transportation network connecting the outer Roman Provinces with Rome.

Masonry materials are ideal for arch construction since they are strong under compression and also very durable. However, it is difficult to construct long span masonry arch bridges. With the development of alternate structural materials such as cast iron and steel at the end of the eighteenth century, there was a shift toward arches formed with metal members. Figure 6.6 shows the Iron Bridge built in 1781. The main span is 100 ft and crosses the Severn Gorge in the UK. Each of the members was formed using cast iron technology which was evolving at the time. Since cast iron is weak in tension and tends to fail in a brittle manner, it was shortly replaced as the material of choice by steel.

The development of railroads created a demand for bridges with more load capacity and longer spans. During this time period, there were many arch bridges constructed. Figure 6.7 shows the Eads Bridge built in 1874 across the Mississippi River in St. Louis, Missouri. This bridge has ribbed steel arch spans of 520 ft, fabricated with tubular structural alloy steel members; the first use of steel in a



Fig. 6.5 Alcantara Toledo bridge

Fig. 6.6 Iron Bridge,
England



major bridge project. Today, the bridge is still carrying pedestrian, vehicular, and light rail traffic across the Mississippi.

At the end of the nineteenth century, reinforced concrete emerged as a major competitor to steel as a structural material. Reinforced concrete allowed one to form arch geometries that were aesthetically more pleasing than conventional steel arch geometries, and therefore became the preferred material. Most of this surge in popularity was due to the work of Robert Maillart, a Swiss Engineer



Fig. 6.7 Eads Bridge, USA



Fig. 6.8 Salginatobel Bridge, Switzerland

(1872–1940), who developed arch concepts that revolutionized the design practice for reinforced concrete arches. An example is the Salginatobel Bridge, shown in Fig. 6.8. This bridge, built in 1930, crosses the Salgina Valley Ravine in Switzerland with a span of 270 ft. It is the ideal solution for this picturesque site and has been recognized by ASCE as a landmark project.

A unique arch bridge in the USA is the New Gorge Steel Arch Bridge located in West Virginia. Opened in 1977, it has the longest main span (1700 ft) and highest height (876 ft) of all arch bridges in North and South America. It held the world record for span and height until 2003 when the Lupu Arch Bridge in Shanghai (1800 ft span) was opened. A type of weathering steel called Corten was used in the New Gorge Arch structure in order to avoid the need for periodic painting.

Another unique arch bridge in the USA is the Hoover Dam Bypass Bridge. Segmented concrete construction was used to fabricate the concrete box elements in situ. The construction process employed a complex tieback scheme, as illustrated in Fig. 6.9b–d. The bridge was completed in 2010.



Fig. 6.9 Modern Arch Bridges in the USA. (a) New Gorge Arch, West Virginia. (b) Hoover Dam Bypass—under construction. (c) Hoover Dam Bypass—under construction. (d) Hoover Dam Bypass—under construction. (e) Hoover Dam Bypass—completed

6.2 Modeling of Arch Structures

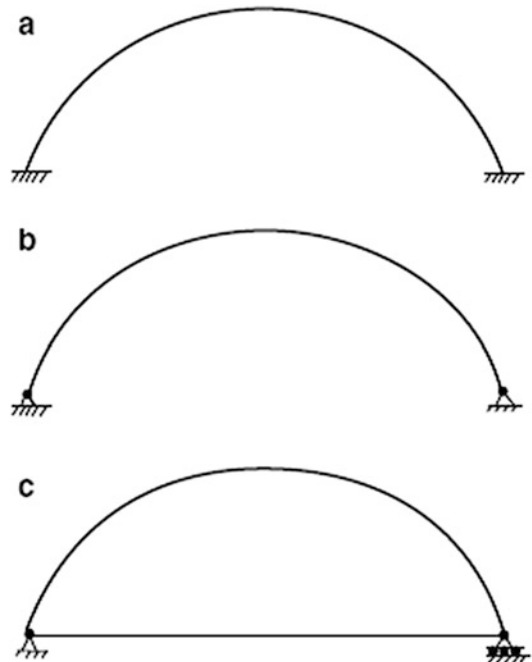
We idealize an arch structure as a curved member restrained at its ends with a combination of fixed, hinged, and roller supports. Figure 6.10 illustrates various types of end conditions. Case (a) corresponds to full end fixity, a condition that is difficult to achieve. The more common case is (b) where the abutments can prevent translation but not rotation. We refer to this structure as a two-hinged arch. The third case, (c), corresponds to a “tied arch structure” where the ends are interconnected with a tension member. This scheme is used when the abutments are not capable of resisting the horizontal thrust action of the arch.

If the arch is a bridge, the roadway may be connected above the structure as in Fig. 6.11a, or below the structure as in Fig. 6.11b. When placed above, the deck weight is transmitted by compression members to the arch. Decks placed below the arch are supported by cables. Both loading cases are idealized as a uniform loading *per horizontal projection* as shown in Fig. 6.11c. In some cases, soil backfill is placed between the roadway and the arch. The soil loading is represented as a nonuniform loading whose shape is defined by the arch geometry. Figures 6.11d, e illustrate this case.

The structures in Fig. 6.10 are statically indeterminate. We can reduce the two-hinge arch to a statically determinate structure by converting it to a three-hinge arch. The additional hinge is usually placed at mid-span as shown in Fig. 6.12.

In this chapter, we first present a general theory of statically determinate curved members and then specialize the general theory for three-hinge arches. We treat statically indeterminate arches later in Chap. 9.

Fig. 6.10 Indeterminate Arch structures with various end fixity conditions. (a) Fully fixed Arch— 3° indeterminate. (b) Two-hinged arch— 1° indeterminate. (c) Tied arch— 1° indeterminate



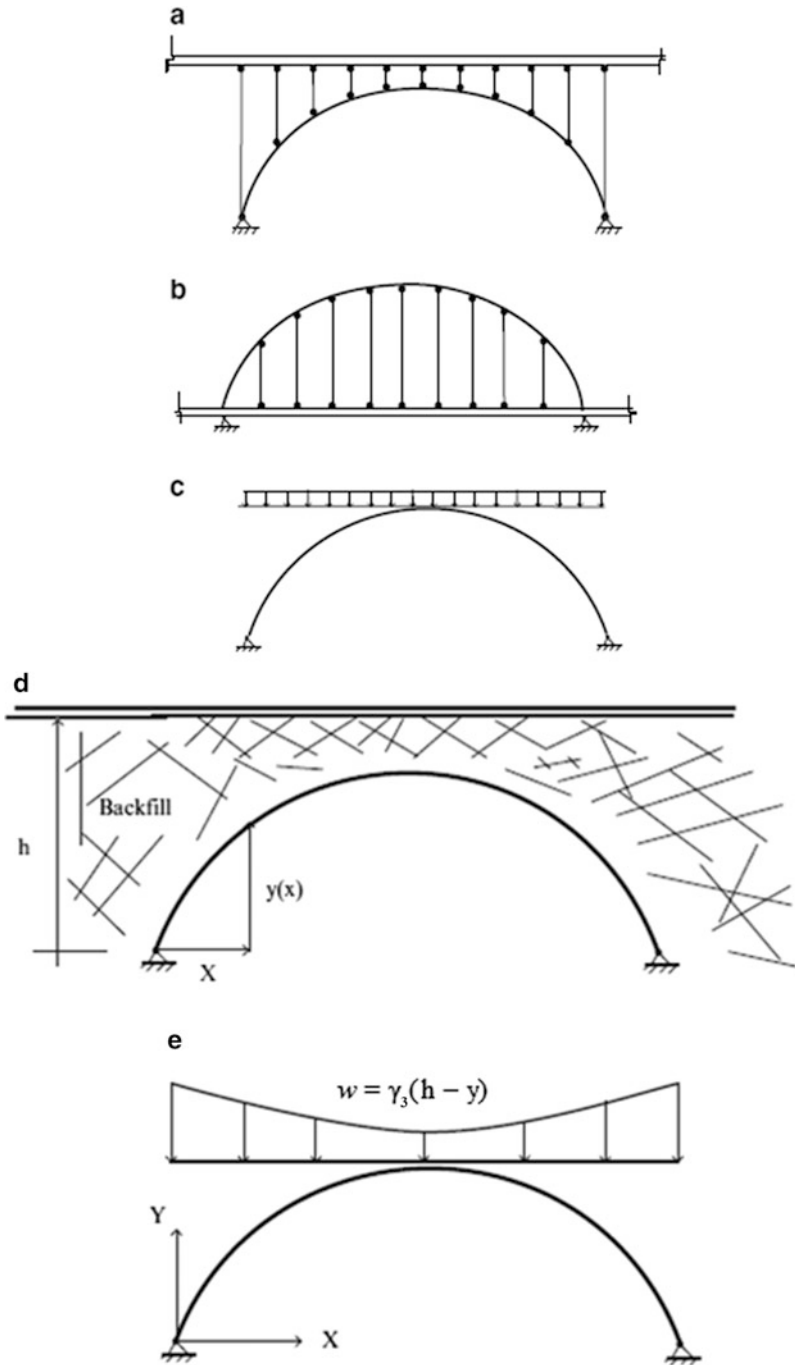
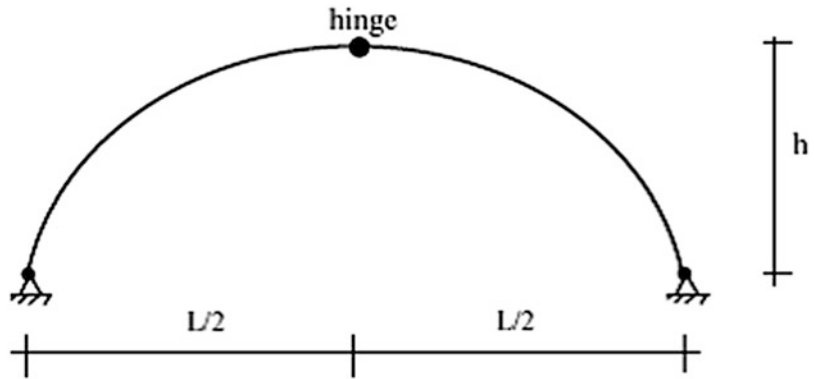


Fig. 6.11 Different roadway arrangements—idealized loading. (a) Roadway above the arch. (b) Roadway below the arch. (c) Idealized uniform dead loading. (d) Soil backfill above the arch. (e) Idealized soil loading

Fig. 6.12 Three-hinge arch

6.3 Internal Forces in Curved Members

We consider the statically determinate curved member shown in Fig. 6.13a. We work with a Cartesian reference frame having axes X and Y and define the centroidal axis of the member by the function, $y = y(x)$. The vertical loading is assumed to be expressed in terms of the horizontal projected length. These choices are appropriate for the arch structures described in the previous section. We determine the reactions using the global equilibrium equations.

The applied load is equilibrated by internal forces, similar to the behavior of a straight beam under transverse load. To determine these internal forces, we isolate an arbitrary segment such as AC defined in Fig. 6.13b. We work initially with the internal forces referred to the $X - Y$ frame and then transform them over to the local tangential/normal frame. Note that now there may be a longitudinal force component as well as a transverse force component, whereas straight beams subjected to transverse loading have no longitudinal component.

Enforcing equilibrium leads to the general solution for the internal forces.

$$\begin{aligned} F_x &= -R_{Ax} \\ F_y &= -R_{Ay} + \int_0^x w(x) d\xi \\ M &= xR_{Ay} - yR_{Ax} - \int_0^x w(x)\xi d\xi \end{aligned} \quad (6.1)$$

Lastly, we transform the Cartesian force components (F_x, F_y) over to the tangential/normal frame (F, V). Noting Fig. 6.14, the transformation law is

$$\begin{aligned} F &= F_y \sin \theta + F_x \cos \theta \\ V &= F_y \cos \theta - F_x \sin \theta \\ \tan \theta &= \frac{dy}{dx} \end{aligned} \quad (6.2)$$

In order to evaluate the axial (F) and shear forces (V), we need to specify the angle θ between the tangent and the horizontal axis. This quantity depends on $y(x)$, the function that defines the shape of the centroidal axis.

Fig. 6.13 (a) Notation for statically determinate curved member. (b) Free body diagram—curved beam. $X - Y$ frame. Local tangential/normal frame

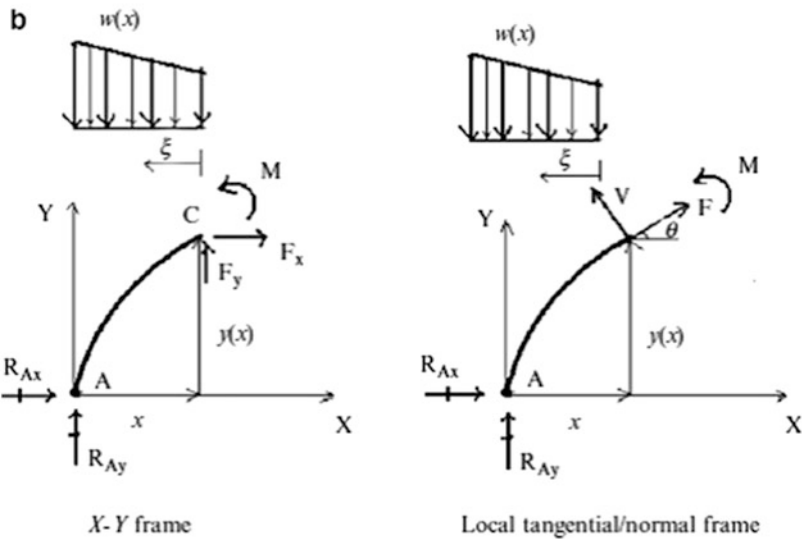
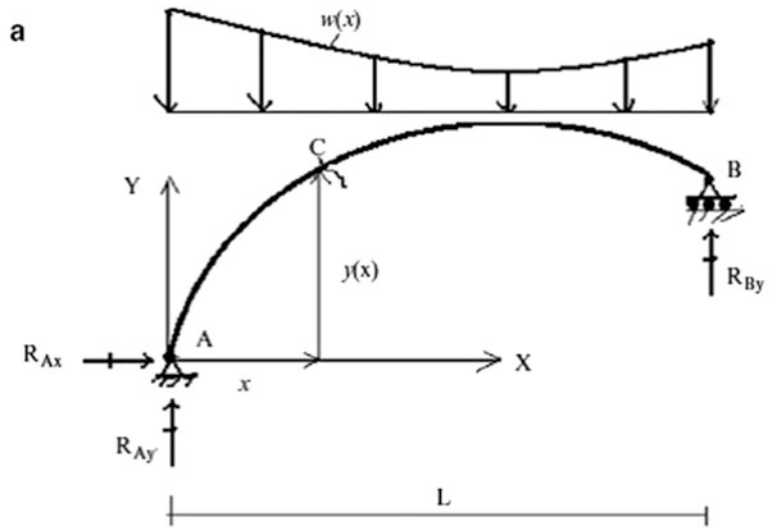


Fig. 6.14 Cartesian—local force components

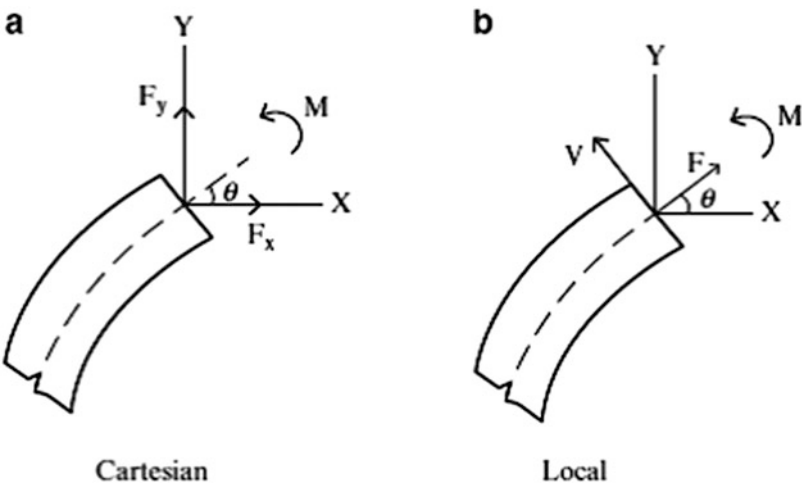
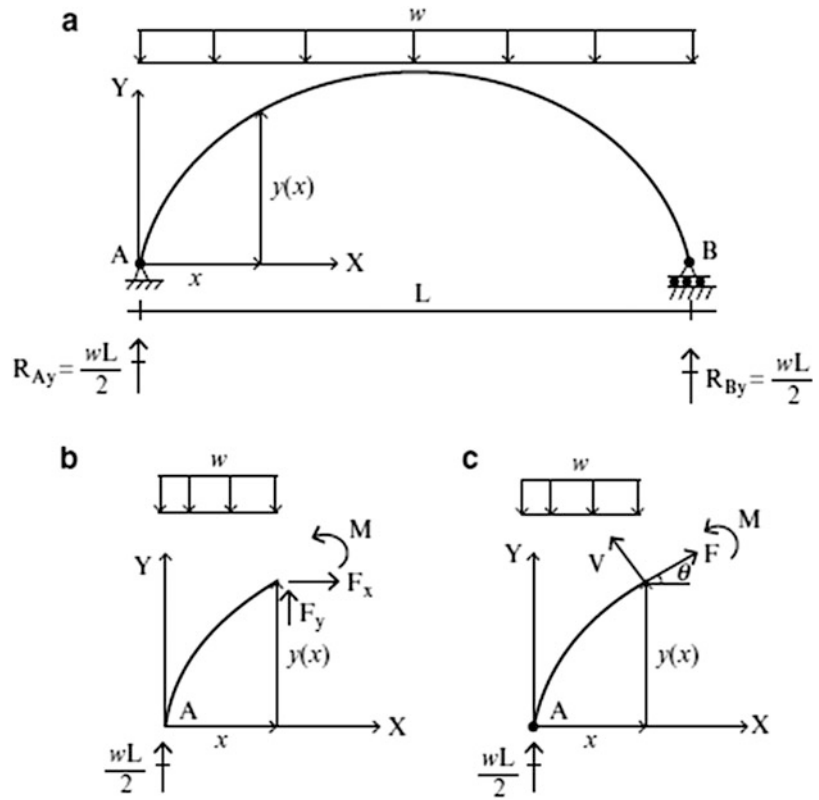


Fig. 6.15 Curved member—uniform vertical loading. (a) Reactions. (b) Internal forces—Cartesian frame. (c) Internal forces—local frame



We specialize the above set of equations for a symmetrical curved member where the loading consists of

- (a) A uniform vertical loading per projected length defined in Fig. 6.15.
- (b) A concentrated load at the crown defined in Fig. 6.16.

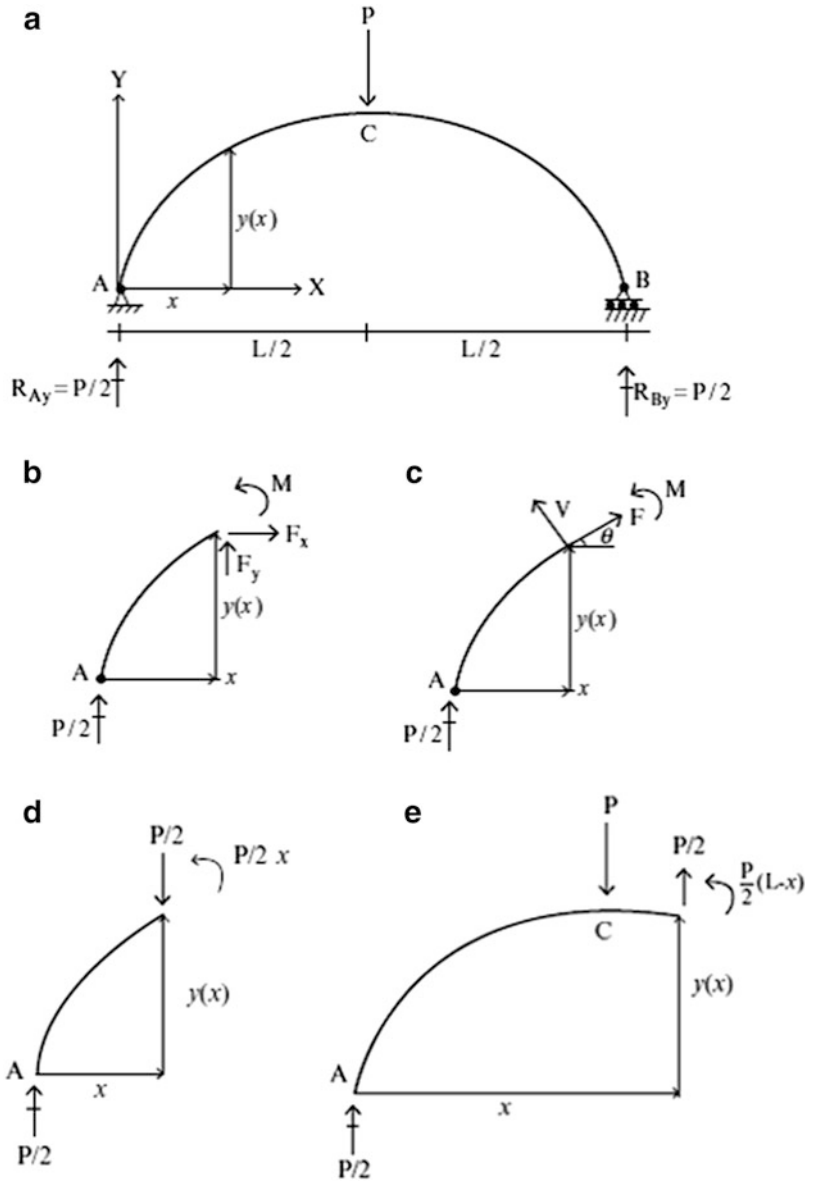
(a) *Uniformly distributed load* (Fig. 6.15):
Enforcing equilibrium and symmetry leads to

$$\begin{aligned}
 R_{Ax} &= 0 & R_{Ay} &= R_{By} = \frac{wL}{2} \\
 F_x &= 0 & F_y &= -\frac{wL}{2} + wx \\
 M &= \frac{wL}{2}x - \frac{wx^2}{2}
 \end{aligned}$$

Note that these results are the *same* as for a simply supported straight beam subjected to transverse loading. Substituting for F_x and F_y in (6.2) results in the internal forces (F, V, M) due to a uniform vertical loading,

$$\begin{aligned}
 F &= \left(-\frac{wL}{2} + wx \right) \sin \theta \\
 V &= \left(-\frac{wL}{2} + wx \right) \cos \theta \\
 M &= \frac{wL}{2}x - \frac{wx^2}{2}
 \end{aligned} \tag{6.3}$$

Fig. 6.16 Curved member—concentrated load. (a) Reactions. (b) Internal forces—Cartesian frame. (c) Internal forces—local frame. (d) Segment AC $0 \leq x < L/2$. (e) Segment CB $L/2 < x \leq L$



(b) Concentrated load (Fig. 6.16):

The internal forces referred to the Cartesian frame are

Segment AC $0 \leq x < L/2$

$$F_x = 0$$

$$F_y = -\frac{P}{2}$$

$$M = \frac{P}{2}x$$

Segment CB $L/2 < x \leq L$

$$F_x = 0$$

$$F_y = \frac{P}{2}$$

$$M = \frac{P}{2}(L-x)$$

Substituting for F_x and F_y in (6.2) results in the internal forces (F , V , M) in the local frame,

$$\begin{array}{ll}
 \text{For } 0 \leq x < L/2 & \text{For } L/2 < x \leq L \\
 F = -\frac{P}{2} \sin \theta & F = +\frac{P}{2} \sin \theta \\
 V = -\frac{P}{2} \cos \theta & V = +\frac{P}{2} \cos \theta \\
 M = \frac{P}{2}x & M = \frac{P}{2}(L - x)
 \end{array} \tag{6.4}$$

6.4 Parabolic Geometry

We will show later that a parabolic arch is the optimal shape for a uniform vertical loading, in the sense that there is essentially no bending, only axial force, introduced by this loading. Using the notation defined in Fig. 6.17, the parabolic curve is expressed in terms of h , the height at mid-span, and the dimensionless coordinate, x/L .

$$y(x) = 4h \left[\frac{x}{L} - \left(\frac{x}{L} \right)^2 \right] \tag{6.5}$$

Differentiating $y(x)$ leads to

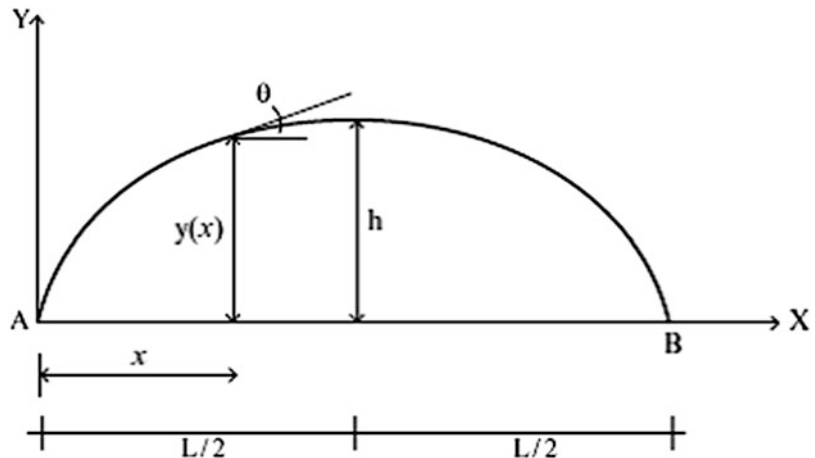
$$\tan \theta = \frac{dy}{dx} = 4\frac{h}{L} \left(1 - 2\frac{x}{L} \right) \tag{6.6}$$

The maximum value of θ is at $x = 0, L$

$$\theta_{\max} = \pm \tan^{-1} \left(\frac{4h}{L} \right)$$

Values of θ_{\max} vs. h/L are tabulated in the table below.

Fig. 6.17 Notation for parabolic shape function



$\frac{h}{L}$	$\theta_{\max}(\text{°})$	$\tan \theta_{\max}$	$\cos \theta_{\max}$	$\sin \theta_{\max}$
0	0	0	1	0
0.01	2.3	0.04	0.999	0.04
0.025	5.7	0.1	0.995	0.099
0.05	11.3	0.2	0.98	0.196
0.1	21.8	0.4	0.93	0.37
0.15	30.9	0.6	0.86	0.51
0.2	38.6	0.8	0.78	0.62
0.25	45	1	0.7	0.7
0.3	50.2	1.2	0.64	0.77
0.35	54.4	1.4	0.58	81
0.4	58	1.6	0.53	0.85
0.45	60.9	1.8	0.48	0.87
0.5	63.4	2	0.45	0.89

The parameter h/L is a measure of the steepness of the curved member. Deep curved members have $h/L \geq \approx 0.25$. A curved member is said to be shallow when h/L is small with respect to unity, on the order of 0.1. The trigonometric measures for a shallow curved member are approximated by

$$\text{shallow parabolic curve} \begin{cases} \tan \theta = \frac{dy}{dx} \approx \theta(\text{rad}) \\ \cos \theta = \frac{1}{\sqrt{1 + \tan^2 \theta}} \approx 1 \\ \sin \theta = \frac{\tan \theta}{\sqrt{1 + \tan^2 \theta}} \approx \tan \theta \approx \theta(\text{rad}) \end{cases} \quad (6.7)$$

Example 6.1 Shallow vs. Deep Parabolic Curved Members

Given: The parabolic curved beam defined in Fig. E6.1a.

Determine: The axial, shear, and moment distributions for (a) $h/L = 0.1$, (b) $h/L = 0.5$.

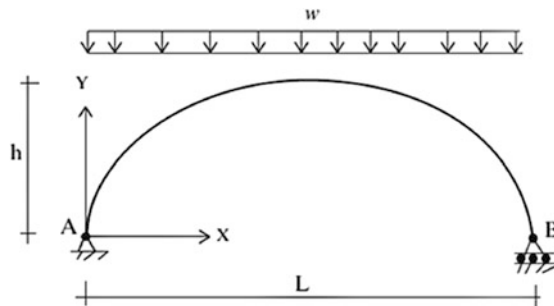


Fig. E6.1a Parabolic geometry

Solution: Enforcing equilibrium and symmetry leads to the reactions listed in Fig. E6.1b.

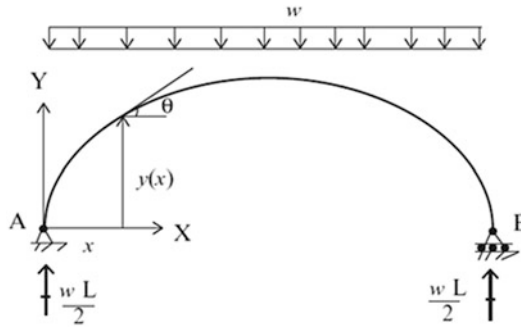


Fig. E6.1b Reactions

Applying (6.3) and (6.5), the internal forces in the local frame are

$$\begin{aligned}
 F &= \left(-\frac{wL}{2} + wx \right) \sin \theta \\
 V &= \left(-\frac{wL}{2} + wx \right) \cos \theta \\
 M &= \frac{wL}{2}x - \frac{wx^2}{2}
 \end{aligned}$$

where

$$\begin{aligned}
 \cos \theta &= \frac{1}{\sqrt{1 + \left(4\frac{h}{L} \left(1 - 2\frac{x}{L} \right) \right)^2}} \\
 \sin \theta &= \frac{4\frac{h}{L} \left(1 - 2\frac{x}{L} \right)}{\sqrt{1 + \left(4\frac{h}{L} \left(1 - 2\frac{x}{L} \right) \right)^2}}
 \end{aligned}$$

The internal forces are listed in the table below and plotted in Figs. E6.1c, E6.1d, and E6.1e for $h/L = 0.1$ and $h/L = 0.5$. Note that the moment is independent of h/L .

$\frac{x}{L}$	$\frac{M}{wL^2}$	$\frac{h}{L} = 0.1$		$\frac{h}{L} = 0.5$	
		$\frac{V}{wL}$	$\frac{F}{wL}$	$\frac{V}{wL}$	$\frac{F}{wL}$
0	0	-0.464	-0.186	-0.224	-0.447
0.1	0.045	-0.381	-0.122	-0.212	-0.339
0.2	0.08	-0.292	-0.07	-0.192	-0.125
0.3	0.105	-0.197	-0.032	-0.156	-0.125
0.4	0.12	-0.1	-0.008	-0.093	-0.037
0.5	0.125	0	0	0	0
0.6	0.12	0.1	-0.008	0.093	-0.037
0.7	0.105	0.197	-0.032	0.156	-0.125
0.8	0.08	0.292	-0.07	0.192	-0.23
0.9	0.045	0.381	-0.122	0.212	-0.339

$\frac{x}{L}$	$\frac{M}{wL^2}$	$\frac{h}{L} = 0.1$		$\frac{h}{L} = 0.5$	
		$\frac{V}{wL}$	$\frac{F}{wL}$	$\frac{V}{wL}$	$\frac{F}{wL}$
1	0	0.464	-0.186	0.224	-0.447

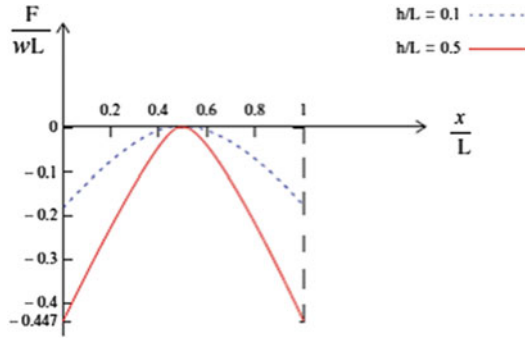


Fig. E6.1c Axial force, F

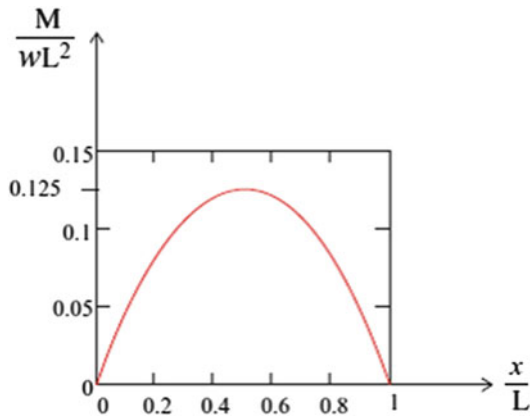


Fig. E6.1d Moment, M

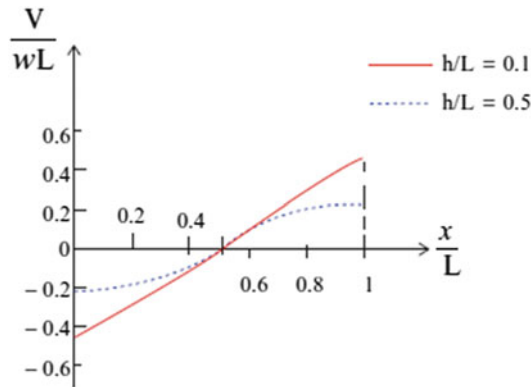


Fig. E6.1e Shear, V

The axial force is compressive and the maximum value occurs at the supports. The maximum shear force also occurs at the supports. The maximum moment occurs at the mid-span. These maximum values are listed below.

$$F_{\max} = \begin{cases} 0.186 wL & \text{for } \frac{h}{L} = 0.1 \\ 0.447 wL & \text{for } \frac{h}{L} = 0.5 \end{cases}$$

$$V_{\max} = \begin{cases} 0.464 wL & \text{for } \frac{h}{L} = 0.1 \\ 0.224 wL & \text{for } \frac{h}{L} = 0.5 \end{cases}$$

$$M_{\max} = 0.125 wL^2$$

Example 6.2 Shallow vs. Deep Parabolic Curved Members

Given: The parabolic curved beam defined in Fig. E6.2a

Determine: The axial, shear, and moment distributions for (a) $h/L = 0.1$, (b) $h/L = 0.5$.

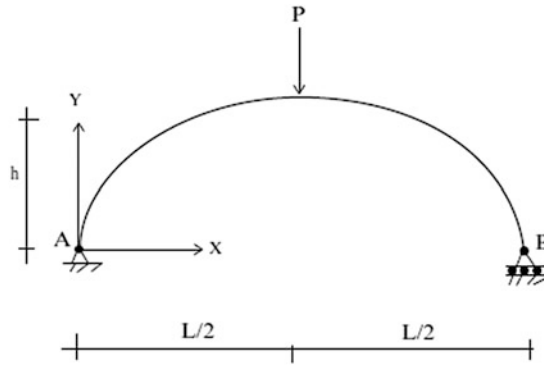


Fig. E6.2a

Solution: Enforcing equilibrium and symmetry leads to the reactions listed in Fig. E6.2b.

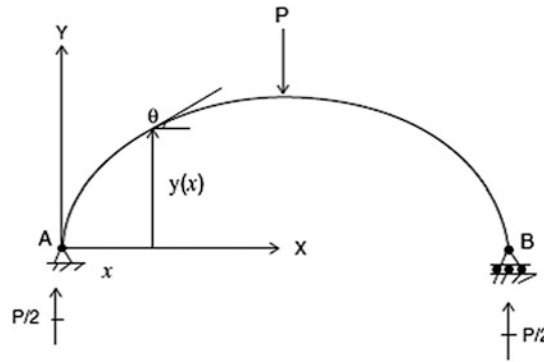


Fig. E6.2b Reactions

Applying (6.4) and (6.5), the internal forces in the local frame are

For $0 \leq x < L/2$	For $L/2 < x \leq L$
$F = -\frac{P}{2} \sin \theta$	$F = +\frac{P}{2} \sin \theta$
$V = -\frac{P}{2} \cos \theta$	$V = +\frac{P}{2} \cos \theta$
$M = \frac{P}{2}x$	$M = +\frac{P}{2}(L - x)$

where

$$\cos \theta = \frac{1}{\sqrt{1 + \left(4\frac{h}{L}\left(1 - 2\frac{x}{L}\right)\right)^2}}$$

$$\sin \theta = \frac{4\frac{h}{L}\left(1 - 2\frac{x}{L}\right)}{\sqrt{1 + \left(4\frac{h}{L}\left(1 - 2\frac{x}{L}\right)\right)^2}}$$

The internal forces are plotted in Figs. E6.1c, E6.1d, and E6.1e and listed in the table which follows for $h/L = 0.1$ and $h/L = 0.5$.

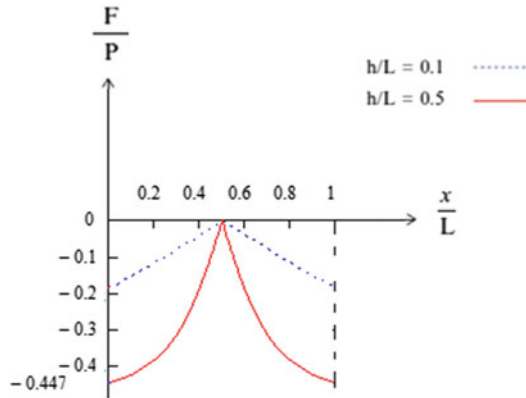


Fig. E6.2c Axial force, F

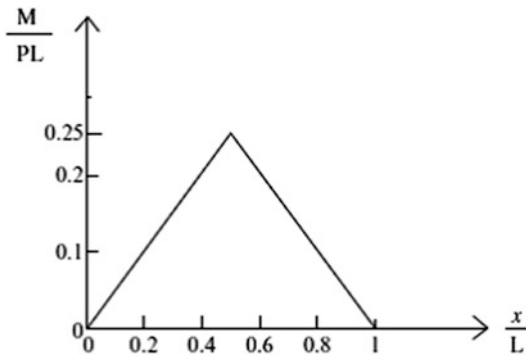


Fig. E6.2d Moment, M

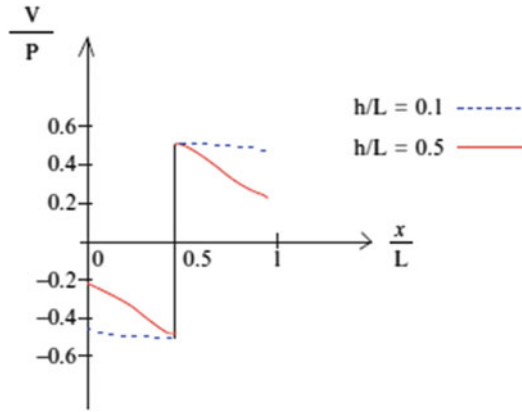


Fig. E6.2e Shear, V

The axial force is compressive and the maximum value occurs at the supports. The maximum shear force and maximum moment occur at the mid-span.

$\frac{x}{L}$	$\frac{M}{PL}$	$\frac{h}{L} = 0.1$		$\frac{h}{L} = 0.5$	
		$\frac{V}{P}$	$\frac{F}{P}$	$\frac{V}{P}$	$\frac{F}{P}$
0	0	-0.464	-0.186	-0.224	-0.447
0.1	0.05	-0.476	-0.152	-0.265	-0.424
0.2	0.1	-0.486	-0.117	-0.32	-0.384
0.3	0.15	-0.494	-0.079	-0.39	-0.312
0.4	0.2	-0.498	-0.04	0.464	-0.186
0.5	0.25	0.5	0	0.5	0
0.6	0.2	0.498	0.04	0.464	0.186
0.7	0.15	0.494	0.079	0.39	0.312
0.8	0.1	0.486	0.117	0.32	0.384
0.9	0.05	0.476	0.152	0.265	0.424
1	0	0.464	0.186	0.244	0.447

6.5 Method of Virtual Forces for Curved Members

Displacements are determined using the form of the method of virtual forces specialized for curved members [1]:

$$d \delta P = \int_s \left\{ \frac{F}{AE} \delta F + \frac{V}{GA_s} \delta V + \frac{M}{EI} \delta M \right\} ds \tag{6.9}$$

where d is the desired displacement, δP , δF , δV , δM denote the virtual force system, and the various terms represent the contribution of axial, shear, and bending deformation. As discussed in Chaps. 3 and 4, the contributions of axial and shear deformation are usually small and only the bending deformation term is retained for slender straight beams and frames composed of slender straight members. For curved members, we distinguish between “non-shallow” and “shallow” members.

6.5.1 Non-shallow Slender Curved Members

For non-shallow slender curved members subjected to transverse loading, the contributions of axial and shear deformation are usually small and only the bending deformation term is retained. In this case, we approximate (6.9) with

$$d\delta P \approx \int_s \frac{M}{EI} \delta M ds = \int_x \frac{M \delta M}{EI \cos \theta} dx \quad (6.10)$$

6.5.2 Shallow Slender Curved Members

For shallow slender curved members subjected to transverse loading, the axial deformation may be as significant as the bending deformation and therefore *must be retained*. In this case, we use

$$d\delta P \approx \int_s \left\{ \frac{F}{AE} \delta F + \frac{M}{EI} \delta M \right\} ds = \int_x \left\{ \frac{F}{AE} \delta F + \frac{M}{EI} \delta M \right\} \frac{dx}{\cos \theta} \quad (6.11)$$

Example 6.3 Deflection of Parabolic Curved Beam—Shallow vs. Deep

Given: The parabolic curved beam defined in Fig. E6.3a. Consider EI is constant.

Determine: The horizontal displacement at B for (a) non-shallow beam and (b) shallow beam.

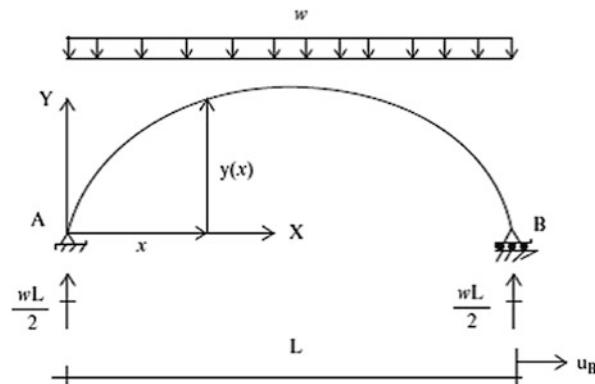


Fig. E6.3a

The internal forces for this loading are

$$\begin{aligned}
 F_x = 0 \\
 F_y = -\frac{wL}{2} + wx \quad \Rightarrow \quad F = \left(-\frac{wL}{2} + wx \right) \sin \theta \\
 V = \left(-\frac{wL}{2} + wx \right) \cos \theta
 \end{aligned}$$

$$M = \frac{wL}{2}x - \frac{wx^2}{2}$$

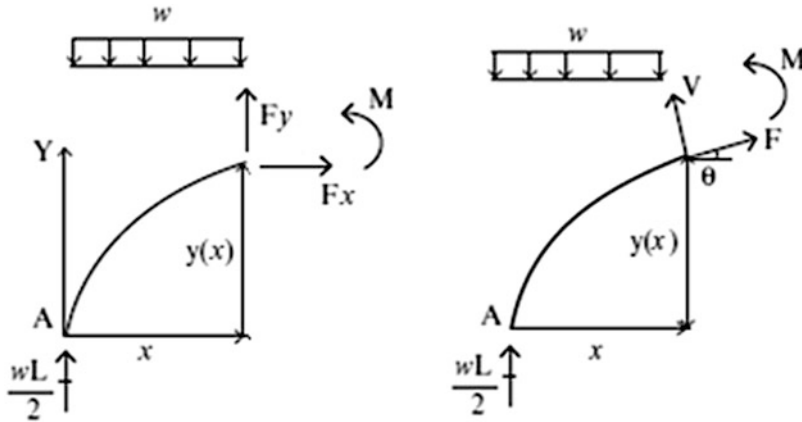


Fig. E6.3b

In order to determine the horizontal displacement at support B, we apply the virtual force system shown in Fig. E6.3c.

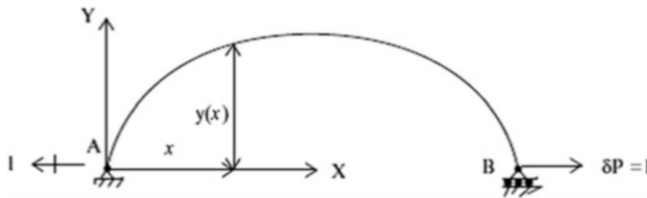


Fig. E6.3c Virtual force system for u_B

The internal virtual forces are

$$\begin{aligned}
 \delta F_x = 1 \\
 \delta F_y = 0 \quad \Rightarrow \quad \delta F = \delta F_y \sin \theta + \delta F_x \cos \theta = \cos \theta \\
 \delta V = \delta F_y \cos \theta - \delta F_x \sin \theta = -\sin \theta \\
 \delta M = y(x) \\
 \tan \theta = \frac{dy}{dx}
 \end{aligned}$$

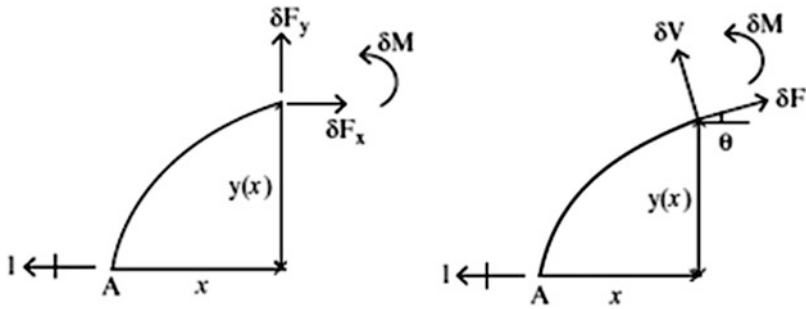


Fig. E6.3d

(a) *Non-shallow curved member:*

We use the approximate form defined by (6.10) for a non-shallow curved member.

$$u_B = \int_0^L \frac{M \delta M}{EI \cos \theta} dx$$

Substituting for M , δM , and $\cos \theta$, this expression expands to

$$u_B = \int_0^L \left(\frac{wL}{2}x - \frac{wx^2}{2} \right) \left\{ 4h \left(\frac{x}{L} - \left(\frac{x}{L} \right)^2 \right) \right\} \sqrt{1 + (\tan \theta)^2} \frac{dx}{EI}$$

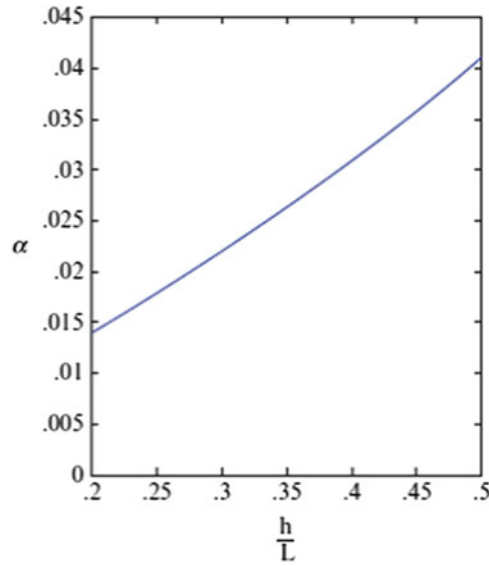
where

$$\tan \theta = 4 \frac{h}{L} \left(1 - 2 \frac{x}{L} \right)$$

For EI constant, the solution is expressed as

$$u_B = \frac{wL^4}{EI} (\alpha)$$

where α is a function of h/L . We evaluate α using numerical integration. The result is plotted below.



(b) *Shallow curved member:*

When the parabola is shallow ($\cos \theta \approx 1$), we need to include the axial deformation term as well as the bending deformation term. Starting with the form specified for a shallow member, (6.11),

$$u_B = \int_x \left(\frac{F}{AE} \delta F + \frac{M}{EI} \delta M \right) dx$$

and noting that

$$F \approx \left(-\frac{wL}{2} + wx \right) \frac{dy}{dx} = -\frac{2wh}{L^2} (L - 2x)^2$$

$$M = \frac{wL}{2}x - \frac{wx^2}{2}$$

$$\delta F_x = 1 \Rightarrow \delta F = \delta F_x \cos \approx 1$$

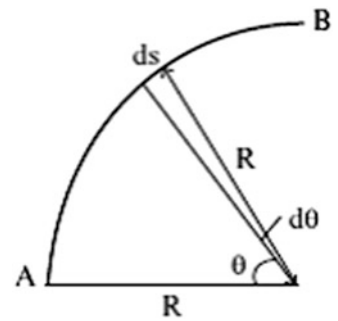
$$\delta M = y = 4h \left\{ \frac{x}{L} - \left(\frac{x}{L} \right)^2 \right\}$$

leads to

$$u_B = -\frac{2}{3} \frac{wLh}{AE} + \frac{1}{15} \frac{whL^3}{EI}$$

Note that the axial deformation causes the ends to move together, whereas the bending deformation causes the ends to move apart.

Fig. 6.18 Geometry—
circular arch



6.5.3 Circular Curved Member

When the arch geometry is a circular segment, it is more convenient to work with polar coordinates. We consider the segment shown in Fig. 6.18. In this case, R is constant and θ is the independent variable. The differential arc length ds is equal to $R d\theta$.

We assume the member is slender and retain only the bending deformation term. Equation (6.10) takes the following form:

$$d\delta P = \int_0^{\theta_B} \frac{M \delta M}{EI} R d\theta \tag{6.12}$$

When EI is constant, the equation simplifies to

$$d\delta P = \frac{R}{EI} \int_0^{\theta_B} M \delta M d\theta \tag{6.13}$$

Example 6.4 Deflection of a Light Pole

Given: The light pole structure defined in Figs. E6.4a, E6.4b, E6.4c, and E6.4d. Consider EI to be constant.

Determine: The horizontal and vertical displacements at C.

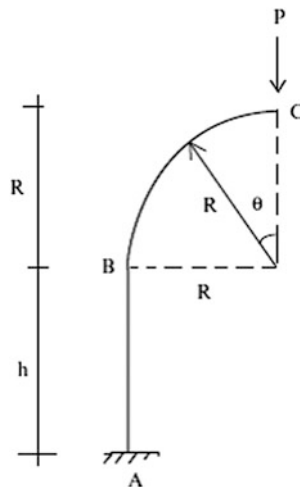


Fig. E6.4a

Solution: Member AB is straight and BC is a circular arc. We take the polar angle from C toward B. The bending moment distribution due to P is

$$\begin{aligned} \text{Segment B - C} \quad M &= -PR \sin \theta & 0 < \theta < \pi/2 \\ \text{Segment A - B} \quad M &= -PR & 0 < x < h \end{aligned}$$

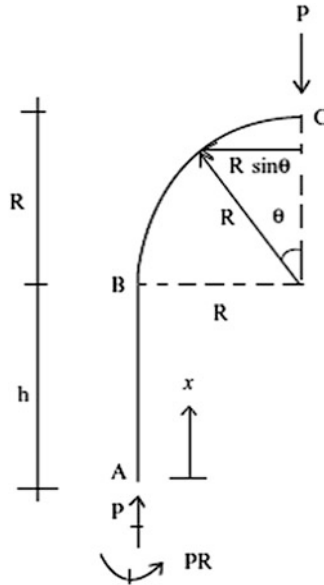


Fig. E6.4b $M(x)$

The vertical displacement at C is determined with the following virtual force system

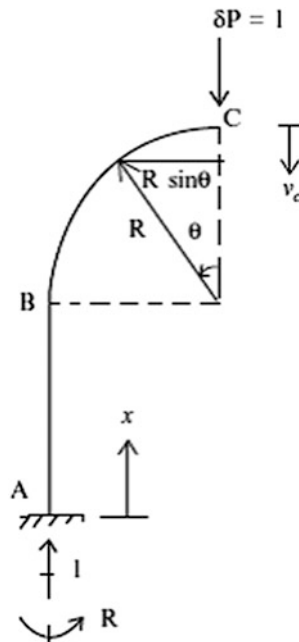


Fig. E6.4c $\delta M(x)$ for v_c

$$\text{Segment B - C} \quad \delta M = -R \sin \theta \quad 0 < \theta < \pi/2$$

$$\text{Segment A - B} \quad \delta M = -R \quad 0 < x < h$$

Considering only bending deformation terms, the displacement is given by

$$\begin{aligned} v_c &= v_c|_{AB} + v_c|_{CB} \\ &= \frac{1}{EI} \int_0^h (-PR)(-R) dx + \frac{1}{EI} \int_0^{\pi/2} (-PR \sin \theta)(-R \sin \theta) R d\theta \\ &= \frac{PR^2 h}{EI} + \frac{1}{EI} \int_0^{\pi/2} PR^3 (\sin \theta)^2 d\theta \\ &= \frac{PR^2}{EI} \left(h + \frac{\pi R}{4} \right) \end{aligned}$$

Following a similar approach, the virtual force system corresponding to the horizontal displacement at C is evaluated

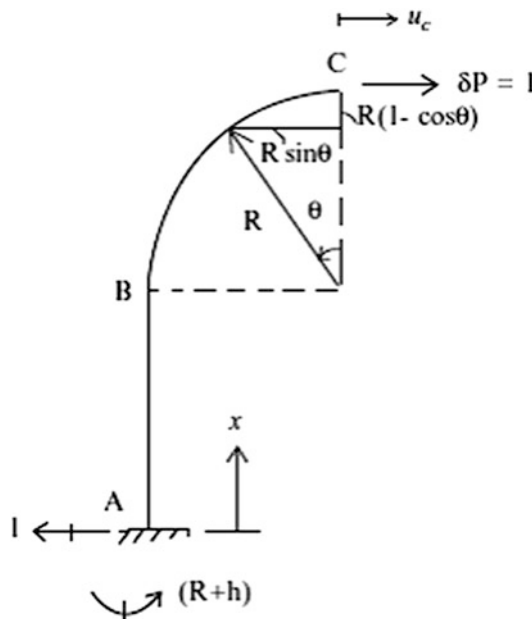


Fig. E6.4d $\delta M(x)$ for u_c

$$\text{Segment B - C} \quad \delta M = -R(1 - \cos \theta) \quad 0 < \theta < \pi/2$$

$$\text{Segment A - B} \quad \delta M = -(R + h) + x \quad 0 < x < h$$

Then

$$\begin{aligned}
 u_c &= u_c|_{AB} + u_c|_{BC} \\
 &= \frac{1}{EI} \int_0^h (-PR)(-R - h + x)dx + \frac{1}{EI} \int_0^{\pi/2} (-PR \sin \theta)R(-1 + \cos \theta)Rd\theta \\
 &= \frac{PRh^2}{2EI} + \frac{PR^2h}{EI} + \frac{1}{EI} \int_0^{\pi/2} PR^3(1 - \cos \theta) \sin \theta d\theta \\
 &= \frac{P}{EI} \left(\frac{R^3}{2} + \frac{h^2R}{2}R^2h \right)
 \end{aligned}$$

6.6 Analysis of Three-Hinged Arches

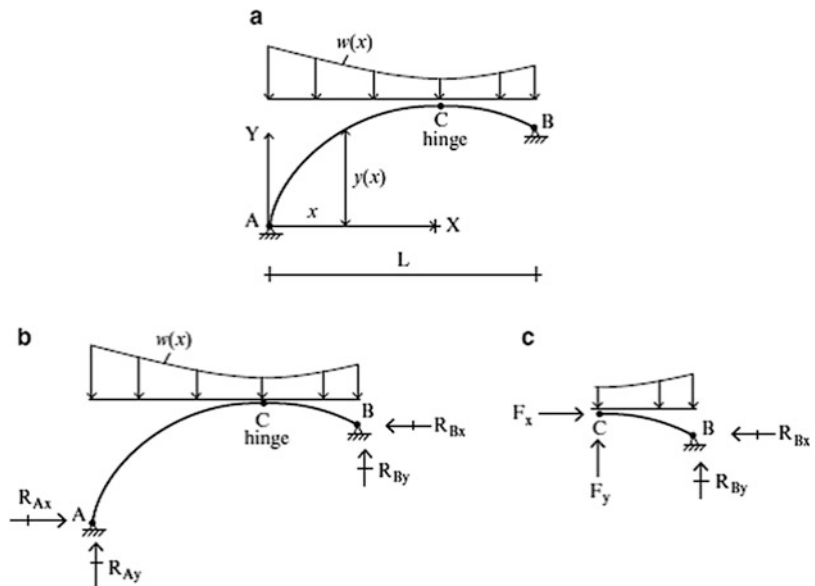
An arch is a particular type of curved member that is restrained against movement at its ends. Since these restraints produce longitudinal forces which counteract the action of vertical loads, arch structures are generally more efficient than straight members. In this section, we examine three-hinged arches, which are a popular form of arch structure. These structures are statically determinate. A more detailed study of statically indeterminate arches is presented in Chap. 9.

Consider the arch shown in Fig. 6.19. This structure is statically determinate since there is a moment release at C. The overall analysis strategy is as follows:

Step 1: Moment summation about A

Step 2: Moment summation about C for segment CB of the arch

Fig. 6.19 Geometry and reactions—three-hinged arch. (a) Geometry. (b) Reactions. (c) Right segment



These steps result in two equations relating R_{Bx} and R_{By} , which can be solved.

Step 3: X force summation $\rightarrow R_{Ax}$

Step 4: Y force summation $\rightarrow R_{Ay}$

Once the reactions are known, one can work in from either end and determine the internal forces and moment using the equations derived in the previous section. The following examples illustrate the approach.

Example 6.5 Three-Hinged Parabolic Arch

Given: The three-hinged arch shown in Fig. E6.5a.

Determine: The reactions. Assume $L_1 = 30$ m, $w = 15$ kN/m.

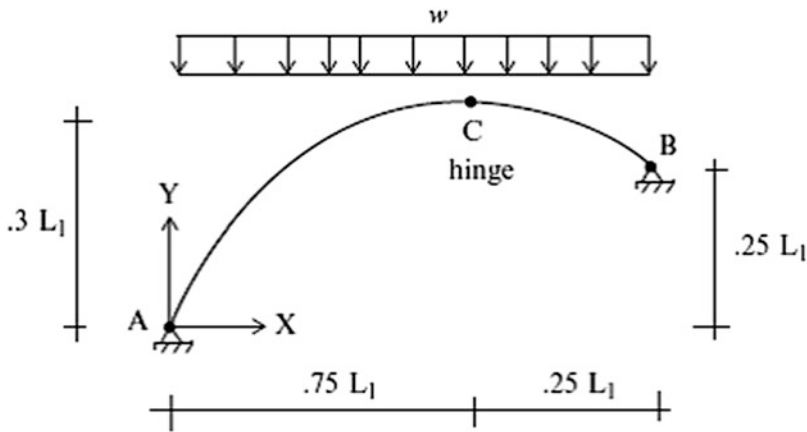


Fig. E6.5a

Solution: Summing moments about A and C leads to (Figs. E6.5b and E6.5c)

$$\sum M_{\text{at A}} = 0 \quad -w \frac{(L_1)^2}{2} + B_x(0.25L_1) + B_y(L_1) = 0$$

$$\sum M_{\text{at C}} = 0 \quad -w \frac{(0.25L_1)^2}{2} - B_x(0.05L_1) + B_y(0.25L_1) = 0$$

The solution of the above equations leads to

$$B_x = \frac{5}{6}wL_1 = 375 \text{ kN} \leftarrow$$

$$B_y = \frac{7}{24}wL_1 = 131.25 \text{ kN} \uparrow$$

Lastly, the reactions at A are determined using force equilibrium:

$$\sum F_y = 0 \quad A_y = -B_y + wL_1 = \frac{17}{24}wL_1 = 318.75 \text{ kN} \uparrow$$

$$\sum F_x = 0 \quad A_x = -B_x = 375 \text{ kN} \rightarrow$$

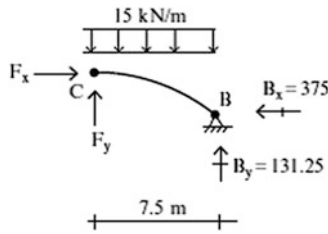


Fig. E6.5b

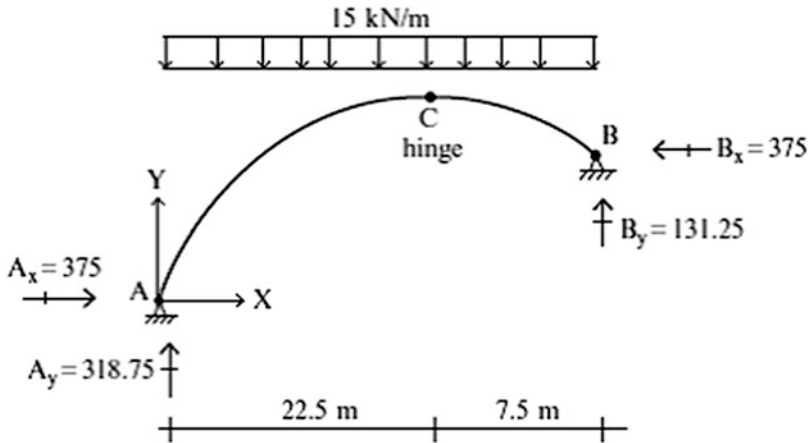


Fig. E6.5c

Example 6.6 Three-Hinged Parabolic Arch—Uniform Vertical Loading

Given: The parabolic arch shown in Fig. E6.6a.

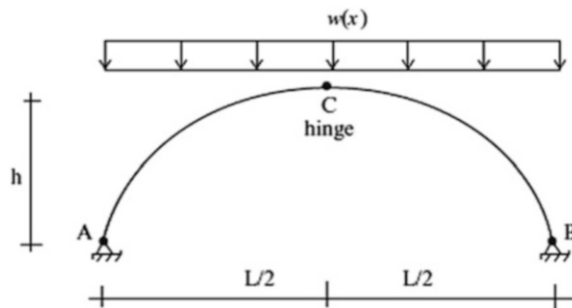


Fig. E6.6a

Determine: The internal forces and the vertical displacement at C (v_c).

Solution: The loading and arch geometry are symmetrical with respect to mid-span. It follows that the vertical reactions are equal to $wL/2$. Setting the moment at C equal to zero, we obtain an expression for R_{Bx} (Fig. E6.6b).

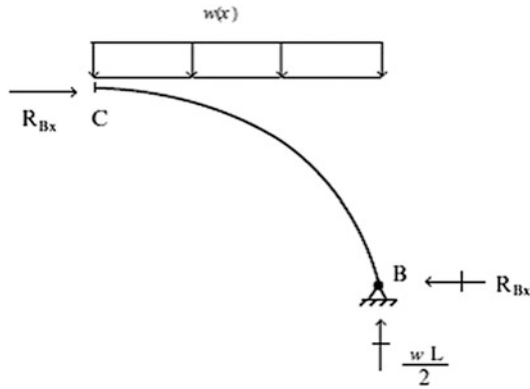


Fig. E6.6b

$$\sum M_c^{\curvearrowright} = 0$$

$$\frac{w}{2} \left(\frac{L}{2} \right)^2 + hR_{Bx} = \frac{wL}{2} \frac{L}{2} \rightarrow R_{Bx} = \frac{wL^2}{8h} \leftarrow$$

Then, summing X forces,

$$\sum F_x = 0$$

$$R_{Ax} = \frac{wL^2}{8h} \rightarrow$$

The results are listed below (Figs. E6.6b and E6.6c).

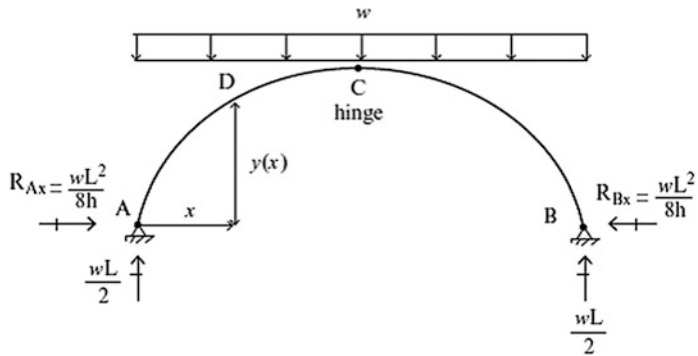


Fig. E6.6c

Cutting the member at D, isolating the segment AD, and applying the equilibrium conditions lead to:

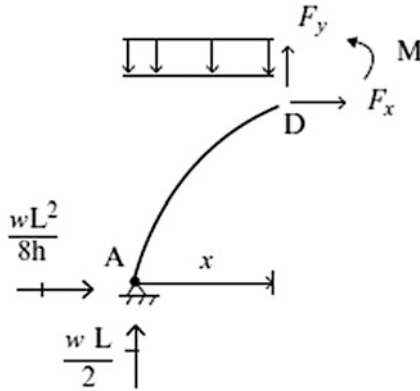


Fig. E6.6d

$$F_x = -\frac{wL^2}{8h}$$

$$F_y = wx - \frac{wL}{2}$$

$$M = \frac{wL}{2}x - \frac{wL^2}{8h}y - \frac{wx^2}{2}$$

Substituting for y , the expression for M reduces to

$$M = \frac{wL}{2}x - \frac{wL^2}{8h} \left\{ 4h \left[\frac{x}{L} - \left(\frac{x}{L} \right)^2 \right] \right\} - \frac{wx^2}{2} = 0$$

It follows that there is no bending moment in a three-hinged parabolic arch subjected to uniform loading per horizontal projection.

We could have deduced this result from the theory of cables presented in Chap. 5. We showed there that a cable subjected to a uniform vertical loading per horizontal projection adopts a parabolic shape. A cable, by definition, has no moment. Therefore, if one views a parabolic arch as an inverted cable, it follows that the moment in the arch will be zero. *This result applies only for uniform vertical loading; there will be bending for other types of loading applied to a parabolic arch.*

The axial force and transverse shear are determined with (6.2).

$$F = F_x \cos \theta + F_y \sin \theta = -\frac{wL^2}{8h} \cos \theta + \left(wx - \frac{wL}{2} \right) \sin \theta$$

$$V = -F_x \sin \theta + F_y \cos \theta = -\frac{wL^2}{8h} \sin \theta + \left(wx - \frac{wL}{2} \right) \cos \theta$$

where

$$\tan \theta = \frac{4h}{L} \left(1 - 2\frac{x}{L} \right)$$

$$\cos \theta = \frac{1}{\sqrt{1 + \tan^2 \theta}}$$

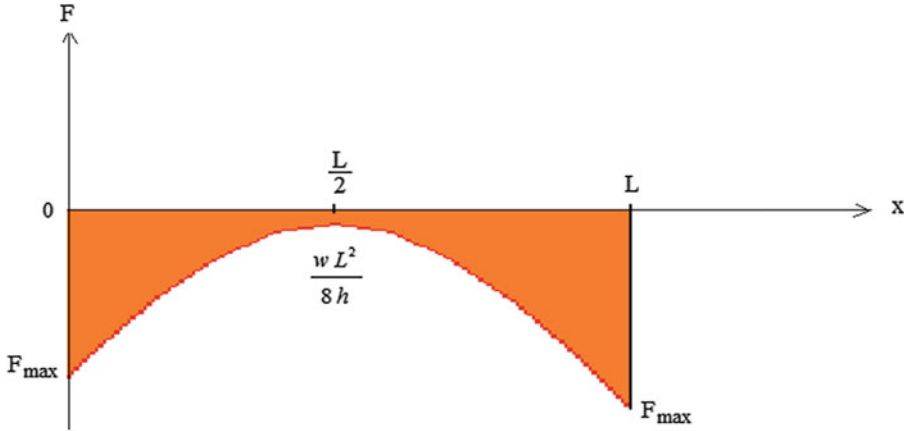
$$\sin \theta = \frac{\tan \theta}{\sqrt{1 + \tan^2 \theta}}$$

Expanding the expression for V and substituting for $\tan \theta$, one finds

$$V = \left[\tan \theta \frac{wL^2}{8h} + wx - \frac{wL}{2} \right] \cos \theta \equiv 0$$

The shear must be zero since the moment is zero. Only axial force exists for this loading.

The axial force distribution is plotted below. The maximum value is also tabulated as a function of h/L .



h/L	F_{\max}
0.1	$-1.35wL$
0.2	$-0.8wL$
0.3	$-0.65wL$
0.4	$-0.59wL$
0.5	$-0.56wL$

The solution, $M = V = 0$, is valid for a uniformly loaded three-hinged parabolic arch, i.e., it applies for both *deep* and *shallow* arches.

If we use the approximate form of the method of virtual forces specialized for a “deep” arch,

$$v_c = \int_S \frac{M \delta M}{EI} ds$$

it follows that the arch does not displace due to bending deformation. However, there will be displacement due to the axial deformation. We need to start with the exact expression,

$$v_c = \int_S \left(\frac{M \delta M}{EI} + \frac{F \delta F}{EA} \right) ds$$

and then set $M = 0$

$$v_c \cong \int_S \frac{F \delta F}{EA} ds$$

Suppose the vertical displacement at mid-span is desired. The virtual force system for $\delta P = 1$ is

$$\begin{aligned} \delta F_x &= -\frac{L}{4h} \\ \delta F_y &= -\frac{1}{2} \end{aligned} \Rightarrow \delta F = \left(-\frac{L}{4h} \right) \cos \theta + \left(-\frac{1}{2} \right) \sin \theta$$

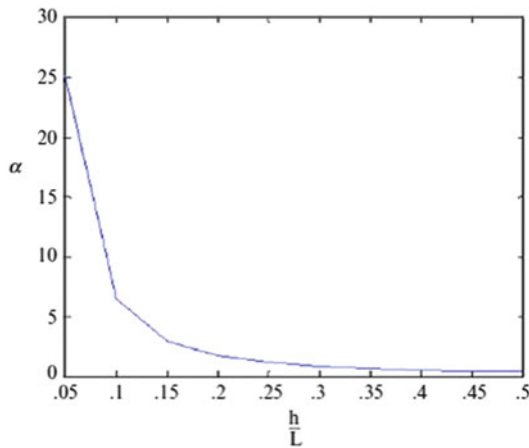
Substituting for the forces and assuming AE is constant result in the following integral

$$v_c = \frac{1}{AE} \int_0^L \left\{ \left(-\frac{wL^2}{8h} \right) + \left(-\frac{wL}{2} + wx \right) \tan \theta \right\} \left(-\frac{L}{4h} - \frac{1}{2} \tan \theta \right) \cos \theta dx$$

We express the solution as

$$v_c = \frac{wL^2}{AE} \{ \alpha \}$$

where α is a function of h/L . The following plot shows the variation of α . Note that v_c approaches 0 for a deep arch.



Example 6.7 Three-Hinged Parabolic Arch—Concentrated Load Applied at Mid-Span

Given: The parabolic arch defined in Fig. E6.7a

Determine: The internal forces and vertical displacement at C (v_c).

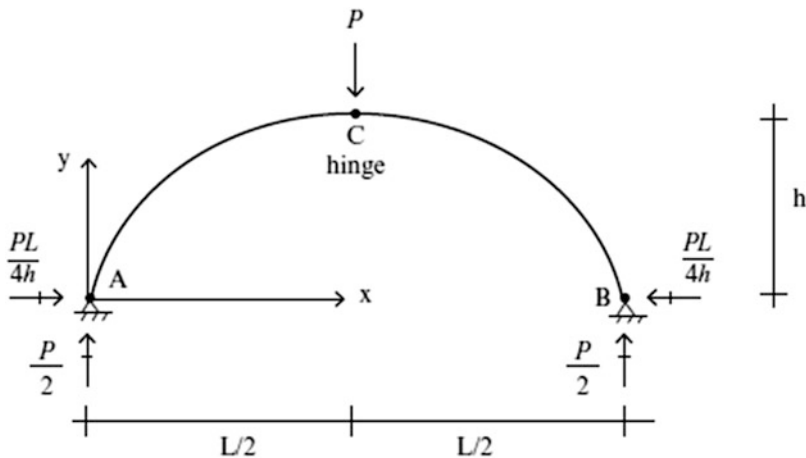


Fig. E6.7a

Solution: Enforcing equilibrium leads to the following expressions for the internal forces (Fig. E6.7b):

Segment AC $0 \leq x < L/2$

$$F_x = -\frac{PL}{4h}$$

$$F_y = -\frac{P}{2}$$

$$M = \frac{P}{2}x - \frac{PL}{4h}y$$

Segment CB $L/2 < x \leq L$

$$F_x = -\frac{PL}{4h}$$

$$F_y = \frac{P}{2}$$

$$M = -\frac{P}{2}x - \frac{PL}{4h}y + \frac{PL}{2}$$

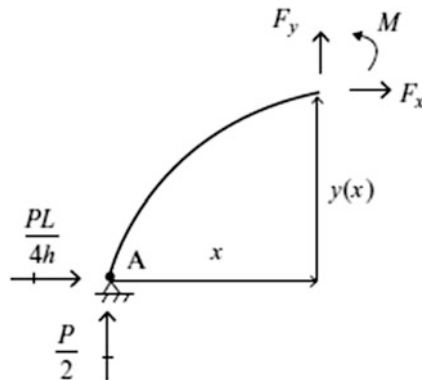


Fig. E6.7b

The corresponding transformed internal forces are
Segment AC $0 \leq x < L/2$

$$F = -\frac{P}{2}\sin\theta - \frac{PL}{4h}\cos\theta$$

$$V = -\frac{P}{2}\cos\theta + \frac{PL}{4h}\sin\theta$$

$$M = \frac{P}{2}x - PL\left[\frac{x}{L} - \left(\frac{x}{L}\right)^2\right] = PL\left(-\frac{x}{2L} + \frac{x^2}{L^2}\right)$$

Segment CB $L/2 < x \leq L$

$$F = \frac{P}{2} \sin \theta - \frac{PL}{4h} \cos \theta$$

$$V = \frac{P}{2} \cos \theta + \frac{PL}{4h} \sin \theta$$

$$M = PL \left(-\frac{3x}{2L} + \frac{x^2}{L^2} + \frac{1}{2} \right)$$

The values of F , V , and M are listed below.

X/L	M/PL	$h/L = 0.5$		$h/L = 0.1$	
		F/P	V/P	F/P	V/P
0	0	-0.67	0.22	-2.51	0.46
0.1	-0.04	-0.69	0.16	-2.53	0.3
0.2	-0.06	-0.7	0.06	-2.55	0.1
0.3	-0.06	-0.7	-0.08	-2.55	-0.1
0.4	-0.04	-0.65	0.28	-2.53	-0.3
0.5	0	-0.5	±0.5	-2.5	±0.5
0.6	-0.04	-0.65	0.28	-2.53	0.3
0.7	-0.06	-0.7	0.08	-2.55	0.1
0.8	-0.06	-0.7	0.06	-2.55	-0.1
0.9	-0.04	-0.69	-0.16	-2.53	-0.3
1	0	-0.67	-0.22	-2.51	-0.46

The maximum moment occurs at the location where $dM/dx = 0$. Note that $M_{\max} = +PL/4$ for a straight member.

$$\frac{dM}{dx} = 0 \Rightarrow x|_{M_{\max}} = \frac{L}{4} \Rightarrow M_{\max} = -\frac{PL}{16}$$

The distribution of F , V , and M is plotted below. The reversal in sense of M is due to the influence of the horizontal thrust force on the bending moment (Figs. E6.7c, E6.7d, and E6.7e).

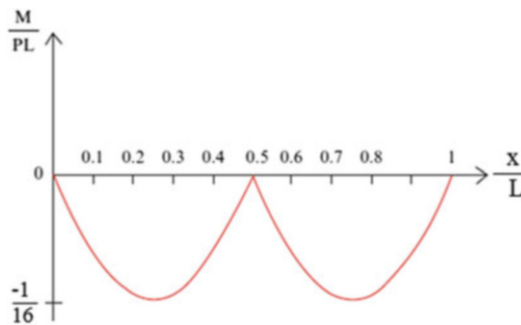


Fig. E6.7c

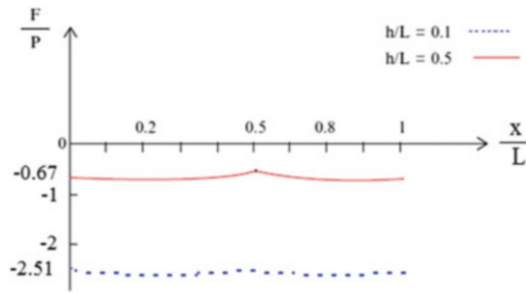


Fig. E6.7d

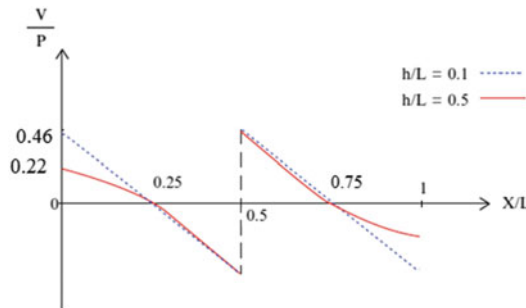


Fig. E6.7e

The virtual forces for the computation of v_c are (Fig. E6.7f)

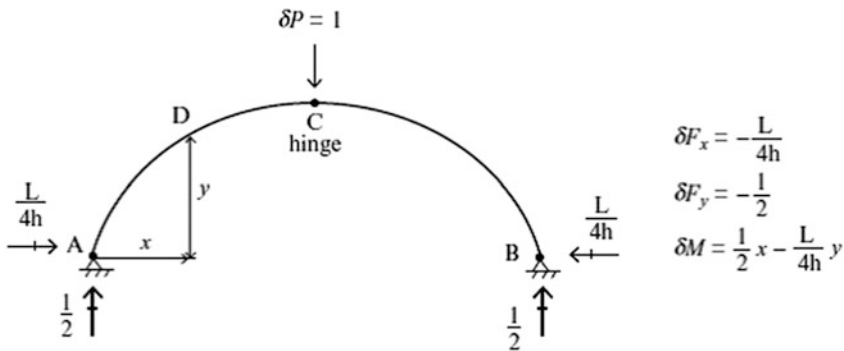


Fig. E6.7f

We consider only bending deformation. The displacement at C is given by

$$v_c = 2 \int_0^{L/2} \frac{P}{2} \left(x - \frac{L}{2h}y\right) \frac{1}{2} \left(x - \frac{L}{2h}y\right) \frac{dx}{EI \cos \theta}$$

When I is a function of x , we use either symbolic or numerical integration. However, when I is taken as $I_0/\cos \theta$, the integral simplifies and one can obtain an analytical solution. The analytical solution corresponding to this assumption is

$$v_c = \frac{PL^3}{EI_0} \left(\frac{1}{30}\right)$$

Example 6.8 Three-Hinged Parabolic Arch with Horizontal and Vertical Loads

Given: The parabolic arch and loading defined in Fig. E6.8a.

Determine: (a) Determine the analytical expressions for the axial force, shear force, and bending moment. (b) Using computer software, determine the vertical and horizontal displacements at C due to the loading. Take $E = 29,000$ ksi, $I = 5000$ in.⁴, and $A = 500$ in.² Discretize the arch using segments of length $\Delta x = 1$ ft. Also determine profiles for displacement, moment, and axial force.

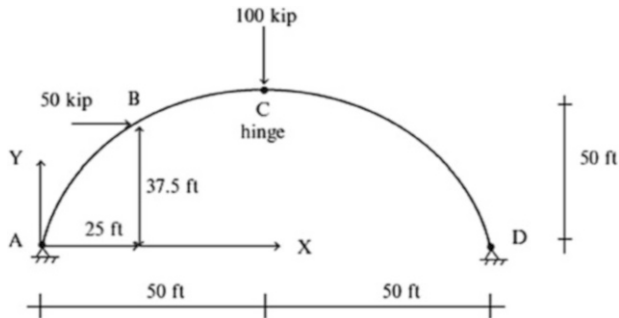


Fig. E6.8a

Solution: (a) The reactions are listed on Fig. E6.8b.

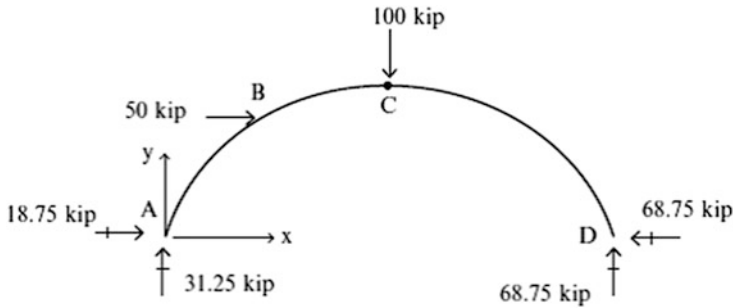


Fig. E6.8b

Noting that $y = 2(x - x^2/100)$ and isolating different segments along the centroidal axis lead to the following expressions for moment (M), axial force (F), and shear (V).

Segment AB $0 \leq x < 25$

$$\begin{aligned}
 F_x &= -18.75 & F &= -18.75 \cos \theta - 31.25 \sin \theta \\
 F_y &= -31.25 & \Rightarrow V &= -18.75 \sin \theta - 31.25 \cos \theta \\
 M &= 31.25x - 18.75y & M &= 31.25x - 18.75y
 \end{aligned}$$

Segment BC $25 < x < 50$

$$\begin{aligned}
 F_x &= -68.75 & F &= -68.75 \cos \theta - 31.25 \sin \theta \\
 F_y &= -31.25 & \Rightarrow V &= -68.75 \sin \theta - 31.25 \cos \theta \\
 M &= 31.25x - 18.75y - 50(y - 37.5) & M &= 31.25x - 18.75y - 50(y - 37.5)
 \end{aligned}$$

Segment CD $50 < x \leq 100$

$$\begin{aligned}
 F_x &= -68.75 & F &= -68.75 \cos \theta + 68.75 \sin \theta \\
 F_y &= 68.75 & \Rightarrow V &= 68.75 \sin \theta + 68.75 \cos \theta \\
 M &= 68.75(100 - x) - 68.75y & M &= 68.75(100 - x) - 68.75y
 \end{aligned}$$

(b) The computer generated moment, axial force, and deflection profiles are listed below (Figs. E6.8c, E6.8d, and E6.8e). Hand computation is not feasible for this task.



Fig. E6.8c Moment, M

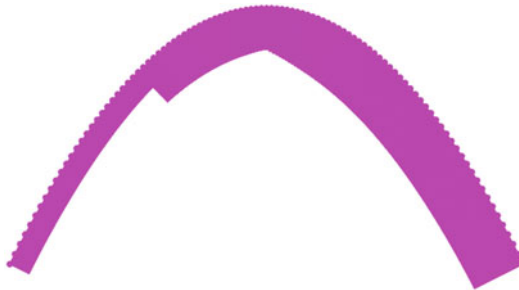


Fig. E6.8d Axial, F

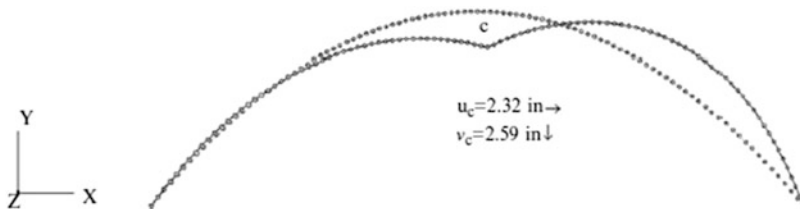


Fig. E6.8e Deflection profile

Example 6.9 Optimal Shape for a Statically Determinate Arch

Given: The loading defined in Fig. E6.9a and support locations A and B. Assume H is a variable.

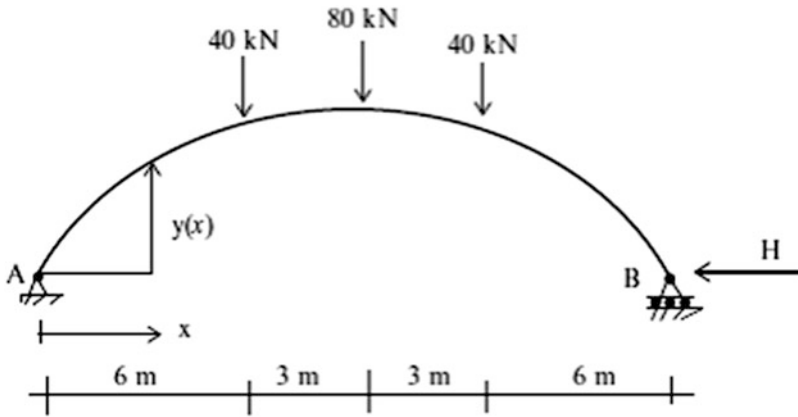


Fig. E6.9a

Determine: The optimal shape of the arch passing through A and B. Consider H to vary from 80 to 200 kN. Note that the optimum shape corresponds to zero bending moment.

Solution: We first generate the bending moment distribution in a simply supported beam spanning between A and B (Fig. E6.9b).

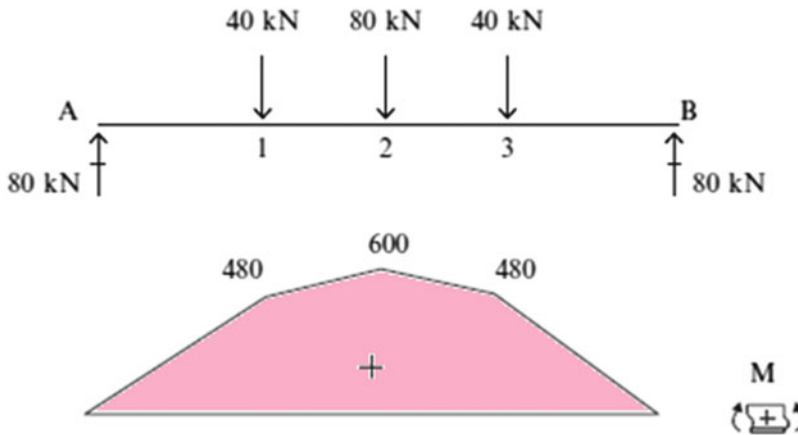


Fig. E6.9b

Requiring the bending moment to vanish at points 1, 2, 3 leads to the following y coordinates of points 1, 2, and 3:

$$y_1 = \frac{480}{H} \quad y_2 = \frac{600}{H} \quad y_3 = \frac{480}{H}$$

This piecewise solution is the general solution for the optimal shape (Fig. E6.9c). One specifies H and then determines the coordinates. The value of H selected depends on the capacity of the supports to resist lateral loading.

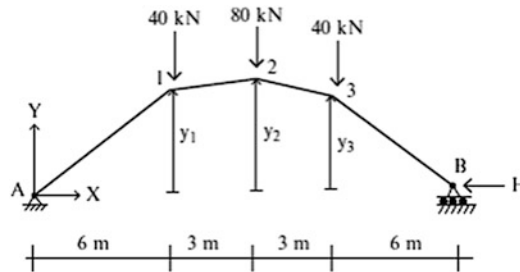


Fig. E6.9c Optimal shape

Configurations corresponding to various values of H are listed below. Note that as H increases, the shape becomes shallower.

H (kN)	y_1 (m)	y_2 (m)	y_3 (m)
80	6	7.5	6
120	4	5	4
160	2	3.75	3
200	1.4	3	2.4

6.7 Summary

6.7.1 Objectives

- To develop the equilibrium equations for planar curved members and illustrate their application to parabolic and circular arches.
- To introduce and apply the Principle of Virtual Forces for planar curved members.
- To describe the analysis process for three-hinged arches.
- To illustrate the behavior of statically determinate parabolic arches subjected to vertical and lateral loading.

6.7.2 Key Factors and Concepts

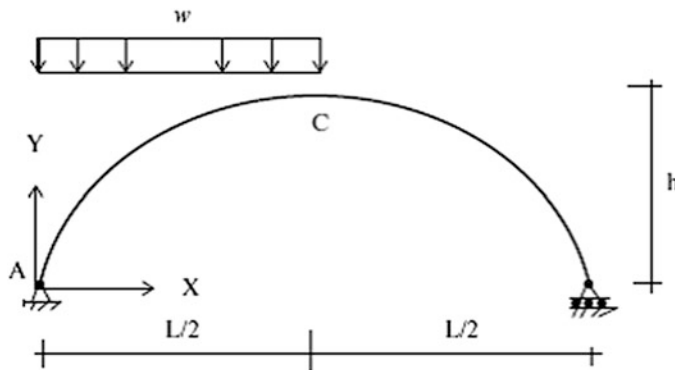
- Depending upon the loading distribution, the geometry of the member, and the support conditions, a curved member may support transverse loading mainly by axial action. This feature makes curved members very attractive for long span structures.
- Curved members are classified as either shallow or non-shallow, depending upon the ratio of height to span length. For shallow members, bending and axial actions are coupled. In the limit, a shallow curved member reduces to a beam.
- When applying the principle of virtual forces to compute displacements of a slender non-shallow (deep) curved member, the contributions due to axial and shear deformation are usually negligible compared to the contribution from bending deformation.

- In general, three-hinged arches carry load through both bending and axial action. However, when the arch shape is parabolic and the vertical loading is uniform, there is no bending moment in the three-hinged arch.
- Two-hinged curved members are statically indeterminate. A general theory for these structures is presented in Chap. 9. One can show that, based on this theory, a moment free state can be obtained for an arbitrary loading by adjusting the shape of the curved member. In this case, two-hinged curved members behave similar to cables.

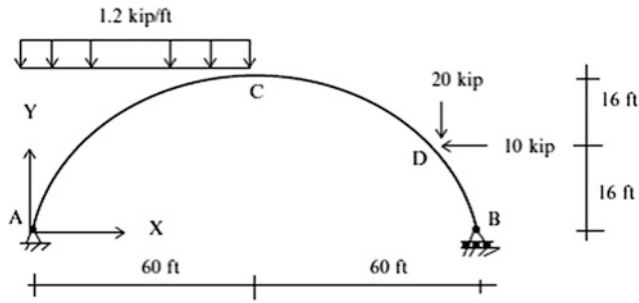
6.8 Problems

Problem 6.1 Consider the parabolic member shown below. Find the reactions and member forces (F , V , and M).

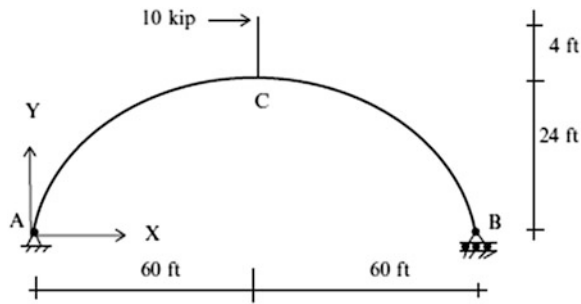
- (a) Assume $w = 1.2$ kip/ft, $h = 24$ ft, $L = 120$ ft
 (b) Assume $w = 18$ kN/m, $h = 7$ m, $L = 36$ m



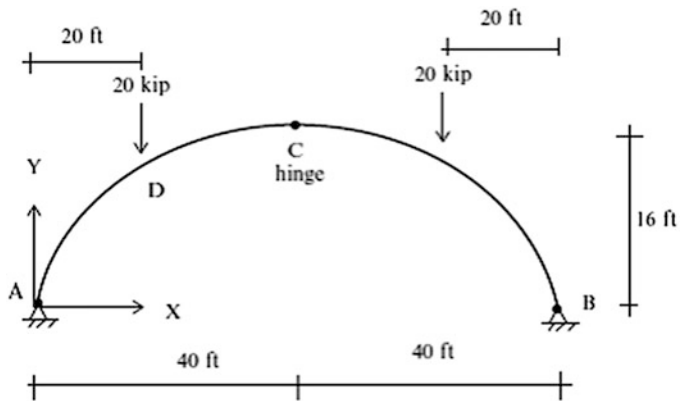
Problem 6.2 Consider the parabolic member shown below. Find the reactions and member forces at $x = 20$ and 80 ft.



Problem 6.3 Consider the parabolic member shown below. Find the reactions and member forces (F , V , and M).

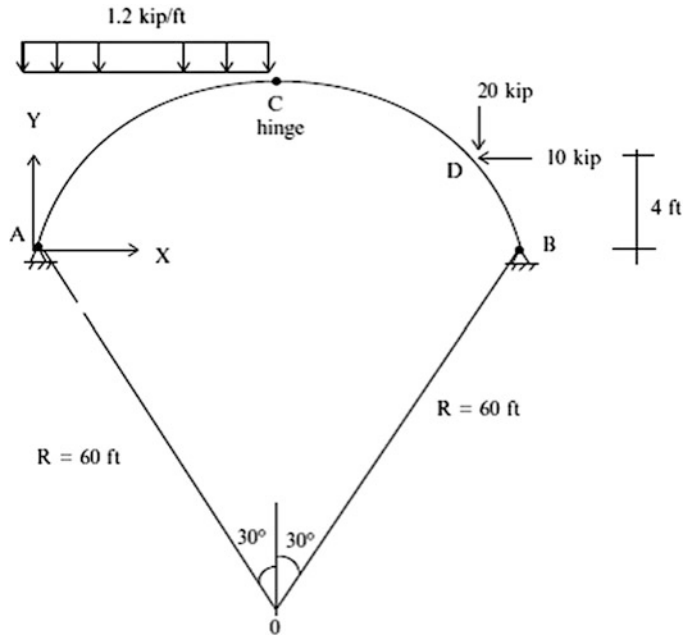


Problem 6.4 Determine the reactions, the axial and shear forces, and the moments at $x = 30$ ft for the three-hinged parabolic arch shown below.

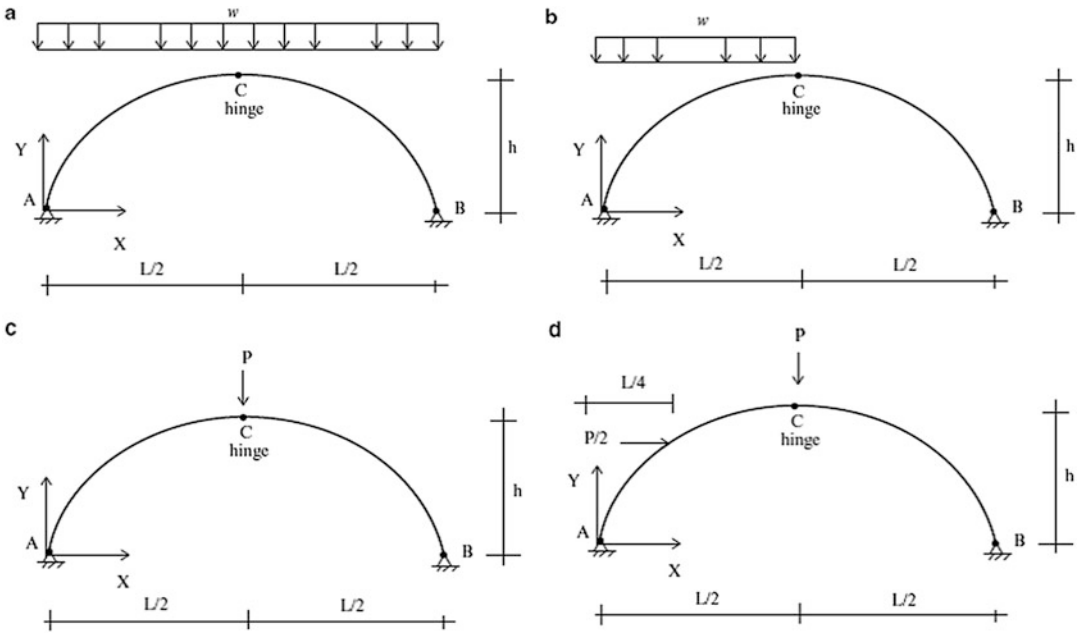


Problem 6.5 Consider the three-hinged circular arch shown below

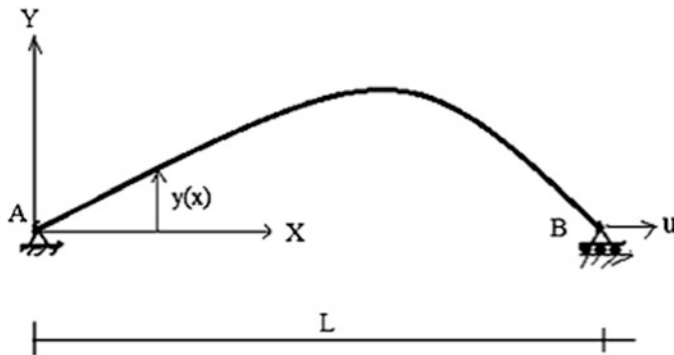
- (a) Find the reactions.
- (b) Determine the axial and shear forces and the moments at $x = 20$ ft and $x = 40$ ft.



Problem 6.6 Consider the three-hinged parabolic arches shown below. Determine analytical expression for the axial force, shear force, and bending moment. Using computer software, determine displacement profiles. Take $h = 9$ m, $L = 30$ m, $P = 450$ kN, $w = 30$ kN/m, $E = 200$ GPa, $I = 160$ (10^6) mm^4 , and $A = 25,800$ mm^2

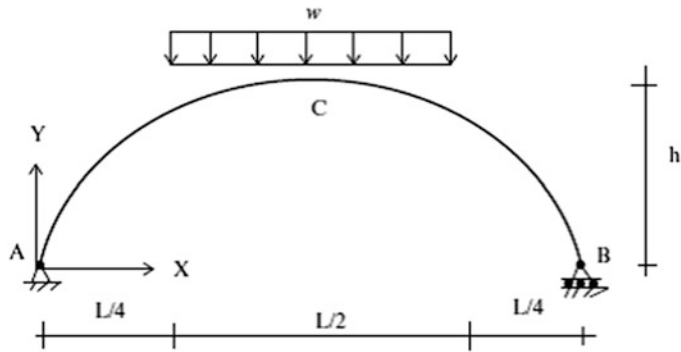


Problem 6.7 Consider the simply supported curved member shown below. Assume the shape is defined by an arbitrary function, $y = y(x)$. Suppose the member experiences a uniform temperature increase, ΔT , over its entire length. Determine the horizontal displacement of B .



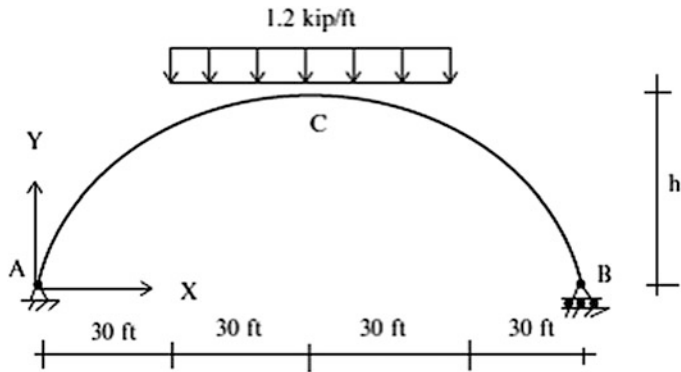
Problem 6.8 Consider the parabolic member shown below. Determine the horizontal displacement at B .

- (a) Assume $w = 1.2$ kip/ft, $h = 24$ ft, $L = 120$ ft, $E = 29,000$ ksi
- (b) Assume $w = 18$ kN/m, $h = 7$ m, $L = 36$ m, $E = 200$ GPa



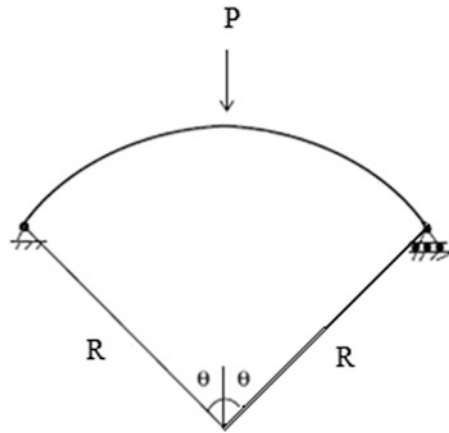
Problem 6.9 Consider the parabolic member shown below. Determine the vertical displacement at C. Take $I = 400 \text{ in.}^4$, $A = 40 \text{ in.}^2$, $E = 29,000 \text{ kip/in.}^2$

- (a) $h = 10 \text{ ft}$
- (b) $h = 30 \text{ ft}$



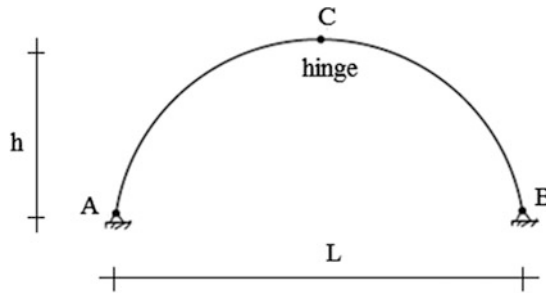
Problem 6.10

- (a) Determine analytical expressions for the member forces for the circular curved member shown below. Take $R = 40 \text{ ft}$, $P = 10 \text{ kip}$, and $\theta = 30^\circ$.
- (b) Repeat part (a) using a computer software package. Discretize the arc length into 3° segments. Assume the following values for the member properties: $E = 29,000 \text{ ksi}$, $I = 400 \text{ in.}^4$, and $A = 40 \text{ in.}^2$ Compare the analytical and computer generated values for moment and axial force.



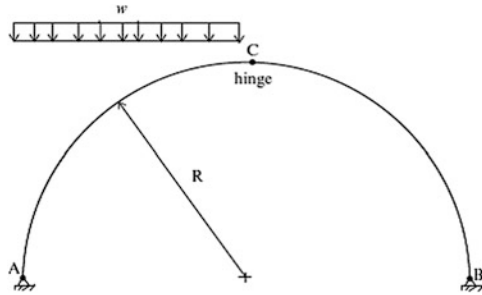
Problem 6.11 Consider the three-hinged arch shown below. Discuss how the arch behaves when:

- There is a uniform temperature increase.
- The support at B settles.



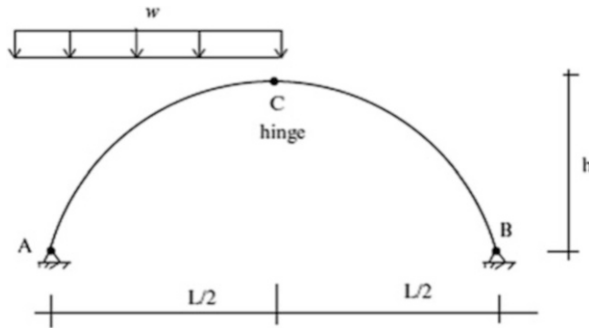
Problem 6.12 Consider the semicircular three-hinged arch shown below. Determine the vertical and horizontal displacements at C due to the loading.

- Assume $E = 29,000$ ksi, $I = 400$ in.⁴, $A = 40$ in.², $R = 50$ ft, and $w = 2$ kip/ft
- Assume $E = 200$ GPa, $I = 160(10^6)$ mm⁴, $A = 25,800$ mm², $R = 15$ m, and $w = 30$ kN/m

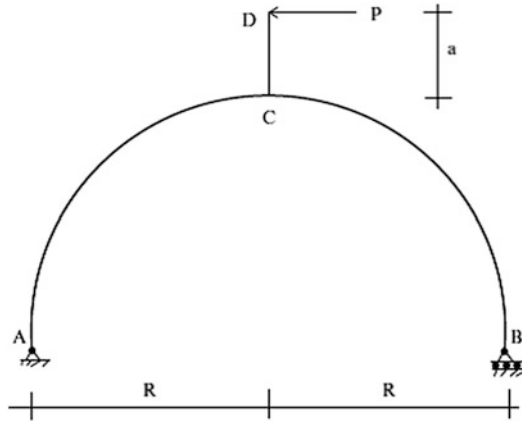


Problem 6.13 Consider the parabolic three-hinged arch shown below. Using computer software, determine the vertical and horizontal displacements at C due to the loading. Discretize the arch using segments of length $\Delta x = L/10, L/20,$ and $L/40$. Compare the convergence rate for these segment sizes.

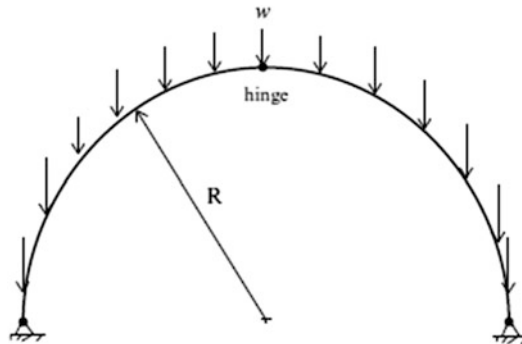
- (a) Take $E = 29,000$ ksi, $I = 400$ in.⁴, $A = 40$ in.², $L = 120$ ft, $h = 60$ ft, and $w = 2$ kip/ft
- (b) Take $E = 200$ GPa, $I = 160(10^6)$ mm⁴, $A = 2500$ mm², $L = 36$ m, $h = 18$ m, and $w = 30$ kN/m



Problem 6.14 Consider the semicircular curved member shown below. Member CD is rigidly attached to the curved member at C. Determine an expression for the horizontal displacement at D due to P.

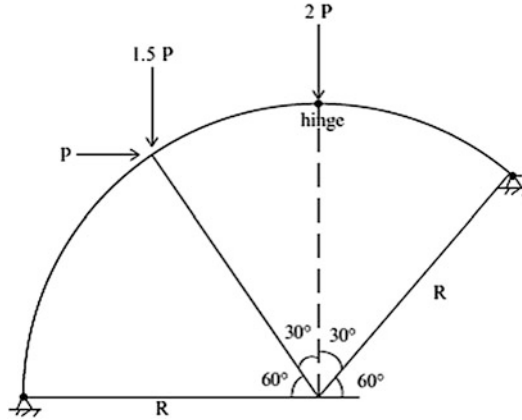
**Problem 6.15**

- (a) Determine analytical solutions for the axial, shear, and moment distribution for the three-hinged semicircular arch shown. Consider the loading to be due to self-weight w . Take $w = 0.6$ kip/ft and $R = 40$ ft.
- (b) Apply computer software using the following discretization: $\Delta\theta = 9^\circ, 4.5^\circ, 2.25^\circ$. Compare the convergence rate of the solution. Take $E = 29,000$ ksi, $I = 400$ in.⁴, and $A = 40$ in.²

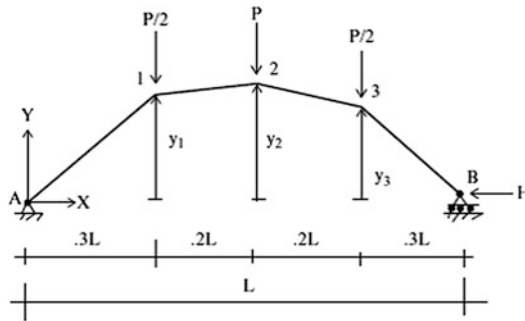


Problem 6.16 Determine the member forces for the three-hinged circular arch shown. Use computer software.

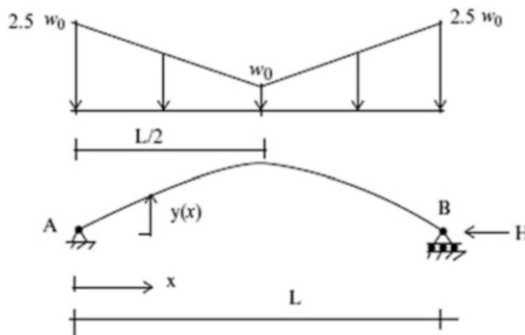
- (a) Take $E = 29,000$ ksi, $R = 40$ ft, $P = 4$ kip, $I = 400$ in.⁴, and $A = 40$ in.²
- (b) Take $E = 200$ GPa, $R = 12$ m, $P = 18$ kN, $I = 160(10^6)$ mm⁴, and $A = 25,800$ mm²



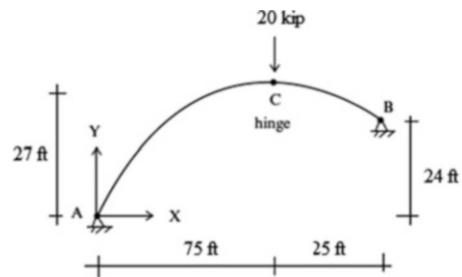
Problem 6.17 Determine the optimal shape of the arch passing through A and B for given value of H . Note that optimum shape corresponds to zero moment. Assume $L = 120$ ft and $P = 25$ kip.



Problem 6.18 Determine the optimal shape of the arch for a given value of H . Assume $L = 30$ m and $w_0 = 15$ kN/m.



Problem 6.19 Consider the three-hinged arch shown below. Determine the reactions and the internal forces.



Reference

1. Tauchert TR. Energy principles in structural mechanics. New York: McGraw-Hill; 1974.

Abstract

Civil structures such as bridges and buildings are placed on the ground. The particular segment of the structure which interfaces with the ground is called the foundation. In this chapter, we focus on a particular type of foundation called a shallow foundation. Shallow foundations are composed of footings which are plate-type elements placed on the ground. Their function is to transmit the loads in the columns and walls to the ground. In this chapter, we describe the various types of shallow footings and identify the conditions under which each type is deployed. Then, we develop an analytical procedure for establishing the soil pressure distribution under a footing due to an arbitrary column loading. Given the soil pressure distribution, one can generate the shear and moment distribution in the footing and establish the peak values required for design. Lastly, we describe how to determine these design values and also present various strategies for dimensioning shallow footings.

7.1 Introduction

7.1.1 Types of Foundations

Civil structures are viewed as having two parts. That part of the structure which is above ground is called the superstructure; the remaining part in contact with the ground is referred to as either the substructure or the foundation. Up to this point, we have focused on the superstructure. Structural Engineers are responsible for the foundation design as well as the superstructure design. They are aided by Geotechnical Engineers who provide information on the soil properties such as the allowable soil bearing pressure at the site.

Figure 7.1 illustrates the different types of foundations. Shallow foundations are located near ground level. The structural loads are transferred directly to the soil through plate-type elements placed under the columns. These plate elements are called footings. This scheme is feasible only when the soil strength is adequate to resist the applied loading. If the soil near the surface is weak, it is

Fig. 7.1 Types of foundations. (a) Shallow foundation. (b) Deep foundation

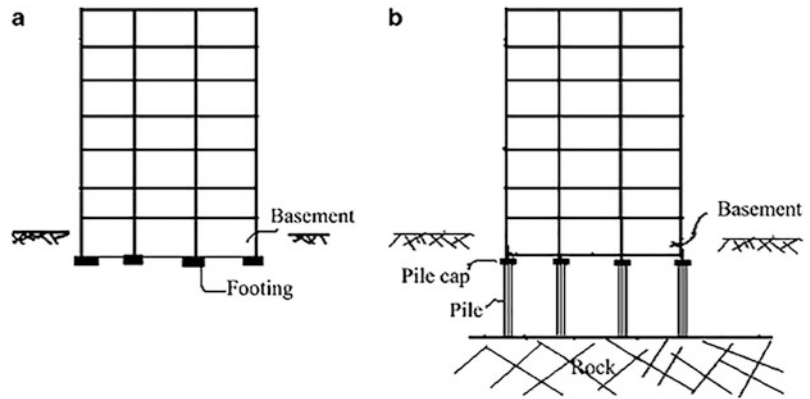
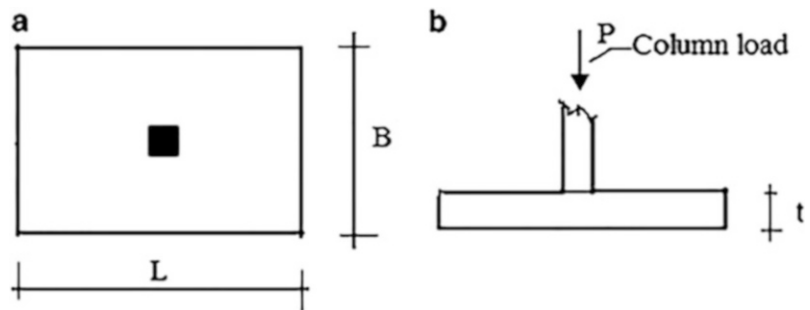


Fig. 7.2 Single footing—axial loading. (a) Plan. (b) Elevation



necessary to transfer the loads to a deeper soil layer having adequate strength. Piles or caissons are typically used to transmit loads through weak soil media. Basements which serve as underground parking facilities may also be incorporated in foundations.

7.1.2 Types of Shallow Foundations

A spread footing is a reinforced concrete plate-type structural component that rests directly on the ground and supports one or more columns or walls. Different geometrical arrangements of footings are used, depending on the column spacing and soil strength. The simplest scheme is a single footing per column, shown in Fig. 7.2. One usually works with a square area. However, there sometimes are constraints such as proximity to a boundary line which necessitate shifting to a rectangular geometry. We describe later a procedure for determining the “dimensions” of the footing given certain geometric constraints. In what follows, we consider the column load to be an axial force. Later, we extend the analysis to deal with both axial force and bending moment.

When adjacent columns are located too close to each other such that their footings would overlap, or when one of the adjacent columns is located close to a property line, the adjacent footings are combined into a single “mega” footing which is designed to support the multiple column loads. Figure 7.3 illustrates this footing layout which is called a “*combined footing*.”

A different strategy is employed when the spacing between columns is large and one of the columns is located too close to a property line to support the entire column load with a single footing. It is necessary to shift some of the column loads over to an adjacent footing by connecting the footings with a strap beam. This scheme is called a “*strap footing*” (see Fig. 7.4).

Fig. 7.3 Combined footing layout. (a) Elevation. (b) Plan view

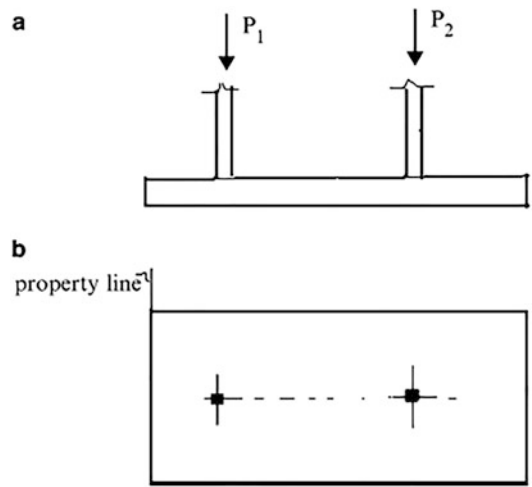
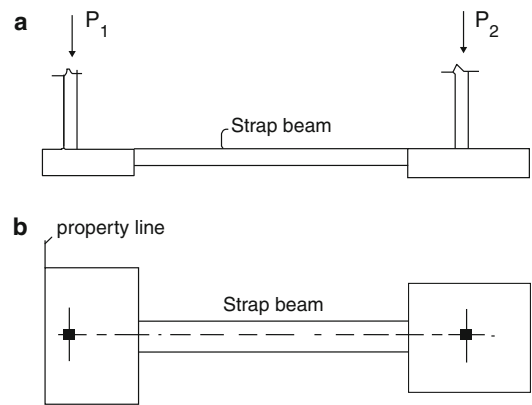


Fig. 7.4 Strap footing layout. (a) Elevation. (b) Plan view



7.1.3 Soil Pressure Distribution

A vertical loading applied to the footing is resisted by soil pressure acting on the lower surface of the footing. The distribution of pressure depends on the type of soil at the site. Typical distributions for sand and clay type soils are shown in Fig. 7.5. In practice, we approximate the actual pressure distribution due to a concentric load with an “average uniform” distribution.

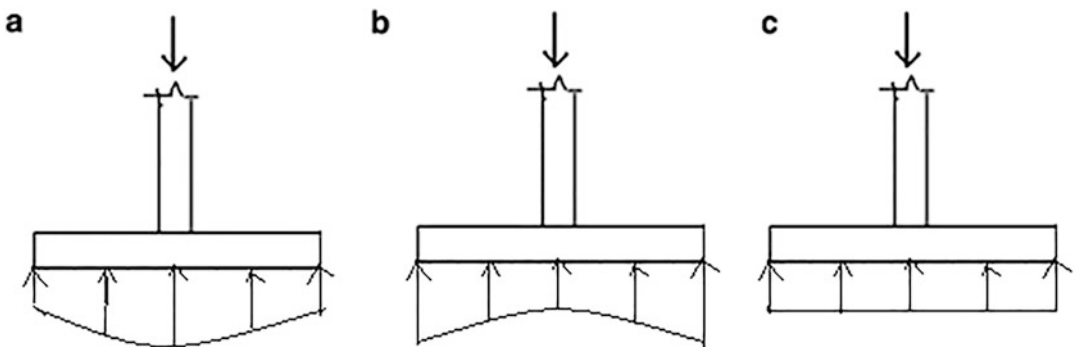
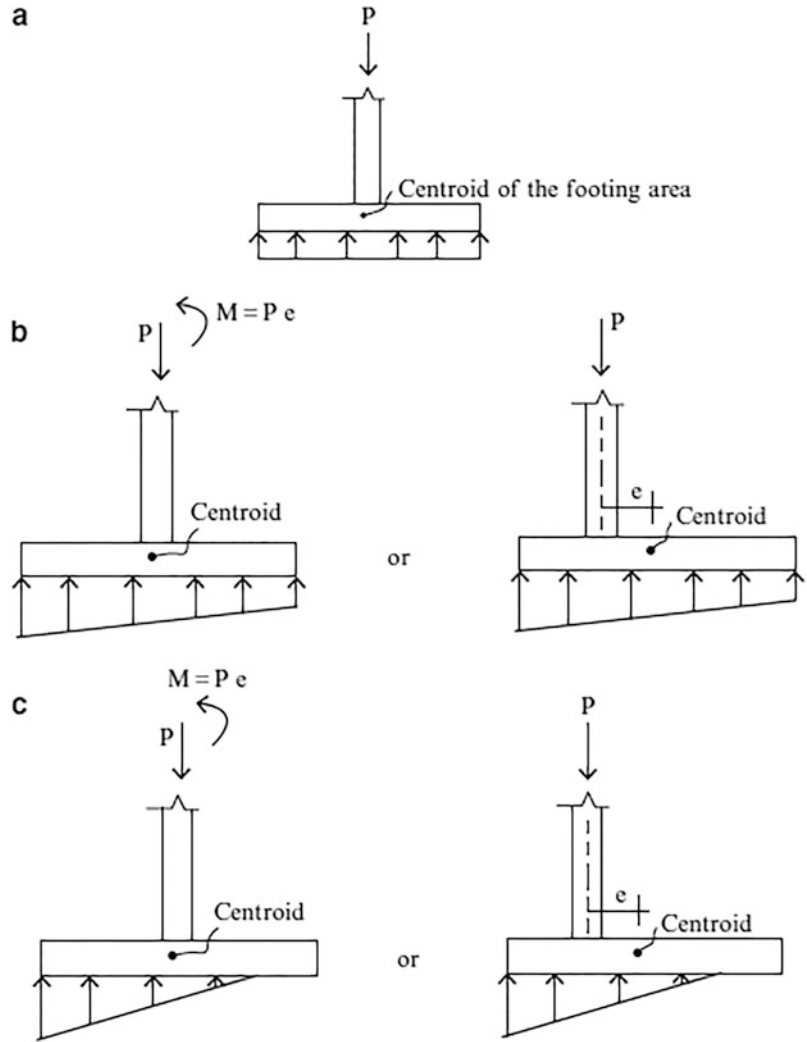


Fig. 7.5 Soil pressure distributions—concentric load. (a) Sandy soil. (b) Clayey soil. (c) Average soil pressure

Fig. 7.6 Idealized pressure distributions. (a) Uniform. (b) Trapezoidal. (c) Triangular



Depending on the column loading and the location of the column with respect to the centroid of the footing area, one of the distributions shown in Fig. 7.6 is normally assumed in order to establish the dimensions of the footing. A uniform distribution is the most desirable distribution. Since soil cannot resist tensile stress, one wants to avoid the case illustrated in Fig. 7.6c. We will describe a strategy for selecting the footing dimensions so as to avoid this situation in the following section.

The allowable pressure varies with the type of soil. Soil is a natural material in contrast to steel, which is manufactured with close quality control. Consequently, there is considerable variability in soil properties. Typical allowable soil pressures for various types of soils are listed in Table 7.1. These values are useful for estimating initial footing dimensions.

Table 7.1 Allowable soil pressures—Reference Terzaghi and Peck [1]

Soil type	Allowable bearing pressure [kip/ft ² (kN/m ²)]
Compact coarse sand	8 (383)
Hard clay	8 (383)
Medium stiff clay	6 (287)
Compact inorganic sand	4 (191)
Loose sand	3 (144)
Soft sand/clay	2 (96)
Loose inorganic sand–silt mixture	1 (48)

7.2 An Analytical Method for Evaluating the Soil Pressure Distribution Under a Footing

We consider the single footing shown in Fig. 7.7. The force P represents the resultant of the column loading. We suppose it has an eccentricity e with respect to the centroid of the footing area. We also suppose the footing area is symmetrical with respect to the x -axis and locate the area such that the column load is on the axis of symmetry. It follows that the pressure loading is symmetrical with respect to this axis. Taking the origin for x at the centroid of the footing area, we express the pressure distribution as a linear function,

$$q(x) = b + ax \quad (7.1)$$

where a and b are unknown parameters. We determine these parameters by enforcing the equilibrium conditions for the footing.

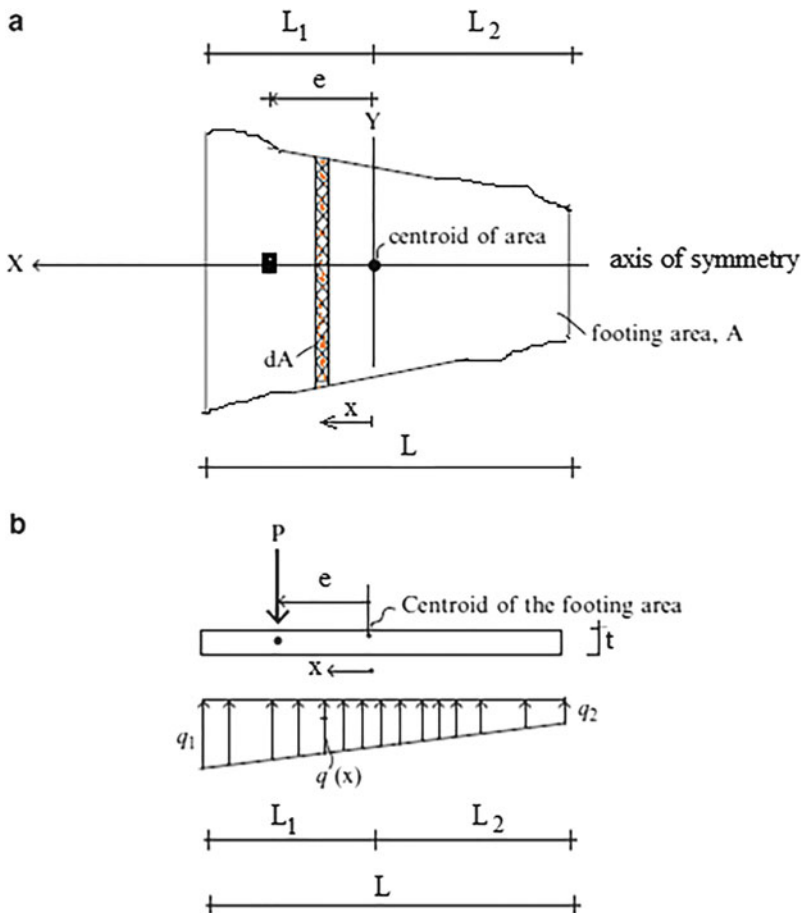


Fig. 7.7 Notation—pressure distribution—single footing. (a) Plan. (b) Elevation

Since x is measured from the centroid, the first moment of area vanishes. Then, $\int x dA = 0$. Requiring force and moment equilibrium to be satisfied, and noting that the column axial loading has an eccentricity, e , with respect to the centroid of the footing area, leads to the following expressions for b and a .

Vertical force equilibrium:

$$P = \int q(x) dA = \int (b + ax) dA = b \int dA + a \int x dA = bA + 0$$

$$\Downarrow$$

$$b = \frac{P}{A}$$

Moment equilibrium:

$$Pe = \int q(x)x dA$$

$$\Downarrow$$

$$Pe = \int (b + ax)x dA = b \int x dA + a \int x^2 dA = 0 + aI_y$$

$$\Downarrow$$

$$a = \frac{Pe}{I_y}$$

where I_y is the second moment of the footing area with respect to the Y -axis, $I_y = \int x^2 dA$. Substituting for a and b , (7.1) takes the form

$$q(x) = \frac{P}{A} + \frac{Pe}{I_y}x \quad (7.2)$$

The peak pressures are shown in Fig. 7.7b.

$$q_1 = \left\{ \frac{P}{A} + \frac{(Pe)L_1}{I_y} \right\}$$

$$q_2 = \left\{ \frac{P}{A} - \frac{(Pe)L_2}{I_y} \right\} \quad (7.3)$$

One uses (7.3) to determine the pressure when the footing area is defined.

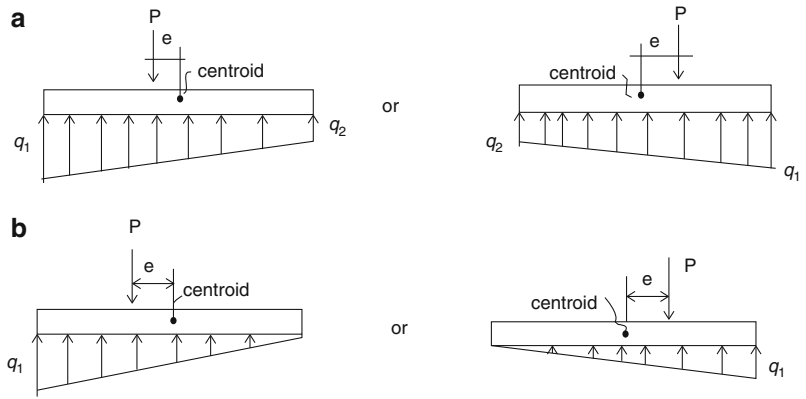
When the resultant acts at the centroid, $e = 0$ and the pressure distribution reduces to a uniform distribution.

$$q = q_1 = q_2 = \frac{P}{A} \quad (7.4)$$

When $e \neq 0$, the distribution is trapezoidal. As e increases, q_2 decreases. The critical state occurs when $q_2 = 0$. This case is shown in Fig. 7.8.

Fig. 7.8 Pressure distributions

for $e \leq e_{\text{critical}}$.
(a) $e < e_{\text{critical}}$.
(b) $e = e_{\text{critical}}$



$$\frac{P}{A} - \frac{(Pe)L_2}{I_y} = 0$$

$$\Downarrow$$

$$e_{\text{critical}} = \frac{I_y}{A} \frac{1}{L_2} \tag{7.5}$$

Applying this reasoning to a rectangular shape of width B and length L , and noting that

$$A = BL \quad I_y = \frac{BL^3}{12} \quad L_1 = L_2 = \frac{L}{2}$$

the expressions for the peak pressures take the form

$$q_1 = \frac{P}{BL} + \frac{6Pe}{BL^2}$$

$$q_2 = \frac{P}{BL} - \frac{6Pe}{BL^2} \tag{7.6}$$

The critical value for e , which corresponds to either q_1 or q_2 equal to 0, is given by

$$e = e_{\text{critical}} = \frac{L}{6} \tag{7.7}$$

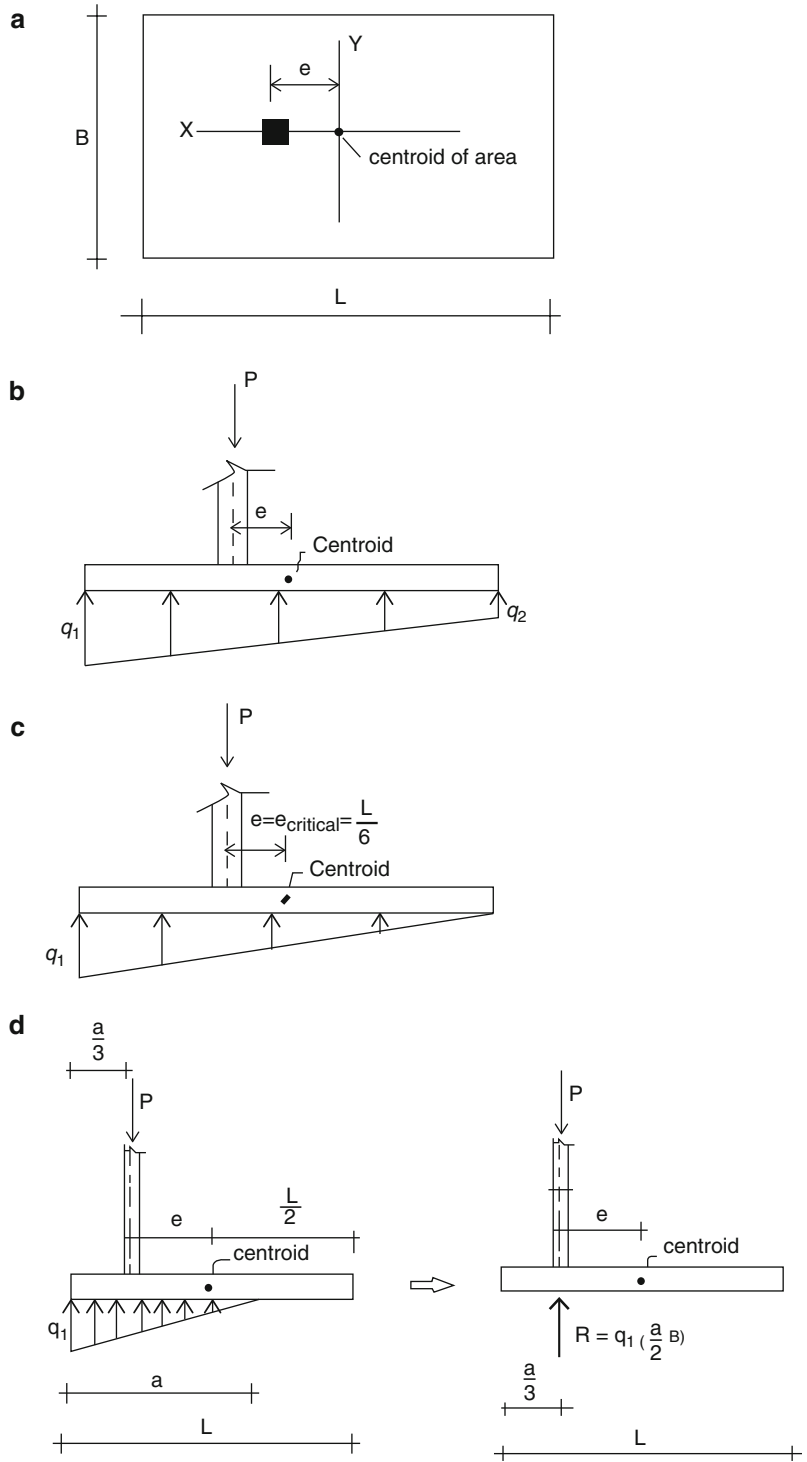
In order for the soil pressure to be compressive throughout the footing area, the point of application of the applied loading must be within a zone of width $L/3$ centered on the centroid. When loaded outside this region, (7.2) does not apply. In this case, the triangular distribution acting on a portion of the surface shown in Fig. 7.9d is used. The soil pressure adjusts its magnitude and extent such that the line of action of the resultant coincides with the line of action of the column force. The expressions for q_1 takes the form

$$R = P = q_1 \left(\frac{a}{2} B \right)$$

$$\Downarrow$$

$$q_1 = \frac{2P}{Ba}$$

Fig. 7.9 (a) Plan—rectangular area. (b) Elevation $e < e_{critical}$. (c) Elevation $e = e_{critical}$. (d) Pressure distribution for $e > e_{critical}$



7.3 Dimensioning a Single Rectangular Footing

Normally, the column position is fixed by the geometry of the structure, and one can only adjust the location of the footing with respect to the column. We consider the case where the design goal is a uniform soil pressure. The optimal dimensions of the footing are achieved by locating the centroid of the footing on the line of action of the column force, i.e., by taking $e = 0$ in Fig. 7.7. The first choice is a square footing. If there is insufficient space in one direction, one can shift to a rectangular footing. If the design is still constrained by space restrictions, one can then follow a different strategy and work with a strap-type footing which is discussed later.

We have shown that the soil pressure distribution is uniform for symmetrically positioned footings. The footing area is *determined using service loads, P , and the effective soil pressure, q_e* , which accounts for the weight of the footing and the soil above the footing. This notation is defined in Fig. 7.10. The relevant computations are

$$q_e = q_{\text{allowable}} - \gamma_{\text{conc.}}t - \gamma_{\text{soil}}(h - t) \approx q_{\text{allowable}} - \left(\frac{\gamma_{\text{conc.}} + \gamma_{\text{soil}}}{2}\right)h$$

$$A_{\text{required}} \geq \frac{\sum P_{\text{service}}}{q_e} \rightarrow L \quad \text{and} \quad B \rightarrow A = LB$$

Current practice estimates the peak values of shear force and moment in the footing using the factored ultimate load P_u and determines the footing thickness and the required reinforcement steel area based on these values. Figure 7.11 illustrates this procedure for a single axial loaded footing. The expressions for the factored ultimate shear and moment are:

$$V_u(x) = Bq_u x$$

$$M_u(x) = \frac{Bq_u x^2}{2} \tag{7.8}$$

where $q_u = \frac{P_u}{A}$. Positive bending moment requires reinforcing steel placed in two directions at the lower surface. One needs to check for two types of shearing actions, one way shear and punching shear.

Fig. 7.10 Notation-effective soil pressure (q_e). (a) Plan. (b) Elevation

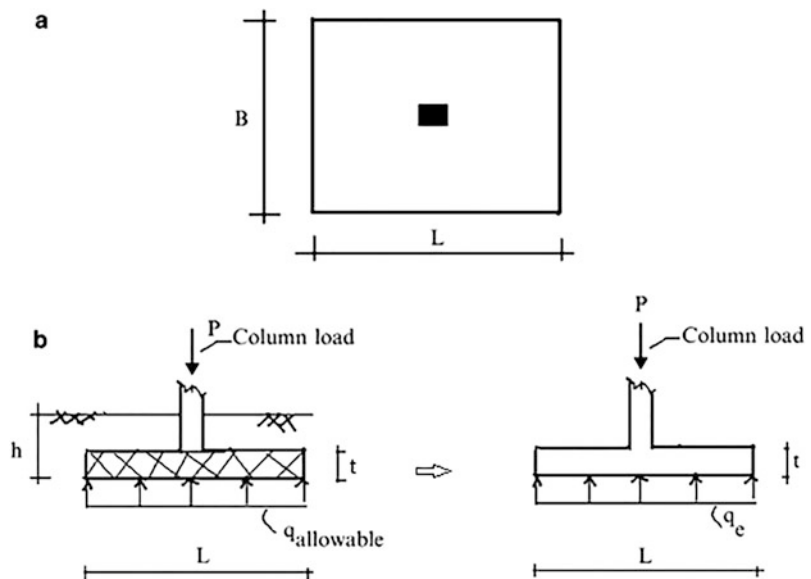


Fig. 7.11 Footing dimensioning process. (a) Factored soil pressure. (b) Shear and moment diagrams. (c) One way shear. (d) Punching shear

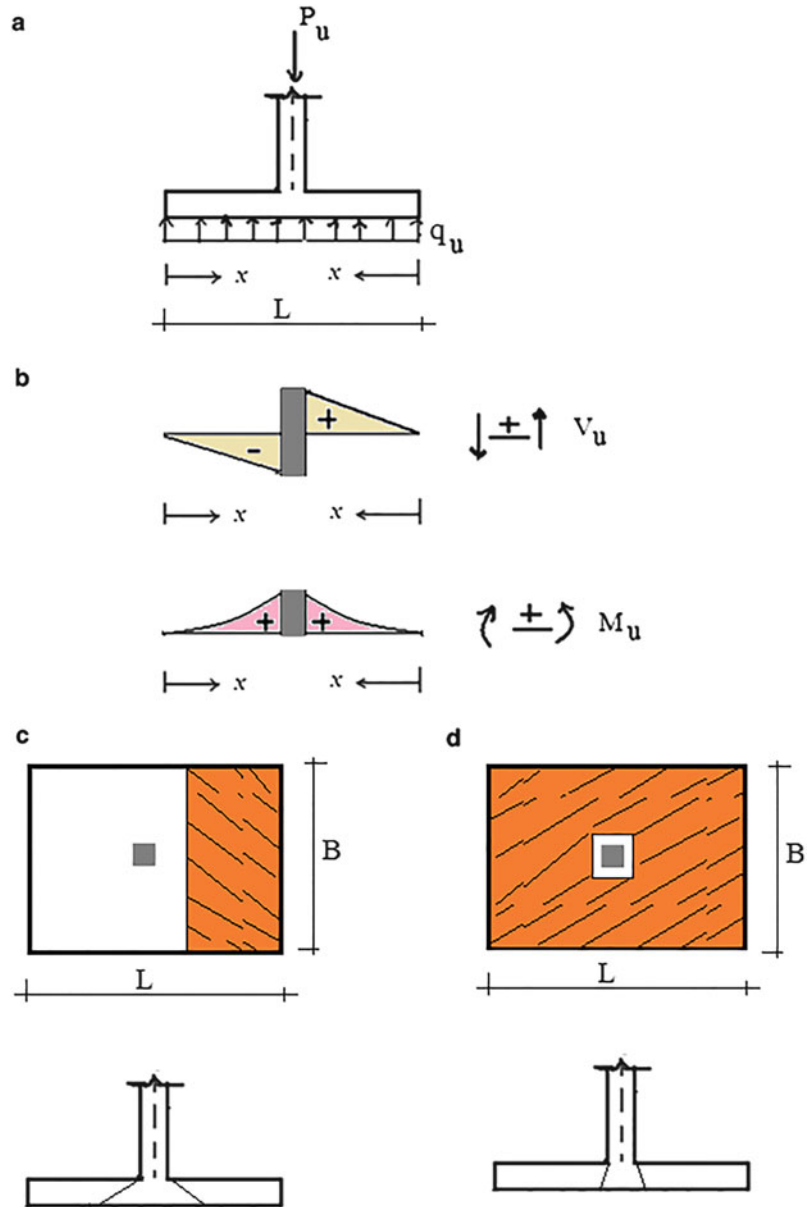


Figure 7.11 shows the location of the critical sections for shear. The distance parameter depends on the column type (steel, concrete) and the specific design code.

Most footings are constructed using reinforced concrete. The location and magnitude of the steel reinforcement is dictated by the sense of the bending moment distribution (i.e., positive or negative). The function of the reinforcement is to provide the tensile force required by the moment. It follows that the moment diagrams shown in Fig. 7.11b require the reinforcement patterns defined in Fig. 7.12. The actual size/number of the rebar depends on the magnitude of the moment and particular design code used to dimension the member.

Fig. 7.12 Single footing steel details. (a) Steel column. (b) Reinforced concrete column

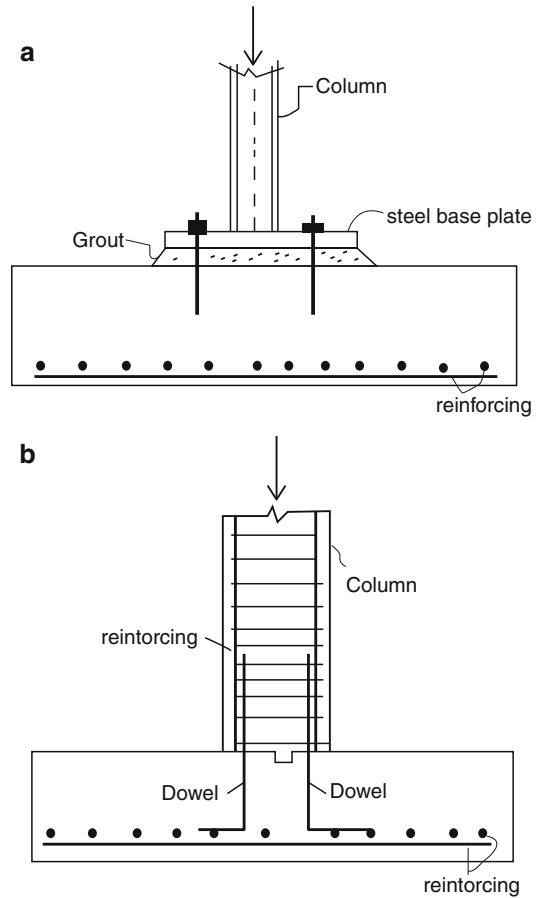


Figure 7.12 illustrates steel reinforcement for steel and concrete columns. A steel plate is welded to the base of a steel column and anchored to the footing with bolts embedded in the concrete. Dowels are used to connect the longitudinal steel in the concrete column to the footing. Usually the column loading is purely axial and the support is considered to be simply supported. However, there are situations where moment as well as axial force is present in the column. The design strategy is the same for both cases.

Example 7.1 Single Footing

Given: A $400 \text{ mm} \times 400 \text{ mm}$ concentrically load column with axial dead load ($P_D = 890 \text{ kN}$), and axial live load ($P_L = 1070 \text{ kN}$) to be supported on a shallow foundation. The effective soil pressure is $q_e = 165 \text{ kN/m}^2$ (Fig. E7.1a, b).

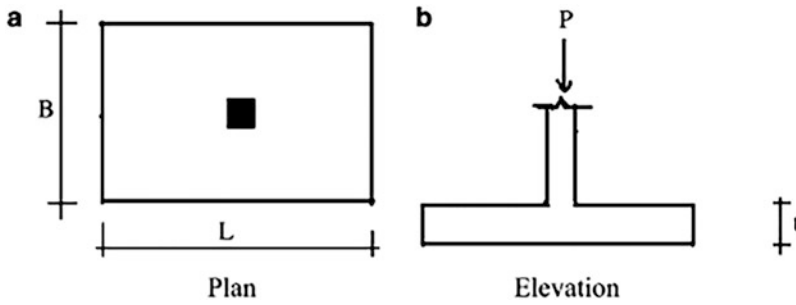


Fig. E7.1 Geometry and loading

Determine: The footing dimensions using service loads. Draw shear and moment diagrams using a factored load of $P_u = 1.2P_D + 1.6P_L$. Consider (a) A square footing, (b) A rectangular footing with $B = 3$ m.

Solution:

Footing dimensions

The required footing area is based on the service load and effective soil pressure.

$$P_{\text{service}} = \sum (P_D + P_L) = 890 + 1070 = 1960 \text{ kN}$$

$$A_{\text{required}} = \frac{P_{\text{service}}}{q_e} = \frac{1960}{165} = 11.88 \text{ m}^2$$

Assuming a square shape, the required dimension is $\sqrt{11.88} = 3.44$ m

We use $L = B = 3.5$ m.

Assuming a rectangular footing $B = 3$ m, the required dimension is $L = \frac{11.88}{3} = 3.96$ m. We use $L = 4$ m

Shear and moment distributions

The factored load is

$$P_u = 1.2P_D + 1.6P_L = 1.2(890) + 1.6(1070) = 2780 \text{ kN}$$

The corresponding factored soil pressure, q_u and V_u , M_u are:

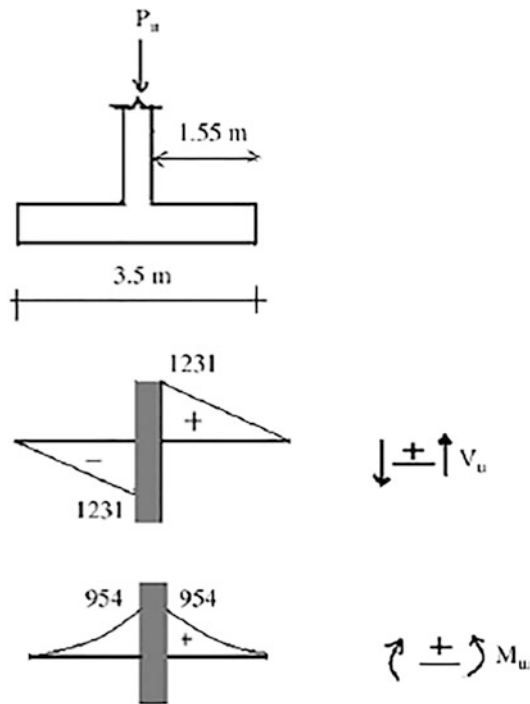
Square shape:

$$q_u = \frac{P_u}{LB} = \frac{2780}{(3.5)(3.5)} = 226.94 \text{ kN/m}^2$$

$$V_{u \text{ max}} = 226.94(3.5)(1.55) = 1231 \text{ kN}$$

$$M_{u \text{ max}} = 226.94(3.5) \frac{(1.55)^2}{2} = 954 \text{ kNm}$$

The shear and moment diagrams are plotted below.



Rectangular shape:

$$q_u = \frac{P_u}{LB} = \frac{2780}{(3)(4)} = 231.67 \text{ kN/m}^2$$

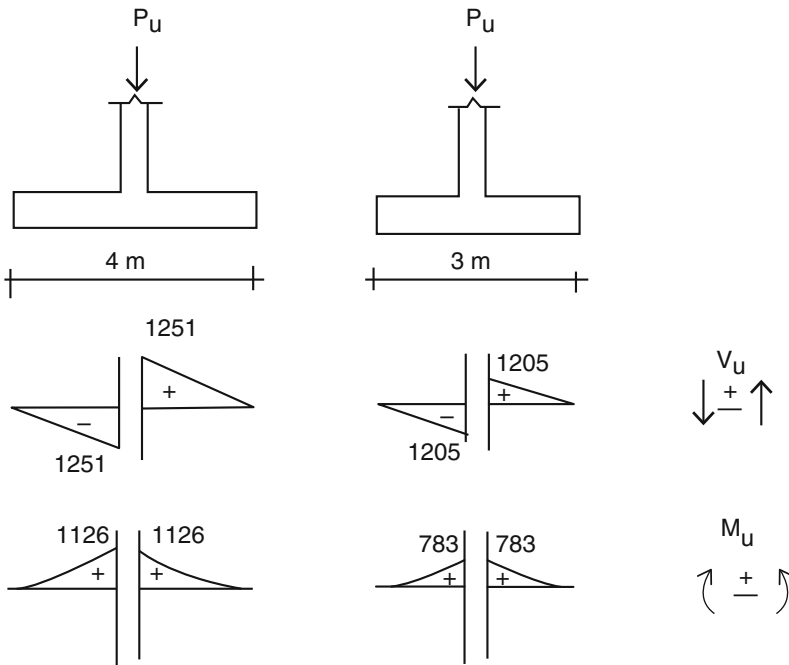
$$V_{u_{\max \text{ long}}} = 231.67(3)(1.8) = 1251 \text{ kN}$$

$$M_{u_{\max \text{ long}}} = 231.67(3) \frac{(1.8)^2}{2} = 1126 \text{ kNm}$$

$$V_{u_{\max \text{ short}}} = 231.67(4)(1.3) = 1205 \text{ kN}$$

$$M_{u_{\max \text{ short}}} = 231.67(4) \frac{(1.3)^2}{2} = 783 \text{ kNm}$$

The shear and moment diagrams are plotted below.



Example 7.2 Dimensioning a Footing Under a Column with Eccentric Loading

Given: A 12 in. × 12 in. column supporting the following loads: $P_D = 120$ kip, $P_L = 80$ kip, $M_D = 60$ kip ft, and $M_L = 40$ kip ft. The effective soil pressure is $q_e = 4.5$ kip/ft².

$$P = P_D + P_L = 120 + 80 = 200 \text{ kip}$$

$$M = M_D + M_L = 60 + 40 = 100 \text{ kip ft}$$

Determine: Dimension square/rectangular footings for the following cases.

Case (a): the center line of the column coincides with the centroid of the footing. M is counterclockwise (Fig. E7.2a).

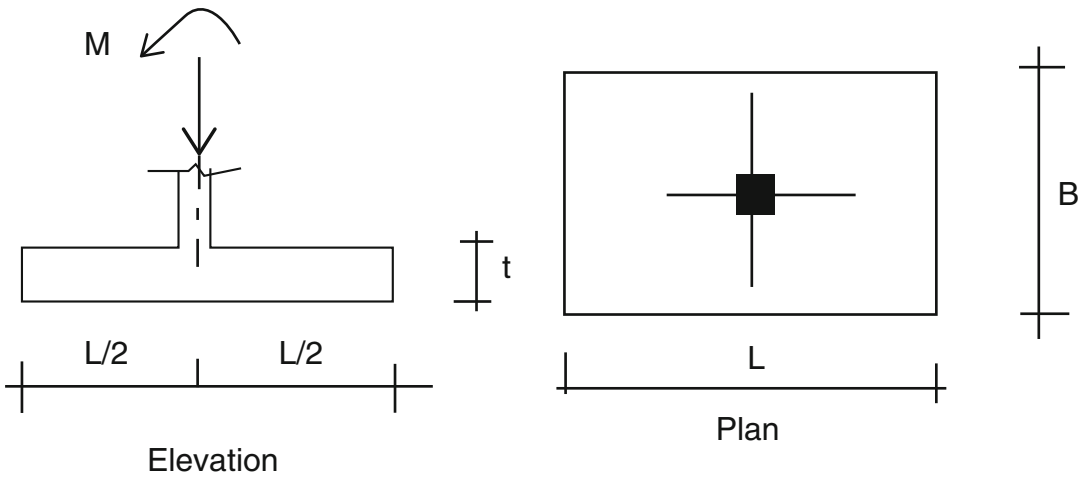


Fig. E7.2a Geometry and loading

Solution: Case (a)

Square footing ($L = B$): We use (7.6) and set $q_1 = q_c$

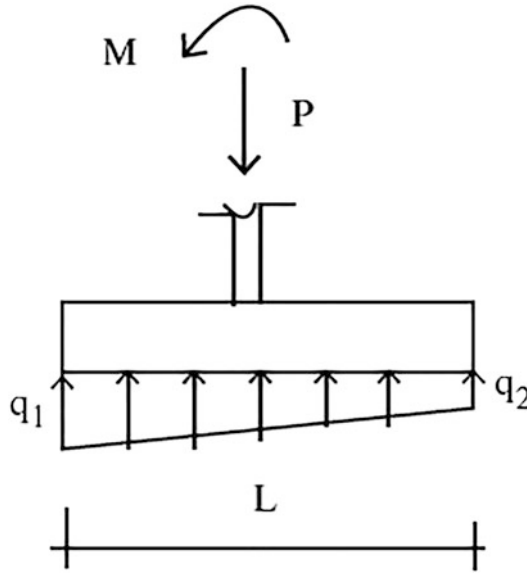
$$\frac{200}{L^2} + \frac{6(100)}{L^3} = 4.5 \Rightarrow L = 7.9 \text{ ft}$$

$$\text{For } L = B = 8 \text{ ft} \Rightarrow q_1, q_2 = 3.125 \pm 1.17 = \begin{cases} 4.3 \text{ kip/ft}^2 \\ 1.95 \text{ kip/ft}^2 \end{cases}$$

Rectangular footing: We take $B = 6$ ft. The pressure equation has the form

$$\begin{aligned} \frac{P}{6L} + \frac{6M}{6L^2} &= q_c \\ \downarrow \\ \frac{200}{6L} + \frac{6(100)}{6L^2} &= 4.5 \Rightarrow L = 9.7 \text{ ft} \end{aligned}$$

$$\text{For } L = 10 \text{ ft and } B = 6 \text{ ft} \Rightarrow q_1, q_2 = 3.33 \pm 1.0 = \begin{matrix} 4.33 \text{ kip/ft}^2 \\ 2.33 \text{ kip/ft}^2 \end{matrix}$$



Case (b): the center line of the column is 3 ft from the property line. M is clockwise (Fig. E7.2b).

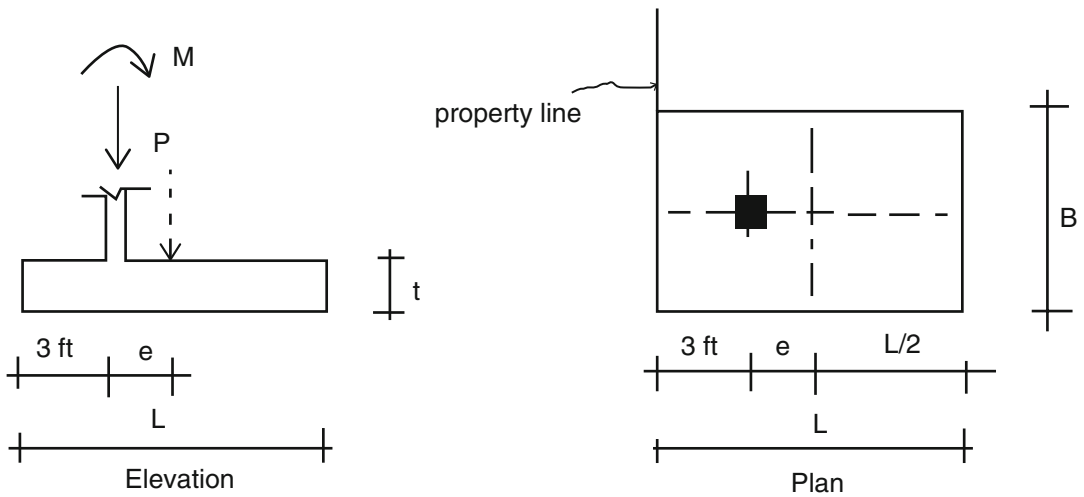


Fig. E7.2b Geometry and loading

Solution: Case (b) We position the centroid of the footing so that it is on the line of action of the resultant force. The location of the resultant is

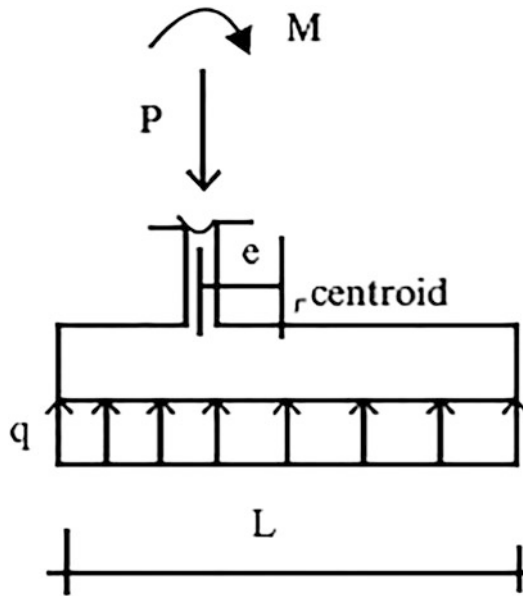
$$M_{total} = M - Pe = 100 - 200(e) = 0 \Rightarrow e = 0.5 \text{ ft}$$

Then

$$3 + e = \frac{L}{2} \Rightarrow L = 2(3 + e) = 7 \text{ ft}$$

$$q_1 = q_2 = \frac{P}{LB} \leq q_e \rightarrow B \geq \frac{200}{7(4.5)} = 6.35$$

For $L = 7 \text{ ft}$ and $B = 6.5 \text{ ft} \Rightarrow q_1 = q_2 = q = \frac{p}{LB} = \frac{200}{7(6.5)} = 4.39 \text{ kip/ft}^2$



Case (c): the center line of the column is 3 ft from the property line. M is zero (Fig. E7.2c).

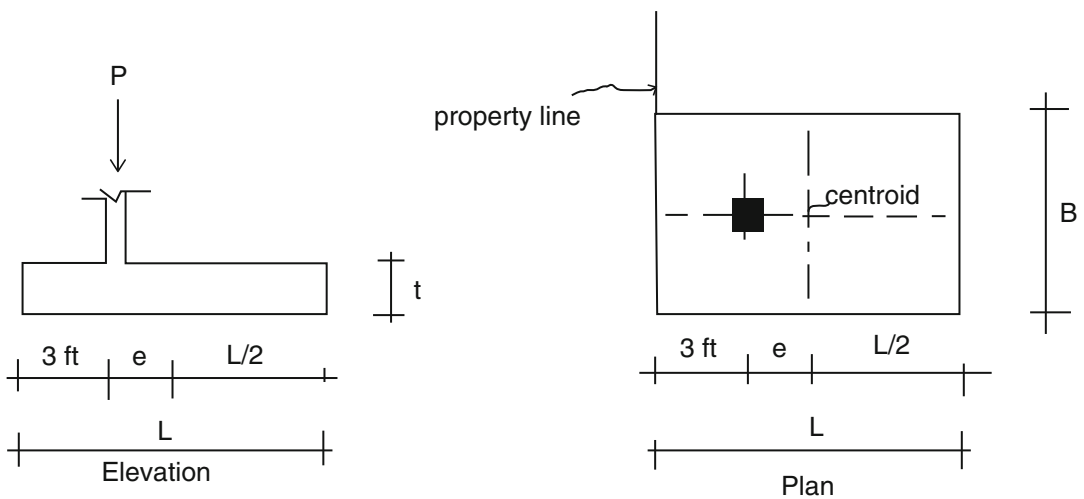


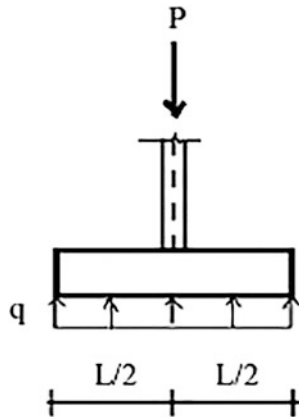
Fig. E7.2c Geometry and loading

Solution: Case (c) For this case, we locate the centroid on the center of the column. Then $e = 0$ and $L = 6.0 \text{ ft}$. The area is determined with

$$q = q_1 = q_2 = \frac{P}{LB} \leq q_e \rightarrow B \geq \frac{200}{6(4.5)} = 7.4$$

Use $L = 6$ ft and $B = 7.5$ ft

$$q = \frac{P}{LB} = \frac{200}{7.5(6)} = 4.44 \text{ kip/ft}^2$$



Case (d): the center line of the column is 3 ft from the property line. M is counterclockwise (Fig. E7.2d).

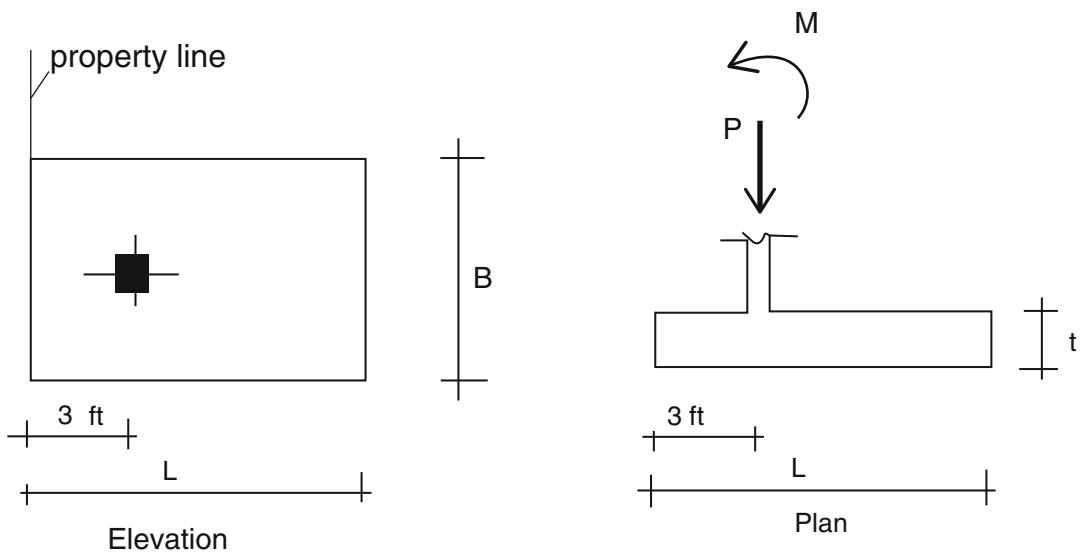
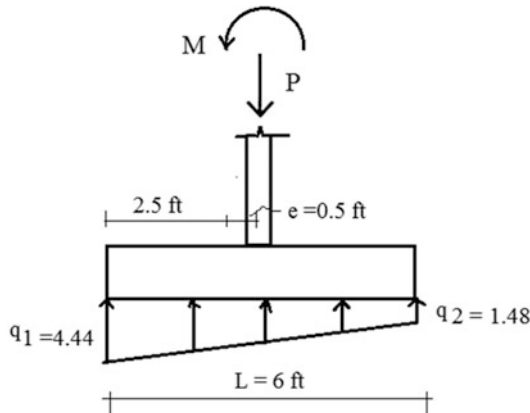


Fig. E7.2d Geometry and loading

Solution: Case (d) We decide to locate the centroid on the column line. Then $e = 0.5$ ft. This leads to the trapezoidal pressure distribution shown below. Taking $L = 6$ ft, and noting (7.3),

$$q_1 = \frac{200}{6B} + \frac{6(100)}{B(6)^2} \leq 4.5 \Rightarrow B \geq 11.1$$

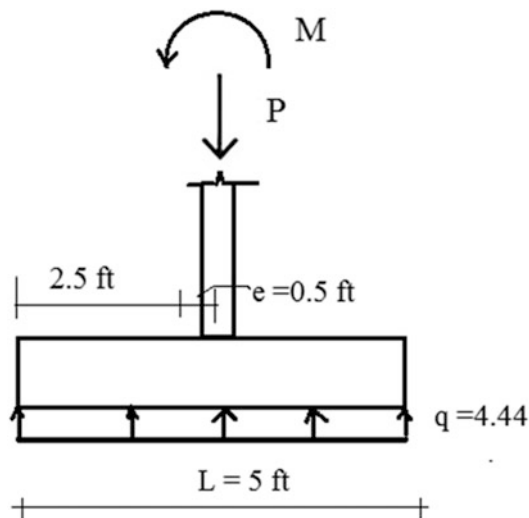
$$\text{For } L = 6 \text{ ft and } B = 11.25 \text{ ft} \rightarrow q_1, q_2 = 2.96 \pm 1.48 = \begin{cases} 4.44 \text{ kip/ft}^2 \\ 1.48 \text{ kip/ft}^2 \end{cases}$$



Another option is to take the centroid on the line of action of the resultant force. Then, $e = 0$ ft, $L = 5$ ft, and (7.6) yields

$$\frac{200}{5B} = 4.5 \rightarrow B = 8.9$$

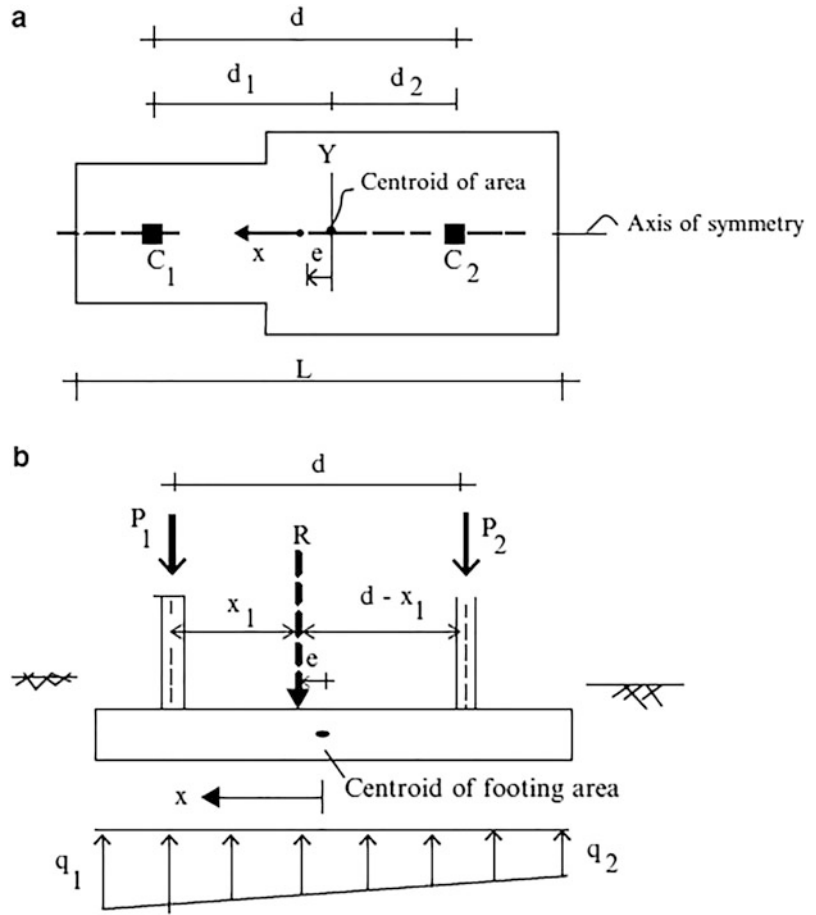
$$\text{For } L = 5 \text{ ft and } B = 9 \text{ ft } q = q_1 = q_2 = \frac{200}{5(9)} = 4.44 \text{ kip/ft}^2$$



7.4 Dimensioning Combined Footings

A combined footing has multiple column loads acting on a single area. This design is adopted when the column spacing is too small to allow for separate footings. Figure 7.13 illustrates the case of two columns. The analytical method described in Sect. 7.2 is also applicable here. One just has to *first replace the column loads with their resultant force*, and then apply (7.2) to determine the pressure distribution.

Fig. 7.13 Notation-combined footing. (a) Plan. (b) Elevation



Specializing (7.2) for this case, and noting the notations defined in Fig. 7.13, the pressure distribution is given by

$$q(x) = \frac{R}{A} + \left(\frac{Re}{I_y}\right)x \tag{7.9}$$

$$R = P_1 + P_2$$

where e is positive when R is located to the left of the centroid of the footing area.

The location of the resultant force can be determined by summing moments about the line of action of P_1

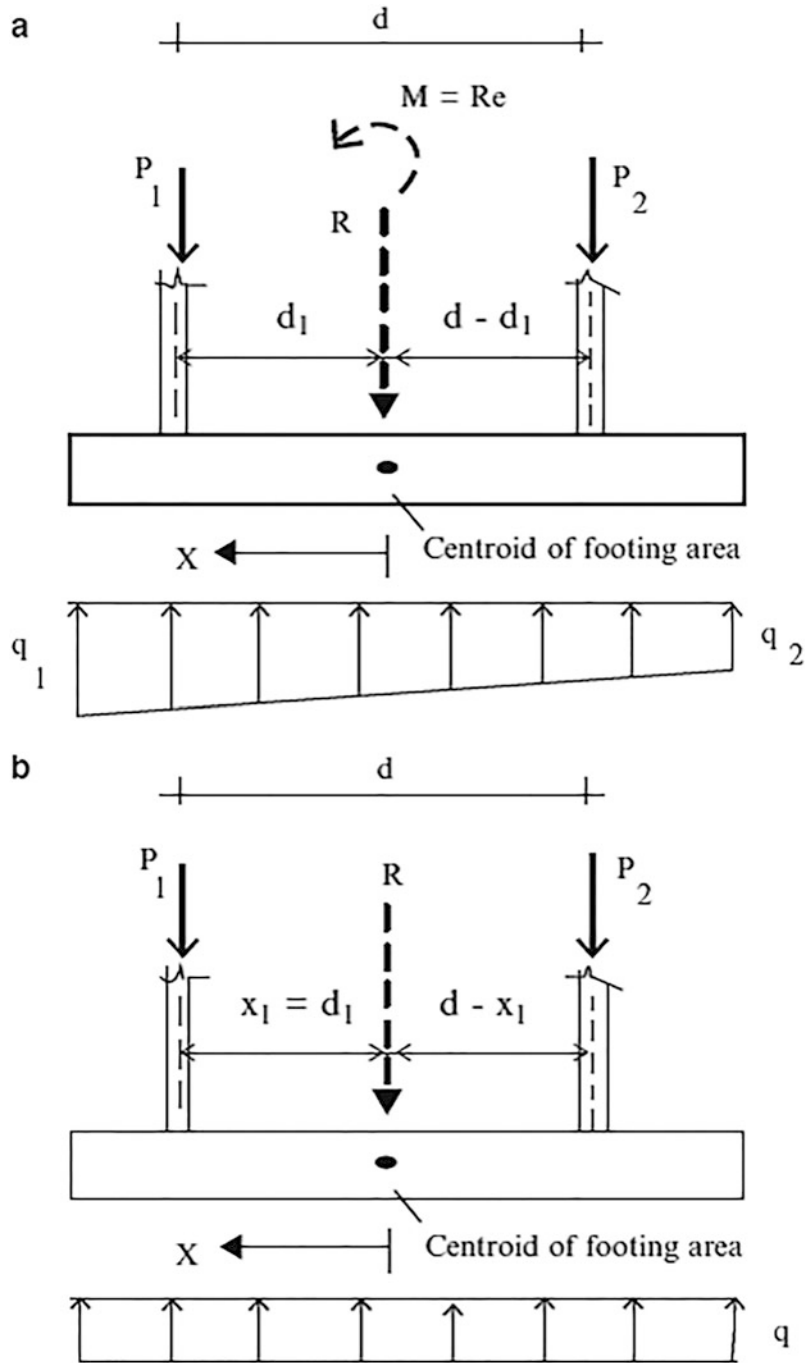
$$x_1 = \frac{P_2 d}{(P_1 + P_2)} \tag{7.10}$$

$$e = d_1 - x_1$$

It follows that *the soil pressure distribution is uniform when the centroid of the footing area is located on the line of action of the resultant force* (Fig. 7.14). For this case, $e = 0$ and $q = R/A$.

We compute the peak shear and moment, using factored loads. The position of the resultant with respect to the centroid may change when factored loads are used.

Fig. 7.14 Conditions for soil pressure distribution. (a) $e > 0$. (b) $e = 0$



$$R_u = P_{1u} + P_{2u}$$

Then,

$$x_{1u} = d_1 - e_u = \frac{P_{2u}}{R_u} d \tag{7.11}$$

If $e_u \neq 0$, the distribution of pressure is trapezoidal, and we use (7.9) to find the corresponding peak pressures due to the factored loads.

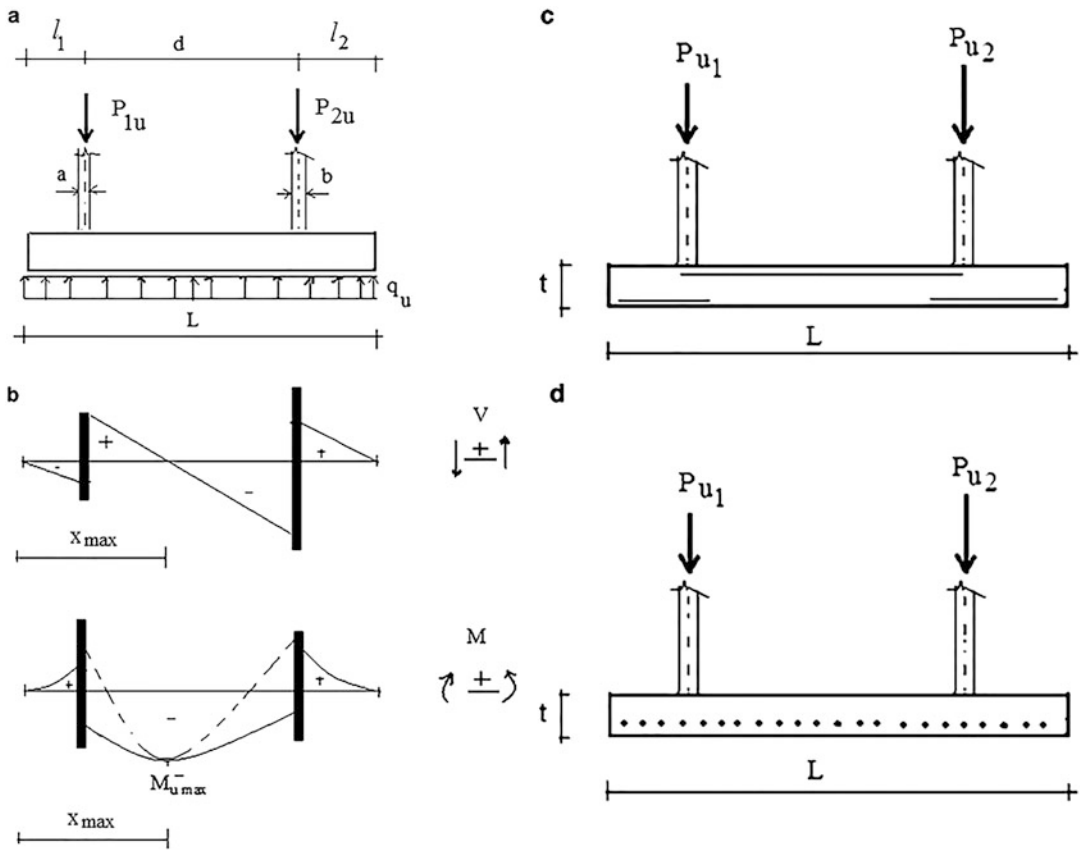


Fig. 7.15 (a) Rectangular footing with uniform ultimate soil pressure $e_u = 0$. (b) Shear and Moment diagrams $e_u = 0$. (c) Steel reinforcing pattern for longitudinal bending. (d) Steel reinforcing pattern for transverse bending

The shear and moment diagrams corresponding to uniform soil pressure are plotted in Fig. 7.15b. Note that for this type of footing, the bending moment distribution in the footing in the longitudinal direction has *both positive and negative regions*. The peak moment values are

$$V_u = 0 \rightarrow Bq_u x_{\max} - P_{u1} = 0 \rightarrow x_{\max} = \frac{P_{u1}}{Bq_u}$$

$$\therefore M_{u\max}^- = Bq_u \frac{x_{\max}^2}{2} - P_{u1}(x_{\max} - l_1)$$

$$\text{At edges of columns } V_u \begin{cases} -Bq_u \left(l_1 - \frac{a}{2} \right) \\ -Bq_u \left(l_1 + \frac{a}{2} \right) + P_{u1} \\ Bq_u \left(l_2 - \frac{b}{2} \right) \\ Bq_u \left(l_2 + \frac{b}{2} \right) - P_{u2} \end{cases}$$

$$\text{At edges of columns } M_u \begin{cases} \frac{Bq_u}{2} \left(l_1 - \frac{a}{2} \right)^2 \\ \frac{Bq_u}{2} \left(l_1 + \frac{a}{2} \right)^2 - P_{u1} \left(\frac{a}{2} \right) \\ \frac{Bq_u}{2} \left(l_2 - \frac{b}{2} \right)^2 \\ \frac{Bq_u}{2} \left(l_2 + \frac{b}{2} \right)^2 - P_{u2} \left(\frac{b}{2} \right) \end{cases}$$

Since the moment diagram for a combined footing generally has both positive and negative values, the steel placement pattern for a combined footing involves placing steel in the top zone as well as the bottom zone of the cross section. The required steel reinforcing patterns are shown in Fig. 7.15c, d. In general, the reinforcement pattern is two way. For the transverse direction, we treat the footing similar to the single footing and the steel for tension is placed at the lower surface.

Example 7.3 Dimensioning a Combined Footing

Given: A combined footing supporting two square columns. Column A is 400 mm × 400 mm and carries a dead load of 700 kN and a live load of 900 kN. Column B is 500 mm × 500 mm and carries a dead load of 900 kN and a live load of 1000 kN. The effective soil pressure is $q_e = 160 \text{ kN/m}^2$ (Figs. E7.3a and E7.3b).

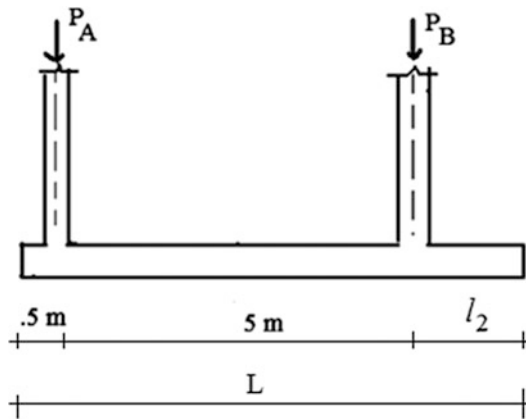


Fig. E7.3a Elevation

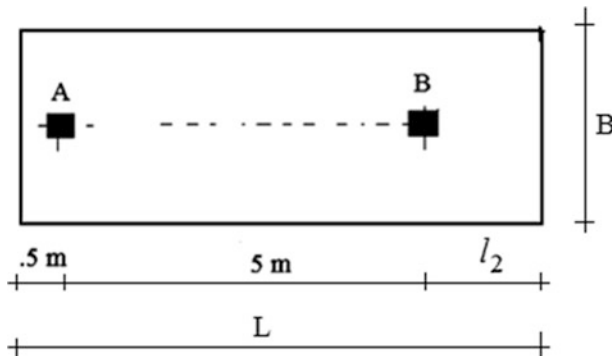


Fig. E7.3b Plan

Determine: The dimensions B and L for service load of $P = P_D + P_L$, assuming the soil pressure distribution is uniform. Draw shear and moment diagrams for factored load of $P_u = 1.2P_D + 1.6P_L$.

Solution:

Step I: Locate the resultant force

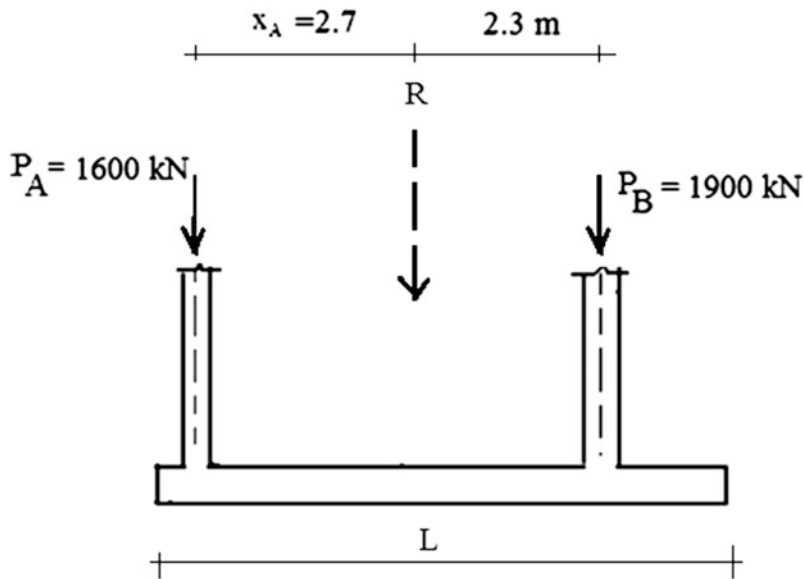
$$P_A = P_D + P_L = 700 + 900 = 1600 \text{ kN}$$

$$P_B = P_D + P_L = 900 + 1000 = 1900 \text{ kN}$$

$$R = P_A + P_B = 3500 \text{ kN}$$

$$x_A = \frac{1900(5)}{3500} = 2.71 \text{ m}$$

The resultant equals 3500 kN located 2.71 m from column A.



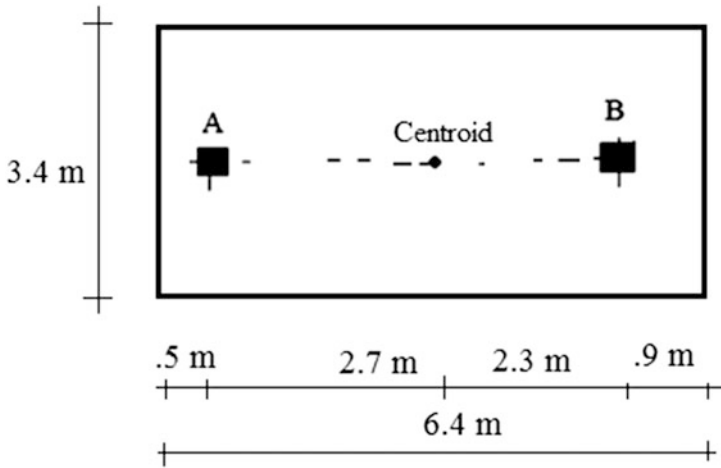
Step II: Select a rectangular geometry. We position the rectangle so that its centroid is on the line of action of the resultant. The design requirement is

$$\frac{L}{2} = x_A + 0.5 = (2.71) + 0.5 = 3.21$$

$$A_{\text{required}} = \frac{R}{q_e} = \frac{3500}{165} = 21.2 \text{ m}^2$$

Take $L = 6.4$ m and $B = 3.4$ m $\rightarrow A = B \times L = 21.76$ m²

The final geometry is shown below



Step III: Draw the shear and moment diagrams corresponding to the factored loads $P_u = 1.2P_D + 1.6P_L$. We work with the soil pressure integrated over the width of the footing. This leads to the “total” shear and “total” moment. These distributions are plotted below. Note that we treat the column loads as concentrated forces. One can also model them as distributed loads over the width of the column.

$$P_{Au} = 1.2P_D + 1.6P_L = 1.2(700) + 1.6(900) = 2280 \text{ kN}$$

$$P_{Bu} = 1.2P_D + 1.6P_L = 1.2(900) + 1.6(1000) = 2680 \text{ kN}$$

$$R_u = P_{Au} + P_{Bu} = 4960 \text{ kN}$$

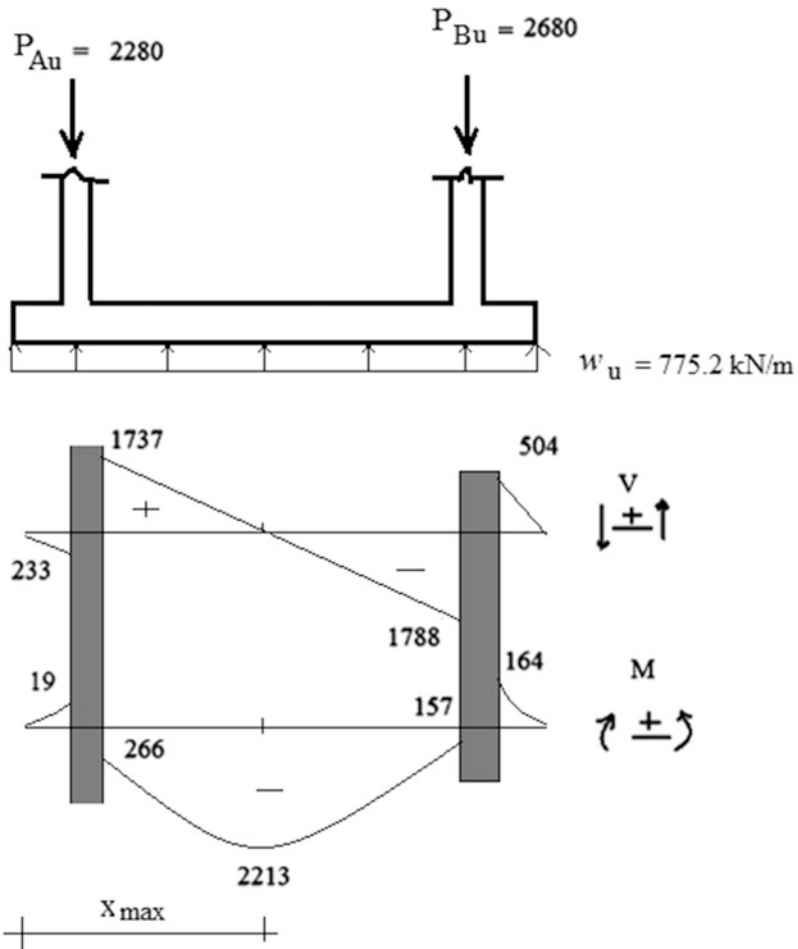
$$x_{Au} = \frac{2680(5)}{4960} = 2.701 \text{ m}$$

The factored resultant acts 2.701 m from column A. It follows that $e = 12$ mm. We neglect this eccentricity and assume the pressure is uniform.

$$q_u = \frac{R_u}{A} = \frac{4960}{6.4(3.4)} = 228 \text{ kN/m}^2$$

Then for $B = 3.4$ m, $w_u = 228(3.4) = 775.2$ kN/m.

The shear and moment diagrams are plotted below.



Example 7.4

Given: A combined footing supporting two square columns. Column C_1 is 16 in. \times 16 in. and carries a service load of 220 kip. Column C_2 is 18 in. \times 18 in. and carries a service load of 440 kip (Figs. E7.4a and E7.4b).

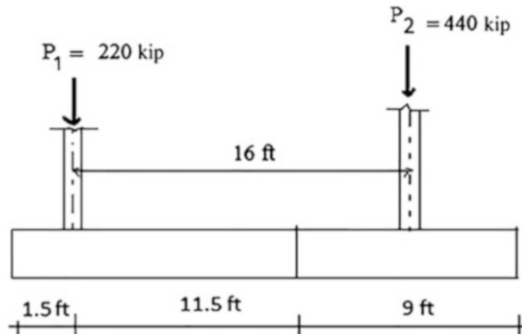


Fig. E7.4a Elevation

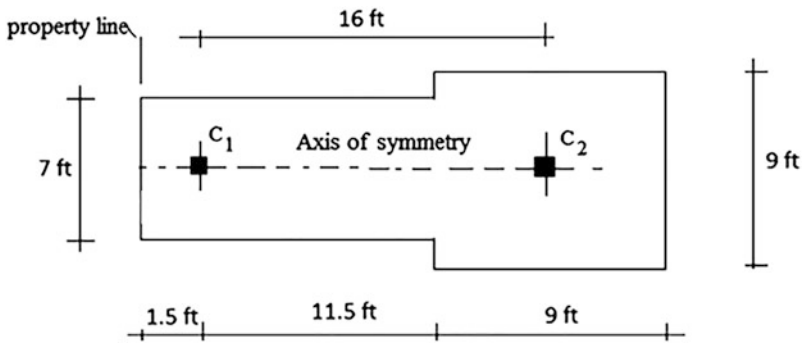


Fig. E7.4b Plan

Determine: The soil pressure distribution caused by the service loads P_1 and P_2 .

Solution:

Locate the centroid of the area

$$A = (9)(9) + (13)(7) = 172 \text{ ft}^2$$

$$L_1 = \frac{81(17.5) + 91(6.5)}{172} = 11.68 \text{ ft}$$

$$d_1 = 11.68 - 1.5 = 10.18 \text{ ft}$$

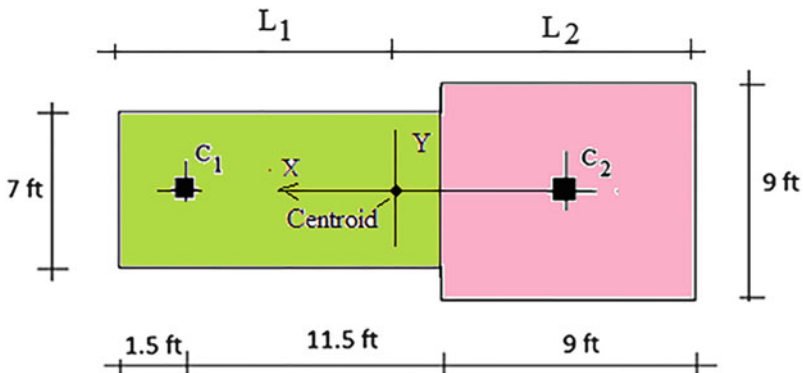


Fig. E7.4c

Locate the resultant force

$$R = P_1 + P_2 = 220 + 440 = 660 \text{ kip}$$

$$x_1 = \frac{P_2 d}{R} = \frac{440(16)}{660} = 10.67 \text{ ft}$$

$$e = -0.49 \text{ ft}$$

The peak pressures are

$$q_1 = \left\{ \frac{R}{A} + \frac{(Re)L_1}{I_y} \right\} = \frac{660}{172} + \frac{660(-0.49)11.68}{7014} = 3.3 \text{ kip/ft}^2$$

$$q_2 = \left\{ \frac{R}{A} - \frac{(Re)L_2}{I_y} \right\} = \frac{660}{172} - \frac{660(-0.49)10.32}{7014} = 4.3 \text{ kip/ft}^2$$

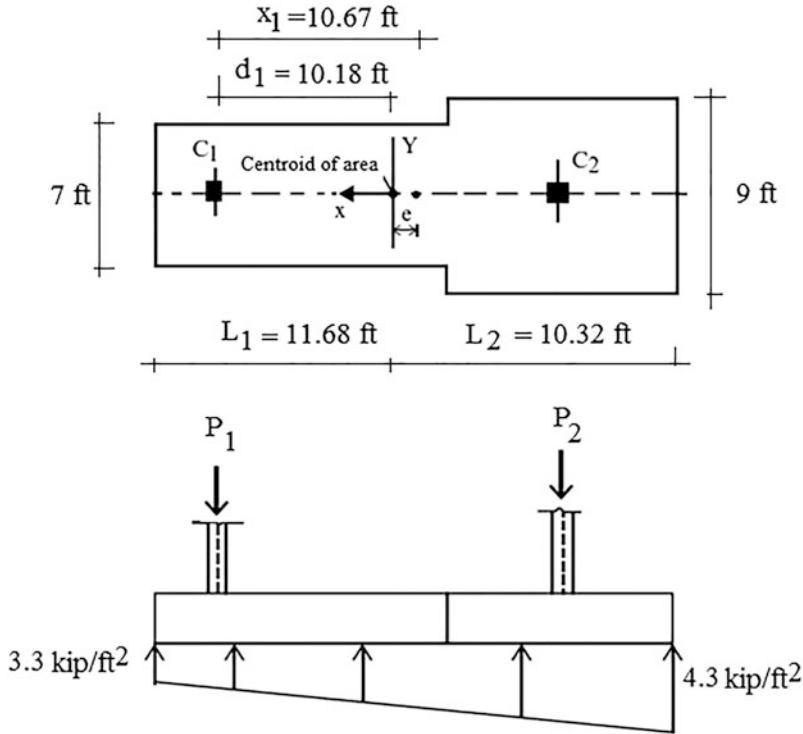


Fig. E7.4d

7.5 Dimensioning Strap Footings

Strap footings consist of individual footings placed under each column and connected together with a rigid beam to form a single unit. Figure 7.16 illustrates the geometric arrangement for two columns supported by two rectangular footings. The centroid for the interior footing (footing #2) is usually taken to be on the line of action of the interior column. The zone under the rigid beam is generally filled with a geofoam material that has essentially no stiffness and provides negligible pressure on the beam. Therefore, all of the resistance to the column loads is generated by the soil pressure acting on the individual footing segments.

We suppose the axis connecting the columns is an axis of symmetry for the area segments. The approach follows essentially the same procedure as employed for combined footings. Figure 7.17 defines the notation for this method.

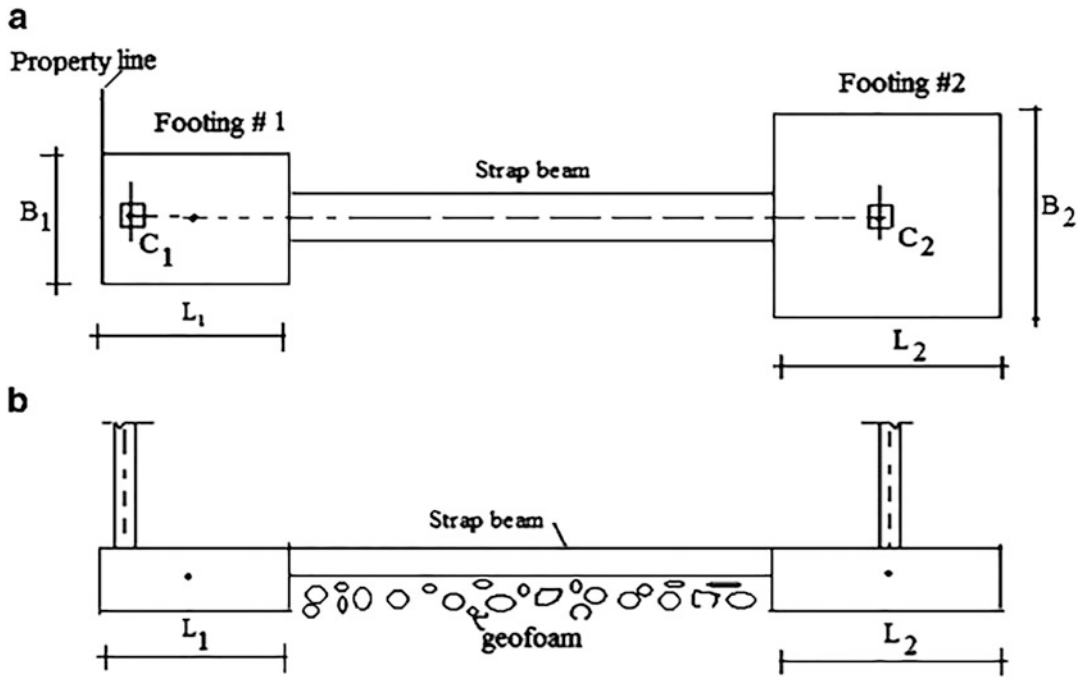


Fig. 7.16 Strap footing. (a) Plan. (b) Elevation

First, we locate the resultant of the column loads.

$$x_1 = \frac{P_2 d}{R}$$

$$R = P_1 + P_2$$

$$e = d_1 - x_1$$

Note that when e is negative, R is located to the right of the centroid (see Fig. 7.17b).

Next, we take footing #2 to be located such that its centroid coincides with the line of action of load P_2 .

We locate the origin of the x -axis at an arbitrary point on the axis of symmetry and use (7.1) to determine the soil pressure acting on the individual footings. We assume there is no soil pressure acting on the link member. Noting (7.1), the soil pressure is taken as

$$q(x) = b + ax \quad \text{for footings \#1 and \#2}$$

$$q(x) = 0 \quad \text{for the strap beam.}$$

The coefficients are evaluated by *integrating over the footing areas*. Enforcing equilibrium leads to

$$R = \int q(x) dA = b(A_1 + A_2) + a \left[\int_{A_1} x dA + \int_{A_2} x dA \right]$$

$$Re = \int x q(x) dA = b \left[\int_{A_1} x dA + \int_{A_2} x dA \right] + a \left[\int_{A_1} x^2 dA + \int_{A_2} x^2 dA \right] \tag{7.12}$$

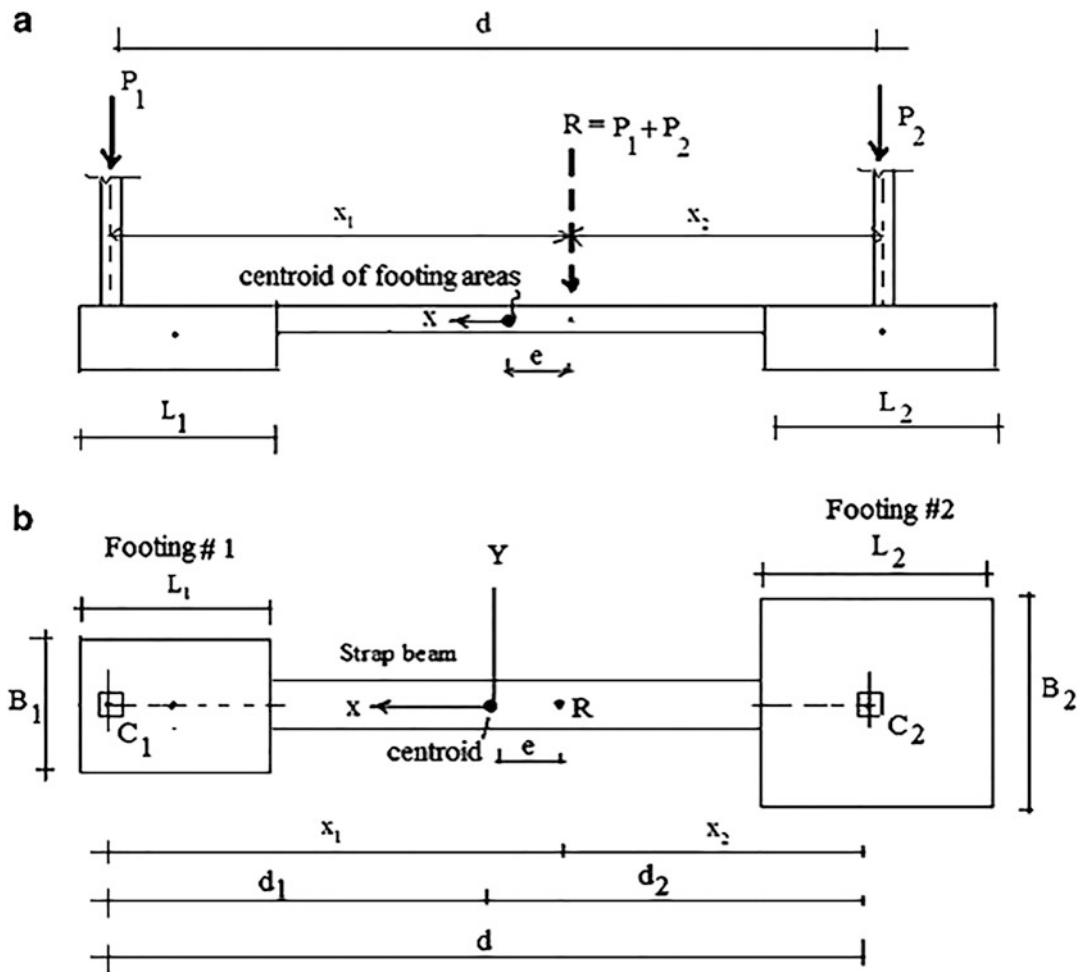


Fig. 7.17 Notation and pressure distribution for strap footing. (a) Elevation. (b) Plan

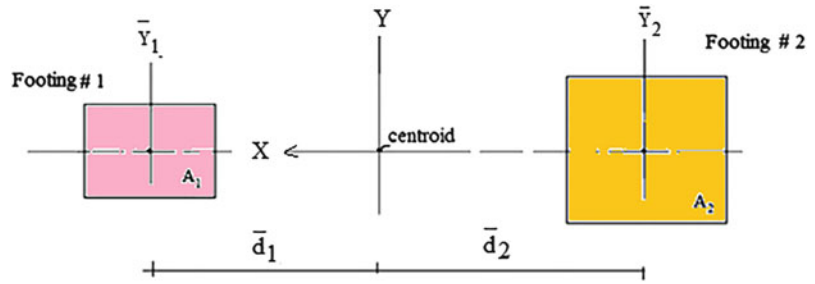
Now, we take the origin for x at the centroid of the combined section. Then $\int_{A_1} x dA + \int_{A_2} x dA = 0$ and (7.12) reduces to

$$\begin{aligned} R &= b(A_1 + A_2) \\ Re &= a(I_{Y1} + I_{Y2}) \end{aligned} \tag{7.13}$$

where $(I_{Y1} + I_{Y2})$ is sum of the second moments of area of the two footing cross sections about the Y -axis through the centroid. The I_Y s are computed using the following equations:

$$\begin{aligned} I_{Y1} &= \bar{I}_{Y1} + A_1 \bar{d}_1^2 \\ I_{Y2} &= \bar{I}_{Y2} + A_2 \bar{d}_2^2 \end{aligned}$$

Fig. 7.18 Geometry–strap footing



Lastly, the pressure equation takes the form:

$$q(x) = \frac{R}{(A_1 + A_2)} + \frac{Re}{(I_{Y1} + I_{Y2})}x \quad (7.14)$$

We use (7.14) to determine the pressure for a given geometry and loading.

When dimensioning the footing, we locate the centroid of the combined footing area on the line of action of the resultant. This step results in a uniform pressure,

$$e = 0 \quad \rightarrow \quad q = \frac{R}{(A_1 + A_2)} = \frac{P_1 + P_2}{(A_1 + A_2)} \quad (7.15)$$

Given the effective soil pressure, we determine the total area with

$$A_1 + A_2 \geq \frac{P_1 + P_2}{q_e} \quad (7.16)$$

The solution procedure is as follows:

We assume the magnitude of either A_1 or A_2 and compute the other area with (7.16). Since we are locating footing #2 such that its centroid coincides with the line of action of P_2 , it follows from Fig. 7.17 that $x_2 \equiv d_2$. Then noting Fig. 7.18, $\bar{d}_2 \equiv d_2$. Lastly, we determine \bar{d}_1 with (7.17)

$$A_1 \bar{d}_1 = A_2 \bar{d}_2 \quad (7.17)$$

This equation corresponds to setting $e = 0$.

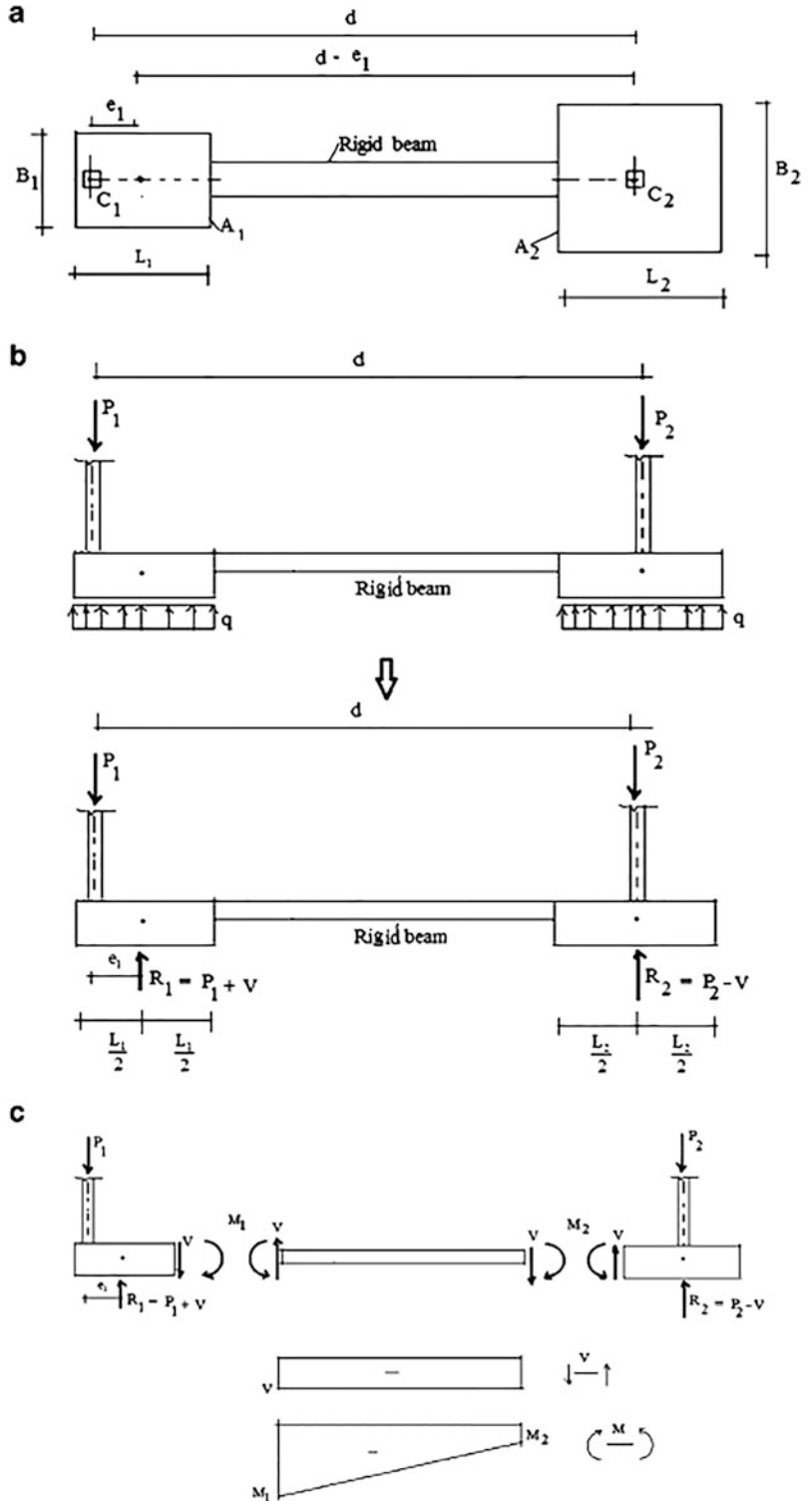
An alternative design approach proceeds as follows. Consider Fig. 7.19. The resultants of the pressure distributions acting on the footings are indicated by R_1 and R_2 . Summing moments about the line of action of R_1 leads to

$$R_2 = P_2 - \frac{P_1 e_1}{d - e_1} \quad (7.18)$$

Summing forces leads to

$$R_1 + R_2 = P_1 + P_2$$

Fig. 7.19 Approximate strap footing analysis. (a) Plan (b) Elevation (c) Components of footing



Then

$$R_1 = P_1 + \frac{P_1 e_1}{d - e_1} \quad (7.19)$$

Let

$$V = \frac{P_1 e_1}{d - e_1} \quad (7.20)$$

then

$$\begin{aligned} R_1 &= P_1 + V \\ R_2 &= P_2 - V \\ R &= R_1 + R_2 = P_1 + P_2 \end{aligned} \quad (7.21)$$

The quantity, V , is the shear force in the strap beam.

Once e_1 is specified, one can determine R_1 and R_2 . We also *assume* the soil pressure acting on the footing is constant and equal to the effective soil pressure (q_e). Then,

$$\begin{aligned} A_{1 \text{ required}} &= \frac{R_1}{q_e} \\ A_{2 \text{ required}} &= \frac{R_2}{q_e} \end{aligned} \quad (7.22)$$

Typical reinforcing patterns required for bending in strap footings are illustrated in Fig. 7.20.

Fig. 7.20 Typical reinforcing patterns



Example 7.5

Given: The eccentrically loaded footing A connected to the concentrically loaded footing B by strap beam as shown below. Assume the strap is placed such that it does not bear directly on the soil (Figs. E7.5a and E7.5b).

Determine: The soil pressure profile under the footings.

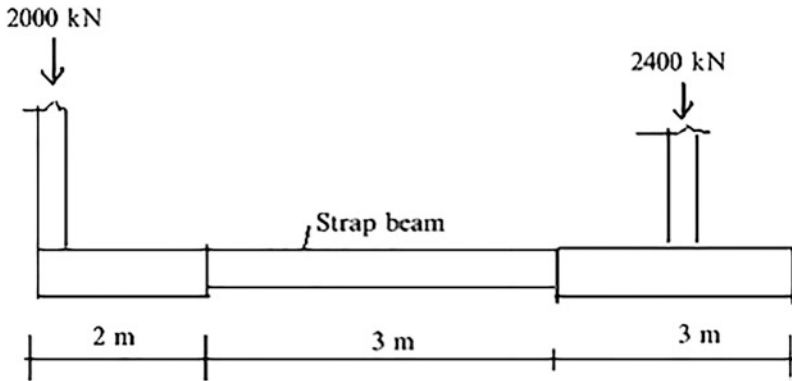


Fig. E7.5a Elevation

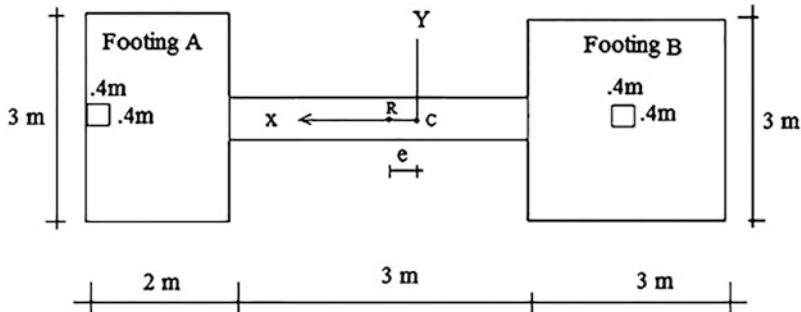


Fig. E7.5b Plan view

Solution: Noting Fig. 7.17, the various measures are

$$d = 6.3 \text{ m}$$

$$x_1 = \frac{2400(6.3)}{4400} = 3.436 \text{ m}$$

$$A_1 = 2(3) = 6 \text{ m}^2$$

$$A_2 = 3(3) = 9 \text{ m}^2$$

$$R = 2000 + 2400 = 4400 \text{ m}^2$$

$$6\bar{d}_1 = 9(5.5 - \bar{d}_1) \Rightarrow \bar{d}_1 = 3.3 \text{ m} \quad \bar{d}_2 = 2.2 \text{ m}$$

$$d_1 = \bar{d}_1 + 0.8 = 4.1 \text{ m}$$

$$e = d_1 - x_1 = 0.66 \text{ m}$$

$$I_{Y1} + I_{Y2} = \frac{3(2)^3}{12} + 6(3.3)^2 + \frac{3(3)^3}{12} + 9(2.2)^2 = 117.65 \text{ m}^4$$

Note that e is positive when R is located to the left of the centroid

$$q(x) = \frac{R}{(A_1 + A_2)} + \frac{Re}{(I_{Y1} + I_{Y2})}x$$

$$= \frac{4400}{15} - \frac{4400(0.66)}{117.65}x = 293.3 + 24.7x$$

∴

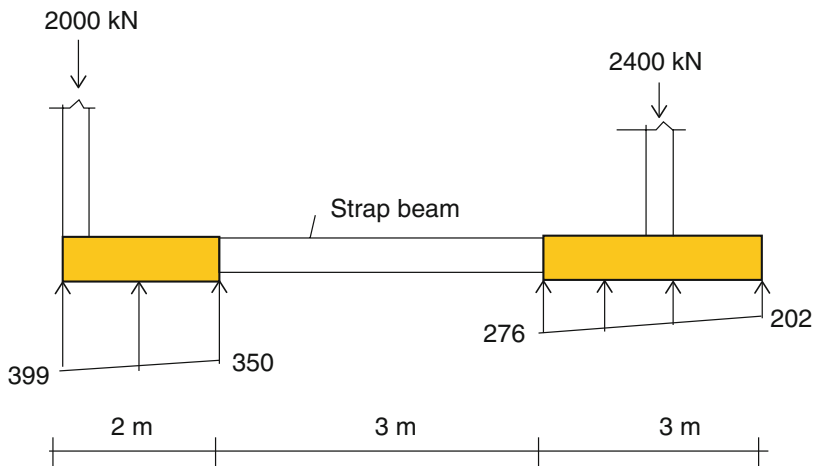
$$q(4.3) = 399 \text{ kN/m}^2$$

$$q(2.3) = 350 \text{ kN/m}^2$$

$$q(-0.7) = 276 \text{ kN/m}^2$$

$$q(-3.7) = 202 \text{ kN/m}^2$$

The corresponding soil pressure is shown below.



Example 7.6 Dimensioning a Strap Footing

Given: The exterior column C_1 is 12 in. \times 12 in. and carries a dead load of 160 kip and a live load of 130 kip. The interior column C_2 is 16 in. \times 16 in. and carries a dead load of 200 kip and a live load of 185 kip. The property line is at the edge of column #1 and the distance between the center lines of the columns #1 and #2 is 20 ft. The effective soil pressure is $q_e = 4.625 \text{ kip/ft}^2$ (Figs. E7.6a and E7.6b).

Determine: The dimensions of the footings for both columns using the two methods described above.

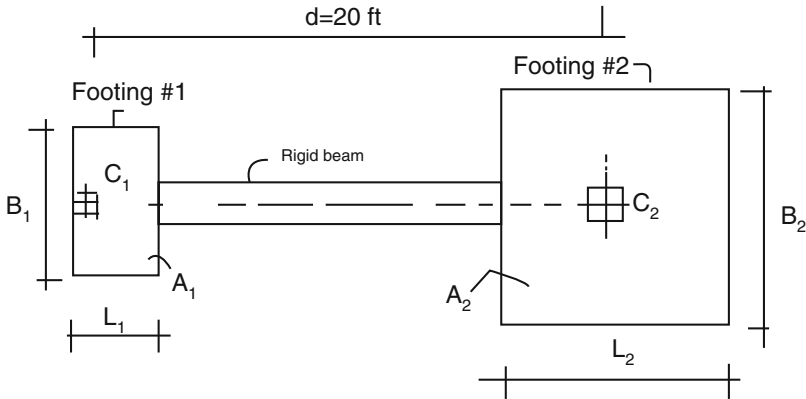


Fig. E7.6a Plan

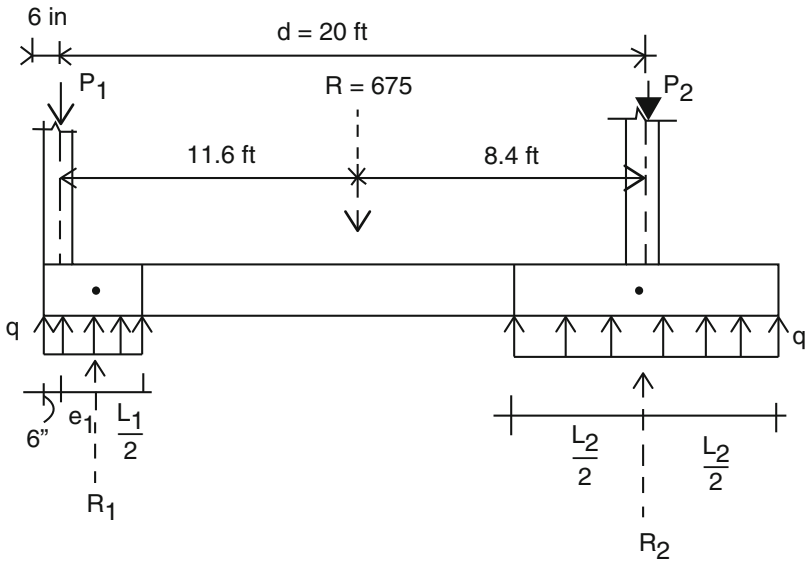


Fig. E7.6b Elevation

Solution:

Procedure #1: The individual column loads are:

$$P_1 = 160 + 130 = 290 \text{ kip}$$

$$P_2 = 200 + 185 = 385 \text{ kip}$$

Next, we locate the resultant of the column loads.

$$R = P_1 + P_2 = 675 \text{ kip}$$

$$d_1 = x_1 = \frac{385}{675}(20) = 11.407 \text{ ft}$$

$$d_2 = x_2 = 20 - 11.407 = 8.593 \text{ ft}$$

Noting (7.16), we obtain:

$$A_1 + A_2 = \frac{675}{4.625} \geq 146 \text{ ft}^2$$

We estimate A_2 knowing R_2 , the resultant of the pressure distribution acting on footing # 2, is less than P_2 .

$$A_2 \approx \frac{385}{4.625} = 83 \text{ ft}^2$$

We take $L_2 = B_2 = 8.5 \text{ ft}$ ($A_2 = 72.25 \text{ ft}^2$).

Then $A_1 \geq 73.75 \text{ ft}^2$

Noting (7.17),

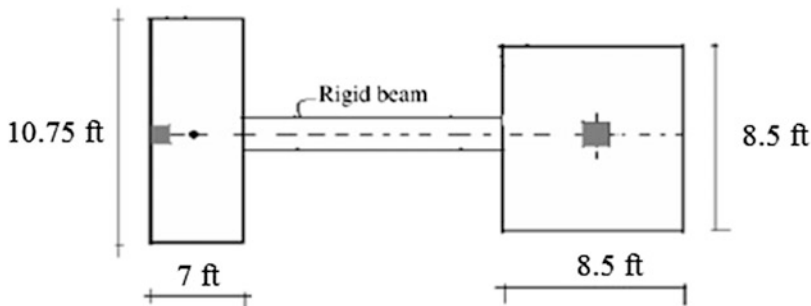
$$73.75\bar{d}_1 = 72.25(8.593) \Rightarrow \bar{d}_1 = 8.418 \text{ ft}$$

Then

$$\frac{L_1}{2} \approx e_1 + (d_1 - \bar{d}) = 0.5 + (11.407 - 8.418) = 3.49 \text{ ft}$$

Take $L_1 = 7 \text{ ft}$ and $B_1 = 10.75 \text{ ft}$ ($A_1 = 75.25 \text{ ft}^2$)

The final dimensions are shown below.



Procedure #2: We illustrate the second design approach here. We estimate A_1 by requiring the pressure under the footing #1 to be equal to q_e .

$$A_1 > \frac{P_1}{q_e} = \frac{290}{4.625} = 62.7 \text{ ft}^2$$

We take $L_1 = 6$ ft as a first estimate. Then, noting Fig. E7.6b

$$e_1 = \frac{L_1}{2} - 0.5 \approx 2.5 \text{ ft}$$

The remaining steps are listed below

$$V = \frac{P_1 e_1}{d - e_1} = \frac{290(2.5)}{20 - 2.5} = 41.43 \text{ kip}$$

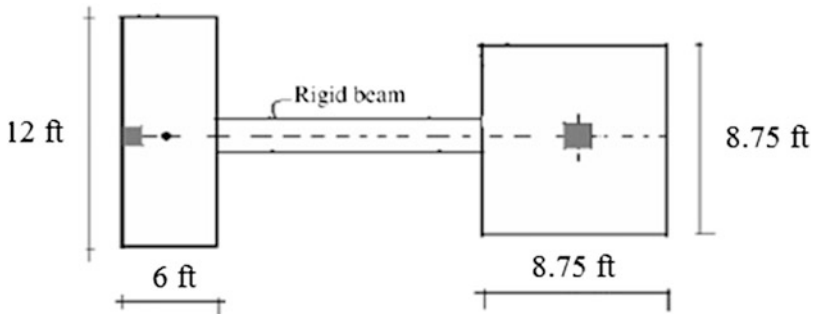
$$R_1 = P_1 + V = 290 + 41.43 = 331.43 \text{ kip}$$

$$R_2 = P_2 - V = 385 - 41.43 = 343.57 \text{ kip}$$

$$A_{1\text{required}} = \frac{331.43}{4.625} = 71.66 \text{ ft}^2 \Rightarrow B_1 = \frac{71.66}{6} = 11.94 \Rightarrow L_1 = 6 \text{ ft} \quad B_1 = 12 \text{ ft}$$

$$A_{2\text{required}} = \frac{343.57}{4.625} = 74.29 \text{ ft}^2 \Rightarrow L_2 = B_2 = \sqrt{74.29} = 8.62 \Rightarrow B_2 = L_2 = 8.75 \text{ ft}$$

The final dimensions are shown below.



Repeating this computation for the ultimate loading case,

$$P_{1u} = 1.2P_D + 1.6P_L = 1.2(160) + 1.6(130) = 400 \text{ kip}$$

$$P_{2u} = 1.2P_D + 1.6P_L = 1.2(200) + 1.6(185) = 536 \text{ kip}$$

and assuming the same value for e_1 leads to

$$V_u = \frac{P_{1u}e_1}{d - e_1} = \frac{400(2.5)}{17.5} = 57.14 \text{ kip}$$

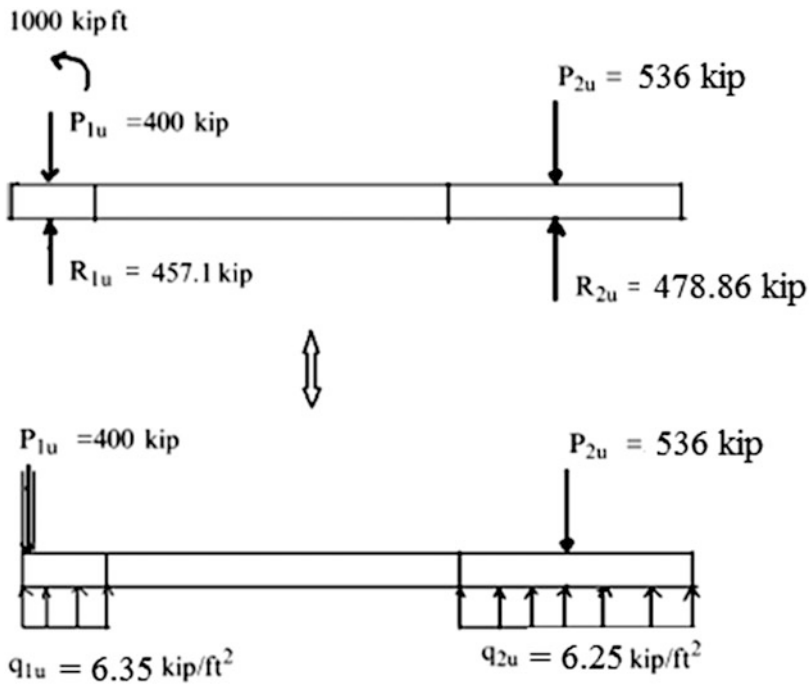
$$R_{1u} = P_{1u} + V_u = 400 + 57.14 = 457.14 \text{ kip}$$

$$q_{1u} = \frac{R_{1u}}{B_1L_1} = \frac{457.14}{6(12)} = 6.35 \text{ kip/ft}^2$$

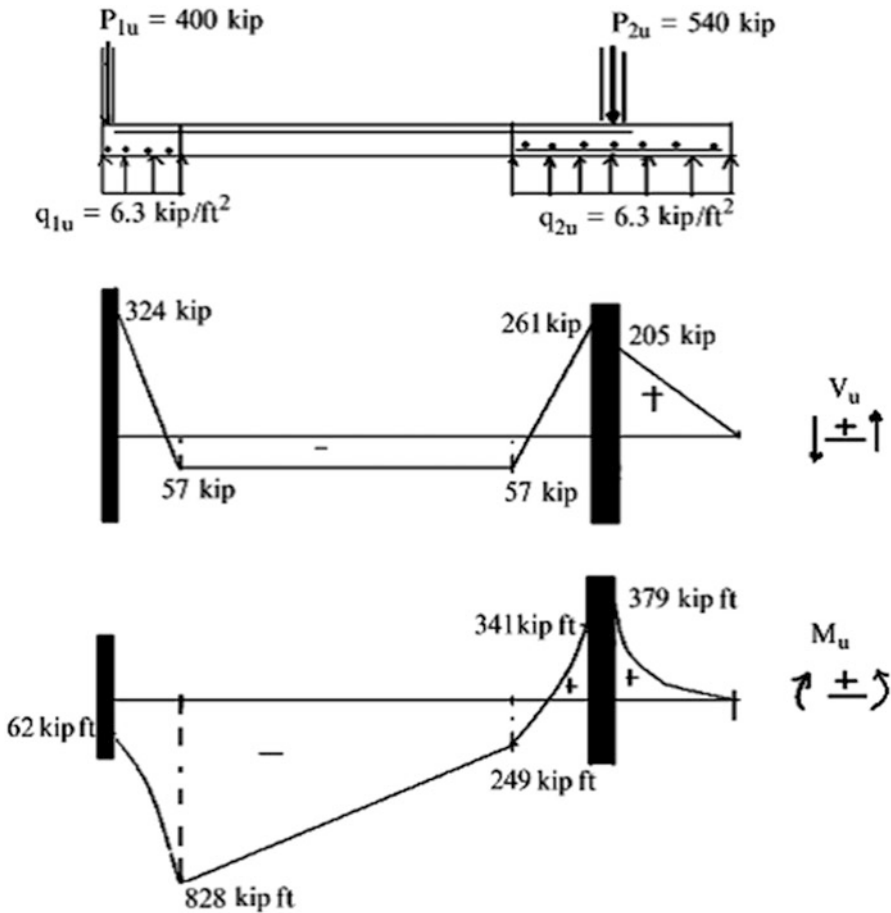
$$R_{2u} = P_{2u} - V_u = 536 - 57.14 = 478.86 \text{ kip}$$

$$q_{2u} = \frac{R_{2u}}{B_2L_2} = \frac{478.86}{8.75(8.75)} = 6.25 \text{ kip/ft}^2$$

The corresponding forces are shown in the sketches below.



The shear and moment diagrams are plotted below.



7.6 Summary

7.6.1 Objectives of the Chapter

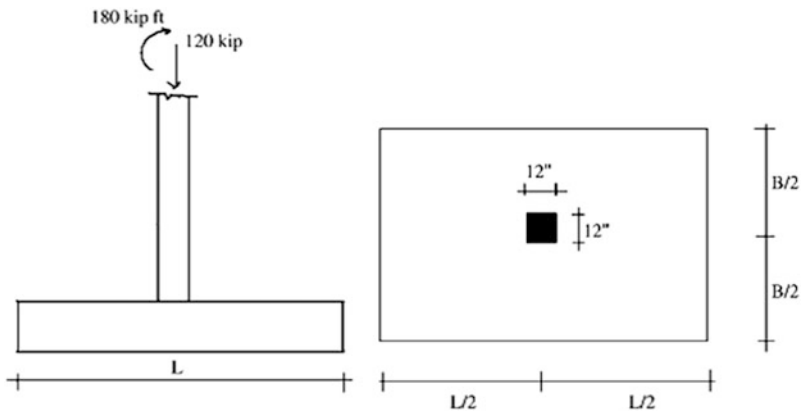
- To describe the various types of footings used in shallow foundations.
- To develop an analytical procedure for dimensioning footings.
- To develop a general analytical procedure for generating the shear and moment distribution in footings based on the assumption of a linear soil pressure distribution.
- To identify critical loading conditions which produce pressure loading distributions with high peak magnitudes.

7.7 Problems

Problem 7.1

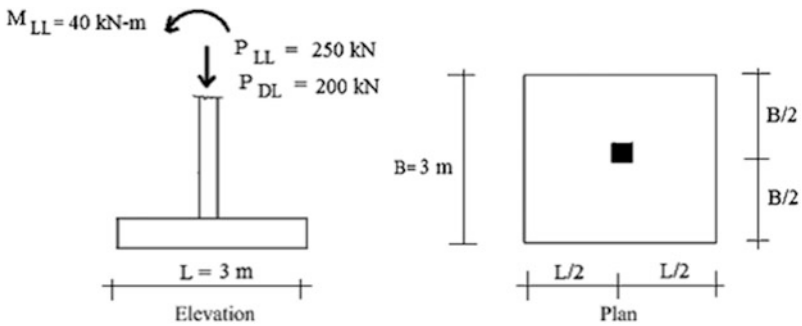
Consider the footing geometry shown below. Determine the soil pressure distribution corresponding to

- (a) $B = L = 8$ ft
- (b) $L = 10$ ft, $B = 5$ ft



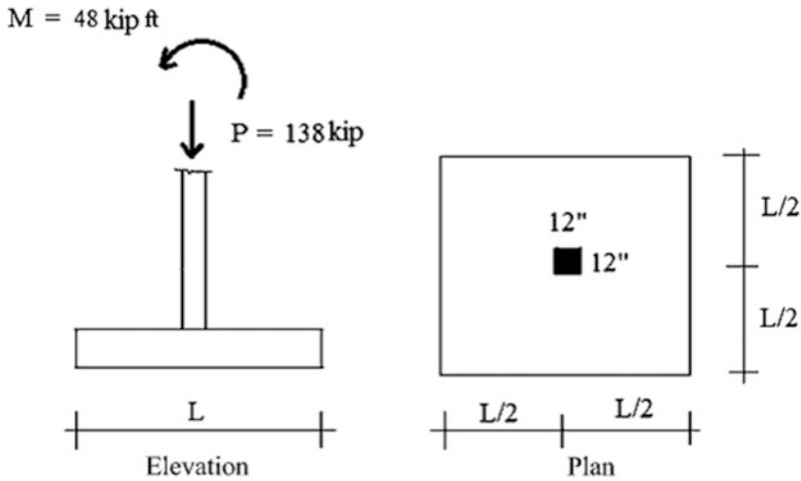
Problem 7.2

The plan view and elevation of a single footing supporting a 300 mm \times 300 mm column are shown below. Determine the soil pressure distribution under the footing. Use a factor of 1.2 for DL and 1.6 for LL.

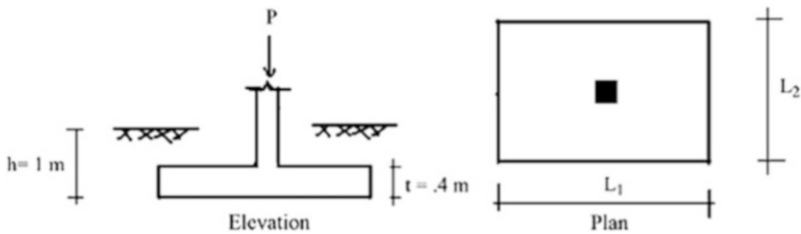


Problem 7.3

The plan view and elevation of a single footing supporting a column are shown below. The effective soil pressure is 4 kip/ft^2 . Determine the required value of L .

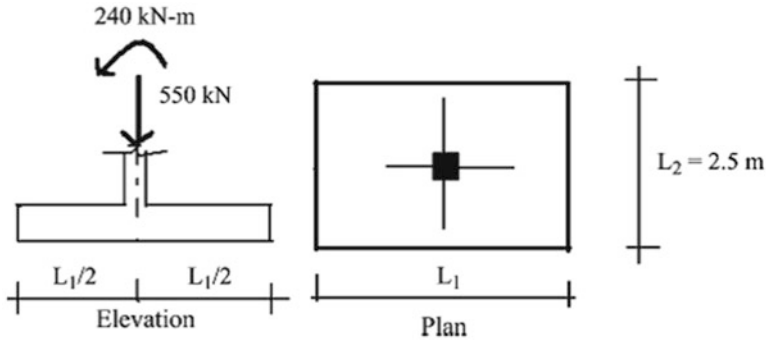
**Problem 7.4**

A $450 \text{ mm} \times 450 \text{ mm}$ concentrically load column is to be supported on a shallow foundation. The base of the footing is 1 m below grade. Estimate the size of the footing using service loads. Draw shear and moment diagrams using a factor load of $P_u = 1.2P_D + 1.6P_L$. The allowable soil pressure is $q_{\text{allowable}} = 250 \text{ kN/m}^2$, $\gamma_{\text{soil}} = 18 \text{ kN/m}^3$, $\gamma_{\text{conc}} = 24 \text{ kN/m}^3$, $P_D = 1000 \text{ kN}$, and $P_L = 1400 \text{ kN}$. Consider: (a) A square footing ($L_1 = L_2 = L$) and (b) A rectangular footing with $L_2 = 2.5 \text{ m}$.

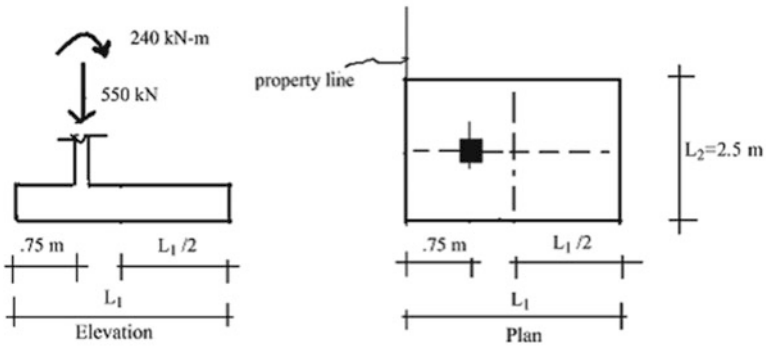
**Problem 7.5**

A $350 \text{ mm} \times 350 \text{ mm}$ column is to be supported on a shallow foundation. Determine the dimensions (either square or rectangular) for the following conditions. The effective soil pressure is $q_{\text{effective}} = 180 \text{ kN/m}^2$.

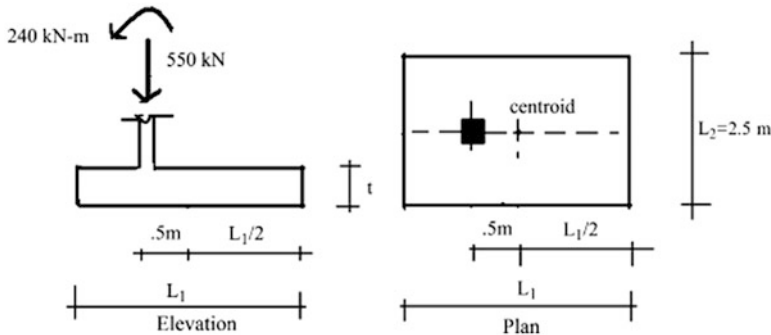
- (a) The center line of the column coincides with the center line of the footing.



- (b) The center line of the column is 0.75 m from the property line.

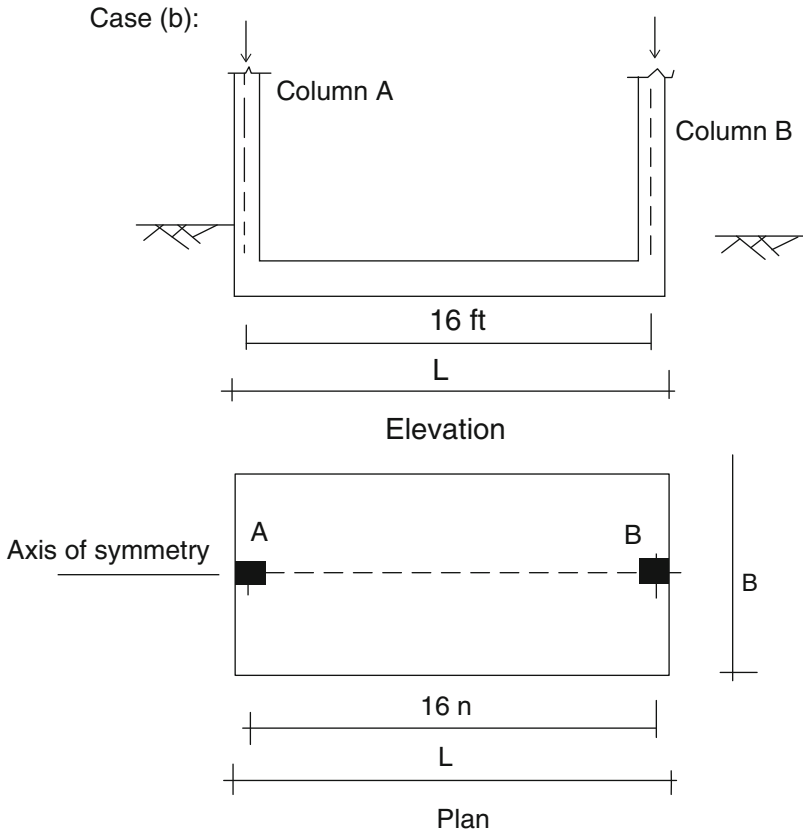
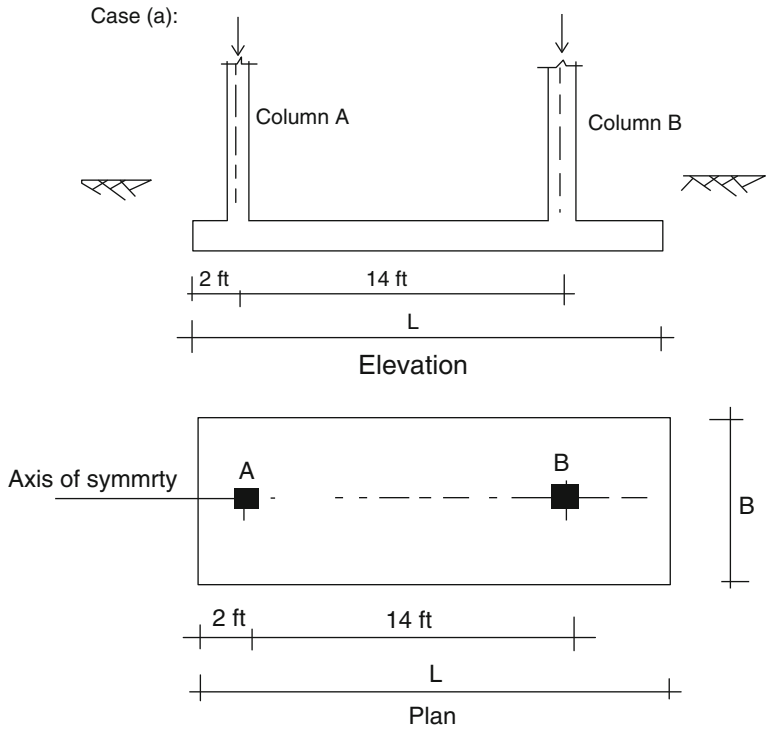


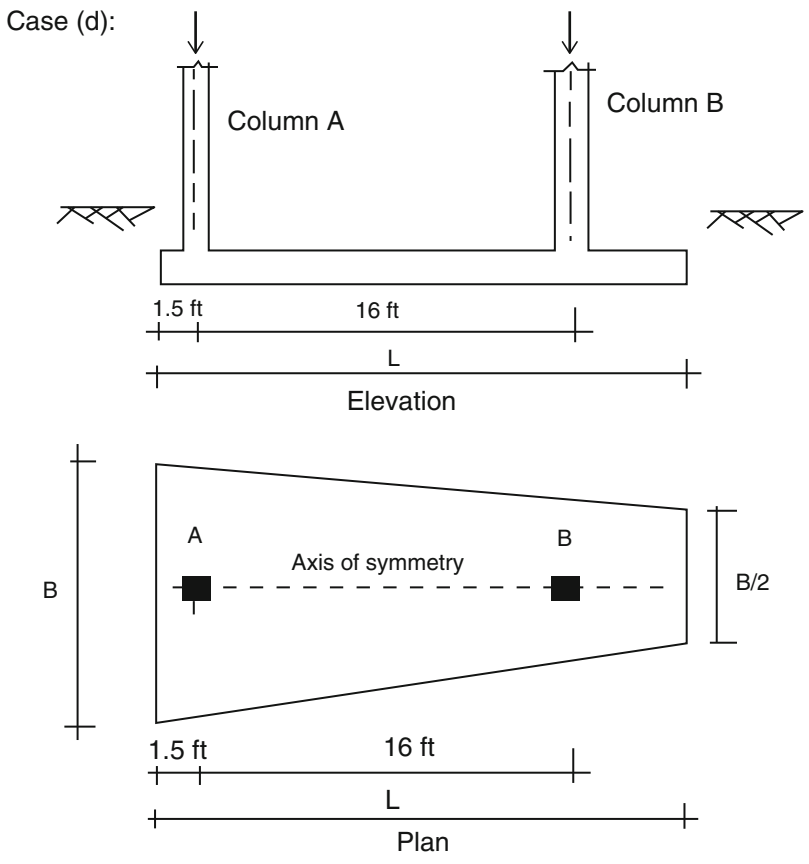
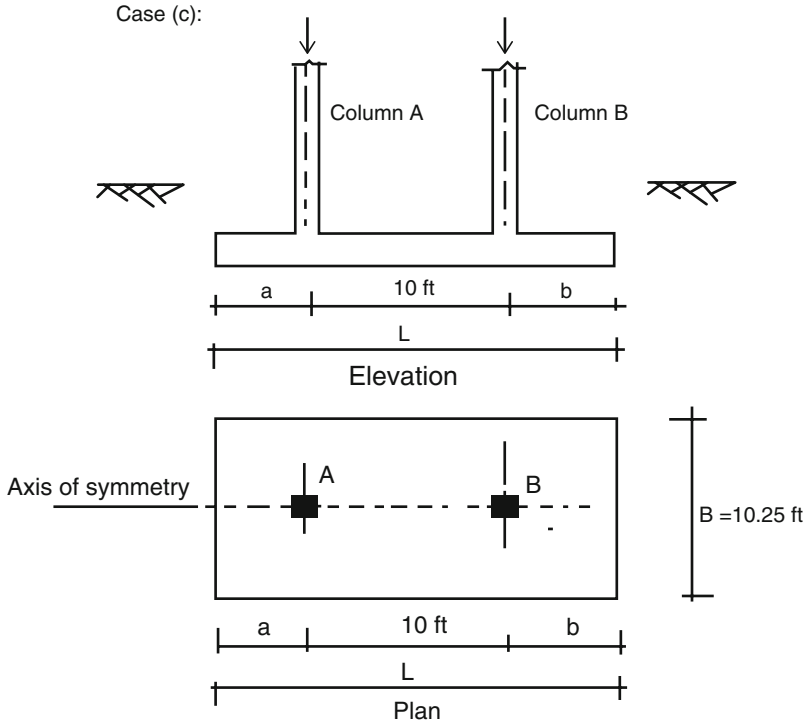
- (c) The center line of the column is 0.5 m from the centroid of the footing.



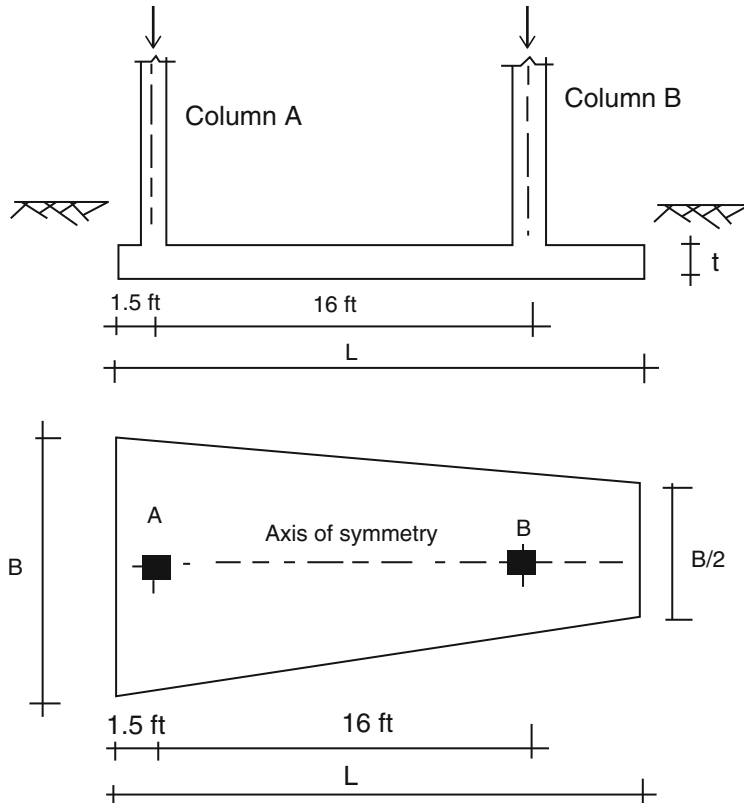
Problem 7.6

A combined footing supports two square columns: Column A is 14 in. \times 14 in. and carries a dead load of 140 kip and a live load of 220 kip. Column B is 16 in. \times 16 in. and carries a dead load of 260 kip and a live load of 300 kip. The effective soil pressure is $q_e = 4.5 \text{ kip/ft}^2$. Assume the soil pressure distribution is uniform, except for case (b). Determine the footing dimensions for the following geometric configurations. Establish the shear and moment diagrams corresponding to the factored loading, $P_u = 1.2P_D + 1.6P_L$.

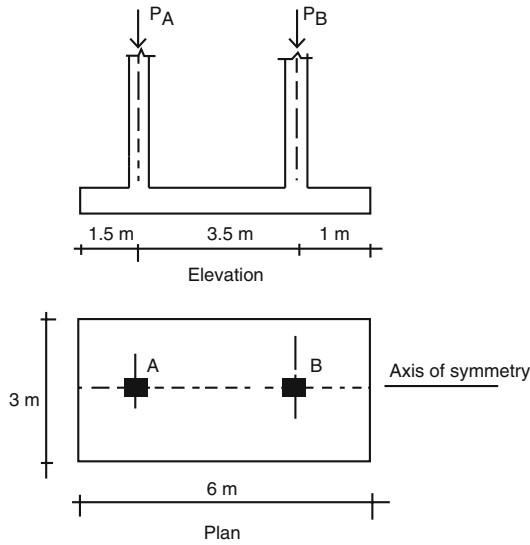




Case (e):

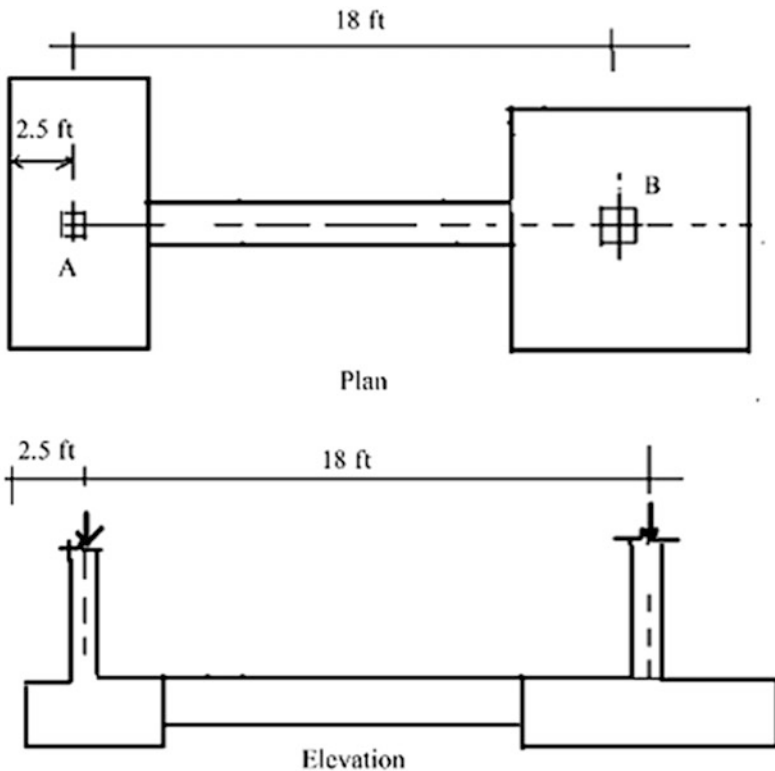
**Problem 7.7**

Column A is $350 \text{ mm} \times 350 \text{ mm}$ and carries a dead load of 1300 kN and a live load of 450 kN. Column B is $450 \text{ mm} \times 450 \text{ mm}$ and carries a dead load of 1400 kN and a live load of 800 kN. The combined footing shown below is used to support these columns. Determine the soil pressure distribution and the shear and bending moment distributions along the longitudinal direction corresponding to the factored loading, $P_u = 1.2P_D + 1.6P_L$.



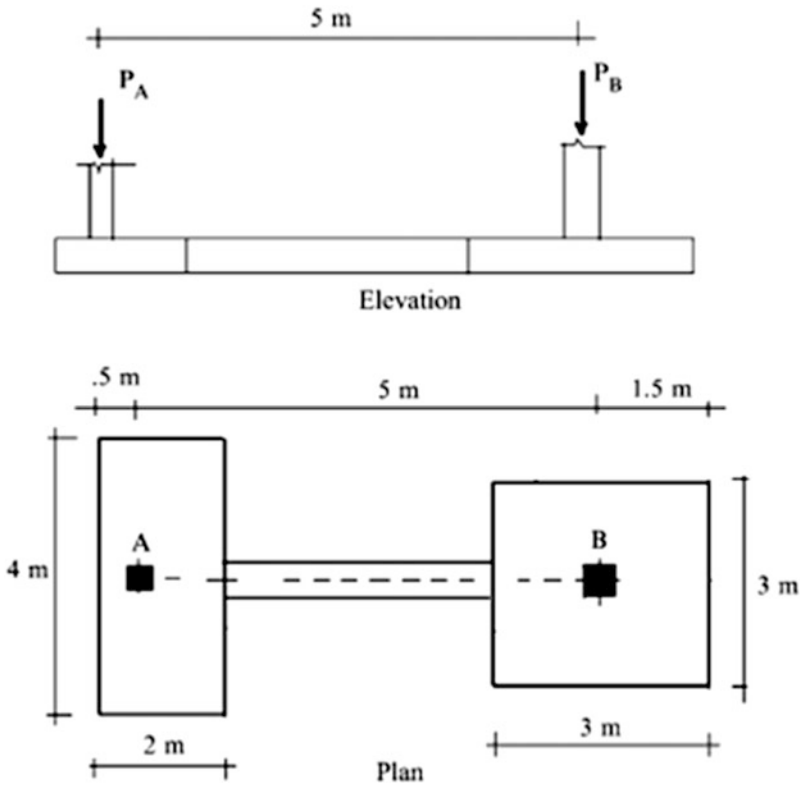
Problem 7.8

Dimension a strap footing for the situation shown. The exterior column A is 14 in. × 14 in. and carries a dead load of 160 kip and a live load of 130 kip; the interior column B is 18 in. × 18 in. and carries a dead load of 200 kip and a live load of 187.5 kip; the distance between the center lines of the columns is 18 ft. Assume the strap is placed such that it does not bear directly on the soil. Take the effective soil pressure as $q_e = 4.5 \text{ kip/ft}^2$. Draw shear and moment diagrams using a factored load of $P_u = 1.2P_D + 1.6P_L$.



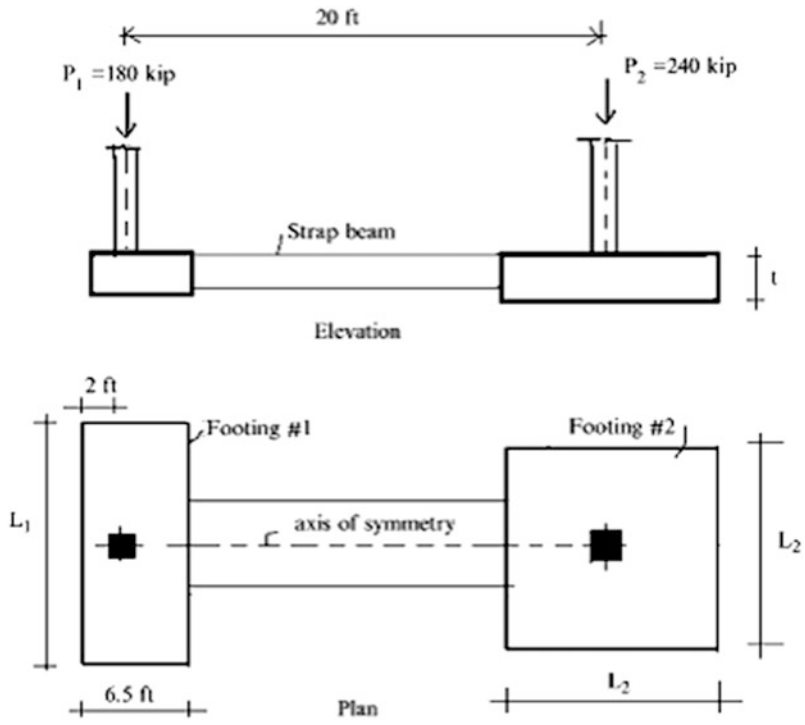
Problem 7.9

Column A is 350 mm × 350 mm and carries a dead load of 1300 kN and a live load of 450 kN. Column B is 450 mm × 450 mm and carries a dead load of 1400 kN and a live load of 800 kN. A strap footing is used to support the columns and the center line of Column A is 0.5 m from the property line. Assume the strap is placed such that it does not bear directly on the soil. Determine the soil pressure distribution and the shear and bending moment distributions along the longitudinal direction corresponding to the factored loading, $P_u = 1.2P_D + 1.6P_L$.

**Problem 7.10**

An exterior 18 in. × 18 in. column with a total vertical service load of $P_1 = 180$ kip and an interior 20 in. × 20 in. column with a total vertical service load of $P_2 = 240$ kip are to be supported at each column by a pad footing connected by a strap beam. Assume the strap is placed such that it does not bear directly on the soil.

- Determine the dimensions L_1 and L_2 for the pad footings that will result in a uniform effective soil pressure not exceeding 3 kip/ft² under each pad footing. Use ¼ ft increments.
- Determine the soil pressure profile under the footings determined in part (a) when an additional loading, consisting of an uplift force of 80 kip at the exterior column and an uplift force of 25 kip at the interior column, is applied.



Reference

1. Terzaghi K, Peck RB. Soil mechanics in engineering practice. New York: Wiley; 1967.

Abstract

Vertical wall type structures function as barriers whose purpose is to prevent a material from entering a certain space. Typical applications are embankment walls, bridge abutments, and underground basement walls. Structural Engineers are responsible for the design of these structures. The loading acting on a retaining wall is generally due to the soil that is confined behind the wall. Various theories have been proposed in the literature, and it appears that all the theories predict similar loading results. In this chapter, we describe the Rankine theory which is fairly simple to apply. We present the governing equations for various design scenarios and illustrate their application to typical retaining structures. The most critical concerns for retaining walls are *ensuring stability with respect to sliding and overturning, and identifying the regions of positive and negative moment in the wall segments*. Some of the material developed in Chap. 7 is also applicable for retaining wall structures.

8.1 Introduction

8.1.1 Types of Retaining Walls

Vertical retaining wall structures are used to form a vertical barrier that retains a fluid or other material such as soil. Figure 8.1 illustrates different types of vertical retaining wall structures. They are constructed using unreinforced concrete for gravity walls and reinforced concrete for cantilever walls and bridge abutments. The base of the wall/footing is placed below the frost level. The material behind the wall is called backfill and is composed of granular material such as sand.

8.1.2 Gravity Walls

A free body diagram of a gravity structure is shown in Fig. 8.2. The force acting on the structure due to the backfill material is represented by P ; the forces provided by the soil at the base are represented

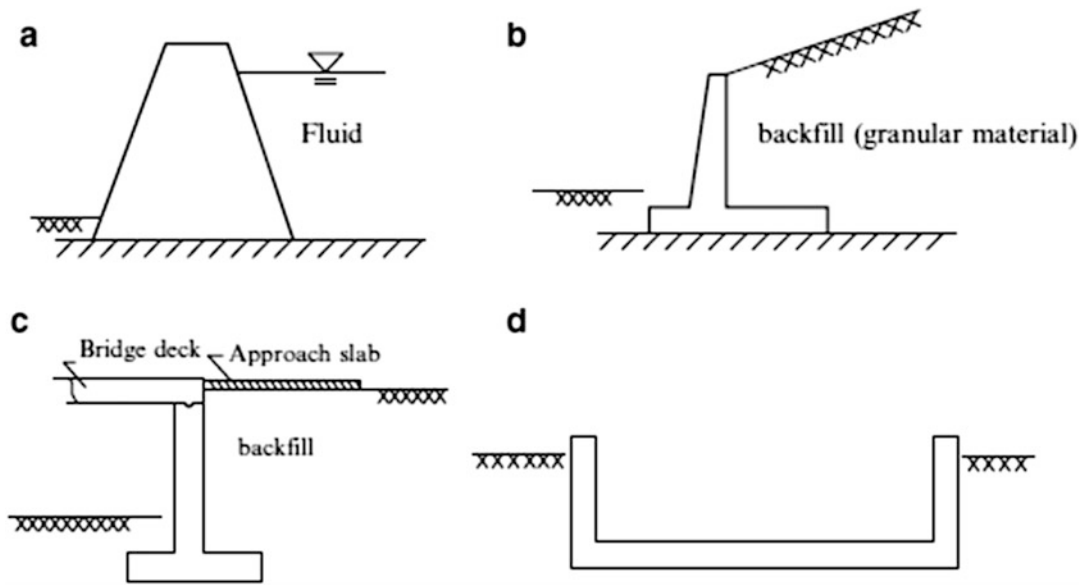


Fig. 8.1 Vertical retaining wall structures. (a) Gravity dam. (b) Cantilever retaining wall. (c) Bridge abutment. (d) Underground basement

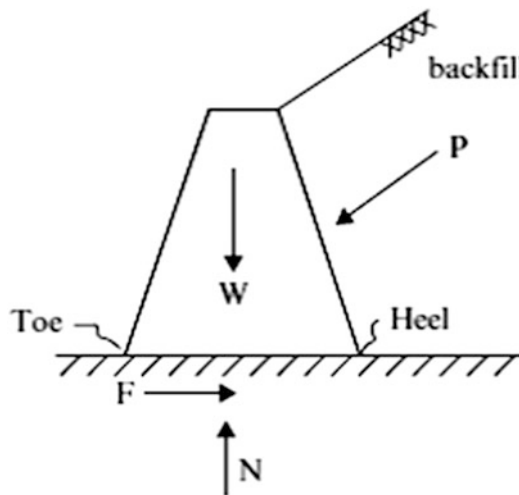


Fig. 8.2 Free body diagram—gravity structure

by the friction force F and the normal force N ; lastly, the weight of the structure is represented by W . The end points of the base are called the “toe” and the “heel.” We observe that P tends to overturn the wall about its toe and also to slide the structure in the horizontal direction. The overturning tendency is resisted by the gravity force W which has a counterbalancing moment about the toe. Sliding is resisted by the friction which is proportional to the normal force. Therefore, since both resisting mechanisms are due to gravity, this type of structure is called a “Gravity” structure.

Of critical concern are the *sliding and overturning failure modes*. The key design parameter is the length of the base. We need to select this parameter such that the factors of safety for sliding and overturning are sufficient to ensure global stability of the structure.

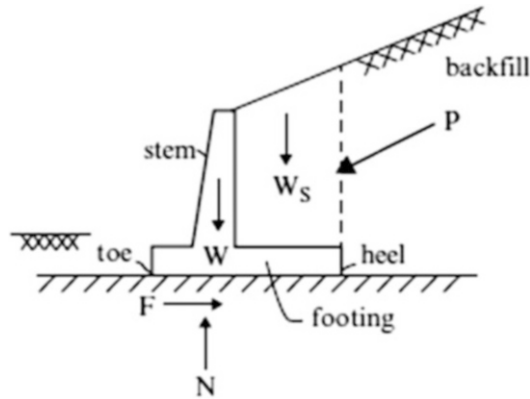


Fig. 8.3 Free body diagram—cantilever structure

8.1.3 Cantilever Walls

The amount of concrete required for a gravity type wall increases with height. Therefore, in order to minimize the concrete volume, the cantilever type retaining wall geometry shown in Fig. 8.3 is used. A portion of the concrete wall is removed and a “footing” extending out from both the heel and toe is added. This change has a stabilizing effect in that the weight of the backfill above the footing, represented by W_s , now contributes to the counterbalancing moment and also to the normal force. The wall stem segment of a cantilever wall carries load through bending action, whereas the gravity wall carries load primarily through *horizontal shear action*. These behavior modes dictate the type of construction.

Cantilever retaining walls, such as shown in Fig. 8.4, are reinforced concrete structures; gravity type walls tend to be unreinforced concrete. The key design issue is the width of the footing. This parameter is controlled by the requirements on the factors of safety with respect to overturning about the toe and sliding of the wall.



Fig. 8.4 Cantilever wall construction

8.2 Force Due to the Backfill Material

8.2.1 Different Types of Materials

8.2.1.1 Fluid

We consider first the case where the backfill material is an ideal fluid. By definition, an ideal fluid has no shear resistance; the state of stress is pure compression. The vertical and horizontal pressures at a point z unit below the free surface are (see Fig. 8.5):

$$p_v = p_h = p = \gamma z \tag{8.1}$$

where γ is the weight density.

We apply this theory to the inclined surface shown in Fig. 8.6. Noting (8.1), the fluid pressure is normal to the surface and varies linearly with depth. The resultant force acts $H/3$ units up from the base and is equal to

$$P = \frac{1}{2} p \frac{H}{\sin \theta} = \frac{1}{2} \gamma \left(\frac{H^2}{\sin \theta} \right) \tag{8.2}$$

Resolving P into horizontal and vertical components leads to

$$P_h = P \sin \theta = \frac{1}{2} \gamma H^2 \tag{8.3}$$

$$P_v = P \cos \theta = \frac{1}{2} \gamma H^2 \frac{1}{\tan \theta}$$

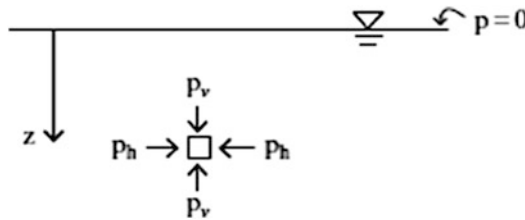
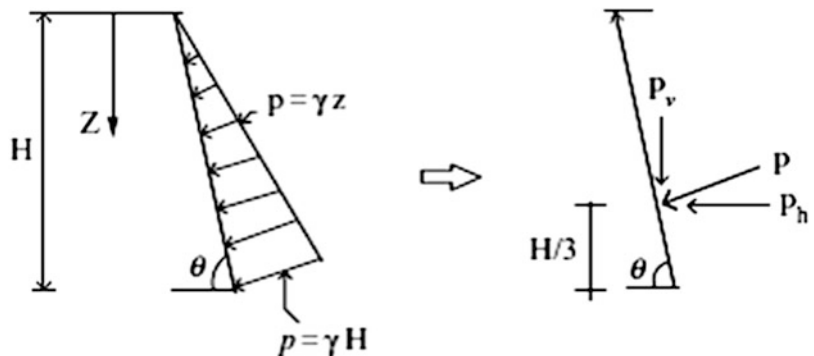


Fig. 8.5 Hydrostatic pressure

Fig. 8.6 Hydrostatic forces on an inclined surface



8.2.1.2 Granular Material

We consider next the case where the backfill behind the wall is composed of a granular material such as dry loose sand (Fig. 8.7). Loose sand behaves in a different manner than a fluid in that sand can resist shearing action as well as compressive action. The maximum shear stress for a sandy soil is expressed as

$$\tau = \sigma_n \tan \varphi$$

where σ_n is the normal stress and φ is defined as the internal friction angle for the soil. A typical value of φ for loose sand is approximately 30° . One can interpret φ as being related to the angle of repose that a volume of sand assumes when it is formed by dumping the sand loosely on the pile. Figure 8.8 illustrates this concept.

The presence of shear stress results in a shift in orientation of the resultant force exerted on the wall by the backfill. A typical case is shown in Fig. 8.9; P is assumed to act at an angle of φ' with respect to the horizontal, where φ' ranges from 0 to φ .

Fig. 8.7 Granular material-stress state

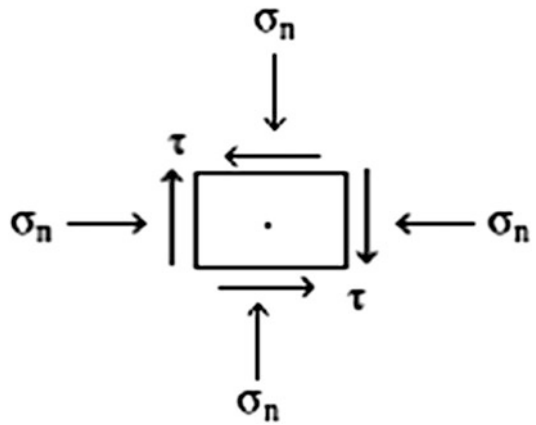


Fig. 8.8 Angle of repose

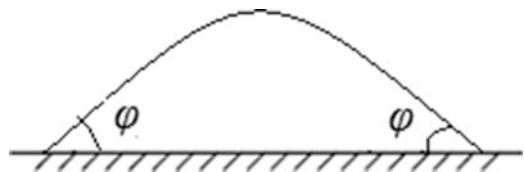
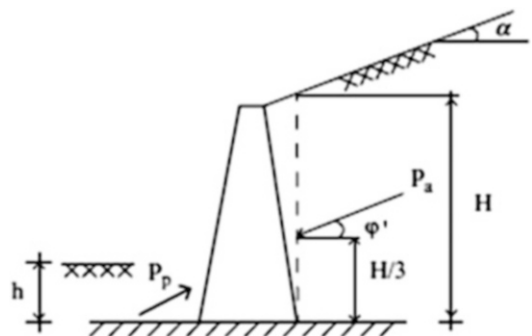


Fig. 8.9 Active and passive failure states



The magnitude of the soil pressure force depends on how the wall moved when the backfill was placed. If the wall moved away from the backfill (to the left in Fig. 8.9), the soil is said to be in an *active failure state*. The other extreme case is when the wall is pushed into the soil; the failure state is said to be in the *passive mode*. There is a significant difference in the force magnitudes corresponding to these states.

In general, the active force is *an order of magnitude* less than the passive force. For the applications that we are considering, the most likely case is when the wall moves away from the soil, and therefore we assume “*active*” conditions. The downward component tends to increase the stability with respect to overturning about the toe and also increases the friction force.

Different theories for the soil pressure distribution have been proposed which relate to the choice of ϕ' . The Rankine theory assumes $\phi' = 0$ (i.e., no shear stress), and the Coulomb theory assumes $\phi' = \phi$. Considering that there is significant variability in soil properties, both theories predict pressure distributions which are suitable for establishing the wall dimensions.

In what follows we present the key elements of the Rankine theory. There are many textbooks that deal with mechanics of soil. In particular, we suggest Lamb and Whitman [1], Terzaghi and Peck [2], and Huntington [3].

8.2.2 Rankine Theory: Active Soil Pressure

Figure 8.10 defines the geometry and the soil pressure distribution. The pressure is applied to vertical surfaces through the heel and toe and is assumed to vary linearly with depth as shown. The magnitudes of the forces acting on a strip of unit width in the longitudinal direction of the wall are:

$$\begin{aligned} P_a &= \frac{1}{2} \gamma H^2 k_a \\ P_p &= \frac{1}{2} \gamma h^2 k_p \end{aligned} \quad (8.4)$$

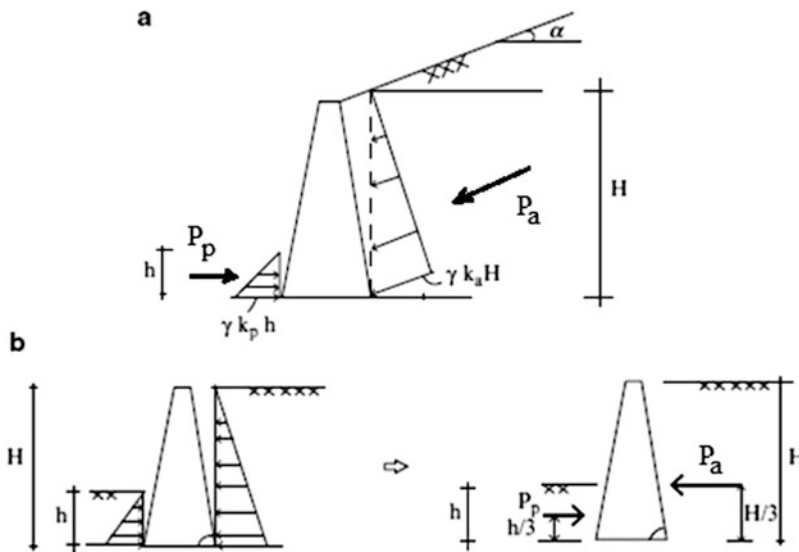


Fig. 8.10 (a) Soil pressure distribution for Rankine theory $\alpha \neq 0$. (b) Soil pressure distribution for Rankine theory $\alpha = 0$

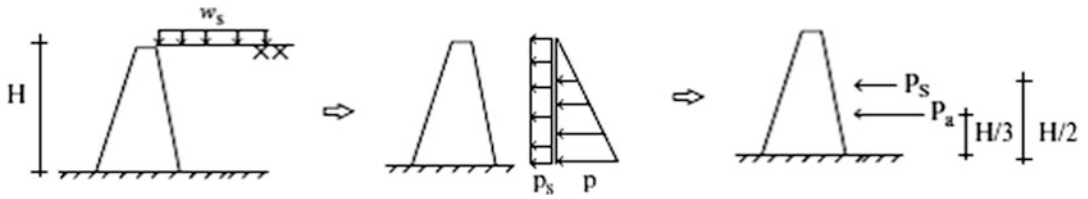


Fig. 8.11 Pressure distributions due to surcharge and active soil pressure

where γ is the unit weight of the soil backfill, k_a and k_p are defined as the active and passive soil pressure coefficients,

$$k_a = \cos \alpha \left\{ \frac{\cos \alpha - \sqrt{(\cos \alpha)^2 - (\cos \varphi)^2}}{\cos \alpha + \sqrt{(\cos \alpha)^2 - (\cos \varphi)^2}} \right\} \tag{8.5}$$

$$k_p = \frac{1 + \sin \varphi}{1 - \sin \varphi}$$

where φ is the internal friction angle, and α is the angle of inclination for the backfill.

When the backfill is level, $\alpha = 0$ and k_a reduces to

$$k_a = \frac{1 - \sin \varphi}{1 + \sin \varphi} \tag{8.6}$$

In this case, both resultants are horizontal forces.

8.2.2.1 Soil Pressure Due to Surcharge

When a surcharge is applied to the top of a backfill, additional soil pressure is developed. This pressure is assumed to be uniform over the depth. In the case of a uniform surcharge applied to a horizontal backfill, the *added* pressure is estimated as

$$p_s \approx k_a w_s$$

$$P_s \approx k_a w_s H \tag{8.7}$$

where k_a is defined by (8.6). The soil pressure distributions due to the surcharge and the active soil pressure are illustrated in Fig. 8.11.

8.3 Stability Analysis of Retaining Walls

The key concerns for a retaining wall are overturning about the toe and sliding. In order to address these issues, one needs to determine the forces acting on the wall. This step requires that we carry out an equilibrium analysis.

Consider the typical gravity wall shown in Fig. 8.12. The weights of the wall and soil segments are denoted by W_j ; P_a and P_p represent the lateral soil pressure forces; N and F are the normal and tangential (friction) forces due to the soil pressure acting on the base. \bar{x} defines the line of action of the normal force acting on the base.

Summing forces in the vertical direction leads to

$$N = \sum W_j \tag{8.8}$$

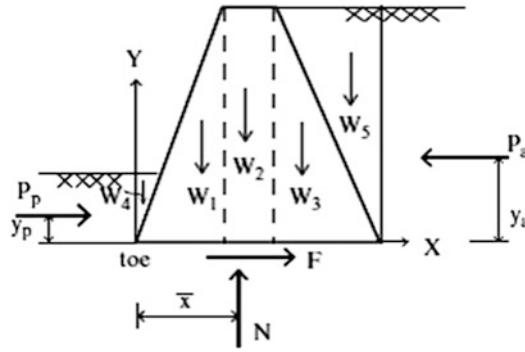


Fig. 8.12 Typical gravity wall

Similarly, horizontal force summation yields

$$F = \sum P_i \quad (8.9)$$

The maximum horizontal force is taken as $F_{\max} = \mu N$, where μ is a friction coefficient for the soil/base interface. This quantity is used to define the factor of safety for sliding:

$$\text{F.S.}_{\text{sliding}} = \frac{F_{\max}}{F} = \frac{\mu N}{F} \quad (8.10)$$

The line of action of N is found by summing the moments about the toe.

$$\begin{aligned} N\bar{x} &= P_p y_p - P_a y_a + \sum W_j x_j = M_{\text{net}} \\ &\Downarrow \\ \bar{x} &= \frac{M_{\text{net}}}{N} \end{aligned} \quad (8.11)$$

For stability with respect to overturning, \bar{x} must be positive. A negative value of \bar{x} implies that the line of action of N lies outside the base. The safety measure for overturning is defined as the ratio of the resisting moment about the toe to the overturning moment.

$$\text{F.S.}_{\text{overturning}} = \frac{M_{\text{resisting}}}{M_{\text{overturning}}} \quad (8.12)$$

Noting Fig. 8.12, this definition expands to

$$\text{F.S.}_{\text{overturning}} = \frac{P_p y_p + \sum W_j x_j}{P_a y_a} \quad (8.13)$$

Typical desired values are $\text{F.S.}_{\text{sliding}} > 1.5$ and $\text{F.S.}_{\text{overturning}} > 2$.

In order to increase the factors of safety against sliding and overturning, either one can increase the width of the concrete wall or one can add a footing extending out from the original base. These schemes are illustrated in Fig. 8.13.

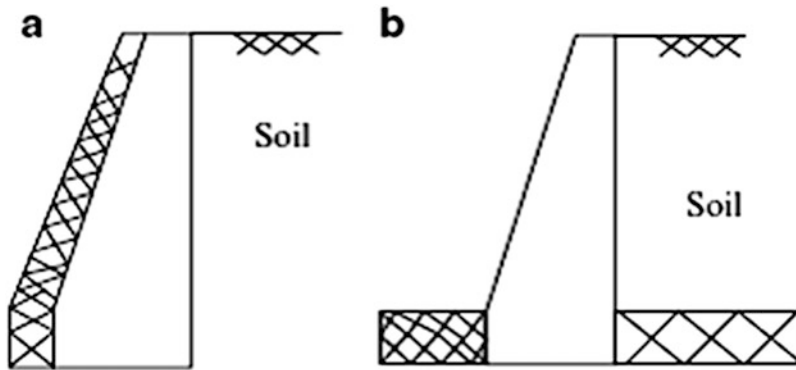


Fig. 8.13 (a) Gravity wall and (b) cantilever retaining wall

8.4 Pressure Distribution Under the Wall Footing

We consider the pressure acting on the footing is assumed to vary linearly. There are two design constraints: firstly, the peak pressures must be less than the allowable bearing pressure for the soil and secondly the pressure cannot be negative, i.e., tension. Noting the formulation presented in Sect. 7.2, the peak pressures are given by (7.6) (we work with a unit width strip of the footing along the length of the wall, i.e., we take $B = 1$ and N as the resultant) which we list below for convenience. Figure 8.14 shows the soil pressure distributions for various values of e .

$$\begin{aligned} q_1 &= \frac{N}{L} \left\{ 1 + \frac{6e}{L} \right\} \\ q_2 &= \frac{N}{L} \left\{ 1 - \frac{6e}{L} \right\} \end{aligned} \quad (8.14)$$

The second design constraint requires $|e| \leq L/6$ or equivalently, the line of action of N must be located within the middle third of the footing width, L . The first constraint limits the maximum peak pressure,

$$|q|_{\max} \leq q_{\text{allowable}}$$

where $q_{\text{allowable}}$ is the allowable soil pressure at the base of the wall. We note that the pressure distribution is uniform when N acts at the centroid of the footing area which, for this case, is the midpoint. Since e depends on the wall height and footing length, we define the optimal geometry as that combination of dimensions for which the soil pressure is *uniform*. Note that the line of action of the resultant N always coincides with the line of action of the applied vertical load.

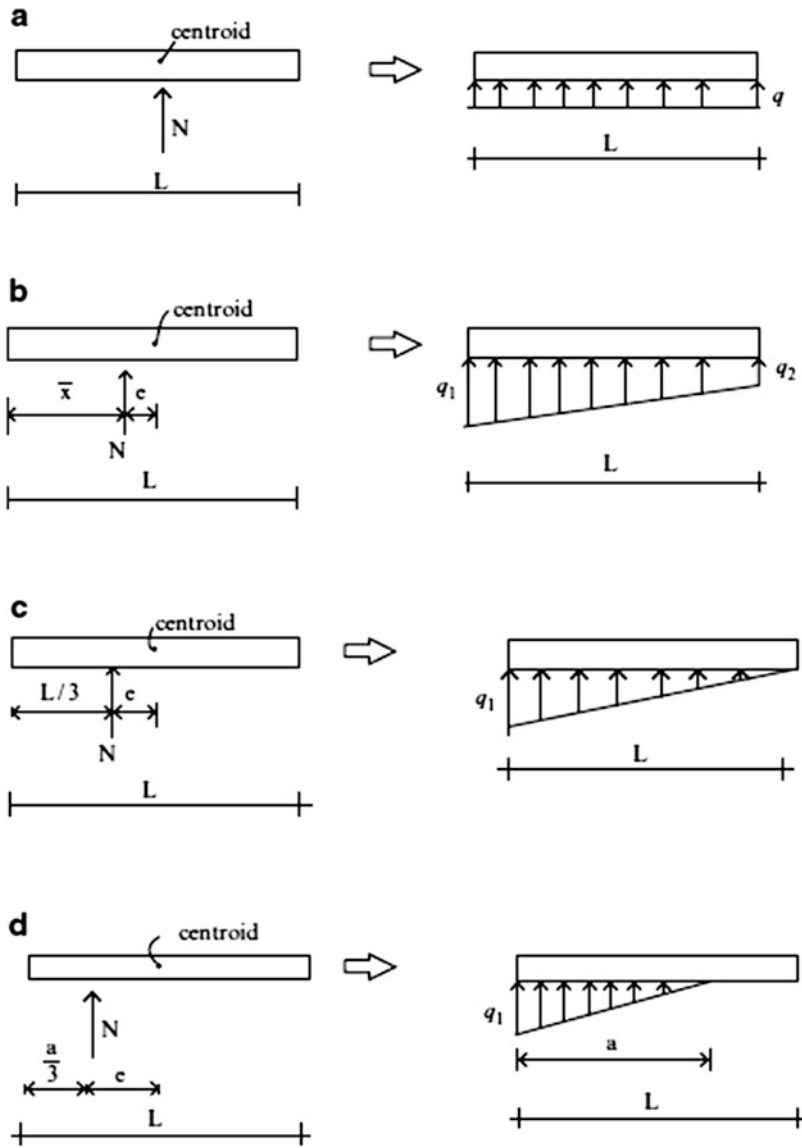


Fig. 8.14 Pressure distributions on footing/wall base. (a) $e = 0$. (b) $e < L/6$. (c) $e = L/6$. (d) $e > L/6$

Example 8.1 Gravity Retaining Wall Analysis

Given: The concrete gravity wall and soil backfill shown in Fig. E8.1a.

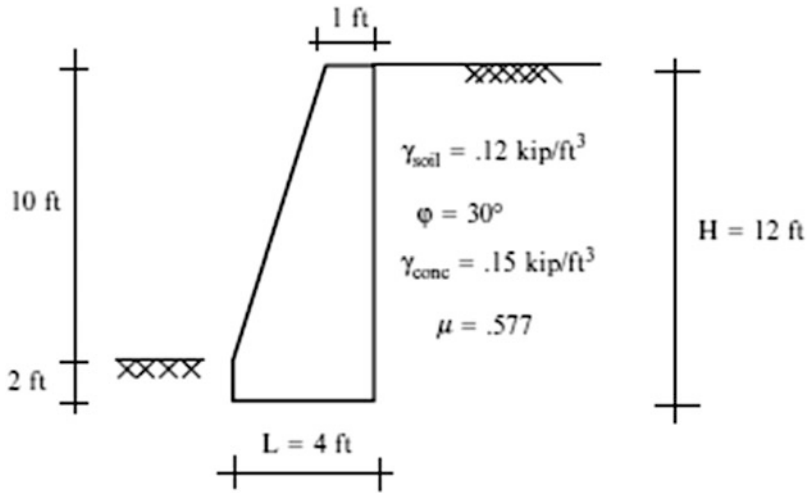


Fig. E8.1a Wall geometry

Determine: The factor of safety against sliding; the factor of safety against overturning; the line of action of the resultant. Use the Rankine theory for soil pressure computations. Neglect the passive pressure acting on the toe.

Solution:

$$\text{For } \varphi = 30^\circ k_a = \frac{1 - \sin \varphi}{1 + \sin \varphi} = \frac{1}{3}$$

$$\text{Then } P_a = \frac{1}{2}(0.12)(12)^2 \left(\frac{1}{3}\right)(1 \text{ ft}) = 2.88 \text{ kip/ft of wall}$$

Next, we compute the weight of the concrete wall segments per foot of wall. Noting Fig. E8.1b,

$$W_1 = (0.150)(10)(1)(1 \text{ ft}) = 1.5 \text{ kip}$$

$$W_2 = (0.150) \left(\frac{10}{2}\right)(3)(1 \text{ ft}) = 2.25 \text{ kip}$$

$$W_3 = (0.150)(4)(2)(1 \text{ ft}) = 1.2 \text{ kip}$$

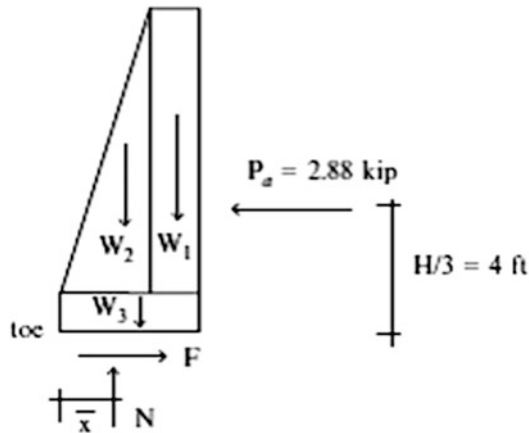


Fig. E8.1b Free body diagram

Applying vertical force equilibrium yields

$$N = W_1 + W_2 + W_3 = 1.5 + 2.25 + 1.2 = 4.95 \text{ kip}$$

The factor of safety with respect to sliding is defined as the ratio of the maximum available friction force F_{\max} to the actual horizontal force.

$$F_{\max} = \mu N = N \tan \phi = 0.577(4.95) = 2.86 \text{ kip}$$

$$\text{F.S.}_{\text{sliding}} = \frac{\mu N}{P_a} = \frac{2.86}{2.88} = 0.99$$

The line of action of N is determined by summing moments about the toe. The factor of safety with respect to overturning is defined as the ratio of the resisting moment to the overturning moment, both quantities with respect to the toe.

$$M_{B_{\text{overturning}}} = P_a \left(\frac{H}{3} \right) = 2.88(4) = 11.52 \text{ kip ft}$$

$$M_{B_{\text{resisting}}} = W_1(3.5) + W_2(2) + W_3(2)$$

$$= 1.5(3.5) + 2.25(2) + 1.2(2) = 12.15 \text{ kip ft}$$

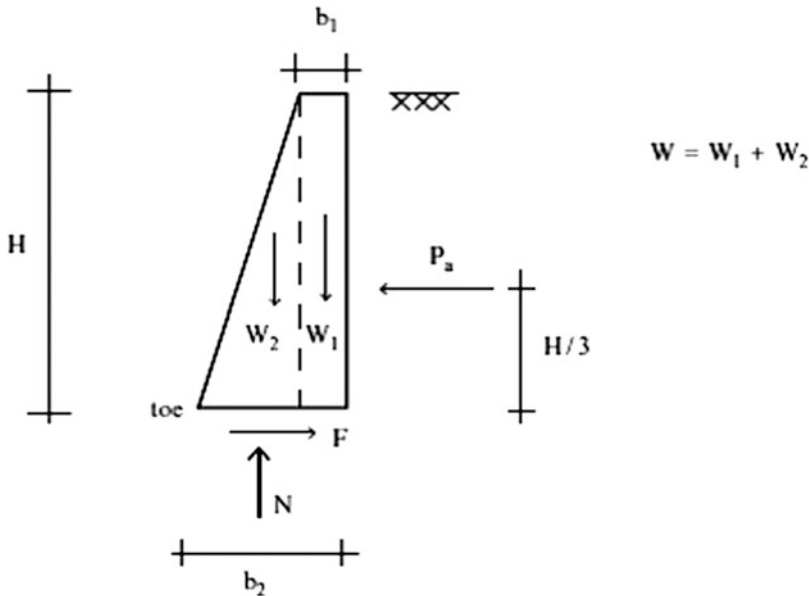
$$\text{F.S.}_{\text{overturning}} = \frac{M_{B_{\text{resisting}}}}{M_{B_{\text{overturning}}}} = \frac{12.15}{11.52} = 1.05$$

$$M_{\text{net}} = M_{B_{\text{overturning}}} - M_{B_{\text{resisting}}} = 0.63 \text{ kip ft clockwise}$$

$$\bar{x} = \frac{M_{\text{net}}}{N} = \frac{0.63}{4.95} = 0.13 \text{ ft}$$

In order to increase the factors of safety, the geometry needs to be modified.

The following procedure is useful for estimating appropriate values for b_1 and b_2 . Given the wall height, one can derive expressions for the factors of safety. The details are listed below.

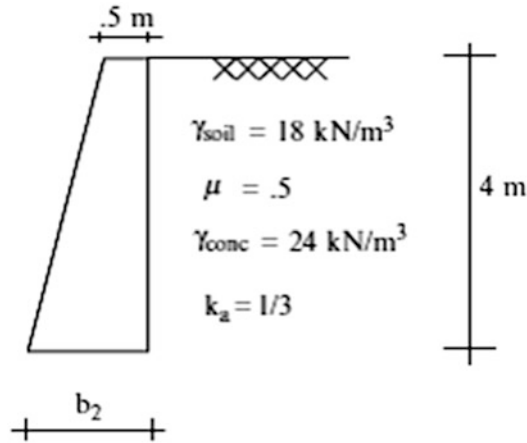


$$\begin{aligned}
 W &= \frac{(b_1 + b_2)}{2} H \gamma_c = N \\
 P_a &= k_a \left\{ \frac{1}{2} \gamma_s H^2 \right\} \\
 \text{F.S.}_{\text{sliding}} &= \frac{\mu N}{P_a} \\
 &\downarrow \\
 \text{F.S.}_{\text{sliding}} &= \left(\frac{\mu \gamma_c}{k_a \gamma_s} \right) \left(\frac{b_2}{H} \right) \left(1 + \frac{b_1}{b_2} \right) \\
 M_{\text{overturning}} &= \frac{H}{3} P_a = \frac{1}{6} k_a \gamma_s H^3 \\
 M_{\text{resisting}} &= \frac{2}{3} (b_2 - b_1) W_2 + \left(b_2 - \frac{b_1}{2} \right) W_1 \\
 &= \frac{H \gamma_c b_2^2}{3} \left\{ 1 - \frac{1}{2} \left(\frac{b_1}{b_2} \right)^2 + \frac{b_1}{b_2} \right\} \\
 \text{F.S.}_{\text{overturning}} &= \frac{M_{\text{Bresisting}}}{M_{\text{Boverturning}}} = \frac{\frac{H \gamma_c b_2^2}{3} \left\{ 1 - \frac{1}{2} \left(\frac{b_1}{b_2} \right)^2 + \frac{b_1}{b_2} \right\}}{\frac{1}{6} k_a \gamma_s H^3} \\
 &\downarrow \\
 \text{F.S.}_{\text{overturning}} &= \frac{2 \gamma_c}{k_a \gamma_s} \left(\frac{b_2}{H} \right)^2 \left\{ 1 - \frac{1}{2} \left(\frac{b_1}{b_2} \right)^2 + \frac{b_1}{b_2} \right\}
 \end{aligned}$$

One specifies the factor of safety with respect to overturning, and the ratio b_1/b_2 , and then computes the value for b_2/H . With b_2/H known, one checks for sliding and if necessary modifies the value of b_2/H .

Example 8.2

Given: The concrete gravity wall and soil backfill shown in Fig. E8.2a.

**Fig. E8.2a**

Determine: The required value for b_2 . Take the factors of safety for overturning and sliding to be equal to 2 and 1.5, respectively.

Solution: Given $b_1 = 0.5 \text{ m}$, $H = 4 \text{ m}$, $\text{F.S.}_{\text{overturning}} = 2$, and $\text{F.S.}_{\text{sliding}} = 1.5$, we determine b_2 corresponding to the two stability conditions.

$$\text{F.S.}_{\text{overturning}} = \frac{2\gamma_c}{k_a\gamma_s} \left(\frac{b_2}{H}\right)^2 \left\{ 1 - \frac{1}{2} \left(\frac{b_1}{b_2}\right)^2 + \frac{b_1}{b_2} \right\}$$

$$\frac{2(24)}{\left(\frac{1}{3}\right)(18)} \left(\frac{b_2}{4}\right)^2 \left\{ 1 - \frac{1}{2} \left(\frac{0.5}{b_2}\right)^2 + \frac{0.5}{b_2} \right\} = 2$$

$$\therefore b_2^2 + 0.5b_2 - 4.125 = 0 \quad b_{2\text{required}} = 1.8 \text{ m}$$

$$\text{F.S.}_{\text{sliding}} = \left(\frac{\mu\gamma_c}{k_a\gamma_s}\right) \left(\frac{b_2}{H}\right) \left(1 + \frac{b_1}{b_2}\right)$$

$$1.5 = \frac{0.5(24)}{\left(\frac{1}{3}\right)(18)} \left(\frac{b_2}{4}\right) \left(1 + \frac{0.5}{b_2}\right) \quad b_{2\text{required}} = 2.5 \text{ m}$$

Use $b_2 = 2.5 \text{ m}$

Example 8.3 Retaining Wall with Footing

Given: The walls defined in Figs. E8.3a, E8.3b, and E8.3c. These schemes are modified versions of the wall analyzed in Example 8.1. We have extended the footing to further stabilize the wall.

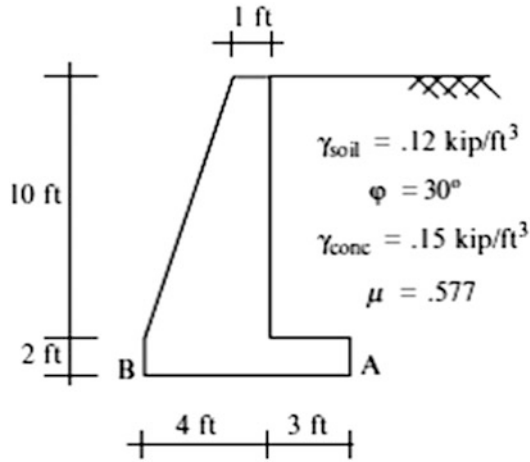


Fig. E8.3a Case "A"

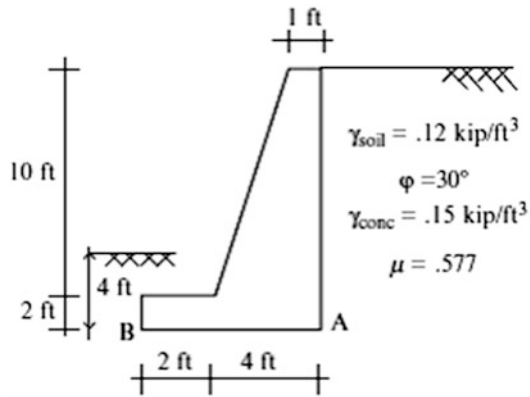


Fig. E8.3b Case "B"

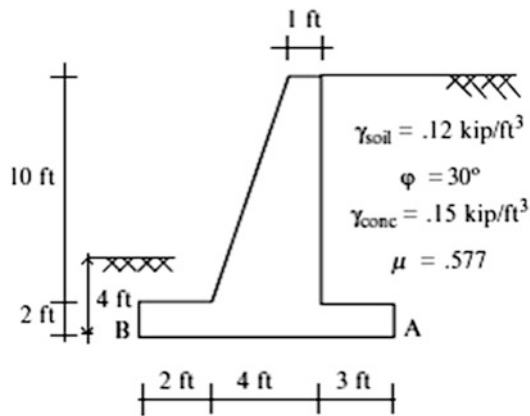


Fig. E8.3c Case "C"

Determine: The factor of safety against sliding; the factor of safety against overturning; the base pressure distribution. Use the Rankine theory for soil pressure computations. Neglect the passive pressure acting on the toe.

Solution:

Case "A": We work with the free body diagram shown in Fig. E8.3d. The vertical surface is taken to pass through the heel.

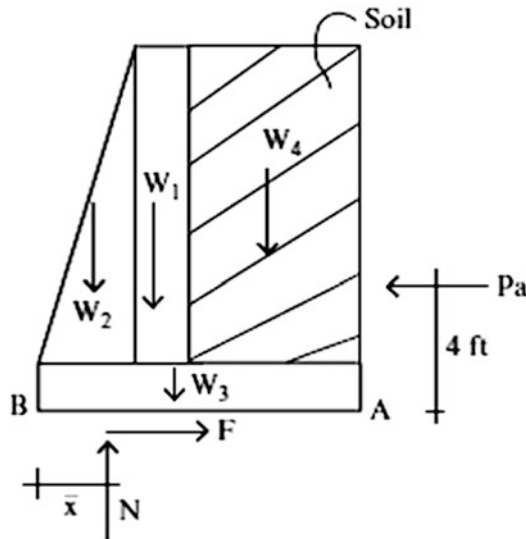


Fig. E8.3d

From Example 8.1:

$$W_1 = 1.5 \text{ kip} \quad W_2 = 2.25 \text{ kip} \quad P_a = 2.88 \text{ kip} \quad M_{B_{\text{overturning}}} = 11.52 \text{ kip ft}$$

The weight of the footing is

$$W_3 = (0.150)(7)(2)(1 \text{ ft}) = 2.1 \text{ kip}$$

The weight of soil is $W_4 = (0.120)(10)(3)(1 \text{ ft}) = 3.6 \text{ kip}$

Then

$$N = \sum W_i = 1.5 + 2.25 + 2.1 + 3.6 = 9.45 \text{ kip}$$

$$W_4 + W_3 + W_2 + W_1$$

$$F_{\text{max}} = \mu N = 0.577(9.45) = 5.45 \text{ kip}$$

$$\text{F.S.}_{\text{sliding}} = \frac{F_{\text{max}}}{P_a} = \frac{5.45}{2.88} = 1.89$$

We sum moments about the toe:

$$\begin{aligned} M_{B_{\text{resisting}}} &= W_1(3.5) + W_2(2) + W_3(3.5) + W_4(5.5) \\ &= 1.5(3.5) + 2.25(2) + 2.1(3.5) + 3.6(5.5) = 36.69 \text{ kip ft} \end{aligned}$$

$$M_{B_{\text{overturning}}} = 11.52 \text{ kip ft}$$

Using these moments, the factor of safety is

$$F.S._{overturning} = \frac{M_{B_{resisting}}}{M_{B_{overturning}}} = \frac{36.9}{11.52} = 3.2$$

Next, we determine the line of action of the resultant

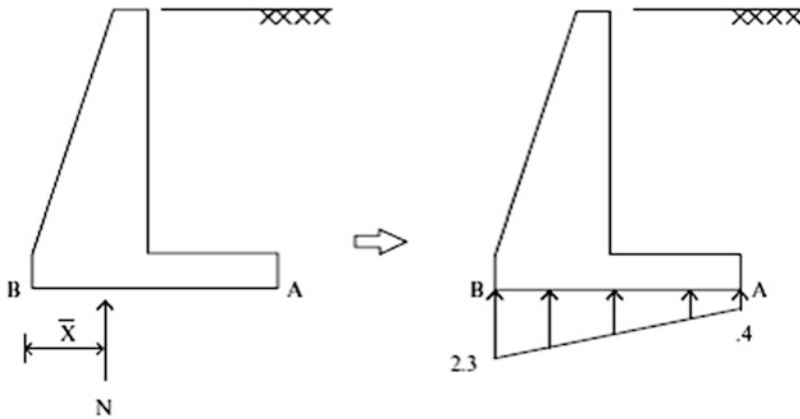
$$M_{net} = M_{B_{overturning}} - M_{B_{resisting}} = 25.38 \text{ kip ft}$$

$$\bar{x} = \frac{M_{net}}{N} = \frac{25.38}{9.45} = 2.68 \text{ ft}$$

$$e = \frac{L}{2} - \bar{x} = 3.5 - 2.68 = 0.82 \text{ ft} < \frac{L}{6} = 1.167 \text{ ft}$$

Lastly, we compute the pressure loading acting on the base.

$$q = \frac{N}{L} \left(1 \pm \frac{6e}{L} \right) = \frac{9.45}{7} \left(1 \pm \frac{6(0.82)}{7} \right) \Rightarrow q_1 = 2.3 \text{ kip/ft}^2, q_2 = 0.4 \text{ kip/ft}^2$$



Case “B”: For this case, we work with the free body diagram shown in Fig. E8.3e. The dimensions are defined in Fig. E8.3b. $W_3 = (0.150)(6)(2)(1 \text{ ft}) = 1.8 \text{ kip}$. $W_5 = (0.120)(2)(2)(1 \text{ ft}) = 0.48 \text{ kip}$

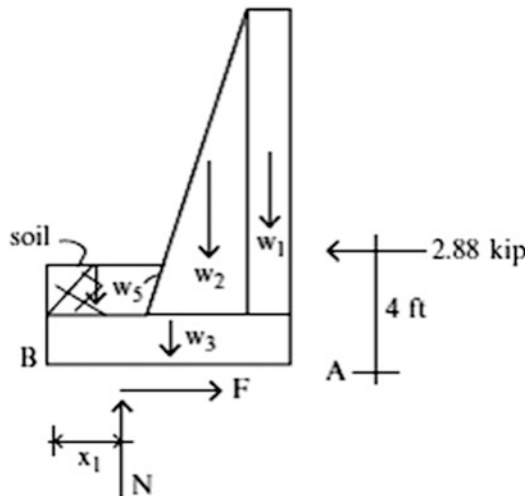


Fig. E8.3e

The calculations proceed as follows:

$$N = W_1 + W_2 + W_3 + W_5 = 1.5 + 2.25 + 1.8 + 0.48 = 6.03 \text{ kip}$$

$$F_{\max} = \mu N = 0.577(6.03) = 3.48 \text{ kip}$$

$$\text{F.S.}_{\text{sliding}} = \frac{F_{\max}}{P_a} = \frac{3.48}{2.88} = 1.2$$

We sum moments about the toe:

$$\begin{aligned} M_{\text{Bresisting}} &= W_1(5.5) + W_2(4) + W_3(3) + W_5(1) \\ &= 1.5(5.5) + 2.25(4) + 1.8(3) + 0.48(1) = 23.13 \text{ kip ft} \end{aligned}$$

$$M_{\text{Boverturning}} = 11.52 \text{ kip ft}$$

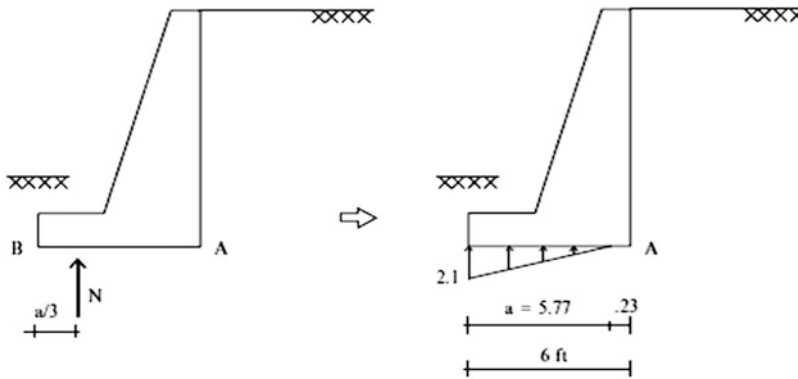
$$\text{F.S.}_{\text{overturning}} = \frac{M_{\text{Bresisting}}}{M_{\text{Boverturning}}} = \frac{23.13}{11.52} = 2.0$$

$$M_{\text{net}} = M_{\text{Boverturning}} - M_{\text{Bresisting}} = 11.61 \text{ kip ft}$$

$$\bar{x} = \frac{M_{\text{net}}}{N} = \frac{11.61}{6.03} = 1.925 \text{ ft}$$

$$e = \frac{L}{2} - \bar{x} = 3 - 1.925 = 1.07 \text{ ft} > \frac{L}{6} = 1.0 \text{ ft} \quad \therefore \bar{x} = \frac{a}{2} \quad a = 5.77 \text{ ft}$$

$$q_1 = \frac{2N}{a} = \frac{2(6.03)}{5.77} = 2.1 \text{ kip/ft}^2$$



Note that the line of action of the normal force is within the base but the pressure is negative at the heel.

Case “C”: We work with the free body diagram shown in Fig. E8.3f. The dimensions are defined in Fig. E8.3c. The revised value of W_3 is $W_3 = (0.15)(9)(2)(1 \text{ ft}) = 2.7 \text{ kip}$

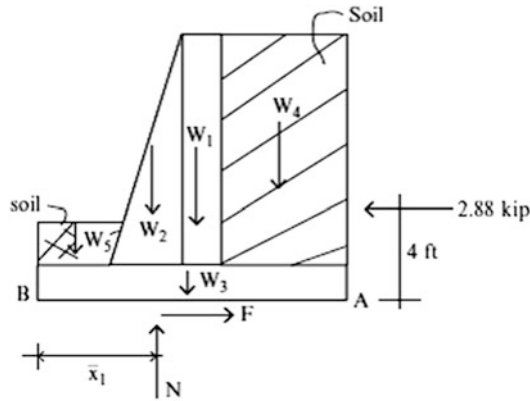


Fig. E8.3f

Then

$$N = W_1 + W_2 + W_3 + W_4 + W_5 = 1.5 + 2.25 + 2.7 + 3.6 + 0.48 = 10.53 \text{ kip}$$

$$F_{\max} = \mu N = 0.577(10.53) = 6.1 \text{ kip}$$

$$\text{F.S.}_{\text{sliding}} = \frac{F_{\max}}{P_a} = \frac{6.1}{2.88} = 2.12$$

We sum moments about the toe:

$$\begin{aligned} M_{\text{Bbalancing}} &= W_1(5.5) + W_2(4) + W_3(4.5) + W_4(7.5) + W_5(1) \\ &= 1.5(5.5) + 2.25(4) + 2.7(4.5) + 3.6(7.5) + 0.48(1) = 56.88 \text{ kip ft} \end{aligned}$$

$$\text{F.S.}_{\text{overturning}} = \frac{M_{\text{Bresisting}}}{M_{\text{Boverturning}}} = \frac{56.88}{11.52} = 4.94$$

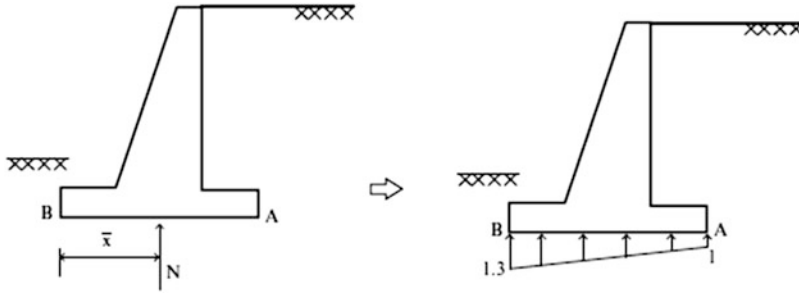
$$M_{\text{net}} = M_{\text{Boverturning}} - M_{\text{Bresisting}} = 45.36 \text{ kip ft}$$

$$\bar{x} = \frac{M_{\text{net}}}{N} = \frac{45.36}{10.53} = 4.3 \text{ ft}$$

$$e = \frac{L}{2} - \bar{x} = 4.5 - 4.3 = 0.2 \text{ ft}$$

$$|e| < L/6 = 1.5 \text{ ft}$$

$$\therefore q = \frac{N}{L} \left(1 \pm \frac{6e}{L} \right) = \frac{10.53}{9} \left(1 \pm \frac{6(0.2)}{9} \right) \Rightarrow q_1 = 1.3 \text{ kip/ft}^2, q_2 = 1.0 \text{ kip/ft}^2$$



We point out that case C has the lowest peak pressure. The analysis results are summarized in the table below.

	Case A	Case B	Case C
N	9.45 kip	6.03 kip	10.53 kip
Friction	5.45 kip	3.48 kip	6.1 kip
F.S.sliding	1.89	1.2	2.12
$M_{balancing}$	36.9 kip ft	23.13 kip ft	56.88 kip ft
$M_{overturning}$	11.52 kip ft	11.52 kip ft	11.52 kip ft
F.S.overturning	3.2	2.0	4.94
\bar{x}	2.68 ft	1.925 ft	4.3 ft
e	0.82 ft < $L/6$	1.07 ft > $L/6$	0.2 ft < $L/6$
q_1	2.3 kip/ft	2.1 kip/ft	1.3 kip/ft ²
q_2	0.4 kip/ft	–	1.0 kip/ft ²

Example 8.4 Cantilever retaining wall

Given: The retaining wall and soil backfill shown in Fig. E8.4a

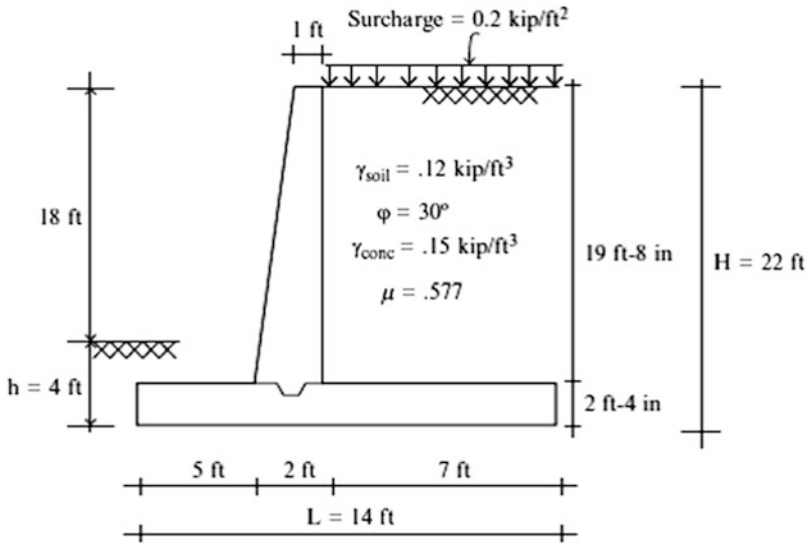


Fig E8.4a

$$N = W_1 + W_2 + W_3 + W_4 + W_5 = 26.84 \text{ kip}$$

$$F_{\max} = \mu N = 0.577(26.84) = 15.5 \text{ kip}$$

$$\sum F_{\text{horizontal}} = P_a + P_s - P_p = 9.68 + 1.47 - 2.88 = 8.27 \text{ kip} \leftarrow$$

Next, we compute the factors of safety.

$$F.S._{\text{sliding}} = \frac{F_{\max}}{\sum F_{\text{horizontal}}} = \frac{15.5}{8.27} = 1.87$$

$$M_{B_{\text{overturning}}} = P_a \left(\frac{H}{3} \right) + P_s \left(\frac{H}{2} \right) = 9.68 \left(\frac{22}{3} \right) + 1.47 \left(\frac{22}{2} \right) = 87.2 \text{ kip ft}$$

$$\begin{aligned} M_{B_{\text{resisting}}} &= W_1(6.5) + W_2(5.67) + W_3(7) + W_4(10.5) + W_5(2.5) + P_p(1.33) \\ &= 2.95(6.5) + 1.47(5.67) + 4.91(7) + 16.5(10.5) \\ &\quad + 1.0(2.5) + 2.88(1.33) \\ &= 241.5 \text{ kip ft} \end{aligned}$$

$$F.S._{\text{ovreturning}} = \frac{M_{B_{\text{resisting}}}}{M_{B_{\text{overturning}}}} = \frac{241.5}{87.2} = 2.77$$

Lastly, we determine the location of the line of action of N .

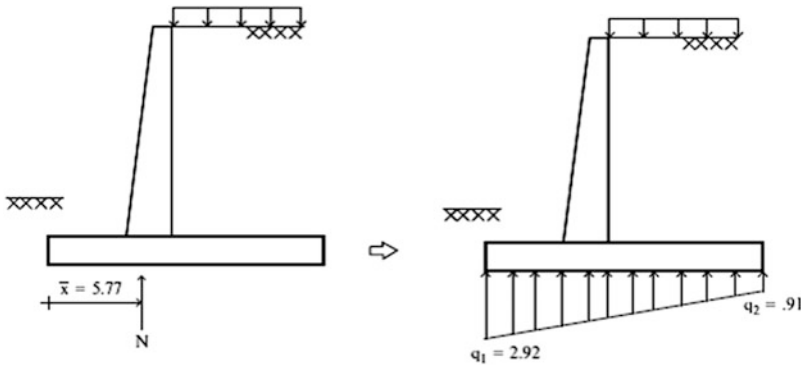
$$M_{\text{net}} = M_{B_{\text{overturning}}} - M_{B_{\text{resisting}}} = 154.8 \text{ kip ft}$$

$$\bar{x} = \frac{M_{\text{net}}}{N} = \frac{154.8}{26.84} = 5.77 \text{ ft}$$

$$e = \frac{L}{2} - \bar{x} = \frac{14}{2} - 5.77 = 1.23 \text{ ft} < \frac{L}{6} = 2.33 \text{ ft}$$

Using the above values, the peak pressures are

$$q = \frac{N}{L} \left(1 \pm \frac{6e}{L} \right) = \frac{26.84}{14} \left(1 \pm \frac{6(1.23)}{14} \right) \Rightarrow q_1 = 2.92 \text{ kip/ft}^2 \quad q_2 = 0.91 \text{ kip/ft}^2$$



Example 8.5 Retaining Wall Supported by Concrete Piles

Given: The structure shown in Fig. E8.5a. Assume all the loads acting on the wall are resisted by the axial loads in the concrete piles. Consider the pile spaced at 6 ft on center. Use Rankine theory.

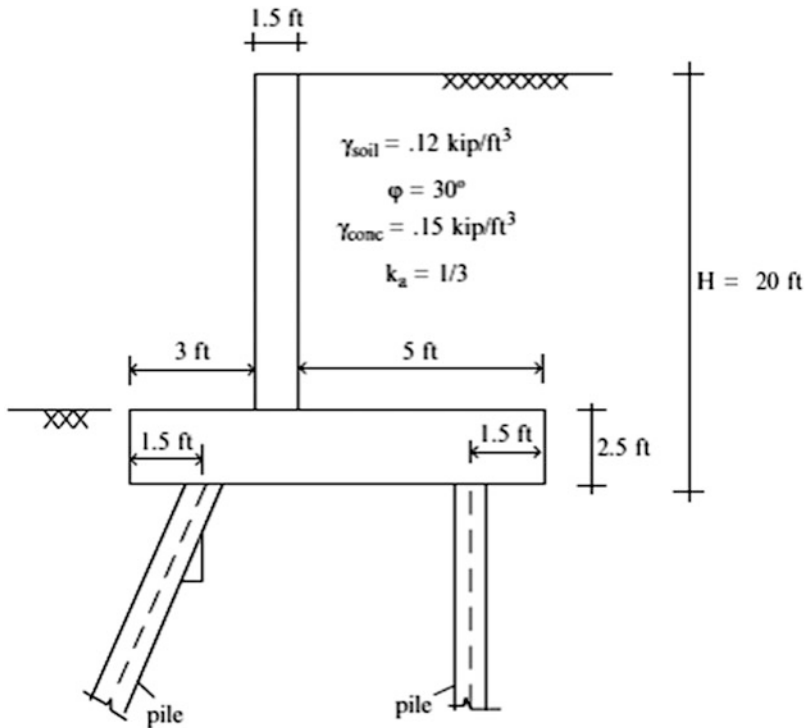


Fig. E8.5a

Determine: The axial loads in the piles.

Solution: We consider a 6 ft segment of the wall. The free body diagram for this segment is shown in Fig. E8.5b. F_1 and F_2 denote the pile forces; P_a is the active lateral soil force; and the W term relates to various weights. We neglect the passive soil force and assume the horizontal load is carried by the inclined pile.

$$P_a = \frac{1}{2} \left(\frac{1}{3} \right) (0.12)(20)^2(6) = 48 \text{ kip}$$

$$W_1 = (5)(17.5)(6)(0.12) = 63 \text{ kip}$$

$$W_2 = (1.5)(17.5)(6)(0.15) = 23.6 \text{ kip}$$

$$W_3 = (2.5)(9.5)(6)(0.15) = 21.4$$

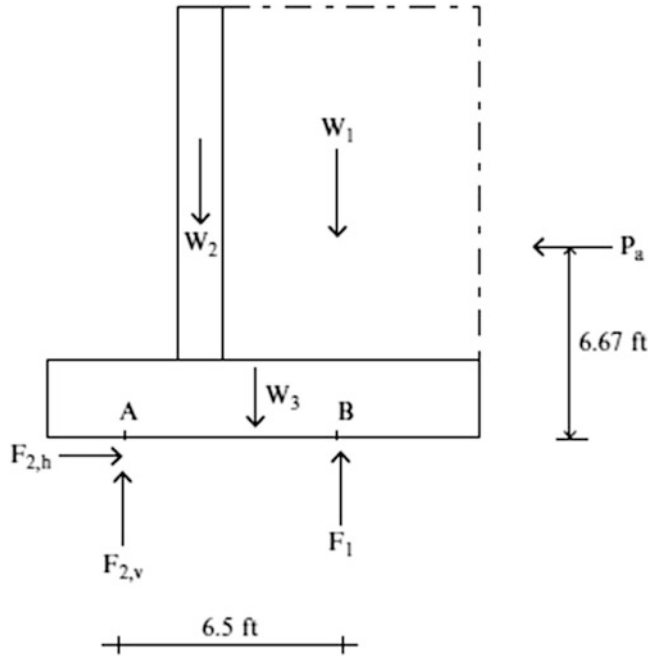


Fig. E8.5b

By summing the moments about A, we determine F_1 :

$$\sum M_A = 0 \quad (2.25)W_2 + (5.5)W_1 = 6.67P_a + 6.5F_1 \Rightarrow F_1 = 22.92 \text{ kips}$$

Summing the vertical forces leads to

$$\sum F_y = 0 \Rightarrow F_{2,v} = 85.1 \text{ kip}$$

Similarly, the horizontal loads yields

$$\sum F_x = 0 \Rightarrow F_{2,h} = P_a = 48 \text{ kip}$$

Then, the axial force in the battered pile is

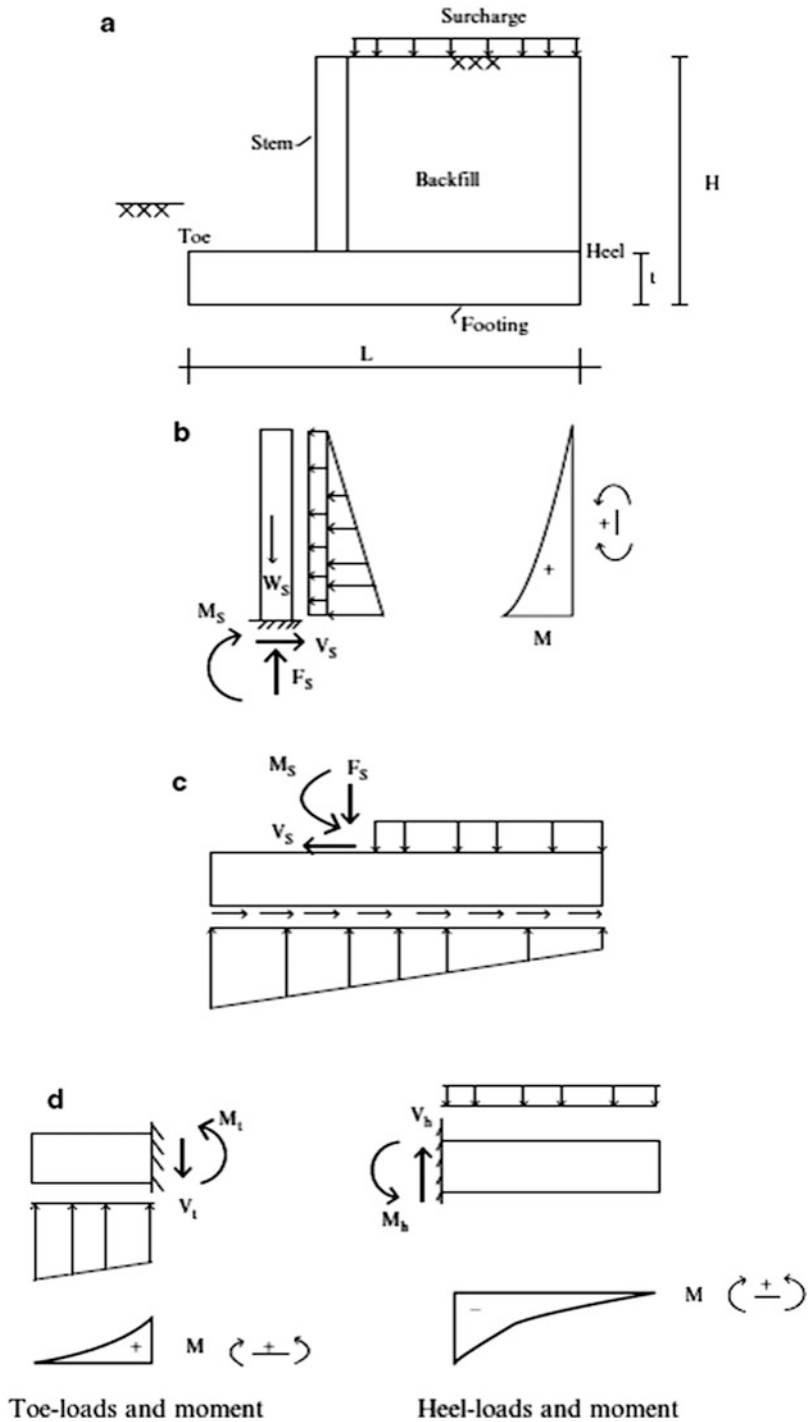
$$F_2 = \sqrt{F_h^2 + F_v^2} = 97.7$$

And the required batter is $48/85.1 = 0.56$

8.5 Critical Sections for Design of Cantilever Walls

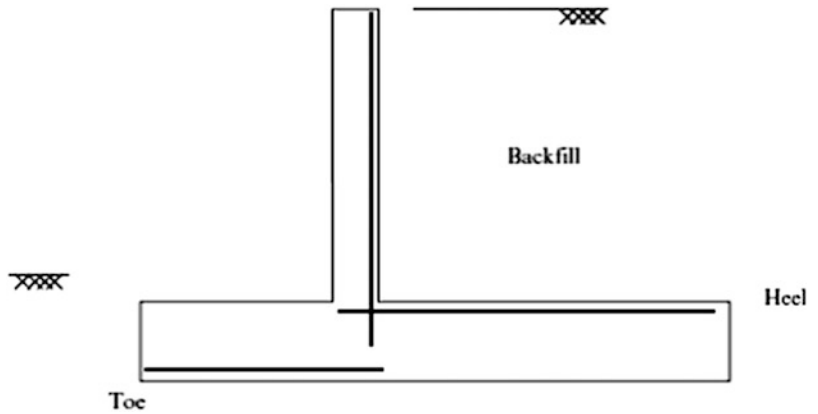
The different segments of a typical cantilever retaining wall structure are shown in Fig. 8.15. The stem functions as a cantilever beam supported by the footing. Gravity and lateral loading are transmitted by the stem onto the footing which then distributes the loading onto the soil. The footing has two counteracting loadings at the heel; the loading due to the weight of the soil, and the pressure loading. The latter is usually neglected when estimating the peak negative moment in the footing. The

Fig. 8.15 Loadings and response pattern for cantilever retaining wall structure. (a) Cantilever retaining wall components. (b) Stem—loads and bending moment. (c) Footing—loads. (d) Components of footing



bending moment distributions are also plotted in Fig. 8.15d. Note that for this type of structure, the bending moment distribution in the footing has both positive and negative regions. *The critical region for design is the stem-footing junction.*

Fig. 8.16 Typical bending steel reinforcement patterns



Retaining wall structures are constructed using reinforced concrete. The thickness of the footing sections is governed by the shear capacity. The location and magnitude of the bending steel reinforcement is dictated by the sense of the bending moment distribution (i.e., positive or negative). Noting that the function of the reinforcement is to provide the tensile force required by the moment, the moment diagrams shown in Fig. 8.15d require the reinforcement patterns defined in Fig. 8.16. The actual size/number of the rebars depends on the magnitude of the moment and the particular design code used to dimension the member.

Example 8.6

Given: The structure shown in Fig. E8.6a.

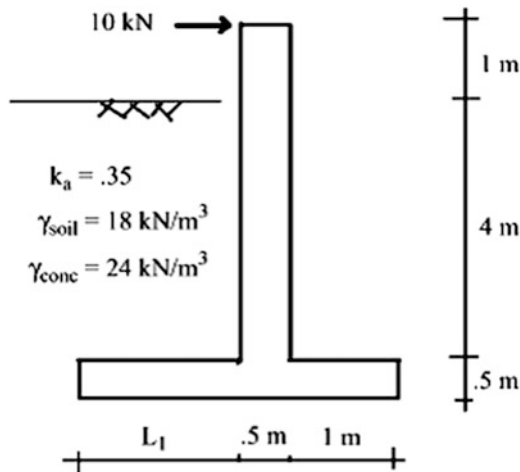
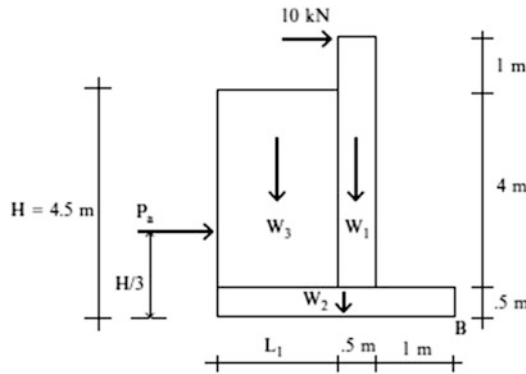


Fig. E8.6a

Determine:

- (a) The required L_1 such that the factor of safety with respect to overturning is equal to 2.
- (b) The tension areas in the stem, toe, and heel and show the reinforcing pattern.

Solution:



$$P_a = \frac{1}{2} k_a \gamma_s H^2 = \frac{1}{2} (0.35)(18)(4.5)^2 = 63.8 \text{ kN}$$

$$W_1 = (0.5)(5)(24) = 60 \text{ kN}$$

$$W_2 = (0.5)(1.5 + L_1)(24)$$

$$W_3 = (4)(L_1)(18)$$

$$M_{B_{\text{overturning}}} = 63.8 \left(\frac{4.5}{3} \right) + 10(5.5) = 150.7$$

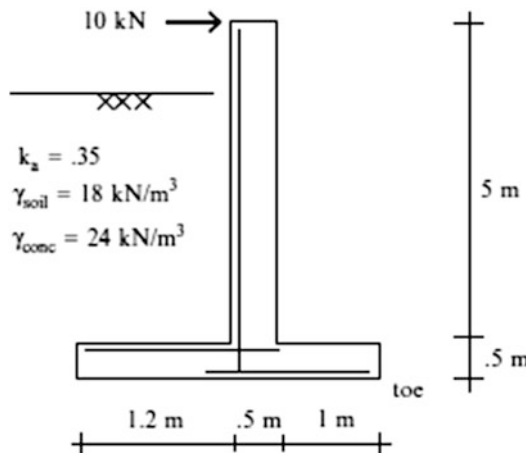
$$M_{B_{\text{resisting}}} = W_1(1.25) + W_2 \left(\frac{L_1 + 1.5}{2} \right) + W_3 \left(\frac{L_1}{2} + 1.5 \right)$$

$$\text{F.S.}_{\text{overturning}} = 2 = \frac{M_{B_{\text{resisting}}}}{M_{B_{\text{overturning}}}} = \frac{W_1(1.25) + W_2 \left(\frac{L_1 + 1.5}{2} \right) + W_3 \left(\frac{L_1}{2} + 1.5 \right)}{150.7}$$

$$\downarrow$$

$$L_1 \text{ required} = 1.2 \text{ m}$$

The figure below shows the reinforcing pattern required for the tension areas.



8.6 Summary

8.6.1 Objectives of the Chapter

- To introduce the topic of vertical retaining wall structures used for embankments, abutments, and underground structures.
- To present a theory for establishing the lateral loading exerted by soil backfill on vertical walls.
- To develop a methodology for evaluating the stability of cantilever retaining walls when subjected to lateral loading due to backfill and surcharges.

8.6.2 Key Concepts and Facts

- The Rankine theory predicts a linear distribution of soil pressure which acts normal to a vertical face and increases with depth. The resultant force is given by

$$P_a = \frac{1}{2} \gamma H^2 k_a$$

where H is the vertical wall height, γ is the soil density, and k_a is a dimensionless coefficient that depends on the soil type and nature of the relative motion between the wall and the backfill. For active conditions,

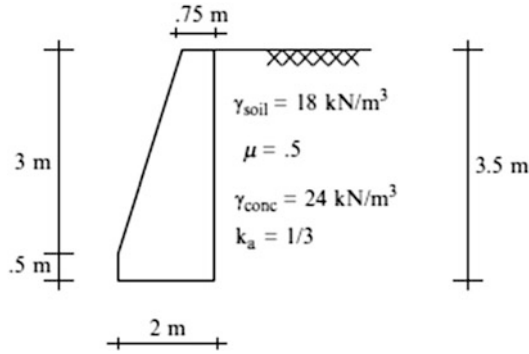
$$k_a = \frac{1 - \sin \varphi}{1 + \sin \varphi}$$

where φ is the soil friction angle, typically $\approx 30^\circ$.

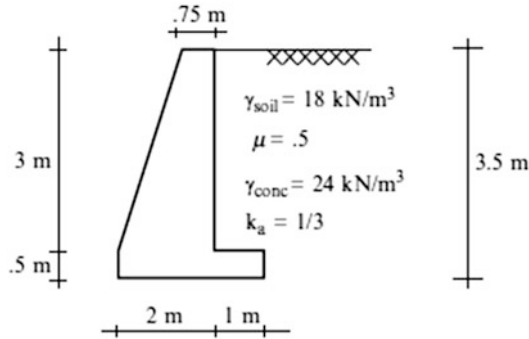
- Stability is addressed from two perspectives: Sliding and overturning. The factor of safety with respect to sliding is defined as the ratio of the peak available horizontal friction force to the actual friction force. The factor of safety with respect to overturning about the toe is taken as the ratio of the restoring moment to the unbalancing moment.
- One selects the dimensions of the footing, such that these factors of safety are greater than one and the resultant force due to the structural weight and the soil loads acts within the middle third of the footing width.

8.7 Problems

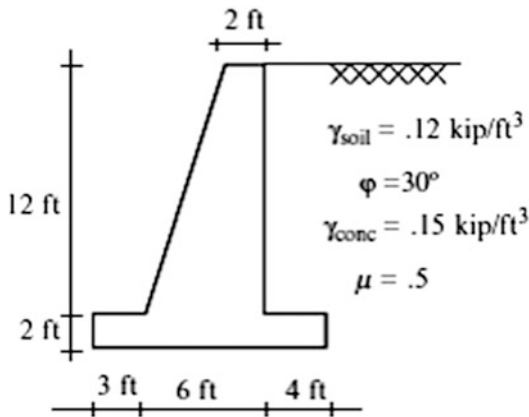
Problem 8.1 For the concrete retaining wall shown, determine the factors of safety against sliding and overturning and the base pressure distribution. Use the Rankine theory for soil pressure computations.



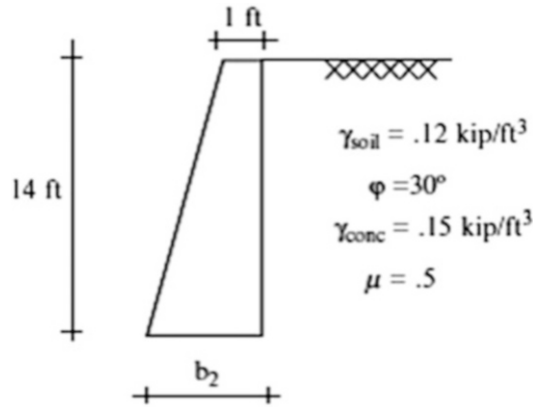
Problem 8.2 For the concrete retaining wall shown, determine the factors of safety against sliding and overturning and the base pressure distribution. Use the Rankine theory for soil pressure computations.



Problem 8.3 For the concrete retaining wall shown, determine the factors of safety against sliding and overturning and the base pressure distribution. Use the Rankine theory for soil pressure computations.



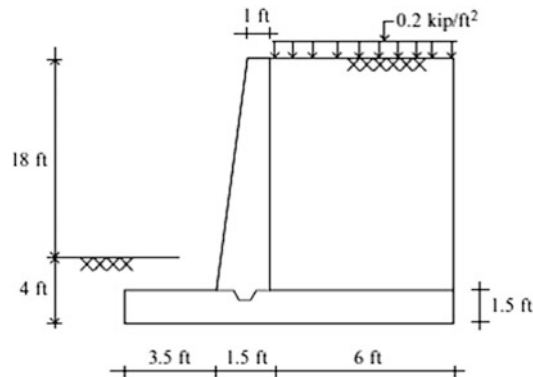
Problem 8.4 For the concrete retaining wall shown, determine the required value for b_2 . Take the factors of safety for overturning and sliding to be equal to 1.75 and 1.25, respectively. Use the Rankine theory for soil pressure computations.



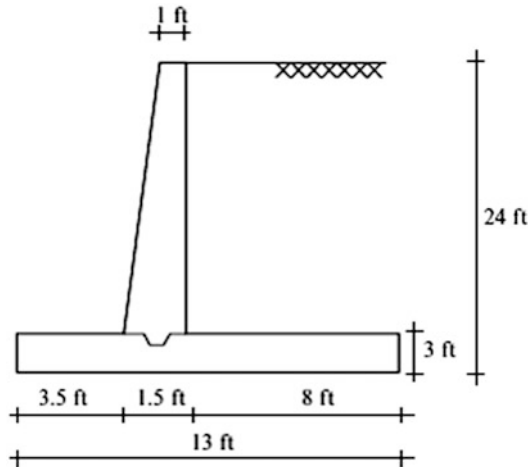
Problem 8.5 For the retaining wall shown, determine

- The soil pressure acting on the wall
- The factor of safety for overturning
- The factor of safety for sliding
- The soil pressure distribution under the footing

Assume: $\mu = 0.5$, $\gamma_{\text{soil}} = 0.12 \text{ kip/ft}^3$, $k_a = 1/3$, $\gamma_{\text{concrete}} = 0.15 \text{ kip/ft}^3$, $\mu = 0.5$, and $\Phi = 30^\circ$.



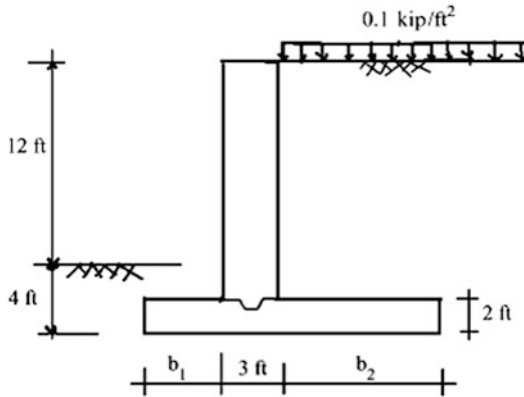
Problem 8.6



- (a) Determine the factors of safety against overturning and sliding.
- (b) Determine the soil pressure distribution under the footing (q_1, q_2).
- (c) Determine the moment distribution in the stem.
- (d) Determine the bending moment distribution in the heel.

Assume: Allowable soil pressure = 5.0 ksf, $\gamma_{\text{soil}} = 0.12 \text{ kip/ft}^3$, $k_a = 1/3$, and $\gamma_{\text{concrete}} = 0.15 \text{ kip/ft}^3$

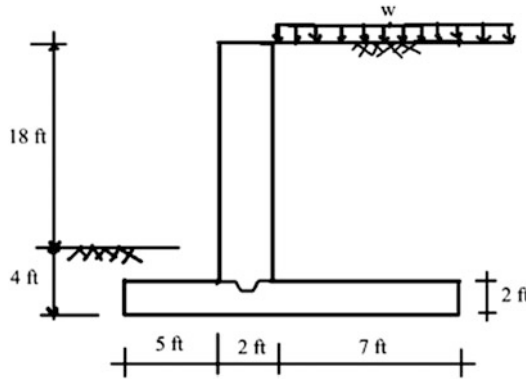
Problem 8.7



Suggest values for b_1 and b_2 . Take the safety factors for sliding and overturning to be equal to 2.

Assume: $\gamma_{\text{soil}} = 0.12 \text{ kip/ft}^3$, $\gamma_{\text{concrete}} = 0.15 \text{ kip/ft}^3$, $\mu = 0.57$, and $\Phi = 30^\circ$.

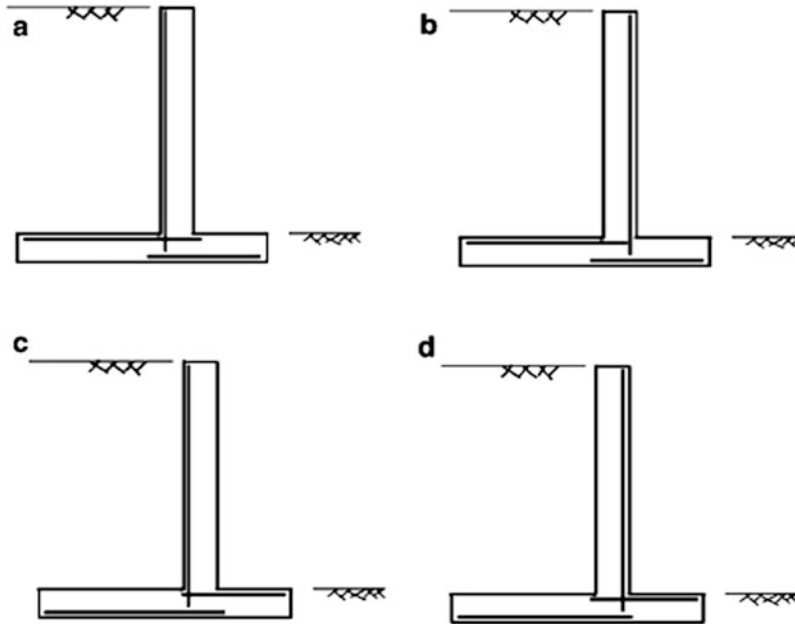
Problem 8.8



Determine the minimum value of w at which soil failure occurs (i.e., the soil pressure exceeds the allowable soil pressure).

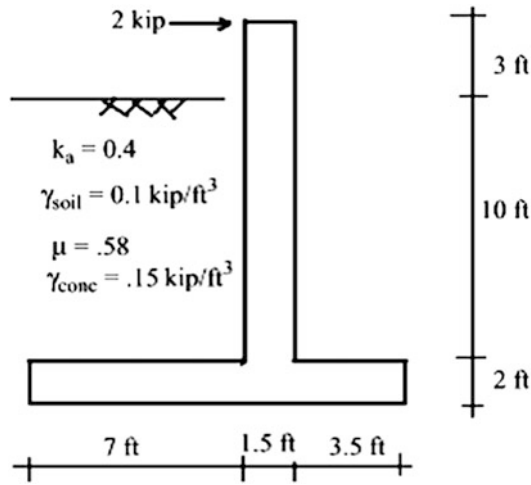
Assume: $q_{\text{allowable}} = 5 \text{ kip/ft}^2$, $\gamma_{\text{soil}} = 0.12 \text{ kip/ft}^3$, $\gamma_{\text{concrete}} = 0.15 \text{ kip/ft}^3$, $\mu = 0.57$, and $\Phi = 30^\circ$.

Problem 8.9 Which of the retaining walls shown below is adequately reinforced for bending?



Problem 8.10

- (a) Determine the factor of safety with respect to overturning and sliding.
- (b) Identify the tension areas in the stem, toe, and heel and show the reinforcing pattern.
- (c) Determine the location of the line of action of the resultant at the base of the footing



References

1. Lambe TW, Whitman RV. Soil mechanics. New York: Wiley; 1969.
2. Terzaghi K, Peck RB. Soil mechanics in engineering practice. New York: Wiley; 1967.
3. Huntington WC. Earth pressures and retaining walls. New York: Wiley; 1957.

Statically Indeterminate Structures

Statically indeterminate structures are over-restrained in the sense that there are more force unknowns than available equilibrium equations. This situation arises when there are more supports than needed to prevent rigid body motion. Multi-span continuous beams and two-hinged frames are examples of this case. Indeterminacy may also result when there is an excess of members, such as a truss with multiple diagonals. Two dominant methods of analysis are used for indeterminate structures.

The traditional approach for analyzing statically indeterminate structures is based on the assumption that the structure behaves in a linear elastic manner, and therefore displacement patterns corresponding to different systems of forces can be superimposed to achieve a desired displacement pattern. One replaces the displacement constraints with unknown forces, determines the deflected shapes for each unit force, and then combines and scales these shapes to obtain a final deflected shape that satisfies the constraints. Since one works with force unknowns, this approach is called the “Force Method.” It is also called the “Flexibility Method.” Engineers find the method appealing since the process of superimposing the different deflected shapes can be easily visualized and the computational details, which are suited for hand computation, provide insight into the deflection behavior.

A second method is based on solving a set of equilibrium equations expressed in terms of certain displacement measures that define the loaded configuration. It views the structure as an assemblage of members and uses a set of member end force–end displacement relations called the slope deflection equations. In general, the number of displacement unknowns is larger than the number of force unknowns, but the method is readily programmed and numerous software packages now exist. We refer to this approach as the “Displacement Method.” It is also called the “Stiffness Method” since the equations involve stiffness coefficients.

In what follows, we discuss both methods. We also describe some approximate hand calculation-based methods that are suitable for rapidly estimating the response due to gravity and lateral loads. Finally, we describe the underlying theory for the Displacement Method and illustrate how to apply the method using computer software.

Abstract

Up to this point, we have focused on the analysis of statically determinate structures because the analysis process is fairly straightforward; only the force equilibrium equations are required to determine the member forces. However, there is another category of structures, called statically indeterminate structures, which are also employed in practice. Indeterminate structures require another set of equations, in addition to the force equilibrium equations, in order to solve for the member forces. There are two general methods for analyzing indeterminate structures, the force (flexibility) method and the displacement (stiffness) method. The force method is more suited to hand computation whereas the displacement method is more procedural and easily automated using a digital computer.

In this chapter, we present the underlying theory of the force method and illustrate its applications to a range of statically indeterminate structures including trusses, multi-span beams, arches, and frames. We revisit the analysis of these structures in the next chapter using the displacement method, and also in Chap. 12, “Finite Element Displacement Method for Framed Structures,” which deals with computer-based analysis.

9.1 Introduction

The force method is a procedure for analyzing statically indeterminate structures that works with force quantities as the primary variables. It is applicable for linear elastic structures. The method is based on superimposing structural displacement profiles to satisfy a set of displacement constraints. *From a historical perspective*, the force method was the “classical” analysis tool prior to the introduction of digital-based methods. The method is qualitative in the sense that one reasons about deflected shapes and visualizes how they can be combined to satisfy the displacement constraints. We find the method very convenient for deriving analytical solutions that allow one to identify key behavior properties and to assess their influence on the structural response. The key step

is establishing the displacement constraints which are referred to as the geometric compatibility equations.

Consider the structure shown in Fig. 9.1. Since there are four displacement restraints, the structure is indeterminate to the first degree, i.e., one of the restraints is not needed for stability, and the corresponding reaction force cannot be determined using only the force equilibrium equations.

The steps involved in applying the force method to this structure are as follows:

1. We select one of the force redundants and remove it. The resulting structure, shown in Fig. 9.2, is called the primary structure. Note that one cannot arbitrarily remove a restraint. One needs to ensure that the resulting structure is stable.
2. We apply the external loading to the primary structure and determine the displacement at C in the direction of the restraint at C. This quantity is designated as $\Delta_{C,0}$. Figure 9.3 illustrates this notation.
3. Next, we apply a unit value of the reaction force at C to the primary structure and determine the corresponding displacement. We designate this quantity as δ_{CC} (see Fig. 9.4).
4. We obtain the total displacement at C of the primary structure by superimposing the displacement profiles generated by the external loading and the reaction force at C.

$$\Delta_C|_{\text{primary structure}} = \Delta_{C,0} + \delta_{CC}R_C \quad (9.1)$$

5. The key step is to require the displacement at C of the primary structure to be equal to the displacement at C of the actual structure.

Fig. 9.1 Actual structure

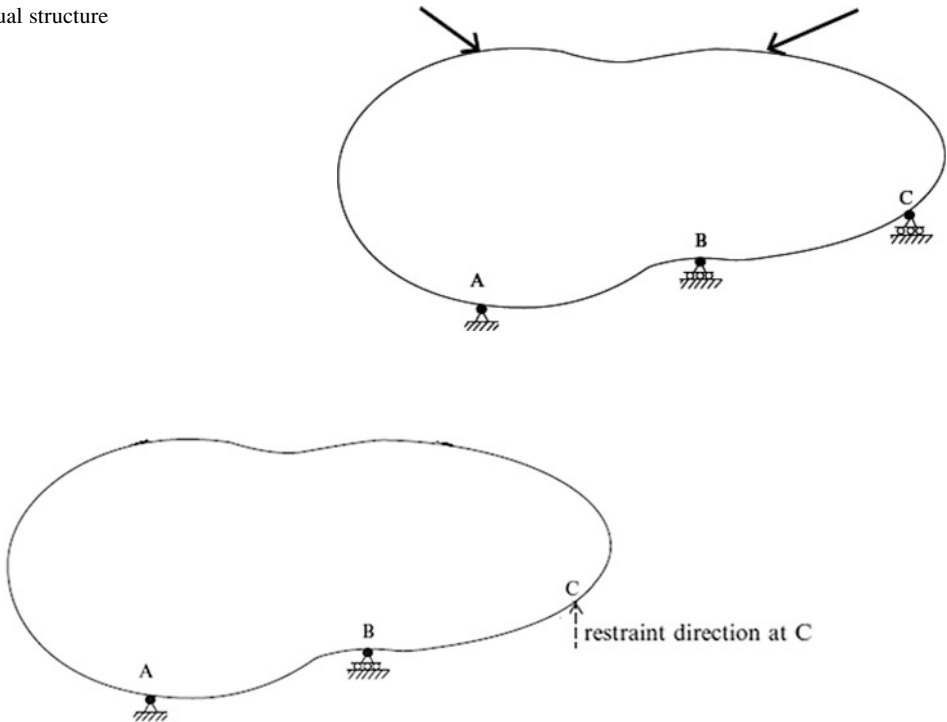


Fig. 9.2 Primary structure

Fig. 9.3 Displacements due to the external loading

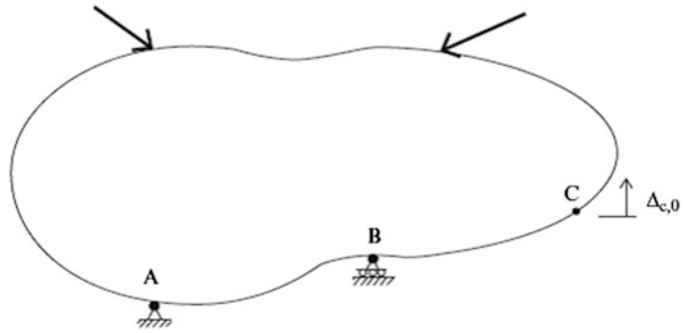
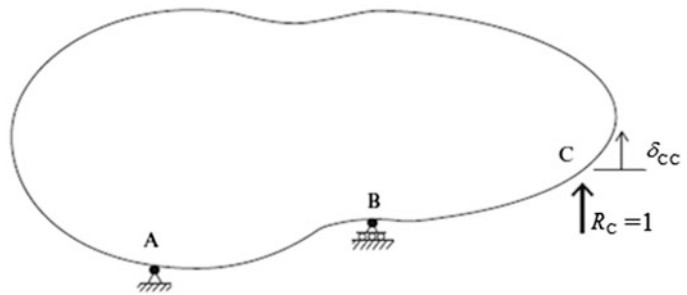


Fig. 9.4 Displacement due to unit value of R_C



$$\Delta_C|_{\text{actual}} = \Delta_C|_{\text{primary}} = \Delta_{C,0} + \delta_{CC}R_C \tag{9.2}$$

Equation (9.2) is referred to as the “geometric compatibility equation.” When this equation is satisfied, the final displacement profiles for the actual and the primary structure will be identical. It follows that the forces in the primary structure and the actual structure will also be identical.

6. We solve the compatibility equation for the reaction force, R_C .

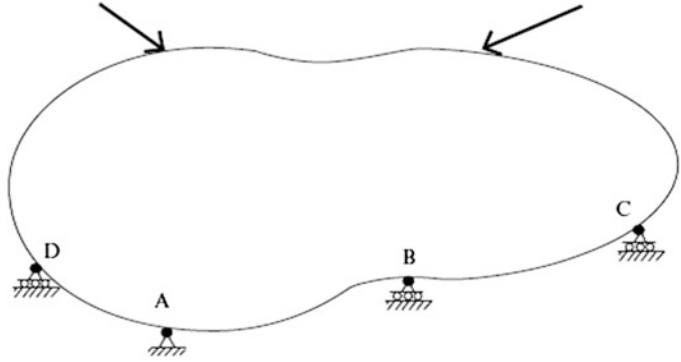
$$R_C = \frac{1}{\delta_{CC}} (\Delta_C|_{\text{actual}} - \Delta_{C,0}) \tag{9.3}$$

Note that $\Delta_C|_{\text{actual}} = 0$ when the support is unyielding. When R_C is negative, the sense assumed in Fig. 9.4 needs to be reversed.

7. The last step involves computing the member forces in the actual structure. We superimpose the member forces computed using the primary structure according to the following algorithm:

$$\text{Force} = \text{Force}|_{\text{external load}} + R_C(\text{Force}|_{R_C=1}) \tag{9.4}$$

Since the primary structure is statically determinate, all the material presented in Chaps. 2, 3, 4, 5, and 6 is applicable. The force method involves scaling and superimposing displacement profiles. The method is particularly appealing for those who have a solid understanding of structural behavior. For simple structures, one can establish the sense of the redundant force through qualitative reasoning.

Fig. 9.5 Actual structure

Essentially, the same approach is followed for structures having more than one degree of indeterminacy. For example, consider the structure shown in Fig. 9.5. There are two excess vertical restraints.

We obtain a primary structure by removing two of the vertical restraints. Note that there are multiple options for choosing the restraints to be removed. The only constraint is that the primary structure must be “stable.” Figure 9.6 shows the different choices.

Suppose we select the restraints at C and D as the redundants. We apply the external loading to the primary structure (Fig. 9.7) and determine the vertical displacements at C and D shown in Fig. 9.8.

The next step involves applying unit forces corresponding to $R_C = 1$ and $R_D = 1$ and computing the corresponding displacements at C and D. Two separate displacement analysis are required since there are two redundant reactions (Fig. 9.9).

Combining the three displacement profiles leads to the total displacement of the primary structure.

$$\begin{aligned}\Delta_C|_{\text{primary structure}} &= \Delta_{C,0} + \delta_{CC}R_C + \delta_{CD}R_D \\ \Delta_D|_{\text{primary structure}} &= \Delta_{D,0} + \delta_{DC}R_C + \delta_{DD}R_D\end{aligned}\quad (9.5)$$

The coefficients of R_C and R_D are called flexibility coefficients. It is convenient to shift over to matrix notation at this point. We define

$$\begin{aligned}\underline{\Delta}_0 &= \begin{Bmatrix} \Delta_{C,0} \\ \Delta_{D,0} \end{Bmatrix} \quad \underline{\mathbf{X}} = \begin{Bmatrix} R_C \\ R_D \end{Bmatrix} \\ \text{flexibility matrix} &= \underline{\boldsymbol{\delta}} = \begin{bmatrix} \delta_{CC} & \delta_{CD} \\ \delta_{DC} & \delta_{DD} \end{bmatrix}\end{aligned}\quad (9.6)$$

Using this notation; the geometric compatibility equation takes the form

$$\underline{\Delta}|_{\text{actual structure}} = \underline{\Delta}_0 + \underline{\boldsymbol{\delta}}\underline{\mathbf{X}}\quad (9.7)$$

Note that $\underline{\Delta}|_{\text{actual structure}} = \underline{0}$ when the supports are unyielding. Given the choice of primary structure, the flexibility coefficients are properties of the primary structure whereas $\underline{\Delta}_0$ depends on the both the external loading and the primary structure. We solve (9.7) for $\underline{\mathbf{X}}$,

Fig. 9.6 Choices for primary structure. (a) Option 1. (b) Option 2. (c) Option 3

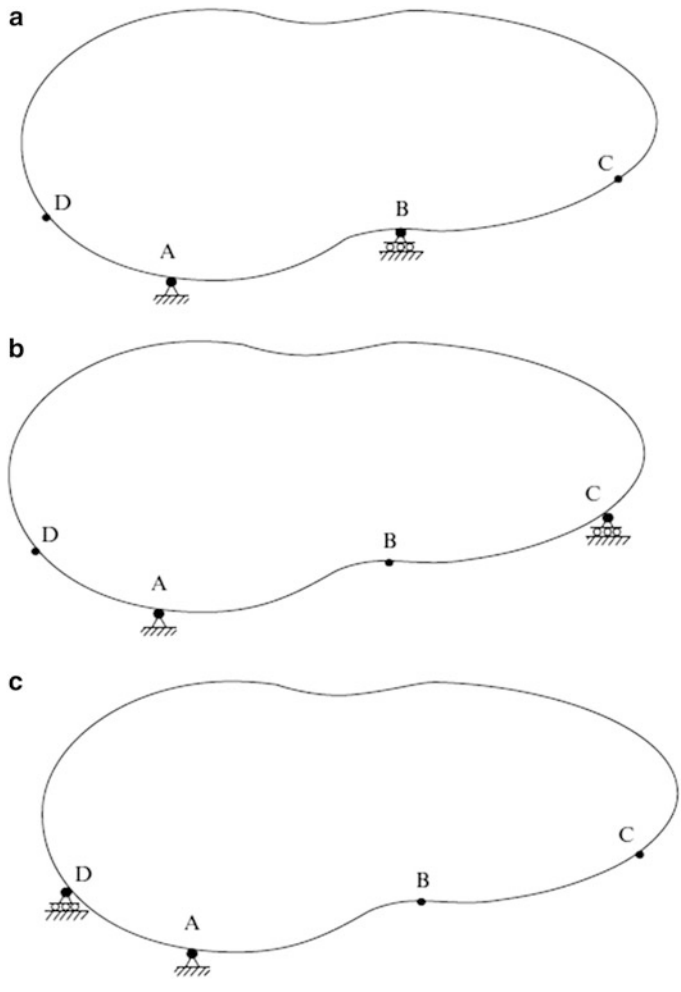


Fig. 9.7 Primary structure

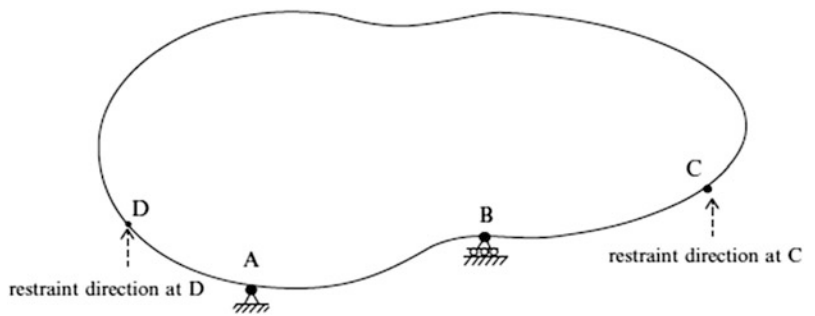


Fig. 9.8 Displacements due to external loading

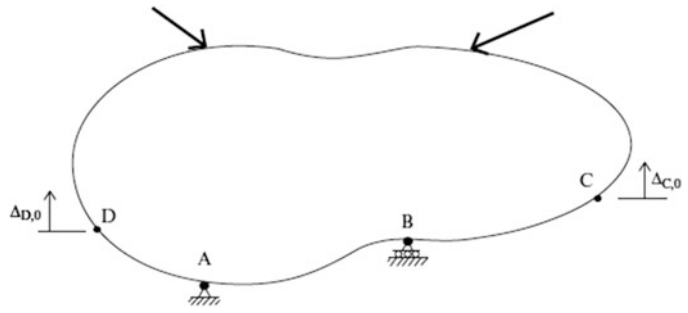
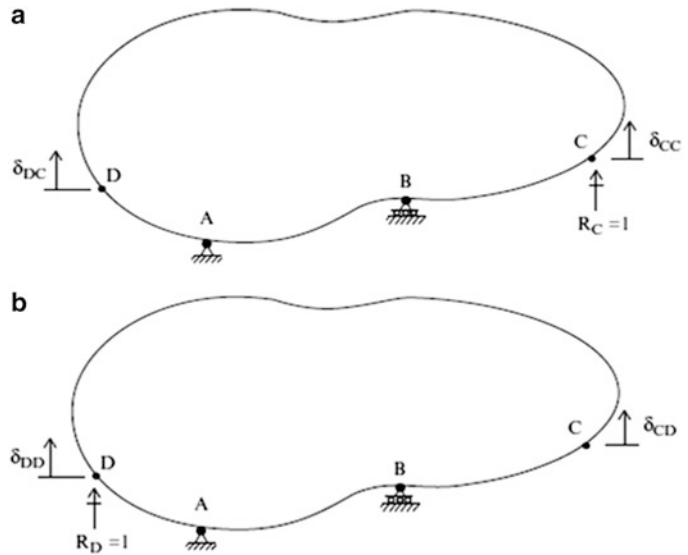


Fig. 9.9 Displacement due to unit values of the redundant. (a) $R_C = 1$. (b) $R_D = 1$



$$\underline{\mathbf{X}} = \underline{\delta}^{-1}(\underline{\Delta}|_{\text{actual structure}} - \underline{\Delta}_0) \tag{9.8}$$

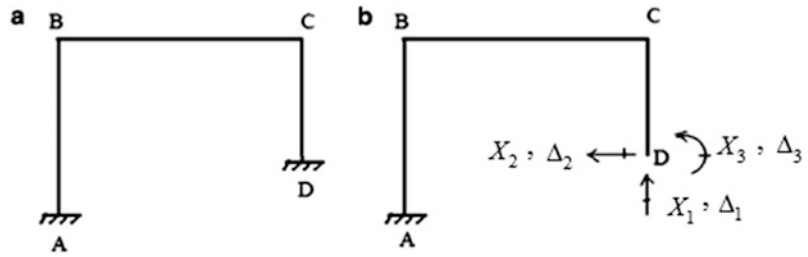
and then determine the member forces by superimposing the individual force states as follows:

$$\underline{\mathbf{F}} = \underline{\mathbf{F}}|_{\text{external load}} + (\underline{\mathbf{F}}|_{R_C=1})R_C + (\underline{\mathbf{F}}|_{R_D=1})R_D \tag{9.9}$$

The extension of this approach to an n th degree statically indeterminate structure just involves more computation since the individual matrices are now of order n . Since there are more redundant force quantities, we need to introduce a more systematic notation for the force and displacement quantities.

Consider the frame structure shown in Fig. 9.10a. It is indeterminate to the third degree. One choice of primary structure is shown in Fig. 9.10b. We remove the support at D, take the reactions as the force redundants, and denote the j th redundant force as X_j and the corresponding measure as Δ_j .

Fig. 9.10 (a) Actual structure. (b) Primary structure—redundant reactions



The resulting displacements of the primary structure due to the external loading and the three force redundants are expressed as

$$\begin{aligned}
 \Delta_1|_{\text{primary structure}} &= \Delta_{1,0} + \delta_{11}X_1 + \delta_{12}X_2 + \delta_{13}X_3 \\
 \Delta_2|_{\text{primary structure}} &= \Delta_{2,0} + \delta_{21}X_1 + \delta_{22}X_2 + \delta_{23}X_3 \\
 \Delta_3|_{\text{primary structure}} &= \Delta_{3,0} + \delta_{31}X_1 + \delta_{32}X_2 + \delta_{33}X_3
 \end{aligned}
 \tag{9.10}$$

The matrix form of (9.10) is

$$\underline{\Delta}|_{\text{primary structure}} = \underline{\Delta}_0 + \underline{\delta}\underline{X}
 \tag{9.11}$$

where

$$\underline{\delta} = \begin{bmatrix} \delta_{11} & \delta_{12} & \delta_{13} \\ \delta_{21} & \delta_{22} & \delta_{23} \\ \delta_{31} & \delta_{32} & \delta_{33} \end{bmatrix} \quad \underline{\Delta}_0 = \begin{Bmatrix} \Delta_{1,0} \\ \Delta_{2,0} \\ \Delta_{3,0} \end{Bmatrix} \quad \underline{X} = \begin{Bmatrix} X_1 \\ X_2 \\ X_3 \end{Bmatrix}$$

Note that the displacement measures may be either a translation or a rotation. A major portion of the computational effort is involved with computing the flexibility coefficients using the Principle of Virtual Forces. The matrix form of the geometric compatibility equation (9.7) is generic, i.e., it is applicable for all structures. One just has to establish the appropriate form for $\underline{\Delta}_0$ and $\underline{\delta}$.

Other possible choices of primary structures are shown in Fig. 9.11. We can retain the two fixed supports, but cut the structure at an arbitrary interior point (Fig. 9.11a). The redundants are taken as the internal forces (axial, shear, and moment) at the point. The flexibility coefficients are now interpreted as the relative displacements of the adjacent cross sections (e.g., spreading, sliding, relative rotation). Another choice involves removing excess reactions as in Fig. 9.11b.

For multi-bay multistory frames, one needs to work with internal force redundants since removing fixed supports is not sufficient to reduce the structure to a statically determinate structure. Figure 9.12 illustrates this case.

Multi-span beam-type structures are handled in a similar way when choosing a primary structure. Consider Fig. 9.13. One can either select certain excess reactions or work with bending moments at interior points. We prefer the latter choice since the computation of the corresponding flexibility coefficients is simpler due to the fact that the deflection profiles associated with the redundant moments are confined to adjacent spans.

For truss-type structures, various cases arise. The truss may have more supports than needed, such as shown in Fig. 9.14a. One choice would be to remove sufficient supports such that the resulting structure is statically determinate (Fig. 9.14b).

We can also keep the original restraints, and remove some members, as indicated in Fig. 9.14c.

Another example is shown in Fig. 9.15a. The truss has too many members and therefore the only option is to remove some of the diagonals. Figure 9.15b illustrates one choice of redundants.

Fig. 9.11 (a) Primary structure—redundant internal forces. (b) Primary structure—redundant reactions

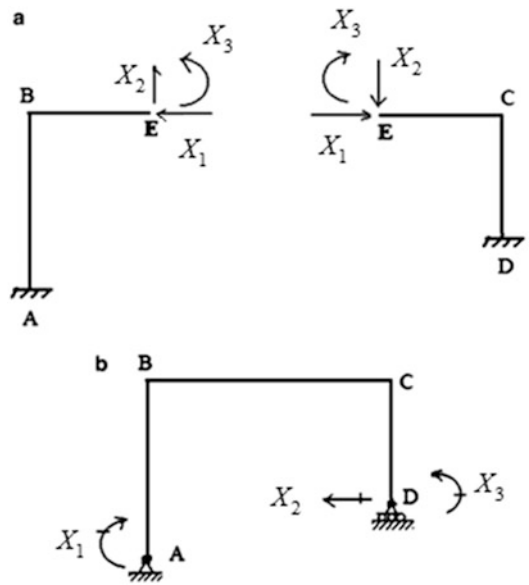


Fig. 9.12 (a) Actual structure. (b) Primary structure

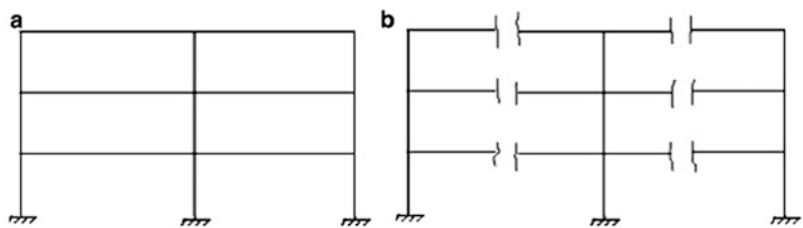


Fig. 9.13 Multi-span beam. (a) Actual structure. (b) Primary structure—redundant reactions. (c) Primary structure—redundant moments

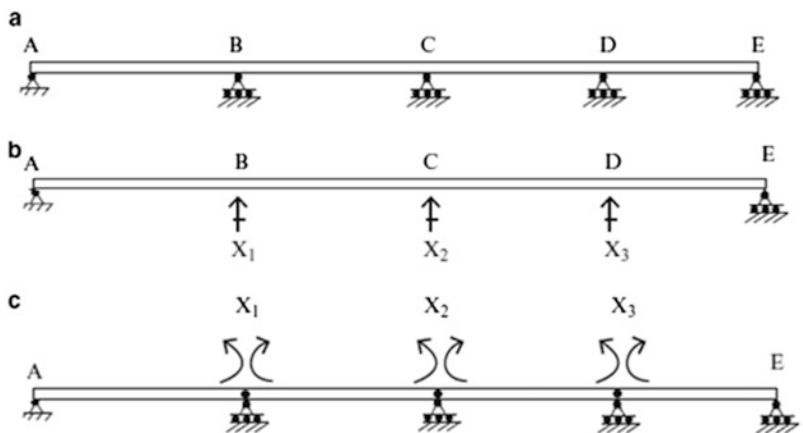


Fig. 9.14 (a) Actual structure. (b) Primary structure—redundant reactions. (c) Primary structure—redundant internal forces

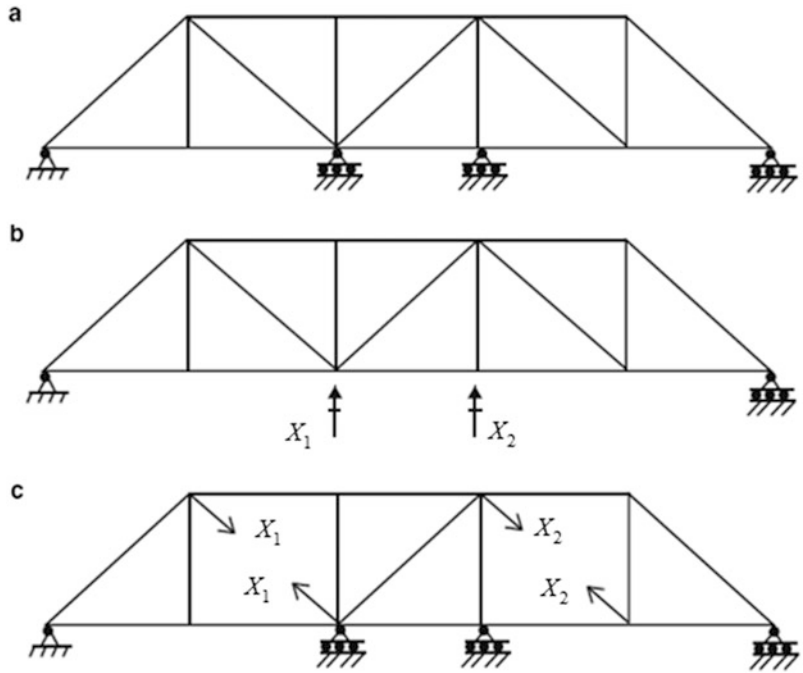
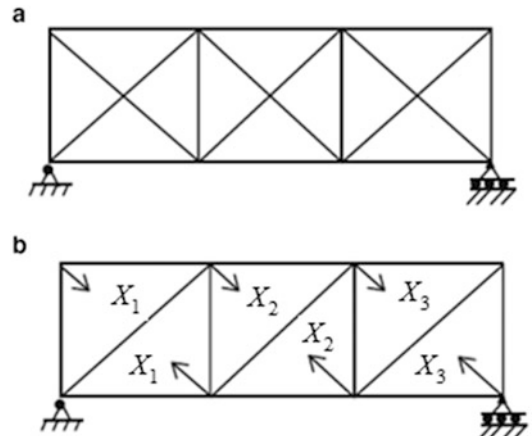


Fig. 9.15 (a) Actual structure. (b) Primary structure—redundant internal forces

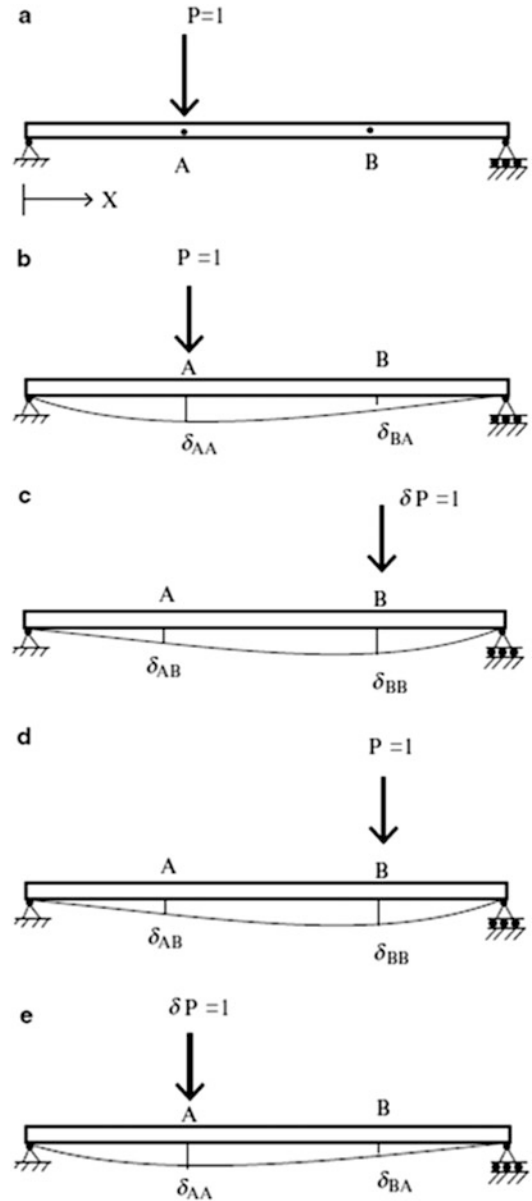


9.2 Maxwell's Law of Reciprocal Displacements

The geometric compatibility equations involve the flexibility matrix, $\underline{\delta}$. One computes the elements of $\underline{\delta}$ using one of the methods described in Part I, such as the Principal of Virtual Forces. Assuming there are n force redundants, $\underline{\delta}$ has n^2 elements. For large n , this computation task becomes too difficult to deal with manually. However, there is a very useful relationship between the elements of $\underline{\delta}$, called "Maxwell's Law," which reduces the computational effort by approximately 50%. In what follows, we introduce Maxwell's Law specialized for member systems.

We consider first a simply supported beam on unyielding supports subjected to a single concentrated unit force. Figure 9.16a defines the geometry and notation. The deflected shape due to

Fig. 9.16 Reciprocal loading conditions. (a) Actual structure. (b) Actual loading (M_A). (c) Virtual loading (δM_B). (d) Actual loading (M_B). (e) Virtual loading (δM_A)



the unit force applied at A is plotted in Fig. 9.16b. Suppose we want to determine the deflection at B due to this load applied at A. We define this quantity as δ_{BA} . Using the Principle of Virtual Forces specialized for beam bending; we apply a unit virtual force at B (see Fig. 9.16c) and evaluate the following integral:

$$\delta_{BA} = \int M_A \delta M_B \frac{dx}{EI} \quad (9.12)$$

where M_A is the moment due to the unit load applied at A, and δM_B is the moment due to the virtual unit load applied at B.

Now, suppose we want the deflection at A due to a unit load at B. The corresponding virtual force expression is

$$\delta_{AB} = \int M_B \delta M_A \frac{dx}{EI} \tag{9.13}$$

where δM_A is the virtual moment due to a unit force applied at A and M_B is the moment due to the load at B. Since we are applying unit loads, it follows that

$$\begin{aligned} M_A &= \delta M_A \\ M_B &= \delta M_B \end{aligned} \tag{9.14}$$

and we find that the expressions for δ_{AB} and δ_{BA} are identical.

$$\delta_{AB} \equiv \delta_{BA} \tag{9.15}$$

This identity is called *Maxwell’s Law*. It is applicable for linear elastic structures [1]. Returning back to the compatibility equations, defined by (9.7), we note that the coupling terms, δ_{ij} and δ_{ji} , are equal. We say the coefficients are symmetrical with respect to their subscripts and it follows that δ is symmetrical. Maxwell’s Law leads to another result called Müller–Breslau Principle which is used to establish influence lines for indeterminate beams and frames. This topic is discussed in Chaps. 13 and 15.

9.3 Application of the Force Method to Beam-Type Structures

We apply the theory presented in the previous section to a set of beam-type structures. For completeness, we also include a discussion of some approximate techniques for analyzing partially restrained single-span beams that are also useful for analyzing frames.

Example 9.1

Given: The beam defined in Fig. E9.1a. Assume $I = 120(10)^6 \text{ mm}^4$, $L = 6 \text{ m}$, $w = 30 \text{ kN/m}$, $v_B = 40 \text{ mm}$, and $E = 200 \text{ GPa}$

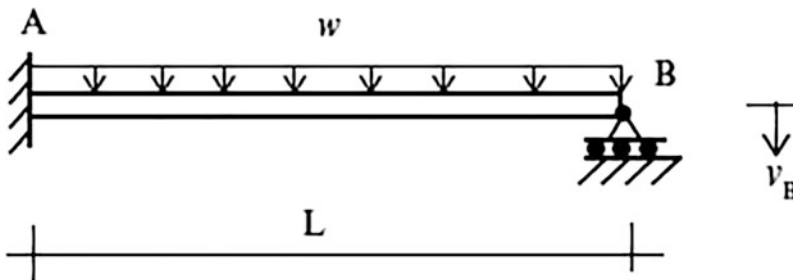


Fig. E9.1a

Determine: The reactions for the following cases:

- (i) $w = 30 \text{ kN/m}$, $v_B = 0$
- (ii) $w = 0$, $v_B = 40 \text{ mm}$
- (iii) $w = 30 \text{ kN/m}$, $v_B = 40 \text{ mm}$

Solution: The beam is indeterminate to the first degree. We work with the primary structure shown below (Fig. E9.1b).

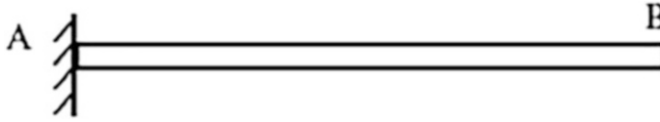


Fig. E9.1b Primary structure

Applying the external loading and the unit load results in the following deflected shapes (Figs. E9.1c and E9.1d):

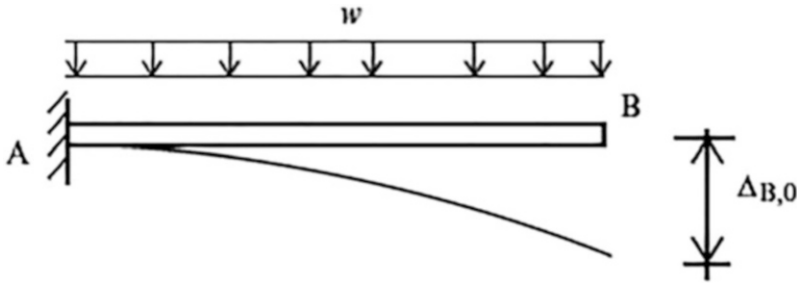


Fig. E9.1c Displacement due to external loading

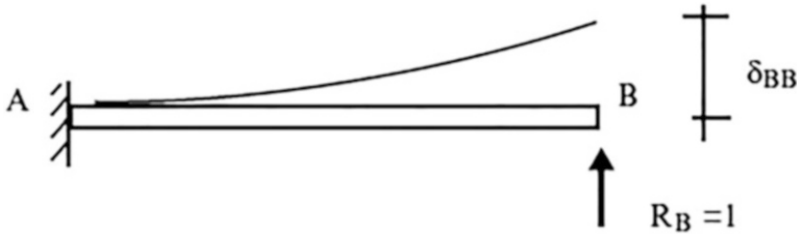


Fig. E9.1d Displacement due to the unit values of R_B The deflection terms are given in Table 3.1.

$$\Delta_{B,0} = \frac{wL^4}{8EI} \downarrow$$

$$\delta_{BB} = \frac{L^3}{3EI} \uparrow$$

Then

$$+ \uparrow \Delta_B|_{\text{actual}} = \Delta_{B,0} + \delta_{BB}R_B$$

↓

$$\Delta_B|_{\text{actual}} = -\frac{wL^4}{8EI} + \frac{L^3}{3EI}R_B \quad \therefore R_B = \frac{\Delta_B|_{\text{actual}} + (wL^4/8EI)}{(L^3/3EI)}$$

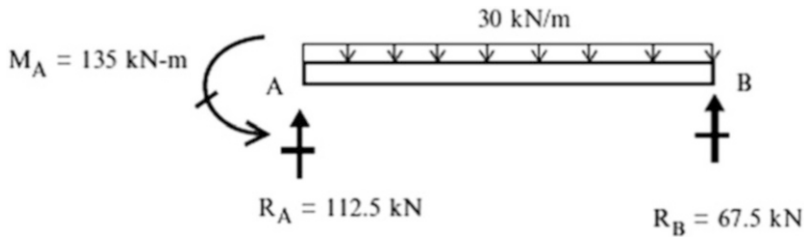
Case (i): For $\Delta_B|_{\text{actual}} = 0$

$$R_B = ((wL^4/8EI)/(L^3/3EI)) = \frac{3}{8}wL = \frac{3}{8}(30)(6) = 67.5 \text{ kN } \uparrow$$

Knowing the value of R_B , we determine the remaining reactions by using the static equilibrium equations.

$$\sum F_y = 0 \quad R_A = \frac{5}{8}wL = \frac{5}{8}(30)(6) = 112.5 \text{ kN } \uparrow$$

$$\sum M_{@A} = 0 \quad M_A = \frac{wL^2}{8} = 135 \text{ kNm } \text{ counterclockwise}$$



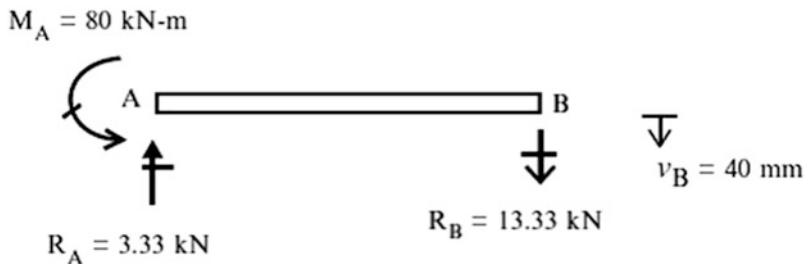
Case (ii): For $w = 0$, $\Delta_B|_{\text{actual}} = -v_B$

$$R_B = \frac{(-v_B)}{(L^3/3EI)} = -\frac{3EI}{L^3}v_B = -\frac{3(200)(10)^6 120(10)^{-6}}{(6)^3}(0.040) = -13.33 \text{ kN } \therefore R_B = 13.33 \text{ kN } \downarrow$$

The reactions are

$$\sum F_y = 0 \quad R_A = \frac{3EI}{L^3}v_B = 13.3 \text{ kN } \uparrow$$

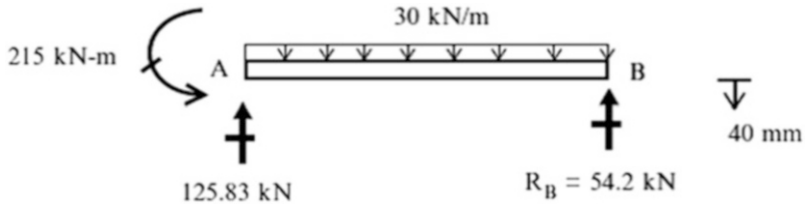
$$\sum M_{@A} = 0 \quad M_A = \frac{3EI}{L^2}v_B = 80 \text{ kNm } \text{ counterclockwise}$$



Case (iii): For $w \neq 0$ and $\Delta_B|_{\text{actual}} = -v_B$

$$R_B = \frac{-v_B + (wL^4/8EI)}{(L^3/3EI)} = +\frac{3}{8}wL - \frac{3EI}{L^3}v_B = 67.5 - 13.33 = 54.2 \text{ kN } \uparrow$$

The reactions are as follows:



Note that since the structure is linear, one can superimpose the solutions for cases (i) and (ii).

Example 9.2

Given: The beam and loading defined in Fig. E9.2a. Assume $I = 400 \text{ in.}^4$, $L = 54 \text{ ft}$, $w = 2.1 \text{ kip/ft}$, $\delta_A = 2.4 \text{ in.}$, and $E = 29,000 \text{ ksi}$.

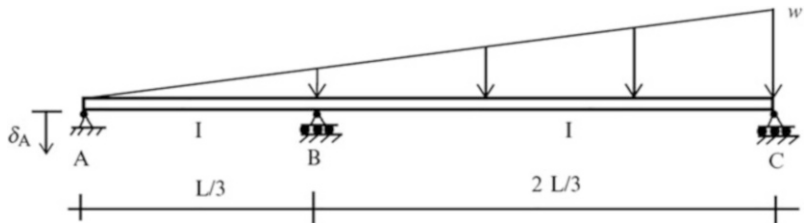


Fig. E9.2a

Determine: The reactions due to

- (i) The distributed load shown
- (ii) The support settlement at A

Solution: The beam is indeterminate to the first degree. We take the vertical reaction at B as the force unknown and compute the deflected shapes due to w and $R_B = 1$ applied to the primary structure (Figs. E9.2b and E9.2c).

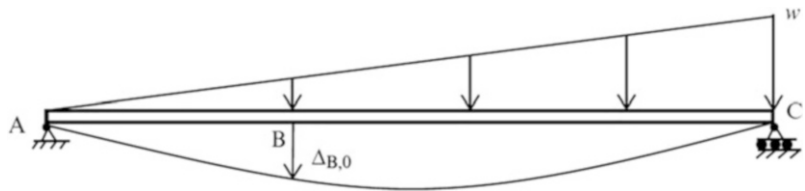


Fig. E9.2b Deflected shape due to w

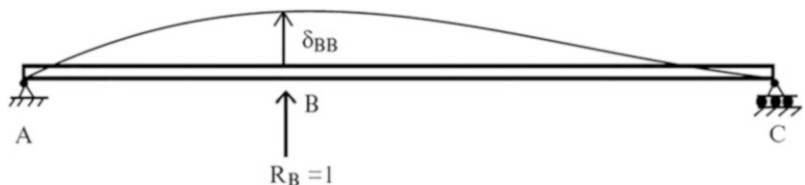


Fig. E9.2c Deflected shape due to unit value of R_B

Case (i): The distributed load shown

$$\begin{aligned}
 + \uparrow \Delta_B|_{\text{actual}} &= \Delta_{B,0} + \delta_{BB}R_B \\
 &\downarrow \\
 \Delta_{B,0} + \delta_{BB}R_B &= 0 \quad \therefore R_B = -\frac{\Delta_{B,0}}{\delta_{BB}}
 \end{aligned}$$

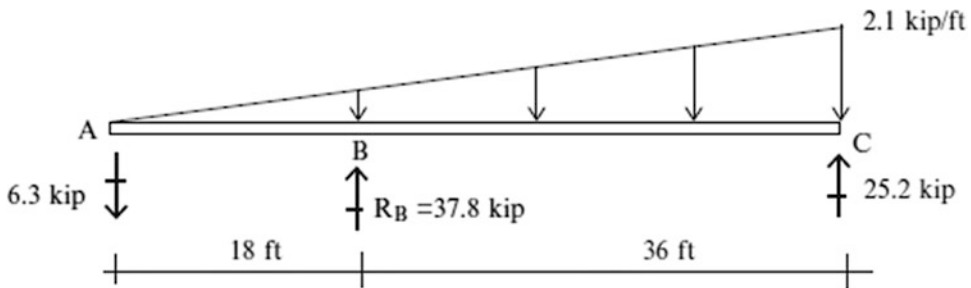
The deflection terms can be determined using (3.34).

$$\begin{aligned}
 \Delta_{B,0} &= -\frac{4wL^4}{729EI} \\
 \delta_{BB} &= \frac{4L^3}{243EI}
 \end{aligned}$$

Then

$$R_B = -\frac{\Delta_{B,0}}{\delta_{BB}} = \frac{(4wL^4/729EI)}{(4L^3/243EI)} = \frac{wL}{3} = 37.8 \text{ kip } \uparrow$$

Knowing the value of R_B , we determine the remaining reactions by using the static equilibrium equations.



Case (ii): The support settlement at A (Fig. E9.2d)

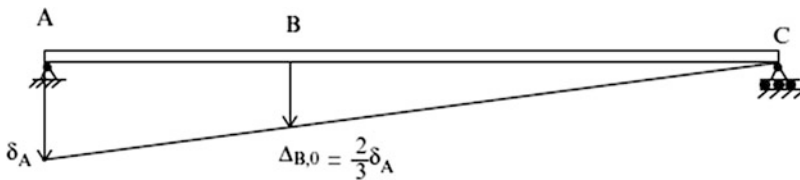


Fig. E9.2d Displacement due to support settlement at A

$$+ \uparrow \Delta_B|_{\text{actual}} = \Delta_{B,0} + \delta_{BB}R_B$$

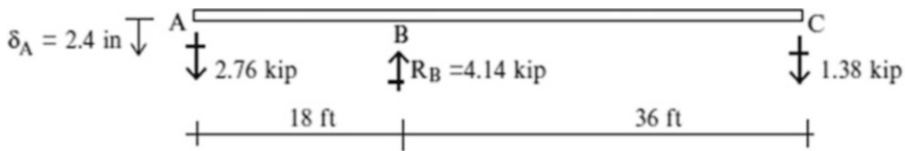
where

$$\begin{aligned}
 \delta_{BB} &= \frac{4L^3}{243EI} = \frac{4(54)^3(12)^3}{243(29,000)(400)} = 0.386 \text{ in.} \\
 \Delta_{B,0} &= \frac{2}{3}\delta_A = -1.6 \text{ in.}
 \end{aligned}$$

Therefore

$$R_B = -\frac{\Delta_{B,0}}{\delta_{BB}} = -\frac{(-1.6)}{0.386} = 4.14 \text{ kip } \uparrow$$

We determine the remaining reactions using the static equilibrium equations.



Example 9.3

Given:

The three-span beam defined in Fig. E9.3a. Assume EI is constant, $L = 9 \text{ m}$, and $w = 20 \text{ kN}$.

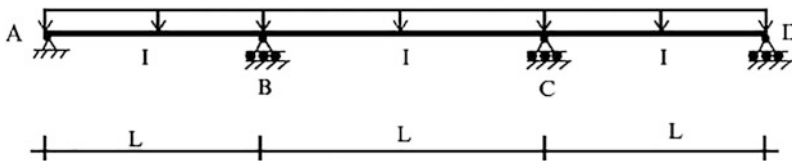


Fig. E9.3a

Determine: The reactions

Solution: The beam is indeterminate to the second degree. We remove the supports at B and C, take the vertical reactions at B and C as the force redundants, and compute the deflected shapes due to w , $X_1 = 1$, and $X_2 = 1$ applied to the primary structure (Figs. E9.3b, E9.3c, E9.3d).

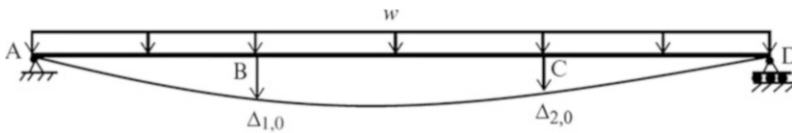


Fig. E9.3b Deflected shape due to external loading



Fig. E9.3c Deflected shape due to $X_1 = 1$



Fig. E9.3d Deflected shape due to $X_2 = 1$

The displacements of the primary structure due to the external loading and the two force redundants are expressed as:

$$\Delta_{1,0} + \delta_{11}X_1 + \delta_{12}X_2 = 0$$

$$\Delta_{2,0} + \delta_{21}X_1 + \delta_{22}X_2 = 0$$

Noting symmetry and the deflection results listed in Table 3.1, it follows that:

$$X_1 = X_2$$

$$\Delta_{1,0} = \Delta_{2,0} = -\frac{11wL^4}{12EI}$$

$$\delta_{11} = \delta_{22} = \frac{4L^3}{9EI}$$

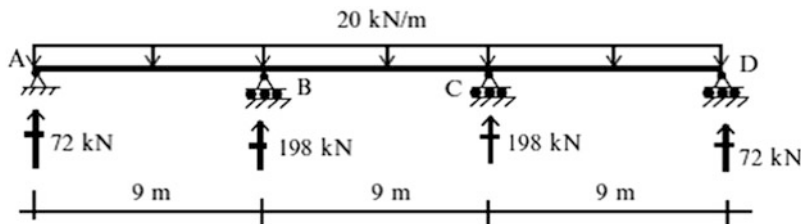
$$\delta_{21} = \delta_{12} = \frac{7L^3}{18EI}$$

Then

$$X_1 = X_2 = \frac{-\Delta_{1,0}}{\delta_{11} + \delta_{12}} = \frac{(11wL^4/12EI)}{(4L^3/9EI) + (7L^3/18EI)} = 1.1wL = 1.1(20)(9) = 198 \text{ kN}$$

Lastly, we determine the remaining reactions

$$\sum F_Y = 0 \quad R_A = R_D = 0.4wL = 72 \text{ kN} \uparrow$$



9.3.1 Beam with Yielding Supports

We consider next the case where a beam is supported by another member, such as another beam or a cable. Examples are shown in Fig. 9.17. When the beam is loaded, reactions are developed, and the supporting members deform. Assuming linear elastic behavior, the supporting members

Fig. 9.17 Beam on flexible supports. (a) Beam. (b) Cable. (c) Column

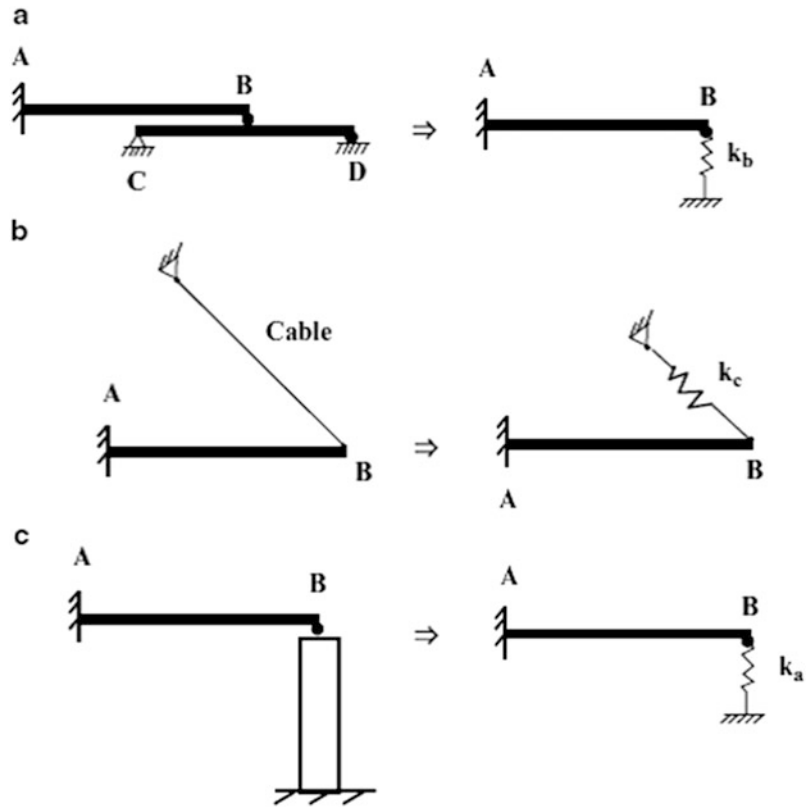
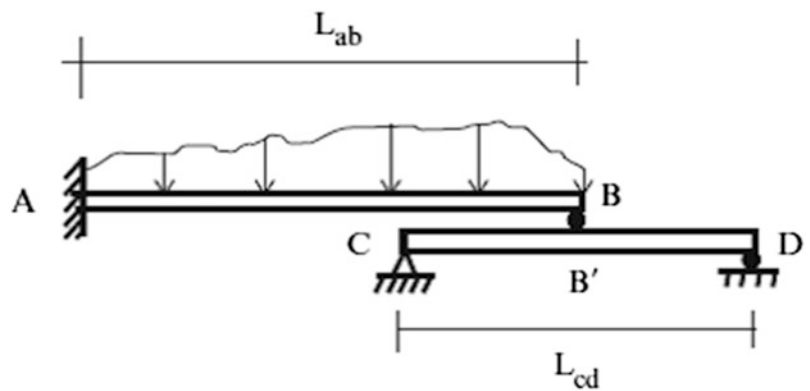


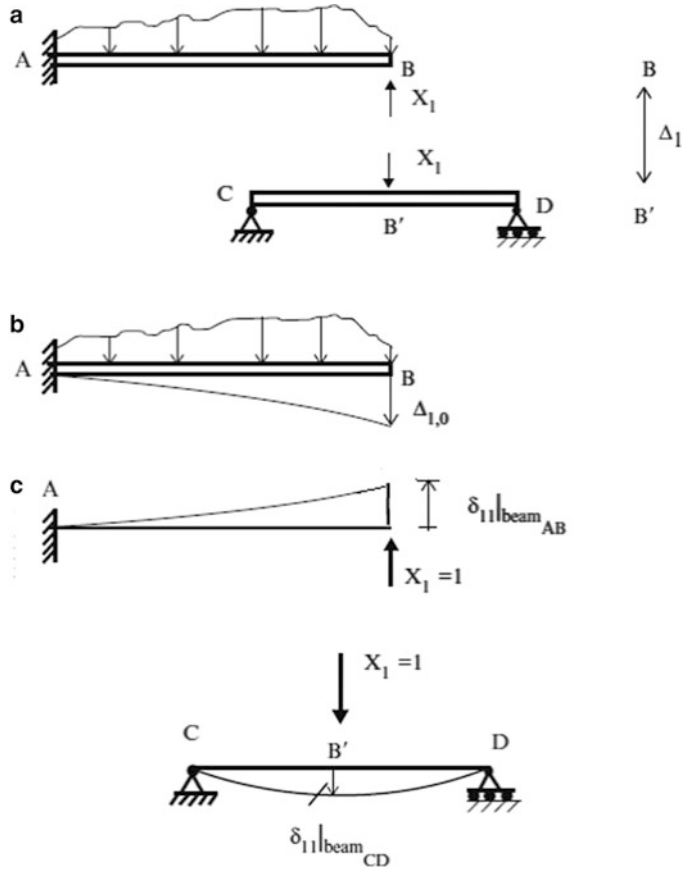
Fig. 9.18 Beam supported by another beam



behave as linear elastic restraints, and can be modeled as equivalent spring elements, as indicated in Fig. 9.17.

We consider here the case where a vertical restraint is provided by another beam. Figure 9.18 illustrates this case. Point B is supported by beam CD which is parallel to beam AB. In this case, point B deflects when the load is applied to beam AB. One strategy is to work with a primary structure that includes both beams such as shown in Fig. 9.19. The force redundant is now a pair of self-equilibrating forces acting at B, and the corresponding displacement measure is the relative displacement apart between the upper and lower contact points, designated as B and B'.

Fig. 9.19 Choice of force redundant and displacement profiles. (a) Primary structure—force redundant system. (b) Deflection due to external loading. (c) Deflection due to redundant force at B



The total displacement corresponding to $X_1 = 1$ is the sum of two terms,

$$\begin{aligned} \delta_{11} &= \delta_{11}|_{AB} + \delta_{11}|_{CD} \\ &= \frac{L^3}{3EI} + \delta_{11}|_{CD} \end{aligned}$$

Beam CD functions as a restraint on the movement of beam AB. The downward movement of B' is resisted by the bending action of beam CD. Assuming linear elastic behavior, this restraint can be modeled as a linear spring of stiffness k . One chooses the magnitude of k such that the spring deflection due to the load P is the same as the beam deflection.

Then, it follows from Fig. 9.20 that

$$\delta_{11}|_{CD} = \frac{1}{k_{CD}} \tag{9.16}$$

Assuming the two beams are rigidly connected at B, the net relative displacement must be zero.

$$\Delta_1 = \Delta_{1,0} + X_1 \left(\frac{1}{k_{CD}} + \frac{L^3}{3EI} \right) = 0 \tag{9.17}$$

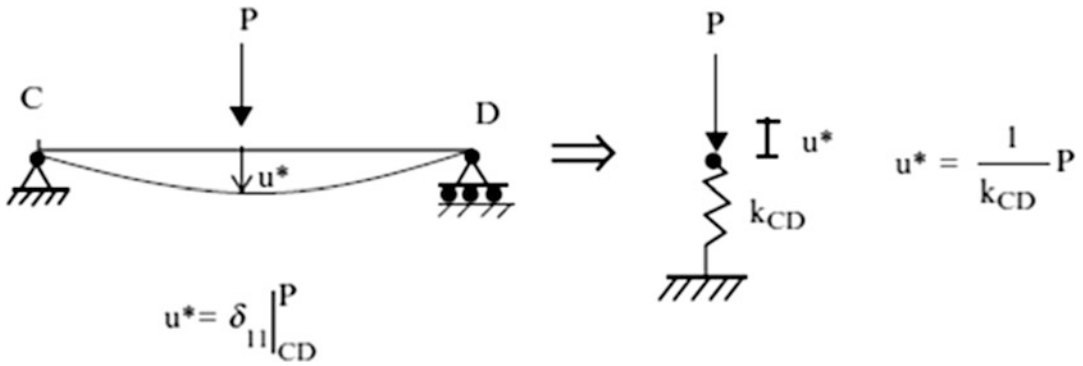


Fig. 9.20 Equivalent spring

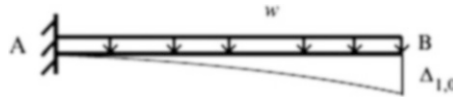
Solving (9.17) for X_1 leads to

$$X_1 = \left\{ \frac{-1}{(L^3/3EI) + (1/k_{CD})} \right\} \Delta_{1,0} \tag{9.18}$$

Note that the value of X_1 depends on the stiffness of beam CD. Taking $k_{CD} = \infty$ corresponds to assuming a rigid support, i.e., a roller support. When $k_{CD} = 0$, $X_1 = 0$. It follows that the bounds on X_1 are

$$0 < X_1 < \left(\frac{3EI}{L^3} \right) \Delta_{1,0} \tag{9.19}$$

When the loading is uniform,



$$\Delta_{1,0} = \frac{wL^4}{8EI} \downarrow$$

Another type of elastic restraint is produced by a cable. Figure 9.21 illustrates this case. We replace the cable with its equivalent stiffness, $k_C = \frac{A_c E_c}{h}$ and work with the primary structure shown in Fig. 9.21b.

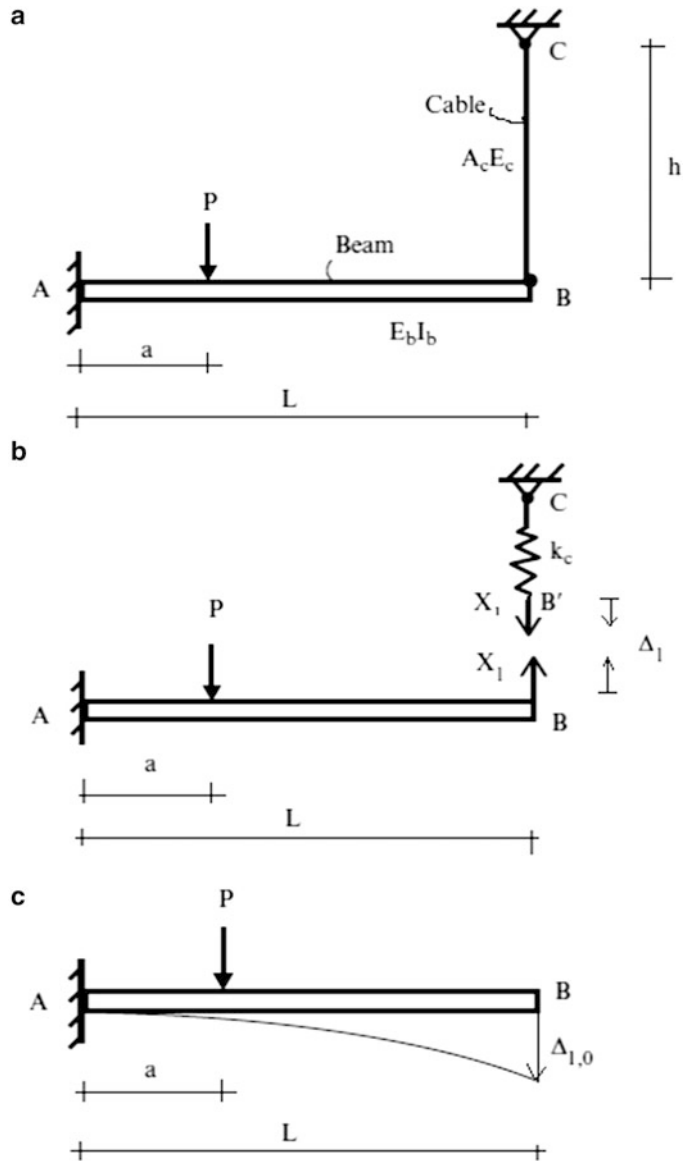
Using the results derived above, and noting that $\Delta_1 = 0$, the geometric compatibility equation is

$$\Delta_1 = \Delta_{1,0} + (\delta_{11}|_{AB} + \delta_{11}|_{BC})X_1 = 0$$

For the external concentrated loading,

$$\Delta_{1,0} = \frac{P}{EI} \left(\frac{a^2 L}{2} - \frac{a^3}{3} \right)$$

Fig. 9.21 (a) Actual structure. (b) Primary structure—force redundant system. (c) Deflection due to applied load



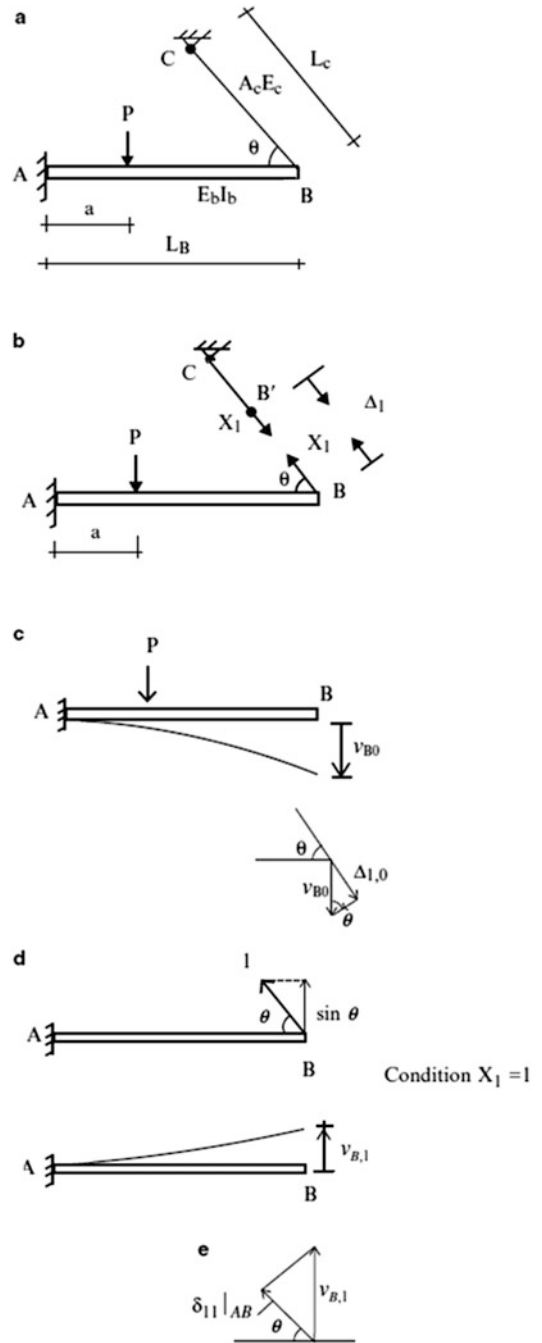
Substituting for the various flexibility terms leads to

$$X_1 = \left[\frac{-1}{(L^3/3E_bI_b) + (1/k_c)} \right] \Delta_{1,0} \tag{9.20}$$

If $\frac{1}{k_c}$ is small with respect to $\frac{L^3}{3E_bI_b}$, the cable acts like a rigid support, i.e., X_1 approaches the value for a rigid support. When $\frac{1}{k_c}$ is large with respect to $\frac{L^3}{3E_bI_b}$, the cable is flexible and provides essentially no resistance, i.e., $X_1 \Rightarrow 0$. The ratio of cable to beam flexibilities is a key parameter for the behavior of this system.

Cable-stayed schemes are composed of beams supported with inclined cables. Figure 9.22a shows the case where there is just one cable. We follow essentially the same approach as described earlier

Fig. 9.22 (a) Cable-stayed scheme. (b) Force redundant. (c) Deflection due to applied load. (d) Deflection due to $X_1 = 1$. (e) Displacement components



except that now the cable is inclined. We take the cable force as the redundant and work with the structure defined in Fig. 9.22b.

Note that Δ_1 is the relative movement together of points B and B' along the inclined direction. Up to this point, we have been working with vertical displacements. Now we need to project these movements on an inclined direction.

We start with the displacement profile shown in Fig. 9.22c. The vertical deflection is v_{B0} . Projecting on the direction of the cable leads to

$$\Delta_{1,0} = -\sin \theta v_{B0} = -\sin \theta \left\{ \frac{P}{E_B I_B} \left(\frac{a^2 L_B}{2} - \frac{a^3}{6} \right) \right\} \tag{9.21}$$

Next, we treat the case where $X_1 = 1$ shown in Fig. 9.22d. The total movement consists of the elongation of the cable and the displacement of the beam.

$$\delta_{11} = \delta_{11}|_{BC} + \delta_{11}|_{AB}$$

The elongation of the cable is

$$\delta_{11}|_{BC} = \frac{L_c}{A_C E_C} = \frac{1}{k_c}$$

The beam displacement follows from Fig. 9.22e.

$$\delta_{11}|_{AB} = v_{B,1} \sin \theta = \sin \theta \left\{ \frac{\sin \theta L_B^3}{3 E_B I_B} \right\} = (\sin \theta)^2 \left(\frac{L_B^3}{3 E_B I_B} \right)$$

Requiring $\Delta_1 = 0$ leads to

$$X_1 = \frac{1}{(\sin \theta)^2 (L_B^3 / 3 E_B I_B) + (1/k_c)} \left[\frac{P \sin \theta}{E_B I_B} \left(\frac{a^2 L_B}{2} - \frac{a^3}{6} \right) \right] \tag{9.22}$$

Finally, we express X_1 in terms of the value of the vertical reaction corresponding to a rigid support at B.

$$X_1 = \frac{\sin \theta}{(\sin \theta)^2 + 3 (E_B I_B / L_B^3) (L_C / E_C A_C)} R|_{\text{rigid support at B}} \tag{9.23}$$

There are two geometric parameters, θ , and the ratio of I_B / L_B^3 to A_C / L_C . Note that X_1 varies with the angle θ . When cables are used to stiffen beams, such as for cable-stayed bridges, the optimum cable angle is approximately 45° . The effective stiffness provided by the cable degrades rapidly with decreasing θ .

Example 9.4

Given: The structure defined in Fig. E9.4a.

Assume $I = 400 \text{ in.}^4$, $L = 54 \text{ ft}$, $w = 2.1 \text{ kip/ft}$, $k_v = 25 \text{ kip/in.}$, and $E = 29,000 \text{ ksi}$.

Determine: The reactions, the axial force in the spring, and the displacement at B.

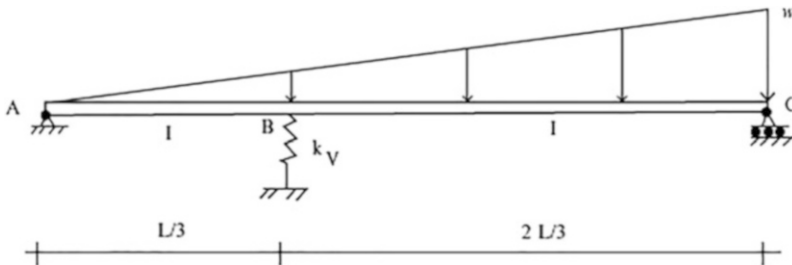


Fig. E9.4a

Solution: The structure is indeterminate to the first degree. We take the axial force in the spring at B as the force unknown.

The geometric compatibility equation is

$$\Delta_{1,0} + \left(\delta_{11}|_{ABC} + \frac{1}{k_v} \right) X_1 = 0$$

The deflection terms can be determined using (3.34).

$$\Delta_{1,0} = -\frac{4wL^4}{729EI} = 14.6 \text{ in.}$$

$$\delta_{11}|_{ABC} = \frac{4L^3}{243EI} = 0.386 \text{ in.}$$

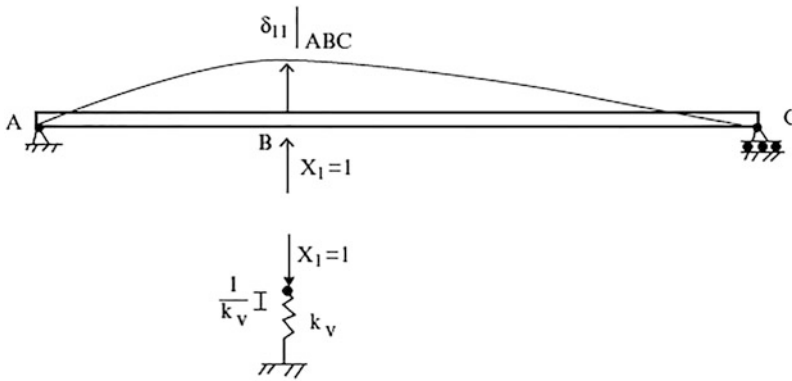


Fig. E9.4b Deflected shape due to $X_1 = 1$

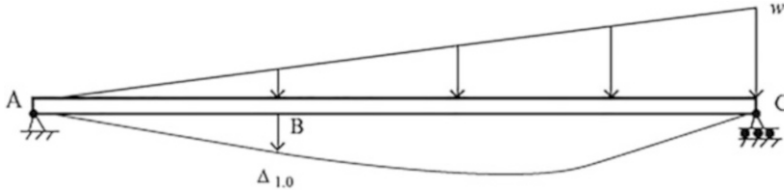
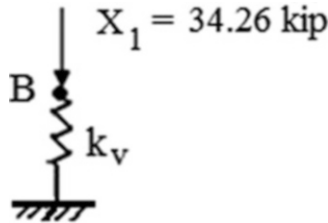


Fig. E9.4c Deflected shape due to external loading

Solving for X_1 , leads to:

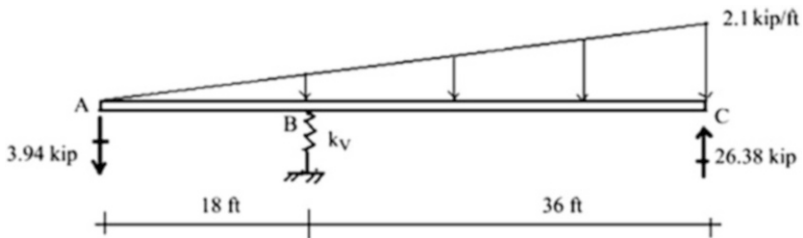
$$X_1 = \frac{\Delta_{1,0}}{\delta_{11}|_{ABC} + (1/k_v)} = \frac{14.6}{0.386 + (1/25)} = 34.26 \text{ kip } \uparrow$$



The displacement at B is

$$v_B = \frac{X_1}{k_v} = \frac{34.26}{25} = 1.37 \text{ in. } \downarrow$$

Next, we determine the remaining reactions by using the static equilibrium equations.



Example 9.5

Given: The structure defined in Fig. E9.5a. Assume $I = 200(10)^6 \text{ mm}^4$, $L = 18 \text{ m}$, $P = 45 \text{ kN}$, $A_C = 1300 \text{ mm}^2$, and $E = 200 \text{ GPa}$.

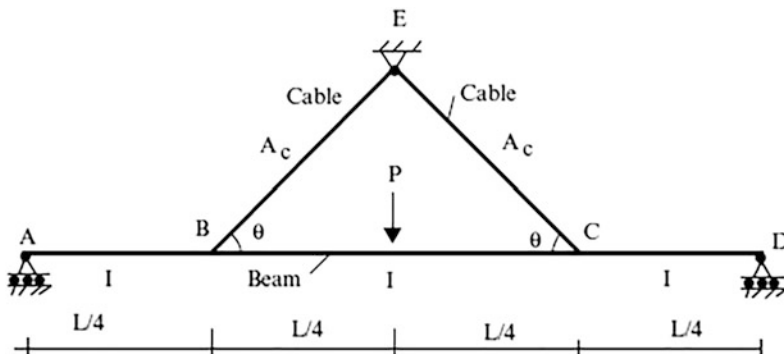


Fig. E9.5a

Determine: The forces in the cables, the reactions, and the vertical displacement at the intersection of the cable and the beam.

- (a) $\theta = 45^\circ$
- (b) $\theta = 15^\circ$

Solution: The structure is indeterminate to the second degree. We take the cable forces as the force redundants and work with the structure defined below (Fig. E9.5b).

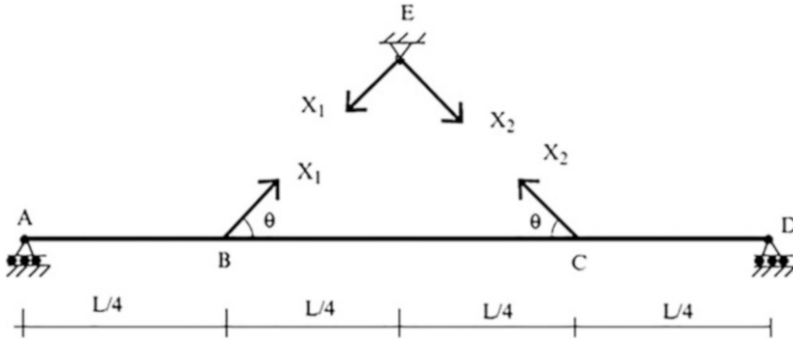


Fig. E9.5b Primary structure

Next, we compute the deflected shapes due to external loading P , $X_1 = 1$, and $X_2 = 1$ applied to the primary structure (Figs. E9.5c, E9.5d, E9.5e).

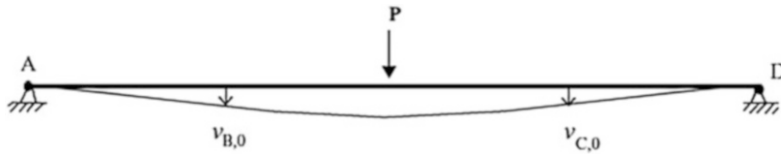


Fig. E9.5c External loading P



Fig. E9.5d $X_1 = 1$

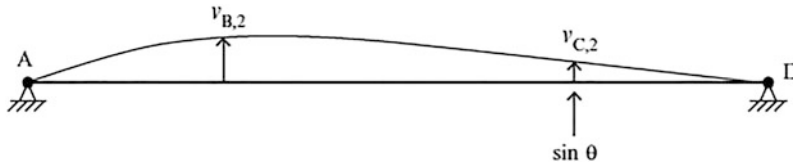


Fig. E9.5e $X_2 = 1$

The displacements of the primary structure due to the external loading and the two force redundants are expressed as

$$\Delta_{1,0} + \delta_{11}X_1 + \delta_{12}X_2 = 0$$

$$\Delta_{2,0} + \delta_{21}X_1 + \delta_{22}X_2 = 0$$

where

$$\delta_{11} = \delta_{11}|_{\text{Beam}} + \delta_{11}|_{\text{cable}}$$

$$\delta_{22} = \delta_{22}|_{\text{Beam}} + \delta_{22}|_{\text{cable}}$$

$$\delta_{12} = \delta_{12}|_{\text{Beam}}$$

$$\delta_{21} = \delta_{21}|_{\text{Beam}}$$

also

$$\Delta_{1,0} = v_{B,0} \sin \theta$$

$$\Delta_{2,0} = v_{C,0} \sin \theta$$

$$\delta_{11}|_{\text{Beam}} = v_{B,1} \sin \theta$$

$$\delta_{21}|_{\text{Beam}} = v_{C,1} \sin \theta$$

$$\delta_{21}|_{\text{Beam}} = v_{B,2} \sin \theta$$

$$\delta_{22}|_{\text{Beam}} = v_{C,2} \sin \theta$$

Because of symmetry:

$$\delta_{11}|_{\text{Beam}} = \delta_{22}|_{\text{Beam}} = v_{B,1} \sin \theta = \frac{3 \sin \theta^2 L^3}{256EI}$$

$$\delta_{12}|_{\text{Beam}} = \delta_{21}|_{\text{Beam}} = v_{B,2} \sin \theta = \frac{7 \sin \theta^2 L^3}{768EI}$$

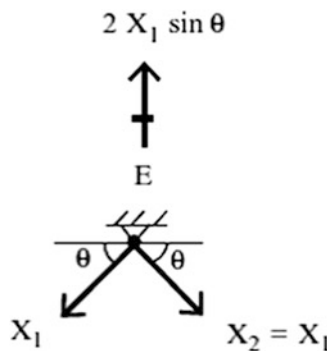
$$\Delta_{1,0} = \Delta_{2,0} = v_{B,0} \sin \theta = \frac{11 \sin \theta PL^3}{768EI}$$

$$\delta_{11}|_{\text{Cable}} = \delta_{22}|_{\text{Cable}} = \frac{L_C}{A_C E} = \frac{L}{4 \cos \theta A_C E}$$

$$X_1 = X_2$$

Lastly, the redundant forces are

$$X_1 = X_2 = \frac{\Delta_{1,0}}{(\delta_{11}|_{\text{Beam}} + \delta_{11}|_{\text{Cable}}) + \delta_{12}|_{\text{Beam}}}$$

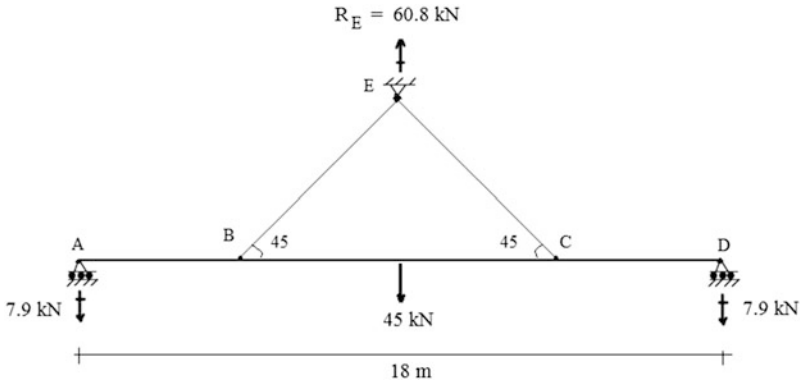


(a) For $\theta = 45^\circ$

$$X_1 = X_2 = \frac{\Delta_{1,0}}{(\delta_{11}|_{\text{Beam}} + \delta_{11}|_{\text{Cable}}) + \delta_{12}|_{\text{Beam}}} = 43 \text{ kN}$$

$$\therefore 2X_1 \sin \theta = 2(43) \sin 45 = 60.8 \text{ kN}$$

The remaining reactions are determined using the static equilibrium equations.

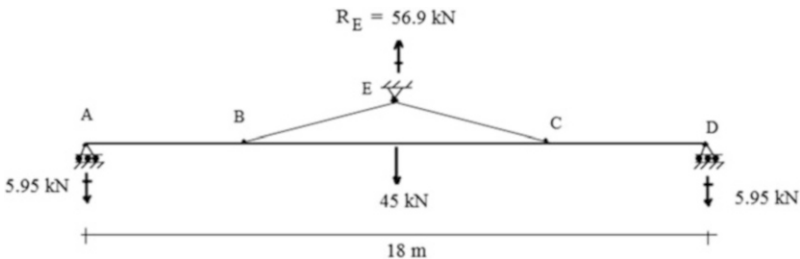


(b) For $\theta = 15^\circ$

$$X_1 = X_2 = \frac{\Delta_{1,0}}{(\delta_{11}|_{\text{Beam}} + \delta_{11}|_{\text{Cable}}) + \delta_{12}|_{\text{Beam}}} = 109.8 \text{ kN}$$

$$\therefore 2X_1 \sin \theta = 2(109.8) \sin 15 = 56.9 \text{ kN}$$

The remaining reactions are determined using the static equilibrium equations.

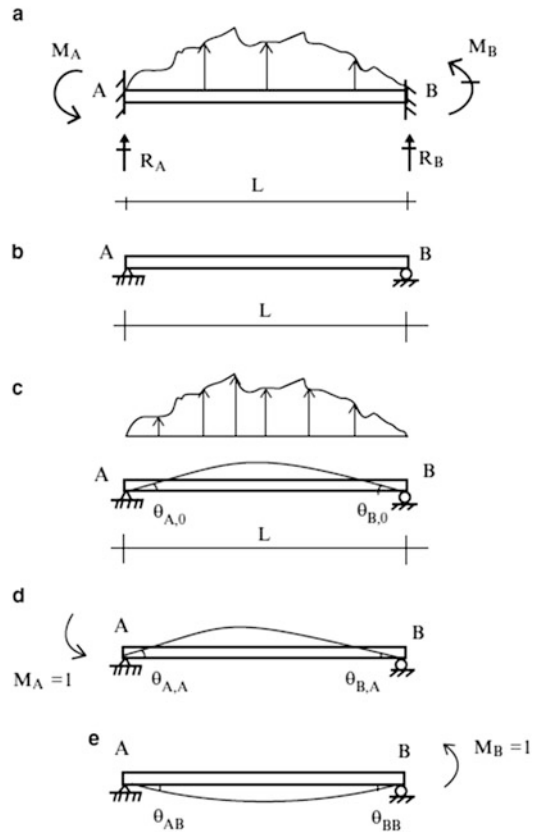


9.3.2 Fixed-Ended Beams

We treat next the beam shown in Fig. 9.23a. The structure is fully restrained at each end and therefore is indeterminate to the second degree. We take as force redundants the counterclockwise end moments at each end. The corresponding displacement measures are the counterclockwise end rotations, θ_A and θ_B .

We write the general form of the compatibility equations as (we use θ instead of Δ to denote the displacement measures and M instead of X for the force measures):

Fig. 9.23 (a) Beam with full end restraint. (b) Primary structure. (c) External loading—displacement profile. (d) Displacement profile for $M_A = 1$. (e) Displacement profile for $M_B = 1$



$$\begin{aligned} \theta_A &= \theta_{A,0} + M_A \theta_{AA} + M_B \theta_{AB} \\ \theta_B &= \theta_{B,0} + M_A \theta_{BA} + M_B \theta_{BB} \end{aligned} \tag{9.24}$$

where $\theta_{A,0}$ and $\theta_{B,0}$ depend on the nature of the applied loading, and the other flexibility coefficients are

$$\begin{aligned} \theta_{AA} &= \frac{L}{3EI} \\ \theta_{BB} &= \frac{L}{3EI} \\ \theta_{AB} &= \theta_{BA} = -\frac{L}{6EI} \end{aligned}$$

We solve (9.24) for M_A and M_B

$$\begin{aligned} M_A &= \frac{2EI}{L} \{2(\theta_A - \theta_{A,0}) + (\theta_B - \theta_{B,0})\} \\ M_B &= \frac{2EI}{L} \{2(\theta_B - \theta_{B,0}) + (\theta_A - \theta_{A,0})\} \end{aligned} \tag{9.25}$$

When the ends are fixed, $\theta_A = \theta_B = 0$, and the corresponding values of M_A and M_B are called the fixed end moments. They are usually denoted as M_A^F and M_B^F

$$M_A^F = -\frac{2EI}{L}\{2\theta_{A,0} + \theta_{B,0}\}$$

$$M_B^F = -\frac{2EI}{L}\{2\theta_{B,0} + \theta_{A,0}\}$$
(9.26)

Introducing this notation in (9.25), the expressions for the end moments reduce to

$$M_A = \frac{2EI}{L}\{2\theta_A + \theta_B\} + M_A^F$$

$$M_B = \frac{2EI}{L}\{2\theta_B + \theta_A\} + M_B^F$$
(9.27)

We will utilize these equations in Chap. 10.

Example 9.6 Fixed End Moments for Uniformly Distributed Loading

Given: The uniform distributed loading applied to a fixed end beam (Fig. E9.6a).

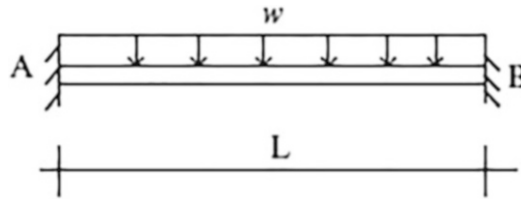


Fig. E9.6a

Determine: The fixed end moments.

Solution: We take the end moments at A and B as force redundant (Fig. E9.6b).

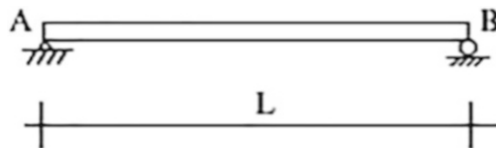


Fig. E9.6b Primary structure

Noting Table 3.1, the rotations due to the applied load are (Fig. E9.6c)

$$EI\theta_{A,0} = -\frac{wL^3}{24} \quad EI\theta_{B,0} = \frac{wL^3}{24}$$

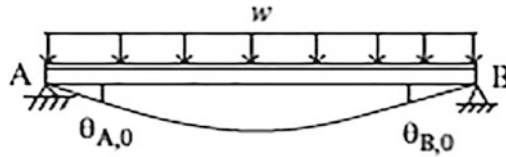


Fig. E9.6c Deformation of primary structure due to applied load

Substituting their values in (9.26) leads to

$$M_A^F = -\frac{2EI}{L} \{2\theta_{A,0} + \theta_{B,0}\} = \frac{wL^2}{6} - \frac{wL^2}{12} = \frac{wL^2}{12}$$

$$M_B^F = -\frac{2EI}{L} \{2\theta_{B,0} + \theta_{A,0}\} = -\frac{wL^2}{6} + \frac{wL^2}{12} = -\frac{wL^2}{12}$$

$$M_A^F = \frac{wL^2}{12} \curvearrowright$$

$$M_B^F = \frac{wL^2}{12} \curvearrowleft$$

The shear and moment diagrams are plotted in Fig. E9.6d.

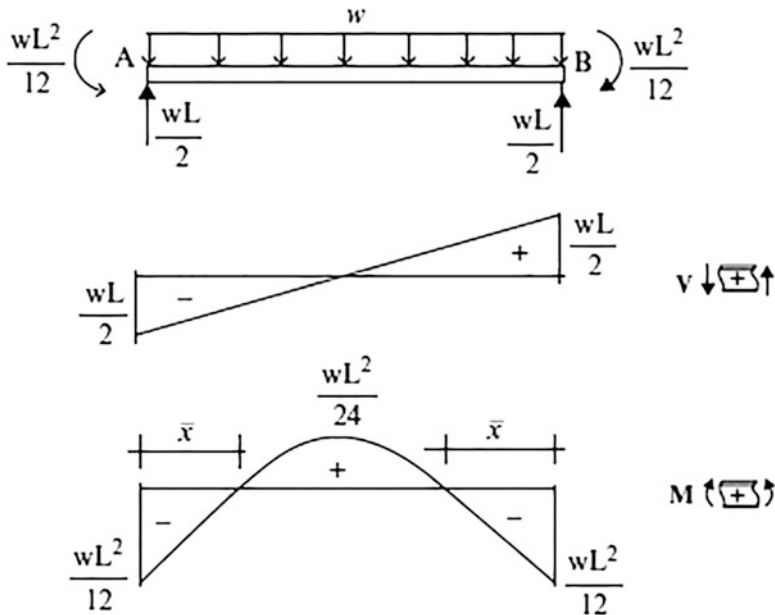


Fig. E9.6d

Note that the peak positive moment for the simply supported case is $+(wL^2/8)$. Points of inflection are located symmetrically at

$$\bar{x} = \frac{L}{2} \left(1 - \frac{1}{\sqrt{3}} \right) \approx 0.21L$$

This solution applies for full fixity. When the member is part of a frame, the restraint is provided by the adjacent members, and the end moments will generally be less than the fully fixed value.

Example 9.7 Fixed End Moment—Single Concentrated Force

Given: A single concentrated force applied at an arbitrary point $x = a$ on the fixed end beam shown in Fig. E9.7a.

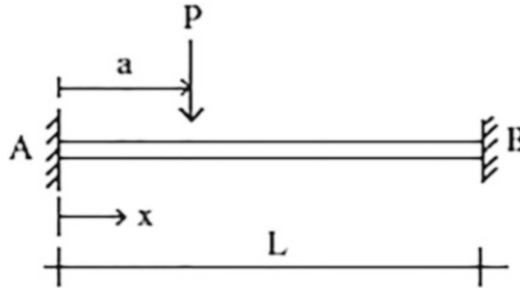


Fig. E9.7a

Determine: The fixed end moments.

Solution: We work with the primary structure defined in Fig. E9.7b.

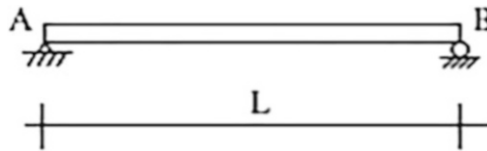


Fig. E9.7b Primary structure

Using the results listed in Table 3.1, the rotations are given by (Fig. E9.7c)

$$EI\theta_{A,0} = -\frac{Pa(L-a)(2L-a)}{6L}$$

$$EI\theta_{B,0} = \frac{Pa(L-a)(L+a)}{6L}$$

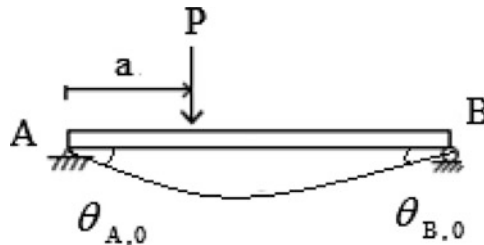


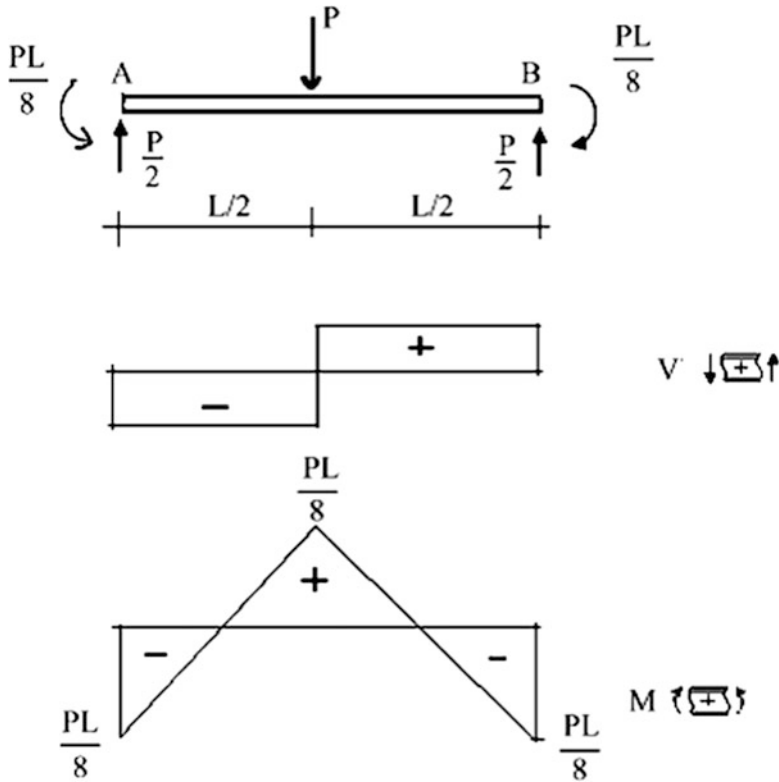
Fig. E9.7c Deformation of primary structure due to external loading

Substituting into (9.26) leads to

$$M_A^F = \frac{Pa(L - a)^2}{L^2}$$

$$M_B^F = -\frac{P(L - a)a^2}{L^2}$$

The critical location for maximum fixed end moment is $a = L/2$; the corresponding maximum values are $M_A^F = -M_B^F = \frac{PL}{8}$. The shear and moment diagrams are plotted below.



Note that there is a 50 % reduction in peak moment due to end fixity.

Results for various loadings and end conditions are summarized in Tables 9.1 and 9.2.

Table 9.1 Fixed end actions for fully fixed

<p>Diagram showing a beam of length L fixed at both ends A and B. A uniformly distributed load w is applied downwards. The fixed end moments are $\frac{wL^2}{12}$ at both ends. The fixed end reactions are $\frac{wL}{2}$ at both ends.</p>	<p>Diagram showing a beam of length L fixed at both ends A and B. A point load P is applied downwards at a distance a from end A and b from end B. The fixed end moments are $\frac{Pab^2}{L^2}$ at A and $\frac{Pba^2}{L^2}$ at B. The fixed end reactions are $\frac{Pb^2(3a+b)}{L^3}$ at A and $\frac{Pa^2(3b+a)}{L^3}$ at B.</p>
<p>Diagram showing a beam of length L fixed at both ends A and B. A triangular load w is applied downwards, increasing from 0 at A to w at B. The fixed end moments are $\frac{5wL^2}{96}$ at both ends. The fixed end reactions are $\frac{wL}{4}$ at both ends.</p>	<p>Diagram showing a beam of length L fixed at both ends A and B. A point load P is applied downwards at the center, $L/2$ from both ends. The fixed end moments are $\frac{PL}{8}$ at both ends. The fixed end reactions are $\frac{P}{2}$ at both ends.</p>
<p>Diagram showing a beam of length L fixed at both ends A and B. A triangular load w is applied downwards, increasing from $\frac{w}{30}$ at A to $\frac{w}{20}$ at B. The fixed end moments are $\frac{wL^2}{30}$ at A and $\frac{wL^2}{20}$ at B. The fixed end reactions are $\frac{3wL}{20}$ at A and $\frac{7wL}{20}$ at B.</p>	<p>Diagram showing a beam of length L fixed at both ends A and B. A vertical displacement Δ is applied at end B. The fixed end moments are $\frac{6EI\Delta}{L^2}$ at both ends. The fixed end reactions are $\frac{12EI\Delta}{L^3}$ at both ends.</p>
<p>Diagram showing a beam of length L fixed at both ends A and B. A uniformly distributed load w is applied downwards over a segment of length $L/2$ starting from end A. The fixed end moments are $\frac{11wL^2}{192}$ at A and $\frac{5wL^2}{192}$ at B. The fixed end reactions are $\frac{13wL}{32}$ at A and $\frac{3wL}{32}$ at B.</p>	<p>Diagram showing a beam of length L fixed at both ends A and B. A point moment M is applied at a distance a from end A and b from end B. The fixed end moments are $\frac{Mb(2a-b)}{L^3}$ at A and $\frac{Ma(2b-a)}{L^3}$ at B. The fixed end reactions are $\frac{6Mab}{L^2}$ at both ends.</p>

Table 9.2 Fixed end actions for partially fixed

9.3.3 Analytical Solutions for Multi-Span Beams

Consider the two-span beam shown in Fig. 9.24a. We allow for different lengths and different moments of inertia for the spans. Our objective here is to determine analytically how the maximum positive and negative moments vary as the load moves across the total span. We choose the negative moment at B as the redundant. The corresponding primary structure is shown in Fig. 9.24b. Here, $\Delta\theta_B$ is the relative rotation together of adjacent cross sections at B.

The geometric compatibility equation involves the relative rotation at B.

$$\Delta\theta_B = \Delta\theta_{B,0} + \delta\theta_{BB}M_B = 0$$

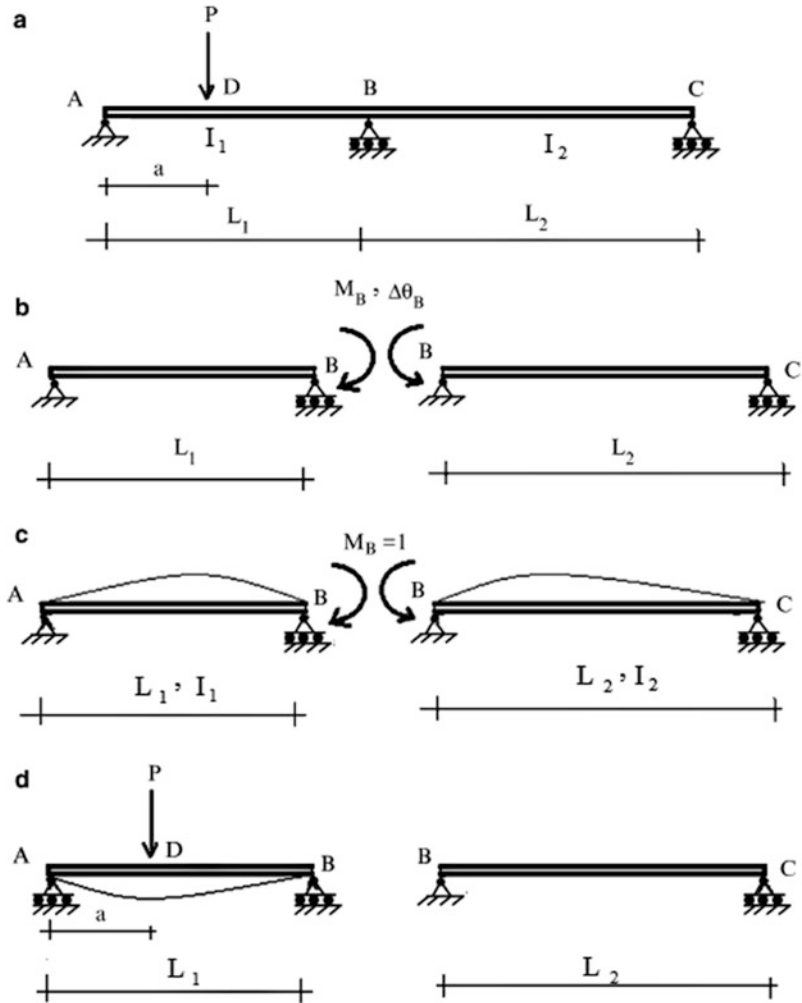
The various rotation terms are given in Table 3.1. Note that the $\delta\theta_{BB}$ term is independent of the applied loading.

$$\delta\theta_{BB} = \frac{1}{3E} \left(\frac{L_1}{I_1} + \frac{L_2}{I_2} \right)$$

When the loading is on span AB (see Table 3.1),

$$\Delta\theta_{B,0} = -\frac{P}{6EI_1L_1} a(a^2 - L_1^2)$$

Fig. 9.24 (a) Actual structure—notation for a two-span beam. (b) Primary structure—redundant moment. (c) Displacement due to a unit value of the redundant moment. (d) Rotation due to external loading



Then

$$M_B = \frac{-\Delta\theta_{B,0}}{\delta\theta_{BB}} = \left\{ \frac{(L_1/I_1)}{(L_1/I_1) + (L_2/I_2)} \right\} \frac{1}{2} Pa \left(1 - \frac{a^2}{L_1^2} \right) \tag{9.28}$$

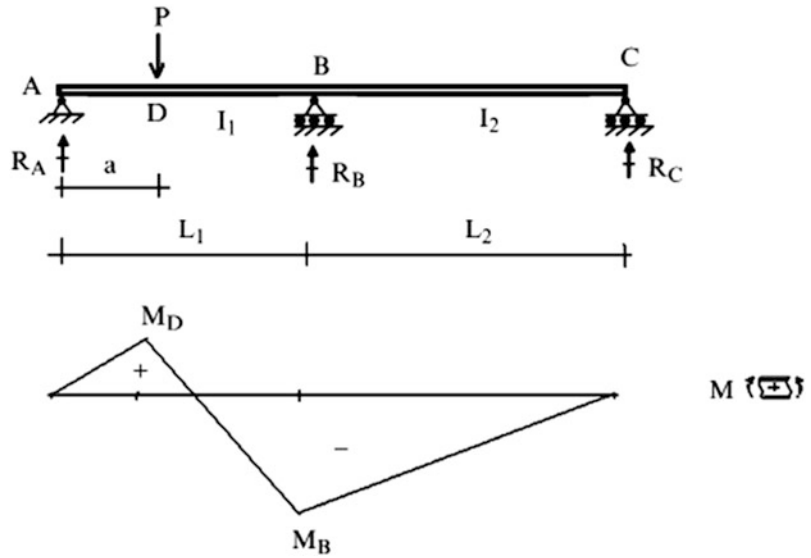
Given the value of M_B , we can determine the reactions by using the static equilibrium equations. Noting (9.28), the peak moments are given by:

$$\begin{aligned} \text{Negative moment } M_B &= -\frac{PL_1}{2} f \frac{a}{L_1} \left(1 - \frac{a^2}{L_1^2} \right) \\ \text{Positive moment } M_D &= PL_1 \left(\frac{a}{L_1} \right) \left\{ \left(1 - \frac{a}{L_1} \right) - \frac{f}{2} \frac{a^2}{L_1^2} \left(1 - \frac{a^2}{L_1^2} \right) \right\} \end{aligned} \tag{9.29}$$

where

$$f = \frac{1}{1 + (I_1/L_1)(L_2/I_2)}$$

Fig. 9.25 Bending moment distribution for load on span AB



We define the ratio of I to L as the “relative stiffness” for a span and denote this parameter by r .

$$r_i = \frac{I}{L} \Big|_{\text{span } i} \tag{9.30}$$

With this notation, f takes the form

$$f = \frac{1}{1 + (r_1/r_2)}$$

The typical bending moment diagram is plotted in Fig. 9.25.

When the load is on span BC, one just has to use a different expression for $\Delta\theta_{B,0}$. Redefining the location of P as shown in Fig. 9.26a, the solution takes the following form:

$$\Delta\theta_{B,0} = -\frac{Pb\left(1 - \frac{b}{L_2}\right)\left(2 - \frac{b}{L_2}\right)}{6EI_2}$$

Then

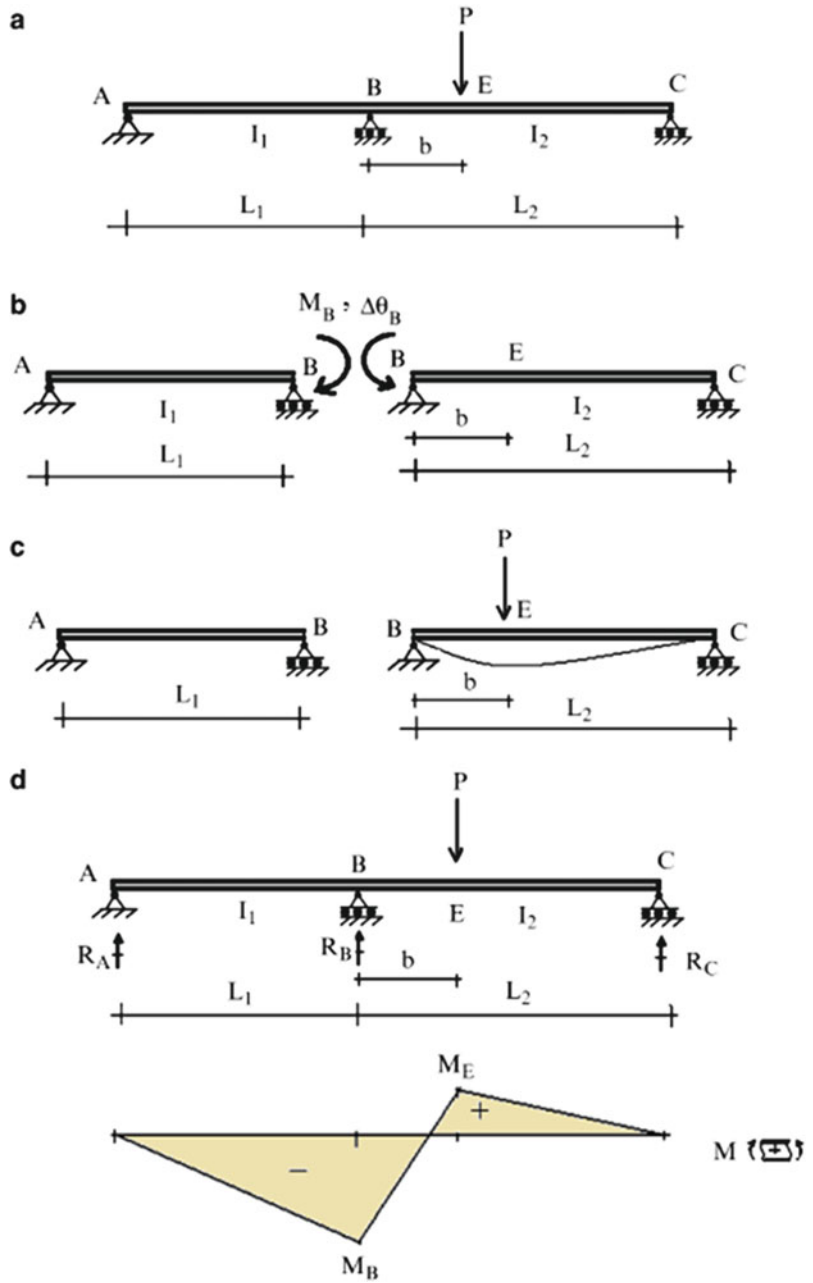
$$M_B = \frac{-\Delta\theta_{B,0}}{\delta\theta_{BB}} = \frac{1}{(1 + (r_2/r_1))} \left(\frac{1}{2}PL_2\right) \frac{b}{L_2} \left(1 - \frac{b}{L_2}\right) \left(2 - \frac{b}{L_2}\right) \tag{9.31}$$

Given M_B , one can construct the moment diagram. It is similar to Fig. 9.25, but rotated 180°.

Example 9.8

Given: The two-span beam shown in Figs. E9.8a and E9.8ab.

Fig. 9.26 (a) Actual structure—loading on span BC. (b) Primary structure—redundant moment. (c) Rotation due to external loading. (d) Bending moment distribution for load on span BC



Determine: The variation of the bending moment at B with relative stiffness of the adjacent spans ($r_1/r_2 = 0.1, 1, \text{ and } 10$).

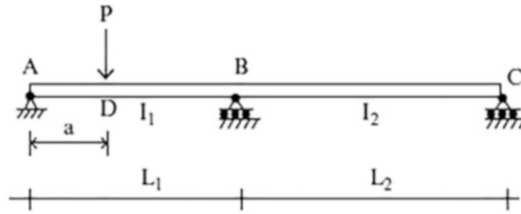


Fig. E9.8a

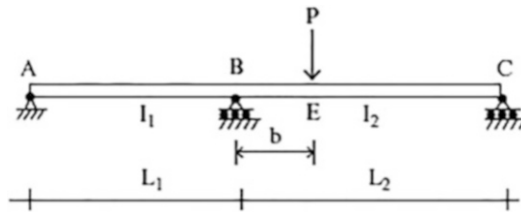


Fig. E9.8b

Solution: We determine the variation of the moment at B for a range of relative stiffness ratios covering the spectrum from one span being very flexible to one span being very rigid with respect to the other span using (9.29) and (9.31). Results for the individual spans are plotted in Figs. E9.8c and E9.8d.

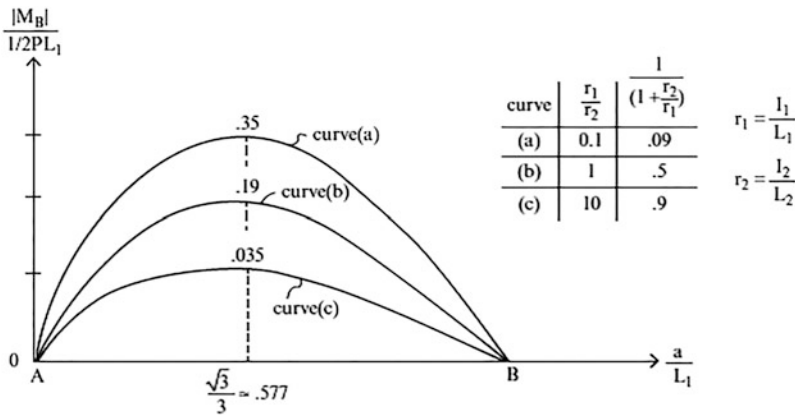


Fig. E9.8c Load on the left span (9.29)

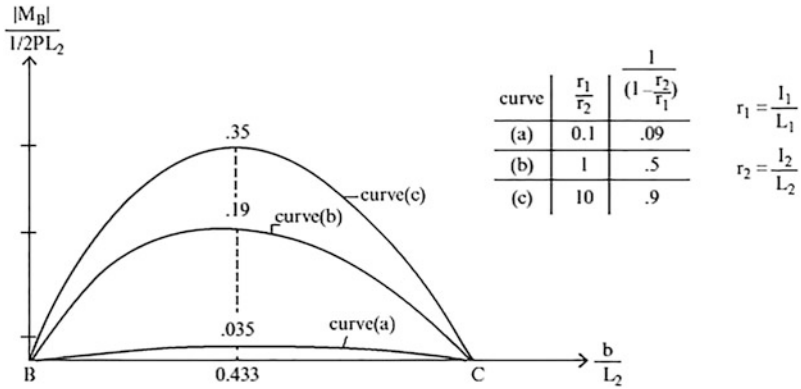


Fig. E9.8d Load on the right span (9.31)

Example 9.9 Two-Span Continuous Beam—Uniform Loading

Given: The two-span beam shown in Fig. E9.9a.

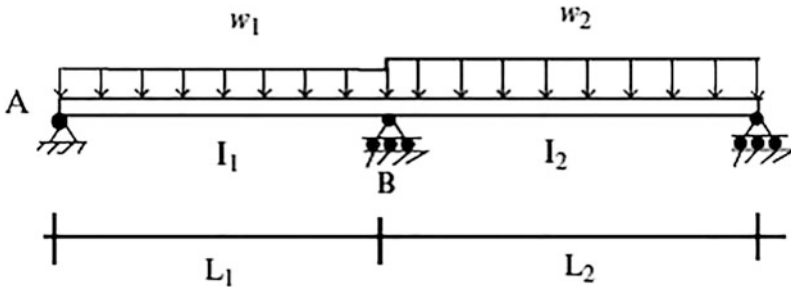


Fig. E9.9a

Determine: The bending moment at support B.

Solution: We take the negative moment at the interior support as the force redundant. The solution process is similar to that followed for the case of a concentrated load. One determines the relative rotations at B, and then enforces continuity at B (Fig. E9.9b).

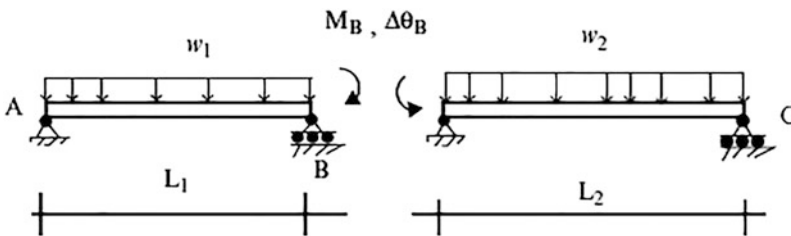


Fig. E9.9b

The various terms are (see Table 3.1)

$$\Delta\theta_{B,0} = -\frac{w_1L_1^3}{24EI_1} - \frac{w_2L_2^3}{24EI_2}$$

$$\delta\theta_{BB} = \frac{L_1}{3EI_1} + \frac{L_2}{3EI_2}$$

Requiring the relative rotation at B equal to zero leads to

$$M_B = \frac{-\Delta\theta_{B,0}}{\delta\theta_{BB}} = \left(\frac{w_1L_1^2}{8}\right) \frac{1 + (w_2/w_1)(L_2/L_1)^2(r_1/r_2)}{1 + (r_1/r_2)}$$

where

$$r_1 = \frac{I_1}{L_1}, \quad r_2 = \frac{I_2}{L_2}$$

Suppose the loading and span lengths are equal. In this case,

$$M_B = \frac{wL^2}{8}$$

for all combinations of I_1 and I_2 . The moment diagram is plotted below (Fig. E9.9c).

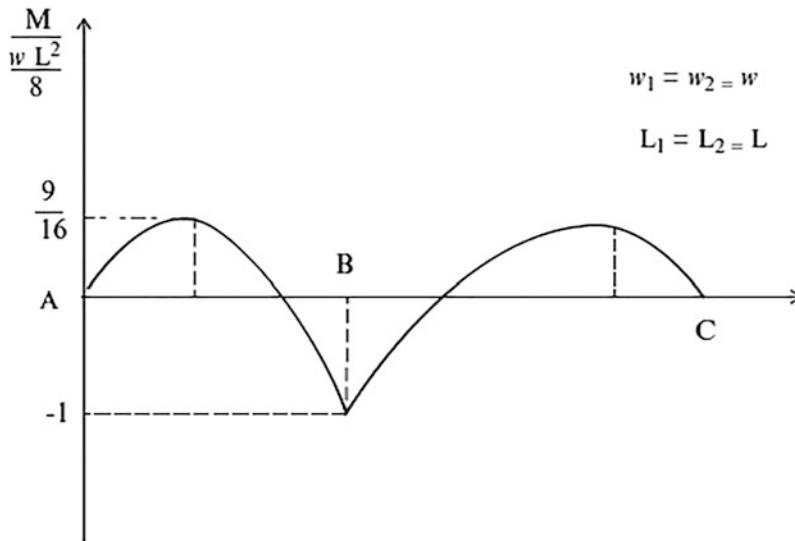
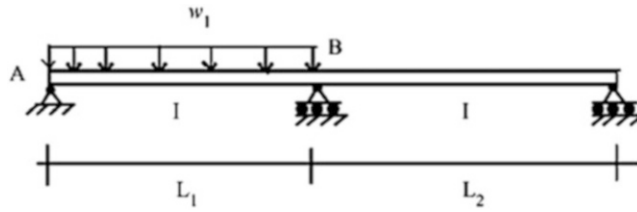


Fig. E9.9c

Another interesting case is where $w_2 = 0$ and $I_1 = I_2$. The solution depends on the ratio of span lengths.

$$M_B = \frac{w_1L_1^2}{8} \frac{1}{1 + (L_2/L_1)}$$



Suppose $L_2 = L_1$ and $I_1 = I_2$, then

$$M_B = \frac{1}{2} \left(\frac{w_1 L_1^2}{8} \right)$$

Example 9.10 Two-Span Continuous Beam with Support Settlement

Given: The two-span beam shown in Fig. E9.10a. The supports at B or A experience a vertical displacement downward due to settlement of the soil under the support.

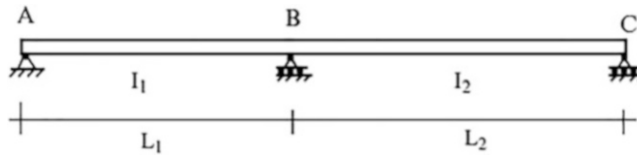


Fig. E9.10a

Determine: The bending moment at B.

Solution: We work with the primary structure shown in Fig. E9.10b.

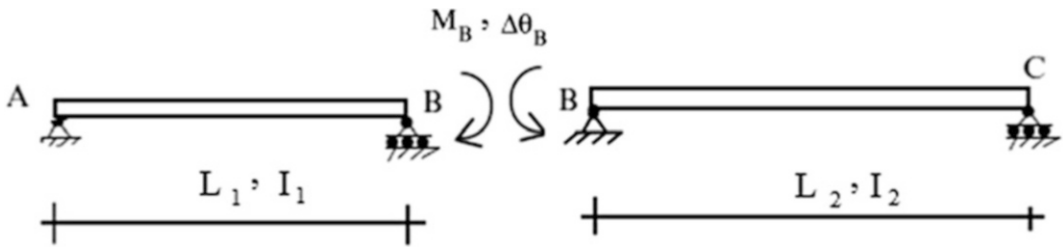
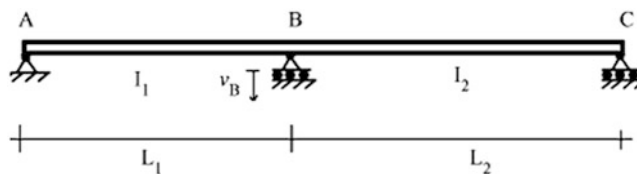


Fig. E9.10b Primary structure—redundant moment

If the support at B moves downward an amount v_B , the relative rotation of the section at B is

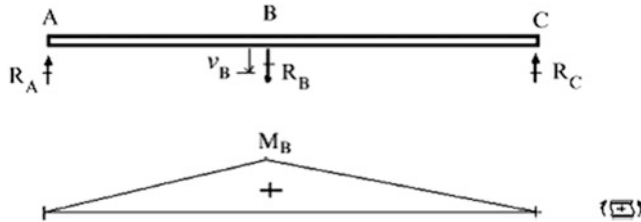
$$\Delta\theta_{B,0} = \frac{v_B}{L_1} + \frac{v_B}{L_2}$$



Compatibility requires the moment at B to be equal to

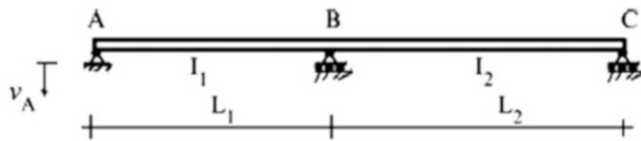
$$M_B = \frac{-\Delta\theta_{B,0}}{\delta\theta_{BB}} = -\frac{v_B((1/L_1) + (1/L_2))}{(1/3E)((L_1/I_1) + (L_2/I_2))}$$

The minus sign indicates that the bending moment is of opposite sense to that assumed in Fig. E9.10b.

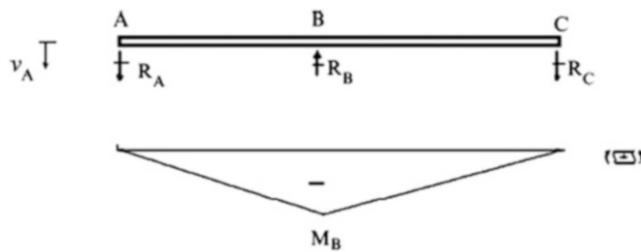


When the properties are the same for both spans ($I_1 = I_2$ and $L_1 = L_2$), M_B reduces to $M_B = \frac{3EI_1}{L_1^2} v_B$.

When the support at A moves downward an amount v_A , the behavior is reversed.



In this case, $\Delta\theta_{B,0} = -v_A/L_1$ and $M_B = \frac{v_A/L_1}{(1/3E)((L_1/I_1) + (L_2/I_2))}$

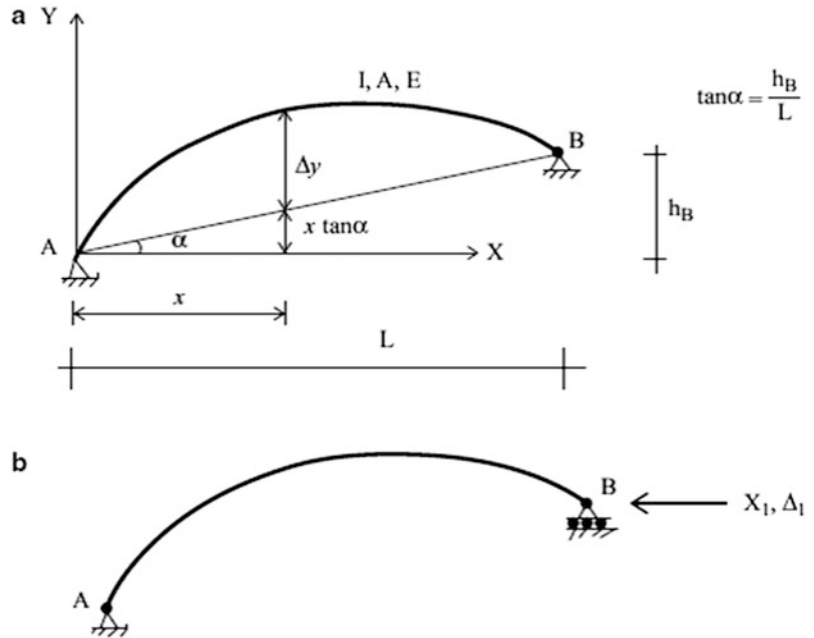


When the properties are the same for both spans ($I_1 = I_2$ and $L_1 = L_2$), M_B reduces to $M_B = \frac{3EI_1}{2L_1^2} v_A$.

9.4 Application to Arch-Type Structures

Chapter 6 introduced the topic of arch structures. The discussion was concerned with how the geometry of arch structures is defined and how to formulate the equilibrium equations for statically determinate arches. Various examples were presented to illustrate how arch structures carry

Fig. 9.27 (a) Actual structure—geometry. (b) Primary structure—redundant reaction



transverse loading by a combination of both axial and bending actions. This feature makes them more efficient than beam structures for long-span applications.

In what follows we extend the analytical formulation to statically indeterminate arches. We base our analysis procedure on the force method and use the principle of virtual forces to compute displacement measures. One of our objectives here is to develop a strategy for finding the geometry for which there is minimal bending moment in the arch due to a particular loading.

We consider the two-hinged arch shown in Fig. 9.27a. This structure is indeterminate to the first degree. We take the horizontal reaction at the right support as the force redundant and use the Principle of Virtual Forces described in Sect. 6.5 to determine $\Delta_{1,0}$, the horizontal displacement due to loading, and δ_{11} , the horizontal displacement due to a unit value of X_1 .

The general expressions for these displacement measures follow from (6.9)

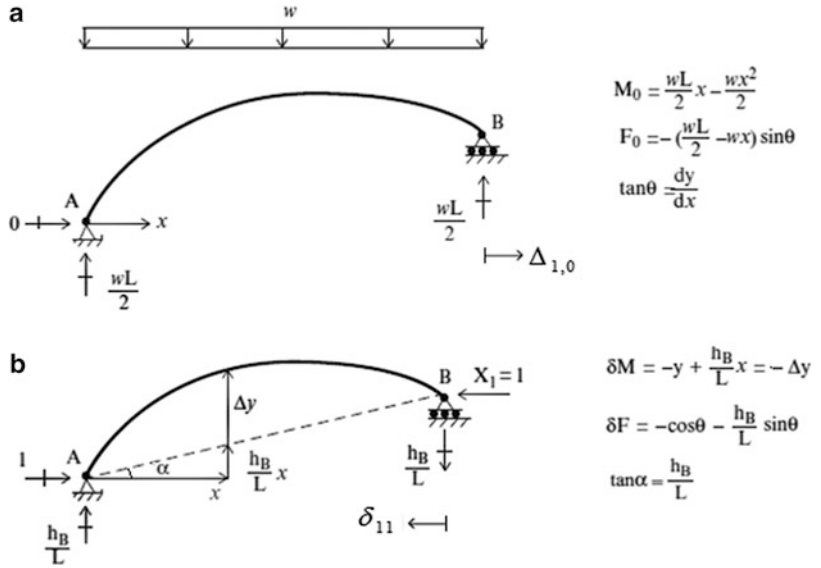
$$\begin{aligned} \Delta_{1,0} &= \int_s \left\{ \frac{F_0}{AE} \delta F + \frac{V_0(x)}{GA_s} \delta V + \frac{M_0(x)}{EI} \delta M \right\} ds \\ \delta_{11} &= \int_s \left\{ \frac{(\delta F)^2}{AE} + \frac{(\delta V)^2}{GA_s} + \frac{(\delta M)^2}{EI} \right\} ds \end{aligned} \tag{9.32}$$

We usually neglect the shear deformation term. Whether one can also neglect the axial deformation term depends on the arch geometry. For completeness, we will retain this term. The two internal force systems are summarized below. We assume the applied load is uniform per projected length (Fig. 9.28).

Substituting for the force terms leads to the following expressions for the displacement measures:

$$\begin{aligned} \Delta_{1,0} &= \int_0^L \left\{ \frac{1}{AE \cos \theta} \left(\frac{wL}{2} - wx \right) \sin \theta (\cos \theta + \tan \alpha \sin \theta) - \left(\frac{wL}{2} x - \frac{wx^2}{2} \right) \frac{\Delta y}{EI \cos \theta} \right\} dx \delta_{11} \\ &= \int_0^L \left\{ \frac{(\cos \theta + \tan \alpha \sin \theta)^2}{AE \cos \theta} + \frac{(\Delta y)^2}{EI \cos \theta} \right\} dx \end{aligned} \tag{9.33}$$

Fig. 9.28 (a) Force due to applied loading (F_0, M_0).
 (b) Force due to $X_1 = 1$ ($\delta F, \delta M$)



Geometric compatibility requires

$$X_1 = -\frac{\Delta_{1,0}}{\delta_{11}} \tag{9.34}$$

One can use either symbolic integration or numerical integration to evaluate the flexibility coefficients. We prefer to use the numerical integration scheme described in Sect. 3.6.6.

The solution simplifies considerably when axial deformation is neglected with respect to bending deformation. One sets $A = \infty$ in (9.33). This leads to

$$\begin{aligned} \Delta_{1,0} &= -\int_0^L \left(\frac{wL}{2}x - \frac{wx^2}{2} \right) \frac{\Delta y}{EI \cos\theta} dx = -\int_0^L \frac{M_0 \Delta y}{EI \cos\theta} dx \\ \delta_{11} &= +\int_0^L \frac{(\Delta y)^2}{EI \cos\theta} dx \end{aligned} \tag{9.35}$$

Suppose Δy is chosen such that

$$\Delta y = \beta \left[\frac{wL}{2}x - \frac{wx^2}{2} \right] \equiv \beta M_0 \tag{9.36}$$

Then,

$$\Delta_{1,0} = -\frac{1}{\beta} \delta_{11}$$

and it follows that

$$\begin{aligned} X_1 &= \frac{1}{\beta} \\ M &= M_0 + X_1 \delta M = M_0 + \left(\frac{1}{\beta} \right) (-\beta M_0) = 0 \end{aligned} \tag{9.37}$$

With this choice of geometry, the arch carries the exterior load by axial action only; there is no bending. *Note that this result is based on the assumption that axial deformation is negligible.* In general, there will be a small amount of bending when h is not small with respect to L , i.e., when the arch is “shallow.” *One cannot neglect axial deformation for a shallow arch.*

Example 9.11 Parabolic Arch with Uniform Vertical Loading

Given: The two-hinged parabolic arch defined in Fig. E9.11a.

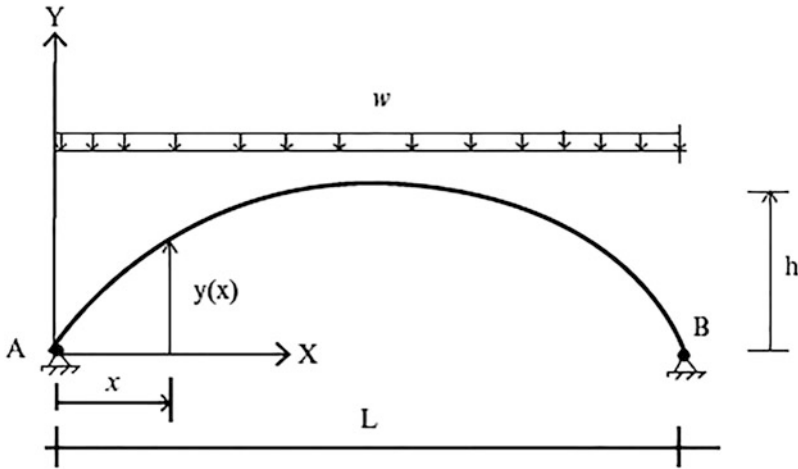


Fig. E9.11a

Determine: The bending moment distribution.

Solution: The centroidal axis for the arch is defined by

$$y = 4h \left[\frac{x}{L} - \left(\frac{x}{L} \right)^2 \right]$$

The bending moment in the primary structure due to the uniform loading per unit x is

$$M_0 = \frac{wL}{2}x - \frac{wx^2}{2} = \frac{wL^2}{2} \left[\frac{x}{L} - \left(\frac{x}{L} \right)^2 \right]$$

We note that the expressions for y and M_0 are similar in form. One is a scaled version of the other.

$$M_0 = \frac{wL^2}{2} \frac{1}{4h} y = \frac{wL^2}{8h} y$$

Then, noting (9.36),

$$\beta = \frac{8h}{wL^2}$$

and $X_1 = \frac{wL^2}{8h}$.

The total moment is the sum of M_0 and the moment due to X_1 .

$$M = M_0 - yX_1 = \frac{wL^2}{8h}y - \frac{wL^2}{8h}y = 0$$

We see that there is no bending for this loading and geometry. We should have anticipated this result since a uniformly loaded cable assumes a parabolic shape. By definition, a cable has no bending rigidity and therefore no moment. We can consider an arch as an inverted cable. It follows that a two-hinged uniformly loaded parabolic arch behaves like an inverted cable.

Example 9.12 Approximate Solutions

Given: The two-hinged arch and the loading defined in Fig. E9.12a. The integral expression for X_1 is given by 9.3.4. Noting (9.35), the solution equals to

$$X_1 \approx + \frac{\int \Delta y \frac{M_0}{EI} ds}{\int (\Delta y)^2 \frac{ds}{EI}}$$

This result applies when there is no support movement.

Determine: An approximate expression for X_1 . Assume the cross section of the arch is deeper at the abutment than at the crown, and use the following approximation to define I ,

$$I = \frac{I_0}{\cos \theta}$$

where I_0 is the cross-sectional inertia at the crown.

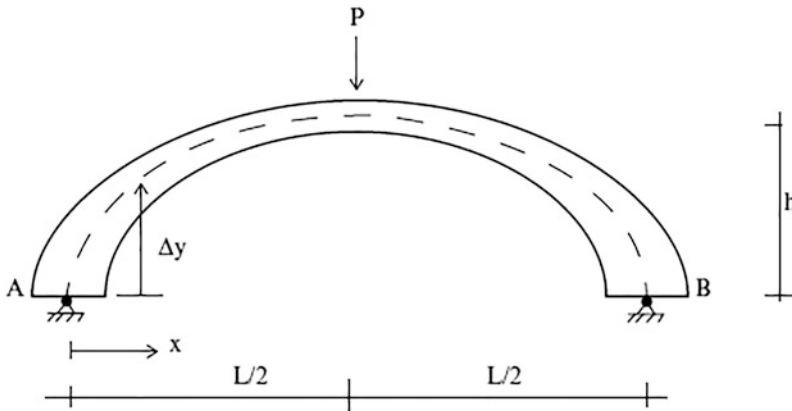


Fig. E9.12a Variable depth arch

Solution: Substituting for I and $ds = \frac{dx}{\cos \theta}$, the integrals simplify to

$$X_1 = \frac{+(1/EI_0) \int \Delta y M_0 dx}{(1/EI_0) \int (\Delta y)^2 dx}$$

and now one can easily determine analytical solutions.

Suppose a concentrated force, P , is applied at mid-span. The corresponding terms for a symmetrical parabolic arch are:

$$\Delta y = \frac{4y}{L} \left(x - \frac{x^2}{L} \right)$$

$$\frac{1}{EI_0} \int \Delta y M_0 dx \Rightarrow \frac{5}{48} \frac{PhL^2}{EI_0}$$

$$\frac{1}{EI_0} \int (\Delta y)^2 dx = \frac{8}{15} \frac{h^2 L}{EI_0}$$

$$X_1 = \frac{25}{128} P \left(\frac{L}{h} \right)$$

Note that the bending moment is *not* zero in this case.

Example 9.13

Given: The two-hinged arch and the loading defined in Fig. E9.13a

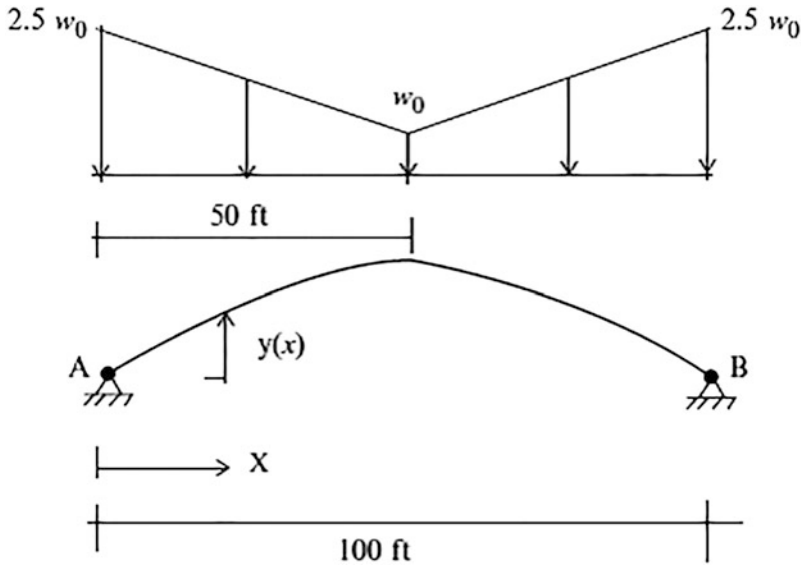


Fig. E9.13a

Determine: The particular shape of the arch which corresponds to negligible bending.

Solution: This two-hinged arch is indeterminate to the first degree. We take the horizontal reaction at the right support as the force redundant (Fig. E9.13b).

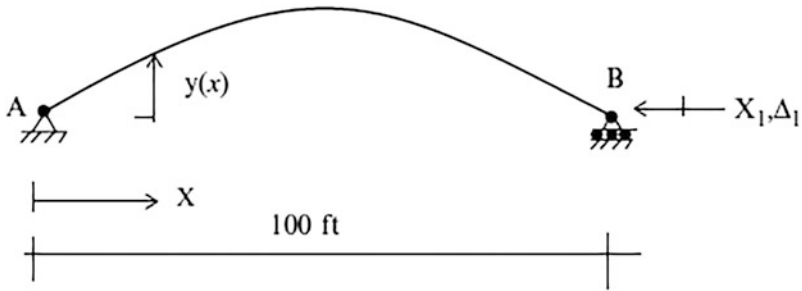


Fig. E9.13b Primary structure—redundant reaction

The applied loading is given by (Fig. E9.13c)

$$w(x) = w_0 \left\{ 2.5 - \frac{1.5}{50}x \right\} \quad 0 < x \leq 50$$

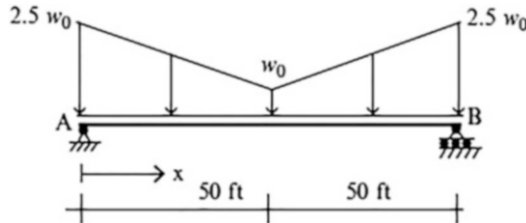


Fig. E9.13c

The corresponding shear and moment in the simply supported beam spanning AB are

$$\frac{dV}{dx} = w(x) \Rightarrow V = w_0 \left\{ 2.5x - \frac{1.5}{100}x^2 \right\} + C_1$$

$$\frac{dM}{dx} = -V \Rightarrow M = -w_0 \left\{ \frac{2.5}{2}x^2 - \frac{1.5}{300}x^3 \right\} + C_1x + C_2$$

Enforcing the boundary conditions,

$$M(0) = 0$$

$$M(100) = 0$$

leads to

$$C_2 = 0$$

$$C_1 = w_0 \left\{ 1.25(100) - \frac{1.5(100)^2}{300} \right\} = 75w_0$$

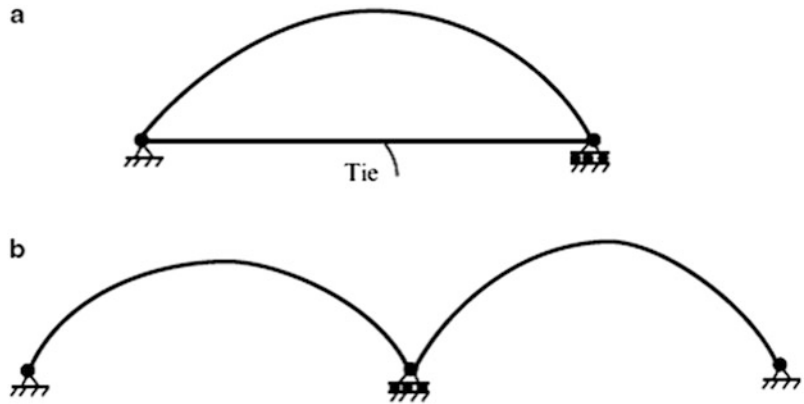
Finally, the expression for M reduces to

$$M = w_0 \{ 75x - 1.25x^2 + 0.005x^3 \} \quad 0 < x \leq 50$$

follows (9.36) and (9.37).

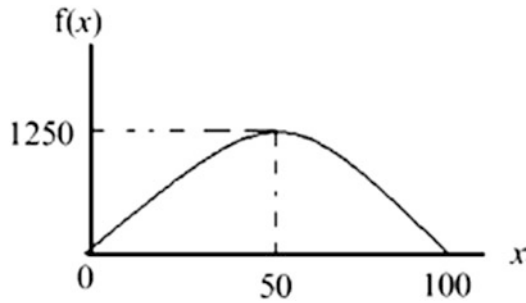
The desired shape is

Fig. 9.29 (a) Single tie arch. (b) Multiple connected arches



$$y(x) = \frac{M(x)}{X_1} = \frac{w_0}{X_1} \{75x - 1.25x^2 + 0.005x^3\} = \frac{w_0}{X_1} f(x)$$

The function $f(x)$ is plotted below. Note that the shape is symmetrical.



When the abutments are inadequate to resist the horizontal thrust, different strategies are employed to resist the thrust. One choice is to insert a tension tie connecting the two supports, as illustrated in Fig. 9.29a. Another choice is to connect a set of arches in series until a suitable anchorage is reached (see Fig. 9.29b). The latter scheme is commonly used for river crossings.

We take the tension in the tie as the force redundant for the tied arch. The corresponding primary structure is shown in Fig. 9.30. We just have to add the extension of the tie member to the deflection δ_{11} . The extended form for δ_{11} is

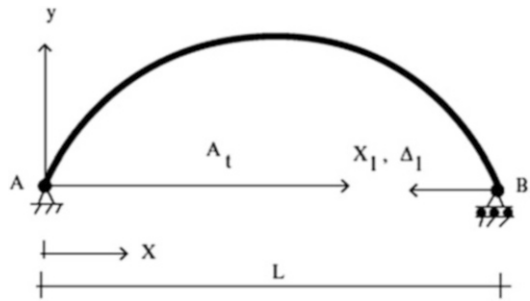
$$\rightarrow \leftarrow \delta_{11} = \int y^2 \frac{ds}{EI} + \frac{L}{A_t E} \tag{9.38}$$

The expression for $\Delta_{1,0}$ does not change. Then, the tension in the tie is given by:

$$X_1 = \frac{-\Delta_{1,0}}{\delta_{11}} = \frac{\int y(M_0 ds/EI)}{\left(\int y^2 (ds/EI) \right) + (L/A_t E)} \tag{9.39}$$

Note that the horizontal reaction is reduced by inserting a tie member. However, now there is bending in the arch.

Fig. 9.30 Choice of redundant



Example 9.14

Given: A parabolic arch with a tension tie connecting the supports. The arch is loaded with a uniformly distributed load per horizontal projection. Consider I to be defined as $\frac{I_0}{\cos \theta}$.

Determine: The horizontal thrust and the bending moment at mid-span (Fig. E9.14a).

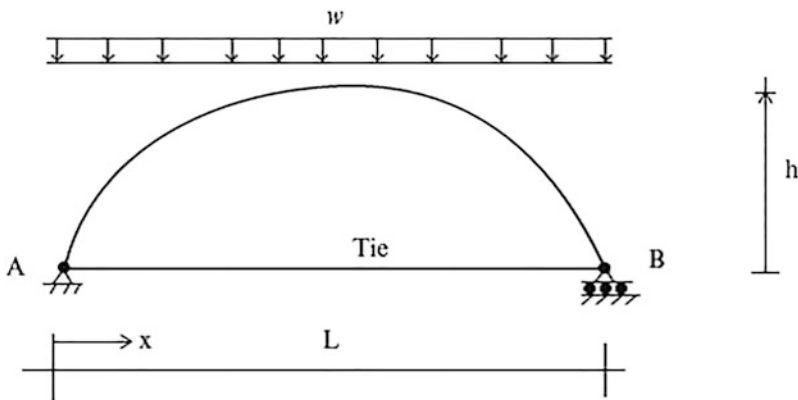


Fig. E9.14a

Solution: We note the results generated in Example 9.12 which correspond to taking $I = \frac{I_0}{\cos \theta}$.

$$\begin{aligned} \Delta_{1,0} &= - \int y M_0 \frac{ds}{EI} = - \frac{1}{EI_0} \int_0^L y M_0 dx \\ &= - \frac{1}{EI_0} \left(\frac{wL^2}{8h} \right) \int_0^L y^2 dx \\ &= - \frac{1}{EI_0} \left(\frac{8}{15} h^2 L \right) \left(\frac{wL^2}{8h} \right) = - \frac{whL^3}{15EI_0} \\ \delta_{11} &= \frac{L}{AE} + \frac{8}{15} \frac{h^2 L}{EI_0} \end{aligned}$$

The tension in the tie is

$$X_1 = \frac{-\Delta_{1,0}}{\delta_{11}} = \frac{wL^2}{8h} \frac{1}{\left(1 + (15/8)(I_0/Ah^2)\right)}$$

Using this value, we determine the moment at mid-span.

$$\begin{aligned} M\left(\frac{L}{2}\right) &= M_0 - hX_1 \\ &= \frac{wL^2}{8} \left\{ 1 - \frac{1}{\left(1 + (15/8)(I_0/Ah^2)\right)} \right\} \\ M\left(\frac{L}{2}\right) &= \frac{wL^2}{8} \left\{ \frac{(15/8)(I_0/Ah^2)}{\left(1 + (15/8)(I_0/Ah^2)\right)} \right\} = \frac{wL^2}{8} \left\{ \frac{1}{\left(1 + (8/15)(Ah^2/I_0)\right)} \right\} \end{aligned}$$

Note that the effect of the tension tie is to introduce bending in the arch.

9.5 Application to Frame-Type Structures

Chapter 4 dealt with statically determinate frames. We focused mainly on three-hinge frames since this type of structure provides an efficient solution for enclosing a space. In this section, we analyze indeterminate frames with the force method. In the next chapter, we apply the displacement method. The analytical results generated provide the basis for comparing the structural response of determinate vs. indeterminate frames under typical loadings.

9.5.1 General Approach

We consider the arbitrary-shaped single bay frame structure shown in Fig. 9.31. The structure is indeterminate to the first degree. We select the horizontal reaction at the right support as the force redundant. The corresponding compatibility equation is

$$\Delta_{1,0} + \delta_{11}X_1 = \Delta_1$$

where Δ_1 is the horizontal support movement at D.

We compute δ_{11} and $\Delta_{1,0}$ with the Principle of the Virtual Forces described in Sect. 4.6. The corresponding form for a plane frame specialized for negligible transverse deformation is given by (4.8)

Fig. 9.31 (a) Actual structure. (b) Primary structure—redundant reaction

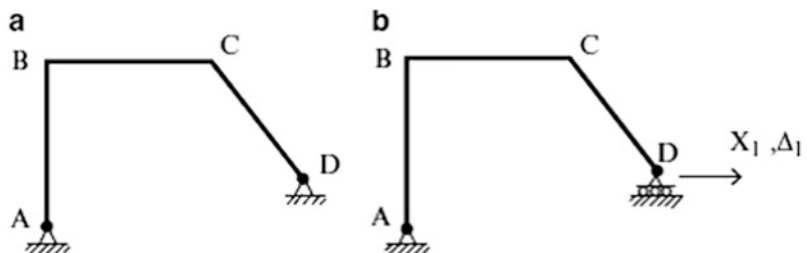
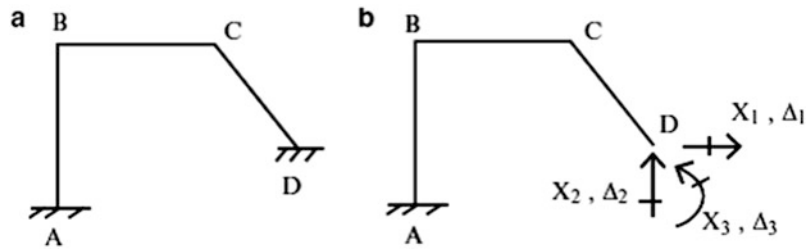


Fig. 9.32 (a) Actual structure. (b) Primary structure—redundant reactions



$$d\delta P = \sum_{\text{members}} \int_s \left\{ \left(\frac{M}{EI} \right) M + \left(\frac{F}{AE} \right) \delta F \right\} ds$$

Axial deformation is small for typical non-shallow frames and therefore is usually neglected. The δ_{11} term is the horizontal displacement due to a horizontal unit load at D. This term depends on the geometry and member properties, not on the external loads, and therefore has to be computed only once. The $\Delta_{1,0}$ term is the horizontal displacement due to the external loading and needs to be evaluated for each loading. Different loading conditions are treated by determining the corresponding values of $\Delta_{1,0}$. Given these displacement terms, one determines X_1 with

$$X_1 = -\frac{\Delta_{1,0}}{\delta_{11}}$$

Consider the frame shown in Fig. 9.32. Now there are three force redundant and three geometric compatibility conditions represented by the matrix equation (see (9.11)),

$$\underline{\Delta}|_{\text{primary structure}} = \underline{\Delta}_0 + \underline{\delta}\underline{X}$$

The flexibility matrix $\underline{\delta}$ is independent of the loading, i.e., it is a property of the primary structure. Most of the computational effort is involved with computing $\underline{\delta}$ and $\underline{\Delta}_0$ numerically. The integration can be tedious. Sometimes numerical integration is used. However, one still has to generate the moment and axial force diagrams numerically.

If the structure is symmetrical, one can reduce the computational effort by working with simplified structural models and decomposing the loading into symmetrical and anti-symmetrical components. It is very useful for estimating, in a qualitative sense, the structural response. We discussed this strategy in Chap. 3.

In what follows, we list results for different types of frames. Our primary objective is to show how these structures respond to typical loadings. We use moment diagrams and displacement profiles as the measure of the response.

9.5.2 Portal Frames

We consider the frame shown in Fig. 9.33a. We select the horizontal reaction at D as the force redundant.

The corresponding flexibility coefficient, δ_{11} , is determined with the Principle of Virtual Forces (see Chap. 4).

Fig. 9.33 Portal Frame.
 (a) Geometry.
 (b) Redundant.
 (c) Reactions due to $X_1 = 1$

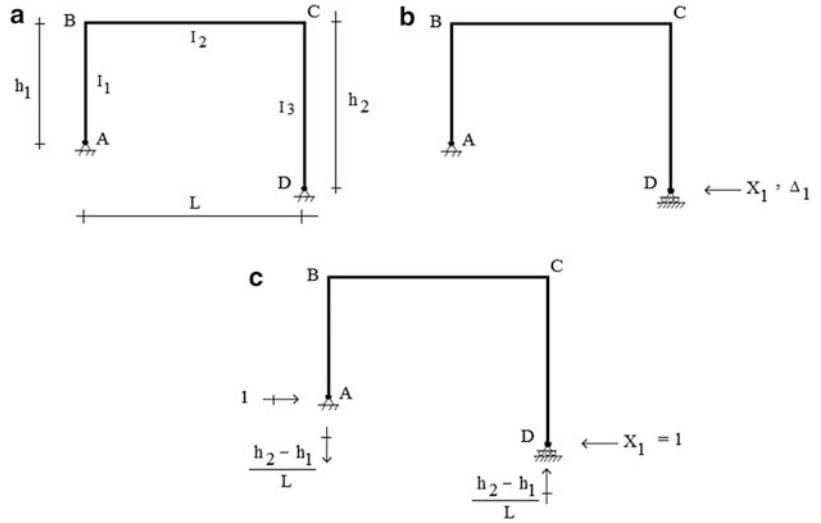
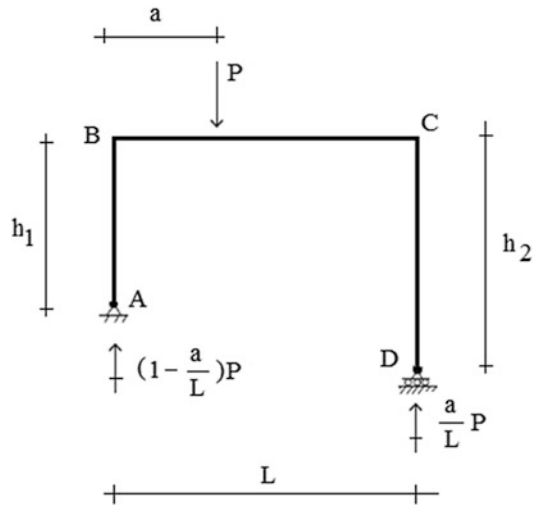


Fig. 9.34 Reactions—gravity loading

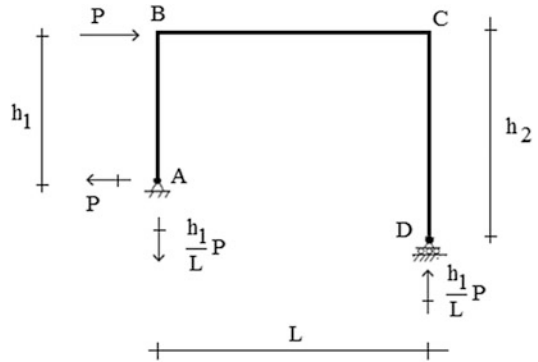


$$\delta_{11} = \frac{h_1^3}{3EI_1} + \frac{h_2^3}{3EI_3} + \frac{L}{3EI_2} \{h_1^2 + h_2^2 + h_1h_2\} \tag{9.40}$$

This coefficient applies for all loading. Considering the arbitrary gravity loading shown in Fig. 9.34, the expression for the displacement, $\Delta_{1,0}$, is determined in a similar way.

$$\Delta_{1,0}|_{\text{gravity}} = -\frac{Pa(L-a)}{2EI_2L} \{(L-a)h_2 + ah_1\} + \frac{Pa(h_2-h_1)}{3EI_2L} (L^2 + 2a^2 - 3aL) \tag{9.41}$$

Fig. 9.35 Reactions—
lateral loading



Lastly, we consider the lateral loading shown in Fig. 9.35. The displacement term due to loading is

$$\Delta_{1,0}|_{\text{lateral}} = -\frac{1}{EI_1} \left\{ \frac{Ph_1^3}{3} \right\} + \frac{1}{EI_2} \left\{ \frac{Ph_1L}{3} \left(\frac{h_2}{2} + h_1 \right) \right\} \quad (9.42)$$

When $h_2 = h_1 = h$ and $I_2 = I_1 = I$, these expressions simplify to

$$\begin{aligned} \delta_{11} &= \frac{2h^3}{3EI} + \frac{L}{EI}(h^2) \\ \Delta_{1,0}|_{\text{gravity}} &= -\frac{Ph}{2EI}(a)(L-a) \\ \Delta_{1,0}|_{\text{lateral}} &= -\frac{Ph^3}{3EI} - \frac{Ph^2L}{2EI} \end{aligned} \quad (9.43)$$

Gravity loading:

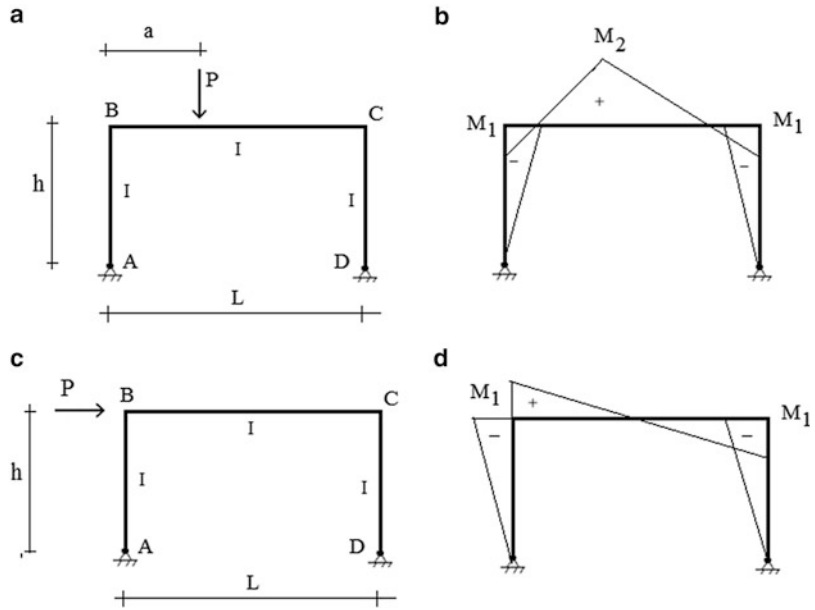
$$\begin{aligned} X_1|_{\text{gravity}} &= \left(\frac{PL}{2h} \right) \frac{(a/L)(1-(a/L))}{1+(2/3)(h/L)} \\ M_1|_{\text{gravity}} &= hX_1|_{\text{gravity}} \\ M_2|_{\text{gravity}} &= a \left(1 - \frac{a}{L} \right) P - M_1|_{\text{gravity}} \end{aligned}$$

Lateral loading:

$$\begin{aligned} X_1|_{\text{lateral}} &= \frac{P}{2} \\ M_1|_{\text{lateral}} &= hX_1|_{\text{lateral}} \end{aligned}$$

The corresponding bending moment diagrams for these two loading cases are shown in Fig. 9.36.

Fig. 9.36 Two-hinged frame (a) Gravity loading. (b) Moment diagram. (c) Lateral loading. (d) Moment diagram

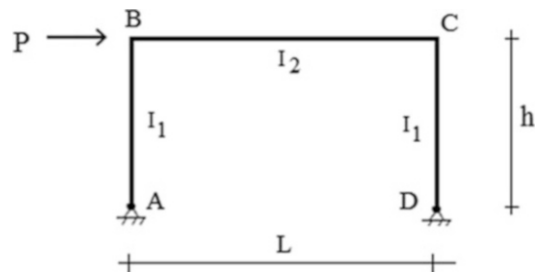


9.5.2.1 Lateral-Loading Symmetrical Portal Frame

We consider first the two-hinged symmetrical frame shown in Fig. 9.37. This structure is indeterminate to the first degree. We decompose the loading into symmetrical and anti-symmetrical components and generate the corresponding symmetrical and anti-symmetrical structural modes using the material presented in Sect. 3.9. These results are shown in Fig. 9.38b. Point E is at mid-span. The anti-symmetrical model is statically determinate since the bending moment at mid-span must equal zero for anti-symmetrical behavior (Fig. 9.38c).

The symmetrical loading introduces no bending in the structure, only axial force in member BE. The bending moment distribution due to the anti-symmetrical component is plotted in Fig. 9.39.

Fig. 9.37 Geometry of two-hinged portal frame



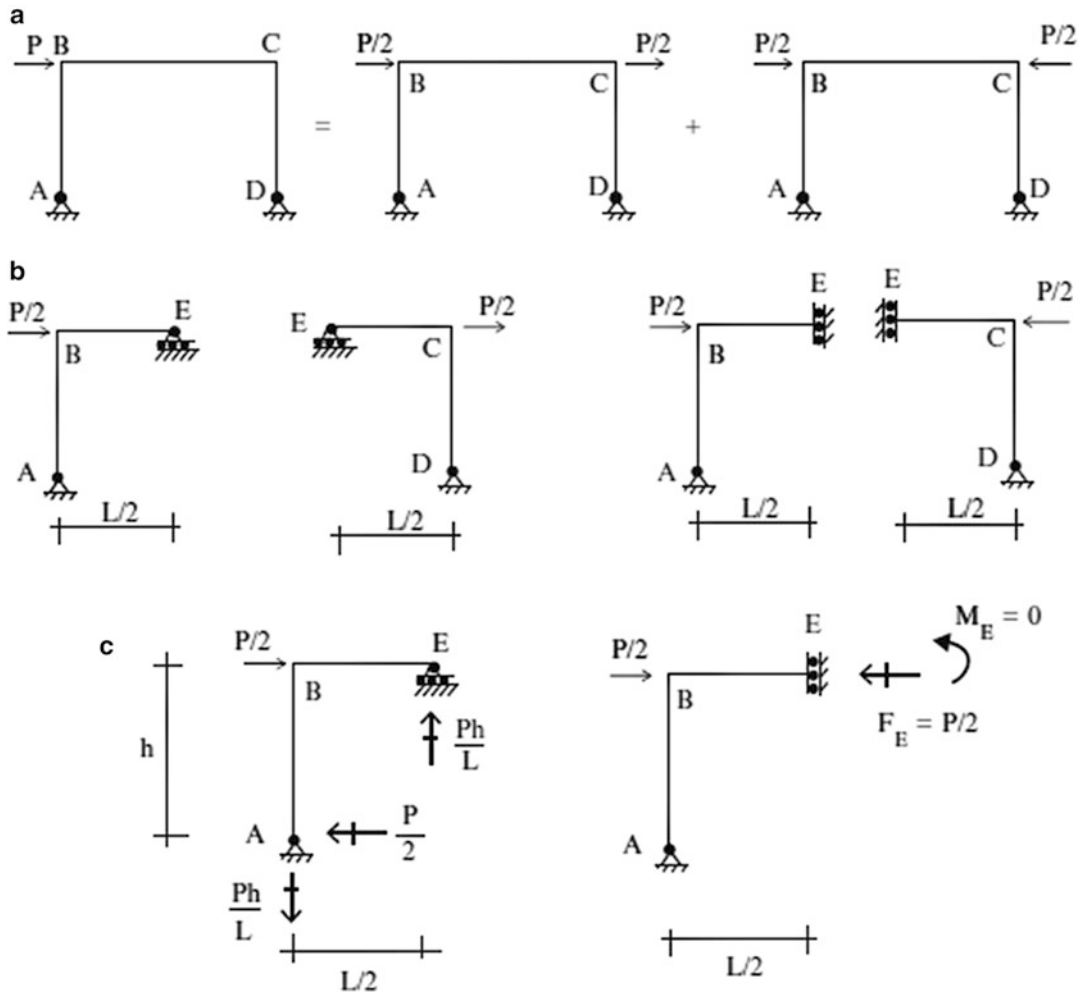
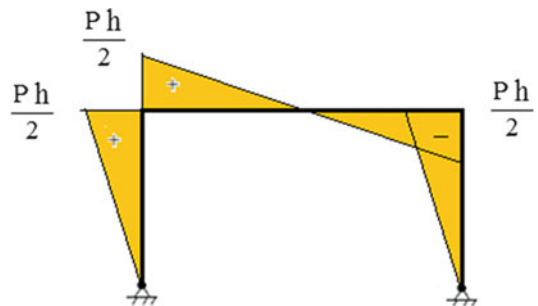


Fig. 9.38 Structural models. (a) Decomposition into anti-symmetrical and symmetrical loadings. (b) Anti-symmetrical and symmetrical models. (c) Free body diagrams of anti-symmetrical and symmetrical segments

Fig. 9.39 Bending moment distribution due to the anti-symmetrical lateral loading



9.5.2.2 Gravity-Loading Symmetrical Portal Frame

We consider next the case of gravity loading applied to a two-hinged portal frame. Figure 9.40a defines the loading and geometry. Again, we decompose the loading and treat separately the two loading cases shown in Fig. 9.40b.

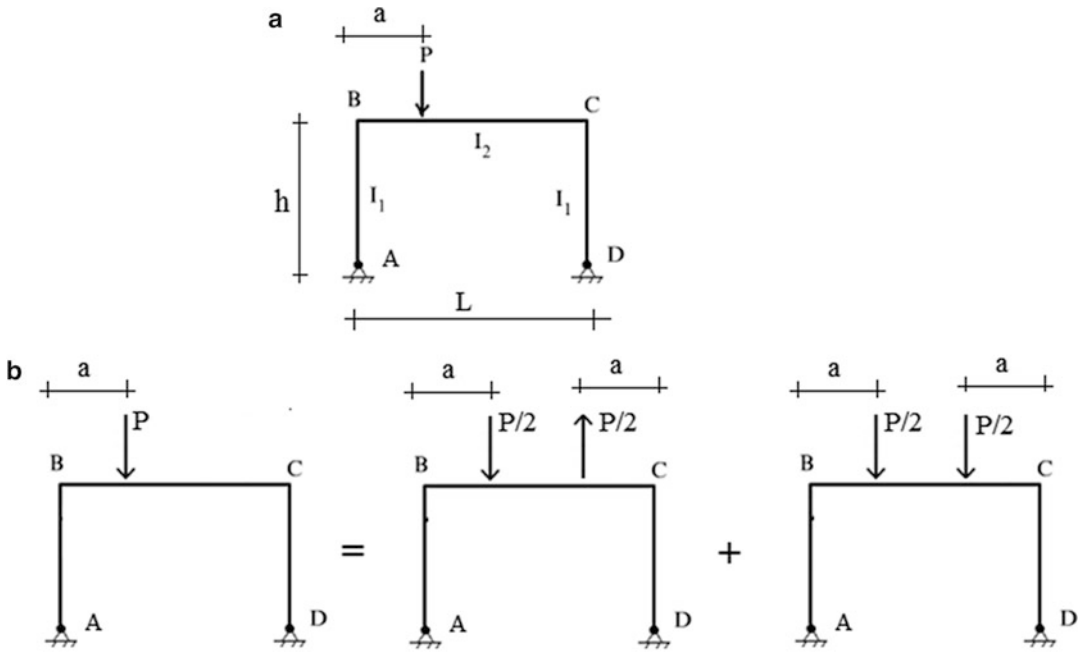


Fig. 9.40 (a) Two-hinged frame under gravity loading. (b) Decomposition of loading into symmetrical and anti-symmetrical components

Geometry and Loading

The anti-symmetrical model is statically determinate. Figure 9.41 shows the model, the corresponding free body diagram and the bending moment distribution.

The symmetrical model is statically indeterminate to one degree. We take the horizontal reaction at the right support as the force redundant and work with the primary structure shown in Fig. 9.42.

Assuming unyielding supports, the compatibility equation has the following form

$$\Delta_{D,0} + \delta_{DD}H_D = 0$$

where $\Delta_{D,0}$ and δ_{DD} are the horizontal displacements at D due to the applied loading and a unit value of H_D . We use the Principle of Virtual Forces specialized for only bending deformation to evaluate these terms. The corresponding expressions are

$$\begin{aligned} \Delta_{D,0} &= \int M_0 \delta M \frac{dS}{EI} \\ \delta_{DD} &= \int_S (\delta M)^2 \frac{dS}{EI} \end{aligned} \tag{9.44}$$

Fig. 9.41 (a) Anti-symmetrical model. (b) Free body diagram—anti-symmetrical segment. (c) Bending moment distribution—anti-symmetrical loading

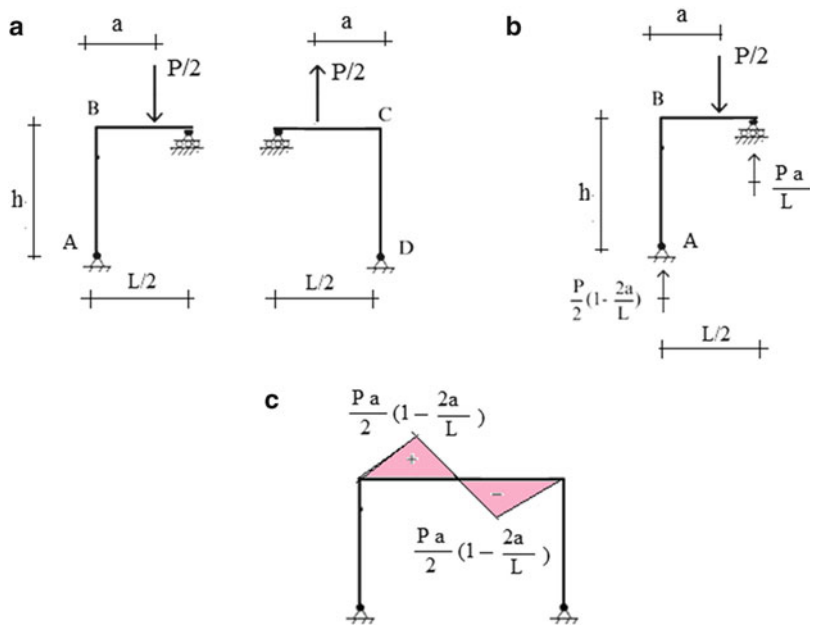
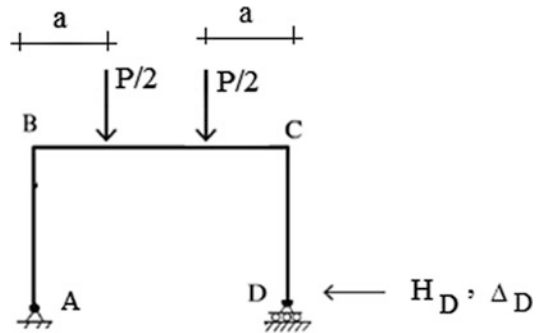


Fig. 9.42 Primary structure for two-hinged frame—symmetrical loading case



where M_0 is the moment due to the applied loading and δM is the moment due to a unit value of H_D . These moment distributions are plotted in Fig. 9.43.

Evaluating the integrals leads to:

$$\begin{aligned} \Delta_{B,0} &= -\frac{P}{2} \frac{ha}{EI_2} (L - a) \\ \delta_{BB} &= \frac{2h^3}{3EI_1} + \frac{h^2L}{EI_2} \end{aligned} \tag{9.45}$$

Finally, the horizontal reaction at support D is

$$H_D = P \frac{a(L - a)}{2hL} \left[\frac{1}{1 + (2/3)(r_g/r_c)} \right] \tag{9.46}$$

where

Fig. 9.43 Bending moment distributions—symmetrical loading—primary structure

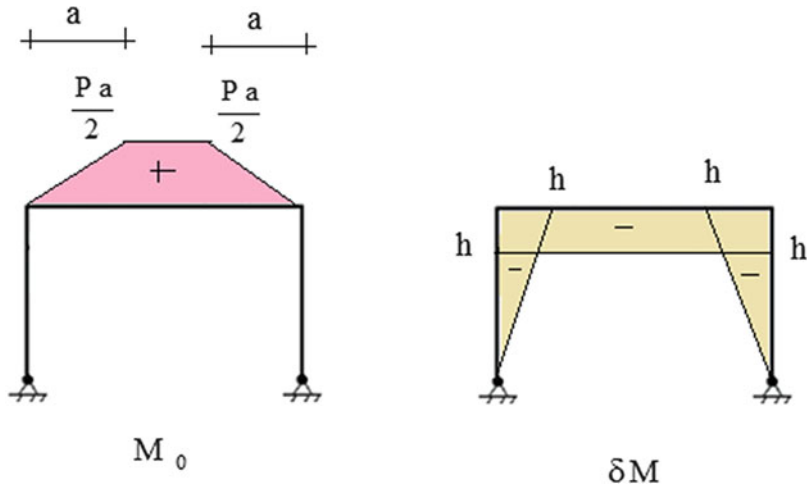
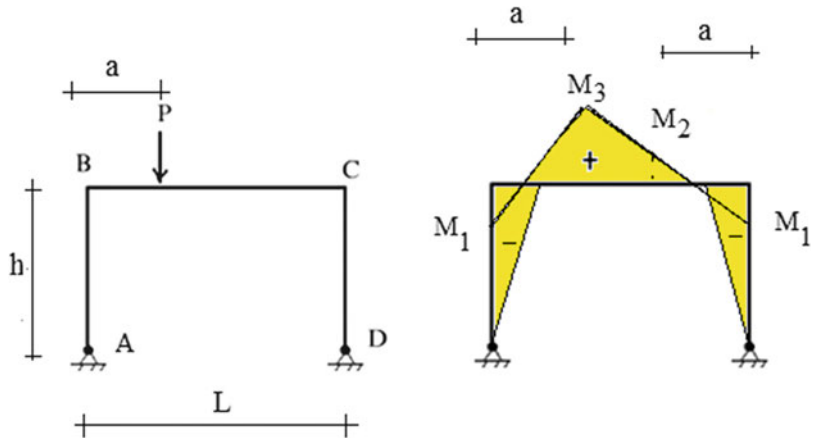


Fig. 9.44 Final bending moment distribution



$$r_c = \frac{I_1}{h} \quad r_g = \frac{I_2}{L} \tag{9.47}$$

are the relative stiffness factors for the column and girder members.

Combining the results for the symmetrical and anti-symmetrical loadings results in the net bending moment distribution plotted in Fig. 9.44. The peak moments are defined by (9.48).

$$\begin{aligned} M_1 &= -\frac{Pa}{2} \left(1 - \frac{a}{L}\right) \frac{1}{1 + (2/3)(r_g/r_c)} \\ M_2 &= +\frac{Pa}{2} \left[\frac{(a/L) + (2/3)(r_g/r_c)}{1 + (2/3)(r_g/r_c)} \right] - \frac{Pa}{2} \left(1 - \frac{2a}{L}\right) \\ M_3 &= +\frac{Pa}{2} \left[\frac{(a/L) + (2/3)(r_g/r_c)}{1 + (2/3)(r_g/r_c)} \right] + \frac{Pa}{2} \left(1 - \frac{2a}{L}\right) \end{aligned} \tag{9.48}$$

Example 9.15 Two-Hinged Symmetrical Frame—Uniform Gravity Load

Given: The frame and loading defined in Fig. E9.15a.

Determine: The bending moment distribution.

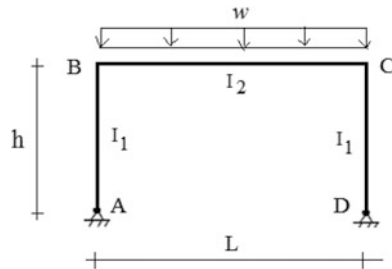


Fig. E9.15a

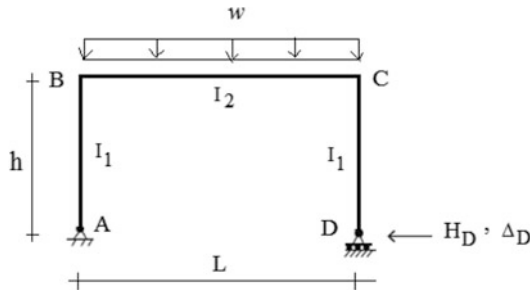


Fig. E9.15b

Solution: We work with the primary structure shown in Fig. E9.15b. We only need to determine the $\Delta_{D,0}$ term corresponding to the uniform loading since the δ_{DD} term is independent of the applied loading. The solution for H_D is

$$H_D = \frac{wL^2}{12h} \frac{1}{1 + (2/3)(r_g/r_c)}$$

where

$$r_g = \frac{I_2}{L}$$

$$r_c = \frac{I_1}{h}$$

Figure E9.15c shows the bending moment distribution. The peak values are

$$M_1 = \frac{wL^2}{12} \frac{1}{1 + (2/3)(r_g/r_c)}$$

$$M_2 = \frac{wL^2}{8} \left[1 - \frac{2}{3} \frac{1}{1 + (2/3)(r_g/r_c)} \right]$$

When members AB and CD are very stiff, $r_c \rightarrow \infty$ and $H_D \rightarrow wL^2/12h$. In this case, the moment at B approaches $wL^2/12$ which is the fixed end moment for member BC.

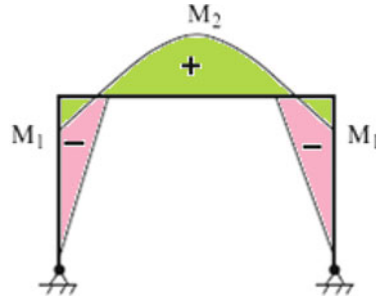


Fig. E9.15c Bending moment distribution

9.5.2.3 Symmetrical Portal Frames with Fixed Supports

We consider the symmetrical frame shown in Fig. 9.45. Because the structure is symmetrical, we consider the loading to consist of symmetrical and anti-symmetrical components. The structure is indeterminate to the second degree for symmetrical loading and to the first degree for anti-symmetrical loading (there is zero moment at mid-span which is equivalent to a hinge at that point). Figure 9.45b defines the structures corresponding to these two loading cases.

Fig. 9.45 (a) Geometry. (b) Decomposition into symmetrical and anti-symmetrical loadings

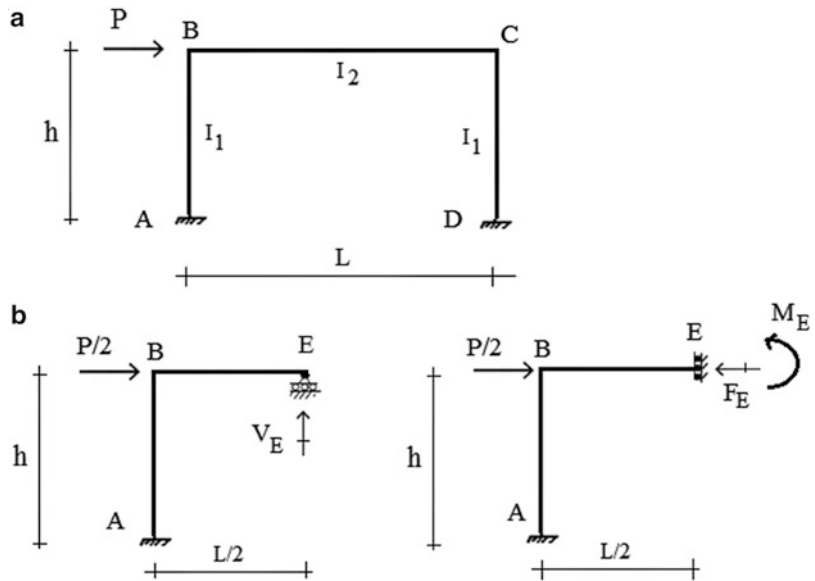
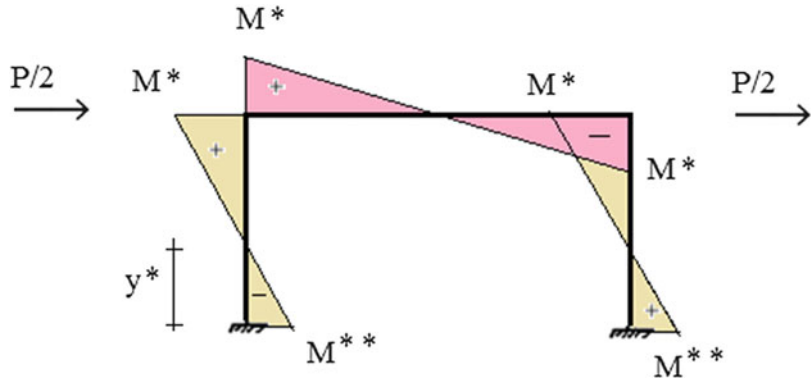


Fig. 9.46 Bending moment distribution—anti-symmetric loading



Evaluating the various displacement terms for the anti-symmetrical loading, one obtains:

$$\Delta_{E,0} = -\frac{PLh^2}{8EI_1}$$

$$\delta_{EE} = \frac{L^3}{24EI_2} + \frac{L^2h}{4EI_1}$$

$$V_E = \frac{-\Delta_{E,0}}{\delta_{EE}} = \left(\frac{Ph}{2L}\right) \frac{1}{\left(1 + (1/6)(L/I_2)(I_1/h)\right)}$$

The moment diagrams are plotted in Fig. 9.46. The peak values are

$$M^* = \pm \frac{Ph}{4} \frac{1}{1 + (1/6)(r_c/r_g)}$$

$$M^{**} = \pm \frac{Ph}{2} \left[-1 + \frac{1}{2(1 + (1/6)(r_c/r_g))} \right] \tag{9.49}$$

$$r_c = \frac{I_1}{h} \quad r_g = \frac{I_2}{L}$$

There are inflection points located in the columns at y^* units up from the base where

$$y^* = h \left[1 - \frac{1}{2} \frac{1}{1 + (1/6)(r_c/r_g)} \right] \tag{9.50}$$

When the girder is very stiff relative to the column, $r_c/r_g \rightarrow 0$ and $y^* \rightarrow h/2$. A reasonable approximation for y^* for typical column and girder properties is $\approx 0.6 h$.

Figure 9.47 shows the corresponding bending moment distribution for the two-hinged portal frame. We note that the peak positive moment is reduced approximately 50 % when the supports are fixed.

We consider next the case where the girder is uniformly loaded. We skip the intermediate details and just list the end moments for member AB and the moment at mid-span (Fig. 9.48).

Fig. 9.47 Moment distribution for two-hinged frame

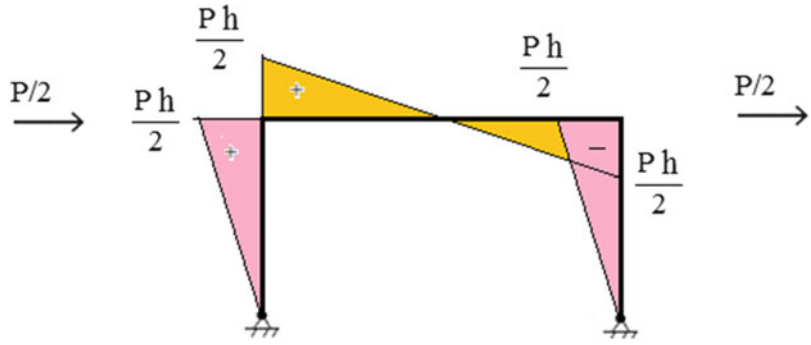
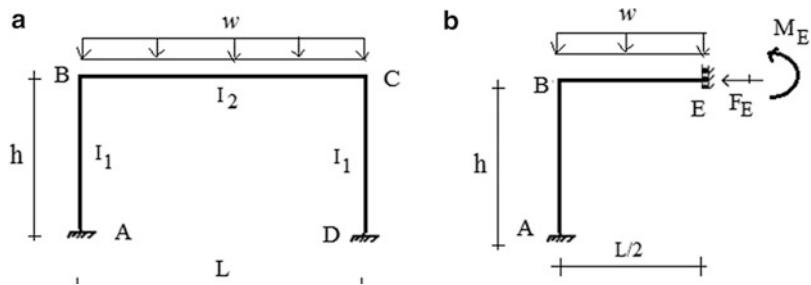


Fig. 9.48 (a) Portal frame with fixed supports under gravity loading. (b) Moment at mid-span



$$M_{BA} = -\frac{wL^2}{12} \frac{1}{1 + (1/2)(r_g/r_c)}$$

$$M_{AB} = \frac{1}{2}M_{BA} \tag{9.51}$$

$$M_E = \frac{wL^2}{8} \left[1 - \frac{2}{3} \frac{1}{1 + (1/2)(r_g/r_c)} \right]$$

The bending moment distribution is plotted in Fig. 9.49. The solution for the two-hinged case is shown in Fig. 9.50. These results show that the bending moment distribution is relatively insensitive to end fixity of the base.

$$M_2 = M_E \frac{1 - \frac{2/3}{1 + 2/3(r_g/r_c)}}{1 - \frac{2/3}{1 + 1/2(r_g/r_c)}} = \frac{wL^2}{8} \left(1 - \frac{(2/3)}{1 + 2/3(r_g/r_c)} \right) \tag{9.52}$$

$$M_1 = M_{BA} \frac{1 + 1/2(r_g/r_c)}{1 + 2/3(r_g/r_c)} = -\frac{wL^2}{12} \left(\frac{1}{1 + 2/3(r_g/r_c)} \right)$$

Fig. 9.49 Bending moment distribution—symmetrical loading—fixed supports

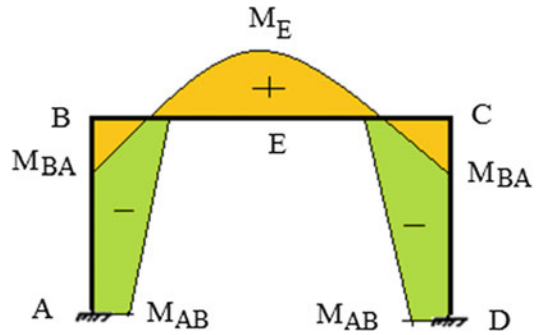
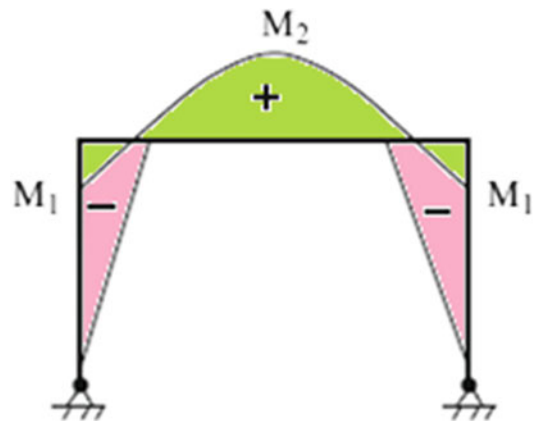


Fig. 9.50 Bending moment distribution—symmetrical loading—hinged supports



9.5.3 Pitched Roof Frames

We consider next a class of portal frames where the roof is pitched, as shown in Fig. 9.51a. We choose to work with the primary structure defined in Fig. 9.51b.

We suppose the structure is subjected to a uniform load per horizontal projection on members BC and CD. The bending moment distribution in the primary structure due to the applied loading, M_0 , is parabolic with a peak value at C (Fig. 9.52). Taking $H_E = 1$ leads to the bending moment distribution shown in Fig. 9.53. It is composed of linear segments.

Assuming the supports are unyielding, the flexibility coefficients are

$$\begin{aligned} \Delta_{E,0} &= -\frac{wL^3}{12 \cos \theta} \left\{ h_1 + \frac{5}{8}h_2 \right\} \frac{1}{EI_2} \\ \delta_{EE} &= \frac{2}{3} \frac{h_1^3}{EI_1} + \frac{L}{EI_2 \cos \theta} \left\{ h_1^2 + h_1h_2 + \frac{h_2^2}{3} \right\} \end{aligned} \tag{9.53}$$

We define the relative stiffness factors as

$$r_1 = \frac{I_1}{h_1} \quad r_2^* = \frac{I_2}{L^*} \tag{9.54}$$

where L^* is the length of the inclined roof members BC and CD.

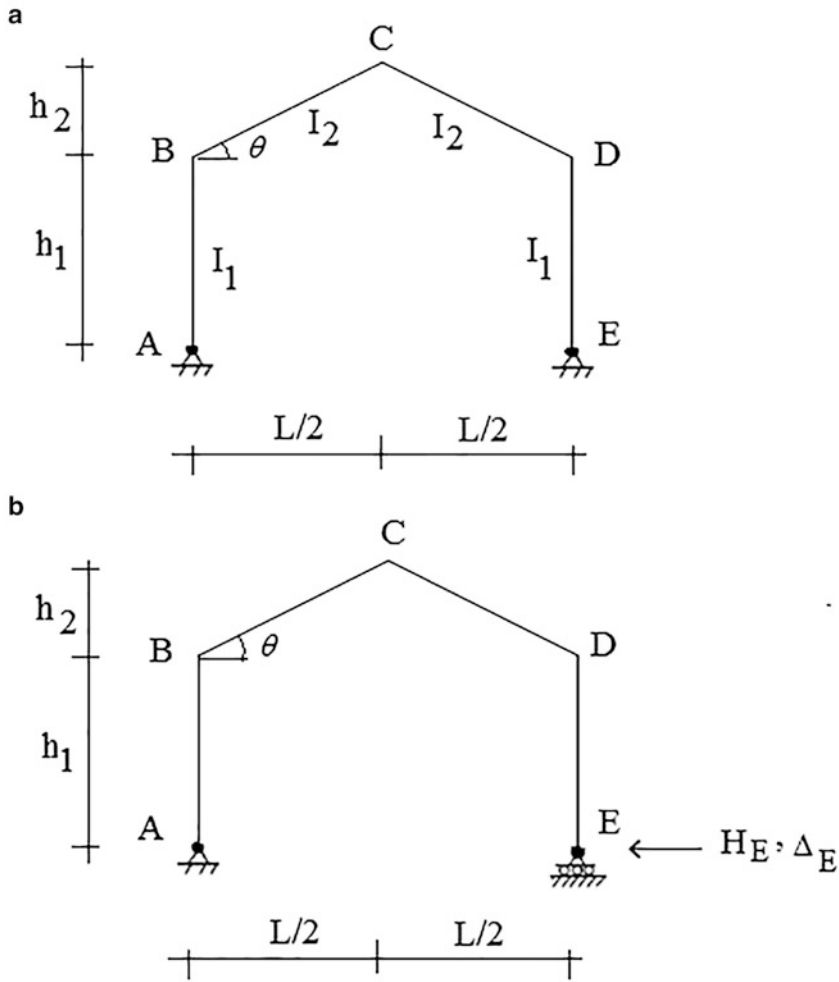


Fig. 9.51 (a) Pitched roof frame—definition sketch. (b) Primary structure—redundant reaction

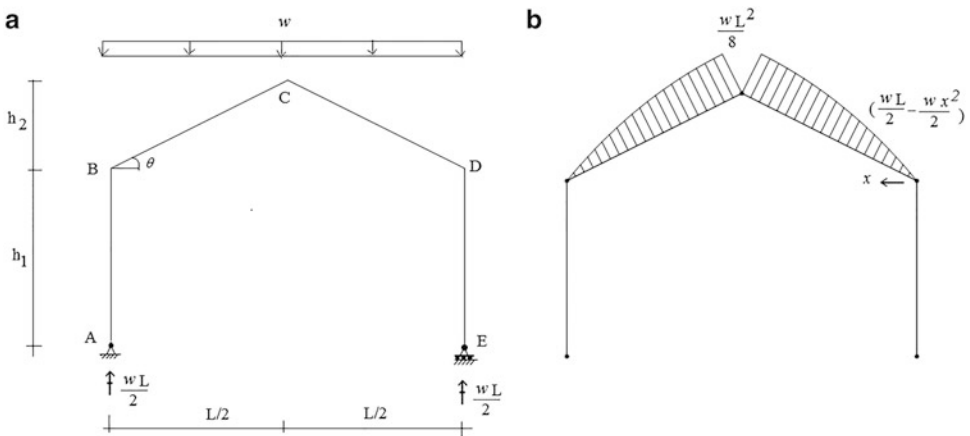


Fig. 9.52 (a) Primary structure-external loading. (b) Bending moment distribution for applied loading, M_0

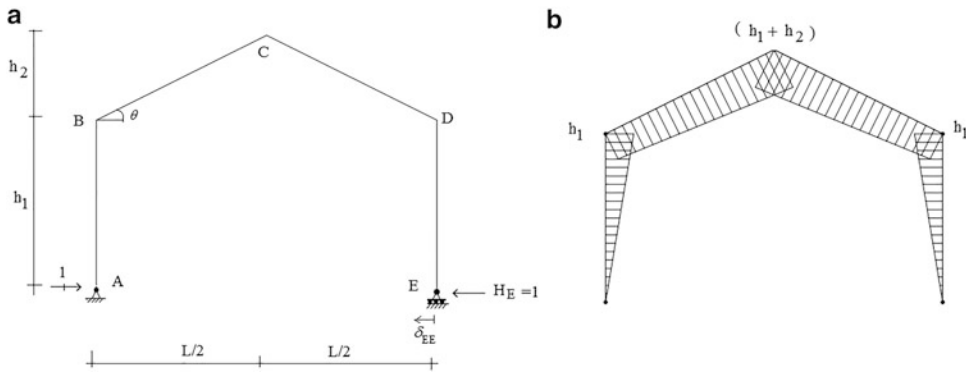
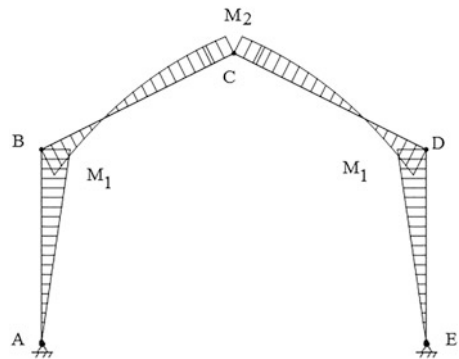


Fig. 9.53 (a) Primary structure-unit load. (b) Bending moment distribution for $H_E = 1$

Fig. 9.54 Distribution of total bending moments



$$L^* = \frac{L}{2 \cos \theta} \tag{9.55}$$

Using this notation, the expression for the horizontal reaction at E takes the form

$$H_E = \frac{wL^2}{12h_1} \frac{1 + (5/8)(h_2/h_1)}{(1/3)(r_2^*/r_1) + 1 + (h_2/h_1) + (1/3)(h_2/h_1)^2} \tag{9.56}$$

The total bending moment distribution is plotted in Fig. 9.54. Equation (9.57) contains the expressions for the peak values.

$$\begin{aligned} M_1 &= -\frac{wL^2}{12} a_1 \\ M_2 &= +\frac{wL^2}{8} a_2 \end{aligned} \tag{9.57}$$

where

$$\begin{aligned} a_1 &= \frac{1 + (5/8)(h_2/h_1)}{(1/3)(r_2^*/r_1) + 1 + (h_2/h_1) + (1/3)(h_2/h_1)^2} \\ a_2 &= 1 - \frac{2}{3} \left(1 + \frac{h_2}{h_1} \right) a_1 \end{aligned} \tag{9.58}$$

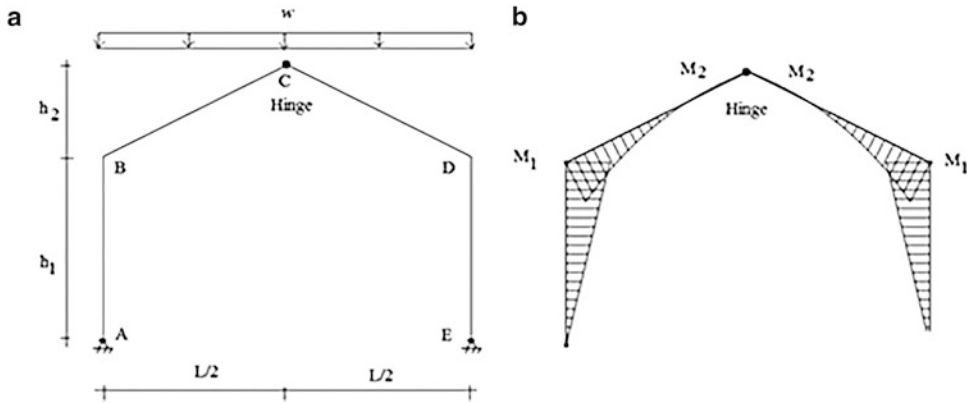


Fig. 9.55 Three-hinge solution. (a) Loading. (b) Bending moment distribution

These values depend on the ratio of heights h_2/h_1 and relative stiffness, r_2^*/r_1 . One sets $h_2 = 0$ and $r_2^* = 2r_2$ to obtain the corresponding two-hinged portal frame solution. For convenience, we list here the relevant solution for the three-hinge case, with the notation modified to be consistent with the notation used in this section. The corresponding moment distributions are shown in Fig. 9.55.

The peak negative and positive moments are

$$M_1 = \frac{wL^2}{8} \frac{h_1}{(h_1 + h_2)} \quad (9.59)$$

$$M_2 = \frac{wL^2}{8} \left\{ \frac{1}{4} - \frac{1}{2} \frac{h_1}{h_1 + h_2} + \frac{1}{4} \left(\frac{h_1}{h_1 + h_2} \right)^2 \right\}$$

In order to compare the solutions, we assume $r_2^* = r_1$, and $h_2 = h_1$ in the definition equations for the peak moments. The resulting peak values are

Three-hinge case (9.59):

$$M_1 = -\frac{wL^2}{8} \left(\frac{1}{2} \right)$$

$$M_2 = +\frac{wL^2}{8} \left(\frac{1}{16} \right)$$

Two-hinge case (9.57):

$$M_1 = -\frac{wL^2}{8} \left(\frac{13}{32} \right) = -\frac{wL^2}{8} (0.406)$$

$$M_2 = +\frac{wL^2}{8} \left(\frac{3}{16} \right)$$

We see that the peak negative moment is reduced by approximately 20 % when the structure is reduced to a two-hinged frame. However, the positive moment is increased by a factor of 3.

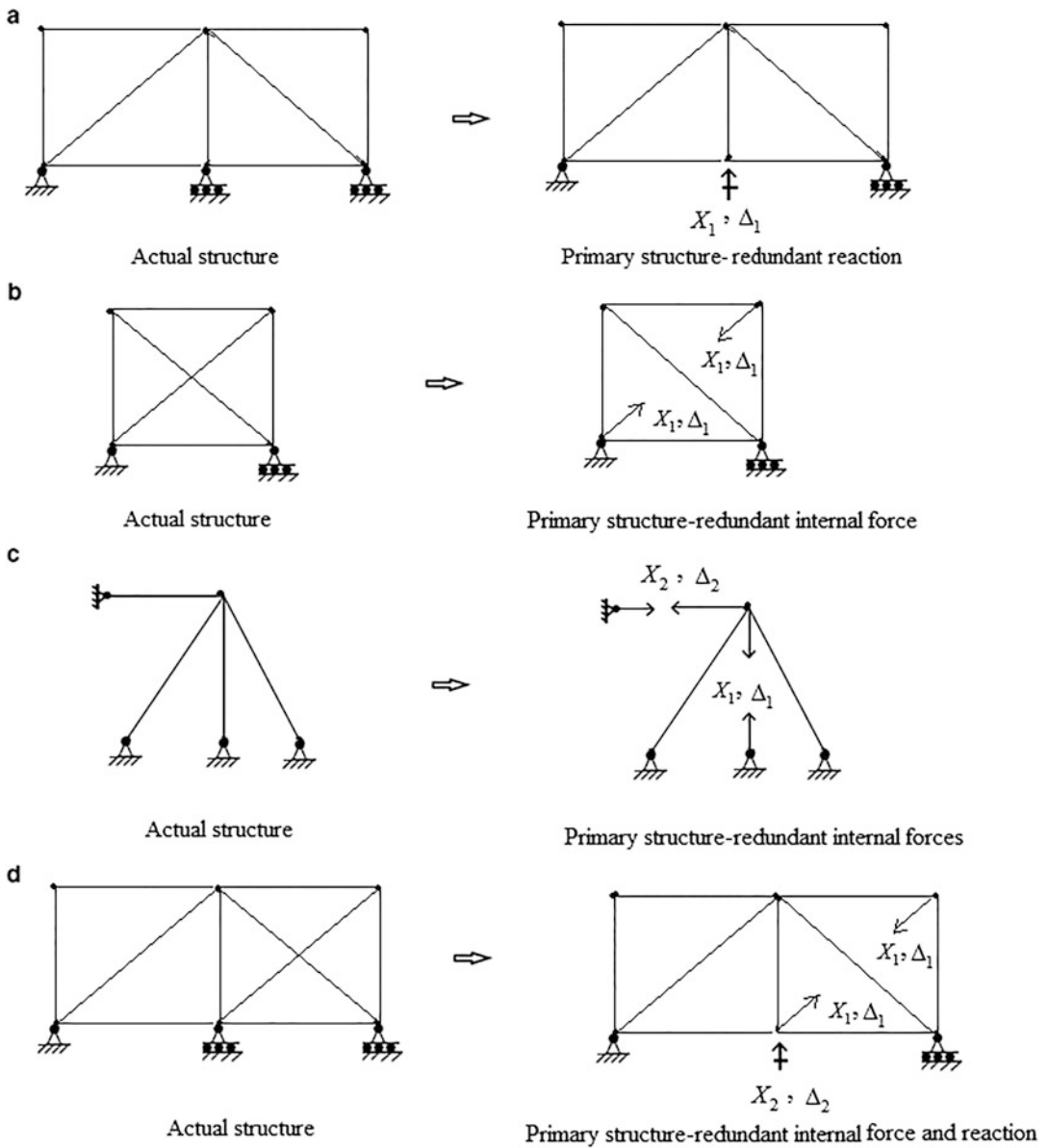


Fig. 9.56 Examples of statically indeterminate trusses

9.6 Indeterminate Trusses

Examples of indeterminate truss structures are shown in Fig. 9.56. One can choose a primary structure by taking either reactions or member forces or a combination as the force redundants. When working with member forces, one visualizes the member as being cut and works with the relative displacement of the adjacent faces. Continuity requires that the net relative displacement is zero.

We illustrate the Force Method procedure for the three-member truss shown in Fig. 9.57a. The truss is indeterminate to the first degree. The force in member BC is taken as the force redundant and

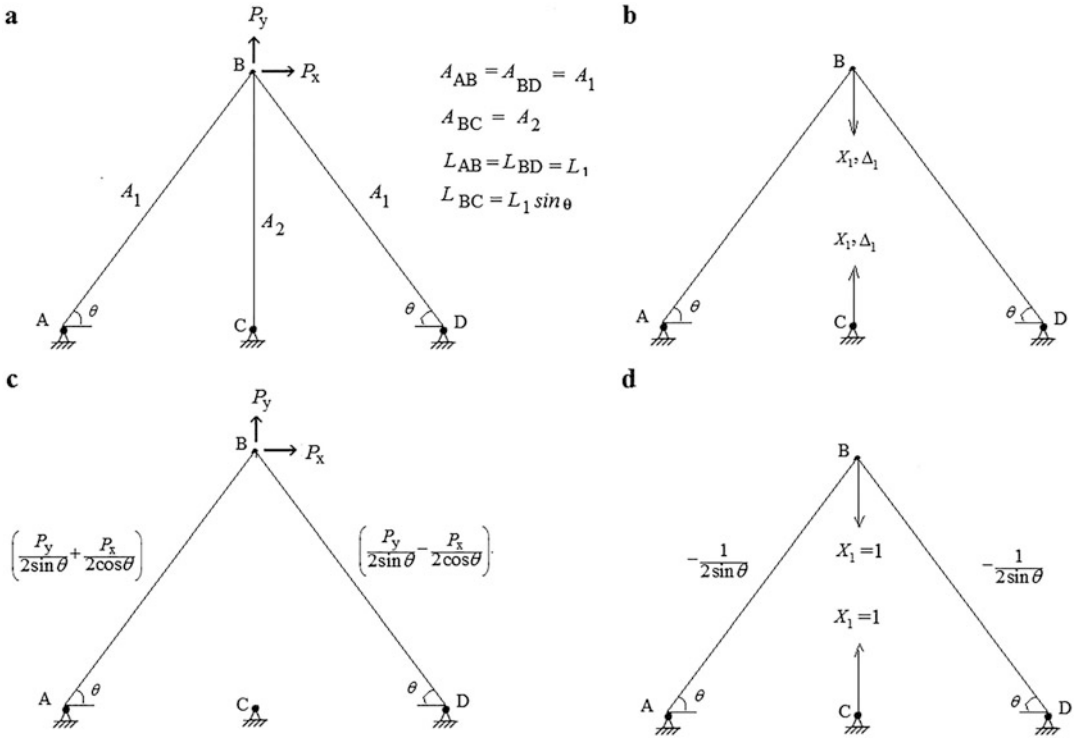


Fig. 9.57 (a) Three-member truss. (b) Primary structure—redundant internal force. (c) F_0 . (d) $\delta F(X_1 = 1)$

Δ_1 is the relative displacement together at the end sections. Two deflection computations are required, one due to the external loads and the other due to $X_1 = 1$. We use the Principle of Virtual Forces discussed in Sect. 2.3.4 for these computations. Results are summarized below.

Displacement due to external loads:

$$\begin{aligned} \Delta_{1,0} &= \sum \left(\frac{F_0 L}{AE} \right) \delta F \\ &= -\frac{1}{2\sin\theta} \left(\frac{P_y}{2\sin\theta} + \frac{P_x}{2\cos\theta} \right) \frac{L_1}{A_1 E} + \left(-\frac{1}{2\sin\theta} \right) \left(\frac{P_y}{2\sin\theta} - \frac{P_x}{2\cos\theta} \right) \frac{L_1}{A_1 E} \\ &= -\frac{P_y}{2\sin^2\theta} \frac{L_1}{A_1 E} \end{aligned}$$

Displacement due to $X_1 = 1$:

$$\begin{aligned} \delta_{11} &= \sum (\delta F)^2 \frac{L}{AE} \\ &= \frac{1}{4\sin^2\theta} \frac{L_1}{A_1 E} + \frac{L_1 \sin\theta}{A_2 E} + \frac{1}{4\sin^2\theta} \frac{L_1}{A_1 E} = \frac{1}{2\sin^2\theta} \frac{L_1}{A_1 E} + \frac{L_1 \sin\theta}{A_2 E} \end{aligned}$$

Enforcing compatibility (9.3) leads to

$$\Delta_{1,0} + \delta_{11} X_1 = 0$$

$$\begin{aligned}
 F_{BC} = X_1 &= -\frac{\Delta_{1,0}}{\delta_{11}} = \frac{(P_y/2 \sin^2\theta)(L_1/A_1E)}{(1/2 \sin^2\theta)(L_1/A_1E) + (L_1 \sin\theta/A_2E)} \\
 &= P_y \frac{(A_2/\sin\theta)}{(A_2/\sin\theta) + 2A_1 \sin^2\theta}
 \end{aligned}
 \tag{9.60}$$

Lastly, the remaining forces are determined by superimposing the individual solutions.

$$\begin{aligned}
 F &= F_0 + \delta F X_1 \\
 F_{AB} &= \frac{P_x}{2 \cos\theta} + P_y \left\{ \frac{A_1 \sin\theta}{(A_2/\sin\theta) + 2A_1 \sin^2\theta} \right\} \\
 F_{DB} &= -\frac{P_x}{2 \cos\theta} + P_y \left\{ \frac{A_1 \sin\theta}{(A_2/\sin\theta) + 2A_1 \sin^2\theta} \right\}
 \end{aligned}
 \tag{9.61}$$

As expected for indeterminate structures, the internal force distribution depends on the relative stiffness of the members. When A_2 is very large in comparison to A_1 , P_y is essentially carried by member BC. Conversely, if A_2 is small in comparison to A_1 , member BC carries essentially none of P_y .

Example 9.16

Given: The indeterminate truss shown in Fig. E9.16a. Assume AE is constant, $A = 2 \text{ in.}^2$, and $E = 29,000 \text{ ksi}$.

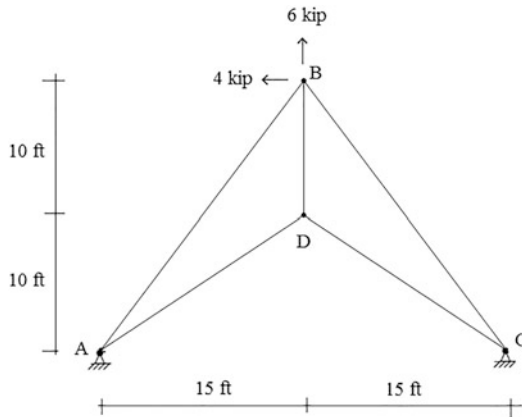


Fig. E9.16a

Determine: The member forces.

Solution: The truss is externally indeterminate to the first degree. The horizontal component of the reaction at C is taken as the force redundant (Fig. E9.16b).

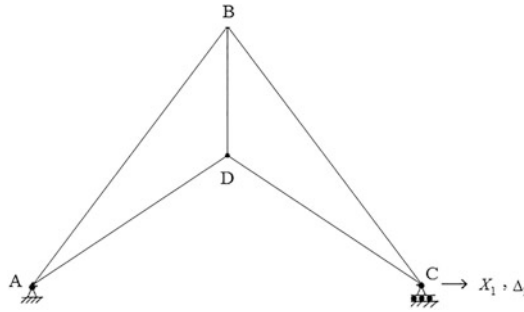


Fig. E9.16b Primary structure—redundant reaction

We apply the geometric compatibility equation to this truss,

$$\Delta_{1,0} + \delta_{11}X_1 = 0$$

where

$$\Delta_{1,0} = \sum F_0 \delta F \frac{L}{AE}$$

$$\delta_{11} = \sum (\delta F)^2 \frac{L}{AE}$$

The corresponding forces are listed in Figs. E9.16c and E9.16d.

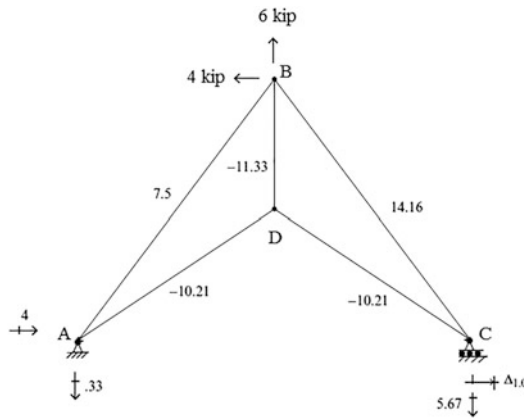


Fig. E9.16c F_0

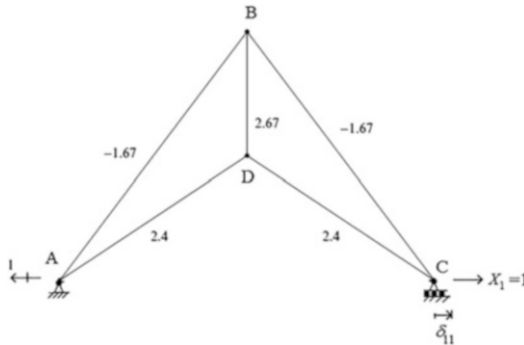


Fig. E9.16d $\delta F(X_1 = 1)$

Member	L (in.)	A (in. ²)	$\frac{L}{A}$	F_0	δF	$(\delta F)^2 \frac{L}{AE}$	$F_0 \delta F \frac{L}{AE}$
AB	300	2	150	7.5	-1.67	418.3/E	-1878.7/E
BC	300	2	150	14.16	-1.67	418.3/E	-3547/E
CD	216.3	2	108.2	-10.21	2.4	625.1/E	2656/E
DA	216.3	2	108.2	-10.21	2.4	625.1/E	2656/E
BD	120	2	60	-11.33	2.67	422.7/E	-1815/E
Σ						2509.5/E	-12,552.7/E

Inserting this data in the compatibility equation leads to

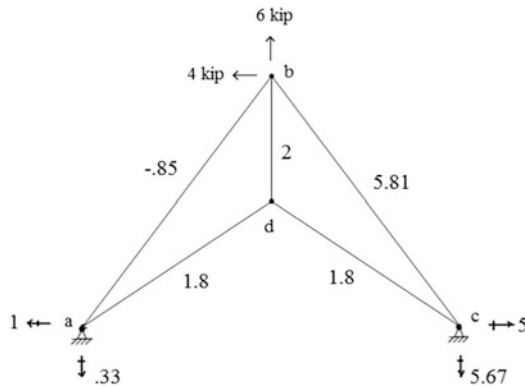
$$X_1 = -\frac{\Delta_{1,0}}{\delta_{11}} = \frac{12552.7}{2509.5} = 5$$

Then, the forces are determined by superimposing the individual solutions

$$F = F_0 + \delta F X_1$$

The final member forces and the reactions are listed below:

Member	F_0	$\delta F X_1$	F
AB	7.5	-8.35	-0.85
BC	14.16	-8.35	5.81
CD	-10.21	12.0	1.8
DA	-10.21	12.0	1.8
BD	-11.33	13.35	2
R_{ax}	4.0	-5.0	-1.0
R_{ay}	-0.33	0	-0.33
R_{cx}	0.0	+5.0	+5.0
R_{cy}	-5.67	0	-5.67



Example 9.17

Given: The indeterminate truss shown in Fig. E9.17a.

Determine: The member forces. Assume AE is constant, $A = 200 \text{ mm}^2$, and $E = 200 \text{ GPa}$.

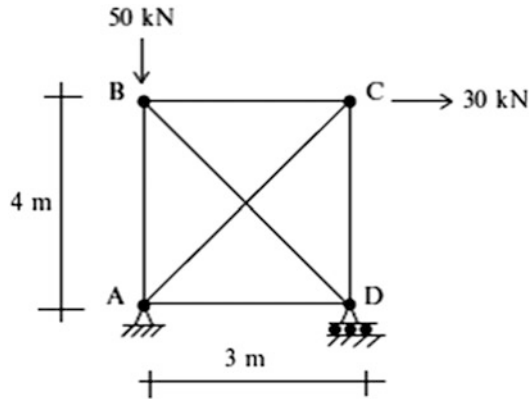


Fig. E9.17a

Solution: The truss is internally indeterminate to the first degree. The force in member BD is taken as the force redundant (Fig. E9.17b).

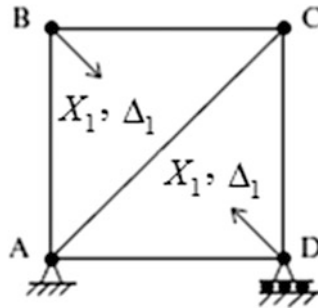


Fig. E9.17b Primary structure—internal force redundant

We apply the geometric compatibility equation to this truss,

$$\Delta_{1,0} + \delta_{11}X_1 = 0$$

where

$$\Delta_{1,0} = \sum F_0 \delta F \frac{L}{AE}$$

$$\delta_{11} = \sum (\delta F)^2 \frac{L}{AE}$$

The corresponding forces are listed in Figs. E9.17c and E9.17d.

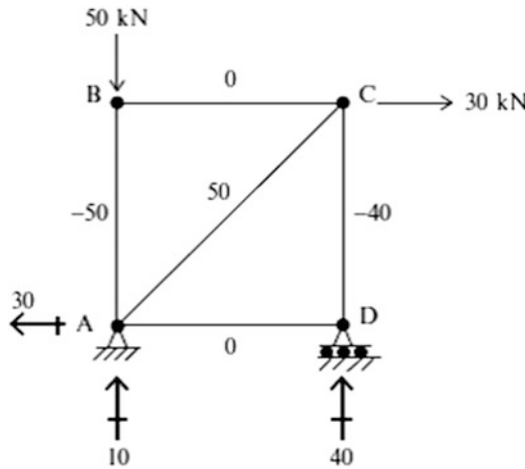


Fig. E9.17c F_0

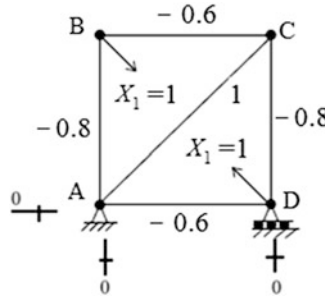


Fig. E9.17d $\delta F(X_1 = 1)$

Member	L (mm)	A (mm ²)	$\frac{L}{A}$	F_0	δF	$(\delta F)^2(L/AE)$	$F_0\delta F(L/AE)$
AB	4000	200	20	-50	-0.8	12.8	800
BC	3000	200	15	0	-0.6	5.4	0
CD	4000	200	20	-40	-0.8	12.8	640
DA	3000	200	15	0	-0.6	5.4	0
BD	5000	200	25	0	1	25	0
AC	5000	200	25	50	1	25	1250
Σ						86.4/E	2690/E

Enforcing comparability leads to

$$X_1 = F_{BD} = -\frac{\Delta_{1,0}}{\delta_{11}} = -\frac{2690}{86.4} = -31.13$$

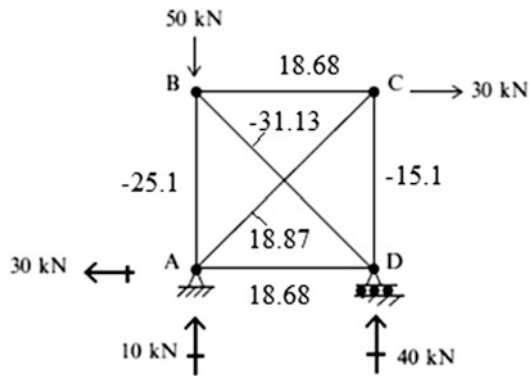
$$\therefore F_{BD} = 31.13 \text{ kN compression}$$

Then, the forces are determined by superimposing the individual solutions.

$$F = F_0 + \delta FX_1$$

The final member forces and the reactions are listed below.

Member	F_0	δFX_1	F
AB	-50	24.9	-25.1
BC	0	18.68	18.68
CD	-40	24.9	-15.1
DA	0	18.68	18.68
BD	0	-31.13	-31.13
AC	50	-31.13	18.87
R_{Ax}	-30	0	-30
R_{Ay}	10	0	10
R_{Dy}	40	0	40



9.7 Summary

9.7.1 Objectives

- The primary objective of this chapter is to present the force method, a procedure for analyzing statically indeterminate structures that work with force quantities as the unknown variables.
- Another objective is to use the force method to develop analytical solutions which are useful for identifying the key parameters that control the response and for conducting parameter sensitivity studies.

9.7.2 Key Factors and Concepts

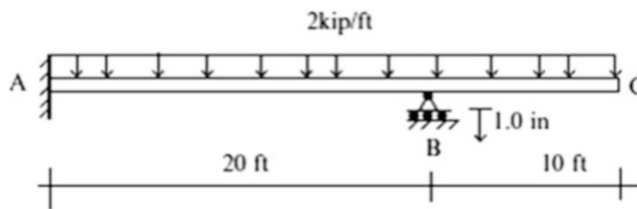
- The force method is restricted to linear elastic behavior.
- The first step is to reduce the structure to a statically determinate structure by either removing a sufficient number of redundant restraints or inserting force releases at internal points. The resulting determinate structure is called the primary structure.
- Next one applies the external loading to the primary structure and determines the resulting displacements at the points where the restraints were removed.
- For each redundant force, the displacements produced by a unit force acting on the primary structure are evaluated.
- Lastly, the redundant forces are scaled such that the total displacement at each constraint point is equal to the actual displacement. This requirement is expressed as

$$\Delta|_{\text{actual}} = \Delta|_{\text{loading}} + \sum_{\text{redundant forces}} (\delta_{\text{unit force}})X$$

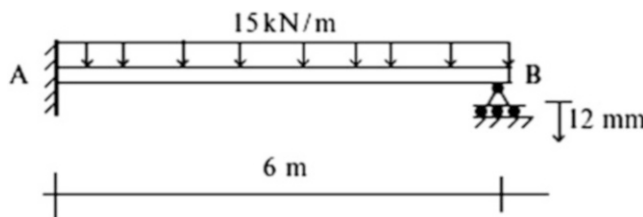
where the various terms are displacements at the constraint points. One establishes a separate equation for each constraint point. Note that all calculations are carried out on the primary structure.

9.8 Problems

Problem 9.1 Determine the vertical reaction at B. Take $E = 29,000$ ksi and $I = 200 \text{ in.}^4$



Problem 9.2 Determine the vertical reaction at B. Take $E = 200$ GPa and $I = 80(10)^6 \text{ mm}^4$.

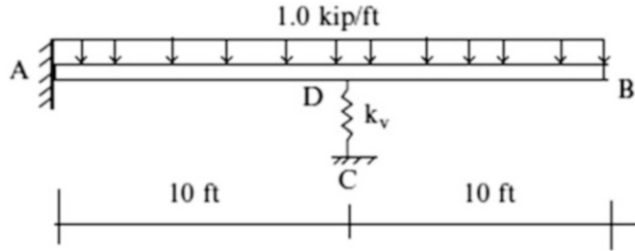


Problem 9.3 Determine the force in spring CD.

$$k_v = 60 \text{ kip/in.}$$

$$E = 29,000 \text{ ksi}$$

$$I = 200 \text{ in.}^4$$



Problem 9.4 Given the following properties and loadings, determine the reactions.

$$P = 40 \text{ kN}$$

$$w = 20 \text{ kN/m}$$

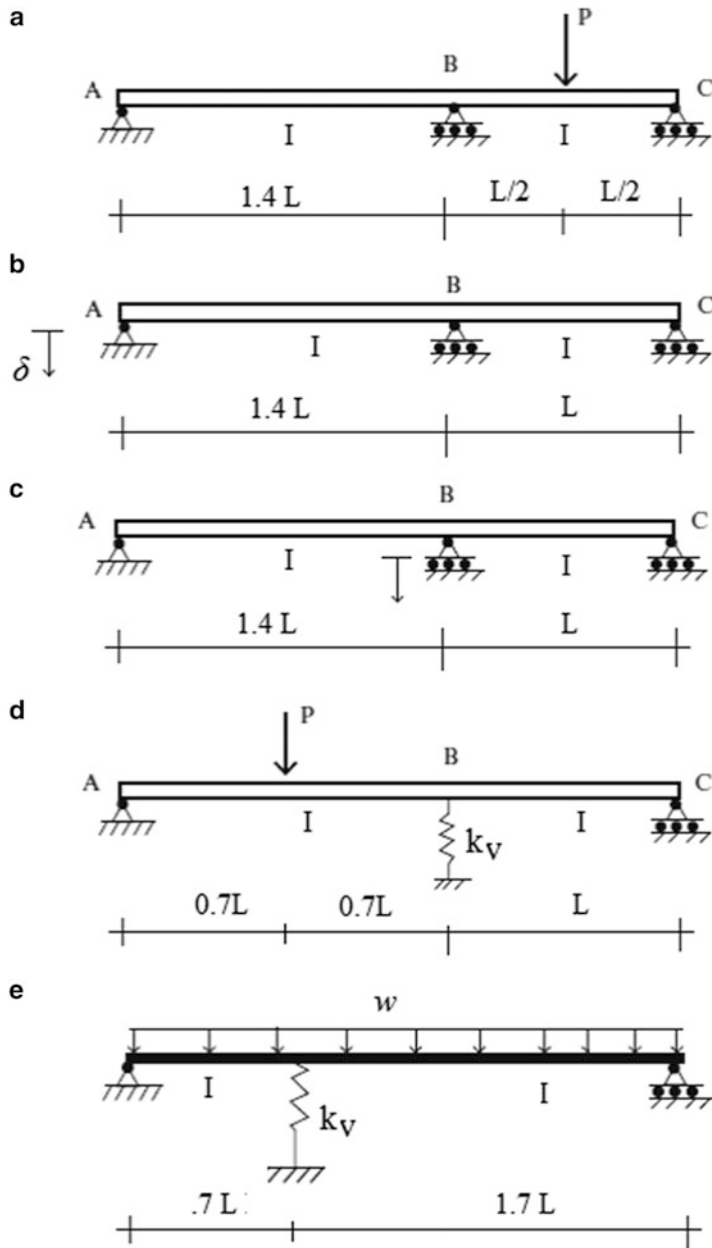
$$L = 10 \text{ m}$$

$$E = 200 \text{ GPa}$$

$$I = 170(10)^6 \text{ mm}^4$$

$$k_v = 40 \text{ kN/mm}$$

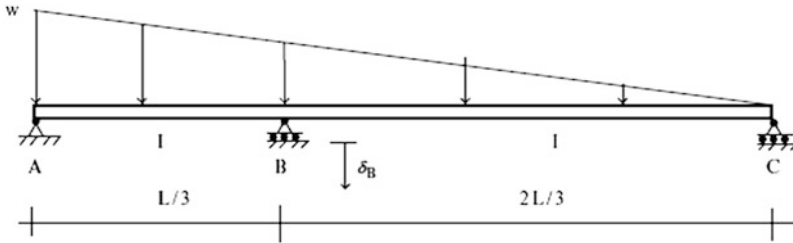
$$\delta = 20 \text{ mm}$$



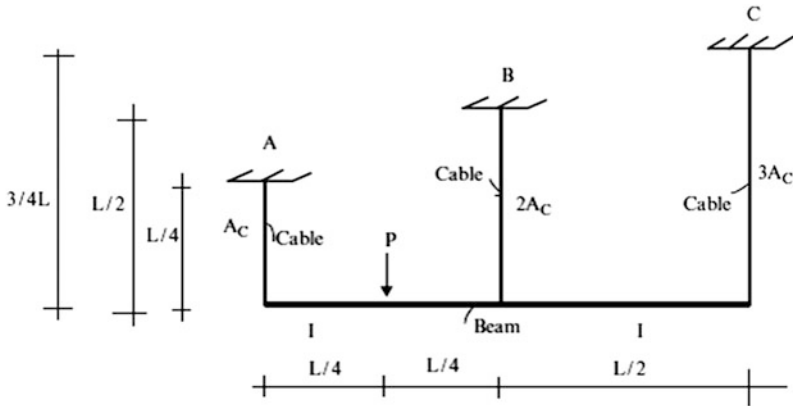
Problem 9.5 Use the force method to determine the reaction at B caused by:

1. The distributed load shown
2. The support settlement at B

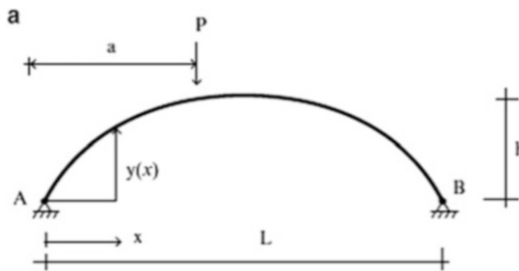
$$\begin{aligned}
 I &= 400 \text{ in.}^4 \\
 L &= 54 \text{ ft} \\
 w &= 2.1 \text{ kip/ft} \\
 \delta_B &= 1.2 \text{ in.} \downarrow \\
 E &= 29,000 \text{ ksi}
 \end{aligned}$$



Problem 9.6 Use the force method to determine the forces in the cables. Assume beam is rigid. $A_C = 1200 \text{ mm}^2$, $L = 9 \text{ m}$, $P = 40 \text{ kN}$, and $E = 200 \text{ GPa}$.



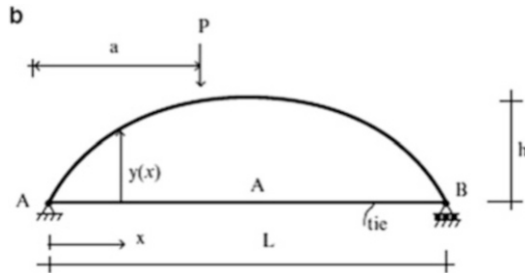
Problem 9.7 Consider the parabolic arch shown below. Assume the arch is non-shallow, i.e., h/L is order of $(1/2)$.



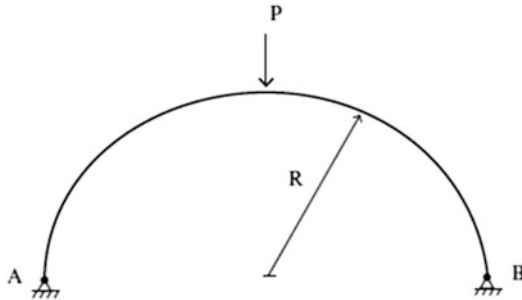
$$y = 4h \left(\frac{x}{L} - \left(\frac{x}{L} \right)^2 \right)$$

$$I = \frac{I_0}{\cos \theta}$$

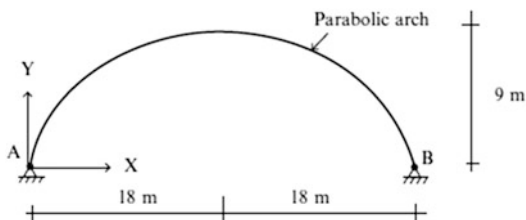
- (a) Determine the horizontal reaction at B due to the concentrated load.
- (b) Utilize the results of part (a) to obtain an analytical expression for the horizontal reaction due to a distributed loading, $w(x)$.
- (c) Specialize (b) for a uniform loading, $w(x) = w_0$.
- (d) Suppose the horizontal support at B is replaced by a member extending from A to B. Repeat part (a).



Problem 9.8 Consider the semicircular arch shown below. Determine the distribution of the axial and shear forces and the bending moment. The cross-section properties are constant.

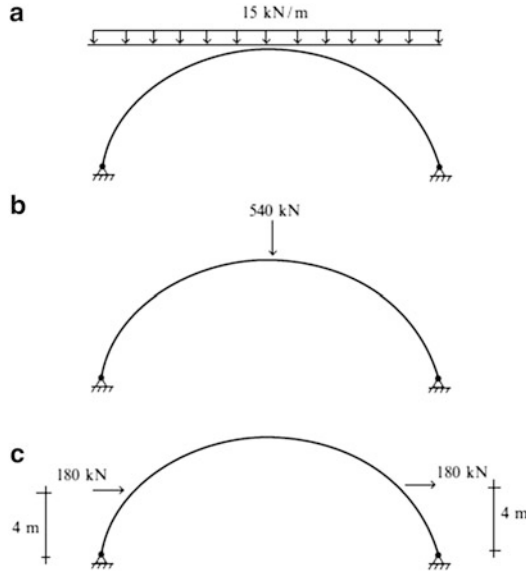


Problem 9.9



Use a computer software system to determine the bending moment distribution and deflected shape produced by the following loadings.

$$\text{Take } A = 20,000 \text{ mm}^2, \quad I = 400(10)^6 \text{ mm}^4 \quad \text{and} \quad E = 200 \text{ GPa}$$

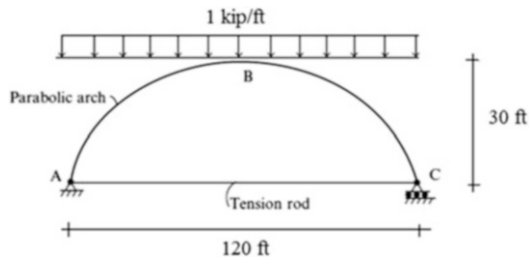


Problem 9.10

$$A = 30 \text{ in.}^2 \quad I = 1000 \text{ in.}^4 \quad E = 29,000 \text{ ksi}$$

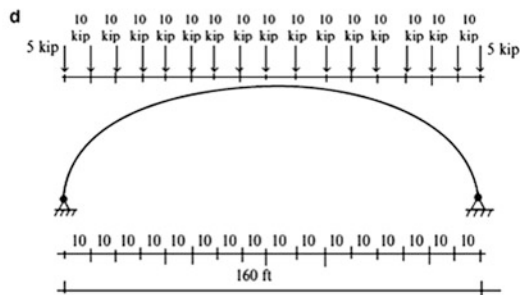
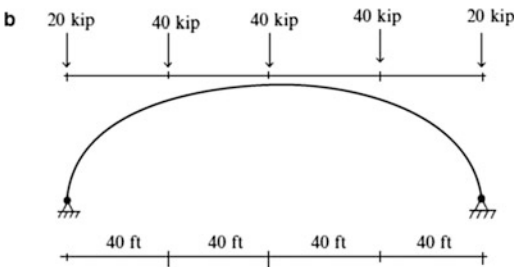
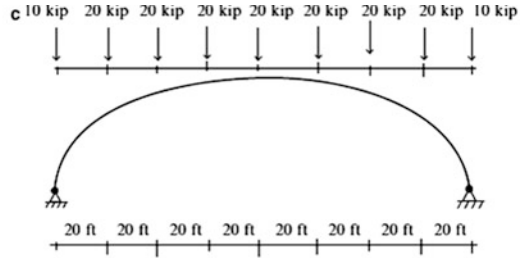
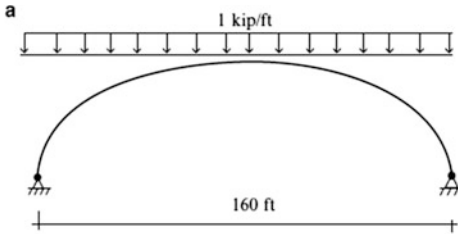
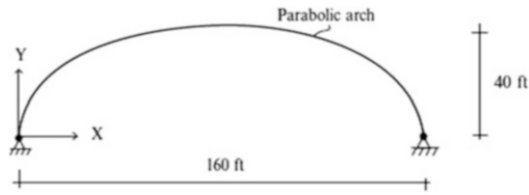
Use a computer software system to determine the maximum bending moment and the axial force in member ABC. Consider the following values for the area of the tension rod AC: 4, 8, and 16 in.^2

Problem 9.11

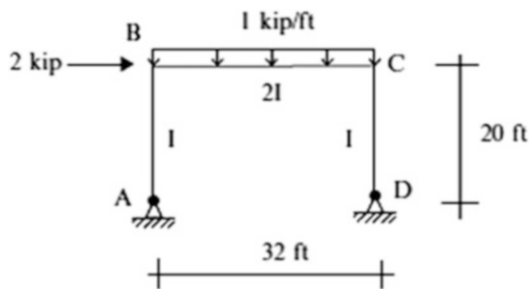


$$A = 40 \text{ in.}^2 \quad I = 1200 \text{ in.}^4 \quad E = 29,000 \text{ ksi}$$

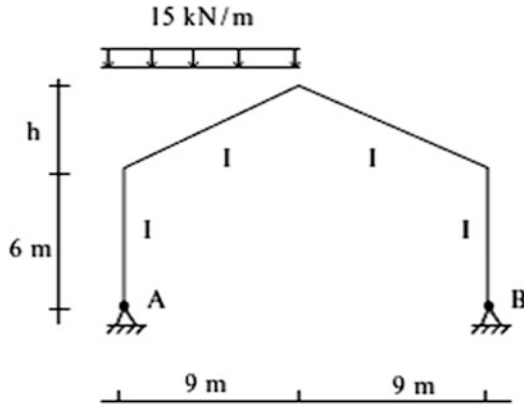
Use a computer software system to compare the bending moment distributions generated by the following loadings:



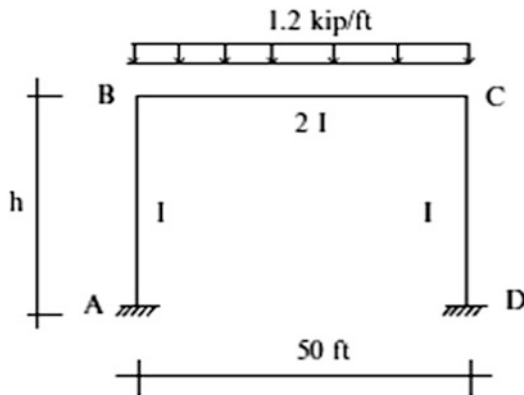
Problem 9.12 Determine the horizontal reaction at support D.



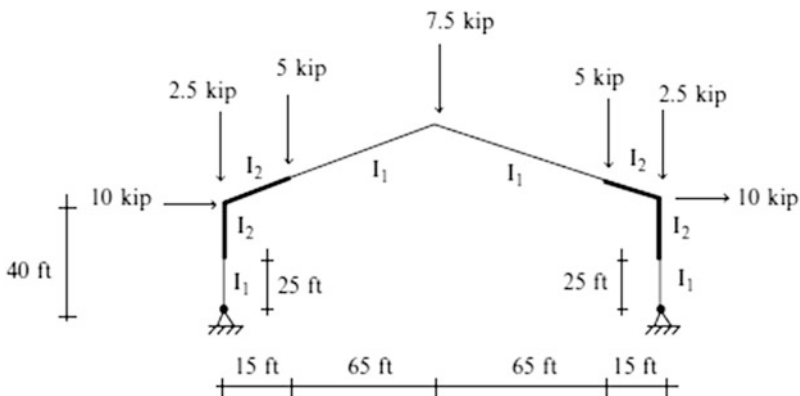
Problem 9.13 Determine the peak positive and negative moments as a function of h . Consider $h = 2, 4, 6$ m.



Problem 9.14 Determine the peak positive and negative moments as a function of h . Consider $h = 10, 20, 30$ ft.

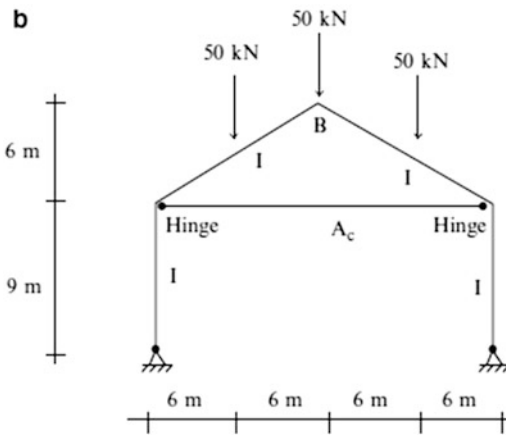
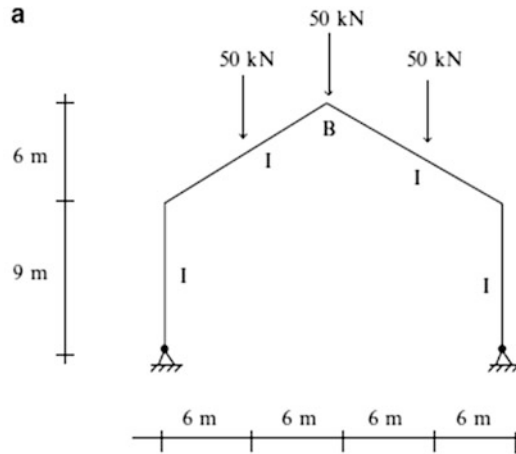


Problem 9.15 Using a computer software system, determine the bending moment distribution and deflected shape due to the loading shown.

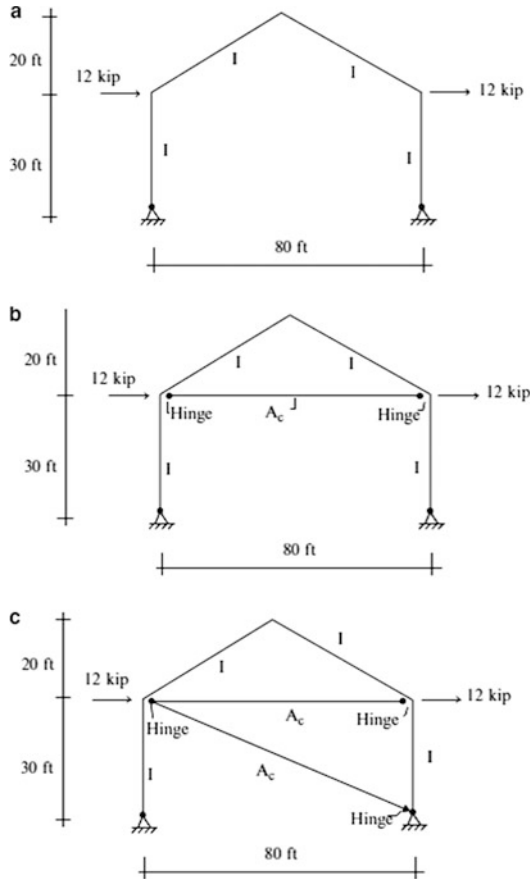


Take $I_1 = 1000 \text{ in.}^4$, $I_2 = 2000 \text{ in.}^4$, $E = 29,000 \text{ ksi}$, and $A = 20 \text{ in.}^2$ all members.

Problem 9.16 Compare the bending moment distributions and the vertical displacement at B for the structures defined below. Take $E = 200 \text{ GPa}$, $I = 400(10)^6 \text{ mm}^4$, $A = 100,000 \text{ mm}^2$, and $A_c = 1200, 2400, 4800 \text{ mm}^2$. Use a computer software system.

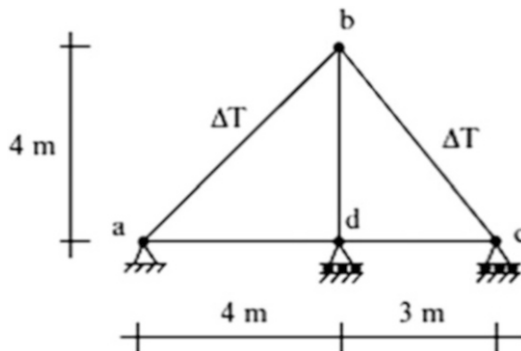


Problem 9.17 Is there any difference in behavior for the structures shown below? Answer the question without resorting to calculations.

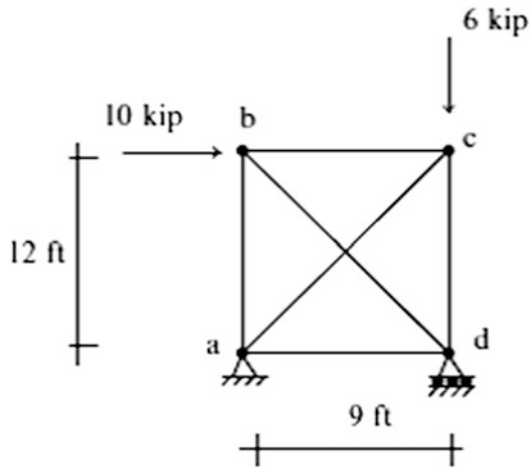


Problem 9.18 Determine the reactions and the member forces for the truss shown. Assume the vertical reaction at d as the force redundant.

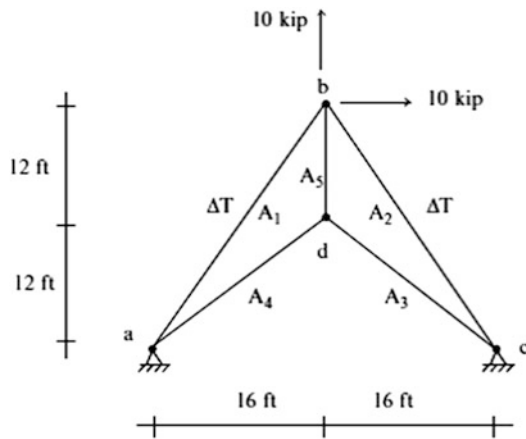
$E = 200 \text{ GPa}$
 $A = 660 \text{ mm}^2$ all members
 $\alpha = 12 \times 10^{-6}/^\circ\text{C}$
 $\Delta T = 10^\circ\text{C}$



Problem 9.19 Determine the forces in the members. $E = 29,000$ ksi and $A = 1 \text{ in.}^2$ all members.



Problem 9.20 Determine the member forces of the truss shown. Assume the horizontal reaction at c as the force redundant.



$$A_1 = A_2 = A_3 = A_4 = 10 \text{ in.}^2$$

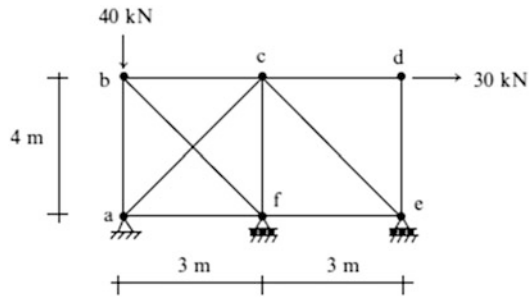
$$A_5 = 5 \text{ in.}^2$$

$$\alpha = 6.5 \times 10^{-6}/^\circ\text{F}$$

$$\Delta T = 60 \text{ F}$$

$$E = 29,000 \text{ ksi}$$

Problem 9.21 Determine the member forces for the truss shown. Assume $A = 1000 \text{ mm}^2$ and $E = 200 \text{ GPa}$ for all the members. Take the force in member ac and the reaction at support f as the force redundants.



Reference

1. Tauchert TR. Energy principles in structural mechanics. New York: McGraw-Hill; 1974.

Abstract

The previous chapter dealt with the force method, one of two procedures for analyzing statically indeterminate structures. In this chapter, we describe the second procedure, referred to as the displacement method. This method works with equilibrium equations expressed in terms of variables that correspond to displacement measures that define the position of a structure, such as translations and rotations of certain points on the structure. We start by briefly introducing the method specialized for frame-type structures and then apply it to truss, beam, and frame structures. Our focus in this chapter is on deriving analytical solutions and using these solutions to explain structural behavior trends. We also include a discussion of the effect of geometrically nonlinear behavior on the stiffness. Later in Chap. 12, we describe how the method can be transformed to a computer-based analysis procedure.

10.1 Introduction

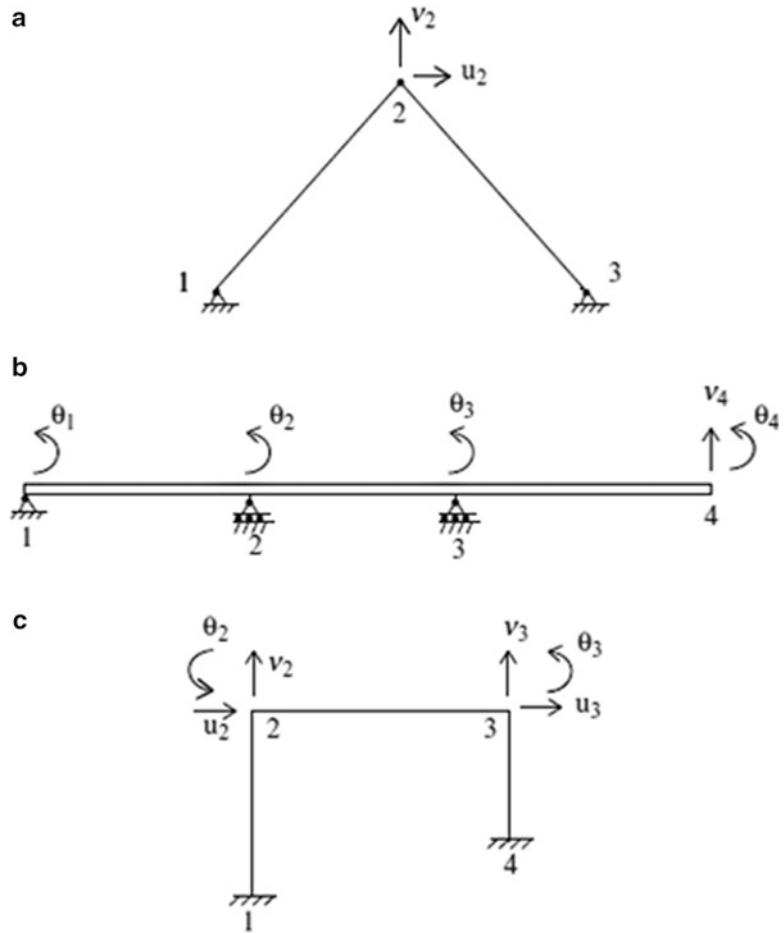
The displacement method works with equilibrium equations expressed in terms of displacement measures. For truss and frame-type structures, which are composed of members connected at node points, the translations and rotations of the nodes are taken as the displacement measures.

Plane truss structures have two displacement measures per node. For example, the plane truss shown in Fig. 10.1a has two unknown displacements (u_2, v_2). The available equilibrium equations are the two force equilibrium equations for node 2.

Planar beam-type structures have two displacement measures per node, the transverse displacement and the cross-section rotation. The corresponding equations are the shear, and moment equilibrium equations for each node. For example, the planar beam shown in Fig. 10.1b has five unknown displacements ($\theta_1, \theta_2, \theta_3, \theta_4, v_4$).

Plane frame-type structures have three displacement measures per node: two translations and one rotation. One works with the force and moment equilibrium equations for each unrestrained node. In general, the number of node equilibrium equations will always be equal to the number of displacements. For example, the plane frame shown in Fig. 10.1c has six unknown displacements ($u_2, v_2, \theta_2, u_3, v_3, \theta_3$).

Fig. 10.1 (a) Plane truss. (b) Planar beam. (c) Plane frame



The approach followed to generate equations involves the following steps:

1. Firstly, we decompose the structure into nodes and members. Note that the forces applied by a member to the node at its end are equal in magnitude but oppose in sense to the forces acting on the end of the member. The latter are called end actions.
2. Secondly, we relate the end actions for a member to the displacement measures for the nodes at the ends of the member. We carry out this procedure for each member.
3. Thirdly, we establish the force equilibrium equations for each node. This step involves summing the applied external loads and the end actions for those members which are incident on the node.
4. Fourthly, we substitute for the member end actions expressed in terms of the nodal displacements. This leads to a set of equilibrium equations relating the applied external loads and the nodal displacements.
5. Lastly, we introduce the prescribed values of nodal displacements corresponding to the supports in the equilibrium equations. The total number of unknowns is now reduced by the number of prescribed displacements. We solve this reduced set of equations for the nodal displacements and then use these values to determine the member end actions.

The solution procedure is systematic and is applicable for both statically determinate and statically indeterminate structures. Applications of the method to various types of structure are described in the following sections.

10.2 Displacement Method Applied to a Plane Truss

Consider the truss shown in Fig. 10.2. We suppose nodes 2, 3, and 4 are unyielding. We analyzed this structure with the force method in Sect. 9.6. We include it here to provide a comparison between the two approaches. There are two displacement measures, the horizontal and vertical translations for node 1. The structure is statically indeterminate to the first degree, so it is a trade-off whether one uses the force method or the displacement method.

The first step is to develop the equations relating the member forces and the nodal displacements. We start by expressing the change in length, e , of each member in terms of the displacements for node 1. This analysis is purely geometrical and involves projecting the nodal displacements on the initial direction of the member. We define an extension as positive when the length is increased. Noting Fig. 10.3, the extensions of members (1), (2), and (3) due to nodal displacements are given by:

$$\begin{aligned} e_{(1)} &= u_1 \cos \theta + v_1 \sin \theta \\ e_{(2)} &= v_1 \\ e_{(3)} &= -u_1 \cos \theta + v_1 \sin \theta \end{aligned} \tag{10.1}$$

Next, we express the member force in terms of the corresponding extension using the stress–strain relation for the material. Noting Fig. 10.3b, the generic equations are:

Fig. 10.2 Truss geometry and loading

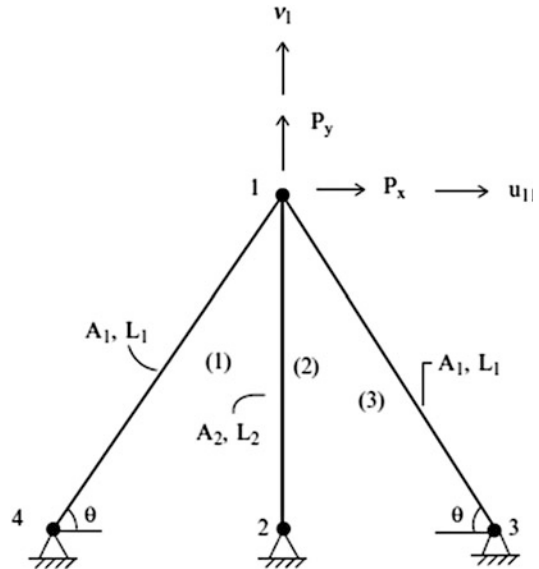
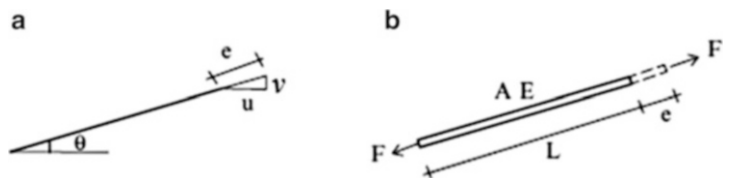


Fig. 10.3 Extension and force quantities—axial loaded member



$$\begin{aligned}\epsilon_{\text{total}} &= \epsilon_0 + \frac{1}{E} \sigma = \frac{e}{L} \\ \sigma &= \frac{F}{A}\end{aligned}$$

where ϵ_0 is the initial strain due to temperature change and fabrication error. Then,

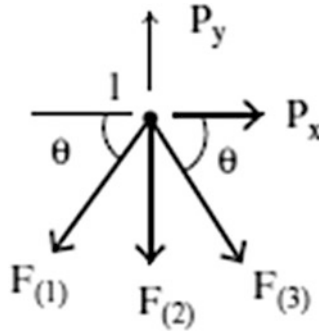
$$\begin{aligned}F &= \frac{AE}{L} e - AE\epsilon_0 \\ &= \frac{AE}{L} e + F^F\end{aligned}\tag{10.2}$$

where F^F is the magnitude of the member force due to initial strain.

Substituting for the extensions leads to the desired expressions relating the member forces and the corresponding nodal displacements.

$$\begin{aligned}F_{(1)} &= \frac{A_1 E}{L_1} \cos \theta u_1 + \frac{A_1 E}{L_1} \sin \theta v_1 + F_{(1)}^F \\ F_{(2)} &= \frac{A_2 E}{L_2} v_1 = \frac{A_2 E}{L_1 \sin \theta} v_1 + F_{(2)}^F \\ F_{(3)} &= -\frac{A_1 E}{L_1} \cos \theta u_1 + \frac{A_1 E}{L_1} \sin \theta v_1 + F_{(3)}^F\end{aligned}\tag{10.3}$$

We generate the force equilibrium equations for node 1 using the free body diagram shown below.



$$\begin{aligned}\sum F_x = 0 &\rightarrow P_x = \cos \theta (F_{(1)} - F_{(3)}) \\ \sum F_y = 0 &\uparrow P_y = \sin \theta (F_{(1)} + F_{(3)}) + F_{(2)}\end{aligned}\tag{10.4}$$

Substituting for the member forces, one obtains a set of uncoupled equations for u_1 and v_1 .

$$\begin{aligned}P_x &= \left\{ \frac{2A_1 E}{L_1} \cos^2 \theta \right\} u_1 + \cos \theta (F_{(1)}^F - F_{(3)}^F) \\ P_y &= \left\{ \frac{A_2 E}{L_1 \sin \theta} + \frac{2A_1 E}{L_1} \sin^2 \theta \right\} v_1 + \sin \theta (F_{(1)}^F + F_{(3)}^F) + F_{(2)}^F\end{aligned}\tag{10.5}$$

One solves these equations for u_1 and v_1 and then determines the member forces using (10.3). The resulting expressions are:

$$\begin{aligned} F_{(1)} &= \frac{P_x^*}{2 \cos \theta} + P_y \left\{ \frac{A_1 \sin \theta}{A_2 / \sin \theta + 2A_1 \sin^2 \theta} \right\} + F_{(1)}^F \\ F_{(2)} &= P_y^* \left\{ \frac{A_2 / \sin \theta}{A_2 / \sin \theta + 2A_1 \sin^2 \theta} \right\} + F_{(2)}^F \\ F_{(3)} &= -\frac{P_x^*}{2 \cos \theta} + P_y^* \left\{ \frac{A_1 \sin \theta}{A_2 / \sin \theta + 2A_1 \sin^2 \theta} \right\} + F_{(3)}^F \end{aligned} \quad (10.6)$$

where

$$\begin{aligned} P_x^* &= P_x - \cos \theta (F_{(1)}^F - F_{(3)}^F) \\ P_y^* &= P_y - \sin \theta (F_{(1)}^F + F_{(3)}^F) + F_{(2)}^F \end{aligned}$$

For this example, it may seem like more effort is required to apply the displacement method vs. the force method (Sect. 9.6). However, the displacement method generates the complete solution, i.e., both the member forces and the nodal displacements. A separate computation is required to compute the displacements when using the force method.

10.3 Member Equations for Frame-Type Structures

The members in frame-type structures are subjected to both bending and axial actions. The key equations for bending behavior of a member are the equations which relate the shear forces and moments acting on the ends of a member to the deflection and rotation of each end. These equations play a very important role in the analysis of statically indeterminate beams and frames and also provide the basis for the matrix formulation of the displacement method for structural frames. In what follows, we develop these equations using the force method.

We consider the structure shown in Fig. 10.4a. We focus specifically on member AB. Both of its ends are rigidly attached to nodes. When the structure is loaded, the nodes displace and the member bends as illustrated in Fig. 10.4b. This motion produces a shear force and moment at each end. The positive sense of these quantities is defined in Figs. 10.4b, c.

We refer to the shear and moment acting at the ends as *end actions*. Our objective here is to relate the end actions (V_B, M_B, V_A, M_A) and the end displacements ($v_B, \theta_B, v_A, \theta_A$). Our approach is based on treating the external loading and end actions as separate loadings and superimposing their responses. We proceed as follows:

- Step 1. Firstly, we assume the nodes at A and B are fixed and apply the external loading to member AB. This leads to a set of end actions that we call *fixed end actions*. This step is illustrated in Fig. 10.5.
- Step 2. Next, we allow the nodes to displace. This causes additional bending of the member AB resulting in additional end actions ($\Delta V_B, \Delta M_B, \Delta V_A, \Delta M_A$). Figure 10.6 illustrates this notation.
- Step 3. Superimposing the results obtained in these two steps leads to the final state shown in Fig. 10.7.

Fig. 10.4 Member deformation and end actions. (a) Initial geometry. (b) Deformed configuration for member AB. (c) Notation for end shear and moment

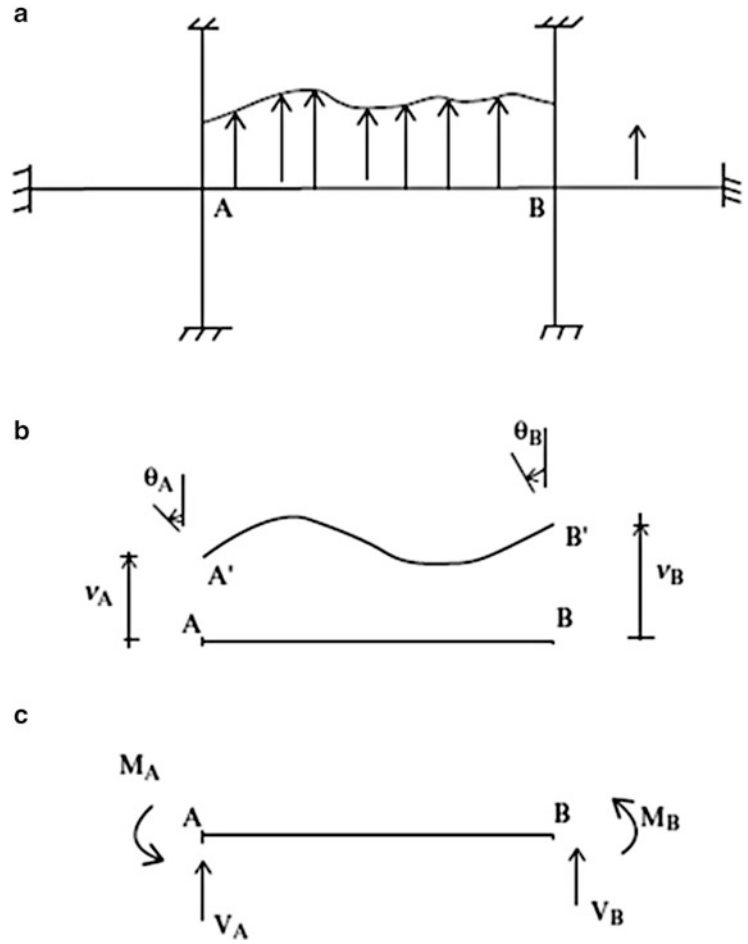


Fig. 10.5 Fixed end Actions. (a) Initial. (b) Deformed

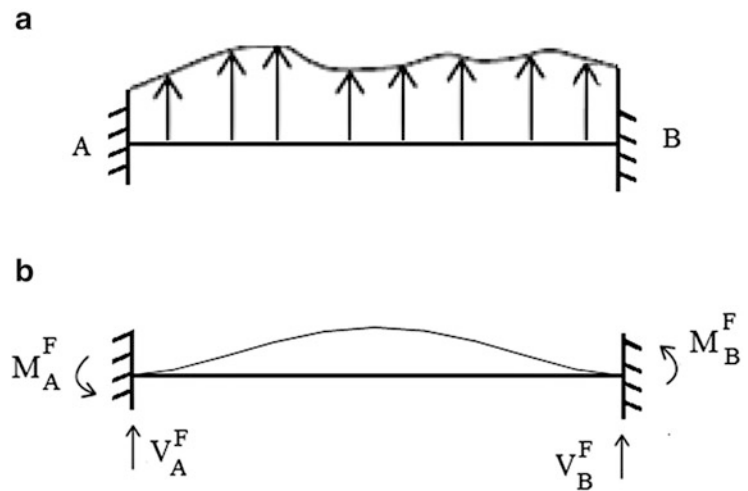
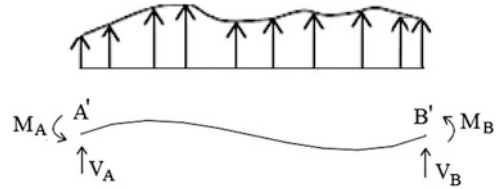


Fig. 10.6 Response to nodal displacements



Fig. 10.7 Final state



$$\begin{aligned}
 M_B &= M_B^F + \Delta M_B \\
 M_A &= M_A^F + \Delta M_A \\
 V_B &= V_B^F + \Delta V_B \\
 V_A &= V_A^F + \Delta V_A
 \end{aligned}$$

We determine the fixed end actions corresponding to the first step using the force method. Details are described in Chap. 9. Fixed end actions for various loading cases are listed in Table 9.1.

For the second step, we visualize the process as consisting of two substeps. First, we displace node B holding A fixed. Then, we displace node A, holding B fixed. Combining these cases result in the response shown in Fig. 10.8c. Superposition is valid since the behavior is linear.

These two substeps are similar and can be analyzed using the same procedure. We consider first case (a) shown in Fig. 10.8a. We analyze this case by considering AB to be a cantilever beam fixed at A and subjected to unknown forces, $\Delta V_B^{(1)}$ and $\Delta M_B^{(1)}$ at B (see Fig. 10.9a).

The displacements at B are (see Table 3.1):

$$\begin{aligned}
 v_B &= \frac{\Delta V_B^{(1)} L^3}{3EI} + \frac{\Delta M_B^{(1)} L^2}{2EI} \\
 \theta_B &= \frac{\Delta V_B^{(1)} L^2}{2EI} + \frac{\Delta M_B^{(1)} L}{EI}
 \end{aligned}
 \tag{10.7}$$

We determine $\Delta V_B^{(1)}$ and $\Delta M_B^{(1)}$ by requiring these displacements to be equal to the actual nodal displacements v_B and θ_B . Solving for $\Delta V_B^{(1)}$ and $\Delta M_B^{(1)}$ leads to

$$\begin{aligned}
 \Delta V_B^{(1)} &= \frac{12EI}{L^3} v_B - \frac{6EI}{L^2} \theta_B \\
 \Delta M_B^{(1)} &= \frac{4EI}{L} \theta_B - \frac{6EI}{L} v_B
 \end{aligned}
 \tag{10.8}$$

Fig. 10.8 Superposition of nodal motions. (a) Support A fixed. (b) Support B fixed. (c) Superimposed motions

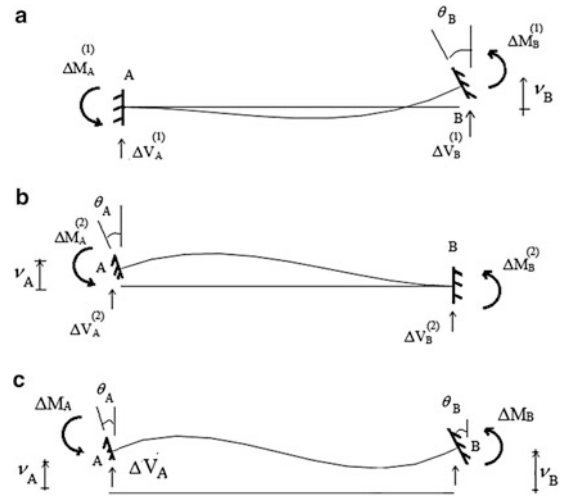
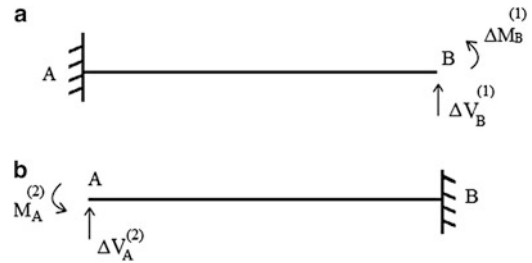


Fig. 10.9 (a) Support A fixed. (b) Support B fixed



The corresponding end actions at A are determined using the equilibrium conditions for the member.

$$\sum F_y = 0 \Rightarrow \Delta V_B^{(1)} + \Delta V_A^{(1)} = 0$$

$$\sum_{\text{at A}} M = 0 \Rightarrow \Delta M_B^{(1)} + \Delta M_A^{(1)} + L\Delta V_B^{(1)} = 0$$

Then

$$\Delta V_A^{(1)} = -\frac{12EI}{L^3}v_B + \frac{6EI}{L^2}\theta_B$$

$$\Delta M_A^{(1)} = -\frac{6EI}{L^2}v_B + \frac{2EI}{L}\theta_B$$
(10.9)

Equations (10.8) and (10.9) define the end actions due to the displacement of node B with A fixed.

Case (b) of Fig. 10.8 is treated in a similar way (see Fig. 10.9b). One works with a cantilever fixed at B and solves for $\Delta V_A^{(2)}$ and $\Delta M_A^{(2)}$. The result is

$$\begin{aligned}\Delta V_A^{(2)} &= \frac{12EI}{L^3} v_A + \frac{6EI}{L^2} \theta_A \\ \Delta M_A^{(2)} &= \frac{6EI}{L^2} v_A + \frac{4EI}{L} \theta_A\end{aligned}\quad (10.10)$$

The end actions at B follow from the equilibrium conditions for the member.

$$\begin{aligned}\Delta V_B^{(2)} &= -\frac{12EI}{L^3} v_A - \frac{6EI}{L^2} \theta_A \\ \Delta M_B^{(2)} &= \frac{6EI}{L^2} v_A + \frac{4EI}{L} \theta_A\end{aligned}\quad (10.11)$$

Equations (10.10) and (10.11) define the end actions due to the displacement of node A with B fixed.

The complete solution is generated by superimposing the results for these two loading conditions and the fixed end actions.

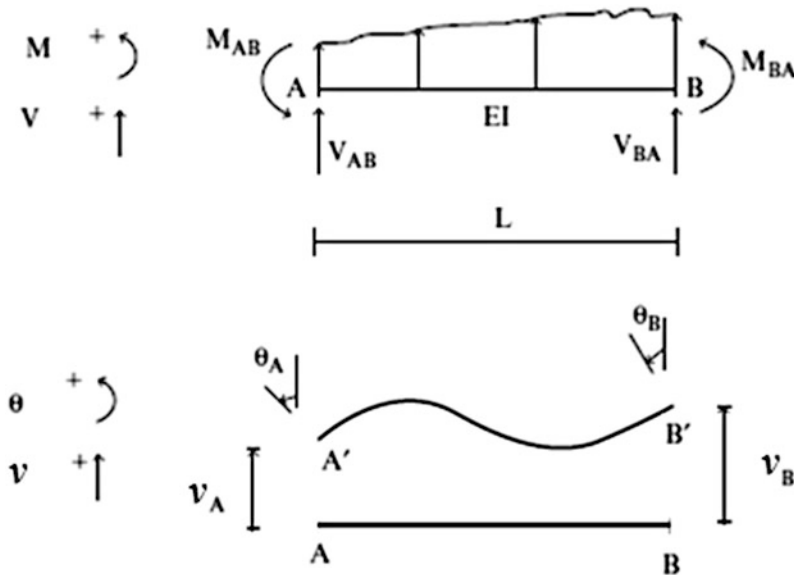
$$\begin{aligned}V_B &= \Delta V_B^{(1)} + \Delta V_B^{(2)} + V_B^F = -\frac{6EI}{L^2} (\theta_B + \theta_A) + \frac{12EI}{L^3} (v_B - v_A) + V_B^F \\ M_B &= \Delta M_B^{(1)} + \Delta M_B^{(2)} + M_B^F = +\frac{2EI}{L} (2\theta_B + \theta_A) - \frac{6EI}{L^2} (v_B - v_A) + M_B^F \\ V_A &= \Delta V_A^{(1)} + \Delta V_A^{(2)} + V_A^F = +\frac{6EI}{L^2} (\theta_B + \theta_A) - \frac{12EI}{L^3} (v_B - v_A) + V_A^F \\ M_A &= \Delta M_A^{(1)} + \Delta M_A^{(2)} + M_A^F = +\frac{2EI}{L} (\theta_B + 2\theta_A) - \frac{6EI}{L^2} (v_B - v_A) + M_A^F\end{aligned}$$

We rearrange these equations according to moment and shear quantities. The final form is written as

$$\begin{aligned}M_{AB} &= \frac{2EI}{L} \left\{ 2\theta_A + \theta_B - 3 \left(\frac{v_B - v_A}{L} \right) \right\} + M_{AB}^F \\ M_{BA} &= \frac{2EI}{L} \left\{ \theta_A + 2\theta_B - 3 \left(\frac{v_B - v_A}{L} \right) \right\} + M_{BA}^F\end{aligned}\quad (10.12a)$$

and

$$\begin{aligned}
 V_{AB} &= +\frac{6EI}{L^2} \left\{ \theta_A + \theta_B - 2\left(\frac{v_B - v_A}{L}\right) \right\} + V_{AB}^F \\
 V_{BA} &= -\frac{6EI}{L^2} \left\{ \theta_A + \theta_B - 2\left(\frac{v_B - v_A}{L}\right) \right\} + V_{BA}^F
 \end{aligned}
 \tag{10.12b}$$



Equations (10.12a, 10.12b) are referred to as the *slope-deflection equations*. They are based on the sign conventions and notation defined above.

10.4 The Displacement Method Applied to Beam Structures

In what follows, we first describe how the slope-deflection equations are employed to analyze horizontal beam structures, starting with two-span beams and then moving on to multi-span beams and frames. The displacement measures for beams are taken as the nodal rotations; the transverse displacements are assumed to be specified.

10.4.1 Two-Span Beams

We consider the two-span beam shown in Fig. 10.10a. One starts by subdividing the beam into two beam segments and three nodes, as indicated in Figs. 10.10b, c. There are only two rotations unknowns: the rotations at nodes \$A\$ and \$B\$; the rotation at node \$C\$ is considered to be zero.

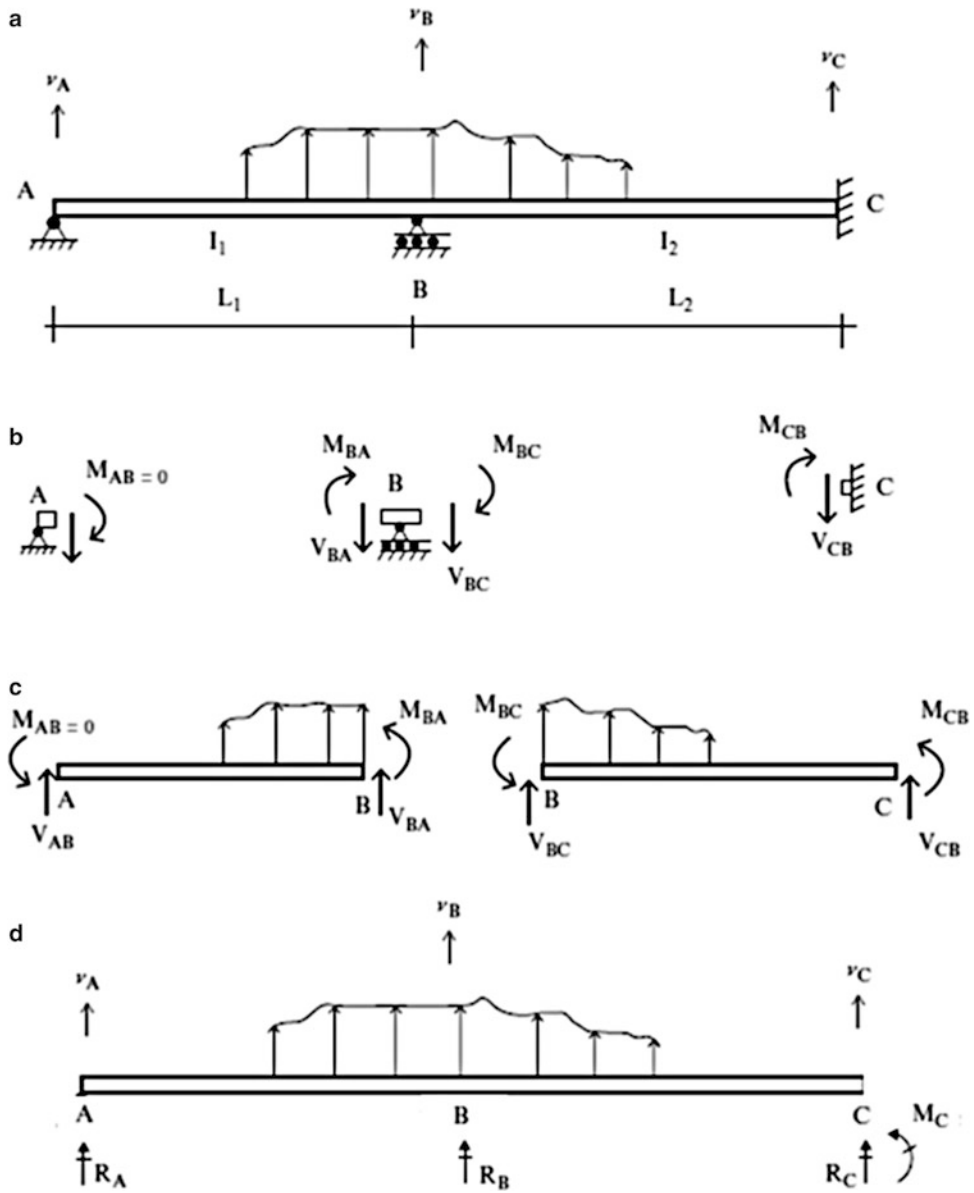


Fig. 10.10 Decomposition of two-span beam into beam segments and nodes. (a) Beam geometry and loading. (b) Segments and nodes. (c) Segments. (d) Reactions

Next we apply the slope-deflection equations (10.12a) to members AB and BC.

$$\begin{aligned}
 M_{AB} &= \frac{2EI_1}{L} \left\{ 2\theta_A + \theta_B - 3 \left(\frac{v_B - v_A}{L_1} \right) \right\} + M_{AB}^F \\
 M_{BA} &= \frac{2EI_1}{L_1} \left\{ 2\theta_B + \theta_A - 3 \left(\frac{v_B - v_A}{L_1} \right) \right\} + M_{BA}^F \\
 M_{BC} &= \frac{2EI_2}{L_2} \left\{ 2\theta_B - 3 \left(\frac{v_C - v_B}{L_2} \right) \right\} + M_{BC}^F \\
 M_{CB} &= \frac{2EI_2}{L_2} \left\{ \theta_B - 3 \left(\frac{v_C - v_B}{L_2} \right) \right\} + M_{CB}^F
 \end{aligned} \tag{10.13}$$

Then, we enforce moment equilibrium at the nodes. The corresponding equations are:

$$\begin{aligned}
 M_{AB} &= 0 \\
 M_{BA} + M_{BC} &= 0
 \end{aligned} \tag{10.14}$$

Substituting for the end moments in the nodal moment equilibrium equations yields

$$\begin{aligned}
 \frac{4EI_1}{L_1} \theta_A + \frac{2EI_1}{L_1} \theta_B &= \frac{6EI_1}{L_1} \left(\frac{v_B - v_A}{L_1} \right) - M_{AB}^F \\
 \frac{2EI_1}{L_1} \theta_A + \left(\frac{4EI_1}{L_1} + \frac{4EI_2}{L_2} \right) \theta_B &= \frac{6EI_1}{L_1} \left(\frac{v_B - v_A}{L_1} \right) + \frac{6EI_2}{L_2} \left(\frac{v_C - v_B}{L_2} \right) - (M_{BA}^F + M_{BC}^F)
 \end{aligned} \tag{10.15}$$

Once the loading, support motion, and member properties are specified, one can solve for θ_B and θ_A . Substituting for the θ s in (10.13) leads to the end moments. Lastly, we calculate the end shears. Since the end moments are known, we can determine the end shear forces using either the static equilibrium equations for the members AB and BC or by using (10.12b).

$$\begin{aligned}
 V_{AB} &= \frac{6EI_1}{L_1^2} (\theta_A + \theta_B) - \frac{12EI_1}{L_1^2} \left(\frac{v_B - v_A}{L_1} \right) + V_{AB}^F \\
 V_{BA} &= -\frac{6EI_1}{L_1^2} (\theta_B + \theta_A) + \frac{12EI_1}{L_1^2} \left(\frac{v_B - v_A}{L_1} \right) + V_{BA}^F \\
 V_{BC} &= \frac{6EI_2}{L_2^2} (\theta_B) - \frac{12EI_2}{L_2^2} \left(\frac{v_C - v_B}{L_2} \right) + V_{BC}^F \\
 V_{CB} &= -\frac{6EI_2}{L_2^2} (\theta_B) + \frac{12EI_2}{L_2^2} \left(\frac{v_C - v_B}{L_2} \right) + V_{CB}^F
 \end{aligned} \tag{10.16}$$

The reactions are related to the end actions by (see Fig. 10.10d)

$$\begin{aligned}
 R_A &= V_{AB} \\
 M_A &= M_{AB} = 0 \\
 R_B &= V_{BA} + V_{BC} \\
 R_C &= V_{CB} \\
 M_C &= M_{CB}
 \end{aligned}$$

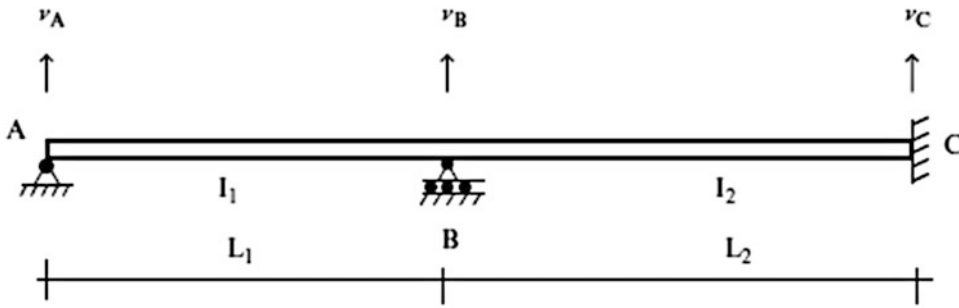


Fig. 10.11 Beam geometry and support settlements

Suppose the only external action on the above two-span beam is prescribed support settlements v_A , v_B , and v_C as shown in Fig. 10.11. We compute the corresponding chord rotation terms and include these terms in the slope-deflection equations. The chord rotations are

$$\begin{aligned}\rho_{AB} &= \frac{v_B - v_A}{L_1} \\ \rho_{BC} &= \frac{v_C - v_B}{L_2}\end{aligned}\quad (10.17)$$

Noting (10.13), the chord rotation terms introduce additional end moments for each member connected to the support which experiences the settlement. The corresponding expressions for the end moments due to this support settlement are

$$\begin{aligned}M_{AB} &= \frac{2EI_1}{L_1} \{2\theta_A + \theta_B - 3\rho_{AB}\} \\ M_{BA} &= \frac{2EI_1}{L_1} \{2\theta_B + \theta_A - 3\rho_{AB}\} \\ M_{BC} &= \frac{2EI_2}{L_2} \{2\theta_B - 3\rho_{BC}\} \\ M_{CB} &= \frac{2EI_2}{L_2} \{\theta_B - 3\rho_{BC}\}\end{aligned}\quad (10.18)$$

Substituting for the support movements, the nodal moment equilibrium equations reduce to

$$\begin{aligned}2\theta_A + \theta_B &= 3\rho_{AB} \\ \frac{2EI_1}{L_1} \{2\theta_B + \theta_A\} + \frac{2EI_2}{L_2} \{2\theta_B\} &= \frac{6EI_1}{L_1} \rho_{AB} + \frac{6EI_2}{L_2} \rho_{BC}\end{aligned}\quad (10.19)$$

Note that the solution depends on the ratio of EI to L for each span. One specifies ρ for each member, solves (10.19) for the θ s, and then evaluates the end actions.

Example 10.1

Given: The two-span beam defined in Fig. E10.1a. Assume the supports are unyielding. Take $E = 29,000$ ksi, $I = 428$ in.⁴, and $L = 20$ ft.

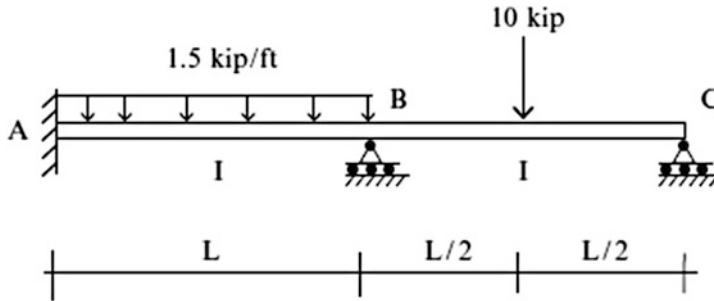
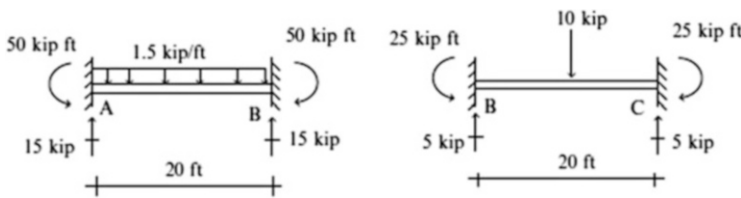


Fig. E10.1a

Determine: The end actions and the shear and moment diagrams due to the applied loading.

Solution: First, we compute the fixed end actions by using Table 9.1.



$$M_{AB}^F = \frac{1.5(20)^2}{12} = 50 \text{ kip ft} \quad V_{AB}^F = \frac{1.5(20)}{2} = 15 \text{ kip}$$

$$M_{BA}^F = -50 \text{ kip ft} \quad V_{BA}^F = \frac{1.5(20)}{2} = 15 \text{ kip}$$

$$M_{BC}^F = \frac{10(20)}{8} = 25 \text{ kip ft} \quad V_{BC}^F = \frac{10}{2} = 5 \text{ kip}$$

$$M_{CB}^F = -25 \text{ kip ft} \quad V_{CB}^F = \frac{10}{2} = 5 \text{ kip}$$

We define the relative member stiffness for each member as

$$k_{\text{members AB}} = k_{\text{members BC}} = \frac{EI}{L} = k_1 = \frac{29,000(428)}{20} \frac{1}{(12)^2} = 4310 \text{ kip ft}$$

Next, we generate the expressions for the end moments using the slope-deflection equation (10.12a) and noting that $\theta_A = 0$ and the supports are unyielding ($v_A = v_B = v_C = 0$).

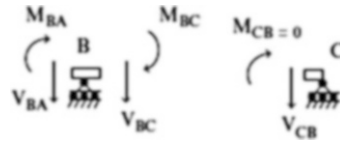
$$M_{AB} = 2k_1(\theta_B) + 50$$

$$M_{BA} = 2k_1(2\theta_B) - 50$$

$$M_{BC} = 2k_1(2\theta_B + \theta_C) + 25$$

$$M_{CB} = 2k_1(\theta_B + 2\theta_C) - 25$$

Enforcing moment equilibrium at nodes B and C



$$M_{BA} + M_{BC} = 0$$

$$M_{CB} = 0$$

leads to

$$2k_1\theta_B + 4k_1\theta_C = 25$$

$$8k_1\theta_B + 2k_1\theta_C = 25$$

↓

$$k_1\theta_B = 1.786$$

$$k_1\theta_C = 5.357$$

↓

$$\theta_B = 0.0004 \text{ rad} \quad \text{counter clockwise}$$

$$\theta_C = 0.0012 \text{ rad} \quad \text{counter clockwise}$$

These rotations produce the following end moments

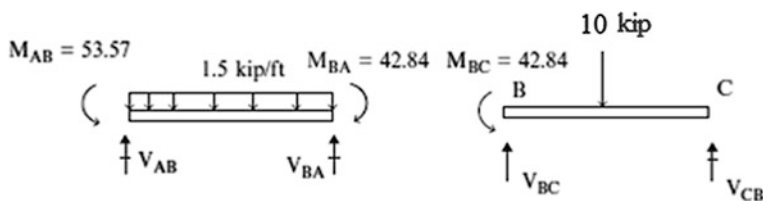
$$M_{AB} = 53.57 \text{ kip ft}$$

$$M_{BA} = -42.84 \text{ kip ft}$$

$$M_{BC} = +42.84 \text{ kip ft}$$

$$M_{CB} = 0$$

Since the end moments are known, we can determine the end shear forces either by using the static equilibrium equations for the members or by using (10.12b).



Noting (10.12b), we find

$$V_{AB} = \frac{6}{L}(k_1\theta_B) + V_{AB}^F = \frac{6}{20}(1.786) + 15 = 15.53 \text{ kip}$$

$$V_{AB} = -\frac{6}{L}(k_1\theta_B) + V_{AB}^F = -\frac{6}{20}(1.786) + 15 = 14.47 \text{ kip}$$

$$V_{BC} = \frac{6}{L}(k_1\theta_B + k_1\theta_C) + V_{BC}^F = \frac{6}{20}(1.786 + 5.357) + 5 = 7.14 \text{ kip}$$

$$V_{AB} = -\frac{6}{L}(k_1\theta_B + k_1\theta_C) + V_{CB}^F = -\frac{6}{20}(1.786 + 5.357) + 5 = 2.86 \text{ kip}$$

The reactions are:

$$R_A = V_{AB} = 15.53 \text{ kip } \uparrow$$

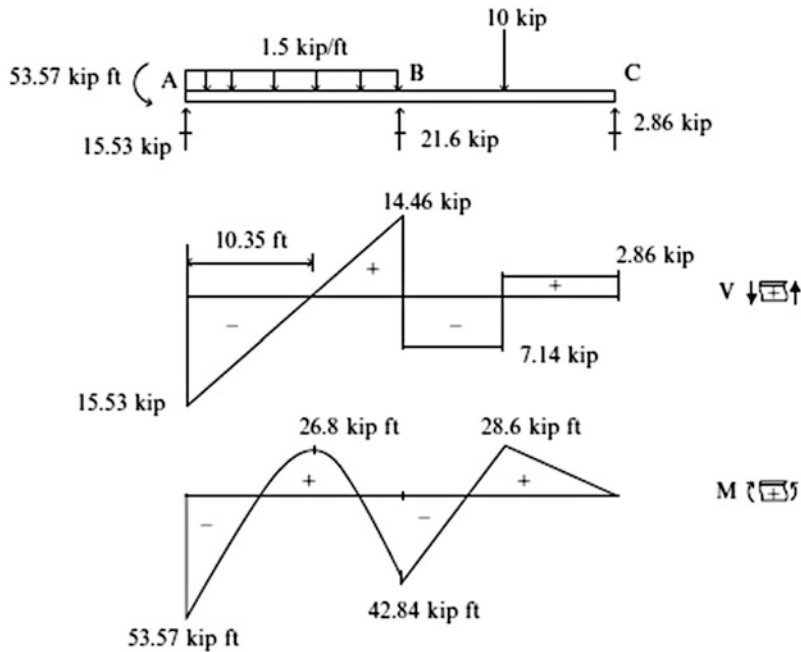
$$M_A = M_{AB} = 53.57 \text{ kip ft}$$

$$R_B = V_{BA} + V_{BC} = 21.6 \text{ kip } \uparrow$$

$$R_C = V_{CB} = 2.86 \text{ kip } \uparrow$$

$$M_C = M_{CB} = 0$$

Lastly, the shear and moment diagrams are plotted below.



Example 10.2: Two-Span Symmetrical Beam—Settlement of the Supports

Given: The symmetrical beam shown in Fig. E10.2a. Assume EI is constant. Take $L = 6$ m, $I = 180(10)^6 \text{ mm}^4$, and $E = 200 \text{ kN/mm}^2$.

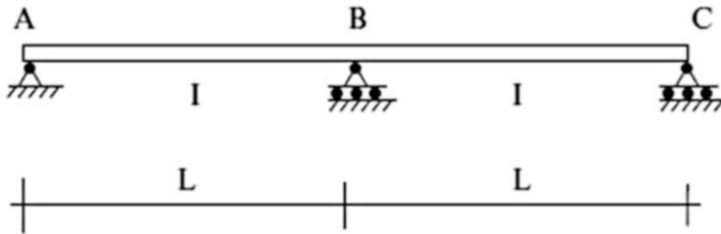


Fig. E10.2a

Case (i), the middle support settles an amount $v_B = 40$ mm.

Case (ii), the left support settles an amount $v_A = 40$ mm.

Determine: The end actions, the shear and bending moment diagrams.

Solution:

Case (i): Support settlement at B (Fig. E10.2b)

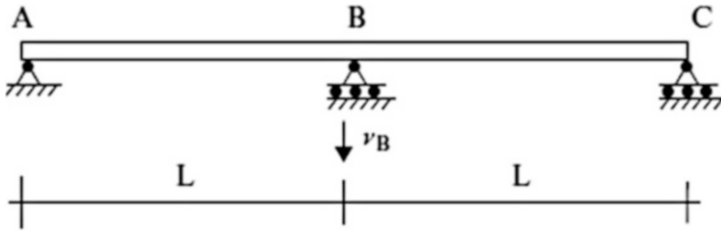


Fig. E10.2b Settlement at B

Noting (10.17), the chord rotations due to settlement at B are:

$$\rho_{AB} = \frac{v_B - v_A}{L} = -\frac{v_B}{L}$$

$$\rho_{BC} = \frac{v_C - v_B}{L} = +\frac{v_B}{L}$$

Substituting for ρ_{AB} and ρ_{BC} , the corresponding slope-deflection equation (10.12a) take the form

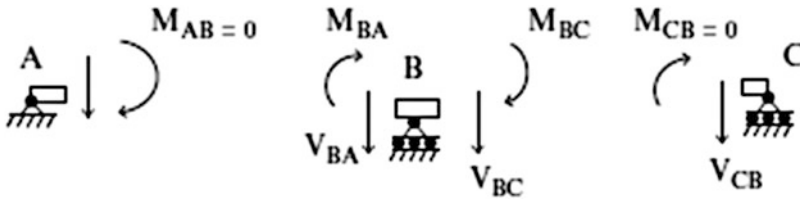
$$M_{AB} = \frac{2EI}{L}(2\theta_A + \theta_B) - \frac{6EI}{L}\rho_{AB}$$

$$M_{BA} = \frac{2EI}{L}(2\theta_B + \theta_A) - \frac{6EI}{L}\rho_{AB}$$

$$M_{BC} = \frac{2EI}{L}(2\theta_B + \theta_C) - \frac{6EI}{L}\rho_{BC}$$

$$M_{CB} = \frac{2EI}{L}(2\theta_C + \theta_B) - \frac{6EI}{L}\rho_{BC}$$

We enforce moment equilibrium at nodes A, B, and C.



The corresponding equations are:

$$\begin{aligned} M_{AB} = 0 &\Rightarrow 2\theta_A + \theta_B = -3\frac{v_B}{L} \\ M_{BA} + M_{BC} = 0 &\Rightarrow \theta_A + 4\theta_B + \theta_C = 0 \\ M_{CB} = 0 &\Rightarrow 2\theta_C + \theta_B = 3\frac{v_B}{L} \end{aligned}$$

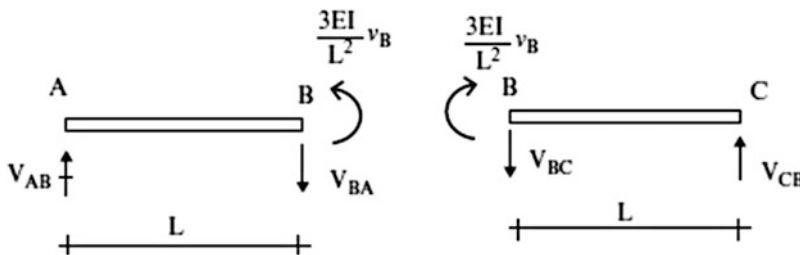
Solving for the θ s leads to

$$\begin{aligned} \theta_B &= 0 \\ \theta_A &= -\frac{3v_B}{2L} \\ \theta_C &= +\frac{3v_B}{2L} \end{aligned}$$

The corresponding end moments are:

$$\begin{aligned} M_{BA} &= \frac{2EI}{L} \left(-\frac{3v_B}{2L} \right) - \frac{6EI}{L} \left(-\frac{v_B}{L} \right) = +\frac{3EI}{L^2} v_B = \frac{3(200)(180)10^6}{(6000)^2} (40) \\ &= 120,000 \text{ kNmm} = 120 \text{ kNm} \\ M_{BC} &= \frac{2EI}{L} \left(\frac{3v_B}{2L} \right) - \frac{6EI}{L} \left(\frac{v_B}{L} \right) = -\frac{3EI}{L^2} v_B = -120 \text{ kNm} \end{aligned}$$

Next, we determine the end shear forces using the static equilibrium equations for the members.



$$\begin{aligned} V_{AB} = V_{CB} &= +\frac{3EI}{L^3} v_B = \frac{3(200)(180)10^6}{(6000)^3} (40) = 20 \text{ kN } \uparrow \\ V_{BA} = V_{BC} &= -\frac{3EI}{L^3} v_B = 20 \text{ kN } \downarrow \end{aligned}$$

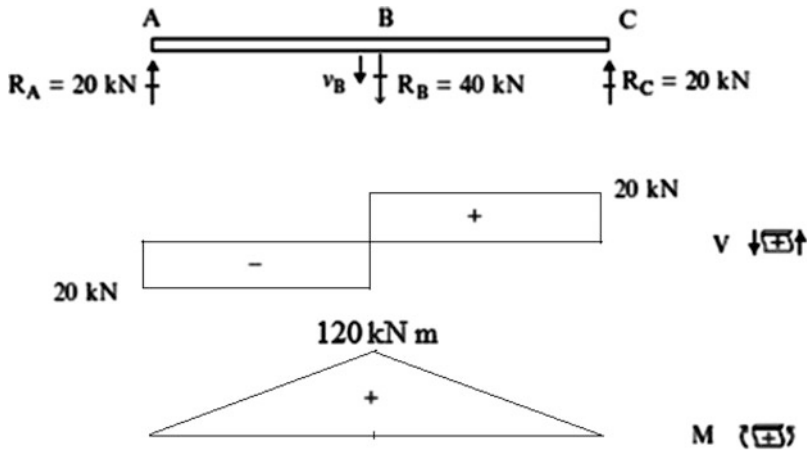
The corresponding reactions are:

$$R_A = V_{AB} = 20 \text{ kN } \uparrow$$

$$R_B = V_{BA} + V_{BC} = 40 \text{ kN } \downarrow$$

$$R_C = V_{CB} = 20 \text{ kN } \uparrow$$

One should expect that $\theta_B = 0$ because of symmetry. The shear and moment diagrams are plotted below.



Case (ii): Support settlement at A (Fig. E10.2c)

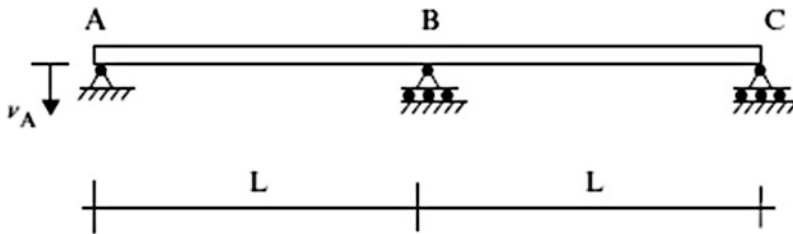


Fig. E10.2c Settlement at A

Settlement at A produces chord rotation in member AB only. The chord rotation for member AB due to settlement of node A is $\rho_{AB} = v_A/L$. Substituting for ρ_{AB} , the corresponding slope-deflection equation (10.12a) take the form

$$M_{AB} = \frac{2EI}{L}(2\theta_A + \theta_B) - \frac{6EI}{L}\rho_{AB}$$

$$M_{BA} = \frac{2EI}{L}(2\theta_B + \theta_A) - \frac{6EI}{L}\rho_{AB}$$

$$M_{BC} = \frac{2EI}{L}(2\theta_B + \theta_C)$$

$$M_{CB} = \frac{2EI}{L}(2\theta_C + \theta_B)$$

Setting $M_{AB} = M_{CB} = 0$ and $M_{BA} + M_{BC} = 0$ leads to

$$2\theta_A + \theta_B = 3\rho_{AB}$$

$$2\theta_C + \theta_B = 0$$

$$4\theta_B + \theta_A + \theta_C = 3\rho_{AB}$$

Solving for the θ s leads to

$$\theta_A = \frac{5}{4}\rho_{AB}$$

$$\theta_B = \frac{1}{2}\rho_{AB}$$

$$\theta_C = -\frac{1}{4}\rho_{AB}$$

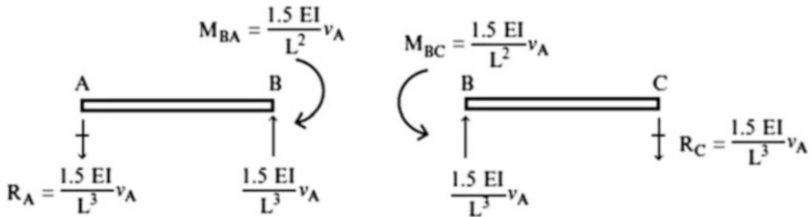
Finally, the bending moment at B due to support settlement at A is:

$$M_{BA} = \frac{2EI}{L} \left(\frac{v_A}{L} + \frac{5v_A}{4L} \right) - \frac{6EIv_A}{L^2} = -\frac{1.5EI}{L^2}v_A = \frac{1.5(200)(180)10^6}{(6000)^2} \quad (40)$$

$$= -60,000 \text{ kNmm} = -60 \text{ kNm}$$

$$M_{BC} = -M_{BA} = 60 \text{ kNm} \quad \text{counterclockwise}$$

Next, we determine the end shear forces using the static equilibrium equations for the members.

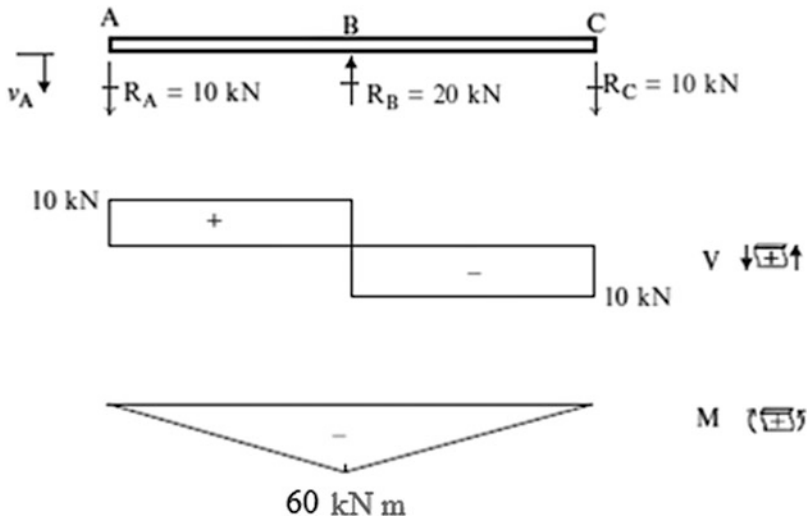


Then,

$$R_A = R_C = -\frac{1.5EI}{L^3}v_A = -\frac{1.5(200)(180)10^6}{(6000)^3} \quad (40) = -10 \text{ kN}$$

$$R_B = \frac{1.5EI}{L^3}v_A + \frac{1.5EI}{L^3}v_A = +20 \text{ N}$$

The shear and moment diagrams are plotted below.



Example 10.3: Two-Span Beam with Overhang

Given: The beam shown in Fig. E10.3a. Assume EI is constant.

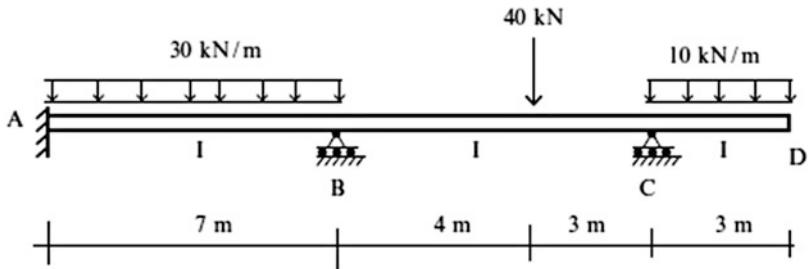
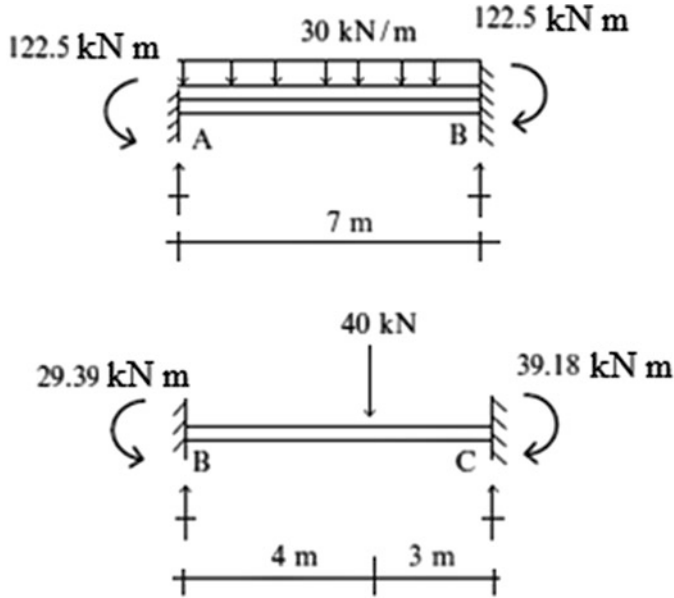


Fig. E10.3a

Determine: The end actions and the shear and moment diagrams.

Solution: First, we compute the fixed end moments by using Table 9.1.



$$M_{AB}^F = + \frac{30(7)^2}{12} = +122.5 \text{ kN m}$$

$$M_{BA}^F = -122.5 \text{ kN m}$$

$$M_{BC}^F = \frac{40(4)(3)^2}{(7)^2} = +29.39 \text{ kN m}$$

$$M_{CB}^F = - \frac{40(4)^2(3)}{(7)^2} = -39.18 \text{ kN m}$$

We define the relative member stiffness for each member as

$$k_{\text{member AB}} = k_{\text{member BC}} = \frac{EI}{L} = k_1$$

Noting that $\theta_A = 0$ and the supports are unyielding ($v_A = v_B = v_C = 0$), the corresponding slope-deflection equation (10.12a) take the form

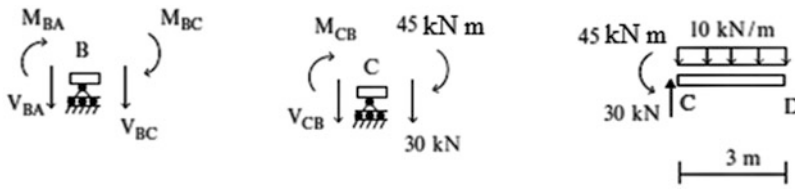
$$M_{AB} = 2k_1(\theta_B) + 122.5$$

$$M_{BA} = 2k_1(2\theta_B) - 122.5$$

$$M_{BC} = 2k_1(2\theta_B + \theta_C) + 29.39$$

$$M_{CB} = 2k_1(2\theta_C + \theta_B) - 39.18$$

We enforce moment equilibrium at the nodes B and C.



The corresponding equations are:

$$M_{BA} + M_{BC} = 0 \Rightarrow 2k_1\theta_C + 6k_1\theta_B = 93.11$$

$$M_{CB} + 45 = 0 \Rightarrow 4k_1\theta_C + 2k_1\theta_B = -5.82$$

Solving these equations leads to

$$k_1\theta_B = 13.71$$

$$k_1\theta_C = -8.31$$

The corresponding end moments are:

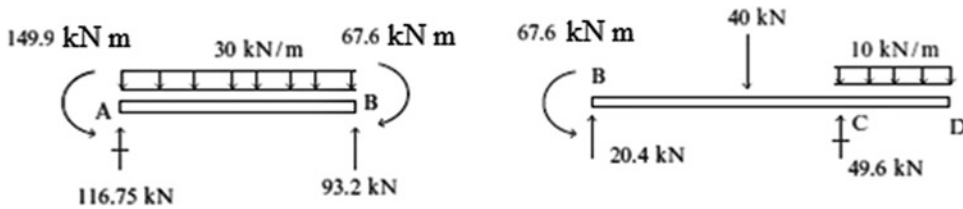
$$M_{AB} = +149.9 \text{ kN m}$$

$$M_{BA} = -67.6 \text{ kN m}$$

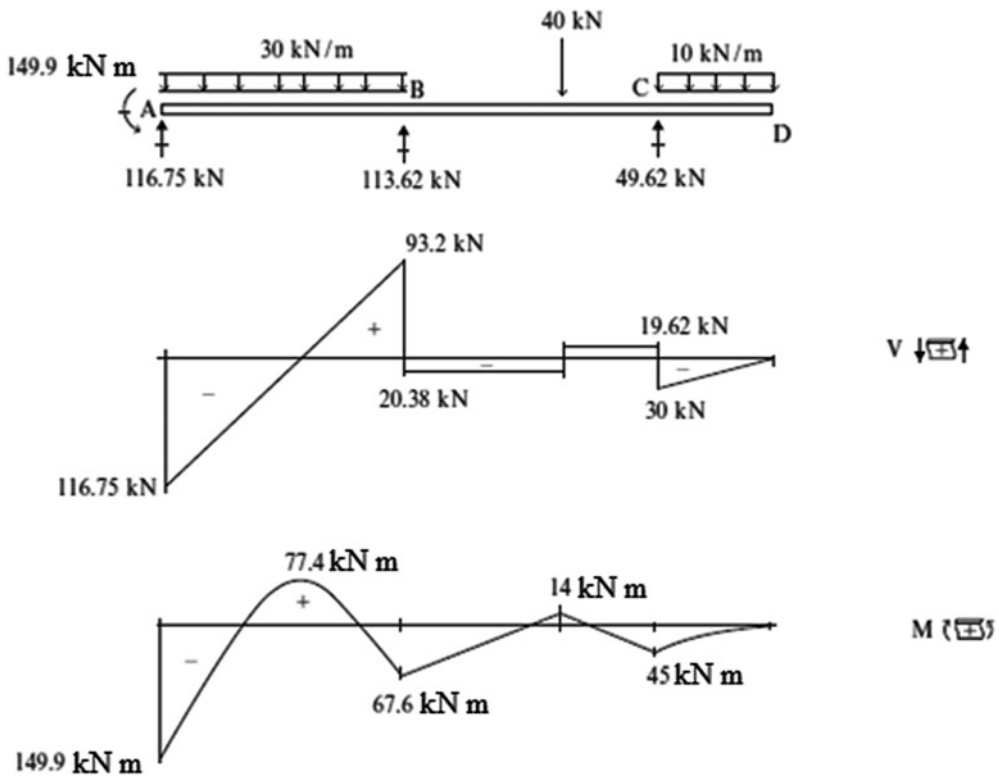
$$M_{BC} = +67.6 \text{ kN m}$$

$$M_{CB} = -45 \text{ kN m}$$

Next, we determine the end shear forces using the static equilibrium equations for the members.



The shear and moment diagrams are plotted below.



10.4.2 Multi-Span Beams

In what follows, we modify the slope-deflection equations for the end members of a multi-span continuous beam when they have either a pin or roller support. Consider the three-span beam shown in Fig. 10.12a. There are three beam segments and four nodes. Since the end nodes have zero moment, we can simplify the slope-deflection equations for the end segments by eliminating the end rotations. We did this in the previous examples, as part of the solution process. Now, we formalize the process and modify the slope-deflection equations before setting up the nodal moment equilibrium equations for the interior nodes.

Consider member AB. The end moment of A is zero, and we use this fact to express θ_A in terms of θ_B . Starting with the expression for M_{AB} ,

$$M_{AB} = \frac{2EI_1}{L_1} \left(2\theta_A + \theta_B - 3 \left(\frac{v_B - v_A}{L_1} \right) \right) + M_{AB}^F = 0$$

and solving for θ_A leads to

$$\theta_A = -\frac{1}{2}\theta_B + \frac{3}{2} \left(\frac{v_B - v_A}{L_1} \right) - \frac{L_1}{4EI_1} M_{AB}^F$$

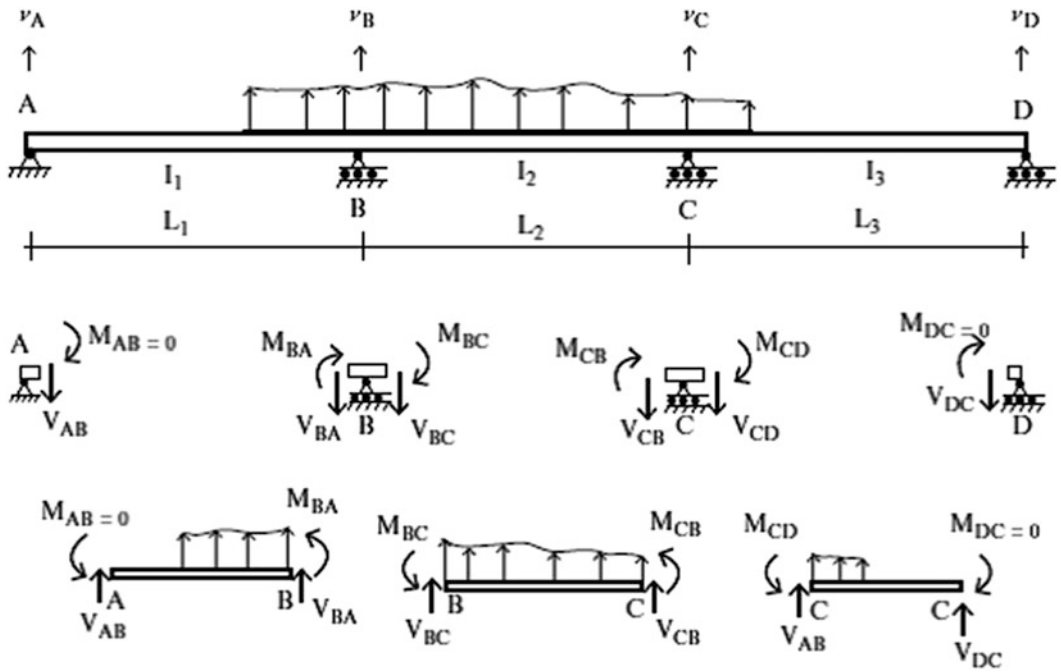


Fig. 10.12 Three-span beam

Then, we substitute for θ_A in the expression M_{BA} ,

$$M_{BA} = \frac{2EI_1}{L_1} \left(2\theta_B + \theta_A - 3 \frac{v_B - v_A}{L_1} \right) + M_{BA}^F$$

and obtain the following form,

$$M_{BA, \text{modified}} = \frac{3EI_1}{L_1} \left(\theta_B - \left(\frac{v_B - v_A}{L} \right) \right) + \left(M_{BA}^F - \frac{1}{2} M_{AB}^F \right) \tag{10.20}$$

Note that the presence of a pin or roller at A *reduces* the rotational stiffness at B from $4EI/L$ to $3EI/L$. Substituting for θ_A in the expression V_{AB} and V_{BA} leads to the following expressions,

$$V_{AB, \text{modified}} = + \frac{6EI}{L^2} \left\{ \frac{1}{2} \theta_B - \frac{1}{2} \left(\frac{v_B - v_A}{L} \right) \right\} + V_{AB}^F - \frac{3M_{AB}^F}{2L}$$

$$V_{BA, \text{modified}} = - \frac{6EI}{L^2} \left\{ \frac{1}{2} \theta_B - \frac{1}{2} \left(\frac{v_B - v_A}{L} \right) \right\} + V_{BA}^F + \frac{3M_{AB}^F}{2L}$$

For member BC, we use the general unchanged form

$$M_{BC} = \frac{2EI_2}{L_2} \left(2\theta_B + \theta_C - 3 \frac{v_C - v_B}{L_2} \right) + M_{BC}^F$$

$$M_{CB} = \frac{2EI_2}{L_2} \left(2\theta_C + \theta_B - 3 \frac{v_C - v_B}{L_2} \right) + M_{CB}^F$$

The modified form for member CD is

$$M_{DC} = 0$$

$$M_{CD} = \frac{3EI_3}{L_3} \left(\theta_C - \frac{v_D - v_C}{L_3} \right) + \left(M_{CD}^F - \frac{1}{2} M_{DC}^F \right)$$

Nodal moment equilibrium equations

Now, we return back to Fig. 10.12. If we use the modified form of the moment expressions for members AB and CD, we *do not* have to enforce moment equilibrium at nodes A and D since we have already employed this condition to modify the equations. Therefore, we need only to consider nodes B and C. Summing moments at these nodes,

$$M_{BA} + M_{BC} = 0$$

$$M_{CB} + M_{CD} = 0$$

and substituting for the end moments expressed in terms of θ_B and θ_C leads to

$$\begin{aligned} & \theta_B \left\{ \frac{3EI_1}{L_1} + \frac{4EI_2}{L_2} \right\} + \theta_C \left\{ \frac{2EI_2}{L_2} \right\} - \left\{ \frac{6EI_2}{L_2} \left(\frac{v_C - v_B}{L_2} \right) + \frac{3EI_1}{L_1} \left(\frac{v_B - v_A}{L_1} \right) \right\} \\ & + \left\{ M_{BC}^F + \left(M_{BA}^F - \frac{1}{2} M_{AB}^F \right) \right\} = 0 \\ & \theta_B \left\{ \frac{2EI_2}{L_2} \right\} + \theta_C \left\{ \frac{4EI_2}{L_2} + \frac{3EI_3}{L_3} \right\} - \left\{ \frac{6EI_2}{L_2} \left(\frac{v_C - v_B}{L_2} \right) + \frac{3EI_3}{L_3} \left(\frac{v_D - v_C}{L_3} \right) \right\} \\ & + \left\{ \left(M_{CD}^F - \frac{1}{2} M_{DC}^F \right) + M_{CB}^F \right\} = 0 \end{aligned} \quad (10.21)$$

Given the nodal fixed end moments due to the loading and the chord rotations due to support settlement, one can solve the above simultaneous equations for θ_B and θ_C and determine the end moments by back substitution. Note that the solution depends on the relative magnitudes of the ratio, l/L , for each member.

In what follows, we list the modified slope-deflection equations for an end member with a pin or roller support.

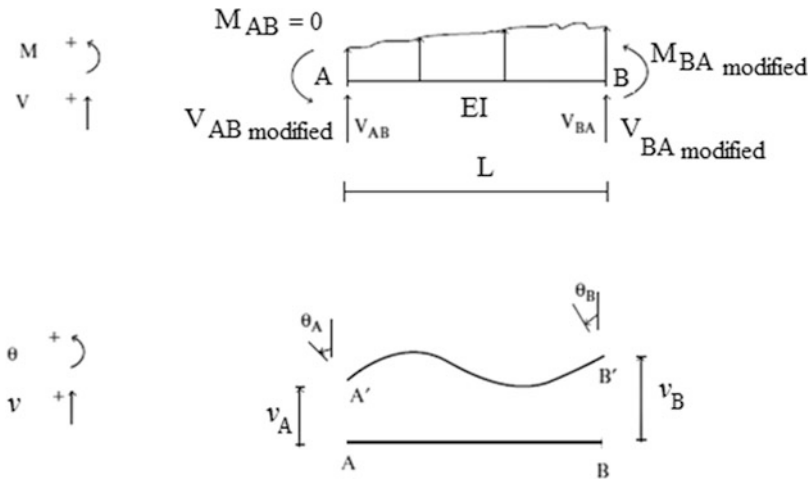
End member AB (exterior pin or roller at A end):

$$M_{AB} = 0$$

$$M_{BA_{\text{modified}}} = \frac{3EI}{L} \left\{ \theta_B - \left(\frac{v_B - v_A}{L} \right) \right\} + \left(M_{BA}^F - \frac{1}{2} M_{AB}^F \right) \quad (10.22a)$$

$$V_{AB_{\text{modified}}} = \frac{3EI}{L^2} \left\{ \theta_B - \left(\frac{v_B - v_A}{L} \right) \right\} + V_{AB}^F - \frac{3M_{AB}^F}{2L} \quad (10.22b)$$

$$V_{BA_{\text{modified}}} = -\frac{3EI}{L^2} \left\{ \theta_B - \left(\frac{v_B - v_A}{L} \right) \right\} + V_{BA}^F + \frac{3M_{AB}^F}{2L}$$



Equations (10.22a, 10.22b) are referred to as the *modified slope-deflection equations*.

Example 10.4: Two-Span Beam with Moment Releases at Both Ends

Given: The two-span beam shown in Fig. E10.4a. Assume EI is constant.

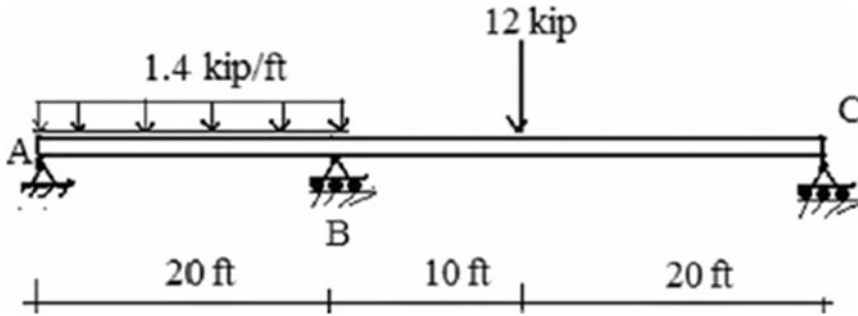


Fig. E10.4a

Determine: The end actions and the shear and moment diagrams.

Solution: The fixed end moments are (see Table 9.1):

$$M_{AB}^F = \frac{1.4(20)^2}{12} = 46.67 \text{ kip ft}$$

$$M_{BA}^F = -46.67 \text{ kip ft}$$

$$M_{BC}^F = \frac{12(10)(20)^2}{(30)} = 53.33 \text{ kip ft}$$

$$M_{CB}^F = -\frac{12(20)(10)^2}{(30)^2} = -26.67 \text{ kip ft}$$

We define the relative member stiffness for each member as

$$k_{\text{member BC}} = \frac{EI}{L_{BC}} = k_1$$

$$k_{\text{member AB}} = \frac{EI}{L_{AB}} = 1.5k_1$$

Next, we generate the expressions for the end moments using the modified slope-deflection equation (10.22a).

$$M_{AB} = 0$$

$$M_{BA} = M_{BA_{\text{modified}}} = 3(1.5k_1)(\theta_B) + \left(M_{BA}^F - \frac{1}{2}M_{AB}^F \right) = 3(1.5k_1)(\theta_B) + \left\{ -46.67 - \frac{1}{2}(46.67) \right\} = 4.5k_1\theta_B - 70$$

$$M_{BC} = M_{BC_{\text{modified}}} = 3(k_1)(\theta_B) + \left(M_{BC}^F - \frac{1}{2}M_{CB}^F \right) = 3(k_1)(\theta_B) + \left\{ +53.33 - \frac{1}{2}(-26.67) \right\} = 3k_1\theta_B + 66.66$$

$$M_{CB} = 0$$

The moment equilibrium equation for node B expands to

$$M_{BA} + M_{BC} = 0$$

$$\Downarrow$$

$$7.5k_1\theta_B - 3.34 = 0$$

$$\Downarrow$$

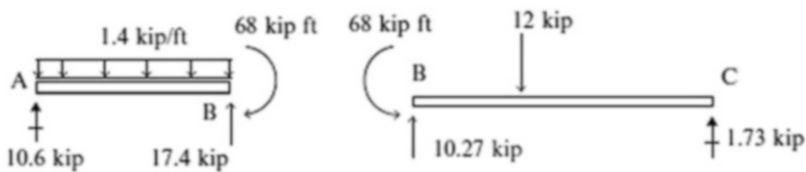
$$k_1\theta_B = 0.4453$$

Finally, the bending moment at B is

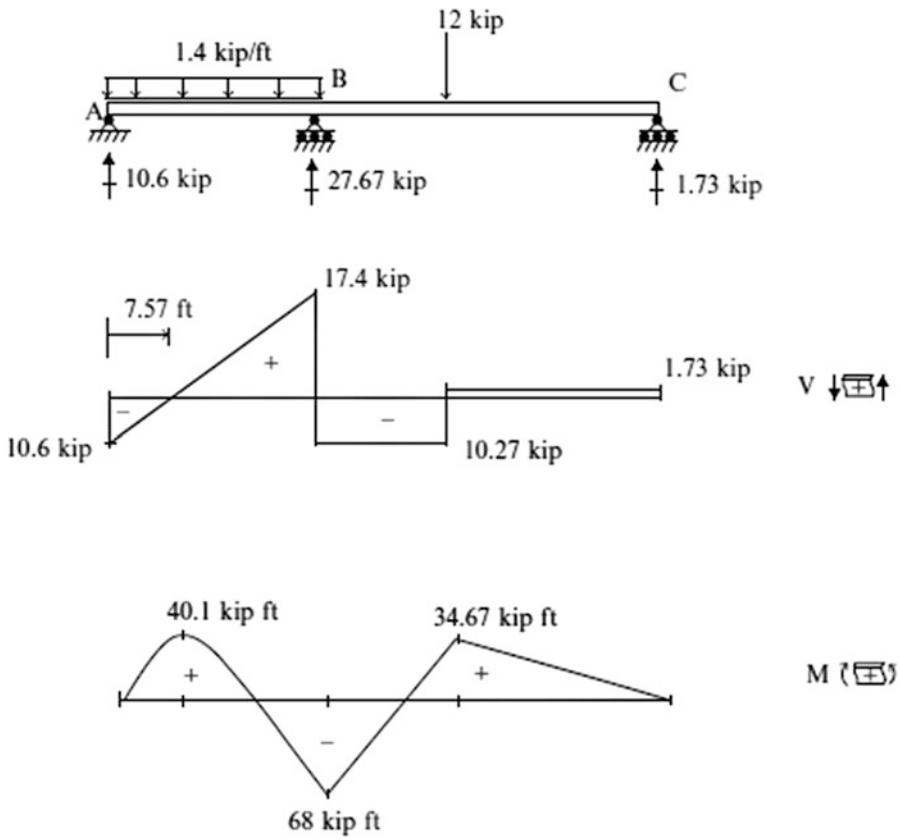
$$M_{BA} = -68 \text{ kip ft}$$

$$M_{BC} = -M_{BA} = 68 \text{ kip ft}$$

Noting the free body diagrams shown below, we find the remaining end actions.



The shear and moment diagrams are plotted below.



Example 10.5: Three-Span Beam

Given: The three-span beam shown in Figs. E10.5a, E10.5b, E10.5c.

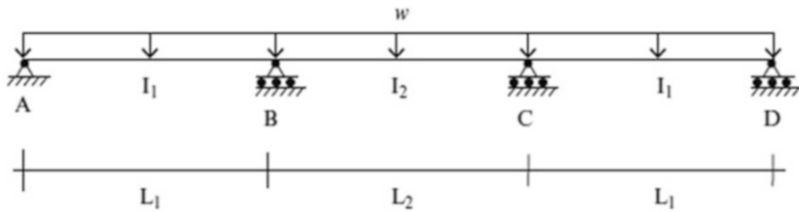


Fig. E10.5a Uniform load

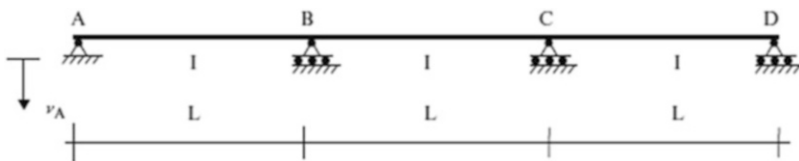


Fig. E10.5b Settlement at A

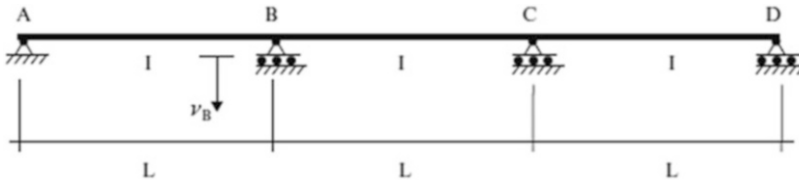


Fig. E10.5c Settlement at B

Determine: The end moments and draw the moment diagram for

Case (i): uniform load w . No support settlement.

Case (ii): No loading. Support settlement at A. Consider I and L are constants.

Case (iii): No loading. Support settlement at B. Consider I and L are constants.

Solution:

Case (i): Uniform loading

The supports are unyielding. Therefore $v_A = v_B = v_C = 0$. The fixed end moments due to the uniform loading are (see Table 9.1)

$$\begin{aligned} M_{AB}^F &= +\frac{wL_1^2}{12} & M_{BA}^F &= -\frac{wL_1^2}{12} \\ M_{BC}^F &= +\frac{wL_2^2}{12} & M_{CB}^F &= -\frac{wL_2^2}{12} \\ M_{CD}^F &= +\frac{wL_1^2}{12} & M_{DC}^F &= -\frac{wL_1^2}{12} \end{aligned}$$

We use (10.22a) for members AB and CD and (10.12a) for member BC.

$$M_{AB} = 0$$

$$M_{BA} = M_{BA_{\text{modified}}} = \frac{3EI_1}{L_1}\theta_B + \left(M_{BA}^F - \frac{1}{2}M_{AB}^F\right) = \frac{3EI_1}{L_1}\theta_B - \frac{wL_1^2}{8}$$

$$M_{BC} = \frac{2EI_2}{L_2}\{2\theta_B + \theta_C\} + M_{BC}^F = \frac{2EI_2}{L_2}\{2\theta_B + \theta_C\} + \frac{wL_2^2}{12}$$

$$M_{CB} = \frac{2EI_2}{L_2}\{\theta_B + 2\theta_C\} + M_{CB}^F = \frac{2EI_2}{L_2}\{\theta_B + 2\theta_C\} - \frac{wL_2^2}{12}$$

$$M_{CD} = M_{CD_{\text{modified}}} = \frac{3EI_1}{L_1}\theta_C + \left(M_{CD}^F - \frac{1}{2}M_{DC}^F\right) = \frac{3EI_1}{L_1}\theta_C + \frac{wL_1^2}{8}$$

$$M_{DC} = 0$$

The nodal moment equilibrium equations are

$$M_{BA} + M_{BC} = 0$$

$$M_{CB} + M_{CD} = 0$$

Substituting for the end moments, the above equilibrium equations expand to

$$\theta_B \left\{ \frac{3EI_1}{L_1} + \frac{4EI_2}{L_2} \right\} + \theta_C \left\{ \frac{2EI_2}{L_2} \right\} = -\frac{wL_2^2}{12} + \frac{wL_1^2}{8}$$

$$\theta_B \left\{ \frac{2EI_2}{L_2} \right\} + \theta_C \left\{ \frac{4EI_2}{L_2} + \frac{3EI_1}{L_1} \right\} = -\frac{wL_1^2}{8} + \frac{wL_2^2}{12}$$

$$\Downarrow$$

$$\frac{EI_2}{L_2} \theta_B = \frac{wL_2^2}{12} \left\{ \frac{-1 + \frac{3}{2}(L_1/L_2)^2}{2 + 3(I_1/I_2)(L_2/L_1)} \right\}$$

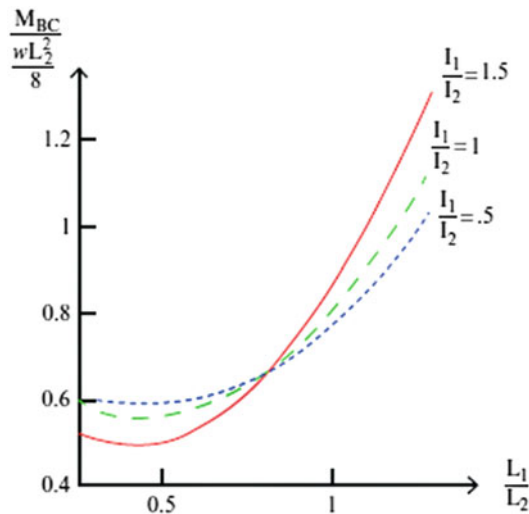
$$\theta_C = -\theta_B$$

The corresponding moments are

$$M_{BC} = \frac{wL_2^2}{8} \left\{ \frac{(L_1/L_2)^2 + (I_1/I_2)(L_2/L_1)}{1 + 3/2(I_1/I_2)(L_2/L_1)} \right\}$$

$$M_{CB} = -M_{BC}$$

We note that the moments are a function of (I_1/I_2) and (L_1/L_2) . The sensitivity of M_{BC} to the ratio (L_1/L_2) is plotted below for various values of (I_1/I_2) .



When I and L are constants for all the spans, the solution is

$$\theta_B = \frac{wL^3}{120EI}$$

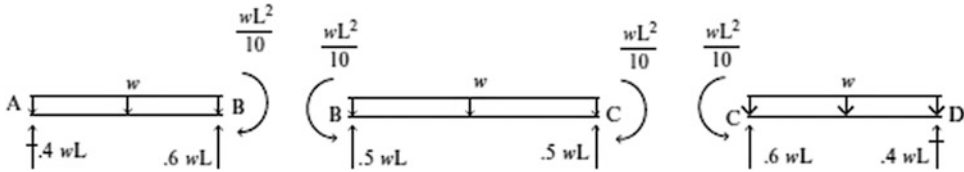
$$\theta_C = -\frac{wL^3}{120EI}$$

and

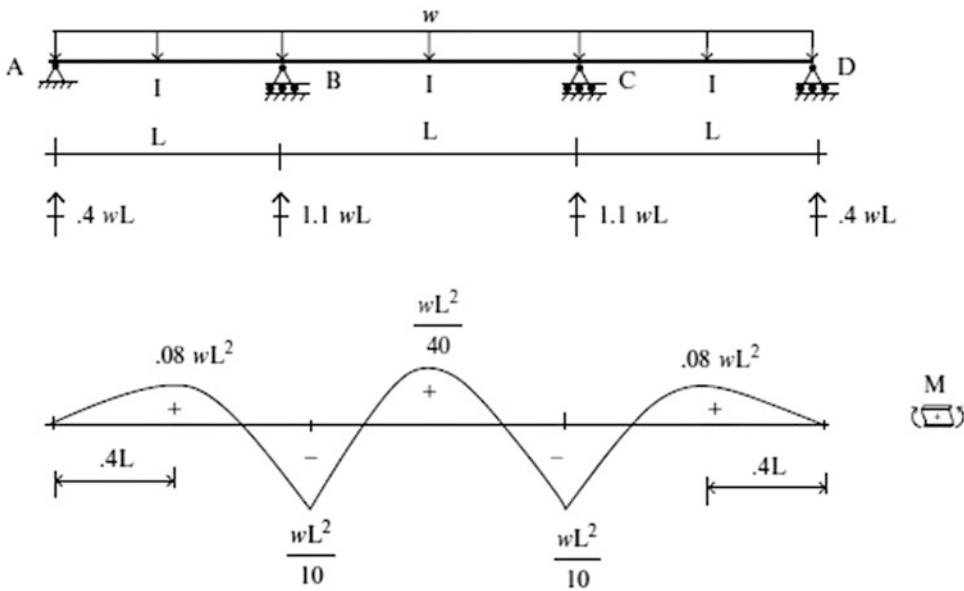
$$M_{BA} = M_{CB} = -\frac{wL^2}{10}$$

$$M_{BC} = M_{CD} = \frac{wL^2}{10}$$

We determine the end shear forces using the static equilibrium equations for the members.



The moment diagram is plotted below.



Case (ii): Support settlement at A, no loading, I and L are constants

The chord rotations are

$$\rho_{AB} = +\frac{v_A}{L}$$

$$\rho_{AB} = \rho_{CD} = 0$$

Specializing (10.22a) for members AB and CD and (10.12a) for member BC for I and L constant, and the above notation results in

$$M_{BA_{\text{modified}}} = \frac{3EI}{L} \left\{ \theta_B - \frac{v_A}{L} \right\}$$

$$M_{BC} = \frac{2EI}{L} \{ 2\theta_B + \theta_C \}$$

$$M_{CB} = \frac{2EI}{L} \{ \theta_B + 2\theta_C \}$$

$$M_{CD_{\text{modified}}} = \frac{3EI}{L} \{ \theta_C \}$$

The nodal moment equilibrium equations are

$$\begin{aligned} M_{BA} + M_{BC} &= 0 & 7\theta_B + 2\theta_C &= \frac{3v_A}{L} \\ &\Rightarrow & & \\ M_{CB} + M_{CD} &= 0 & 2\theta_B + 7\theta_C &= 0 \end{aligned}$$

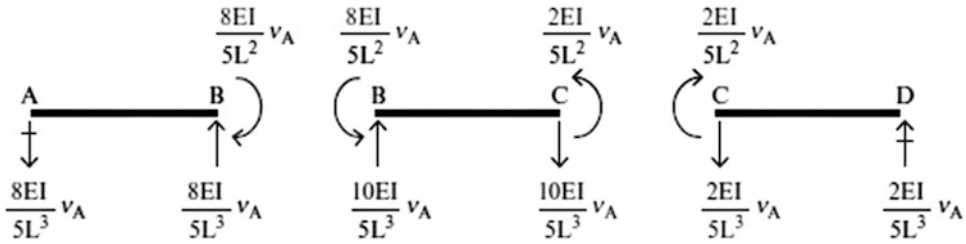
The solution is

$$\begin{aligned} \theta_B &= \frac{7v_A}{15L} \\ \theta_C &= -\frac{2v_A}{15L} \end{aligned}$$

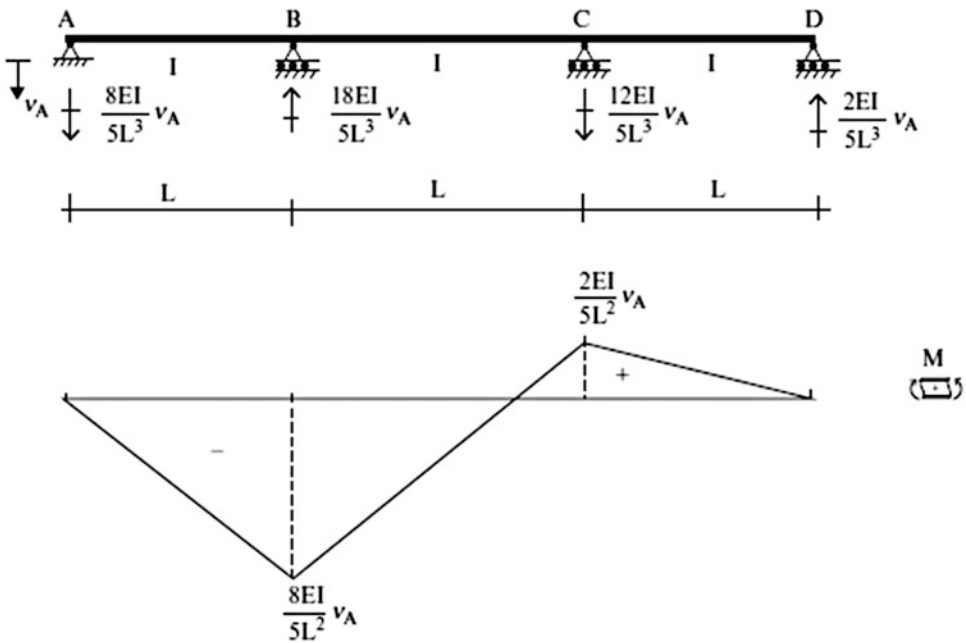
and the corresponding moments are

$$\begin{aligned} M_{BA} &= -\frac{8EI}{5L^2} v_A \\ M_{CD} &= -\frac{2EI}{5L^2} v_A \end{aligned}$$

We determine the end shear forces using the static equilibrium equations for the members.



The moment diagram is plotted below.



Case (iii): Support settlement at B, no loading, I and L are constants

The chord rotations are

$$\begin{aligned}\rho_{AB} &= -\frac{v_B}{L} \\ \rho_{BC} &= +\frac{v_B}{L} \\ \rho_{CD} &= 0\end{aligned}$$

Specializing (10.22a) for members AB and CD and (10.12a) for member BC for I and L constant, and the above notation results in

$$\begin{aligned}M_{BA\text{modified}} &= \frac{3EI}{L} \left\{ \theta_B + \left(\frac{v_B}{L} \right) \right\} \\ M_{BC} &= \frac{2EI}{L} \left\{ 2\theta_B + \theta_C - 3\frac{v_B}{L} \right\} \\ M_{CB} &= \frac{2EI}{L} \left\{ \theta_B + 2\theta_C - 3\frac{v_B}{L} \right\} \\ M_{CD\text{modified}} &= \frac{3EI}{L} \{ \theta_C \}\end{aligned}$$

The nodal moment equilibrium equations are

$$\begin{aligned}M_{BA} + M_{BC} &= 0 & 7\theta_B + 2\theta_C &= \frac{3v_B}{L} \\ & \Rightarrow \\ M_{CB} + M_{CD} &= 0 & 2\theta_B + 7\theta_C &= \frac{6v_B}{L}\end{aligned}$$

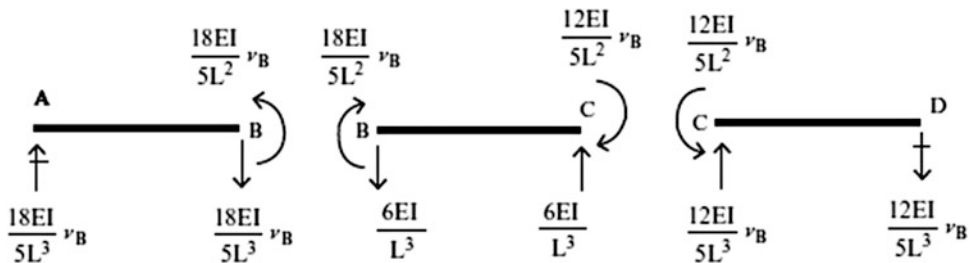
The solution is

$$\begin{aligned}\theta_B &= \frac{v_B}{5L} \\ \theta_C &= \frac{4v_B}{5L}\end{aligned}$$

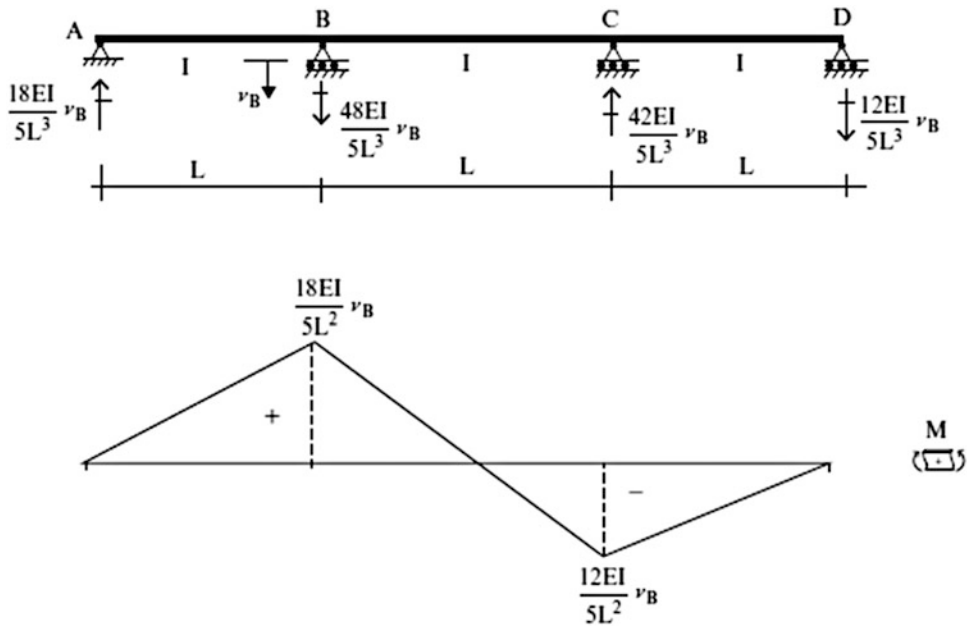
and the corresponding moments are

$$\begin{aligned}M_{BA} &= \frac{18EI}{5L^2} v_B \\ M_{CD} &= \frac{12EI}{5L^2} v_B\end{aligned}$$

We determine the end shear forces using the static equilibrium equations for the members.



Noting the free body diagrams, we find the reactions. The moment diagram is plotted below.



Example 10.6: Uniformly Loaded Three-Span Symmetrical Beam—Fixed Ends

Given: The three-span symmetrical fixed end beam defined in Fig. E10.6a. This model is representative of an integral bridge with very stiff abutments at the ends of the beam.

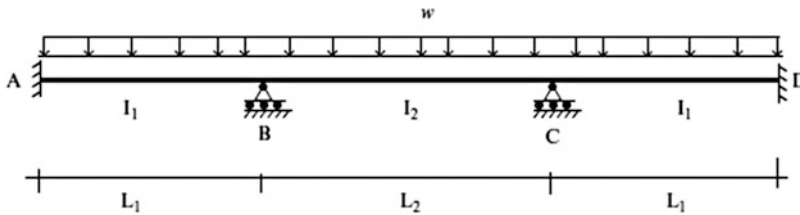


Fig. E10.6a

Determine: The end moments.

Solution: The slope-deflection equations for unyielding supports, $\theta_A = \theta_D = 0$ and symmetry $\theta_B = -\theta_C$ are

$$M_{AB} = -M_{DC} = \frac{2EI_1}{L_1}(\theta_B) + M_{AB}^F$$

$$M_{BA} = \frac{2EI_1}{L_1}(2\theta_B) + M_{BA}^F$$

$$M_{BC} = -M_{CB} = \frac{2EI_2}{L_2}(\theta_B) + M_{BC}^F$$

where

$$M_{AB}^F = M_{CD}^F = +\frac{wL_1^2}{12}$$

$$M_{BA}^F = M_{DC}^F - \frac{wL_1^2}{12}$$

$$M_{BC}^F = +\frac{wL_2^2}{12}$$

$$M_{CB}^F = -\frac{wL_2^2}{12}$$

Summing end moments at node B

$$M_{BA} + M_{BC} = 0$$

$$\theta_B \left\{ \frac{4EI_1}{L_1} + \frac{2EI_2}{L_2} \right\} = -(M_{BA}^F + M_{BC}^F)$$

and solving for θ_B leads to

$$\theta_B = -\theta_C = \frac{((wL_1^2/12) - (wL_2^2/12))}{((4EI_1/L_1) + (2EI_2/L_2))}$$

Suppose I and L are constants. The end rotations corresponding to this case are

$$\theta_B = \theta_C = 0$$

It follows that the end moments are equal to the fixed end moments.

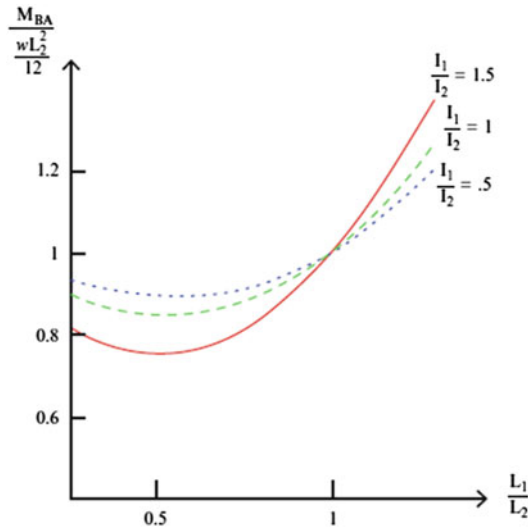
$$M_{AB} = \frac{wL^2}{12}$$

$$M_{BA} = -M_{BC} = -\frac{wL^2}{12}$$

The general solution for the moment at B follows by substituting for θ_B in either the expression for M_{BA} or M_{BC} . After some algebraic manipulation, the expression for M_{BA} reduces to

$$M_{BA} = \frac{wL_2^2}{12} \frac{\left\{ (L_1/L_2)^2 + 2(I_1/I_2)(L_2/L_1) \right\}}{(1 + 2(I_1/I_2)(L_2/L_1))}$$

We note that the moments are a function of (I_1/I_2) and (L_1/L_2) . The sensitivity of M_{BA} to the ratio (L_1/L_2) is plotted below for various values of (I_1/I_2) .



10.5 The Displacement Method Applied to Rigid Frames

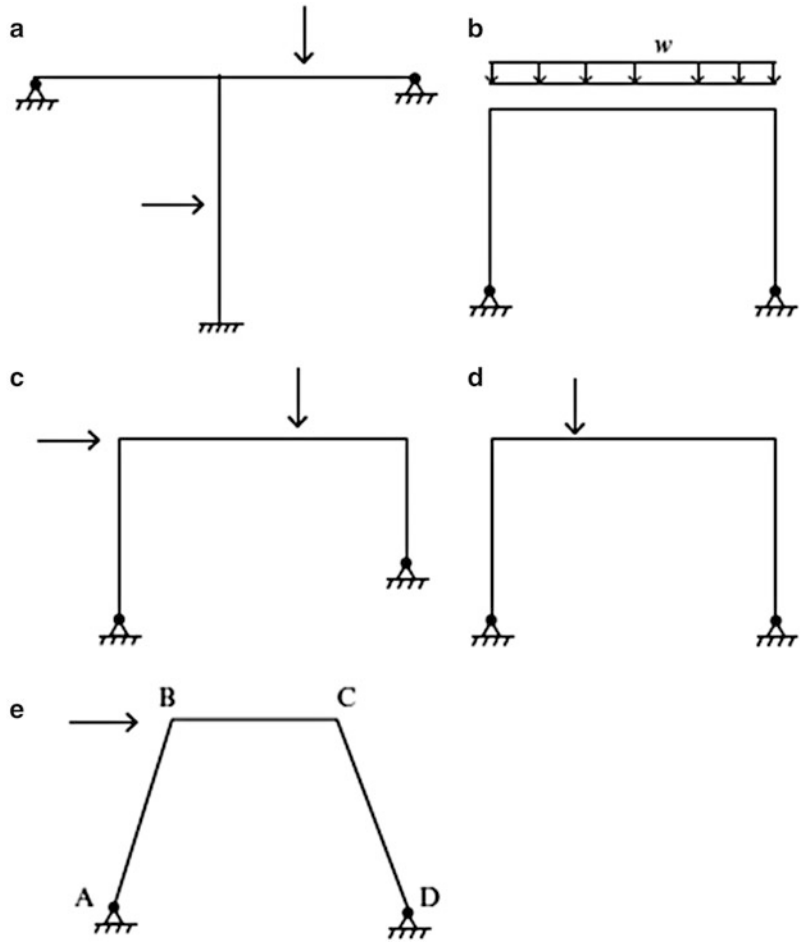
The essential difference between the analysis of beams and frames is the choice of the nodal displacements. The nodal variables for a beam are taken as the rotations. When there is support movement, we prescribe the nodal translation and compute the corresponding fixed end moments. In this way, the equilibrium equations always involve only rotation variables. Rigid frames are considered to be an assemblage of members rigidly connected at nodes. Since frame structures are formed by joining members at an arbitrary angle, the members rotate as well as bend. When this occurs, we need to include the chord rotation terms in the slope-deflection equations, and work with both translation and rotation variables. Using these relations, we generate a set of equations relating the nodal translations and rotations by enforcing equilibrium for the nodes. The approach is relatively straightforward when there are not many displacement variables. However, for complex structures involving many displacement unknowns, one would usually employ a computer program which automates the generation and solution of the equilibrium equations.

The term “sideway” is used to denote the case where some of the members in a structure experience chord rotation resulting in “sway” of the structure. Whether sideway occurs depends on how the members are arranged and also depends on the loading applied. For example, consider the frame shown in Fig. 10.13a. Sideway is not possible because of the horizontal restraint. The frame shown in Fig. 10.13b is symmetrical and also loaded symmetrically. Because of symmetry, there will be no sway. The frame shown in Fig. 10.13c will experience sideway. The symmetrical frame shown in Fig. 10.13d will experience sideway because of the unsymmetrical loading. All three members will experience chord rotation for the frame shown in Fig. 10.13e.

When starting an analysis, one first determines whether sideway will occur in order to identify the nature of the displacement variables. The remaining steps are relatively straightforward. One establishes the free body diagram for each node and enforces the equilibrium equations. The essential difference is that now one needs to consider force equilibrium as well as moment equilibrium. We illustrate the analysis process with the following example.

Consider the frame shown in Fig. 10.14. Under the action of the applied loading, nodes B and C will displace horizontally an amount Δ . Both members AB and CD will have chord rotation. There are

Fig. 10.13 Examples of sideway



three displacement unknowns θ_B , θ_C , and Δ . In general, we neglect the axial deformation. The free body diagrams for the members and nodes are shown in Fig. 10.15. We take the positive sense of the members to be from $A \rightarrow B$, $B \rightarrow C$, and $C \rightarrow D$. Note that this fixes the sense of the shear forces. The end moments are always positive when counterclockwise.

Moment equilibrium for nodes B and C requires

$$\begin{aligned} \sum M_B = 0 &\Rightarrow M_{BA} + M_{BC} = 0 \\ \sum M_C = 0 &\Rightarrow M_{CB} + M_{CD} = 0 \end{aligned} \tag{10.23a}$$

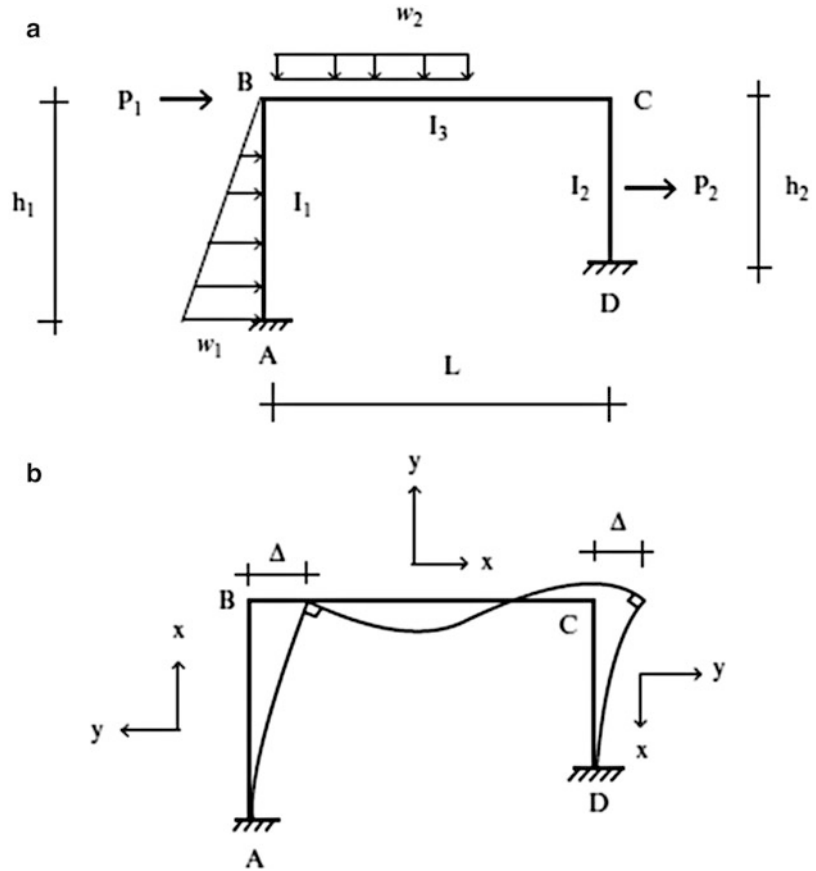
We also need to satisfy horizontal force equilibrium for the entire frame.

$$\sum F_x = 0 \rightarrow + \Rightarrow -V_{AB} + V_{DC} + \sum F_x = 0 \tag{10.23b}$$

where $\sum F_x = P_1 + P_2 + \frac{1}{2}w_1h_1$.

The latter equation is associated with sideway.

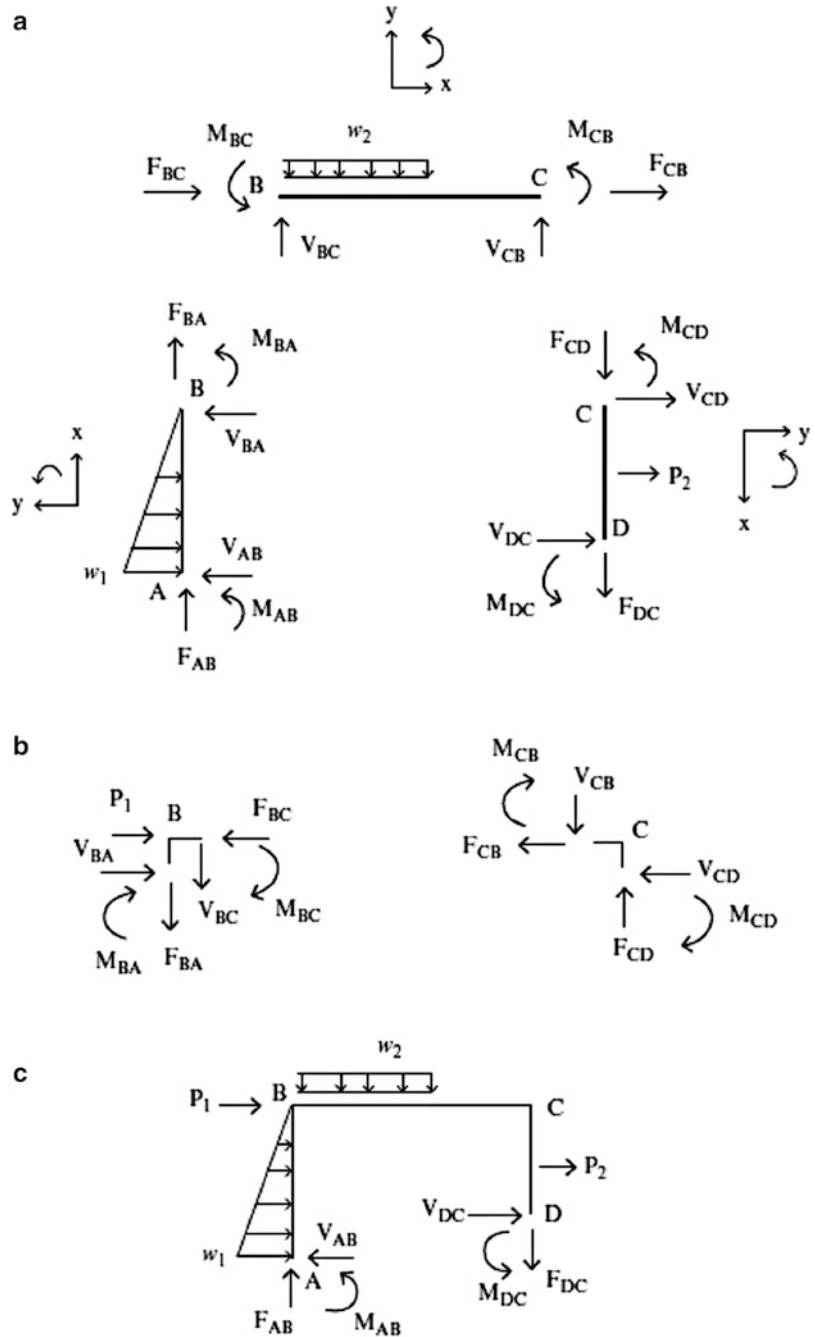
Fig. 10.14 (a) Loading.
(b) Deflected shape



Noting that $\theta_A = \theta_D = 0$, $v_A = v_D = 0$, $v_B = -\Delta$, and $v_C = +\Delta$, the slope-deflection equations (10.12a, 10.12b) simplify to

$$\begin{aligned}
 M_{AB} &= \frac{2EI_1}{h_1} \left\{ \theta_B - 3 \left(\frac{-\Delta}{h_1} \right) \right\} + M_{AB}^F \\
 M_{BA} &= \frac{2EI_1}{h_1} \left\{ 2\theta_B - 3 \left(\frac{-\Delta}{h_1} \right) \right\} + M_{BA}^F \\
 M_{BC} &= \frac{2EI_3}{L} \{ 2\theta_B + \theta_C \} + M_{BC}^F \\
 M_{CB} &= \frac{2EI_3}{L} \{ 2\theta_C + \theta_B \} + M_{CB}^F \\
 M_{CD} &= \frac{2EI_2}{h_2} \left\{ 2\theta_C - 3 \left(\frac{-\Delta}{h_2} \right) \right\} + M_{CD}^F \\
 M_{DC} &= \frac{2EI_2}{h_2} \left\{ \theta_C - 3 \left(\frac{-\Delta}{h_2} \right) \right\} + M_{DC}^F \\
 V_{AB} &= \frac{6EI_1}{h_1^2} \left\{ \theta_B + 2 \frac{\Delta}{h_1} \right\} + V_{AB}^F \\
 V_{DC} &= -\frac{6EI_2}{h_2^2} \left\{ \theta_C + 2 \frac{\Delta}{h_2} \right\} + V_{DC}^F
 \end{aligned} \tag{10.24}$$

Fig. 10.15 Free body diagrams for members and nodes of the frame. (a) Members. (b) Nodes. (c) Reactions



Substituting for the end moments and shear forces in (10.23a, 10.23b) leads to

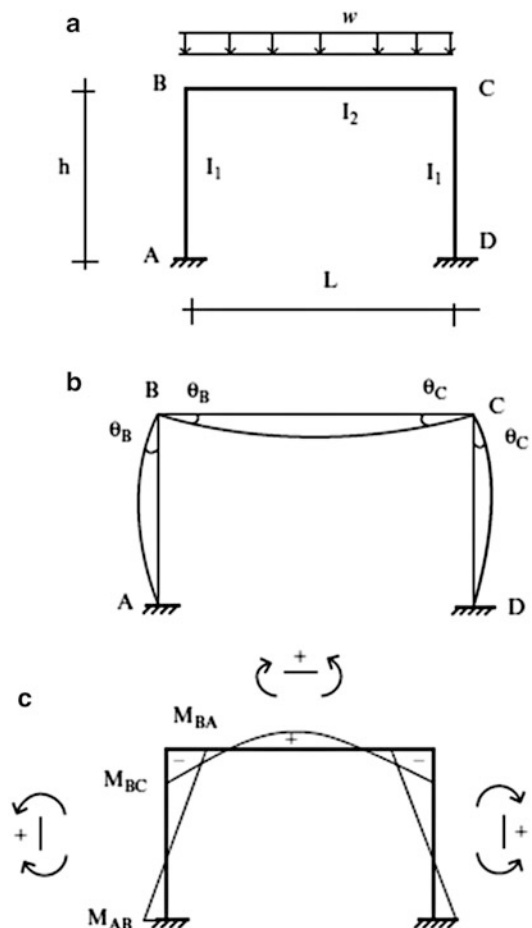
$$\begin{aligned} \left(\frac{4EI_1}{h_1} + \frac{4EI_3}{L}\right)\theta_B + \frac{2EI_3}{L}\theta_C + \frac{6EI_1}{h_1}\left(\frac{\Delta}{h_1}\right) + (M_{BC}^F + M_{BA}^F) &= 0 \\ \frac{2EI_3}{L}\theta_B + \left(\frac{4EI_3}{L} + \frac{4EI_2}{h_2}\right)\theta_C + \frac{6EI_2}{h_2}\left(\frac{\Delta}{h_2}\right) + (M_{CD}^F + M_{CB}^F) &= 0 \\ -\frac{6EI_1}{h_1^2}\theta_B - \frac{6EI_2}{h_2^2}\theta_C + \left(-\frac{12EI_1}{h_1^3} - \frac{12EI_2}{h_2^3}\right)\Delta - V_{AB}^F + V_{DC}^F + \sum F_x &= 0 \end{aligned} \tag{10.25}$$

Once the loading and properties are specified, one can solve (10.25) for θ_B , θ_C , and Δ . The end actions are then evaluated with (10.24).

10.5.1 Portal Frames: Symmetrical Loading

Consider the symmetrical frame defined in Fig. 10.16. When the loading is also symmetrical, nodes B and C do not displace laterally, and therefore there is no chord rotation for members AB and CD. Also, the rotations at B and C are equal in magnitude but opposite in sense ($\theta_B = -\theta_C$). With these simplifications, the expressions for the end moments reduce to

Fig. 10.16 Portal frame—symmetrical loading. (a) Loading. (b) Deflected shape. (c) Moment diagram



$$\begin{aligned}
 M_{BC} &= \frac{2EI_2}{L}(\theta_B) + M_{BC}^F \\
 M_{BA} &= \frac{2EI_1}{h}(2\theta_B) \\
 M_{AB} &= \frac{1}{2}M_{BA}
 \end{aligned} \tag{10.26}$$

Moment equilibrium for node B requires

$$M_{BC} + M_{BA} = 0 \tag{10.27}$$

Substituting for the moments, the equilibrium equation expands to

$$2E\theta_B \left\{ 2\frac{I_1}{h} + \frac{I_2}{L} \right\} = -M_{BC}^F$$

We solve for θ_B and then evaluate the end moments.

$$M_{BA} = 2M_{AB} = -M_{BC} = \frac{-1}{1 + (I_2/L)/2(I_1/h)} M_{BC}^F \tag{10.28}$$

The bending moment diagram is plotted in Fig. 10.16c.

10.5.2 Portal Frames: Anti-symmetrical Loading

Lateral loading produces anti-symmetrical behavior, as indicated in Fig. 10.17, and chord rotation for members AB and CD. In this case, the nodal rotations at B and C are equal in both magnitude and sense ($\theta_B = \theta_C$). The chord rotation is related to the lateral displacement of B by

$$\rho_{AB} = -\frac{v_B}{h} \tag{10.29}$$

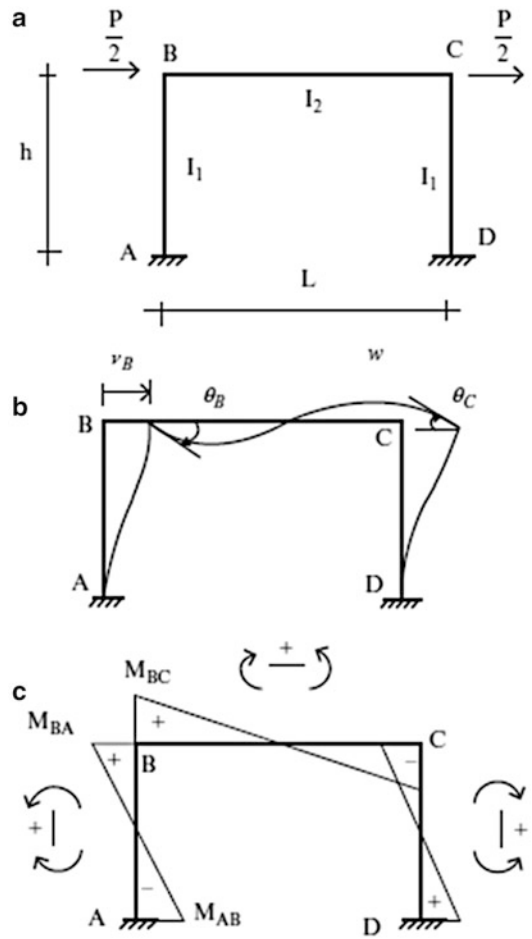
Note that the chord rotation sign convention for the slope-deflection equations (10.12a, 10.12b) is positive when counterclockwise. Therefore for this choice of the sense of v_B , the chord rotation for AB is negative. The corresponding expressions for the end moments are

$$\begin{aligned}
 M_{BC} &= 2E\frac{I_2}{L}(3\theta_B) \\
 M_{BA} &= 2E\frac{I_1}{h}\left(2\theta_B + \frac{3v_B}{h}\right) \\
 M_{AB} &= 2E\frac{I_1}{h}\left(\theta_B + \frac{3v_B}{h}\right)
 \end{aligned} \tag{10.30}$$

Equilibrium requires

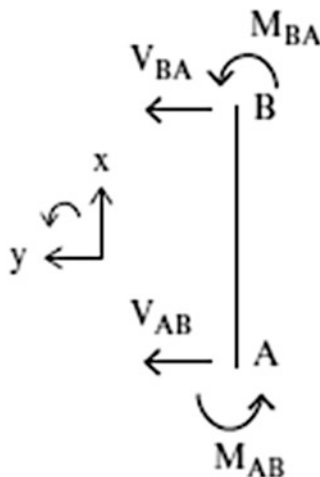
$$\begin{aligned}
 M_{BC} + M_{BA} &= 0 \\
 -V_{AB} + \frac{P}{2} &= 0
 \end{aligned} \tag{10.31}$$

Fig. 10.17 Portal frame—anti-symmetric loading.
 (a) Loading. (b) Deflected shape. (c) Moment diagram



We determine the end shear with the moment equilibrium equation for member AB.

$$\begin{aligned}
 V_{AB} &= \frac{M_{BA} + M_{AB}}{h} \\
 &= \frac{2EI_1}{h^2} \left(3\theta_B + 6\frac{v_B}{h} \right)
 \end{aligned}
 \tag{10.32}$$



Substituting for the moments and shear in (10.31) leads to two equations with two unknowns, θ_B and v_B . The solution has the following form

$$\begin{aligned}\theta_B &= \frac{-h^2 P}{4EI_1} \frac{1}{1 + 6(I_2/L)/(I_1/h)} \\ v_B &= \frac{h^3 P}{24EI_1} \left(\frac{1 + \frac{2}{3}((I_1/h)/(I_2/L))}{1 + (I_1/h)/6(I_2/L)} \right)\end{aligned}\quad (10.33)$$

We evaluate M_{BA} and M_{AB} using (10.30).

$$\begin{aligned}M_{BA} &= \frac{Ph}{4} \frac{1}{1 + \frac{1}{6}(I_1/h)/(I_2/L)} \\ M_{AB} &= \frac{Ph}{4} \frac{1 + 1/3(I_1/h)/(I_2/L)}{1 + 1/6(I_1/h)/(I_2/L)}\end{aligned}\quad (10.34)$$

A typical moment diagram is shown in Fig. 10.17c. Note the sign convention for bending moment. When the girder is very stiff with respect to the column, $I_2/L \gg I_1/h$ the solution approaches

$$\begin{aligned}\theta_B &\rightarrow 0 \\ v_B &\rightarrow \frac{h^3 P}{24EI_1} \\ M_{BA} &\rightarrow \frac{Ph}{4} \\ M_{AB} &\rightarrow \frac{Ph}{4}\end{aligned}\quad (10.35)$$

Example 10.7: Frame with No Sideway

Given: The frame defined in Fig. E10.7a.

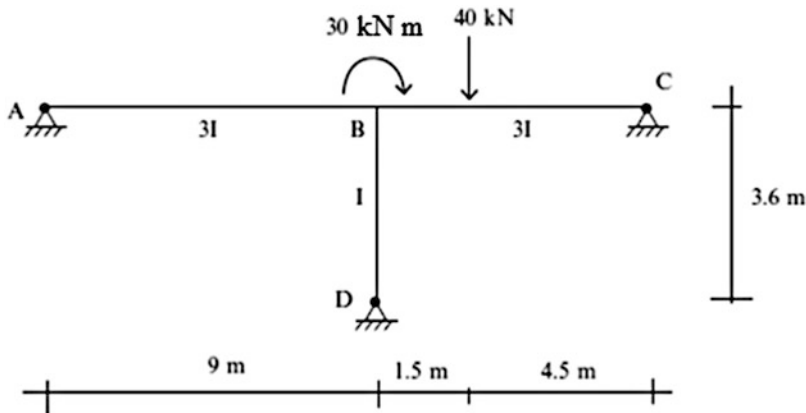


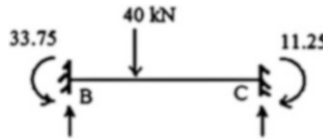
Fig. E10.7a

Determine: The end actions.

Solution: The fixed end moments are (see Table 9.1)

$$M_{BC}^F = \frac{40(1.5)(4.5)^2}{(6)^2} = 33.75 \text{ kNm}$$

$$M_{CB}^F = \frac{40(4.5)(1.5)^2}{(6)^2} = -11.25 \text{ kNm}$$



The modified slope-deflection equations (10.22a) which account for moment releases at A, C, and D are

$$M_{AB} = M_{DB} = M_{CB} = 0$$

$$M_{BA} = M_{BA_{\text{modified}}} = 3 \frac{E(3I)}{9} (\theta_B) = EI\theta_B$$

$$M_{BD} = M_{BD_{\text{modified}}} = 3 \frac{E(I)}{3.6} (\theta_B) = (0.83)EI\theta_B$$

$$M_{BC} = M_{BC_{\text{modified}}} = 3 \frac{E(3I)}{6} (\theta_B) + \left\{ M_{BC}^F - \frac{1}{2} M_{CB}^F \right\} = (1.5)EI\theta_B + 39.375$$

Moment equilibrium for node B requires (Fig. E10.7b)

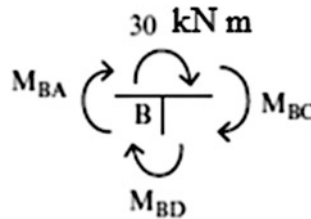


Fig. E10.7b

$$M_{BA} + M_{BC} + M_{BD} + 30 = 0$$

$$\Downarrow$$

$$EI\theta_B + (0.83)EI\theta_B + (1.5)EI\theta_B + 39.375 + 30 = 0$$

$$\Downarrow$$

$$EI\theta_B = -20.83$$

The final bending moments at B are

$$M_{BA} = -20.8 \Rightarrow M_{BA} = 20.8 \text{ kN m clockwise}$$

$$M_{BD} = -17.3 \Rightarrow M_{BD} = 17.3 \text{ kN m clockwise}$$

$$M_{BC} = 8.1 \Rightarrow M_{BC} = 8.1 \text{ kN m counterclockwise}$$

Noting the free body diagrams below, we find the remaining end actions (Figs. E10.7c and E10.7d).

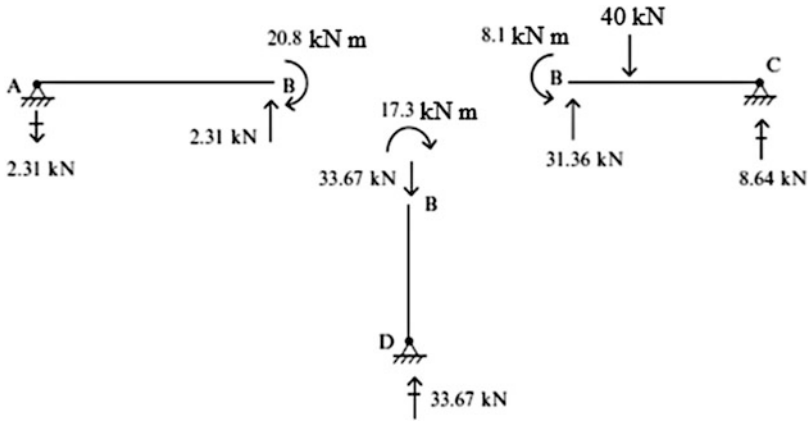


Fig. E10.7c Free body diagrams

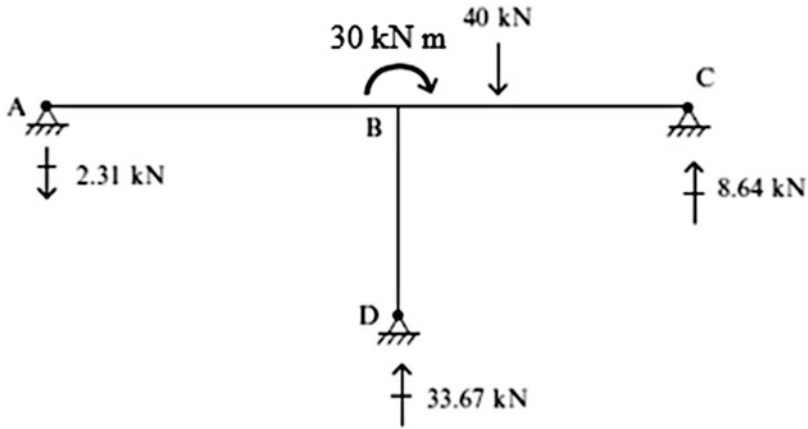


Fig. E10.7d Reactions

Example 10.8: Frame with Sideway

Given: The frame defined in Fig. E10.8a.

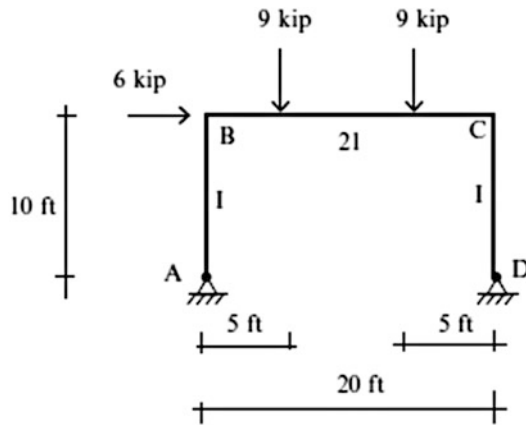


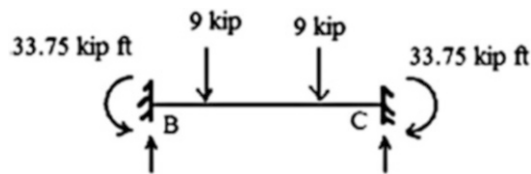
Fig. E10.8a

Determine: The end actions.

Solution: The fixed end moments are (see Table 9.1)

$$M_{BC}^F = \frac{9(5)(15)^2}{20^2} + \frac{9(15)(5)^2}{20^2} = 33.75 \text{ kip ft}$$

$$M_{CB}^F = -M_{BC}^F = -33.75 \text{ kip ft}$$



The chord rotations follow from the sketch below (Fig. E10.8b):

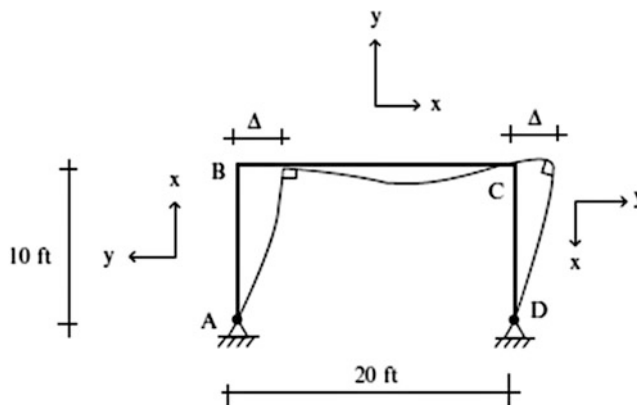


Fig. E10.8b

$$\rho = \rho_{AB} = \rho_{CD} = -\frac{\Delta}{10}$$

$$\rho_{BC} = 0$$

Substituting for the chord rotations in the slope-deflection equations [(10.12a, 10.12b) and (10.22a, 10.22b)] results in (Figs. E10.8c and E10.8d)

$$M_{AB} = M_{DC} = 0$$

$$M_{BA} = M_{BA_{\text{modified}}} = \frac{3E(I)}{10} \{\theta_B + \rho\} = 0.3EI\theta_B + 0.3EI\rho$$

$$M_{BC} = \frac{2E(2I)}{20} \{2\theta_B + \theta_C\} + 33.75 = 0.4EI\theta_B + 0.2EI\theta_C + 33.75$$

$$M_{CB} = \frac{2E(2I)}{20} \{\theta_B + 2\theta_C\} - 33.75 = 0.2EI\theta_B + 0.4EI\theta_C - 33.75$$

$$M_{CD} = M_{CD_{\text{modified}}} = \frac{3E(I)}{10} \{\theta_C + \rho\} = 0.3EI\theta_C + 0.3EI\rho$$

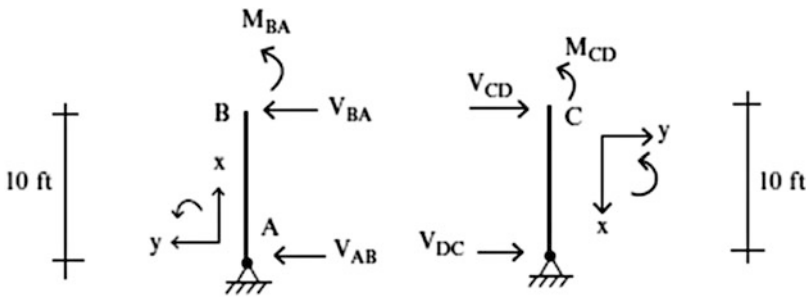


Fig. E10.8c

Also

$$V_{AB} = \frac{M_{BA}}{10}$$

$$V_{DC} = -\frac{M_{CD}}{10}$$

The end actions are listed in Fig. E10.8c.

Enforcing equilibrium at nodes B and C yields two equations,

$$M_{BC} + M_{BA} = 0 \rightarrow 0.7EI\theta_B + 0.2EI\theta_C + 0.3EI\rho + 33.75 = 0$$

$$M_{CB} + M_{CD} = 0 \rightarrow 0.2EI\theta_B + 0.7EI\theta_C + 0.3EI\rho - 33.75 = 0$$

Summing horizontal forces for the entire frame leads to an additional equation,

$$\begin{aligned} \sum F_x = 0 \quad \rightarrow \quad & -V_{AB} + V_{DC} + 6 = 0 \\ & \downarrow \\ & -0.3EI\theta_B - 0.3EI\theta_C - 0.6EI\rho + 60 = 0 \end{aligned}$$

Solving these three equations, one obtains

$$\begin{cases} EI\theta_B = -117.5 \text{ kip ft}^2 \\ EI\theta_C = 17.5 \text{ kip ft}^2 \\ EI\rho = 150 \text{ kip ft}^2 \end{cases}$$

and then

$$\left\{ \begin{array}{l} M_{BA} = +9.75 \\ M_{BC} = -9.75 \\ M_{CB} = -50.25 \\ M_{CD} = +50.25 \\ V_{AB} = .975 \\ V_{DC} = -5.25 \end{array} \right. \Rightarrow \left\{ \begin{array}{ll} M_{BA} = 9.75 \text{ kip ft} & \text{counterclockwise} \\ M_{BC} = 9.75 \text{ kip ft} & \text{clockwise} \\ M_{CB} = 50.25 \text{ kip ft} & \text{clockwise} \\ M_{CD} = 50.25 \text{ kip ft} & \text{counterclockwise} \\ V_{AB} = .975 \text{ kip} & \leftarrow \\ V_{DC} = 5.25 \text{ kip} & \leftarrow \end{array} \right.$$

Noting the free body diagrams below, we find the remaining end actions (Figs. E10.8d and E10.8e).

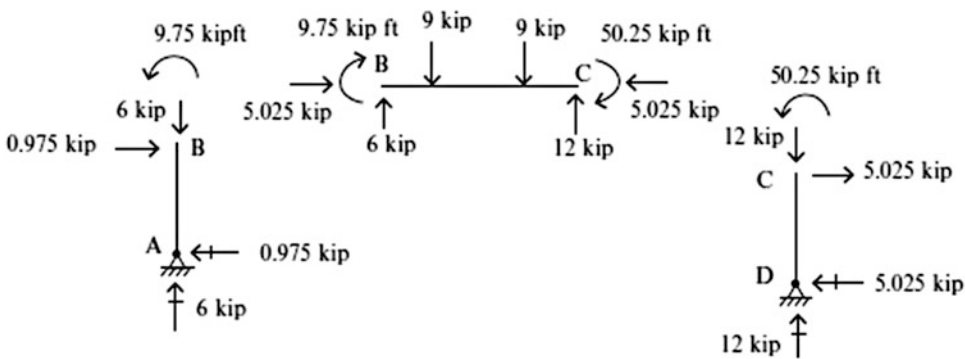


Fig. E10.8d Free body diagrams

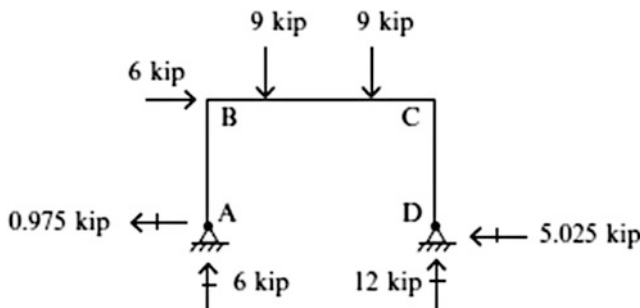


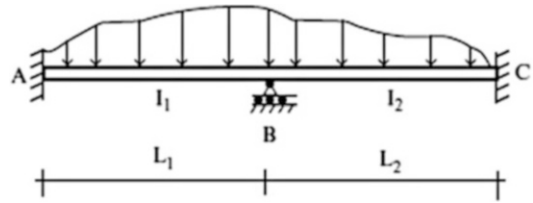
Fig. E10.8e Reactions

10.6 The Moment Distribution Solution Procedure for Multi-span Beams

10.6.1 Introduction

In the previous sections, we developed an analysis procedure for multi-span beams that is based on using the slope-deflection equations to establish a set of simultaneous equations relating the nodal rotations. These equations are equivalent to the nodal moment equilibrium equations. We generated the solution by solving these equations for the rotations and then, using these values, we determined the end moments and end shears. The solution procedure is relatively straightforward from a

Fig. 10.18 Two-span beam with fixed ends



mathematical perspective, but it is difficult to gain some physical insight as to how the structure is responding during the solution process. This is typical of mathematical procedures which involve mainly number crunching and are ideally suited for computer-based solution schemes.

The Moment Distribution Method is a solution procedure developed by Structural Engineers to solve the nodal moment equilibrium equations. The method was originally introduced by Cross [1] and has proven to be an efficient hand-based computational scheme for beam- and frame-type structures. Its primary appeal is its computational simplicity.

The solution is generated in an iterative manner. Each iteration cycle involves only two simple computations. Another attractive feature is the fact that one does not have to formulate the nodal equilibrium equations expressed in terms of the nodal displacements. The method works directly with the end moments. This feature allows one to assess convergence by comparing successive values of the moments as the iteration progresses. In what follows, we illustrate the method with a series of beam-type examples. Later, we extend the method to frame-type structures.

Consider the two-span beam shown in Fig. 10.18. Supports A and C are fixed, and we assume that there is no settlement at B.

We assume initially that there is no rotation at B. Noting Fig. 10.19, the net unbalanced clockwise nodal moment at B is equal to the sum of the fixed end moments for the members incident on node B.

Fig. 10.19 Nodal moments

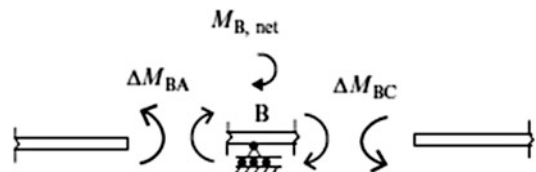


$$+ \curvearrowright M_{B,net} = + \sum M_B^F = +M_{BA}^F + M_{BC}^F \tag{10.36}$$

This unbalanced moment will cause node B to rotate until equilibrium is restored. Using the slope-deflection equations, we note that the increment in the end moment for a member which is incident on B due to a counterclockwise rotation at B is proportional to the relative stiffness I/L for the member.

The moments acting on the node are of opposite sense, i.e., clockwise, from Newton's law. The equilibrium state for the node is shown in Fig. 10.20.

Fig. 10.20 Moment equilibrium for node B



Equilibrium requires the moment sum to vanish.

$$\Delta M_{BA} + \Delta M_{BC} + M_{B,\text{net}} = 0$$

Substituting for the moment increments yields an equation for θ_B

$$\left(\frac{4EI_1}{L_1} + \frac{4EI_2}{L_2}\right)\theta_B = -M_{B,\text{net}}$$

$$\Downarrow$$

$$\theta_B = \frac{1}{((4EI_1/L_1) + (4EI_2/L_2))}(-M_{B,\text{net}}) \quad (10.37)$$

Lastly, we use this value of θ_B to evaluate the incremental end moments.

$$\Delta M_{BA} = \frac{(4EI_1/L_1)}{((4EI_1/L_1) + (4EI_2/L_2))}(-M_{B,\text{net}})$$

$$\Delta M_{BC} = \frac{(4EI_2/L_2)}{((4EI_1/L_1) + (4EI_2/L_2))}(-M_{B,\text{net}}) \quad (10.38)$$

The form of the solution suggests that we define a dimensionless factor, DF, for each member as follows:

$$DF_{BA} = \frac{I_1/L_1}{(I_1/L_1) + (I_2/L_2)}$$

$$DF_{BC} = \frac{I_2/L_2}{(I_1/L_1) + (I_2/L_2)} \quad (10.39)$$

Note that $DF_{BA} + DF_{BC} = 1.0$. With this notation, the expressions for the incremental end moments reduce to

$$\Delta M_{BA} = -DF_{BA}(M_{B,\text{net}})$$

$$\Delta M_{BC} = -DF_{BC}(M_{B,\text{net}}) \quad (10.40)$$

One distributes the unbalanced fixed end moment to the members incident on the node according to their distribution factors which depend on their relative stiffness.

The nodal rotation at B produces end moments at A and C. Again, noting the slope-deflection equations, these incremental moments are related to θ_B by

$$\Delta M_{AB} = \frac{2EI_1}{L_1}\theta_B = \frac{2EI_1/L_1}{\{(4EI_1/L_1) + (4EI_2/L_2)\}}(-M_{B,\text{net}}) = -\frac{1}{2}DF_{BA}(M_{B,\text{net}})$$

$$\Delta M_{CB} = \frac{2EI_2}{L_2}\theta_B = \frac{2EI_2/L_2}{\{(4EI_1/L_1) + (4EI_2/L_2)\}}(-M_{B,\text{net}}) = -\frac{1}{2}DF_{BC}(M_{B,\text{net}}) \quad (10.41)$$

Comparing (10.41) with (10.40), we observe that the incremental moments at the far end are 1/2 the magnitude at the distributed moments at the near end.

$$\begin{aligned}\Delta M_{AB} &= \frac{1}{2} \Delta M_{BA} \\ \Delta M_{CB} &= \frac{1}{2} \Delta M_{BC}\end{aligned}\quad (10.42)$$

We summarize the moment distribution procedure for this example. The steps are:

1. Determine the distribution factors at each free node (only node B in this case)
2. Determine the fixed end moments due to the applied loading and chord rotation for the beam segments.
3. Sum the fixed end moments at node B. This sum is equal to the unbalanced moment at node B.
4. Distribute the unbalanced nodal moment to the members incident on node B.
5. Distribute one half of the incremental end moment to the other end of each member incident on node B.

Executing these steps is equivalent to formulating and solving the nodal moment equilibrium equations at node B. Moment distribution avoids the operation of setting up and solving the equations. It reduces the effort to a series of simple computations.

Example 10.9: Moment Distribution Method Applied to a Two-Span Beam

Given: The two-span beams shown in Fig. E10.9a.

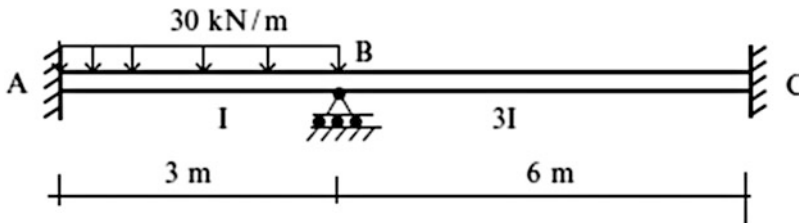


Fig. E10.9a

Determine: The end moments using moment distribution.

Solution: The fixed end moments and the distribution factors for node B are listed below.

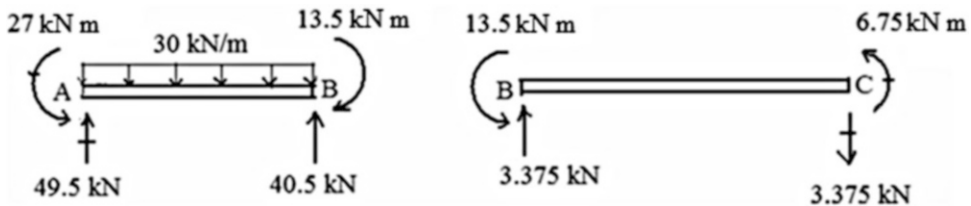
$$\begin{aligned}M_{AB}^F &= 30 \frac{(3)^2}{12} = 22.5 \text{ kN m} & M_{BC}^F &= 0 \\ M_{BA}^F &= -22.5 \text{ kN m} & M_{CB}^F &= 0\end{aligned}$$

$$\text{At joint B} \left\{ \begin{array}{l} \sum \frac{I}{L} = \frac{1}{3} + \frac{3I}{6} = \frac{5I}{6} \\ DF_{BA} = \frac{I/3}{5I/6} = 0.4 \quad DF_{BC} = \frac{3I/6}{5I/6} = 0.6 \end{array} \right.$$

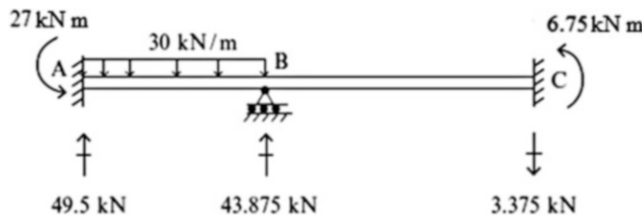
It is convenient to list the end moments and distribution factors on a sketch superimposed on the multi-span beam. A typical sketch is shown below. We distribute the 22.5 kN m unbalanced moment at B and carry over the moments to A and C. After one distribution, moment equilibrium at B is restored.

	A	B		C
DF's	1	0.4	0.6	1
FEM's	22.5	-22.5	0	0
	4.5 ←	9	13.5 →	6.75
ΣM	27	-13.5	13.5	6.75

Since the end moments are known, one can determine the end shear forces using the static equilibrium equations for the member.



Lastly, the reactions are listed below.



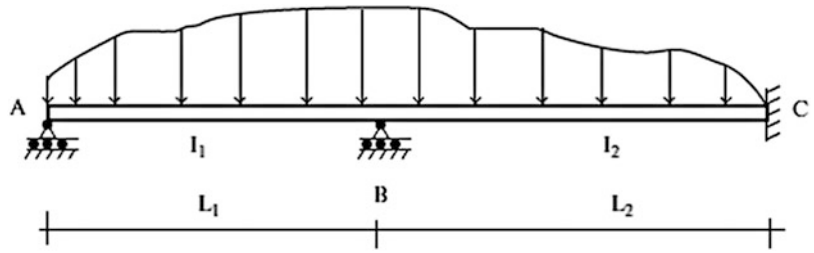
10.6.2 Incorporation of Moment Releases at Supports

We consider next the case where an end member has a moment release, as shown in Fig. 10.21. We work with the modified slope-deflection equation for member AB developed in Sect. 10.3. The end moments are given by (10.22a, 10.22b) which is listed below for convenience.

$$M_{BA_{\text{modified}}} = \frac{3EI_1}{L_1} \theta_B + \left\{ M_{BA}^F - \frac{1}{2} M_{AB}^F \right\} = \frac{3EI_1}{L_1} \theta_B + M_{BA_{\text{modified}}}^F$$

$$M_{AB} = 0$$

Fig. 10.21 Two-span beam with a moment release at a support



Then, the increment in moment for member BA due to a rotation at B is

$$\Delta M_{BA} = 4E \left(\frac{3I_1}{4L_1} \right) \theta_B \tag{10.43}$$

$$\Delta M_{AB} = 0$$

We use a *reduced relative rigidity* factor $(3/4)I_1/L_1$ when computing the distribution factor for node B. Also, we use a *modified fixed end moment* (see Table 9.2). There is *no* carry-over moment to A.

Example 10.10: Two-Span Beam with a Moment Release at One End

Given: The beam shown in Fig. E10.10a.

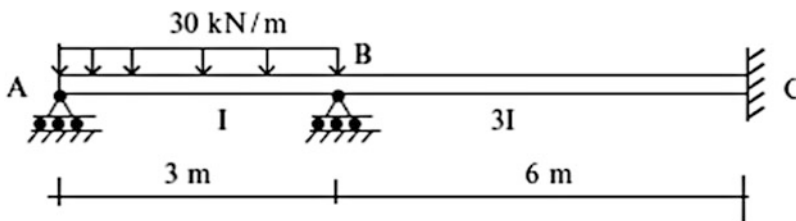
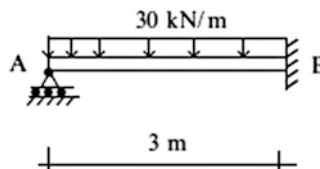


Fig. E10.10a

Determine: The end actions.

Solution: Since member AB has a moment release, we work with the modified slope-deflection equation for member AB. The computational details are listed below.

The modified fixed end moments (see Table 9.2):



$$M_{BA}^F = M_{BA}^F - \frac{1}{2} M_{AB}^F = -\frac{30(3)^2}{8} = -33.75 \text{ kN m}$$

$$M_{AB}^F = 0$$

The modified distribution factors for node B:

$$\sum_{\text{joint B}} \frac{1}{L} = \frac{3}{4} \left(\frac{I}{3} \right) + \left(\frac{3I}{6} \right) = \frac{3I}{4}$$

$$DF_{BA} = \frac{(3/4)(I/3)}{(3I/4)} = \frac{1}{3}$$

$$DF_{BC} = 1 - DF_{BA} = \frac{2}{3}$$

The distribution details are listed below.

	A	B		C
DF'S	0	1/3	2/3	1
FEM's	0	-33.75	0	0
		11.25	22.5	11.25
ΣM	0	-22.5	22.5	11.25

Noting the free body diagrams below, we find the remaining end actions (Figs. E10.10b and E10.10c).

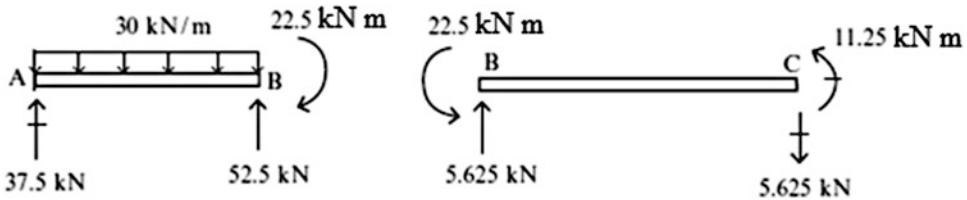


Fig. E10.10b Free body diagrams

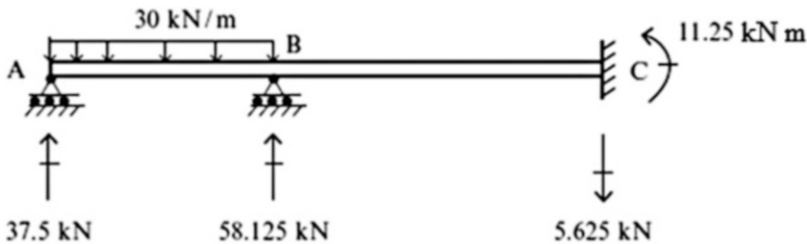


Fig. E10.10c Reactions

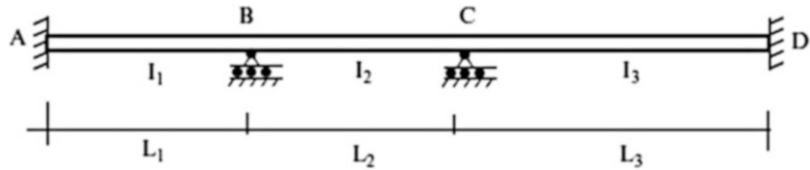
10.6.3 Moment Distribution for Multiple Free Nodes

The previous examples have involved only a single free node. We now extend the method for multiple free nodes. The overall approach is the same. We just have to incorporate an *iterative* procedure for successively balancing the nodal moments.

Consider the three-span beam shown in Fig. 10.22. We assume nodes B and C are fixed, determine the fixed end moments for the members, and compute the unbalanced nodal moments at nodes B and C. If these moments are not equal to zero, the nodes will rotate until equilibrium is restored. Allowing a node, such as B, to rotate produces incremental end moments in members AB and BC equal to

$$\begin{aligned} \Delta M_{BA} &= \frac{4EI_1}{L_1} \theta_B & \Delta M_{AB} &= \frac{1}{2} \Delta M_{BA} \\ \Delta M_{BC} &= \frac{4EI_2}{L_2} \theta_B & \Delta M_{CB} &= \frac{1}{2} \Delta M_{BC} \end{aligned} \tag{10.44}$$

Fig. 10.22 Three span beam



Similarly, a rotation at node C produces incremental end moments in segment BC and CD.

$$\begin{aligned} \Delta M_{CB} &= \frac{4EI_2}{L_2} \theta_C & \Delta M_{BC} &= \frac{1}{2} \Delta M_{CB} \\ \Delta M_{CD} &= \frac{4EI_3}{L_3} \theta_C & \Delta M_{DC} &= \frac{1}{2} \Delta M_{CD} \end{aligned} \tag{10.45}$$

The distribution and carry-over process is the same as described previously. One evaluates the distribution factors using (10.39) and takes the carry-over factor as 1/2. Since there is more than one node, we start with the node having the *largest unbalanced moment*, distribute this moment, and carry over the distributed moment to the adjacent nodes. This operation changes the magnitudes of the remaining unbalanced moments. We then select the node with the “largest” new unbalanced moment and execute a moment distribution and carry-over at this node. The solution process proceeds by successively eliminating residual nodal moments at various nodes throughout the structure. At any step, we can assess the convergence of the iteration by examining the nodal moment residuals. Usually, only a few cycles of distribution and carry-over are sufficient to obtain reasonably accurate results.

Example 10.11: Moment Distribution Method Applied to a Three-Span Beam

Given: The three-span beam defined in Fig. E10.11a.

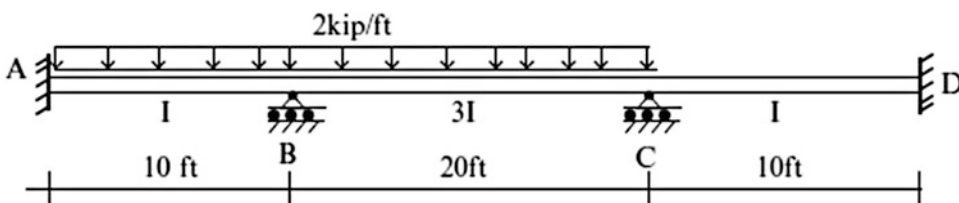


Fig. E10.11a

Determine: The end actions.

Solution: The sequence of nodal moment balancing is at the following nodes: C, B, C, B, C. We stop when the unbalanced nodal moment is approximately less than 0.5 kip ft.

The computations and distribution details are listed below.

$$M_{AB}^F = 2 \frac{(10)^2}{12} = 16.67 \text{ kip ft} \quad M_{BA}^F = -16.67 \text{ kip ft}$$

$$M_{BC}^F = 2 \frac{(20)^2}{12} = 66.67 \text{ kip ft} \quad M_{CB}^F = -66.67 \text{ kip ft}$$

$$M_{CD}^F = M_{DC}^F = 0$$

$$\text{At joint B or C} \left\{ \begin{array}{l} \sum_{\text{modified}} \frac{I}{L} = \frac{I}{10} + \frac{3I}{20} = \frac{5I}{20} \\ DF_{BA} = DF_{CD} = \frac{I/10}{5I/20} = 0.4 \\ DF_{CB} = DF_{BC} = 1 - 0.4 = 0.6 \end{array} \right.$$

$$DF_{DC} = DF_{AB} = 1$$

	A	B		C		D
DF's	1	.4	.6	.4	.6	1
FEM's	16.67	-16.67	66.67	-66.67	0	0
			20 ←	40	26.67 →	13.33
	-14 ←	-28	-42 →	-21		
			6.3 ←	12.6	8.4 →	4.2
	-1.26 ←	-2.52	-3.78 →	-1.89		
			.56 ←	1.13	.75 →	.37
			-.22	-.34		
ΣM	1.4	-47.4	+47.4	-35.8	35.8	17.9

Noting the free body diagrams below, we find the remaining end actions (Figs. E10.11b and E10.11c).

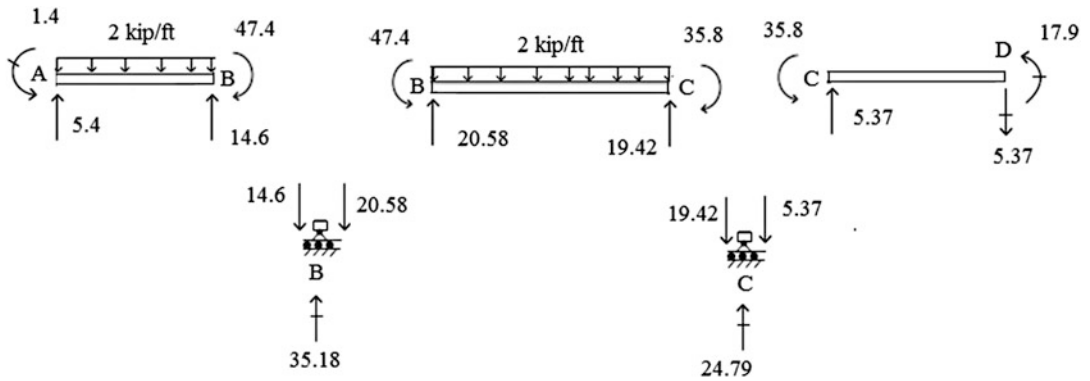


Fig. E10.11b Free body diagrams

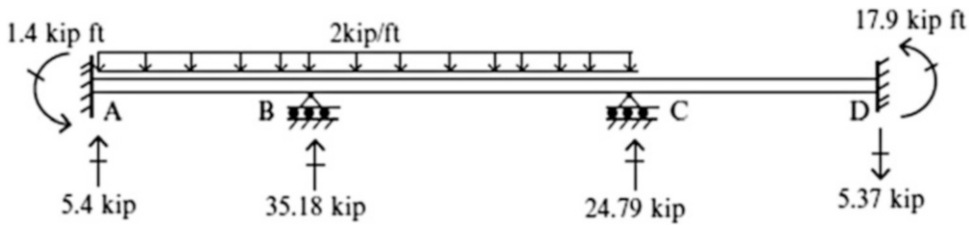


Fig. E10.11c Reactions

Example 10.12: Example 10.11 with Moment Releases at the End Supports

Given: A three-span beam with moment releases at its end supports (Figs. E10.12a, E10.12b, E10.12c).

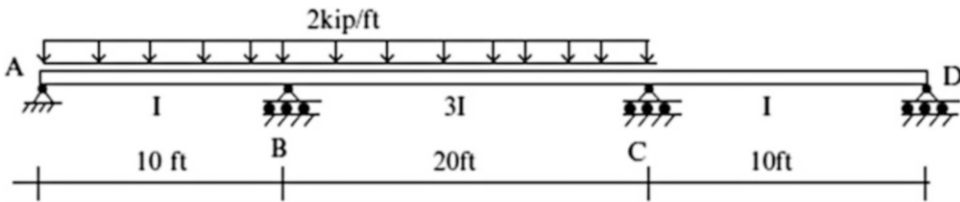
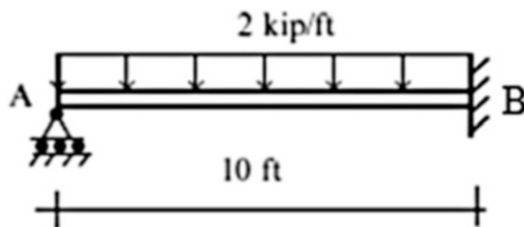


Fig. E10.12a

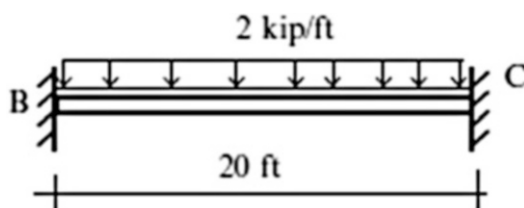
Determine: The end actions.

Solution: We rework Example 10.11 with moment releases at A and D. We use reduced relative rigidities for members AB and CD, and a modified fixed end moment for AB. There is no carry-over from B to A or from C to D. Details are listed below.



$$M_{BA_{\text{modified}}}^F = M_{BA}^F - \frac{1}{2}M_{AB}^F = -\frac{2(10)^2}{8} = -25 \text{ kip ft}$$

$$M_{AB_{\text{modified}}}^F = 0$$



$$M_{BC}^F = \frac{2(20)^2}{12} = 66.67 \text{ kip ft}$$

$$M_{CB}^F = -66.67 \text{ kip ft}$$

$$M_{CD}^F = M_{DC}^F = 0$$

$$\text{At joint B or C} \left\{ \begin{array}{l} \sum_{\text{modified}} \frac{I}{L} = \frac{3}{4} \left(\frac{I}{10} \right) + \left(\frac{3I}{20} \right) = \frac{9I}{40} \\ DF_{BA_{\text{modified}}} = DF_{CD_{\text{modified}}} = \frac{3I/40}{9I/40} = \frac{1}{3} \\ DF_{CB} = DF_{BC} = 1 - \frac{1}{3} = \frac{2}{3} \\ DF_{DC} = DF_{AB} = 0 \end{array} \right.$$

The distribution details and end actions are listed below.

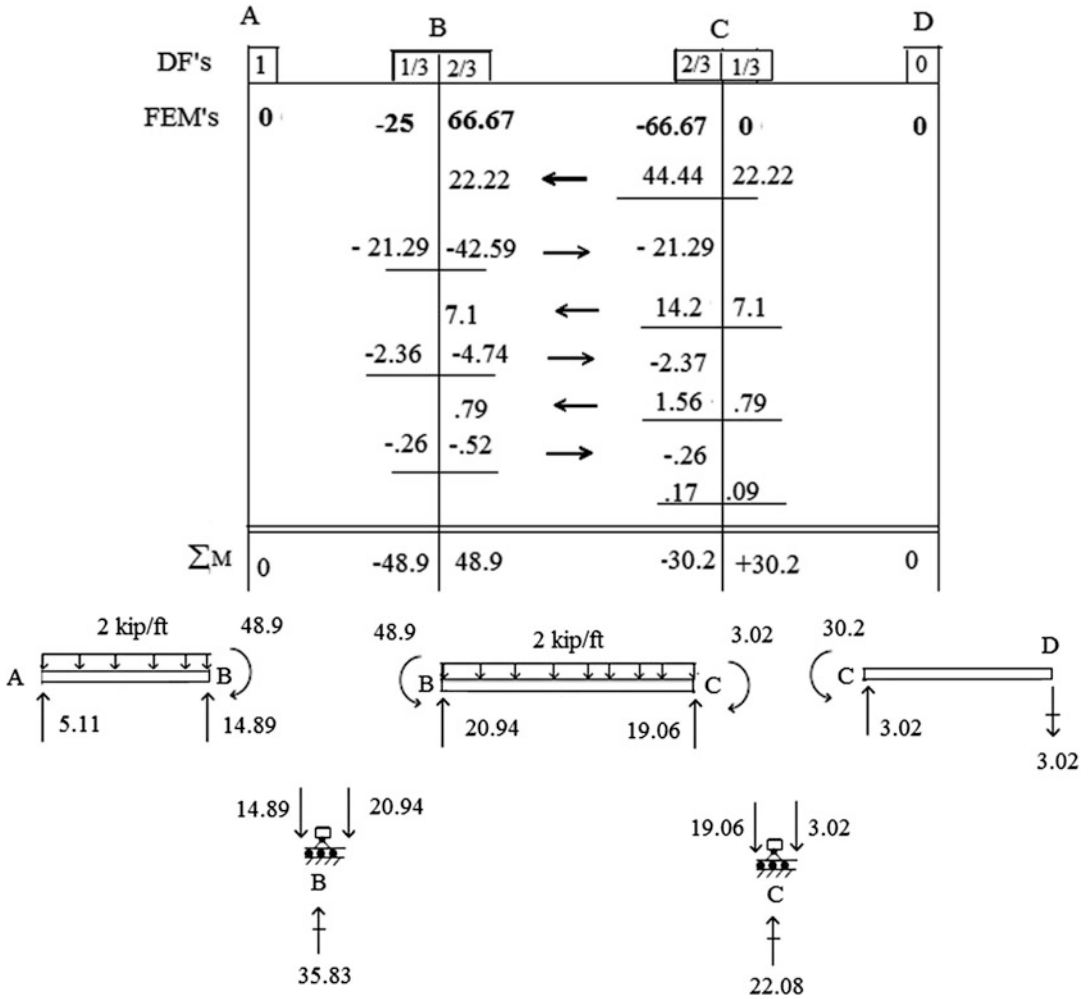


Fig. E10.12b Free body diagrams

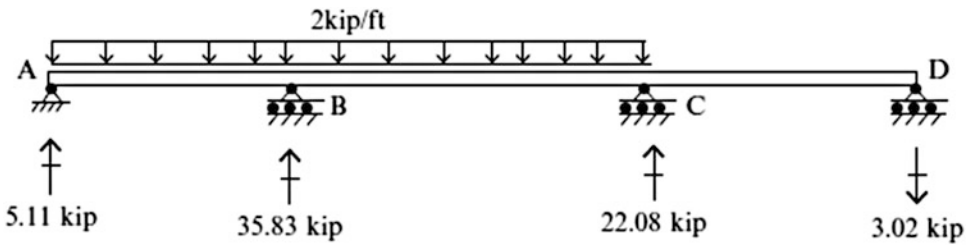


Fig. E10.12c Reactions

10.7 Moment Distribution: Frame Structures

10.7.1 Frames: No Sideway

Sideway does not occur if there is a lateral restraint. Frames with no sideway are treated in a similar way as beams. The following examples illustrate the process.

Example 10.13: Moment Distribution Method for a Frame with No Sideway

Given: The frame shown in Fig. E10.13a.

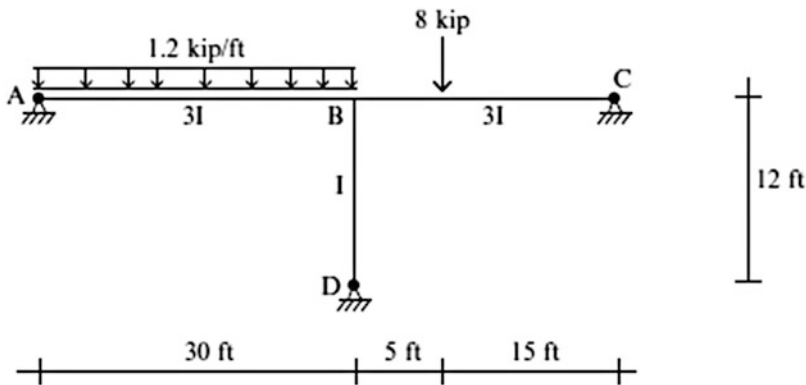


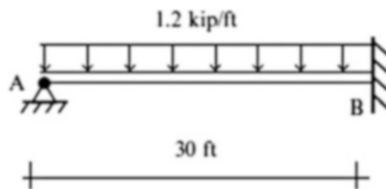
Fig. E10.13a

Determine: The end actions.

Solution: The distribution details and the fixed end moments and end actions are listed below.

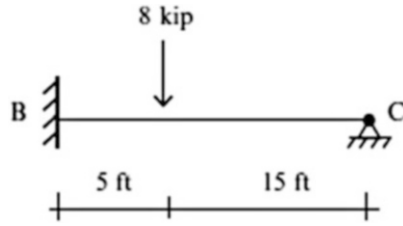
$$M_{BA_{\text{modified}}}^F = M_{BA}^F - \frac{1}{2}M_{AB}^F = -\frac{1.2(30)^2}{8} = -135 \text{ kip ft}$$

$$M_{AB_{\text{modified}}}^F = 0$$



$$M_{BC_{\text{modified}}}^F = M_{BC}^F - \frac{1}{2}M_{CB}^F = +\frac{21PL}{128} = 26.25 \text{ kip ft}$$

$$M_{CB_{\text{modified}}}^F = 0$$



$$\text{At joint B} \left\{ \begin{array}{l} \sum_{\text{modified}} \frac{I}{L} = \frac{3}{4} \left(\frac{3I}{30} + \frac{3I}{20} + \frac{I}{12} \right) = \frac{I}{4} \\ DF_{BA_{\text{modified}}} = \frac{3/4(3I/30)}{I/4} = 0.3 \\ DF_{BC_{\text{modified}}} = \frac{3/4(3I/20)}{I/4} = 0.45 \\ DF_{BC_{\text{modified}}} = \frac{3/4(I/12)}{I/4} = 0.25 \end{array} \right.$$

The distribution details are listed in Fig. E10.13b.

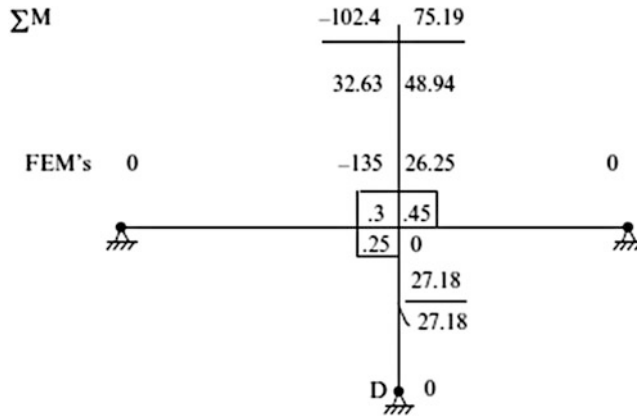


Fig. E10.13b

Noting the free body diagrams below, we find the remaining end actions (Fig. E10.13c).

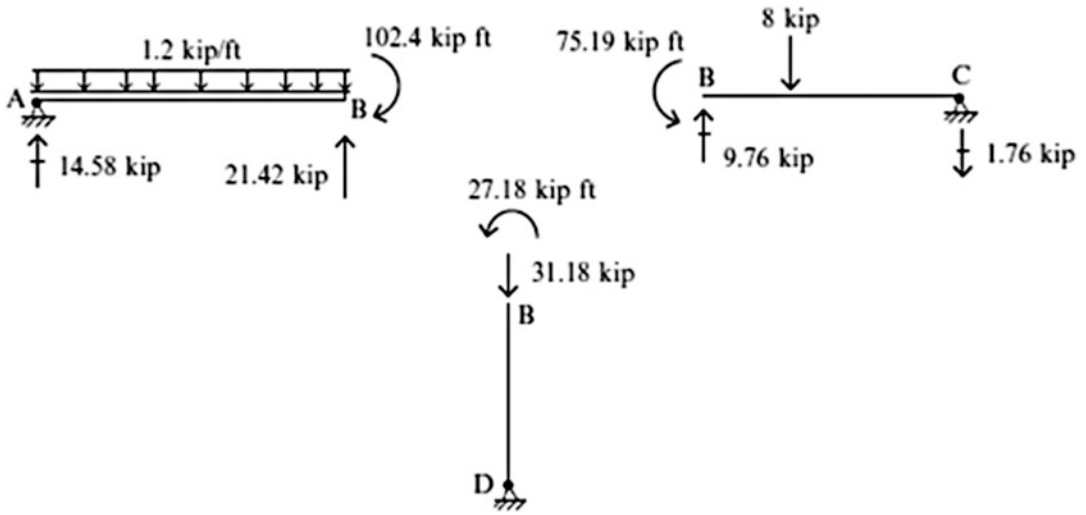


Fig. E10.13c End actions

Example 10.14: Symmetrical Two-Bay Portal Frame—Symmetrical Loading

Given: The two-bay frame defined in Fig. E10.14a.

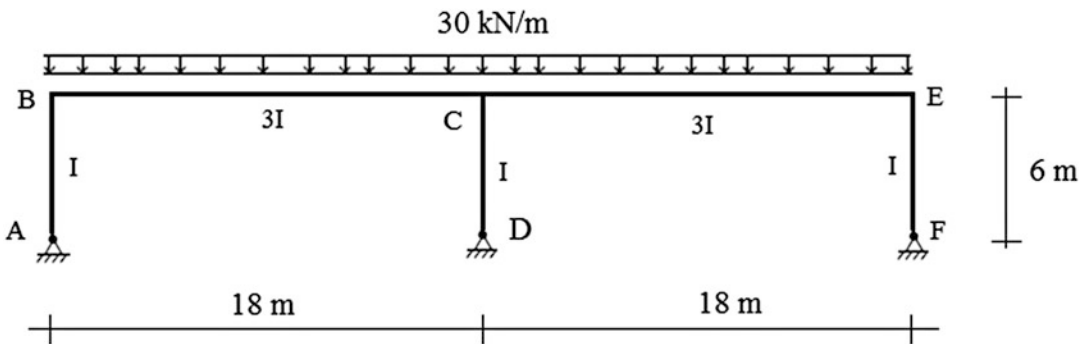


Fig. E10.14a

Determine: The bending moment distribution and end actions using moment distribution.

Solution: We use reduced rigidity factors for the column members and *no* carry-over to the hinged ends at nodes A, D, and F (Fig. E10.14b).

$$\text{At node B or E} \left\{ \begin{aligned} \sum \frac{I}{L} &= \left(\frac{I}{6}\right)\frac{3}{4} + \left(\frac{3I}{18}\right) \\ DF_{BA_{\text{modified}}} = DF_{EF_{\text{modified}}} &= \frac{(I/6)3/4}{(I/6)3/4 + (3I/18)} = \frac{3}{7} \\ DF_{BC} = DF_{EC} &= 1 - \frac{3}{7} = \frac{4}{7} \end{aligned} \right.$$

$$\text{At node C} \left\{ \begin{aligned} \sum \frac{I}{L} &= \left(\frac{I}{6}\right)\frac{3}{4} + \frac{3I}{18} + \frac{3I}{18} = \frac{11}{24}I \\ DF_{CD_{\text{modified}}} &= \frac{(I/6)3/4}{(11/24)I} = \frac{3}{11} \\ DF_{CB} = DF_{CE} &= \frac{1}{2}\left(1 - \frac{3}{11}\right) = \frac{4}{11} \end{aligned} \right.$$

The fixed end moments are

$$M_{BC}^F = -M_{CB}^F = M_{CE}^F = -M_{EC}^F = +\frac{30(18)^2}{12} = +810 \text{ kNm}$$

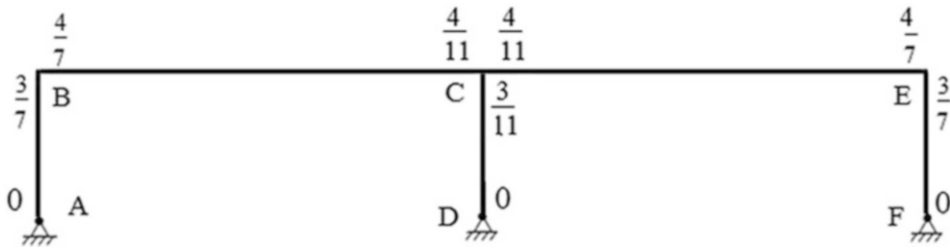


Fig. E10.14b Distribution factors

The moment distribution sequence is listed in Fig. E10.14c. Note that there is never any redistribution at node C because of symmetry (Fig. E10.14d).

ΣM	0	<u>-348.3</u>	<u>348.3</u>		<u>-1040.85</u>	<u>1040.85</u>		<u>-348.3</u>	<u>348.3</u>	0
FEM's	0	-348.3	-461.7	→	-230.85	230.85	←	461.7	348.3	0
	0	0	810		-810	810		-810	0	0
		B	B		C	C		E	E	
		A	A		D	D		F	F	

Fig. E10.14c

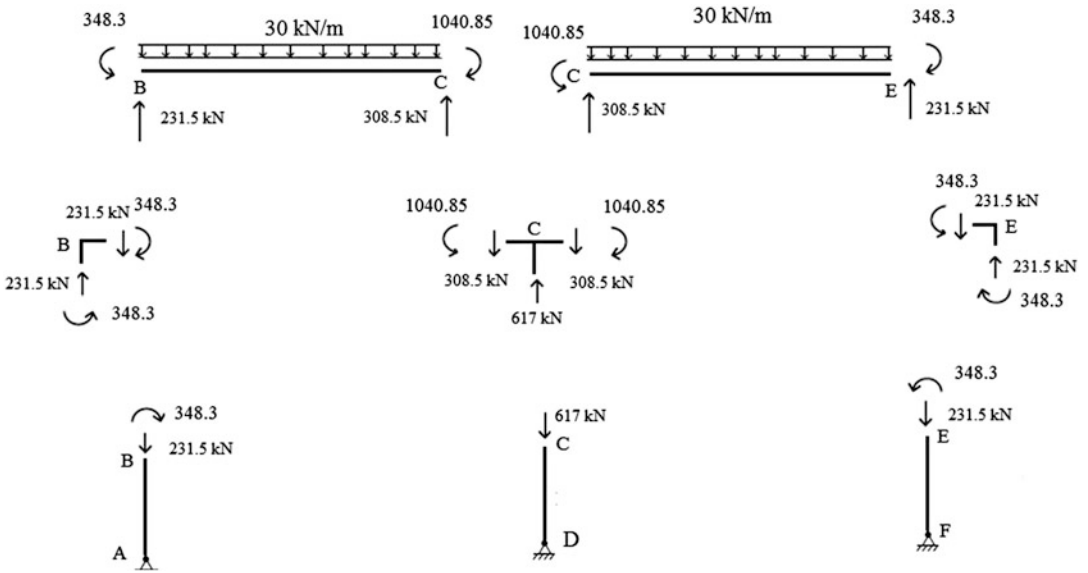


Fig. E10.14d Free body diagram

The final bending moment distributions are plotted in Fig. E10.14e.

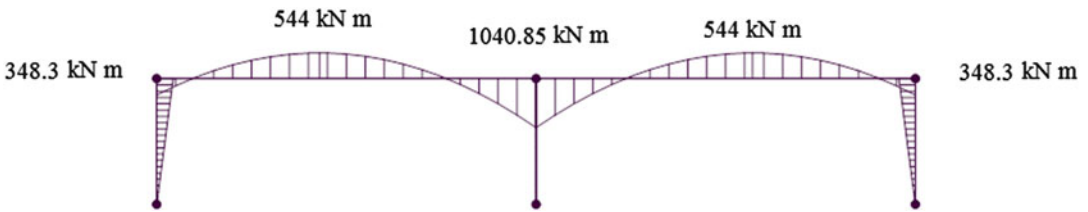


Fig. E10.14e

Example 10.15: Two-Bay Portal Frame—Support Settlement

Given: The frame shown in Fig. E10.15a. Consider Support D to experience a downward settlement of $\delta = 1$ in.

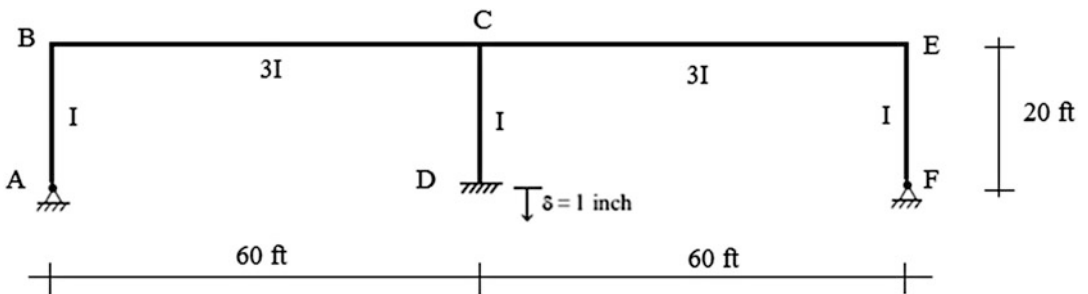


Fig. E10.15a

Determine: The end moments. Take $E = 29,000$ ksi and $I = 2000$ in.⁴

Solution: We use reduced factors for the column members AB and EF and no carry-over to the hinged ends. The distribution factors are listed on the following sketch (Fig. E10.15b).

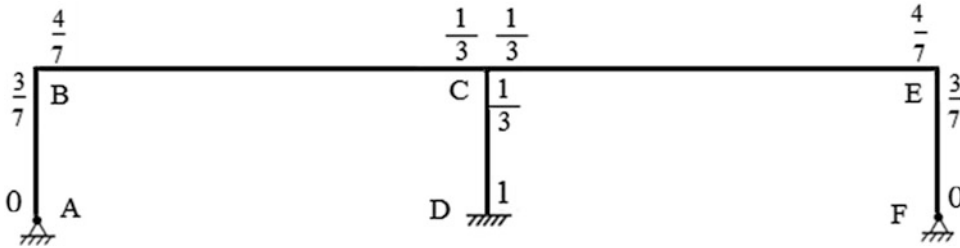


Fig. E10.15b Distribution factors

$$\text{At node B or E} \begin{cases} \sum \frac{I}{L} = \left(\frac{I}{20}\right)\frac{3}{4} + \left(\frac{3I}{60}\right) = \frac{7I}{80} \\ DF_{BA_{\text{modified}}} = DF_{EF_{\text{modified}}} = \frac{(I/20)3/4}{7I/80} = \frac{3}{7} \\ DF_{BC} = DF_{EC} = 1 - \frac{3}{7} = \frac{4}{7} \end{cases}$$

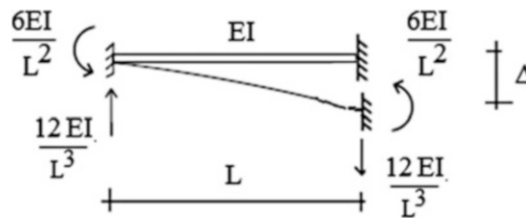
$$\text{At node C} \begin{cases} \sum \frac{I}{L} = \frac{I}{20} + \frac{3I}{60} + \frac{3I}{60} = \frac{3I}{20} \\ DF_{CD} = DF_{CB} = DF_{CE} = \frac{I/20}{3I/20} = \frac{1}{3} \end{cases}$$

Settlement at D produces chord rotation in members BC and CE. The corresponding rotations for a 1 in. settlement are

$$\rho_{BC} = -\frac{\delta}{L}$$

$$\rho_{CE} = +\frac{\delta}{L}$$

These rotations produce the following fixed end moments (see Table 9.1),



$$M_{BC}^F = M_{CB}^F = \frac{6E(3I)\delta}{L^2} = +\frac{18EI\delta}{L^2} = \frac{18(29,000)(2000)(1)}{(60)^2} \frac{1}{(12)^3} = 167.8 \text{ kipft}$$

$$M_{CE}^F = M_{EC}^F = -\frac{6E(3I)\delta}{L^2} = -\frac{18EI\delta}{L^2} = -167.8 \text{ kipft}$$

These moments are distributed at nodes B and E. Note that no unbalanced moment occurs at node C (Fig. E10.15c).

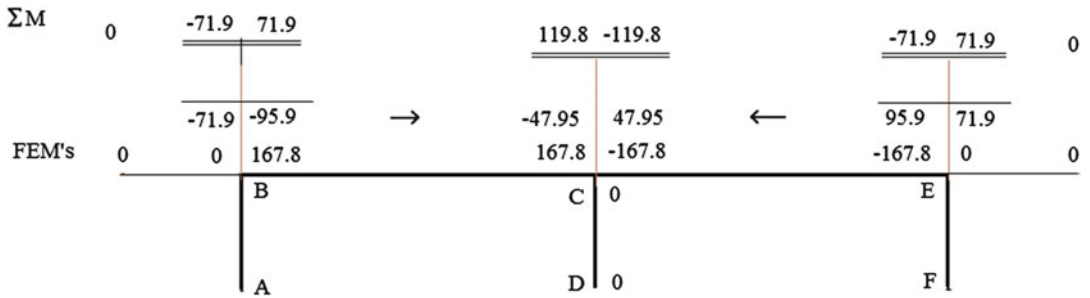


Fig. E10.15c

The final bending moment distributions are plotted in Fig. E10.15d.

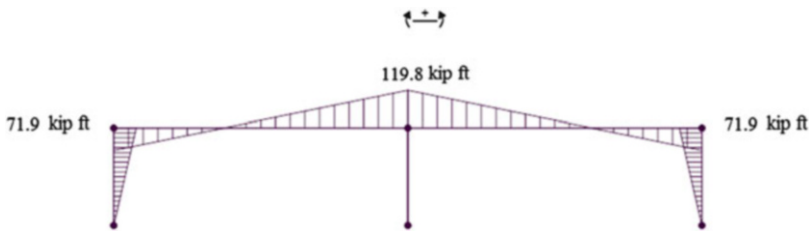


Fig. E10.15d

Example 10.16: Two-Bay Portal Frame—Temperature Increase

Given: The frame shown in Fig. E10.16a. Consider members BC and CE to experience a temperature increase of ΔT .

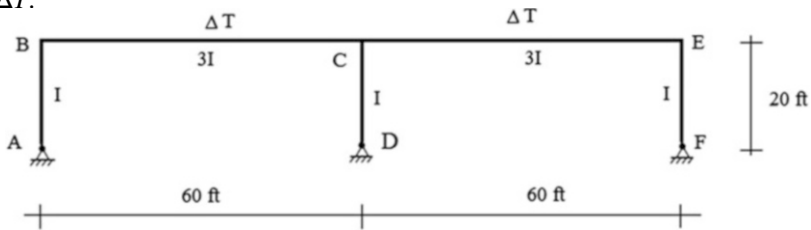


Fig. E10.16a

Determine: The end moments.

Solution: The top members will expand, causing members AB and EF to rotate. Member CD will not rotate because of symmetry. Noting Fig. E10.16b, the rotations are

$$\rho_{AB} = \frac{u/2}{L_{AB}}$$

$$\rho_{EF} = -\frac{u/2}{L_{EF}}$$

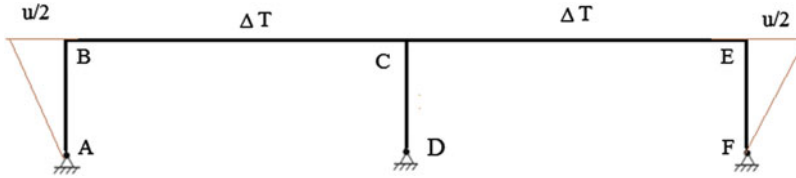


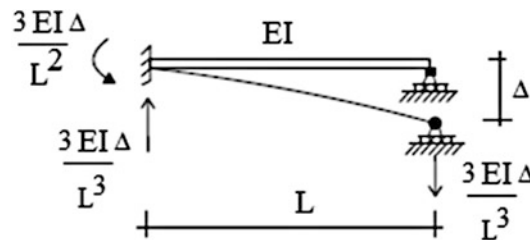
Fig. E10.16b

Assuming a uniform temperature increase over the total span, u is equal to

$$u = (\alpha\Delta T) \sum L = 120\alpha\Delta T$$

This motion is symmetrical and known. Therefore, there will be no additional displacement (therefore no additional sideways).

Noting Table 9.2, the fixed end actions corresponding to the case where there is a hinge at one end are



$$M_{BA}^F \text{modified} = -\frac{3EI}{L_{AB}} \rho_{AB} = -\frac{3EI}{20(12)} (3\alpha\Delta T) = -\frac{3}{80} EI\alpha\Delta T$$

$$M_{EF}^F \text{modified} = +\frac{3}{80} EI\alpha\Delta T$$

We assume the material is steel ($E = 3 \times 10^4$ ksi, $\alpha = 6.6 \times 10^{-6}/^\circ\text{F}$), $\Delta T = 120$ °F, and $I = 2000$ in.⁴.

The corresponding fixed end moments are

$$M_{BA}^F \text{modified} = -1782 \text{ kip in.} = -148.5 \text{ kip ft}$$

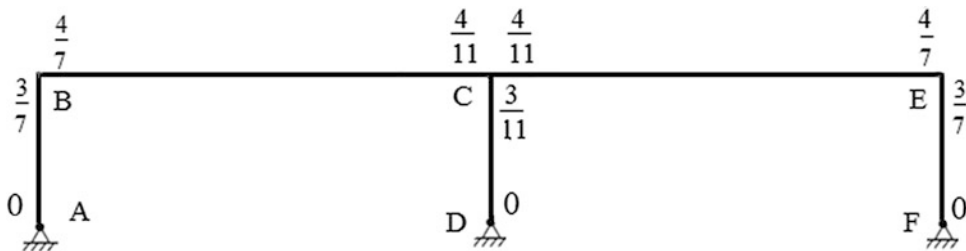
$$M_{EF}^F \text{modified} = +1782 \text{ kip in.} = +148.5 \text{ kip ft}$$

The distribution factors are

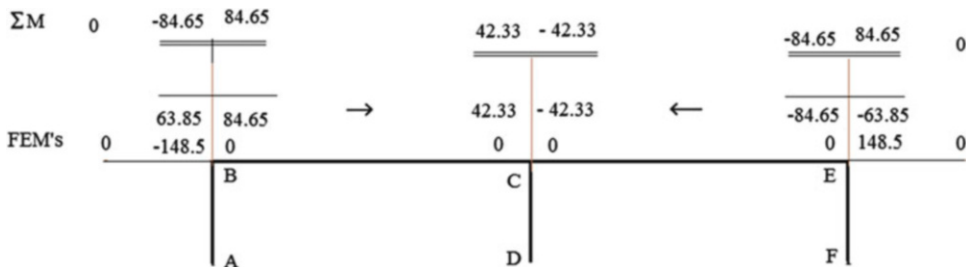
$$\text{At node B or E} \left\{ \begin{array}{l} \sum \frac{I}{L} = \left(\frac{I}{20}\right)\frac{3}{4} + \left(\frac{3I}{60}\right) = \frac{7I}{80} \\ DF_{BA_{\text{modified}}} = DF_{EF_{\text{modified}}} = \frac{(I/20)\frac{3}{4}}{7I/80} = 0.43 \\ DF_{BC} = DF_{EC} = 1 - 0.43 = 0.57 \end{array} \right.$$

$$\text{At node C} \left\{ \begin{array}{l} \sum \frac{I}{L} = \left(\frac{I}{20}\right)\frac{3}{4} + \frac{3I}{60} + \frac{3I}{60} = \frac{11I}{80} \\ DF_{CD_{\text{modified}}} = \frac{(I/20)\frac{3}{4}}{11I/80} = 0.28 \\ DF_{CB} = DF_{CE} = \frac{1 - 0.28}{2} = 0.36 \end{array} \right.$$

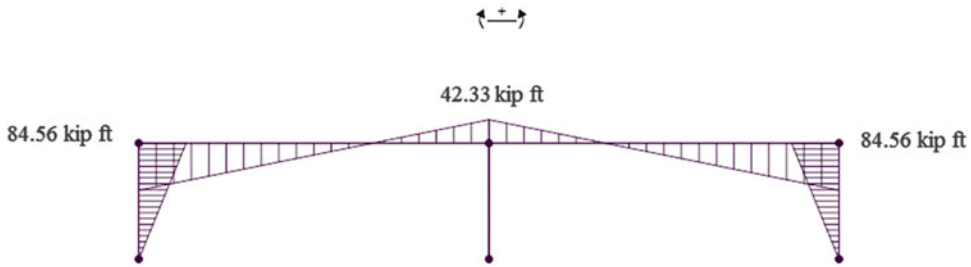
The distribution factors are listed on the following sketch.



The distribution details are listed below.



The final bending moment distributions are plotted in the following figure.

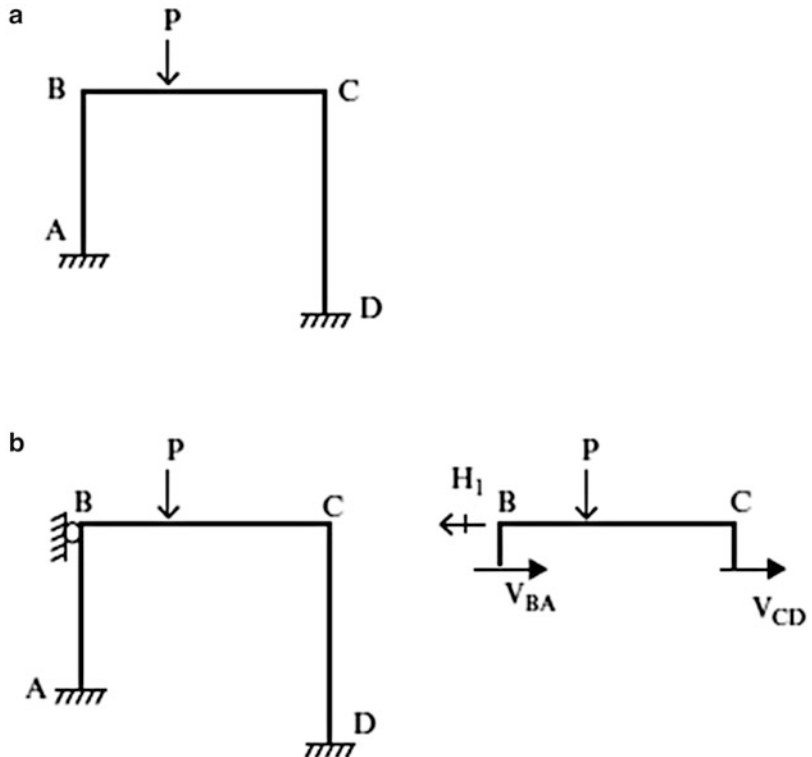


10.7.2 Frames with Sideway

Given a frame structure, one needs to identify whether there will be chord rotation due to lateral displacement. If sideway is possible, we introduce “holding” forces applied at certain nodes to prevent this motion and carry out a conventional moment distribution based on distribution and carry-over factors. Once the fixed end moments are distributed, we can determine the member shear forces, and using these values, establish the magnitude of the holding forces. This computation is illustrated in Fig. 10.23. There is one degree of sideway, and we restrain node B. The corresponding lateral force is H_1 . Note that we generally neglect axial deformation for framed structures so fixing B also fixes C.

The next step involves introducing an arbitrary amount of the lateral displacement that we had restrained in Step 1, computing the chord rotations and corresponding fixed end moments, applying

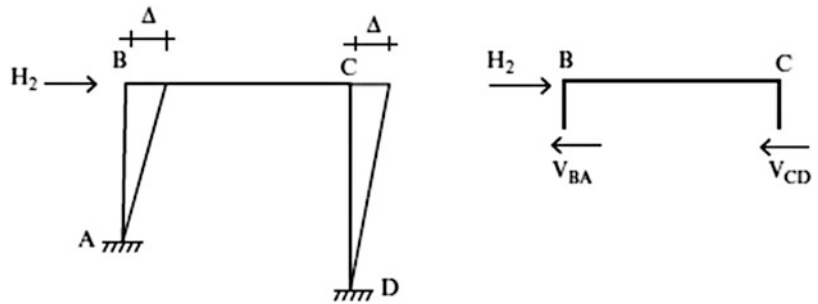
Fig. 10.23 (a) Frame with sideway. (b) Sideway restraining force—case I



the holding force again, and then distributing the fixed end moments using the conventional distribution procedure. The holding force produced by this operation is illustrated in Fig. 10.24. One combines the two solutions such that the resulting sideway force is zero.

$$\text{Final solution} = \text{case I} + \left(\frac{H_1}{H_2}\right) \text{case II} \tag{10.46}$$

Fig. 10.24 Sideway introduced—case II



The fixed end moments due to the chord rotation produced by the horizontal displacement, Δ , are (see Table 9.1)

$$M_{BA}^F = M_{AB}^F = \pm \frac{6EI_{AB}}{L_{AB}^2} \Delta = \pm \frac{6EI_{AB}}{L_{AB}} \rho_{AB}$$

$$M_{DC}^F = M_{CD}^F = \pm \frac{6EI_{CD}}{L_{CD}^2} \Delta = \pm \frac{6EI_{CD}}{L_{CD}} \rho_{CD}$$

where moment quantities are counterclockwise when positive. Following this approach, one works only with chord rotation quantities and converts these measures into equivalent fixed end moments. The standard definition equations for the distribution and carry-over factors are employed to distribute the moments.

Example 10.17: Portal Bent—Sideway Analysis

Given: The portal frame defined in Fig. E10.17a.

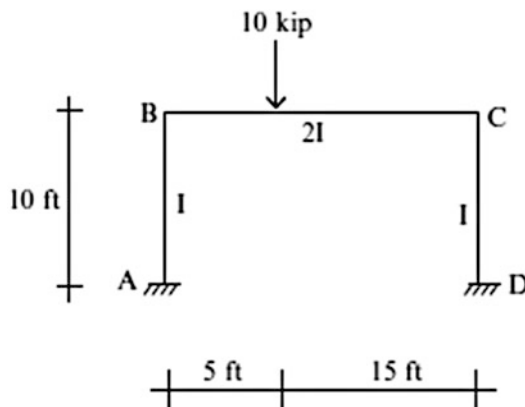


Fig. E10.17a

Determine: The end actions.

Solution: Since the loading is not symmetrical, there will be lateral motion (sideway). We restrain node B as indicated in Fig. E10.17b. The distribution factors are also indicated in the sketch.



Fig. E10.17b

We compute the fixed end moments due to the 10 kip load.

$$M_{BC}^F = \frac{10(5)(15)^2}{20^2} = +28.13 \text{ kip ft}$$

$$M_{CB}^F = -\frac{10(15)(5)^2}{20^2} = -9.38 \text{ kip ft}$$

Details of the moment distribution and the end moments for case I are listed below (Fig. E10.17c). The holding force is determined by summing the shear forces in the columns and is equal to 1.1 kip.

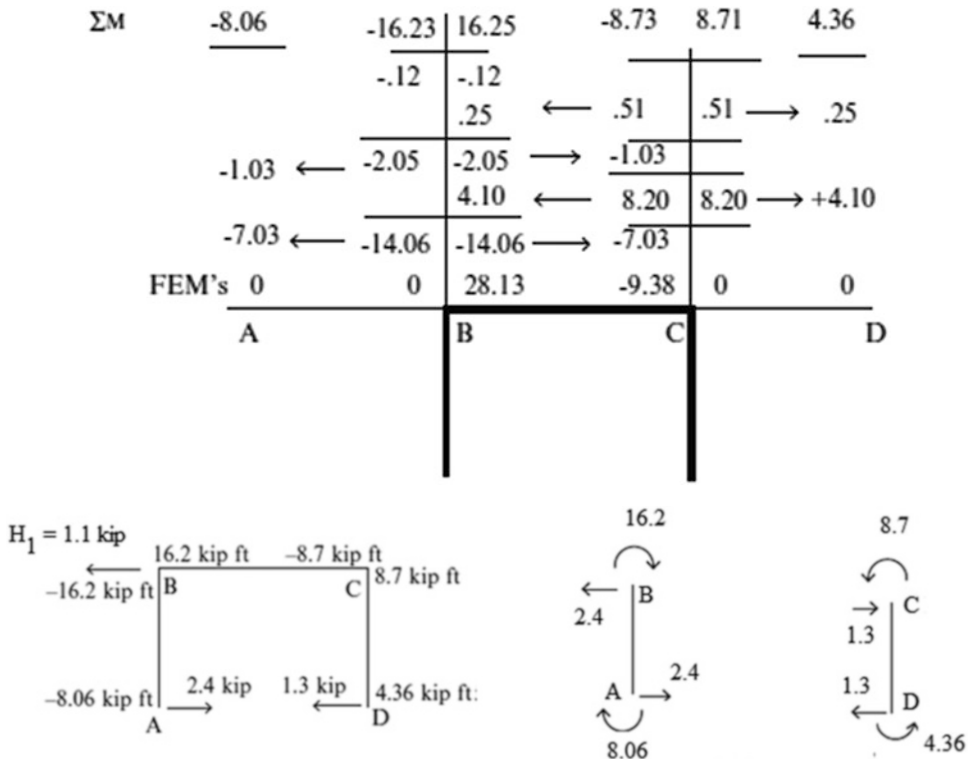


Fig. E10.17c Case I—end moments and column shear

Next, we introduce a lateral displacement to the left equal to Δ . Figure E10.17d shows this operation.

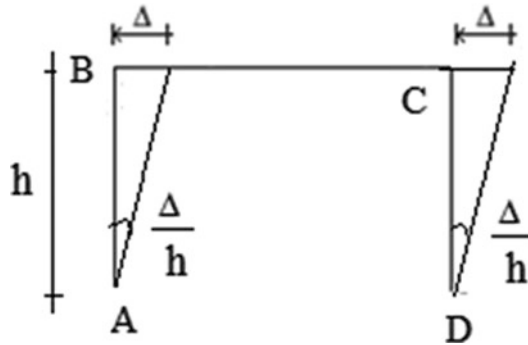


Fig. E10.17d Case II—sideway introduced

The chord rotations and corresponding fixed end moments are

$$M_{BA}^F = M_{AB}^F = M_{DC}^F = M_{CD}^F = -\frac{6EI\Delta}{h^2}$$

Since we are interested only in relative moments, we take $EI\Delta/h^2 = 1$. Details of the moment distribution and the end moments for case II are listed below (Fig. E10.17e).

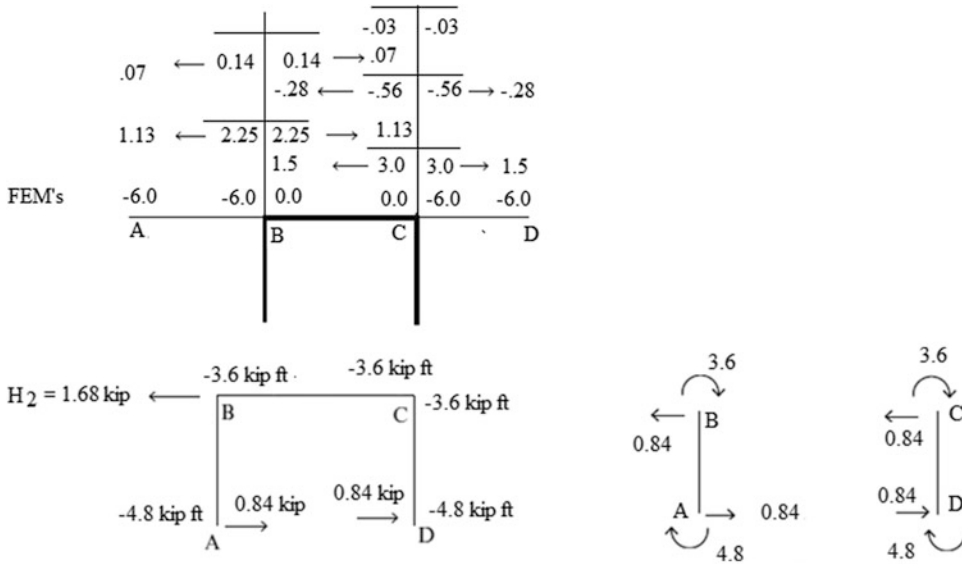


Fig. E10.17e Case II—end moments and column shear

We scale this solution by $H_1/H_2 = -1.1/1.68$ and then combine these scaled results with the results for case I.

Final end moments = end moments case I + end moments case II (H_1/H_2).

The final moments are summarized in Fig. E10.17f followed by free body diagrams.

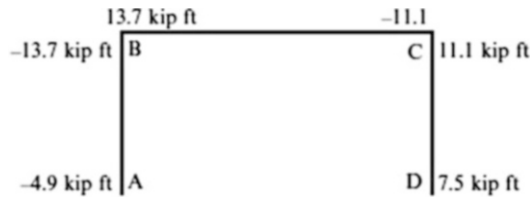
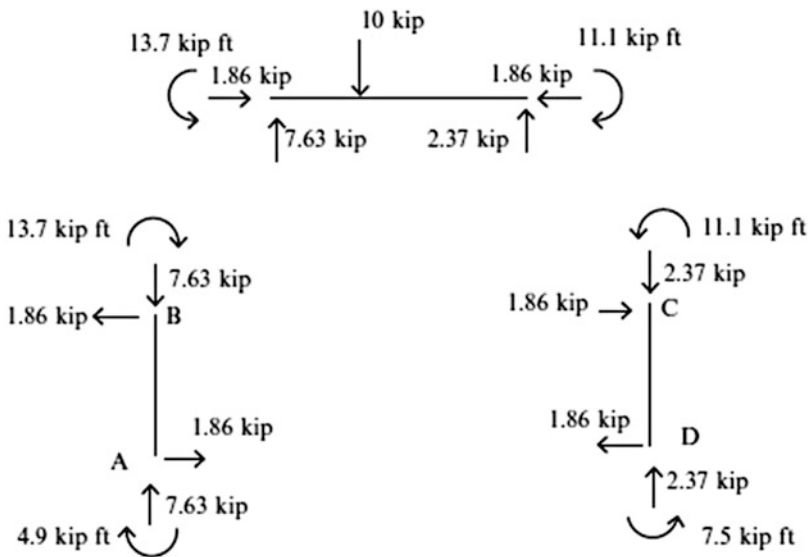


Fig. E10.17f Final end moments

Using these moments, we find the axial and shear forces.



Example 10.18: Frame with Inclined Legs

Given: The frame shown in Fig. E10.18a.

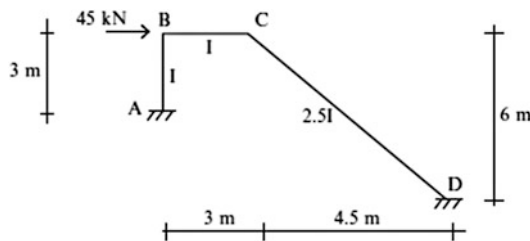


Fig. E10.18a

Determine: The end actions.

Solution: The distribution factors are listed in the sketch below (Fig. E10.18b).

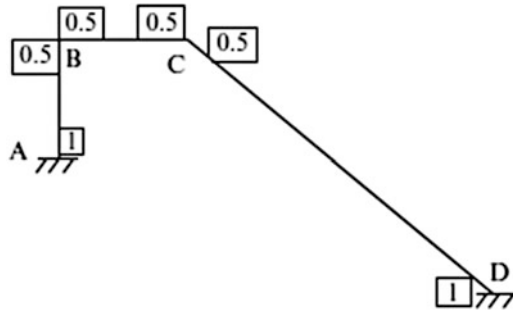
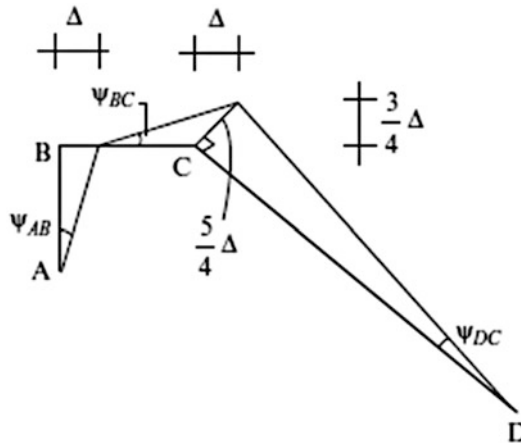


Fig. E10.18b

There are no fixed end moments due to member loads. However, we need to carry out a sideway analysis (case II). We introduce a horizontal displacement at B and compute the corresponding rotation angles.



The rotation of members BC and CD is determined by requiring the horizontal displacement of node C to be equal to Δ . The angles follow from the above sketch

$$\psi_{AB} = \frac{\Delta}{3}$$

$$\psi_{BC} = \frac{3/4\Delta}{3} = \frac{\Delta}{4}$$

$$\psi_{DC} = \frac{5/4\Delta}{7.5} = \frac{\Delta}{6}$$

Finally, the chord rotations are (note: positive sense is counterclockwise)

$$\rho_{AB} = -\frac{\Delta}{3}$$

$$\rho_{BC} = +\frac{\Delta}{4}$$

$$\rho_{DC} = -\frac{\Delta}{6}$$

Using these values, we compute the fixed end moments due to chord rotation.

$$M_{AB}^F = M_{BA}^F = \frac{6(EI)}{(3)} \left(\frac{\Delta}{3}\right) = +\frac{2}{3}(EI\Delta)$$

$$M_{BC}^F = M_{CB}^F = -\frac{6(EI)}{(3)} \left(\frac{\Delta}{4}\right) = -\frac{1}{2}(EI\Delta)$$

$$M_{CD}^F = M_{DC}^F = \frac{6(2.5EI)}{(7.5)} \left(\frac{\Delta}{6}\right) = +\frac{1}{3}(EI\Delta)$$

Since we need only relative moments, we take $EI\Delta = 90$

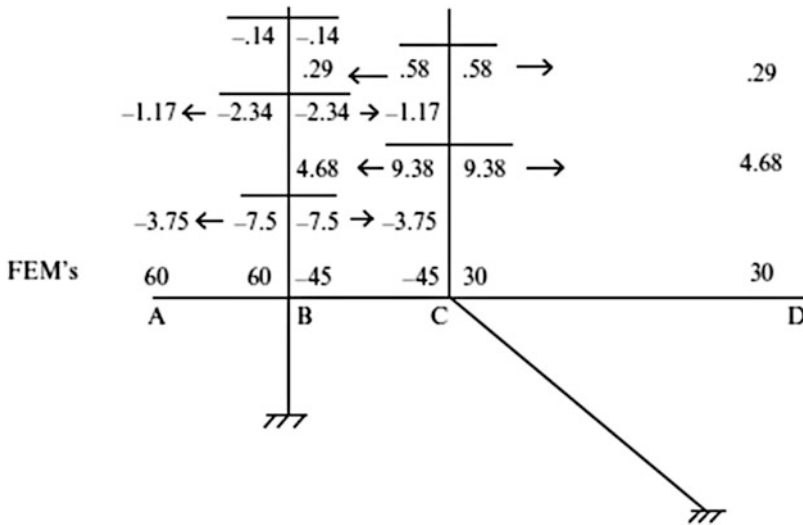
Then

$$M_{AB}^F = M_{BA}^F = +60 \text{ kNm}$$

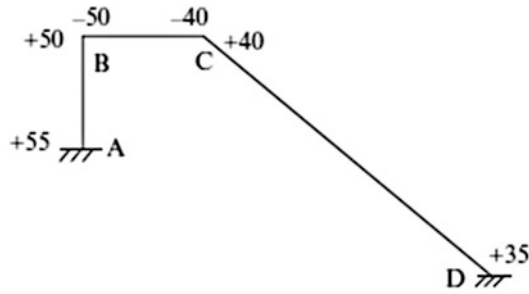
$$M_{CB}^F = M_{BC}^F = -45 \text{ kNm}$$

$$M_{DC}^F = M_{CD}^F = +30 \text{ kNm}$$

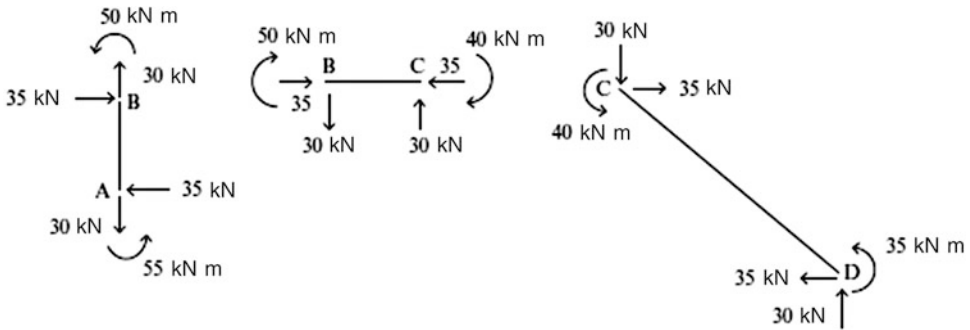
Next, we distribute the moments as shown below



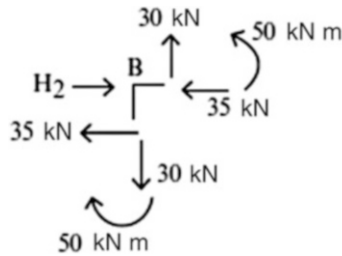
The end moments values are



Using these moments, we find the axial and shear forces.



Note that one needs the axial force in member BC in order to determine H_2 . Summing horizontal force components at B leads to H_2 .



Therefore

$$H_2 = 35 + 35 = 70 \text{ kN}$$

Given that the actual horizontal force is 45 kN, we scale the sideway moments by $H_1/H_2 = 45/70 = 9/14$.

$$\text{Final end moments} = \text{end moments case II} \left(\frac{H_1}{H_2} \right)$$

The final end moments (kN m) are listed below (Fig. E10.18c).

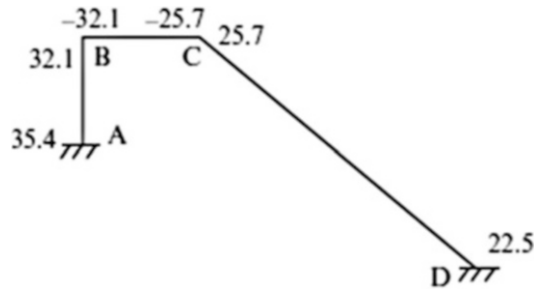
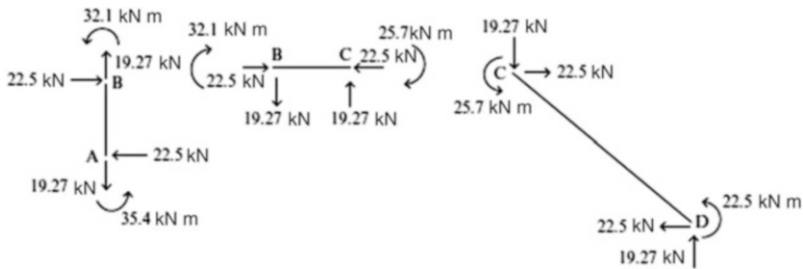


Fig. E10.18c Final end moments

Using these moments, we find the axial and shear forces.



Example 10.19: Computer-Based Analysis—Frame with Inclined Legs

Given: The frame shown in Fig. E10.19a.

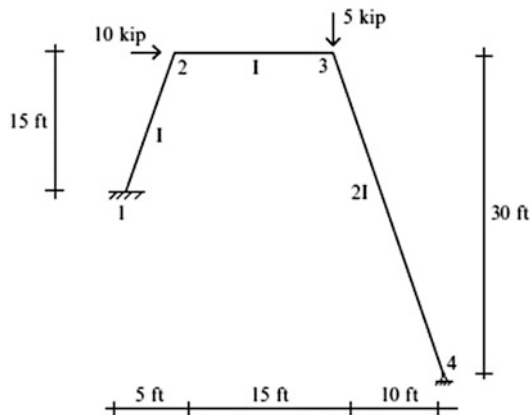


Fig. E10.19a

Determine: The displacement components at nodes 2 and 3, the bending moment distribution, and the reactions. Consider a range of values for I ($I = 100, 200, \text{ and } 400 \text{ in.}^4$). Take $A = 20 \text{ in.}^2$. Use computer software.

Solution: The computer generated deflection profiles and the reactions and moment diagram are listed below (Figs. E10.19b, E10.19c, E10.19d, E10.19e, E10.19f). Hand computation is not feasible for this task.

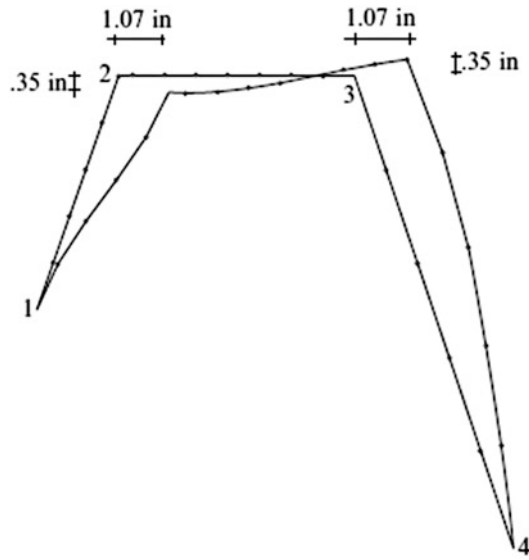


Fig. E10.19b Deflection profile— $I = 100 \text{ in.}^4$

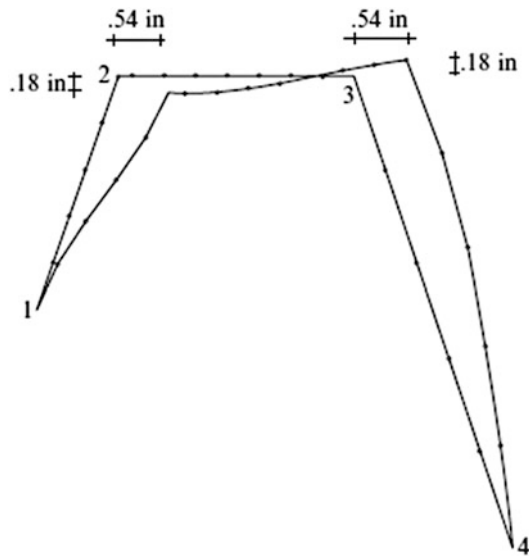


Fig. E10.19c Deflection profile— $I = 200 \text{ in.}^4$

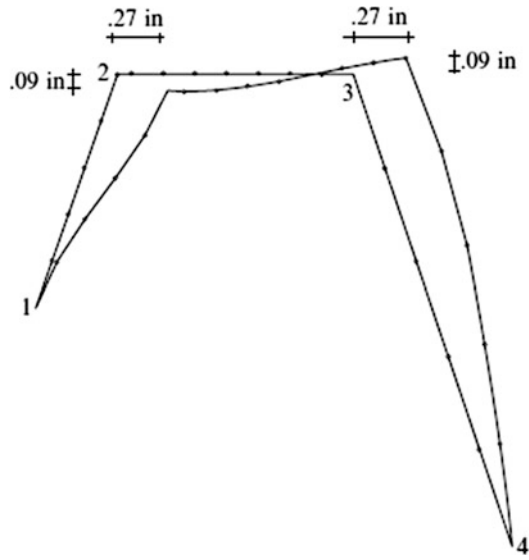


Fig. E10.19d Deflection Profile— $I = 400 \text{ in.}^4$

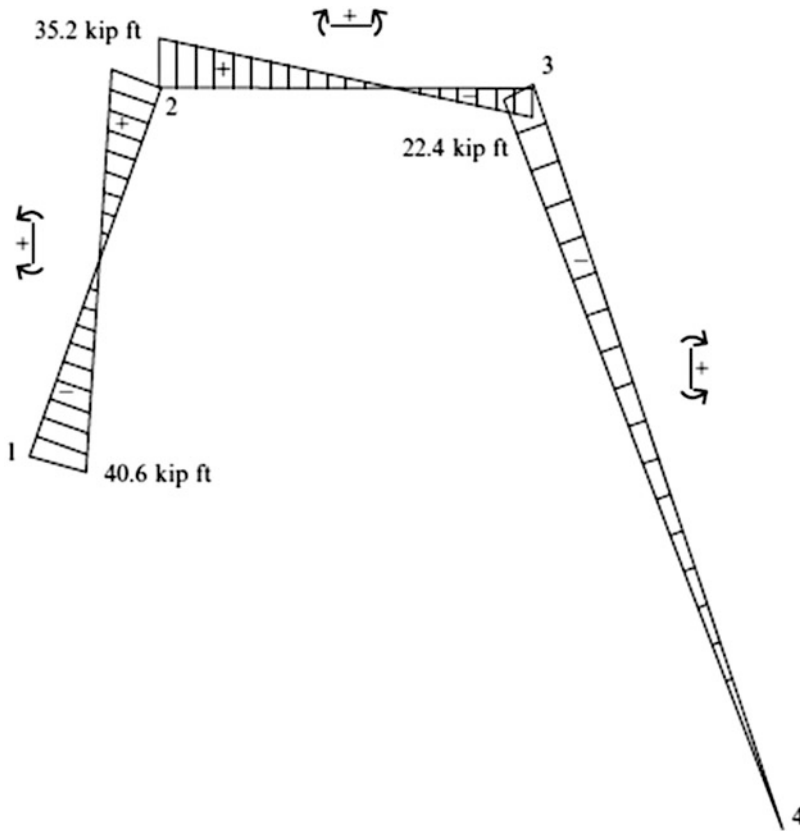


Fig. E10.19e Moment diagram

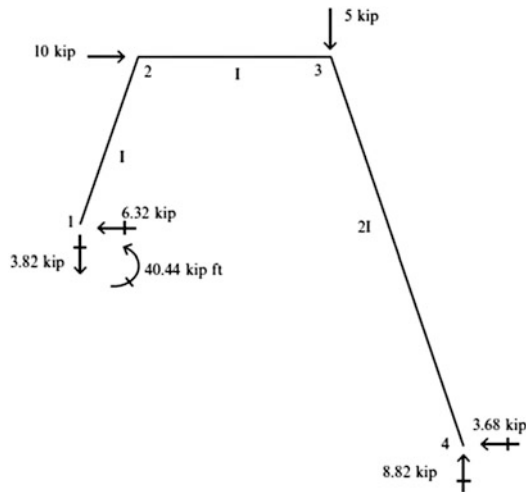


Fig. E10.19f Reactions

Note that the member forces are *invariant* since the relative stiffness of the members is the same. Also, the displacement varies linearly with l .

10.8 Plane Frames: Out of Plane Loading

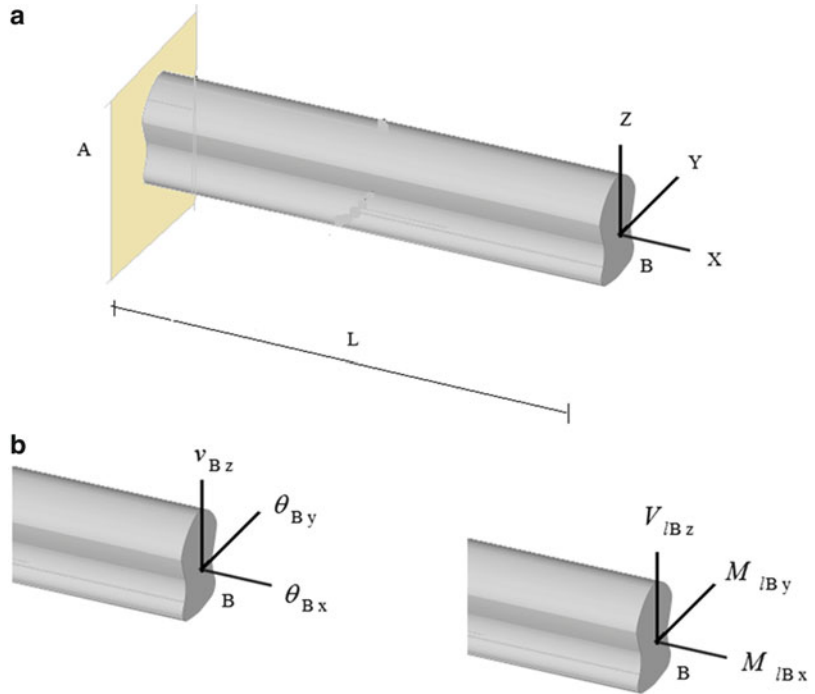
We discussed this case briefly in Chap. 4 when we dealt with statically determinate plane frame structures loaded normal to the plane such as highway signs. We extend the analysis methodology here to deal with statically indeterminate cases. Our strategy is based on the displacement method, i.e., we use generalized slope-deflection equations for the members and enforce equilibrium at the nodes. This approach is more convenient than the force method and has the additional advantage that it can be readily adopted for digital computation.

10.8.1 Slope-Deflection Equations: Out of Plane Loading

Consider the prismatic member shown in Fig. 10.25a. We assume that the member is loaded in the X - Z plane (note that all the previous discussions have assumed the loading is in the X - Y plane). The relevant displacement measures for this loading are the rotation θ_x , the rotation θ_y , and the transverse displacement v_z . Figure 10.25b defines the positive sense for these quantities and the corresponding end actions at B.

Following the procedure described in Sect. 10.3, one can establish the equations relating the end actions at A and B to the end displacements at A and B. Their form is

Fig. 10.25 (a) Prismatic member (b) Positive sense



$$\begin{aligned}
 V_{IAz} &= \frac{6EI_y}{L^2}(\theta_{By} + \theta_{Ay}) - \frac{12EI_y}{L^3}(v_{Bz} - v_{Az}) + V_{IAz}^F \\
 M_{IAx} &= -\frac{GJ}{L}(\theta_{Bx} - \theta_{Ax}) + M_{IAx}^F \\
 M_{IAy} &= \frac{2EI_y}{L}(\theta_{By} + 2\theta_{Ay}) - \frac{6EI_y}{L^2}(v_{Bz} - v_{Az}) + M_{IAy}^F \\
 V_{IBz} &= -\frac{6EI_y}{L^2}(\theta_{By} + \theta_{Ay}) + \frac{12EI_y}{L^3}(v_{Bz} - v_{Az}) + V_{IBz}^F \\
 M_{IBx} &= \frac{GJ}{L}(\theta_{Bx} - \theta_{Ax}) + M_{IBx}^F \\
 M_{IBy} &= \frac{2EI_y}{L}(2\theta_{By} + \theta_{Ay}) - \frac{6EI_y}{L^2}(v_{Bz} - v_{Az}) + M_{IBy}^F
 \end{aligned} \tag{10.47}$$

where GJ is the torsional rigidity for the cross section, and I_y is the second moment of area with respect to y -axis.

$$I_y = \int_A z^2 dA \tag{10.48}$$

The remaining steps are essentially the same as for the planar case. One isolates the members and nodes and enforces equilibrium at the nodes. In what follows, we illustrate the steps involved.

Consider the structure shown in Fig. 10.26. We suppose the supports are rigid. There are three unknown nodal displacement measures, θ_x , θ_y , and v_z at node 1.

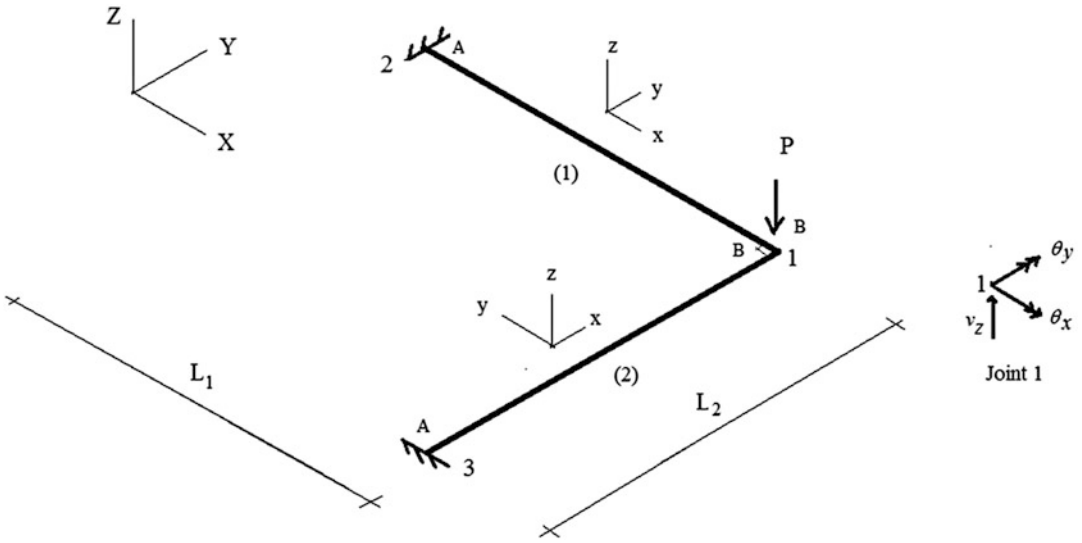


Fig. 10.26 Plane grid

Free body diagrams for the members incident on node 1 are shown below in Fig. 10.27. Requiring equilibrium at node 1 leads to the following equations:

$$\begin{aligned}
 V_{Bz}^{(1)} + V_{Bz}^{(2)} + P &= 0 \\
 M_{Bx}^{(1)} - M_{By}^{(2)} &= 0 \\
 M_{By}^{(1)} + M_{Bx}^{(2)} &= 0
 \end{aligned}
 \tag{10.49}$$

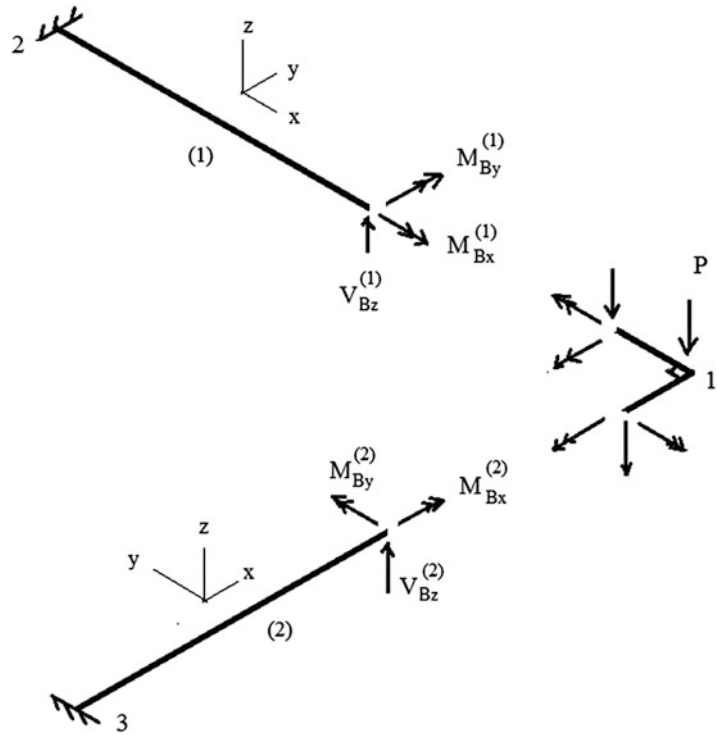
Noting the relationship between the variables,

$$\begin{aligned}
 \theta_{Bx}^{(1)} &= \theta_{1x} \\
 \theta_{Bx}^{(2)} &= \theta_{1y} \\
 \theta_{By}^{(1)} &= \theta_{1y} \\
 \theta_{By}^{(2)} &= -\theta_{1x} \\
 v_{Bz}^{(1)} &= v_{Bz}^{(2)} = v_{1z}
 \end{aligned}
 \tag{10.50}$$

the member equations take the following form,

$$\begin{aligned}
 M_{Bx}^{(1)} &= \frac{GJ_1}{L_1} \theta_{1x} \\
 M_{By}^{(1)} &= \frac{4EI_1}{L_1} \theta_{1y} + \frac{6EI_1}{L_1^2} v_{1z} \\
 V_{Bz}^{(1)} &= \frac{12EI_1}{L_1^3} v_{1z} - \frac{6EI_1}{L_1^2} \theta_{1y} \\
 \text{and} \\
 M_{Bx}^{(2)} &= \frac{GJ_2}{L_2} \theta_{1y} \\
 M_{By}^{(2)} &= \frac{4EI_2}{L_2} (-\theta_{1x}) + \frac{6EI_2}{L_2^2} v_{1z} \\
 V_{Bz}^{(2)} &= \frac{12EI_2}{L_2^3} v_{1z} - \frac{6EI_2}{L_2^2} (-\theta_{1x})
 \end{aligned}
 \tag{10.51}$$

Fig. 10.27 Free body diagrams



Lastly, we substitute for the end actions in the equilibrium equations (10.49) leading to

$$\begin{aligned}
 12E \left(\frac{I_1}{L_1^3} + \frac{I_2}{L_2^3} \right) v_{1z} + \frac{6EI_2}{L_2^2} \theta_{1x} - \frac{6EI_1}{L_1^2} \theta_{1y} + P &= 0 \\
 -\frac{6EI_2}{L_2^2} v_{1z} + \left(\frac{GJ_1}{L_1} + \frac{4EI_2}{L_2} \right) \theta_{1x} &= 0 \\
 \frac{6EI_1}{L_1^2} v_{1z} + \left(\frac{GJ_2}{L_2} + \frac{4EI_1}{L_1} \right) \theta_{1y} &= 0
 \end{aligned} \tag{10.52}$$

The solution is

$$\begin{aligned}
 \theta_{1x} &= \frac{6EI_2/L_2^2}{(GJ_1/L_1 + 4EI_2/L_2)} v_{1z} \\
 \theta_{1y} &= \frac{-6EI_1/L_1^2}{(GJ_2/L_2 + 4EI_1/L_1)} v_{1z} \\
 \left\{ 12E \left(\frac{I_1}{L_1^3} + \frac{I_2}{L_2^3} \right) + \frac{(6EI_1/L_1^2)^2}{(GJ_2/L_2 + 4EI_1/L_1)} + \frac{(6EI_2/L_2^2)^2}{(GJ_1/L_1 + 4EI_2/L_2)} \right\} v_{1z} &= -P
 \end{aligned} \tag{10.53}$$

When the member properties are equal,

$$I_1 = I_2$$

$$L_1 = L_2$$

$$J_1 = J_2$$

the solution reduces to

$$v_{1z} = \frac{-P}{\left(\frac{6EI}{L^3}\right) \left(1 + \frac{\frac{12EI}{L^2}}{(GJ + 4EI)}\right)}$$

$$\theta_{1y} = -\theta_{1x} = \frac{6EI/L^3}{(GJ + 4EI)} v_{1z} = \frac{-P}{(GJ + 4EI) + \left(\frac{12EI}{L^2}\right)} \tag{10.54}$$

end shear forces $V_{Bz}^{(1)} = V_{Bz}^{(2)} = \frac{P}{2}$

Note that even for this case, the vertical displacement depends on both I and J . In practice, we usually use a computer-based scheme to analyze grid-type structures.

Example 10.20: Grid Structure

Given: The grid structure defined in Fig. E10.20a. The members are rigidly connected at all the nodes. Assume the members are steel and the cross-sectional properties are constant. $I = 100 \text{ in.}^4$, $J = 160 \text{ in.}^4$.

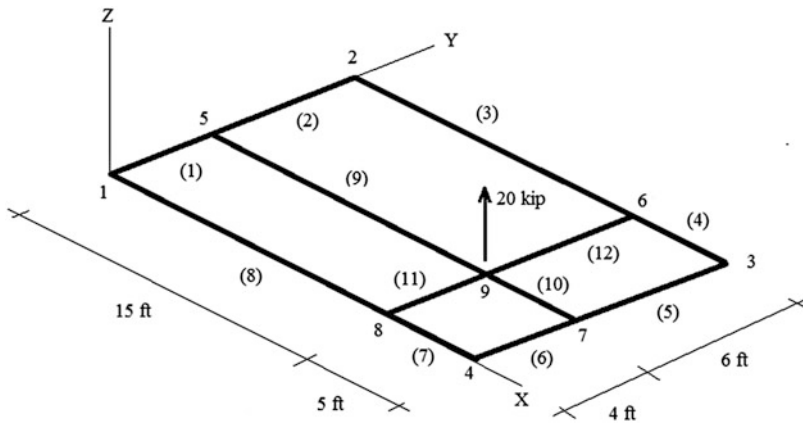


Fig. E10.20a

The nodal displacement restraints are as follows:

Node 1: x, y, z translation

Node 2: z translation

Node 3: z translation

Node 4: y, z translation

Determine: The displacement measures and member end forces at node 9. Use computer software.

Solution: The computer output data for this structure is

Displacement measures at node 9:

$$\text{Node 9} \begin{cases} w = 0.189 \text{ in.} \\ \theta_x = 0.00051 \text{ rad} \\ \theta_y = 0.00192 \text{ rad} \end{cases}$$

Member end forces at node 9:

$$\begin{array}{l} \text{Member (9)} \\ \text{Member (11)} \end{array} \begin{cases} V_Z = 1.31 \text{ kip} \\ M_x = 0.25 \text{ kip ft} \\ M_y = 14.5 \text{ kip ft} \end{cases} \quad \begin{array}{l} \text{Member (10)} \\ \text{Member (12)} \end{array} \begin{cases} V_Z = 5.2 \text{ kip} \\ M_x = 0.55 \text{ kip ft} \\ M_y = -16.6 \text{ kip ft} \end{cases} \quad \begin{cases} V_Z = 8.2 \text{ kip} \\ M_x = 0.86 \text{ kip ft} \\ M_y = 27 \text{ kip ft} \end{cases} \quad \begin{cases} V_Z = 5.3 \text{ kip} \\ M_x = 1.2 \text{ kip ft} \\ M_y = -26.2 \text{ kip ft} \end{cases}$$

One checks the results by noting that the sum of the end shears at node 9 must equal the applied load of 20 kip.

10.9 Nonlinear Member Equations for Frame-Type Structures

10.9.1 Geometric Nonlinearity

Although we did not mention it explicitly, when dealing with equilibrium equations, we always showed the forces acting on the initial geometry position of the structure. However, the geometry changes due to deformation under the action of the loading, and this assumption is justified only when the change in geometry (deformation) is negligible. This is true in most cases. However, there are exceptions, and it is of interest to explore the consequence of accounting for geometric change when establishing the equilibrium equations. This approach is referred to as geometric nonlinear analysis since the additional geometric terms result in nonlinear equations. In what follows, we illustrate this effect for different types of structures.

Consider the two-member truss shown in Fig. 10.28a. We suppose the angle θ is small, say about 15° . When a vertical force is applied, the structure deforms as shown in Fig. 10.28b. The load is resisted by the member forces generated by the deformation resulting from the displacement, v .

Due to the displacement, the angle changes from θ to β , where β is a function of v .

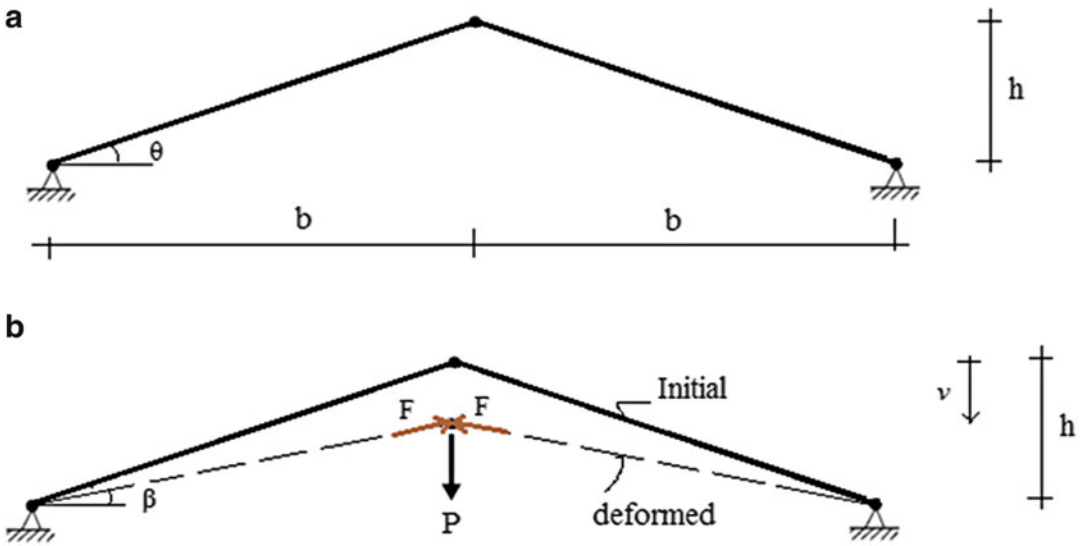


Fig. 10.28 Nonlinear truss example

$$\tan \beta = \frac{h - v}{b} \tag{10.55}$$

The equilibrium equation also depends on v .

$$P = 2F \sin \beta \tag{10.56}$$

When v is small with respect to h , β can be approximated as

$$\tan \beta \approx \frac{h}{b} \equiv \tan \theta \tag{10.57}$$

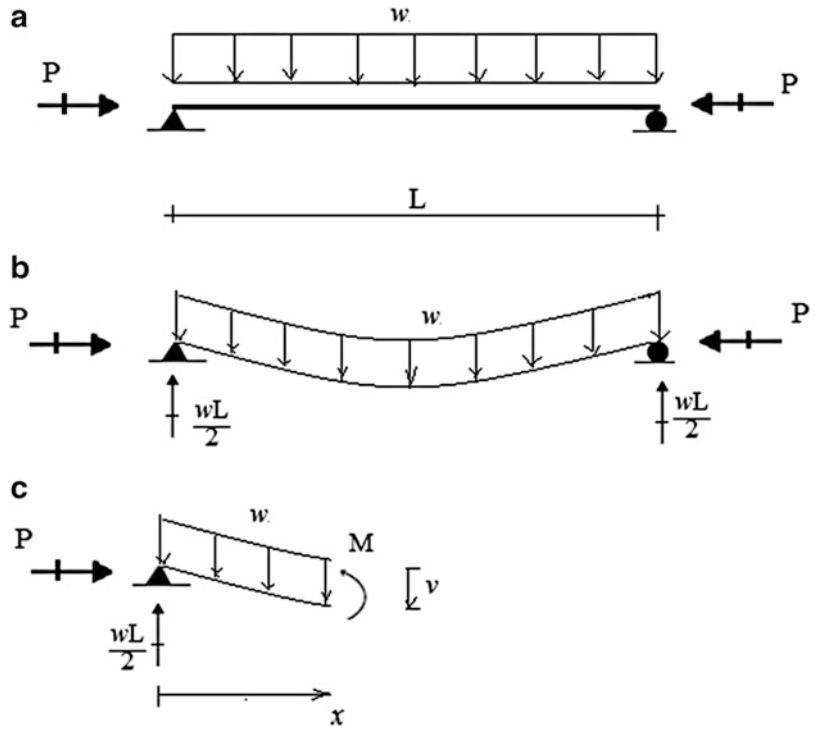
and it follows that

$$P \approx 2F \sin \theta \tag{10.58}$$

which is the “linearized” form of the equilibrium equation. One cannot neglect the change in angle when h is also small which is the case when θ is on the order of 15° .

Another example of geometric nonlinearity is a beam subjected to axial compression and transverse loading. Fig. 10.29 shows the loading condition and deformed geometry.

Fig. 10.29 Nonlinear beam example



Noting Fig. 10.29c, the bending moment at location x is

$$M = \left(\frac{wL}{2}\right)x - \frac{wx^2}{2} + Pv \tag{10.59}$$

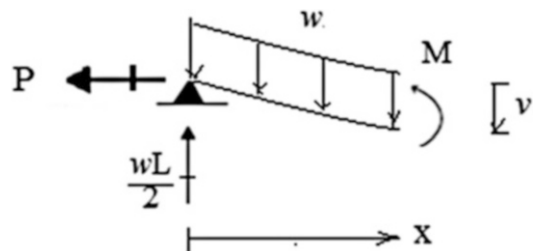
The last term is due to accounting for the displacement from the initial position of the beam. We will show later that this term has a destabilizing effect on the response, i.e., it magnifies the response.

Up to this point in the text, we have neglected the geometric term and always worked with the initial undeformed geometry. For example, we have been taking M as

$$M \approx \left(\frac{wL}{2}\right)x - \frac{wx^2}{2} \tag{10.60}$$

When P is compressive, and the beam is flexible, this linearized expression is not valid and one needs to use the nonlinear form, (10.59). If P is a tensile force, the free body diagram shown in Fig. 10.30 now applies and the appropriate expression for M is

Fig. 10.30 Nonlinear beam – axial tension



$$M = \left(\frac{wL}{2}\right)x - \frac{wx^2}{2} - Pv \tag{10.61}$$

In this case, the nonlinear contribution has a *stabilizing* effect.

Generalizing these observations, whenever a member is subjected to a *compressive* axial load, one needs to consider the potential destabilizing effect of geometric nonlinearity on the axial stiffness of the member. This type of behavior is usually referred to as “buckling.” From a design perspective, buckling must be avoided. This is achieved by appropriately dimensioning the cross section and providing bracing to limit transverse displacement.

In what follows, we extend the planar beam bending formulation presented in Sects. 3.5 and 3.6 to account for geometric nonlinearities. This revised formulation is applied to establish the nonlinear form of the member equations described in Sect. 10.3. Lastly, these equations are used to determine the nonlinear behavior of some simple frame structures.

10.9.2 Geometric Equations Accounting for Geometric Nonlinearity

Figure 10.31a shows the initial and deformed position of a differential element experiencing planar bending in the x - y plane. The geometric variables are the axial displacement, u ; the transverse displacement, v ; and the rotation of the cross section, β .

Fig. 10.31 (a) Initial and deformed positions
(b) Position of tangent

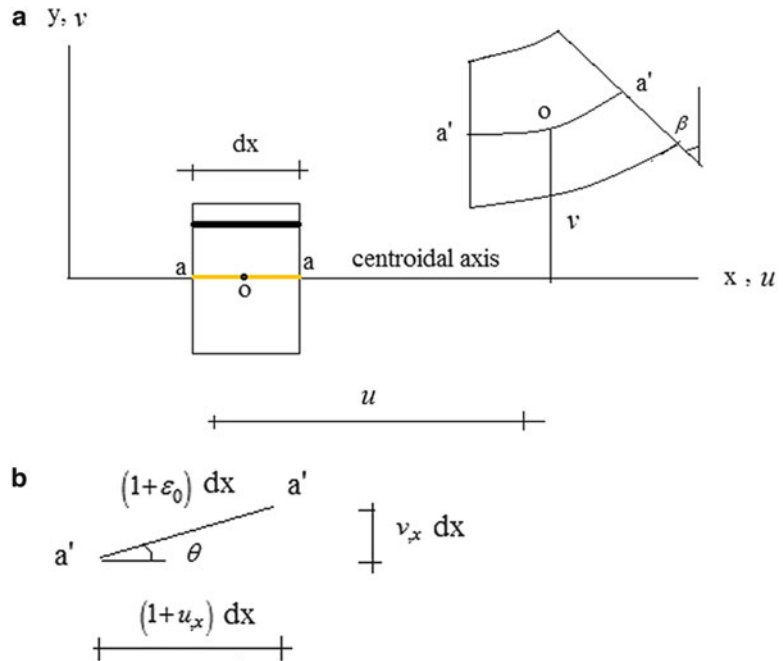


Figure 10.31b defines the deformed position of line a-a; θ denotes the rotation of the centroidal axis. Assuming $\theta = 0$ leads to the linearized expression for the strain, ϵ_0 .

$$\theta \approx 0 \Rightarrow \epsilon_0 = u_{,x} \tag{10.62}$$

The next level of approximation is based on assuming θ is sufficiently small such that $\theta^2 \ll 1$. This leads to

$$\begin{aligned}\tan \theta &\approx \sin \theta \approx \theta \\ \cos \theta &\approx 1\end{aligned}\quad (10.63)$$

Then, the exact expressions for ε_0 and $\tan \theta$

$$\begin{aligned}(1 + \varepsilon_0)^2 &= (1 + u_{,x})^2 + (v_{,x})^2 \\ \tan \theta &= \frac{v_{,x}}{1 + u_{,x}}\end{aligned}\quad (10.64)$$

reduce to

$$\begin{aligned}\varepsilon_0 &= u_{,x} + \frac{1}{2}(v_{,x})^2 \\ \theta &\approx v_{,x}\end{aligned}\quad (10.65)$$

Equation (10.65) applies for small strain, i.e., $\varepsilon \ll 1$. Note that the nonlinearity involves the rotation of the centroidal axis.

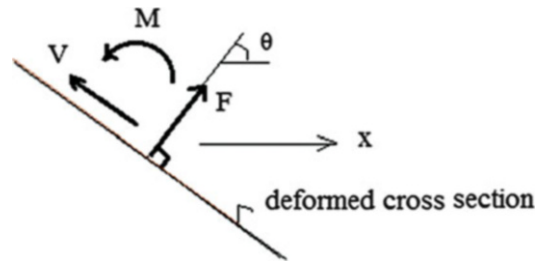
The remaining steps are similar to those followed for the linear case. We assume the cross section remains a plane and neglect the transverse shear deformation. These assumptions lead to (see Fig. 10.32):

$$\begin{aligned}\gamma &= 0 \quad \Rightarrow \quad \beta \approx \theta = \frac{dv}{dx} \\ \text{and} \\ \varepsilon &= \varepsilon_0 - y\chi\end{aligned}\quad (10.66)$$

$$\chi = \frac{d\beta}{dx} = \frac{d\theta}{dx} = \frac{d^2v}{dx^2}$$

Given the strains, one can determine the internal axial force and moment using the linear elastic

Fig. 10.32 Orientation of deformed cross section



stress–strain relations.

$$\begin{aligned}F &= \int \sigma dA = AE\varepsilon_0 \\ M &= \int -y\sigma dA = EI\chi\end{aligned}\quad (10.67)$$

Note that F acts at an angle θ with respect to the x -axis. Since we have neglected the transverse shear deformation, V has to be determined using an equilibrium requirement.

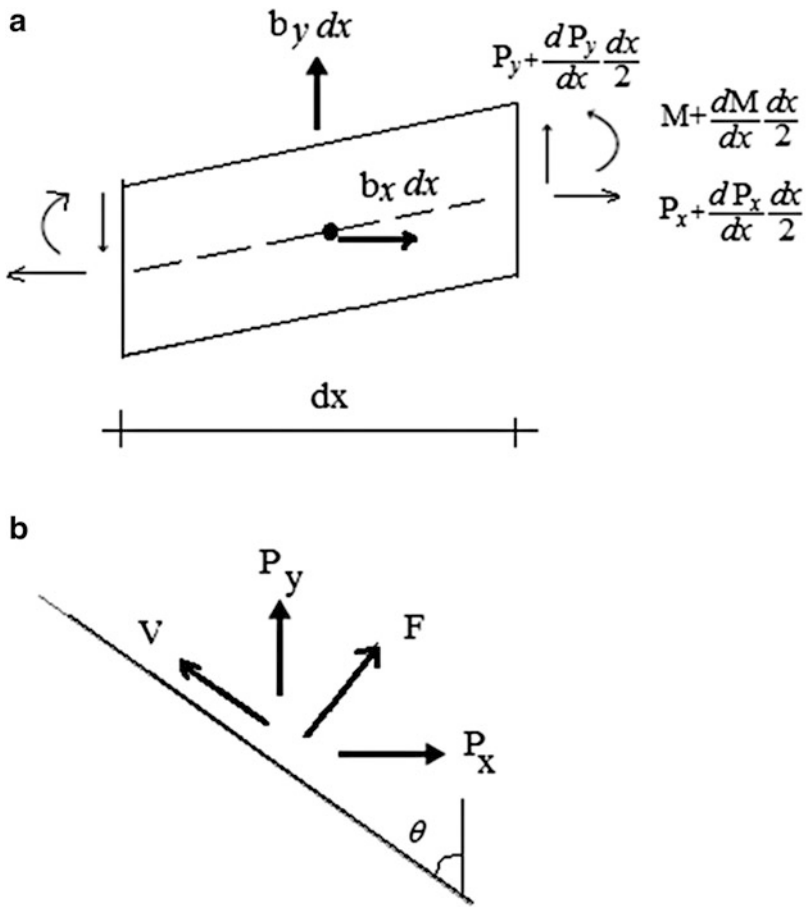


Fig. 10.33 (a) Differential element (b) Cartesian components

The last step involves enforcing the equilibrium condition. We work with the differential element shown in Fig. 10.33a; b_x and b_y are the loads per unit length. The Cartesian components are related to the internal forces in terms of the rotation angle, θ .

$$\begin{aligned} P_x &= F \cos \theta - V \sin \theta \\ P_y &= F \sin \theta + V \cos \theta \end{aligned} \tag{10.68}$$

Noting Fig. 10.33b, it follows that

$$\begin{aligned} F &= P_x \cos \theta + P_y \sin \theta \\ V &= -P_x \sin \theta + P_y \cos \theta \end{aligned}$$

Assuming θ is small, we simplify Eq. (10.68) to

$$\begin{aligned} P_x &\approx F \\ P_y &\approx F \cdot \theta + V = F_{V,x} + V \end{aligned} \tag{10.69}$$

The equilibrium equations for the element are

$$\begin{aligned}\frac{d}{dx}P_x + b_x &= 0 \\ \frac{d}{dx}P_y + b_y &= 0 \\ \frac{dM}{dx} + P_y - v_{,x}P_x &= 0\end{aligned}\quad (10.70)$$

Substituting for P_x and P_y , Equation (10.70) reduce to

$$\begin{aligned}\frac{dF}{dx} + b_x &= 0 \\ \frac{d}{dx}\left(F\frac{dv}{dx}\right) + \frac{dV}{dx} + b_y &= 0 \\ \frac{dM}{dx} + V &= 0\end{aligned}\quad (10.71)$$

The nonlinearity is present in the transverse equilibrium equation in the form of a coupling between axial and bending actions. Lastly, the boundary conditions are:

$$\left. \begin{array}{ll} u \text{ or } P_x = F & \text{prescribed} \\ v \text{ or } P_x = Fv_{,x} + V & \text{prescribed} \\ \theta \text{ or } M & \text{prescribed} \end{array} \right\} \text{at each end} \quad (10.72)$$

We illustrate the boundary condition for various types of supports.

Case 1: Free end



$$P_x = P_y = M = 0 \Rightarrow F = V = M = 0$$

Case 2: Axial load



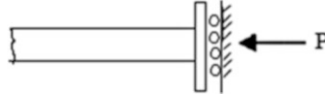
$$\begin{cases} P_x = -P \\ P_y = 0 \\ M = 0 \end{cases} \Rightarrow \begin{cases} F = -P \\ V = v_{,x}P \\ M = 0 \end{cases}$$

Case 3: Roller support



$$\begin{cases} P_x = -P \\ v = 0 \\ M = 0 \end{cases} \Rightarrow \begin{cases} F = -P \\ v = M = 0 \end{cases}$$

Case 4: Rotation restraint



$$\begin{cases} P_x = -P \\ P_y = 0 \\ \theta = 0 \end{cases} \Rightarrow \begin{cases} F = -P \\ V = 0 \\ \theta = 0 \end{cases}$$

10.9.3 Solution for Compressive Axial Load

We consider here the case where the axial load is compressive (e.g., see Fig. 10.29). Taking

$$F = -P = \text{constant} \quad (10.73)$$

the remaining equations in (10.71) reduce to

$$\begin{aligned} V &= -\frac{dM}{dx} \\ \frac{d^2M}{dx^2} + P\frac{d^2v}{dx^2} &= b_y \end{aligned} \quad (10.74)$$

The corresponding boundary conditions are:

$$\left. \begin{array}{l} v \text{ or } V - P\frac{dv}{dx} \text{ prescribed} \\ \frac{dv}{dx} \text{ or } M \text{ prescribed} \end{array} \right\} \text{at each end} \quad (10.75)$$

Noting (10.67), the expression for M expands to

$$M = EI\frac{d^2v}{dx^2} \quad (10.76)$$

Integrating the second equation in (10.74) leads to

$$M + Pv = \int \int_x b_y dx + c_1x + c_2$$

where c_1 and c_2 are integration constants. Then, substituting for M , we obtain the governing equation for v .

$$EI\frac{d^2v}{dx^2} + Pv = \int \int_x b_y dx + c_1x + c_2 \quad (10.77)$$

We suppose b_y and EI are constant. For this case,

$$\int \int_x b_y dx = \frac{1}{2}b_yx^2 \equiv \frac{1}{2}bx^2 \quad (10.78)$$

and the corresponding solution of (10.77) is:

$$v = \frac{1}{\mu^2} \left\{ \frac{b}{2EI} \left(x^2 - \frac{2}{\mu^2} \right) + \frac{1}{EI} (c_1 x + c_2) \right\} + c_3 \cos \mu x + c_4 \sin \mu x \quad (10.79)$$

where

$$\mu^2 = \frac{P}{EI}$$

The integration constants are determined using the boundary conditions, (10.75).

Example 10.21

Given: The axially loaded member shown in Fig. E10.21a.

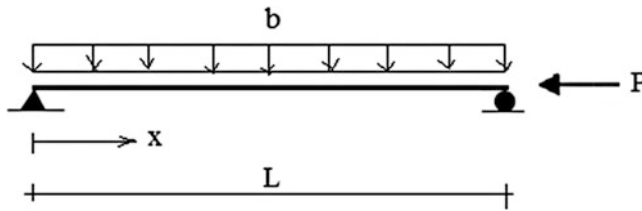


Fig. E10.21a

Determine: The transverse displacement as a function of the axial load, P .

Solution: The boundary conditions for the simply supported axially loaded member shown in Fig. E10.21a are

$$v(0) = v(L) = 0$$

$$M(0) = M(L) = 0$$

Substituting for v in (10.76) leads to

$$M = -\mu^2 \{ c_3 \cos \mu x + c_4 \sin \mu x \} + \frac{b}{\mu^2 EI}$$

Enforcing the boundary conditions, the corresponding integration constants are:

$$c_1 = -\frac{bL}{2}$$

$$c_2 = 0$$

$$c_3 = \frac{b}{\mu^4 EI}$$

$$c_4 = \frac{b}{\mu^4 EI} \left(\frac{1 - \cos \mu L}{\sin \mu L} \right)$$

Using these values, the solution for v expands to

$$v = \frac{b}{\mu^4 EI} \left\{ \cos \mu x + \sin \mu x \left(\frac{1 - \cos \mu L}{\sin \mu L} \right) \right\} + \frac{b}{\mu^2 EI} \left\{ \frac{1}{2} \left(x^2 - \frac{2}{\mu^2} \right) - \frac{xL}{2} \right\}$$

The nonlinear behavior is generated by the axial force parameter, μ . To illustrate this effect, we evaluate v at $x = L/2$.

$$v\left(\frac{L}{2}\right) = \frac{b}{\mu^4 EI} \left\{ \cos \frac{\mu L}{2} + \sin \frac{\mu L}{2} \left(\frac{1 - \cos \mu L}{\sin \mu L} \right) \right\} + \frac{b}{\mu^2 EI} \left\{ -\frac{1}{\mu^2} - \frac{L^2}{8} \right\}$$

The linear (i.e., $P = 0$) solution is

$$v\left(\frac{L}{2}\right) = \frac{5}{384} \frac{bL^4}{EI}$$

Figure E10.21b shows the variation of the ratio $\frac{v}{v_{\text{linear}}}$ vs. $\frac{P}{P_{\text{cr}}}$, where P_{cr} is the value of P for which $\sin \mu L = 0$.

$$\sin \mu L = 0 \Rightarrow \mu L = \pi$$

$$\mu L = \left(\frac{P}{EI}\right)^{\frac{1}{2}} L = \pi$$

$$P_{\text{cr}} = \frac{\pi^2 EI}{L^2}$$

The effect of axial load becomes pronounced when P approaches P_{cr} .

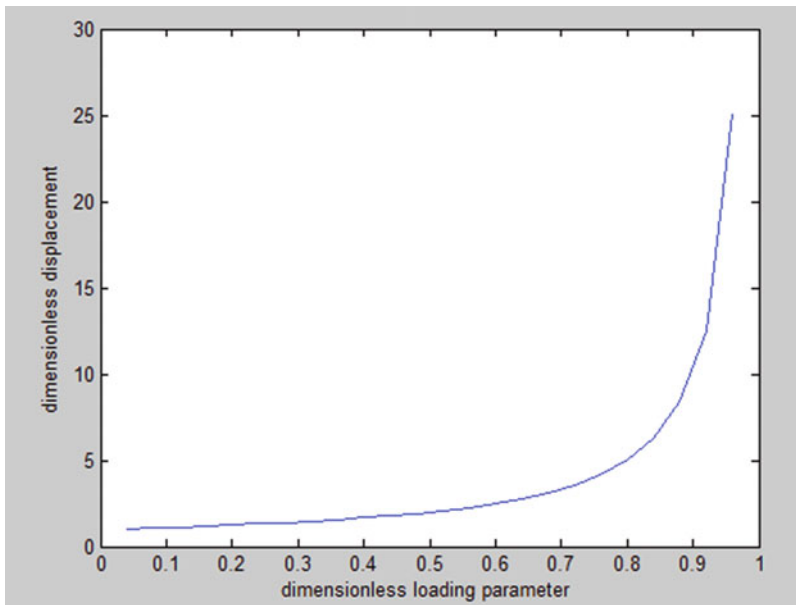


Fig. E10.21b

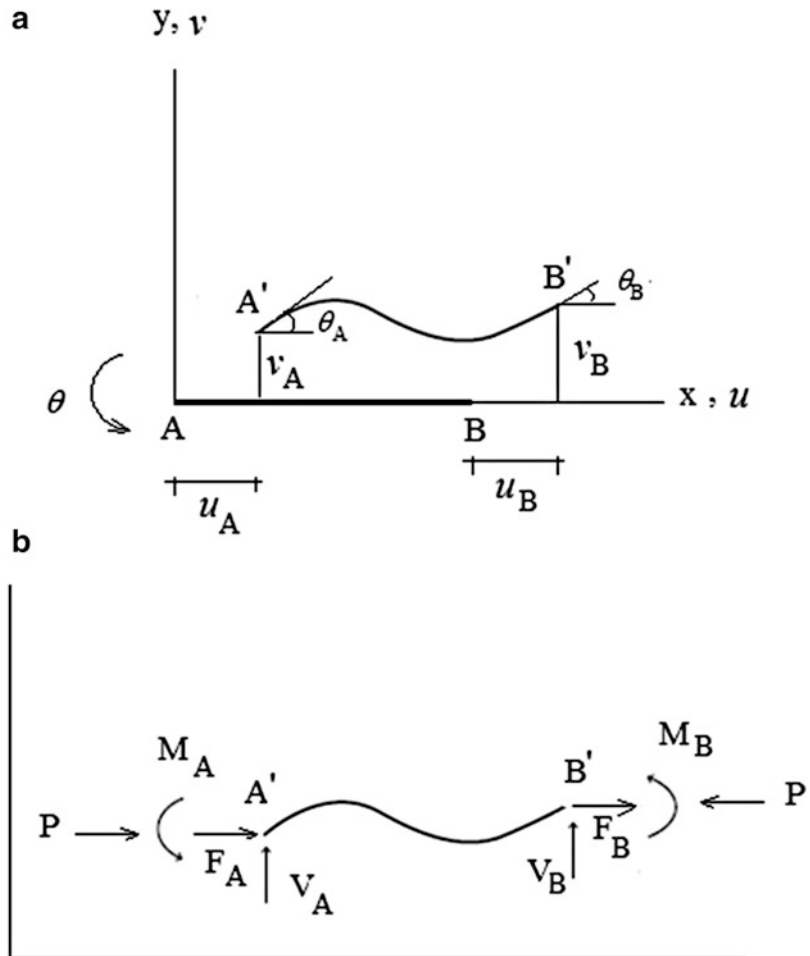
10.9.4 Nonlinear Member End Actions–End Displacement Equations

In order to deal with framed structures, one needs the set of equations relating the forces acting on the ends of a member and the displacement measures for the ends. The linear form of these equations is developed in Sect. 10.3. We derive the nonlinear form here using the general solution represented by (10.79).

Figures 10.34a, b define the notation for the displacement measures and the end actions. The only difference for the nonlinear case is the presence of the axial load, P . All quantities are referred to the local member frame. Note that the end actions act on the deformed configuration.

Equation (10.79) defines the solution for the case of a uniform load. To allow for an arbitrary load, we express the solution as

Fig. 10.34 Notation for nonlinear case.
 (a) Displacements.
 (b) End actions



$$v = v_p + \frac{1}{\mu^2 EI} (C_1 x + C_2) + C_3 \cos \mu x + C_4 \sin \mu x \tag{10.80}$$

The boundary conditions now involve the displacement measures at $x = 0$ and L .

$$\begin{aligned}
 v(0) &= v_A & \frac{dv}{dx}(0) &= \omega_A \\
 v(L) &= v_B & \frac{dv}{dx}(L) &= \omega_B
 \end{aligned}
 \tag{10.81}$$

Specializing (10.80) for these conditions leads to expressions for the integration constants.

$$\begin{aligned}
 C_1 &= \omega_A - \omega_{A,p} - \mu C_4 \\
 C_2 &= u_A - u_{A,p} - C_3 \\
 C_3 &= -C_4 \frac{1 - \cos \mu L}{\sin \mu L} - \frac{\omega_B - \omega_A - \omega_{B,p} + \omega_{A,p}}{\mu \sin \mu L} \\
 C_4 &= \frac{1}{D} \left\{ [u_B - u_{B,p} - u_A + u_{A,p} - (\omega_A + \omega_{A,p})L] \sin \mu L \right. \\
 &\quad \left. - \frac{1 - \cos \mu L}{\mu} [\omega_B - \omega_{B,p} - \omega_A + \omega_{A,p}] \right\} \\
 D &= 2(1 - \cos \mu L) - \mu L \sin \mu L
 \end{aligned}
 \tag{10.82}$$

Note that $D \rightarrow 0$ as $\mu L \rightarrow 2\pi$. Then $C_4 \rightarrow \infty$ and it follows that $v \rightarrow \infty$ for any arbitrary loading. The limiting value of P is

$$P|_{\max} = P_{cr} = \frac{4\pi^2 EI}{L^2} \tag{10.83}$$

Given v , one can evaluate the end actions. The bending moment is defined as

$$M = EI \frac{d^2 v}{dx^2} \tag{10.84}$$

Noting Fig. 10.34b, the end actions are related to the bending moment by

$$\begin{aligned}
 V_B &= \frac{-1}{L} (M_A + M_B) - P \frac{(v_B - v_A)}{L} \\
 V_A &= -V_B
 \end{aligned}
 \tag{10.85}$$

The second term in the expression for V_B is due to the rotation of the chord connecting A and B. This term is neglected in the linear formulation. We will show later that it leads to a loss in lateral stiffness (commonly referred to as the P -delta effect).

Using the above equations, we express the final equations as:

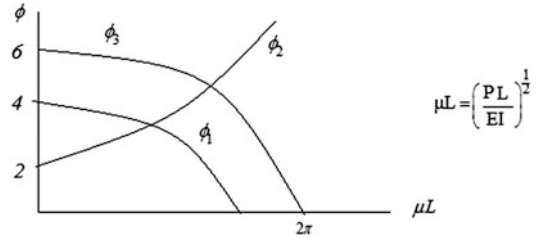
$$\begin{aligned}
 M_A &= M_A^F + \frac{EI}{L} \left[\phi_1 \omega_A + \phi_2 \omega_B - \frac{\phi_3}{L} (v_B - v_A) \right] \\
 M_B &= M_B^F + \frac{EI}{L} \left[\phi_1 \omega_B + \phi_2 \omega_A - \frac{\phi_3}{L} (v_B - v_A) \right] \\
 V_A &= V_A^F + \frac{\phi_3 EI}{L^2} \left[\omega_B + \omega_A - \frac{2}{L} (v_B - v_A) \right] + \frac{P}{L} (v_B - v_A) \\
 V_B &= V_B^F - \frac{\phi_3 EI}{L^2} \left[\omega_B + \omega_A - \frac{2}{L} (v_B - v_A) \right] - \frac{P}{L} (v_B - v_A)
 \end{aligned}
 \tag{10.86}$$

where

$$\begin{aligned} D\phi_1 &= \mu L (\sin \mu L - \mu L \cos \mu L) \\ D\phi_2 &= \mu L (\mu L - \sin \mu L) \\ \phi_3 &= \phi_1 + \phi_2 \end{aligned} \quad (10.87)$$

The ϕ functions were introduced by Livesley [2]. Figure 10.35 shows the variation with μL . For small μL , the coefficients reduce to the corresponding linear values

Fig. 10.35 ϕ functions



$$\begin{aligned} \mu L &\rightarrow 0 \\ \phi_1 &\rightarrow 4 \\ \phi_2 &\rightarrow 2 \\ \phi_3 &\rightarrow 6 \end{aligned} \quad (10.88)$$

For large μL , the functions behave in a nonlinear manner

$$\begin{aligned} \mu L &\rightarrow 2\pi \\ \phi_1 &\rightarrow -\infty \\ \phi_2 &\rightarrow +\infty \\ \phi_3 &\rightarrow 0 \end{aligned} \quad (10.89)$$

One can assume linear behavior and use these results to obtain an initial estimate for the axial load. Equations (10.86) are applicable for those members which have a compressive axial load. As the external loading is increased, the internal axial loads also increase, resulting in a reduction in stiffness and eventually to large displacements similar to the behavior shown in Fig. E10.21b. This trend is clearly evident in the expressions for V_A and V_B listed in (10.86). As P increases, ϕ_3 decreases, and the overall stiffness decreases. The following examples illustrate this effect.

Example 10.22

Given: The portal frame shown in Fig. E10.22a.

Determine: The effect of axial load on the lateral stiffness.

Solution: We assume $I_g \gg I_c$ so that member BC just translates under the action of the horizontal load. We also assume there is a gravity loading which creates compression in the columns. Of interest

is the interaction between the gravity loading and the lateral loading. Due to the compressive nature of the gravity loading, we should expect a reduction in lateral stiffness, leading eventually to an unstable condition.

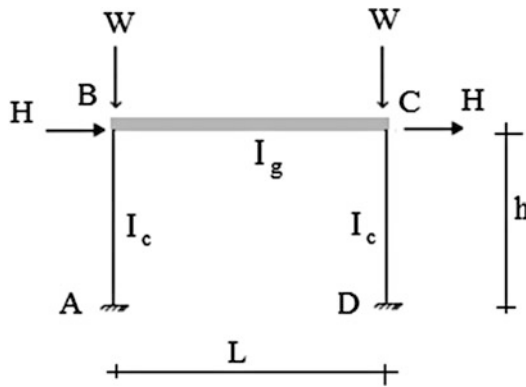


Fig. E10.22a

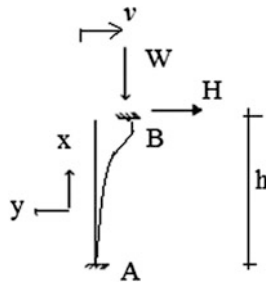


Fig. E10.22b

Noting the free body diagram shown in Fig. E10.22b, the end conditions for member AB are

$$\theta_A = v_A = 0 \quad \theta_B = 0 \quad \bar{V}_B = -H$$

$$v_B = -v \quad P = W$$

Using these values, the expression for \bar{V}_B follows from Equation (10.86).

$$V_B = \frac{-2EI_c\phi_3}{h^3}v + \frac{P}{h}v$$

Then

$$H = \left\{ \frac{2EI_c\phi_3}{h^3} - \frac{P}{h} \right\} v \equiv kv$$

Figure E10.22c shows how k degrades with increasing P . The P -delta term dominates this process; it leads to an 80 % reduction at the critical loading, $\alpha = 1$. As the load approaches this load level, the lateral stiffness approaches zero, resulting in large displacement, and eventual failure due to excessive inelastic deformation.

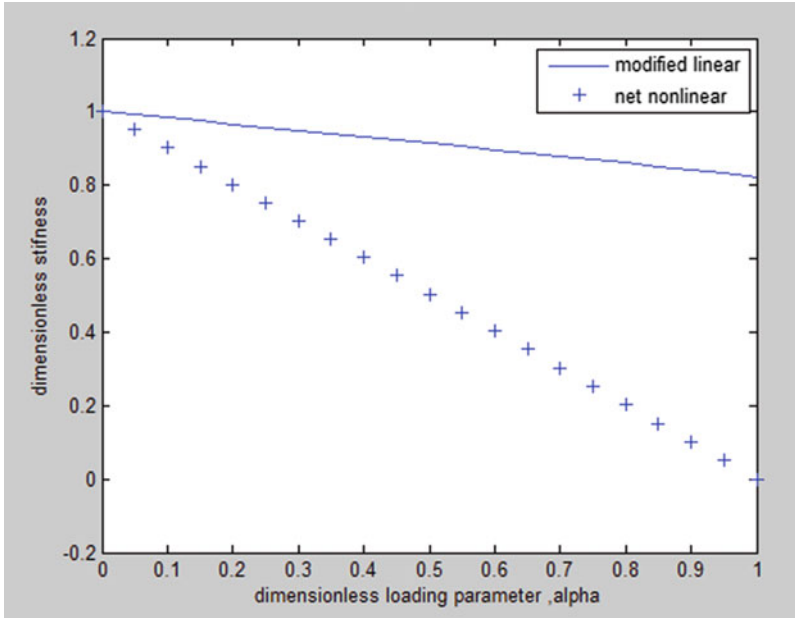


Fig. E10.22c

Example 10.23

Given: The pin-ended portal frame shown in Fig. E10.23a.

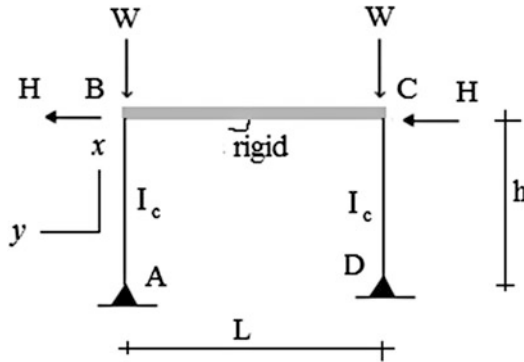


Fig. E10.23a

Determine: (a) The effect of axial load on the lateral stiffness. (b) The additional stiffness provided by diagonal bracing (Fig. E10.23c).

Solution:

Part(a)

The response is anti-symmetrical so one has only to analyze member AB. Noting Fig. E10.23a, the end conditions are

$$\begin{aligned}v_A = M_A = 0 \quad P = W \\ \theta_B = 0 \quad V_B = +H\end{aligned}$$

Setting $M_A = 0$ leads to

$$\frac{EI_c}{h} \left[\phi_1 \theta_A + \phi_2 \theta_B - \phi_3 \left(\frac{v_B - v_A}{h} \right) \right] = 0$$

Then, noting the end conditions, and solving for θ_A yields

$$\theta_A = \frac{\phi_3}{\phi_1} \frac{EI_c}{h} \left(\frac{v_B}{h} \right)$$

Substituting for θ_A , the expression for V_B becomes

$$V_B = -\frac{EI_c}{h} \phi_3 \left[\left(\frac{\phi_3}{\phi_1} - 2 \right) \left(\frac{v_B}{h} \right) \right] - \frac{P}{h} v_B$$

Lastly, we require $V_B = +H$.

Then

$$H = \frac{EI_c}{h^3} \left[\phi_3 \left(2 - \frac{\phi_3}{\phi_1} \right) \right] v_B - \frac{P}{h} v_B$$

We express H as

$$\begin{aligned}H &= k v_B \\ k &= \frac{3EI_c}{h^3} \left[\frac{1}{3} \phi_3 \left(2 - \frac{\phi_3}{\phi_1} \right) - \frac{\alpha \pi^2}{12} \right] = \frac{3EI_c}{h^3} (k_1 - k_2)\end{aligned}$$

where

$$\begin{aligned}\alpha &= \frac{P}{P_{cr}} = \frac{P}{\frac{\pi^2 EI_c}{4h^2}} \\ k_2 &= \frac{Ph^2}{3EI_c}\end{aligned}$$

Note that k_2 represents the P -delta effect on stiffness. Figure E10.23b shows that k_2 dominates the stiffness reduction due to the axial compression in the columns.

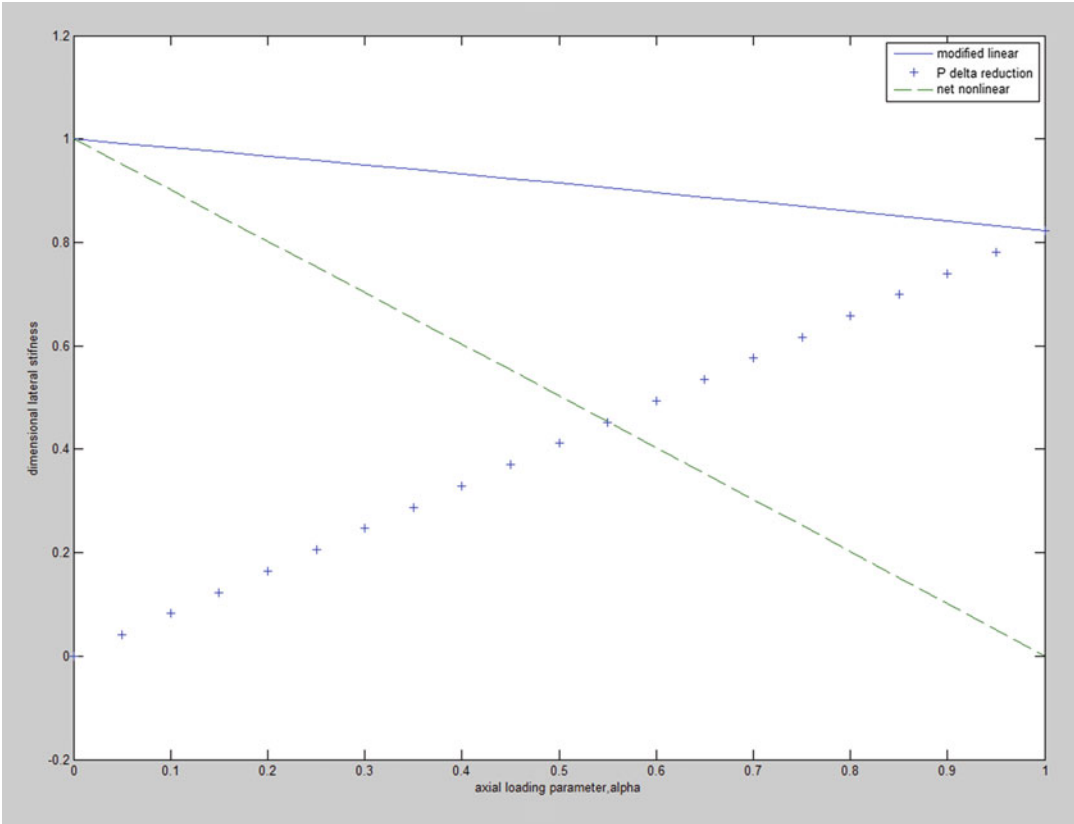


Fig. E10.23b

Part(b)

Suppose the diagonal braces shown in Fig. E10.23c are added. They provide additional stiffness which offsets the loss in stiffness due to P -delta effect. Noting the expression for V_B derived above, the force H is now equal to the sum of V_B and the horizontal component of the bracing force.

$$H = V_B + F_{\text{brace}} \cos \theta = (k + k_{\text{brace}})v_B$$

where

$$k_{\text{brace}} = \frac{A_{\text{brace}}E}{L_{\text{brace}}} (\cos \theta)^2 = \frac{A_{\text{brace}}E}{h} (\cos \theta)^2 \sin \theta$$

One selects k_{brace} such that

$$k_{\text{brace}} = \frac{A_{\text{brace}}E}{h} (\cos \theta)^2 \sin \theta = \frac{3EI_c}{h^3} = K|_{P=0}$$

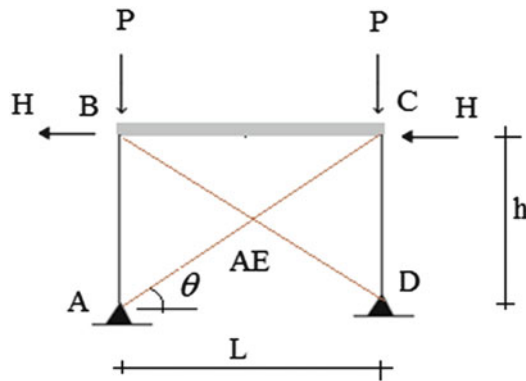


Fig. E10.23c

10.10 Summary

10.10.1 Objectives

- To describe the displacement method of analysis specialized for frame-type structures.
- To develop the slope-deflection equations for planar bending of beams
- To illustrate how to apply the displacement method for beams and rigid frame systems using the slope-deflection equations.
- To formulate the moment distribution procedure and demonstrate its application to indeterminate beams and rigid frames.
- To determine the effect of geometric nonlinearity and to formulate the geometric nonlinear form of the slope-deflection equations.

10.10.2 Key Factors and Concepts

- The displacement method works with nodal Force Equilibrium Equations expressed in terms of displacements
- The slope-deflection equations relate the end shears and moments to the end translations and rotations. Their general linear form for planar bending of a prismatic member AB is

$$M_{AB} = \frac{2EI}{L} \{2\theta_A + \theta_B\} + \frac{6EI}{L} \left(\frac{v_A - v_B}{L} \right) + M_{AB}^F$$

$$M_{BA} = \frac{2EI}{L} \{2\theta_B + \theta_A\} + \frac{6EI}{L} \left(\frac{v_A - v_B}{L} \right) + M_{BA}^F$$

$$V_{AB} = \frac{6EI}{L^2} (\theta_A + \theta_B) + \frac{12EI}{L^3} (v_A - v_B) + V_{AB}^F$$

$$V_{BA} = -\frac{6EI}{L^2} (\theta_B + \theta_A) - \frac{12EI}{L^3} (v_A - v_B) + V_{BA}^F$$

- Moment distribution is a numerical procedure for distributing the unbalanced nodal moments into the adjacent members based on relative stiffness. If one continued the process until the moment

residuals are reduced to zero, one would obtain the exact solution. Normally, the process is terminated when the residuals are relatively small.

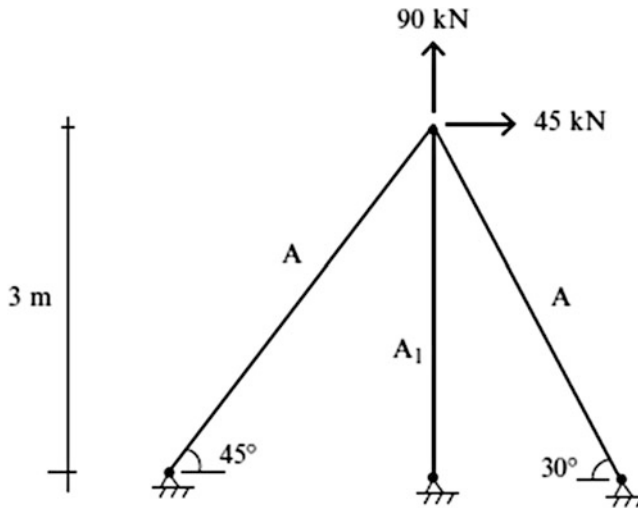
- The slope-deflection equations provide the basis for the computer-based analysis procedure described in Chap. 12.
- Geometric nonlinear behavior is due to the coupling between compressive axial load and transverse displacement. It results in a loss of stiffness and leads to unstable behavior.

10.11 Problems

Problem 10.1 Determine the displacements and member forces for the truss shown. Consider the following values for the areas:

- $A_1 = \frac{1}{2}A$
- $A_1 = 2A$
- Check your results with computer-based analysis.

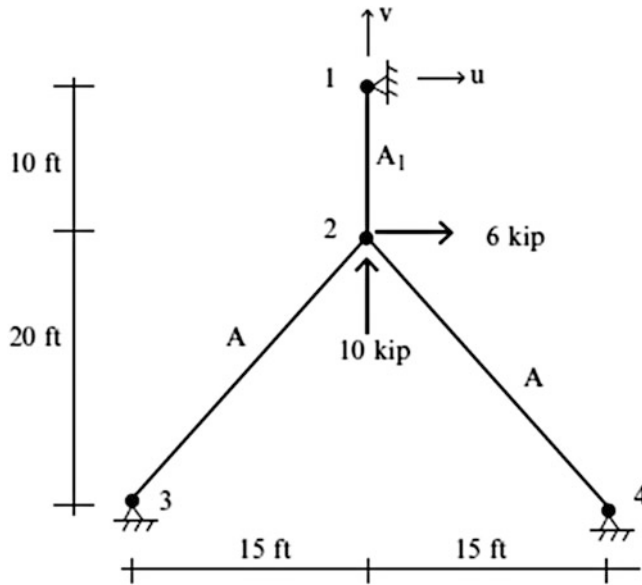
Take $E = 200 \text{ GPa}$ and $A = 2000 \text{ mm}^2$



Problem 10.2 For the truss shown below, determine the member forces for:

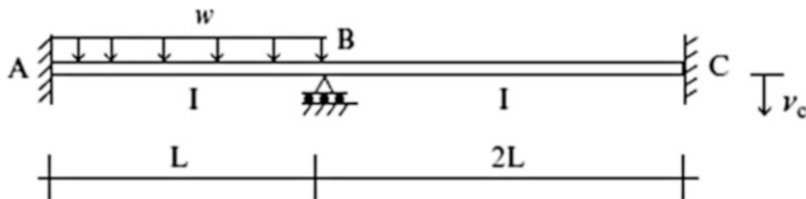
- The loading shown
- Support #1 moves as follows: $u = \frac{1}{8} \text{ in.}$ \rightarrow and $v = \frac{1}{2} \text{ in.}$ \uparrow

Take $A = 0.1 \text{ in.}^2$, $A_1 = 0.4 \text{ in.}^2$, and $E = 29,000 \text{ ksi}$.



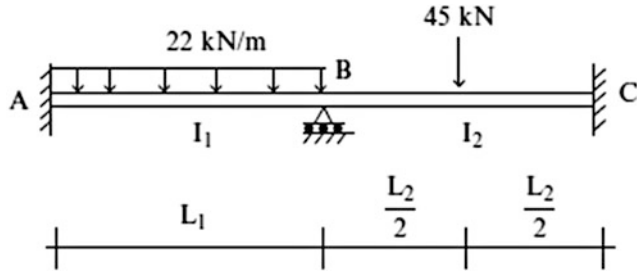
For the following beams and frames defined in Problems 10.3–10.18, determine the member end moments using the slope-deflection equations.

Problem 10.3 Assume $E = 29,000$ ksi, $I = 200$ in.⁴, $L = 30$ ft, $v_C = 0.6$ in. \downarrow , and $w = 1.2$ kip/ft.



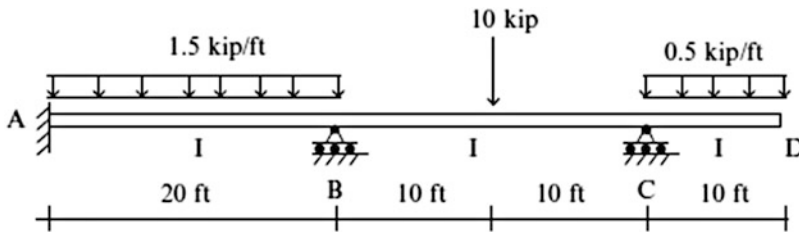
Problem 10.4

- (a) $I_1 = I_2$ and $L_1 = L_2$
- (b) $I_1 = 2I_2$ and $L_1 = L_2$
- (c) $I_1 = 2I_2$ and $L_1 = 2L_2$



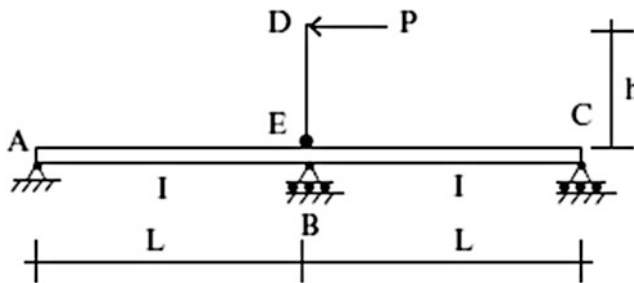
Assume $E = 200 \text{ GPa}$, $I_2 = 80(10)^6 \text{ mm}^4$, and $L_2 = 6 \text{ m}$.

Problem 10.5

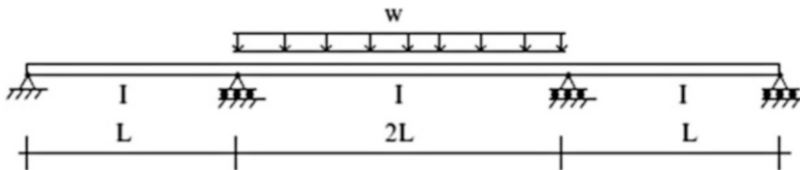


$E = 29,000 \text{ ksi}$ and $I = 300 \text{ in.}^4$

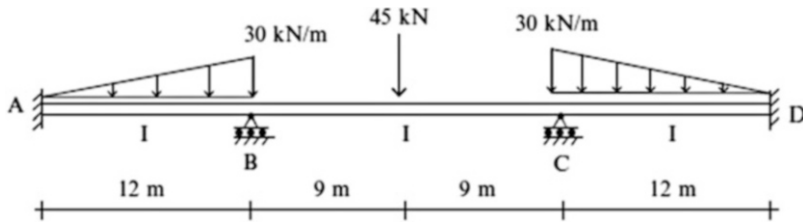
Problem 10.6 Assume $E = 200 \text{ GPa}$, $I = 80(10)^6 \text{ mm}^4$, $P = 45 \text{ kN}$, $h = 3 \text{ m}$, and $L = 9 \text{ m}$.



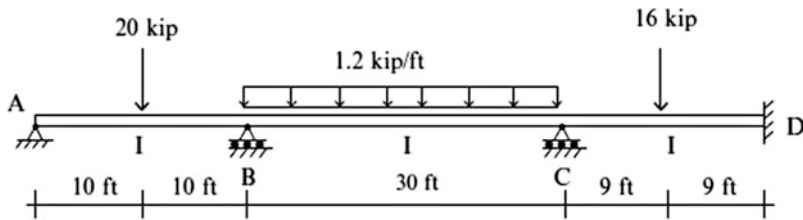
Problem 10.7 Assume $E = 29,000 \text{ ksi}$, $I = 200 \text{ in.}^4$, $L = 18 \text{ ft}$, and $w = 1.2 \text{ kip/ft}$.



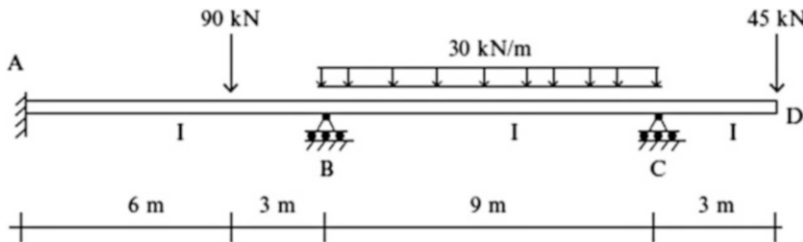
Problem 10.8 Assume $E = 200 \text{ GPa}$ and $I = 80(10)^6 \text{ mm}^4$.



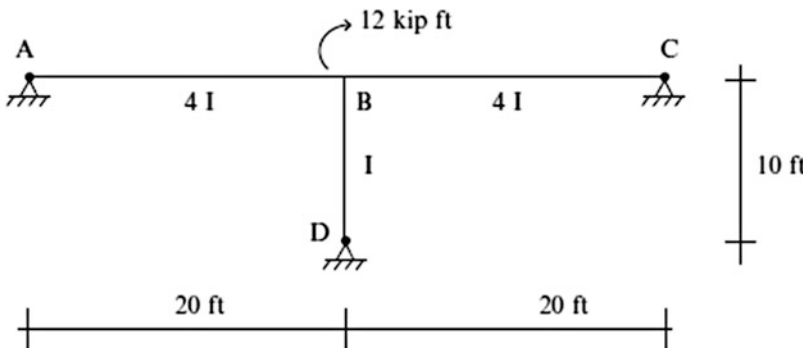
Problem 10.9 Assume $E = 29,000 \text{ ksi}$ and $I = 400 \text{ in.}^4$



Problem 10.10 Assume $E = 200 \text{ GPa}$ and $I = 100(10)^6 \text{ mm}^4$.

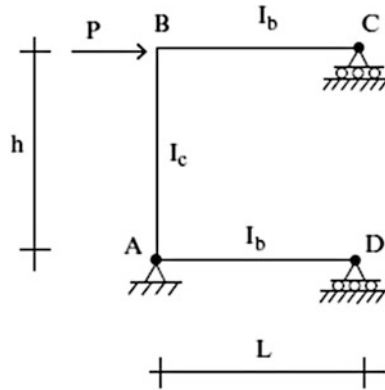


Problem 10.11 Assume $E = 29,000 \text{ ksi}$ and $I = 100 \text{ in.}^4$

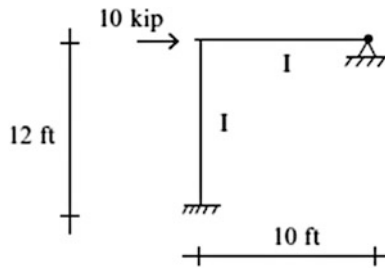
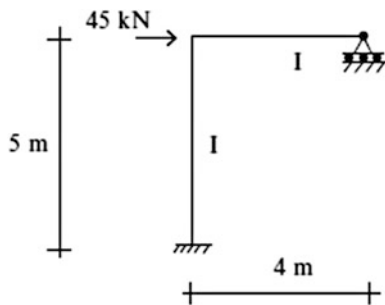


Problem 10.12

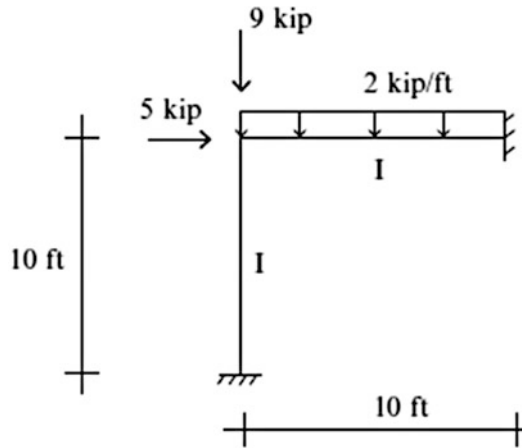
- (a) $I_b = I_c$
 (b) $I_b = 1.5I_c$



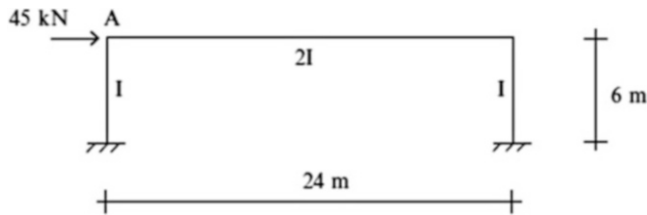
Assume $E = 200 \text{ GPa}$, $I_c = 120(10)^6 \text{ mm}^4$, $L = 8 \text{ m}$, $h = 4 \text{ m}$, and $P = 50 \text{ kN}$.

Problem 10.13 Assume $E = 29,000 \text{ ksi}$ and $I = 200 \text{ in.}^4$ **Problem 10.14** Assume $E = 200 \text{ GPa}$ and $I = 80(10)^6 \text{ mm}^4$.

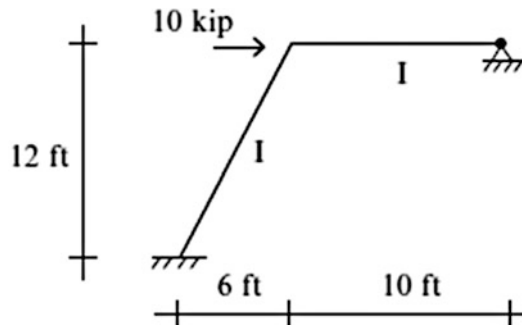
Problem 10.15 $I = 600 \text{ in.}^4$
 $E = 29,000 \text{ kip/in.}^2$



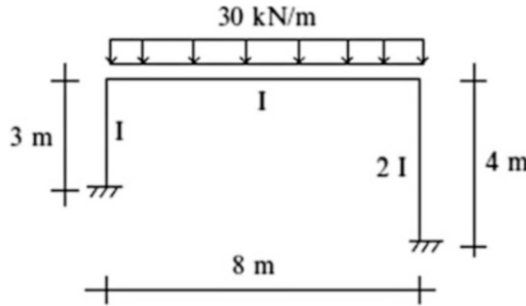
Problem 10.16 Assume $E = 200 \text{ GPa}$ and $I = 120(10)^6 \text{ mm}^4$.



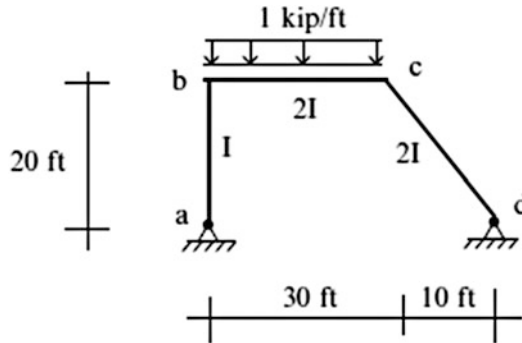
Problem 10.17 Assume $E = 29,000 \text{ ksi}$ and $I = 200 \text{ in.}^4$



Problem 10.18 Assume $E = 200 \text{ GPa}$ and $I = 80(10)^6 \text{ mm}^4$.



Problem 10.19 For the frame shown below, use computer software to determine the moment diagram and displacement profile. Assume $E = 29,000 \text{ ksi}$ and $I = 200 \text{ in.}^4$



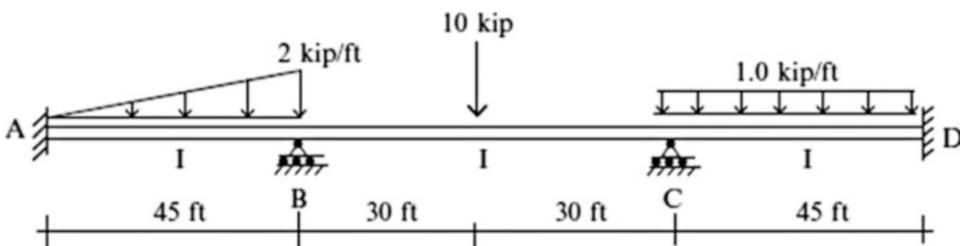
For the following beams and frames defined in Problems 10.20–10.34, determine the member end moments using moment distribution.

Problem 10.20 The loading shown

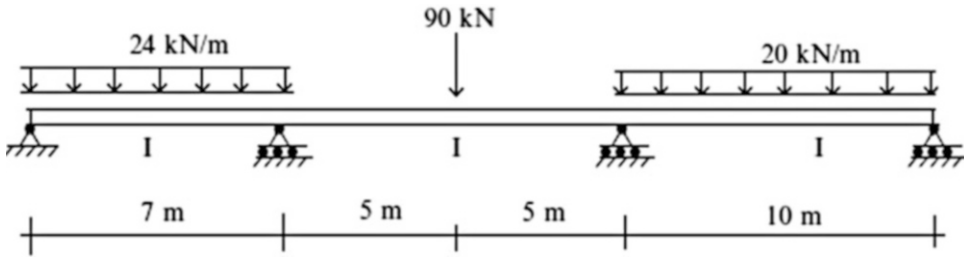
- (a) A support settlement of .5 in. downward at joint B in addition to the loading
- (b) Check your results with computer-based analysis.

$$E = 29,000 \text{ ksi,}$$

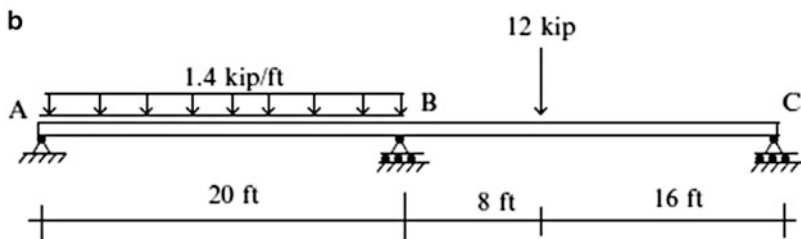
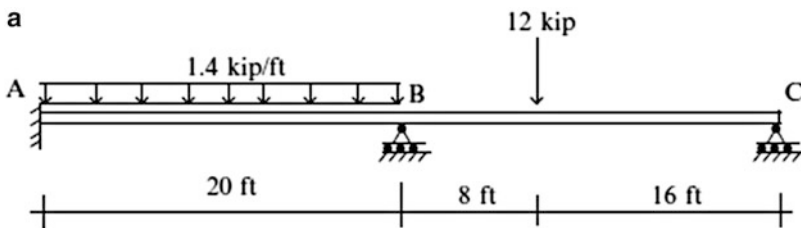
$$I = 300 \text{ in.}^4$$



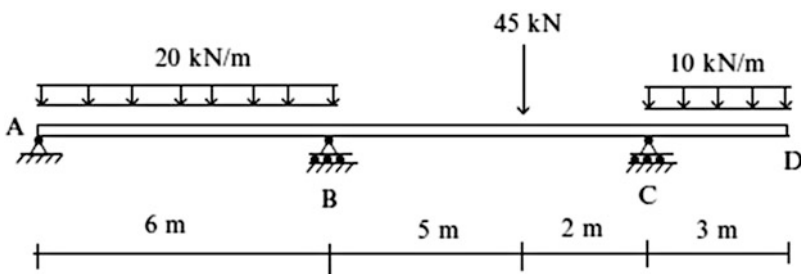
Problem 10.21 Compute the end moments and reactions. Draw the shear and moment diagrams. Check your results with computer analysis. Assume $E = 200 \text{ GPa}$ and $I = 75(10)^6 \text{ mm}^4$.



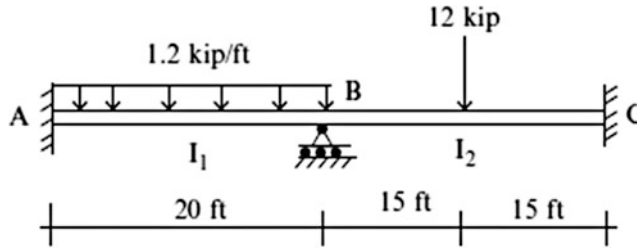
Problem 10.22 Determine the bending moments and the reactions for the following cases. Assume EI is constant



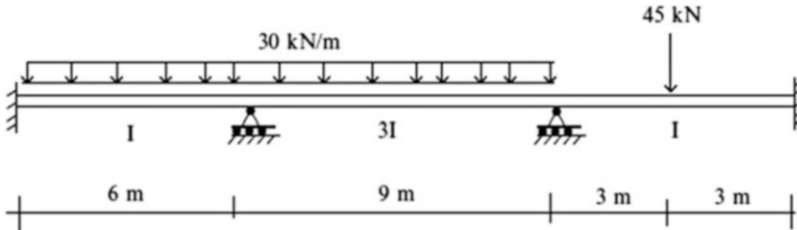
Problem 10.23 Determine the bending moment distribution for the beam shown below. Assume EI is constant.



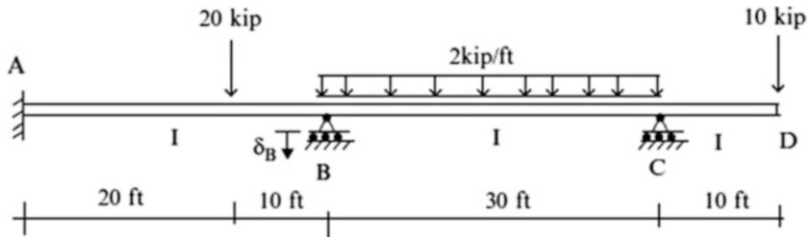
Problem 10.24 Determine the bending moment distribution. Assume $I_1 = 1.4I_2$.



Problem 10.25 Determine the bending moment distribution.



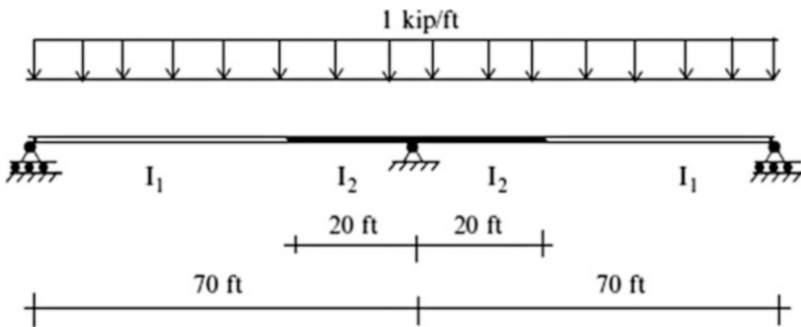
Problem 10.26 Solve for the bending moments. $\delta_B = 0.4 \text{ in. } \downarrow$, $E = 29,000 \text{ ksi}$, and $I = 240 \text{ in.}^4$.



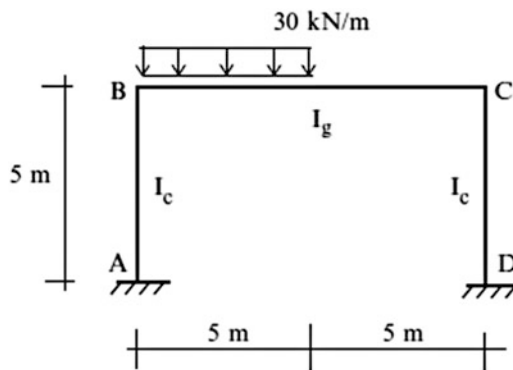
Problem 10.27 Determine the bending moment distribution and the deflected shape. $E = 29,000 \text{ ksi}$

- (a) Take $I_1 = I_2 = 1000 \text{ in.}^4$
- (b) Take $I_1 = 1.5I_2$. Use computer analysis.

Discuss the difference in behavior between case (a) and (b).



Problem 10.28 Determine the axial, shear, and bending moment distributions. Take $I_g = 2I_c$



Problem 10.29 Determine the member forces and the reactions.

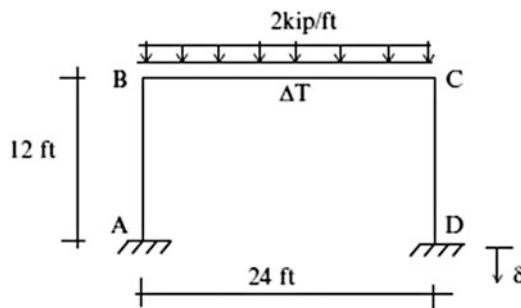
- (a) Consider only the uniform load shown
- (b) Consider only the support settlement of joint D ($\delta = 0.5$ in. \downarrow)
- (c) Consider only the temperature increase of $\Delta T = 80$ °F for member BC.

$$E = 29,000 \text{ ksi}$$

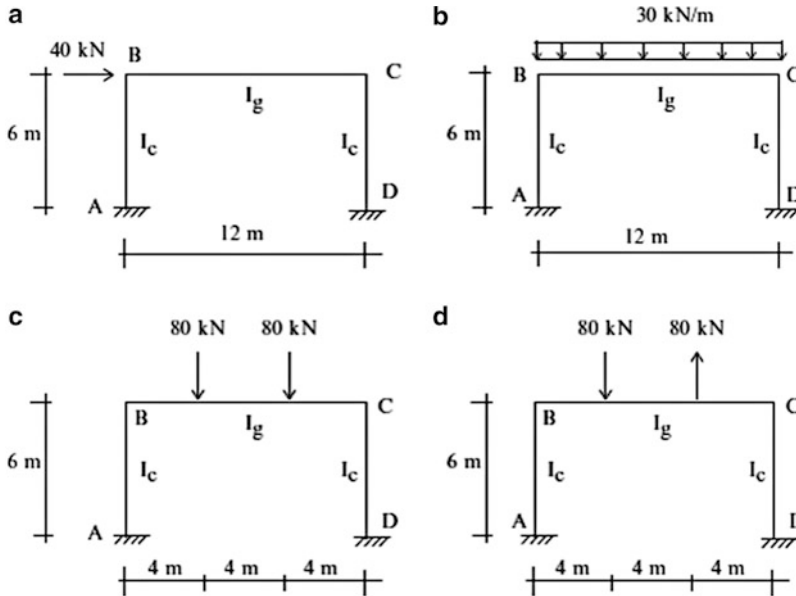
$$I_{AB} = I_{CD} = 100 \text{ in.}^4$$

$$I_{BC} = 400 \text{ in.}^4$$

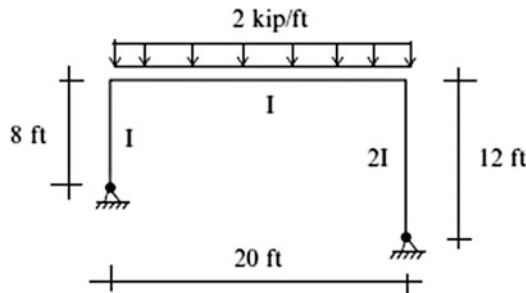
$$\alpha = 6.5 \times 10^{-6} / ^\circ\text{F}$$



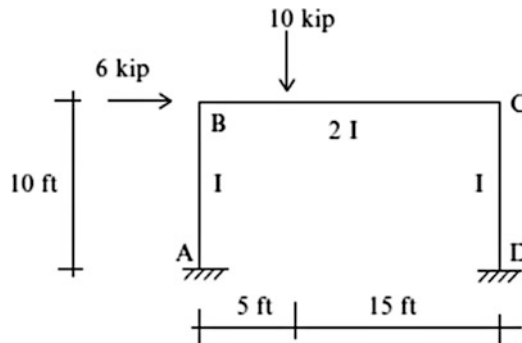
Problem 10.30 Determine the bending moment distribution for the following loadings. Take $I_g = 5I_c$.



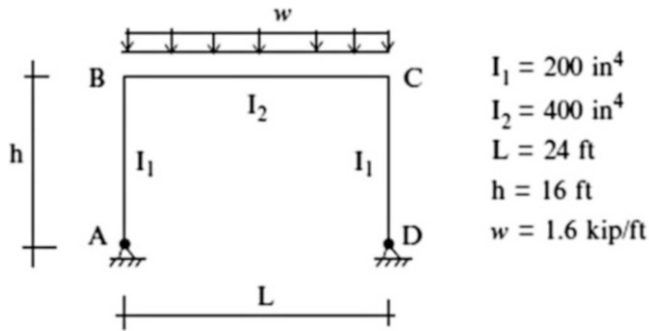
Problem 10.31 Solve for the bending moments.



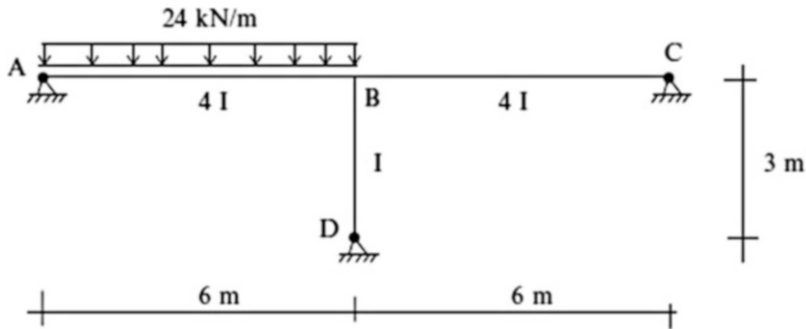
Problem 10.32 Determine the bending moment distribution.



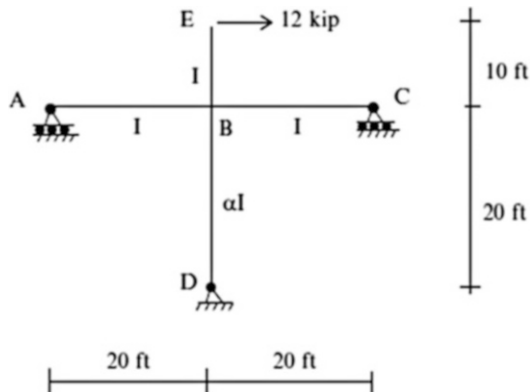
Problem 10.33 Solve for the bending moments.



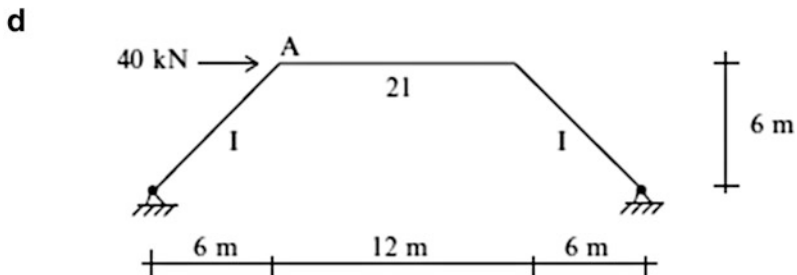
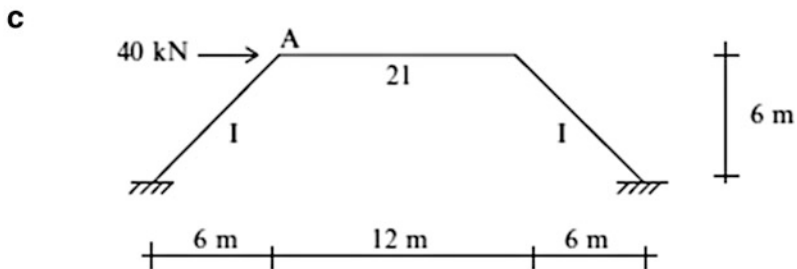
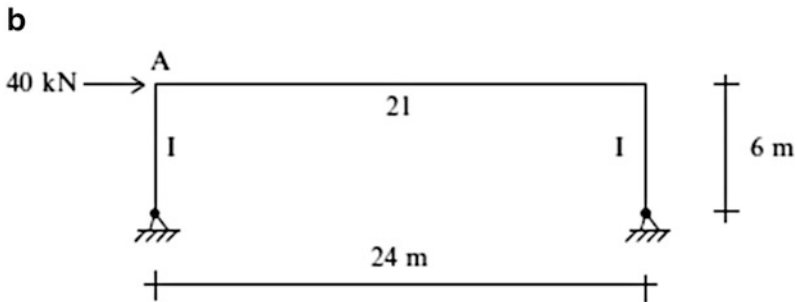
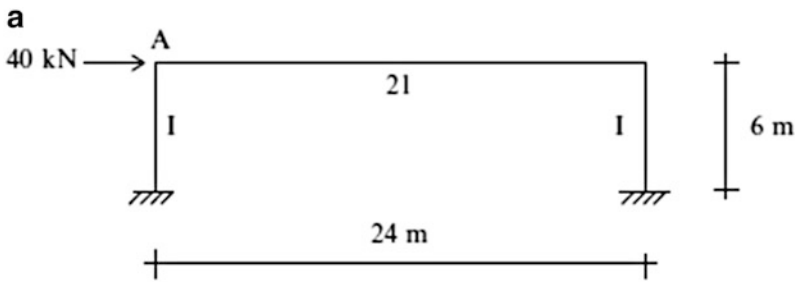
Problem 10.34 For the frame shown, determine the end moments and the reactions. Assume $E = 200 \text{ GPa}$ and $I = 40(10)^6 \text{ mm}^4$.



Problem 10.35 Determine analytic expression for the rotation and end moments at B. Take $I = 1000 \text{ in}^4$, $A = 20 \text{ in}^2$ for all members, and $\alpha = 1.0, 2.0, 5.0$. Is there an upper limit for the end moment, M_{BD} ?



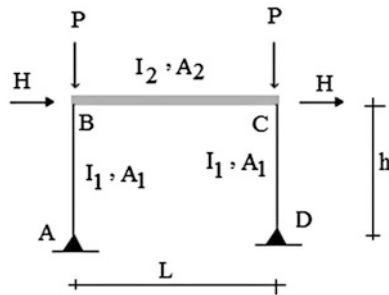
Problem 10.36 Compare the end moments and horizontal displacement at A for the rigid frames shown below. Check your results for parts (c) and (d) with a computer-based analysis. Take $E = 200$ GPa and $I = 120(10)^6 \text{ mm}^4$. $A = 10,000 \text{ mm}^2$ for all members.



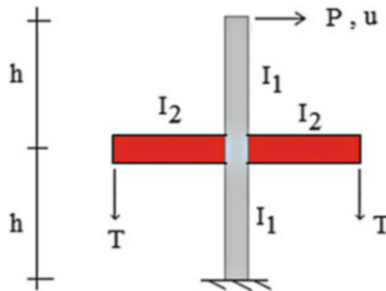
Problem 10.37 Compute displacement at node C for

- (a) No P -delta effect
- (b) With P -delta effect included

Take $I_1 = 881 \text{ in.}^4$, $A_1 = 24 \text{ in.}^2$, $I_2 = 2960 \text{ in.}^4$, $A_2 = 35.9 \text{ in.}^2$, $H = 100 \text{ kip}$, $P = 200 \text{ kip}$, $E = 29,000 \text{ ksi}$, $L = 20 \text{ ft}$, and $h = 10 \text{ ft}$.



Problem 10.38 Generate the plots of P vs. u for various values of T . Starting at $T=0$ and increasing to $T = \frac{\pi^2 EI_1}{4h^2}$. Take $I_1 = 400 \text{ in.}^4$, $I_2 = \infty$, and $h = 10 \text{ ft}$.



References

1. Cross H. Analysis of continuous frames by distributing fixed-end moments. Trans ASCE. 1932;96:1-10. Paper 1793.
2. Livesley RK. Matrix methods of structural analysis. London: Pergamon; 1964.

Approximate Methods for Estimating Forces in Statically Indeterminate Structures

11

Abstract

In this chapter, we describe some approximate methods for estimating the forces in indeterminate structures. We start with multi-span beams subjected to gravity loading. Next, we treat rigid frame structures under gravity loading. Then, we consider rigid frame structures under lateral loading. For this case, we distinguish between short and tall buildings. For short buildings, we first describe the portal method, an empirical procedure, for estimating the shear forces in the columns, and then present an approximate stiffness approach which is more exact but less convenient to apply. For tall buildings, we model them as beams and use beam theory to estimate the forces in the columns. With all the approximate methods, our goal is to use simple hand calculation-based methods to estimate the forces which are needed for preliminary design and also for checking computer-based analysis methods.

11.1 Introduction

The internal forces in a statically indeterminate structure depend on the member cross-sectional properties. We demonstrated this dependency with the examples presented in the previous two chapters. However, in order to design a structure, one needs the internal forces. Therefore, when starting the design process, it is necessary to estimate a sufficient number of force quantities so that the structure is reduced to a statically determinate structure for which the distribution of internal forces is independent of the material properties. For bending type structures, such as multi-span beams and frames, the approximations are usually introduced by assuming moment releases at certain locations. The choice of the release locations is based on an understanding of the behavior of the structure for the particular loading under consideration. For indeterminate trusses, we assume the magnitude of certain forces. A typical case for a truss would be when there are two diagonals in a bay. We usually assume the transverse shear is divided equally between the two diagonals.

11.2 Multi-span Beams: Gravity Loading

11.2.1 Basic Data-Moment Diagrams

Figures 11.1, 11.2, and 11.3 show moment diagrams due to a uniform distributed loading for a range of beam geometries and support conditions. These results are presented in Chaps. 9 and 10. They provide the basis for assuming the location of moment releases (points of zero moment) for different combinations of span lengths and loading distributions. We utilize this information to develop various strategies for generating approximate solutions for multi-span beams.

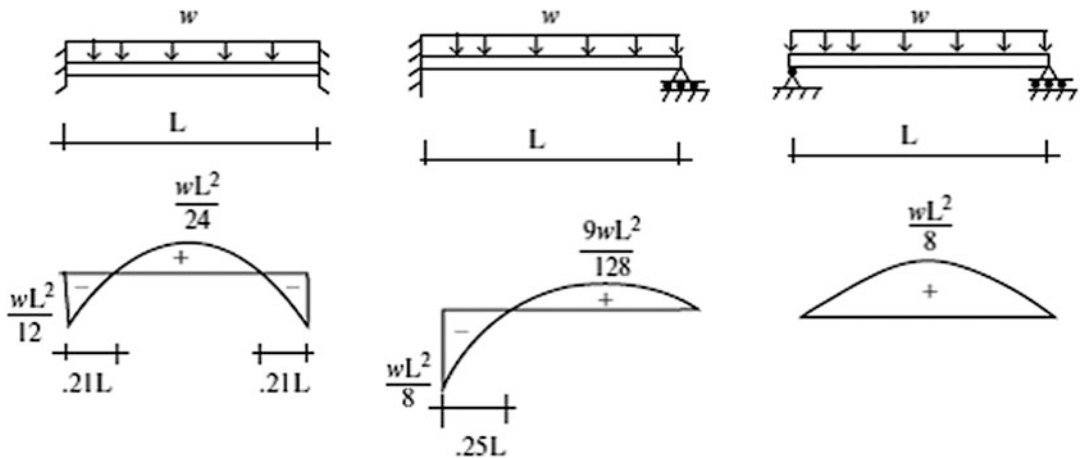
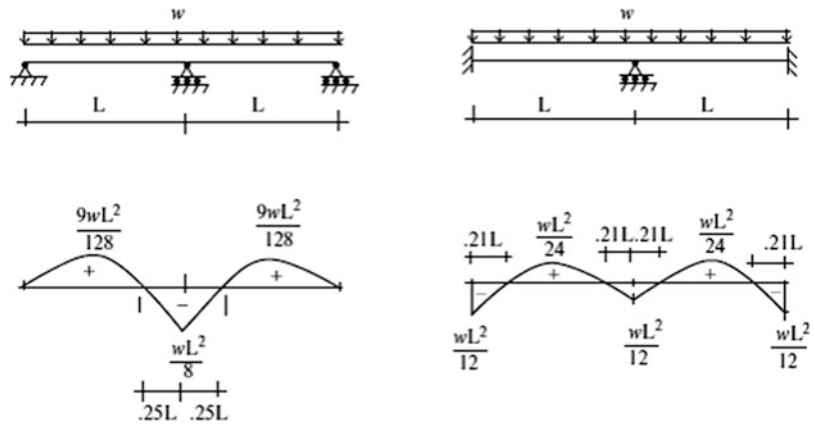


Fig. 11.1 Moment diagrams for single-span beams

Fig. 11.2 Moment diagrams for two-span beams



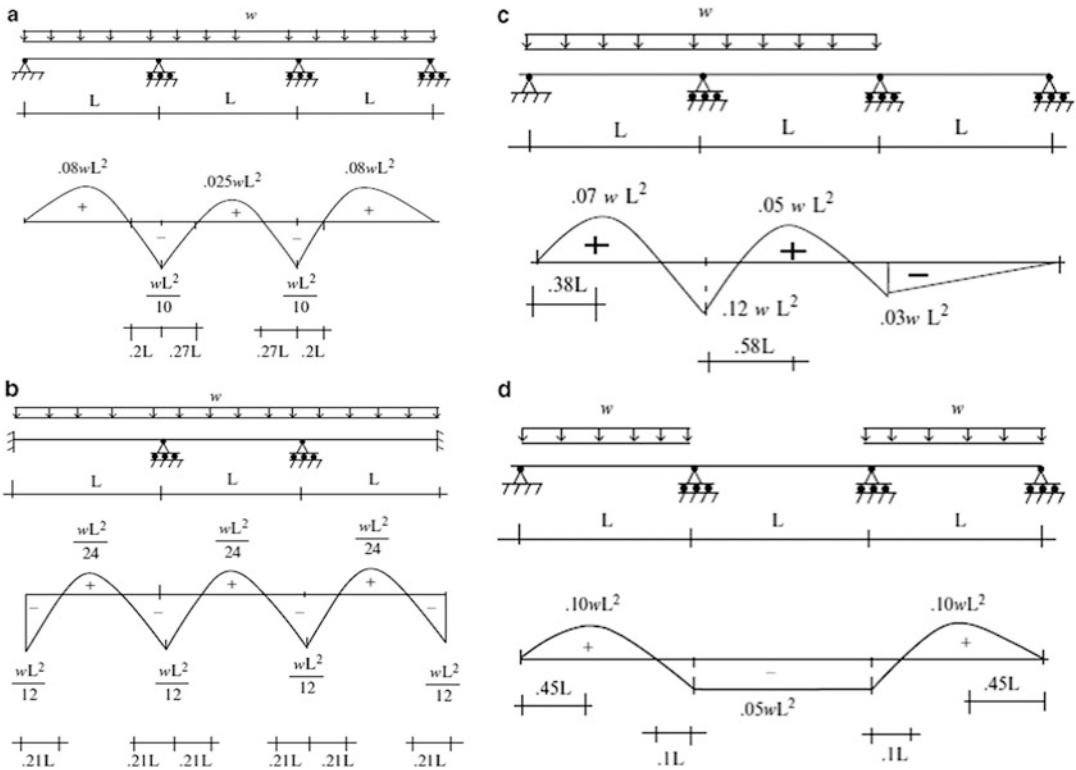
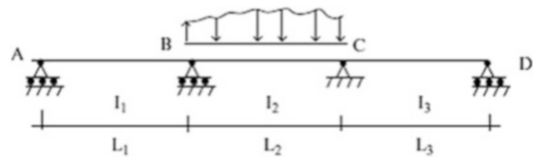


Fig. 11.3 Moment diagrams for three-span beams. (a) Simply supported. (b) Fixed at each end. (c) Partial loading. (d) Partial loading symmetrical

Fig. 11.4 Multi-span beam



11.2.2 Quantitative Reasoning Based on Relative Stiffness

Consider the multi-span beam shown in Fig. 11.4. Our objective is to estimate the peak positive and negative moments in span BC. As a first step, we estimate the end moments for this span using the member distribution factors which are related to the relative stiffness factors for the members. We consider node B. The distribution factors for members BA and BC are as follows (see Sect. 10.6):

$$DF_{BA} = \frac{I_1/L_1}{((I_1/L_1) + (I_2/L_2))} \tag{11.1}$$

$$DF_{BC} = \frac{I_2/L_2}{((I_1/L_1) + (I_2/L_2))}$$

Note that when I is constant for all spans, the relative stiffness parameters reduce to the inverse of the span length. Given the initial unbalanced moment at B, we distribute it according to

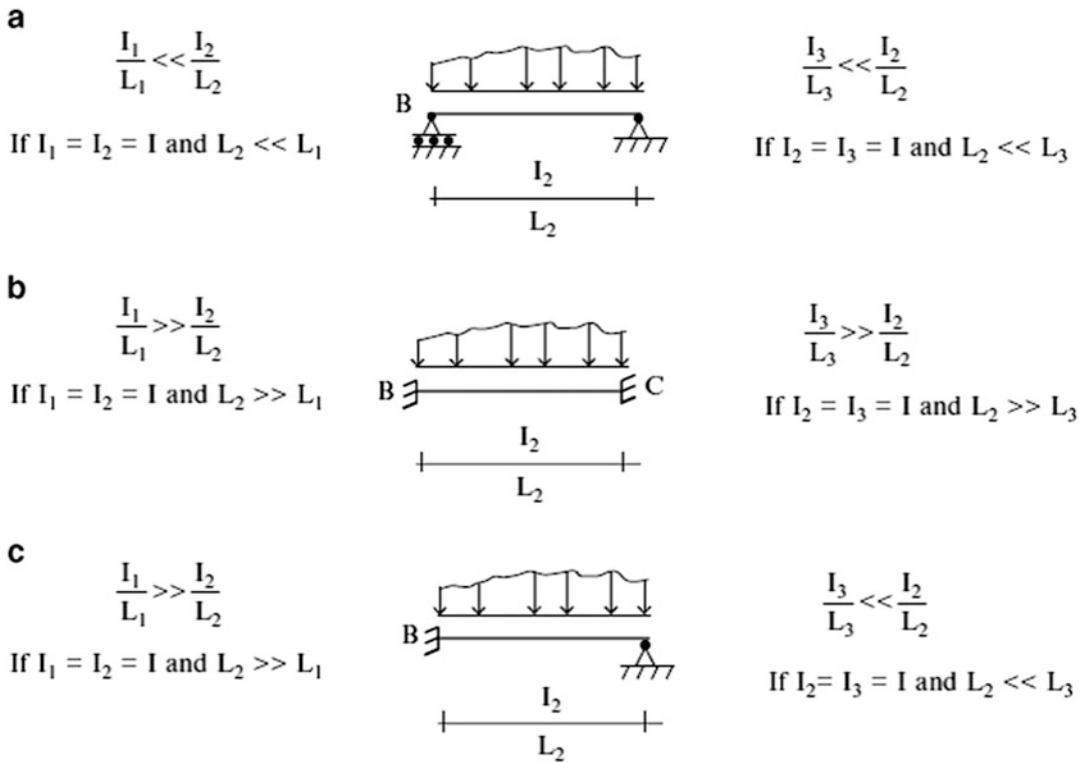


Fig. 11.5 Summary of approximate models for extreme values of L_1/L_2 and L_3/L_2 . (a) Hinged model. (b) Clamped end model. (c) Clamped/hinged model

$$\begin{aligned} \Delta M_{BA} &= -DF_{BA} \left(\text{FEM} \Big|_B \right) \\ \Delta M_{BC} &= -DF_{BC} \left(\text{FEM} \Big|_B \right) \end{aligned} \tag{11.2}$$

We consider no carry-over movement to the other ends.

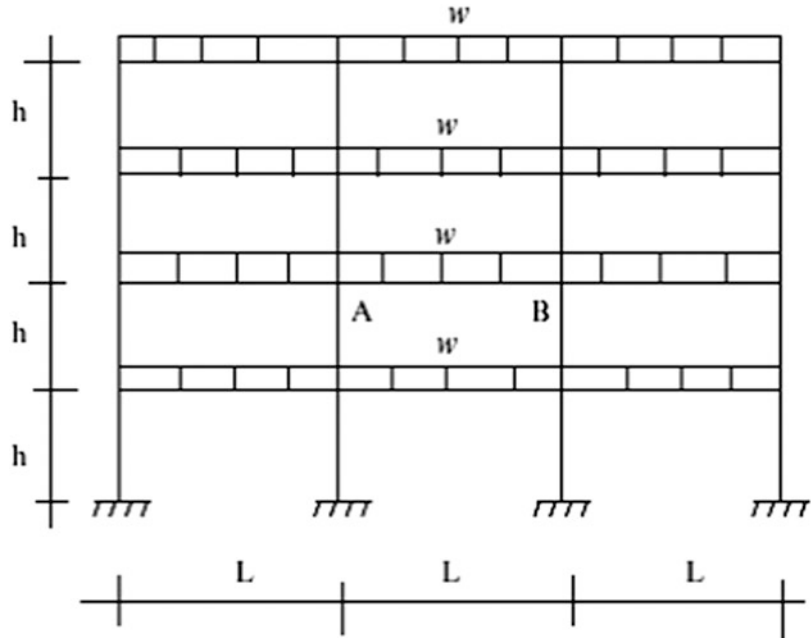
If $\frac{I_1}{L_1}$ is small in comparison to $\frac{I_2}{L_2}$, then DF_{BA} will be small in comparison to DF_{BC} . It follows that only a small portion of the unbalanced nodal moment at node B will be distributed to member BA. The opposite case is where I_1/L_1 is large in comparison to I_2/L_2 . Now DF_{BC} is small vs. DF_{BA} . Essentially all of the unbalanced nodal moment is distributed to member BA. The final end moment in member BC is close to its initial value (the initial fixed end moment) since there is relatively little distribution.

When I is constant for all the spans, the relative stiffness parameters reduce to the inverse of the span lengths. In this case, one compares the ratio of adjacent span lengths. The limiting cases for extreme values of these ratios are listed in Fig. 11.5.

11.3 Multistory Rigid Frames: Gravity Loading

Gravity type loading is usually the dominant loading for multistory frames. It consists of both dead and live loading. Consider the frame shown in Fig. 11.6. We suppose the loading is a uniform gravity load, w . Our objective here is to determine the positive and negative moments in beam AB.

Fig. 11.6 Multistory frame—gravity loading



One can estimate moments at the ends and at the center by assuming moment releases in the beams. Assuming moment releases at $0.1L$ leads to

$$M_{\text{center}}^+ = \frac{w(0.8L)^2}{8} = 0.08wL^2$$

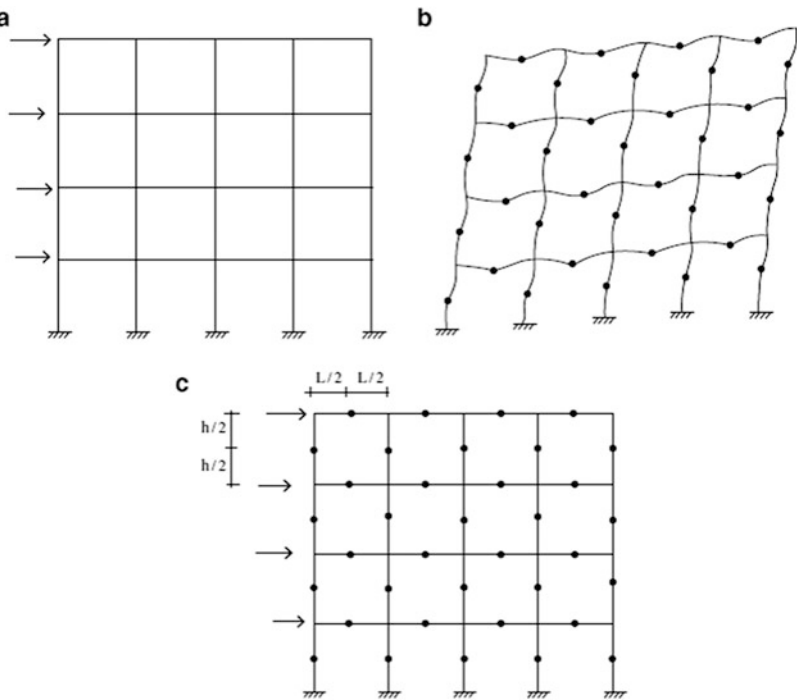
$$M_A = M_B = w \frac{(0.1L)^2}{2} + w(0.4L)(0.1L) = 0.045wL^2$$

11.4 Multistory Rigid Frames: Lateral Loading

Consider the rigid frame shown in Fig. 11.7a. Under a lateral loading, the frame develops inflection points (points where the bending moment is equal to zero) in the columns and beams. Most of the approximate methods published in the literature are based on the assumption that the inflection points occur at mid-height of the columns and mid-span of the beams, as indicated in Fig. 11.7c. This assumption, coupled with an assumption concerning how the column axial and shear forces are distributed within a story, is sufficient to allow us to compute estimates for the end moments, the axial forces, and the shear forces in the columns.

In what follows, we present two different approaches for estimating the forces in the columns. The first approach (11.4.1–11.4.3) estimates the column shears in a story, and is applicable mainly for *low-rise rigid frames*. The second approach (11.5) estimates the axial forces in the columns. Because of the nature of the underlying assumptions, the latter procedure is appropriate only for *tall, narrow rigid frames*. Both procedures are derived using the idealized model of the structure shown in Fig. 11.7c, i.e., with inflection points at mid-height of the columns and mid-span of the beams.

Fig. 11.7 Multistory rigid frame. (a) Initial position. (b) Deflected Position. (c) Assumed location of inflection points



11.4.1 Portal Method

The portal method is an empirical procedure for estimating the forces in low-rise rigid frames subjected to lateral loads. In addition to assuming inflection points in the columns and beams, *the shear in the exterior columns is assumed to be one-half the shear in the interior columns*, which is taken to be equal for all the interior columns. We use this method to generate the first estimate of the member forces. Of particular interest are the end moments in the columns.

Example 11.1 Application of the Portal Method

Given: The rigid frame shown in Fig. E11.1a.

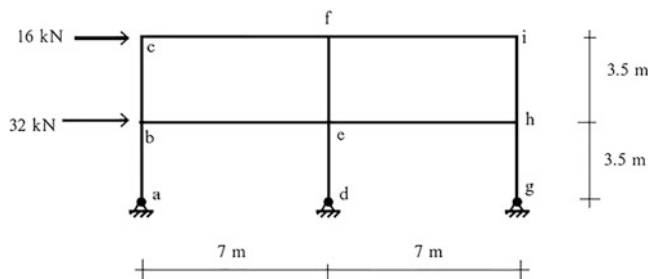


Fig. E11.1a

Determine: The axial force, shear force, and bending moment in the beams and columns using the Portal method.

Solution: The portal method assumes the exterior column shear, V_E , is equal to one-half the interior column shear V_I , which is taken to be equal for all the interior columns.

$$V_E = \frac{1}{2} V_I$$

Summing the column shear forces for this structure leads to an expression for the total story shear.

$$\begin{aligned} V_T &= 2V_E + V_I \\ &= 2V_I \end{aligned}$$

Then,

$$V_I = \frac{1}{2} V_T$$

$$V_E = \frac{1}{2} V_I = \frac{1}{4} V_T$$

We range over the stories and generate the column shear for each story. The calculations are summarized below.

Story	V_T (kN)	V_I (kN)	V_E (kN)
Top	16	8	4
Bottom	48	24	12

Given the column shear forces, one can determine the column end moments using the assumption that there are inflection points at certain locations in the columns. For this structure, since the base is pinned, the inflection points for the first story are at the base. The inflection points for the second story are taken at mid-height. The free body diagrams for the various segments are shown below along with the final results. Once the column end moments are known, we can determine the end moments and shear forces in the beams and lastly, the axial forces in the columns using equilibrium equations (Figs. E11.1b, E11.1c, E11.1d, E11.1e, E11.1f, E11.1g, E11.1h).

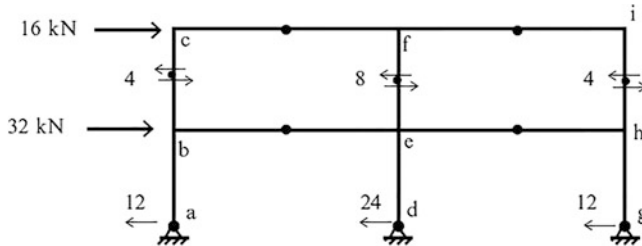


Fig. E11.1b Shear distribution for the columns (kN)

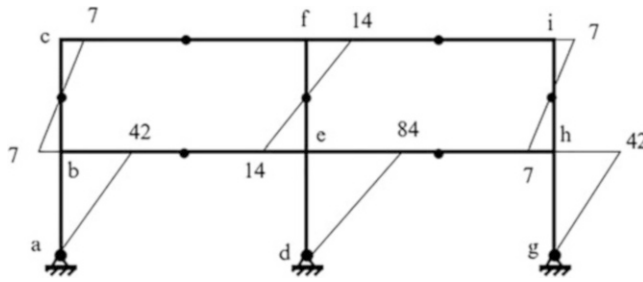


Fig. E11.1c Bending moment distribution for the columns (kN m)

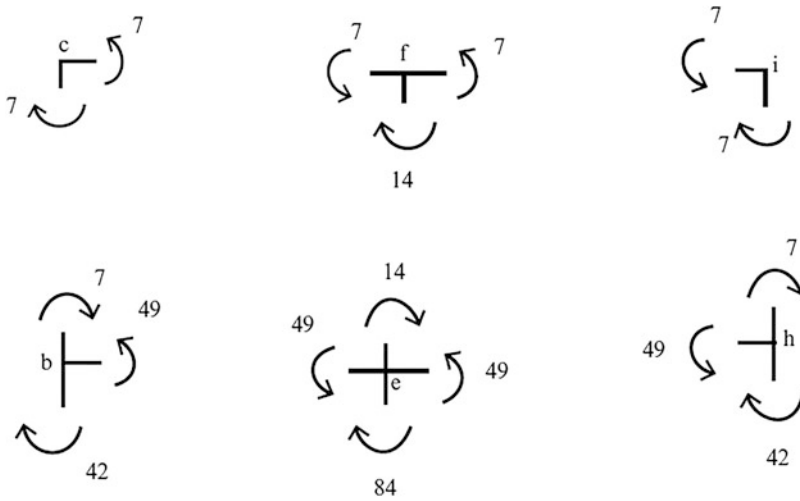


Fig. E11.1d Moments at the joints (kN m)

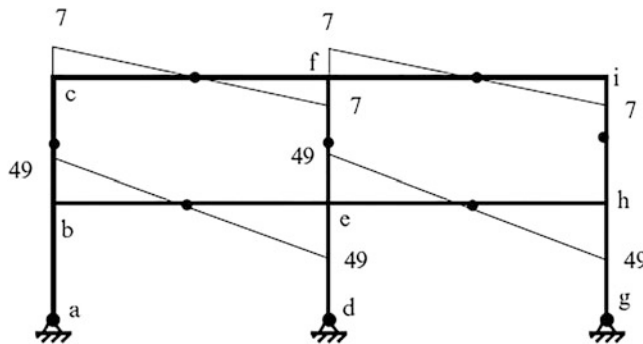


Fig. E11.1e Bending moment distribution for the beams (kN m)

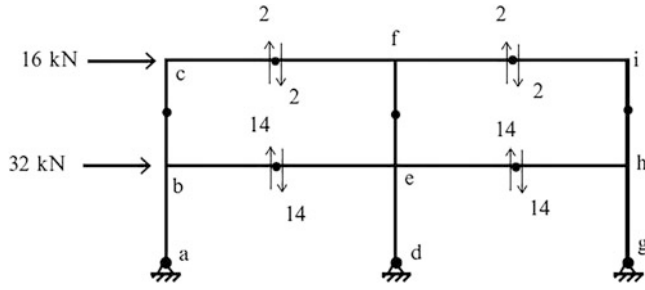


Fig. E11.1f Shear distribution for the beams (kN)

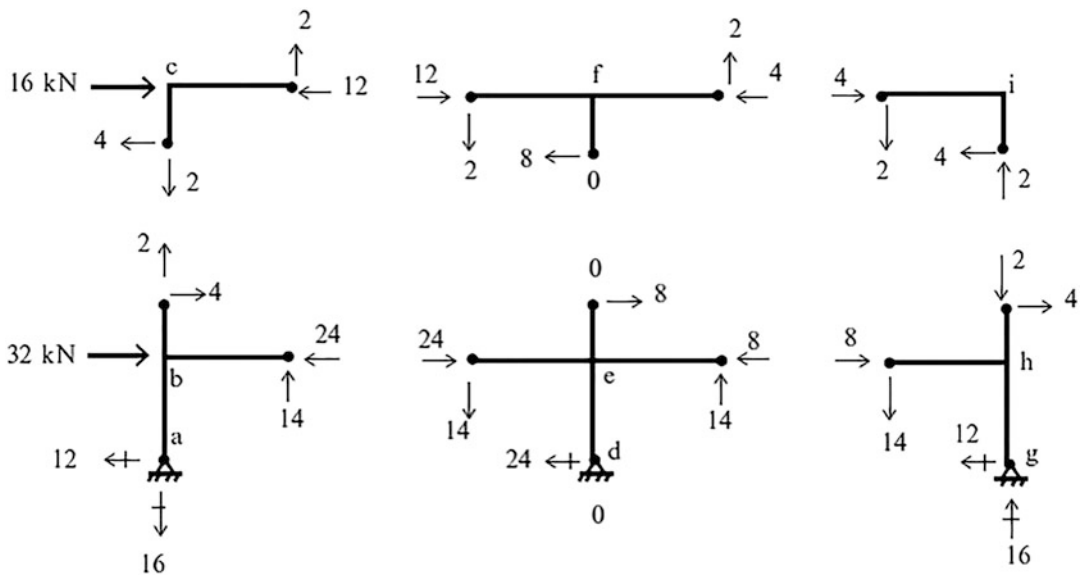


Fig. E11.1g Axial and shear forces (kN)

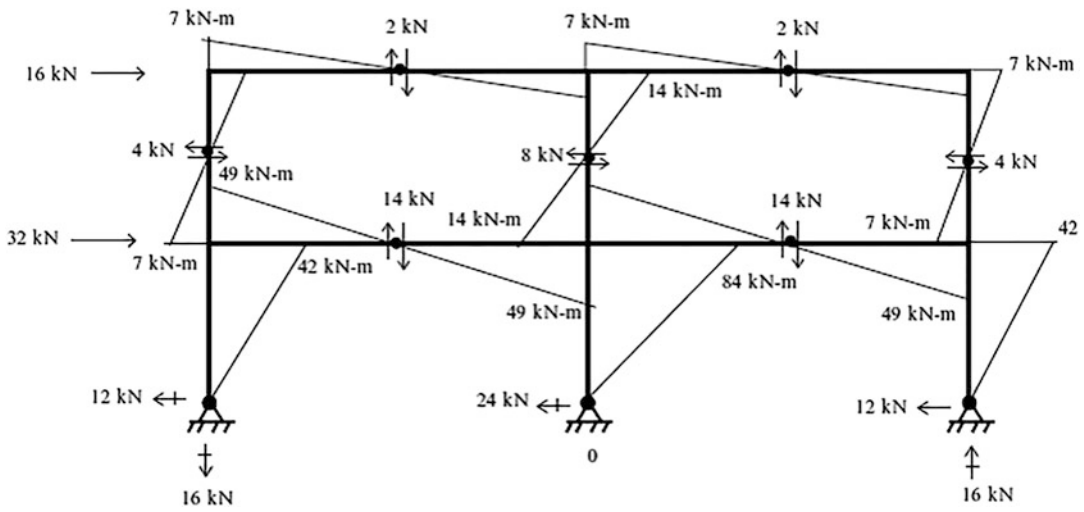


Fig. E11.1h Reactions, shear forces, and moment distribution

Example 11.2 Application of the Portal Method

Given: The rigid frame shown in Fig. E11.2a.

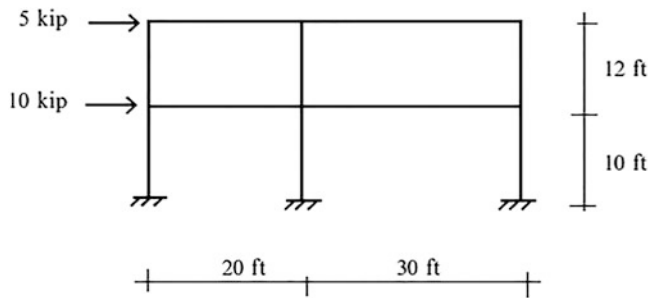


Fig. E11.2a

Determine: The reactions and the bending moments in the beams and columns using the Portal method.

Solution: The Portal method assumes the exterior column shear, V_E , is equal to one-half the interior column shear force V_I . The calculations are summarized in the table below. Note that, since the base is fixed, we assume inflection points at mid-height for the first story (Figs. E11.2b, E11.2c, E11.2d, E11.2e, E11.2f, E11.2g, E11.2h).

Story	V_T (kip)	V_I (kip)	V_E (kip)
Top	5	2.5	1.25
Bottom	15	7.5	3.75

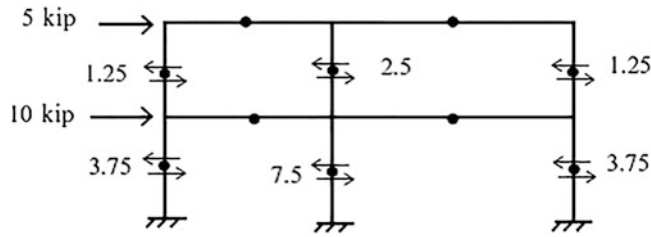


Fig. E11.2b Shear distribution for the columns (kip)

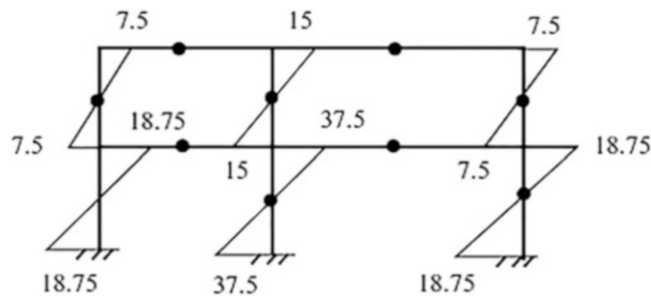


Fig. E11.2c Bending moment distribution for the columns (kip ft)

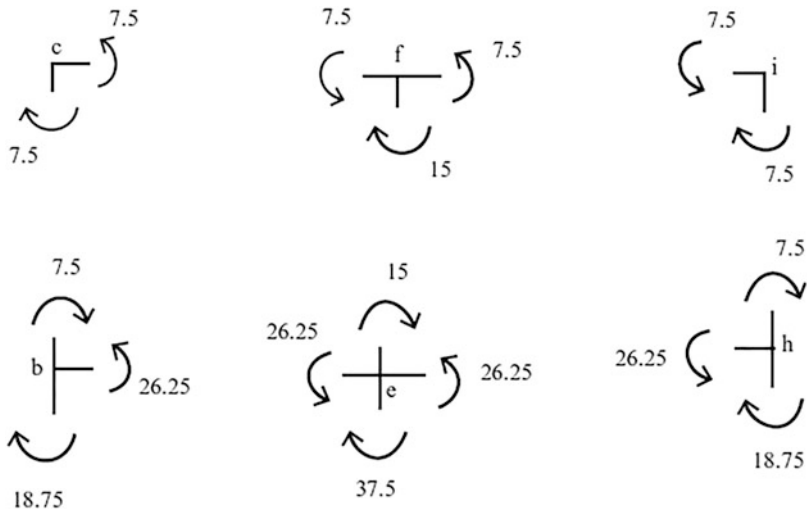


Fig. E11.2d Moments at the joints (kip ft)

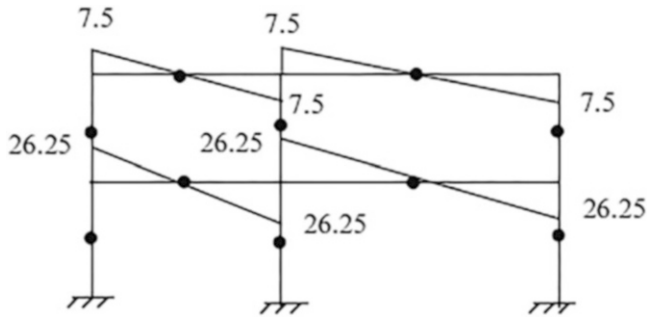


Fig. E11.2e Bending moment distribution for the beams (kip ft)

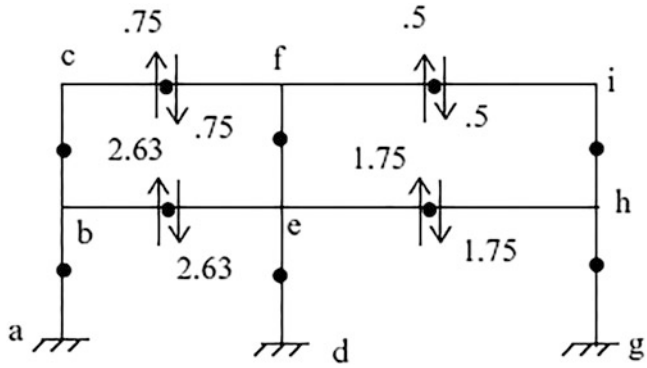


Fig. E11.2f Shear distribution for the beams (kip)

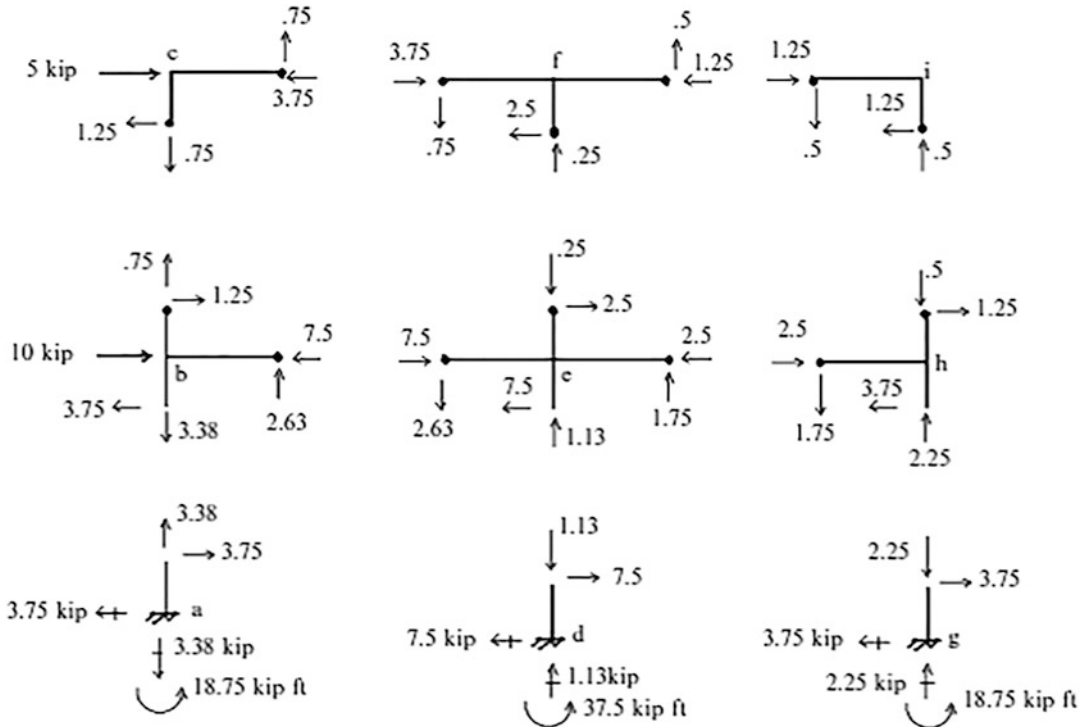


Fig. E11.2g Axial and shear forces (kip)

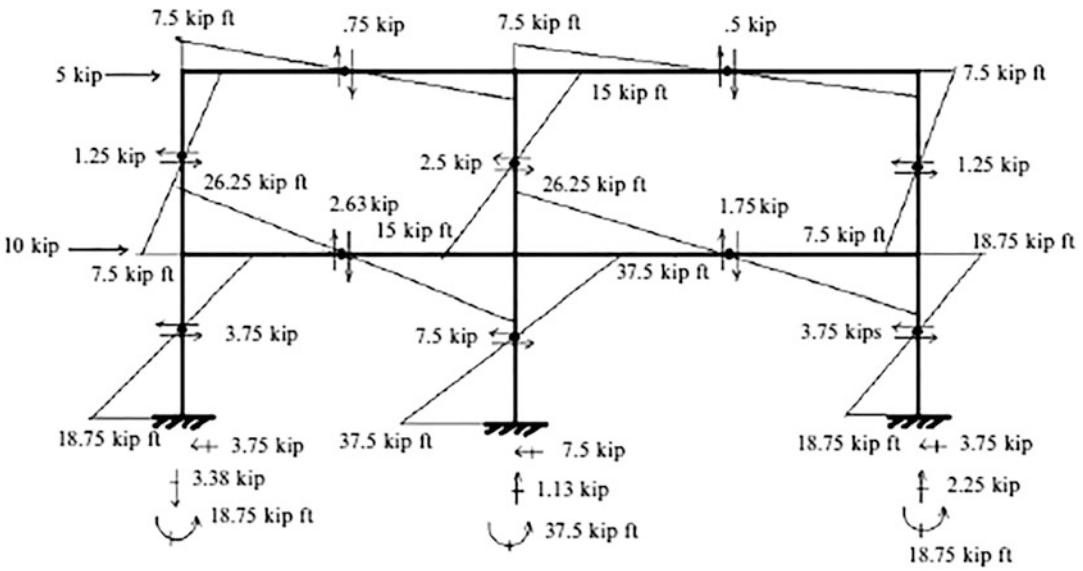


Fig. E11.2h Reactions, shear forces and moment distribution

11.4.2 Shear Stiffness Method: Low-Rise Rigid Frames

In this approach, we model a frame as a set of substructures, which resist the lateral shear in the stories through shearing action. First, we idealize the frame as a rigid frame with moment releases at the midpoints of the columns and beams such as shown in Fig. 11.8. We consider a segment bounded by floor $i + 1$ and floor i . For convenience, we assume I_b and L are *constant* in a story. We allow for different values of I for the exterior and interior columns. We define V_T as the sum of the lateral loads acting on floor $i + 1$, and all the floors above floor $i + 1$. This quantity represents the *total transverse shear* for the story. Next, we define Δu as the *differential lateral displacement between floor i and floor $i + 1$* . We assume the floor beams are *rigid* with respect to axial deformation so that all points on a floor experience the same lateral displacement. Lastly, we assume the floors do not move in the vertical direction, and insert lines as indicated in Fig. 11.9. Our objective in this section is to establish an expression for the column shear forces in a story as a function of the total transverse shear for the story.

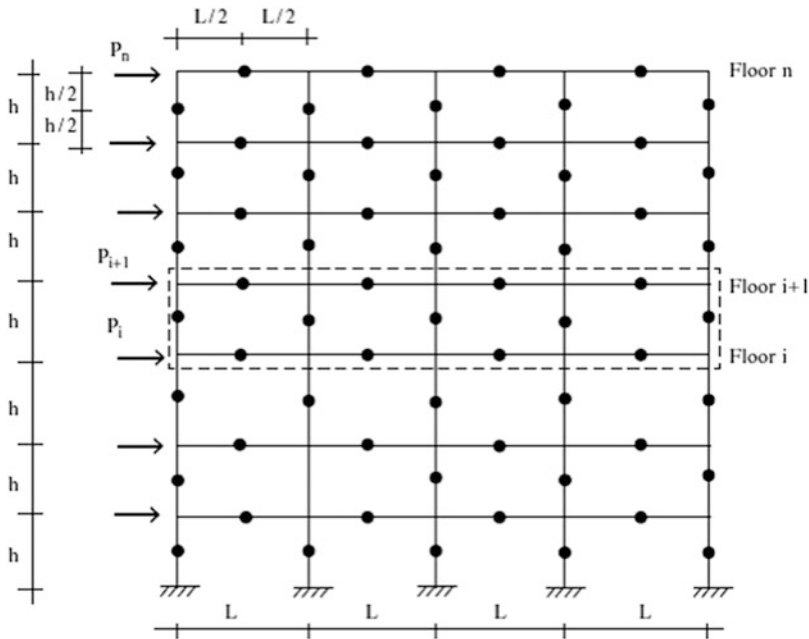


Fig. 11.8 Low-rise, frame

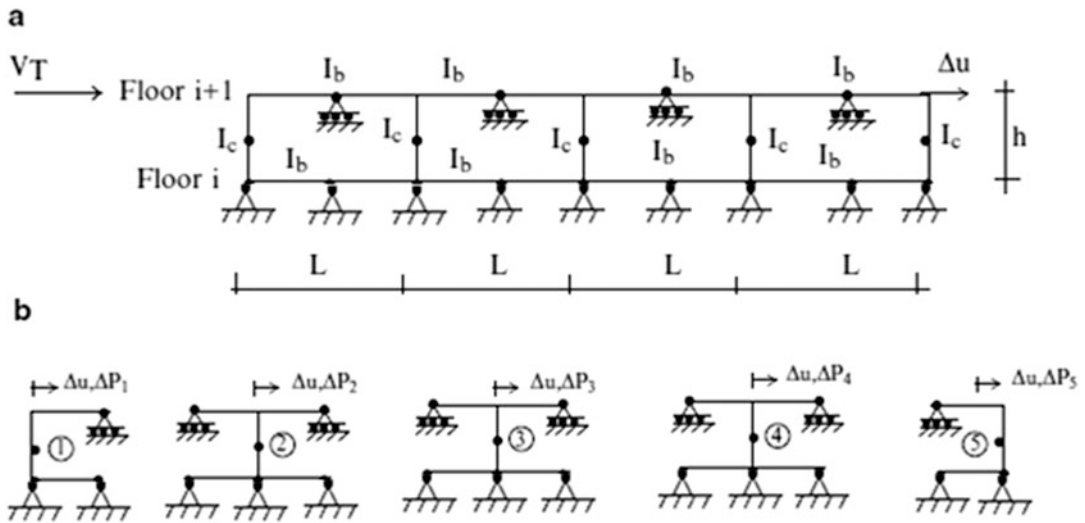


Fig. 11.9 (a) Idealized model for a story in a low-rise frame. (b) Sub-elements of the idealized model—low-rise frame

We visualize the model to consist of the sub-elements shown in Fig. 11.9b. Each sub-element experiences the same Δu . The resistance force ΔP_i for sub-element i depends on the stiffness of the element.

$$\Delta P_i = k_i \Delta u \equiv V_i \tag{11.3}$$

Then, summing the forces over the number of sub-elements leads to

$$V_T = \sum V_i = \left(\sum k_i \right) \Delta u = k_T \Delta u \tag{11.4}$$

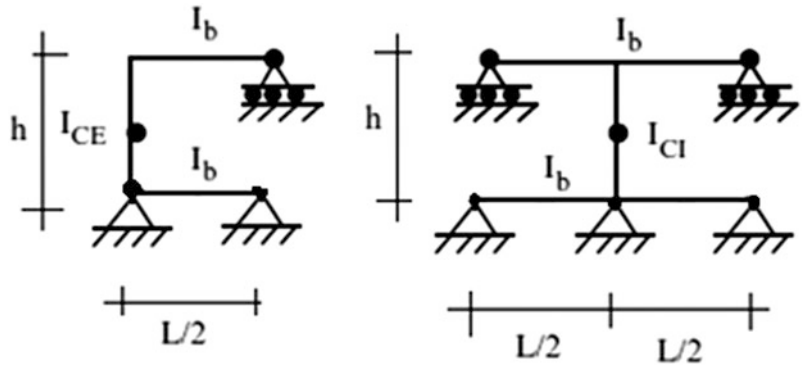
Noting (11.3) and (11.4), the shear carried by sub-element i is given by

$$V_i = \Delta P_i = \left(\frac{k_i}{\sum k_i} \right) V_T = \left(\frac{k_i}{k_T} \right) V_T \tag{11.5}$$

According to (11.5), the shear in a column depends on the ratio of the shear stiffness of the corresponding sub-element to the total story shear stiffness.

Using the slope-deflection equations presented in Sect. 10.3, one can derive the following expressions for the sub-element shear stiffness factors (Fig. 11.10):

Fig. 11.10 Typical sub-elements. (a) Exterior. (b) Interior



Exterior Element: Upper Story

$$k_E = \frac{12EI_{CE}}{h^3} \left\{ \frac{1}{1 + (I_{CE}/h)/(I_b/L)} \right\} = \frac{12EI_{CE}}{h^3} f_E \tag{11.6}$$

Interior Element: Upper Story

$$k_I = \frac{12EI_{CI}}{h^3} \left\{ \frac{1}{1 + (1/2)((I_{CI}/h)/(I_b/L))} \right\} = \frac{12EI_{CI}}{h^3} f_I \tag{11.7}$$

where the dimensionless factor $(I_b/h)/(I_b/L)$ accounts for the flexibility of the beam.

Values of k_E/k_I for a range of values of $(I_{CI}/h)/(I_b/L)$ and I_{CE}/I_{CI} are tabulated in (Table 11.1).

Table 11.1 Stiffness ratios: upper stories

$(I_{CI}/h)/(I_b/L)$	$\frac{k_E}{k_I}$	
	$\frac{I_{CE}}{I_{CI}} = 1/2$	$\frac{I_{CE}}{I_{CI}} = 1$
0	0.5	1
0.25	0.5	0.9
0.5	0.5	0.83
1.0	0.5	0.75
1.5	0.5	0.75
1.5	0.5	0.7
2.0	0.5	0.67

Noting (11.5), we observe that the ratio of the shear in the external column to the shear in the interior column is given by

$$\frac{V|_{E-col}}{V|_{I-col}} = \frac{k_E}{k_I} \tag{11.8}$$

The derivation listed above applies for the upper stories, and needs to be modified for the bottom story. Figure 11.11 shows the idealized model used to estimate the story stiffness for the case where the base is fixed. The sub-elements are illustrated in Fig. 11.12 and the corresponding story stiffness factors are defined by (11.9) and (11.10).

Fig. 11.11 Transverse shear model for bottom story—fixed support

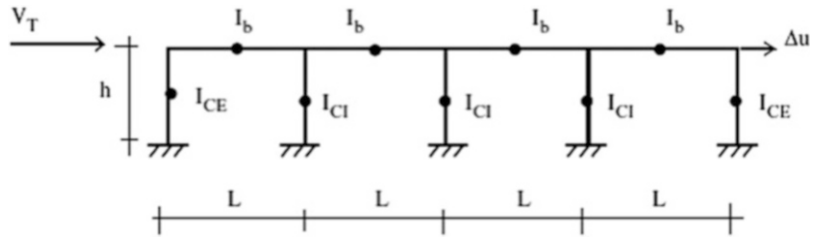
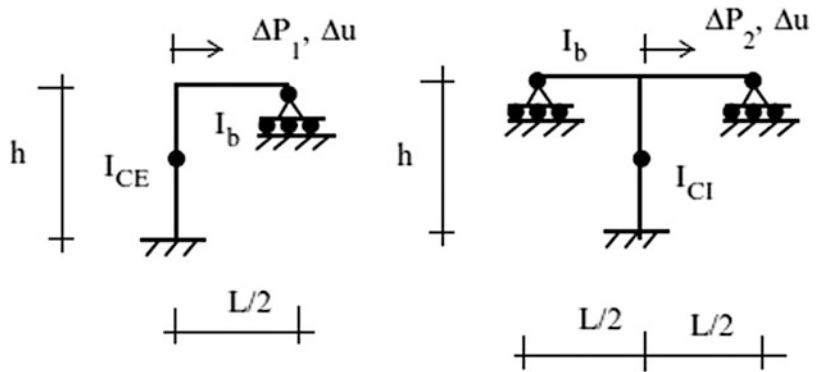


Fig. 11.12 Typical sub-elements for base story—fixed support. (a) Exterior. (b) Interior



Exterior Element: Base Story (Fixed Support)

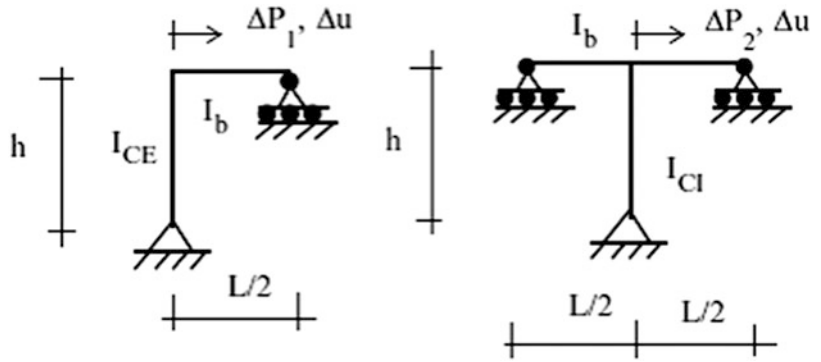
$$k_{BE} = \frac{12EI_{CE}}{h^3} \left\{ \frac{1 + \frac{1}{6} \left(\frac{I_{CE}/h}{I_b/L} \right)}{1 + \frac{2}{3} \left(\frac{I_{CE}/h}{I_b/L} \right)} \right\} = \frac{12EI_{CE}}{h^3} f_{BE} \tag{11.9}$$

Interior Element: Base Story (Fixed Support)

$$k_{BI} = \frac{12EI_{CI}}{h^3} \left\{ \frac{1 + \frac{1}{12} \left(\frac{I_{CI}/h}{I_b/L} \right)}{1 + \frac{1}{3} \left(\frac{I_{CI}/h}{I_b/L} \right)} \right\} = \frac{12EI_{CI}}{h^3} f_{BI} \tag{11.10}$$

When the base is hinged, we use the expressions listed in (11.11) and (11.12). In this case, we do not assume an inflection point at mid-height of the first story (Fig. 11.13).

Fig. 11.13 Typical sub-elements for base story—hinged support. (a) Exterior. (b) Interior



Exterior Element: Base Story (Hinged Support)

$$k_{BE} = \frac{3EI_{CE}}{h^3} \left\{ \frac{1}{1 + (1/2)((I_{CE}/h)/(I_b/L))} \right\} = \frac{3EI_{CE}}{h^3} f_{BE} \tag{11.11}$$

Interior Element: Base Story (Hinged Support)

$$k_{BI} = \frac{3EI_{CI}}{h^3} \left\{ \frac{1}{1 + (1/4)((I_{CI}/h)/(I_b/L))} \right\} = \frac{3EI_{CI}}{h^3} f_{BI} \tag{11.12}$$

The base shears are related by

$$V|_{E-col} = V|_{I-col} \frac{k_{BE}}{k_{BI}} \tag{11.13}$$

Values of k_{BE}/k_{BI} for a range of $(I_{CI}/h)/(I_b/L)$ for both hinged and fixed supports are listed in Table 11.2.

Table 11.2 Stiffness ratios: lowest story

$(I_{CI}/h)/(I_b/L)$	Hinged support		Fixed support	
	$\frac{k_E}{k_I}$		$\frac{k_E}{k_I}$	
	$I_{CE} = 1/2 I_{CI}$	$I_{CE} = I_{CI}$	$I_{CE} = 1/2 I_{CI}$	$I_{CE} = I_{CI}$
0	0.5	1	0.5	1
0.25	0.5	0.944	0.5	0.948
1.0	0.5	0.9	0.5	0.91
1.0	0.5	0.833	0.5	0.862
1.5	0.5	0.786	0.5	0.833
2.0	0.5	0.75	0.5	0.816

Example 11.3 Approximate Analysis Based on the Shear Stiffness Method

Given: The frame shown in Fig. E11.3a.

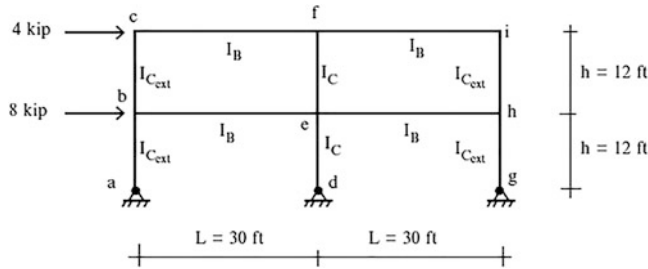


Fig. E11.3a

Determine: The column shear forces using the shear stiffness model and the member properties defined as cases A, B, C, and D.

Case A: $I_{C_{ext}} = \frac{1}{2}I_C$ and $I_B = 4I_C \Rightarrow \frac{I_{C_{ext}}/h}{I_B/L} = 0.31 \frac{I_C/h}{I_B/L} = 0.62$.

Case B: $I_{C_{ext}} = I_C$ and $I_B = 4I_C \Rightarrow \frac{I_{C_{ext}}/h}{I_B/L} = \frac{I_C/h}{I_B/L} = 0.625$.

Case C: $I_{C_{ext}} = I_C$ and $I_B = 2I_C \Rightarrow \frac{I_{C_{ext}}/h}{I_B/L} = \frac{I_C/h}{I_B/L} = 1.25$.

Case D: $I_{C_{ext}} = \frac{1}{2}I_C$ and $I_B = 2I_C \Rightarrow \frac{I_{C_{ext}}/h}{I_B/L} = 0.625 \frac{I_C/h}{I_B/L} = 1.25$.

Solution: Using (11.6), (11.7), and (11.11), (11.12) the sub-element stiffnesses are:

	Case A	Case B	Case C	Case D
Top story	$f_E = 0.762$	$f_E = 0.615$	$f_E = 0.444$	$f_E = 0.615$
	$f_I = 0.762$	$f_I = 0.762$	$f_I = 0.615$	$f_I = 0.615$
	$k_E = 0.5$	$k_E = 0.808$	$k_E = 0.722$	$k_E = 0.5$
	k_I	k_I	k_I	k_I
Bottom story	$f_{BE} = 0.865$	$f_{BE} = 0.762$	$f_{BE} = 0.615$	$f_{BE} = 0.762$
	$f_{BI} = 0.865$	$f_{BI} = 0.865$	$f_{BI} = 0.762$	$f_{BI} = 0.762$
	$k_{BE} = 0.5$	$k_{BE} = 0.881$	$k_{BE} = 0.808$	$k_{BE} = 0.5$
	k_{BI}	k_{BI}	k_{BI}	k_{BI}

Noting that

$$\frac{V_E}{V_I} = \frac{k_E}{k_I}$$

we express the total shear as

$$V_{Total} = 2V_E + V_I = \left[2 \left(\frac{k_E}{k_I} \right) + 1 \right] V_I$$

Once I is specified for the interior and exterior columns, we can evaluate the ratio, k_E/k_I , and then V_I . The computations corresponding to Cases A, B, C, and D are summarized below. We also list the results predicted by the portal method. Note that the portal method agrees exactly with the stiffness method when $I_{C_{exterior}} = \frac{1}{2}I_{C_{interior}}$ (Cases A and D).

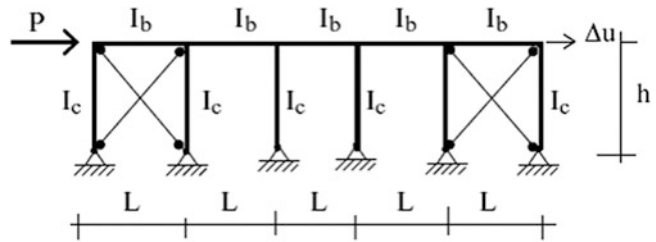
Story	V_T (kip)	Stiffness method								Portal method	
		Case A		Case B		Case C		Case D		V_E (kip)	V_I (kip)
		V_E (kip)	V_I (kip)	V_E (kip)	V_I (kip)	V_E (kip)	V_I (kip)	V_E (kip)	V_I (kip)		
Top	4	1	2	1.235	1.53	1.18	1.64	1	2	1	2
Bottom	12	3	6	3.83	4.34	3.7	4.59	3	6	3	6

11.4.3 Low-Rise Rigid Frames with Bracing

11.4.3.1 Lateral Load

A rigid frame resists lateral loading through bending action of the columns. When a bracing system is combined with the frame, both of these systems participate in carrying the lateral load. From a stiffness perspective, the load is distributed according to the relative stiffness, i.e., the stiffer element carries more load. For low-rise frames, the transverse shear stiffness is the controlling parameter. Figure 11.14 illustrates the structural scheme for a one-story structure. A similar arrangement is used for multistory structures. Of particular interest is the distribution of lateral load between the rigid frame and the brace.

Fig. 11.14 Rigid frame with bracing

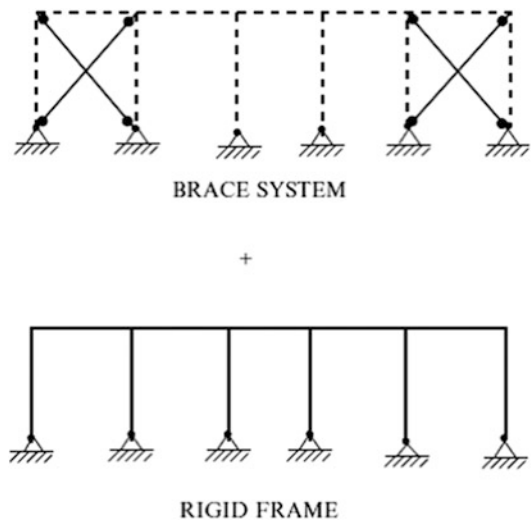


The individual systems are defined in Fig. 11.15. We assume all sub-elements experience the same lateral displacement Δu , and express the lateral loads carried by each structural system as

$$\begin{aligned} P_{\text{frame}} &= k_{\text{frame}} \Delta u \\ P_{\text{brace}} &= k_{\text{brace}} \Delta u \end{aligned} \tag{11.14}$$

where k_{frame} , k_{brace} denote the frame and brace stiffness factors. Summing these forces, we write

Fig. 11.15 Individual systems



$$P = P_{\text{frame}} + P_{\text{brace}} = (k_{\text{brace}} + k_{\text{frame}}) \Delta u = k_T \Delta u \tag{11.15}$$

Solving for Δu and back substituting in (11.14) results in

$$\begin{aligned}
 P_{\text{frame}} &= \frac{k_{\text{frame}}}{k_T} P \\
 P_{\text{brace}} &= \frac{k_{\text{brace}}}{k_T} P
 \end{aligned}
 \quad (11.16)$$

Also,

$$\frac{P_{\text{frame}}}{P_{\text{brace}}} = \frac{k_{\text{frame}}}{k_{\text{brace}}}
 \quad (11.17)$$

According to (11.16), the lateral force carried, by a system depends on its relative stiffness. Increasing k_{brace} shifts load onto the bracing system.

Considering a single story, the lateral load required to introduce an inter-story lateral displacement Δu is equal to

$$P_{\text{frame}} = k_{\text{frame}} \Delta u
 \quad (11.18)$$

where k_{frame} is estimated by combining (11.11) and (11.12).

$$k_{\text{frame}} = \frac{3E}{h^3} \left\{ \frac{2I_{CE}}{1 + (1/2)((I_{CE}/h)/(I_b/L))} + \sum_{\text{intercol}} \frac{I_{CI}}{1 + (1/4)((I_{CI}/h)/(I_b/L))} \right\}
 \quad (11.19)$$

Once the member properties are known, one can evaluate k_{frame} . We need to develop a similar expression for a brace.

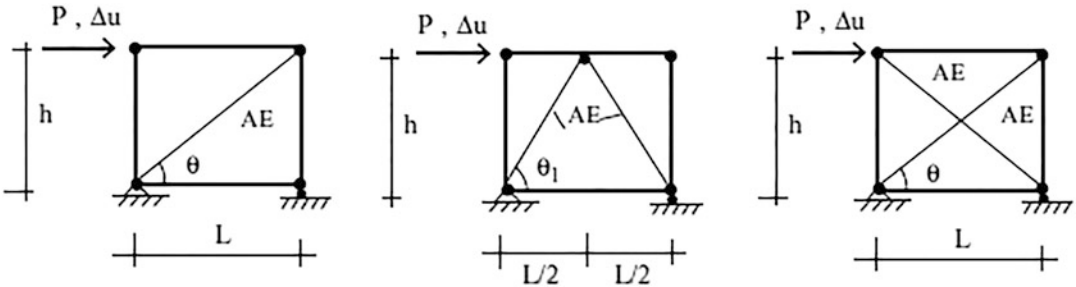


Fig. 11.16 Diagonal bracing systems. (a) Single. (b) Chevron. (c) X Brace

Typical bracing schemes are shown in Fig. 11.16. The lateral load is carried equally by the diagonal members. One determines k_{brace} using structural mechanics concepts such as deformation and equilibrium. The analytical expressions for the different schemes are

$$\begin{aligned}
 k_{\text{brace}(\text{single})} &= \frac{AE}{h} (\sin \theta \cos^2 \theta) \\
 k_{\text{brace}(\text{chevron})} &= \frac{2AE}{h} (\sin \theta_1 \cos^2 \theta_1) \\
 k_{\text{brace}(\text{x brace})} &= \frac{2AE}{h} (\sin \theta \cos^2 \theta)
 \end{aligned}
 \quad (11.20)$$

The diagonal forces reverse when the lateral load reverses, which occurs for wind and earthquake loading.

Example 11.4 Shear Force Distribution

Given: The one-story frame defined in Fig. E11.4a.

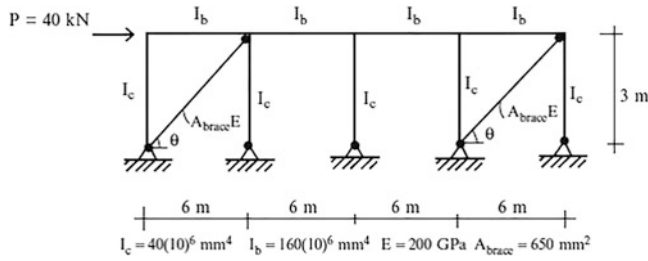


Fig. E11.4a

Determine: The column shears and the diagonal brace forces.

Solution: Using (11.19), the frame stiffness is

$$k_{\text{frame}} = \frac{3EI_c}{h^3} \left(\frac{2}{1 + (1/2)((I_c/h)/(I_b/L))} + \frac{3}{1 + (1/4)((I_c/h)/(I_b/L))} \right)$$

$$= \frac{3EI_c}{h^3} \left(\frac{8}{5} + \frac{8}{3} \right) = 12.8 \frac{EI_c}{h^3}$$

The brace stiffness follows from (11.20). Note that there are two braces.

$$k_{\text{brace}} = 2 \frac{A_{\text{brace}}E}{h} (\sin \theta \cos^2 \theta) = \frac{A_{\text{brace}}E}{h} 2(0.447)(0.894)^2 = 0.714 \frac{A_{\text{brace}}E}{h}$$

Noting (11.16), the individual forces are related by

$$P_{\text{frame}} = \left(\frac{k_{\text{frame}}}{k_{\text{brace}}} \right) P_{\text{brace}} = 17.9 \left(\frac{I_c}{A_{\text{brace}}h^2} \right) P_{\text{brace}}$$

Summing the forces leads to

$$P_{\text{frame}} + P_{\text{brace}} = P \Rightarrow \left(17.9 \frac{I_c}{A_{\text{brace}}h^2} + 1 \right) P_{\text{brace}} = 40$$

Then

$$P_{\text{brace}} = \frac{40}{1 + (17.9) \left(\frac{(40(10)^6)}{(650)(3000)^2} \right)} = 35.6 \text{ kN}$$

$$P_{\text{frame}} = 4.36 \text{ kN}$$

The force in each diagonal brace is given by

$$F_b = \frac{P_{\text{brace}}}{2 \cos \theta} = 19.9 \text{ kN}$$

We evaluate the column shear forces using the corresponding stiffness factors defined by (11.11) and (11.12).

$$k_E = \frac{3EI_c}{h^3} \left(\frac{4}{5} \right)$$

$$k_I = \frac{3EI_c}{h^3} \left(\frac{8}{9} \right)$$

$$\frac{V_E}{V_I} = \frac{k_E}{k_I} = \frac{4/5}{8/9} = \frac{9}{10}$$

$$\therefore V_E = 0.9V_I$$

Summing the shears,

$$2V_E + 3V_I = 4.36 \Rightarrow 1.8V_I + 3V_I = 4.36$$

Then

$$V_I = 0.91 \text{ kN}$$

$$V_E = 0.82 \text{ kN}$$

Note that the brace carries the major portion of the story shear.

Example 11.5 Shear Force Distribution

Given: The braced rigid frame defined in Fig. E11.5a. $A_b = 0.8 \text{ in.}^2$, $E = 29,000 \text{ ksi}$, and $I = 150 \text{ in.}^4$.

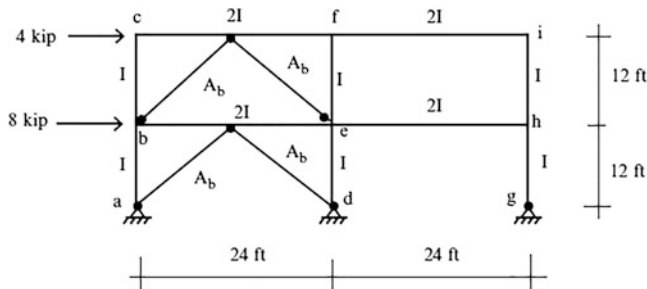


Fig. E11.5a

Determine: The lateral forces carried by the frame and brace systems.

Solution:

$$P_{\text{frame}} + P_{\text{brace}} = 4 \text{ kip Upper floor}$$

$$P_{\text{frame}} + P_{\text{brace}} = 12 \text{ kip Lower floor}$$

Frame:

Upper story sub-element: Equations (11.6) and (11.7)

$$k_E = \frac{6EI_c}{h^3} \Rightarrow k_{\text{frame}} = \frac{EI_c}{h^3} (2(6) + 8) = \frac{20EI_c}{h^3} = \frac{20(29,000)150}{(12 \times 12)^3} = 29.14 \text{ kip/in.}$$

$$k_I = \frac{8EI_c}{h^3}$$

Base story sub-element: Equations (11.11) and (11.12)

$$k_E = \frac{2EI_c}{h^3} \Rightarrow k_{\text{frame}} = \frac{EI_c}{h^3} (2(2) + 2.4) = \frac{6.4EI_c}{h^3} = 9.32 \text{ kip/in.}$$

$$k_I = \frac{2.4EI_c}{h^3}$$

Brace:

$$k_{\text{brace}} = \frac{2EA_b}{h} \sin \theta_1 (\cos \theta_1)^2 = 0.707 \frac{EA_b}{h} = \frac{0.707(0.8)(29,000)}{12(12)} = 113.9 \text{ kip/in.}$$

Shear distributions

$$P_{\text{frame}} = \left(\frac{k_{\text{frame}}}{k_{\text{brace}}} \right) P_{\text{brace}} \Rightarrow \begin{aligned} P_{\text{frame}} &= \left(\frac{29.14}{113.9} \right) P_{\text{brace}} = 0.256 P_{\text{brace}} && \text{Upper floor} \\ P_{\text{frame}} &= \left(\frac{9.32}{113.9} \right) P_{\text{brace}} = 0.082 P_{\text{brace}} && \text{Lower floor} \end{aligned}$$

Then

$$(0.256 + 1)P_{\text{brace}} = 4 \text{ kip} \Rightarrow P_{\text{brace}} = 3.18 \text{ kip} \quad \text{Upper floor}$$

$$(0.082 + 1)P_{\text{brace}} = 12 \text{ kip} \Rightarrow P_{\text{brace}} = 11.09 \text{ kip} \quad \text{Lower floor}$$

Therefore

$$P_{\text{frame}} = 0.256 P_{\text{brace}} = 0.81 \text{ kip} \quad \text{Upper floor}$$

$$P_{\text{frame}} = 0.082 P_{\text{brace}} = 0.91 \text{ kip} \quad \text{Lower floor}$$

Example 11.6 Shear Force Distribution

Given: The braced frame defined in Fig. E11.6a.

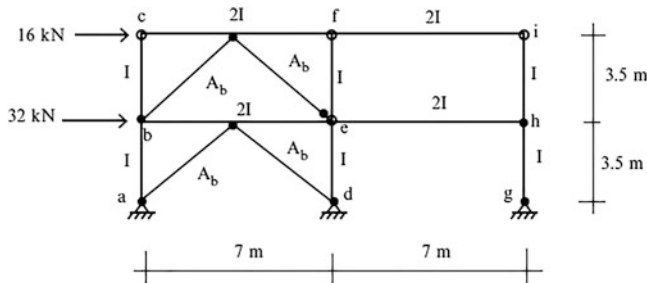


Fig. E11.6a

Determine: The required brace area A_b , to limit the inter-story displacement to 10 mm for each story. Assume $E = 200$ GPa.

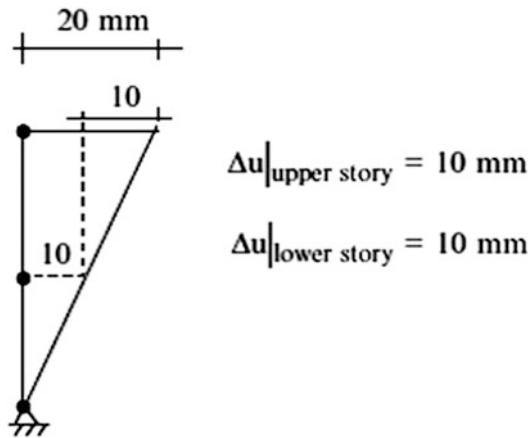
Solution:

$$P_{\text{brace}} = 16 \text{ Upper floor}$$

$$P_{\text{brace}} = 16 + 32 = 48 \text{ Lower floor}$$

$$k_{\text{brace}} = \frac{2EA_b}{h} \sin \theta_1 (\cos \theta_1)^2 = 0.707 \frac{EA_b}{h}$$

$$P_{\text{brace}} = k_{\text{brace}} u$$



$$\text{Upper floor } 16 = 0.707 \frac{EA_b}{h} \Delta u_{\text{upper}} \Rightarrow A_b \geq \frac{16(3500)}{0.707(10)(200)} = 39.6 \text{ mm}^2$$

$$\text{Lower floor } 48 = 0.707 \frac{EA_b}{h} \Delta u_{\text{upper}} \Rightarrow A_b \geq \frac{48(3500)}{0.707(10)(200)} = 118.8 \text{ mm}^2$$

The value for the lower floor controls the design.

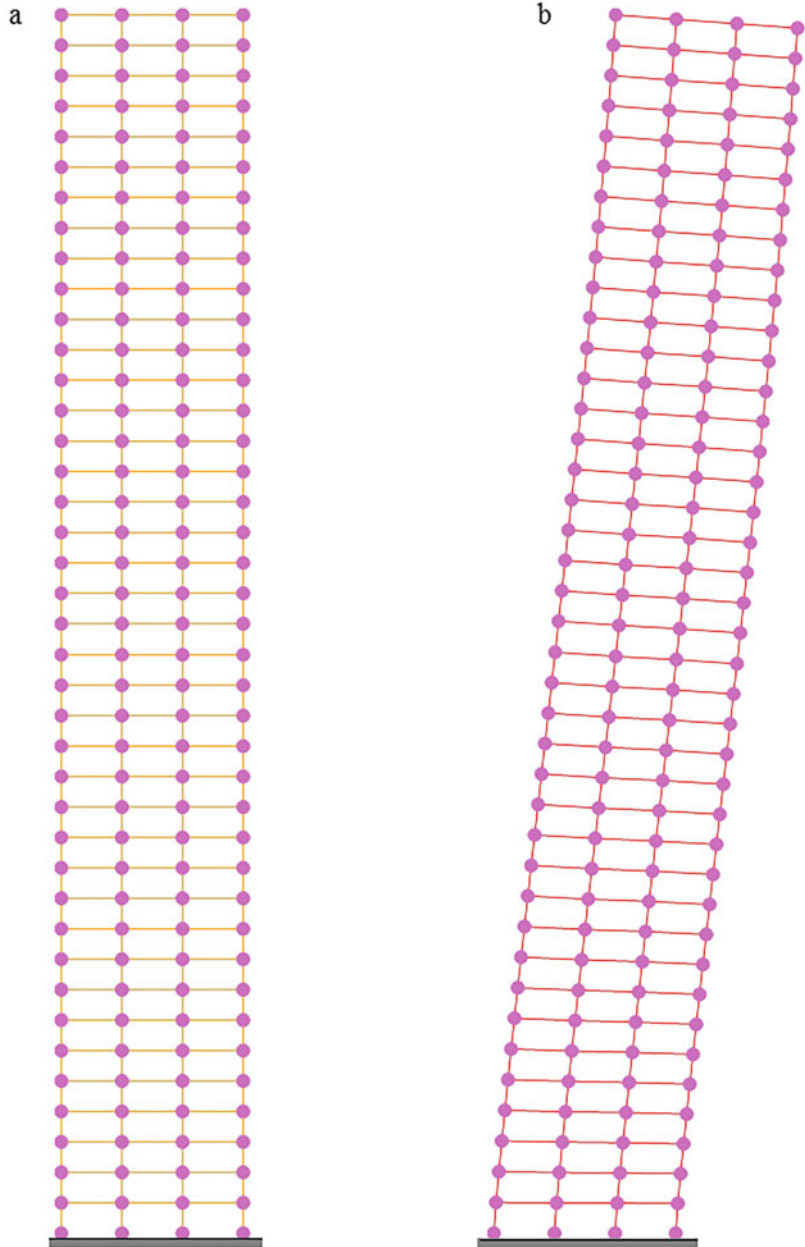
$$\therefore A_{b_{\text{required}}} = 118.8 \text{ mm}^2$$

11.5 High-Rise Rigid Frames: The Cantilever Method

The approximate procedure described above is applicable for low-rise rigid frames, which behave as “shear type” frames, i.e., the floors displace laterally but do not rotate. One determines the axial forces in the columns using the shear forces in the floor beams. High-rise frames behave more like a cantilever beam. As illustrated in Fig. 11.17b, the floors rotate as rigid planes. Their behavior is

similar to what is assumed for the cross section of a beam in the formulation of the bending theory of beams; the floors experience both a translation and a rotation. Just as for beams, the rotational component produces axial strain in the columns. The column shears and moments are found from equilibrium considerations, given the axial forces in the columns. In what follows, we describe an idealized structural model that is used to establish the distribution of column axial forces in a story. This approach is called the “Cantilever Method.”

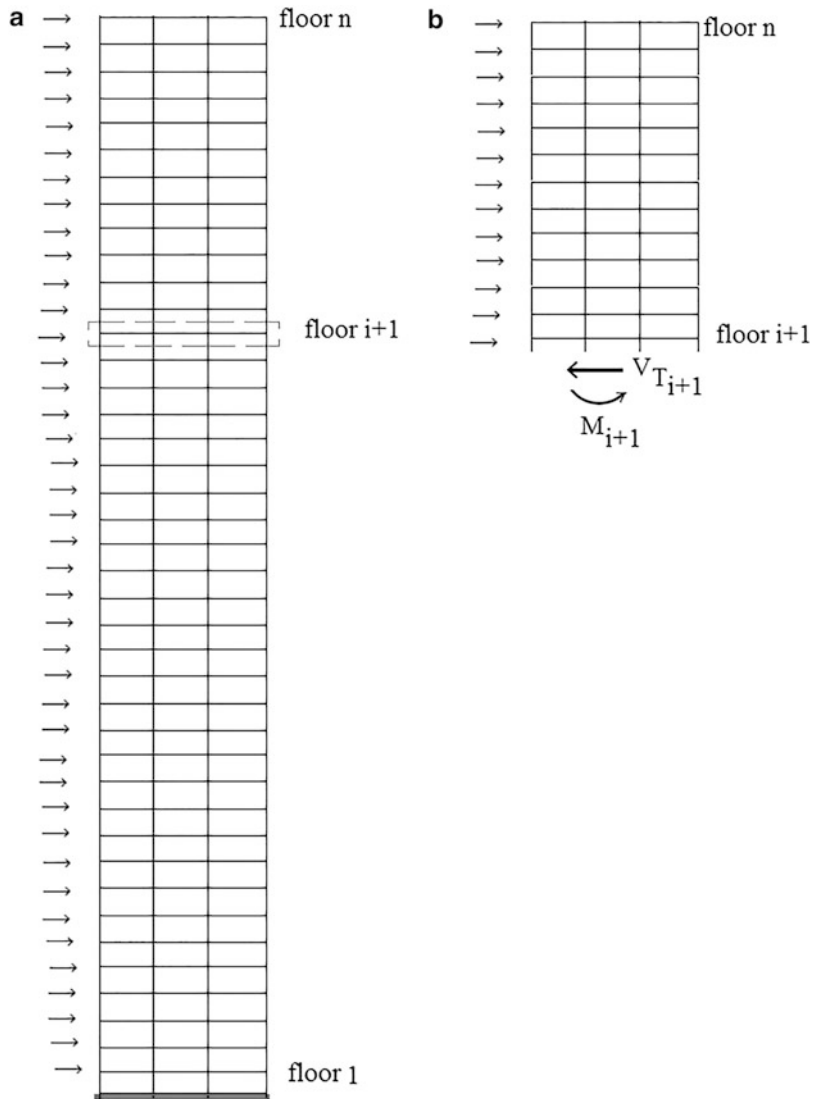
Fig. 11.17 Tall building model—lateral deflections



One normally applies this method to estimate the axial forces in the columns at the base of the building, i.e., where the bending moment due to lateral loading is a maximum.

We consider the typical tall building shown in Fig. 11.18. Given the lateral load, we can determine the bending moment and transverse shear at mid-height of each story. We denote these quantities as M_{i+1} and $V_{T_{i+1}}$.

Fig. 11.18 Tall building model (a) under lateral loading (b) Segment of building above floor i



Now, we isolate a segment of the building consisting of floors $i + 1$, i , and the columns connecting these floors. Figure 11.19 shows this segment. The floors are assumed to be rigid plates, and the columns are represented as axial springs. Floor $i + 1$ experiences a rotation, $\Delta\beta$, with respect to floor i due to the moment M_{i+1} .

We position a reference axis at point O and define x_i as the X coordinate for spring i . The corresponding axial stiffness is k_i . The origin of the reference axis is located such that

Fig. 11.19 Column-beam model for a story bounded by floors i and $i + 1$

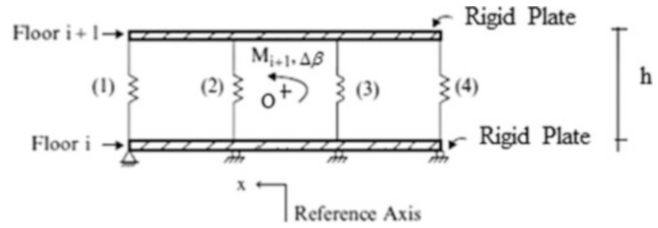
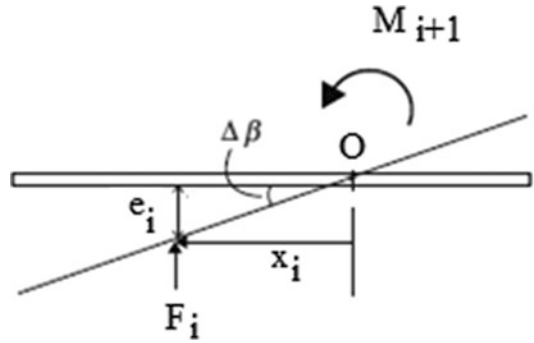


Fig. 11.20 Deformation due to relative rotation



$$\sum k_i x_i = 0 \tag{11.21}$$

Note that the axial stiffness is equal to the column stiffness,

$$k_i = \frac{A_i E}{h} \tag{11.22}$$

where A_i is the cross-sectional axis and h is the column height. Then, when E is constant, (11.21) can be written as

$$\sum A_i x_i = 0 \tag{11.23}$$

In this case, one can interpret the reference axis as equivalent to the centroidal axis for the column areas in the story.

We suppose the floors rotate about O and define $\Delta\beta$ as the relative rotation between adjacent floors. The deformation introduced in spring i follows from Fig. 11.20.

$$\begin{aligned} e_i &= x_i \Delta\beta \\ F_i &= k_i e_i = k_i x_i \Delta\beta \end{aligned} \tag{11.24}$$

Summing moments about O , and equating the result to the applied moment, M_{i+1} results in

$$M_{i+1} = \left(\sum k_i x_i^2 \right) \Delta\beta \tag{11.25}$$

Here, M_{i+1} represents the moment due to the lateral loads applied *on and above* floor $i + 1$. We solve for $\Delta\beta$ and then back substitute in the expression for F_i . The result is

$$F_i = k_i x_i \frac{M_{i+1}}{\left(\sum k_i x_i^2 \right)} = x_i A_i \left(\frac{E}{h \sum k_i x_i^2} \right) M_{i+1} \tag{11.26}$$

We see that the column force distribution is proportional to the distance from the reference axis and the relative column cross-sectional area. One does not need to specify the actual areas, only the ratio of areas.

One should note that this result is based on the assumption that the *floor acts as a rigid plate*. Stiff belt-type trusses are frequently incorporated at particular floors throughout the height so that the high-rise frame behaves consistent with this hypothesis.

Example 11.7 Approximate analysis based on the cantilever method

Given: The symmetrical 42-story plane frame shown in Fig. E11.7a. Assume the building is supported on two caissons located at the edges of the base. Consider the base to be rigid.

Determine: The axial forces in the caissons.

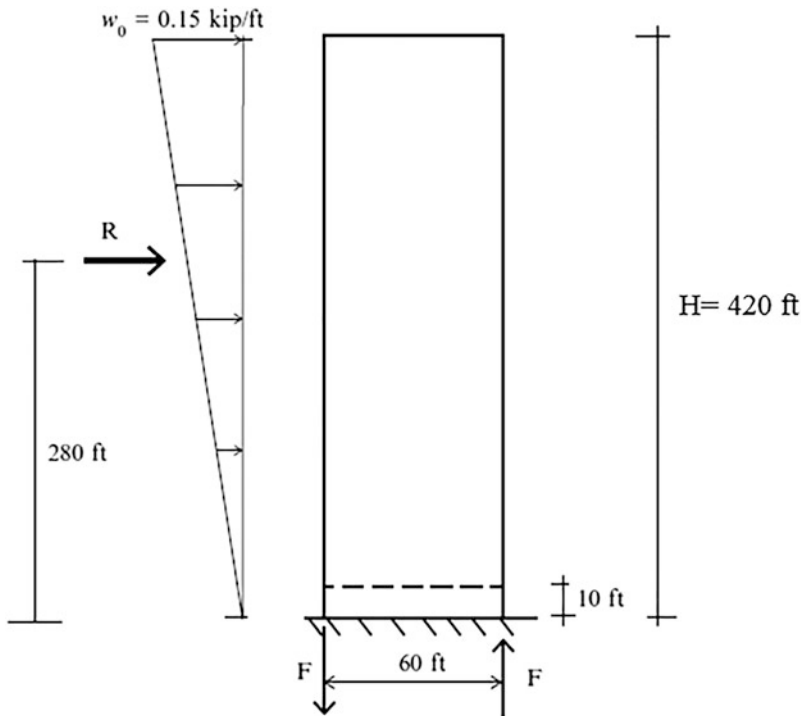


Fig. E11.7a

Solution: The Moment at the base is given by

$$R = \frac{w_0 H}{2} = 210w_0$$

$$M = \frac{2H}{3}R = 58,800w_0 = 8820 \text{ kip ft}$$

This moment is resisted by the pair of caisson forces which are equivalent to a couple.

$$60F = 8820$$

$$F = 147 \text{ kip}$$

Example 11.8 Approximate Analysis Based on the Cantilever Method

Given: The symmetrical plane frame shown in Fig. E11.8a.

Determine: The column axial forces in the bottom story for the distribution of column areas shown.

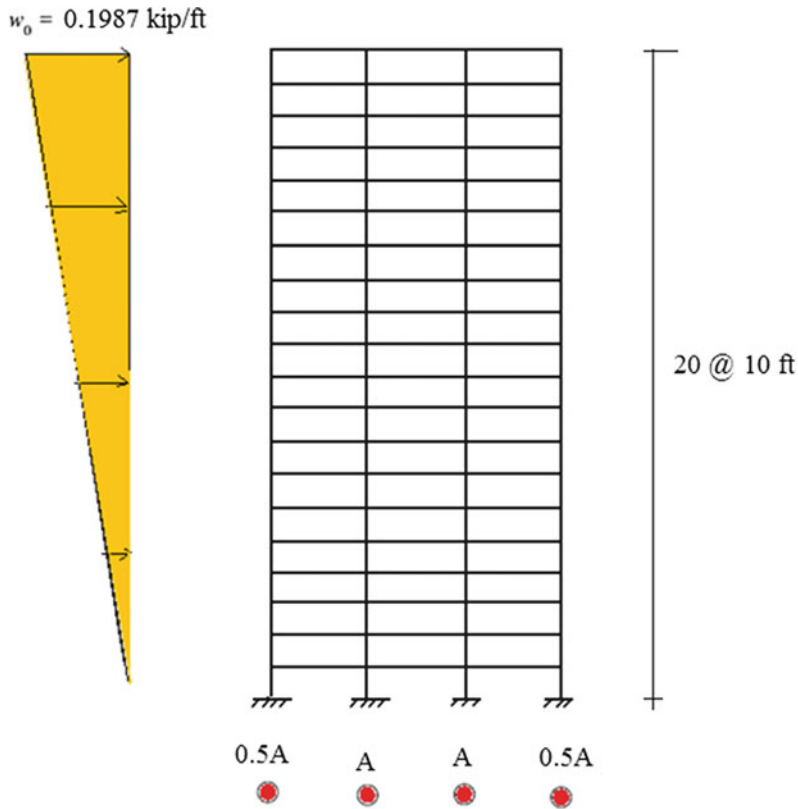


Fig. E11.8a

Solution: The rotational stiffness for the story is:

$$K_x = \sum k_i x_i^2 = \frac{E}{h} \sum A_i x_i^2 = 1100 \left(\frac{EA}{h} \right)$$

The bending moment at mid-height of the first story is 2550 kip ft. Then, substituting for M_{i+1} and K_x in (11.26) leads to the axial forces in the columns (Fig. E11.8b),

$$F_2 = (10) \frac{AE}{h} \left(\frac{2550}{1100(AE/h)} \right) = 23.2 \text{ kip } \downarrow$$

$$F_1 = (30) \frac{.5AE}{h} \left(\frac{2550}{1100(AE/h)} \right) = 34.8 \text{ kip } \downarrow$$

$$F_3 = -F_2 = 23.2 \text{ kip } \uparrow$$

$$F_4 = -F_1 = 34.8 \text{ kip } \uparrow$$

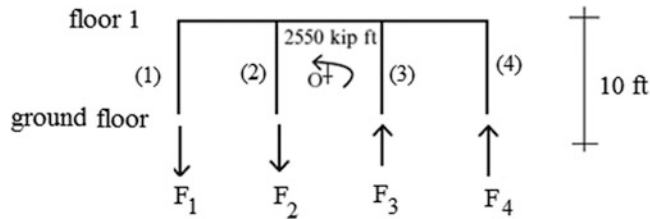


Fig. E11.8b

This computation is repeated for successive stories. Once all the column axial forces are known, one can compute the column shears by assuming inflection points at the midpoints of the columns and beams and applying static equilibrium conditions. The procedure is similar to that followed in Example 11.2.

11.6 Summary

11.6.1 Objectives of the Chapter

Our goals in this chapter are

- To describe some approximate methods for estimating the bending moment distribution in multi-span beams and multi-bay frames subjected to gravity loading.
- To present approximate methods for analyzing multistory rigid frames subjected to lateral loading.

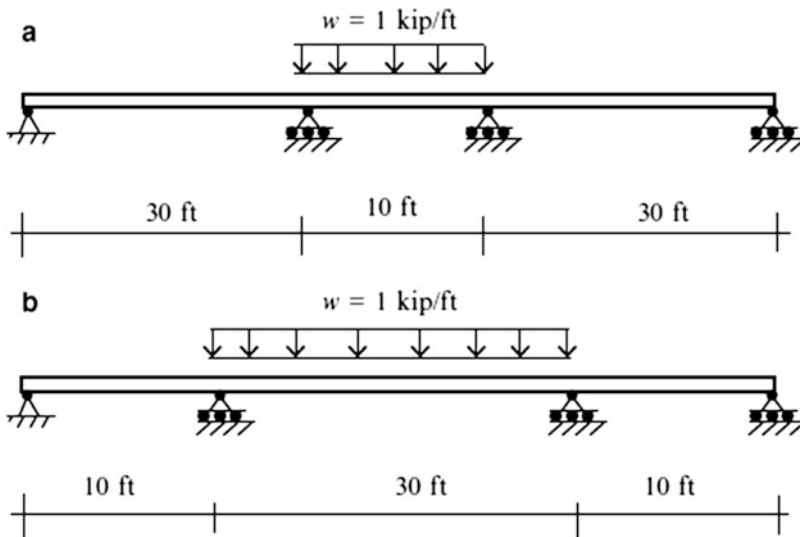
11.6.2 Key Concepts

- Reasoning in a qualitative sense about the behavior using the concept of relative stiffness provides the basis for a method to estimate the bending moment distribution in multi-span beams.
- Two methods are described for analyzing low-rise rigid frame structures.
- The Portal method: The Portal method assumes the shear forces in the interior columns are equal to a common value, and the shears in the exterior columns are equal to $\frac{1}{2}$ this value. This is an empirical-based procedure.
- The shear stiffness method: The shear stiffness method uses simplified structural models to estimate the shear forces in the columns given the total shear force for a story. This procedure predicts that the shear force in a particular column is proportioned to the relative stiffness. It follows that a stiff column attracts more load than a flexible column.

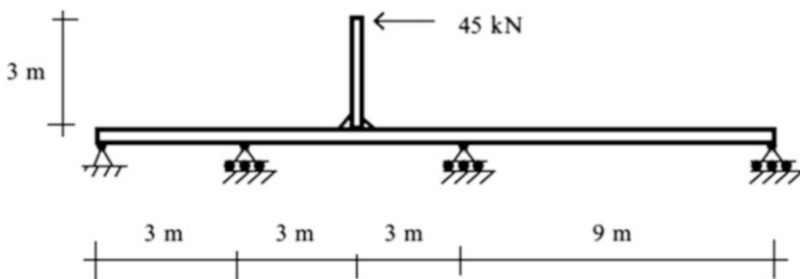
- High-rise rigid frames are modeled as equivalent cantilever beams. The floor slabs are considered rigid and the bending rigidity is generated through the axial action of the columns. One starts with the bending moment at the midpoint between a set of floors and determines the axial forces in the columns. According to this method, the axial force depends on the axial rigidity of the column and the distance from the centroidal axis.

11.7 Problems

Problem 11.1. Estimate the bending moment distribution for the cases listed below. Use qualitative reasoning based on relative stiffness. Assume I as constant.



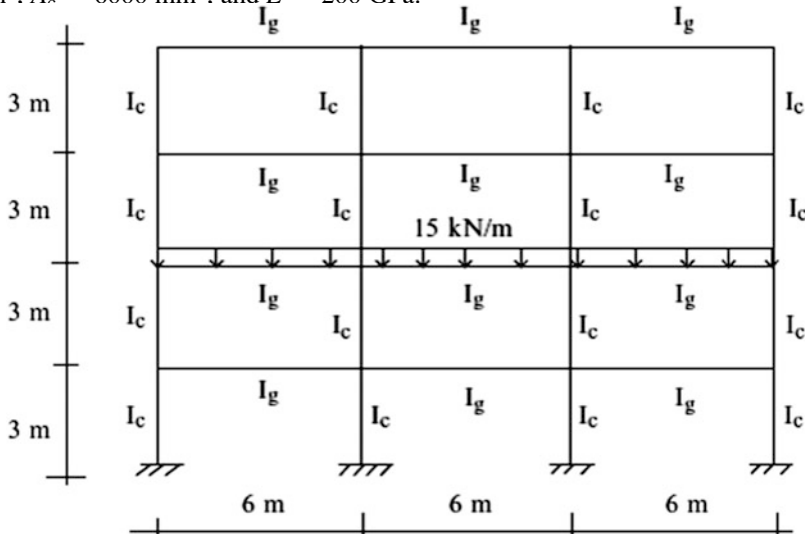
Problem 11.2. Estimate the bending moment distribution. Use qualitative reasoning based on relative stiffness. Assume I as constant.



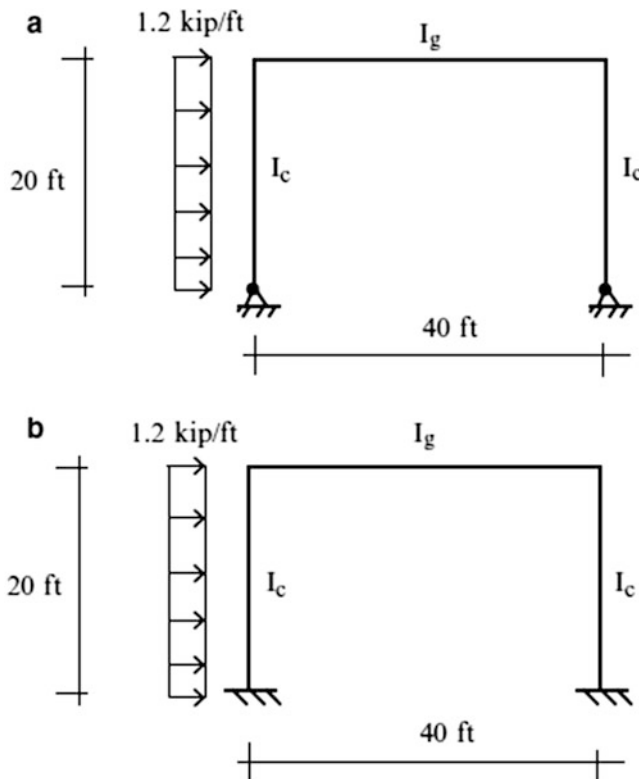
Problem 11.3. Solve Problem 11.1 cases (a) and (b) using moment distribution. Compare the approximate and exact results.

Problem 11.4. Consider the multistory steel frame shown below. Determine the maximum positive and negative moments in the beams using the following approaches:

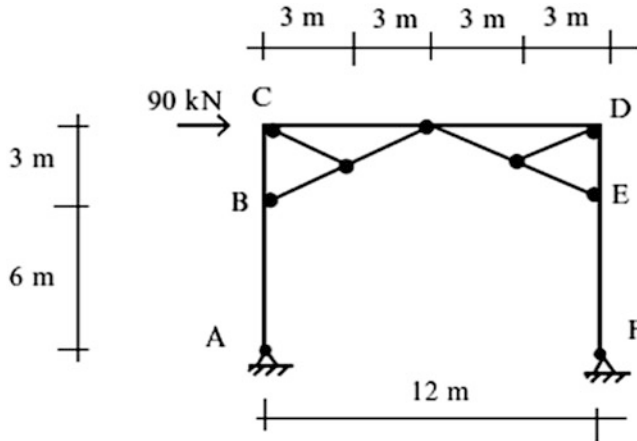
1. Assume inflection points at $0.1L$ from each end of the beams.
2. Use a computer software system. Assume $I_g = 200(10)^6 \text{ mm}^4$, $A_g = 16,000 \text{ mm}^2$, $I_c = 100(10)^6 \text{ mm}^4$, $A_c = 6000 \text{ mm}^2$, and $E = 200 \text{ GPa}$.



Problem 11.5. Estimate the axial force, shear force, and bending moment distributions. Assume $I_g = 2I_c$



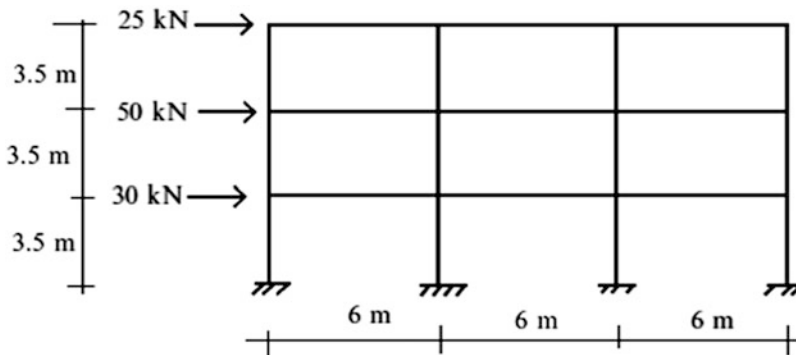
Problem 11.6. Members AC and FD are continuous. Estimate the bending moment distribution in AC and FD, and the axial forces in the pin-ended members. Compare your results with results generated with a computer software system. Assume $I = 100(10)^6 \text{ mm}^4$, $A = 6000 \text{ mm}^2$, $A_{\text{pin-ended}} = 4000 \text{ mm}^2$, and $E = 200 \text{ GPa}$.



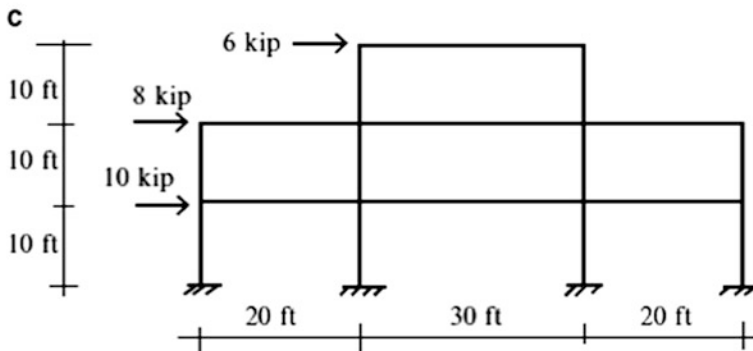
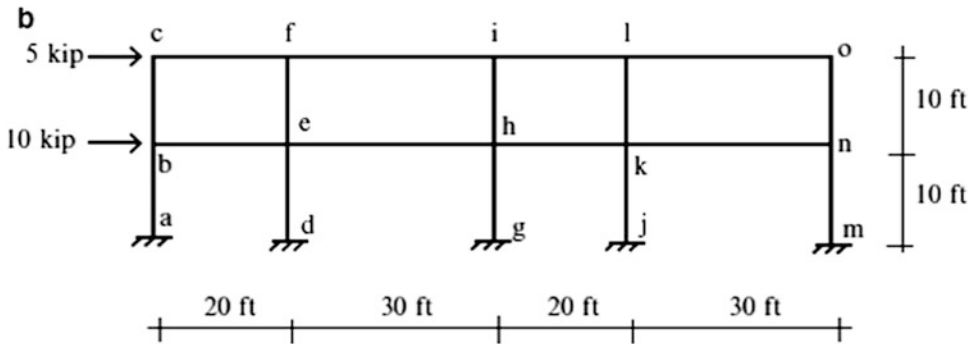
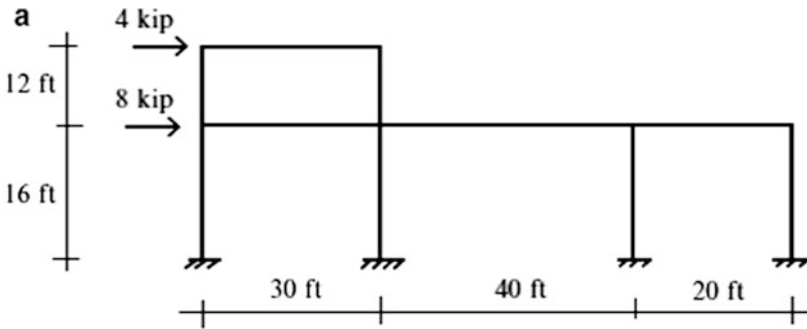
Problem 11.7. Repeat Problem 11.6 assuming fixed supports at A and F.

Problem 11.8. Consider the steel frame shown below. Determine the moment at each end of each member using

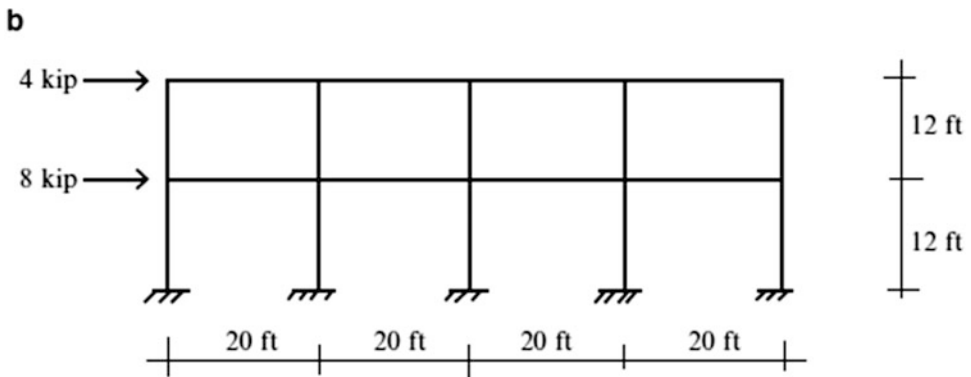
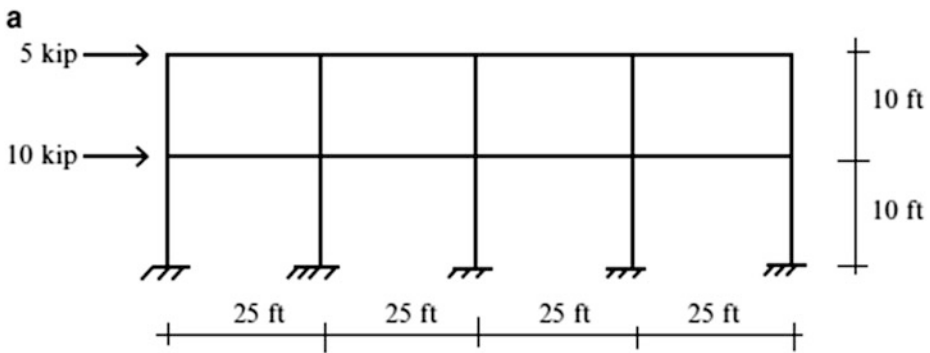
- (a) The Portal method.
- (b) The shear stiffness method. Take $I_g = 300(10)^6 \text{ mm}^4$, $A_g = 18,000 \text{ mm}^2$ for all the girders, $I_c = 100(10)^6 \text{ mm}^4$, and $A_c = 6000 \text{ mm}^2$ for all the columns.



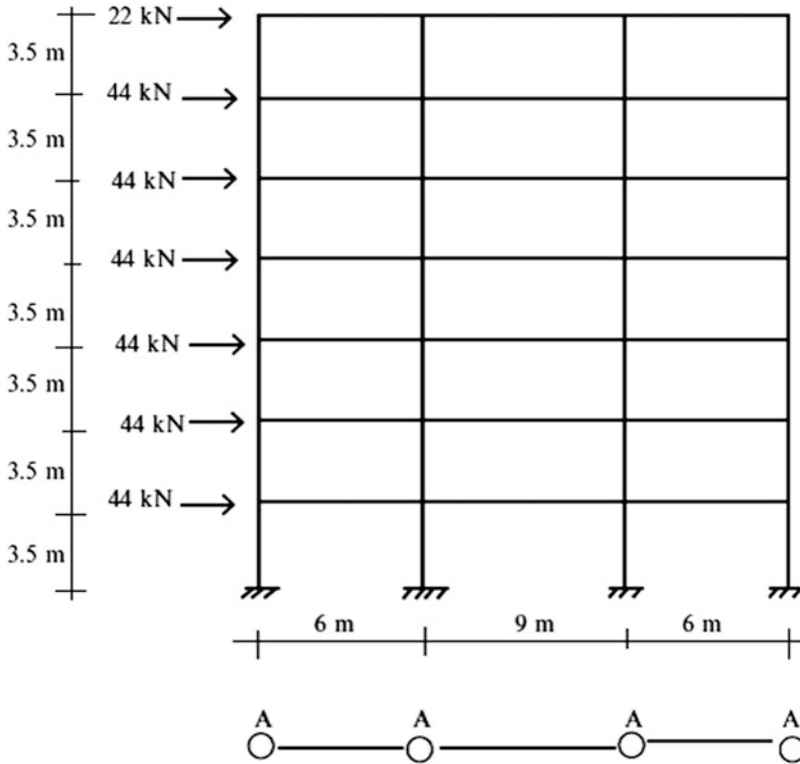
Problem 11.9. For the steel frames shown, estimate the axial force, shear force, and moments for all of the members using the Portal method. Compare your results with results generated with a computer software system. Take $I_c = 480 \text{ in.}^4$, $A_c = 40 \text{ in.}^2$ for all the columns and $I_b = 600 \text{ in.}^4$, $A_b = 60 \text{ in.}^2$ for all the beams.



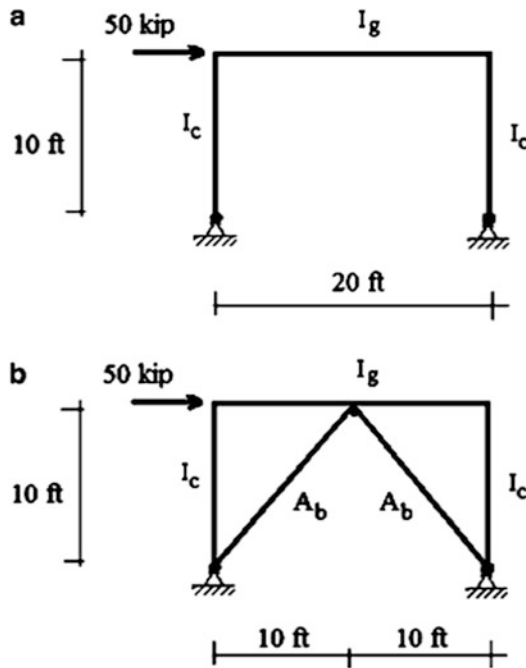
Problem 11.10. For the steel frames shown, estimate the axial force, shear force, and moments for all of the members. Use the Stiffness method. Take $I_c = 480 \text{ in.}^4$, $A_c = 40 \text{ in.}^2$ for all the columns and $I_b = 600 \text{ in.}^4$, $A_b = 60 \text{ in.}^2$ for all the beams.



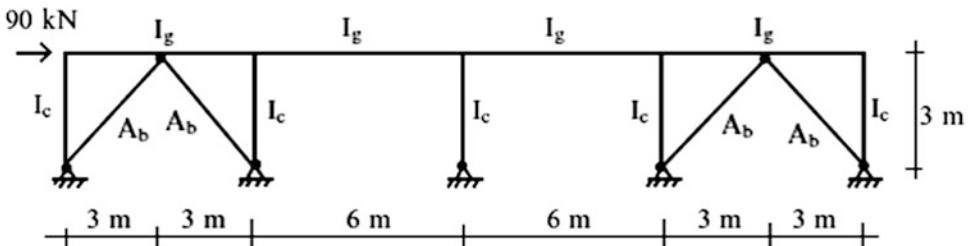
Problem 11.11. Estimate the column axial forces in the bottom story for the distribution of column areas shown.



Problem 11.12. Estimate the column shears for cases (a) and (b). Compare your results with computer-based solutions. Assume $I_g = 300 \text{ in.}^4$, $A_g = 20 \text{ in.}^2$, $I_c = 100 \text{ in.}^4$, $A_c = 10 \text{ in.}^2$, $A_b = 0.5 \text{ in.}^2$, and $E = 29,000 \text{ ksi}$.



Problem 11.13. Consider the rigid steel frame with bracing shown below. Estimate the column shears and brace forces. Compare your results with a computer-based solution. Take $I_g = 120 (10)^6 \text{ mm}^4$, $A_g = 6000 \text{ mm}^2$, $I_c = 40(10)^6 \text{ mm}^4$, $A_c = 2000 \text{ mm}^2$, $A_b = 650 \text{ mm}^2$, and $E = 2000 \text{ GPa}$.



Abstract

In this chapter, we revisit the Displacement Method for structures such as trusses, beams, and frames which are composed of member type elements. *Our objective is to identify the basic steps involved in applying the Displacement Method that can be represented as computer procedures.* We utilize matrix notation since it is the natural language of computation, and systematically reformulate the different steps as a sequence of matrix operations. This reformulation is referred to as the Finite Element Displacement Method. It is relatively straightforward to convert these matrix operations into computer code once one selects a computer language.

12.1 Introduction

In Chaps. 9 and 10, we described two methods for analyzing indeterminate structures, namely the Force and Displacement Methods. The examples that we presented were deliberately kept simple to minimize the computational effort since our objective was to demonstrate “how” the methods are applied rather than the computational details. However, one can appreciate that as a structure becomes more complex, the computational effort becomes the limiting issue for hand computation. Therefore, it is necessary to resort to computer-based procedures in order to execute the various phases of the analysis process. One needs to be familiar with commercial computer-based analysis codes since the extensive use of digital computers in structural analysis and design has revolutionized the practice of structural engineering over the past 40 years.

12.2 Key Steps of the Finite Element Displacement Method for Member Systems

Chapter 10 discussed the methodology of the Displacement Method and presented examples of beam and frame structures analyzed by this method. We summarize here the key steps involved in applying

the Displacement Method to member type structures. In later sections, we reexamine each step and represent the set of actions as a set of matrix operations.

Step #1. *Formulate the member end force–end displacement equations*

Using beam theory, we express the forces acting on the ends of a member in terms of the displacement measures for the ends. These equations are referred to as member end action–end displacement equations. Their derivation is contained in Sect. 10.2. A subset of these equations are called the slope-deflection equations. In the derivation, the force and displacement quantities are referred to a local reference frame associated with the orientation of the member.

Step #2. *Select a global reference frame and transform member variables*

We select a common reference frame and refer both the nodal and member force and displacement quantities to this common frame. This step involves shifting back and forth from member frames to the global frame and allows one to deal with structures having arbitrary geometries.

Step #3. *Establish the nodal force equilibrium equations*

We enforce force equilibrium at each node. This step involves summing the end actions for those members which are incident on the node. Then, using the member equations, we substitute for the end actions in terms of the nodal displacements that correspond to the end displacements for the member. This operation leads to a set of linear algebraic equations which relate the external forces applied to the nodes and the nodal displacements. The coefficient matrix for this set is called the “System Stiffness Matrix.”

Step #4. *Introduce displacement constraints*

Supports at nodes introduce constraints on certain nodal displacements. For example, if a node is fully fixed, all the displacement measures associated with the node are equal to zero. Introducing displacement constraints reduces the total number of displacement variables, and one works with a “reduced” set of equilibrium equations. Depending on the structure, a certain number of supports are required to prevent initial instability.

Step #5. *Solve the nodal equilibrium equations*

We solve the nodal force equilibrium equations for the nodal displacements. When the number of unknown displacements is large, this step is not feasible without a digital computer.

Step #6. *Determine member end actions*

We substitute the values of the nodal displacements obtained from the solution of the nodal equilibrium equations into the member force–displacement relations and solve for the member end forces.

Step #7. *Check on nodal force equilibrium*

The last step involves substituting for the member end forces in the nodal force equilibrium equations to check that the external nodal forces are equilibrated by the member forces. This step provides information on the reactions; it also provides a check on statics. Static discrepancy is generally related to the computational accuracy associated with solving the nodal equilibrium equations. Most computers now use double precision representation and numerical accuracy is usually not a problem.

12.3 Matrix Formulation of the Member Equations: Planar Behavior

In what follows, we present the member equations for the two-dimensional case where bending occurs in the x - y plane. Figure 12.1 shows the end actions and end displacements *referred to the local member frame*. We use a subscript l to denote quantities referred to the local frame. The x -axis coincides with the centroidal axis for the member, and the y and z axes are the principal inertia directions for the cross section. Subscripts B and A denote the positive and negative ends of the member. It is convenient to represent the set of end forces and end displacements as matrices defined as follows:

- End Displacements

$$\mathbf{U}_{\ell B} = \begin{Bmatrix} u_{\ell B} \\ v_{\ell B} \\ \theta_B \end{Bmatrix} \quad \mathbf{U}_{\ell A} = \begin{Bmatrix} u_{\ell A} \\ v_{\ell A} \\ \theta_A \end{Bmatrix} \quad (12.1)$$

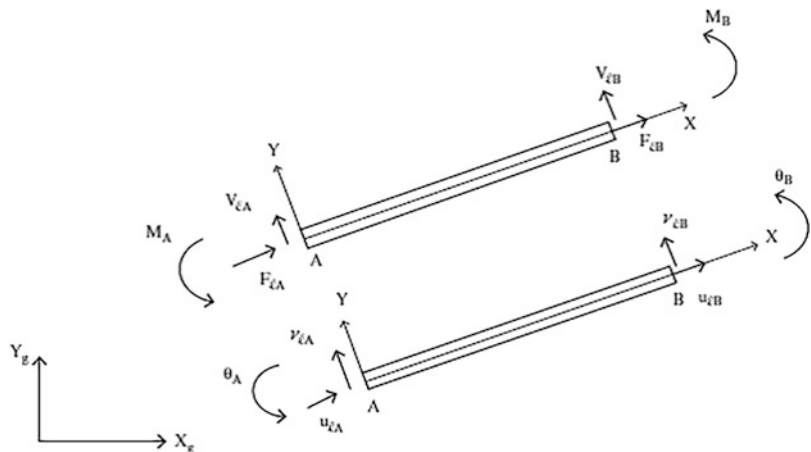
- End Forces

$$\mathbf{P}_{\ell B} = \begin{Bmatrix} F_{\ell B} \\ V_{\ell B} \\ M_B \end{Bmatrix} \quad \mathbf{P}_{\ell A} = \begin{Bmatrix} F_{\ell A} \\ V_{\ell A} \\ M_A \end{Bmatrix} \quad (12.2)$$

Note that the positive sense for moment and rotation is taken as counterclockwise, i.e., from X toward Y .

We derived the complete set of equations relating the end forces and end displacements in Chap. 10 and used a subset of these equations (10.12) to analyze bending of beams and frames. That analysis was approximate in the sense that the axial deformation of the members was neglected. Consequently, the axial forces had to be determined from the force equilibrium conditions. In what follows, we remove this assumption. The resulting analysis is now applicable for both truss and frame type structures. The formulation is now more involved since there are now more unknowns, but this is

Fig. 12.1 End forces and displacements—local member frame—planar behavior



not a problem when a computer is used to solve the equations. The complete set of planar equations for the end actions at B are:

$$\begin{aligned} F_{\ell B} &= \frac{AE}{L}(u_{\ell B} - u_{\ell A}) + F_{\ell B}^F \\ V_{\ell B} &= -\frac{6EI}{L^2}(\theta_B + \theta_A) + \frac{12EI}{L^3}(v_{\ell B} - v_{\ell A}) + V_{\ell B}^F \\ M_B &= \frac{2EI}{L}(2\theta_B + \theta_A) - \frac{6EI}{L^2}(v_{\ell B} - v_{\ell A}) + M_B^F \end{aligned} \quad (12.3)$$

where $F_{\ell B}^F$, $V_{\ell B}^F$, and M_B^F are the fixed end actions generated by the loading applied to the member with the ends fixed. Using the global equilibrium equations for the member, one obtains a similar set of equations for the end actions at A.

$$\begin{aligned} F_{\ell A} &= -\frac{AE}{L}(u_{\ell B} - u_{\ell A}) + F_{\ell A}^F \\ V_{\ell A} &= \frac{6EI}{L^2}(\theta_B + \theta_A) - \frac{12EI}{L^3}(v_{\ell B} - v_{\ell A}) + V_{\ell A}^F \\ M_A &= \frac{2EI}{L}(\theta_B + 2\theta_A) - \frac{6EI}{L^2}(v_{\ell B} - v_{\ell A}) + M_A^F \end{aligned} \quad (12.4)$$

Both sets of (12.3) and (12.4) are restricted to prismatic members, i.e., members with constant cross-sectional properties.

We introduce the matrix notation defined by (12.1) and (12.2) and express the end action equations as

$$\begin{aligned} \mathbf{P}_{\ell B} &= \mathbf{k}_{\ell BB} \mathbf{U}_{\ell B} + \mathbf{k}_{\ell BA} \mathbf{U}_{\ell A} + \mathbf{P}_{\ell B}^F \\ \mathbf{P}_{\ell A} &= \mathbf{k}_{\ell AB} \mathbf{U}_{\ell B} + \mathbf{k}_{\ell AA} \mathbf{U}_{\ell A} + \mathbf{P}_{\ell A}^F \end{aligned} \quad (12.5)$$

where the expanded form of the individual stiffness and force matrices are

$$\begin{aligned} \mathbf{k}_{\ell BB} &= \begin{bmatrix} \frac{AE}{L} & 0 & 0 \\ 0 & \frac{12EI}{L^3} & -\frac{6EI}{L^2} \\ 0 & -\frac{6EI}{L^2} & \frac{4EI}{L} \end{bmatrix} & \mathbf{k}_{\ell BA} &= \begin{bmatrix} -\frac{AE}{L} & 0 & 0 \\ 0 & -\frac{12EI}{L^3} & -\frac{6EI}{L^2} \\ 0 & \frac{6EI}{L^2} & \frac{2EI}{L} \end{bmatrix} & \mathbf{P}_{\ell B}^F &= \begin{Bmatrix} F_{\ell B}^F \\ V_{\ell B}^F \\ M_B^F \end{Bmatrix} \\ \mathbf{k}_{\ell AA} &= \begin{bmatrix} \frac{AE}{L} & 0 & 0 \\ 0 & \frac{12EI}{L^3} & \frac{6EI}{L^2} \\ 0 & \frac{6EI}{L^2} & \frac{4EI}{L} \end{bmatrix} & \mathbf{k}_{\ell AB} &= \begin{bmatrix} -\frac{AE}{L} & 0 & 0 \\ 0 & -\frac{12EI}{L^3} & \frac{6EI}{L^2} \\ 0 & -\frac{6EI}{L^2} & \frac{2EI}{L} \end{bmatrix} & \mathbf{P}_{\ell A}^F &= \begin{Bmatrix} F_{\ell A}^F \\ V_{\ell A}^F \\ M_A^F \end{Bmatrix} \end{aligned} \quad (12.6)$$

The matrices $\mathbf{k}_{\ell BB}$, $\mathbf{k}_{\ell AA}$, $\mathbf{k}_{\ell BA}$, $\mathbf{k}_{\ell AB}$ are called the member stiffness matrices referred to the local member frame. Note that once the end displacements $\mathbf{U}_{\ell B}$ and $\mathbf{U}_{\ell A}$ are known, one can determine the end actions $\mathbf{P}_{\ell B}$ and $\mathbf{P}_{\ell A}$. The member stiffness matrices are functions of the member properties (A, I, L) and the material property E . The fixed end actions ($\mathbf{P}_{\ell B}^F$ and $\mathbf{P}_{\ell A}^F$) depend on the external loading applied to the member.

Example 12.1: The Fixed End Actions

Given: The linearly loaded beam shown in Fig. E12.1.

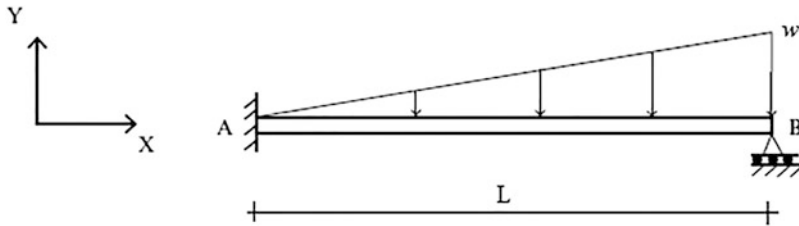
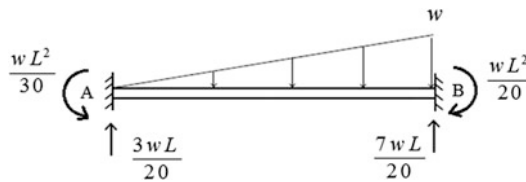


Fig. E12.1

Determine: The fixed end forces.

Solution: The fixed end forces are determined using the Force Method described in Chap. 9 (Table 9.1).



$$\mathbf{P}_{\ell_B}^F = \begin{Bmatrix} 0 \\ \frac{7wL}{20} \\ -\frac{wL^2}{20} \end{Bmatrix} \quad \mathbf{P}_{\ell_A}^F = \begin{Bmatrix} 0 \\ \frac{3wL}{20} \\ \frac{wL^2}{30} \end{Bmatrix}$$

12.4 Local and Global Reference Frames

Consider the structure shown in Fig. 12.2. There are five nodes and four members. We number these artifacts consecutively starting with one. The local X -axis for a member is selected to coincide with the longitudinal axis, as indicated on the figure; the Y -axis is taken to be 90° counterclockwise from the X -axis. The member equations presented in the previous section involve force and displacement quantities referred to the *local member* frames. Figure 12.3 illustrates the situation for node two. The end displacements are related to the nodal displacements. However, one must first select a *common reference frame* for the nodal displacements. We choose the global frame shown in Fig. 12.2. Once the local frames are specified with respect to the global frame (X_g, Y_g), one can derive the relationships between the displacement and force variables.

Consider the reference frames shown in Fig. 12.4. Starting with quantities referred to the local member frame, we project them on the global directions using trigonometric relations. One obtains

$$\begin{aligned} u &= u_l \cos \alpha - v_l \sin \alpha \\ v &= u_l \sin \alpha + v_l \cos \alpha \end{aligned} \quad (12.7)$$

Fig. 12.2 Local and global reference frames

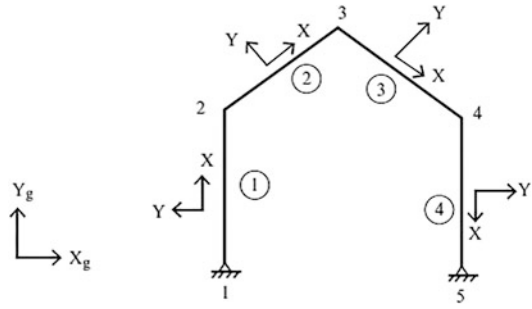


Fig. 12.3 Member and nodal frames at node 1

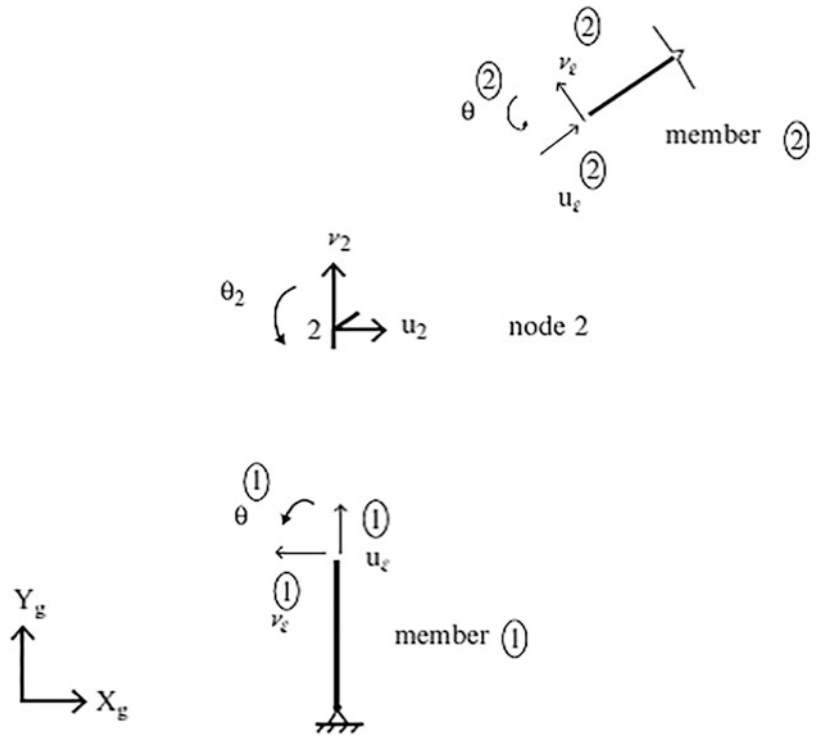
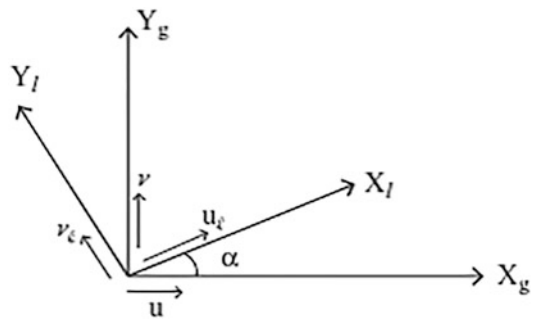


Fig. 12.4 Rotation of axes



Introducing matrix notation, we write $\mathbf{U} = \begin{Bmatrix} u \\ v \\ \theta \end{Bmatrix}$ and $\mathbf{U}_\ell = \begin{Bmatrix} u_\ell \\ v_\ell \\ \theta \end{Bmatrix}$ and express (12.7) as a matrix product.

$$\mathbf{U} = \mathbf{R}_{lg}\mathbf{U}_\ell \tag{12.8}$$

where

$$\mathbf{R}_{lg} = \begin{bmatrix} \cos \alpha & -\sin \alpha & 0 \\ \sin \alpha & \cos \alpha & 0 \\ 0 & 0 & 1 \end{bmatrix}$$

We interpret \mathbf{R}_{lg} as a rotation transformation matrix from the local to the global frame. The transformation from the global to the local frame is expressed in a similar way,

$$\mathbf{U}_l = \mathbf{R}_{gl}\mathbf{U} \tag{12.9}$$

where \mathbf{R}_{gl} has the following form:

$$\mathbf{R}_{gl} = \begin{bmatrix} \cos \alpha & \sin \alpha & 0 \\ -\sin \alpha & \cos \alpha & 0 \\ 0 & 0 & 1 \end{bmatrix}$$

Comparing these two forms for \mathbf{R} , we observe that one is both the inverse and the transpose of the other.

$$\mathbf{R}_{gl} = (\mathbf{R}_{lg})^T = (\mathbf{R}_{lg})^{-1} \tag{12.10}$$

A matrix having this property is said to be orthogonal.

Example 12.2 Rotation Matrices

Given: The structure defined in Fig. E12.2a.

Determine: The rotation matrices for the members.

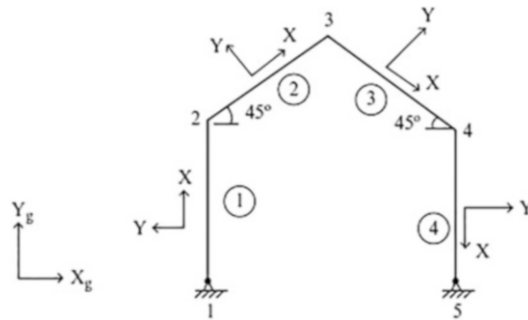


Fig. E12.2a

Solution:

Member (1)	$\alpha = +90^\circ$ $\mathbf{R}_{lg} = \begin{bmatrix} 0 & -1 & 0 \\ 1 & 0 & 0 \\ 0 & 0 & 1 \end{bmatrix}$ $\mathbf{R}_{gl} = \begin{bmatrix} 0 & 1 & 0 \\ -1 & 0 & 0 \\ 0 & 0 & 1 \end{bmatrix}$
Member (2)	$\alpha = +45^\circ$ $\mathbf{R}_{lg} = \begin{bmatrix} 0.707 & -0.707 & 0 \\ 0.707 & 0.707 & 0 \\ 0 & 0 & 1 \end{bmatrix}$
Member (3)	$\alpha = -45^\circ$ $\mathbf{R}_{lg} = \begin{bmatrix} 0.707 & 0.707 & 0 \\ -0.707 & 0.707 & 0 \\ 0 & 0 & 1 \end{bmatrix}$
Member (4)	$\alpha = -90^\circ$ $\mathbf{R}_{lg} = \begin{bmatrix} 0 & 1 & 0 \\ -1 & 0 & 0 \\ 0 & 0 & 1 \end{bmatrix}$

We suppose the external nodal forces are referred to the global frame. Then, we need to transform the member end forces from the member frame to the global frame. End forces transform in a similar way as displacements, i.e.,

$$\mathbf{P} = \mathbf{R}_{lg} \mathbf{P}_\ell \quad (12.11)$$

Operating on the member matrix equations defined by (12.5) and noting (12.9) and (12.11), the “transformed” equations expressed in terms of quantities referred to the global frame take the following form:

$$\begin{aligned} \mathbf{P}_B &= \mathbf{k}_{BB} \mathbf{U}_B + \mathbf{k}_{BA} \mathbf{U}_A + \mathbf{P}_B^F \\ \mathbf{P}_A &= \mathbf{k}_{AB} \mathbf{U}_B + \mathbf{k}_{AA} \mathbf{U}_A + \mathbf{P}_A^F \end{aligned} \quad (12.12)$$

where the member stiffness and end action matrices referred to the global frames are defined by

$$\begin{aligned} \mathbf{k}_{BB} &= \mathbf{R}_{lg} \mathbf{k}_{\ell BB} (\mathbf{R}_{lg})^T & \mathbf{k}_{BA} &= \mathbf{R}_{lg} \mathbf{k}_{\ell BA} (\mathbf{R}_{lg})^T \\ \mathbf{k}_{AA} &= \mathbf{R}_{lg} \mathbf{k}_{\ell AA} (\mathbf{R}_{lg})^T & \mathbf{k}_{AB} &= \mathbf{R}_{lg} \mathbf{k}_{\ell AB} (\mathbf{R}_{lg})^T \\ \mathbf{P}_B^F &= \mathbf{R}_{lg} \mathbf{P}_{\ell B}^F & \mathbf{P}_A^F &= \mathbf{R}_{lg} \mathbf{P}_{\ell A}^F \end{aligned} \quad (12.13)$$

Given \mathbf{R}_{lg} , one operates, according to (12.13), on the “local” stiffness matrices given by (12.6) to obtain their global forms.

12.5 Nodal Force Equilibrium Equations

The force equilibrium equations for a node involve the end actions for those members which are incident on the node. We need to distinguish between positive and negative incidence, i.e., whether the positive or negative end of the member is incident on the node. Up to this point, we have used subscript B to denote the *positive* end, and A for the *negative* end of a member. To allow for automating the process of assembling the nodal equilibrium equations and computing the member end forces given the member end displacements, we introduce a numbering scheme for the members and the associated end nodes.

We number the members consecutively from 1 to N_m , where N_m is the total number of members. We also define

$$\begin{aligned} n_+ &= \text{node number located at the positive end of member } m \\ n_- &= \text{node number located at the negative end of member } m \end{aligned} \quad (12.14)$$

The connectivity of the members and nodes is defined by a table, which lists for each member the node numbers corresponding to the positive end and negative end. The following table is the member–node incidence table for the structure defined in Fig. 12.2.

Member–node incidence table

Member m	Negative node n_-	Positive node n_+
(1)	1	2
(2)	2	3
(3)	3	4
(4)	4	5

The incidence table provides the “instructions” for assembling the nodal equations. We will illustrate this feature later.

Example 12.3: Construction of a Member–Node Incidence Table

Given: The structure shown in Fig. E12.3a.

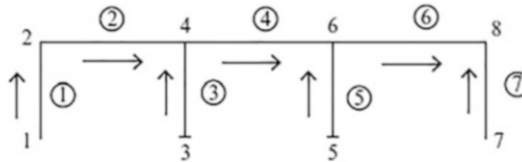


Fig. E12.3a

Determine: The member–node incidence table.

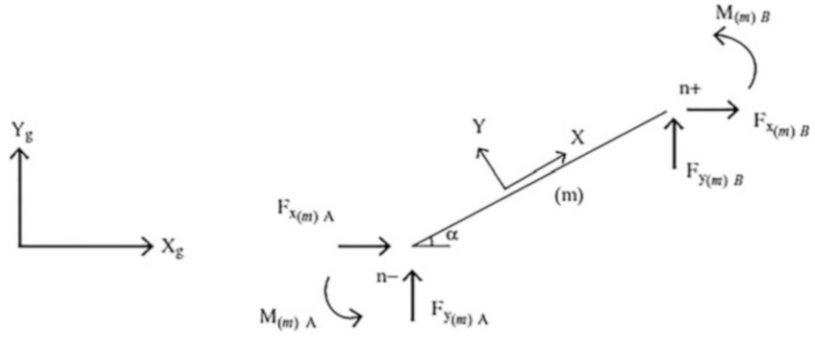
Solution: There are seven members and eight nodes. One loops over the members and lists the node numbers at the positive and negative ends of each member (the positive sense for a member is indicated with an arrow). The result is listed below.

Member–node incidence table

Member m	Negative node n_-	Positive node n_+
(1)	1	2
(2)	2	4
(3)	3	4
(4)	4	6
(5)	5	6
(6)	6	8
(7)	7	8

Using the notation introduced above and noting (12.12), we denote the global end actions for member m with a subscript (m).

Fig. 12.5 Member end actions referred to global frame

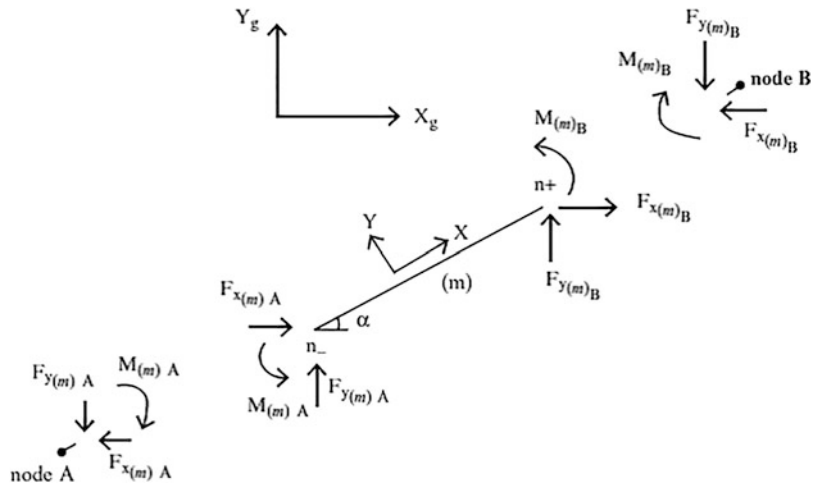


$$\begin{aligned} \mathbf{P}_{(m)B} &= \mathbf{k}_{(m)BB} \mathbf{U}_{(m)B} + \mathbf{k}_{(m)BA} \mathbf{U}_{(m)A} + \mathbf{P}_{(m)B}^F \\ \mathbf{P}_{(m)A} &= \mathbf{k}_{(m)AB} \mathbf{U}_{(m)B} + \mathbf{k}_{(m)AA} \mathbf{U}_{(m)A} + \mathbf{P}_{(m)A}^F \end{aligned} \quad (12.15)$$

The expanded forms of the matrices in (12.15) referred to the global frame follow from (12.13). We assume member m is oriented at the angle, α (see Fig. 12.5).

$$\begin{aligned} \mathbf{k}_{(m)AA} &= \begin{bmatrix} \left(\frac{AE}{L} \cos^2 \alpha + \frac{12EI}{L^3} \sin^2 \alpha \right) & \left(\frac{AE}{L} - \frac{12EI}{L^3} \right) \sin \alpha \cos \alpha & -\frac{6EI}{L^2} \sin \alpha \\ \left(\frac{AE}{L} - \frac{12EI}{L^3} \right) \sin \alpha \cos \alpha & \left(\frac{AE}{L} \sin^2 \alpha + \frac{12EI}{L^3} \cos^2 \alpha \right) & \frac{6EI}{L^2} \cos \alpha \\ -\frac{6EI}{L^2} \sin \alpha & \frac{6EI}{L^2} \cos \alpha & \frac{4EI}{L} \end{bmatrix} \\ \mathbf{k}_{(m)AB} &= \begin{bmatrix} -\left(\frac{AE}{L} \cos^2 \alpha + \frac{12EI}{L^3} \sin^2 \alpha \right) & -\left(\frac{AE}{L} - \frac{12EI}{L^3} \right) \sin \alpha \cos \alpha & -\frac{6EI}{L^2} \sin \alpha \\ -\left(\frac{AE}{L} - \frac{12EI}{L^3} \right) \sin \alpha \cos \alpha & -\left(\frac{AE}{L} \sin^2 \alpha + \frac{12EI}{L^3} \cos^2 \alpha \right) & \frac{6EI}{L^2} \cos \alpha \\ \frac{6EI}{L^2} \sin \alpha & -\frac{6EI}{L^2} \cos \alpha & \frac{2EI}{L} \end{bmatrix} \\ \mathbf{k}_{(m)BA} &= \begin{bmatrix} -\left(\frac{AE}{L} \cos^2 \alpha + \frac{12EI}{L^3} \sin^2 \alpha \right) & -\left(\frac{AE}{L} - \frac{12EI}{L^3} \right) \sin \alpha \cos \alpha & \frac{6EI}{L^2} \sin \alpha \\ -\frac{AE}{L} - \frac{12EI}{L^3} \sin \alpha \cos \alpha & -\left(\frac{AE}{L} \sin^2 \alpha + \frac{12EI}{L^3} \cos^2 \alpha \right) & -\frac{6EI}{L^2} \cos \alpha \\ -\frac{6EI}{L^2} \sin \alpha & \frac{6EI}{L^2} \cos \alpha & \frac{2EI}{L} \end{bmatrix} \\ \mathbf{k}_{(m)BB} &= \begin{bmatrix} \left(\frac{AE}{L} \cos^2 \alpha + \frac{12EI}{L^3} \sin^2 \alpha \right) & \left(\frac{AE}{L} - \frac{12EI}{L^3} \right) \sin \alpha \cos \alpha & \frac{6EI}{L^2} \sin \alpha \\ \left(\frac{AE}{L} - \frac{12EI}{L^3} \right) \sin \alpha \cos \alpha & \left(\frac{AE}{L} \sin^2 \alpha + \frac{12EI}{L^3} \cos^2 \alpha \right) & -\frac{6EI}{L^2} \cos \alpha \\ \frac{6EI}{L^2} \sin \alpha & -\frac{6EI}{L^2} \cos \alpha & \frac{4EI}{L} \end{bmatrix} \end{aligned} \quad (12.16)$$

Fig. 12.6 Member reaction forces



$$\begin{aligned}
 U_{(m)B} &= \begin{Bmatrix} u_{(m)B} \\ v_{(m)B} \\ \theta_{(m)B} \end{Bmatrix} & U_{(m)A} &= \begin{Bmatrix} u_{(m)A} \\ v_{(m)A} \\ \theta_{(m)A} \end{Bmatrix} \\
 P_{(m)B} &= \begin{Bmatrix} F_{x(m)B} \\ F_{y(m)B} \\ M_{(m)B} \end{Bmatrix} & P_{(m)A} &= \begin{Bmatrix} F_{x(m)A} \\ F_{y(m)A} \\ M_{(m)A} \end{Bmatrix} \\
 P_{(m)B}^F &= \begin{Bmatrix} F_{x(m)B}^F \\ F_{y(m)B}^F \\ M_{(m)B}^F \end{Bmatrix} & P_{(m)A}^F &= \begin{Bmatrix} F_{x(m)A}^F \\ F_{y(m)A}^F \\ M_{(m)A}^F \end{Bmatrix}
 \end{aligned} \tag{12.17}$$

Note that all terms in (12.16) and (12.17) are referred to the *global reference frame*.

Figure 12.6 shows the forces (end actions) acting on member AB and the nodes located at each end. The nodal forces are $-\mathbf{P}_{(m)A}$ and $-\mathbf{P}_{(m)B}$, i.e., their sense is opposite to the actual end actions.

To generate the force equilibrium equations for a node, one sums up the applied external forces and the member reaction forces associated with the node. We express the matrix equilibrium equation for node j as

$$\mathbf{P}_{Ej} + \sum_{n_+=j} (-\mathbf{P}_{(m)B}) + \sum_{n_-=j} (-\mathbf{P}_{(m)A}) = 0 \tag{12.18}$$

where \mathbf{P}_{Ej} is the applied external force vector for node j and the Σ is for those members having one end incident on node j . Noting (12.15), we observe that the equilibrium equation for node j involves the displacements of those nodes which are connected to node j by members. We utilize this observation later.

We generate the complete set of nodal equilibrium equations by evaluating (12.18) for all the nodes. It is convenient to work with matrices expressed in a form that is partitioned according to the “natural” size of the nodal vectors. For a planar frame, the size of the nodal vectors is 3×1 . For a plane truss, the size is 2×1 . For a horizontal beam, the size is 2×1 . We suppose there are Nn

nodes. Then, there will be Nn matrix equations similar in form to (12.18). We express the total set of equations as a single matrix equation,

$$\mathbf{P}_E = \mathbf{K}\mathbf{U} + \mathbf{P}_I \quad (12.19)$$

where the partitioned forms of the individual matrices are

$$\mathbf{U} = \text{system displacement vector} = \begin{Bmatrix} \mathbf{U}_1 \\ \mathbf{U}_2 \\ \vdots \\ \mathbf{U}_{N_n} \end{Bmatrix}$$

$$\mathbf{P}_E = \text{external nodal force vector} = \begin{Bmatrix} \mathbf{P}_{E1} \\ \mathbf{P}_{E2} \\ \vdots \\ \mathbf{P}_{EN_n} \end{Bmatrix}$$

$$\mathbf{P}_I = \text{nodal force vector due to member fixed end actions} = \begin{Bmatrix} \mathbf{P}_{I1}^F \\ \mathbf{P}_{I2}^F \\ \vdots \\ \mathbf{P}_{IN_n}^F \end{Bmatrix}$$

$$\mathbf{K} = \text{system stiffness matrix} = [\mathbf{K}_{ij}] \quad i, j = 1, 2, \dots, N_n$$

Note that the system stiffness matrix, \mathbf{K} , has Nn partitioned rows and columns.

We generate the partitioned forms of the system stiffness matrix and internal nodal force vector by looping over the members and noting (12.18). The information for n_+ and n_- for a given member m is provided by the member–node incidence table and leads to the following assembly algorithms for $m = 1, 2, \dots, N_m$:

For \mathbf{K} :

$$\begin{aligned} \mathbf{k}_{(m)AA} & \text{ in row } n_-, \text{ column } n_- \\ \mathbf{k}_{(m)AB} & \text{ in row } n_-, \text{ column } n_+ \\ \mathbf{k}_{(m)BA} & \text{ in row } n_+, \text{ column } n_- \\ \mathbf{k}_{(m)B} & \text{ in row } n_+, \text{ column } n_+ \end{aligned} \quad (12.20)$$

For \mathbf{P}_I :

$$\begin{aligned} \mathbf{P}_{(m)A}^F & \text{ in row } n_- \\ \mathbf{P}_{(m)B}^F & \text{ in row } n_+ \end{aligned} \quad (12.21)$$

This assembly process is called the “Direct Stiffness Method.” It is generally employed by most commercial analysis software codes since it is relatively straightforward to implement. We can deduce from the assembly algorithm that the system stiffness matrix is square and symmetrical. The nonzero elements tend to be clustered in a band centered on the diagonal.

Example 12.4: Assembly Process

Given: The plane frame shown in Fig. E12.4a.

Determine: The system stiffness and nodal force matrices.

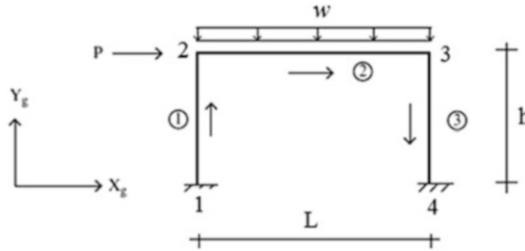


Fig. E12.4a

Solution: We first number the members and nodes as indicated in Fig. E12.4a, and then generate the member–node incidence table listed below.

Member–node incidence table

Member m	Negative node n_-	Positive node n_+
(1)	1	2
(2)	2	3
(3)	3	4

Using the member–node incident table, we replace the member end force and displacement matrices with

$$\begin{aligned} \mathbf{U}_B &\Rightarrow \mathbf{U}_{n_+} & \mathbf{P}_B &\Rightarrow \mathbf{P}_{n_+} \\ \mathbf{U}_A &\Rightarrow \mathbf{U}_{n_-} & \mathbf{P}_A &\Rightarrow \mathbf{P}_{n_-} \end{aligned}$$

In (12.15), the operation is carried out for each member. The resulting expressions for the end forces expressed in terms of the nodal displacements are

$$\begin{aligned} \mathbf{P}_{(1)2} &= \mathbf{k}_{(1)BB} \mathbf{U}_2 + \mathbf{k}_{(1)BA} \mathbf{U}_1 + \mathbf{P}_{(1)B}^F \\ \mathbf{P}_{(1)1} &= \mathbf{k}_{(1)AB} \mathbf{U}_2 + \mathbf{k}_{(1)AA} \mathbf{U}_1 + \mathbf{P}_{(1)A}^F \end{aligned}$$

$$\begin{aligned} \mathbf{P}_{(2)3} &= \mathbf{k}_{(2)BB} \mathbf{U}_3 + \mathbf{k}_{(2)BA} \mathbf{U}_2 + \mathbf{P}_{(2)B}^F \\ \mathbf{P}_{(2)2} &= \mathbf{k}_{(2)AB} \mathbf{U}_3 + \mathbf{k}_{(2)AA} \mathbf{U}_2 + \mathbf{P}_{(2)A}^F \end{aligned}$$

$$\begin{aligned} \mathbf{P}_{(3)4} &= \mathbf{k}_{(3)BB} \mathbf{U}_4 + \mathbf{k}_{(3)BA} \mathbf{U}_3 + \mathbf{P}_{(3)B}^F \\ \mathbf{P}_{(3)3} &= \mathbf{k}_{(3)AB} \mathbf{U}_4 + \mathbf{k}_{(3)AA} \mathbf{U}_3 + \mathbf{P}_{(3)A}^F \end{aligned}$$

Next, we equate the external nodal force to the sum of the member forces at each node. This step leads to the nodal force equilibrium equations (see (12.18)).

$$\begin{aligned} \mathbf{P}_{E1} &= \mathbf{P}_{(1)1} \\ \mathbf{P}_{E2} &= \mathbf{P}_{(2)2} + \mathbf{P}_{(1)2} \\ \mathbf{P}_{E3} &= \mathbf{P}_{(2)3} + \mathbf{P}_{(3)3} \\ \mathbf{P}_{E4} &= \mathbf{P}_{(3)4} \end{aligned}$$

Substituting for the end forces expressed in terms of the nodal displacements, these equations expand to

$$\begin{aligned}\mathbf{P}_{E1} &= \mathbf{k}_{(1)AA}\mathbf{U}_1 + \mathbf{k}_{(1)AB}\mathbf{U}_2 + \mathbf{P}_{(1)A}^F \\ \mathbf{P}_{E2} &= \mathbf{k}_{(1)BA}\mathbf{U}_1 + (\mathbf{k}_{(1)BB} + \mathbf{k}_{(2)AA})\mathbf{U}_2 + \mathbf{k}_{(2)AB}\mathbf{U}_3 + \mathbf{P}_{(2)A}^F + \mathbf{P}_{(1)B}^F \\ \mathbf{P}_{E3} &= \mathbf{k}_{(2)BA}\mathbf{U}_2 + (\mathbf{k}_{(2)BB} + \mathbf{k}_{(3)AA})\mathbf{U}_3 + \mathbf{k}_{(3)AB}\mathbf{U}_4 + \mathbf{P}_{(3)A}^F + \mathbf{P}_{(2)B}^F \\ \mathbf{P}_{E4} &= \mathbf{k}_{(3)BA}\mathbf{U}_3 + \mathbf{k}_{(3)BB}\mathbf{U}_4 + \mathbf{P}_{(3)B}^F\end{aligned}$$

Lastly, we write these equations as a single equation in terms of “system” matrices [see (12.19)]. The forms of the system matrices are listed below.

$$\mathbf{U} = \begin{Bmatrix} \mathbf{U}_1 \\ \mathbf{U}_2 \\ \mathbf{U}_3 \\ \mathbf{U}_4 \end{Bmatrix} \quad \mathbf{P}_E = \begin{Bmatrix} \mathbf{P}_{E1} \\ \mathbf{P}_{E2} \\ \mathbf{P}_{E3} \\ \mathbf{P}_{E4} \end{Bmatrix} \quad \mathbf{P}_I = \begin{Bmatrix} \mathbf{P}_{(1)A}^F \\ (\mathbf{P}_{(1)B}^F + \mathbf{P}_{(2)A}^F) \\ (\mathbf{P}_{(2)B}^F + \mathbf{P}_{(3)A}^F) \\ \mathbf{P}_{(3)B}^F \end{Bmatrix}$$

$$\mathbf{K} = \begin{bmatrix} \mathbf{k}_{(1)AA} & \mathbf{k}_{(1)AB} & 0 & 0 \\ \mathbf{k}_{(1)BA} & (\mathbf{k}_{(1)BB} + \mathbf{k}_{(2)AA}) & \mathbf{k}_{(2)AB} & 0 \\ 0 & \mathbf{k}_{(2)BA} & (\mathbf{k}_{(2)BB} + \mathbf{k}_{(3)AA}) & \mathbf{k}_{(3)AB} \\ 0 & 0 & \mathbf{k}_{(3)BA} & \mathbf{k}_{(3)BB} \end{bmatrix}$$

There are four nodes in this example, so the partitioned form of \mathbf{K} is 4×4 . The expanded size of \mathbf{K} for this two-dimensional plane frame will be 12×12 since there are three variables per node.

In this example, we chose to list all the equations first and then combine them in a single “system” equation. Normally, one would apply the algorithms defined by (12.20) and (12.21) and directly assemble the system matrices.

12.6 Introduction of Nodal Supports

Introducing a support at a node corresponds to prescribing the value of certain nodal displacements. For example, a hinge prevents translation in two orthogonal directions. Full fixity eliminates both translation and rotation at a node. When supports are introduced, the number of displacement unknowns is decreased by the number of displacement restraints. However, each displacement constraint produces an unknown reaction so that the “total” number of unknowns (nodal displacements and nodal reaction forces) remains constant. In order to determine the unknown displacements, we work with a reduced set of equilibrium equations. We illustrate this process with the following example.

Example 12.5: Example of Fully Fixed Supports

Given: The structure defined in Fig. E12.5a. Suppose nodes one and four are fully fixed.

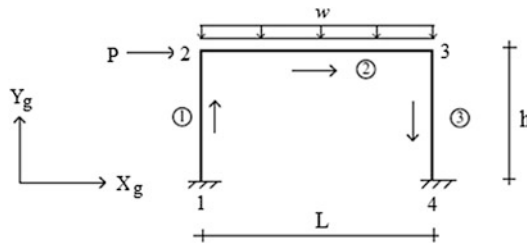


Fig. E12.5a

Determine: The reduced system matrices.

Solution: The system matrices are presented in Example 12.4. We start with the complete set of nodal force equilibrium equations generated in the previous example.

$$\begin{aligned}\mathbf{P}_{E1} &= \mathbf{k}_{(1)AA}\mathbf{U}_1 + \mathbf{k}_{(1)AB}\mathbf{U}_2 + \mathbf{P}_{(1)A}^F \\ \mathbf{P}_{E2} &= \mathbf{k}_{(1)BA}\mathbf{U}_1 + (\mathbf{k}_{(1)BB} + \mathbf{k}_{(2)AA})\mathbf{U}_2 + \mathbf{k}_{(2)AB}\mathbf{U}_3 + \mathbf{P}_{(2)A}^F + \mathbf{P}_{(1)B}^F \\ \mathbf{P}_{E3} &= \mathbf{k}_{(2)BA}\mathbf{U}_2 + (\mathbf{k}_{(2)BB} + \mathbf{k}_{(3)AA})\mathbf{U}_3 + \mathbf{k}_{(3)AB}\mathbf{U}_4 + \mathbf{P}_{(3)A}^F + \mathbf{P}_{(2)B}^F \\ \mathbf{P}_{E4} &= \mathbf{k}_{(3)BA}\mathbf{U}_3 + \mathbf{k}_{(3)BB}\mathbf{U}_4 + \mathbf{P}_{(3)B}^F\end{aligned}$$

Nodes 1 and 4 are fully fixed. The external nodal forces \mathbf{P}_{E1} and \mathbf{P}_{E2} represent the reactions at these nodes. We set $\mathbf{U}_1 = \mathbf{U}_4 = 0$ and rearrange the order of the equations so that \mathbf{P}_{E1} and \mathbf{P}_{E4} are last. This step leads to two sets of equations,

$$\begin{aligned}\mathbf{P}_{E2} &= (\mathbf{k}_{(1)BB} + \mathbf{k}_{(2)AA})\mathbf{U}_2 + \mathbf{k}_{(2)AB}\mathbf{U}_3 + \mathbf{P}_{(2)A}^F + \mathbf{P}_{(1)B}^F \\ \mathbf{P}_{E3} &= \mathbf{k}_{(2)BA}\mathbf{U}_2 + (\mathbf{k}_{(2)BB} + \mathbf{k}_{(3)AA})\mathbf{U}_3 + \mathbf{P}_{(3)A}^F + \mathbf{P}_{(2)B}^F \\ &\Downarrow \\ \begin{Bmatrix} \mathbf{P}_{E2} \\ \mathbf{P}_{E3} \end{Bmatrix} &= \begin{bmatrix} (\mathbf{k}_{(1)BB} + \mathbf{k}_{(2)AA}) & \mathbf{k}_{(2)AB} \\ \mathbf{k}_{(2)BA} & (\mathbf{k}_{(2)BB} + \mathbf{k}_{(3)AA}) \end{bmatrix} \begin{Bmatrix} \mathbf{U}_2 \\ \mathbf{U}_3 \end{Bmatrix} + \begin{Bmatrix} \mathbf{P}_{(2)A}^F + \mathbf{P}_{(1)B}^F \\ \mathbf{P}_{(3)A}^F + \mathbf{P}_{(2)B}^F \end{Bmatrix}\end{aligned}$$

and

$$\begin{aligned}\mathbf{P}_{E1} &= \mathbf{k}_{(1)AB}\mathbf{U}_2 + \mathbf{P}_{(1)A}^F \\ \mathbf{P}_{E4} &= \mathbf{k}_{(3)BA}\mathbf{U}_3 + \mathbf{P}_{(3)B}^F \\ &\Downarrow \\ \begin{Bmatrix} \mathbf{P}_{E1} \\ \mathbf{P}_{E4} \end{Bmatrix} &= \begin{bmatrix} \mathbf{k}_{(1)AB} & 0 \\ 0 & \mathbf{k}_{(3)BA} \end{bmatrix} \begin{Bmatrix} \mathbf{U}_2 \\ \mathbf{U}_3 \end{Bmatrix} + \begin{Bmatrix} \mathbf{P}_{(1)A}^F \\ \mathbf{P}_{(3)B}^F \end{Bmatrix}\end{aligned}$$

We solve the first set for \mathbf{U}_2 and \mathbf{U}_3 . Then, we use these displacements to determine the reactions \mathbf{P}_{E1} and \mathbf{P}_{E4} with the second set of equations. Note that the total number of unknowns remains the same when displacement constraint is introduced.

12.6.1 Systematic Approach

The systematic approach for introducing displacement constraints involves rearranging the system displacement vector \mathbf{U} into two segments and also rearranging the rows and columns of \mathbf{P} and \mathbf{K} consistent with this reordering of \mathbf{U} . We write the rearranged system matrices as

$$\mathbf{K} \rightarrow \mathbf{K}' = \begin{pmatrix} \mathbf{K}'_{11} & | & \mathbf{K}'_{12} \\ \hline & | & \\ \mathbf{K}'_{21} & | & \mathbf{K}'_{22} \end{pmatrix} \quad (12.23)$$

$$\mathbf{U} \rightarrow \begin{Bmatrix} \mathbf{U}' \\ \mathbf{U}'' \end{Bmatrix} \quad \mathbf{P}_E \rightarrow \begin{Bmatrix} \mathbf{P}'_E \\ \mathbf{P}''_E \end{Bmatrix} \quad \mathbf{P}_I \rightarrow \begin{Bmatrix} \mathbf{P}'_I \\ \mathbf{P}''_I \end{Bmatrix}$$

where \mathbf{U}' contains the *unknown* displacements, \mathbf{U}'' contains the *prescribed* support movements, \mathbf{P}'_E contains the *prescribed* joint loads, and \mathbf{P}''_E contains the *unknown forces* (reactions).

With this reordering, the system equation takes the following form:

$$\begin{Bmatrix} \mathbf{P}'_E \\ \hline \mathbf{P}''_E \end{Bmatrix} = \begin{pmatrix} \mathbf{K}'_{11} & | & \mathbf{K}'_{12} \\ \hline & | & \\ \mathbf{K}'_{21} & | & \mathbf{K}'_{22} \end{pmatrix} \begin{Bmatrix} \mathbf{U}' \\ \hline \mathbf{U}'' \end{Bmatrix} + \begin{Bmatrix} \mathbf{P}'_I \\ \hline \mathbf{P}''_I \end{Bmatrix} \quad (12.24)$$

Expanding the matrix product results in two matrix equations

$$\begin{aligned} \mathbf{P}'_E &= \mathbf{K}'_{11}\mathbf{U}' + \mathbf{K}'_{12}\mathbf{U}'' + \mathbf{P}'_I \\ \mathbf{P}''_E &= \mathbf{K}'_{21}\mathbf{U}' + \mathbf{K}'_{22}\mathbf{U}'' + \mathbf{P}''_I \end{aligned} \quad (12.25)$$

We solve the first equation for \mathbf{U}'

$$\mathbf{U}' = (\mathbf{K}'_{11})^{-1} (\mathbf{P}'_E - \mathbf{K}'_{12}\mathbf{U}'' - \mathbf{P}'_I) \quad (12.26)$$

Note that the prescribed support movements are converted to equivalent nodal forces. Given \mathbf{U}' , we use the second equation in (12.25) to determine the reaction forces. This step involves only matrix multiplication. With this approach, one can deal separately with the nodal loads, member loads, and support movements.

Expanding the right hand side of (12.26) leads to solutions due to the different loading conditions

External joint loads only: ($\mathbf{P}'_E \neq 0, \mathbf{P}'_I = 0, \mathbf{P}''_I = 0, \mathbf{U}'' = 0$)

$$\begin{aligned} \mathbf{U}' &= (\mathbf{K}'_{11})^{-1} (\mathbf{P}'_E) \\ \mathbf{P}''_E &= \mathbf{K}'_{21}\mathbf{U}' \end{aligned}$$

Support settlements only: ($\mathbf{P}'_E = 0, \mathbf{P}'_I = 0, \mathbf{P}''_I \neq 0, \mathbf{U}'' \neq 0$)

$$\begin{aligned} \mathbf{U}' &= (\mathbf{K}'_{11})^{-1} (-\mathbf{K}'_{12}\mathbf{U}'' - \mathbf{P}'_I) \\ \mathbf{P}''_E &= \mathbf{K}'_{21}\mathbf{U}' + \mathbf{K}'_{22}\mathbf{U}'' \end{aligned}$$

Member fixed end actions only: ($\mathbf{P}'_E = 0, \mathbf{P}'_I \neq 0, \mathbf{P}''_I \neq 0, \mathbf{U}'' = 0$)

$$\begin{aligned} \mathbf{U}' &= (\mathbf{K}'_{11})^{-1} (-\mathbf{P}'_I) \\ \mathbf{P}''_E &= \mathbf{K}'_{21}\mathbf{U}' + \mathbf{P}''_I \end{aligned}$$

Lastly, we determine the end member forces in the global coordinate frame and then transform them to the local frame. The operations for member m are

$$\begin{aligned}
 \mathbf{P}^{(m)B} &= \mathbf{k}^{(m)BB} \mathbf{U}_{n^+} + \mathbf{k}^{(m)BA} \mathbf{U}_{n^-} + \mathbf{P}^{(m)B}_F \\
 \mathbf{P}^{(m)A} &= \mathbf{k}^{(m)AB} \mathbf{U}_{n^+} + \mathbf{k}^{(m)AA} \mathbf{U}_{n^-} + \mathbf{P}^{(m)A}_F \\
 \mathbf{P}^{\ell(m)B} &= \mathbf{R}_{g\ell} \mathbf{P}^{(m)B} \\
 \mathbf{P}^{\ell(m)A} &= \mathbf{R}_{g\ell} \mathbf{P}^{(m)A}
 \end{aligned}
 \tag{12.27}$$

Example 12.6 Support Movement

Given: The structure defined in Fig. E12.6a. Consider nodes 1 and 4 to experience support settlements of δ_1 and δ_4 .

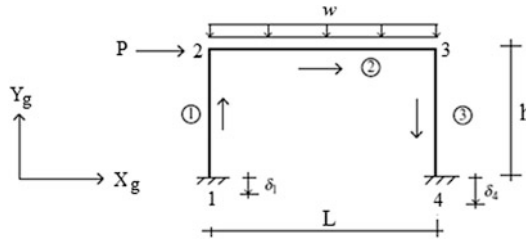


Fig. E12.6a

Determine: The rearranged system matrices

Solution: The system matrices are presented in Example 12.4. We place the displacement matrices corresponding to the partially fixed nodes in \mathbf{U}'' .

$$\mathbf{K} = \begin{bmatrix} \mathbf{k}^{(1)AA} & \mathbf{k}^{(1)AB} & \mathbf{0} & \mathbf{0} \\ \mathbf{k}^{(1)BA} & (\mathbf{k}^{(1)BB} + \mathbf{k}^{(2)AA}) & \mathbf{k}^{(2)AB} & \mathbf{0} \\ \mathbf{0} & \mathbf{k}^{(2)BA} & (\mathbf{k}^{(2)BB} + \mathbf{k}^{(3)AA}) & \mathbf{k}^{(3)AB} \\ \mathbf{0} & \mathbf{0} & \mathbf{k}^{(3)BA} & \mathbf{k}^{(3)BB} \end{bmatrix}$$

$$\mathbf{U}' = \begin{Bmatrix} \mathbf{U}_2 \\ \mathbf{U}_3 \end{Bmatrix} = \begin{Bmatrix} u_2 \\ v_2 \\ \theta_2 \\ u_3 \\ v_3 \\ \theta_3 \end{Bmatrix} \quad \mathbf{U}'' = \begin{Bmatrix} \mathbf{U}_1 \\ \mathbf{U}_4 \end{Bmatrix} = \begin{Bmatrix} u_1 = 0 \\ v_1 = -\delta_1 \\ \theta_1 = 0 \\ u_4 = 0 \\ v_4 = -\delta_4 \\ \theta_4 = 0 \end{Bmatrix}$$

The modified form of \mathbf{K} consistent with this reordering of \mathbf{U} is generated by moving the first partitioned row and column back to the third location. The steps are

$$\mathbf{K}' = \left[\begin{array}{cc|cc} (\mathbf{k}^{(1)BB} + \mathbf{k}^{(2)AA}) & \mathbf{k}^{(2)AB} & \mathbf{k}^{(1)AB} & \mathbf{0} \\ \mathbf{k}^{(2)BA} & (\mathbf{k}^{(2)BB} + \mathbf{k}^{(3)AA}) & \mathbf{0} & \mathbf{k}^{(3)AB} \\ \hline \mathbf{k}^{(1)AB} & \mathbf{0} & \mathbf{k}^{(1)AA} & \mathbf{0} \\ \mathbf{0} & \mathbf{k}^{(3)BA} & \mathbf{0} & \mathbf{k}^{(3)BB} \end{array} \right]$$

Noting (12.24), the partitioned form of \mathbf{K}' is

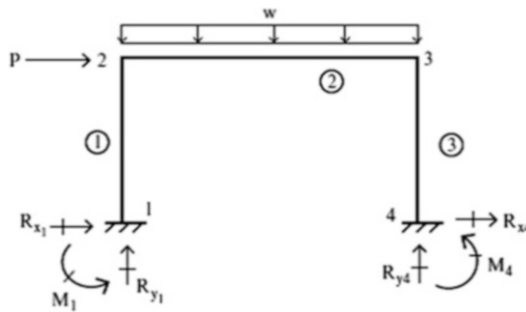
$$\mathbf{K}'_{11} = \begin{bmatrix} (\mathbf{k}_{(1)BB} + \mathbf{k}_{(2)AA}) & \mathbf{k}_{(2)AB} \\ \mathbf{k}_{(2)BA} & (\mathbf{k}_{(2)BB} + \mathbf{k}_{(3)AA}) \end{bmatrix} \quad \mathbf{K}'_{12} = \begin{bmatrix} \mathbf{k}_{(1)BA} & 0 \\ 0 & \mathbf{k}_{(3)BA} \end{bmatrix}$$

$$\mathbf{K}'_{21} = \begin{bmatrix} \mathbf{k}_{(1)AB} & 0 \\ 0 & \mathbf{k}_{(3)BA} \end{bmatrix} \quad \mathbf{K}'_{22} = \begin{bmatrix} \mathbf{k}_{(1)AA} & 0 \\ 0 & \mathbf{k}_{(3)BB} \end{bmatrix}$$

We perform a similar operation on the rows of \mathbf{P}_E and \mathbf{P}_I . The corresponding reordered partitioned nodal forces are:

$$\mathbf{P}'_E = \begin{Bmatrix} \mathbf{P}_{E2} \\ \mathbf{P}_{E3} \end{Bmatrix} \quad \mathbf{P}'_I = \begin{Bmatrix} \mathbf{P}^F_{(1)B} + \mathbf{P}^F_{(2)A} \\ \mathbf{P}^F_{(2)B} + \mathbf{P}^F_{(3)A} \end{Bmatrix}$$

$$\mathbf{P}''_E = \begin{Bmatrix} \mathbf{P}_{E1} \\ \mathbf{P}_{E4} \end{Bmatrix} = \begin{Bmatrix} R_{x1} \\ R_{y1} \\ M_1 \\ R_{x4} \\ R_{y4} \\ M_4 \end{Bmatrix} \quad \mathbf{P}''_I = \begin{Bmatrix} \mathbf{P}^F_{(1)A} \\ \mathbf{P}^F_{(3)B} \end{Bmatrix}$$



Throughout the chapter, matrix computations are carried out using computer software such as MATLAB (29) or MATHCAD (30).

Example 12.7: Two-Member Plane Frame—Partially Fixed

Given: The frame shown in Fig. E12.7a. E , I , and A are constant for both members.

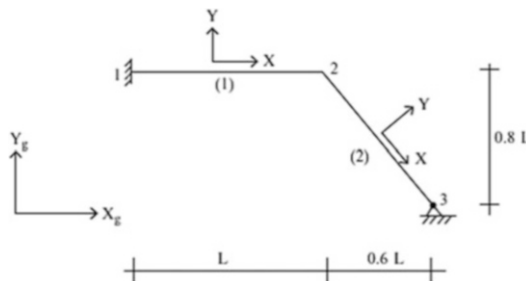


Fig. E12.7a

Determine: (a) The various matrices for the matrix displacement formulation. (b) Solve for the joint displacements, member forces, and reactions due to the loading defined in Fig. E12.7b. Use the following values for the parameters: $L = 15$ ft, $I = 170$ in.⁴, $A = 10$ in.², and $E = 29,000$ ksi.

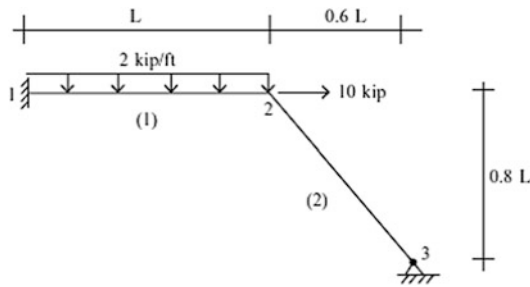


Fig. E12.7b

Solution:

We start with the geometric data. The topological and geometric information is listed below.

Geometric data:

Member m	n_-	n_+	α
(1)	1	2	0
(2)	2	3	-53.13°

Member m	α	$\cos \alpha$	$\sin \alpha$	$\sin \alpha \cos \alpha$	$\cos^2 \alpha$	$\sin^2 \alpha$
(1)	0	1	0	0	1	0
(2)	-53.13°	0.6	-0.8	-0.48	0.36	0.64

Generate stiffness matrices:

The system stiffness matrix and displacement vector have the following form:

$$\mathbf{K} = \begin{bmatrix} \mathbf{k}_{(1)AA} & \mathbf{k}_{(1)AB} & 0 \\ \mathbf{k}_{(1)BA} & \mathbf{k}_{(1)BB} & 0 \\ 0 & 0 & 0 \end{bmatrix} + \begin{bmatrix} 0 & 0 & 0 \\ 0 & \mathbf{k}_{(2)AA} & \mathbf{k}_{(2)AB} \\ 0 & \mathbf{k}_{(2)BA} & \mathbf{k}_{(2)BB} \end{bmatrix} = \begin{bmatrix} \mathbf{k}_{(1)AA} & \mathbf{k}_{(1)AB} & 0 \\ \mathbf{k}_{(1)BA} & (\mathbf{k}_{(1)BB} + \mathbf{k}_{(2)AA}) & \mathbf{k}_{(2)AB} \\ 0 & \mathbf{k}_{(2)BA} & \mathbf{k}_{(2)BB} \end{bmatrix}$$

$$\mathbf{U} = \left\{ \begin{matrix} \mathbf{U}_1 \\ \mathbf{U}_2 \\ \mathbf{U}_3 \end{matrix} \right\} = \begin{pmatrix} u_1 \\ v_1 \\ \theta_1 \\ u_2 \\ v_2 \\ \theta_2 \\ u_3 \\ v_3 \\ \theta_3 \end{pmatrix}$$

We determine the individual member matrices using (12.16). These matrices are referred to the global reference frame.

$$\begin{aligned}
\mathbf{k}_{(1)AA} &= \begin{bmatrix} \frac{AE}{L} & 0 & 0 \\ 0 & \frac{12EI}{L^3} & \frac{6EI}{L^2} \\ 0 & \frac{6EI}{L^2} & \frac{4EI}{L} \end{bmatrix} & \mathbf{k}_{(1)AB} &= \begin{bmatrix} -\frac{AE}{L} & 0 & 0 \\ 0 & -\frac{12EI}{L^3} & \frac{6EI}{L^2} \\ 0 & -\frac{6EI}{L^2} & \frac{2EI}{L} \end{bmatrix} \\
\mathbf{k}_{(1)BA} &= \begin{bmatrix} -\frac{AE}{L} & 0 & 0 \\ 0 & -\frac{12EI}{L^3} & -\frac{6EI}{L^2} \\ 0 & \frac{6EI}{L^2} & \frac{2EI}{L} \end{bmatrix} & \mathbf{k}_{(1)BB} &= \begin{bmatrix} \frac{AE}{L} & 0 & 0 \\ 0 & \frac{12EI}{L^3} & -\frac{6EI}{L^2} \\ 0 & -\frac{6EI}{L^2} & \frac{4EI}{L} \end{bmatrix} \\
\mathbf{k}_{(2)AA} &= \begin{bmatrix} \left(\frac{AE}{L} 0.36 + \frac{12EI}{L^3} 0.64\right) & \left(\frac{AE}{L} - \frac{12EI}{L^3}\right)(-0.48) & -\frac{6EI}{L^2}(-0.8) \\ \left(\frac{AE}{L} - \frac{12EI}{L^3}\right)(-0.48) & \left(\frac{AE}{L} 0.64 + \frac{12EI}{L^3} 0.36\right) & \frac{6EI}{L^2} 0.6 \\ -\frac{6EI}{L^2}(-0.8) & \frac{6EI}{L^2} 0.6 & \frac{4EI}{L} \end{bmatrix} \\
\mathbf{k}_{(2)AB} &= \begin{bmatrix} -\left(\frac{AE}{L} 0.36 + \frac{12EI}{L^3} 0.64\right) & (-0.48)\left(-\frac{AE}{L} + \frac{12EI}{L^3}\right) & -\frac{6EI}{L^2}(-0.8) \\ \left(-\frac{AE}{L} + \frac{12EI}{L^3}\right)(-0.48) & -\left(\frac{AE}{L} 0.64 + \frac{12EI}{L^3} 0.36\right) & \frac{6EI}{L^2} 0.6 \\ \frac{6EI}{L^2}(-0.8) & -\frac{6EI}{L^2} 0.6 & \frac{2EI}{L} \end{bmatrix} \\
\mathbf{k}_{(2)BA} &= \begin{bmatrix} -\left(\frac{AE}{L} 0.36 + \frac{12EI}{L^3} 0.64\right) & (-0.48)\left(-\frac{AE}{L} + \frac{12EI}{L^3}\right) & -\frac{6EI}{L^2}(-0.8) \\ -(-0.48)\left(\frac{AE}{L} + \frac{12EI}{L^3}\right) & -\left(\frac{AE}{L} 0.64 + \frac{12EI}{L^3} 0.36\right) & -\frac{6EI}{L^2} 0.6 \\ -\frac{6EI}{L^2}(-0.8) & \frac{6EI}{L^2} 0.6 & \frac{2EI}{L} \end{bmatrix} \\
\mathbf{k}_{(2)BB} &= \begin{bmatrix} \left(\frac{AE}{L} 0.36 + \frac{12EI}{L^3} 0.64\right) & (-0.48)\left(\frac{AE}{L} - \frac{12EI}{L^3}\right) & \frac{6EI}{L^2}(-0.8) \\ \left(\frac{AE}{L} - \frac{12EI}{L^3}\right)(-0.48) & \left(\frac{AE}{L} 0.64 + \frac{12EI}{L^3} 0.36\right) & -\frac{6EI}{L^2} 0.6 \\ \frac{6EI}{L^2}(-0.8) & -\frac{6EI}{L^2} 0.6 & \frac{4EI}{L} \end{bmatrix}
\end{aligned}$$

Substituting for these matrices, the system stiffness matrix takes the following form:

$$\mathbf{K} = \begin{bmatrix}
 \frac{AE}{L} & 0 & 0 & -\frac{AE}{L} & 0 & 0 & 0 & 0 & 0 & 0 \\
 0 & \frac{12EI}{L^3} & \frac{6EI}{L^2} & 0 & \frac{12EI}{L^3} & -\frac{6EI}{L^2} & 0 & \frac{6EI}{L^2} & 0 & 0 \\
 0 & \frac{6EI}{L^2} & \frac{4EI}{L} & 0 & \frac{6EI}{L^2} & -\frac{2EI}{L} & 0 & \frac{2EI}{L} & 0 & 0 \\
 -\frac{AE}{L} & 0 & 0 & \left(\frac{AE}{L} \cdot 1.36 + \frac{12EI}{L^3} \cdot 0.64\right) & -0.48 \left(\frac{AE}{L} - \frac{12EI}{L^3}\right) & -\frac{6EI}{L^2} (-0.8) & -\left(\frac{AE}{L} \cdot 0.36 + \frac{12EI}{L^3} \cdot 0.64\right) & -0.48 \left(-\frac{AE}{L} + \frac{12EI}{L^3}\right) & 0 & -\frac{6EI}{L^2} (-0.8) \\
 0 & -\frac{12EI}{L^3} & \frac{6EI}{L^2} & -0.48 \left(\frac{AE}{L} - \frac{12EI}{L^3}\right) & \left(\frac{AE}{L} \cdot 0.64 + \frac{12EI}{L^3} \cdot 1.36\right) & \frac{6EI}{L^2} (-0.4) & -0.48 \left(-\frac{AE}{L} + \frac{12EI}{L^3}\right) & -\left(\frac{AE}{L} \cdot 0.64 + \frac{12EI}{L^3} \cdot 0.36\right) & \frac{6EI}{L^2} \cdot 0.6 & \frac{6EI}{L^2} \cdot 0.6 \\
 0 & \frac{6EI}{L^2} & \frac{2EI}{L} & -\frac{6EI}{L^2} (-0.8) & \frac{6EI}{L^2} (-0.4) & \frac{8EI}{L} & \frac{6EI}{L^2} (-0.8) & -\frac{6EI}{L^2} (0.6) & \frac{2EI}{L} & \frac{2EI}{L} \\
 0 & 0 & 0 & -\left(\frac{AE}{L} \cdot 0.36 + \frac{12EI}{L^3} \cdot 0.64\right) & -0.48 \left(-\frac{AE}{L} + \frac{12EI}{L^3}\right) & \frac{6EI}{L^2} (-0.8) & \left(\frac{AE}{L} \cdot 0.36 + \frac{12EI}{L^3} \cdot 0.64\right) & -0.48 \left(\frac{AE}{L} - \frac{12EI}{L^3}\right) & \frac{6EI}{L^2} (-0.8) & \frac{6EI}{L^2} (-0.8) \\
 0 & 0 & 0 & 0.48 \left(\frac{AE}{L} + \frac{12EI}{L^3}\right) & -\left(\frac{AE}{L} \cdot 0.64 + \frac{12EI}{L^3} \cdot 0.36\right) & -\frac{6EI}{L^2} (0.6) & -0.48 \left(\frac{AE}{L} - \frac{12EI}{L^3}\right) & \left(\frac{AE}{L} \cdot 0.64 + \frac{12EI}{L^3} \cdot 0.36\right) & -\frac{6EI}{L^2} (0.6) & -\frac{6EI}{L^2} (0.6) \\
 0 & 0 & 0 & -\frac{6EI}{L^2} (-0.8) & \frac{6EI}{L^2} (0.6) & \frac{2EI}{L} & \frac{6EI}{L^2} (-0.8) & -\frac{6EI}{L^2} (0.6) & \frac{4EI}{L} & \frac{4EI}{L}
 \end{bmatrix}$$

Introduce displacement constraints:

We note that node 1 is fully fixed but node 3 is partially fixed, i.e., the rotation θ_3 is unknown. We rearrange the rows and columns of \mathbf{K} , and the rows of \mathbf{U} , \mathbf{P}_E , and \mathbf{P}_F . This step leads to the resulting partitioned vectors and matrices listed below.

$$\mathbf{U}' = \begin{Bmatrix} u_2 \\ v_2 \\ \theta_2 \\ \theta_3 \end{Bmatrix} \quad \mathbf{U}'' = \begin{Bmatrix} u_1 \\ v_1 \\ \theta_1 \\ u_3 \\ v_3 \end{Bmatrix}$$

$$\mathbf{K}'_{11} = \begin{bmatrix} \left(\frac{AE}{L} 1.36 + \frac{12EI}{L^3} 0.64\right) & (-0.48)\left(\frac{AE}{L} - \frac{12EI}{L^3}\right) & -\frac{6EI}{L^2}(-0.8) & -\frac{6EI}{L^2}(-0.8) \\ (-0.48)\left(\frac{AE}{L} - \frac{12EI}{L^3}\right) & \left(\frac{AE}{L} 0.64 + \frac{12EI}{L^3} 1.36\right) & \frac{6EI}{L^2}(-0.4) & \frac{6EI}{L^2}(0.6) \\ -\frac{6EI}{L^2}(-0.8) & \frac{6EI}{L^2}(-0.4) & \frac{8EI}{L} & \frac{2EI}{L} \\ -\frac{6EI}{L^2}(-0.8) & \frac{6EI}{L^2}(0.6) & \frac{2EI}{L} & \frac{4EI}{L} \end{bmatrix}$$

$$\mathbf{K}'_{12} = \begin{bmatrix} -\frac{AE}{L} & 0 & 0 & -\left(\frac{AE}{L} 0.36 + \frac{12EI}{L^3} 0.64\right) & -0.48\left(-\frac{AE}{L} + \frac{12EI}{L^3}\right) \\ 0 & -\frac{12EI}{L^3} & -\frac{6EI}{L^2} & \left(-\frac{AE}{L} + \frac{12EI}{L^3}\right)(-0.48) & -\left(\frac{AE}{L} 0.64 + \frac{12EI}{L^3} 0.36\right) \\ 0 & \frac{6EI}{L^2} & \frac{2EI}{L} & -\frac{6EI}{L^2}(-0.8) & -\frac{6EI}{L^2} 0.6 \\ 0 & 0 & 0 & \frac{6EI}{L^2}(-0.8) & -\frac{6EI}{L^2} 0.6 \end{bmatrix}$$

$$\mathbf{K}'_{21} = \begin{bmatrix} -\frac{AE}{L} & 0 & 0 & 0 & 0 \\ 0 & -\frac{12EI}{L^3} & \frac{6EI}{L^2} & 0 & 0 \\ 0 & \frac{6EI}{L^2} & \frac{2EI}{L} & 0 & 0 \\ -\left(\frac{AE}{L} 0.36 + \frac{12EI}{L^3} 0.64\right) & (-0.48)\left(-\frac{AE}{L} + \frac{12EI}{L^3}\right) & \frac{6EI}{L^2}(-0.8) & \frac{6EI}{L^2}(-0.8) \\ -\left(\frac{AE}{L} + \frac{12EI}{L^3}\right)(-0.48) & -\left(\frac{AE}{L} 0.64 + \frac{12EI}{L^3} 0.36\right) & -\frac{6EI}{L^2} 0.6 & -\frac{6EI}{L^2} 0.6 \end{bmatrix}$$

$$\mathbf{K}'_{22} = \begin{bmatrix} \frac{AE}{L} & 0 & 0 & 0 & 0 \\ 0 & \frac{12EI}{L^3} & \frac{6EI}{L^2} & 0 & 0 \\ 0 & \frac{6EI}{L^2} & \frac{4EI}{L} & 0 & 0 \\ 0 & 0 & 0 & \left(\frac{AE}{L} 0.36 + \frac{12EI}{L^3} 0.64\right) & \left(\frac{AE}{L} - \frac{12EI}{L^3}\right)(-0.48) \\ 0 & 0 & 0 & \left(\frac{AE}{L} - \frac{12EI}{L^3}\right)(-0.48) & \left(\frac{AE}{L} 0.64 + \frac{12EI}{L^3} 0.36\right) \\ 0 & 0 & 0 & \frac{6EI}{L^2}(-0.8) & -\frac{6EI}{L^2} 0.6 \end{bmatrix}$$

Introduce the member properties and evaluate the stiffness terms:

We evaluate the individual stiffness matrices using the following values for the parameters ($L = 15$ ft, $I = 170$ in.⁴, $A = 10$ in.², $E = 29,000$ ksi).

$$\mathbf{K}'_{11} = \begin{bmatrix} 2.198 \times 10^3 & -768.464 & 730.37 & 730.37 \\ -768.464 & 1.045 \times 10^3 & -365.185 & 547.778 \\ 730.37 & -365.185 & 2.191 \times 10^5 & 5.475 \times 10^4 \\ 730.37 & 547.778 & 5.478 \times 10^4 & 1.096 \times 10^5 \end{bmatrix}$$

$$\mathbf{K}'_{21} = \begin{bmatrix} -1.61 \times 10^3 & 0 & 0 & 0 \\ 0 & -10.14 & 913 & 0 \\ 0 & -913 & 548 \times 10^4 & 0 \\ -586.5 & -768.5 & -730.4 & -730.4 \\ 778.2 & -1.035 \times 10^3 & -547.8 & -547.8 \end{bmatrix}$$

We need the inverse of \mathbf{K}'_{11} to solve for the displacement due to a given loading. Its form is

$$\left(\mathbf{K}'_{11}\right)^{-1} = \begin{bmatrix} 6.17 \times 10^{-4} & 4.574 \times 10^{-4} & 3.492 \times 10^{-7} & -6.575 \times 10^{-6} \\ 4.574 \times 10^{-4} & 1.301 \times 10^{-3} & 3.464 \times 10^{-6} & -1.128 \times 10^{-5} \\ 3.492 \times 10^{-7} & 3.464 \times 10^{-6} & 5.227 \times 10^{-6} & -2.633 \times 10^{-6} \\ -6.575 \times 10^{-6} & -1.128 \times 10^{-5} & -2.633 \times 10^{-6} & 1.054 \times 10^{-5} \end{bmatrix}$$

Specify loading:

Next, we consider the loading shown in Fig. E12.7b. The fixed end actions due to the uniform loading applied to member 1 are defined in Fig. E12.7c.

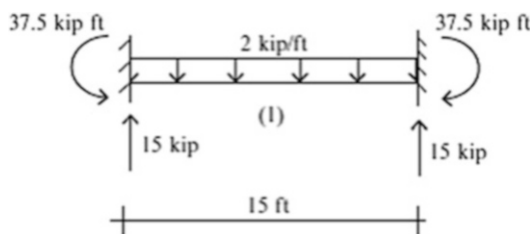


Fig. E12.7c

The system load vectors corresponding to these loads are:

$$\mathbf{P}'_E = \begin{Bmatrix} 10 \\ 0 \\ 0 \\ 0 \end{Bmatrix} \quad \mathbf{P}'_1 = \begin{Bmatrix} 0 \\ 15.0 \text{ kip in} \\ -37.5(12) \text{ kip in} \\ 0 \end{Bmatrix} \quad \mathbf{P}''_1 = \begin{Bmatrix} 0 \\ 15.0 \text{ kip} \\ 37.5(12) \text{ kip in} \\ 0 \\ 0 \end{Bmatrix}$$

Determine the unknown displacements:

Finally, we determine the unknown displacements using (12.26):

$$\mathbf{U}' = (\mathbf{K}'_{11})^{-1} (\mathbf{P}'_E - \mathbf{P}'_1)$$

$$\begin{aligned} & \downarrow \\ \begin{Bmatrix} u_2 \\ v_2 \\ \theta_2 \\ \theta_3 \end{Bmatrix} &= \begin{bmatrix} 6.17 \times 10^{-4} & 4.574 \times 10^{-4} & 3.492 \times 10^{-7} & -6.575 \times 10^{-6} \\ 4.574 \times 10^{-4} & 1.301 \times 10^{-3} & 3.464 \times 10^{-6} & -1.128 \times 10^{-5} \\ 3.492 \times 10^{-7} & 3.464 \times 10^{-6} & 5.227 \times 10^{-6} & -2.633 \times 10^{-6} \\ -6.575 \times 10^{-6} & -1.128 \times 10^{-5} & -2.633 \times 10^{-6} & 1.054 \times 10^{-5} \end{bmatrix} \\ & \times \left[\begin{bmatrix} 10 \\ 0 \\ 0 \\ 0 \end{bmatrix} - \begin{bmatrix} 0 \\ 15.0 \\ -(37.5 \times 12) \\ 0 \end{bmatrix} \right] = \begin{Bmatrix} -5.329 \times 10^{-4} \\ -0.013 \\ 2.304 \times 10^{-3} \\ -1.081 \times 10^{-3} \end{Bmatrix} \end{aligned}$$

$$u_2 = 0.00053 \text{ in. } \leftarrow$$

$$v_2 = 0.013 \text{ in. } \downarrow$$

$$\theta_2 = 0.002304 \text{ rad counterclockwise}$$

$$\theta_3 = 0.001081 \text{ rad counterclockwise}$$

Determine unknown forces (reactions):

Given the displacements, one determines the reactions with

$$\mathbf{P}''_E = \mathbf{K}'_{21} \mathbf{U}' + \mathbf{K}'_{22} \mathbf{U}'' + \mathbf{P}'_1 \Rightarrow \begin{Bmatrix} R_{x1} \\ R_{y1} \\ M_1 \\ R_{x3} \\ R_{y3} \end{Bmatrix} = \mathbf{K}'_{21} \begin{Bmatrix} u_2 \\ v_2 \\ \theta_2 \\ \theta_3 \end{Bmatrix} + \mathbf{P}'_1$$

$$\begin{aligned} \begin{Bmatrix} R_{x1} \\ R_{y1} \\ M_1 \\ R_{x3} \\ R_{y3} \end{Bmatrix} &= \begin{bmatrix} -1.61 \times 10^3 & 0 & 0 & 0 \\ 0 & -10.14 & 913 & 0 \\ 0 & -913 & 548 \times 10^4 & 0 \\ -586.5 & -768.5 & -730.4 & -730.4 \\ 778.2 & -1.035 \times 10^3 & -547.8 & -547.8 \end{bmatrix} \\ & \times \begin{Bmatrix} -5.329 \times 10^{-4} \\ -0.013 \\ 2.304 \times 10^{-3} \\ -1.081 \times 10^{-3} \end{Bmatrix} + \begin{Bmatrix} 0 \\ 15.0 \\ (37.5 \times 12) \\ 0 \\ 0 \end{Bmatrix} \\ &= \begin{Bmatrix} 0.86 \text{ kip} \\ 17.24 \text{ kip} \\ 588.4 \text{ kip in} \\ -10.86 \text{ kip} \\ 12.76 \text{ kip} \end{Bmatrix} \end{aligned}$$

The reactions are listed on Fig. E12.7d

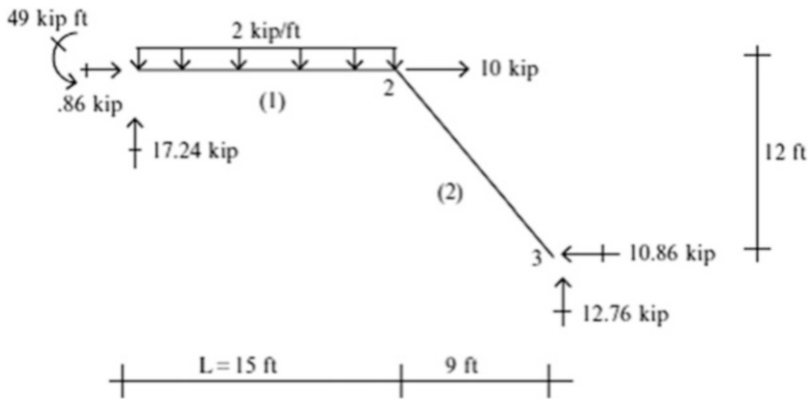


Fig. E12.7d

Determine member forces in the local coordinates:

Lastly, we determine the member end actions in the global and local coordinate system using (12.27). Applying these equations for members 1 and 2 leads to the following results:

Fixed end actions

$$\mathbf{P}_{(1)A}^F = \begin{Bmatrix} 0 \\ 15 \text{ kip} \\ 37.5(12) \text{ kip in} \end{Bmatrix} \quad \mathbf{P}_{(1)B}^F = \begin{Bmatrix} 0 \\ 15 \text{ kip} \\ -37.5(12) \text{ kip in} \end{Bmatrix} \quad \mathbf{P}_{(2)A}^F = \mathbf{P}_{(2)B}^F = 0$$

Global end actions

$$P_{(1)A} = k_{(1)AB} \begin{Bmatrix} u_2 \\ v_2 \\ \theta_2 \end{Bmatrix} + P_{(1)A}^F = \begin{Bmatrix} 0.86 \text{ kip} \\ 17.24 \text{ kip} \\ 588.4 \text{ kip in} \end{Bmatrix}$$

$$P_{(1)B} = k_{(1)BB} \begin{Bmatrix} u_2 \\ v_2 \\ \theta_2 \end{Bmatrix} + P_{(1)B}^F = \begin{Bmatrix} -0.86 \text{ kip} \\ 12.76 \text{ kip} \\ -183.4 \text{ kip in} \end{Bmatrix}$$

$$P_{(2)A} = k_{(2)AB} \begin{Bmatrix} 0 \\ 0 \\ \theta_3 \end{Bmatrix} + k_{(2)AA} \begin{Bmatrix} u_2 \\ v_2 \\ \theta_2 \end{Bmatrix} = \begin{Bmatrix} 10.86 \text{ kip} \\ -12.76 \text{ kip} \\ 183.4 \text{ kip in} \end{Bmatrix}$$

$$P_{(2)B} = k_{(2)BB} \begin{Bmatrix} 0 \\ 0 \\ \theta_3 \end{Bmatrix} + k_{(2)BA} \begin{Bmatrix} u_2 \\ v_2 \\ \theta_2 \end{Bmatrix} = \begin{Bmatrix} -10.86 \text{ kip} \\ 12.76 \text{ kip} \\ 0.0 \end{Bmatrix}$$

Local end actions

$$P_{\ell(1)A} = \begin{Bmatrix} F_{(1)A} \\ V_{(1)A} \\ M_{(1)A} \end{Bmatrix} = \mathbf{R}_{gl} \mathbf{P}_{(1)A} = \begin{bmatrix} 1 & 0 & 0 \\ 0 & 1 & 0 \\ 0 & 0 & 1 \end{bmatrix} \begin{Bmatrix} 0.86 \\ 17.24 \\ 588.4 \end{Bmatrix} = \begin{Bmatrix} 0.86 \text{ kip} \\ 17.24 \text{ kip} \\ 588.4 \text{ kip in} \end{Bmatrix}$$

$$P_{\ell(1)B} = \begin{Bmatrix} F_{x(1)B} \\ V_{(1)B} \\ M_{(1)B} \end{Bmatrix} = \mathbf{R}_{gl} \mathbf{P}_{(1)A} = \begin{bmatrix} 1 & 0 & 0 \\ 0 & 1 & 0 \\ 0 & 0 & 1 \end{bmatrix} \begin{Bmatrix} -0.86 \\ 12.76 \\ -213.96 \end{Bmatrix} = \begin{Bmatrix} -0.86 \text{ kip} \\ 12.76 \text{ kip} \\ -183.4 \text{ kip in} \end{Bmatrix}$$

$$P_{\ell(2)A} = \begin{Bmatrix} F_{(2)A} \\ V_{(2)A} \\ M_{(2)A} \end{Bmatrix} = \mathbf{R}_{gl} \mathbf{P}_{(2)A} = \begin{bmatrix} 0.6 & -0.8 & 0 \\ 0.8 & 0.6 & 0 \\ 0 & 0 & 1 \end{bmatrix} \begin{Bmatrix} 10.86 \\ -12.76 \\ 183.4 \end{Bmatrix} = \begin{Bmatrix} 16.72 \text{ kip} \\ 1.03 \text{ kip} \\ 183.4 \text{ kip in} \end{Bmatrix}$$

$$P_{\ell(2)B} = \begin{Bmatrix} F_{(2)B} \\ V_{(2)B} \\ M_{(2)B} \end{Bmatrix} = \mathbf{R}_{gl} \mathbf{P}_{(2)B} = \begin{bmatrix} 0.6 & -0.8 & 0 \\ 0.8 & 0.6 & 0 \\ 0 & 0 & 1 \end{bmatrix} \times \begin{Bmatrix} -10.86 \\ 12.76 \\ 0.0 \end{Bmatrix} = \begin{Bmatrix} -16.72 \text{ kip} \\ -1.03 \text{ kip} \\ 0.0 \end{Bmatrix}$$

The local member end actions are listed in Fig. E12.7e.

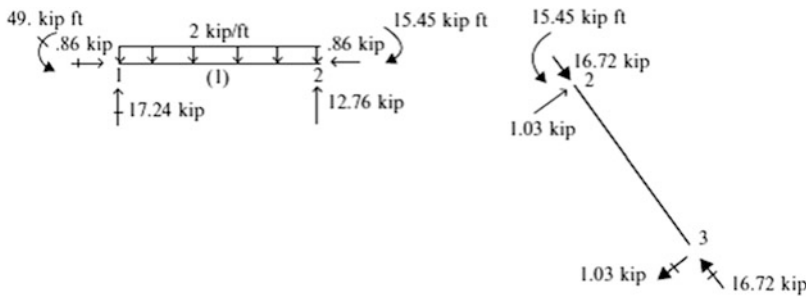


Fig. E12.7e

Example 12.8: Two-Member Plane Frame—Fully Fixed

Given: The frame shown in Fig. E12.8a. E , I , and A are constant for both members. Take $L = 5$ m, $I = 70(10)^6 \text{ mm}^4$, $A = 6500 \text{ mm}^2$, $M = 20 \text{ kN m}$, and $E = 200 \text{ GPa}$.

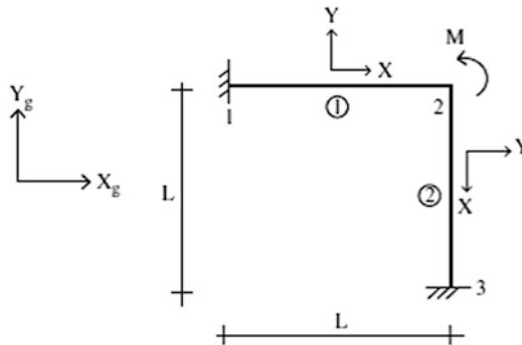


Fig. E12.8a

Determine: The reactions

Solution: We start with the geometric data. The topological and geometric information is listed below.

Geometric data:

Member m	n_-	n_+	α
(1)	1	2	0
(2)	2	3	-90°

Member m	α	$\cos \alpha$	$\sin \alpha$	$\sin \alpha \cos \alpha$	$\cos^2 \alpha$	$\sin^2 \alpha$
(1)	0	1	0	0	1	0
(2)	-90°	0	-1	0	0	1

The system stiffness matrix and displacement vector have the following form:

$$\mathbf{K} = \begin{bmatrix} \mathbf{k}_{(1)AA} & \mathbf{k}_{(1)AB} & 0 \\ \mathbf{k}_{(1)BA} & \mathbf{k}_{(1)BB} & 0 \\ 0 & 0 & 0 \end{bmatrix} + \begin{bmatrix} 0 & 0 & 0 \\ 0 & \mathbf{k}_{(2)AA} & \mathbf{k}_{(2)AB} \\ 0 & \mathbf{k}_{(2)BA} & \mathbf{k}_{(2)BB} \end{bmatrix}$$

$$= \begin{bmatrix} \mathbf{k}_{(1)AA} & \mathbf{k}_{(1)AB} & 0 \\ \mathbf{k}_{(1)BA} & (\mathbf{k}_{(1)BB} + \mathbf{k}_{(2)AA}) & \mathbf{k}_{(2)AB} \\ 0 & \mathbf{k}_{(2)BA} & \mathbf{k}_{(2)BB} \end{bmatrix}$$

We determine the individual member matrices using (12.16). These matrices are referred to the global reference frame.

$$\mathbf{k}_{(1)AA} = \begin{bmatrix} \frac{AE}{L} & 0 & 0 \\ 0 & \frac{12EI}{L^3} & \frac{6EI}{L^2} \\ 0 & \frac{6EI}{L^2} & \frac{4EI}{L} \end{bmatrix} \quad \mathbf{k}_{(1)AB} = \begin{bmatrix} -\frac{AE}{L} & 0 & 0 \\ 0 & -\frac{12EI}{L^3} & \frac{6EI}{L^2} \\ 0 & -\frac{6EI}{L^2} & \frac{2EI}{L} \end{bmatrix}$$

$$\mathbf{k}_{(1)BA} = \begin{bmatrix} -\frac{AE}{L} & 0 & 0 \\ 0 & -\frac{12EI}{L^3} & -\frac{6EI}{L^2} \\ 0 & \frac{6EI}{L^2} & \frac{2EI}{L} \end{bmatrix} \quad \mathbf{k}_{(1)BB} = \begin{bmatrix} \frac{AE}{L} & 0 & 0 \\ 0 & \frac{12EI}{L^3} & -\frac{6EI}{L^2} \\ 0 & -\frac{6EI}{L^2} & \frac{4EI}{L} \end{bmatrix}$$

$$\mathbf{k}_{(2)AA} = \begin{bmatrix} \frac{12EI}{L^3} & 0 & \frac{6EI}{L^2} \\ 0 & \frac{AE}{L} & 0 \\ \frac{6EI}{L^2} & 0 & \frac{4EI}{L} \end{bmatrix} \quad \mathbf{k}_{(2)AB} = \begin{bmatrix} -\frac{12EI}{L^3} & 0 & \frac{6EI}{L^2} \\ 0 & -\frac{AE}{L} & 0 \\ \frac{6EI}{L^2} & 0 & \frac{2EI}{L} \end{bmatrix}$$

$$\mathbf{k}_{(2)BA} = \begin{bmatrix} -\frac{12EI}{L^3} & 0 & -\frac{6EI}{L^2} \\ 0 & -\frac{AE}{L} & 0 \\ \frac{6EI}{L^2} & 0 & \frac{2EI}{L} \end{bmatrix} \quad \mathbf{k}_{(2)BB} = \begin{bmatrix} \frac{12EI}{L^3} & 0 & \frac{6EI}{L^2} \\ 0 & \frac{AE}{L} & 0 \\ \frac{6EI}{L^2} & 0 & \frac{4EI}{L} \end{bmatrix}$$

Substituting for these matrices, the system stiffness matrix takes the following form using the following values for the parameters $L = 5 \text{ m}$, $I = 70(10)^6 \text{ mm}^4$, $A = 6500 \text{ mm}^2$, and $E = 200 \text{ GPa}$.

$$\mathbf{K} = \begin{bmatrix} 260 & 0 & 0 & -260 & 0 & 0 & 0 & 0 & 0 \\ 0 & 1.344 & 3.36 \times 10^3 & 0 & -1.344 & 3.36 \times 10^3 & 0 & 0 & 0 \\ 0 & 3.36 \times 10^3 & 1.12 \times 10^7 & 0 & -3.36 \times 10^3 & 5.6 \times 10^6 & 0 & 0 & 0 \\ -260 & 0 & 0 & 261.344 & -1.584 \times 10^{-14} & 3.36 \times 10^3 & -1.344 & 1.584 \times 10^{-14} & 3.36 \times 10^3 \\ 0 & -1.344 & -3.36 \times 10^3 & -1.584 \times 10^{-14} & 261.344 & -3.36 \times 10^3 & 1.584 \times 10^{-14} & -260 & 2.057 \times 10^{-13} \\ 0 & 3.36 \times 10^3 & 5.6 \times 10^6 & 3.36 \times 10^3 & -3.36 \times 10^3 & 2.24 \times 10^7 & -3.36 \times 10^3 & -2.057 \times 10^{-13} & 5.6 \times 10^6 \\ 0 & 0 & 0 & -1.344 & 1.584 \times 10^{-14} & -3.36 \times 10^3 & 1.344 & -1.584 \times 10^{-14} & -3.36 \times 10^3 \\ 0 & 0 & 0 & 1.584 \times 10^{-14} & -260 & -2.057 \times 10^{-13} & -1.584 \times 10^{-14} & 260 & -2.057 \times 10^{-13} \\ 0 & 0 & 0 & 3.36 \times 10^3 & 2.057 \times 10^{-13} & 5.6 \times 10^6 & -3.36 \times 10^3 & -2.057 \times 10^{-13} & 1.12 \times 10^7 \end{bmatrix}$$

We note that nodes 1 and 3 are fully fixed. We rearrange the rows and columns of \mathbf{K} , and the rows of \mathbf{U} , \mathbf{P}_E accordingly. This step leads to the resulting partitioned vectors and matrices listed below (Fig. E12.8b).

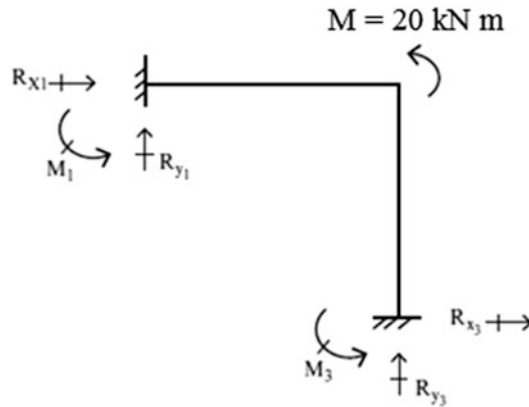


Fig. E12.8b Nodal forces

$$\mathbf{U}' = \begin{Bmatrix} u_2 \\ v_2 \\ \theta_2 \end{Bmatrix} \quad \mathbf{U}'' = 0 \quad \mathbf{P}_E'' = \begin{Bmatrix} R_{x1} \\ R_{y1} \\ M_1 \\ R_{x3} \\ R_{y3} \\ M_3 \end{Bmatrix} \quad \mathbf{P}_E' = \begin{Bmatrix} 0 \\ 0 \\ 20(10)^3 \text{ kNmm} \end{Bmatrix} \quad \mathbf{P}_1' = \mathbf{P}_1'' = 0$$

$$\mathbf{K}'_{11} = \begin{pmatrix} 261.344 & -1.584 \times 10^{-14} & 3.36 \times 10^3 \\ -1.584 \times 10^{-14} & 261.344 & -3.36 \times 10^3 \\ 3.36 \times 10^3 & -3.36 \times 10^3 & 2.24 \times 10^7 \end{pmatrix}$$

$$\mathbf{K}'_{21} = \begin{pmatrix} -260 & 0 & 0 \\ 0 & -1.344 & 3.36 \times 10^3 \\ 0 & -3.36 \times 10^3 & 5.6 \times 10^6 \\ -1.344 & 1.584 \times 10^{-14} & -3.36 \times 10^3 \\ 1.584 \times 10^{-14} & -260 & -2.057 \times 10^{-13} \\ 3.36 \times 10^3 & 2.057 \times 10^{-13} & 5.6 \times 10^6 \end{pmatrix}$$

Then

$$\mathbf{K}'_{11}{}^{-1} = \begin{pmatrix} 3.834 \times 10^{-3} & -7.408 \times 10^{-6} & -5.762 \times 10^{-7} \\ -7.408 \times 10^{-6} & 3.834 \times 10^{-3} & 5.762 \times 10^{-7} \\ -5.762 \times 10^{-7} & -5.762 \times 10^{-7} & 4.482 \times 10^{-8} \end{pmatrix}$$

Then, we determine the unknown displacements using the following equation:

$$\mathbf{U}' = \begin{Bmatrix} u_2 \\ v_2 \\ \theta_2 \end{Bmatrix} = (\mathbf{K}'_{11})^{-1} (\mathbf{P}'_E) \Rightarrow \begin{Bmatrix} u_2 \\ v_2 \\ \theta_2 \end{Bmatrix} = (\mathbf{K}'_{11})^{-1} \begin{Bmatrix} 0 \\ 0 \\ 20(10)^3 \end{Bmatrix} = \begin{Bmatrix} -0.0115 \text{ mm} \\ 0.0115 \text{ mm} \\ 8.964(10)^{-4} \text{ rad} \end{Bmatrix}$$

Given the displacements, one determines the reactions

$$\mathbf{P}'_E = \begin{Bmatrix} R_{x1} \\ R_{y1} \\ M_1 \\ R_{x3} \\ R_{y3} \\ M_3 \end{Bmatrix} = \mathbf{K}'_{21} \mathbf{U}' \Rightarrow \begin{Bmatrix} R_{x1} \\ R_{y1} \\ M_1 \\ R_{x3} \\ R_{y3} \\ M_3 \end{Bmatrix} = \begin{Bmatrix} 3 \text{ kN} \\ 3 \text{ kN} \\ 5000 \text{ kN m} \\ -3 \text{ kN} \\ -3 \text{ kN} \\ 5000 \text{ kN m} \end{Bmatrix}$$

The results are shown in Fig. E12.8c.

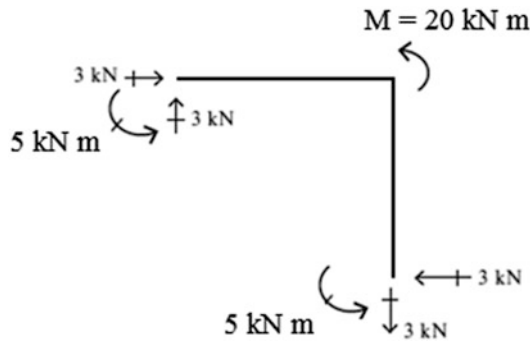


Fig. E12.8c

12.7 Specialized Formulation for Beam and Truss Structures

The formulation presented in the previous sections applies for frame type structures which involve both axial and bending actions. Beams and trusses are special cases where only one type of action occurs. Trusses support loads by axial action; beams support transverse loads through bending action. It is relatively easy to specialize the general frame formulation for these limiting cases.

12.7.1 The Steps Involved for Plane Truss Structures

The member end actions for a truss member consist of only an axial force, i.e., there is no shear or moment. Also, each node of a plane truss has only two displacement unknowns; the nodal rotation occurs independent of the translation and has no effect on the member force. We take these simplifications into account by defining “reduced” member force and nodal matrices. The formulation is exactly the same as described in Sects. 12.3–12.6. One only has to work with modified stiffness, end action, and nodal displacement matrices.

We start with the member equations. Figure 12.7 shows the member force and displacement measures referred to the local member frame. Note that now the member matrices are just scalar quantities.

$$\begin{aligned} \mathbf{U}_{\ell B} &= u_{\ell B} & \mathbf{U}_{\ell A} &= u_{\ell A} \\ \mathbf{P}_{\ell A} &= F_{\ell A} & \mathbf{P}_{\ell B} &= F_{\ell B} \end{aligned} \quad (12.28)$$

We consider (12.5) to be the general matrix expression for the member equations but interpret the various terms as “reduced” matrices. Their form follows by deleting the second and third row and column of the matrices listed in (12.6).

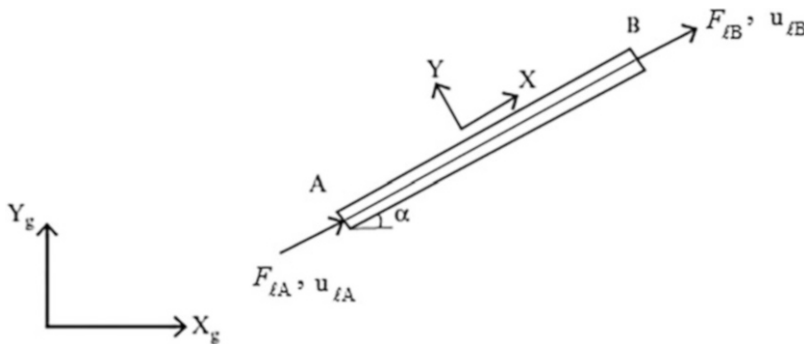


Fig. 12.7 End force and end displacement—local member truss—planar behavior

$$\begin{aligned}
 \mathbf{k}_{\ell_{BB}} &= \frac{AE}{L} & \mathbf{k}_{\ell_{BA}} &= -\frac{AE}{L} \\
 \mathbf{k}_{\ell_{BA}} &= -\frac{AE}{L} & \mathbf{k}_{\ell_{AA}} &= \frac{AE}{L} \\
 \mathbf{P}_{\ell_B}^F &= F_{\ell_B}^F & \mathbf{P}_{\ell_A}^F &= F_{\ell_A}^F
 \end{aligned} \tag{12.29}$$

We need to modify the rotation matrix in a similar way. Now, there are two nodal displacement measures and only one local displacement measure.

$$\begin{aligned}
 \mathbf{U} &= \begin{Bmatrix} u \\ v \end{Bmatrix} \\
 \mathbf{U}_{\ell} &= u_{\ell}
 \end{aligned} \tag{12.30}$$

Noting (12.8), we write

$$\begin{aligned}
 \mathbf{U} &= \mathbf{R}_{\ell_g} u_{\ell} \\
 \mathbf{R}_{\ell_g} &= \begin{Bmatrix} \cos \alpha \\ \sin \alpha \end{Bmatrix}
 \end{aligned} \tag{12.31}$$

We use this form for \mathbf{R}_{ℓ_g} to transform between the local and global frames.

Given \mathbf{R}_{ℓ_g} , we generate the global form of the member matrices using (12.13). A typical term is

$$\mathbf{k} = \mathbf{R}_{\ell_g} \mathbf{k}_{\ell} (\mathbf{R}_{\ell_g})^T \tag{12.32}$$

where \mathbf{k}_{ℓ} is defined by (12.29). Expanding (12.32) leads to

$$\begin{aligned}
 \mathbf{k}_{AA} = \mathbf{k}_{BB} = \mathbf{k} &= \left(\frac{AE}{L}\right) \begin{bmatrix} \cos^2 \alpha & \sin \alpha \cos \alpha \\ \sin \alpha \cos \alpha & \sin^2 \alpha \end{bmatrix} \\
 \mathbf{k}_{AB} = \mathbf{k}_{BA} = -\mathbf{k} &= -\left(\frac{AE}{L}\right) \begin{bmatrix} \cos^2 \alpha & \sin \alpha \cos \alpha \\ \sin \alpha \cos \alpha & \sin^2 \alpha \end{bmatrix}
 \end{aligned} \tag{12.33}$$

Noting (12.33), we observe that now \mathbf{k} is of order of (2×2) for a plane truss vs. (3×3) for a plane frame.

Lastly, we determine the end member forces for member m in the local frame.

$$\begin{aligned}
 F_{\ell_{(m)B}} &= \left(\frac{AE}{L}\right)_{(m)} [\cos \alpha_{(m)} \sin \alpha_{(m)}] (\mathbf{U}_{n^+} - \mathbf{U}_{n^-}) + F_{\ell_{(m)B}}^F \\
 F_{\ell_{(m)A}} &= -\left(\frac{AE}{L}\right)_{(m)} [\cos \alpha_{(m)} \sin \alpha_{(m)}] (\mathbf{U}_{n^+} - \mathbf{U}_{n^-}) + F_{\ell_{(m)A}}^F
 \end{aligned} \tag{12.34}$$

Example 12.9: Statically Determinate Truss

Given: The truss shown in Fig. E12.9a.

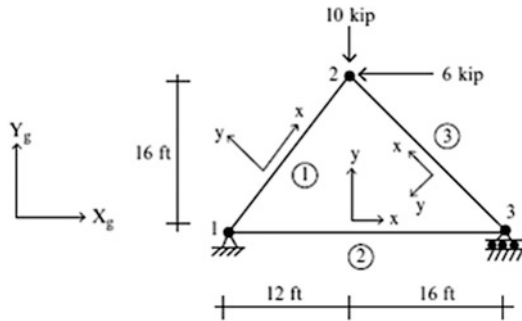


Fig. E12.9a

Determine: The joint displacements, reactions, and member forces using the Displacement Method. $A_{(1)} = A_{(2)} = A_{(3)} = A = 2 \text{ in.}^2$, $\alpha = 6.5 \times 10^{-6}/^\circ\text{F}$, and $E = 29,000 \text{ ksi}$.

- (a) Due to the loading shown
- (b) Due to temperature decrease of 40°F for all members.

Solution: We start with the geometric data. The topological and geometric information is listed below.

Member m	n_-	n_+	α	L (in.)	$\frac{AE}{L}$ (kip/in.)
(1)	1	2	53.13°	$20(12)$	241.7
(2)	1	3	0	$28(12)$	172.6
(3)	3	2	135°	$22.63(12)$	213.6

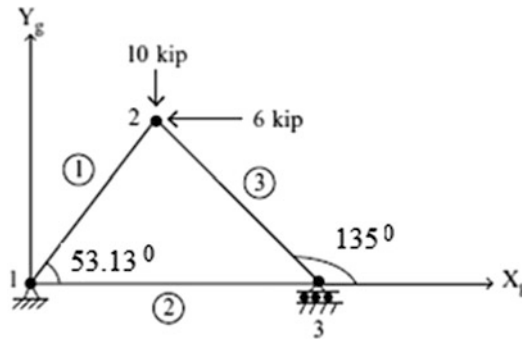


Fig. E12.9b

Member m	α	$\sin \alpha$	$\cos \alpha$	$\sin \alpha \cos \alpha$	$\sin \alpha^2$	$\cos \alpha^2$
(1)	53.13	0.8	0.6	0.48	0.64	0.36
(2)	0	0	1	0	0	1
(3)	135	.707	-0.707	-0.5	0.5	0.5

We determine the individual member matrices using (12.33).

$$\mathbf{k}_{(m)AA} = \mathbf{k}_{(m)BB} = \mathbf{k}_{(m)} = \left(\frac{AE}{L}\right)_{(m)} \begin{bmatrix} \cos^2 \alpha_{(m)} & \sin \alpha_{(m)} \cos \alpha_{(m)} \\ \sin \alpha_{(m)} \cos \alpha_{(m)} & \sin^2 \alpha_{(m)} \end{bmatrix}$$

$$\mathbf{k}_{(m)AB} = \mathbf{k}_{(m)BA} = -\mathbf{k}_{(m)} = -\left(\frac{AE}{L}\right)_{(m)} \begin{bmatrix} \cos^2 \alpha_{(m)} & \sin \alpha_{(m)} \cos \alpha_{(m)} \\ \sin \alpha_{(m)} \cos \alpha_{(m)} & \sin^2 \alpha_{(m)} \end{bmatrix}$$

The system stiffness matrix and displacement vector have the following form:

$$\mathbf{K} = \begin{bmatrix} \mathbf{k}_{(1)AA} & \mathbf{k}_{(1)AB} & 0 \\ \mathbf{k}_{(1)BA} & \mathbf{k}_{(1)BB} & 0 \\ 0 & 0 & 0 \end{bmatrix} + \begin{bmatrix} \mathbf{k}_{(2)AA} & 0 & \mathbf{k}_{(2)AB} \\ 0 & 0 & 0 \\ \mathbf{k}_{(2)BA} & 0 & \mathbf{k}_{(2)BB} \end{bmatrix} \begin{bmatrix} 0 & 0 & 0 \\ 0 & \mathbf{k}_{(3)AA} & \mathbf{k}_{(3)AB} \\ 0 & \mathbf{k}_{(3)BA} & \mathbf{k}_{(3)BB} \end{bmatrix}$$

$$= \begin{bmatrix} (\mathbf{k}_{(1)AA} + \mathbf{k}_{(2)AA}) & & \\ & \mathbf{k}_{(1)AB} & \mathbf{k}_{(2)AB} \\ & (\mathbf{k}_{(1)BB} + \mathbf{k}_{(3)AA}) & \mathbf{k}_{(3)AB} \\ & \mathbf{k}_{(2)BA} & (\mathbf{k}_{(2)BB} + \mathbf{k}_{(3)BB}) \\ & & & \mathbf{k}_{(3)BA} & & \end{bmatrix}$$

$$\mathbf{U} = \left\{ \begin{matrix} \mathbf{U}_1 \\ \mathbf{U}_2 \\ \mathbf{U}_3 \end{matrix} \right\} = \begin{Bmatrix} u_1 \\ v_1 \\ u_2 \\ v_2 \\ u_3 \\ v_3 \end{Bmatrix}$$

By substituting for individual matrices using (12.33), the system stiffness matrix takes the following form:

$$\mathbf{K} = \begin{pmatrix} 259.62 & 116 & -87 & -116 & -172.62 & 0 \\ 116 & 154.66 & -116 & -154.66 & 0 & 0 \\ -87 & -116 & 193.79 & 9.21 & -106.79 & 106.79 \\ -116 & -154.66 & 9.21 & 261.457 & 106.79 & -106.79 \\ -172.62 & 0 & -106.9 & 106.79 & 279.409 & -106.79 \\ 0 & 0 & 106.9 & -106.79 & -106.79 & 106.79 \end{pmatrix}$$

We note that node 1 is fully fixed but node 3 is partially fixed. We rearrange the rows and columns of \mathbf{K} , and the rows of \mathbf{U} . This step leads to the resulting partitioned vectors and matrices listed below.

$$\mathbf{U}' = \begin{Bmatrix} u_2 \\ v_2 \\ u_3 \end{Bmatrix} \quad \mathbf{U}'' = \begin{Bmatrix} u_1 \\ v_1 \\ v_3 \end{Bmatrix}$$

$$\mathbf{K}'_{11} = \begin{pmatrix} 193.79 & 9.21 & -106.79 \\ 9.21 & 261.46 & 106.79 \\ -106.79 & 106.79 & 279.41 \end{pmatrix} \quad \mathbf{K}'_{12} = \begin{pmatrix} -87 & -116 & 106.79 \\ -116 & -154.66 & -106.79 \\ -172.62 & 0 & -106.79 \end{pmatrix}$$

$$\mathbf{K}'_{21} = \begin{pmatrix} -87 & -116 & -172.62 \\ -116 & -154.66 & 0 \\ 106.79 & -106.79 & -106.79 \end{pmatrix} \quad \mathbf{K}'_{22} = \begin{pmatrix} 259.62 & 116 & 0 \\ 116 & 154.66 & 0 \\ 0 & 0 & 106.79 \end{pmatrix}$$

We need the inverse of \mathbf{K}'_{11} to solve for the displacement due to a given loading. Its form is

$$\left(\mathbf{K}'_{11}\right)^{-1} = \begin{pmatrix} 0.007 & -0.002 & 0.003 \\ -0.002 & 0.005 & -0.002 \\ 0.003 & -0.002 & 0.006 \end{pmatrix}$$

Part (a): Loading shown in Fig. E12.9a

The system load vectors corresponding to this loading are

$$\mathbf{P}'_E = \begin{Bmatrix} -6 \\ -10 \\ 0 \end{Bmatrix} \quad \mathbf{P}'_I = \mathbf{P}''_I = 0$$

We determine the unknown displacements using

$$\mathbf{U}' = \left(\mathbf{K}'_{11}\right)^{-1} \left(\mathbf{P}'_E\right) \Rightarrow \begin{Bmatrix} u_2 \\ v_2 \\ u_3 \end{Bmatrix} = \left(\mathbf{K}'_{11}\right)^{-1} \left(\mathbf{P}'_E\right) = \begin{Bmatrix} -0.026 \\ -0.039 \\ 0.005 \end{Bmatrix}$$

Given the displacements, one determines the reactions with

$$\mathbf{P}''_E = \mathbf{K}'_{21} \mathbf{U}' \Rightarrow \begin{Bmatrix} R_{1x} \\ R_{1y} \\ R_{3y} \end{Bmatrix} = \mathbf{K}'_{21} \mathbf{U}' = \begin{Bmatrix} 6 \\ 9.14 \\ 0.86 \end{Bmatrix}$$

Finally, we determine member forces:

$$F_{\ell(m)B} = \left(\frac{AE}{L}\right)_{(m)} [\cos \alpha_{(m)} \sin \alpha_{(m)}] (\mathbf{U}_{n^+} - \mathbf{U}_{n^-}) + F_{\ell(m)B}^F$$

$$F_{\ell(1)B} = 241.7[0.6 \quad 0.8] \begin{Bmatrix} -0.026 \\ -0.039 \end{Bmatrix} + 0 = -11.43 \text{ kip}$$

$$F_{\ell(2)B} = 172.6[1 \quad 0] \begin{Bmatrix} 0.005 \\ 0 \end{Bmatrix} + 0 = +0.86 \text{ kip}$$

$$F_{\ell(3)B} = 213.6[-0.707 \quad 0.707] \begin{Bmatrix} (-0.026 - 0.005) \\ -0.039 \end{Bmatrix} + 0 = -1.21 \text{ kip}$$

Part (b): $\Delta T = -40^\circ$ for all members

We determine the fixed end actions caused by the temperature decrease (Figs. E12.9c and E12.9d).

$$F_{l(m)}^F = EA\alpha\Delta T = (29,000)(2)(6.5 \times 10^{-6})(40) = 15.08 \text{ kip}$$

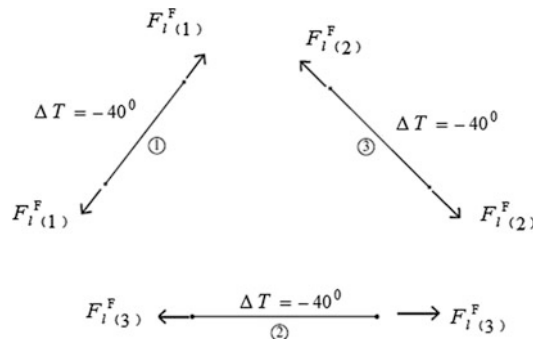


Fig. E12.9c Fixed end actions—members

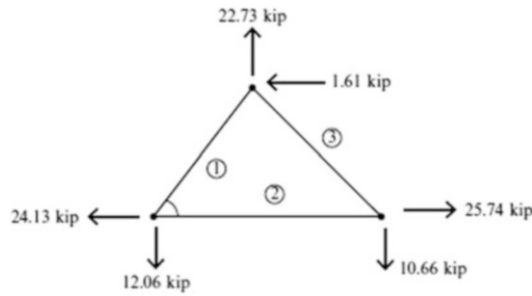


Fig. E12.9d Fixed end actions—joints

The system load vectors corresponding to these loads are

$$\mathbf{P}'_E = 0 \quad \mathbf{P}'_1 = \begin{Bmatrix} -1.61 \\ 22.73 \\ 25.74 \end{Bmatrix} \quad \mathbf{P}''_1 = \begin{Bmatrix} -24.13 \\ -12.06 \\ -10.66 \end{Bmatrix}$$

We determine the unknown displacements using

$$\mathbf{U}' = (\mathbf{K}'_{11})^{-1} (-\mathbf{P}'_1) \Rightarrow \begin{Bmatrix} u_2 \\ v_2 \\ u_3 \end{Bmatrix} = (\mathbf{K}'_{11})^{-1} (-\mathbf{P}'_1) = \begin{Bmatrix} -0.037 \text{ in.} \\ -0.05 \text{ in.} \\ -0.087 \text{ in.} \end{Bmatrix} \Rightarrow \begin{cases} u_2 = 0.037 \text{ in.} \leftarrow \\ v_2 = 0.05 \text{ in.} \downarrow \\ u_3 = 0.087 \text{ in.} \leftarrow \end{cases}$$

Given the displacements, one determines the reactions. For a determinate truss, the reactions will be zero. Also the member forces will be zero.

$$\mathbf{P}''_E = \mathbf{K}'_{21} \mathbf{U}' + \mathbf{P}''_1 \Rightarrow \begin{Bmatrix} R_{1x} \\ R_{1y} \\ R_{3y} \end{Bmatrix} = \mathbf{K}'_{21} \mathbf{U}' + \mathbf{P}''_1 = \begin{Bmatrix} 0 \\ 0 \\ 0 \end{Bmatrix}$$

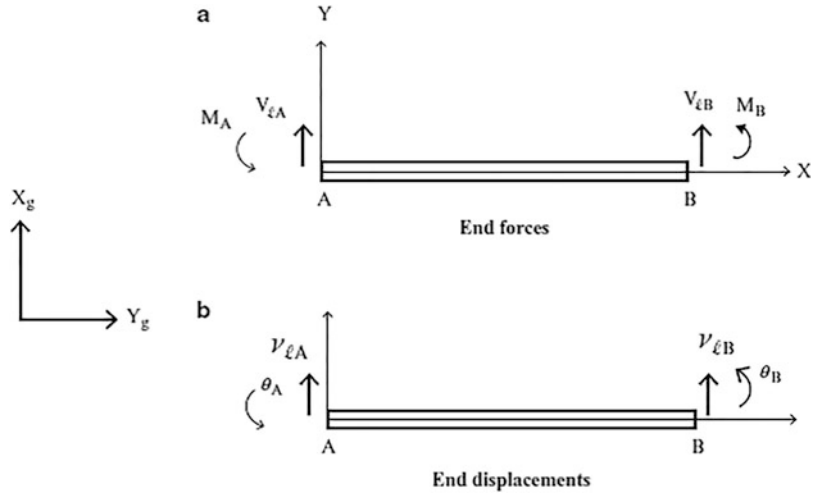
$$F_{\ell(m)B} = \left(\frac{AE}{L}\right)_{(m)} [\cos \alpha_{(m)} \sin \alpha_{(m)}] (\mathbf{U}_{n^+} - \mathbf{U}_{n^-}) + F_{\ell(m)B}^F$$

$$F_{\ell(1)B} = F_{\ell(2)B} = F_{\ell(3)B} = 0$$

12.7.2 The Steps Involved for Beam Structures with Transverse Loading—Planar Behavior

The member forces for a beam member subjected to transverse loading consist only of shear and moment, i.e., there is no axial force. Also, each node of a beam has only *two displacement unknowns: the rotation and transverse displacement*. We take these simplifications into account by defining “reduced” member and nodal matrices. The procedure is similar to that followed for the trusses.

Fig. 12.8 Member end forces and displacements



We start with the member equations. Figure 12.8 shows the member force and displacement measures. For beam structures, the local and global frames are taken to be the same. The “reduced” displacement and end action matrices are

$$\begin{aligned} \mathbf{U}_{\ell B} &= \begin{Bmatrix} v_{\ell B} \\ \theta_B \end{Bmatrix} & \mathbf{U}_{\ell A} &= \begin{Bmatrix} v_{\ell A} \\ \theta_A \end{Bmatrix} \\ \mathbf{P}_{\ell B} &= \begin{Bmatrix} V_{\ell B} \\ M_B \end{Bmatrix} & \mathbf{P}_{\ell A} &= \begin{Bmatrix} V_{\ell A} \\ M_A \end{Bmatrix} \end{aligned} \quad (12.35)$$

We obtain the “reduced” member stiffness matrices by deleting the first row and column of the matrices listed in (12.6).

$$\begin{aligned} \mathbf{k}_{AA} &= \begin{bmatrix} \frac{12EI}{L^3} & \frac{6EI}{L^2} \\ \frac{6EI}{L^2} & \frac{4EI}{L} \end{bmatrix} & \mathbf{k}_{AB} &= \begin{bmatrix} -\frac{12EI}{L^3} & \frac{6EI}{L^2} \\ -\frac{6EI}{L^2} & \frac{2EI}{L} \end{bmatrix} \\ \mathbf{k}_{BB} &= \begin{bmatrix} \frac{12EI}{L^3} & -\frac{6EI}{L^2} \\ -\frac{6EI}{L^2} & \frac{4EI}{L} \end{bmatrix} & \mathbf{k}_{BA} &= \begin{bmatrix} -\frac{12EI}{L^3} & -\frac{6EI}{L^2} \\ \frac{6EI}{L^2} & \frac{2EI}{L} \end{bmatrix} \end{aligned} \quad (12.36)$$

The remaining steps involved in assembling the system matrices and introducing the support fixity are the *same* as described earlier for the general frame. Note that no rotation transformations are required here since the local and global frames coincide.

Example 12.10: Two-Span Beam

Given: The beam shown in Fig. E12.10a. The properties are taken as

$$L_{(1)} = L_{(2)} = L = 20 \text{ ft}, I_{(1)} = I_{(2)} = I = 428 \text{ in.}^4, E = 29,000 \text{ ksi}$$

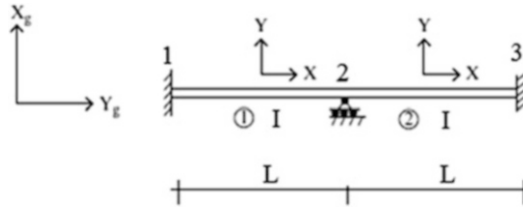


Fig. E12.10a

Determine: The joint displacements and member forces due to (i) the loading in Fig. E12.10b, (ii) support settlement in Fig. E12.10c.

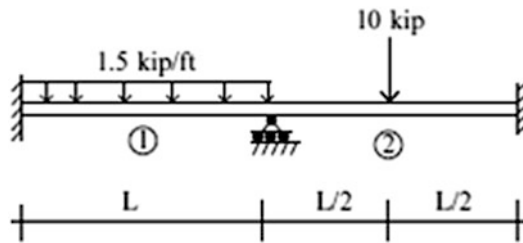


Fig. E12.10b

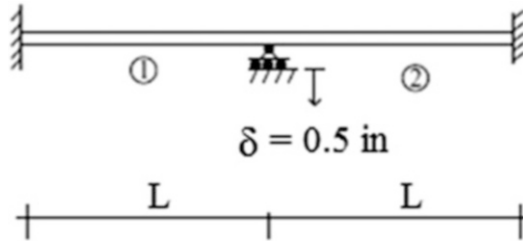


Fig. E12.10c

Solution:

We start with the geometric data listed below.

Member m	n_-	n_+
(1)	1	2
(2)	2	3

The system stiffness matrix has the following form:

$$\mathbf{K} = \begin{bmatrix} \mathbf{k}_{(1)AA} & \mathbf{k}_{(1)AB} & 0 \\ \mathbf{k}_{(1)BA} & \mathbf{k}_{(1)BB} & 0 \\ 0 & 0 & 0 \end{bmatrix} + \begin{bmatrix} 0 & 0 & 0 \\ 0 & \mathbf{k}_{(2)AA} & \mathbf{k}_{(2)AB} \\ 0 & \mathbf{k}_{(2)BA} & \mathbf{k}_{(2)BB} \end{bmatrix}$$

$$= \begin{bmatrix} \mathbf{k}_{(1)AA} & \mathbf{k}_{(1)AB} & 0 \\ \mathbf{k}_{(1)BA} & (\mathbf{k}_{(1)BB} + \mathbf{k}_{(2)AA}) & \mathbf{k}_{(2)AB} \\ 0 & \mathbf{k}_{(2)BA} & \mathbf{k}_{(2)BB} \end{bmatrix}$$

The member stiffness matrices follow from Equation (12.36). Since the lengths and cross-sectional properties are equal, the corresponding matrices are equal.

$$\mathbf{k}_{(1)AA} = \mathbf{k}_{(2)AA} = \begin{bmatrix} \frac{12EI}{L^3} & \frac{6EI}{L^2} \\ \frac{6EI}{L^2} & \frac{4EI}{L} \end{bmatrix} \quad \mathbf{k}_{(1)AB} = \mathbf{k}_{(2)AB} = \begin{bmatrix} -\frac{12EI}{L^3} & -\frac{6EI}{L^2} \\ \frac{6EI}{L^2} & \frac{2EI}{L} \end{bmatrix}$$

$$\mathbf{k}_{(1)BA} = \mathbf{k}_{(2)BA} = \begin{bmatrix} -\frac{12EI}{L^3} & -\frac{6EI}{L^2} \\ \frac{6EI}{L^2} & \frac{2EI}{L} \end{bmatrix} \quad \mathbf{k}_{(1)BB} = \mathbf{k}_{(2)BB} = \begin{bmatrix} \frac{12EI}{L^3} & -\frac{6EI}{L^2} \\ -\frac{6EI}{L^2} & \frac{4EI}{L} \end{bmatrix}$$

Substituting for the member matrices, the system matrix expands to:

$$\mathbf{K} = \begin{pmatrix} \frac{12EI}{L^3} & \frac{6EI}{L^2} & -\frac{12EI}{L^3} & -\frac{6EI}{L^2} & 0 & 0 \\ \frac{6EI}{L^2} & \frac{4EI}{L} & -\frac{6EI}{L^2} & \frac{2EI}{L} & 0 & 0 \\ \frac{12EI}{L^3} & \frac{6EI}{L^2} & \frac{12EI}{L^3} & \frac{6EI}{L^2} & -\frac{12EI}{L^3} & \frac{6EI}{L^2} \\ -\frac{6EI}{L^2} & -\frac{2EI}{L} & -\frac{6EI}{L^2} & -\frac{2EI}{L} & \frac{6EI}{L^2} & \frac{2EI}{L} \\ \frac{6EI}{L^2} & \frac{2EI}{L} & 0 & \frac{8EI}{L} & -\frac{6EI}{L^2} & \frac{2EI}{L} \\ 0 & 0 & -\frac{12EI}{L^3} & -\frac{6EI}{L^2} & \frac{12EI}{L^3} & -\frac{6EI}{L^2} \\ 0 & 0 & \frac{6EI}{L^2} & \frac{2EI}{L} & -\frac{6EI}{L^2} & \frac{4EI}{L} \end{pmatrix}$$

The system nodal displacement and nodal load terms follow from (12.19).

$$\mathbf{U} = \begin{Bmatrix} v_1 \\ \theta_1 \\ v_2 \\ \theta_2 \\ v_3 \\ \theta_3 \end{Bmatrix} \quad \mathbf{P}_E = \begin{Bmatrix} R_{y1} \\ M_1 \\ R_{y2} \\ M_2 \\ R_{y3} \\ M_3 \end{Bmatrix} \quad \mathbf{P}_1 = \begin{Bmatrix} V_{(1)A}^F \\ M_{(1)A}^F \\ (V_{(1)B}^F + V_{(2)A}^F) \\ (M_{(1)B}^F + M_{(2)A}^F) \\ V_{(2)B}^F \\ M_{(2)B}^F \end{Bmatrix}$$

Nodes 1 and 3 are fully fixed and node 2 is partially fixed. The only unknown displacement is θ_2 . We rearrange the rows and columns according to the systematic approach described in Sect. 12.6.1. Noting (12.23) and (12.24), the rearranged terms are

$$\mathbf{U}' = \{\theta_2\} \quad \mathbf{U}'' = \begin{Bmatrix} v_1 \\ \theta_1 \\ v_2 \\ v_3 \\ \theta_3 \end{Bmatrix}$$

and

$$\mathbf{P}'_E = \{M_2\} \quad \mathbf{P}''_E = \begin{Bmatrix} R_{y1} \\ M_1 \\ R_{y2} \\ R_{y3} \\ M_3 \end{Bmatrix}$$

$$\mathbf{P}'_I = \left\{ \left(M_{(1)B}^F + M_{(2)A}^F \right) \right\} \quad \mathbf{P}''_I = \begin{Bmatrix} V_{(1)A}^F \\ M_{(1)A}^F \\ \left(V_{(1)B}^F + V_{(2)A}^F \right) \\ V_{(2)B}^F \\ M_{(2)B}^F \end{Bmatrix}$$

$$\mathbf{K}' = \begin{pmatrix} \frac{8EI}{L} & \frac{6EI}{L^2} & \frac{2EI}{L} & 0 & \frac{-6EI}{L^2} & \frac{2EI}{L} \\ \frac{6EI}{L^2} & \frac{12EI}{L^3} & \frac{6EI}{L^2} & \frac{-12EI}{L^3} & 0 & 0 \\ \frac{2EI}{L} & \frac{6EI}{L^2} & \frac{4EI}{L} & \frac{-6EI}{L^2} & 0 & 0 \\ 0 & \frac{-12EI}{L^3} & \frac{-6EI}{L^2} & \frac{24EI}{L^3} & \frac{-12EI}{L^3} & \frac{6EI}{L^2} \\ \frac{-6EI}{L^2} & 0 & 0 & \frac{-12EI}{L^3} & \frac{12EI}{L^3} & \frac{-6EI}{L^2} \\ \frac{2EI}{L} & 0 & 0 & \frac{6EI}{L^2} & \frac{-6EI}{L^2} & \frac{4EI}{L} \end{pmatrix}$$

$$\mathbf{K}'_{11} = \left\{ \frac{8EI}{L} \right\} \quad \mathbf{K}'_{12} = \left\{ \frac{6EI}{L^2} \quad \frac{2EI}{L} \quad 0 \quad \frac{-6EI}{L^2} \quad \frac{2EI}{L} \right\}$$

$$\mathbf{K}'_{21} = \begin{Bmatrix} \frac{6EI}{L^2} \\ \frac{2EI}{L} \\ 0 \\ \frac{-6EI}{L^2} \\ \frac{2EI}{L} \end{Bmatrix} \quad \mathbf{K}'_{22} = \begin{bmatrix} \frac{12EI}{L^3} & \frac{6EI}{L^2} & \frac{-12EI}{L^3} & 0 & 0 \\ \frac{6EI}{L^2} & \frac{4EI}{L} & \frac{-6EI}{L^2} & 0 & 0 \\ \frac{-12EI}{L^3} & \frac{-6EI}{L^2} & \frac{24EI}{L^3} & \frac{-12EI}{L^3} & \frac{6EI}{L^2} \\ 0 & 0 & \frac{-12EI}{L^3} & \frac{12EI}{L^3} & \frac{-6EI}{L^2} \\ 0 & 0 & \frac{6EI}{L^2} & \frac{-6EI}{L^2} & \frac{4EI}{L} \end{bmatrix}$$

The inverse of \mathbf{K}'_{11} is

$$\left(\mathbf{K}'_{11}\right)^{-1} = \frac{L}{8EI} = \frac{20(12)}{8(29,000)(428)} = 2.417(10^{-6})$$

(i) *Loading:*

We consider the loading shown in Fig. E12.10b. The fixed end actions due to the loading applied to members 1 and 2 are defined in Fig. E12.10d.

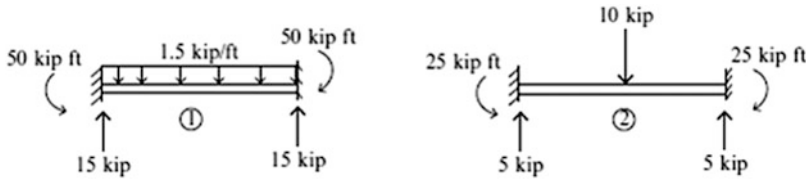


Fig. E12.10d

Substituting for the fixed end actions, the various nodal displacement and load terms reduce to $\mathbf{U}' = \{\theta_2\}$ $\mathbf{U}'' = 0$ (No support movement)

$$\mathbf{P}'_E = \{0\} \quad \mathbf{P}'_1 = \{(-50 + 25)\} = \{-25 \text{ kip ft}\} \quad \mathbf{P}''_1 = \left\{ \begin{array}{l} 15.0 \text{ kip} \\ 50.0 \text{ kip ft} \\ (15.0 + 5.0) \text{ kip} \\ 5.0 \text{ kip} \\ -25.0 \text{ kip ft} \end{array} \right\}$$

The unknown displacement is determined with (12.26) specialized for this example

$$\begin{aligned} \mathbf{U}' &= (\mathbf{K}'_{11})^{-1} (\mathbf{P}'_E - \mathbf{K}'_{12} \mathbf{U}'' - \mathbf{P}'_1) \\ &\downarrow \\ \mathbf{U}' &= (\mathbf{K}'_{11})^{-1} (-\mathbf{P}'_1) \\ &\downarrow \\ \theta_2 &= \left(\frac{L}{8EI} \right) (25.0 \text{ kip ft}) = \frac{3.125L}{EI} = \frac{3.125(20)(12)^2}{29,000(428)} = 0.000725 \text{ rad} \end{aligned}$$

Given the displacement, one determines the reactions with the second equation in (12.25):

$$\begin{aligned} \mathbf{P}''_E &= \mathbf{K}'_{21} \mathbf{U}' + \mathbf{K}'_{22} \mathbf{U}'' + \mathbf{P}''_1 \\ &\downarrow \\ \mathbf{P}''_E &= \mathbf{K}'_{21} \mathbf{U}' + \mathbf{P}''_1 \\ &\downarrow \\ \left\{ \begin{array}{l} R_{y1} \\ M_1 \\ R_{y2} \\ R_{y3} \\ M_3 \end{array} \right\} &= \left\{ \begin{array}{l} \frac{6EI}{L^2} \\ \frac{2EI}{L} \\ 0 \\ -\frac{6EI}{L^2} \\ \frac{2EI}{L} \end{array} \right\} \left(\frac{3.125L}{EI} \right) + \left\{ \begin{array}{l} 15 \\ 50 \\ 20 \\ 5 \\ -25 \end{array} \right\} = \left\{ \begin{array}{l} 15.94 \text{ kip} \\ 56.25 \text{ kip ft} \\ 20.0 \text{ kip} \\ 4.06 \text{ kip} \\ -18.75 \text{ kip ft} \end{array} \right\} \end{aligned}$$

The reactions are listed on Fig. E12.10e.

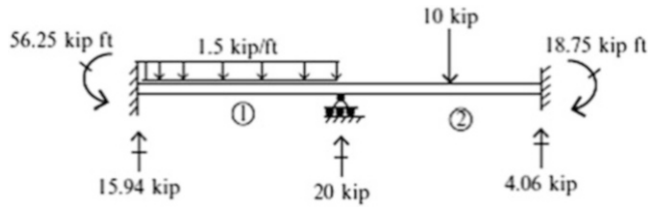


Fig. E12.10e

Lastly, we compute the member end actions.

$$\begin{aligned} \mathbf{P}_{(1)A} &= \begin{Bmatrix} V_{(1)A} \\ M_{(1)A} \end{Bmatrix} = \mathbf{k}_{(1)AB} \begin{Bmatrix} v_2 \\ \theta_2 \end{Bmatrix} + \begin{Bmatrix} V_{(1)A}^F \\ M_{(1)A}^F \end{Bmatrix} \\ &= \begin{bmatrix} -\frac{12EI}{L^3} & \frac{6EI}{L^2} \\ \frac{6EI}{L^2} & \frac{2EI}{L} \end{bmatrix} \begin{Bmatrix} 0 \\ \frac{3.125L}{EI} \end{Bmatrix} + \begin{Bmatrix} 15.0 \\ 50.0 \end{Bmatrix} = \begin{Bmatrix} 15.94 \\ 56.25 \end{Bmatrix} \end{aligned}$$

$$\begin{aligned} \mathbf{P}_{(1)B} &= \begin{Bmatrix} V_{(1)B} \\ M_{(1)B} \end{Bmatrix} = \mathbf{k}_{(1)BB} \begin{Bmatrix} v_2 \\ \theta_2 \end{Bmatrix} + \begin{Bmatrix} V_{(1)B}^F \\ M_{(1)B}^F \end{Bmatrix} \\ &= \begin{bmatrix} \frac{12EI}{L^3} & -\frac{6EI}{L^2} \\ -\frac{6EI}{L^2} & \frac{4EI}{L} \end{bmatrix} \begin{Bmatrix} 0 \\ \frac{3.125L}{EI} \end{Bmatrix} + \begin{Bmatrix} 15.0 \\ -50.0 \end{Bmatrix} = \begin{Bmatrix} 14.06 \\ -37.50 \end{Bmatrix} \end{aligned}$$

$$\begin{aligned} \mathbf{P}_{(2)A} &= \begin{Bmatrix} V_{(2)A} \\ M_{(2)A} \end{Bmatrix} = \mathbf{k}_{(2)AA} \begin{Bmatrix} v_2 \\ \theta_2 \end{Bmatrix} + \begin{Bmatrix} V_{(2)A}^F \\ M_{(2)A}^F \end{Bmatrix} \\ &= \begin{bmatrix} \frac{12EI}{L^3} & \frac{6EI}{L^2} \\ \frac{6EI}{L^2} & \frac{4EI}{L} \end{bmatrix} \begin{Bmatrix} 0 \\ \frac{3.125L}{EI} \end{Bmatrix} + \begin{Bmatrix} 5.0 \\ 25.0 \end{Bmatrix} = \begin{Bmatrix} 5.94 \\ 37.50 \end{Bmatrix} \end{aligned}$$

$$\begin{aligned} \mathbf{P}_{(2)B} &= \begin{Bmatrix} V_{(2)B} \\ M_{(2)B} \end{Bmatrix} = \mathbf{k}_{(1)BA} \begin{Bmatrix} v_2 \\ \theta_2 \end{Bmatrix} + \begin{Bmatrix} V_{(2)B}^F \\ M_{(2)B}^F \end{Bmatrix} \\ &= \begin{bmatrix} -\frac{12EI}{L^3} & -\frac{6EI}{L^2} \\ \frac{6EI}{L^2} & \frac{2EI}{L} \end{bmatrix} \begin{Bmatrix} 0 \\ \frac{3.125L}{EI} \end{Bmatrix} + \begin{Bmatrix} 5.0 \\ -25.0 \end{Bmatrix} = \begin{Bmatrix} 4.06 \\ -18.75 \end{Bmatrix} \end{aligned}$$

The results are summarized in Fig. E12.10f.

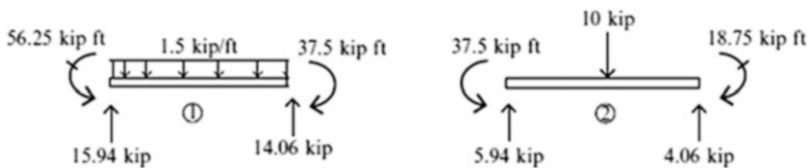


Fig. E12.10f

(ii) *Support Settlement:*

We consider a support settlement of $\delta = 0.5$ in. \downarrow at joint 2. The corresponding loading terms are

$$\mathbf{U}' = \{\theta_2\} \quad \mathbf{U}'' = \begin{Bmatrix} 0 \\ 0 \\ \delta \\ 0 \\ 0 \end{Bmatrix} \quad \mathbf{P}'_E = \{0\} \quad \mathbf{P}'_1 = 0 \quad \mathbf{P}''_1 = 0$$

Then noting (12.26),

$$\mathbf{U}' = (\mathbf{K}'_{11})^{-1} (-\mathbf{K}'_{12} \mathbf{U}'')$$

$$\theta_2 = -\frac{L}{8EI} \left\{ \frac{6EI}{L^2} \quad \frac{2EI}{L} \quad 0 \quad -\frac{6EI}{L^2} \quad \frac{2EI}{L} \right\} \begin{Bmatrix} 0 \\ 0 \\ \delta \\ 0 \\ 0 \end{Bmatrix} = 0.0$$

We evaluate the reactions with (12.25). In this case, $\mathbf{U}' = 0$.

$$\mathbf{P}''_E = \mathbf{K}''_{22} \mathbf{U}''$$

$$\begin{Bmatrix} R_{y1} \\ M_1 \\ R_{y2} \\ R_{y3} \\ M_3 \end{Bmatrix} = \begin{bmatrix} \frac{12EI}{L^3} & \frac{6EI}{L^2} & -\frac{12EI}{L^3} & 0 & 0 \\ \frac{6EI}{L^2} & \frac{4EI}{L} & -\frac{6EI}{L^2} & 0 & 0 \\ \frac{12EI}{L^3} & \frac{6EI}{L^2} & \frac{24EI}{L^3} & -\frac{12EI}{L^3} & \frac{6EI}{L^2} \\ -\frac{12EI}{L^3} & -\frac{6EI}{L^2} & \frac{24EI}{L^3} & -\frac{12EI}{L^3} & \frac{6EI}{L^2} \\ 0 & 0 & -\frac{12EI}{L^3} & \frac{12EI}{L^3} & -\frac{6EI}{L^2} \\ 0 & 0 & \frac{6EI}{L^2} & -\frac{6EI}{L^2} & \frac{4EI}{L} \end{bmatrix} \begin{Bmatrix} 0 \\ 0 \\ \delta \\ 0 \\ 0 \end{Bmatrix} = \begin{Bmatrix} -\frac{12EI}{L^3} \delta \\ -\frac{6EI}{L^2} \delta \\ \frac{24EI}{L^3} \delta \\ -\frac{12EI}{L^3} \delta \\ \frac{6EI}{L^2} \delta \end{Bmatrix}$$

Using the given properties and taking $\delta = -0.5$ in. result in the forces shown in Figs. E12.10g and E12.10h.

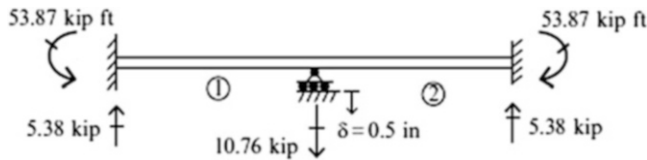


Fig. E12.10g

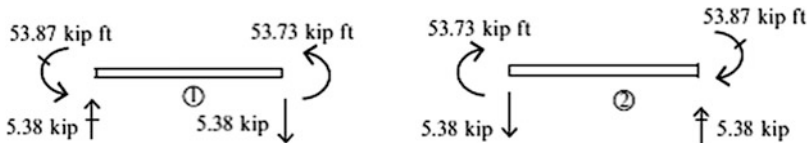


Fig. E12.10h

Example 12.11. Two-Span Beam with a Spring Support at Mid-span

Given: The structure shown in Fig. E12.11a. Node 2 is supported with a spring of stiffness $k_v = 200$ kip/ft. Taken $L = 20$ ft, $I = 428$ in.⁴, and $E = 29,000$ ksi.

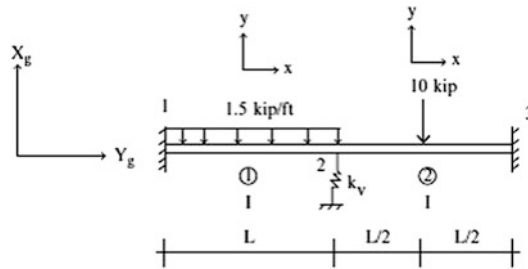


Fig. E12.11a

Determine: The displacements at node 2 and the member end forces (Fig. E12.11b)

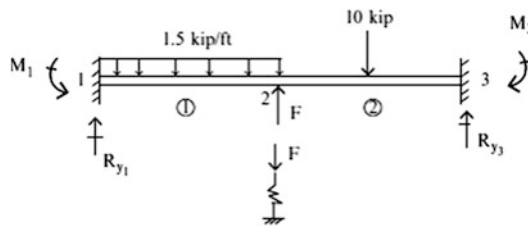


Fig. E12.11b

Solution:

Nodes 1 and 3 are fully fixed and node 2 is restrained by a linear elastic spring. The unknown displacements at node 2 are the vertical displacement v_2 and the rotation θ_2 . We arrange the rows and columns of the system matrix consistent with this support condition. The spring is introduced by adding an external nodal force at node 2 with a magnitude equal to $F = -k_v v_2$. The minus sign is needed since the spring force acts in the opposite direction to the displacement. We utilize the results for \mathbf{K} and \mathbf{P}_1 contained in Example 12.10. The initial and rearranged matrices are

$$\mathbf{K} = \begin{pmatrix} \frac{12EI}{L^3} & \frac{6EI}{L^2} & -\frac{12EI}{L^3} & \frac{6EI}{L^2} & 0 & 0 \\ \frac{6EI}{L^2} & \frac{4EI}{L} & -\frac{6EI}{L^2} & \frac{2EI}{L} & 0 & 0 \\ \frac{L^2}{12EI} & \frac{L}{6EI} & -\frac{L^2}{24EI} & \frac{L}{6EI} & \frac{12EI}{L^3} & \frac{6EI}{L^2} \\ -\frac{L^3}{6EI} & -\frac{L^2}{2EI} & \frac{L^3}{6EI} & \frac{L^2}{2EI} & -\frac{L^3}{6EI} & \frac{L^2}{2EI} \\ \frac{L^2}{6EI} & \frac{L}{2EI} & 0 & \frac{L}{2EI} & -\frac{L^2}{6EI} & \frac{L}{2EI} \\ 0 & 0 & -\frac{12EI}{L^3} & -\frac{6EI}{L^2} & \frac{12EI}{L^3} & -\frac{6EI}{L^2} \\ 0 & 0 & \frac{L^3}{6EI} & \frac{L^2}{2EI} & -\frac{L^3}{6EI} & \frac{L^2}{2EI} \end{pmatrix}$$

$$\mathbf{U} = \begin{Bmatrix} v_1 \\ \theta_1 \\ v_2 \\ \theta_2 \\ v_3 \\ \theta_3 \end{Bmatrix} \quad \mathbf{P}_E = \begin{Bmatrix} R_{y1} \\ M_1 \\ (V_{(1)B} + V_{(2)A}) \\ (M_{(1)B} + M_{(2)A}) \\ R_{y3} \\ M_3 \end{Bmatrix}$$

and

$$\mathbf{U}' = \begin{Bmatrix} v_2 \\ \theta_2 \end{Bmatrix} \quad \mathbf{U}'' = \begin{Bmatrix} v_1 \\ \theta_1 \\ v_3 \\ \theta_3 \end{Bmatrix}$$

$$\mathbf{P}'_E = \begin{Bmatrix} -k_v v_2 \\ 0 \end{Bmatrix} \quad \mathbf{P}'_I = \begin{Bmatrix} 20 \text{ kip} \\ -25 \text{ kip ft} \end{Bmatrix} \quad \mathbf{P}'_{II} = \begin{Bmatrix} 15 \text{ kip} \\ 50 \text{ kip ft} \\ 5 \text{ kip} \\ -25 \text{ kip ft} \end{Bmatrix}$$

$$\mathbf{K}' = \begin{bmatrix} \frac{24EI}{L^3} & 0 & -\frac{12EI}{L^3} & -\frac{6EI}{L^2} & -\frac{12EI}{L^3} & \frac{6EI}{L^2} \\ 0 & \frac{8EI}{L} & \frac{6EI}{L^2} & \frac{2EI}{L} & -\frac{6EI}{L^2} & \frac{2EI}{L} \\ -\frac{12EI}{L^3} & \frac{6EI}{L} & \frac{12EI}{L^2} & \frac{6EI}{L} & 0 & 0 \\ -\frac{6EI}{L^3} & \frac{2EI}{L^2} & \frac{6EI}{L^3} & \frac{4EI}{L^2} & 0 & 0 \\ \frac{12EI}{L^3} & \frac{6EI}{L} & -\frac{6EI}{L^2} & 0 & \frac{12EI}{L^3} & -\frac{6EI}{L^2} \\ \frac{6EI}{L^3} & \frac{2EI}{L^2} & 0 & 0 & -\frac{6EI}{L^3} & \frac{4EI}{L^2} \\ \frac{12EI}{L^3} & \frac{6EI}{L} & -\frac{6EI}{L^2} & 0 & \frac{12EI}{L^3} & -\frac{6EI}{L^2} \\ \frac{6EI}{L^3} & \frac{2EI}{L^2} & 0 & 0 & -\frac{6EI}{L^3} & \frac{4EI}{L^2} \end{bmatrix}$$

$$\mathbf{K}'_{11} = \begin{bmatrix} \frac{24EI}{L^3} & 0 \\ 0 & \frac{8EI}{L} \end{bmatrix} \quad \mathbf{K}'_{12} = \begin{bmatrix} -\frac{12EI}{L^3} & -\frac{6EI}{L^2} & -\frac{12EI}{L^3} & \frac{6EI}{L^2} \\ \frac{6EI}{L^2} & \frac{2EI}{L} & \frac{6EI}{L^2} & \frac{2EI}{L} \end{bmatrix}$$

$$\mathbf{K}'_{21} = \begin{bmatrix} -\frac{12EI}{L^3} & \frac{6EI}{L^2} \\ -\frac{6EI}{L^2} & \frac{2EI}{L} \\ \frac{12EI}{L^3} & -\frac{6EI}{L^2} \\ \frac{6EI}{L^3} & \frac{2EI}{L^2} \end{bmatrix} \quad \mathbf{K}'_{22} = \begin{bmatrix} \frac{12EI}{L^3} & \frac{6EI}{L^2} & 0 & 0 \\ \frac{6EI}{L^2} & \frac{4EI}{L} & 0 & 0 \\ 0 & 0 & \frac{12EI}{L^3} & -\frac{6EI}{L^2} \\ 0 & 0 & -\frac{6EI}{L^3} & \frac{4EI}{L^2} \end{bmatrix}$$

Assuming nodes 1 and 3 are fixed, the reduced equations are

$$\mathbf{P}'_E = \mathbf{K}'_{11} \mathbf{U}' + \mathbf{P}'_I$$

Noting the matrices listed above, this equation expands to

$$\begin{Bmatrix} -k_v v_2 \\ 0 \end{Bmatrix} = \begin{Bmatrix} 20.0 \\ -25.0 \end{Bmatrix} + \frac{EI}{L} \begin{bmatrix} \frac{24}{L^2} & 0 \\ 0 & 8 \end{bmatrix} \begin{Bmatrix} v_2 \\ \theta_2 \end{Bmatrix}$$

We transfer the term involving v_2 over to the right hand side and solve for v_2, θ_2 .

$$\begin{bmatrix} \left(\frac{24EI}{L^3} + k_v \right) & 0 \\ 0 & \frac{8EI}{L} \end{bmatrix} \begin{Bmatrix} v_2 \\ \theta_2 \end{Bmatrix} = \begin{Bmatrix} -20.0 \\ +25.0 \end{Bmatrix}$$

When a particular nodal displacement is elastically restrained, we modify the system stiffness matrix \mathbf{K} , by adding the spring stiffness to the *diagonal entry that corresponds to the displacement*. We then rearrange the rows and columns to generate \mathbf{K}' . Continuing with the computation, the displacements at node 2 are

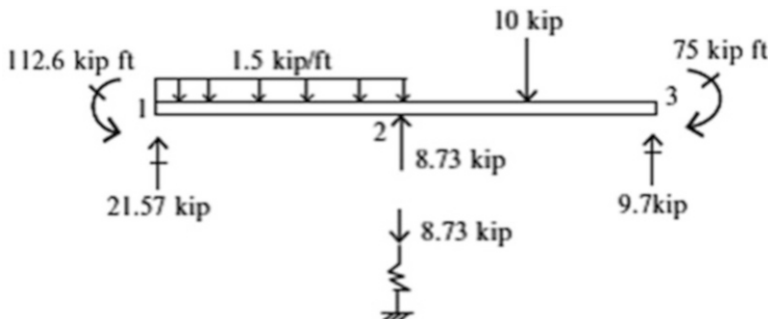
$$\begin{aligned} (\mathbf{K}'_{11})^{-1} &= \begin{bmatrix} \left(\frac{24EI}{L^3} + k_v \right) & 0 \\ 0 & \frac{8EI}{L} \end{bmatrix}^{-1} = \begin{bmatrix} \frac{1}{\left(\frac{24EI}{L^3} + k_v \right)} & 0 \\ 0 & \frac{L}{8EI} \end{bmatrix} \\ \Rightarrow \mathbf{U}' = \begin{Bmatrix} v_2 \\ \theta_2 \end{Bmatrix} &= (\mathbf{K}'_{11})^{-1} (-\mathbf{P}'_1) = \begin{bmatrix} -\frac{(20 \text{ kip})}{\left(\frac{24EI}{L^3} + k_v \right)} \\ +\frac{L(25 \text{ kip})}{8EI} \end{bmatrix} = \begin{Bmatrix} -0.523 \text{ in.} \\ 0.000725 \text{ rad} \end{Bmatrix} \end{aligned}$$

Lastly, the reactions are determined with

$$\begin{aligned} \mathbf{P}''_E &= \mathbf{K}'_{21} \mathbf{U}' + \mathbf{P}'_1 \\ \Downarrow \\ \begin{Bmatrix} R_{y1} \\ M_1 \\ R_{y3} \\ M_3 \end{Bmatrix} &= \begin{bmatrix} -\frac{12EI}{L^3} & \frac{6EI}{L^2} \\ \frac{6EI}{L^2} & \frac{2EI}{L} \\ -\frac{12EI}{L^3} & -\frac{6EI}{L^2} \\ \frac{6EI}{L^2} & \frac{2EI}{L} \end{bmatrix} \begin{Bmatrix} \frac{(20 \text{ kip})}{\left(\frac{24EI}{L^3} + k_v \right)} \\ +\frac{L(25 \text{ kip ft})}{8EI} \end{Bmatrix} + \begin{Bmatrix} 15.0 \text{ kip} \\ 50 \text{ kip ft} \\ 5.0 \text{ kip} \\ -25 \text{ kip ft} \end{Bmatrix} = \begin{Bmatrix} 21.57 \text{ kip} \\ 112.6 \text{ kip ft} \\ 9.7 \text{ kip} \\ -75 \text{ kip ft} \end{Bmatrix} \end{aligned}$$

$$F = -k_v v_2 = -(200 \text{ kip/ft}) \left(\frac{1}{12} \right) (-0.5230) = 8.73 \text{ kip}$$

The results are listed below.



12.8 Three-Dimensional Formulation

In what follows, we extend the planar formulation presented in the previous sections to deal with the case where the loading is three dimensional (3D). The basic approach is the same; one just has to expand the definition of the displacement, end action, and member stiffness matrices. The three-dimensional formulation is much more detailed, and is generally executed using a digital computer.

We start by defining the local coordinate system for a prismatic member. We take the X_1 direction to coincide with the centroidal axis, and X_2 and X_3 as the principle inertia directions for the cross section. Figure 12.9 shows this notation. The inertia properties for X_2 and X_3 are defined as

$$\begin{aligned} I_2 &= \int_A x_3^2 \, dA \\ I_3 &= \int_A x_2^2 \, dA \end{aligned} \quad (12.37)$$

There are six displacement measures for the 3D case, three translations and three rotations. The corresponding force measures are defined in a similar manner. We refer these quantities to the local directions and use the notation defined in Fig. 12.10.

Using this notation, the 3D versions of the displacement and end action matrices at the end points A and B are

Fig. 12.9 Local coordinate system for a prismatic member

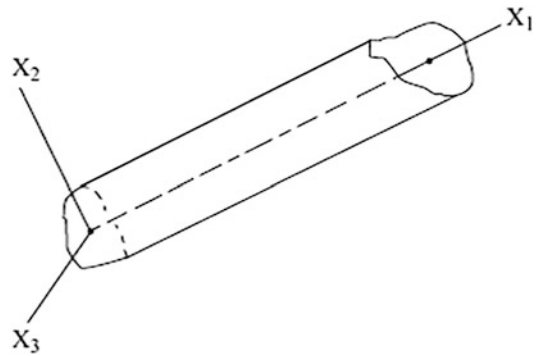
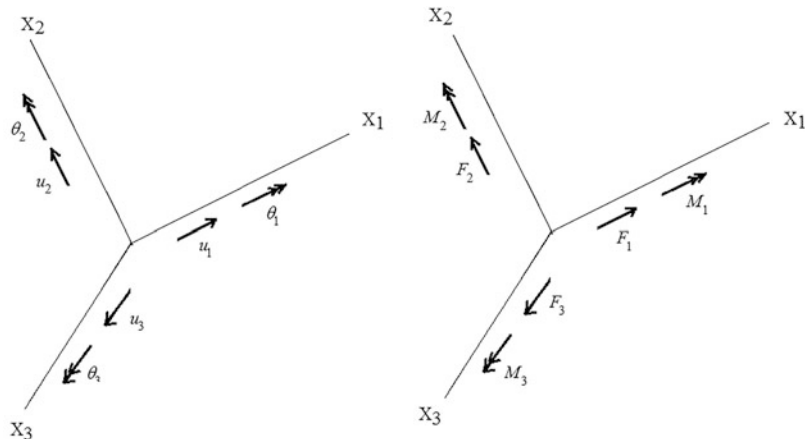


Fig. 12.10 End displacements and forces in local coordinate system



$$\begin{aligned}
F_{1\ell_A} &= -\frac{AE}{L}(u_{1\ell_B} - u_{1\ell_A}) + F_{1\ell_A}^F \\
F_{2\ell_A} &= \frac{6EI_3}{L^2}(\theta_{3B} + \theta_{3A}) - \frac{12EI_3}{L^3}(u_{2\ell_B} - u_{2\ell_A}) + F_{2\ell_A}^F \\
F_{3\ell_A} &= \frac{6EI_2}{L^2}(\theta_{2B} + \theta_{2A}) - \frac{12EI_2}{L^3}(u_{3\ell_B} - u_{3\ell_A}) + F_{3\ell_A}^F \\
M_{1A} &= -\frac{GJ}{L}(\theta_{1B} - \theta_{1A}) + M_{1A}^F \\
M_{2A} &= \frac{2EI_2}{L}(\theta_{2B} + 2\theta_{2A}) - \frac{6EI_2}{L^2}(u_{3\ell_B} - u_{3\ell_A}) + M_{2A}^F \\
M_{3A} &= \frac{2EI_3}{L}(\theta_{3B} + 2\theta_{3A}) - \frac{6EI_3}{L^2}(u_{2\ell_B} - u_{2\ell_A}) + M_{3A}^F
\end{aligned} \tag{12.38a}$$

$$\begin{aligned}
F_{1\ell_B} &= \frac{AE}{L}(u_{1\ell_B} - u_{1\ell_A}) + F_{1\ell_B}^F \\
F_{2\ell_B} &= -\frac{6EI_3}{L^2}(\theta_{3B} + \theta_{3A}) + \frac{12EI_3}{L^3}(u_{2\ell_B} - u_{2\ell_A}) + F_{2\ell_B}^F \\
F_{3\ell_B} &= -\frac{6EI_2}{L^2}(\theta_{2B} + \theta_{2A}) + \frac{12EI_2}{L^3}(u_{3\ell_B} - u_{3\ell_A}) + F_{3\ell_B}^F \\
M_{1B} &= \frac{GJ}{L}(\theta_{1B} - \theta_{1A}) + M_{1B}^F \\
M_{2B} &= \frac{2EI_2}{L}(2\theta_{2B} + \theta_{2A}) - \frac{6EI_2}{L^2}(u_{3\ell_B} - u_{3\ell_A}) + M_{2B}^F \\
M_{3B} &= \frac{2EI_3}{L}(2\theta_{3B} + \theta_{3A}) - \frac{6EI_3}{L^2}(u_{2\ell_B} - u_{2\ell_A}) + M_{3B}^F
\end{aligned} \tag{12.38b}$$

We express the end action–end displacement relations in the same form as for the planar case.

$$\begin{aligned}
\mathbf{U}_\ell &= \{u_1 \ u_2 \ u_3 \ \theta_1 \ \theta_2 \ \theta_3\} \\
\mathbf{P}_\ell &= \{F_1 \ F_2 \ F_3 \ M_1 \ M_2 \ M_3\}
\end{aligned}$$

Noting (12.5), we write:

$$\begin{aligned}
\mathbf{P}_{\ell_B} &= \mathbf{k}_{\ell_{BB}}\mathbf{U}_{\ell_B} + \mathbf{k}_{\ell_{BA}}\mathbf{U}_{\ell_A} + \mathbf{P}_{\ell_B}^F \\
\mathbf{P}_{\ell_A} &= \mathbf{k}_{\ell_{AB}}\mathbf{U}_{\ell_B} + \mathbf{k}_{\ell_{AA}}\mathbf{U}_{\ell_A} + \mathbf{P}_{\ell_A}^F
\end{aligned}$$

where the \mathbf{k} matrices are now of order 6×6 . Their expanded forms are listed below.

$$\mathbf{k}_{\ell_{AA}} = \begin{bmatrix} \frac{AE}{L} & 0 & 0 & 0 & 0 & 0 \\ 0 & \frac{12EI_3}{L^3} & 0 & 0 & 0 & \frac{6EI_3}{L^2} \\ 0 & 0 & \frac{12EI_2}{L^3} & 0 & +\frac{6EI_2}{L^2} & 0 \\ 0 & 0 & 0 & \frac{GJ}{L} & 0 & 0 \\ 0 & 0 & +\frac{6EI_2}{L^2} & 0 & \frac{4EI_2}{L} & 0 \\ 0 & \frac{6EI_3}{L^2} & 0 & 0 & 0 & \frac{4EI_3}{L} \end{bmatrix}$$

$$\begin{aligned}
 \mathbf{k}_{\ell AB} &= \begin{bmatrix} -\frac{AE}{L} & 0 & 0 & 0 & 0 & 0 \\ 0 & -\frac{12EI_3}{L^3} & 0 & 0 & 0 & +\frac{6EI_3}{L^2} \\ 0 & 0 & -\frac{12EI_2}{L^3} & 0 & +\frac{6EI_2}{L^2} & 0 \\ 0 & 0 & 0 & -\frac{GJ}{L} & 0 & 0 \\ 0 & 0 & -\frac{6EI_2}{L^2} & 0 & \frac{2EI_2}{L} & 0 \\ 0 & -\frac{6EI_3}{L^2} & 0 & 0 & 0 & +\frac{2EI_3}{L} \end{bmatrix} \\
 \mathbf{k}_{\ell BA} &= \begin{bmatrix} -\frac{AE}{L} & 0 & 0 & 0 & 0 & 0 \\ 0 & -\frac{12EI_3}{L^3} & 0 & 0 & 0 & -\frac{6EI_3}{L^2} \\ 0 & 0 & -\frac{12EI_2}{L^3} & 0 & -\frac{6EI_2}{L^2} & 0 \\ 0 & 0 & 0 & -\frac{GJ}{L} & 0 & 0 \\ 0 & 0 & \frac{6EI_2}{L^2} & 0 & +\frac{2EI_2}{L} & 0 \\ 0 & +\frac{6EI_3}{L^2} & 0 & 0 & 0 & +\frac{2EI_3}{L} \end{bmatrix} \\
 \mathbf{k}_{\ell BB} &= \begin{bmatrix} \frac{AE}{L} & 0 & 0 & 0 & 0 & 0 \\ 0 & \frac{12EI_3}{L^3} & 0 & 0 & 0 & -\frac{6EI_3}{L^2} \\ 0 & 0 & \frac{12EI_2}{L^3} & 0 & -\frac{6EI_2}{L^2} & 0 \\ 0 & 0 & 0 & \frac{GJ}{L} & 0 & 0 \\ 0 & 0 & -\frac{6EI_2}{L^2} & 0 & \frac{4EI_2}{L} & 0 \\ 0 & -\frac{6EI_3}{L^2} & 0 & 0 & 0 & \frac{4EI_3}{L} \end{bmatrix} \quad (12.39)
 \end{aligned}$$

These matrices are transformed to the global reference frame using the following matrix:

$$\mathbf{R}_{\ell g} = \begin{bmatrix} \mathbf{R}' & 0 \\ 0 & \mathbf{R}' \end{bmatrix} \quad (12.40)$$

where

$$\mathbf{R}' = \begin{bmatrix} \beta_{11} & \beta_{12} & \beta_{13} \\ \beta_{21} & \beta_{22} & \beta_{23} \\ \beta_{31} & \beta_{32} & \beta_{33} \end{bmatrix}$$

$$\beta_{ij} = \cos(X_{ig}, X_{jl})$$

The operation involves the following computation:

$$\begin{aligned}
 \mathbf{k}|_{\text{global}} &= \mathbf{R}_{\ell_g} \mathbf{k}|_{\text{local}} \mathbf{R}_{\ell_g}^T \\
 &\quad \downarrow \\
 \mathbf{k}_{AA} &= \mathbf{R}_{\ell_g} \mathbf{k}_{lAA} \mathbf{R}_{\ell_g}^T \\
 \mathbf{k}_{AB} &= \mathbf{R}_{\ell_g} \mathbf{k}_{lAB} \mathbf{R}_{\ell_g}^T \\
 \mathbf{k}_{BA} &= \mathbf{R}_{\ell_g} \mathbf{k}_{lBA} \mathbf{R}_{\ell_g}^T \\
 \mathbf{k}_{BB} &= \mathbf{R}_{\ell_g} \mathbf{k}_{lBB} \mathbf{R}_{\ell_g}^T
 \end{aligned} \tag{12.41}$$

The remaining steps are the same as the 2D case.

One assembles the global equations, matrix, the boundary conditions on displacement, and solve for the modal displacements.

Simplifications are possible depending on the type of structure. For a space truss there are only axial forces. One can delete the equilibrium equations associated with nodal rotations and moments, and work with the reduced nodal displacement matrix,

$$\mathbf{U}_\ell = \{u_1 \ u_2 \ u_3\} \quad \mathbf{P}_\ell = \{F_1 \ F_2 \ F_3\}$$

$$\mathbf{R}' = \begin{bmatrix} \beta_{11} \\ \beta_{21} \\ \beta_{31} \end{bmatrix} \quad \mathbf{R}_{\ell_g} = \begin{vmatrix} \beta_{11} & 0 \\ \beta_{21} & 0 \\ \beta_{31} & 0 \\ 0 & \beta_{11} \\ 0 & \beta_{21} \\ 0 & \beta_{21} \end{vmatrix}$$

$$\mathbf{k}|_{\text{global}} = \mathbf{R}_{\ell_g} \mathbf{k}|_{\text{local}} \mathbf{R}_{\ell_g}^T$$

↓

$$\mathbf{k}_{AA} = \mathbf{k}_{BB} = -\mathbf{k}_{AB} = -\mathbf{k}_{BA} = \frac{AE}{L} \mathbf{R}_{\ell_g} \mathbf{R}_{\ell_g}^T = \frac{AE}{L} \begin{bmatrix} \beta_{11}^2 & \beta_{11}\beta_{21} & \beta_{11}\beta_{31} \\ \beta_{21}\beta_{11} & \beta_{21}^2 & \beta_{21}\beta_{31} \\ \beta_{31}\beta_{11} & \beta_{31}\beta_{21} & \beta_{31}^2 \end{bmatrix} \tag{12.42}$$

Another case is a plane frame loaded normal to the plane (out of plane bending). One can delete the equilibrium equations associated with nodal rotations and moments, and work with the reduced nodal displacement matrix.

Taking the z axis (X_3 direction) normal to the plane, the non-zero displacement measures are

$$\mathbf{U}_\ell = \{u_3 \theta_1 \theta_2\} \quad \mathbf{P}_\ell = \{F_3 M_1 M_2\} \quad \mathbf{R}_{\ell g} = \begin{bmatrix} 1 & 0 & 0 \\ 0 & \beta_{11} & \beta_{12} \\ 0 & \beta_{21} & \beta_{22} \end{bmatrix}$$

$$\mathbf{k}_{\ell AA} = \begin{bmatrix} \frac{12EI_2}{L^3} & 0 & \frac{6EI_2}{L^2} \\ 0 & \frac{GJ}{L} & 0 \\ \frac{6EI_2}{L^2} & 0 & \frac{4EI_2}{L} \end{bmatrix} \quad \mathbf{k}_{\ell AB} = \begin{bmatrix} -\frac{12EI_2}{L^3} & 0 & \frac{6EI_2}{L^2} \\ 0 & -\frac{GJ}{L} & 0 \\ -\frac{6EI_2}{L^2} & 0 & \frac{2EI_2}{L} \end{bmatrix} \quad (12.43)$$

$$\mathbf{k}_{\ell BA} = \begin{bmatrix} -\frac{12EI_2}{L^3} & 0 & -\frac{6EI_2}{L^2} \\ 0 & -\frac{GJ}{L} & 0 \\ \frac{6EI_2}{L^2} & 0 & \frac{2EI_2}{L} \end{bmatrix} \quad \mathbf{k}_{\ell BB} = \begin{bmatrix} \frac{12EI_2}{L^3} & 0 & -\frac{6EI_2}{L^2} \\ 0 & \frac{GJ}{L} & 0 \\ -\frac{6EI_2}{L^2} & 0 & \frac{4EI_2}{L} \end{bmatrix}$$

$$\mathbf{k}|_{\text{global}} = \mathbf{R}_{\ell g} \mathbf{k}|_{\text{local}} \mathbf{R}_{\ell g}^T$$

$$\mathbf{k}_{AA} = \mathbf{R}_{\ell g} \mathbf{k}_{\ell AA} \mathbf{R}_{\ell g}^T = \begin{bmatrix} \frac{12EI_y}{L^3} & \frac{6EI_y}{L^2} \beta_{21} & \frac{6EI_y}{L^2} \beta_{22} \\ \frac{6EI_y}{L^2} \beta_{12} & \left(\frac{4EI_y}{L} \beta_{12} \beta_{21} + \frac{GJ}{L} \beta_{11}^2 \right) & \left(\frac{4EI_y}{L} \beta_{12} \beta_{22} + \frac{GJ}{L} \beta_{11} \beta_{12} \right) \\ \frac{6EI_y}{L^2} \beta_{12} & \left(\frac{4EI_y}{L} \beta_{21} \beta_{22} + \frac{GJ}{L} \beta_{11} \beta_{21} \right) & \left(\frac{4EI_y}{L} \beta_{22}^2 + \frac{GJ}{L} \beta_{21} \beta_{12} \right) \end{bmatrix}$$

$$\mathbf{k}_{AB} = \mathbf{R}_{\ell g} \mathbf{k}_{\ell AB} \mathbf{R}_{\ell g}^T = \begin{bmatrix} -\frac{12EI_y}{L^3} & \frac{6EI_y}{L^2} \beta_{21} & \frac{6EI_y}{L^2} \beta_{22} \\ -\frac{6EI_y}{L^2} \beta_{12} & \left(\frac{2EI_y}{L} \beta_{12} \beta_{21} - \frac{GJ}{L} \beta_{11}^2 \right) & \left(\frac{2EI_y}{L} \beta_{12} \beta_{22} - \frac{GJ}{L} \beta_{11} \beta_{12} \right) \\ -\frac{6EI_y}{L^2} \beta_{22} & \left(\frac{2EI_y}{L} \beta_{21} \beta_{22} - \frac{GJ}{L} \beta_{11} \beta_{21} \right) & \left(\frac{2EI_y}{L} \beta_{22}^2 - \frac{GJ}{L} \beta_{21} \beta_{12} \right) \end{bmatrix}$$

$$\mathbf{k}_{BA} = \mathbf{R}_{\ell g} \mathbf{k}_{\ell BA} \mathbf{R}_{\ell g}^T = \begin{bmatrix} -\frac{12EI_y}{L^3} & \frac{6EI_y}{L^2} \beta_{21} & -\frac{6EI_y}{L^2} \beta_{22} \\ \frac{6EI_y}{L^2} \beta_{12} & \left(\frac{2EI_y}{L} \beta_{12} \beta_{21} - \frac{GJ}{L} \beta_{11}^2 \right) & \left(\frac{2EI_y}{L} \beta_{12} \beta_{22} - \frac{GJ}{L} \beta_{11} \beta_{12} \right) \\ \frac{6EI_y}{L^2} \beta_{22} & \left(\frac{2EI_y}{L} \beta_{21} \beta_{22} - \frac{GJ}{L} \beta_{11} \beta_{21} \right) & \left(\frac{2EI_y}{L} \beta_{22}^2 - \frac{GJ}{L} \beta_{21} \beta_{12} \right) \end{bmatrix}$$

$$\mathbf{k}_{BB} = \mathbf{R}_{\ell g} \mathbf{k}_{\ell BB} \mathbf{R}_{\ell g}^T = \begin{bmatrix} \frac{12EI_y}{L^3} & -\frac{6EI_y}{L^2} \beta_{21} & -\frac{6EI_y}{L^2} \beta_{22} \\ -\frac{6EI_y}{L^2} \beta_{12} & \left(\frac{4EI_y}{L} \beta_{12} \beta_{21} + \frac{GJ}{L} \beta_{11}^2 \right) & \left(\frac{4EI_y}{L} \beta_{12} \beta_{22} + \frac{GJ}{L} \beta_{11} \beta_{12} \right) \\ -\frac{6EI_y}{L^2} \beta_{22} & \left(\frac{4EI_y}{L} \beta_{21} \beta_{22} - \frac{GJ}{L} \beta_{11} \beta_{21} \right) & \left(\frac{4EI_y}{L} \beta_{22}^2 + \frac{GJ}{L} \beta_{21} \beta_{12} \right) \end{bmatrix}$$

(12.44)

Note that \mathbf{k} is now a 3×3 matrix.

Example 12.12: Plane Grid

Given: The plane grid shown in Fig. E12.12a.

Determine: joint displacements and reactions. The cross section is square tube (HSS203.2 × 203.2 × 9.5). Take $L = 4$ m, $P = 30$ kN, $E = 200$ GPa, and $G = 77$ GPa.

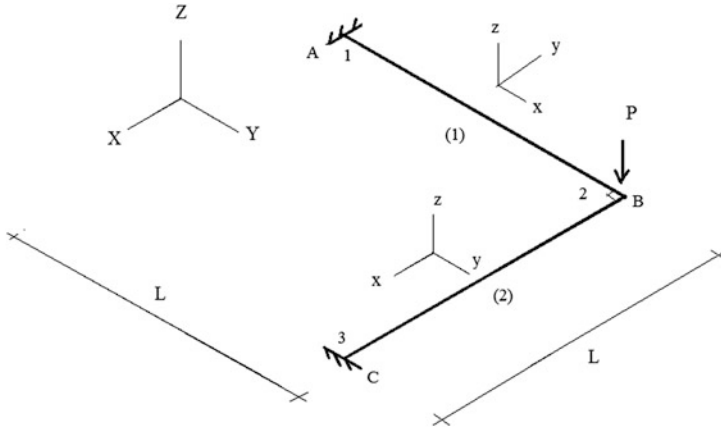


Fig. E12.12a

Solution:

Member m	n_-	n_+
(1)	1	2
(2)	2	3

$$\mathbf{R}'_{(1)} = \begin{bmatrix} \beta_{11}^{(1)} & \beta_{12}^{(1)} & \beta_{13}^{(1)} \\ \beta_{21}^{(1)} & \beta_{22}^{(1)} & \beta_{23}^{(1)} \\ \beta_{31}^{(1)} & \beta_{32}^{(1)} & \beta_{33}^{(1)} \end{bmatrix} = \begin{bmatrix} 0 & -1 & 0 \\ 1 & 0 & 0 \\ 0 & 0 & 1 \end{bmatrix}$$

$$\mathbf{R}'_{(2)} = \begin{bmatrix} \beta_{11}^{(2)} & \beta_{12}^{(2)} & \beta_{13}^{(2)} \\ \beta_{21}^{(2)} & \beta_{22}^{(2)} & \beta_{23}^{(2)} \\ \beta_{31}^{(2)} & \beta_{32}^{(2)} & \beta_{33}^{(2)} \end{bmatrix} = \begin{bmatrix} 1 & 0 & 0 \\ 0 & 1 & 0 \\ 0 & 0 & 1 \end{bmatrix}$$

$$\mathbf{R}_{g(i)} = \begin{bmatrix} \mathbf{R}'_{(i)} & \mathbf{0} \\ \mathbf{0} & \mathbf{R}'_{(i)} \end{bmatrix}$$

$$\begin{aligned}
 \mathbf{k}|_{\text{global}} &= \mathbf{R}_{\ell_g} \mathbf{k}|_{\text{local}} \mathbf{R}_{\ell_g}^T \\
 &\Downarrow \\
 \mathbf{k}_{AA} &= \mathbf{R}_{\ell_g} \mathbf{k}_{/AA} \mathbf{R}_{\ell_g}^T \\
 \mathbf{k}_{AB} &= \mathbf{R}_{\ell_g} \mathbf{k}_{/AB} \mathbf{R}_{\ell_g}^T \\
 \mathbf{k}_{BA} &= \mathbf{R}_{\ell_g} \mathbf{k}_{/BA} \mathbf{R}_{\ell_g}^T \\
 \mathbf{k}_{BB} &= \mathbf{R}_{\ell_g} \mathbf{k}_{/BB} \mathbf{R}_{\ell_g}^T
 \end{aligned}$$

$$\mathbf{K} = \begin{bmatrix} \mathbf{k}_{(1)AA} & \mathbf{k}_{(1)AB} & 0 \\ \mathbf{k}_{(1)BA} & \mathbf{k}_{(1)BB} & 0 \\ 0 & 0 & 0 \end{bmatrix} + \begin{bmatrix} 0 & 0 & 0 \\ 0 & \mathbf{k}_{(2)AA} & \mathbf{k}_{(2)AB} \\ 0 & \mathbf{k}_{(2)BA} & \mathbf{k}_{(2)BB} \end{bmatrix} = \begin{bmatrix} \mathbf{k}_{(1)AA} & \mathbf{k}_{(1)AB} & 0 \\ \mathbf{k}_{(1)BA} & (\mathbf{k}_{(1)BB} + \mathbf{k}_{(2)AA}) & \mathbf{k}_{(2)AB} \\ 0 & \mathbf{k}_{(2)BA} & \mathbf{k}_{(2)BB} \end{bmatrix}$$

$$\begin{aligned}
 \mathbf{K}'_{11} &= (\mathbf{k}_{(1)BB} + \mathbf{k}_{(2)AA}) & \mathbf{K}'_{12} &= [\mathbf{k}_{(1)BA} \quad \mathbf{k}_{(2)AB}] \\
 \mathbf{K}'_{21} &= \begin{bmatrix} \mathbf{k}_{(1)AB} \\ \mathbf{k}_{(2)BA} \end{bmatrix} & \mathbf{K}'_{22} &= \begin{bmatrix} \mathbf{k}_{(1)AA} & 0 \\ 0 & \mathbf{k}_{(2)BB} \end{bmatrix}
 \end{aligned}$$

$$\mathbf{P}'_E = \begin{Bmatrix} 0 \\ 0 \\ -30 \text{ kN} \\ 0 \\ 0 \\ 0 \end{Bmatrix} \quad \mathbf{U}' = \begin{Bmatrix} u_{1\text{joint } 2} \\ u_{2\text{joint } 2} \\ u_{3\text{joint } 2} \\ \theta_{1\text{joint } 2} \\ \theta_{2\text{joint } 2} \\ \theta_{3\text{joint } 2} \end{Bmatrix}$$

Matrix computations are carried out using Mathcad.

$$\mathbf{K}'_{11} = \begin{bmatrix} 283.85 & 0 & 0 & 0 & 0 & 2672.21 \\ 0 & 283.85 & 0 & 0 & 0 & 2672.21 \\ 0 & 0 & 2.67 & 2672.21 & 2672.21 & 0 \\ 0 & 0 & 2672.21 & 8,407,874.79 & 0 & 0 \\ 0 & 0 & 2672.21 & 0 & 8,407,874.79 & 0 \\ 2672.21 & 2672.21 & 0 & 0 & 0 & 14,251,764 \end{bmatrix}$$

We determine the unknown displacements using

$$\mathbf{U}' = \begin{Bmatrix} u_{1\text{joint } 2} \\ u_{2\text{joint } 2} \\ u_{3\text{joint } 2} \\ \theta_{1\text{joint } 2} \\ \theta_{2\text{joint } 2} \\ \theta_{3\text{joint } 2} \end{Bmatrix} \left(\mathbf{K}'_{11} \right)^{-1} \left(\mathbf{P}'_E \right) = \begin{Bmatrix} 0 \\ 0 \\ -30.81 \text{ mm} \\ -.00098 \text{ rad} \\ -.00098 \text{ rad} \\ 0 \end{Bmatrix}$$

Given the displacements, one determines reactions.

$$\mathbf{P}_E'' = \begin{Bmatrix} R_{1x} \\ R_{1y} \\ R_{1z} \\ M_{1x} \\ M_{1y} \\ M_{1z} \\ R_{3x} \\ R_{3y} \\ R_{3z} \\ M_{3x} \\ M_{3y} \\ M_{3z} \end{Bmatrix} = \mathbf{K}'_{21} \mathbf{U}' = \begin{bmatrix} \mathbf{k}^{(1)AB} \\ \mathbf{k}^{(2)BA} \end{bmatrix} \begin{Bmatrix} u_{1\text{joint } 2} \\ u_{2\text{joint } 2} \\ u_{3\text{joint } 2} \\ \theta_{1\text{joint } 2} \\ \theta_{2\text{joint } 2} \\ \theta_{3\text{joint } 2} \end{Bmatrix} = \begin{Bmatrix} 0 \\ 0 \\ 15 \text{ kN} \\ 47.44 \text{ kN m} \\ 12.55 \text{ kN m} \\ 0 \\ 0 \\ 0 \\ 0 \\ 15 \text{ kN} \\ 12.55 \text{ kN m} \\ 47.44 \text{ kN m} \\ 0 \end{Bmatrix}$$

Alternative approach:

We considered analytical methods for out of plane bending in Sect. 10.8.

The approach here is based on the simplified formulate described above (12.43).

$$\mathbf{R}_{\ell_g (1)} = \begin{bmatrix} 1 & 0 & 0 \\ 0 & \beta_{11}^{(1)} & \beta_{12}^{(1)} \\ 0 & \beta_{21}^{(1)} & \beta_{22}^{(1)} \end{bmatrix} = \begin{bmatrix} 1 & 0 & 0 \\ 0 & 0 & -1 \\ 0 & 1 & 0 \end{bmatrix}$$

$$\mathbf{R}_{\ell_g (2)} = \begin{bmatrix} 1 & 0 & 0 \\ 0 & \beta_{11}^{(2)} & \beta_{12}^{(2)} \\ 0 & \beta_{21}^{(2)} & \beta_{22}^{(2)} \end{bmatrix} = \begin{bmatrix} 1 & 0 & 0 \\ 0 & 1 & 0 \\ 0 & 0 & 1 \end{bmatrix}$$

$$\mathbf{P}'_E = \begin{Bmatrix} -30 \text{ kN} \\ 0 \\ 0 \end{Bmatrix} \quad \mathbf{U}' = \begin{Bmatrix} u_{3\text{joint } 2} \\ \theta_{1\text{joint } 2} \\ \theta_{2\text{joint } 2} \end{Bmatrix}$$

$$\mathbf{K}'_{11} = (\mathbf{k}^{(1)BB} + \mathbf{k}^{(2)AA}) \quad \mathbf{K}'_{12} = [\mathbf{k}^{(1)BA} \quad \mathbf{k}^{(2)AB}]$$

$$\mathbf{K}'_{21} = \begin{bmatrix} \mathbf{k}^{(1)AB} \\ \mathbf{k}^{(2)BA} \end{bmatrix} \quad \mathbf{K}'_{22} = \begin{bmatrix} \mathbf{k}^{(1)AA} & 0 \\ 0 & \mathbf{k}^{(2)BB} \end{bmatrix}$$

$$\mathbf{U}' = \begin{Bmatrix} u_{3\text{joint } 2} \\ \theta_{1\text{joint } 2} \\ \theta_{2\text{joint } 2} \end{Bmatrix} (\mathbf{K}'_{11})^{-1} (\mathbf{P}'_E) = \begin{Bmatrix} -30.81 \text{ mm} \\ -.00098 \text{ rad} \\ -.00098 \text{ rad} \end{Bmatrix}$$

$$\mathbf{P}_E'' = \begin{Bmatrix} R_{1z} \\ M_{1x} \\ M_{1y} \\ M_{1z} \\ R_{3z} \\ M_{3x} \\ M_{3y} \end{Bmatrix} = \mathbf{K}'_{21} \mathbf{U}' = \begin{bmatrix} \mathbf{k}^{(1)AB} \\ \mathbf{k}^{(2)BA} \end{bmatrix} \begin{Bmatrix} u_{3\text{joint } 2} \\ \theta_{1\text{joint } 2} \\ \theta_{2\text{joint } 2} \end{Bmatrix} = \begin{Bmatrix} 15 \text{ kN} \\ 47.44 \text{ kN m} \\ 12.55 \text{ kN m} \\ 15 \text{ kN} \\ 12.55 \text{ kN m} \\ 47.44 \text{ kN m} \end{Bmatrix}$$

Example 12.13: Space Truss

Given: The space truss shown in Fig. E12.13a, b.

Determine: Use the direct stiffness method to find displacements, reactions. Take $A = 1300 \text{ mm}^2$, $E = 200 \text{ GPa}$.

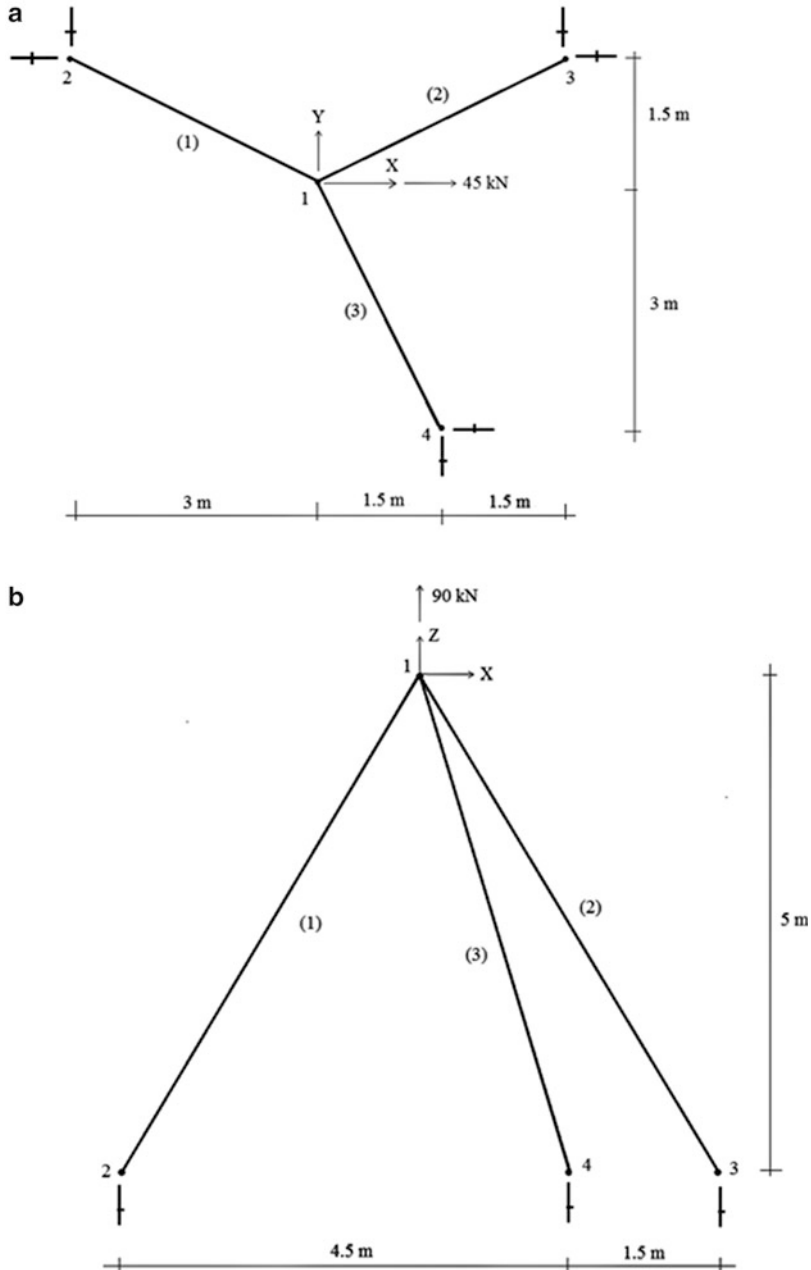


Fig. E12.13 Space truss geometry and supports. (a) x - y plan view. (b) x - z plan view

Member	n_-	n_+	ℓ_x	ℓ_y	ℓ_z	ℓ_m	β_{11}	β_{21}	β_{31}
(1)	1	2	-3.0	1.5	-5	6.0	-0.5	0.25	-0.83
(2)	1	3	3.0	1.5	-5	6.0	0.5	0.25	-0.83
(3)	1	4	1.5	-3	-5	6.0	0.25	-0.5	-0.83

$$\mathbf{k}_{AA} = \mathbf{k}_{BB} = \frac{AE}{L} \begin{bmatrix} \beta_{11}^2 & \beta_{11}\beta_{21} & \beta_{11}\beta_{31} \\ \beta_{21}\beta_{11} & \beta_{21}^2 & \beta_{21}\beta_{31} \\ \beta_{31}\beta_{11} & \beta_{31}\beta_{21} & \beta_{31}^2 \end{bmatrix} \quad \mathbf{k}_{AB} = \mathbf{k}_{BA} = -\frac{AE}{L} \begin{bmatrix} \beta_{11}^2 & \beta_{11}\beta_{21} & \beta_{11}\beta_{31} \\ \beta_{21}\beta_{11} & \beta_{21}^2 & \beta_{21}\beta_{31} \\ \beta_{31}\beta_{11} & \beta_{31}\beta_{21} & \beta_{31}^2 \end{bmatrix}$$

$$\mathbf{K} = \begin{bmatrix} \mathbf{k}_{(1)AA} & \mathbf{k}_{(1)AB} & 0 & 0 \\ \mathbf{k}_{(1)BA} & \mathbf{k}_{(1)BB} & 0 & 0 \\ 0 & 0 & 0 & 0 \\ 0 & 0 & 0 & 0 \end{bmatrix} + \begin{bmatrix} \mathbf{k}_{(2)AA} & 0 & \mathbf{k}_{(2)AB} & 0 \\ 0 & 0 & 0 & 0 \\ \mathbf{k}_{(2)BA} & 0 & \mathbf{k}_{(2)BB} & 0 \\ 0 & 0 & 0 & 0 \end{bmatrix} + \begin{bmatrix} \mathbf{k}_{(3)AA} & 0 & 0 & \mathbf{k}_{(3)AB} \\ 0 & 0 & 0 & 0 \\ 0 & 0 & 0 & 0 \\ \mathbf{k}_{(3)BA} & 0 & 0 & \mathbf{k}_{(3)BB} \end{bmatrix}$$

$$= \begin{bmatrix} (\mathbf{k}_{(1)AA} + \mathbf{k}_{(2)AA} + \mathbf{k}_{(3)AA}) & \mathbf{k}_{(1)AB} & \mathbf{k}_{(2)AB} & \mathbf{k}_{(3)AB} \\ \mathbf{k}_{(1)BA} & \mathbf{k}_{(1)BB} & 0 & 0 \\ \mathbf{k}_{(2)BA} & 0 & \mathbf{k}_{(2)BB} & 0 \\ \mathbf{k}_{(3)BA} & 0 & 0 & \mathbf{k}_{(3)BB} \end{bmatrix}$$

$$\mathbf{K}'_{11} = (\mathbf{k}_{(1)AA} + \mathbf{k}_{(2)AA} + \mathbf{k}_{(3)AA}) \quad \mathbf{K}'_{12} = [\mathbf{k}_{(1)AB} \quad \mathbf{k}_{(2)AB} \quad \mathbf{k}_{(3)AB}]$$

$$\mathbf{K}'_{21} = \begin{bmatrix} \mathbf{k}_{(1)BA} \\ \mathbf{k}_{(2)BA} \\ \mathbf{k}_{(3)BA} \end{bmatrix} \quad \mathbf{K}'_{22} = \begin{bmatrix} \mathbf{k}_{(1)BB} & 0 & 0 \\ 0 & \mathbf{k}_{(2)BB} & 0 \\ 0 & 0 & \mathbf{k}_{(3)BB} \end{bmatrix}$$

$$\mathbf{P}'_E = \begin{Bmatrix} 45 \\ 0 \\ 90 \end{Bmatrix} \text{ kN} \quad \mathbf{U}' = \begin{Bmatrix} u_{1\text{joint1}} \\ u_{2\text{joint1}} \\ u_{3\text{joint1}} \end{Bmatrix}$$

Matrix computations are carried out using MathCAD:

$$\mathbf{K}'_{11} = \begin{pmatrix} 24.123 & -5.361 & -8.935 \\ -5.361 & 16.082 & 0 \\ -8.935 & 0 & 89.345 \end{pmatrix} \Rightarrow (\mathbf{K}'_{11})^{-1} = \begin{pmatrix} 0.047 & 0.016 & 0.005 \\ 0.016 & 0.067 & 0.002 \\ 0.005 & 0.002 & 0.012 \end{pmatrix}$$

We determine the unknown displacements using

$$\mathbf{U}' = \begin{Bmatrix} u_{1\text{joint1}} \\ u_{2\text{joint1}} \\ u_{3\text{joint1}} \end{Bmatrix} = (\mathbf{K}'_{11})^{-1} (\mathbf{P}'_E) = \begin{Bmatrix} 2.52 \\ 0.84 \\ 1.26 \end{Bmatrix} \text{ mm}$$

Given the displacements, one determines reactions.

$$\mathbf{P}''_E = \begin{Bmatrix} R_{2x} \\ R_{2y} \\ R_{2z} \\ R_{3x} \\ R_{3y} \\ R_{3z} \\ R_{4x} \\ R_{4y} \\ R_{4z} \end{Bmatrix} = \mathbf{K}'_{21} \mathbf{U}' = \begin{bmatrix} \mathbf{k}_{(1)BA} \\ \mathbf{k}_{(2)BA} \\ \mathbf{k}_{(3)BA} \end{bmatrix} \begin{Bmatrix} u_{1joint1} \\ u_{2joint1} \\ u_{3joint1} \end{Bmatrix} = \begin{Bmatrix} -45 \\ 22.5 \\ -75 \\ -9 \\ -4.5 \\ 15 \\ 9 \\ -18 \\ -30 \end{Bmatrix} \text{ kN}$$

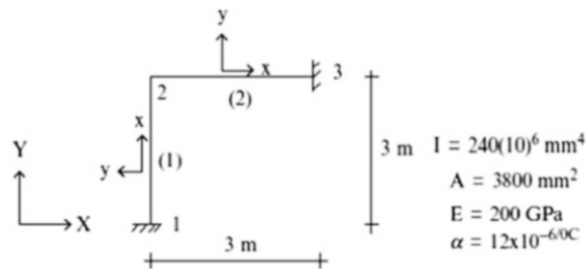
12.9 Summary

12.9.1 Objectives

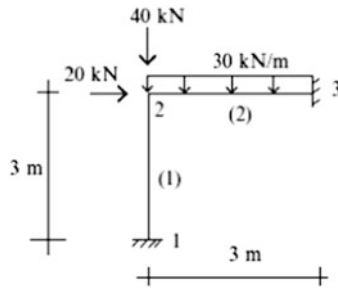
- Formulate the governing equations corresponding to the various steps in the displacement method using matrix notation.
- Introduce the concept of a local reference frame for each member and a fixed global reference frame for the structure.
- Develop the matrix form of the member force–displacement relations.
- Derive expressions for the various member stiffness matrices.
- Introduce the concept of a member–node incidence table and show how it is used to assemble the system equilibrium equations.
- Develop a procedure for introducing nodal displacement restraints.
- Specialize the rigid frame formulation for trusses, multi-span beams, and grids.

12.10 Problems

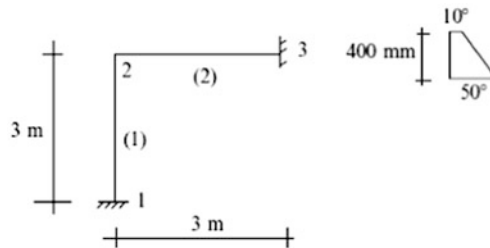
Problem 12.1. For the rigid frame shown below, use the direct stiffness method to find the joint displacements and reactions for the following conditions:



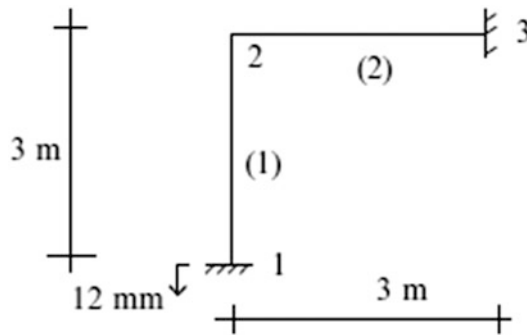
(a) The loading shown



(b) Member 2 experiences a uniform temperature change throughout its span. The temperature varies linearly through the depth, from 10°C at the top to 50°C at the bottom.



(c) Support 1 settles 12 mm.

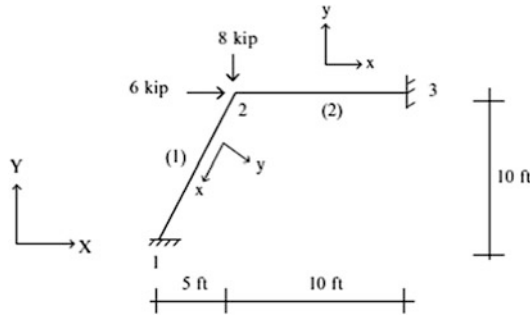


Problem 12.2. For the rigid frame shown below, use the direct stiffness method to find the joint displacements, and reactions.

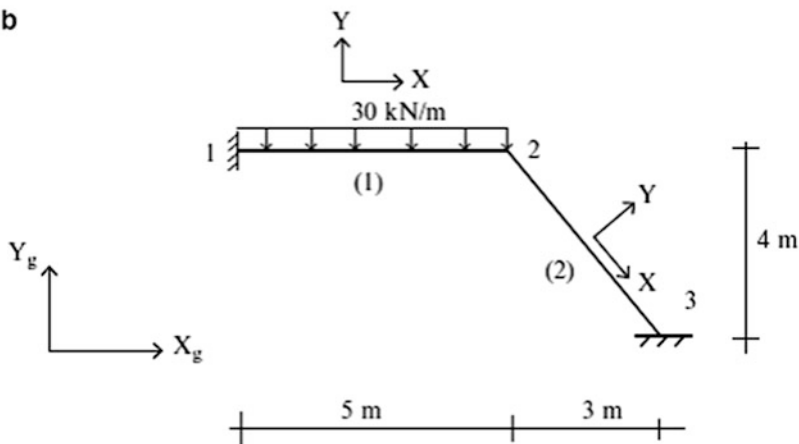
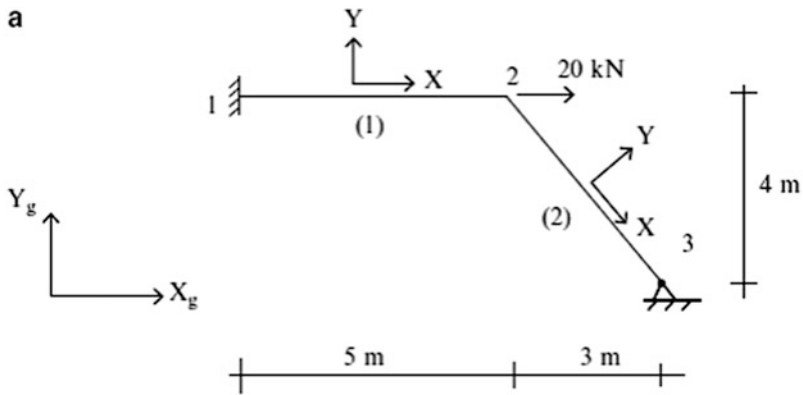
$$I = 400 \text{ in.}^4$$

$$A = 10 \text{ in.}^2$$

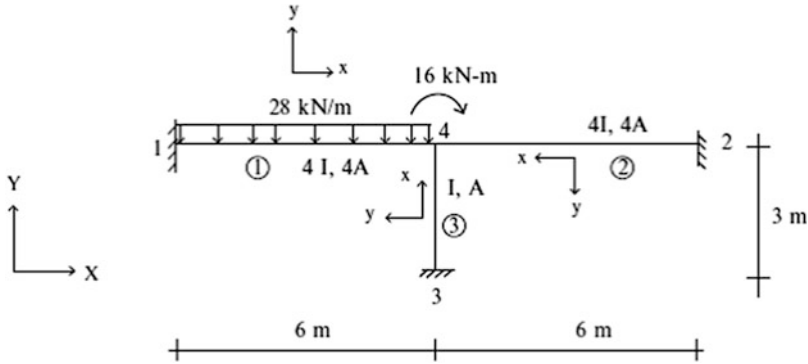
$$E = 29,000 \text{ kip/in.}^2$$



Problem 12.3 For the rigid frames shown below, use the direct stiffness method to find the joint displacements and reactions. Take $I = 160(10)^6 \text{ mm}^4$, $A = 6500 \text{ mm}^2$, and $E = 200 \text{ GPa}$.



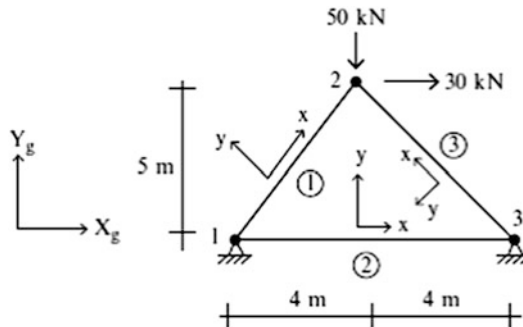
Problem 12.4 For the rigid frame shown, use partitioning to determine \mathbf{K}'_{11} , \mathbf{K}'_{21} , \mathbf{P}'_E , and \mathbf{P}'_I for the loadings shown. $I = 40(10)^6 \text{ mm}^4$, $A = 3000 \text{ mm}^2$, and $E = 200 \text{ GPa}$.



Problem 12.5 For the truss shown, use the direct stiffness method to find the joint displacements, reactions, and member forces.

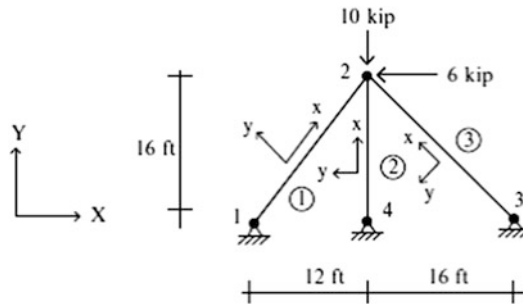
$$A = 1200 \text{ mm}^2$$

$$E = 200 \text{ GPa}$$



Problem 12.6 For the truss shown, use the direct stiffness method to find the joint displacements, reactions, and member forces for

- (a) The loading shown
- (b) A support settlement of 0.5 in. at joint 4

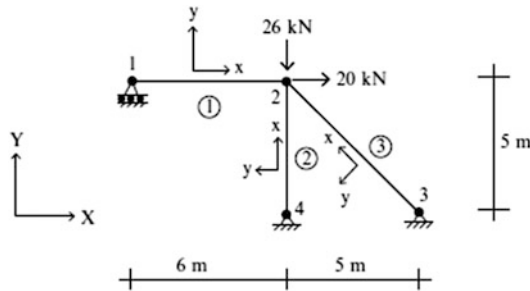


$$A = 2 \text{ in.}^2$$

$$E = 29,000 \text{ ksi}$$

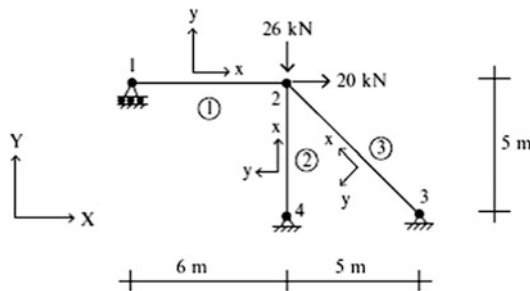
Problem 12.7 For the truss shown, use the direct stiffness method to find the joint displacements, reactions, and member forces due to (a) the loading shown, (b) a temperature decrease of 10°C for all members, (c) a support settlement of $\delta = 2\text{ mm}$ downward at node 4.

$$\begin{aligned} A &= 1200\text{ mm}^2 \\ E &= 200\text{ GPa} \\ \alpha &= 12 \times 10^{-6}/^\circ\text{C} \\ h &= 3\text{ m} \end{aligned}$$



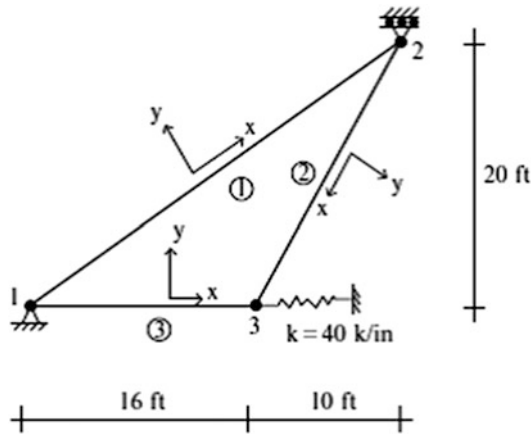
Problem 12.8. For the truss shown, determine \mathbf{K}'_{11} and \mathbf{K}'_{21} .

$$\begin{aligned} A &= 2000\text{ mm}^2 \\ E &= 200\text{ GPa} \end{aligned}$$

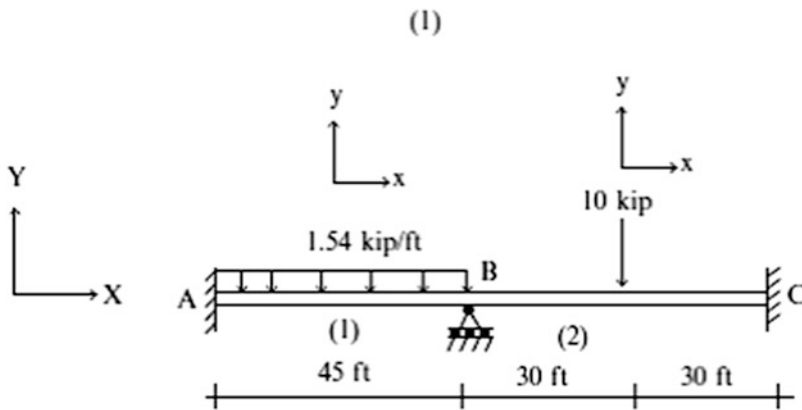


Problem 12.9 For the truss shown, determine \mathbf{K}'_{11} and \mathbf{K}'_{22} .

$$\begin{aligned} A &= 3\text{ in.}^2 \\ E &= 29,000\text{ ksi} \end{aligned}$$



Problem 12.10 For the beam shown, use the direct stiffness method to find the joint displacements, reactions, and member forces for the loading shown.

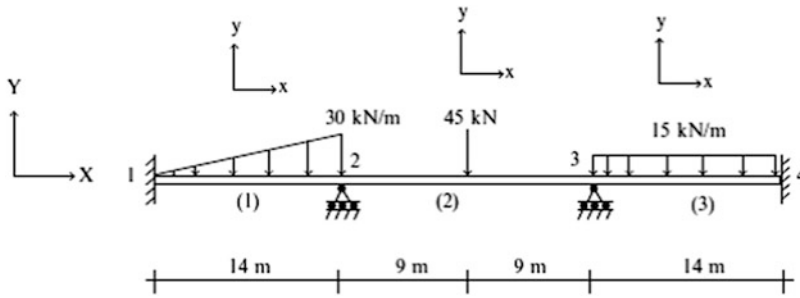


$$I = 300 \text{ in.}^4$$

$$E = 29,000 \text{ ksi}$$

Problem 12.11 For the beam shown, use the direct stiffness method to find the joint displacements, reactions, and member forces for

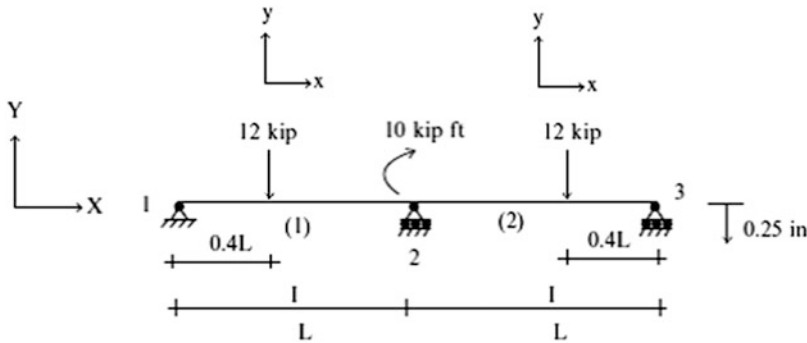
- (a) The loading shown
- (b) A support settlement of 12 mm at joint 2



$$I = 120(10)^6 \text{ mm}^4$$

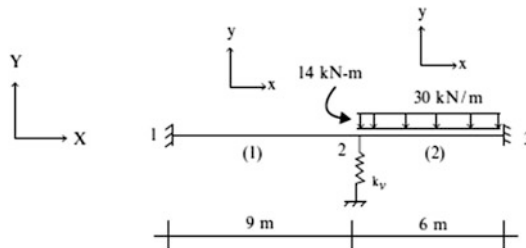
$$E = 200 \text{ GPa}$$

Problem 12.12 For the beam shown, use partitioning to determine \mathbf{K}'_{11} , \mathbf{K}'_{21} , \mathbf{U}'' , \mathbf{P}'_1 , \mathbf{P}''_1 , \mathbf{P}'_E and \mathbf{P}''_E for the loading and displacement constraint shown. $L = 30 \text{ ft}$, $I = 300 \text{ in}^4$, and $E = 29,000 \text{ ksi}$.

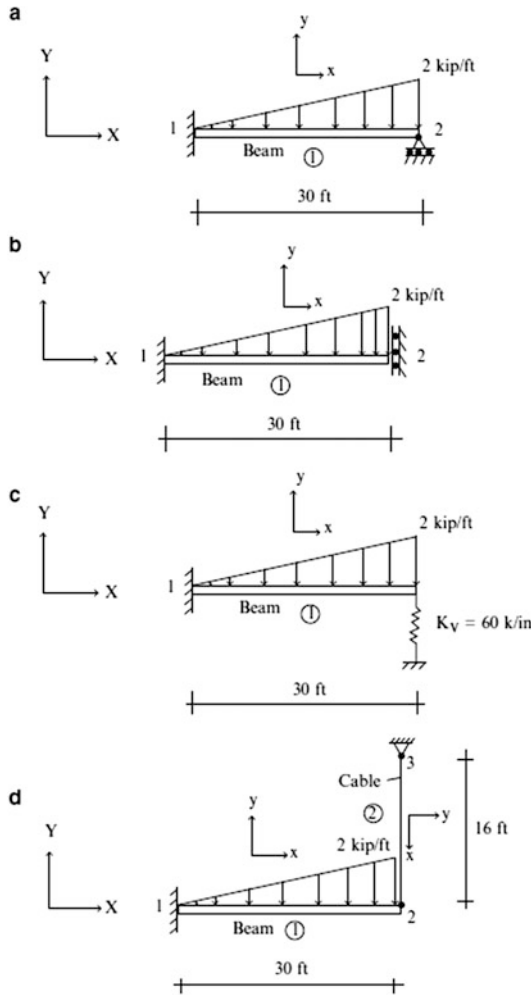


Problem 12.13 Investigate the effect of varying the spring stiffness on the behavior (moment and deflected profile) of the structure shown below. Consider a range of values of k_v .

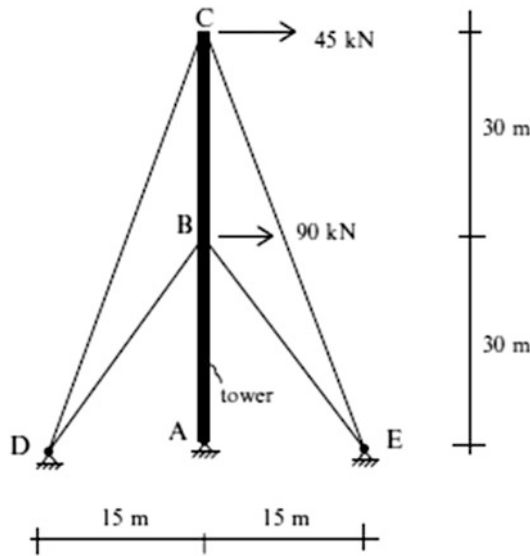
$$I = 120(10)^6 \text{ mm}^4, E = 200 \text{ GPa} \text{ and } k_v = \begin{cases} 18 \text{ kN/mm} \\ 36 \text{ kN/mm} \\ 90 \text{ kN/mm} \end{cases}$$



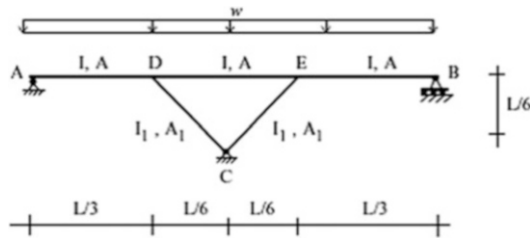
Problem 12.14 Determine the bending moment and deflection profiles for the following structures. Take $I = 300 \text{ in.}^4$, $A_{\text{Cable}} = 3 \text{ in.}^2$, and $E = 29,000 \text{ kip/in.}^2$.



Problem 12.15 Consider the guyed tower defined in the sketch. The cables have an initial tension of 220 kN. Determine the horizontal displacements at B, C, the change in cable tension, and the bending moment distribution in member ABC. Treat the cables as axial elements. Develop a computer-based scheme to solve this problem. Take $I_{\text{tower}} = 200(10)^6 \text{ mm}^4$, $A_{\text{cable}} = 650 \text{ mm}^2$, $A_{\text{tower}} = 6000 \text{ mm}^2$, and the material to be steel.



Problem 12.16



Consider the rigid frame shown above. Investigate how the response changes when A_1 is varied. Use computer software. Vary A_1 from 2 to 10 in.² Take $I = 600$ in.⁴, $A = 5$ in.², $L = 200$ ft, $I_1 = 300$ in.⁴, and $w = 1$ kip/ft. Material is steel.

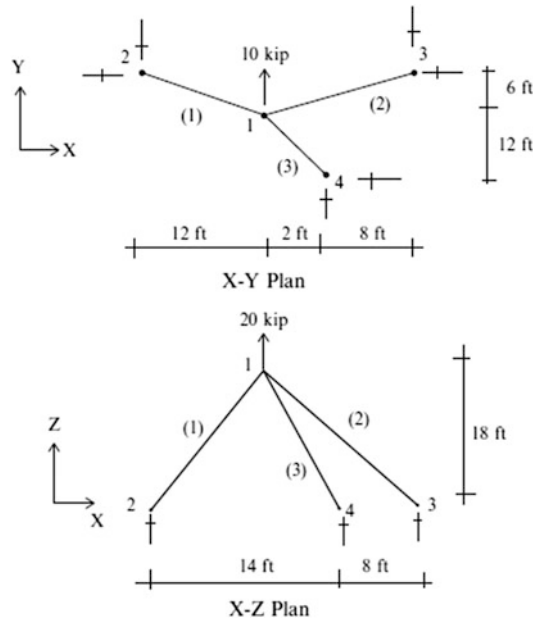
Problem 12.17

- (a) Develop a computer code to automate the generation of the member stiffness matrices defined by (12.6). Assume A , E , I , and L are given.
- (b) Develop a computer code to carry out the operations defined by (12.13).
- (c) Develop a computer code to carry out the operation defined by (12.20) and (12.21).

Problem 12.18 For the space truss shown, use the direct stiffness method to find displacements at joint 1.

$$A = 3 \text{ in.}^2$$

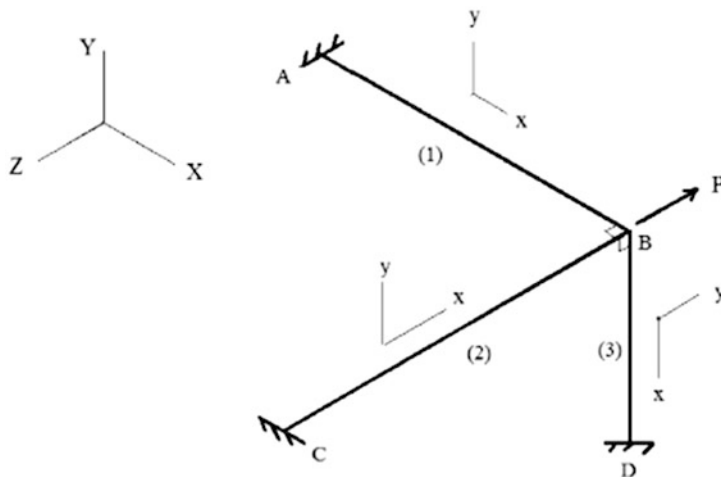
$$E = 29,000 \text{ ksi}$$



Problem 12.19 For the space frame shown, use the direct stiffness method to find displacements at joint B. The load P is applied parallel to member BC. The cross section is circular tube. Take $L_{(1)} = 3.5\text{ m}$, $L_{(2)} = 4\text{ m}$, $L_{(3)} = 3\text{ m}$, $P = 30\text{ kN}$, $E = 200\text{ GPa}$, and $G = 77\text{ GPa}$.



Cross section



Practice of Structural Engineering

The practice of structural engineering involves identifying possible loading patterns, conceptualizing candidate structural systems, developing idealized physical models, applying the possible loading patterns to these idealized models, using analysis methods to determine the peak values of the response variables needed for design detailing, and selecting the design details using an appropriate design code. In this section, we focus on selecting loading patterns, idealizing three-dimensional frame structures, and establishing the peak values of the response variables needed for design detailing. Computer-based analysis is used extensively for this phase.

Multi-span horizontal structures are discussed in the next chapter. The topics range from girder bridges to arch bridges to cable-stayed bridges. The following chapter presents a strategy for modeling three-dimensional low-rise rigid frame structures subjected to varying loads. Then, the succeeding chapter describes in detail the process followed to establish the critical loading patterns for multistory frames. Finally, the last chapter covers the inelastic response of structures.

Abstract

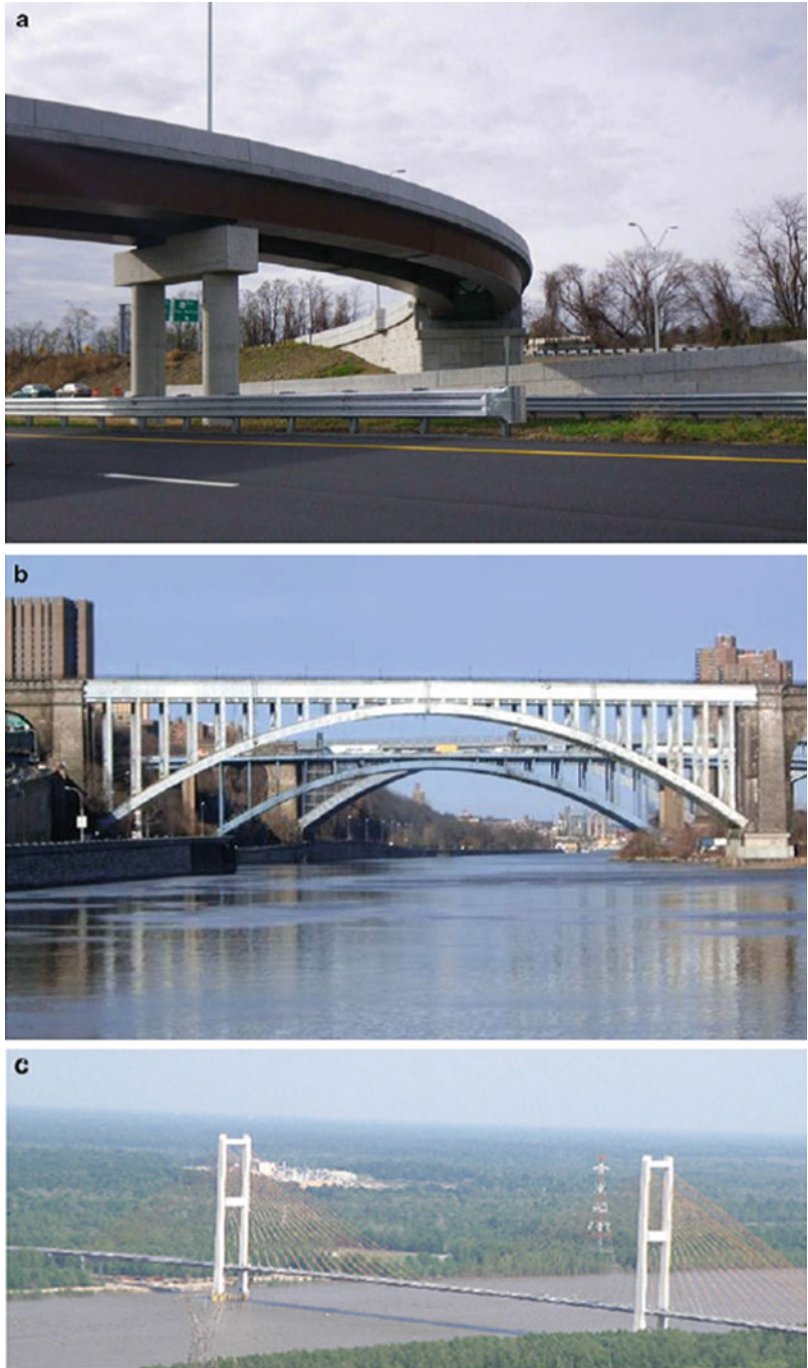
In this chapter, we discuss the role of analysis in the structural engineering process for multi-span horizontal structures such as bridges. Typical examples of a girder bridge, an arch bridge, and a cable-stayed bridge are shown in Fig. 13.1. Multi-span girders are actually variable depth horizontal beams. They are used extensively in medium span highway bridge systems. Arch and cable-stayed structures are efficient for spans ranging up to 1000 m.

Chapters 9 and 10 dealt with analysis methods for indeterminate structures. Some of the analytical results presented in those chapters are utilized here to estimate critical loading patterns. Most of the analysis effort required in the engineering process is related to determining the maximum values of bending moment, axial force, and shear corresponding to the typical bridge loadings. Establishing these values for indeterminate structures requires a considerable amount of computational effort. In what follows, we illustrate this computational process for different types of bridges such as continuous girder, arch, and cable-stayed schemes using a commercial structural analysis software system.

13.1 The Engineering Process for Girders

The objective of the structural engineering process for a beam is to define the physical makeup, i.e., the location of supports, the material, the shape and dimensions of the cross section, and special cross-section features such as steel reinforcement in the case of a reinforced concrete beam. Given the absolute maximum values of shear and moment at a particular location, the choice of material, and the general shape of the cross section, one determines the specific cross-sectional dimensions by applying numerical procedures specified by a design code. This phase of the engineering process is called design detailing. *We focus here on that aspect of the process associated with the determination of the “maximum” values of shear and moment.*

Fig. 13.1 Bridge structures. (a) Multi-span girder bridge. (b) Arch bridge. (c) Cable stayed



In general, shear and bending moment result when an external loading is applied to a beam. Throughout the text, we have shown how one can establish the shear and moment distributions corresponding to a given loading. For statically determinate beams, the internal forces depend only on the external loading and geometry; they are independent of the cross-sectional properties. However, when the beam is indeterminate, such as a multi-span beam, the internal forces also depend on the

relative span lengths and cross-sectional properties. In this case, one needs to iterate on the geometry and properties in order to estimate the internal forces.

Now, the loading consists of two contributions: dead and live. The dead loading is fixed, i.e., its magnitude and spatial distribution are constant over time. Live loading is, by definition, time varying over the life of the structure. This variability poses a problem when we are trying to establish the maximum values of shear and moment. We need to consider a number of live load positions in order to identify the particular live load location that results in the absolute maximum values of shear and moment. One approach for multi-span beams is based on determining, for all positions of the live load, the absolute maximum value at sections along the span. Plots of global maxima at discrete sections along the span are called *force envelopes*.

It is important to distinguish between influence lines and force envelopes. An influence line relates a *force quantity at a particular point to the position of the live load*, whereas a *force envelope relates the absolute maximum value of the force quantity along the span*. We apply both approaches to establish design values.

13.2 Influence Lines for Indeterminate Beams Using Müller-Breslau's Principle

The topic of influence lines for statically determinate beams was introduced in Chap. 3. We include here a discussion of how one can generate influence lines for indeterminate beams using the Müller-Breslau principle [1]. We introduce the principle using the beam structure shown in Fig. 13.2a as an example. Later, in Chap. 15, we apply it to rigid frames.

Suppose one wants the influence line for *the negative moment at A* due to a downward vertical load. According to Müller-Breslau, one works with a modified structure obtained by inserting a moment release at A and applies a negative moment at A. The resulting structure is shown in Fig. 13.2b.

The deflected shapes of the modified structure due to a unit load applied at an arbitrary point, and a unit negative moment at A, are plotted in Fig. 13.2c, d. Since the beam is continuous at A, compatibility requires the net relative rotation at A to vanish. Then

$$\begin{aligned} \theta_{Ax} + \theta_{AA}M_A &= 0 \\ &\Downarrow \\ M_A &= -\frac{\theta_{Ax}}{\theta_{AA}} \end{aligned} \quad (13.1)$$

We note that $\theta_{Ax} = \delta_{xA}$ according to Maxwell's law of reciprocal displacements (see Sect. 9.2). Then (13.1) can be written as

$$M_A = -\frac{\delta_{Ax}}{\theta_{AA}} \quad (13.2)$$

Since δ_{xA} is at an arbitrary point, it follows that the *deflected shape of the modified structure due to a unit value of M_A is a scaled version of the influence line for M_A* . The actual sense of M_A is determined by comparing the direction of the displacement with the direction of the applied load. In this example, the positive direction of the load is *downward*. We had applied a negative moment. Therefore, the sense of M_A needs to be reversed when the displacement is positive, in this case, downward. The loading zones for the positive and negative values of M_A are shown in Fig. 13.3, which is based on the sign convention for moment, i.e., positive when compression on the upper fiber.

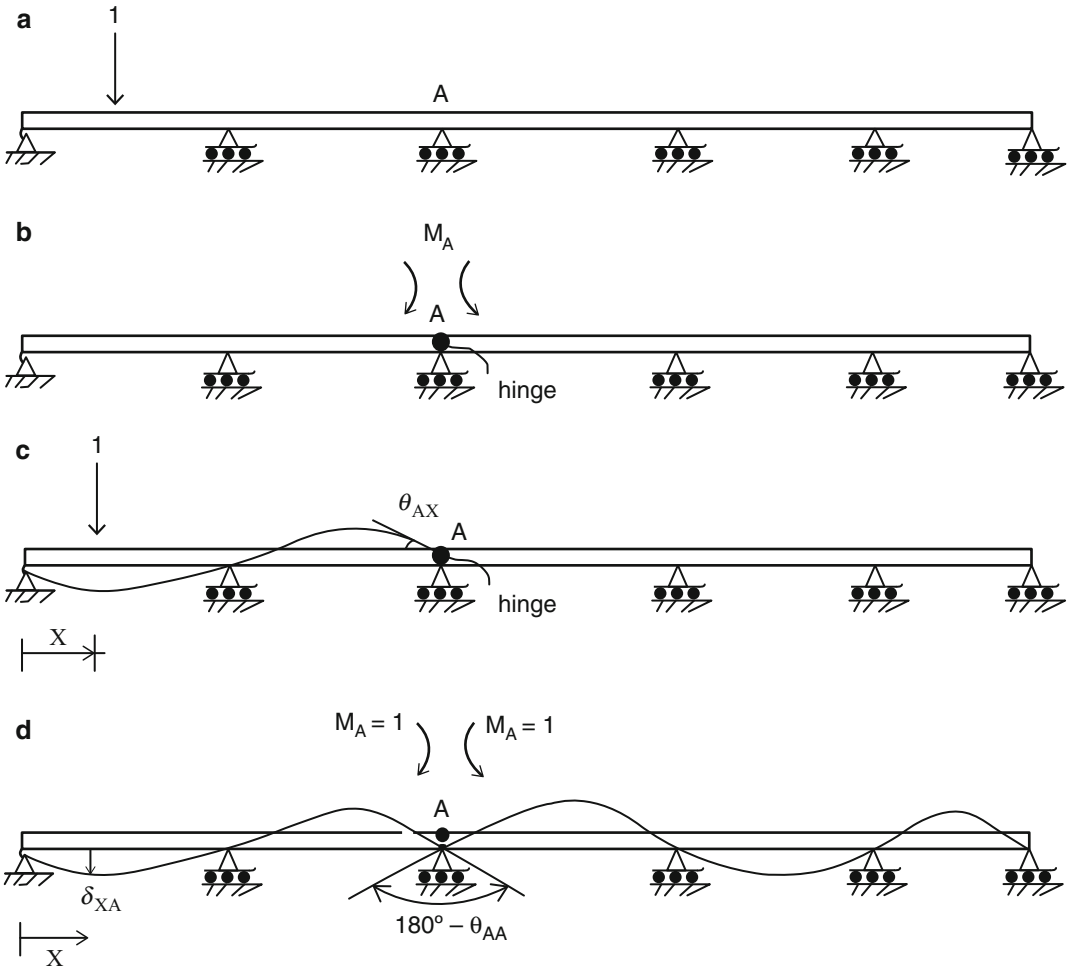


Fig. 13.2 Application of Müller-Breslau principle (a) Example structure. (b) Negative moment. (c) Deflection due to load. (d) Deflection due to moment

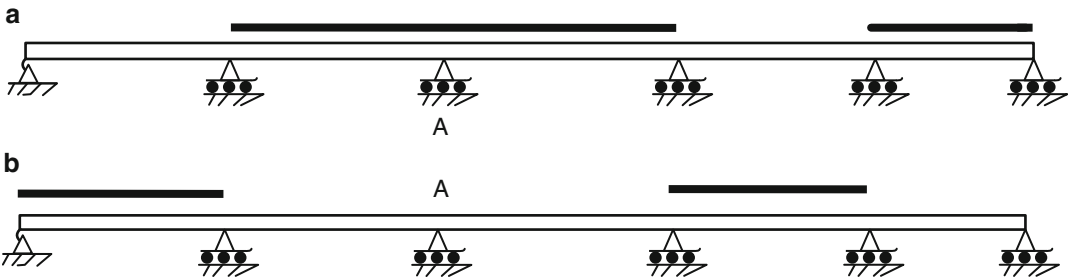


Fig. 13.3 Loading zones for moment at A. (a) Negative moment at A. (b) Positive moment at A

We repeat this process to establish the influence line for the maximum positive moment at D, the center of span AC. The sequence of steps is illustrated in Fig. 13.4. Figure 13.5 defines the loading zones for positive and negative moments.

Summarizing the discussion presented above, the process of applying the Müller-Breslau principle to establish the influence line for a redundant force quantity involves the following steps:

1. Modify the actual structure by removing the restraint corresponding to the force quantity of interest.
2. Apply a unit value of the force quantity at the release and determine the deflected shape.
3. This deflected shape is a scaled version of the influence line. It consists of positive and negative zones for the force quantity. If the applied loading is a unit downward load, the positive zone includes those regions where the deflection is upward.

Since it is relatively easy to sketch deflected shapes, the Müller-Breslau principle allows one with minimal effort to establish the critical loading pattern for a redundant force quantity.

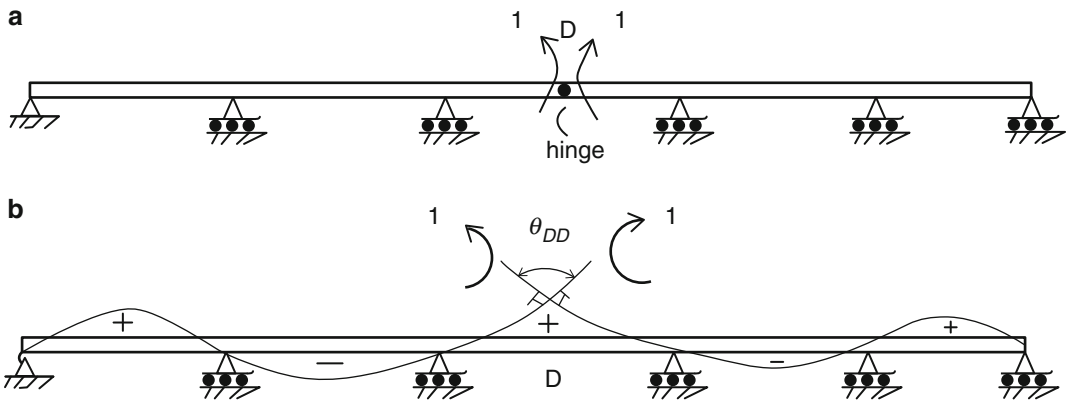


Fig. 13.4 Modified structure and deflected shape for positive moment at D

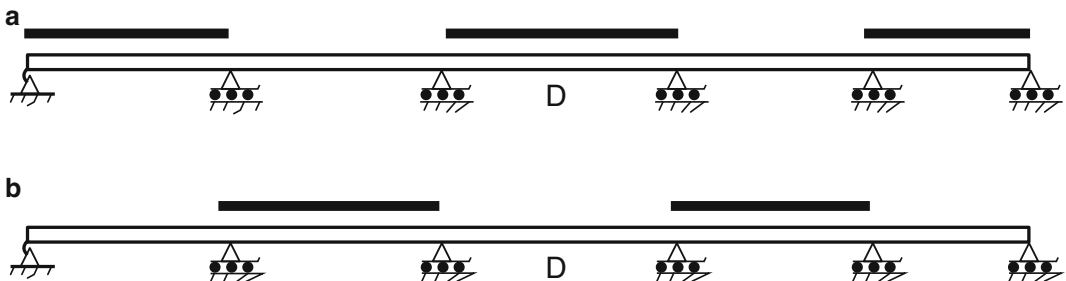


Fig. 13.5 Loading zones for moment at D. (a) Positive value. (b) Negative value

Example 13.1 Application of Müller-Breslau Principle

Given: The four-span beam shown in Fig. E13.1a.

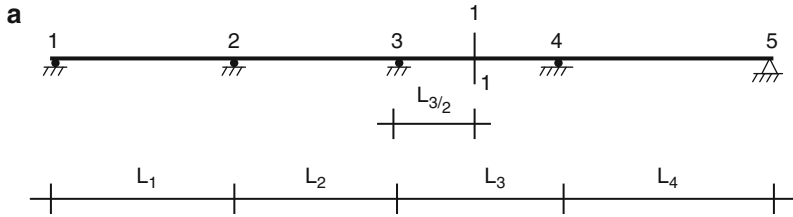


Fig. E13.1a

Determine: The influence lines for the upward vertical reaction at support 3 (R_3), the negative moment at support 3 (M_3), the positive moment at section 1-1 (M_{1-1}), and shear at section 1-1 (V_{1-1}). Also determine the critical loading patterns for a uniformly distributed load that produce the maximum values of R_3 , M_3 , M_{1-1} , and V_{1-1} .

Solution: The deflected shapes and influence lines for a unit downward load are plotted below.

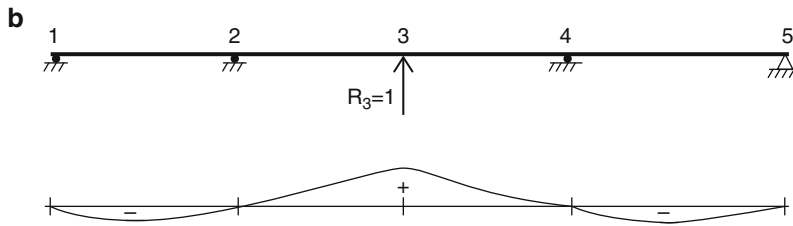


Fig. E13.1b Influence line for R_3

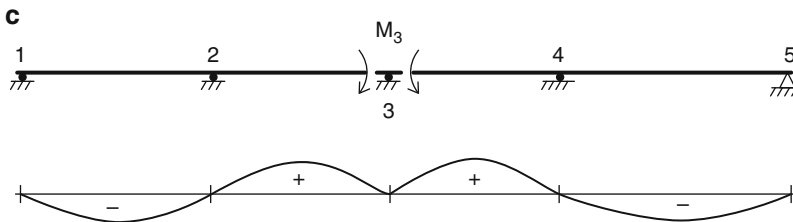


Fig. E13.1c Influence line for M_3

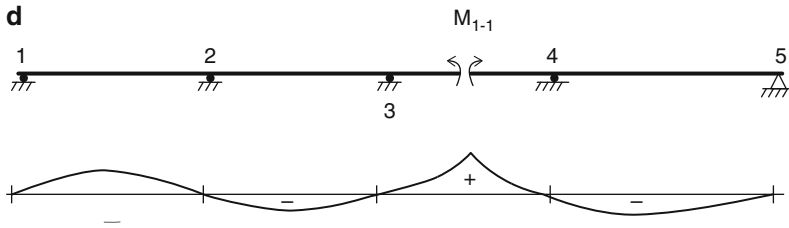


Fig. E13.1d Influence line for M_{1-1}

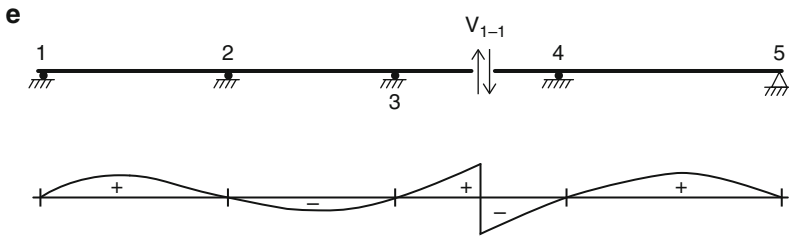


Fig. E13.1e Influence line for V_{1-1}

Loading patterns that produce the peak positive and negative values of these force parameters are shown in Figs. E13.1f, E13.1g, E13.1h, and E13.1i.

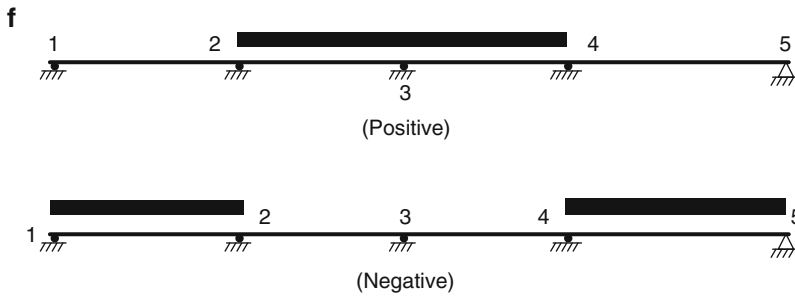


Fig. E13.1f Loading patterns for absolute maximum R_3

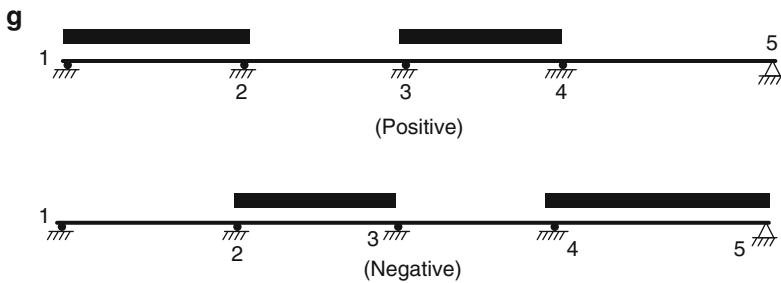


Fig. E13.1g Loading patterns for absolute maximum M_{1-1}

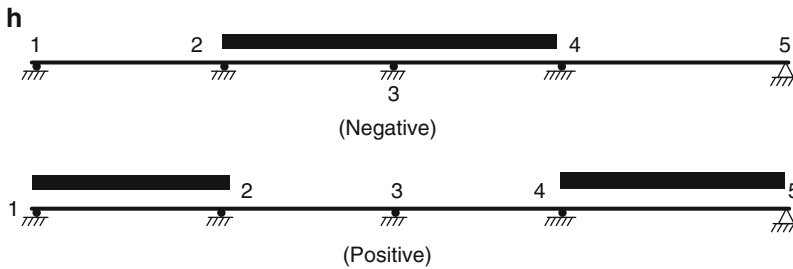


Fig. E13.1h Loading patterns for absolute maximum M_3

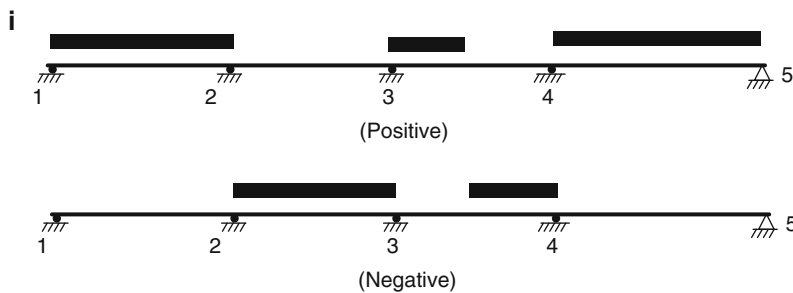


Fig. E13.1i Loading patterns for absolute maximum V_{1-1}

13.3 Engineering Issues for Multi-span Girder Bridges

13.3.1 Geometric Configurations

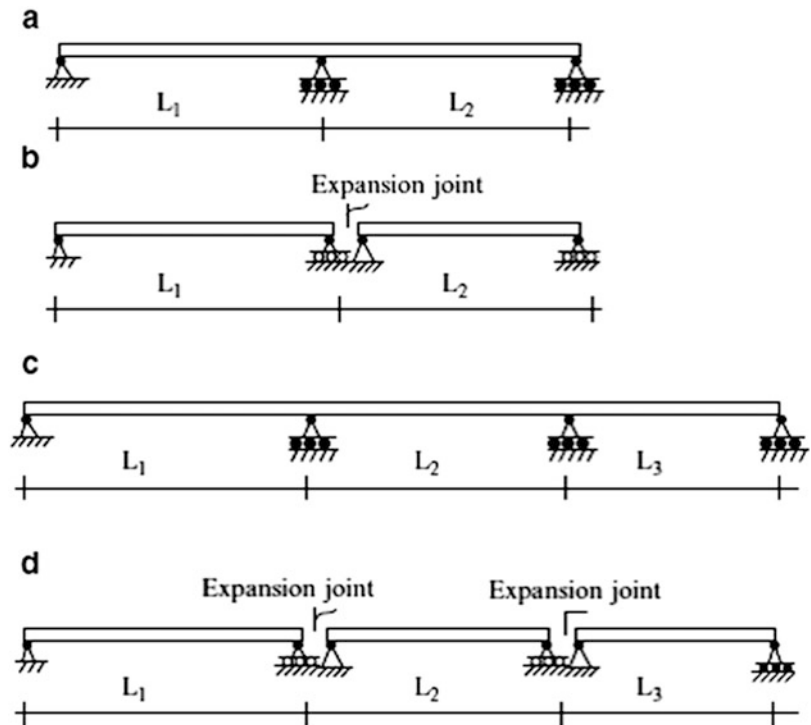
The superstructure of a typical highway girder bridge consists of longitudinal girders which support a concrete deck. The girders may be fabricated from either steel or concrete. The substructure is composed of piers and abutments which are founded on either shallow foundations or piles. In general, the makeup of the substructure depends on the soil conditions at the site. Bearings are employed to connect the girders to the substructure.

Bridge spans are classified as either short, medium, or long according to the total span length. Typical categories are

- Short : less than 125 ft (38 m)
- Medium : 125 – 400 ft (38 – 120 m)
- Long : over 400 ft (120 m)

Typical highway bridge structural systems are composed of continuous beams. One could replace the continuous beam with an arrangement of simply supported beams. However, this choice requires additional bearings and introduces discontinuities in the deck slab at the interior supports that creates a serious problem since it provides a pathway for moisture and leads to corrosion of the bearings at the supports. Using a continuous beam allows one to achieve continuity of the deck slab and also eliminates some bearings. It is the preferred structural scheme for new bridges. Typical span arrangements are shown in Fig. 13.6. The current trend is to use a constant girder cross section throughout the span.

Fig. 13.6 Span arrangements for multi-span beams. (a) Two spans continuous. (b) Two spans simply supported. (c) Three spans continuous. (d) Three spans simply supported

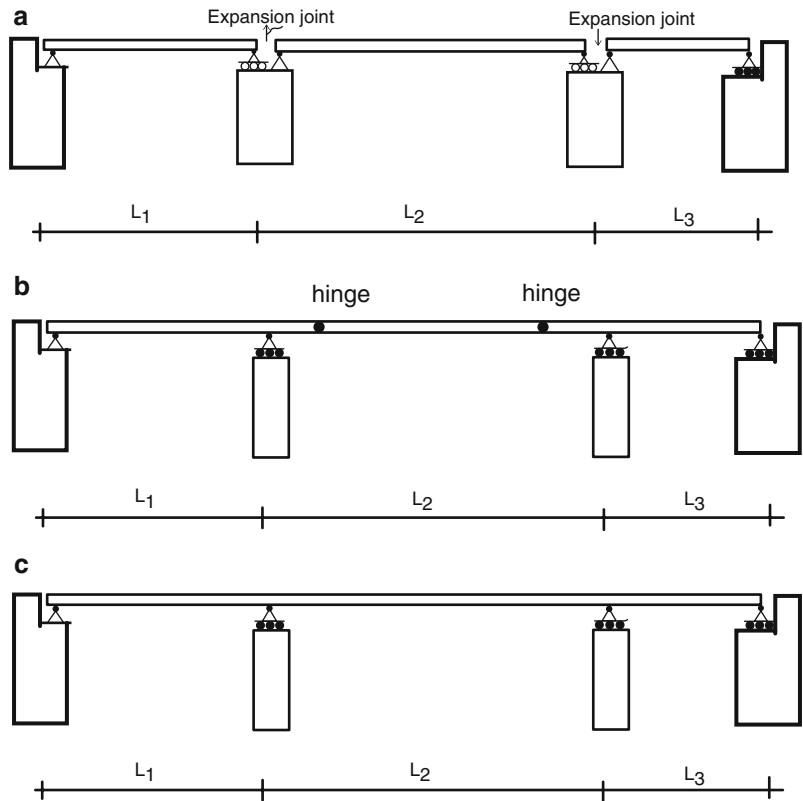


Historically, girder bridges were configured as a collection of single spans. This scheme is illustrated in Fig. 13.7a. In order to deal with longer interior spans, the cantilever scheme shown in Fig. 13.7b was introduced. Both schemes involve discontinuities in the girder/deck which provide pathways for moisture and lead to deterioration. To eliminate the interior discontinuities, the obvious option is to use a continuous girder as shown in Fig. 13.7c. We demonstrated in Chap. 9 that continuous beams are more efficient structurally, i.e., the peak internal forces are less than the corresponding forces for the simply supported case. Therefore, the required cross section tends to be lighter.

Even when a continuous girder is used, there still remains the problem of the discontinuities at the end supports (abutments). The problem is solved by using the scheme shown in Fig. 13.8. The abutments walls are supported on flexible piles that are rigidly connected to the deck/girder system. This concept is called an “integral abutment bridge.” Since the abutment is rigidly attached to the deck/girder, a temperature change of the deck produces a longitudinal displacement of the abutment wall. In order to minimize the effect of the resulting lateral force, the abutments are supported on flexible piles and loose granular backfill is placed behind the wall. The longitudinal displacement due to temperature varies linearly with the span length, and consequently, the maximum span length is limited by the seasonal temperature change.

We generate an idealized model by replacing the action of the soil and piles with equivalent springs [2]. Figure 13.9a illustrates this approach. An estimate of the effect of support stiffness is obtained using the model shown in Fig. 13.9b.

Fig. 13.7 Multi-span bridge schemes (a) Simple spans. (b) Cantilever spans. (c) Continuous spans



13.3.2 Choice of Span Lengths

Given some overall crossing length, one needs to decide on the number and relative magnitude of the spans to be used to achieve the crossing. We utilize here some of the analytical results for multi-span continuous beams with constant I subject to uniform loading generated in Chaps. 9 and 10. Figure 13.10 shows how the maximum moment varies with increasing number of spans. Note that there is a significant reduction in peak moment as the number of spans is increased, for a *given overall length*. Note also that the bending moment distribution for constant I is independent of the value of I .

In general, for constant I , the bending moment distribution depends on the ratio of the span lengths. For the symmetrical case shown in Fig. 13.11, the analytical solution for the negative moment at an interior support has the form (see Example 10.5)

$$M_{\max}^- = g \left(\frac{L_2}{L_1} \right) \frac{wL_1^2}{8} \quad (13.3)$$

where

$$g \left(\frac{L_2}{L_1} \right) = \frac{1 + (L_2/L_1)^2}{1 + (3/2)(L_2/L_1)}$$

We express L_1 and L_2 as

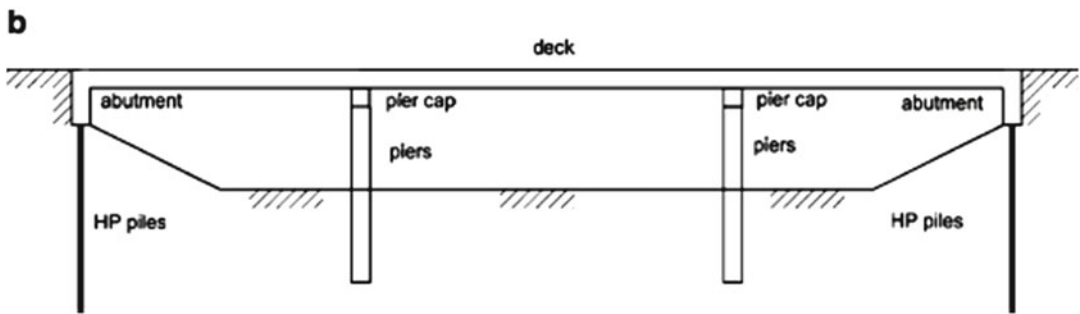


Fig. 13.8 (a) Three-span integral abutment bridge in Orange, Massachusetts. (b) Elevation—three-span integral abutment bridge

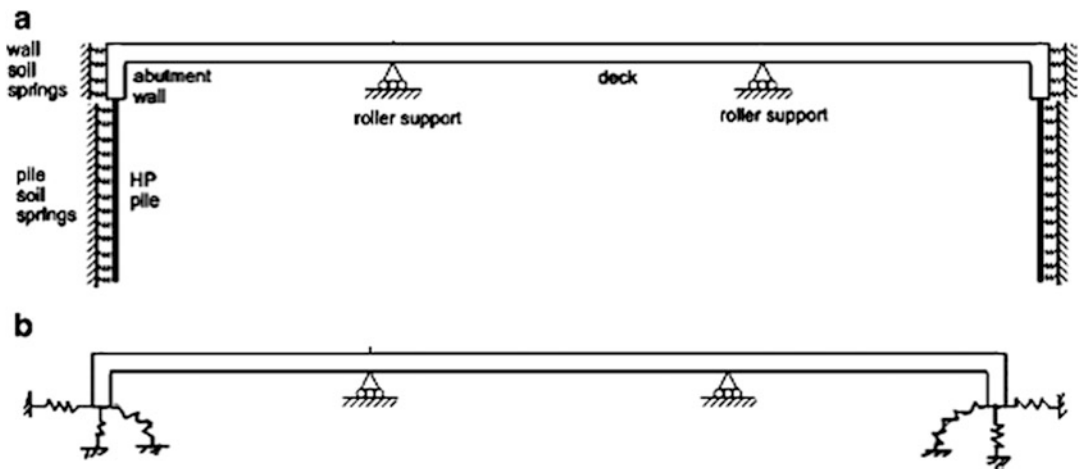


Fig. 13.9 Idealized models for an integral abutment bridge (a) Global model. (b) Simplified model

Fig. 13.10 Variation of the bending moment distribution. (a) Simply supported. (b) Two-span scheme. (c) Three-span scheme

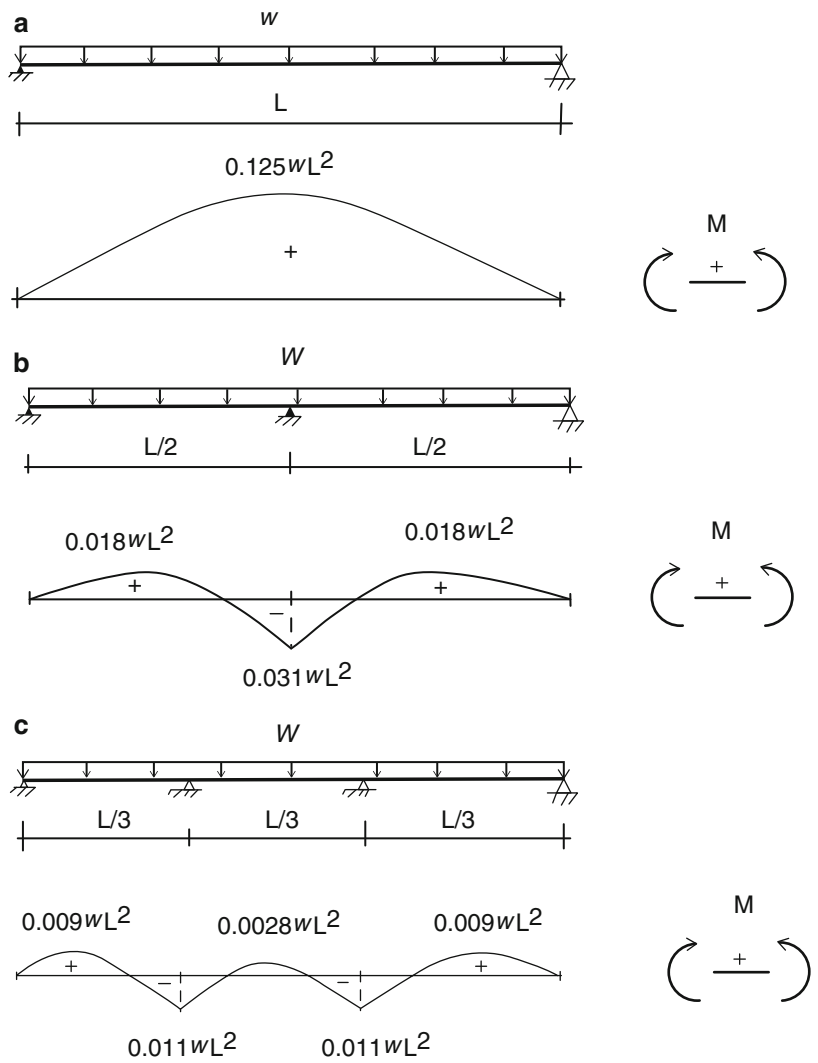
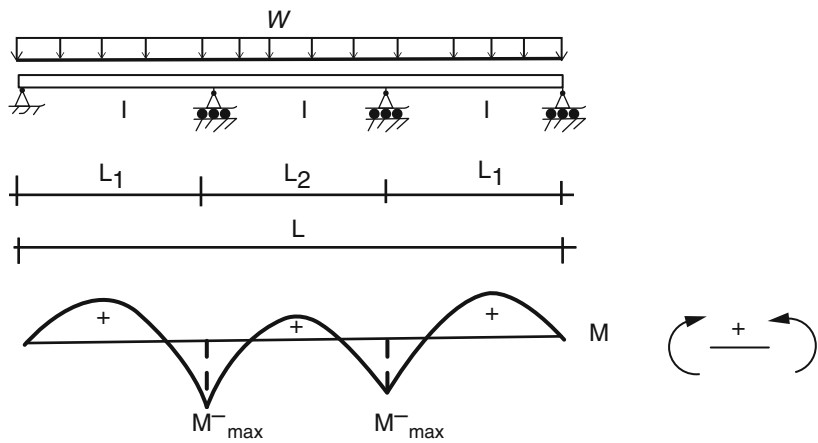


Fig. 13.11 Bending moment distribution—three-span symmetrical scheme

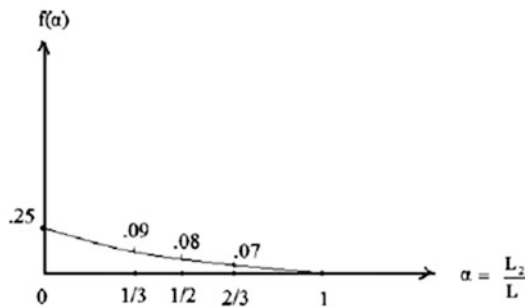


$$\begin{aligned} L_2 &= \alpha L \\ L_1 &= \frac{(1 - \alpha)L}{2} \end{aligned} \quad (13.4)$$

With this notation, (13.3) expands to

$$\begin{aligned} M_{\max}^- &= \frac{wL^2}{8} f(\alpha) \\ f(\alpha) &= \frac{1 - 3\alpha + 7\alpha^2 - 5\alpha^3}{4(1 + 2\alpha)} \end{aligned} \quad (13.5)$$

The variation of f with α is plotted below.



Taking $L_2 = L_1$ corresponds to $\alpha = 1/3$. The more common case is where α is between $1/3$ and $1/2$. When spans L_1 and L_2 are chosen, one applies the uniformly distributed loading and determines the peak value of negative moment using (13.5).

13.3.3 Live Loads for Multi-span Highway Bridge Girders: Moment Envelopes

The live load for a highway bridge is assumed to consist of two components: a uniform loading intended to simulate small vehicles, such as cars, and a set of concentrated loads that characterize heavy vehicles, such as trucks.

13.3.3.1 Set of Concentrated Live Loads

The action of a heavy vehicle traveling across the total span is simulated by positioning a set of concentrated loads at various locations along the span. The load magnitude and axle spacing vary depending on the code that governs the design. For each load position, we determine the bending moment at specific points along the span. When the beam is statically determinate, it is possible to develop an analytical solution for the peak moment. This approach is described in Chap. 3. However, when the beam is indeterminate, one must resort to a numerical procedure. This approach is illustrated in Fig. 13.12. In practice, one first discretizes the spans and then positions the load at the individual discrete points. Assuming there are n discrete points, one needs to carry out n analyses. This results in n bending moment distributions. At each discrete point, we determine the maximum positive and negative values from the set of n values generated by the n analyses. Finally, we construct a plot showing the “maximum” values of moment at each discrete point. This plot allows one to readily identify the absolute “maximum” moment by scanning over the plot. Since the values at each discrete point represent the *peak values at the point for all positions of the loading*, we interpret the plot as a *moment envelope*. Working with a refined span discretization provides detailed

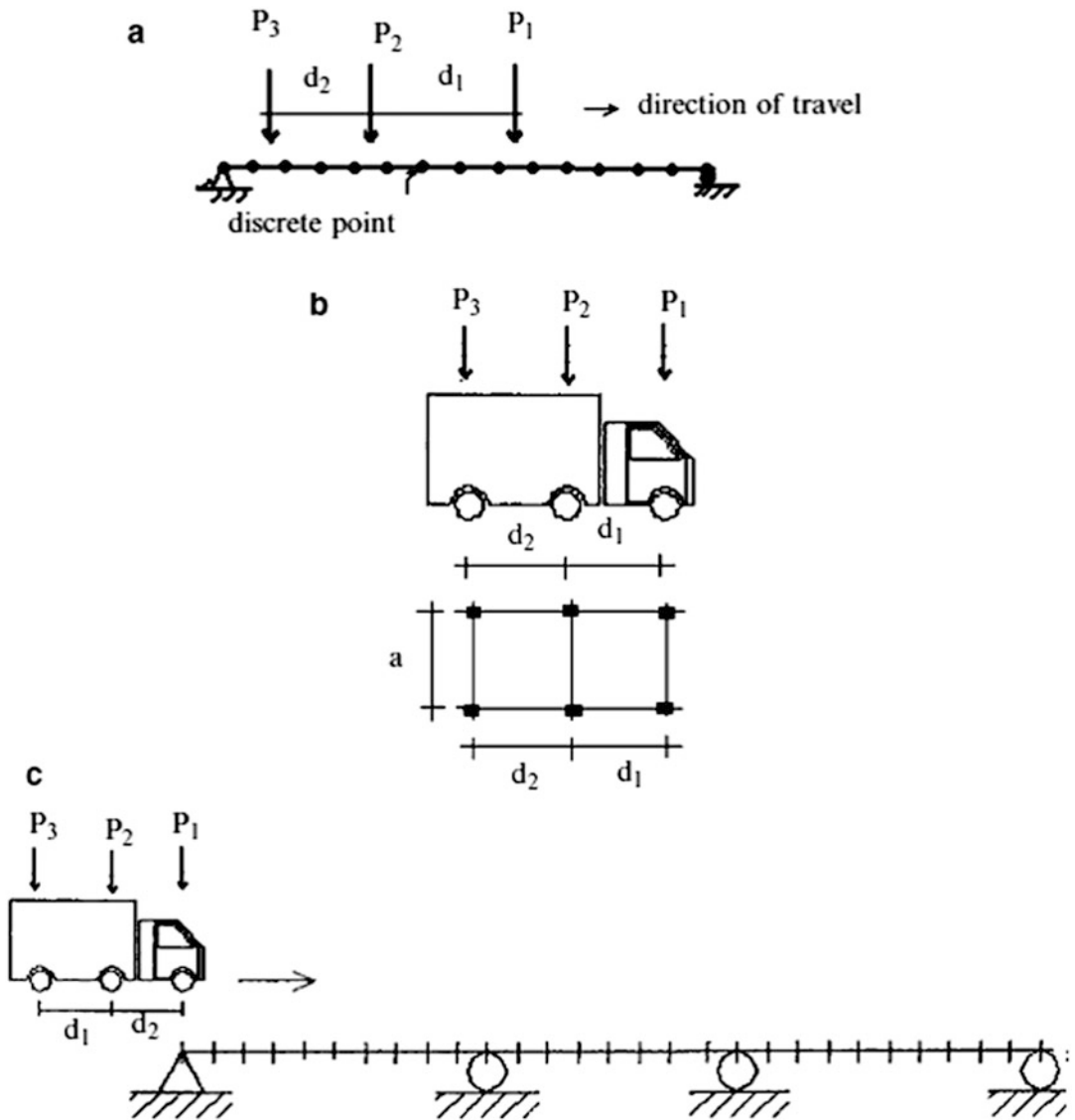


Fig. 13.12 Truck loading and span discretization. (a) Span discretization. (b) Three-axle truck. (c) Multi-span discretization

information on the absolute shear and moment distributions. For example, 30 separate analyses are required to generate the moment envelope for the span discretization shown in Fig. 13.12c. We discuss next how one establishes the magnitudes of the concentrated loads.

13.3.3.2 Transverse Distribution of Truck Load to Stringers

Figure 13.13 shows typical slab stringer highway bridge cross sections. The roadway is supported by a reinforced concrete slab, which rests on a set of longitudinal beams, called stringers. The stringers may be either steel sections or concrete elements.

In order to determine the truck load applied to the stringer, we position the truck such that one set of wheels is directly on the stringer. Figure 13.14 illustrates this case. *Note that P is the axle load.*

Fig. 13.13 Typical slab-stringer bridge deck cross sections (a) Steel girders. (b) Concrete T beams. (c) Precast concrete beams

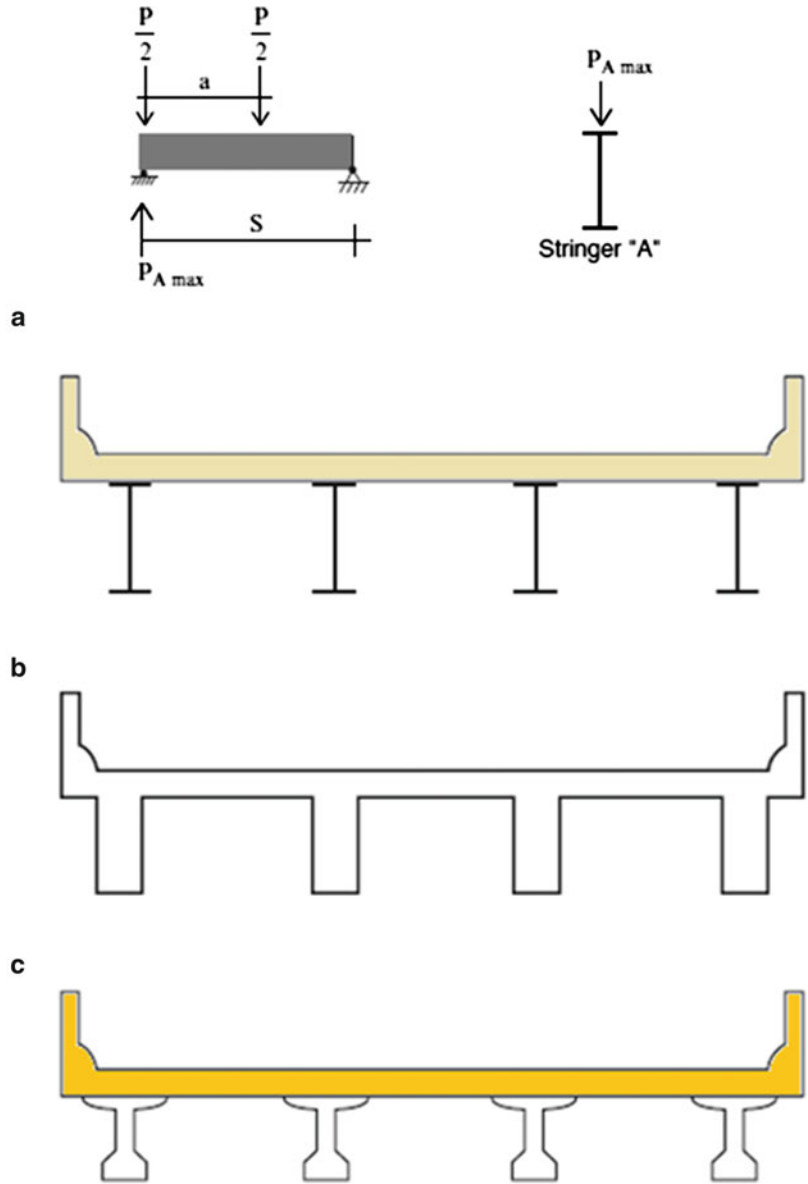
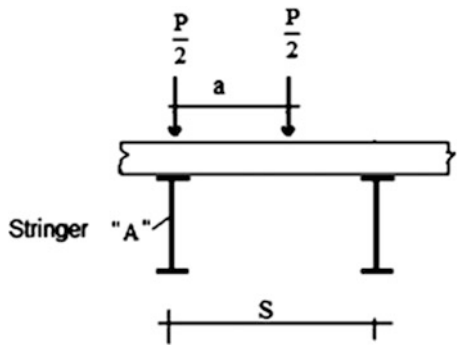


Fig. 13.14 Transverse position of vehicle wheel loads



We assume the slab acts as a simply supported beam spanning between the stringers. This assumption is conservative. Then the load on stringer “A” is

$$P_{A\max} = \frac{P}{2} + \frac{P}{2} \left(\frac{S-a}{S} \right) = \frac{P}{2} \left(2 - \frac{a}{S} \right)$$

The axle distribution factor is defined as

$$DF = \frac{1}{2} \left(2 - \frac{a}{S} \right) \quad (13.6)$$

Using this definition, the load on the stringer is represented as

$$P_{A\max} = P(DF)$$

Taking $S = 8$ ft and $a = 6$ ft yields $P_{A\max} \approx 0.625P$

Another effect that needs to be included is impact. The loading is applied rapidly as the vehicle travels onto the bridge. A measure of the loading duration is the ratio of span length to vehicle velocity. When a loading is applied suddenly and maintained constant, the effect on the response of a structure is equivalent to the application of a static load whose magnitude is equal to twice the actual load. The concept of an impact factor is introduced to handle this effect. Intuitively, one would expect this factor to be larger for short spans, i.e., to vary inversely with span length. An impact magnification factor (I) of 30 % is commonly used. With this notation, the load on the stringer is given by

$$P_{i\text{ design}} = P_i(1 + I)DF \quad (13.7)$$

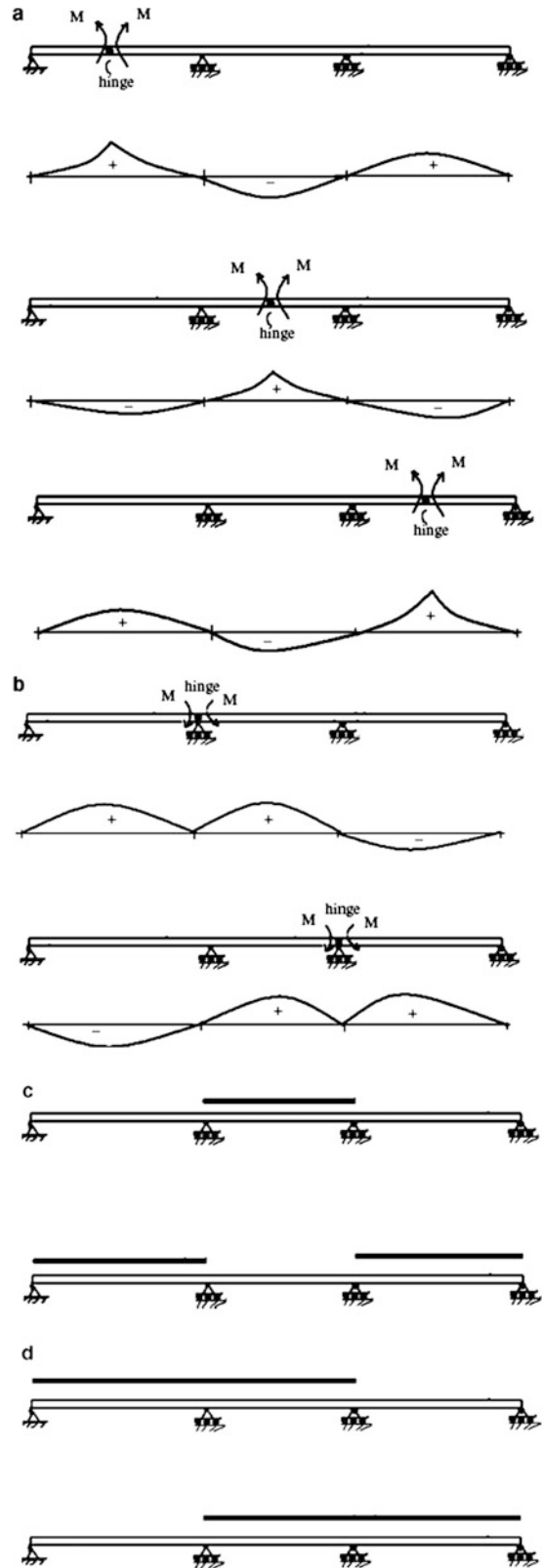
where P_i is the axle load.



13.3.3.3 Uniform Live Load

Small vehicles are modeled as a uniform loading applied selectively to individual spans. The purpose of this loading is to simulate the case where a set of passenger cars is stalled in a lane on one or more spans. *One uses the influence lines for the moments at mid-span and the interior supports to establish the loading patterns for lane loads.* The loading patterns for a three-span system are listed in Fig. 13.15c, d. Loading cases 1 and 2 produce the peak positive moment at the midpoint of the interior span; cases 3 and 4 generate the peak negative moment at the interior supports.

Fig. 13.15 Lane load cases—loading patterns. (a) Influence lines for positive moments at mid-spans. (b) Influence lines for negative moments at the supports. (c) Maximum positive moment at mid-spans (cases 1 and 2). (d) Max negative moments at the supports (cases 3 and 4)

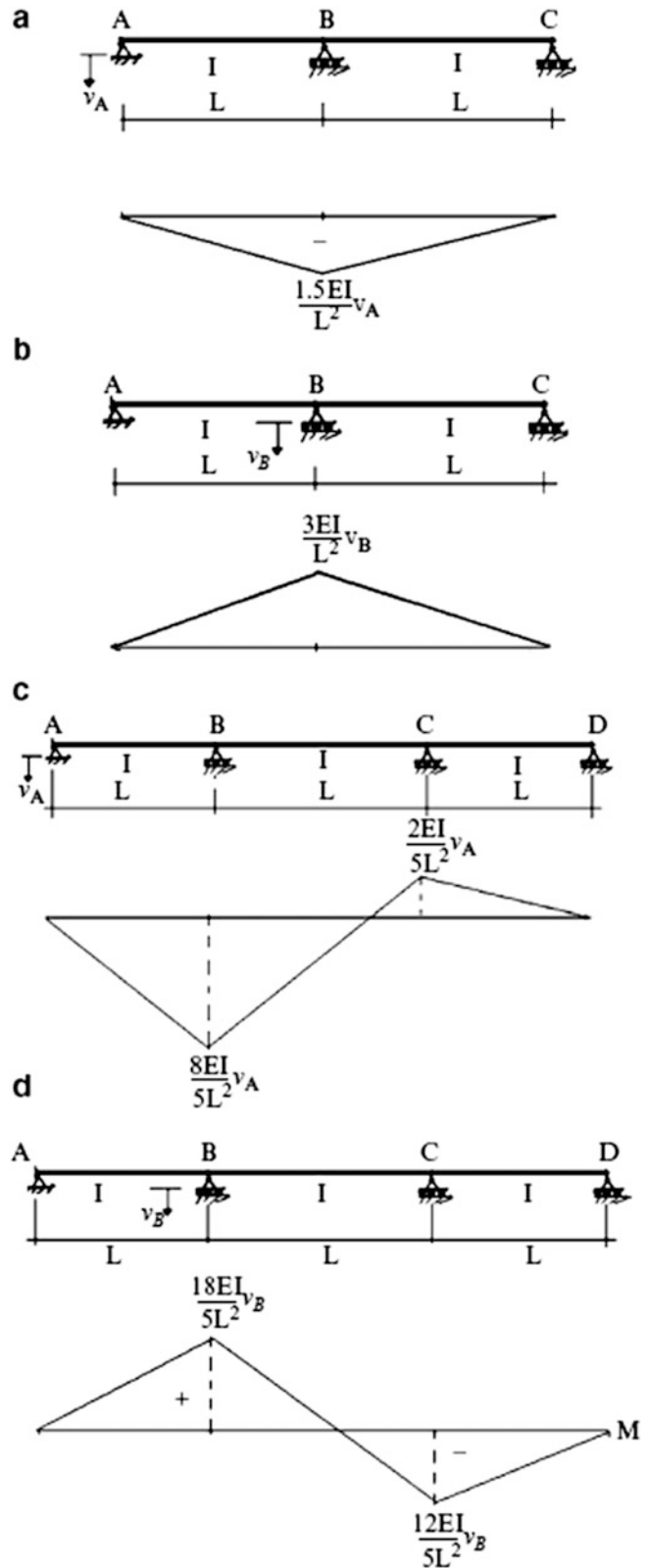


Given the loading patterns, one generates the bending moment distribution for each loading condition and then establishes the maximum values of the positive and negative moments at the *same discrete locations* selected for the truck loading. These results define the discrete moment envelope for the structure. Four separate analyses (cases 1–4) are required to construct the discrete moment envelope corresponding to the lane loading for this three-span example.

13.3.4 Loading Due to Support Settlements

In addition to the gravity loading associated with the weight of the beam and vehicles, one also needs to consider the moments induced in the structure due to support settlement. This calculation is relatively straightforward. The analytical solutions for two- and three-span symmetrical beams are generated in Examples 10.2 and 10.5. We list those results in Fig. 13.16 for convenience. Note that the peak moments are linear functions of EI . Note that the peak moment varies as $1/L^2$. Therefore support settlement is more significant for short spans vs. long spans.

Fig. 13.16 Moments due to support settlements. (a) Two-span case for v_A . (b) Two-span case for v_B . (c) Three-span case for v_A . (d) Three-span case for v_B



Example 13.2: Effect of Span Length on Support Settlement

Given: The three-span beam shown in Fig. E13.2a. The beam properties are $E = 200$ GPa and $I = 9000(10)^6$ mm⁴.

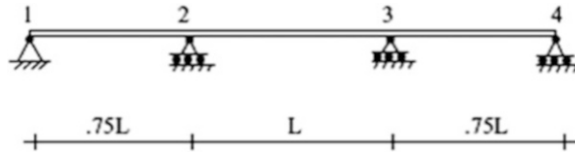


Fig. E13.2a

Determine: The bending moment distribution due to support settlement of 25 mm at supports A and B. Consider the following cases: (a) $L = 10$ m, (b) $L = 20$ m

Solution: The resulting moments are plotted in Figs. E13.2b and E13.2c. These results demonstrate that the effect of support settlement is more critical for the shorter span [case (a)].

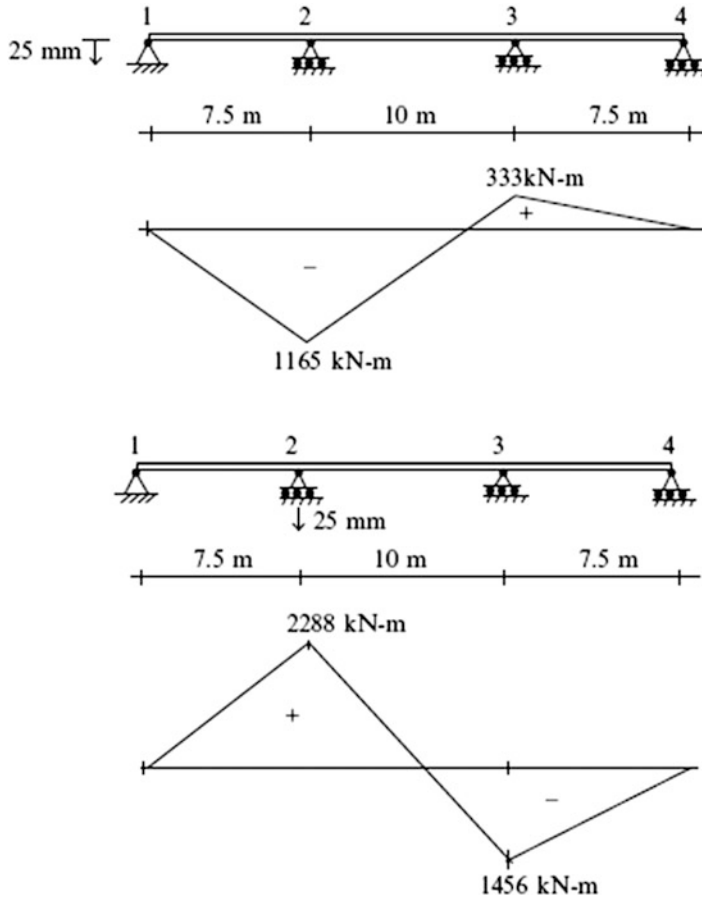


Fig. E13.2b Case a results

Case a: $L = 10$ m

Case b: $L = 20$ m

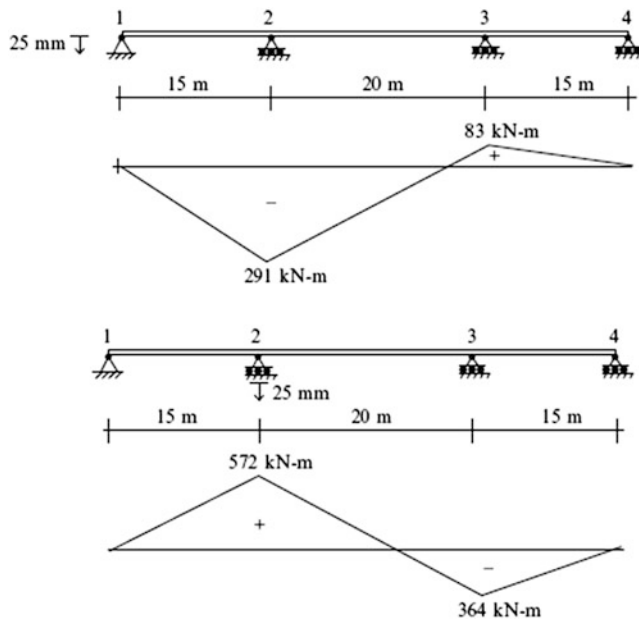


Fig. E13.2c Case b results

13.4 Case Studies

13.4.1 Case Study I: A Three-Span Continuous Girder Bridge

We illustrate the process of establishing design values using an actual bridge as a case study. The bridge is a three-span continuous girder bridge, with spans measuring 80 ft, 110 ft, and with an overall length of 270 ft. The superstructure consists of an 8 in. thick concrete slab acting in composite with four lines of steel girders spaced at 8.67 ft on center. The girder cross section is constant throughout the length. The deck carries two traffic lanes, continuous over the entire length of the bridge. The bearings are either hinge or roller supports. Figures 13.17 and 13.18 show the makeup of the bridge system and the details of the cross section. The bridge is modeled using an equivalent section equal to approximately one-fourth of the cross section of the bridge (one girder plus a 8.67 ft slab). Figure 13.18b defines the model used for this analysis.

Our objectives are

1. To determine the moment envelopes for truck and lane loading corresponding to a live uniform lane loading of 0.64 kip/ft and the truck loading defined in Fig. 13.19.

Fig. 13.17 Girder bridge system



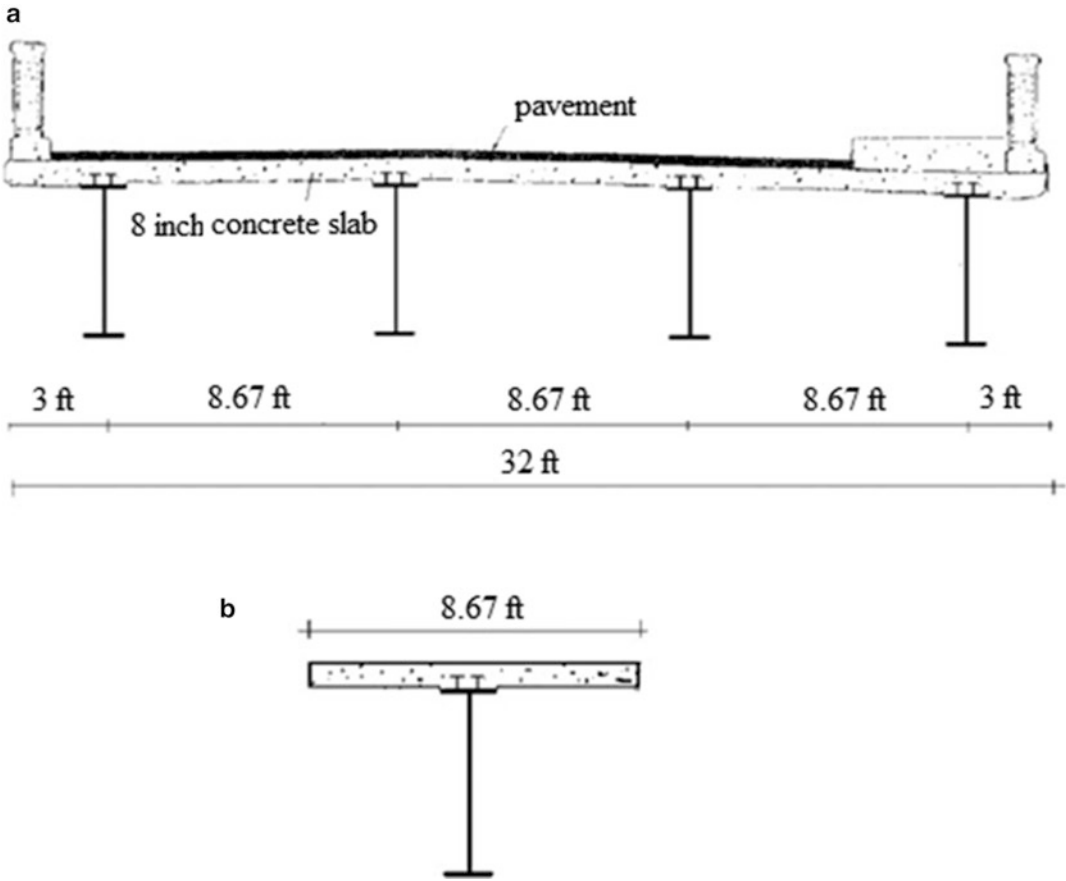
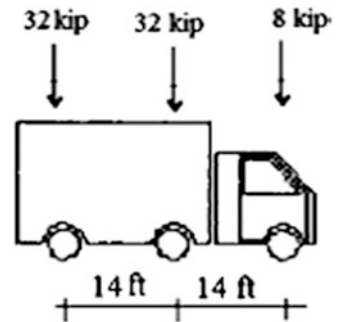


Fig. 13.18 (a) Cross section—bridge deck. (b) Cross section of single composite beam

Fig. 13.19 Truck load



2. To establish the absolute peak values (positive and negative) for moment due to dead loading of 2.1 kip/ft, lane loading, and design truck loading.
3. To determine the moments due to: 1 in. settlement of support A; 1 in. settlement of support B.

Loading patterns:

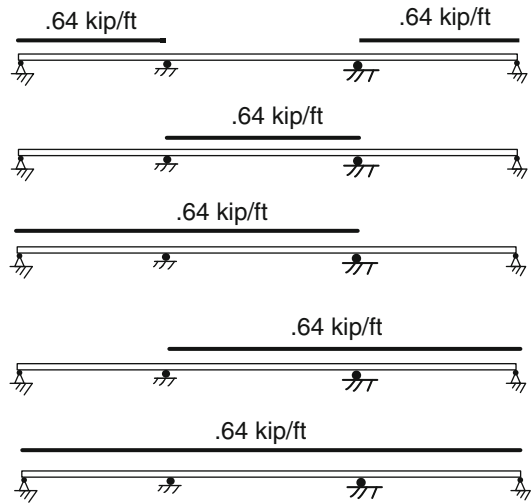
The loading patterns for the uniform dead and lane loading are shown in Figs. 13.20 and 13.21.

We discretize the individual spans into ten segments, as indicated in Fig. 13.22. A computer software system is used to generate the solutions and the moment envelopes. One can assume an

Fig. 13.20 Uniform dead load pattern



Fig. 13.21 Uniform lane load patterns for positive and negative moments



arbitrary value for I since the moment results are independent of I . Computer-based analysis is ideally suited for envelopes. Certain software packages have incorporated special features that automate the process of moving the load across the span and compiling the peak positive and negative moment values at each discrete section. Both the positive and negative moment envelopes are required in order to dimension the beam cross section.

Dead load:

The envelopes for dead load coincide with the actual moment and shear distribution shown below (Fig. 13.23). The peak values of shear, moment, and deflection are listed below.

$$\left\{ \begin{array}{l} M_{DLmax}^- = 1975 \text{ kip ft} \\ M_{DLmax}^+ = 1202 \text{ kip ft} \\ V_{DLmax} = 115.5 \text{ kip} \\ \delta_{DLmax} = 1.1 \text{ in. span II} \\ \delta_{DLmax} = 1.26 \text{ in. span I or III} \end{array} \right.$$

13.4.1.1 Uniform Lane Load

The uniform load patterns defined in Fig. 13.21 are analyzed separately; based on this data, the following envelopes are generated (Fig. 13.24).

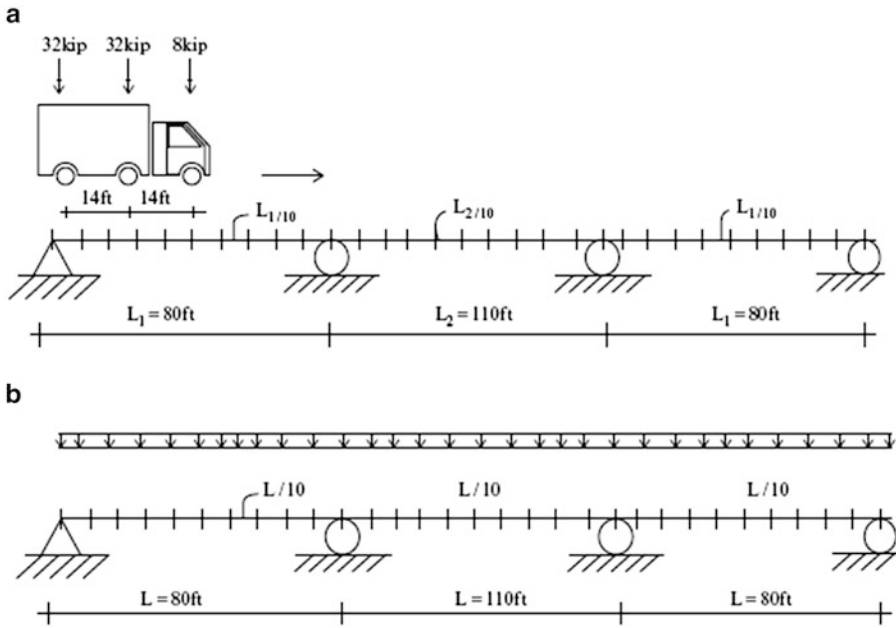


Fig. 13.22 Span discretization for live loads. (a) Truck. (b) Lane load

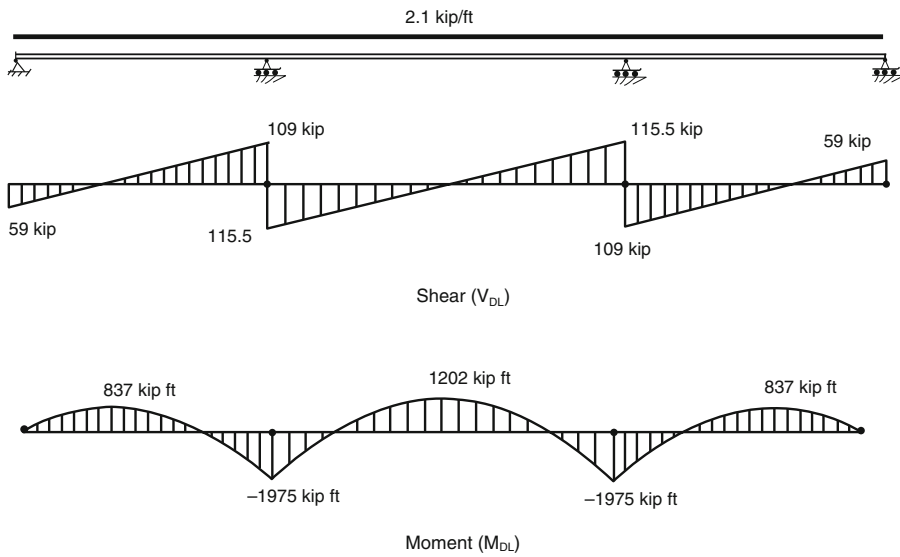
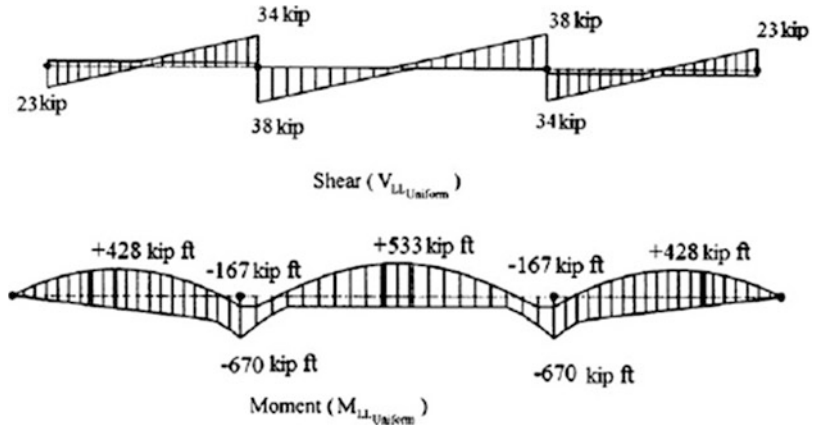


Fig. 13.23 Dead load shear and moment distributions

13.4.1.2 Truck Loading

The truck loading defined in Fig. 13.22a is passed over the span leading to the envelopes plotted in Fig. 13.25. This moment needs to be modified to account for the distribution between adjacent

Fig. 13.24 Uniform lane load envelopes



stringers and impact. The final values are determined using

$$DF = \frac{1}{2} \left(2 - \frac{a}{S} \right) = \frac{1}{2} \left(2 - \frac{6}{8.67} \right) = 0.65$$

$$M_{Design_{truck}} = M_{LL_{truck}} (1 + I) DF = M_{LL_{truck}} 1.3(0.65) = 0.845 M_{LL_{truck}}$$

Numerical results for the modified moment envelope values at the discrete points (interval of $L/10$) are listed in Tables 13.1, 13.2, and 13.3. Note that the results for span III are similar but not identical to the results for span I. Although the structure is symmetrical, the truck loading is not symmetrical.

Fig. 13.25 Truck loading envelopes

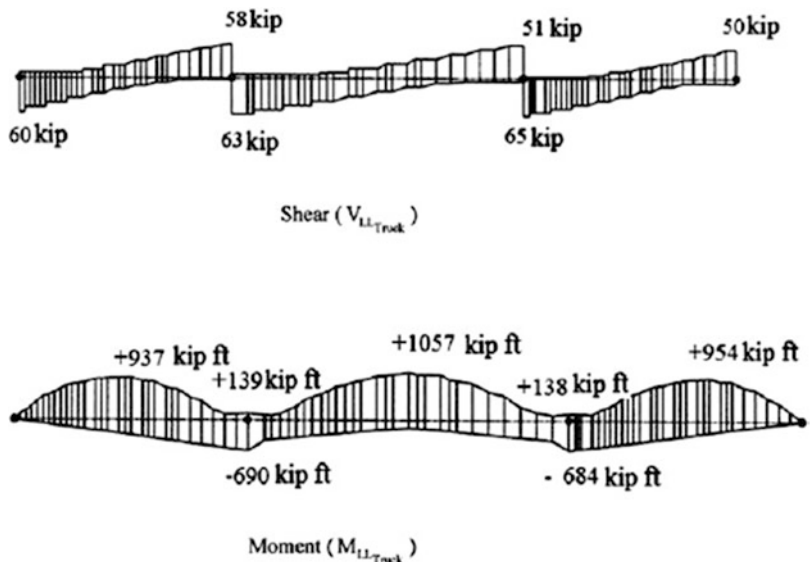


Table 13.1 Discrete envelope values: Span I (kip ft)

Span I					
X	M_{DL}	$M_{Designtruck}^+$	$M_{Designtruck}^-$	$M_{LLuniform}^+$	$M_{LLuniform}^-$
0	0	0	0	0	0
0.1 L	407	344	-58	168	-43
0.2 L	680	576	-117	294	-87
0.3 L	819	703	-175	380	-130
0.4 L	823	775	-233	425	-174
0.5 L	693	792	-292	428	-217
0.6 L	428	718	-350	391	-261
0.7 L	29	568	-408	313	-304
0.8 L	-504	357	-466	194	-348
0.9 L	-1172	106	-525	34	-419
L	-1975	117	-583	-	-670

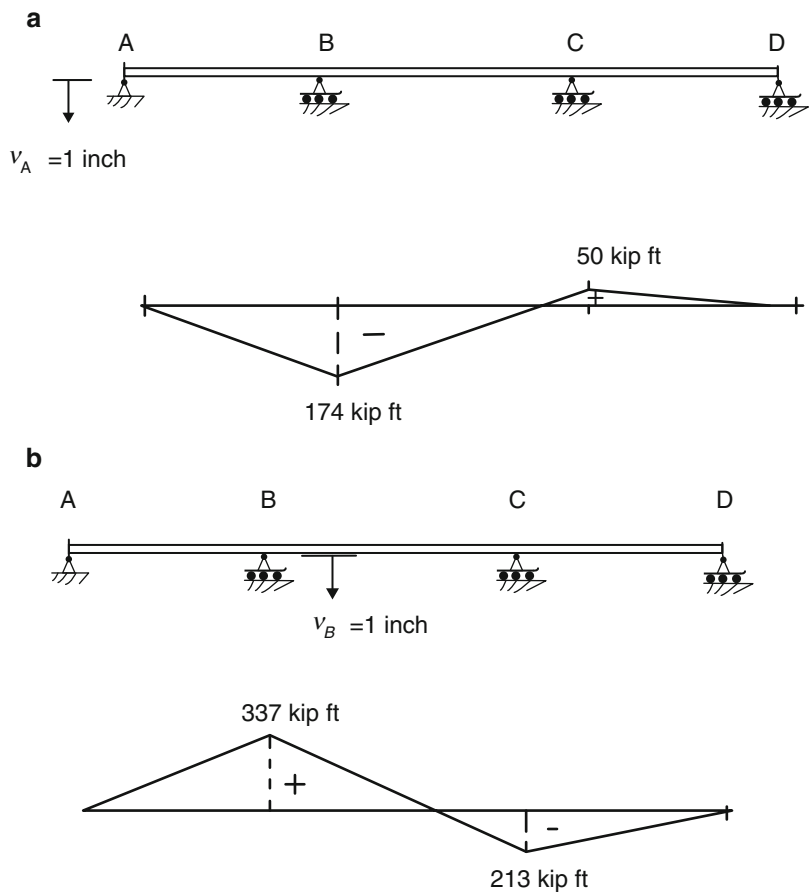
Table 13.2 Discrete envelope values: Span II (kip ft)

Span II					
X	M_{DL}	$M_{Designtruck}^+$	$M_{Designtruck}^-$	$M_{LLuniform}^+$	$M_{LLuniform}^-$
0	-1975	117	-583	-	-670
0.1 L	-831	116	-351	-	-291
0.2 L	58	430	-298	192	-167
0.3 L	693	674	-247	387	-167
0.4 L	1074	823	-194	495	-167
0.5 L	1202	893	-144	533	-167
0.6 L	107	851	-196	495	-167
0.7 L	693	700	-248	378	-167
0.8 L	58	454	-301	192	-167
0.9 L	-831	143	-353	-	-291
L	-1975	117	-583	-	-670

Table 13.3 Discrete envelope values: Span III (kip ft)

Span III					
X	M_{DL}	$M_{Designtruck}^+$	$M_{Designtruck}^-$	$M_{LLuniform}^+$	$M_{LLuniform}^-$
0	-1975	167	-578	-	-670
0.1 L	-1172	105	-520	34	-419
0.2 L	-504	330	-462	194	-348
0.3 L	29	532	-405	313	-304
0.4 L	428	682	-346	391	-261
0.5 L	693	777	-289	428	-217
0.6 L	823	806	-232	425	-174
0.7 L	819	742	-173	380	-130
0.8 L	680	575	-116	294	-130
0.9 L	407	334	-57	168	-43
L	0	0	0	0	0

Fig. 13.26 Moment due to support settlements ($E = 29,000$ ksi and $I = 48,110$ in.⁴). (a) Settlement at A. (b) Settlement at B



13.4.1.3 Support Settlement

We deal with support settlement by assuming a value for EI (in this case, we take $E = 29,000$ ksi and $I = 48,110$ in.⁴). Once the actual EI is established, the moment results can be scaled. The corresponding moment diagrams are plotted in Fig. 13.26.

13.4.2 Case Study II: Two-Hinged Parabolic Arch Response—Truck Loading

This study illustrates how one evaluates the behavior of a typical two-hinged arch bridge subjected to a truck loading. An example structure is shown in Fig. 13.27; the idealized model is defined in Fig. 13.28. We model the roadway as a continuous longitudinal beam supported at 10 ft intervals by

Fig. 13.27 Two-hinged arch bridge



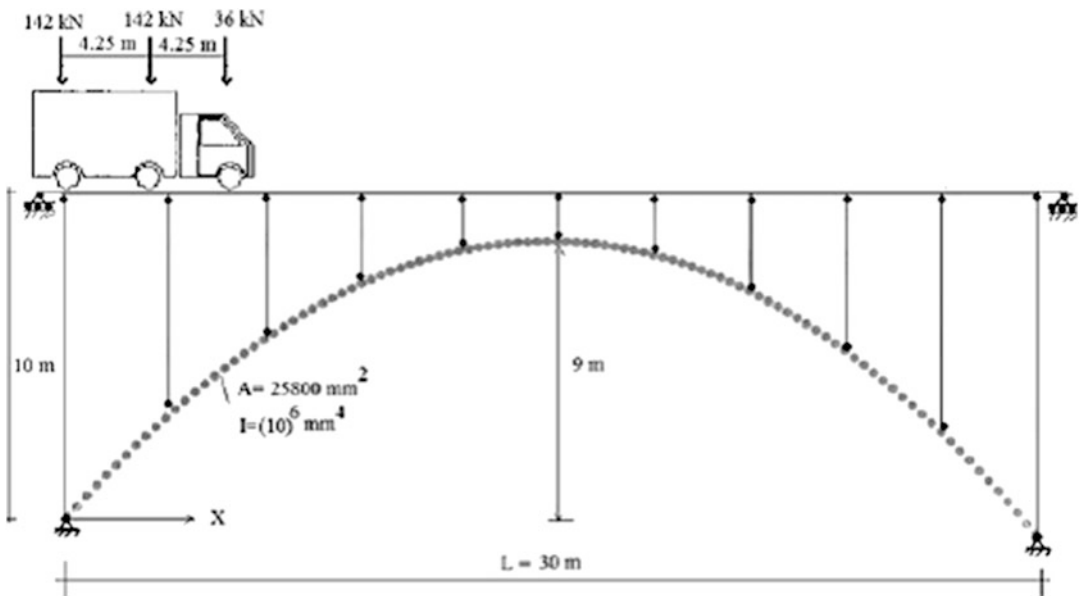


Fig. 13.28 Parabolic-arch geometry and loading-idealized model

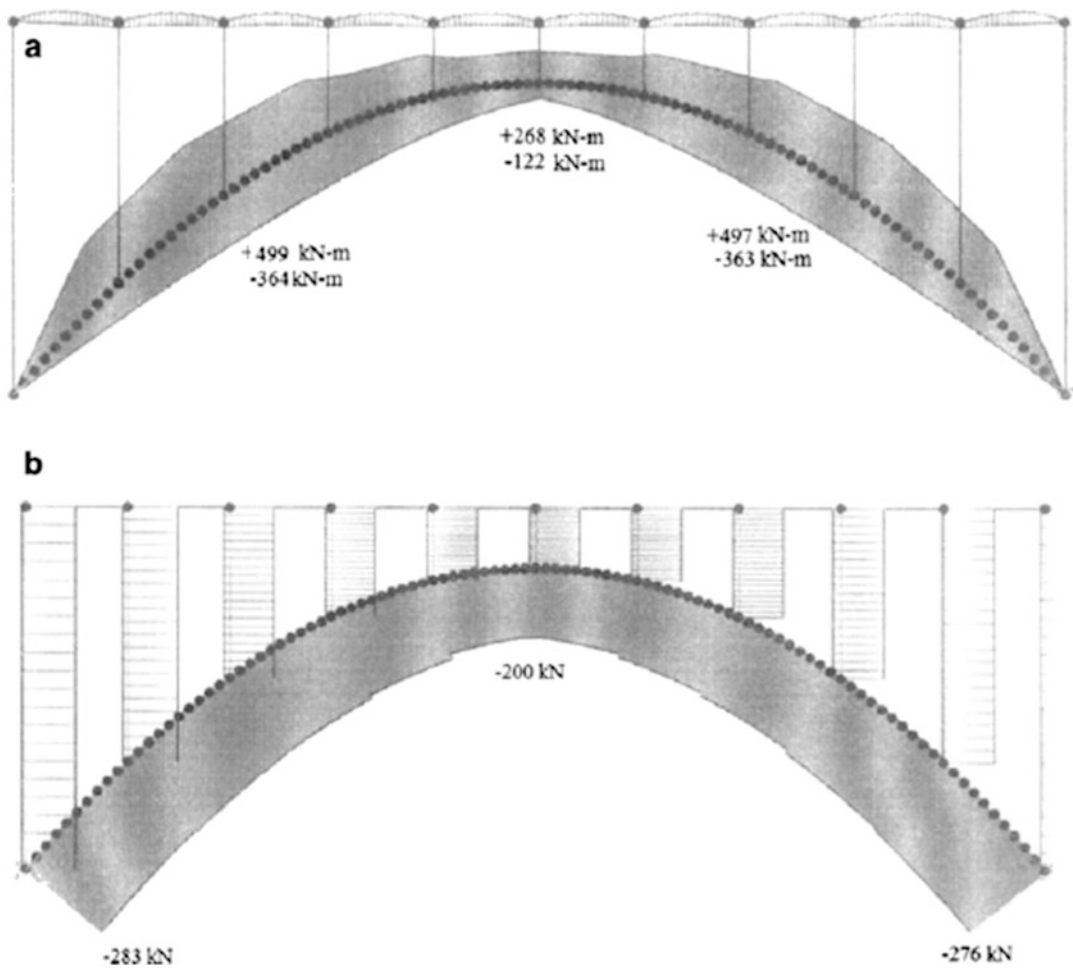


Fig. 13.29 Force envelopes—Truck loading—100 straight segments. (a) Moment envelope. (b) Axial envelope

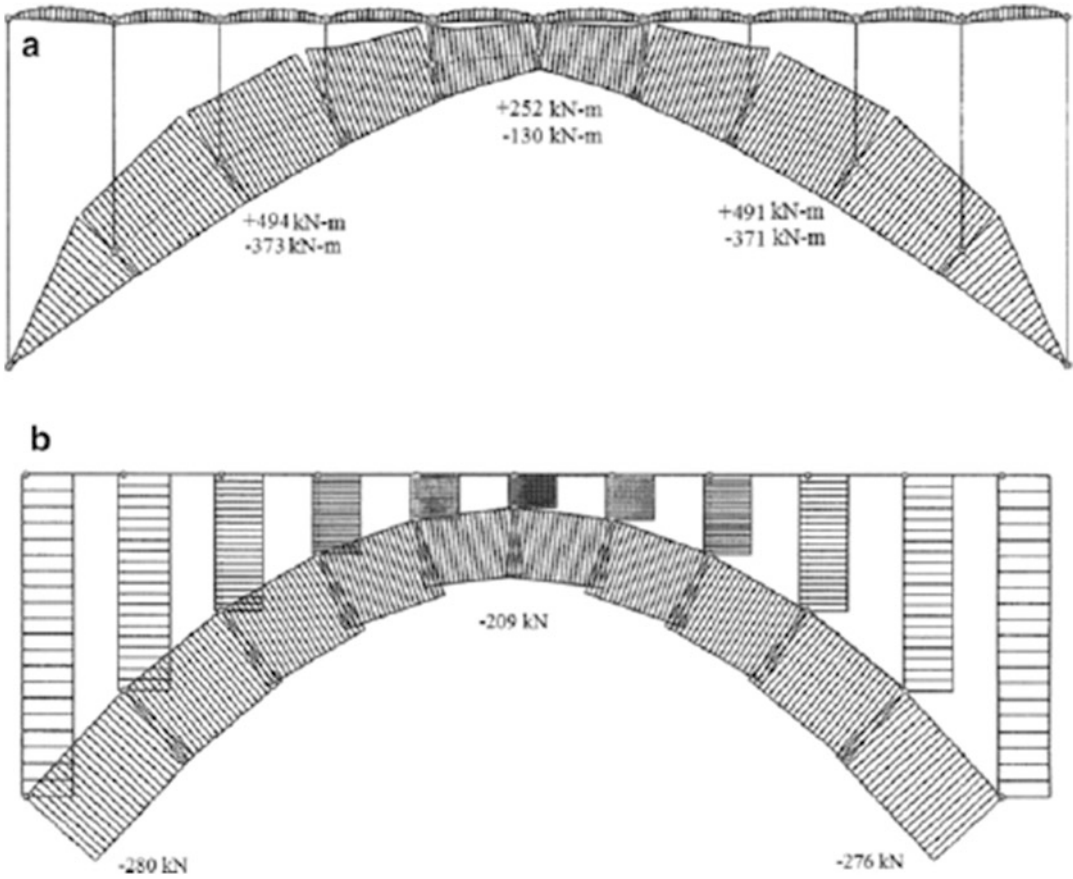


Fig. 13.30 Force envelopes—Truck loading—10 straight segments. (a) Bending envelope. (b) Axial envelope

axial members attached to the parabolic arch. The truck loading is transmitted through the axial elements to the arch. We generate force envelopes for the arch using an analysis software system applied to the discretized model. A similar discretization strategy was employed in Chap. 6. Results for the bending moment and axial force due to the truck loading are plotted in Figs. 13.29 and 13.30. Figure 13.29 is obtained by subdividing the arch into 100 straight segments having a constant projection, Δx , of 0.3 m. Figure 13.30 is generated by subdividing the arch into ten straight segments having a constant projection, Δx , of 3 m.

The force envelope plots are useful for displaying the variation in response, e.g., the range in moment values. However, to determine the absolute extreme values, one has to scan over the data. This process leads to the following “absolute values”

$$100 \text{ straight segment} \begin{cases} M_{\max}^+ = +499 \text{ kN m} \\ M_{\max}^- = -381 \text{ kN m} \\ P_{\max} = -283 \text{ kN} \end{cases} \quad 10 \text{ straight segment} \begin{cases} M_{\max}^+ = +499 \text{ kN m} \\ M_{\max}^- = -381 \text{ kN m} \\ P_{\max} = -283 \text{ kN} \end{cases}$$

In general, it is a good strategy to consider at least two discretizations. In this example, we observe that the ten segment model produces quite reasonable results.

13.4.3 Case Study III: Three-Span Parabolic Arch Response—Truck Loading

We consider next the three-span arch system shown in Fig. 13.31. The span lengths, discretizations, and the truck loading are the same as for case study I. It is of interest to compare the peak values of the force envelopes for the two different structural models. The discretized model consists of straight segments having a constant horizontal projection of 1 ft. A computer software package was used to generate the corresponding force envelopes which are plotted in Figs. 13.32 and 13.33.

Comparing the moment envelopes for the arch and the girder, we note that arch system has lower peak moment values. However, the arch system has axial forces so that the cross section must be designed for combined bending and axial action. There are no axial forces in the girder system, just pure bending.

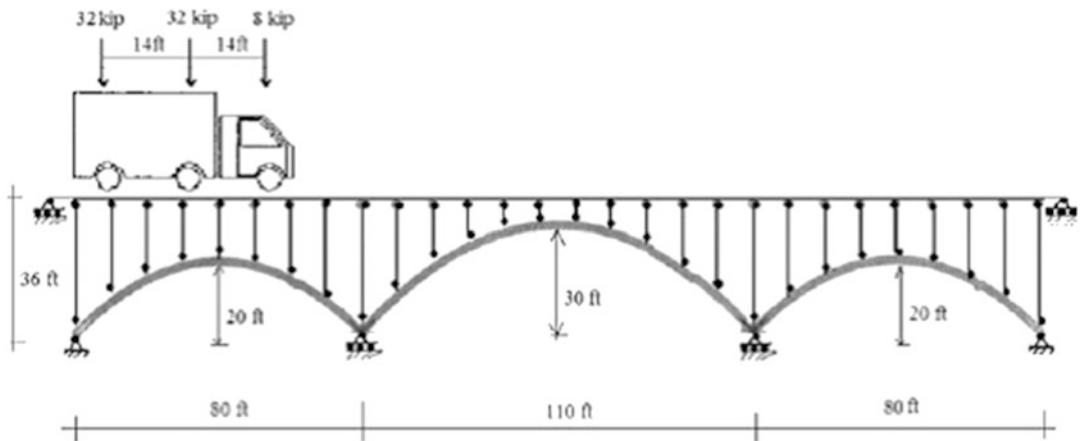


Fig. 13.31 Idealized model—three-span arch

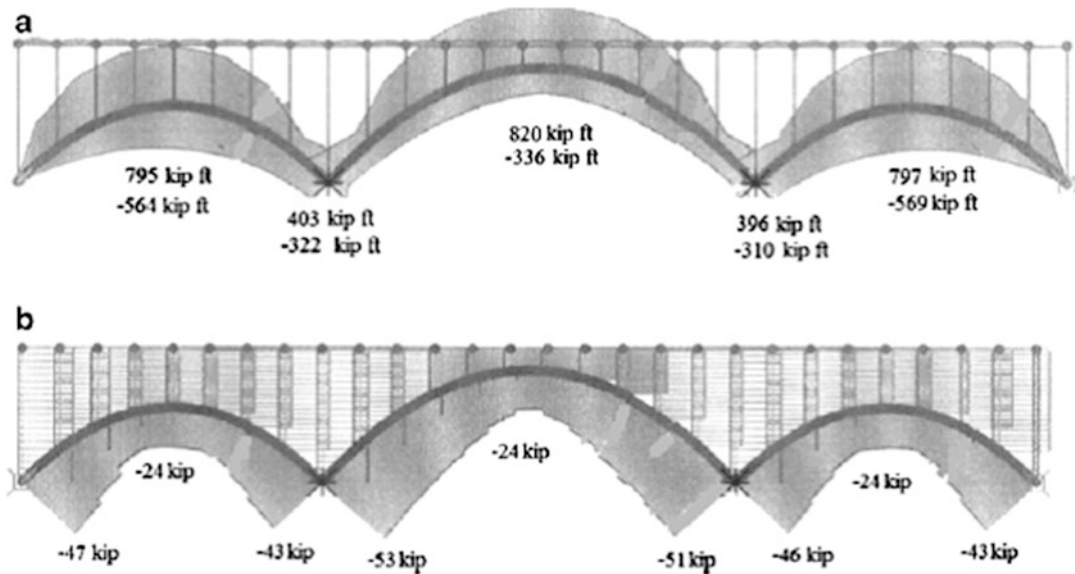


Fig. 13.32 Force envelopes—three-span arch. (a) Moment envelope—three-span arch. (b) Axial envelope—three-span arch

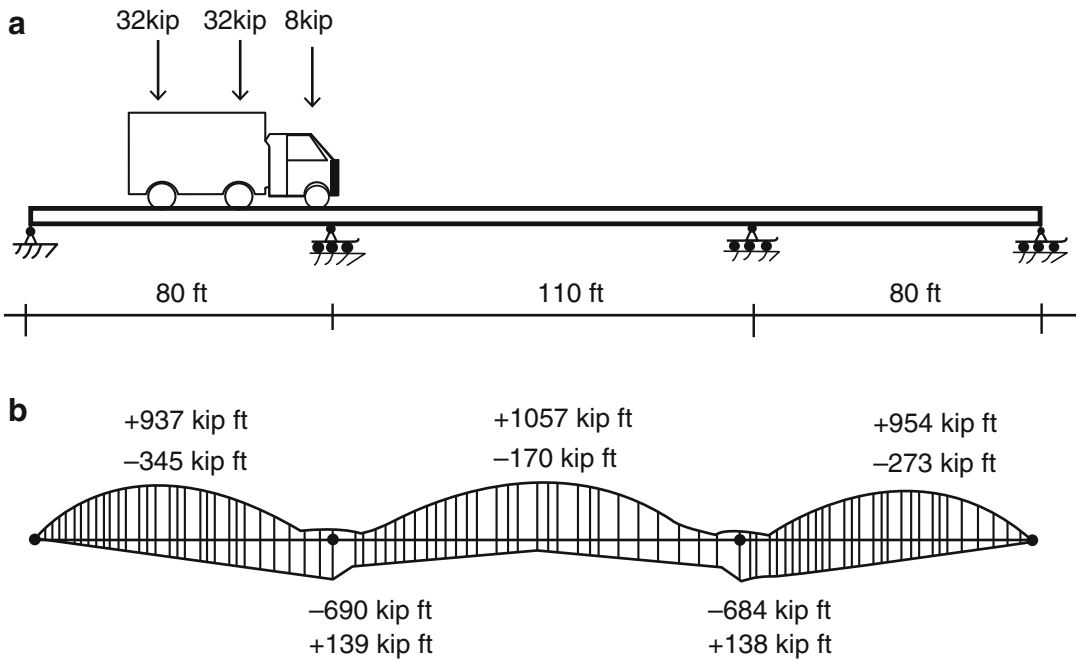


Fig. 13.33 Force envelopes—three-span girder. (a) Geometry and loading. (b) Moment envelope

13.4.4 Case Study IV: Cable-Stayed Bridge

This case study concerns the cable-stayed bridge concept, a type of structure that requires some special modeling strategies and exhibits a completely different behavioral pattern than girder and arch-type structures. It has evolved as the dominant choice for long span crossings. A typical configuration is shown in Fig. 13.34. The terms “harp” and “fan” refer to the positioning of the cables on the tower. A modified fan arrangement is usually adopted to avoid congestion on the tower.

Fig. 13.34 Typical cable-stayed scheme



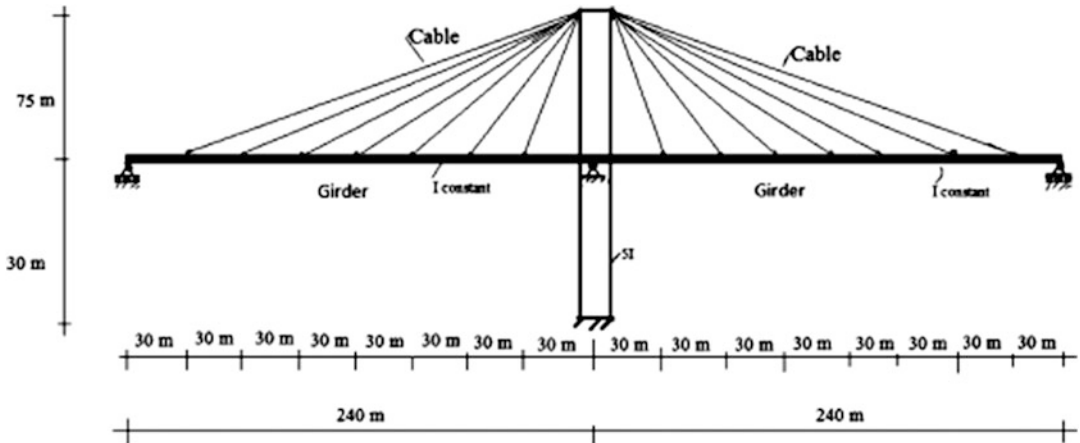


Fig. 13.35 Idealized cable-stayed scheme

Of particular interest is the load path for vertical loading applied to the girder. Without the cables, the girder carries the load by bending action throughout the total span. Since the maximum moment varies as to the square of the span length, this structural concept is not feasible for long spans. The effect of the cables is to provide a set of vertical supports to the girder, thus reducing the moment in the girder. In what follows, we illustrate this effect using the idealized structure shown in Fig. 13.35.

We suppose the girder is continuous, and the cable layout is symmetrical (equally spaced on the longitudinal axis). There are seven pairs of symmetrical cables. Each cable has a different cross-sectional area. The girder is hinged at the tower, but free to expand at the two end supports. We model the cables as straight members that are hinged at their ends to the tower and the girder. In this way, they function as axial elements and transmit the gravity loading applied to the girder up to the tower. The net effect is to reduce the bending moment in the girder.

Starting with nodes at the supports and the cable–girder intersection points, one may also discretize the girder between the cable nodes to obtain more refined displacement and moment profiles. Since the structure is indeterminate, we need to specify member properties in order to execute an analysis. We estimate the cable areas by assuming an individual cable carries the tributary loading on a segment adjacent to the cable. This estimate is based on strength.

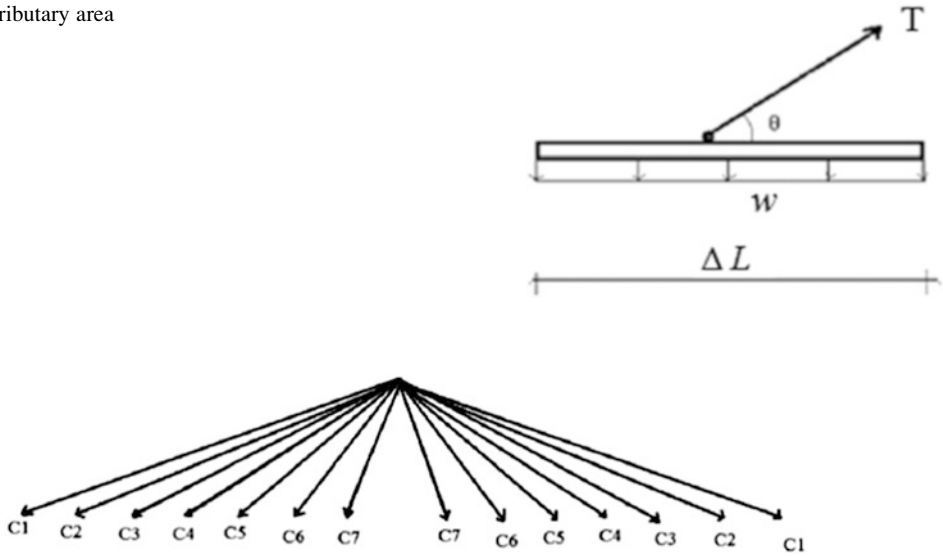
$$A_C = \frac{T}{\sigma_{all}} = \frac{w\Delta L}{\sigma_{all} \sin \theta}$$

where σ_{all} is some fraction of the yield stress and ΔL is the cable spacing. This equation shows that the required area increases with decreasing θ . Therefore, one must increase the cable area as the distance from the tower increases. A lower limit on θ is usually taken as 15° (Fig. 13.36).

Taking $w = 10 \text{ kN/m}$, $\Delta L = 30 \text{ m}$, and $\sigma_{all} = 0.687 \text{ kN/mm}^2$ leads to the estimated cable areas listed below.

Cable	θ°	$\frac{1}{\sin \theta}$	$A_{cable} \text{ (mm}^2\text{)}$
C1	19.6	3	1305
C2	22.6	2.3	1130
C3	26.5	2.2	957
C4	32	1.9	827
C5	39.8	1.6	696
C6	51.3	1.3	566
C7	68.2	1.1	480

Fig. 13.36 Tributary area for cable



We estimate I for the girder by assuming the bending moment diagram is similar to the distribution for a uniformly loaded beam with multiple spans equal to ΔL . The peak negative moment for this case is $\frac{w(\Delta L)^2}{12}$. Given these estimated properties, one analyzes the structure and iterates on the properties until the design requirements are satisfied.

Figure 13.37 shows the forces and displacement profile corresponding to $I_{\text{girder}} = 420(10)^6 \text{ mm}^4$ and the following set of cable areas for cables 1–7, respectively (1305, 1130, 957, 827, 696, 566, and 480 mm^2). The girder cross-sectional area is taken as $120,000 \text{ mm}^2$. Note that the bending moment diagram for the girder is similar to that observed for a multi-span uniformly loaded beam. We also point out that the response is sensitive to the girder cross-sectional area since there is significant compression in the girder.

An estimate of the vertical displacement based on the axial force corresponding to strength is given by

$$v = \frac{\sigma L_{\text{cable}}}{E \sin \theta}$$

The displacement profile for the girder agrees with this approximation. The peak value occurs for the outermost cable which has the largest length and smallest angle.

A suggested peak value for displacement under live load is $L/800$, which for this geometry translates to 300 mm. We can decrease the deflection by increasing the areas for the outer cables. Assuming an individual cable act as a single vertical spring subjected to the loading $w(\Delta L)$, and requiring the displacement to be equal to v_{all} leads to the following estimate for the cable area

$$A_c = \frac{w(\Delta L)L_c}{v_{\text{all}}E(\sin \theta)^2}$$

where L_c is the cable length. Holding the girder properties constant, we use this approximate expression to increase the cable areas to (14,000, 11,500, 8500, 5000, 3000, 3000, 2000 mm^2) and repeat the analysis. The displacement profile of the girder for this case is plotted in Fig. 13.38 and also summarized in the table listed below. Note that the displacement is sensitive to the cable area and the angle of inclination; the cable tension is governed primarily by strength. This case study illustrates the

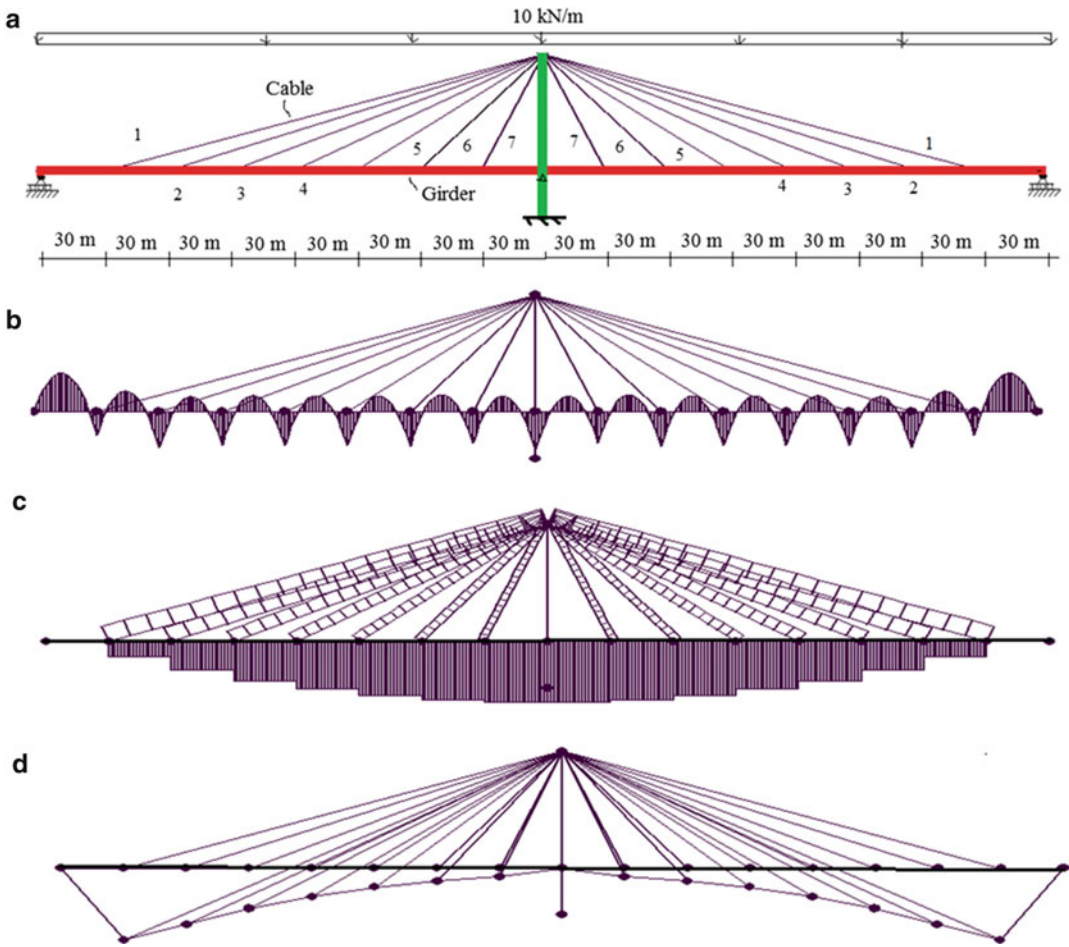
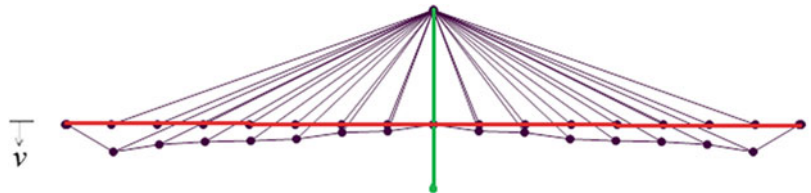


Fig. 13.37 Force and displacement profiles. (a) Geometry and loading. (b) Moment in girder. (c) Axial forces in cables and girder. (d) Displacement profile of girder

Fig. 13.38 Final displacement profile of girder



role of computer simulation in developing the design of cable-stayed structures. One refines the design through iteration. This example also illustrates how cable-stayed structures carry the load primarily through axial action in the cables. The girder functions mainly to transmit the deck loading to the cables, i.e., the bending is localized between the cable support points.

Cable	A_{cable} (mm ²)	Tension (kN)	v_{\downarrow} (mm)	A_{cable} (mm ²)	Tension (kN)	v_{\downarrow} (mm)
C1	1305	914	2382	14,000	998	297
C2	1130	810	1864	11,500	761	217
C3	957	665	1341	8500	675	186
C4	827	567	940	5000	566	176
C5	696	467	630	3000	467	157
C6	566	387	428	3000	386	86
C7	480	315	287	3000	386	48

13.5 Summary

13.5.1 Objectives

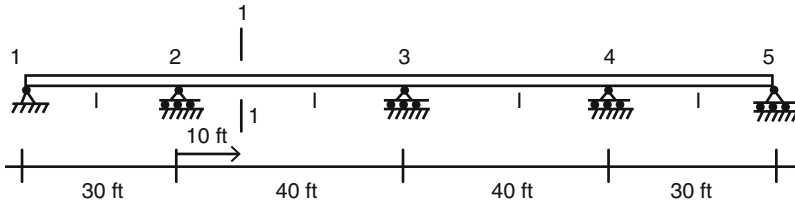
- To present Müller-Breslau's principle and illustrate how it is used to establish loading patterns that produce the maximum value of a force quantity at a particular point on a structure.
- To describe a procedure for determining the load on an individual stringer due to an axle load applied to the deck of a slab-stringer bridge system.
- To describe and illustrate a computer-based procedure for generating force envelopes for indeterminate horizontal structures subjected to a set of concentrated loads.
- To illustrate the different behavioral patterns for multi-span girder, arch, and cable-stayed systems.

13.5.2 Key Facts and Concepts

- Müller-Breslau's principle is used to establish influence lines for indeterminate structures. One works with a structure generated by removing the constraint provided by the force quantity. The deflected shape of the structure due to a unit value of the force quantity is a scaled version of the influence line.
- The moment envelope for a horizontal structure is generated by applying the loading at discrete points on the longitudinal axes, tabulating the bending moment at each discrete point for *all the loading cases*, and selecting the largest positive and negative values. A computer-based procedure is used for this task.
- Support settlement can produce bending moments which are significant for short span bridges.

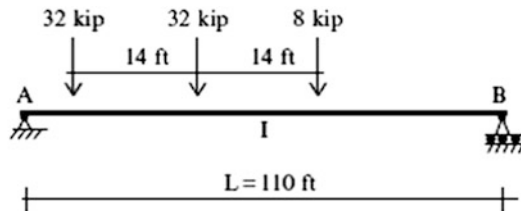
13.6 Problems

Problem 13.1



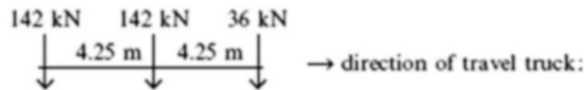
- (a) Using Müller-Breslau principle, sketch the influence lines for the vertical upward reaction at support 3 (R_3), the negative moment at support 2 (M_2), and the negative moment at section 1-1 (M_{1-1})
- (b) Use a software package to determine:
 - (i) The maximum values of R_3 , M_2 , and M_{1-1} cause by a uniformly distributed dead load of 2 kip/ft.
 - (ii) The maximum value of M_2 caused by a uniformly distributed live load of 1 kip/ft.

Problem 13.2 Consider the single span bridge shown below. Using the analytical procedure described in Sect. 3.10.2.1, determine the absolute maximum value of moment developed as the truck loading defined below passes over the span. Repeat the analysis using computer software.

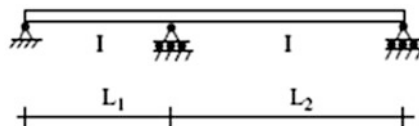


Problem 13.3 Consider the two-span bridges shown below. Use computer software to determine global moment envelopes for both the lane and truck loadings defined below.

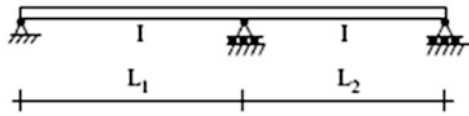
Lane load: $w = 10$ kN/m uniform
 Truck load:



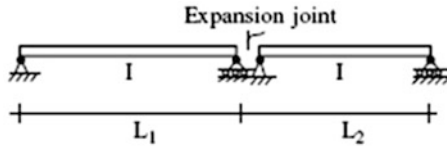
- (a) $L_1 = L_2 = 30$ m, EI is constant



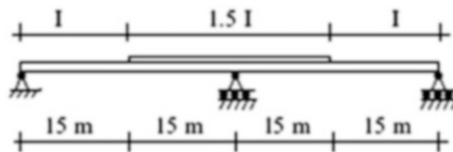
- (b) $L_1 = 15\text{ m}$, $L_2 = 30\text{ m}$, EI is constant



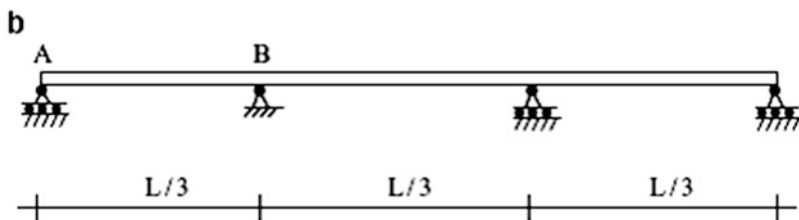
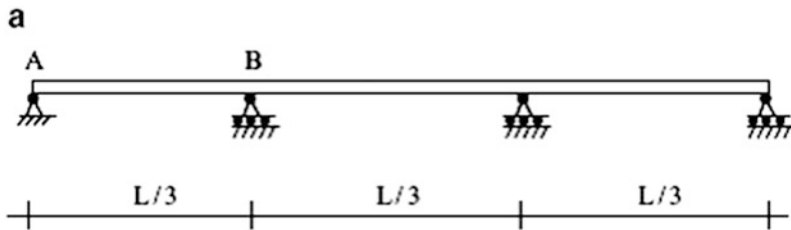
- (c) $L_1 = L_2 = 30\text{ m}$, EI is constant



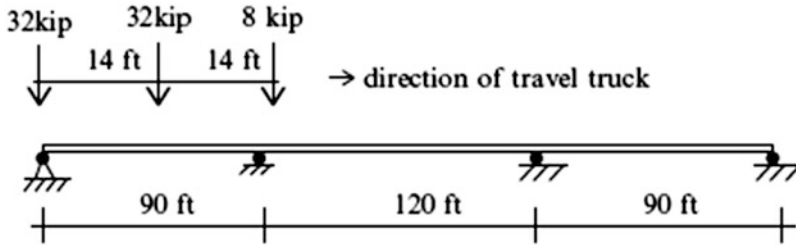
- (d) Compare the global moment envelopes for the structure shown below with the envelopes generated in part (a). Is there any effect of varying I ?



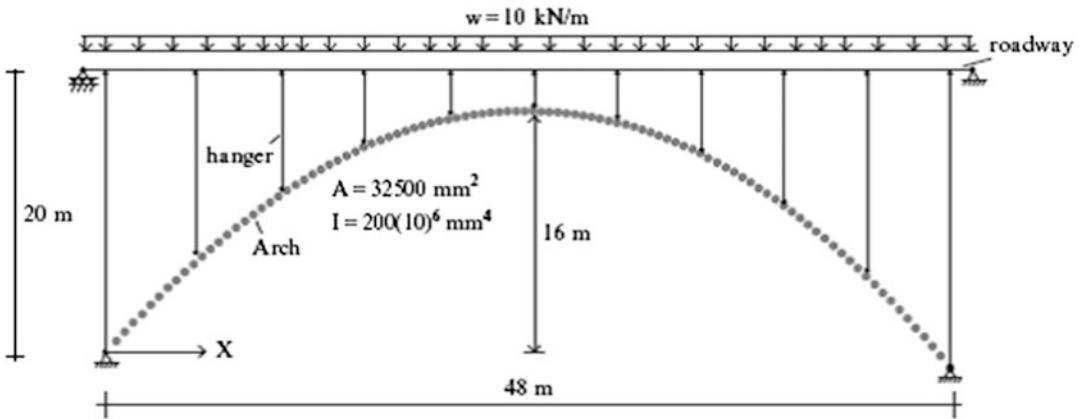
Problem 13.4 Consider the multi-span bridge shown below. Suppose the bridge is expected to experience a temperature change of ΔT over its entire length. Where would you place a hinge support: at A or at B? Determine the end movement corresponding to your choice of support location.



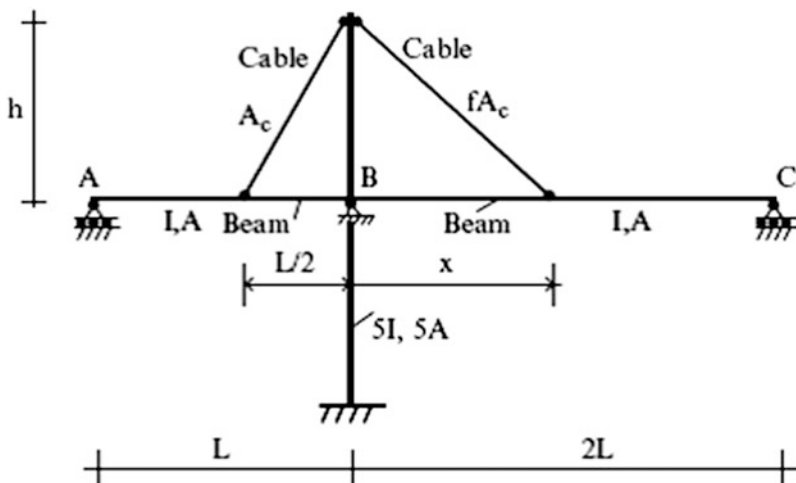
Problem 13.5 Most design codes limit the deflection due to live loading to some fraction of length, say L/α , where α is on the order of 500. Generate the global “deflection” envelope for the multi-span beam and truck loading shown below. Take $E = 29,000$ ksi and $I = 60,000$ in.⁴

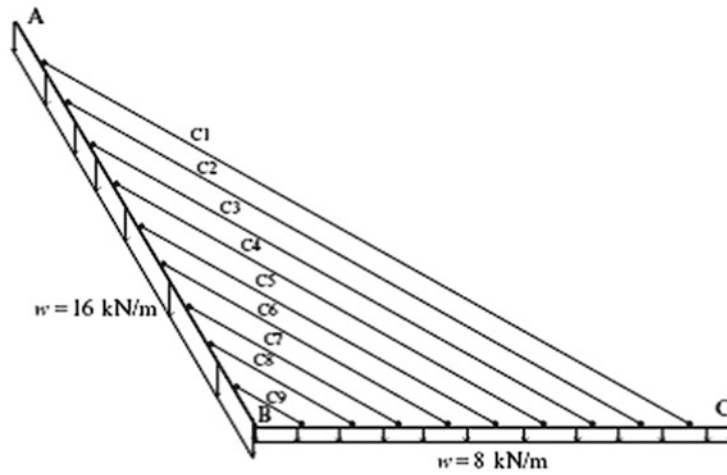
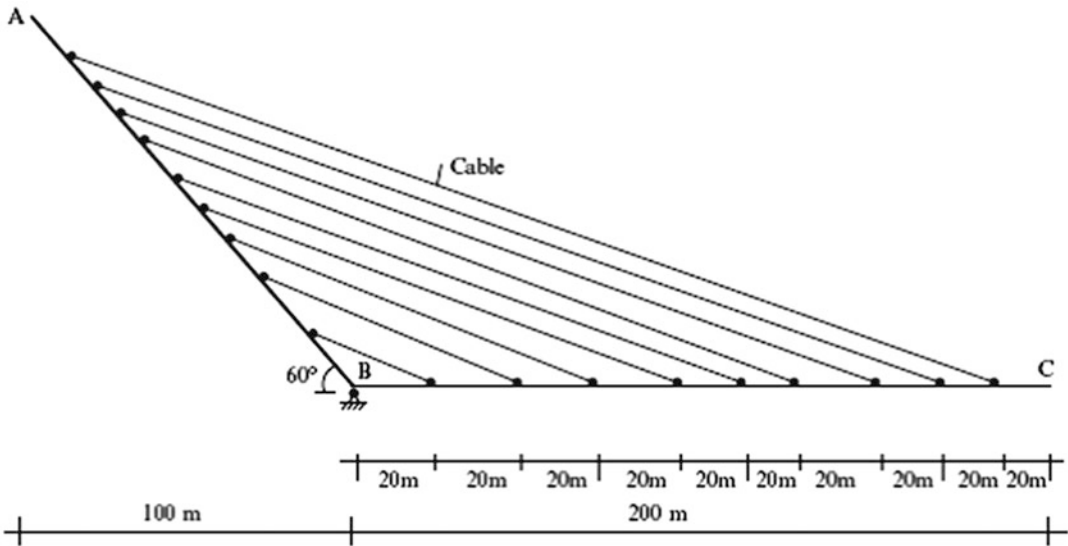


Problem 13.6 Investigate convergence of the internal forces for the parabolic arch shown as the discretization is refined. Take the interval as 2.4, 1.2, and 0.6 m.



Problem 13.7 Suppose a uniform loading is applied to span ABC. Investigate how the response changes as x varies from $L/2$ to L . Take $h = L/2$, $A = 50$ in.², $A_c = 2$ in.², $w = 1$ kip/ft, $f = 1 + (2x/L)^2$.

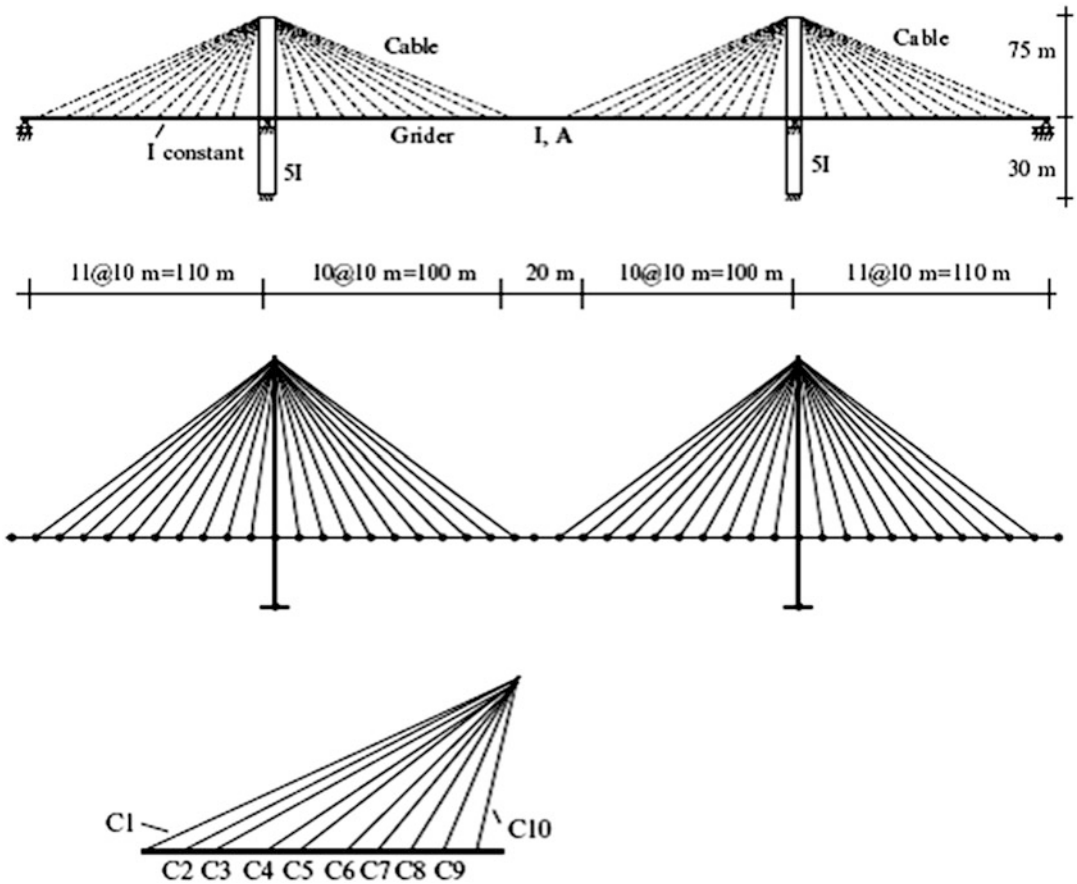




An illustration of this structural concept created by Santiago Calatrava is shown below. This bridge is located in Seville, Spain. Puente del Alamillo in Seville, Spain. This work has been released into the public domain by its author, Consorcio Turismo Sevilla. This applies worldwide. The image was accessed in March 2012 from http://en.wikipedia.org/wiki/File:Puente_del_Alamillo.jpg.



Problem 13.10 Consider the symmetrical cable structure shown below. Determine a set of cable areas (C_1-C_{10}) such that the maximum vertical displacement is less than 375 mm under a uniformly distributed live load of 10 kN/m. Assume $I_{\text{girder}} = 400(10)^6 \text{ mm}^4$, $A_{\text{girder}} = 120(10)^3 \text{ mm}^2$. Take the allowable stress as 700 MPa.



References

1. Wilbur JB, Norris CH. Elementary structural analysis. New York: McGraw-Hill; 1948.
2. Faraji S, Ting J, Crovo DS, Ernst H. Nonlinear analysis of integral bridges: finite element model. ASCE J Geotech Geoenviron Eng. 2001;127(5):454-61.

Abstract

Buildings are complex physical systems. Structural Engineers deal with this complexity by creating idealized structural models that define the key structural components, the overall makeup of the building structure, and the loadings that it needs to withstand. The information provided by the idealized model allows one to apply analysis and design methods directly to the model and then extrapolate the results to the actual building.

We begin the chapter with a description of the various types of building systems and the associated structural components. In general, a building consists of plane frame structures which are interconnected by floor systems. We describe approaches for establishing the *lateral loads* due to wind and earthquake excitation. These loads are evaluated at each floor level and then distributed to the individual plane frames using the concepts of center of mass and center of twist. At this point, one has the appropriate lateral loading to analyze the plane frames. The topic of loading on building frames is discussed further in the next chapter where we also consider gravity loads acting on the floor systems.

14.1 Types of Multistory Building Systems

The majority of the activities in Structural Engineering are concerned with the design of Structural Systems for buildings. Approximately 95 % of the building inventory consists of buildings having less than ten stories. Buildings of this type are classified as low-rise buildings. Figure 14.1 illustrates the typical makeup of a low-rise building. The primary structural components are beams, columns, and floor plates. Members are usually arranged in an orthogonal pattern to form a three-dimensional framework. Plate-type elements span between the beams to form the flooring system. We visualize the three-dimensional (3D) framework to be composed of plane frames which are connected by floor plates. This interpretation allows us to analyze the individual plane frames rather than the complete 3D structure.

Fig. 14.1 Typical makeup of a structural system for a low-rise building

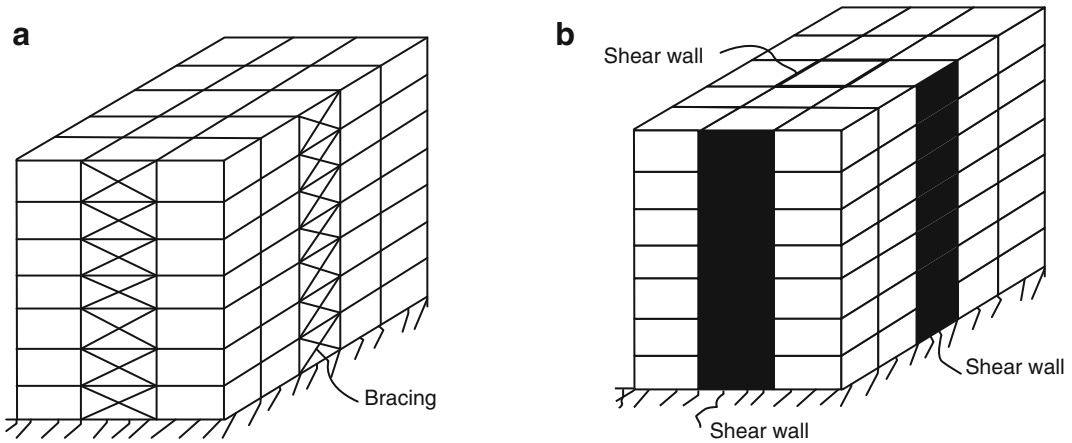


Fig. 14.2 (a) Steel braced frame with bracing. (b) Concrete frame with shear walls

Frames are designated according to how the beams and columns are interconnected at their end points. When the members are rigidly connected so that no relative rotation can occur, end moments develop under loading and the frame is said to be “rigid.” Rigid frames may employ either Steel or Concrete construction.

The opposite case is when the beams are pinned to the columns. No end moments are developed and the frame behaves similar to a truss. Some form of bracing is needed since a rectangular pinned frame is unstable under lateral load. These structures are called “braced” frames. Figure 14.2a shows a typical braced frame structure. The bracing consists of sets of diagonal elements placed within certain bays and extending over the height of the structure. This system is designed to carry all the lateral loading. Note that at least two orthogonal bracing systems are needed to ensure stability under an arbitrary lateral loading. Braced frames are constructed using steel components.

Depending on the magnitude of the lateral loading, lateral stiffness systems may also be incorporated in rigid frames to carry a fraction of the lateral loading. For concrete rigid frames, the stiffening is achieved by incorporating shear walls located either within or on the exterior of the building and extending over the entire height. Figure 14.2b illustrates this scheme. These walls function as cantilever beams and provide additional lateral restraint. For steel rigid frames, the stiffening system may be either a concrete shear wall or a diagonal steel member scheme.

14.2 Treatment of Lateral Loading

Lateral loading may be due to either wind or earthquake acting on the building. These actions may occur in an arbitrary direction. For rectangular buildings, such as shown in Fig. 14.3, the directions are usually taken normal to the faces. One determines the component of the resultant force for each direction. Figure 14.4 illustrates this approach.

The resultant force is distributed to the individual floors, and then each floor load is distributed to the nodes on the floor. This process leads to a set of nodal forces acting on the individual frames. We express the force acting at floor j of frame i as

$$P_x |_{\text{frame } i \text{ floor } j} = f_{ij} R_x \tag{14.1}$$

How one establishes f_{ij} is discussed in Sect. 14.3.

Fig. 14.3 Rectangular building

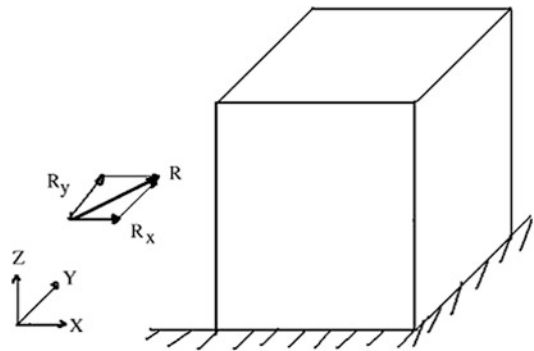
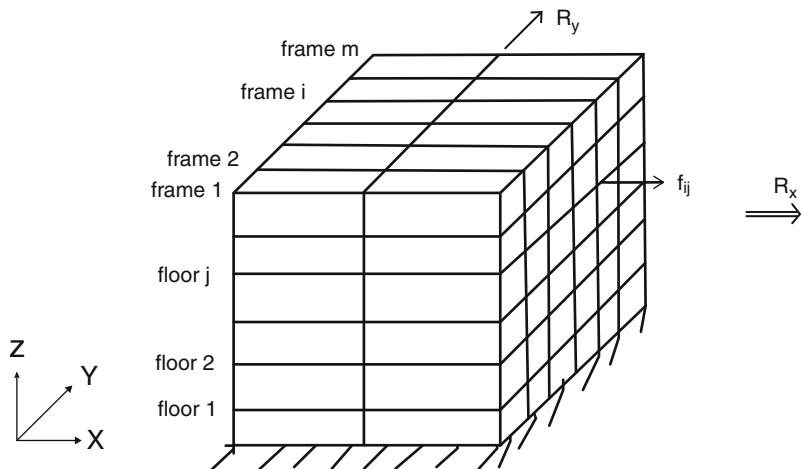


Fig. 14.4 Resultant force components



14.2.1 Wind Loading

We suppose the wind acts in the x direction, as shown in Fig. 14.5a. The normal pressure varies in the vertical direction according to a power law (e.g., $p \sim z^{1/7}$). We approximate the distribution with a set of step functions centered at the floor levels and generate the resultant force for each floor by integrating over the tributary area associated with the floor. This process is illustrated in Fig. 14.5b, c. The individual floor forces are given by

$$P_i = p(z_i) \left[\frac{z_{i+1} - z_i}{2} + \frac{z_i - z_{i-1}}{2} \right] B = p(z_i) \left[\frac{z_{i+1} - z_{i-1}}{2} \right] B \quad (14.2)$$

$i = 1, 2, \dots, n$

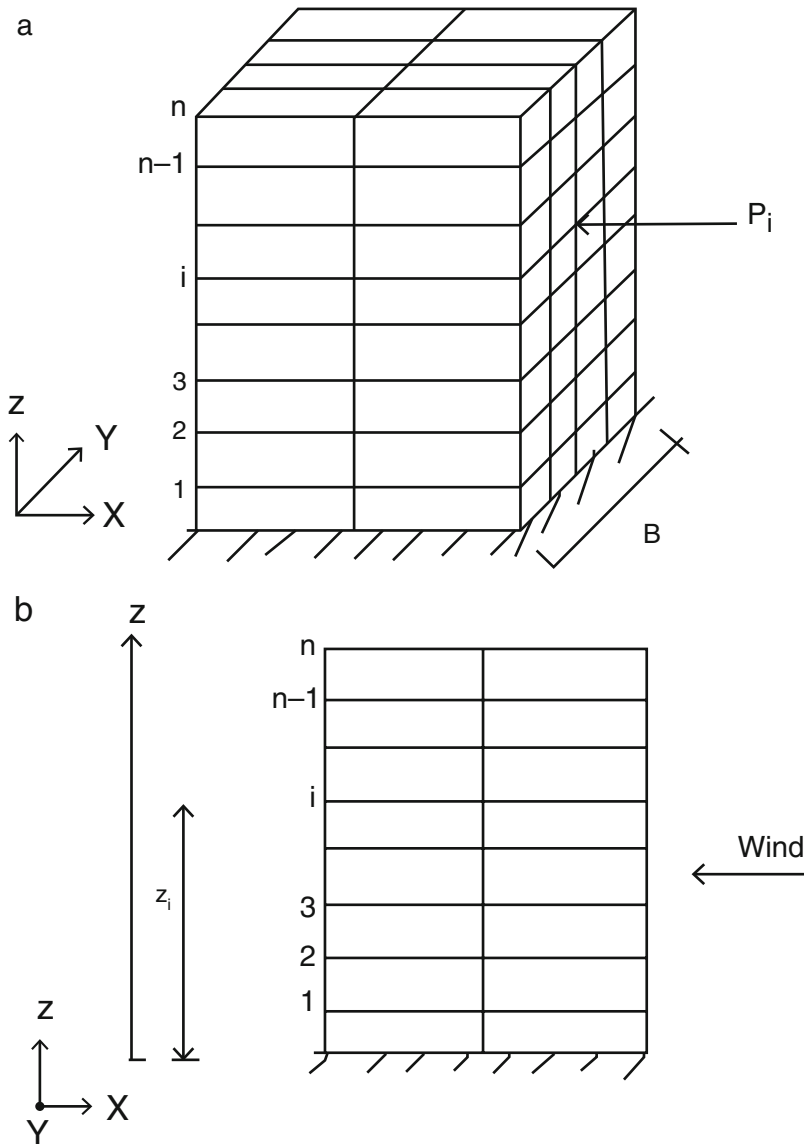


Fig. 14.5 Lateral floor forces due to wind pressure. (a) Wind in X direction. (b) Wind on $Y-Z$ face. (c) Floor loads due to wind load on $Y-Z$ face

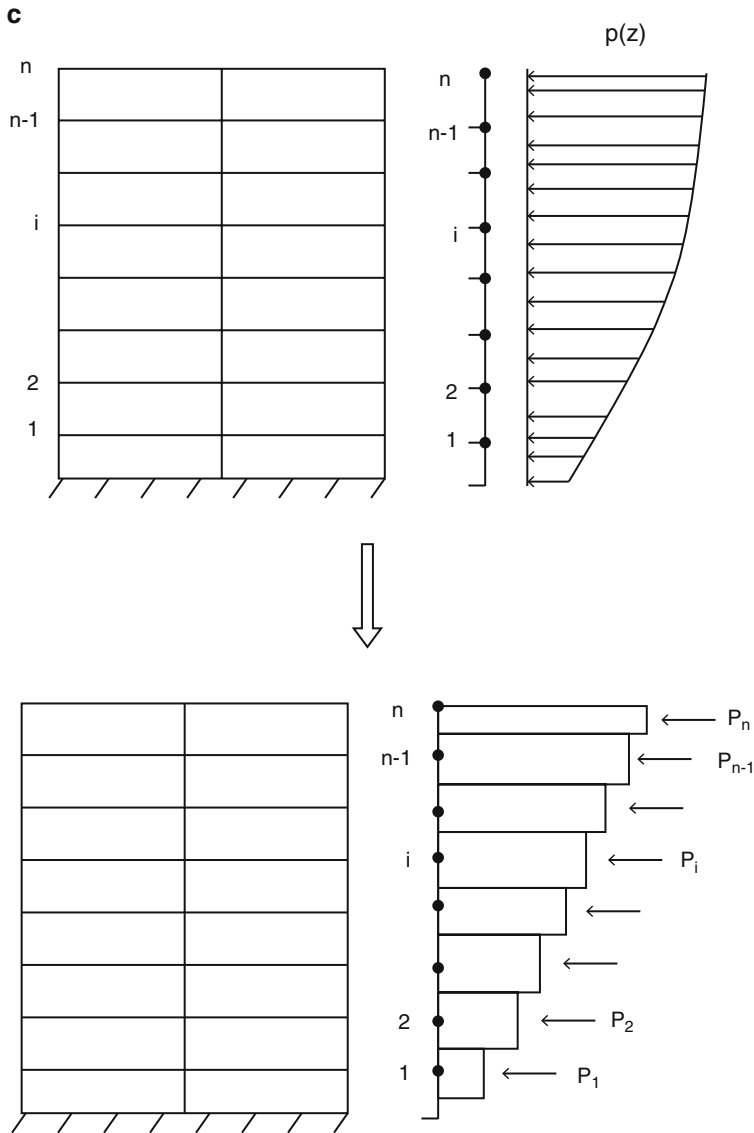


Fig. 14.5 (continued)

This computation is repeated for wind acting in the Y direction. It remains to distribute the loads acting at the floor levels of the façade to nodes of the individual plane frames. The final result is a set of lateral nodal loads for each plane frame.

The underlying strategy for this approach is based on analyzing plane frames vs. a three-dimensional system. This approach works when the structural geometry is composed of parallel plane frames which produce an orthogonal pattern of columns and beams. If the structural geometry is irregular, one has to analyze the full 3D structural system. In this case, one subdivides the façade area into panels centered on the structural nodes contained in the façade area and generates the force for structural node j with

$$P_j = p(z_j)A_j \tag{14.3}$$

where A_j is the tributary area for structural node j .

14.2.2 Earthquake Loading

Seismic loading is generated by an earthquake passing through the site. An earthquake is the result of slippage between adjacent tectonic plates which releases energy in the form of pressure waves that produce both horizontal and vertical ground motion. For civil structures, in seismically active regions, the horizontal motion produces the most critical lateral loading since the design of civil structures is usually controlled by vertical gravity loading. Data on earthquake ground motion is continuously collected and distributed by the US Geological Survey National Earthquake Information Center [1]. Figure 14.6 contains a typical plot of ground acceleration vs. time for the 1994 Northridge California earthquake. The information of interest is the peak ground acceleration, denoted as pga , with respect to g , the acceleration due to gravity. In this case, the pga is equal to $0.6g$. We point out that seismic loading is cyclic, of varying amplitude, and of short duration, on the order of 20–30 s for a typical earthquake.

Seismic loading is discussed in Sect. 1.3.6. We briefly review the important features of seismic loading here and then describe how one uses this information to generate the lateral loading for a building. The lateral forces produced by the horizontal ground motion require the incorporation of lateral bracing systems. Structures located in high seismic activity regions, such as Japan, Greece, and the Western parts of the USA, are required to meet more extreme performance standards, and the design is usually carried out by firms that specialize in seismic design.

Figure 14.7 illustrates how a typical low-rise rigid frame building responds to horizontal ground motion. The floor slabs act like rigid plates and displace horizontally with respect to the ground due to bending of the columns. Since there are no external loads applied to the floors, *the deformation has to be due to the inertia forces associated with the floor masses*. The magnitude of these forces depends on the floor masses and the floor accelerations.

The lateral displacement profile is assumed to be a linear function of Z as indicated in Fig. 14.8.

$$u_i(z) = u_{\text{ground}} + \frac{Z_i}{H} u(H)$$

Fig. 14.6 Ground acceleration time history—Northridge (1994) California Earthquake

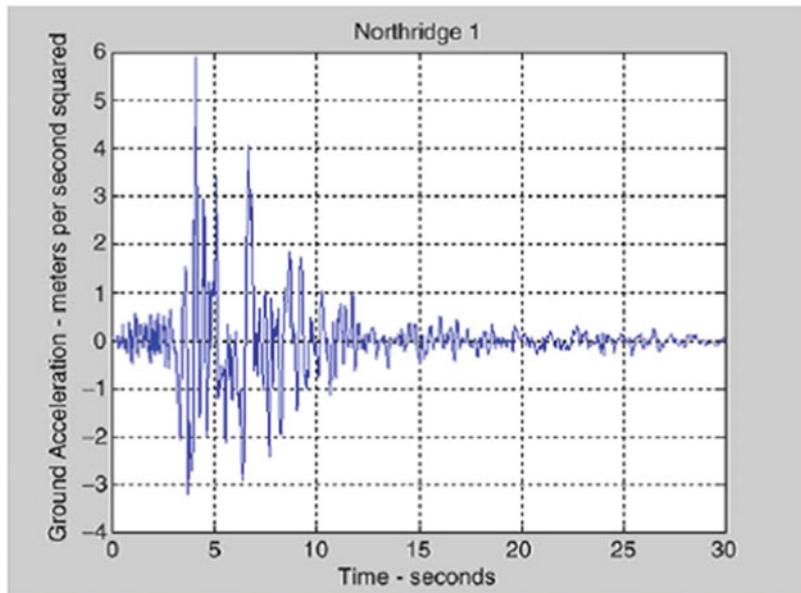


Fig. 14.7 Seismic response of low-rise frames with respect to ground

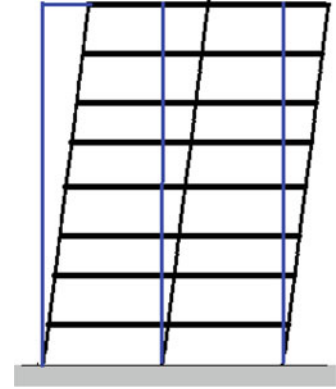
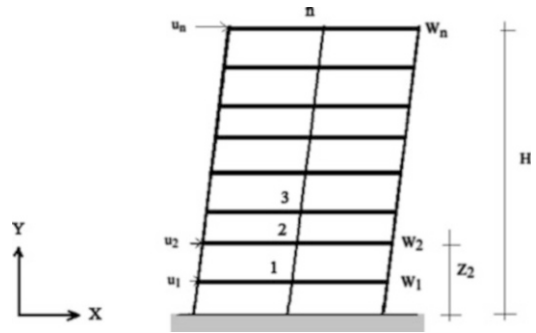


Fig. 14.8 Lateral displacement profile with respect to ground



where $u(H)$ is the relative displacement of the top floor with respect to the ground, and Z_i is the vertical coordinate of floor i . This assumption leads to the following expression for the total acceleration of a typical floor:

$$a|_{\text{floor } i} = a_g(t) + \frac{Z_i}{H} \frac{d^2 u(H)}{dt^2} \tag{14.4}$$

where $a_g(t)$ is the ground acceleration time history. Applying Newton’s law, the force required to accelerate floor i , assuming it moves as a rigid body and the lateral displacement profile is linear, is

$$P|_{\text{floor } i} = \frac{W_i}{g} \left\{ a_g(t) + \frac{Z_i}{H} \frac{d^2 u(H)}{dt^2} \right\} \tag{14.5}$$

This force is provided by the shear forces in the columns adjacent to the floor.

Given an earthquake ground motion time history, one applies this floor loading to a structure and determines the structural response. The solution for the acceleration at the top floor is expressed as [2]:

$$\frac{d^2 u(H)}{dt^2} = -\Gamma(a_g(t) + \theta(t)) \tag{14.6}$$

where $\theta(t)$ depends on the earthquake ground motion and the structural period; Γ is a dimensionless parameter that depends on the distribution of floor masses,

$$\Gamma = \frac{\sum_{i=1}^N m_i \frac{Z_i}{H}}{\sum_{i=1}^N m_i \left(\frac{Z_i}{H}\right)^2} = \frac{H \sum_{i=1}^N W_i Z_i}{\sum_{i=1}^N W_i (Z_i)^2} \quad (14.7)$$

Substituting for the top floor acceleration, the inertia force expands to

$$P|_{\text{floor } i} = \frac{W_i}{g} a_g(t) \left\{ 1 - \Gamma \frac{Z_i}{H} \right\} + \frac{W_i}{g} \left\{ -\Gamma \frac{Z_i}{H} \theta(t) \right\} \quad (14.8)$$

The peak values of $a_g(t)$ and $\theta(t)$ do not generally occur at the same time. Also the magnitude of Γ is of order one and the maximum value of $\theta(t)$ is usually larger than $a_{g_{\max}}$. Therefore, the *peak force* at floor i is approximated as:

$$P|_{\text{floor } i} \approx \frac{Z_i W_i}{H} \left\{ \Gamma \frac{S_a}{g} \right\} \quad (14.9)$$

where S_a is defined as the maximum absolute value of $\theta(t)$. In the seismic literature, S_a is called the spectral acceleration. It is *the maximum acceleration that an equivalent single degree of freedom system experiences when subjected to the earthquake*. Summing up the floor forces leads to the resultant force which is also equal to the maximum shear force at the base.

$$V|_{\text{base}} = \sum P|_{\text{floor } i} \approx \frac{\left(\sum_{i=1}^N W_i Z_i\right)^2 S_a}{\sum_{i=1}^N W_i (Z_i)^2 g} \quad (14.10)$$

Finally, we express the force for floor i in terms of $V|_{\text{base}}$.

$$P|_{\text{floor } i} = \left(\frac{W_i Z_i}{\sum W_i Z_i} \right) V|_{\text{base}} \quad (14.11)$$

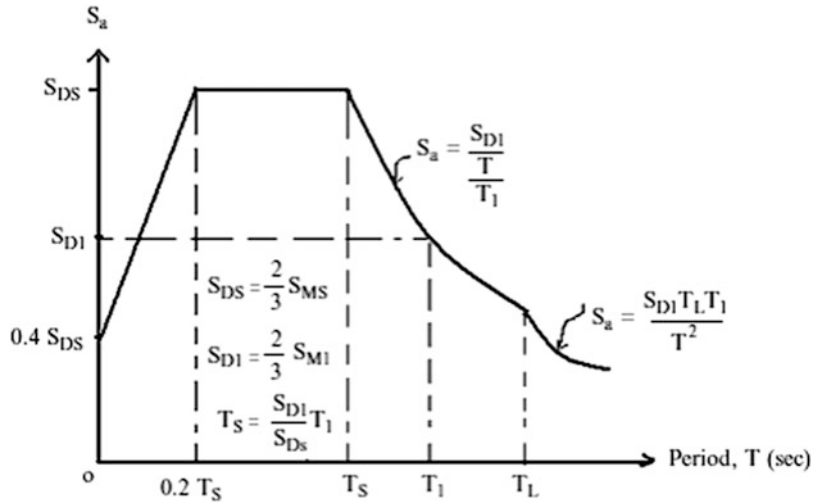
The spectral acceleration measure, S_a , depends on the ground motion time history $a_g(t)$ and the period of the structure, T .

A simple approximation for T for a low-rise building is

$$T \approx \frac{N}{10} \text{ s} \quad (14.12)$$

where N is the number of stories. Values of S_a vs. the structural period, T , have been compiled by various agencies, such as the US Geological Survey's National Earthquake Information Center [1] for a range of earthquakes, and used to construct design plots such as illustrated below in Fig. 14.9. One estimates T and determines S_a with this plot. The limiting values for the plot, such as S_{DS} and S_{D1} , depend on S_{MS} and S_{M1} which are defined for a particular site and seismic design code [3]. Values of S_{MS} , S_{M1} , and T_L are listed on the USGS Web site, usgs.gov/hazards: S_{M1} is usually taken as the spectral acceleration for 5 % damping and 1 s period (i.e., $T_1 = 1$ s); S_{MS} is the spectral acceleration for 5 % damping and 0.2 s period and T_L is the long transition period. The worst case scenario is for the structural period to be between $0.2T_S$ and T_S . When $T \gg T_S$, the seismic load is significantly less than the load corresponding to the region $0.2T_S < T < T_S$.

Fig. 14.9 Peak acceleration vs. structural period [3]



Example 14.1

Given: The three-story building shown in Figs. E14.1a and E14.1b. Assume the building is subjected to an earthquake in the North–South direction. Take the spectral acceleration as $S_a = 0.4 g$

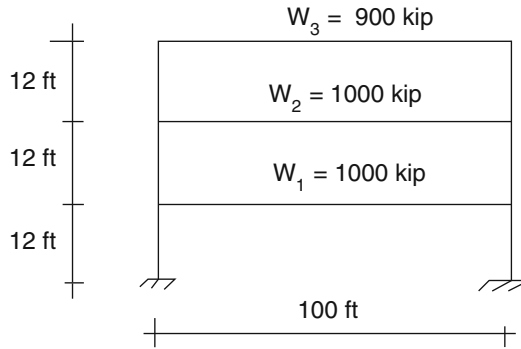


Fig. E14.1a Elevation N-S

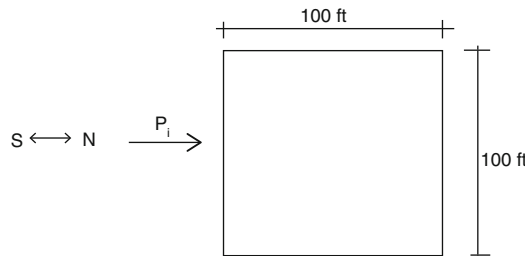


Fig. E14.1b Typical floor plan

Determine: The base shear and earthquake forces on the individual floors.

Solution: We use (14.10). The base shear is given by

$$V|_{\text{base}} = \frac{\left(\sum_{i=1}^3 Z_i W_i\right)^2 S_a}{\sum_{i=1}^3 W_i (Z_i)^2 g} = \frac{\{1000(12) + 1000(24) + 900(36)\}^2 S_a}{\{1000(12)^2 + 1000(24)^2 + 900(36)^2\} g} = 3420(0.4) = 1368 \text{ kip}$$

Then, applying (14.11), we obtain the individual floor loads.

$$\sum_{i=1}^3 W_i Z_i = \{ (12(1000) + 24(1000) + 36(900)) \} = 68,400$$

$$P_1 = \frac{12(1000)}{68,400} V|_{\text{base}} = 0.175(1368) = 239.4 \text{ kip}$$

$$P_2 = \frac{24(1000)}{68,400} V|_{\text{base}} = 0.351(1368) = 480.2 \text{ kip}$$

$$P_3 = \frac{36(900)}{68,400} V|_{\text{base}} = 0.474(1368) = 648.4 \text{ kip}$$



Example 14.2

Given: The three-story building shown in Figs. E14.2a and E14.2b. The floor weights are indicated. There is also an additional weight located on the top floor.

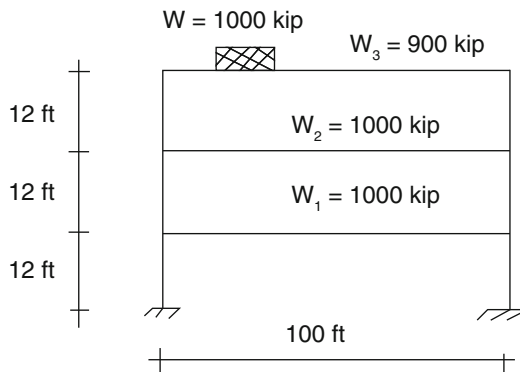


Fig. E14.2a Elevation

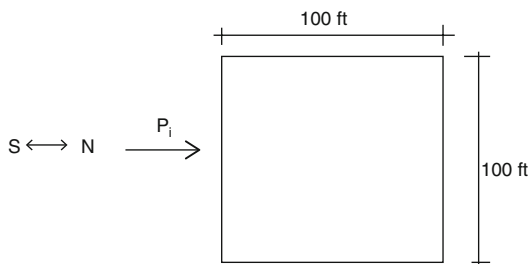


Fig. E14.2b Typical floor plan

Determine: The earthquake floor forces for a North–South earthquake of intensity $S_a = 0.4g$.

Solution: The computations are organized in the following table.

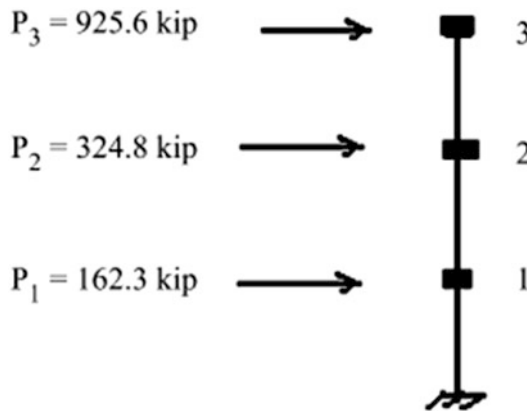
Floor	Z_i	W_i	$W_i Z_i (10^3)$	$W_i (Z_i)^2 (10^3)$
1	12	1000	12	144
2	24	1000	24	596
3	36	900	32.4	1050
Roof	36	1000	36	1296
			104.4×10^3	3086×10^3

$$V|_{\text{base}} = (0.4) \frac{(104.4(1000))^2}{3086(1000)} = 1412.7 \text{ kip}$$

$$P_1 = \frac{12,000}{104.4(1000)} (1412.7) = 162.3 \text{ kip}$$

$$P_2 = \frac{24(1000)}{104.4(1000)} (1412.7) = 324.8 \text{ kip}$$

$$P_3 = \frac{(32.4 + 36)(1000)}{104.4(1000)} (1412.7) = 925.6 \text{ kip}$$



Note that the shear in the top story is increased considerably due to the additional mass on the third floor.

14.3 Building Response Under Lateral Loads

Up to this point, we have discussed how one generates the lateral loads acting at the floor levels. These loads are resisted by the frames which support the floors. In this section, we develop a methodology for distributing a floor load to the frames which support the floor.

We model the building as a set of *rigid floors* supported by columns and braces between the floors. When subjected to horizontal loading, the floor plates displace horizontally, resulting in bending of the columns and shearing deformation in the braces. The horizontal load is resisted by the shear forces developed in the columns and braces. We know from the examples studied in Chaps. 9 and 10 that stiffness attracts force. Therefore, one should expect that the distribution of floor load to the supporting elements, i.e., the columns and braces, will depend on the relative stiffness of these elements.

Fig. 14.10 (a) One-story braced frame. (b) Shear spring model for brace

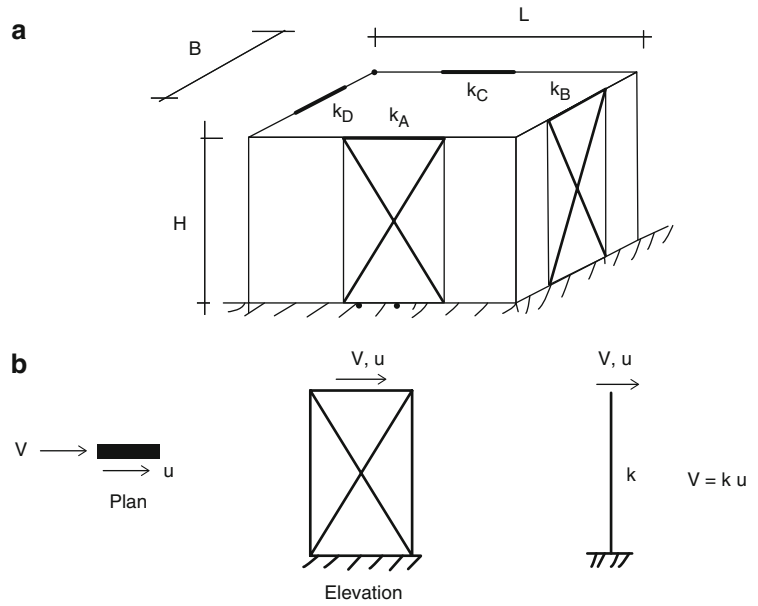
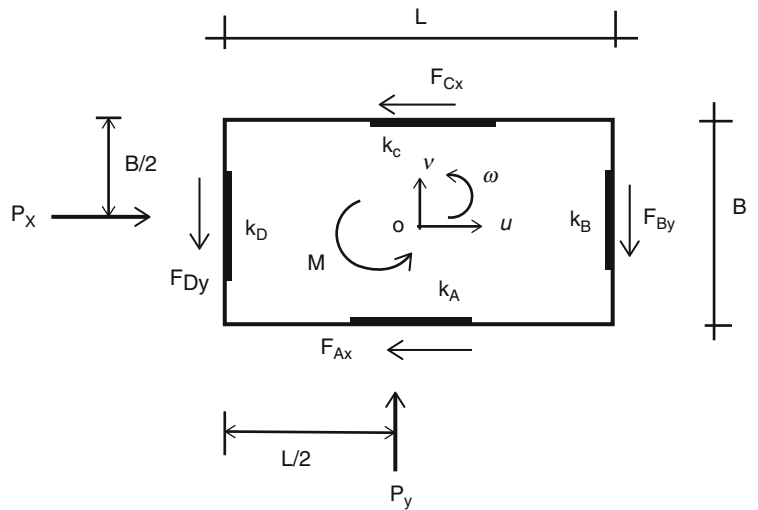


Fig. 14.11 Plan view



14.3.1 Center of Twist: One-Story Frame

We consider first the one-story braced frame structure shown in Fig. 14.10a. The braces located at the midpoints of the sides provide the resistance to horizontal load. We represent the braces as simple shear springs. Figure 14.10b illustrates this modeling strategy. Each brace provides a force which acts in the plane of the wall that contains the brace.

We locate the origin of the X - Y coordinate system at the geometric center of the floor and assume the floor is subjected to external forces, P_x , P_y , M . Under the action of these forces, the floor will experience translation (u , v) and rotation ω about the origin. These displacements produce shear forces in the springs which oppose the motion. The free body diagram for the floor is shown in Fig. 14.11.

Noting the free body diagram shown, the equilibrium equations expand to

$$\begin{aligned}
 + \rightarrow \sum F_x &= P_x - F_{Ax} - F_{Cx} = 0 \\
 + \uparrow \sum F_y &= P_y - F_{By} - F_{Dy} = 0 \\
 \sum M_0 &= M + (F_{Cx} - F_{Ax})\frac{B}{2} + (F_{Dy} - F_{By})\frac{L}{2} = 0
 \end{aligned}
 \tag{14.13}$$

Assuming the floor plate is rigid; the shear forces are related to the displacements by

$$\begin{aligned}
 F_{Ax} &= k_A \left(u + \frac{B}{2}\omega \right) \\
 F_{Cx} &= k_C \left(u - \frac{B}{2}\omega \right) \\
 F_{By} &= k_B \left(v + \frac{L}{2}\omega \right) \\
 F_{Dy} &= k_D \left(v - \frac{L}{2}\omega \right)
 \end{aligned}
 \tag{14.14}$$

Substituting for the forces in (14.13) leads to

$$\begin{aligned}
 P_x &= u(k_A + k_C) + \frac{B}{2}(k_A - k_C)\omega \\
 P_y &= v(k_B + k_D) + \frac{L}{2}(k_B - k_D)\omega \\
 M &= \frac{B}{2}(k_A - k_C)u + \frac{L}{2}(k_B - k_D)v + \left\{ \frac{B^2}{4}(k_A + k_C) + \frac{L^2}{4}(k_B + k_D) \right\} \omega
 \end{aligned}
 \tag{14.15}$$

We see that the response depends on the relative stiffness of the braces. If $k_A \neq k_C$ or $k_B \neq k_D$, the floor will experience rotation when only P_x or P_y is applied at the geometric center. Given the stiffness of the braces, one solves (14.15) for u, v, ω and evaluates the braces forces using (14.14).

Example 14.3

Given: The floor plan, dimensions and layout of the braces, and the brace stiffnesses shown in Fig. E14.3a.

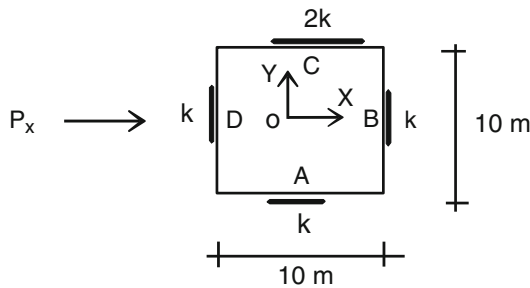


Fig. E14.3a Plan view

Determine: The response due to P_x .

Solution: We note that the braces at A, B, D have equal stiffnesses, and the brace at C is twice as stiff as the others. For convenience, we show these values as just k and $2k$. We set $P_y = M = 0$ in (14.15).

$$\begin{aligned}
 P_x &= (3k)u + 5(-k)\omega = P \\
 P_y &= (2k)v = 0 \\
 M &= 5(-k)u + \left(\frac{500}{4}k\right)\omega = 0
 \end{aligned}$$

Solving these equations, we obtain

$$\begin{aligned}
 u &= \frac{25P}{70k} \\
 v &= 0 \\
 \omega &= \frac{P}{70k}
 \end{aligned}$$

Finally, the brace forces are

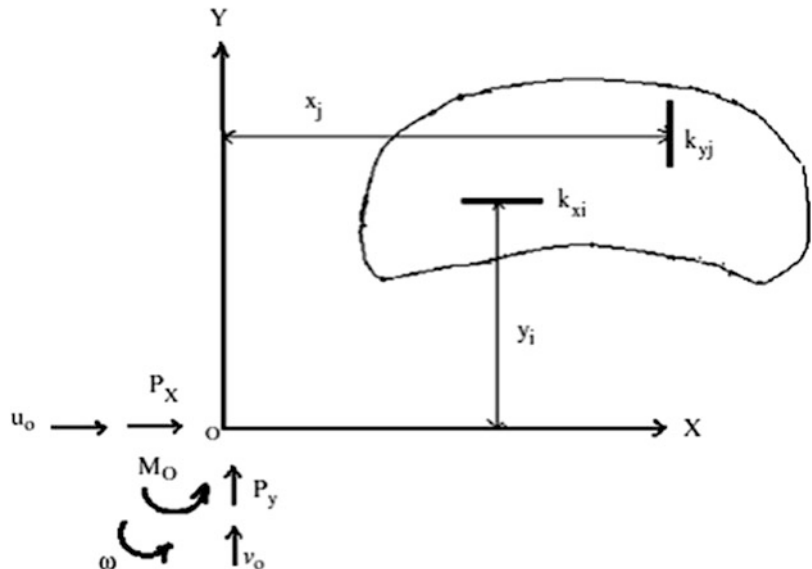
$$\begin{aligned}
 F_{Ax} &= k_A \left(u + \frac{B}{2}\omega\right) = P \left(\frac{25}{70} + \frac{5}{70}\right) = \frac{3}{7}P \\
 F_{Cx} &= k_C \left(u - \frac{B}{2}\omega\right) = 2P \left(\frac{25}{70} - \frac{5}{70}\right) = \frac{4}{7}P \\
 F_{By} &= k_B \left(v + \frac{L}{2}\omega\right) = P \left(\frac{5}{70}\right) = \frac{1}{14}P \\
 F_{Dy} &= k_D \left(v - \frac{L}{2}\omega\right) = P \left(-\frac{5}{70}\right) = -\frac{1}{14}P
 \end{aligned}$$

To avoid rotation, which is undesirable, one needs to modify either the stiffness at A or C. Taking $k_A = k_C = k$, the response is

$$\begin{aligned}
 u &= \frac{P}{2k} \\
 v &= \omega = 0 \\
 F_{Ax} &= F_{Cx} = \frac{P}{2}
 \end{aligned}$$

The formulation described above can be generalized to deal with an arbitrary number of braces or shear walls oriented in either the X or Y direction. We shift to the notation shown in Fig. 14.12 to

Fig. 14.12 Notation



identify the various braces. Each brace is characterized by a stiffness magnitude (k) and the perpendicular distance from the tangent to the origin.

Assuming the floor is rigid, the tangential motion for the X oriented braces due to a rigid body motion of the origin o is

$$+ \rightarrow u_i = u_o - y_i \omega \quad (14.16)$$

Similarly, the Y motion for brace j is given by

$$+ \uparrow v_j = v_o + x_j \omega \quad (14.17)$$

These motions produce shear forces which act to *oppose* the motion of the floor. The individual forces are

$$\begin{aligned} + \rightarrow F_{xi} &= -k_{xi}u_i = -k_{xi}u_o + k_{xi}y_i\omega \\ + \uparrow F_{yj} &= -k_{yj}v_j = -k_{yj}v_o - k_{yj}x_j\omega \end{aligned} \quad (14.18)$$

Summing forces and moments with respect to the origin leads to the equilibrium equations for the floor

$$\begin{aligned} + \rightarrow P_x - u_o \left(\sum k_{xi} \right) + \omega \left(\sum y_i k_{xi} \right) &= 0 \\ + \uparrow P_y - v_o \left(\sum k_{yj} \right) - \omega \left(\sum x_j k_{yj} \right) &= 0 \\ M_0 + u_o \left(\sum y_i k_{xi} \right) - v_o \left(\sum x_j k_{yj} \right) - \omega \left\{ \sum y_i^2 k_{xi} + \sum x_j^2 k_{yj} \right\} &= 0 \end{aligned} \quad (14.19)$$

where P_x , P_y , and M_0 are the external loads on the floor.

We define the following terms:

$$\begin{aligned} \sum k_{xi} &= K_{xx} \\ \sum k_{yj} &= K_{yy} \\ \sum y_i k_{xi} &= K_{xz} \\ \sum x_j k_{yj} &= K_{yz} \\ \sum y_i^2 k_{xi} + \sum x_j^2 k_{yj} &= K_o \end{aligned} \quad (14.20)$$

With this notation, (14.19) takes the following form:

$$\begin{aligned} P_x &= K_{xx}u_o - K_{xz}\omega \\ P_y &= K_{yy}v_o + K_{yz}\omega \\ M_0 &= -K_{xz}u_o + K_{yz}v_o + K_o\omega \end{aligned} \quad (14.21)$$

Equation (14.21) applies for an arbitrary choice of origin. Note that forces applied at the origin will produce rotation when either $K_{xz} \neq 0$ or $K_{yz} \neq 0$. If the stiffness distribution is symmetrical, these terms vanish. Rotation of the floor is a torsional mode of response, which introduces an undesirable anti-symmetric deformation in the perimeter facades. Therefore, one approach is to always choose a symmetrical stiffness layout. Another approach is to shift the origin to some other point in the floor. Obviously, the most desirable point corresponds to $K_{xz} = K_{yz} = 0$.

Consider the floor geometry shown in Fig. 14.13. Point o denotes the initial origin and C some arbitrary point in the floor. We locate a new set of axes at C and express the forces in terms of the coordinates with respect to C .



Fig. 14.13 Floor geometry

$$\begin{aligned} u_i &= u_c - y'_i \omega \\ v_i &= v_c + x'_i \omega \end{aligned} \tag{14.22}$$

$$\begin{aligned} F_{xi} &= -k_{xi} u_c + k_{xi} y'_i \omega \\ F_{yi} &= -k_{yi} v_c - k_{yi} x'_i \omega \end{aligned} \tag{14.23}$$

The equilibrium equations referred to point C have the following form:

$$\begin{aligned} P_{xc} - u_c \left(\sum k_{xi} \right) + \omega \left(\sum y'_i k_{xi} \right) &= 0 \\ P_{yc} - v_c \left(\sum k_{yj} \right) - \omega \left(\sum x'_j k_{yj} \right) &= 0 \\ M_c + u_c \left(\sum y'_i k_{xi} \right) - v_c \left(\sum x'_j k_{yj} \right) + \omega \left(-\sum y_i'^2 k_{xi} - \sum x_j'^2 k_{yj} \right) &= 0 \end{aligned} \tag{14.24}$$

We choose point C such that

$$\sum y'_i k_{xi} = \sum x'_j k_{yj} = 0 \tag{14.25}$$

These conditions define the coordinates of point C. Substituting for x' and y' using

$$\begin{aligned} x' &= -x_c + x \\ y' &= -y_c + y \end{aligned}$$

leads to

$$\begin{aligned} x_c &= \frac{\sum x_j k_{yj}}{\sum k_{yj}} \\ y_c &= \frac{\sum y_i k_{xi}}{\sum k_{xi}} \end{aligned} \tag{14.26}$$

The equilibrium equations referred to these new axes simplify to

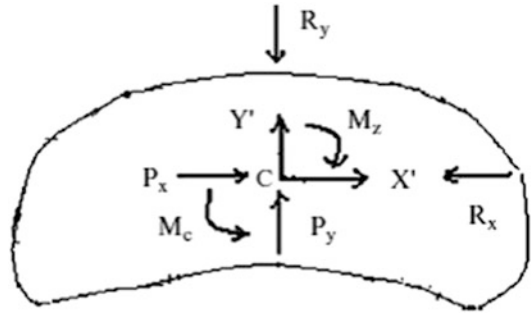
$$\begin{aligned} P_x &= K_{xx} u_C = R_x \\ P_y &= K_{yy} v_C = R_y \\ M_C &= K_C \omega_C = M_z \end{aligned} \tag{14.27}$$

where

$$K_C = \sum y_i'^2 k_{xi} + \sum x_j'^2 k_{yj}$$

The external and internal forces are shown in Fig. 14.14.

Fig. 14.14 External and internal forces



Point C is called the “center of twist.” Figure 14.14 shows that the resultant of the “resisting” forces acts at the center of twist. External forces applied at the center of twist produce only translation; an external moment applied to the floor produces twist about the center of twist. We point out that the coordinates of the center of twist depend on the stiffness of the components located in the story. The location of the center of twist changes when either the position or magnitude of the stiffness components is changed.

Example 14.4

Given: The floor plan shown in Fig. E14.4a. The two shear walls are orthogonal and are located on the X and Y axes.

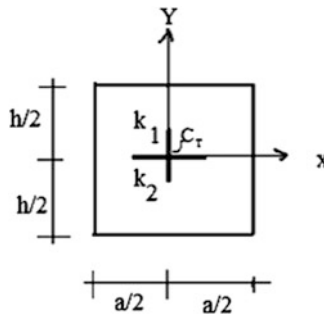


Fig. E14.4a

Determine: The center of twist.

Solution: The center of stiffness lies on an axis of symmetry. In this case, there are two axes of symmetry and therefore the center of twist is at the origin.

Example 14.5

Given: The stiffness distribution shown in Fig. E14.5a.

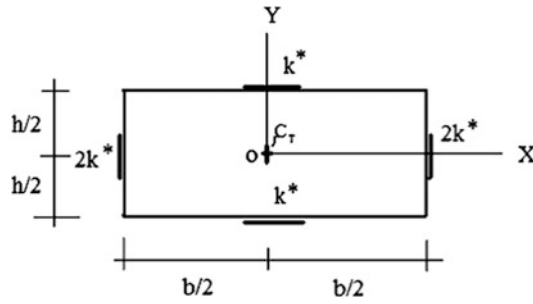


Fig. E14.5a

Determine: The center of twist.

Solution: The stiffness distributions are symmetrical with respect to the X and Y axes. Therefore,

$$X_{CT} = Y_{CT} = 0.$$

Example 14.6

Given: The stiffness distribution shown in Fig. E14.6a.

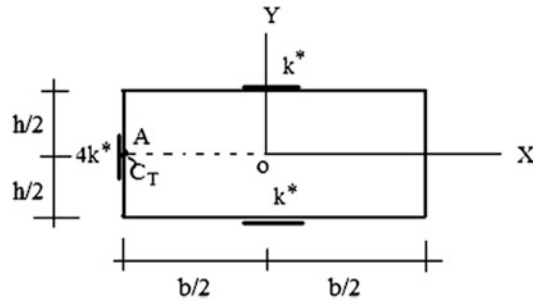


Fig. E14.6a

Determine: The center of twist.

Solution: The center of twist (C_T) lies on the X -axis because the stiffness is symmetrical with respect to the X -axis. Summing moments about the origin leads to

$$x_{CT} = \frac{\sum x_i k_{yi}}{\sum k_{yi}} = \frac{4k^*(-(b/2))}{4k^*} = -\frac{b}{2}$$

Example 14.7

Given: The stiffness distribution and loading shown in Fig. E14.7a.

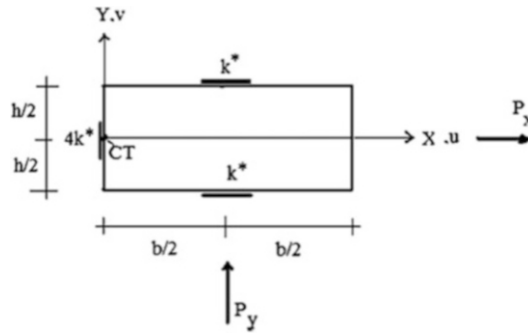


Fig. E14.7a

Determine: The rigid body motion.

Solution: The floor will experience rotation as well as translation since there is a net moment with respect to the center of twist. We determine the motion measures using (14.27). The stiffness measures are

$$K_{xx} = \sum k_{xi} = 2k^*$$

$$K_{yy} = \sum k_{yj} = 4k^*$$

$$K_C = \sum y_i^2 k_{xi} + \sum x_j^2 k_{yj} = 2 \left\{ \left(\frac{b}{2}\right)^2 k^* \right\} = \frac{b^2}{2} k^*$$

Then,

$$u = \frac{P_x}{K_{xx}} = \frac{P_x}{2k^*}$$

$$v = \frac{P_y}{K_{yy}} = \frac{P_y}{4k^*}$$

$$\omega = \frac{P_y(\frac{b}{2})}{K_C} = P_y \frac{\frac{b}{2}}{\frac{b^2}{2} k^*} = \frac{P_y}{k^*} \frac{b}{b^2}$$

The deformed configuration of the floor is shown in Fig. E14.7b.

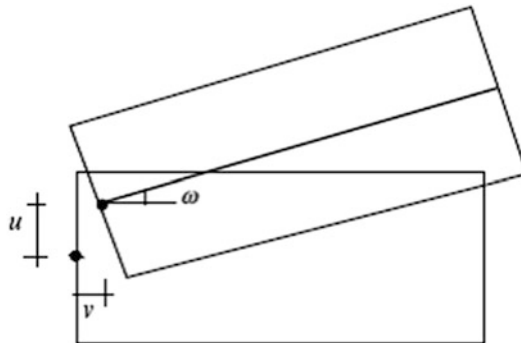


Fig. E14.7b

Example 14.8

Given: The stiffness distribution shown in Fig. E14.8a.

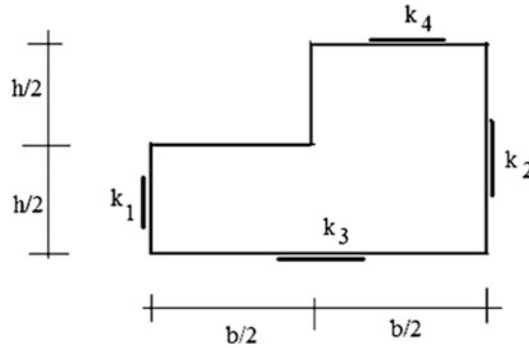


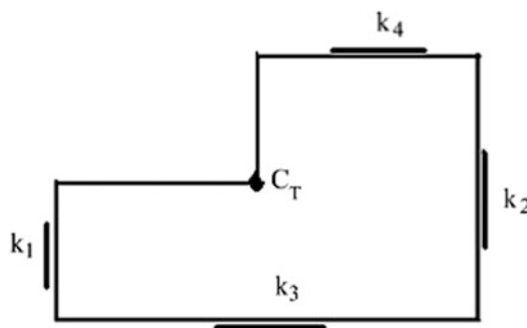
Fig. E14.8a

Determine: The center of twist for the following combination of stiffness factors:

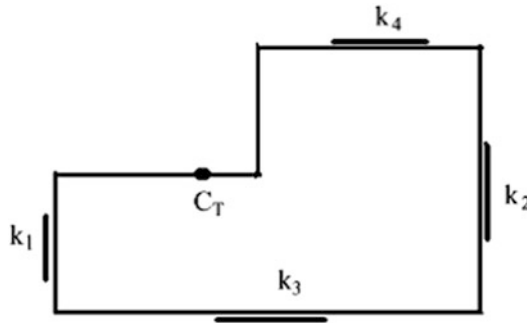
- (a) $k_1 = k_2 = k_3 = k_4$
- (b) $k_4 = k_3$ $k_1 > k_2$
- (c) $k_4 > k_3$ $k_1 = k_2$
- (d) $k_4 > k_3$ $k_1 > k_2$

Solution: The problem can be viewed as being equivalent to finding the centroid of a set of areas, with area replaced by stiffness. One can use qualitative reasoning to estimate the location of the center of twist.

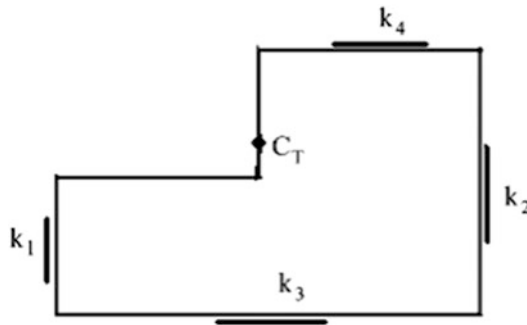
Case (a) $k_1 = k_2 = k_3 = k_4$



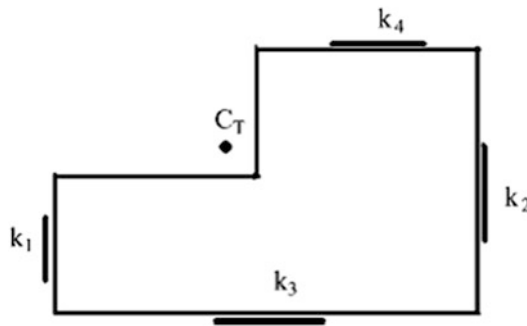
Case (b) $k_4 = k_3$ $k_1 > k_2$



Case (c) $k_4 > k_3$ $k_1 = k_2$



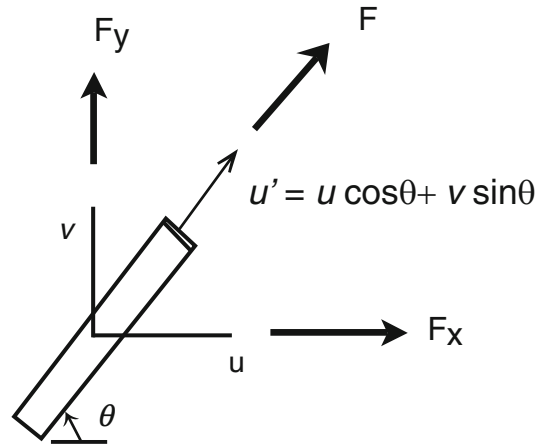
Case (d) $k_4 > k_3$ $k_1 > k_2$



We consider next the single inclined brace shown in Fig. 14.15. Introducing displacements u and v produces a longitudinal force F equal to ku' . Projecting F on the x and y axes leads to

$$\begin{aligned} F_x &= F \cos \theta = k \left[u(\cos \theta)^2 + v \cos \theta \sin \theta \right] \\ F_y &= F \sin \theta = k \left[u \sin \theta \cos \theta + v(\sin \theta)^2 \right] \end{aligned} \tag{14.28}$$

Summing these forces over the number of braces, the resultants are given by

Fig. 14.15 Inclined brace

$$\begin{aligned} R_x &= \sum F_x = u \sum k_i \cos^2 \theta + v \sum k_i \cos \theta \sin \theta \\ R_y &= \sum F_y = u \sum k_i \sin \theta \cos \theta + v \sum k_i \sin^2 \theta \end{aligned} \quad (14.29)$$

We write these equations as

$$\begin{aligned} R_x &= uK_{cc} + vK_{cs} \\ R_y &= uK_{cs} + vK_{ss} \end{aligned} \quad (14.30)$$

where

$$\begin{aligned} K_{cc} &= \sum k_i \cos^2 \theta \\ K_{cs} &= \sum k_i \cos \theta \sin \theta \\ K_{ss} &= \sum k_i \sin^2 \theta \end{aligned}$$

Note that when $\theta = 0^\circ$ or 90° , these expressions reduce to (14.27).

The line of action is determined by summing moments about O . Working first with the X direction (u) and then the Y direction (v) leads to the following pair of equations for x^* and y^* , the coordinates of the center of twist.

$$\begin{aligned} y^* K_{cc} - x^* K_{cs} &= \sum y_i k_i \cos^2 \theta - \sum x_i k_i \sin \theta \cos \theta \\ y^* K_{cs} - x^* K_{ss} &= \sum y_i k_i \sin \theta \cos \theta - \sum x_i k_i \sin^2 \theta \end{aligned} \quad (14.31)$$

When the stiffness elements are parallel to either x or y , these equations reduce to

$$\begin{aligned} K_{cc} &= \sum k_x & K_{cs} &= 0 & K_{ss} &= \sum k_y \\ y^* &= \frac{\sum y k_x}{\sum k_x} & x^* &= \frac{\sum x k_y}{\sum k_y} \end{aligned}$$

Example 14.9

Given: The stiffness distribution shown in Fig. E14.9a. Two of the braces are inclined with respect to the x -axis.

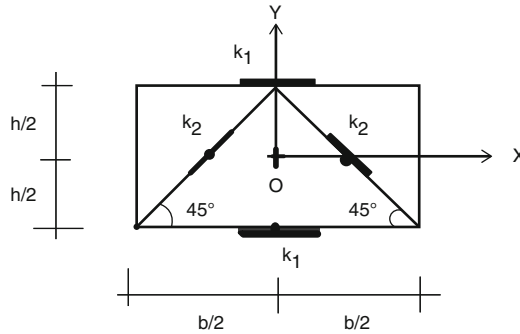


Fig. E14.9a

Determine: The center of twist.

Solution: Evaluating (14.31) leads to

$$K_{cc} = \sum k_i \cos^2 \theta = 2k_1 + 2\left(\frac{1}{2}k_2\right) = 2k_1 + k_2$$

$$K_{cs} = \sum k_i \cos \theta \sin \theta = \left(\frac{1}{2}k_2\right) + \left(-\frac{1}{2}k_2\right) = 0$$

$$K_{ss} = \sum k_i \sin^2 \theta = 2\left(\frac{1}{2}k_2\right) = k_2$$

$$\sum y_i k_i \cos^2 \theta = 0$$

$$\sum x_i k_i \sin^2 \theta = 0$$

$$\sum x_i k_i \sin \theta \cos \theta = k_2 \frac{b}{4} \sum (-1)\frac{1}{2} + (+1)\left(-\frac{1}{2}\right) = -k_2 \frac{b}{4}$$

$$\sum y_i k_i \sin \theta \cos \theta = 0$$

Then,

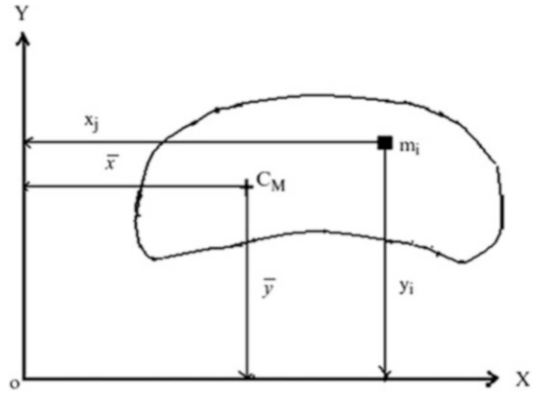
$$y^* = \frac{\frac{bk_2}{4}}{2k_1 + k_2} = \frac{b}{4} \left(\frac{k_2}{k_2 + 2k_1} \right)$$

$$x^* = 0$$

14.3.2 Center of Mass: One-Story Frame

The center of twist for a one-story frame is a property of the stiffness components located in the story below the floor. It defines the point of application of the inter-story resistance forces acting on the floor. These forces depend on the translation and rotation of the floor produced by the applied loading, i.e., they are due to inter-story deformation.

Fig. 14.16 Plan view of floor



When the loading is dynamic, additional inertia forces are generated due to the acceleration of the masses located on the floor. In order to study the equilibrium of the floor, we need to establish the magnitude and location of the resultant of these inertia forces. In what follows, we describe the procedure for locating this resultant.

Figure 14.16 shows a typical plan view of a floor. We locate the origin at some arbitrary point in the floor, and suppose that there are masses located at discrete points in the floor. The center of mass is a particular point in the floor defined by the coordinates \bar{x} and \bar{y} , where

$$\begin{aligned} \bar{x} &= \frac{\sum x_i m_i}{\sum m_i} \\ \bar{y} &= \frac{\sum y_i m_i}{\sum m_i} \end{aligned} \tag{14.32}$$

Example 14.10

Given: The floor mass layout shown in Fig. E14.10a.

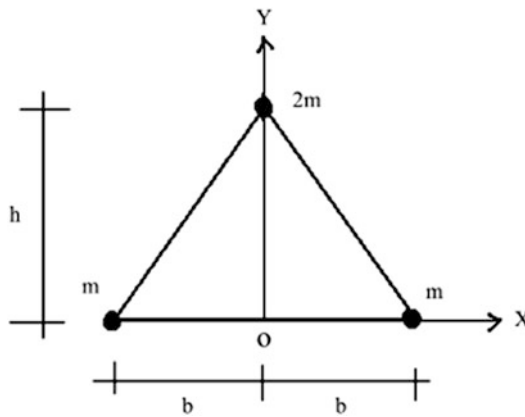


Fig. E14.10a

Determine: The center of mass.

Solution: The center of mass is on the y -axis. In general, if the mass distribution is symmetrical, the center of mass lies on the axis of symmetry. We determine the y coordinate by summing moments about the x -axis (Fig. E14.10b).

$$\bar{y} = \frac{\sum y_i m_i}{\sum m_i} = \frac{(2m)h}{4m} = \frac{h}{2}$$

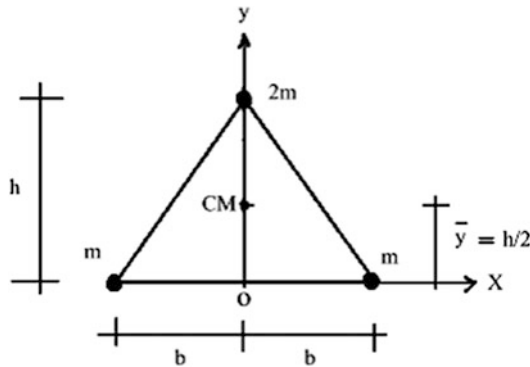


Fig. E14.10b

Example 14.11

Given: The floor mass layout shown in Fig. E14.11a.

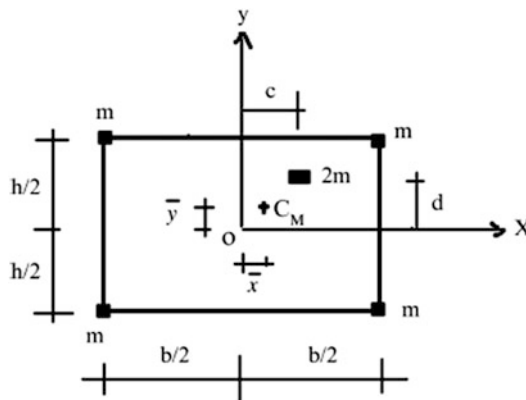


Fig. E14.11a

Determine: The center of mass.

Solution: Summing the moments leads to

$$\begin{aligned}\sum m_i &= 6m \\ \bar{x} &= \frac{2mc + 2m(b/2) + 2m(-b/2)}{6m} = \frac{c}{3} \\ \bar{y} &= \frac{2md + 2m(h/2) + 2m(-h/2)}{6m} = \frac{d}{3}\end{aligned}$$

Example 14.12

Given: The floor mass layout shown in Fig. E14.12a.

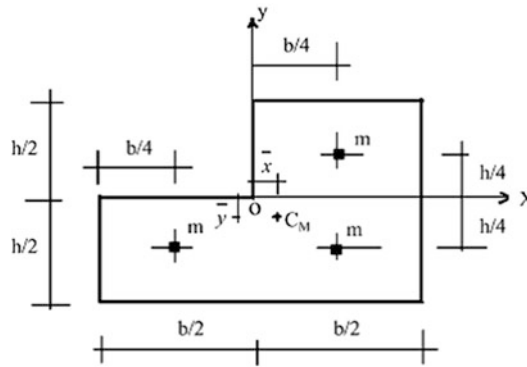


Fig. E14.12a

Determine: The center of mass.

Solution: We sum moments about the \$x\$ and \$y\$ axes and obtain

$$\begin{aligned}\bar{x} &= \frac{m(b/4)}{3m} = \frac{b}{12} \\ \bar{y} &= \frac{-m(h/4)}{3m} = -\frac{h}{12}\end{aligned}$$

14.3.3 One-Story Frame: General Response

We have shown that there are two key points in the floor, *the center of twist and the center of mass*. For quasi-static loading, we work with quantities referred to the center of twist. Noting (14.27), the response of the center of twist due to an arbitrary static loading is (Fig. 14.17)

$$\begin{aligned}u_c &= \frac{P_x}{K_{xx}} \\ v_c &= \frac{P_y}{K_{yy}} \\ \omega_c &= \frac{M_C}{K_C}\end{aligned}\tag{14.33}$$

Note that twist occurs only when there is an external moment with respect to the center of twist; forces applied at the center of twist produce only translation.

Fig. 14.17 Forces acting at the center of twist

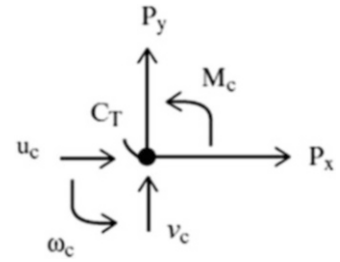
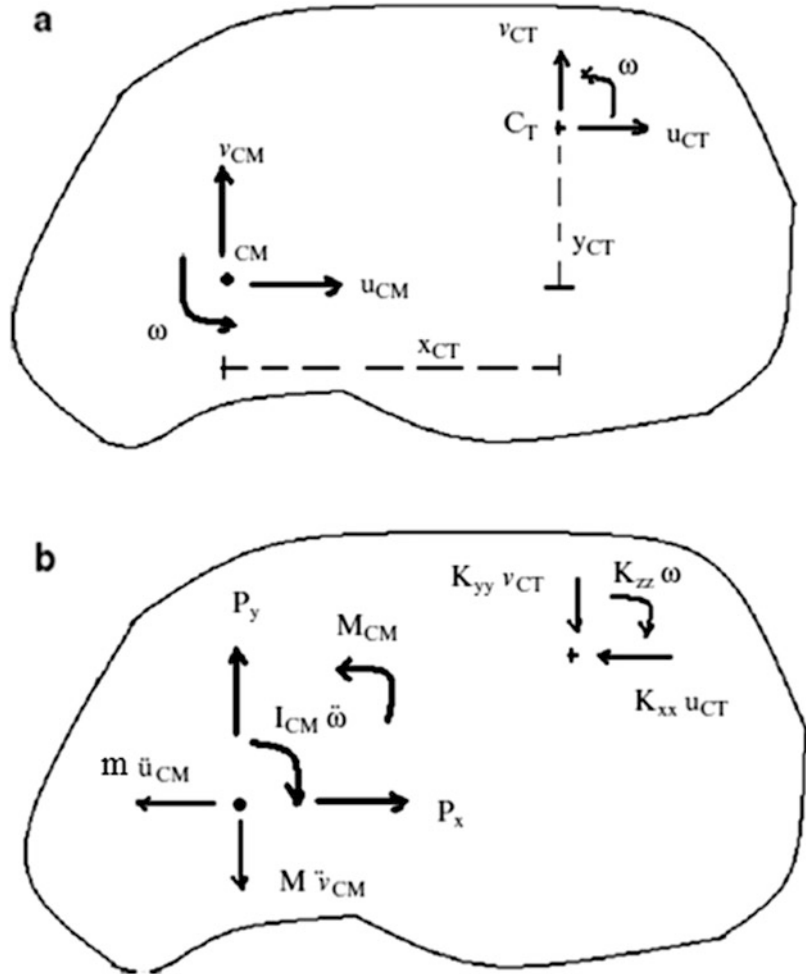


Fig. 14.18 Forces acting at the center of mass (a) Displacements, (b) Forces



When the loading is dynamic, one needs to include the inertia forces. In this case, it is more convenient to place the origin at the center of mass and work with force and displacement quantities referred to the axes centered at the center of mass. Figure 14.18a illustrates this choice. Note that the resistance forces act at the center of twist and produce a moment about the center of mass. The displacements of the two centers are related by

$$\begin{aligned}
 u_{CT} &= u_{CM} - y_{CT}\omega \\
 v_{CT} &= v_{CM} + x_{CT}\omega \\
 \omega_{CT} &= \omega
 \end{aligned}
 \tag{14.34}$$

The equilibrium equations referred to the center of mass have the following form:

$$\begin{aligned}
 P_x &= m\ddot{u}_{CM} + K_{xx}(u_{CM} - y_{CT}\omega) \\
 P_y &= m\ddot{v}_{CM} + K_{yy}(v_{CM} + x_{CT}\omega) \\
 M_{CM} &= I_{CM}\ddot{\omega} + K_C\omega + x_{CT}K_{yy}(v_{CM} + x_{CT}\omega) - y_{CT}K_{xx}(u_{CM} - y_{CT}\omega) \\
 &= I_{CM}\ddot{\omega} + \omega\{K_C + x_{CT}^2K_{yy} + y_{CT}^2K_{xx}\} + x_{CT}K_{yy}v_{CM} - y_{CT}K_{xx}u_{CM}
 \end{aligned}
 \tag{14.35}$$

Equation (14.35) shows that the motion is coupled when the center of twist *does not* coincide with the center of mass. The center of mass is usually fixed by the mass distribution on the floor and one usually does not have any flexibility in shifting masses. Therefore, the most effective strategy is to adjust the location of the braces in the story below the floor such that the centers of mass and twist coincide, i.e., to take $x_{CT} = y_{CT} = 0$.

Example 14.13

Given: The mass and stiffness layout shown in Fig. E14.13a.

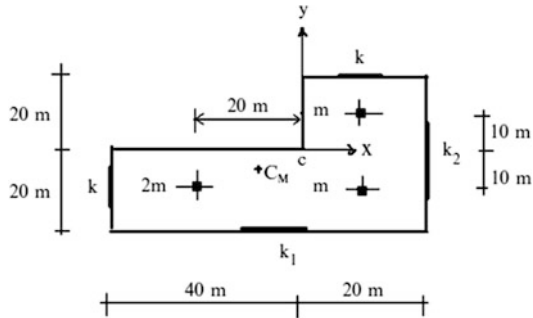


Fig. E14.13a

Determine: The magnitude of the stiffness elements k_1 and k_2 such that the centers of mass and twist coincide.

Solution: First, we locate the center of mass.

$$\begin{aligned}
 \sum m_i &= 4m \\
 \sum x_i m_i &= 10(2m) - 20(2m) = -20m \\
 \bar{x} &= \frac{-20m}{4m} = -5m
 \end{aligned}$$

Similarly,

$$\sum y_i m_i = 10(m) - 10(3m) = -20m$$

$$\bar{y} = \frac{-20m}{4m} = -5m$$

Next, we determine k_1 and k_2 by requiring the center of twist to coincide with the center of mass. The steps are

Step 1:

$$x_{CT} = \frac{\sum x_i k_y}{\sum k_y} = \frac{20k_2 - 40k}{k_2 + k} = -5m$$

$$\Downarrow$$

$$20k_2 - 40k = -5k - 5k_2$$

$$25k_2 = 35k$$

$$k_2 = 1.4k$$

Step 2:

$$y_{CT} = \frac{\sum y_i k_x}{\sum k_x} = \frac{20(k - k_1)}{k_1 + k} = -5m$$

$$\Downarrow$$

$$25k = 15k_1$$

$$k_1 = 1.67k$$

14.3.4 Multistory Response

A typical floor in a multistory structure is connected to the adjacent floors by stiffness elements such as columns, shear walls, and braces. When the floors displace, inter-story deformation due to the relative motion between the floors is developed, resulting in self-equilibrating story forces which act on the adjacent floors. Figure 14.19 illustrates this mode of behavior. Floors i and $i + 1$ experience lateral displacements which produce shear deformations in the braces

$$\gamma = u_{i+1} - u_i$$

and corresponding shear forces

$$F = k\gamma = k(u_{i+1} - u_i)$$

These forces act on both floors $i + 1$ and floor i ; the sense is reversed for the lower floor (this follows from Newton's law of action equal reaction).

In order to express these resistance forces in terms of displacements, we need to specify a common reference frame for all the floors. We suppose the floors translate and rotate with respect to this common reference frame. We consider floor i . We determine the inter-story displacement measures for the two centers of twist associated with the stories above and below floor i and apply (14.27). The resulting expressions for the resultant forces acting on floor i are listed below. Their sense is

Fig. 14.19 Forces due to inter-story deformation

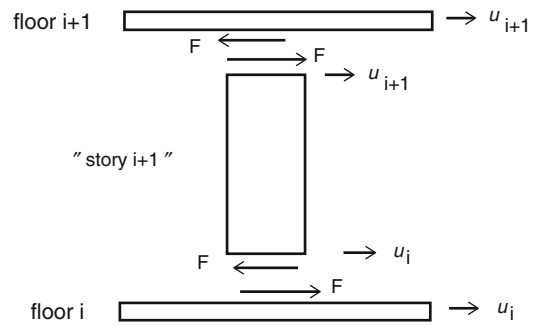
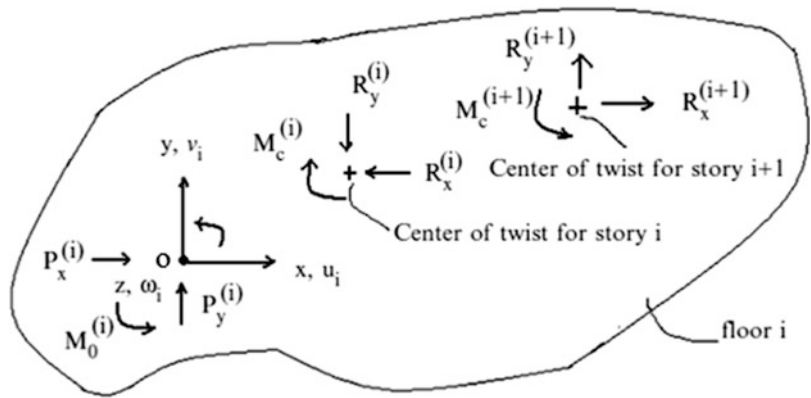


Fig. 14.20 Forces acting on floor i



defined in Fig. 14.20. Note that the direction of the forces due to story $i + 1$ are opposite to those due to story i .

For story i :

$$\begin{aligned}
 R_x^{(i)} &= K_{xx}^{(i)} \left[\left\{ u_i - y_{CT}^{(i)} \omega_i \right\} - \left\{ u_{i-1} - y_{CT}^{(i)} \omega_{i-1} \right\} \right] \\
 R_y^{(i)} &= K_{yy}^{(i)} \left[\left\{ v_i - x_{CT}^{(i)} \omega_i \right\} - \left\{ v_{i-1} - x_{CT}^{(i)} \omega_{i-1} \right\} \right] \\
 M_C^{(i)} &= K_C^{(i)} [\omega_i - \omega_{i-1}]
 \end{aligned}
 \tag{14.36}$$

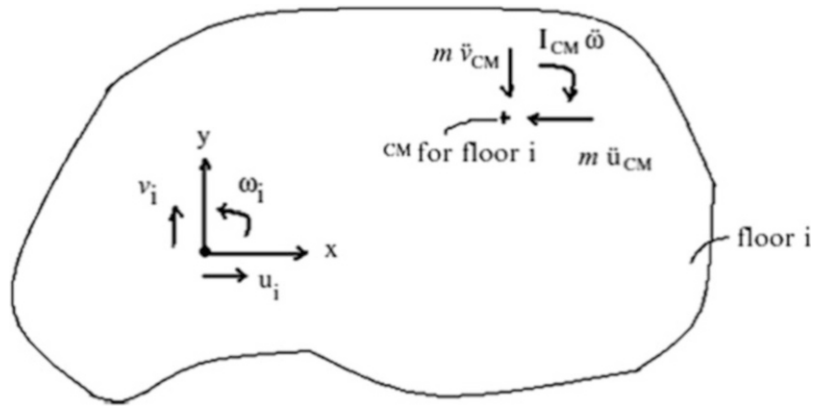
For story $i + 1$:

$$\begin{aligned}
 R_x^{(i+1)} &= K_{xx}^{(i+1)} \left[\left\{ u_{i+1} - y_{CT}^{(i+1)} \omega_{i+1} \right\} - \left\{ u_i - y_{CT}^{(i+1)} \omega_i \right\} \right] \\
 R_y^{(i+1)} &= K_{yy}^{(i+1)} \left[\left\{ v_{i+1} + x_{CT}^{(i+1)} \omega_{i+1} \right\} - \left\{ v_i - x_{CT}^{(i+1)} \omega_i \right\} \right] \\
 M_C^{(i+1)} &= K_C^{(i+1)} [\omega_{i+1} - \omega_i]
 \end{aligned}
 \tag{14.37}$$

The inertia forces for a floor depend on the mass distribution and acceleration of the floor. They act at the center of mass, a property of the floor. Figure 14.21 shows the inertia forces for floor i .

We require floor i to be in equilibrium. Summing forces with respect to the origin at O results in the following equilibrium equations:

Fig. 14.21 Inertia forces for floor i



$$\begin{aligned}
 P_x^{(i)} - m^{(i)}\ddot{u}_{i,CM} - R_x^{(i)} + R_x^{(i+1)} &= 0 \\
 P_y^{(i)} - m^{(i)}\ddot{v}_{i,CM} - R_y^{(i)} + R_y^{(i+1)} &= 0 \\
 M_0^{(i)} - I_{CM}^{(i)}\ddot{\omega} - M_C^{(i)} + M_C^{(i+1)} + m^{(i)}y_{CM}^{(i)}\ddot{u}_{i,CM} - m^{(i)}x_{CM}^{(i)}\ddot{v}_{i,CM} + y_{CT}^{(i)}R_x^{(i)} \\
 - x_{CT}^{(i)}R_y^{(i)} - y_{CT}^{(i+1)}R_x^{(i+1)} + x_{CT}^{(i+1)}R_y^{(i+1)} &= 0
 \end{aligned}
 \tag{14.38}$$

The form of (14.36) and (14.37) shows that the equilibrium equations for floor i involve the displacements for floor $i - 1$, i , and $i + 1$. Assuming there are n floors, there are n sets of equations similar in form to (14.38).

When the location of the center of mass is the same for all the floors, we take the origin at the “common” center of mass. If the center of twist also coincides with the center of mass, the equations simplify to

$$\begin{aligned}
 P_x^{(i)} &= m^{(i)}\ddot{u}_i + K_{xx}^{(i)}(u_i - u_{i-1}) - K_{xx}^{(i+1)}(u_{i+1} - u_i) \\
 P_y^{(i)} &= m^{(i)}\ddot{v}_i + K_{yy}^{(i)}(v_i - v_{i-1}) - K_{yy}^{(i+1)}(v_{i+1} - v_i) \\
 M_0^{(i)} &= I^{(i)}\ddot{\omega}_i + K_C^{(i)}(\omega_i - \omega_{i-1}) + K_C^{(i+1)}(\omega_{i+1} - \omega_i)
 \end{aligned}
 \tag{14.39}$$

where u , v , and ω are the displacement measures for the center of mass.

These equations are useful for qualitative reasoning about the behavior. In general, we want to avoid torsion, if possible. Therefore, we distribute the inter-story stiffness elements such that the location of the center of twist is constant for all stories. In regions where the seismic loading is high, such as California, one needs to consider dynamic response. In this case, the goal in seismic design is to have the center of mass and center of twist coincide throughout the height of the structure.

The formulation obtained above can be interpreted as a “shear beam” formulation for a building system in the sense that the assumptions we introduced concerning the behavior of a floor are similar to those for a beam subjected to shearing and torsional action. These assumptions are applicable for low-rise buildings, where the aspect ratio, defined as the ratio of height to width, is of order 1. Most buildings are in this category. For tall buildings and for those structures having flexible floors, one creates idealized models consisting of 3D frame structures composed of columns, beams, shear walls, and floor plates. These models generally involve a large number of variables and require computer-based analysis methods to generate solutions. The advantage of simple models is that one can reason about behavior through examination of analytical solutions. Both approaches are necessary and each has a role.

14.3.5 Matrix Formulation: Shear Beam Model

In what follows, we introduce matrix notation and express the equations defined in the previous section in a form similar to the equations for a member system that are presented in Chap. 12. We number the floor and stories consecutively, and work with the common X - Y - Z reference frame shown in Fig. 14.22. The following notation is used for floor i :

$$\begin{aligned}\underline{U}_i &= \{u_i, v_i, \omega_i\} = \text{Floor displacement vector} \\ \underline{P}_i &= \{P_{xi}, P_{yi}, M_{zi}\} = \text{External load vector}\end{aligned}\quad (14.40)$$

These quantities are referred to the common global reference frame located at point O .

The inter-story displacements at the center of twist for story i are expressed as a matrix product.

$$\Delta \underline{U}_{CT,i} = \underline{T}_{CT,i} \{ \underline{U}_i - \underline{U}_{i-1} \} \quad (14.41)$$

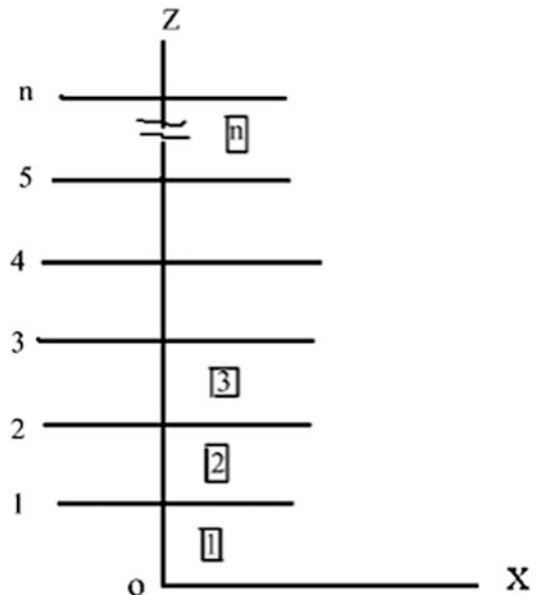
where \underline{T}_{CT} has the following general form:

$$\underline{T}_{CT,i} = \begin{bmatrix} 1 & 0 & -y_{CT}^{(i)} \\ 0 & 1 & x_{CT}^{(i)} \\ 0 & 0 & 1 \end{bmatrix} \quad (14.42)$$

The corresponding story resistance force matrices acting at the centers of twist are related to these inter-story displacements by

$$\begin{aligned}\underline{R}_{CT,i} &= K_i \Delta \underline{U}_{CT,i} \\ \underline{R}_{CT,i+1} &= K_{i+1} \Delta \underline{U}_{CT,i+1}\end{aligned}\quad (14.43)$$

Fig. 14.22 Numbering scheme for floors and stories



where \underline{K}_j depends on the stiffness properties for story j .

$$\underline{K}_j = \begin{bmatrix} \mathbf{K}_{cc}^{(j)} & \mathbf{K}_{cs}^{(j)} & 0 \\ \mathbf{K}_{cs}^{(j)} & \mathbf{K}_{ss}^{(j)} & 0 \\ 0 & 0 & \mathbf{K}_C^{(j)} \end{bmatrix} \quad (14.44)$$

We need to transfer these forces from the center of twist to the origin of the common reference frame. This operation involves the transpose of \underline{T}_{CT} .

$$\begin{aligned} \underline{R}_{o,i} &= \underline{T}_{CT,i}^T \underline{R}_{CT,i} \\ \underline{R}_{o,i+1} &= \underline{T}_{CT,i+1}^T \underline{R}_{CT,i+1} \end{aligned} \quad (14.45)$$

Using (14.41) and (14.43), (14.45) expands to

$$\begin{aligned} \underline{R}_{o,i} &= \underline{K}_{o,i} (\underline{U}_i - \underline{U}_{i-1}) \\ \underline{R}_{o,i+1} &= \underline{K}_{o,i+1} (\underline{U}_{i+1} - \underline{U}_i) \end{aligned} \quad (14.46)$$

where \underline{K}_o is the stiffness matrix referred to the common origin, O.

$$\underline{K}_{o,j} = \underline{T}_{CT,j}^T \underline{K}_j \underline{T}_{CT,j} \quad (14.47)$$

One starts with the properties of the center of twist namely, K_{xx} , K_{yy} , K_C , x_{CT} , y_{CT} , and then generates \underline{K}_o for each story.

We consider next the inertia forces which act at the center of mass of the floor. The displacements are related by

$$\begin{aligned} \underline{U}_{CM,i} &= \underline{T}_{CM,i} \underline{U}_i \\ \underline{T}_{CM,i} &= \begin{bmatrix} 1 & 0 & -y_{CM} \\ 0 & 1 & x_{CM} \\ 0 & 0 & 1 \end{bmatrix} \end{aligned} \quad (14.48)$$

The inertia force matrix acting at the center of mass is related to the acceleration matrix by

$$\underline{F}_{CM,i} = -\underline{m}_i \ddot{\underline{U}}_{CM,i} = \underline{m}_i \underline{T}_{CM,i} \ddot{\underline{U}}_i \quad (14.49)$$

where

$$\underline{m}_i = \begin{bmatrix} m^{(i)} & & \\ & m^{(i)} & \\ & & I_{CM}^{(i)} \end{bmatrix} \quad (14.50)$$

Translating these forces from the center of mass to the origin leads to

$$\begin{aligned} \underline{F}_{o,i} &= \underline{m}_{o,i} \ddot{\underline{U}}_i \\ \underline{m}_{o,i} &= \underline{T}_{CM,i}^T \underline{m}_i \underline{T}_{CM,i} \end{aligned} \quad (14.51)$$

We interpret $\underline{m}_{o,i}$ as the effective mass matrix for floor i .

Finally, summing forces for floor i , the matrix equilibrium equation referred to the common reference frame has the form.

$$\underline{P}_{o,i} = m_{o,i}\ddot{\underline{U}}_i + \underline{R}_{o,i} - \underline{R}_{o,i+1} = 0 \quad (14.52)$$

Substituting for the internal resistance matrices, the expanded form for floor i is

$$\underline{P}_{o,i} = m_{o,i}\ddot{\underline{U}}_i + \underline{K}_{o,i}(U_i - U_{i-1}) - \underline{K}_{o,i+1}(U_{i+1} - U_i) \quad (14.53)$$

We suppose there are N floors and express the complete set of N equations as a single matrix equation,

$$\underline{P} = \underline{m}\ddot{\underline{U}} + \underline{K}\underline{U} \quad (14.54)$$

We assemble \underline{m} and \underline{K} in partitioned form (N rows and N columns). The entries follow from (14.53).

$$\begin{aligned} i = 1, 2, \dots, N \\ \underline{m}_{o,i} \text{ in partitioned row } i \text{ and column } i \text{ of } \underline{m} \\ + \underline{K}_{o,i} \left\{ \begin{array}{l} \text{in row } i \text{ and column } i \\ \text{in row } i-1 \text{ and column } i-1 \end{array} \right\} \text{ of } \underline{K} \\ - \underline{K}_{o,i} \left\{ \begin{array}{l} \text{in row } i \text{ and column } i-1 \\ \text{in row } i-1 \text{ and column } i \end{array} \right\} \text{ of } \underline{K} \\ \underline{P}_{o,i} \text{ in row } i \text{ of } \underline{P} \end{aligned} \quad (14.55)$$

Note that this approach is *identical* to the procedure that we followed in Chap. 12 to assemble the system matrices for a member system. The following example illustrates the steps for a three-story structure.

Example 14.14

Given: The three-story structure shown in Fig. E14.14a. Assume the transformed mass and stiffness properties are known for each floor.

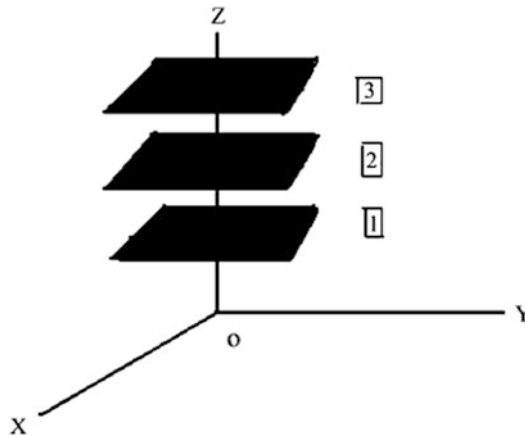


Fig. E14.14a

Determine: The non-zero entries in the system load, mass, and stiffness matrices.

Solution: $N = 3$ for this example. The partitioned form of the equations is listed below.

$$\begin{Bmatrix} P_{o,1} \\ P_{o,2} \\ P_{o,3} \end{Bmatrix} = \begin{bmatrix} m_{o,1} & & \\ & m_{o,2} & \\ & & m_{o,3} \end{bmatrix} \begin{Bmatrix} \ddot{U}_1 \\ \ddot{U}_2 \\ \ddot{U}_3 \end{Bmatrix} + \begin{bmatrix} (K_{o,1} + K_{o,2}) & -K_{o,2} & 0 \\ -K_{o,2} & (K_{o,2} + K_{o,3}) & -K_{o,3} \\ 0 & -K_{o,3} & K_{o,3} \end{bmatrix} \begin{Bmatrix} U_1 \\ U_2 \\ U_3 \end{Bmatrix}$$

14.4 Response of Symmetrical Buildings

We consider the symmetrical structural system shown in Fig. 14.23. We locate the global reference frame on the symmetry axis. By definition, the center of mass and center of twist for all the floors are located on the Z -axis.

We suppose the external floor loading is applied in the X direction. This loading is resisted by the frames supporting the floors. Each frame displaces in the X direction and develops resistance through shearing action between the floors.

A typical frame is modeled as a set of discrete masses supported by shear springs. Figure 14.24 illustrates this idealization. The shear spring stiffness for a story in a frame is determined by summing the contribution of the columns contained in the story. Using the approximate method for estimating lateral stiffness for frames developed in Chap. 11, the equivalent shear stiffness for a story in a frame is estimated as

$$k_{\text{story } i} = \frac{12E}{h^3} \sum_{\text{inter col}} I_c \frac{1}{(1 + (r/2))} + \frac{12E}{h^3} \sum_{\text{exter col}} I_c \frac{1}{(1 + r)} \tag{14.56}$$

where r is the ratio of relative stiffness factors for the column and girder.

$$r = \frac{I_{\text{col}}/h}{I_{\text{girder}}/L}$$

We evaluate the story shear stiffness factors for each frame. When shear walls or braces are present in a story, we combine the stiffness terms corresponding to the braces with the terms due to the columns.

Fig. 14.23 Symmetrical building structure

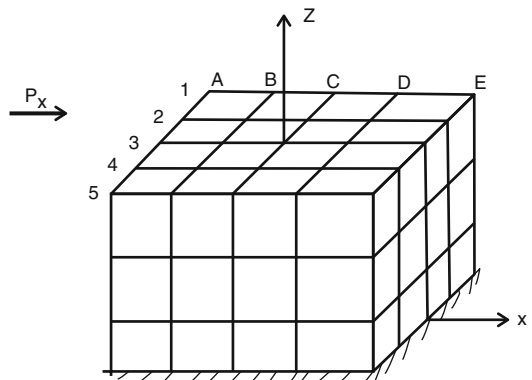


Fig. 14.24 Shear model of typical frame

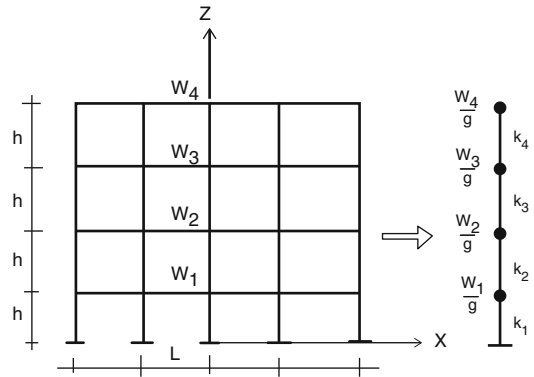
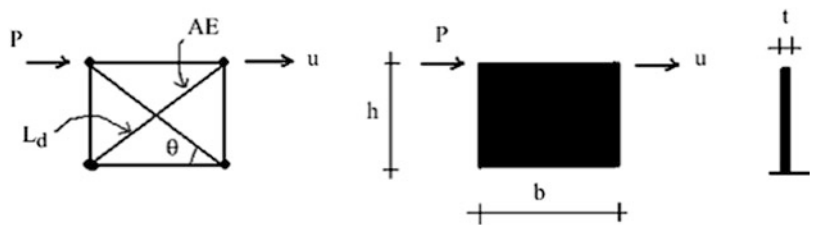


Fig. 14.25 Shear stiffness elements. (a) Steel brace. (b) Concrete shear wall



$$k|_{\text{story } i} = k_{\text{col}}|_{\text{story } i} + k_{\text{brace}}|_{\text{story } i} \tag{14.57}$$

The shear stiffness factors for the shear elements defined in Fig. 14.25 are

$$k_{\text{shearwall}} = \frac{h}{Gbt} \tag{14.58}$$

$$k_{\text{brace}} = \frac{2AE}{L_d} (\cos \theta)^2 \tag{14.59}$$

The complete building system is represented as a set of frames in parallel linked through the “rigid” floor slab. Figure 14.26 illustrates this idealization. At each story level, *all frames experience the same lateral displacement*. It follows that the story shear force in a particular frame is proportional to the ratio of the frame story shear stiffness to the global story shear stiffness which is defined as

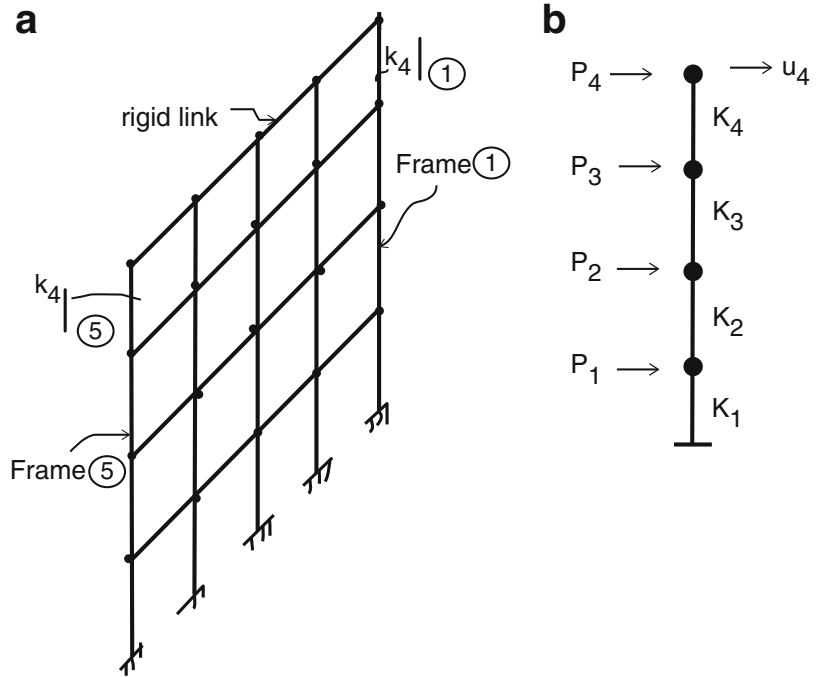
$$K_{\text{global, floor } i} = K_i = \sum_{\text{frames}} k_i|_{\text{frame } j} \tag{14.60}$$

$$V_{\text{frame } j} = \frac{k_i|_{\text{frame } j}}{K_i} V_i|_{\text{global}}$$

Generalizing this result, we can state that the lateral global loads are distributed to the individual parallel frames in proportion to their relative stiffness.

Noting Fig. 14.26, the global shear for a story is equal to the sum of the loads acting on the floors above the particular floor. For example,

Fig. 14.26 Idealized building model. (a) Set of frames with rigid link. (b) Global loads and global story stiffnesses



$$\begin{aligned} V_1|_{\text{global}} &= P_1 + P_2 + P_3 + P_4 \\ V_2|_{\text{global}} &= P_2 + P_3 + P_4 \end{aligned} \tag{14.61}$$

One first evaluates these global shear forces and then determines the individual frame story shears with (14.60).

Suppose the ratio of story stiffness to global story stiffness is constant for all stories in frame j

$$\frac{k_i|_{\text{frame } j}}{K_i} = \alpha_j \tag{14.62}$$

Then, it follows that frame j carries a fraction equal to α_j of the total applied load. This result is useful since it allows one to reason in a qualitative way about how global floor loads are distributed into the frames. For example, suppose that there are n frames having equal stiffness. Then, each frame carries $(1/n)$ of the total lateral load.

Example 14.15

Given: The symmetrical rigid frame structure shown in Fig. E14.15a. Assume the frame properties are constant throughout the building height and also assume the structure is uniformly loaded. (a) The columns in frames 2 and 3 are twice as stiff as the columns in frames 1 and 4 and the floor slab is rigid. (b) Assume equal frame stiffnesses and rigid floor slab. (c) Assume equal frame stiffnesses and a flexible floor slab.

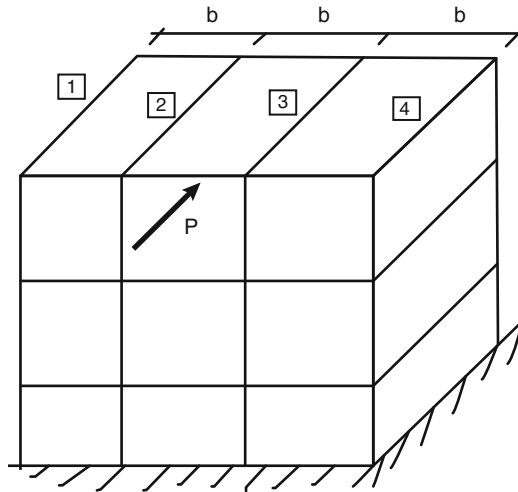


Fig. E14.15a

Determine: The distribution of the total lateral load to the individual frames.

Solution:

Part (a): A typical floor is shown in Fig. E14.15b. The equivalent story shear stiffness factors are defined as k^* and $2k^*$. The resultant global shear force acts at the midpoint of the side, and there is no twist since the stiffness distribution is symmetrical.

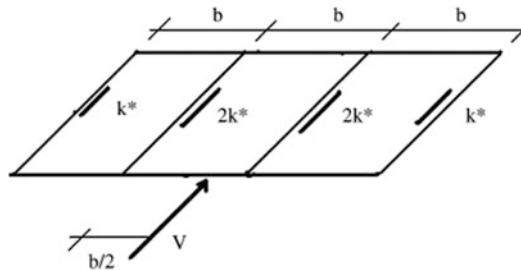


Fig. E14.15b Typical floor

The total story stiffness is

$$\sum k_j = (k^*)(1 + 2 + 2 + 1) = 6k^*$$

According to (14.60), the fraction of the total story shear carried by an individual frame is equal to the ratio of the frame story stiffness to the total story stiffness. Then,

For frames 1 and 4

$$V_1 = V_4 = V \frac{k^*}{6k^*} = \frac{1}{6}V$$

For frames 2 and 3

$$V_2 = V_3 = V \frac{2k^*}{6k^*} = \frac{1}{3}V$$

In this case, *the interior frames carry twice as much load as the exterior frames.*

Part (b): If the floor slab is rigid and equal frame stiffnesses are used, the frame load distribution shown in Fig. E14.15c is now applicable; the shear is assigned uniformly to the frames.

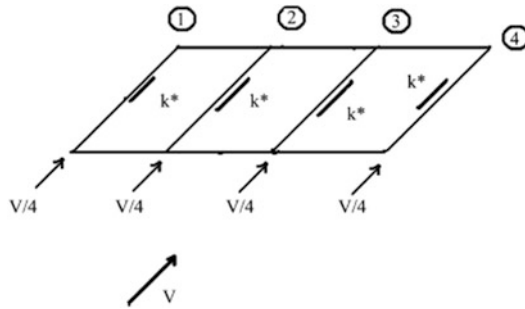


Fig. E14.15c Typical floor

Part (c): Suppose one generates an estimate for the global loading on an individual frame using the tributary areas for the frames. Consider the structure shown in Fig. E14.15a. We divide the façade area into area segments and associate these segmental areas with the frames adjacent to the areas as illustrated in Fig. E14.15d.

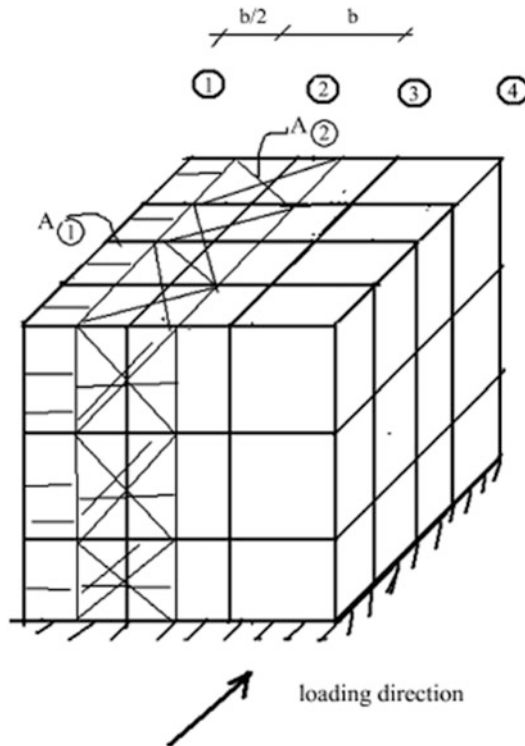


Fig. E14.15d

We note that the width for the segmental areas 1 and 4 is $\frac{1}{2}$ the width for the interior tributary areas. Therefore, assuming the external loading is constant over the width, it follows that the magnitude of the loads for frames 1 and 4 is $\frac{1}{2}$ the load for the interior frames. This breakdown is shown in Fig. E14.15e. This distribution is based on the assumption that the frames act independently, i.e., the floor slabs are flexible.

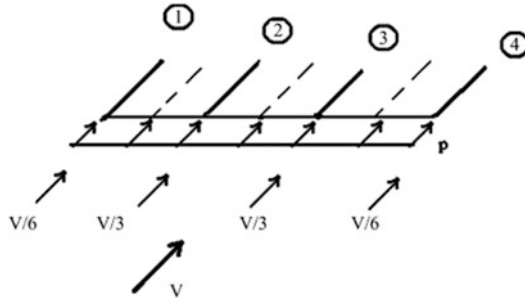


Fig. E14.15e

Example 14.16

Given: The five-story symmetrical rigid frame building shown in Figs. E14.16a and E14.16b. Assume the building can be subjected to an earthquake in either the North–South or East–West directions. Take the spectral acceleration as $S_a = 0.15g$. Consider all the beams to be the same size and all the columns to be the same size. Assume $I_B = 4I_C$.

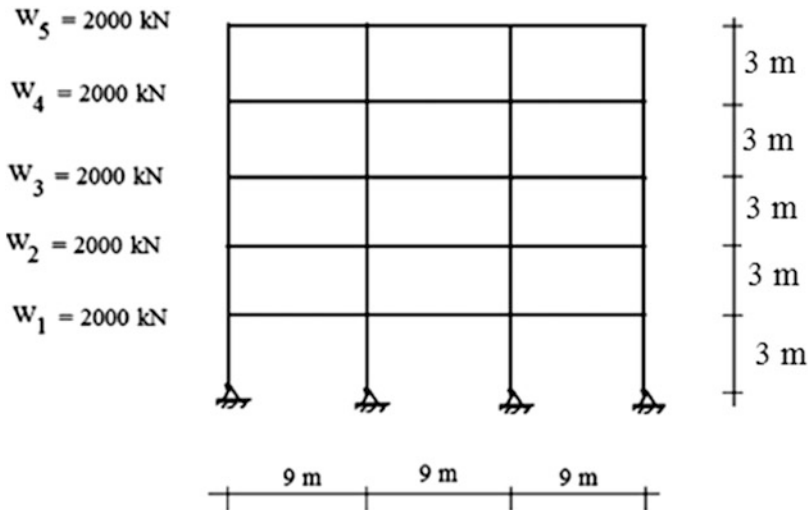


Fig. E14.16a Elevation

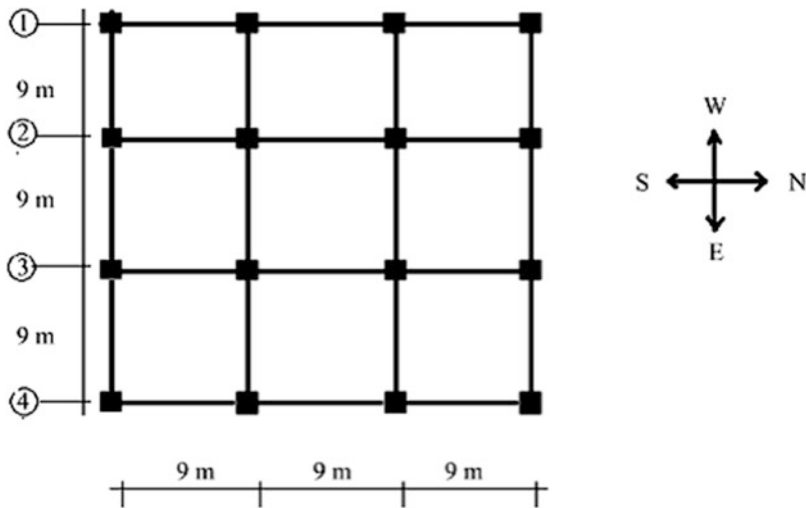


Fig. E14.16b Typical floor plan

Determine: The maximum moments in the columns (a) for rigid floors and (b) for flexible floors.

Solution: We use (14.10). The base shear is given by

$$V|_{\text{base}} = \frac{\left(\sum_{i=1}^5 Z_i W\right)^2}{\sum_{i=1}^5 W_i (Z_i)^2} \frac{S_a}{g} \frac{(2000(3) + 2000(6) + 2000(9) + 2000(12) + 2000(15))^2}{2000(3)^2 + 2000(6)^2 + 2000(9)^2 + 2000(12)^2 + 2000(15)^2} \quad (0.15)$$

$$= 1227 \text{ kN}$$

Then, applying (14.11), we obtain the individual floor loads (Fig. E14.16c).

$$P|_{\text{floor } i} = \left(\frac{W_i Z_i}{\sum W_i Z_i}\right) V|_{\text{base}}$$

$$\sum_{i=1}^5 W_i Z_i = 2000(3) + 2000(6) + 2000(9) + 2000(12) + 2000(15)$$

$$= 90,000 \text{ kN/m}$$

$$P|_{\text{floor } 1} = \frac{3(2000)}{90,000} (1227) = 81.8 \text{ kN}$$

$$P|_{\text{floor } 2} = \frac{6(2000)}{90,000} (1227) = 163.6 \text{ kN}$$

$$P|_{\text{floor } 3} = \frac{9(2000)}{90,000} (1227) = 245.4 \text{ kN}$$

$$P|_{\text{floor } 4} = \frac{12(2000)}{90,000} (1227) = 327.2 \text{ kN}$$

$$P|_{\text{floor } 5} = \frac{15(2000)}{90,000} (1227) = 409 \text{ kN}$$

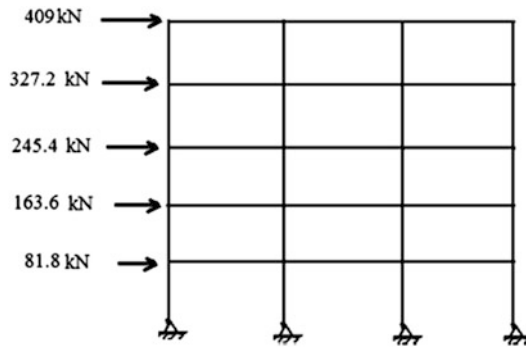


Fig. E14.16c Earthquake floor loads

It remains to distribute the floor loads to the frames. Since the structure is symmetrical, we need to consider only one direction, say the N-S direction (Fig. E14.16d).

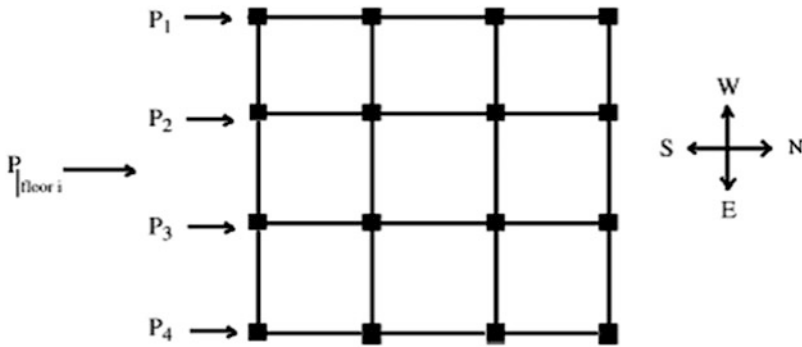


Fig. E14.16d Floor load distribution

Part a:

When the floor slab is rigid, and the frame stiffnesses are equal, the floor load is distributed uniformly to the frames (Fig. E14.16e).

$$P_1 = P_2 = P_3 = P_4 = \frac{1}{4} P_{\text{floor } i}$$

Therefore,

$$P_1 = P_2 = P_3 = P_4 = \begin{cases} 20.5 \text{ kN} \\ 40.9 \text{ kN} \\ 61.4 \text{ kN} \\ 81.8 \text{ kN} \\ 102.3 \text{ kN} \end{cases}$$

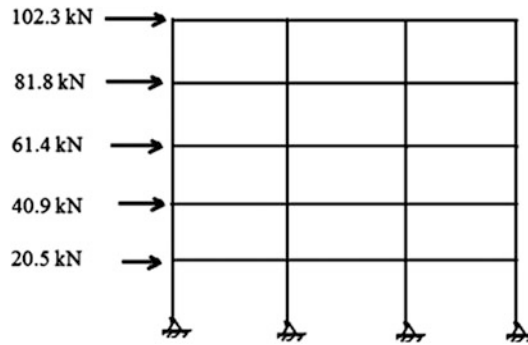


Fig. E14.16e Frame load—rigid floors

Part b:

When the floor slab is flexible, the loads are proportioned to their tributary floor areas. Then, it follows that (Fig. E14.16f)

$$P_2 = P_3 = \frac{1}{3}P_{\text{floor } i} = \begin{cases} 27.3 \text{ kN} \\ 54.5 \text{ kN} \\ 81.8 \text{ kN} \\ 109 \text{ kN} \\ 136.3 \text{ kN} \end{cases}$$

$$P_1 = P_4 = \frac{1}{6}P_{\text{floor } i} = \begin{cases} 13.6 \text{ kN} \\ 27.3 \text{ kN} \\ 40.9 \text{ kN} \\ 54.5 \text{ kN} \\ 68.2 \text{ kN} \end{cases}$$

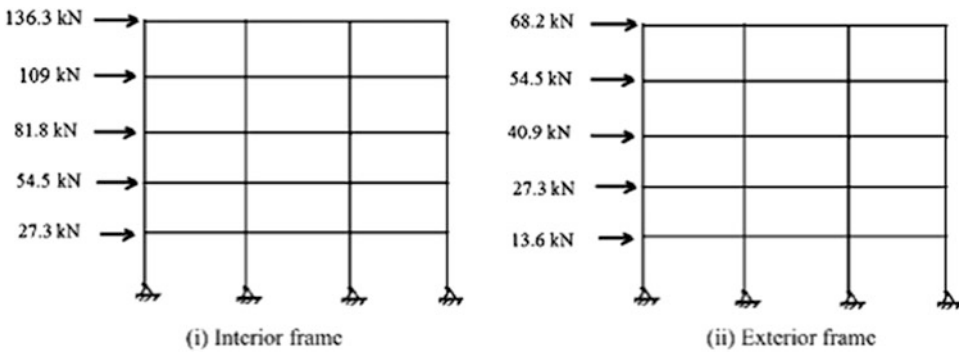


Fig. E14.16f Frame loads—flexible floors

Part c:

We apply the stiffness method described in Chap. 11 to estimate the maximum moments in the exterior and interior columns.

$$I_{C_{ext}} = I_C \text{ and } I_B = 4I_C \Rightarrow \frac{I_{C_{ext}}/h}{I_B/L} = \frac{I_C/h}{I_B/L} = \frac{(I_C/4)}{(4I_C/9)} = 0.5625$$

$$k_E = \frac{3EI_{CE}}{h^3} \left\{ \frac{1}{1 + \frac{1}{2} \left(\frac{I_{CE}/h}{I_b/L} \right)} \right\} = \frac{2.34EI_C}{h^3} \Rightarrow \frac{k_E}{k_I} = 0.89$$

$$k_I = \frac{3EI_{CI}}{h^3} \left\{ \frac{1}{1 + \frac{1}{4} \left(\frac{I_{CI}/h}{I_b/L} \right)} \right\} = \frac{2.63EI_C}{h^3}$$

Noting that

$$\frac{V_E}{V_I} = \frac{k_E}{k_I}$$

we express the total shear as

$$V_{Total} = 2V_E + 2V_I = 2 \left(\frac{k_E}{k_I} + 1 \right) V_I \Rightarrow V_I = 0.265V_{Total}$$

The distributions are shown in Figs. E14.16g and E14.16h.

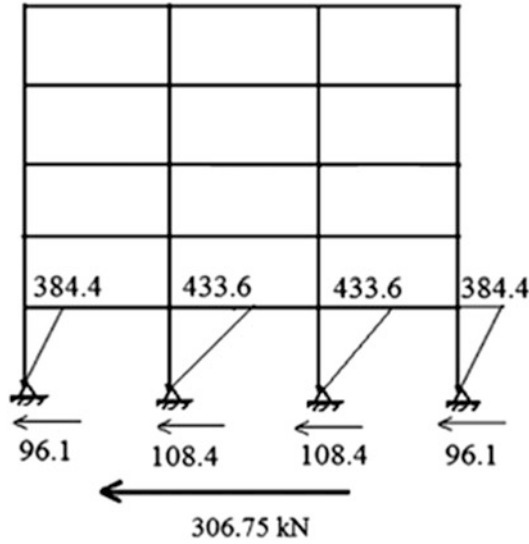


Fig. E14.16g Maximum column moments—rigid floors

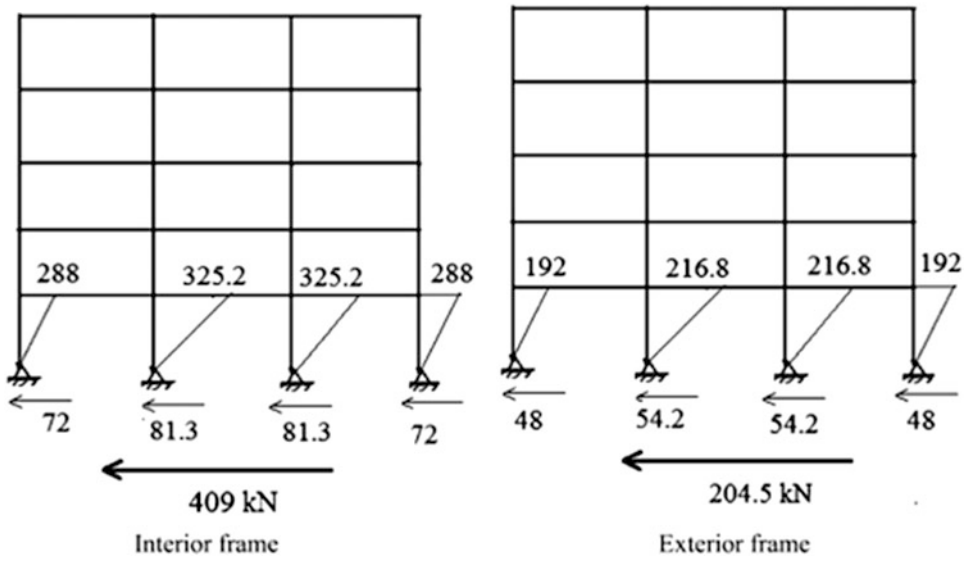


Fig. E14.16h Maximum column moments—flexible floors

Example 14.17

Given: The one-story frame shown in Figs. E14.17a, E14.17b, E14.17c. Assume the cross sections are equal.

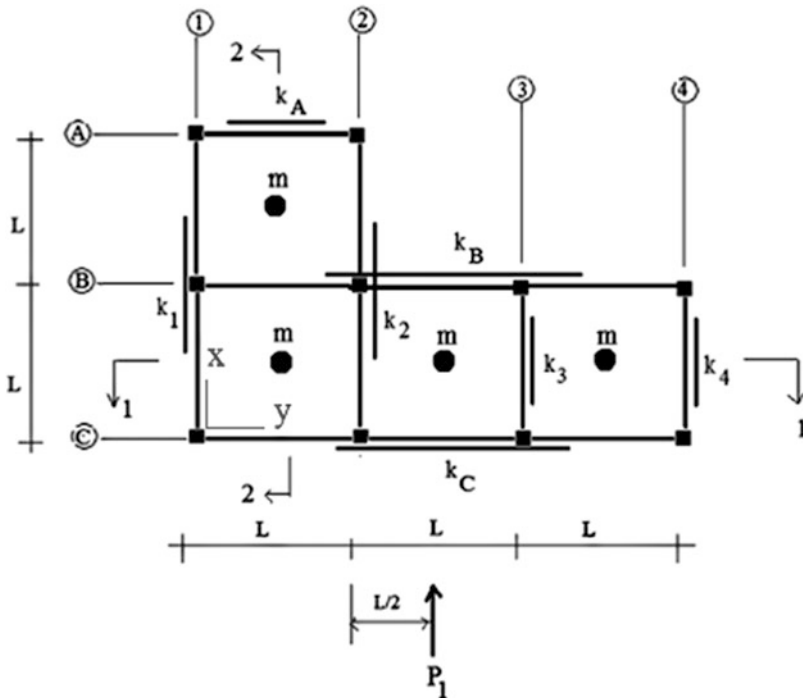


Fig. E14.17a Plan

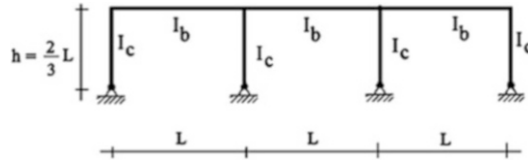


Fig. E14.17b Elevation—section 1-1

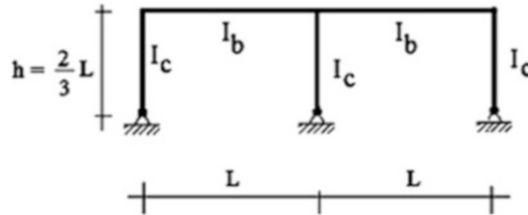


Fig. E14.17c Elevation—section 2-2

Determine:

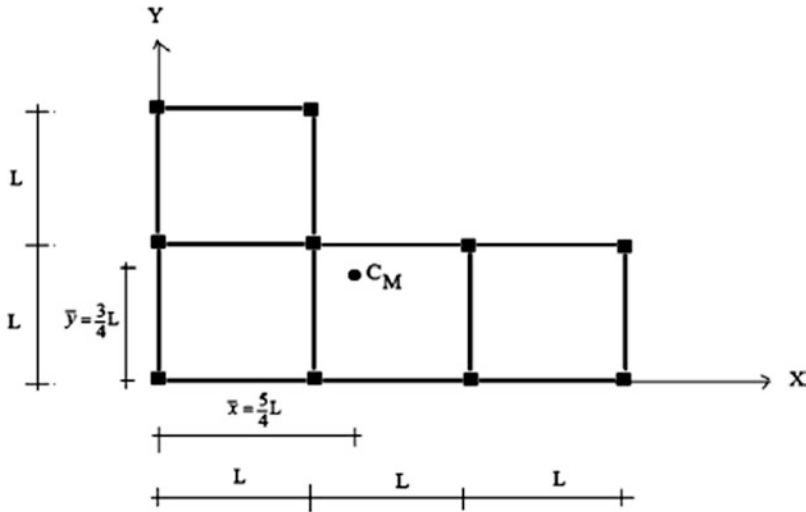
- (a) The center of mass.
- (b) The center of twist. Take $I_b = 2I_c$.
- (c) The revised stiffness required on lines B-B and 2-2 so that the center of stiffness coincides with the center of mass.
- (d) The translation and rotation of the center of twist for the structure determined in part (c) due to load P_1 .

Solution:

- (a) The center of mass

$$\bar{x} = \frac{\sum x_i m_i}{\sum m_i} = \frac{(0.5L)2m + (1.5L)m + (2.5L)m}{4m} = \frac{5}{4}L$$

$$\bar{y} = \frac{\sum y_i m_i}{\sum m_i} = \frac{(0.5L)3m + (1.5L)m}{4m} = \frac{3}{4}L$$



(b) The center of twist

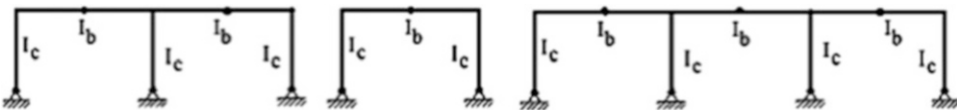
$$\begin{aligned}
 I_{CE} &= I_{CI} = I_c \\
 I_b &= 2I_c \\
 \left(\frac{I_{CI}/h}{I_b/L}\right) &= \left(\frac{I_{CE}/h}{I_b/L}\right) = \left(\frac{3I_c/2L}{2I_c/L}\right) = 0.75
 \end{aligned}$$

Using the shear stiffness equations (11.11) and (11.12), the relevant stiffness factors are

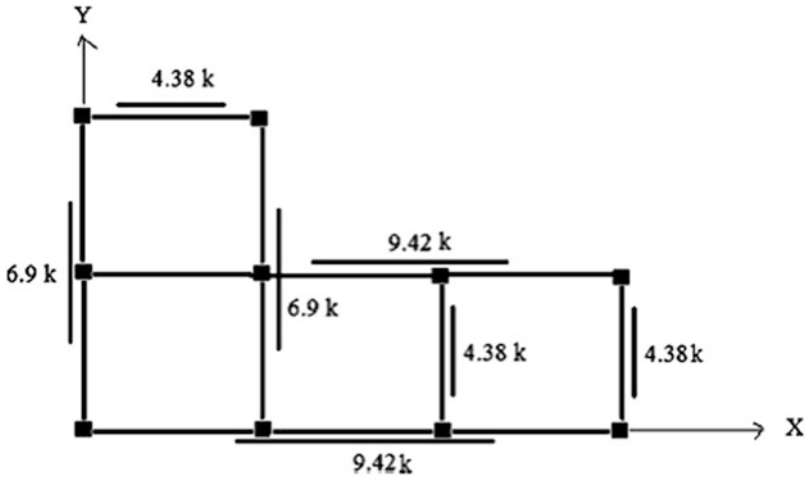
$$\begin{aligned}
 f_{BE} &= \left\{ \frac{1}{1 + \frac{1}{2} \left(\frac{I_{CE}/h}{I_b/L}\right)} \right\} = 0.73 \\
 f_{BI} &= \left\{ \frac{1}{1 + \frac{1}{4} \left(\frac{I_{CI}/h}{I_b/L}\right)} \right\} = 0.84
 \end{aligned}$$

Let $(EI_c/h^3) = k$. Then,

$$\begin{aligned}
 k_{BE} &= \frac{3EI_{CE}}{h^3} \left\{ \frac{1}{1 + \frac{1}{2} \left(\frac{I_{CE}/h}{I_b/L}\right)} \right\} = \frac{3EI_{CE}}{h^3} f_{BE} = 2.19k \\
 k_{BI} &= \frac{3EI_{CI}}{h^3} \left\{ \frac{1}{1 + \frac{1}{4} \left(\frac{I_{CI}/h}{I_b/L}\right)} \right\} = \frac{3EI_{CI}}{h^3} f_{BI} = 2.52k
 \end{aligned}$$

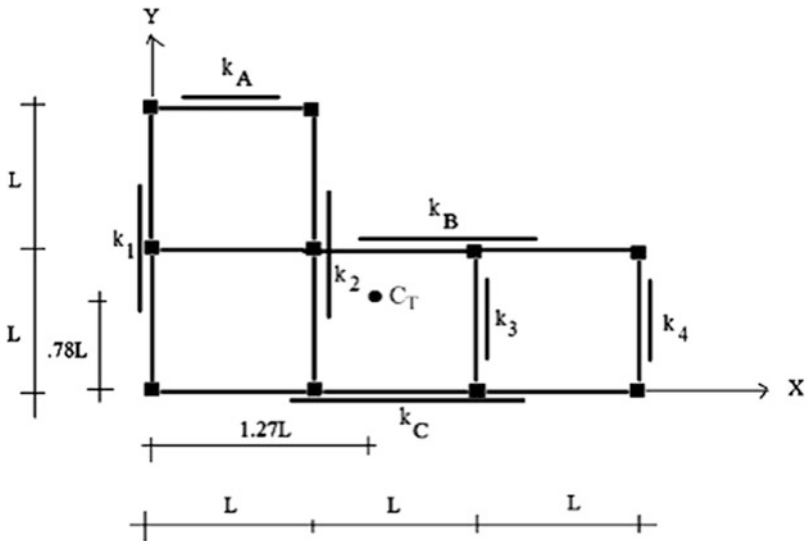


$$\begin{aligned}
 k_1 = k_2 &= 2k_{BE} + k_{BI} = 6.9k \\
 k_3 = k_4 &= k_A = 2k_{BE} = 4.38k \\
 k_B = k_C &= 2k_{BE} + 2k_{BI} = 9.42k
 \end{aligned}$$



Finally, one obtains the coordinates

$$\begin{aligned}
 x_{CT} &= \frac{\sum x_j k_{yj}}{\sum k_{yj}} = \frac{6.9k(L) + 4.38k(2L) + 4.38k(3L)}{2(6.9k + 4.38k)} = 1.27L \\
 y_{CT} &= \frac{\sum y_i k_{xi}}{\sum k_{xi}} = \frac{9.42k(L) + 4.38k(2L)}{2(9.42k) + 4.38k} = 0.78L
 \end{aligned}$$

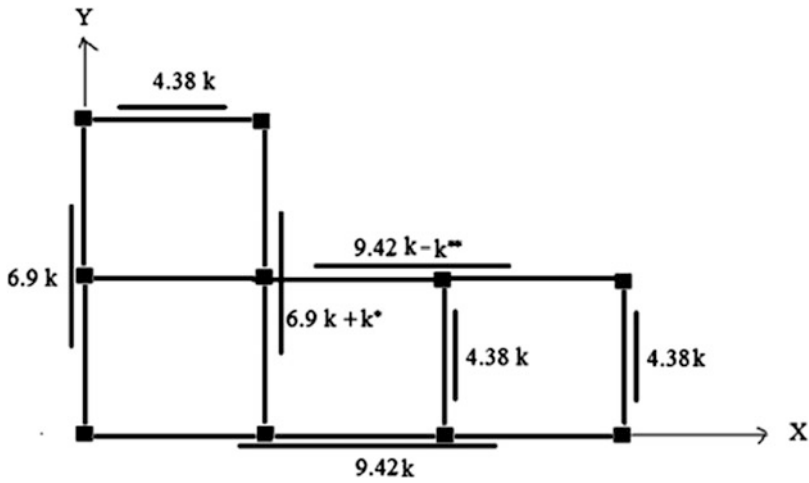


(c) The revised stiffness required on lines B-B and 2-2

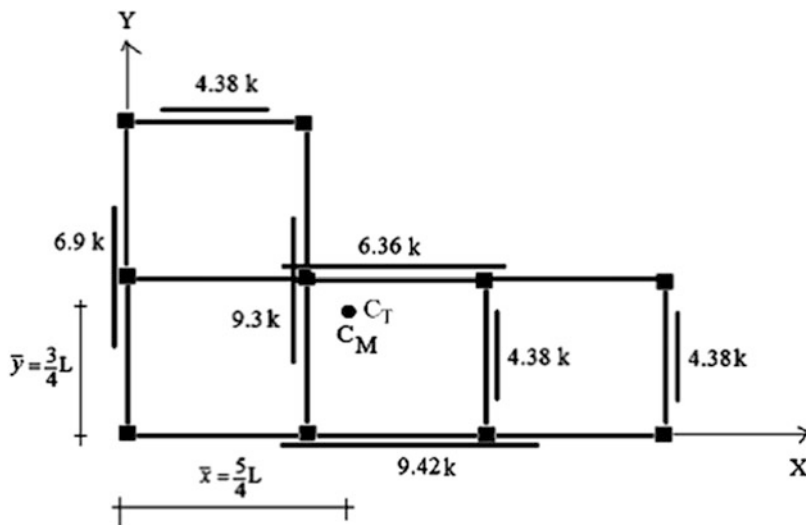
$$x_{CT} = \bar{x} = \frac{5}{4}L = \frac{(6.9k + k^*)(L) + 4.38k(2L) + 4.38k(3L)}{6.9k + (6.9k + k^*) + 2(4.38k)}$$

$$y_{CT} = \bar{y} = \frac{3}{4}L = \frac{(9.42k - k^{**})(L) + 4.38k(2L)}{9.42k + (9.42k - k^{**}) + 4.38k}$$

$$\therefore k^* = 2.4k \quad k^{**} = 3.06k$$



(d) The translation and rotation of the center of twist



Noting the result for part (c) and (14.20) specialized for the center of twist, the displacements of the center of twist due to P_1 are

$$K_{yy} = \sum k_{yj} = k\{6.9 + 9.3 + 2(4.38)\} = 24.96k$$

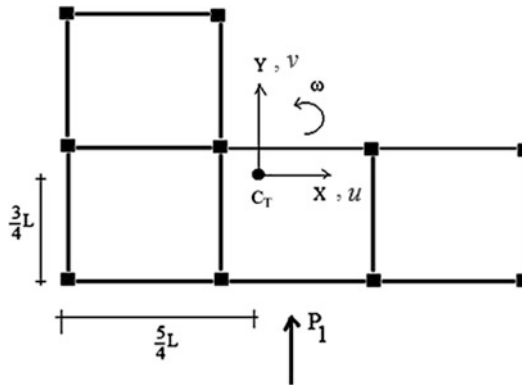
$$K_o = \sum y_j^2 k_{xi} + \sum x_j^2 k_{yj} = \left\{4.38k(1.25L)^2 + 9.42k(0.75L)^2 + 6.36k(0.25L)^2\right\} \\ + \left\{6.9k(1.25L)^2 + 9.3k(0.25L)^2 + 4.38k(0.75L)^2 + 4.38k(1.75L)^2\right\} = 39.78kL^2$$

$$M_o = P_1 \left(\frac{L}{4}\right)$$

$$u = 0$$

$$v = \frac{P_y}{K_{yy}} = \frac{P_1}{24.96k}$$

$$\omega = \frac{M_o}{K_o} = \frac{P_1(L/4)}{39.78kL^2} = 0.00628 \frac{P_1}{kL}$$



14.5 Summary

14.5.1 Objectives

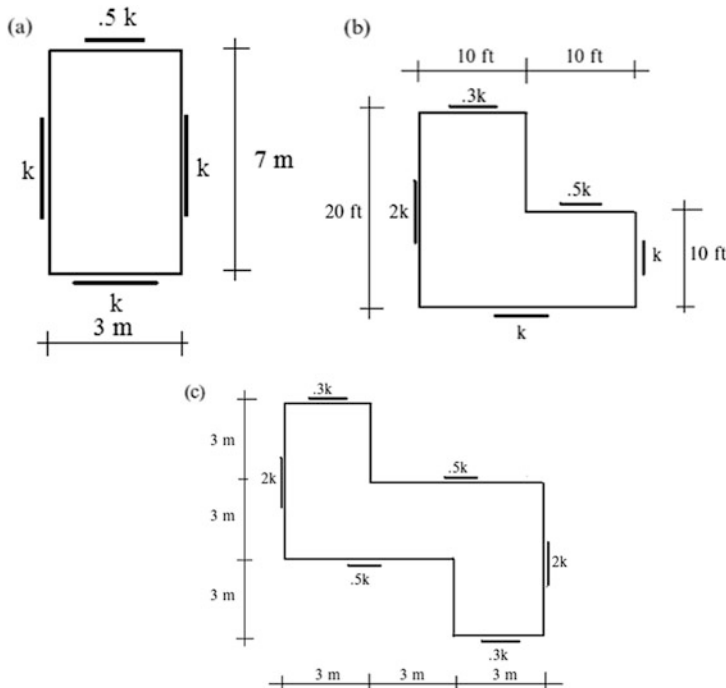
- To describe various idealized models that are used to represent building structures as an assemblage of plane frames and rigid floor slabs.
- To introduce procedures for generating wind and earthquake loads for building structures.
- To introduce the concepts of center of mass and center of stiffness and apply these concepts to typical building structures.
- To formulate the governing equations for a building idealized as a three-dimensional shear beam.
- To represent these equations using matrix notation.
- To specialize the formulation for symmetrical buildings.

14.5.2 Key Facts and Concepts

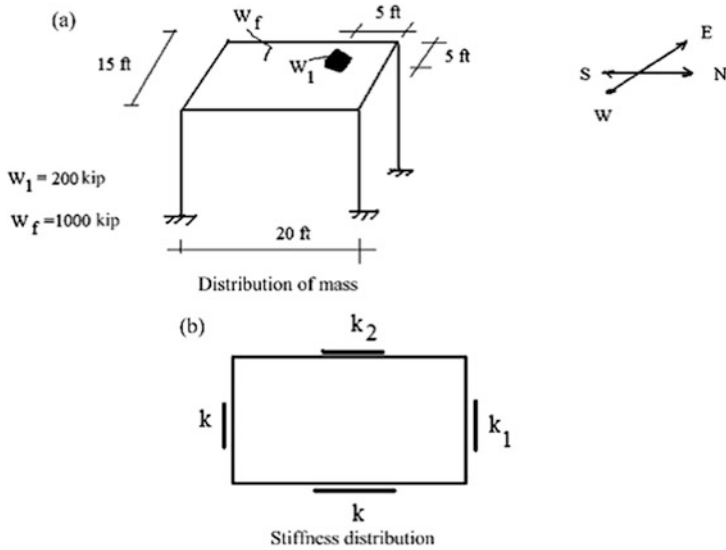
- The normal pressure due to wind varies as a power law ($p \sim z^{1/7}$) in the vertical direction.
- Seismic excitation is represented by a set of inertia forces acting at the floor levels. These forces are defined in terms of certain parameters that depend on the site and are specified by design codes. The vertical force distribution depends on the floor masses and increases with distance from the base.
- The center of mass is a property of a floor, i.e., it depends on the mass distribution within the floor. It is important since the resultant of the inertia forces passes through the center of mass.
- The center of stiffness is a property of the lateral stiffness distribution in a story. Twisting of the floor slab will occur when the resultant force acting on a story does not pass through the center of stiffness. Ideally one positions the center of stiffness to coincide with the center of mass if dynamic loading is one of the design loading conditions.
- Given a set of parallel frames connected by a rigid diaphragm and subjected to a lateral load applied at the center of twist, the load carried by an individual frame is proportional to the relative stiffness of the frame.

14.6 Problems

Problem 14.1 Consider the plan view of one-story rigid frames shown below. Determine the center of twist corresponding to the brace stiffness patterns shown.



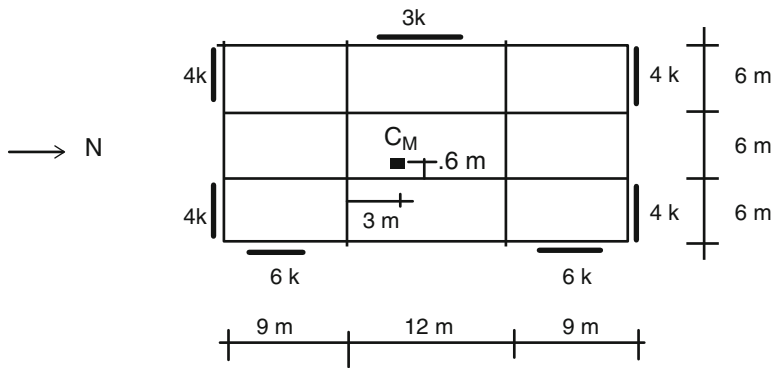
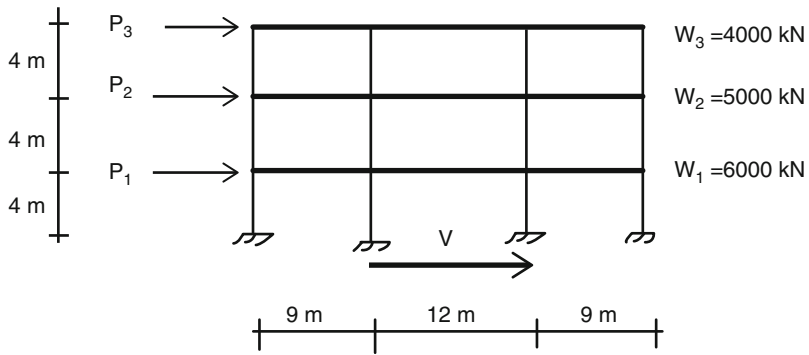
Problem 14.2



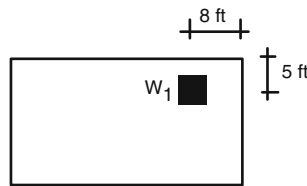
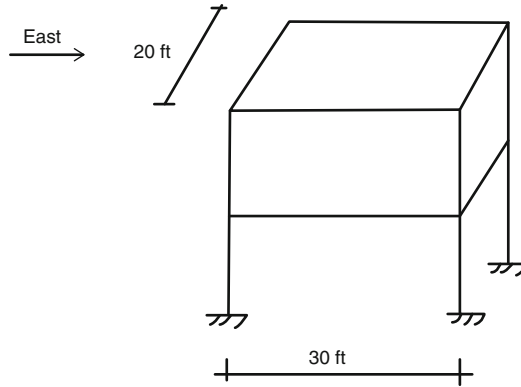
The one-story frame shown has an unsymmetrical mass distribution.

- (a) Determine the center of mass.
- (b) Determine the stiffness parameters k_1 and k_2 such that the center of stiffness coincides with the center of mass.
- (c) Determine the earthquake floor loads corresponding to $S_a = 0.3g$. Consider both direction, i.e., N-S and E-W.

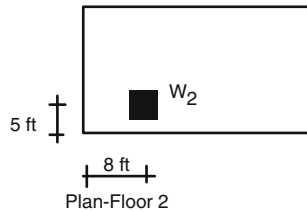
Problem 14.3 For the rigid frame shown below, determine (a) the center of twist (C_T) and (b) the seismic floor loads applied at the center of mass (C_M) for an N-S earthquake with $S_a = 0.3g$. Assume properties are equal for each floor.



Problem 14.4 Consider the two-story rigid frame defined below. Assume the weight of the floor slabs is equal to w_{floor} . Concentrated masses are located on each floor as indicated.

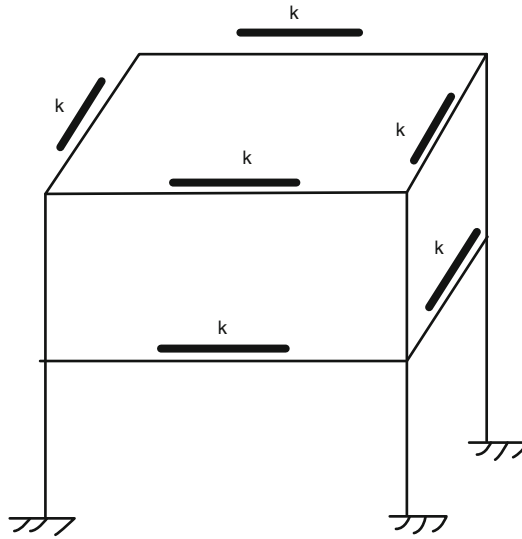


Plan-Floor 1

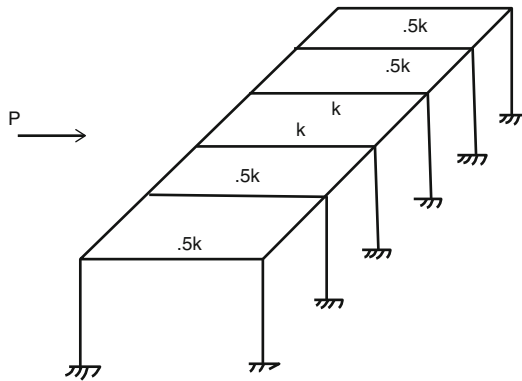


Plan-Floor 2

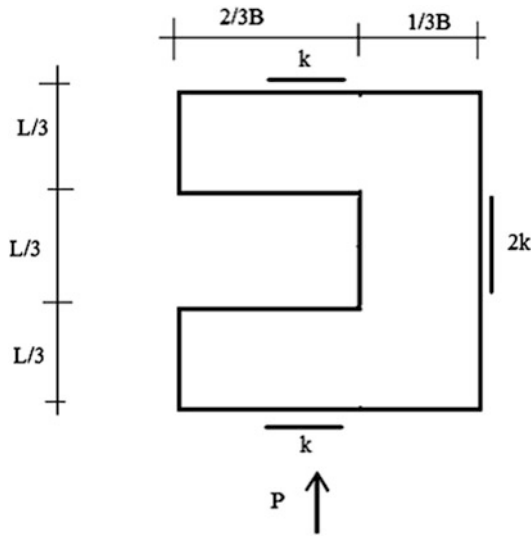
- (a) Determine the position of the center of mass for each floor.
- (b) Assume the structure is subjected to an earthquake acting in the east direction. Determine the earthquake forces for the individual floors. Assume $w_{\text{floor}} = 1000$ kip, $w_1 = w_2 = 1000$ kip, and $S_a = 0.3g$.
- (c) Suppose the story stiffness distribution shown below is used. Describe qualitatively how the structure will displace when subjected to an earthquake. Consider the stiffness distribution to be the same for each floor.



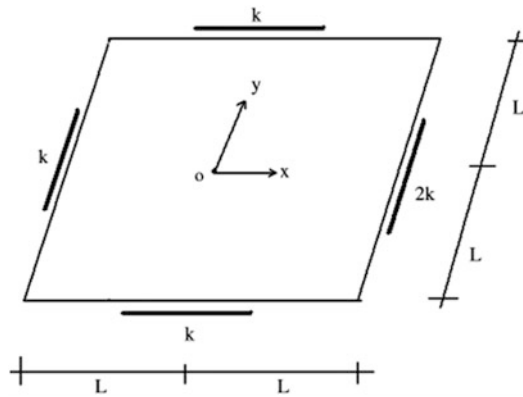
Problem 14.5 Consider the single-story multi-frame structure shown below. Determine the lateral force in the frames due to a global load P . Consider both wind and earthquake loading. Assume the slab is rigid.



Problem 14.6 Consider the stiffness distribution for the one-story rigid frame shown below. Determine the displaced configuration under the action of the loading shown. Assume the slab is rigid.

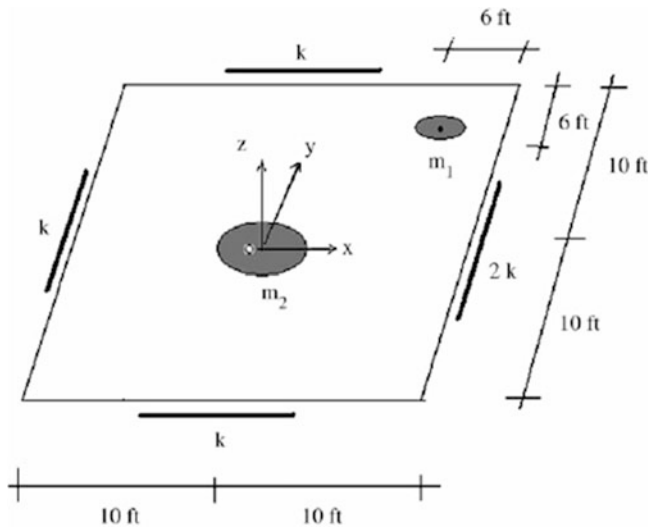


Problem 14.7



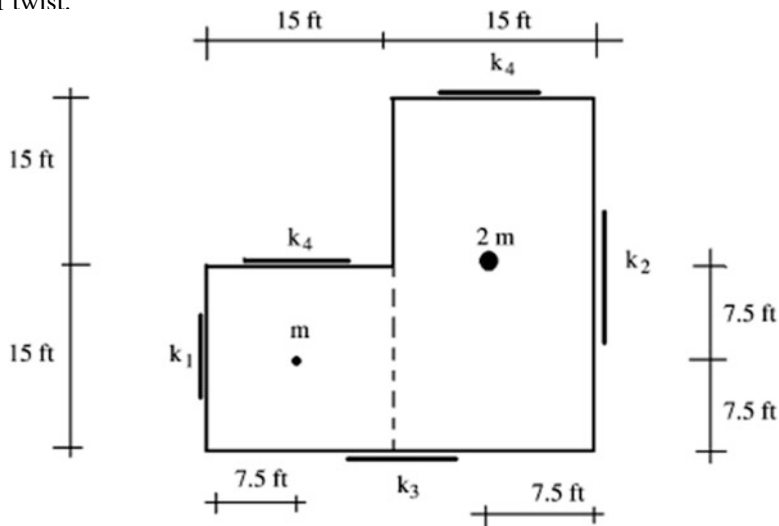
- (a) Determine the center of twist.
- (b) Using (14.47) determine \underline{K}_0 .

Problem 14.8 Consider the plan view of a one-story frame shown below. Using the matrix formulation presented in Sect. 14.3.5 generate the equations of motion for the story. Take $m_1 = 1000$ lb, $m_2 = 500$ lb, and $k = 10$ kip/in.

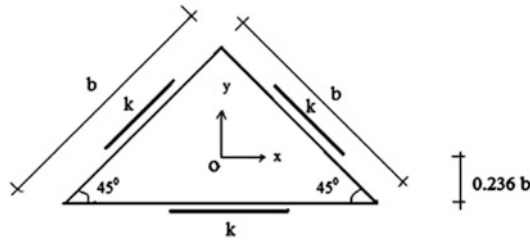


Problem 14.9 Consider the one-story plan view shown below.

- (a) Locate the center of mass.
- (b) Locate the center of twist. Take $k_1 = k_2 = k_3 = k_4 = k$.
- (c) Take $k_1 = k_3 = 10$. Suggest values for k_2 and k_4 such that the center of mass coincides with the center of twist.

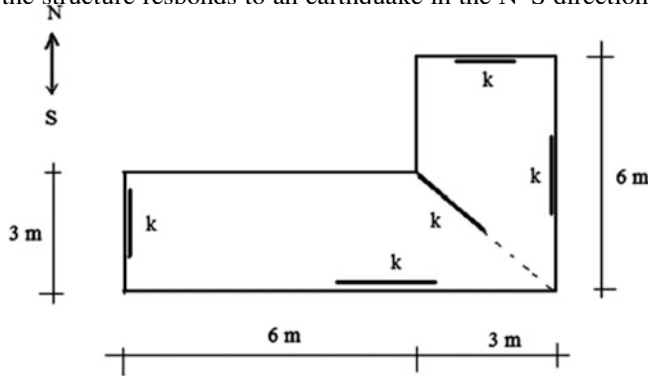


Problem 14.10 Consider the floor plan shown below. Assume the mass is uniformly distributed over the floor area. Establish the equations of motion referred to point O.



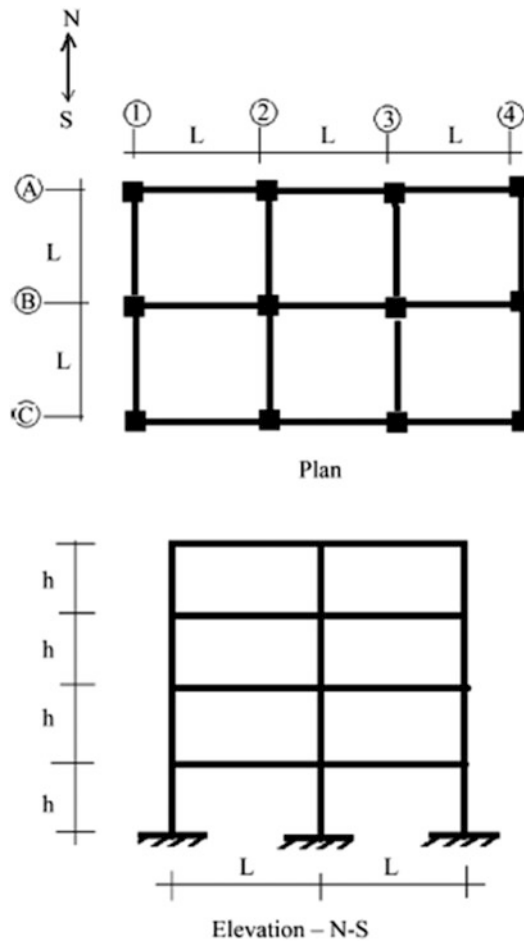
Problem 14.11 Consider the roof plan for a one-story structure shown below. Assume the shear walls have equal stiffness and the roof dead load is uniform.

- (a) Determine the center of mass and the center of stiffness.
- (b) Describe how the structure responds to an earthquake in the N–S direction.



Problem 14.12 The framing shown below has identical rigid frames along column lines 1, 2, 3, and 4, and cross-bracing along lines A, B, and C. Consider all the beams and all the columns to be the same size. Assume $I_b = 3I_c$ and $L = 2h$.

- (a) Assuming the roof/floor slab are rigid with respect to the rigid frames, what part of the total seismic load due to a N–S earthquake is carried by the frame 4?
- (b) Repeat part (a) considering the roof/floor slab to be flexible.



References

1. United States Geological Survey National Earthquake Information Center, Denver, Colorado. <http://earthquake.usgs.gov/earthquakes/shakemap/>
2. Connor JJ. Introduction to structural motion control. Englewood Cliffs: Prentice Hall; 2003. p. 3.
3. Structural Engineering Institute, ASCE. ASCE/SEI 7-05, Minimum design loads for buildings and other structures. New York: ASCE; 2006.

Abstract

The previous chapter dealt with issues related to the lateral loadings on building systems. In that chapter, we described how one can represent the global lateral loading as loads acting on the individual frames contained in the building system. We focus in this chapter on how one treats vertical loads such as gravity loads. Gravity loads applied to a floor slab are converted to distributed loads acting on the beams which support the slab. Since the floor slab loads involve both dead and live loads, one needs to investigate various floor slab loading patterns in order to establish the maximum values of the design parameters such as bending moment. We apply Müller-Breslau principle for this task. The last section of the chapter contains a case study which illustrates the process of combining lateral and vertical loading, and demonstrates the sensitivity of the structural design to the type of structural system.

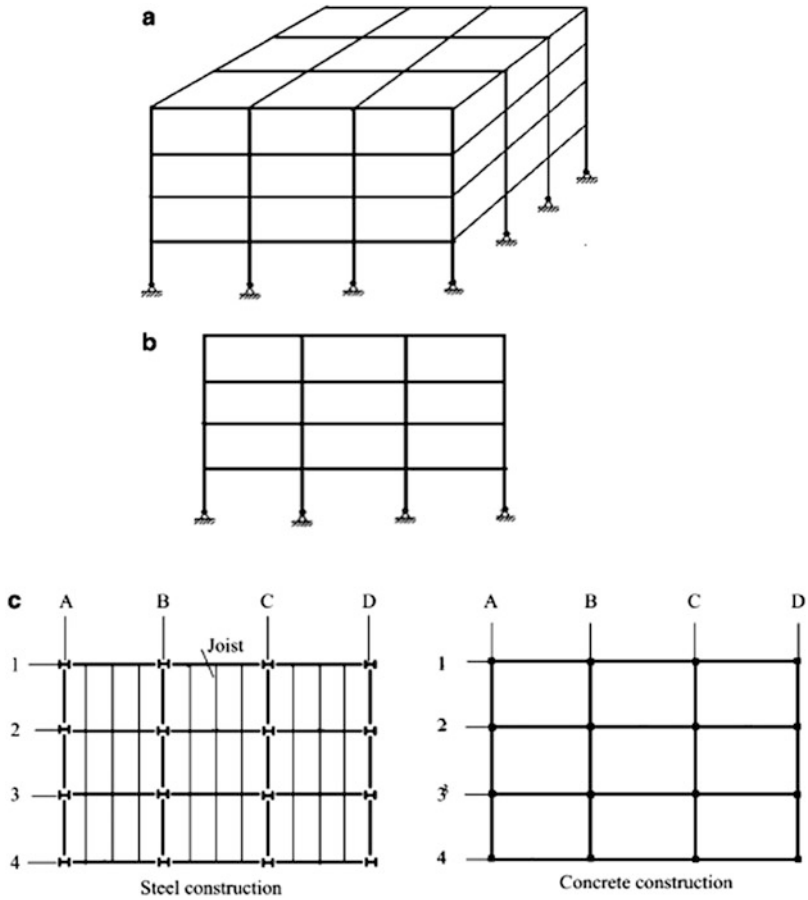
15.1 Loads on Frames

Figure 15.1 shows a multistory building system and Figure 15.2 shows a typical makeup of a rectangular building; the structural system is composed of floor slabs that are supported by frames arranged in an orthogonal pattern. The action of wind and earthquake is represented by concentrated lateral loads applied to the nodes. Gravity loads acting on the floor slabs or roof are transferred to the beams and then to the columns. The nature of these beam loads (uniform, concentrated, triangular, trapezoidal) depends on the makeup of the flooring system. In this chapter, we examine first the mechanism by which the floor loads are transferred to the beams and then describe how to establish the critical loading pattern that produces the peak values of moment in an individual beam. Given the peak moments, one can select appropriate beam cross sections.

Fig. 15.1 Multistory building



Fig. 15.2 Rectangular building. (a) Building frame. (b) Elevation view—individual frame. (c) Typical plan view—flooring system



15.2 Treatment of Gravity Floor Loads

Figure 15.3 shows a rectangular segment of the floor (abcd) bounded by columns at its corners and beams along its sides. In typical concrete construction, the floor slab and beams are framed simultaneously. The floor slab–beam system functions as a rectangular plate supported on all its sides. If the load is transmitted to all the sides, we refer to this behavior as two-way action. When the load tends to be transmitted primarily in one direction, this behavior is called one-way action.

Whether one-way or two-way action occurs depends on the dimensions and makeup of the floor slab. The most common approach is to work with the tributary areas defined in Fig. 15.4. One constructs 45° lines and computes individual areas. The loading on an area is assigned to the adjacent beam. When the members are located in the interior, these areas are doubled to account for the adjacent panels. In general, the areas are either triangular or trapezoidal.

Fig. 15.3 Slab–beam framing scheme—two-way action

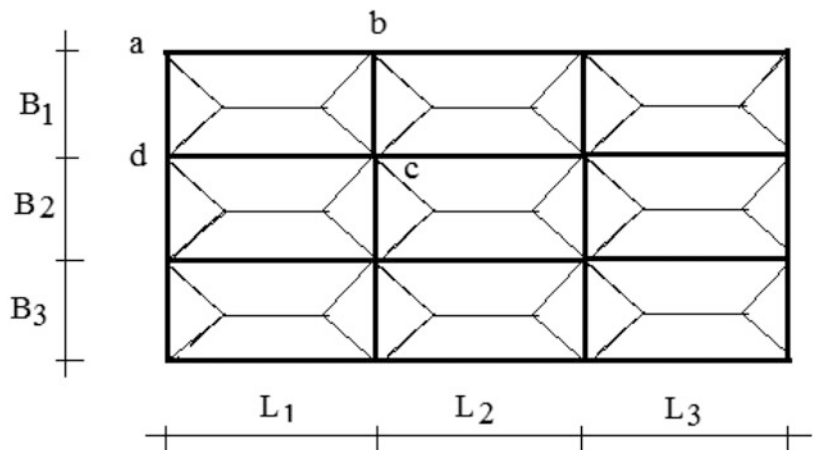


Fig. 15.4 Tributary areas for floor panel abcd

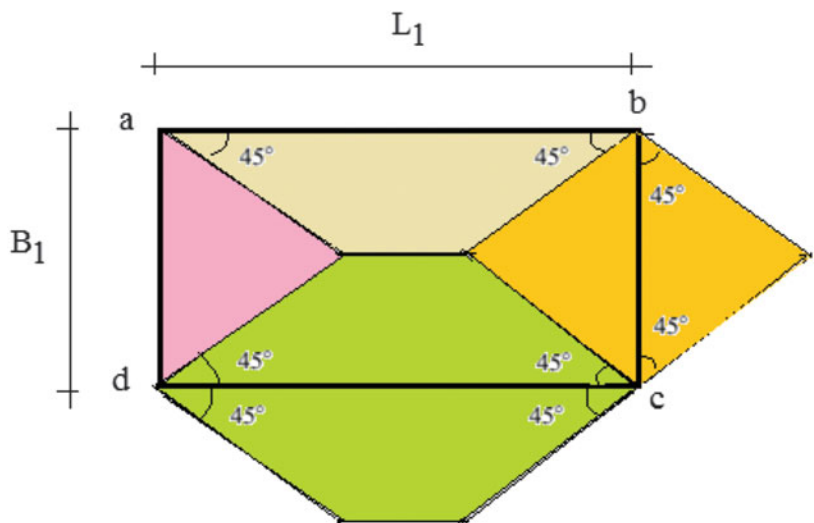
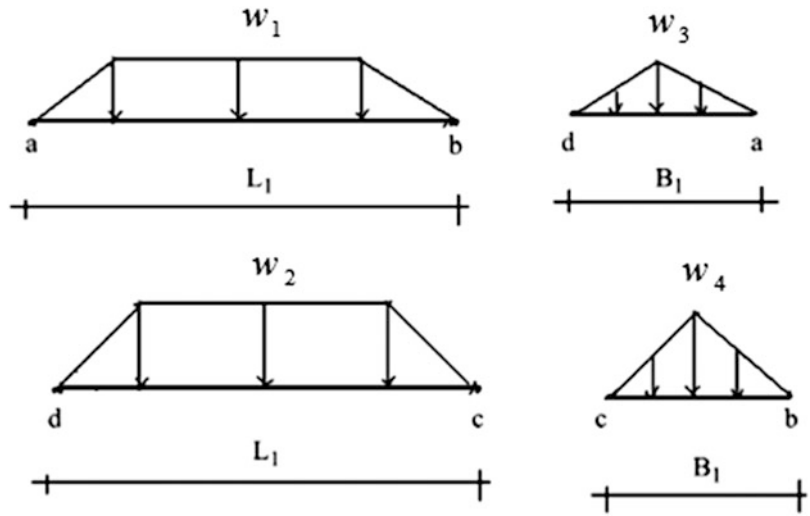


Fig. 15.5 Two-way action perimeter beam loadings for uniform floor loading—panel abcd



The floor loading is represented as a uniform load q (Ib/ft² or N/m²) applied to the floor slab. Using the concept of tributary areas, we convert this loading to a line loading w (Ib/ft or N/m) on the perimeter floor beams. The loading patterns for the beams supporting panel abcd and adjacent panels shown in Fig. 15.5 are listed below.

$$\begin{cases} w_1 = q \left(\frac{B_1}{2} \right) \\ w_2 = q \left(\frac{B_1}{2} + \frac{B_2}{2} \right) \\ w_3 = q \left(\frac{B_1}{2} \right) \\ w_4 = qB_1 \end{cases}$$

When steel members are used, the usual approach is to form the floor by first installing joists, then overlaying steel decking, and lastly casting a thin layer of concrete. Loading applied to the floor is transferred through the decking to the joists and ultimately to the beams supporting the joists. For the geometry shown in Fig. 15.6, beams ab and cd carry essentially all the loads applied to the floor panel abcd. The loads on beams ad and bc are associated with the small tributary areas between them and the adjacent joists. Depending on the joist spacing, the beam loads are represented either as concentrated loads or as a uniformly distributed load. The loading patterns are shown in Fig. 15.7 are listed below.

$$\begin{cases} P_1 = q a_1 \left(\frac{B_1}{2} \right) \\ P_2 = q a_1 \left(\frac{B_1}{2} + \frac{B_2}{2} \right) \\ w_1 = q \left(\frac{B_1}{2} \right) \\ w_2 = q \left(\frac{B_1}{2} + \frac{B_2}{2} \right) \end{cases}$$

Fig. 15.6 Steel joist/beam framing scheme

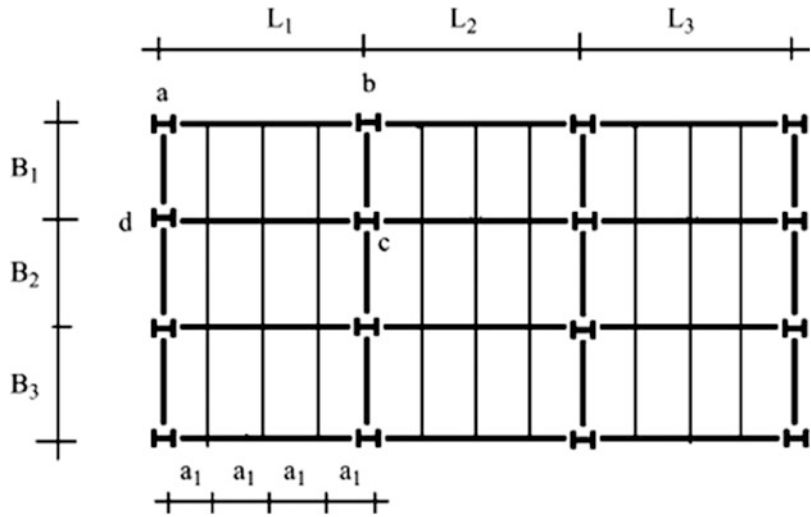
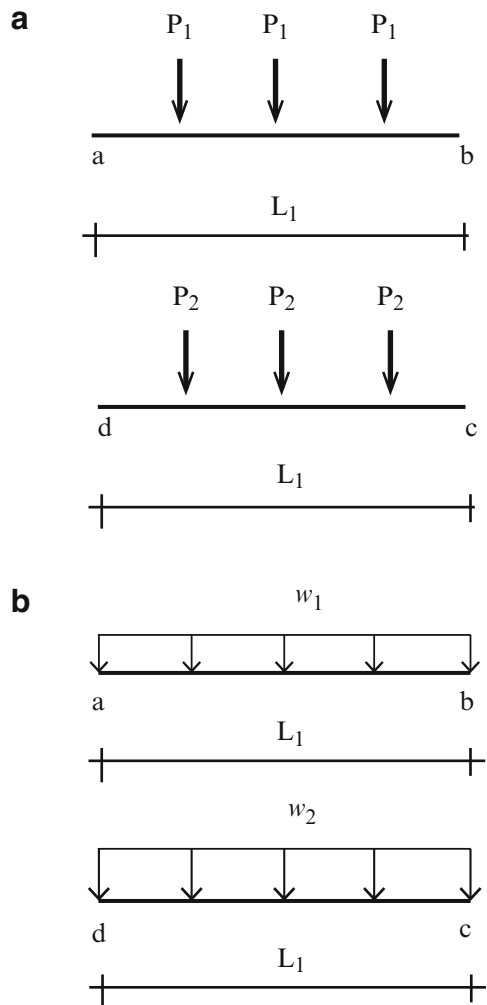


Fig. 15.7 One-way action beam loading for uniform floor loading q . (a) Large joist spacing. (b) Small joist spacing



15.3 Live Load Patterns for Frame Structures

Gravity type loading is usually the dominant loading for low-rise multistory frames. It consists of both dead and live loading. Given a multistory frame, the first step is to establish the critical loading patterns for the individual members. Once the loading patterns are established, one can carry out an approximate analysis to generate peak force values which are used for the initial design. From then on, one iterates on member properties using an exact analysis method. In this section, we describe how Müller-Breslau’s Principle can be employed to establish loading patterns for live gravity loading. We also describe some approximate techniques for estimating the peak positive and negative moments in beams.

Consider the frame shown in Fig. 15.8. We suppose the gravity live loading is a uniformly distributed load, w , that can act on a portion of any member. Our objective here is to determine the loading patterns that produce the maximum positive moment at A and maximum negative moment at B.

To determine the positive moment at A, we insert a moment release at A and apply self-equilibrating couples as indicated in Fig. 15.9. According to the Müller-Breslau Principle, one applies a downward load to those spans where the beam deflection is upward to produce the maximum positive moment at A. The corresponding loading pattern is shown in Fig. 15.10.

Referring back to Fig. 15.8, we establish the loading pattern for the negative moment at B by inserting a moment release at B and applying a negative moment. In this case, there are two possible deflected shapes depending upon whether one assumes the inflection points are in either the columns

Fig. 15.8 Multistory frame example

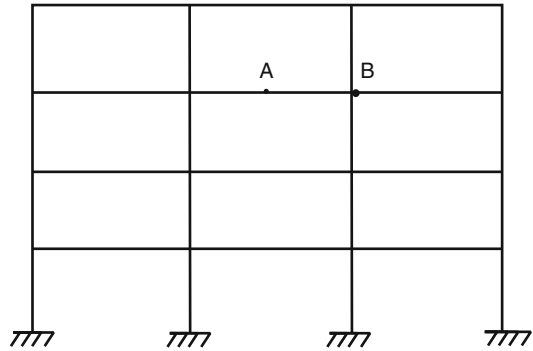


Fig. 15.9 Deflection pattern for positive moment at A

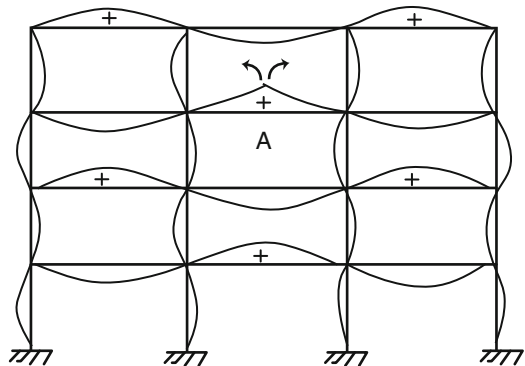


Fig. 15.10 Loading pattern for maximum positive moment at A

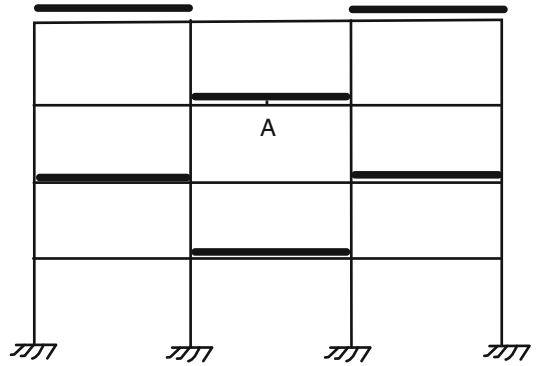


Fig. 15.11 Deflection pattern for negative moment at B—inflection points in beams

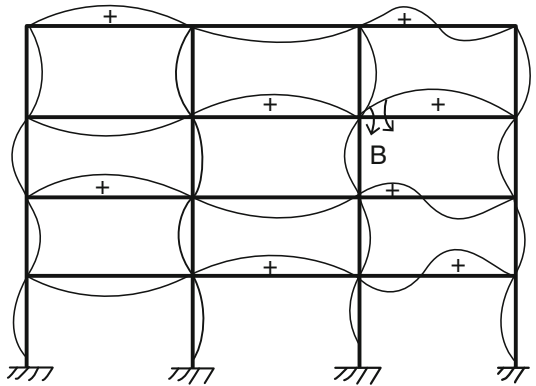
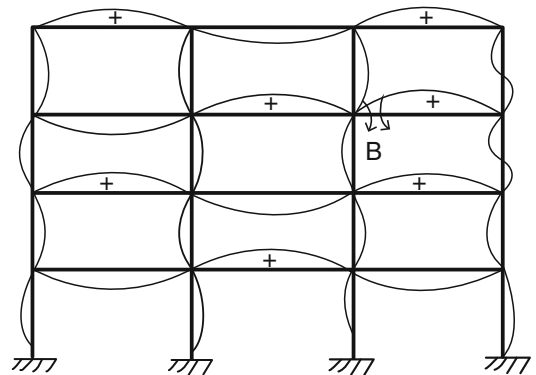
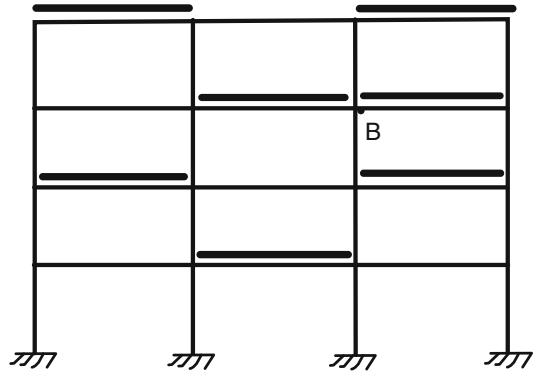


Fig. 15.12 Deflection pattern for negative moment at B—inflection points in columns



or the beams. These shapes are plotted in Figs. 15.11 and 15.12. The exact shape depends on the relative stiffness of the beams and columns which is not known at the preliminary design phase. Although there are cases where there is some ambiguity in the deflected shape, the Müller-Breslau Principle is a very useful tool for generating a qualitative first estimate of the loading pattern (Fig. 15.13). One can refine the estimate later using a structural analysis software system.

Fig. 15.13 Loading pattern for maximum negative moment at B— inflection points in columns



Example 15.1

Given: The rigid steel frame defined in Fig. E15.1a. Assume the member loading is a uniformly distributed live load.

Determine:

- (a) Critical loading patterns for gravity live loading using Müller-Breslau’s Principle that produces the peak value of moments at mid-spans and end points of the beams.
- (b) Use a computer software package to compare the maximum moment corresponding to the critical pattern loading to the results for a uniform loading on all members. Consider all the girders to be the same size and all the columns to be the same size.

Assume $L_1 = 6\text{ m}$, $L_2 = 9\text{ m}$, $h = 4\text{ m}$, $w = 10\text{ kN/m}$, and $I_G = 3.5I_C$

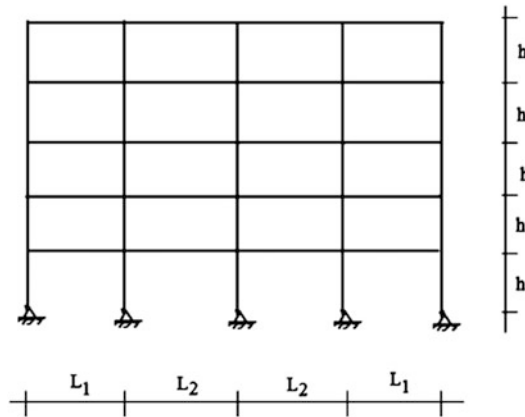


Fig. E15.1a Rigid steel frame

Solution:

Part (a): The process followed to determine the critical loading patterns for bending moment in the beams is described below.

Step 1: Positive Moment at mid-span of the beams.

There are two live load patterns for positive moment at the midpoint of the beams. They are listed in Fig. E15.1b.

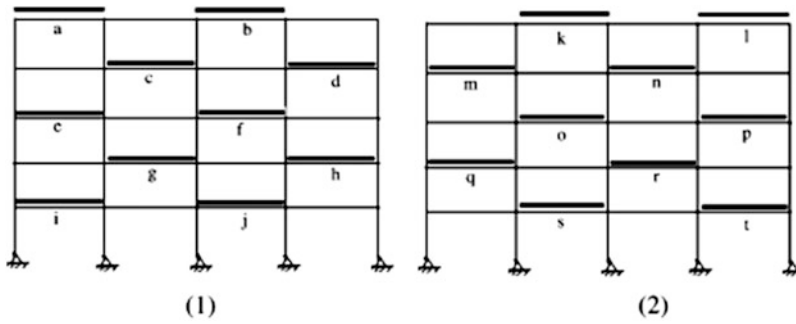


Fig. E15.1b Positive moment loading patterns

Step 2: Negative moment at the end point of the beams

There are 15 patterns of uniform loading for negative moment. Typical patterns are shown in Fig. E15.1c. One carries out analyses for the 15 different loading patterns, and then represents the results by a discrete moment envelope. Figure E15.1d shows the final results.

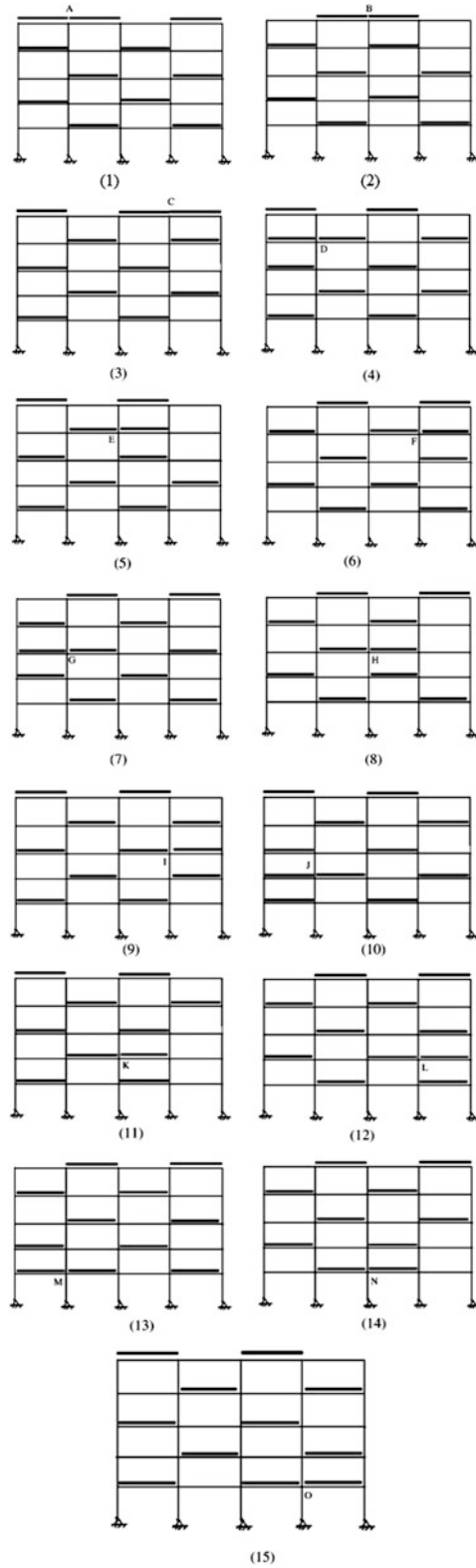


Fig. E15.1c Live load patterns for negative moment

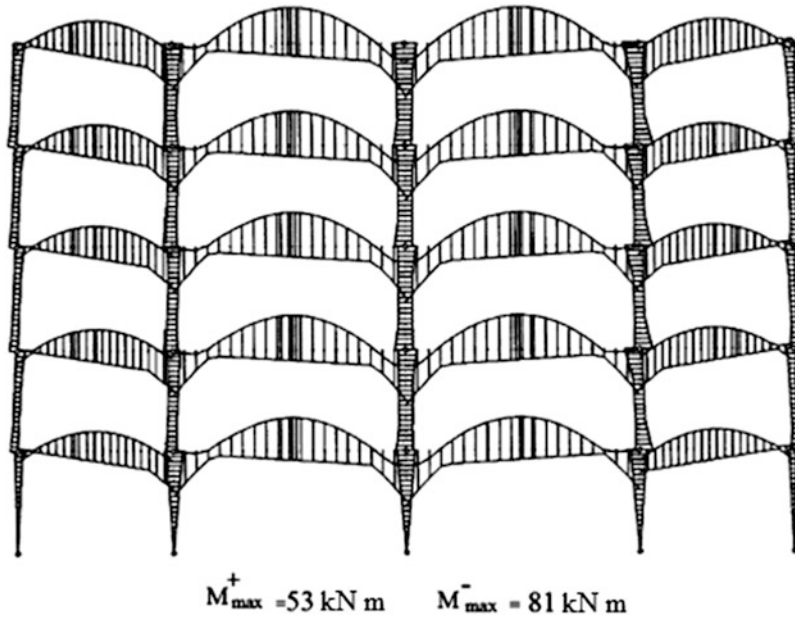


Fig. E15.1d Discrete moment envelope for pattern loading

Part (b): The moment results for uniform loading are plotted in Fig. E15.1e. We note that the uniform loading produces results which underestimate the peak values (30 % for positive moment and 11 % for negative moment). However, since the uniform loading case is easy to implement and provides reasonable results, it frequently is used to generate a first estimate.

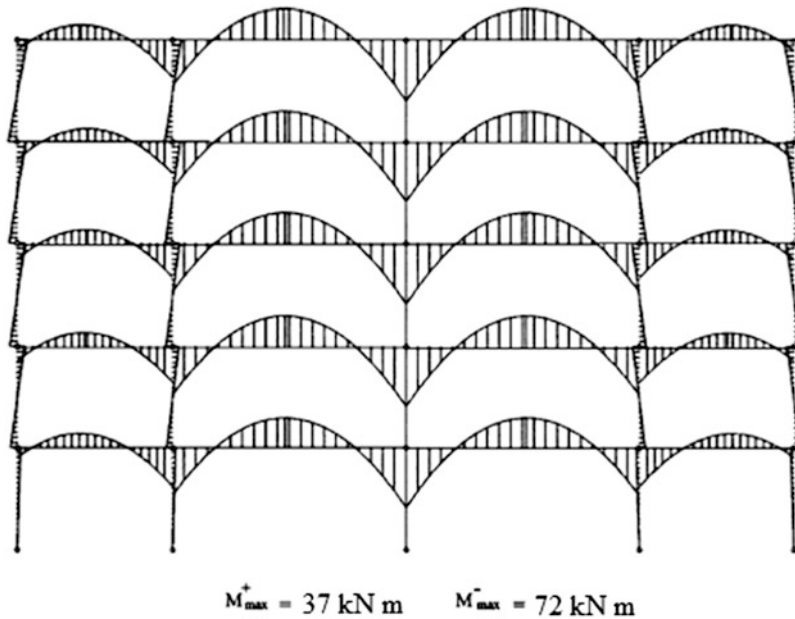


Fig. E15.1e Moment diagram for uniform loading

Example 15.2

Given: The five-story symmetrical rigid frame building shown in Figs. E15.2a, E15.2b, and E15.2c. Assume the building is subjected to uniform gravity dead loading and an earthquake loading in the north–south direction. Consider the floor load to be transmitted to all sides (two-way action). Assume the floors are rigid with respect to lateral motion.

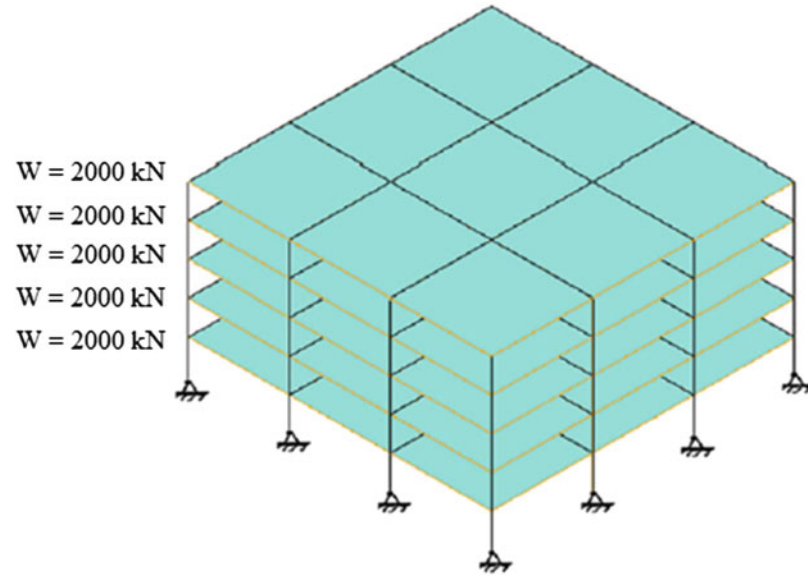


Fig. E15.2a 3D model

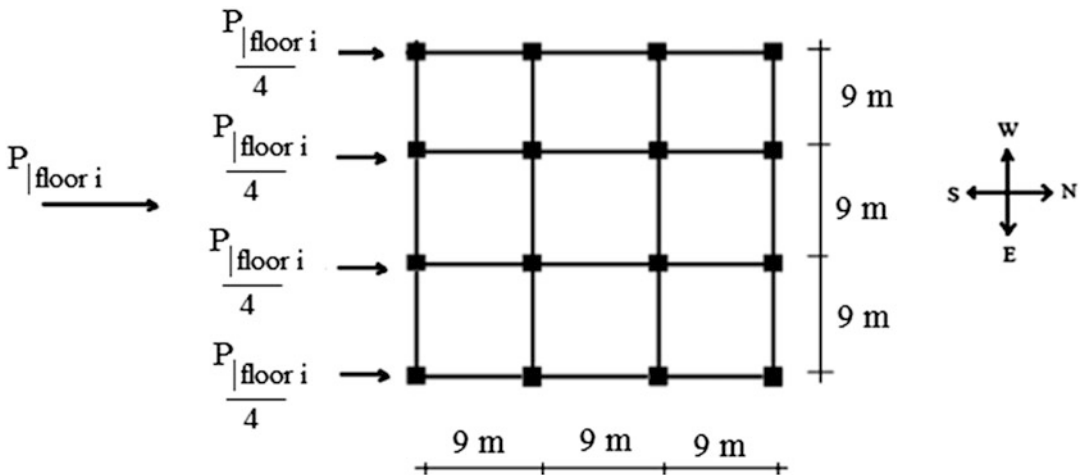


Fig. E15.2b Typical floor plan

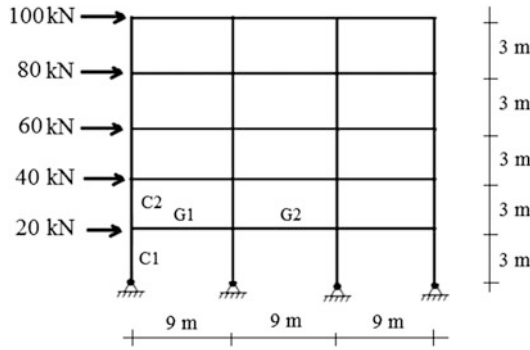


Fig. E15.2c Earthquake in N–S direction—specified floor loads on a typical frame

Determine: The maximum forces in the columns and beams for a typical interior bay and the lateral displacement of the floors using computer software. Assume all the beams to be the same size and all the columns to be the same size.

The corresponding cross-sectional properties are specified for two cases:
 The second case corresponds to doubling the column inertias for case one

$$I \text{ shape beams } \begin{cases} I_z = 445,146,750 \text{ mm}^4 \\ I_y = 22,798,170 \text{ mm}^4 \\ I_x = 1,135,750 \text{ mm}^4 \\ A = 12,320 \text{ mm}^2 \end{cases} \begin{matrix} y \\ | \\ z \end{matrix}$$

$$\text{Hollow square columns } \begin{cases} \text{case (1)} \begin{cases} I_z = I_y = 148,520,925 \text{ mm}^4 \\ I_x = 233,390,025 \text{ mm}^4 \\ A = 10,677 \text{ mm}^2 \end{cases} \\ \text{case (2)} \begin{cases} I_z = I_y = 309,106,575 \text{ mm}^4 \\ I_x = 486,749,250 \text{ mm}^4 \\ A = 15,867 \text{ mm}^2 \end{cases} \end{cases} \begin{matrix} y \\ | \\ z \end{matrix}$$

Solution: The floor loading is uniformly applied to the floor slab. Using the concept of tributary areas, we convert this loading to line loadings w on the perimeter floor beams. Note that the N–S and E–W loading are identical because of the geometry.

$$W_{\text{floor total}} = 2000 \text{ kN}$$

$$\frac{2000}{(27)(27)} = 2.744 \text{ kN/m}^2$$

⇓

$$w_{1\text{gravity}} = 2.744(4.5) = 12.35 \text{ kN/m}$$

$$w_{2\text{gravity}} = 2.744(9) = 24.7 \text{ kN/m}$$

The gravity line loading patterns for the perimeter floor beams are listed below.

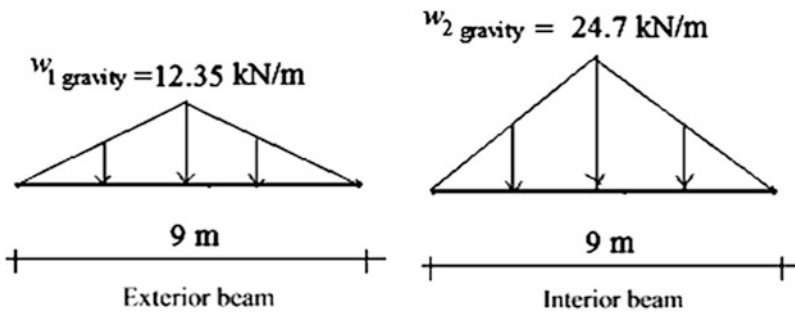


Fig. E15.2d

Using computer software, we analyze a 2D model of the rigid frame for gravity and earthquake loading. This approach is possible because the geometry and stiffness properties are symmetrical.

The critical values for the column forces (axial, shear, moment) occur in the first story. Results for the beams, columns, and lateral displacement corresponding to the two choices for column properties are listed and plotted below.

Column	Gravity	Case(1)	$F_{\max} = 574 \text{ kN}$	Case(2)	$F_{\max} = 567 \text{ kN}$
			$V_{\max} = 36 \text{ kN}$		$V_{\max} = 42 \text{ kN}$
	Earthquake	Case(1)	$M_{\max} = 62 \text{ kN m}$	Case(2)	$M_{\max} = 76 \text{ kN m}$
			$F_{\max} = 130 \text{ kN}$		$F_{\max} = 127 \text{ kN}$
Beam	Gravity	Case(1)	$V_{\max} = 95 \text{ kN}$	Case(2)	$V_{\max} = 99 \text{ kN}$
			$M_{\max} = 252 \text{ kN m}$		$M_{\max} = 258 \text{ kN m}$
	Earthquake	Case(1)	$F_{\max} = 36 \text{ kN}$	Case(2)	$F_{\max} = 42 \text{ kN}$
			$V_{\max} = 61 \text{ kN}$		$V_{\max} = 60 \text{ kN}$
		$M_{\max} = 115 \text{ kN m}$			$M_{\max} = 113 \text{ kN m}$
		$F_{\max} = 82 \text{ kN}$			$F_{\max} = 84 \text{ kN}$
		$V_{\max} = 51 \text{ kN}$			$V_{\max} = 48 \text{ kN}$
		$M_{\max} = 247 \text{ kN m}$			$M_{\max} = 224 \text{ kN m}$

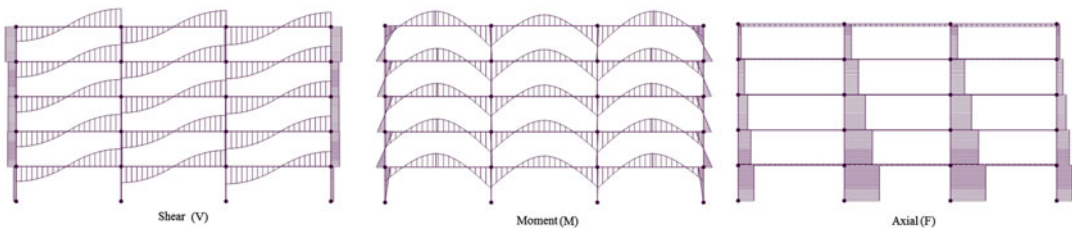


Fig. E15.2e Shear, moment, axial force diagrams—gravity loading

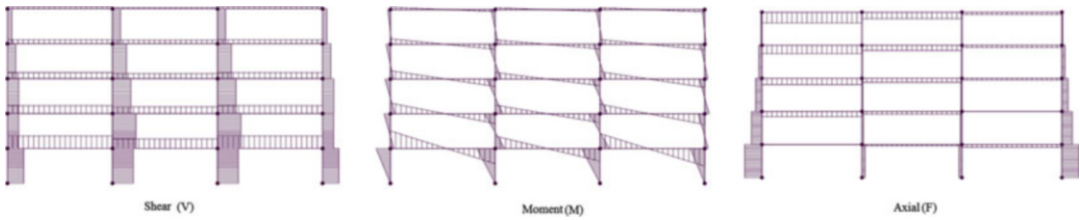


Fig. E15.2f Shear, moment, axial force diagrams—earthquake loading

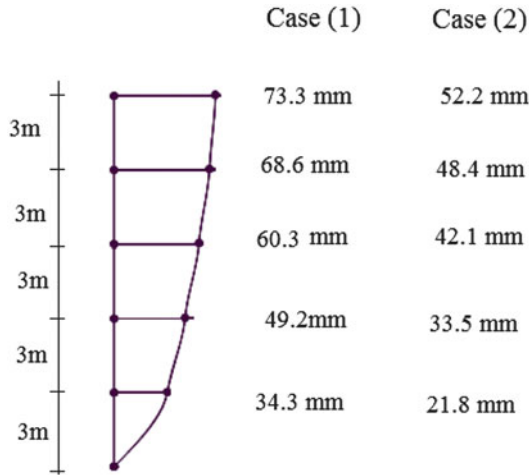


Fig. E15.2g Lateral displacement of the floors—earthquake

Note that there is only a small difference in the force magnitudes when the column inertia values are doubled. The main effect is on the lateral displacement which is to be expected.

15.4 A Case Study: Four-Story Building

In this section, we illustrate the computation of the design parameters for two typical structural systems, a rigid frame and a partially braced frame, having the same loading and geometry. We also use the same code-based procedures to estimate the structural properties. Our objective is to compare the required design parameters which provide an estimate of the relative efficiency of the two systems.

15.4.1 Building Details and Objectives

The building is a four-story steel frame building with a green roof. Figure 15.14 shows the typical floor plan and elevation views. The rigid flooring system transmits the gravity load primarily in the E–W direction to the floor beams oriented in the N–S direction (one-way action).

The loading and member data are as follows:

- Floor dead load = 0.055 kip/ft²
- Floor live load = 0.07 kip/ft²
- Roof dead load = 0.18 kip/ft²

- Roof live load = 0.02 kip/ft²
- Global wind loads acting in the N–S and E–W direction are defined in Fig. 15.15. They correspond to a peak wind speed of 80 mph for a building located in Boston, Massachusetts.
- The weight of exterior walls will be carried by the edge beams.
- Self-weight of exterior walls = 1.1 kip/ft
- Based on economic considerations related to fabrication and construction, the choice of member sizes is restricted to the following:
 - All the roof beams in the N–S direction are the same size.
 - All the floor beams in the N–S direction are the same size.
 - All the floor/roof beams in the E–W direction are the same size.
 - All the columns have the same size.
 - All the braces have the same size.
- The following combinations of loads for strength design are to be considered:

$$w_u = \begin{cases} 1.4w_D \\ 1.2w_D + 1.6w_{L_{\text{floor}}} + 0.5w_{L_{\text{roof}}} \\ 1.2w_D + 0.5w_{L_{\text{floor}}} + 0.5w_{L_{\text{roof}}} + 1.6w_{\text{wind}} \end{cases}$$

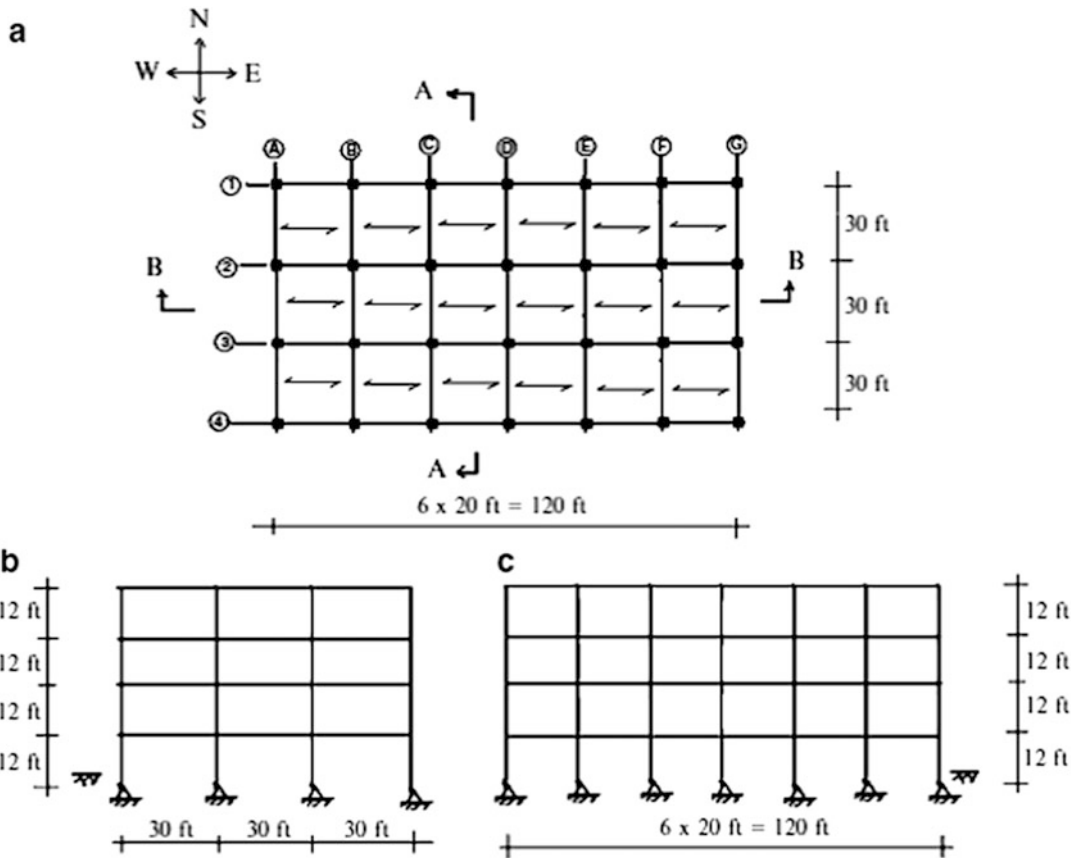


Fig. 15.14 Floor plan and elevation views—case study. (a) Plan. (b) N–S elevation—Section A-A. (c) E–W elevation—Section B-B

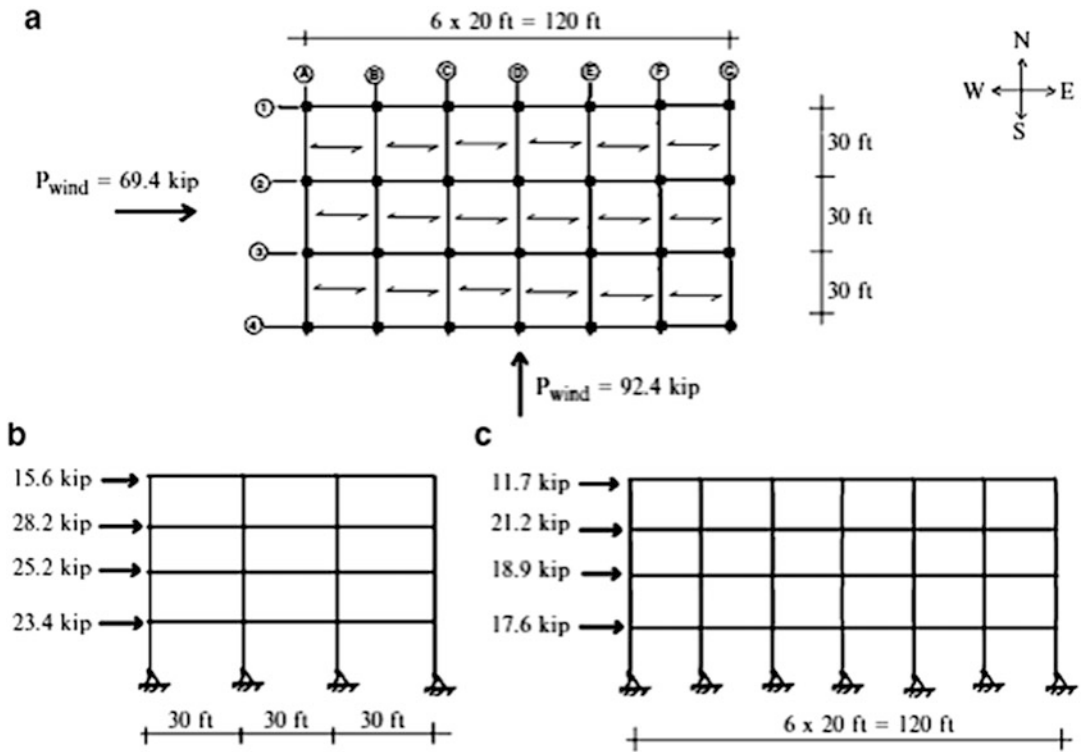


Fig. 15.15 Global Wind loads. (a) Plan. (b) N-S. (c) E-W

- The following limits are required by the serviceability constraint:

$$\text{Limit beam deflection to } \begin{cases} \frac{L_{\text{beam}}}{240} & \text{for (DL + LL)} \\ \frac{L_{\text{beam}}}{360} & \text{for LL} \end{cases}$$

$$\text{Limit building drift to } \frac{H_{\text{building}}}{300}$$

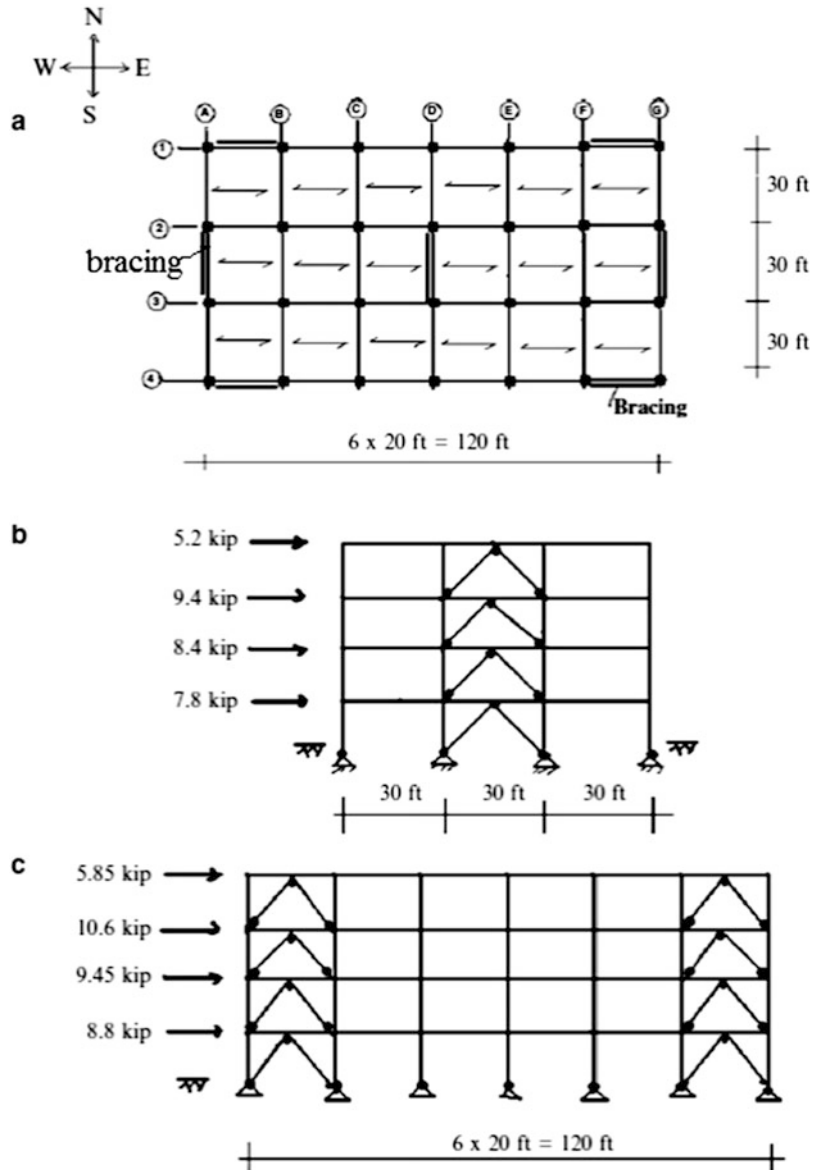
Case (1): The structure is a braced frame, i.e., all the connections between beams and columns are pinned.

Case (2): The structure is a rigid frame in the N-S direction and a braced frame in the E-W direction. All the connections between beams and columns in the N-S direction are moment (rigid) connections; in the E-W direction, they remain pinned.

15.4.2 Case (1) Frames Are Braced in Both N-S and E-W Directions: Computation Details

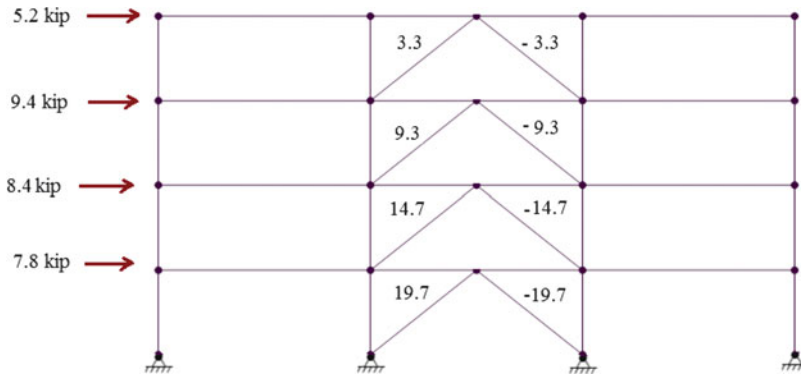
We suppose that since the connections between the beams and the columns are pin connections in both the N-S and E-W directions, the lateral load (wind) is carried by the bracing. The brace layout is governed by architectural considerations. We use the *K* bracing schemes shown in Fig. 15.16.

Fig. 15.16 Braced frame configuration. (a) Plan—braced in both directions. (b) N-S elevation—braced frames A-A, D-D, G-G. (c) E-W elevation braced frames 1-1, 4-4

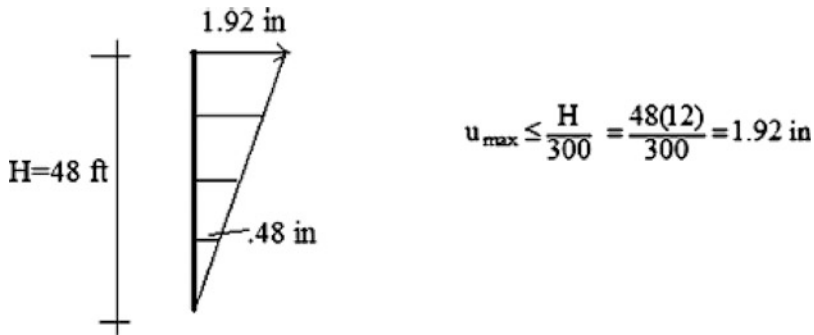


The braces have equal stiffnesses and the floors are rigid. Therefore the global wind load will be distributed equally between braces (see Chap. 14). The column load is purely axial since the members are pinned. We establish the column load per floor working with the tributary floor area associated with the column. The beams are simply supported, and the beam loading is based on one-way action (uniformly loaded).

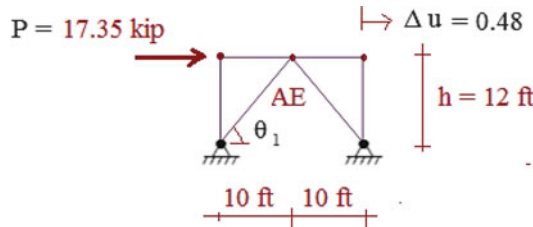
Since all the members are pinned, the total lateral wind load on a floor is carried by the bracing systems. The axial forces in a typical brace are shown on the sketch below. We assume the shear is equally distributed between the diagonals.



The constraint on the maximum lateral deflection at the top floor is $u_{\max} \leq H/300$:



We assume the inter-story displacement is constant for the stories and focus on the first story which has the maximum shear force.



Noting the equations presented in Sect. 11.4.3, we solve for the required area.

$$k_{\text{brace}} = \frac{2AE}{h} (\sin \theta_1 \cos^2 \theta_1)$$

$$P = k_{\text{brace}} \Delta u$$

$$\therefore P = \frac{2AE}{h} (\sin \theta_1 \cos^2 \theta_1) \Delta u \Rightarrow A = \frac{Ph}{2E (\sin \theta_1 \cos^2 \theta_1) \Delta u}$$

leads to

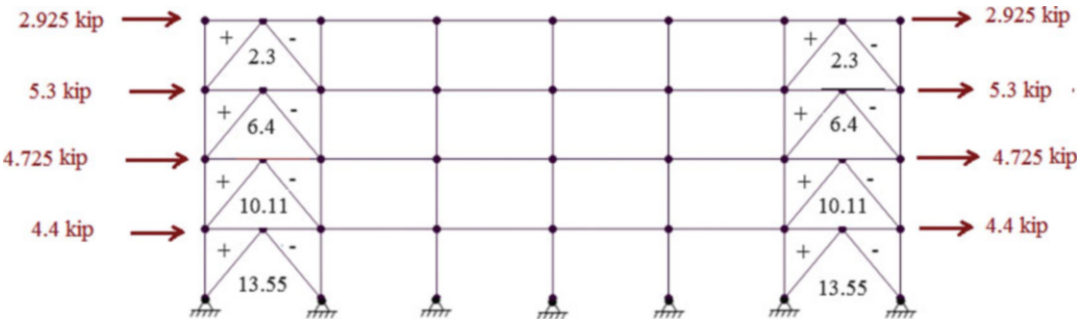
$$A_{\text{required}} = \frac{(30.8)(12 \times 12)}{2(29,000) (\sin(38.66) \cos^2(38.66)) (0.48)} = 0.42 \text{ in.}^2$$

The diagonal elements may be subjected to either tension or compression loading depending on the direction of the wind. The maximum axial force due to wind in the bracing is 19.7 kip. Applying the appropriate load factor, the design value is $P_u = 19.7(1.6) = 31.5$ kip.

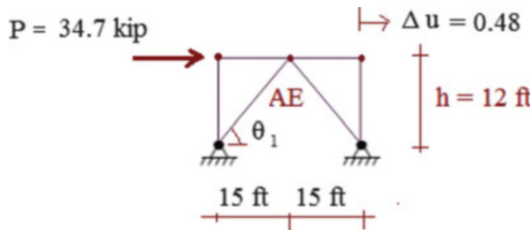
$$\text{NS bracing} \begin{cases} P_{u_{\text{max}}} = 19.7(1.6) = 31.5 \text{ kip} \\ L_{\text{bracing}} = \sqrt{12^2 + 15^2} = 19.2 \text{ ft} \\ \Delta u = 0.48 \text{ in.} \rightarrow A_{\text{req}} = 0.42 \text{ in.}^2 \end{cases}$$

Based on the design axial load $P_u = 31.5$ kip, an effective length of 19.2 ft, and the required area based on the lateral sway of 0.48 in., one selects a cross-sectional area and uses this section for all the brace members in the N–S direction.

We repeat the same type of analysis for the E–W bracing except that now the bracing system is indeterminate. We assume each of the braces carries $\frac{1}{2}$ the lateral load, and estimate the forces in the brace members by hand computations or use computer analysis. The force results are listed below.



The maximum factored axial force in the bracing is $P_u = 13.55(1.6) = 21.7$ kip.



We compute the required brace area following the same approach used for the N–S bracing system. The required area is given by

$$A_{\text{required}} = \frac{(17.35)(12 \times 12)}{2(29,000)(\sin(50.19)\cos^2(50.19))(0.48)} = 0.285 \text{ in.}^2$$

15.4.2.1 Interior Columns

The column load is purely axial since the members are pinned. We establish the column load per floor working with the tributary floor areas for dead and live loads, and the brace forces due to wind. The column on the first floor has the maximum axial force.

The loads in an interior column located in the first story are

$$P_D = 20(30)\{0.18 + .055(3)\} = 207 \text{ kip}$$

$$P_{L_{\text{roof}}} = 20(30)\{0.02\} = 12 \text{ kip}$$

$$P_{L_{\text{floor}}} = 20(30)\{0.07(3)\} = 126 \text{ kip}$$

$$P_{N-S_{\text{Wind}}} = 29.4 \text{ kip}$$

Evaluating the following load combinations

$$P_u = \begin{cases} 1.4P_D = 290 \text{ kip} \\ 1.2P_D + 1.6P_L + 0.5P_{L_r} = 456 \text{ kip} \leftarrow \\ 1.2P_D + 0.5P_L + 0.5P_{L_r} + 1.6P_{\text{Wind}} = 364 \text{ kip} \end{cases}$$

leads to the design value of $P_u = 456 \text{ kip}$. One selects a cross section based on $P_u = 456 \text{ kip}$ and an effective length of 12 ft.

15.4.2.2 Interior Beams

Interior Floor Beams (30 ft span):

$$w_{D_{\text{floor}}} = 0.055(20) = 1.1 \text{ kip/ft} \Rightarrow M_{D_{\text{floor}}} = \frac{w_D L^2}{8} = \frac{1.1(30)^2}{8} = 124 \text{ kip ft}$$

$$w_{L_{\text{floor}}} = 0.07(20) = 1.4 \text{ kip/ft} \Rightarrow M_{L_{\text{floor}}} = \frac{w_L L^2}{8} = \frac{1.4(30)^2}{8} = 157.5 \text{ kip ft}$$

$$w_u = \begin{cases} 1.4w_D = 1.54 \text{ kip/ft} \\ 1.2w_D + 1.6w_L = 3.56 \text{ kip/ft} \leftarrow \end{cases}$$

$$M_u = \frac{w_u L^2}{8} = \frac{3.56(30)^2}{8} = 400.5 \text{ kip ft}$$

$$V_u = \frac{w_u L}{2} = \frac{3.56(30)}{2} = 53.4 \text{ kip}$$

Interior Roof Beams (30 ft span):

$$w_{D_{\text{roof}}} = 0.18(20) = 3.6 \text{ kip/ft} \Rightarrow M_{D_{\text{roof}}} = \frac{w_D L^2}{8} = \frac{3.6(30)^2}{8} = 405 \text{ kip ft}$$

$$w_{L_{\text{roof}}} = 0.02(20) = 0.4 \text{ kip/ft} \Rightarrow M_{L_{\text{roof}}} = \frac{w_L L^2}{8} = \frac{0.4(30)^2}{8} = 45 \text{ kip ft}$$

$$M_{L_{\text{roof}}} = \frac{w_L L^2}{8} = \frac{0.4(30)^2}{8} = 45 \text{ kip ft}$$

$$w_u = \begin{cases} 1.4w_D = 5.04 \text{ kip/ft} \leftarrow \\ 1.2w_D + 1.6w_L = 4.96 \text{ kip/ft} \end{cases}$$

$$M_u = \frac{w_u L^2}{8} = \frac{5.04(30)^2}{8} = 567 \text{ kip ft}$$

$$V_u = \frac{w_u L}{2} = \frac{5.04(30)}{2} = 75.6 \text{ kip}$$

The design is constrained by the deflection at mid-span.

$$\begin{aligned} v_{\text{max}} &= \frac{5wL^4}{384EI} \\ &\leq \frac{L}{240} = \frac{30(12)}{240} = 1.5 \text{ in} \quad \text{for } (w = w_D + w_L) \\ &\leq \frac{L}{360} = \frac{30(12)}{360} = 1.0 \text{ in} \quad \text{for } (w = w_L) \end{aligned}$$

These constraints lead to the following conditions on the required I .

$$\begin{aligned} \text{Floor} &\begin{cases} I_{(D+L)_{\text{req}}} = \frac{5(w_D + w_L)(30)^4(12)^3}{384(29,000)(1.5)} = 418.96(w_D + w_L) = 1,047 \text{ in}^4 \leftarrow \\ I_{L_{\text{req}}} = \frac{5(w_L)(30)^4(12)^3}{384(29,000)(1.0)} = 628.45(w_L) = 880 \text{ in}^4 \end{cases} \\ \text{Roof} &\begin{cases} I_{(D+L)_{\text{req}}} = 418.96(3.6 + 0.4) = 1,676 \text{ in}^4 \leftarrow \\ I_{L_{\text{req}}} = 628.45(0.4) = 251 \text{ in}^4 \end{cases} \end{aligned}$$

15.4.2.3 Summary for Case (1)

The relevant design parameters for the braced frame are listed below.

N-S roof beams	$M_u = 567 \text{ kip ft}$	$I_{\text{req}} = 1676 \text{ in}^4$
N-S floor beams	$M_u = 400 \text{ kip ft}$	$I_{\text{req}} = 1047 \text{ in}^4$
E-W beams	$M_u = 77 \text{ kip ft}$	$I_{\text{req}} = 137 \text{ in}^4$
Columns	$P_u = 456 \text{ kip}$	
E-W braces	$P_u = 21.7 \text{ kip}$	$A_{\text{req}} = .285 \text{ in}^2$
N-S braces	$P_u = 31.5 \text{ kip}$	$A_{\text{req}} = .42 \text{ in}^2 \text{e}$

15.4.3 Case (2) Frames Are Rigid in the N-S Direction But Remain Braced in the E-W Direction

Figure 15.17a shows a plan view of this structural scheme. Our objective here is to generate the response of an individual rigid frame and to compare the design values for the braced vs. rigid frame structural concepts.

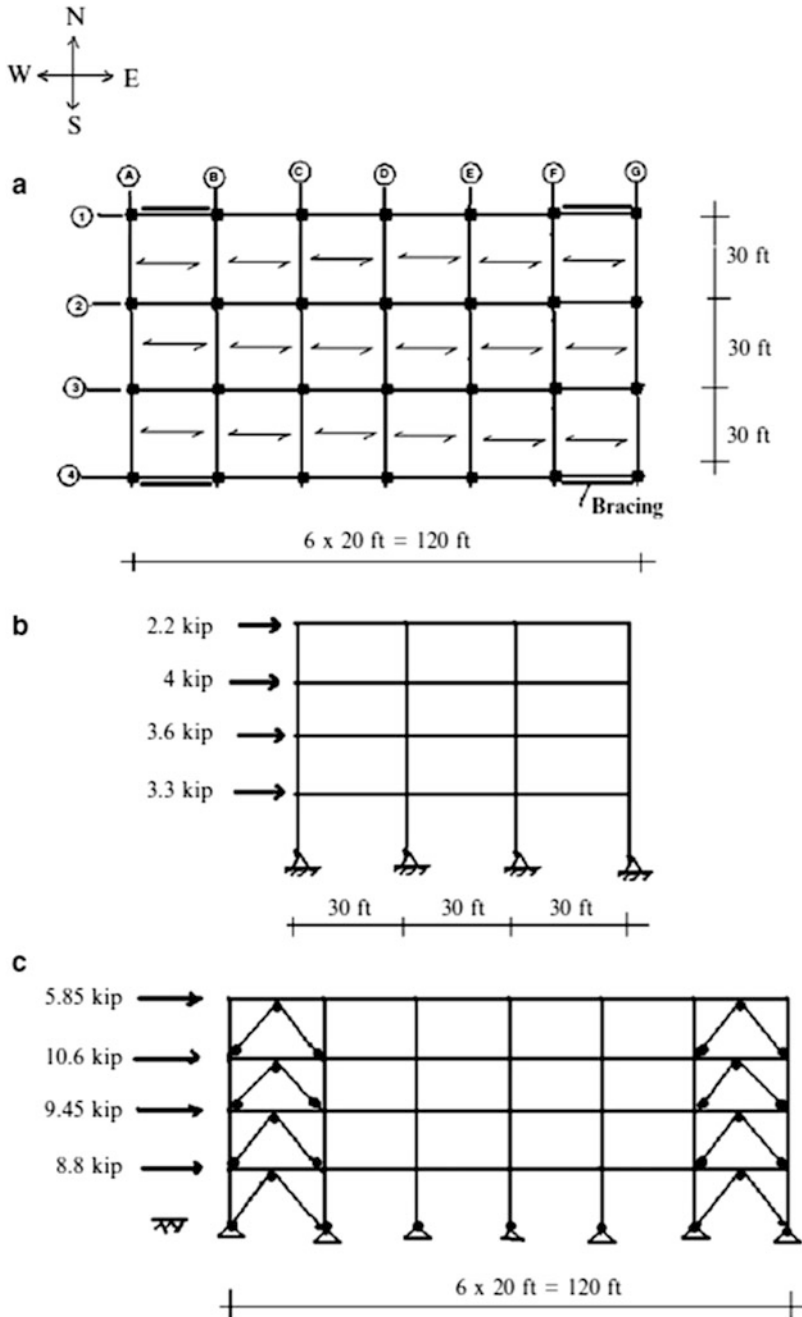
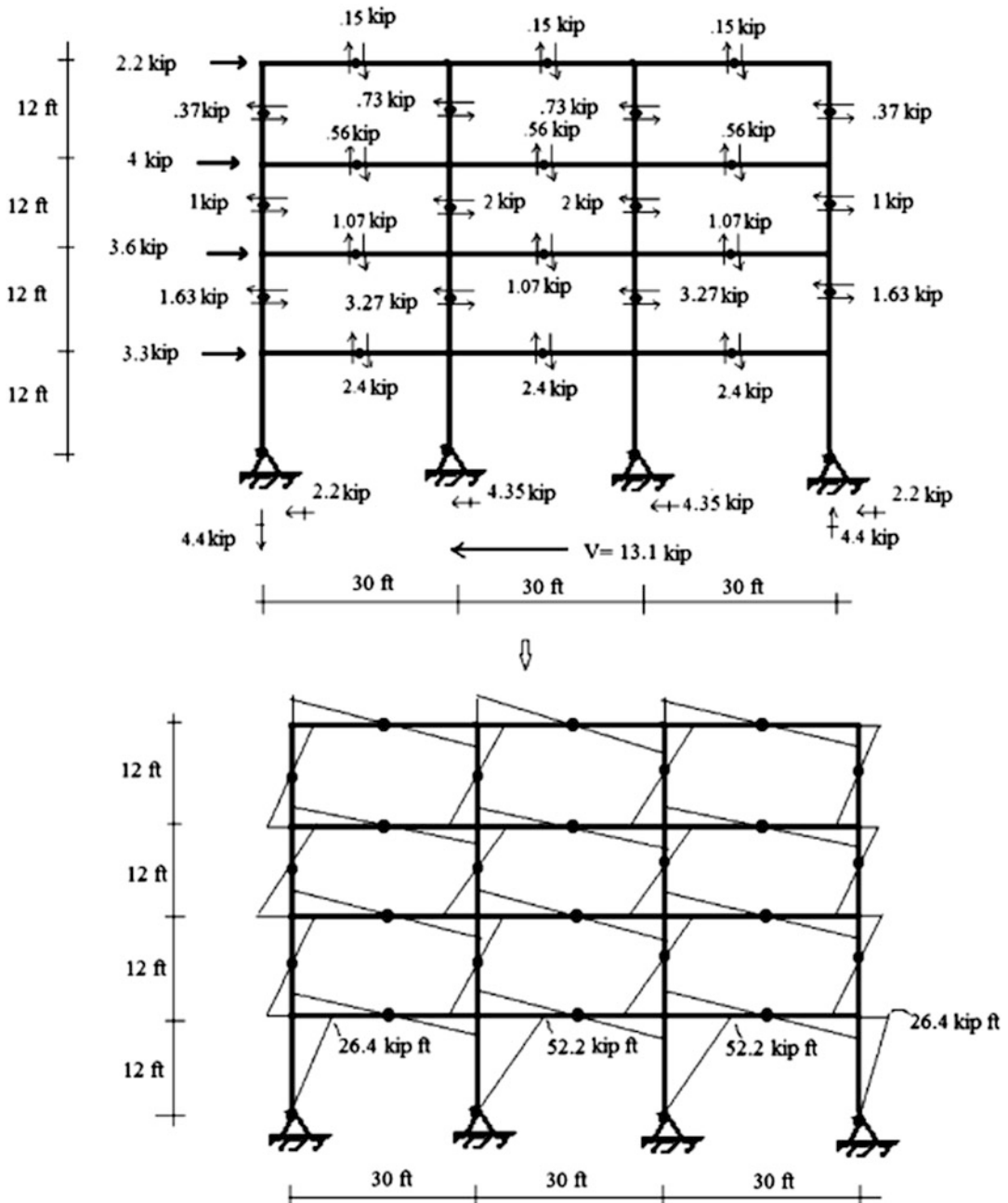


Fig. 15.17 Rigid frame N-S, braced frame E-W. (a) Plan. (b) Typical rigid frame elevation—N-S; wind loading. (c) E-W elevation braced frames 1-1, 4-4; wind loading

15.4.3.1 Strategy for N-S Beams and Columns

We specify moment connections between the beams and the columns in the N-S direction and assume that the lateral wind load will be carried equally by the seven rigid frames, because the floor slabs are rigid and the rigid frames have equal stiffnesses. The E-W direction remains the same as the beams in this direction are pin ended. Since the beams in the N-S direction are now rigidly connected to the columns, end moments will be developed in the beams. *The net effect is a reduction in the maximum moment in the beams.* For a first estimate, assuming full fixity, the peak moment reduces from $wL^2/8$ to $wL^2/12$, a reduction of 33 %. It follows that the beams will be *lighter*; however, the columns will be *heavier* since they now must be designed for both axial force and moment.

Wind loading introduces end moments in the beams and columns. We use the portal method (see Chap. 11) to estimate these values. The results are shown on the sketch below.



15.4.3.2 Estimated Properties: Beams

We estimate the design moment for roof and floor beams based on the following combination of factored moments:

Roof:

$$M_u^- \approx \begin{cases} 1.4 \frac{w_D L^2}{12} = 378 \text{ kip ft} \leftarrow \\ (1.2w_D + 1.6w_L) \frac{L^2}{12} = 372 \text{ kip ft} \\ (1.2w_D + 0.5w_L) \frac{L^2}{12} + 1.6M_{wind} = 343 \text{ kip ft} \end{cases}$$

Floor:

$$M_u^- \approx \begin{cases} 1.4 \frac{w_D L^2}{12} = 115.5 \text{ kip ft} \\ (1.2w_D + 1.6w_L) \frac{L^2}{12} = 267 \text{ kip ft} \leftarrow \\ (1.2w_D + 0.5w_L) \frac{L^2}{12} + 1.6M_{wind} = 209 \text{ kip ft} \end{cases}$$

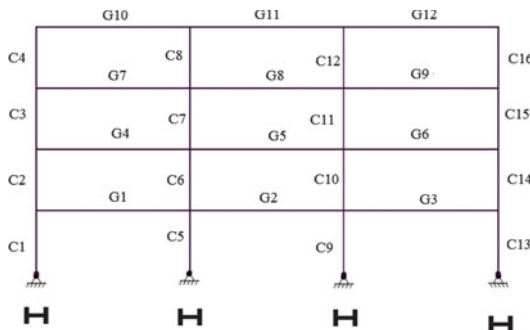
As a first estimate, we use tributary areas to estimate the axial load in the columns due to dead and live loads. The most critical load combinations for the columns are

$$\begin{cases} P_u = 1.2P_D + 1.6P_{wind} + 0.5P_{L_{floors}} + 0.5P_{L_{roof}} \approx 317 \text{ kip} \\ M_u \approx 1.6M_{wind} \approx 1.6(52.2) \approx 84 \text{ kip ft} \\ P_u = 1.2P_D + 1.6P_{L_{floors}} + 0.5P_{L_{roof}} \approx 461 \text{ kip} \\ M_u \approx 10 \text{ kip ft} \end{cases}$$

Based on the above estimated force values, we select the following cross-sectional properties.

$$\begin{cases} I_{col} = 272 \text{ in.}^4 & A_{col} = 14.4 \text{ in.}^2 \\ I_{beam/floor} = 1070 \text{ in.}^4 & A_{beam/floor} = 19.1 \text{ in.}^2 \\ I_{beam/roof} = 1830 \text{ in.}^4 & A_{beam/roof} = 24.3 \text{ in.}^2 \end{cases}$$

Determining the actual properties is an iterative process. We expect the beam sizes to decrease, and the column size to increase as the iteration proceeds due to the shift from braced frame to rigid frame. We orient the cross sections such that the bending occurs about the strong axis as indicated on the sketch below.



15.4.3.3 Live Load Patterns

We determine the live load patterns for the maximum positive and negative moments for the beams and for the maximum axial force for columns and then analyze the model under the combined dead, live, and wind loads. The wind loads are defined in Fig. 15.17b. Figure 15.18 shows live load patterns for maximum moments in beams, and axial force in columns.

Live Load Patterns for Positive Moment—Beams:

There are two load patterns for maximum positive moment at mid-span of the beams.

Negative Moment Live Load Patterns—Beams:

There are eight loading patterns for maximum negative end moments of the beams.

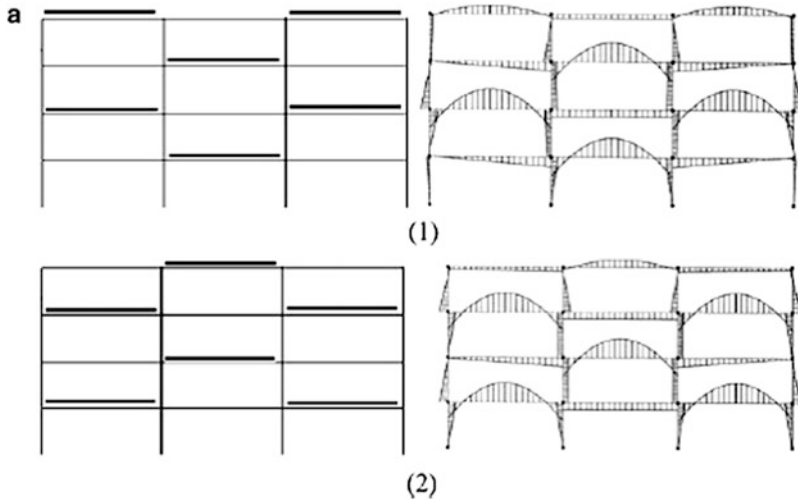


Fig. 15.18 (a) Positive live load (LL) moment patterns (1)–(2). (b) Negative live load (LL) moment patterns (3)–(10). (c) Live load patterns for axial force in column (11)–(12)

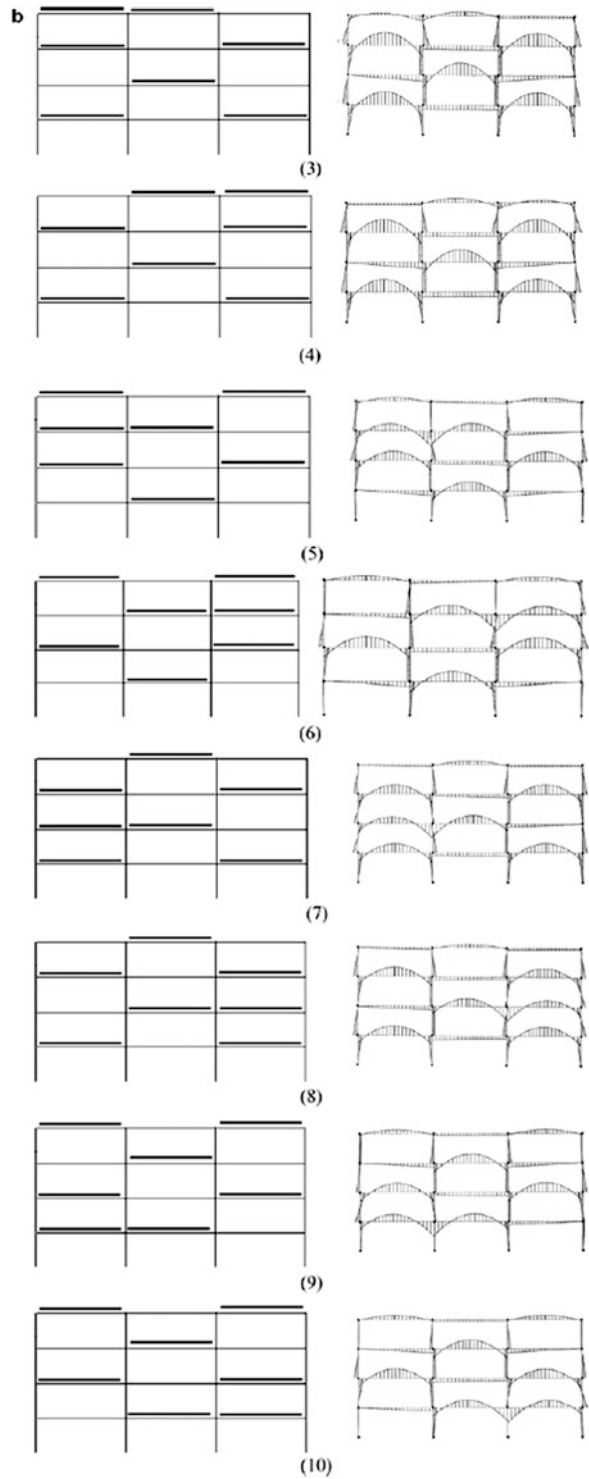


Fig. 15.18 (continued)

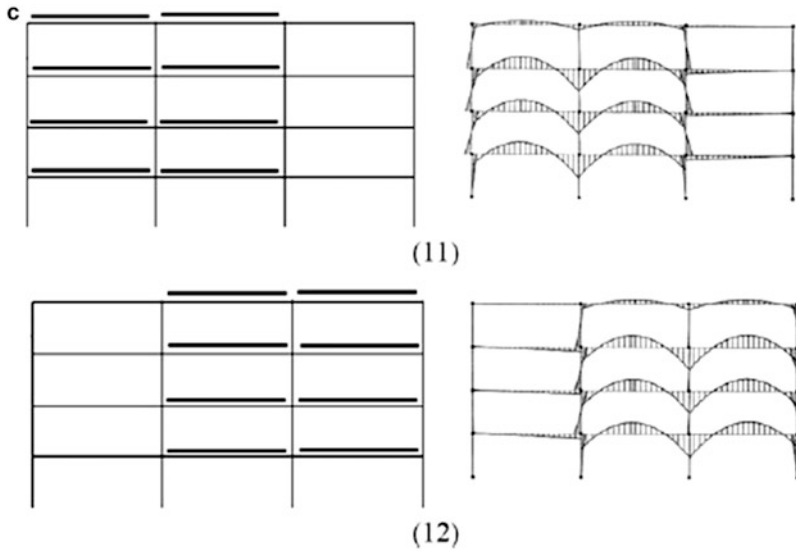


Fig. 15.18 (continued)

Axial Force Live Load Patterns—Columns:

The following two load patterns establish the peak values of the column axial forces.

15.4.3.4 Discrete Moment Envelop Plot-Live Load

Using a computer software system, results of the analyses for the ten live load patterns defined in Fig. 15.18a, b are used to construct the discrete moment envelope plots shown in Fig. 15.19. These plots show the *peak positive and negative moments at various sections along the spans* generated by the ten different loading patterns. The absolute peak values are summarized in Fig. 15.20.

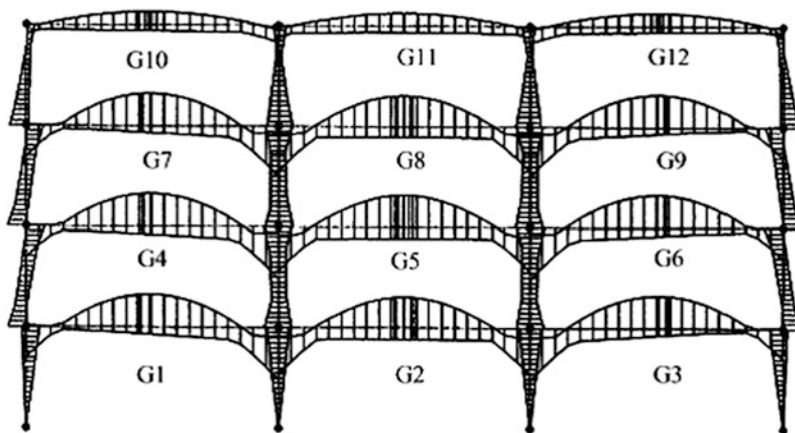
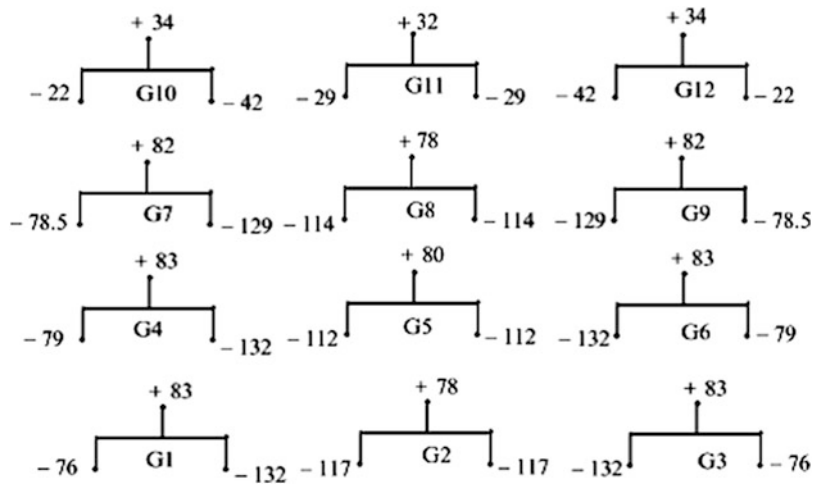


Fig. 15.19 Peak positive and negative discrete moment envelopes due to pattern live loading

Fig. 15.20 Absolute maximum positive and negative moments in the beams due to pattern live loading (kip ft)



The factored discrete envelopes are plotted in Fig. 15.21. Using this updated information, we determine revised values for the cross-sectional

$$\begin{cases} I_{col} = 341 \text{ in.}^4 & A_{col} = 17.7 \text{ in.}^2 \\ I_{beam/floor} = 890 \text{ in.}^4 & A_{beam/floor} = 16.2 \text{ in.}^2 \\ I_{beam/roof} = 1140 \text{ in.}^4 & A_{beam/roof} = 16.2 \text{ in.}^2 \end{cases}$$

Lastly, using these properties, we generate updated values for the design moments shown in Fig. 15.22.

Since the columns are subjected to both axial action and bending, we need to scan the results for the individual loadings and identify the loadings that produce the maximum axial force and the maximum moment in the columns. Carrying out this operation, we identify the combinations for columns C1 and C5 listed in Fig. 15.23.

Given these design values, one generates new estimates for the cross-sectional properties. If these new estimates differ significantly from the original estimates, the analysis needs to be repeated since the results are based on the relative stiffness of the beams and columns. It turns out for this study that the initial estimates are sufficiently accurate.

15.4.3.5 Summary for Case (2)

N-S roof beams	$M_u = 442 \text{ kip ft}$
N-S floor beams	$M_u = 336 \text{ kip ft}$
E-W beams	same as case(1)
Columns	$\begin{cases} P_u = 490 \text{ kip} \\ M_u = 10 \text{ kip ft} \end{cases}$ or $\begin{cases} P_u = 306 \text{ kip} \\ M_u = 111 \text{ kip ft} \end{cases}$
E-W braces	same as case(1)

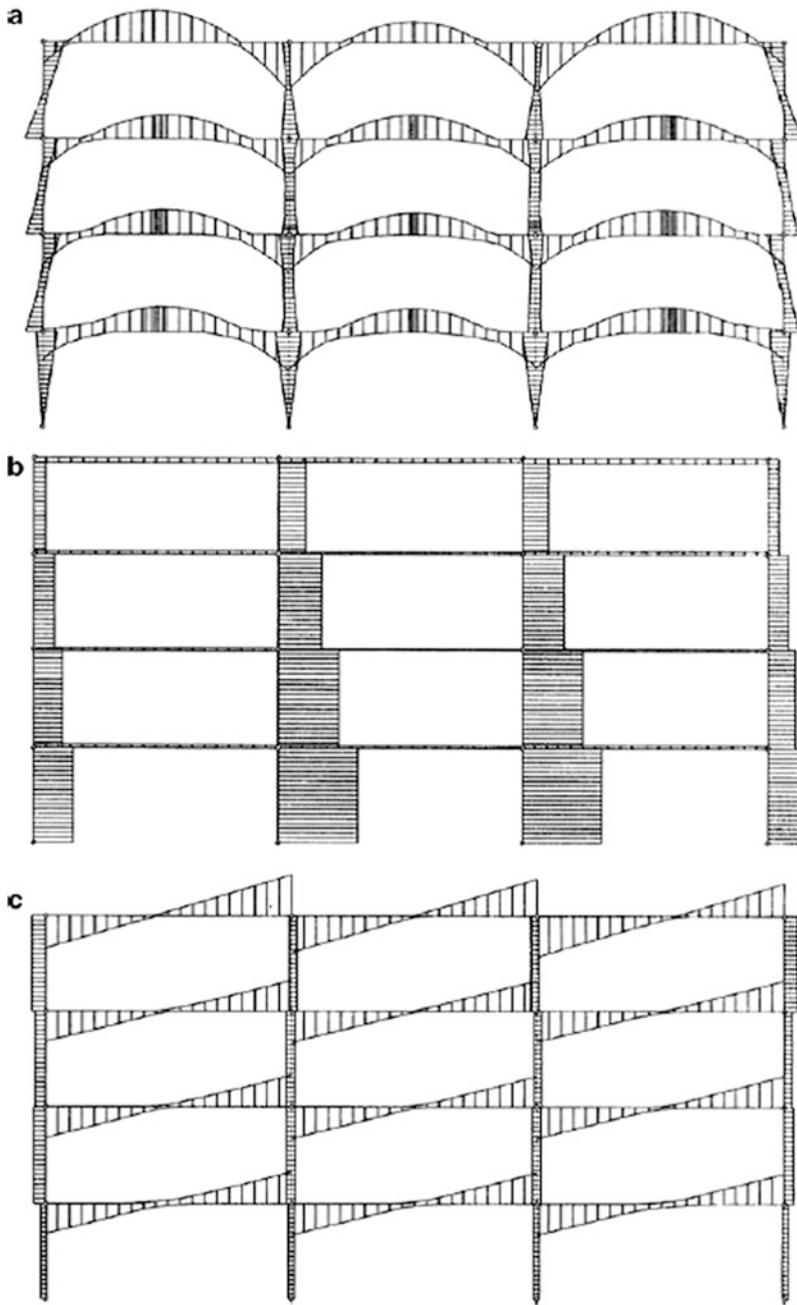


Fig. 15.21 (a) Discrete moment envelope–factored load combination. (b) Discrete axial force envelope–factored load combination. (c) Discrete shear envelope–factored load combination

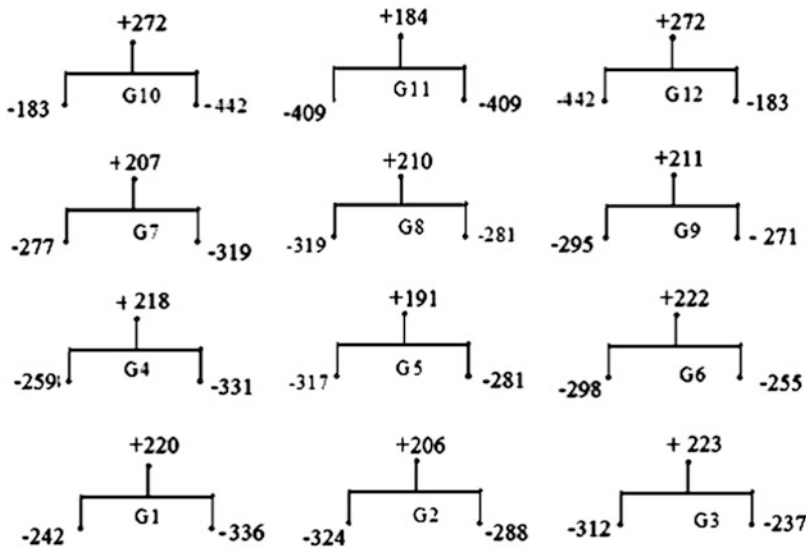
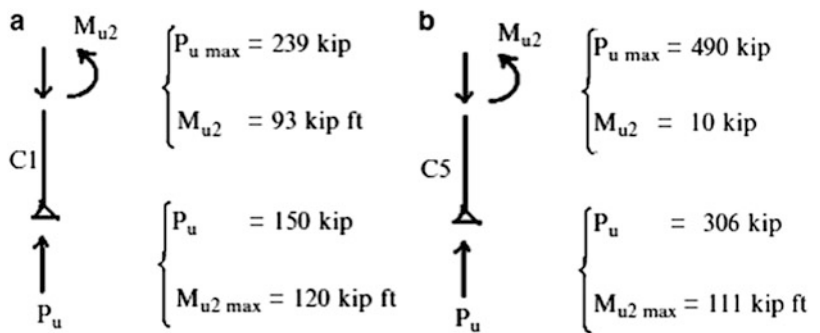


Fig. 15.22 Maximum and minimum design moments (kip ft)

Fig. 15.23 Critical axial load–moment combinations for Columns C1 and C5. (a) Exterior column. (b) Interior column



15.4.4 Discussion

The following table contains the design values corresponding to the two cases.

	Case (1) Braced	Case(2) Rigid in N–S direction
N–S roof beam	$M_u = 567 \text{ kip ft}$	$M_u = 442 \text{ kip ft}$
N–S floor beam	$M_u = 400 \text{ kip ft}$	$M_u = 336 \text{ kip ft}$
E–W beams	$M_u = 77 \text{ kip ft}$	$M_u = 77 \text{ kip ft}$
Columns	$P_u = 456 \text{ kip}$	$\begin{cases} P_u = 490 \text{ kip} \\ M_u = 10 \text{ kip ft} \end{cases}$ or $\begin{cases} P_u = 306 \text{ kip} \\ M_u = 111 \text{ kip ft} \end{cases}$
E–W beams	$P_u = 24 \text{ kip}$	$P_u = 24 \text{ kip}$
N–S beams	$P_u = 31.5 \text{ kip}$	Not required

Comparing values, we see that the N–S rigid frame structure is more efficient in the sense that its design values are less, and therefore the required cross-sections are lighter. However, the lateral displacements will be greater.

15.5 Summary

15.5.1 Objectives

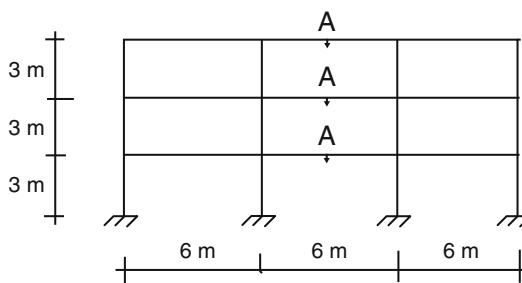
- To describe how gravity floor loading is transformed into distributed loading acting on the supporting beams.
- To show how Müller-Breslau principle can be applied to establish critical patterns of live gravity loading for the peak bending moments in rigid frames.
- To present a case study which integrates all the different procedures for dealing with dead, live, wind, and earthquake loads.

15.5.2 Key Concepts

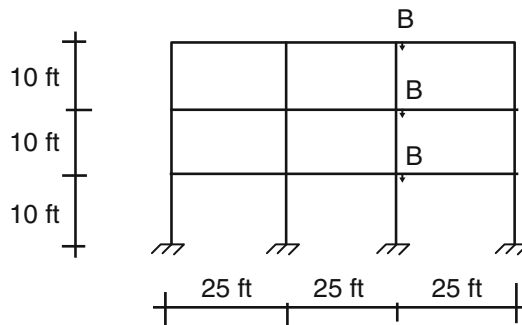
- The floor slabs in concrete buildings are cast simultaneously with the supporting beams. The type of construction provides two possible load paths for gravity loads. Which path dominates depends on the relative magnitude of the side dimensions. The terms one-way and two-way actions are limiting cases where (1) one side is large with respect to the other side and (2) the sides are of the same order of magnitude.
- Gravity loading produces only positive moment in the beams of a braced frame.
- Positive moment at mid-span in the beams of a rigid frame is due only to gravity loading.
- Negative moment in the beams of a rigid frame is generated by both gravity and lateral loads.

15.6 Problems

Problem 15.1

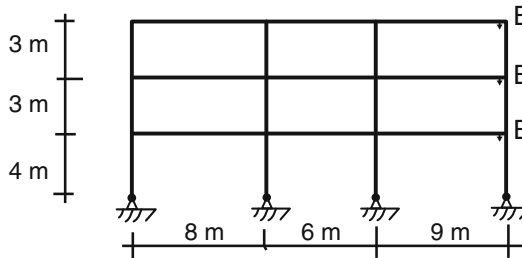


Using Müller-Breslau Principle, determine the loading patterns (uniformly distributed member load) that produce the peak values of positive moment at point A (mid-span) for each story.

Problem 15.2

Using Müller-Breslau Principle, estimate the loading patterns (uniformly distributed member load) that produce the peak value of negative moment at B for each story. Check the results using a software package. Take $I_c = 150 \text{ in.}^4$ for all the columns and $I_g = 300 \text{ in.}^4$ for all the beams.

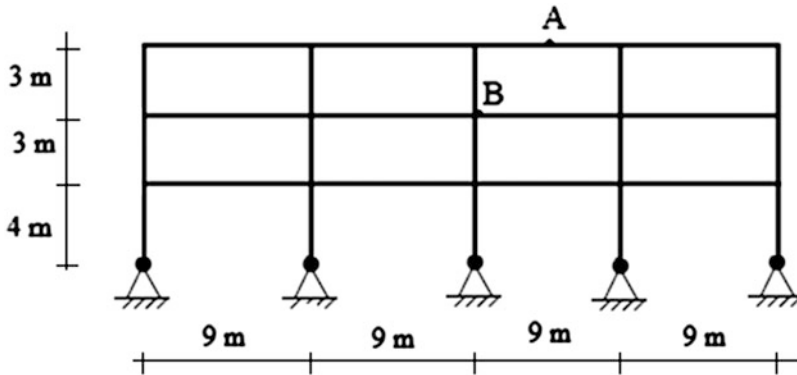
Problem 15.3 Using Müller-Breslau Principle, estimate the loading patterns (uniformly distributed member load) that produce the peak value of negative moment at B for each story. Check the results using a software package. Take $I_b = 300(10)^6 \text{ mm}^4$ for all the beams and $I_c = 100(10)^6 \text{ mm}^4$ for all the columns.



Problem 15.4 For the frame shown below

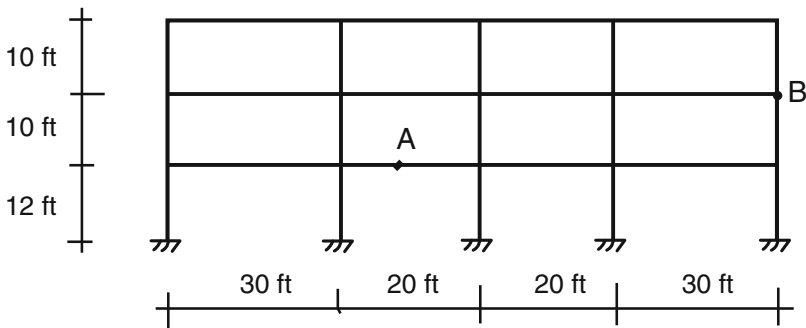
- (a) Using Müller-Breslau Principle, sketch the influence lines for the positive moment at A and the negative moment at B.

- (b) Use a software package to determine the maximum values of these quantities due to a uniformly distributed live load of 30 kN/m and a uniformly distributed dead load of 20 kN/m. Take $I_c = 100(10)^6 \text{ mm}^4$ for all the columns and $I_b = 200(10)^6 \text{ mm}^4$ for all the beams.

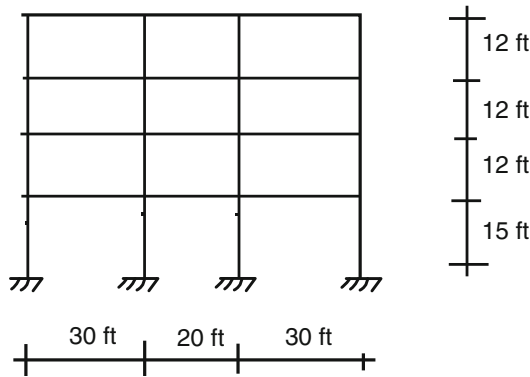


Problem 15.5 For the frame shown below

- (a) Using Müller-Breslau Principle, sketch the influence lines for the positive moment at A and the negative moment at B.
- (b) Use a software package to determine the maximum values of these quantities due to a uniformly distributed live load of 1.8 kip/ft and a uniformly distributed dead load of 1.2 kip/ft. Take $I_c = 480 \text{ in.}^4$ for all the columns and $I_b = 600 \text{ in.}^4$ for all the beams.



Problem 15.6

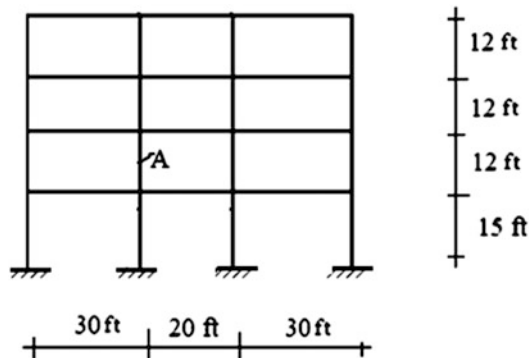


Consider the typical frame defined above. Assume the bay spacing is 20 ft.

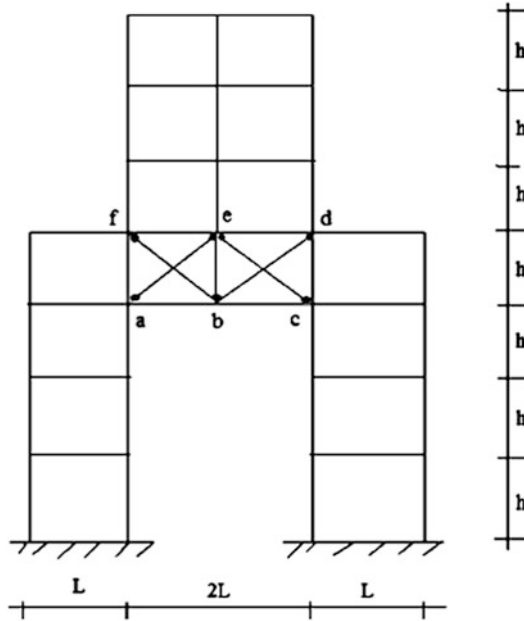
- (a) Determine the floor loads per bay due to an earthquake of intensity $S_a = 0.3g$. Assume the following dead weights. Roof load = 0.08 kip/ft² and floor load = 0.06 kip/ft².
- (b) Estimate the column shear forces due to this earthquake.
- (c) Estimate the column shear forces due to both gravity and earthquake.

Problem 15.7 Consider the frame shown below. Assume a uniform gravity live loading for the beams.

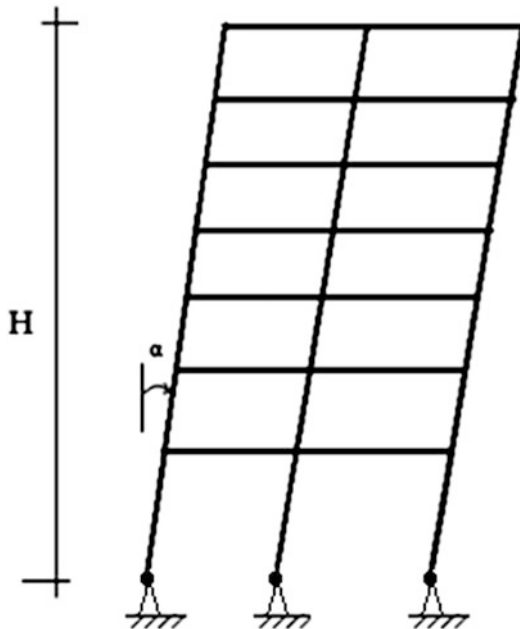
- (a) Describe how you would apply Müller-Breslau Principle to establish the loading pattern for the compressive axial load in column A.
- (b) Compare the axial load in column A of the pattern loading to the uniform loading on all members. Consider all the girders to be of the same size and all the columns to be of the same size. Assume $I_{\text{beam}} = 2.5I_{\text{column}}$ and $w = 1.2$ kip/ft. Use computer software.



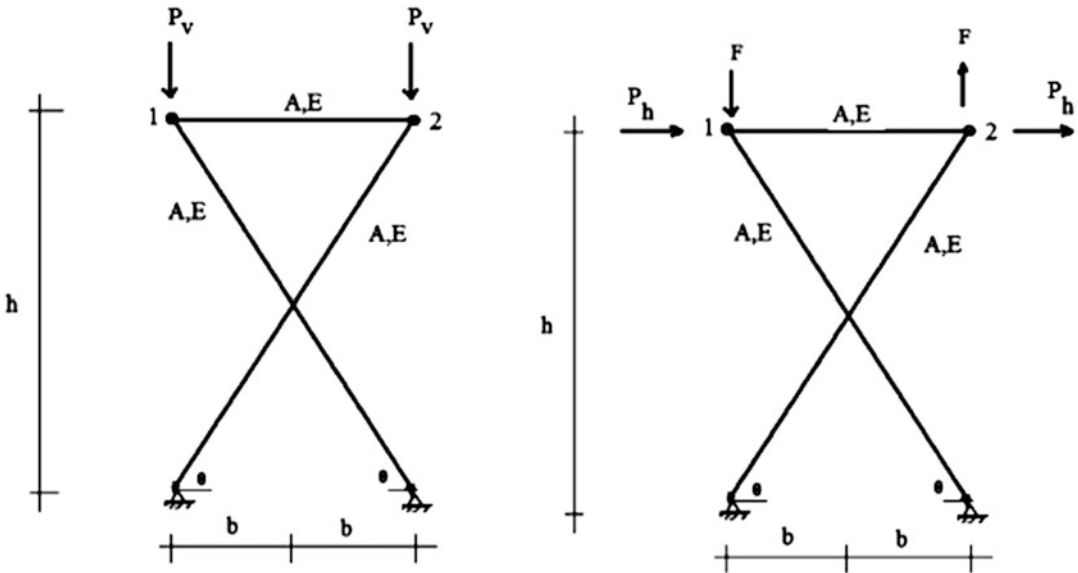
Problem 15.8 Discuss the function of the structure, abcdef. How would you determine the gravity loading acting on it? Assume uniform gravity loading for the beams.



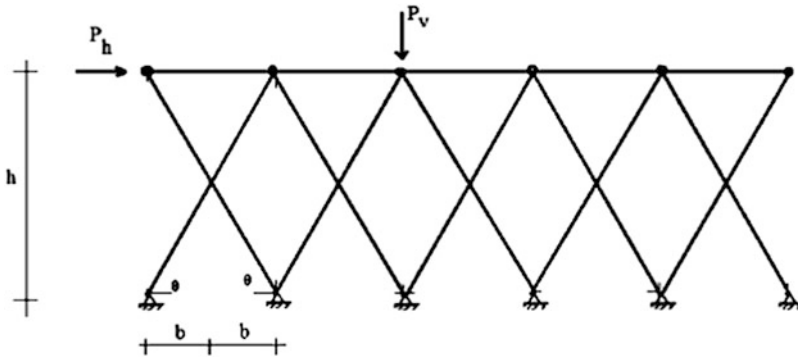
Problem 15.9 Consider a uniform floor gravity loading on the floors of the multistory rigid frame building shown below. Investigate how the internal forces vary with the angle α ranging from 0 to 20° , considering H constant. Is there a limiting value for α ?



Problem 15.10 Consider the structures shown below. All the members are pinned at their ends.



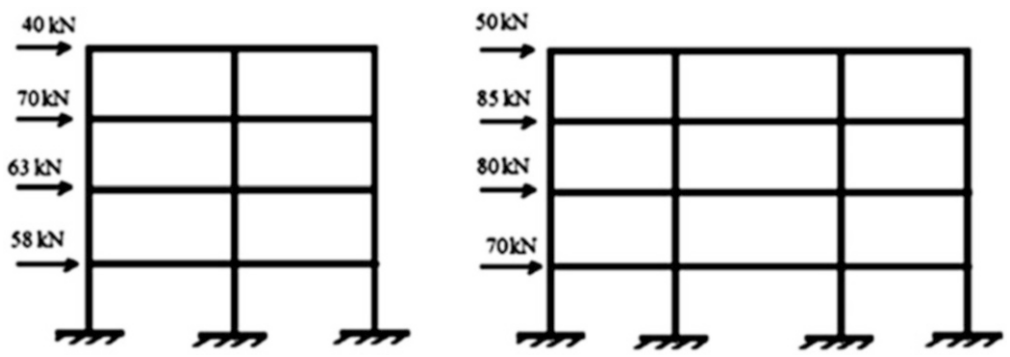
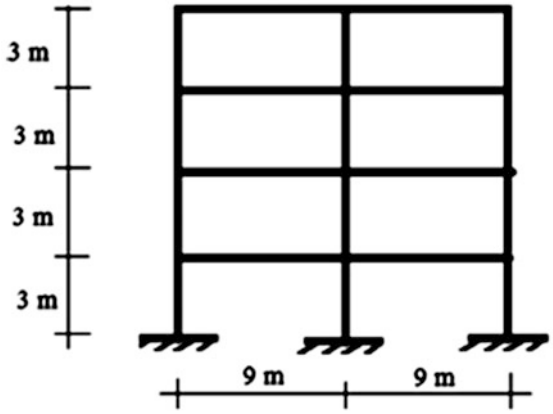
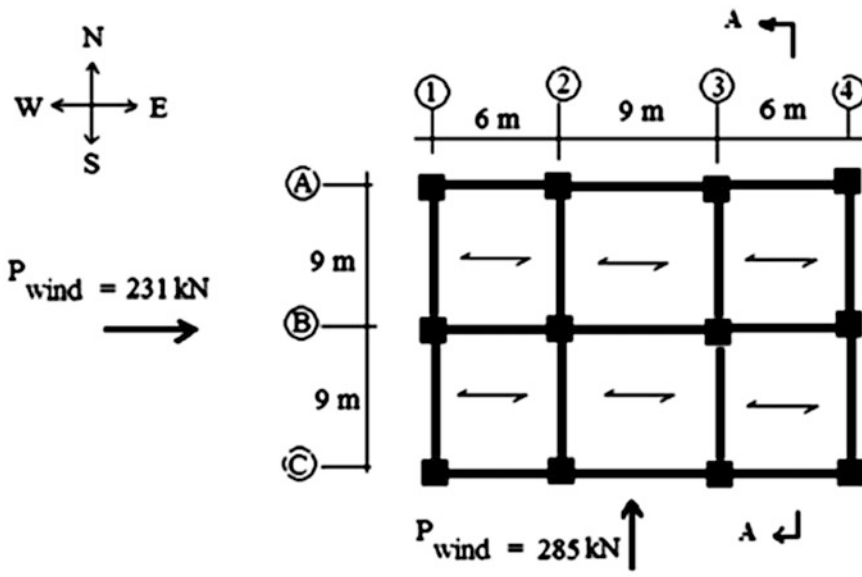
- (a) Determine expression for the axial forces in the diagonal members.
- (b) Determine the horizontal and vertical displacements of the nodes 1 and 2.
- (c) Extend the analysis to the structure shown below. This structure is called a DIAGRID structure.



Problem 15.11 For the structure shown below, assume the floors are flexible and the flooring system transmits the gravity loading to the floor beams in the N-S direction (one-way action). Assume all beams are the same size and all the columns are the same size. $I_{\text{beam}} = 3I_{\text{column}}$, $\text{Floor}_{\text{gravity}} = 175 \text{ kN/m}^2$.

Compare the maximum forces in beams and columns caused by combination of gravity and wind for the following cases.

- 1. The structure is considered to be a braced frame, i.e., all the connections between beams and columns are pinned both in N-S and E-W direction. Assume the frames are suitably braced.
- 2. The structure is considered to be a rigid frame in the N-S direction and a braced frame in the E-W direction, i.e., all the connections between beams and columns are moment connections in N-S direction, but connections in the E-W direction remain pinned.



Abstract

The conventional design approach works with factored loads and reduced material capacities such as strength. When subjected to service loads, the structure is detailed such that it behaves elastically. For extreme loadings, the structure is allowed to experience a limited amount of deformation beyond the elastic limit. This deformation is called “inelastic” since in contrast to elastic deformation, when the loading is removed, the structure does not return to its original position. Up to this point in the text, we have assumed the behavior to be elastic. In Chap. 10, we included geometric nonlinear effects but still assumed elastic behavior. Here, we introduce an additional effect, inelastic behavior. We start with an in-depth discussion of the stress–strain behavior of structural steels and concrete, apply these ideas to beams subjected to inelastic bending, and then develop an analysis procedure to determine the inelastic response of frame-type structures. This approach allows one to estimate the “maximum” loading that a structure can support, i.e., the “limit load.” Examples illustrating the influence of inelastic behavior on the ultimate capacity are included.

16.1 Stress–Strain Behavior of Structural Steels

Steel and concrete are the two most popular construction materials. Steels with low carbon content are usually referred to as “structural” steels since they are used primarily to fabricate structural elements such as W, T, and I shapes. Structural steels have desirable properties such as strength, uniformity, weldability, and ductility. The latter property is related to the ability of structural steels to experience significant deformation prior to fracture.

Figure 16.1 shows a typical stress–strain plot for a mild (low carbon) steel. There are four distinct deformation zones: elastic; yielding; strain hardening; and necking. The stress remains constant as the specimen yields until the strain, ϵ_y , is reached. Beyond this level, strain hardening occurs with the stress increasing to its “ultimate” value and then decreasing to the value at which rupture occurs. The yield zone for mild steel is relatively large, on the order of 20 times the yield strain ϵ_y . Another

Fig. 16.1 Typical stress–strain curve for mild structural steel

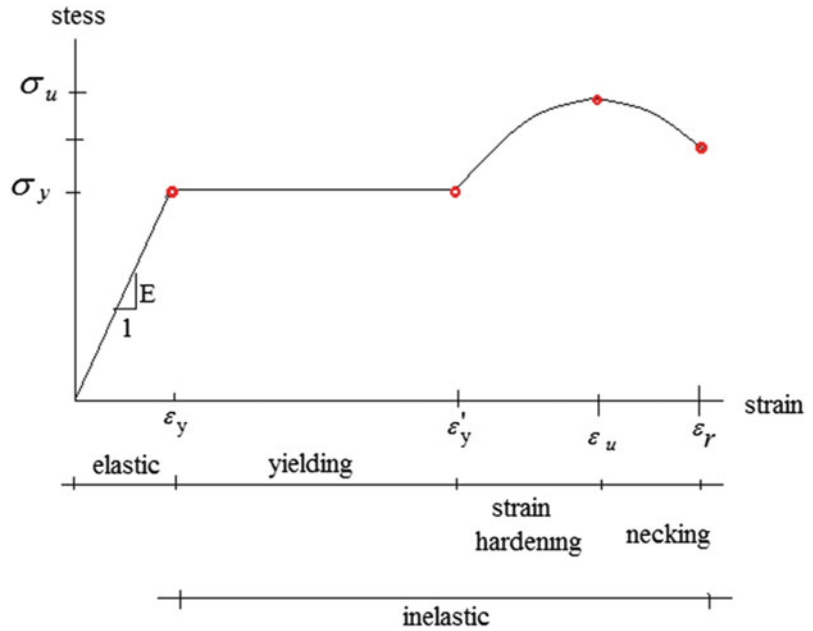
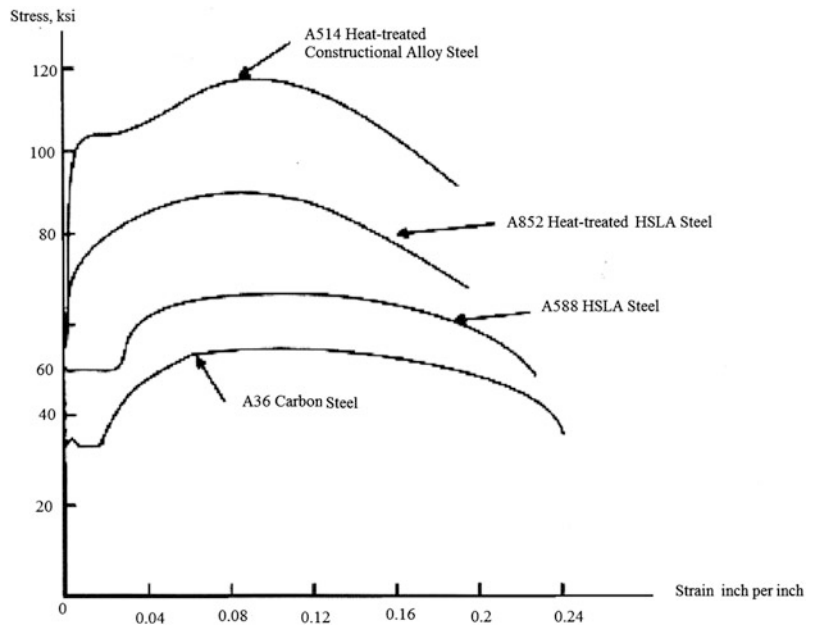


Fig. 16.2 Steel properties—structural steels



measure is the rupture strain ϵ_r . By definition, ϵ_r is the fractional change in length of the specimen and is usually expressed as a percentage. For mild steel, the percent elongation is about 24 %. Ductility refers to the ability to deform plastically without fracturing and is measured by the ratio $\frac{\epsilon_r}{\epsilon_y}$. This ratio

is large compared to 1. The last measure of interest is the toughness, defined as the energy required to fracture the material. Toughness is equal to the area under the stress–strain curve to fracture, and is usually expressed as a multiple of R , the area under the linear portion of the stress–strain curve.

Figure 16.2 lists the stress–strain plots for a range of common structural steels. Note that as the yield stress and the ultimate stress increase, the yield zone and the rupture strains decrease. There is a

trade-off between ductility and strength. The yield zones for the two lower strength steels are essentially equal $\left(\frac{\epsilon'_y}{\epsilon_y} \approx 13\right)$ whereas the higher strength steels shift directly from elastic behavior into strain hardening.

16.2 Inelastic Moment–Curvature Relationships

The fact that structural steels can experience significant deformation before rupturing is the basis for developing an analysis procedure for tracking the response as the structure passes from the elastic range through the yielding zone up to rupture. The starting point for the analysis is establishing the moment capacity of a beam subjected to inelastic bending.

Assuming a cross section remains a plane, the extensional strain varies linearly with distance from the centroidal axis.

$$\epsilon = y\chi \quad (16.1)$$

where χ is the curvature of the centroidal axis. Given χ , one computes ϵ and then determines the stress using a nonlinear stress–strain relation such as shown in Fig. 16.1.

$$\epsilon \rightarrow \sigma = f(\epsilon) \rightarrow \sigma = f(\chi) \quad (16.2)$$

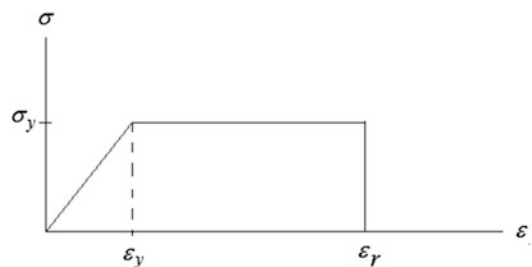
The moment is defined by the following integral,

$$M = \int_A (-y)\sigma dA = M(\chi) \quad (16.3)$$

This integral is usually evaluated numerically; one ranges over χ and constructs a plot of M vs. χ . The exact form depends upon the assumed stress–strain relationship and the shape of the cross section.

In order to obtain an analytical solution, the stress–strain curve is usually approximated with a linear model. The simplest model for steel is based on the assumption of elastic perfectly plastic fracture behavior; the increase in stress due to strain hardening is neglected. Figure 16.3 illustrates this behavior.

Fig. 16.3 Elastic perfectly plastic fracture (EPPF) model



Using this model, and applying (16.1)–(16.3) to a rectangular cross section, one obtains the plot shown in Fig. 16.4.

$$M_y = \sigma_y \left(\frac{bh^2}{6} \right)$$

$$M_r = \frac{3}{2} M_y \left\{ 1 - \frac{1}{3} \left(\frac{\epsilon_y}{\epsilon_r} \right)^2 \right\}$$

$$\chi_y = \frac{2\epsilon_y}{h} \quad \chi_r = \frac{2\epsilon_r}{h}$$

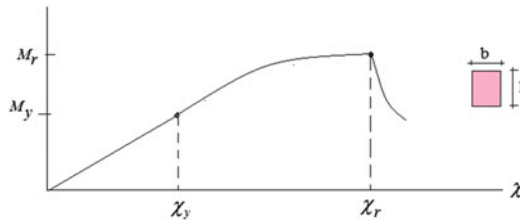


Fig. 16.4 Moment–curvature plot—rectangular sector and EPPF material

The outer fiber fractures at $\chi = \chi_r$, resulting in a discontinuity in the derivative.

For $\chi > \chi_r$, yielding progresses over the section and the moment capacity rapidly decreases.

Wide flange sections behave differently since the moment is carried primarily by the flanges. Fracture in the flanges results in a significant loss of moment capacity, especially when the sections are thin-walled since, in this case, the fracture occurs simultaneously throughout the flange thickness. A typical plot is shown in Fig. 16.5.

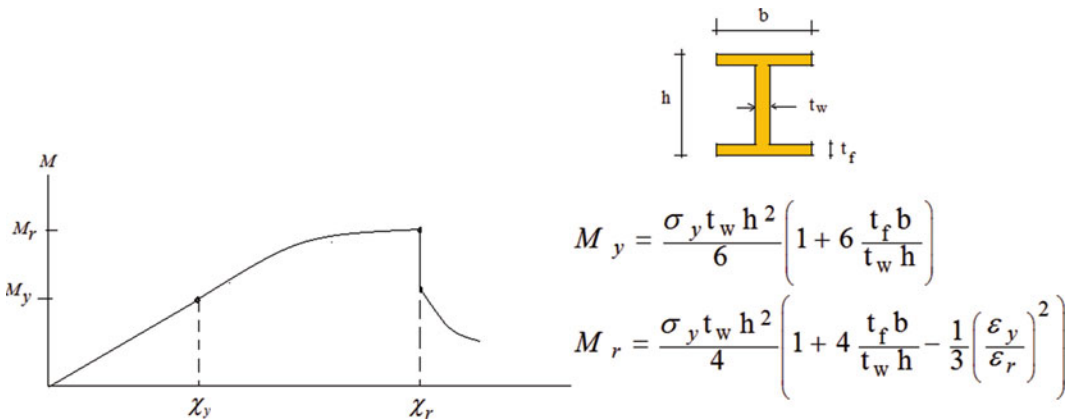


Fig. 16.5 Moment–curvature plot—thin walled wide flange section and EPPF material

From a computer implementation perspective, it is convenient to represent the moment–curvature relations with the bilinear approximation shown in Fig. 16.6. Nonlinear analysis is required to evaluate the load–deflection behavior. With this type of approximation, when yielding occurs, one replaces the elastic stiffness with a “linearized” tangent stiffness. The simplest possible strategy is to

Fig. 16.6 Bilinear moment–curvature models. (a) General bilinear model and (b) EPPF model

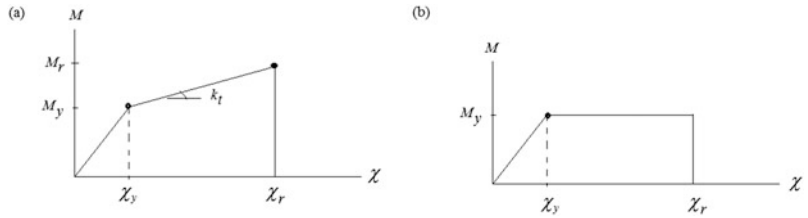
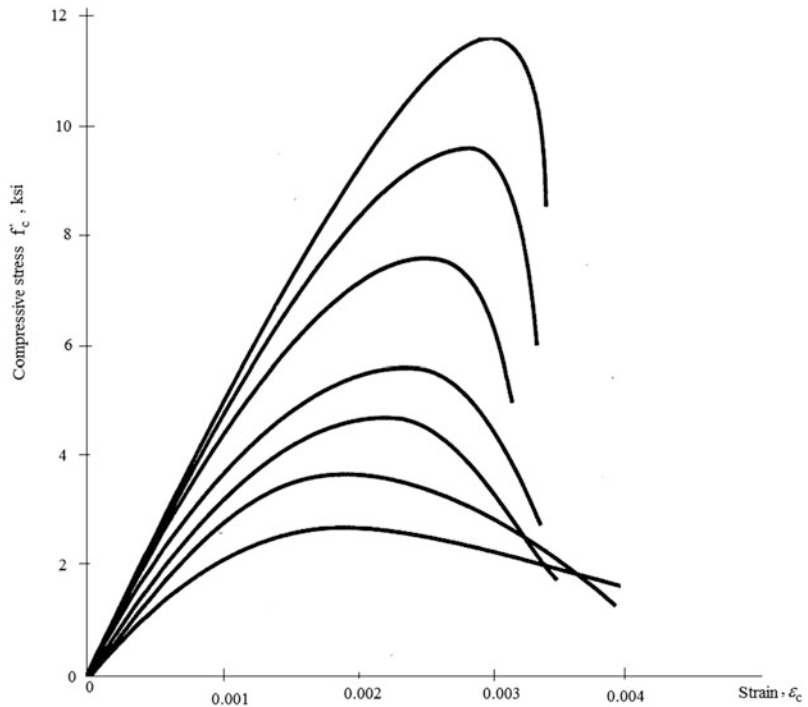


Fig. 16.7 Compressive stress–strain curves for concrete



work with an elastic perfectly plastic fracture model, i.e., to assume the tangent stiffness is negligible for $\chi_y < \chi < \chi_r$. This behavior is introduced by inserting a hinge at the location of the cross section and applying a constant moment equal to M_y . When $\chi \geq \chi_r$, the constant moment is removed, resulting in no moment capacity at the section.

Although the discussion has been focused on steel, the concept of a bilinear moment–curvature model is also adopted for concrete. The behavior of concrete differs from that of steel in that the stress–strain relationship for concrete exhibits strain softening (a reduction in stress beyond the peak value with increasing strain) and the peak strain is several order of magnitude smaller than that of steel. Typical plots are shown in Fig. 16.7. The limiting strain, ϵ_r , corresponds to crushing of the concrete and is of the order of 0.0004.

Assuming the strain varies linearly over the cross section; one can construct the moment–curvature relationship. A typical plot for an under-reinforced section is shown in Fig. 16.8. For computer-based analysis, one uses the nonlinear form. For hand computation, this form is approximated with an elastic perfectly plastic fracture model where M_y' is considered to be the ultimate moment capacity. A detailed discussion of this topic is contained in Winter and Nilson [1].

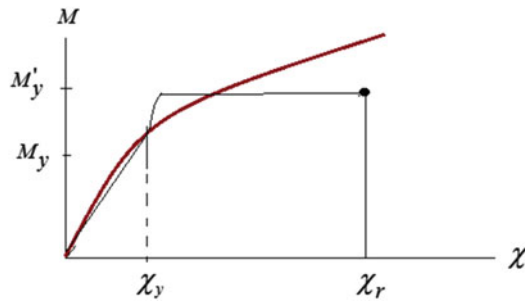


Fig. 16.8 Moment–curvature relationship—concrete beams

16.3 Limit Analysis: A Simplified Approach

Given the properties of a structure and a particular loading distribution, it is of interest to establish the peak magnitude of the loading that the structure can support, i.e., the limit of the loading. In what follows, we describe a procedure based on using an elastic perfectly plastic fracture model. Starting at a low load level, one carries out an elastic analysis and identifies the section where the bending moment is a relative maximum. The loading is then scaled up such that the magnitude of the moment at that particular section equals its moment capacity. In this approach, the capacity is taken as the yield moment. At this loading limit, a hinge is inserted and a set of self-equilibrating concentrated moments equal to M_y are applied at the section. The modified structure is then examined with respect to its stability, i.e., its capacity to support additional load. If stable, the loading is increased until another cross section reaches its moment capacity. The structure is again checked for stability and, if stable, a hinge and the assumed set of moments are inserted. The process is continued until the modified structure is unstable. The following examples illustrate the limit analysis process.

Example 16.1

Given: A simply supported beam subjected to a uniform loading defined in Fig. E16.1a.

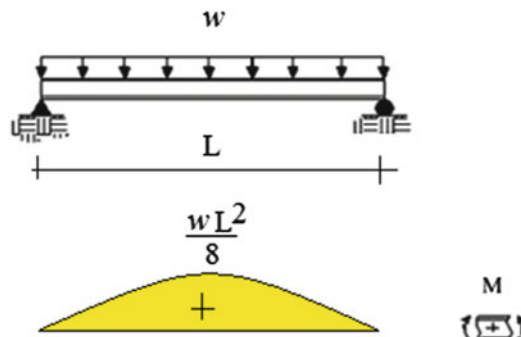


Fig. E16.1a

Determine: The load capacity.

Solution: The peak moment occurs at mid-span.

$$M_{\max} = \frac{wL^2}{8}$$

We increase the loading until $M_{\max} = M_y$.

$$M_y = \frac{w_1 L^2}{8}$$

$$\Downarrow$$

$$w_1 = \frac{8M_y}{L^2}$$

The modified structure for this load level is shown in Fig. E16.1b.

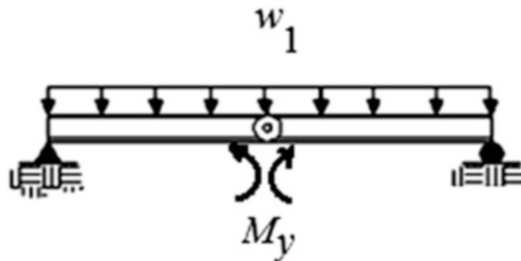


Fig. E16.1b

Any load increase will cause the structure to collapse downward since it has no capacity to carry any additional load. Therefore, $w_1 = w_{\max}$.

Example 16.2

Given: The fixed-ended beam subjected to a uniform loading defined in Fig. E16.2a.

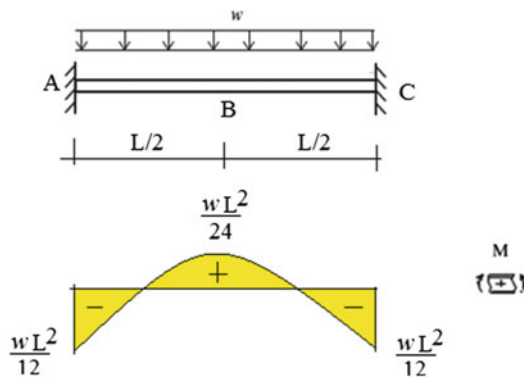


Fig. E16.2a

Determine: The load capacity.

Solution: The peak moment occurs at A and C. Therefore, yielding will first occur at these sections. We increase the loading until $M_{\max} = M_y$.

$$M_y = \frac{w_1 L^2}{12}$$

$$\Downarrow$$

$$w_1 = \frac{12M_y}{L^2}$$

Inserting hinges at A and C results in a simply supported beam with end moments.

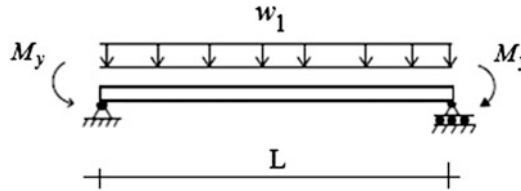


Fig. E16.2b

The next critical section is at mid-span. Applying an incremental load, Δw , increases the moment at mid-span.

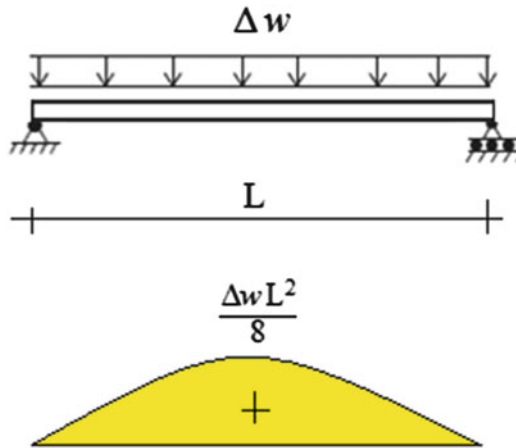


Fig. E16.2c

Then, superimposing the results for the two cases leads to the peak moment at mid-span which is set equal to M_y .

$$\frac{\Delta w L^2}{8} + \frac{w_1 L^2}{24} = M_y$$

Substituting for w_1 ,

$$\frac{\Delta w L^2}{8} = M_y - \frac{1}{2} M_y = \frac{1}{2} M_y$$

leads to

$$\Delta w = \frac{4}{L^2} M_y$$

Lastly,

$$w_{\max} = w_1 + \Delta w = \frac{16}{L^2} M_y$$

The final “limit state” is shown in Fig. E16.2d. This structure is unstable for any *additional transverse loading*.

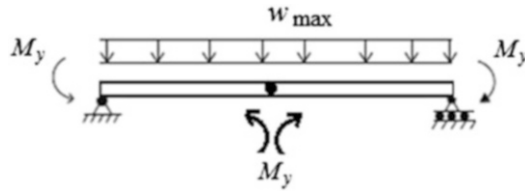


Fig. E16.2d

Example 16.3

Given: The two-span beam shown in Fig. E16.3a. Assume EI is constant.

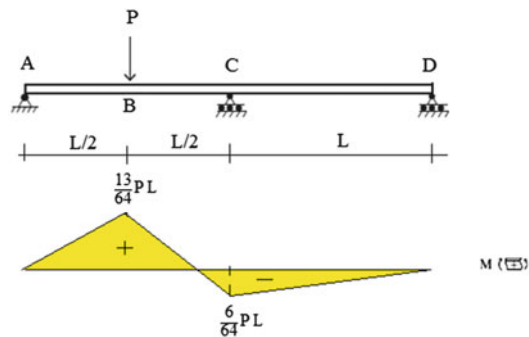


Fig. E16.3a

Determine: The limit state.

Solution: The moments at section B and C are relative maxima; the value at B is the largest, so yielding will occur first at this section.

$$M_B = \frac{13}{64} PL$$

$$M_C = -\frac{6}{64} PL$$

Load level 1:

We set M_B equal to M_y and insert a hinge at B.

$$\begin{aligned} \frac{13}{64} P_1 L &= M_y \\ &\Downarrow \\ P_1 &= \frac{64}{13L} M_y \end{aligned}$$

At this load level, the modified structure is

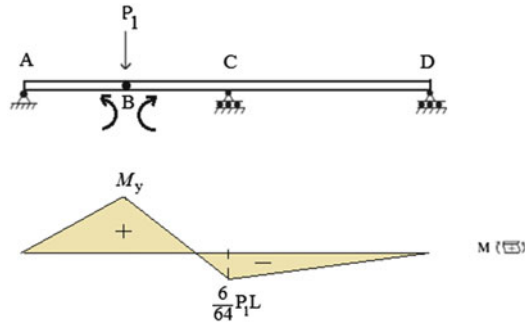


Fig. E16.3b

Load level 2:

We apply an incremental load, ΔP , to the modified structure leading to an incremental moment at C.

$$\Delta M_C = \frac{L}{2} \Delta P$$

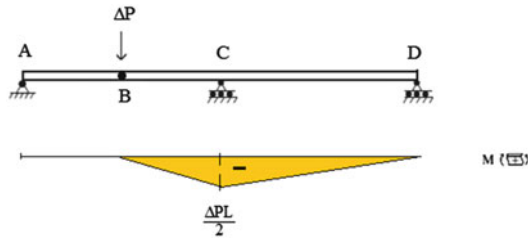


Fig. E16.3c

The total negative moment at C is

$$\left\{ M_C = \frac{6}{64} P_1 L + \frac{\Delta PL}{2} \right\}$$

Setting $M_C = M_y$ leads to the limiting value for ΔP

$$\frac{6}{64} P_1 L + \Delta P \frac{L}{2} = M_y$$

Substituting for P_1 , one obtains

$$\Delta P = \frac{14}{13L} M_y$$

Finally

$$P_{\max} = P_1 + \Delta P = \frac{78}{13L} M_y = \frac{6}{L} M_y$$

The limit state has hinges at B and C.

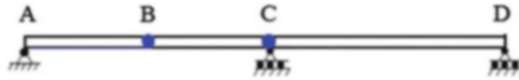


Fig. E16.3d

The procedure followed in the above examples involved applying the loading in increments and analyzing the structure at each load level. When yielding is reached at a particular load level, the structural stiffness is modified by inserting a hinge (i.e., zero rotational stiffness) at the yielded section. The loading process is continued until the structure becomes unstable. In general, instability occurs when the number of plastic hinges is equal to 1 plus the number of degrees of static indeterminacy. From a structural prospective, instability occurs when the tangent stiffness associated with the complete structure vanishes.

When evaluating the response, one must also check that the curvature at a yielded section does not exceed the “rupture” or “crushing” value. When this occurs, the moment capacity is set to zero. We did not carry out this computation in the above examples since it requires a computer-based procedure in order to obtain reliable results. Later in the chapter, we describe a computer procedure based on a finite element beam discretization combined with an incremental nonlinear solution strategy. Most modern structural software systems have this type of capability.

An alternative hand calculation approach to establishing the limit state is based on assuming a pattern of hinges that corresponds to a limit state and evaluating the corresponding load magnitude. One starts with the elastic moment diagram and identifies the sections where the moment is a relative maximum. At the limit state, the number of plastic hinges is equal to 1 plus the number of degrees of freedom. The load magnitude can be obtained either by applying the equilibrium equations or using the principle of virtual work which is an equivalent statement of equilibrium. The latter approach is generally more convenient. We illustrate this procedure with the following examples.

Example 16.4

Given: A two-span beam shown in Fig. E16.4a.

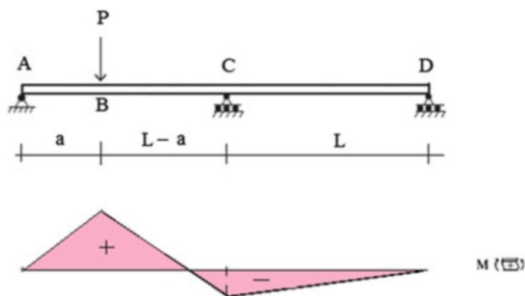


Fig. E16.4a

Determine: The limit state.

Solution: The critical state has two hinges. Noting the moment diagram, we locate them at Points B and C.

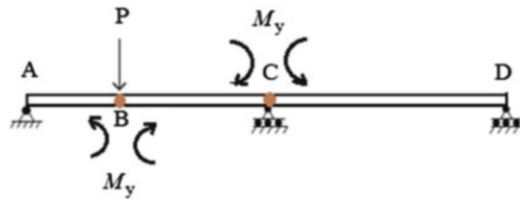


Fig. E16.4b

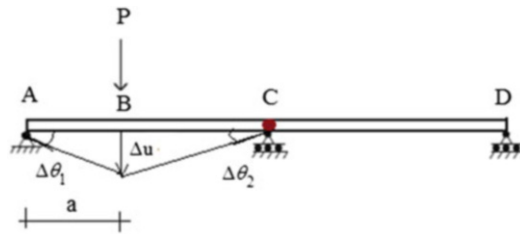


Fig. E16.4c

We use the principle of virtual work to establish the expression for P . Introducing a virtual displacement at B and evaluating the work done by P and the plastic moments lead to

$$P\Delta u - M_y(\Delta\theta_1 + \Delta\theta_2) - M_y\Delta\theta_2 = 0$$

The displacement terms are related by

$$\begin{cases} \Delta\theta_1 = \frac{\Delta u}{a} \\ \Delta\theta_2 = \frac{\Delta u}{L-a} \end{cases}$$

Substituting for the $\Delta\theta$ terms, the work equation reduces to

$$\Delta u \left\{ P - \frac{M_y}{a} - 2M_y \left(\frac{1}{L-a} \right) \right\} = 0$$

This must be satisfied for arbitrary Δu . Then

$$P = M_y \left(\frac{1}{a} + \frac{2}{L-a} \right)$$

Example 16.5

Given: A two-story frame shown in Fig. E16.5a.

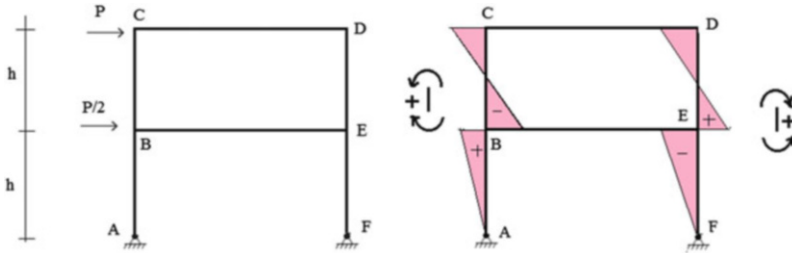


Fig. E16.5a

Determine: The limit state.

Solution: For this structure and loading, the relative moment maxima occur at the nodes. Therefore, plastic hinges will develop at the end of the members. When designing the members, most design codes require that one selects sectional properties such that yielding occurs only in the beams. We assume that condition is satisfied here, and work with the limit state shown below.

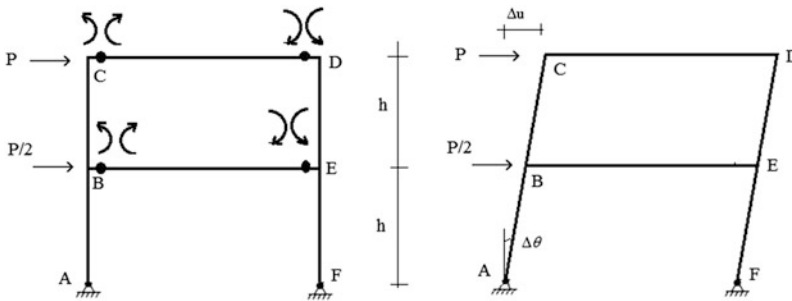


Fig. E16.5b

Introducing a virtual displacement at C, the work terms are

$$\begin{aligned}
 P\Delta u + \frac{P}{2} \frac{\Delta u}{2} - 4M_y\Delta\theta &= 0 \\
 \downarrow \\
 \frac{5}{4}P\Delta u &= 4M_y\Delta\theta = 4M_y \left(\frac{\Delta u}{2(h)} \right) \\
 \downarrow \\
 P_{\max} &= \frac{8M_y}{5h}
 \end{aligned}$$

In the above example, we assumed a particular plastic hinge pattern. Other patterns are also possible, each with a different limit load. One needs to examine *all possible patterns* in order to identify the minimum critical load. This operation is not feasible using hand computation for a complex structure. One needs to employ a computer-based nonlinear analysis scheme which generates the load displacement response allowing for the formation of plastic hinges up to the load level at which collapse is imminent. A particular nonlinear analysis scheme is described in the next section.

16.4 Nonlinear Analysis Scheme

We illustrate this method using the structure analyzed in Example 16.4. The first step involves discretizing the structure with a combination of elastic and plastic finite elements. A refined mesh is used in those zones where the moment is a relative maximum, such as adjacent to interior nodes and concentrated loads. Since the extent of plastic yielding is not known initially, one needs to iterate, starting with a single plastic element and adding additional plastic elements if necessary. This process is illustrated in Fig. 16.9.

The material behavior within a plastic segment is assumed to follow the bilinear moment–curvature model defined in Fig. 16.10. When $\chi < \chi_y$, the behavior is elastic, and the elastic stiffness k_E applies. When $\chi > \chi_y$, the behavior is inelastic and the reduced stiffness, k_t , is used. When $\chi > \chi_r$, the moment is set equal to zero, i.e., the section is considered to have no moment capacity.

The equilibrium equations for a member are generalized using the Principle of Virtual Displacements [2]. Consider the element shown in Fig. 16.11. Nodes are located at each end, and the nodal displacement measures are the translation and rotation.

Introducing matrix notation, these measures are expressed as

$$\underline{U}_1 = \begin{Bmatrix} v_1 \\ \theta_1 \end{Bmatrix} \quad \underline{U}_2 = \begin{Bmatrix} v_2 \\ \theta_2 \end{Bmatrix}$$

The transverse displacement is approximated as

$$v(x) = \underline{\Phi}_1 \underline{U}_1 + \underline{\Phi}_2 \underline{U}_2 \quad (16.4)$$

where $\underline{\Phi}_1$ and $\underline{\Phi}_2$ contain interpolation functions.

Fig. 16.9 Plastic element discretization. (a) Initial mesh and (b) expanded mesh

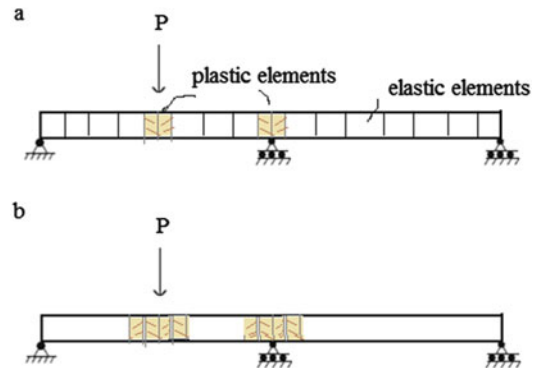


Fig. 16.10 Bilinear model

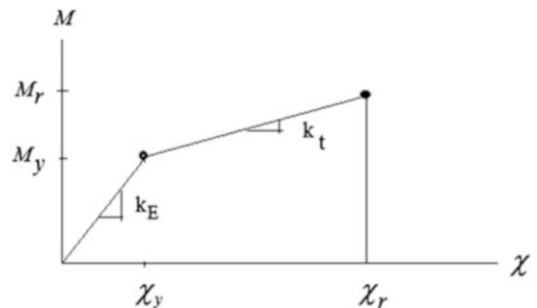
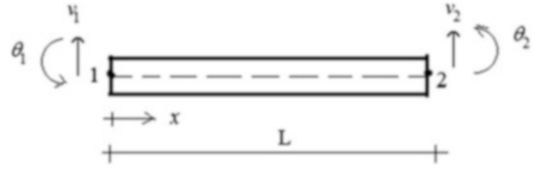


Fig. 16.11 Notation for end displacements



$$\begin{aligned}\underline{\Phi}_1 &= \left[1 - 3\left(\frac{x}{L}\right)^2 + 2\left(\frac{x}{L}\right)^3 \quad x - 2\frac{x^2}{L} + \frac{x^3}{L^2} \right] \\ \underline{\Phi}_2 &= \left[3\left(\frac{x}{L}\right)^2 - 2\left(\frac{x}{L}\right)^3 \quad -\frac{x^2}{L} + \frac{x^3}{L^2} \right]\end{aligned}\quad (16.5)$$

Differentiating twice leads to the curvature

$$\begin{aligned}\chi &= v_{,xx} = \underline{\Phi}_{1,xx} U_1 + \underline{\Phi}_{2,xx} U_2 \\ \underline{\Phi}_{1,xx} &= \left[-\frac{6}{L^2} + \frac{12x}{L^3} \quad -\frac{4}{L} + \frac{6x}{L^2} \right] \\ \underline{\Phi}_{2,xx} &= \left[+\frac{6}{L^2} - \frac{12x}{L^3} \quad -\frac{2}{L} + \frac{6x}{L^2} \right]\end{aligned}\quad (16.6)$$

Note that the curvature varies linearly over the segment in this approach. *Given the end displacements, one evaluates the curvature, and then the bending moment.*

The end forces are determined with the following virtual work requirement:

$$\int M \delta\chi \, dx \equiv \underline{P}_1^T \delta U_1 + \underline{P}_2^T \delta U_2 \quad (16.7)$$

for arbitrary δU_1 and δU_2 . Noting

$$\delta\chi = v_{,xx} = \underline{\Phi}_{1,xx} \delta U_1 + \underline{\Phi}_{2,xx} \delta U_2 \quad (16.8)$$

and expanding (16.7) result in

$$\begin{aligned}\underline{P}_1 &= \int \underline{\Phi}_{1,xx}^T M \, dx \\ \underline{P}_2 &= \int \underline{\Phi}_{2,xx}^T M \, dx\end{aligned}\quad (16.9)$$

When the behavior is inelastic, a numerical integration scheme, such as a 2 point Gaussian approximation, is used to evaluate the integrals. The moment is determined using Fig. 16.10.

Lastly, the global force equilibrium equation for the nodes is written as

$$\underline{P}_E = \underline{P}_I \quad (16.10)$$

where \underline{P}_E contains the external nodal loads and \underline{P}_I represents the nodal loads due to the member end actions which are functions of the nodal displacements. The solution scheme proceeds as follows. Suppose $U|_i$ represents the i th solution for the response due to P_E . The static error is

$$E|_i = P_E|_i - P_I|_i \quad (16.11)$$

We correct the error by introducing an incremental displacement $\Delta U|_i$ which leads to the increment $\Delta P_I|_i$. The equilibrium requirement for $\Delta P_I|_i$ is

$$\Delta P_1|_i = P_E|_i - P_1|_i \quad (16.12)$$

Finally, we approximate the force increment as

$$\Delta \underline{P}_1|_i = K_t|_i \Delta \underline{U}|_i \quad (16.13)$$

where K_t represents a “tangent” stiffness matrix for the structure. The incremental equilibrium equation takes the form

$$K_t|_i \Delta \underline{U}|_i = P_E|_i - P_1|_i \quad (16.14)$$

One cycles on (16.14) until successive value of $\Delta \underline{U}$ agree to a specified tolerance. Instability occurs where K_t is singular.

One determines ΔP_1 by operating on (16.9). For example, noting

$$\begin{aligned} \Delta P_1 &= \int \Phi_{1,xx}^T \Delta M dx \\ \Delta M &= 0 \quad \text{for } \chi > \chi_r \\ \Delta M &= k_t \Delta \chi \quad \text{for } \chi_y < \chi < \chi_r \\ \Delta M &= k_E \Delta \chi \quad \text{for } \chi < \chi_y \\ \Delta \chi &= \Phi_{1,xx} \Delta U_1 + \Phi_{2,xx} \Delta U_2 \end{aligned} \quad (16.15)$$

leads to

$$\Delta P_1 = \left[\int \Phi_{1,xx}^T k^* \Phi_{1,xx} dx \right] \Delta U_1 + \left[\int \Phi_{2,xx}^T k^* \Phi_{2,xx} dx \right] \Delta U_2$$

where $k^* = k_E, k_t$, or 0 depending on the value of χ .

One applies the external load in increments and cycles at each load level. This approach generates the complete nonlinear load-displacement response history for the structure, i.e., it determines the order and location of plastic hinges as the load is increased, and the final limit state. Most commercial structural software have this capability. The following examples illustrate the nonlinear analysis process.

Example 16.6

Given: The portal frame defined in Fig. E16.6a. Consider the gravity loading w to be constant. The lateral load P is due to seismic excitation. Material is steel, $\sigma_y = 50$ ksi, and $w = 4.17$ kip/ft.

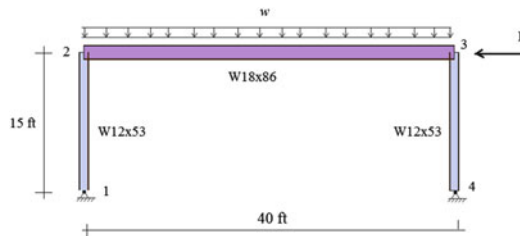


Fig. E16.6a

Determine: The inelastic response of the frame and the limiting values of P and S_a .

Solution: The analysis of gravity loaded frames subjected to lateral loading is referred to as a pushover analysis. One common application is to estimate the capacity of a frame for seismic excitation. One applies the lateral loading in increments and generates the nonlinear response up to the onset of instability. The pushover analysis was done using computer software [3] and the result is plotted in Fig. E16.6b.

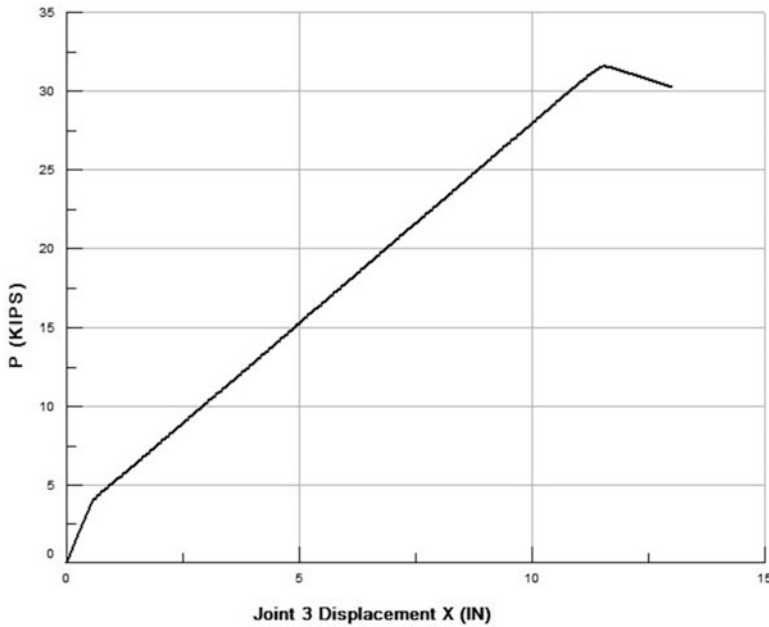


Fig. E16.6b Pushover results, P vs. joint displacement

Using the materials presented in Sect. 14.2.2, one can relate P to the spectral acceleration. For a single degree of freedom system, this relationship reduces to

$$P \approx mS_a$$

where m is the lumped mass and S_a is the spectral acceleration.

$$P_{\max} = 32 \text{ kip}$$

$$m = \frac{4.17(40)}{g} = \frac{166.8}{g}$$

$$S_a = \frac{P_{\max}}{m} = 0.19g$$

Example 16.7

Given: The three-story frame defined in Fig. E16.7a. Consider the gravity floor loading to be constant. The lateral load is due to seismic excitation. The material is steel, $\sigma_y = 50$ ksi, and the gravity floor load $= 0.75$ kip/ft

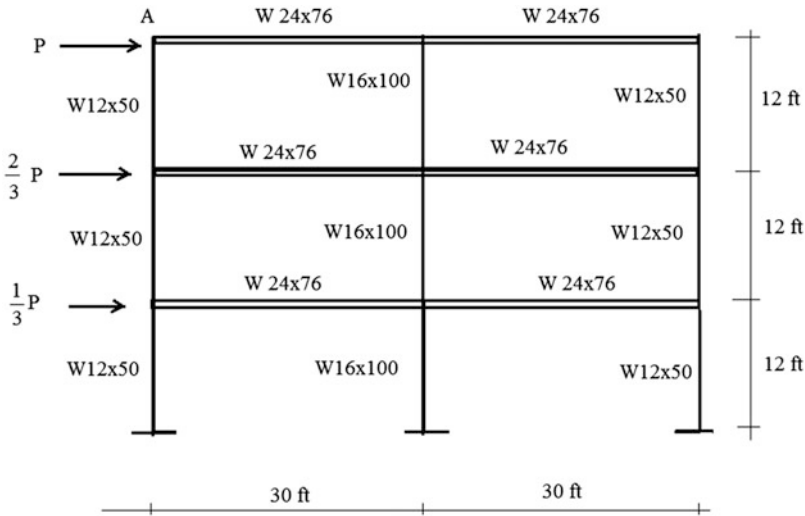


Fig. E16.7a

Determine: The lateral displacement of point A versus P and the limiting value of S_a .

Solution: We use Equation (14.9) specialized for this structure

$$P = m\Gamma S_a$$

where m is the mass of a typical floor, $m = \frac{0.75(60)}{g} = \frac{45}{g}$

Noting (14.7), $\Gamma = \frac{9}{7}$ for this frame.

One applies the lateral loading in increments and generates the nonlinear response up to the onset of instability. The pushover analysis was done using computer software [3] and the result is plotted in Fig. E16.7b.

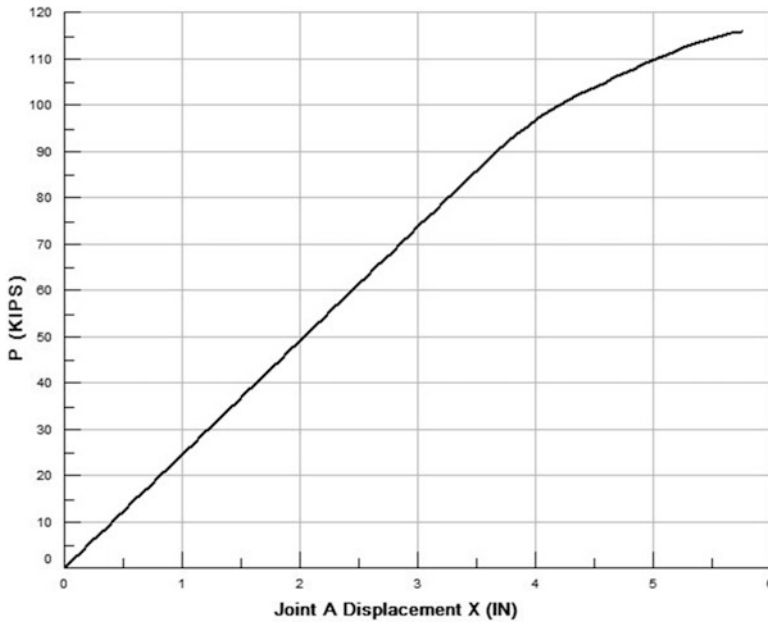


Fig. E16.7b Pushover results, P vs. joint displacement

Then

$$S_a = \frac{P_{\max}}{m\Gamma} = \frac{115}{\left(\frac{45}{g}\right)\left(\frac{9}{7}\right)} = 1.98g$$

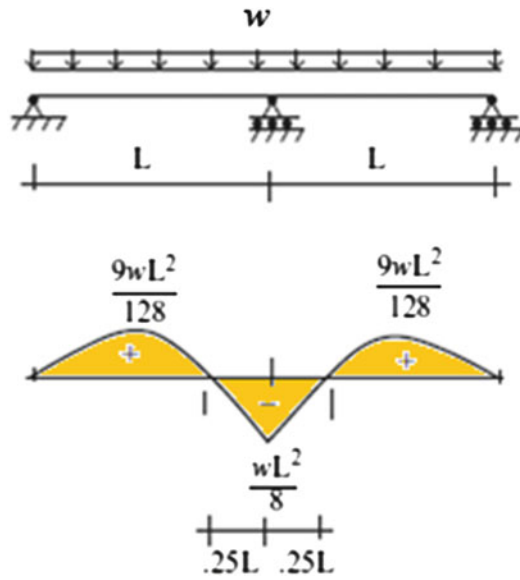
16.5 Summary

16.5.1 Objectives

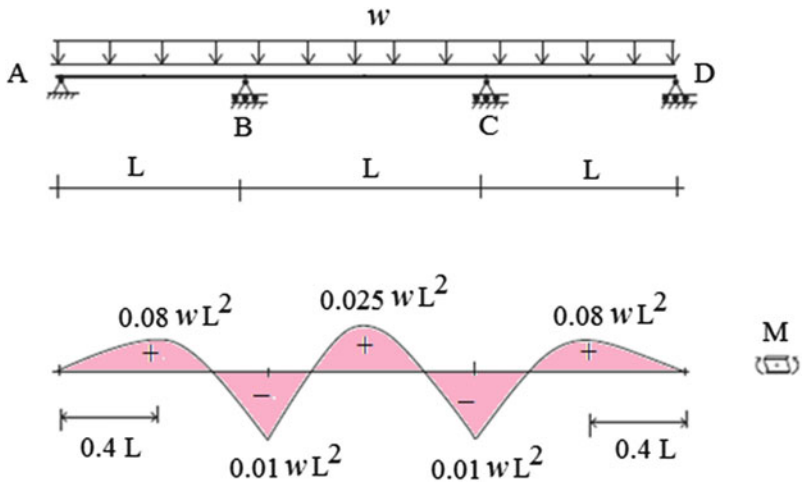
- Describe the different regions of the stress–strain behavior of structural steels and concrete: elastic; inelastic.
- Extend the moment–curvature relationships to the inelastic range and estimate the moment capacity of a beam subjected to inelastic bending.
- Present analysis procedures for determining the maximum external load that a structure can support using: (a) hand calculation methods and (b) finite element computation-based methods. This general topic is called “Limit Analysis.”
- Include some examples which illustrate how analysis is applied to simple rigid frames.

16.6 Problems

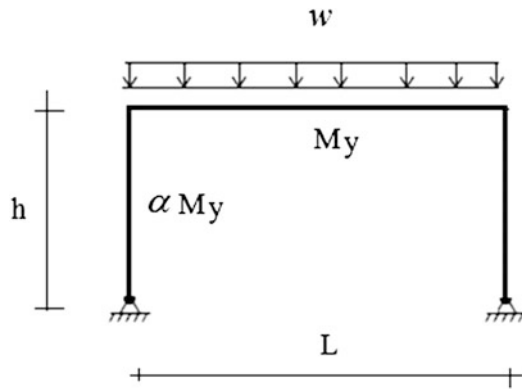
Problem 16.1 Determine the load capacity.



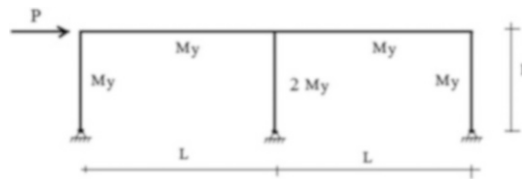
Problem 16.2 Determine the load capacity.



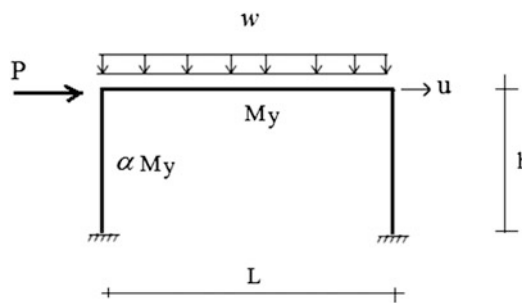
Problem 16.3 Determine w_{\max} as a function of α .



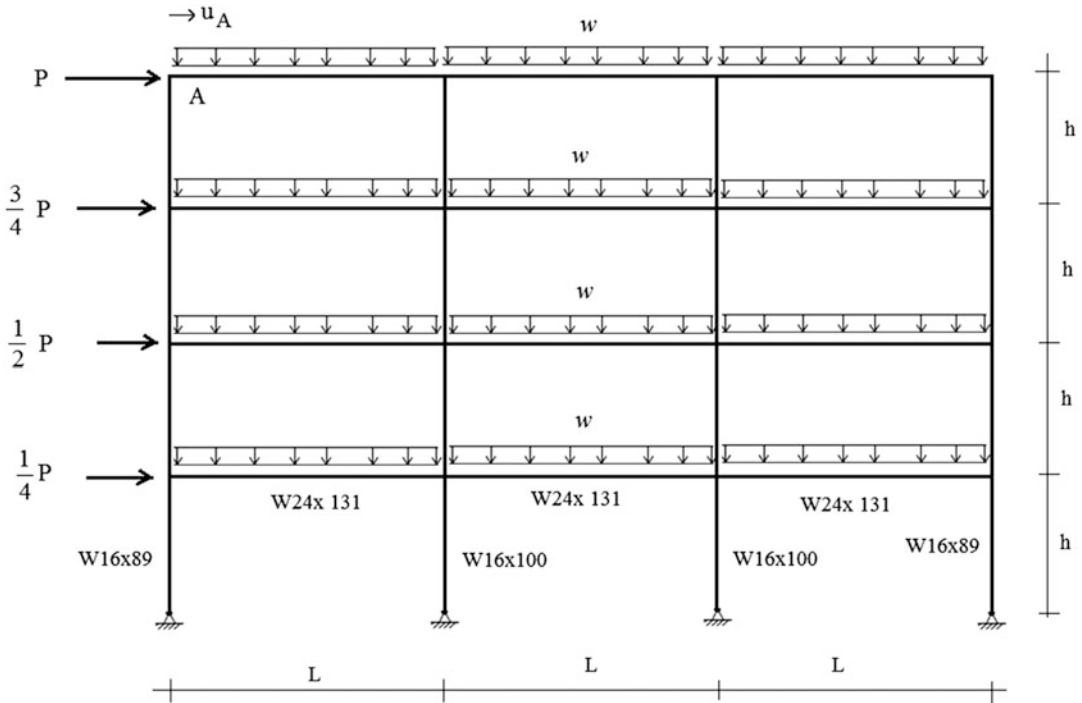
Problem 16.4 Determine an expression for P_{\max} .



Problem 16.5 Generate the plot of P vs. u for the frame shown. Consider w as a dead loading. Assume $\alpha = 1.2$.



Problem 16.6 Using computer software, generate the plot of u_A vs. P , and estimate P_{\max} . Take $w = 1.5$ kip/ft, $h = 12$ ft, and $L = 30$ ft. The material is steel, $\sigma_y = 50$ ksi. The exterior columns are W16 \times 89, the interior columns are a W16 \times 100, and all the beams are W24 \times 131.



References

1. Nilson AH. Design of concrete structures. 14th ed. New York: McGraw Hill; 2013.
2. Bathe KJ. Finite element procedures. 1st ed. Prentice Hall: Upper Saddle River; 1995.
3. GTSTRUDL. Intergraph Corporation PP&M, Norcross, GA, USA.

Index

A

Active failure mode, 530

A-frame

description, 306

indeterminate, 309

loading, reactions and free body, 341–343

moment distribution, 342, 343

reactions and bending moment distribution, 372

Allowable soil pressure, 477, 479

American Association of State Highway and

Transportation Officials (AASHTO), 17, 18

Analysis

statically determinate plane frames

angle-type frame segment, 314–316

cantilever frame, 311–314

moment, shear and axial force, 310

sign convention, 310

Analytical solutions, multi span beams

Bending moment distribution, 597

compatibility equation, 595, 596

lengths and moments, 596

loading, 597, 598

peak moments, 596

static equilibrium equations, 596

support settlement, continuous, 602–603

uniform loading, continuous, 600–602

variation, bending moment, 599–600

Analytical tools, structural analysis

beam response, 35

concept of equilibrium, 27–30

deformations and displacements, 33–34

description, 27

displacements

deformation modes, 38

description, 36

reactions, cable tension and vertical displacement,
36–37

rigid member, springs, 37, 38

spring forces, 3, 9–40

statically indeterminate beam, 40–42

FBD, 30, 31

internal forces, 30–33

study of forces, 36

Anti-symmetry

deflected shapes, 254–257

shear and moment diagrams, 250–254

Approximate methods

bending moment distribution

approximate and exact results, 797

axial force, shear force, 798

qualitative reasoning, relative stiffness, 797

bending type structures, 767

column axial forces, 802, 803

column shears, 803

multi-span beams (gravity loading), 768–770

multistory rigid frames

gravity loading, 770–771

lateral loading, 771–790

positive and negative moments, multistory steel
frame, 798

rigid steel frame, bracing, 803

statically indeterminate structure, 767

steel frame

axial force, shear force and moments, 800–802

portal and shear stiffness method, 799–802

Arc length

differential and total, 403, 404

initial and loaded shapes, cable, 403

maximum tension, determination, 414, 422

sag profile and total arc length, 406

sag ratio, 404

temperature effect, 404, 405, 422

Arch bridge

structure, 874

two-hinged, 899

Arch structures

historical development, 424

models, 429–431

Arches

“false arch”, 424

force method

applied load, 605

axial deformation, 604

description, 604

expressions, horizontal displacement, 604

integral expression, 607–608

- Arches (*cont.*)
 - parabolic, 606–607
 - structure, 603, 604
 - tension tie, 611–612
 - two-hinged arch and loading, 607–608
- ASCE 7-05, 16, 17, 20, 21
- Assuming the supports are unyielding, the flexibility coefficients, 625
- Axial force
 - compressive and maximum value, 442
 - gable frame
 - 3-hinge, 335–337
 - simply supported, 369
 - graphical output, 358, 360
 - shallow vs. deep parabolic curved members, 436–439
 - sign convention, 310
 - and transverse shear, 454, 455
 - triangular rigid frame, 380
- Axial stress, 34, 55
- Axle load, 886, 888
- B**
- Backfill material
 - fluid
 - definition, 527
 - horizontal and vertical components, 529
 - hydrostatic forces, inclined surface, 529
 - granular
 - active and passive failure states, 530
 - angle of repose, 530
 - dry loose, 529
 - shear stress, 529
 - theories, soil pressure distribution, 530
- Base shear, 783, 923, 955
- Beam formulation
 - loading, 827, 844
 - member end forces and displacements, 840
 - nodes, 842
 - spring support, 846–849
 - stiffness matrices, 842
 - support settlement, 846
 - two-span beam, 840
- Beams
 - deep beams, deformation and displacement relations, 244–247
 - differential equations, equilibrium, 190–210
 - displacement process, 35
 - external loads, 285
 - force method
 - single-span beams, analyzing frames, 571–577
 - Yielding Supports, 577–588
 - forced envelope, 286
 - influence line, 286
 - internal force, 258
 - mass system, 25
 - objectives, 285
 - planar bending, 286, 287
 - prismatic beams, 163
 - problems
 - computer software, 303–304
 - deflected shape, 296–297
 - influence lines, 300–301
 - loading system, span, 302
 - rotation, cross-section, 300
 - shear and moment diagrams, 286–292
 - single concentrated load, 301
 - trapezoidal rule, 299
 - vertical deflection, 298–299
 - virtual force method, 293–296
 - statically indeterminate, 40–42
 - symmetry and anti-symmetry
 - deflected shapes, 253–258
 - shear and moment diagrams, 250–254
 - torsion, prismatic members, 247–250
 - transverse displacement, 286
 - two span beams, displacement method
 - chord rotations, 661
 - decomposition, 658, 659
 - end actions, shear and moment, 662–664
 - end shears, 660
 - geometry and support settlements, 661
 - moment releases, 675–677
 - nodal moment equilibrium, 660
 - overhang, modified slope-deflection equations, 670–672
 - symmetrical beam, supports settlement, 665–669
 - three span beam, 677–683
 - uniformly loaded three span symmetrical beam, 683–685
- Behavior
 - brittle, 11
 - combined bending and torsion, 164
 - ductile, 11
 - portal frames
 - hinge, 3, 312–314, 324, 325
 - gravity loading, 323, 324
 - lateral loading, 323, 324
- Bending moment
 - distribution
 - approximate and exact results, 797
 - axial force, shear force, 798, 799
 - beams and columns, portal method, 772–779
 - lateral loading, 792
 - multi-span beams and multi-bay frames, 796
 - qualitative reasoning, relative stiffness, 796
 - transverse shear, 792
 - horizontal thrust force, 458, 459
 - reactions and shear distributions, 204–206
 - uniform loading, parabolic, 283
- Bilinear moment–curvature model, 1026
- Braced frames
 - definition, 789–790
 - multistory, 305, 306
- Braced rigid frame
 - analytical expressions, schemes, 786
 - column shear forces, 787

- definition, one-story, 787
- individual systems defined, 785
- one-story structure, 785
- shear force distribution
 - base story sub-element, 789
 - brace stiffness, 787
 - column shear forces, 787
 - frame stiffness, 787
 - inter-story displacement, 790
 - lateral forces, 788
 - one-story, 787
 - upper story sub-element, 788
 - value, lower floor controls, 790
- Bridge
 - gravity live loads, 17
 - segmented long-span, 14
 - structure
 - geometric arrangement, 71
 - and gravity, 13
 - iron truss bridge, USA, 52
 - plane bridge truss, 105, 106
 - steel truss bridges, 54
 - wooden bridge truss, 51
- Brittle, 11, 12, 15, 43
- Buckling, 12, 43
- Building
 - design, 13
 - effect, wind, 17
 - gravity live loads, 17
 - ground motion, 23
 - low-rise, 21
 - vortex shedding, 22
- Building codes, 13
- Building systems
 - “shear beam” formulation, 945
- C**
- Cable, 4, 7, 15, 36–37
- Cable length, 387, 404–406, 416
- Cable stayed
 - bridges, 383, 404, 409
 - beam displacement, 583
 - composition, 581, 582
 - configuration, 903
 - displacement profile of girder, 906
 - elongation, 582, 583
 - estimated areas, 904
 - force and displacement profiles, 905, 906
 - idealized scheme, 904
 - stiffen beams, 583
 - tributary area, 905
 - vertical displacement, cable and beam, 585–588
- Cable structures
 - Brooklyn Bridge, USA, 383, 385
 - cable-strand arrangements, 383, 384
 - Clifton Suspension Bridge, England, 383, 384
 - coordinates, lowest point, 421
 - deflected shape, 420, 421
 - doubly curved single-layer cable net, 384, 385
 - guyed tower, 422
 - maximum tension, 418–420
 - Normandy Bridge, France, 384, 386
 - peak values, cable tension, 421
 - reactions and tension, 416–418
- Cantilever frame
 - symmetrical, 312–314
 - unsymmetrical, 337–339
- Cantilever method
 - applied moment, 793
 - bending moment, axial forces, columns, 795
 - column-beam model, 793
 - deformation, relative rotation, 793
 - description, 790
 - lateral deflections, 790
 - reference axis, 792
 - stiff belt type trusses, 794
 - symmetrical -story plane frame, 42, 794
 - symmetrical plane frame, 795
 - tall building model, 792
- Catenary shape
 - arc length and tension, 414
 - equilibrium and vertical loading, 412, 413
 - horizontal projection, 412
 - iteration and sag ratio, 414
 - symmetrical case, 412, 414
- Center of mass
 - description, 937
 - floor
 - mass layout, 938–940
 - plan view, 938
- Center of twist
 - braces, 935–937
 - external and internal forces, 930
 - floor
 - configuration, 933
 - geometry, 929
 - free body diagram, floor, 926
 - rigid body motion, 929
 - shear spring model, 926
 - stiffness
 - braces, 927
 - distribution, 931
 - symmetry axes, 931
- Centroid
 - dimension square/rectangular footings, 488
 - single footing, 479–481
 - structure, 477, 478
- Centroidal axis, 1015
- Chord
 - horizontal, 389, 393, 397
 - inclined, 393, 394, 400
- Circular curved members
 - deflection, light pole, 447, 449
 - geometry-circular arch, 447
 - slender and retain, 447
- Clamped end model, 770
- Clamped/hinged model, 770

- Clay soil
 - allowable soil pressure, 477, 479
 - pressure distributions, 477, 478
- Combined footings
 - description, 493
 - factored loads, 496
 - peak moment values, 496
 - shear and moment, 494
 - soil pressure distribution, 494, 495
 - square columns, 497–499
- Complex trusses
 - corresponding nodal force equilibrium equations, 88
 - definition, 48, 86
 - equilibrium at joints, 87
 - geometrically stable, 89
 - individual nodal force systems, 88
 - matrix form, 88
 - planar, 137
 - planar truss, 87
- Compound trusses, 48, 60, 61, 86
- Compression*, 310, 314
- Computation of displacements
 - and deformation relations, 136
 - matrix equilibrium equations, 137
 - nodal displacement, 135, 137
 - planar complex truss, 137
 - scalar equation, 137
 - space truss, 139
 - static-geometric analogy, 136
- Computer based analysis
 - displacement method
 - bending moment distribution, 760, 761
 - frame structures, 728–729
 - and member forces, 752
 - nonlinear form, 1017, 1025
 - plane frames
 - gable, 358
 - graphical output, 358, 360
- Concentrated load
 - horizontal cables
 - free body diagram, segment, 387
 - moment distributions, 389
 - moments and sag, 387
 - multiple concentrated loads, 389, 391–393
 - tension, 388, 389
 - transverse loading, pretensioned cable, 386, 387
 - inclined cables
 - description, 393–397
 - reactions and horizontal force, 393, 394
 - sag determination, 395, 396
- Concept of equilibrium
 - non-concurrent force system, 28–30
- Construction loading, 14
- Containments, 4, 14
- Corbel arch, 424
- Critical loading
 - plan, rectangular area, 481, 482
 - pressure distributions, 481
- Critical sections for design, cantilever walls, 549, 552
- Cross section
 - beam, 164
 - combined bending and torsion, 164
 - properties, 258
- Cross, H., 698
- Curvature
 - positive and negative, deflected shapes, 213
 - relationship, 212–213
- D**
- Deck
 - and beam system, 105
 - segments, 105
 - slab, 49
- Deep beams, deformation and displacement relations
 - symmetry and anti-symmetry, 254–258
- Deep curved members, 464
- Deflection(s)
 - computation
 - deformation–displacement relations, 91–92
 - description, 90
 - force–deformation relationship, 90–91
- Deflection profiles
 - curvature, 356
 - gable frames, 357, 358
 - lateral loading, 357
 - peak deflection, estimation, 377
 - portal and -hinge frame, 3, 357
- Deformations
 - and displacements, 33–34
 - inelastic, 12, 27
 - modes, 38
- Design codes, 16, 21, 43
- Design philosophy, 26–27
- Design strategies, N-S beams and columns, 998–999
- Differential equations of equilibrium, planar loading
 - arbitrary distributed loading, differential element, 190
 - cantilever beam triangular loading, 193–196
 - distributed and concentrated loads, 196–200
 - extreme value, moment, 192
 - integral forms, 19
 - jump conditions, 194
 - moment summation, 191
 - reactions, shear, and bending moment distributions, 204–212
 - shear and moment, interpretation, 193
 - uniform loading, end moments, 199
- Dimensions
 - design code, 551
 - optimal geometry, 535
 - pressure distributions, 530
 - wall footing, 553
- Direct stiffness method, 860–865, 868, 869
- Displacement method
 - description, 649
 - displacements and member forces, truss, 752
 - frame structures
 - member equations, 653–658

- member end moments
 - moment distribution, 753–760
 - slope-deflection equations, 753–758
- member forces, truss, 752
- end moments and horizontal displacement, 764
- planar
 - beam-type structures, 649, 650
 - frame-type structure, 649, 650
 - truss, 649, 650
- plane truss
 - axial loaded member, 651
 - force-equilibrium equations, 651
 - horizontal and vertical translations, 651
 - nodal displacements and member forces, 651
 - rotation and end moments, analytic expression, 763
- Distributed load
 - horizontal cable
 - description, 397, 398
 - tension determination, 398, 399
 - inclined cables
 - arbitrary loading, 399, 400
 - sag expression and lowest point, 400
 - tension determination, 401, 402
 - total moment, 399
 - uniform load, 400, 402
- Ductile, 11, 43
- Ductility, 11, 1013–1015
- E**
- Earthquake loading
 - base shear, 923
 - elevation, 954
 - floor forces, 925
 - ground acceleration time history, 920
 - ground motion, 23
 - lateral displacement profile, 921
 - low-rise rigid frame, 921
 - peak acceleration vs. structural period, 923
 - peak lateral inertia force, 25
 - seismic lateral load profile, 26
 - seismic loading, 920
 - single degree-of-freedom model, 25
- Elastic moment diagram, 1022
- Engineering process
 - bridge structures, 874
 - loading, 874
 - objective, 873
- Equivalent axial stiffness
 - horizontal cable
 - actual and perturbed configurations, 407
 - deflection patterns, 407, 408
 - modified elastic modulus, 408
 - net motion, 408
 - sag ratio, 409
 - inclined cable
 - Ernst's formula, 411
 - guyed tower modeling, 409, 410
 - Millau Viaduct Bridge, France, 409
 - modified elastic modulus, 411
 - steel cable, 411, 412
- Equivalent single degree of freedom system, 922
- Extensional strain, 11, 34
- External loading
 - creation, 182
 - displacements, 562, 563
 - primary structure, 563, 565
 - produce reaction forces, 182
 - shear and bending moment, beams, 258
 - structure, 173
 - and three force redundants, 567
 - and unit load results, 572
- F**
- Factor of safety
 - defined, 533
 - requirements, 527
 - vs. sliding and overturning, 533
- Factored soil pressure, 484, 486
- Failure mode, buckling, 12
- Finite element method
 - beam structures, 839–849
 - bending moment and deflection profiles, 867
 - description, 805
 - direct stiffness method, 860–865, 868, 869
 - horizontal displacements, 867
 - local and global reference frames, 809–812
 - matrix formulation for rigid frames, 807–809
 - nodal supports
 - displacement constraints, 819–820, 826
 - end member forces, 820
 - fixed and global end actions, 829
 - fully fixed supports, 818
 - geometric data, 823
 - loading conditions, 820, 827
 - local end actions, 830
 - matrix displacement formulation, 823
 - member forces, local coordinates, 829
 - member plane frame, 830
 - movement, 821
 - rearranged system matrices, 821–822
 - reduced system matrices, 819
 - stiffness matrices, 823–825, 827
 - system stiffness matrix, 831
 - unknown force and displacements, 827–829
 - spring stiffness, 866
 - steps, 805–806
 - three dimensional (3D) formulation, 850–860
 - truss structures, 834–839
- Fixed support
 - planar loading, 168
 - three dimensional, 170
- Fixed-end beams
 - compatibility equations, 588
 - fully fixed, 594
 - partially fixed, 595
 - single concentrated force, 592–593
 - structure, 588
 - uniformly distributed loading, 590–592
- Fixed-ended beam
 - inelastic response, limit analysis process, 1019–1021

- Flexibility coefficients
 - description, 564
 - pitched roof frames, 625
 - plane frame, 612
 - Principle of Virtual Forces, 567
 - symbolic/numerical integration, 605
- Flexibility method, 41
- Floor loads, wind load, 918
- Force envelopes
 - axial, 1003, 1004
 - definition, 258
 - two-hinged arches, 899
- Force method
 - axial, shear forces and bending moment, 641
 - behavioral differences, 646
 - computer software system, use, 641–643, 645
 - description, 561–562
 - forces, cables, 640
 - horizontal reaction, 643
 - parabolic arch, 640
 - peak positive and negative moments, 643–644
 - properties and loadings, 637–639
 - reactions and member forces, 647–648
 - structure and steps
 - actual, 562
 - choices, primary, 563, 565
 - external loading, displacements, 561–564
 - flexibility coefficients, 564
 - force redundants, 566
 - “geometric compatibility equation”, 563
 - internal forces, 567
 - matrix form, 567
 - multi-bay multistory frame, 567
 - multi-span beam-type, 567
 - primary, 562
 - reaction force, displacements, 562
 - redundant reactions, 563, 567
 - truss-type, 567
 - vertical reaction, 637
- Fracture, 11, 15, 1014–1018
- Frame(s)
 - braced, 22
 - force method
 - arbitrary-shaped single bay frame
 - structure, 612
 - axial deformation, 613
 - compatibility equation, 612
 - description, 612
 - flexibility matrix, 613
 - matrix equations, 613
 - three-story, 25
- Frame type structures, member equations
 - deformation and end actions, 654
 - description, 653
 - equilibrium conditions, 657
 - fixed end actions, 654, 655
 - moment and shear quantities, 657–658
 - nodal displacement, 655
 - slope-deflection equations, 658
 - superposition, 655, 656
- Free body diagram (FBD)
 - beam
 - construction, 174, 175
 - statically indeterminate, 41
 - statically determinate plane frames
 - A-frames, 341, 342
 - forces acting, node B, 307, 308
 - member forces, 307, 308
 - structural analysis, 30, 31
- Fully fixed arch, 429
- G**
- Gable frame
 - 3-hinge
 - lateral load, 335–337
 - shear and moment, 339–342
 - bending moment distributions, 369
 - deflection profiles, 356, 357
 - simply supported
 - lateral load, 369
 - unsymmetrical loading, 337–339
- Geometric compatibility
 - description, 563
 - flexibility coefficients, 564
 - flexibility matrix, 569
 - matrix equations, 613
 - member forces, 631, 634
- Geometric nonlinear analysis, 734
- Geometric nonlinearity, 734–741
- Girder, 7, 15, 43
- Girder bridge system, 893
- Global force equilibrium equations, planar loading, 173
- Global reference frame
 - quantities, 946
 - symmetry axis, 949
- Granular material, 525, 529, 530
- Gravity floor loads
 - floor slab-beam system, 977
 - loading patterns, 977–978
 - one-way action beam loading, 979
 - steel joist/beam framing, 979
 - tributary areas, 977
- Gravity load, 13, 17, 22
- Gravity walls
 - concrete and soil backfill, 535
 - description, 526
 - retaining analysis, 534–536
- Grid structures, 733
- Guyed tower(s), 403, 404, 409, 410, 422
- H**
- Heyman, J., 27
- High-strength steel, 383, 384, 409
- Hinged model, 770
- Hinged support
 - 3-D, 170
 - planar loading, 169
 - portal
 - gravity loading, 323
 - lateral loading, 323
 - variable cross-section, 325

- Horizontal cables
 - distributed load
 - description, 397, 398
 - tension determination, 398
 - equivalent axial stiffness
 - actual and perturbed configurations, 407
 - deflection patterns, 407, 408
 - modified elastic modulus, 408
 - net motion, 407
 - sag ratio, 409
- Horizontal projection
 - catenary shape, 412
 - distributed loading, 397–399
- Huntington, W.C., 530
- I**
- Idealized dead loading, 430
- Idealized model
 - defined, 899
 - integral abutment bridge, 883
 - loading-idealized model, 900
 - story stiffness, 781
 - sub-elements, 780
 - three-span arch, 902
- Idealized models
 - integral abutment bridge, 883
- Impact magnification factor, 888
- Inclined cable, 394
 - concentrated load, description, 394
- Inclined cables
 - cable-stayed schemes, 581
 - concentrated load
 - description, 394
 - reactions and horizontal force, 393
 - sag determination, 396, 397
 - equivalent axial stiffness
 - Ernst's formula, 411
 - guyed tower modeling, 409, 410
 - Millau Viaduct Bridge in France, 409
 - modified elastic modulus, 411
 - steel cable, 411
- Incremental load, 1022
- Indeterminate, 574, 582, 584, 586, 604, 618, 622, 626, 629–636
 - arches, 604, 610
 - beams
 - first degree, 572, 584
 - second degree, 576, 586, 588
 - frames
 - first degree, 604, 616
 - second degree, 622
 - plane truss, 57
 - portal frames, 616, 618
 - trusses
 - internal force distribution, 631
 - member forces, determination, 631–634
 - principle of virtual forces, 630
 - structures, 629
 - three member truss, 629, 630
- Inelastic analysis, 1013–1034
- Inelastic behavior, 1026, 1027
- Inelastic bending, 1015
- Inelastic deformation, 11, 12, 27, 747
- Inelastic response
 - computer software, 1034
 - dead loading, 1033
 - limit analysis process
 - fixed-ended beam, 1019–1021
 - loading, 1018
 - plastic fracture model, 1018
 - simply supported beam, 1018–1019
 - two-span beam, 1021–1025
 - two-story frame, 1025–1026
 - load capacity determination, 1032
 - moment capacity, 1018
 - moment–curvature relations, 1015–1018
 - nonlinear analysis scheme
 - bilinear moment–curvature model, 1026
 - end forces, 1027
 - equilibrium equations, 1026
 - force increment, 1028
 - global force equilibrium equation, 1027
 - matrix notation, 1026
 - 2 point Gaussian approximation, 1027
 - portal frame, 1028–1029
 - refined mesh, 1026
 - three-story frame, 1030–1031
 - transverse displacement, 1026
 - structural steels, stress–strain behavior of, 1013–1015
- Influence lines, 261, 262, 264, 272
 - actual loading distribution, 107
 - chord forces, 109
 - deck-beam system, 105
 - diagonal members, function, 107
 - force parameters, 879
 - live load analysis, gable roof structure, 111–113
 - load positions and corresponding member forces, 105, 106
 - loading, 105
 - loading zones, 875, 876
 - Müller-Breslau principle application, 875, 878
 - peak value, member force, 108
 - shear, 107
 - slender members, compression vs. tension, 108
 - span beam, 878
 - structure and truck loading, 110
 - truss geometry, 105, 106
 - virtual work, principle
 - cantilever construction-concentrated loading, 266
 - construction, 262–266
 - equilibrium equations, 285
 - uniform design loading-cantilever construction, 272
- Integral abutment bridges
 - elevation—three-span, 881, 883
 - idealized model, 881, 883
- Internal bending moment, 182

- Internal forces
 free body diagram, 205
 planar loading
 beam and eccentric lateral load, 188
 cantilever beam and multiple concentrated loads, 184
 internal shear and moment, 194
 maximum bending moment and shear force, 184
 shear and moment diagrams, 184
 sign convention, 183
 uniform loading and cantilever beam, 187
 structural analysis, 30–33
- J**
- Joints
 3-D trusses
 analysis process, 122
 direction cosines, 121
 displacement computation, 127
 force equilibrium equations, 119
 resolution, force, 121
 tetrahedron, analysis, 125–127
 tripod structure, analysis, 122–124
 definition, 47
 deflections, 90
 pin joint connections, 54
- K**
- Keystone arch construction, 422, 423
 Kirchoff's hypothesis, 211
 K-type truss, 82
- L**
- Lambe, T.W., 530
 Lane load, 17
 Lateral loading
 3-hinge gable frame, 335–337
 building response
 center of mass, 937–940
 description, 925
 forces acting, center of mass, 941
 multistory response, 943–945
 portal frames, 323–325
 stiffness elements, 942, 943, 945
 center of mass, 968
 center of twist, 970, 971
 center of twist and seismic floor loads, 967
 deflection profiles, 356
 displaced configuration, 969
 frames, 972
 pitched roof frames, 330–338
 story rigid frames, 965–966
 treatment
 earthquake loading, 920–925
 rectangular buildings, 917
 wind loading, 918–919
 Lateral stiffness, 409, 745–748, 917, 949
 Limit analysis, 1018–1025
 Limit load, 1025
 Limit state, 11, 27, 1021, 1023–1025, 1028
Line elements, 4, 7, 212
 Live load gravity, 16–17
 Live load patterns
 deflection pattern
 beams, negative moment, 980, 981
 columns, negative moment, 980, 981
 positive moment, 980, 1000
 earthquake analysis, 986–988
 gravity type loading, 980
 loading pattern
 columns, maximum negative moment, 980, 982
 maximum positive moment, 980, 1000
 multistory frame, 980
 uniformly distributed live load, 982–985
 Live loads, bridges
 truck loading and span discretization, 885, 886
 uniform live load, 888–890
 Load magnitude, 1023
 Loading(s)
 codes and technical societies, 13
 gravity live loads, 16–17
 properties
 importance factor, values, 16
 occupancy categories, 16
 quasi-static loading, 15
 temporal variation, 15
 snow, 22–24
 source
 construction, 14
 function, 13
 interaction, environment, 30–33
 terrorist loads, 14
 Loading pattern
 computer-based analysis, 895
 dead load, 894–895
 span discretization, 893, 896
 Loading zones, 875–877
 Local reference frame
 member and nodes, 809, 810
 nodal forces, 812
 rotation matrices, 811
 rotation of axes, 809, 810
 structure, 809, 810
 Low-rise rigid frames
 bracing, 785–790
 shear stiffness method, 779–784
- M**
- Mass, 13, 15, 19, 25, 26
 Matrix formulation, 807–809
 displacements, computation, 135–141
 floors and stories, 946
 force equilibrium equations, 133–135
 inertia forces, 947
 manual techniques, 131
 member–node incidence, 133
 notation, 131–133
 rigid frames

- end forces and displacements, 807
 - fixed end forces, 809
 - linearly loaded beam, 809
 - member stiffness matrices, 807–808
- stability, 135
- story structure, 948
- system load, mass and stiffness matrices, 949
- Maxwell's law
 - compatibility equations, 571
 - definition, 569
 - reciprocal loading conditions, 569–571
- Method of joints
 - cantilever truss analysis, 71–74
 - five member truss, 65–71
 - gable roof truss analysis, 75–77
 - plane truss, 61
 - three member truss analysis, 62–65
 - zero force members, 72
- Method of sections
 - chord trusses, 78
 - design, 142
 - equilibrium equations, 77
 - hybrid analysis strategy, 84–86
 - joints, 77
 - K-type trusses, analysis, 82–84
 - parallel chord truss, 79–80
 - roof truss, 80–82
 - shear forces, 78
- Method of virtual forces
 - arches, 447
 - beams, 231
 - bending, slender beams, 231
 - deflection computation, 232
 - displacement, roller support, 376
 - frames, 344
 - horizontal deflection determination, 374, 378
 - horizontal displacement, 376
 - trusses, 78
 - vertical deflection determination, 374, 375, 378
- M1, M2, and M3, maximum value, 277, 878, 908
- Modern cables, 383
- Modern structural software systems, 1023
- Modulus of elasticity, 34, 44
- Moment area theorems, slender beams
 - cantilever beam, 220
 - cross-sectional rotation and deflection, 218
 - double integral, 219
 - First Moment Area theorem, 218
 - integration, x_1 and x_2 , 219
 - Second Moment Area Theorem, 219
 - simply supported beam, 224–230
- Moment capacity, 1015–1018, 1023, 1026
- Moment distribution
 - multi-span beams
 - dimensionless factor (DF), 699
 - incremental moments, 699
 - iteration cycle, 698
 - method, 698
 - moment equilibrium, 699
 - moment release, two span beam, 702–703
 - multiple free nodes, 703–704
 - reduced relative rigidity factor, 702
 - solution procedure, 698
 - three span beam, 704–706
 - two span beam, 700–704
 - unbalanced clockwise nodal moment, 698
- Multi-bay
 - multistory frames, 567
 - portal frame, 306
- Multiple concentrated loads
 - force envelopes
 - absolute maximum moment, 277
 - computation, maximum moments, 277–282
 - critical truck loading position, 283
 - dead + truck loading, 284
 - forces, 275
 - M1 and M2, maximum value, 277
 - maximum bending moments, 278
 - moment diagram-arbitrary position, loading, 276
 - truck moving across, span, 283
 - internal forces, cantilever beam, 184, 188
- Multi-span beams (gravity loading)
 - data-moment diagrams
 - quantitative reasoning, relative stiffness, 769–770
 - single-span, 768
 - three-span, 768, 769
 - two-span, 768
- Multi-span beams force method
 - structures, 567
- Multi-span bridges, 878
 - geometric configurations
 - elevation—three-span, 881, 883
 - idealized model, 881, 883
 - integral abutment bridge, 883
 - sintegral abutment bridge, 882
 - span arrangements, 880, 881
 - span lengths
 - bending moment distribution, 882, 884
 - symmetrical scheme, 882, 884
- Multi-span horizontal structures
 - cable-stayed
 - bridge, 903–907
 - structure, 911
 - engineering process, girders, 873–875
 - global deflection, 910
 - idealized tied arch, 911
 - influence lines, 875–880, 908
 - single span bridge, 908
 - span lengths, 908
 - symmetrical cable structure, 913
 - three-span parabolic arch response, 902–903
 - Two-Hinged Parabolic Arch Response, 899–901
- multistory building systems
 - multistory building systems, 915–917
- Multistory buildings
 - braced frames, N-S and E-W directions
 - beam properties E-W direction, 989
 - configuration, 992
 - deflection, 996
 - floor loading, 1006

- Multistory buildings (*cont.*)
- interior columns, 982
 - result, 998
 - four-story building
 - floor plan and elevation structure, 989
 - global wind loads, 990
 - loading and member data, 989
 - load paths, 1006
 - loading patterns estimation, Müller–Breslau principle, 1006–1009
 - loads, frames
 - rectangular building, 975, 976
 - structure, 975, 976
 - system, 975
 - rigid frames, N-S and E-W direction
 - beams, N-S, 998
 - braced vs. rigid frame, 997
 - columns, N-S, 998
 - connection, N-S beams and columns, 998
 - dead load, 1008
 - design values, 1005
 - live load patterns, 980–989
 - moment diagrams, 1024
 - result, 1006
 - uniform live load, 888–889
 - wind load N-S, 990–992, 997, 998
 - systems
 - braced frame structure, 916
 - lateral stiffness systems, 917
 - low-rise building, 916, 917
- Multistory response
- forces
 - floor, 943
 - inertia, 944
 - interstory deformation, 943
 - shear beam, 945
- Multistory rigid and braced frame, 306
- Multistory rigid frames
- gravity loading, 771
 - lateral loading
 - approaches, estimation, 771
 - inflection points, 771
 - low-rise, bracing, 785–790
 - shear stiffness method, 779–784
- N**
- Nodal equilibrium equations
- direct stiffness method, 816
 - equilibrium equations, 815
 - member end actions, 814
 - member node incidence, 812–813
 - member reaction forces, 815
 - positive/negative end, 812
 - system matrices, 818
- Nodes
- and member incidence, 133
 - concurrent force system, 56
 - description, 47
 - horizontal displacement, 94–99
 - member af and cf, extreme values, 108
 - plane trusses, 118
 - positive and negative, member n , 131
 - scalar equilibrium equations, 57
- Non prismatic members, 241–244
- Nonlinear analysis
- bilinear moment–curvature model, 1026
 - end forces, 1027
 - equilibrium equations, 1026
 - force increment, 1028
 - global force equilibrium equation, 1027
 - matrix notation, 1026
 - 2 point Gaussian approximation, 1027
 - portal frame, 1028–1029
 - refined mesh, 1026
 - three-story frame, 1030–1031
 - transverse displacement, 1026
- Nonlinear equations, 734
- Nonlinear stress–strain relation, 1015
- O**
- Optimal shape
- parabolic arch, 435
 - statically determinate arch, 462–463
- Out of plane loading
- end actions, 729
 - equilibrium equations, 731
 - free body diagrams, 686, 688
 - grid structure, 733–734
 - plane frames
 - 3-D system, 359, 361
 - displacement and rotation, 358
 - gravity load, 359
 - highway signpost, 359
 - transversely loaded grid structure, 362
 - prismatic member, 729
- Overturning
- base pressure distribution, 553
 - defined, 533
 - stability, 553
 - toe and sliding, 532
 - vs. safety, 545
- P**
- Parabolic geometry
- notation, parabolic shape function, 435
 - shallow vs. deep parabolic curved members, 436–442
- Passive soil pressure, 531
- Pattern loading
- three-span system, 888–889
 - uniform dead and lane, 894
- P -delta effect, 745, 749, 750, 764
- Peak acceleration, 23, 25, 26
- Peak pressure, 480, 481, 502
- Peck, R.B., 479, 530
- Piles/caissons, 476, 547–549
- Pitched roof frames
- analytical solutions
 - gravity loading, 330, 331

- displacement profiles, shear and moment diagrams, 379
- expression, horizontal reaction, 627
- member loads
 - equivalent vertical loading, 328
 - inclined member, 326, 327
 - normal and tangential directions, 329
 - reactions, 326–320
- peak negative and positive moments, 628
- primary structure, 625
- relative stiffness factors, 625–626
- structures, 326
- three-hinge solution, 628
- total bending moment distribution, 627
- two vs. three-hinge solution, 628
- Planar beam systems, 171
- Planar bending, 164
 - definition, 164
 - stability and determinacy, beams *see* Stability
 - transverse displacement, 286
- Planar trusses
 - analysis
 - axial force, 90
 - equilibrium considerations, 56
 - statically determinate, 57–58
 - bottom and top nodes, 49
 - complex and compound, 49
 - simple planar truss construction, 48
 - structure, 91
 - two member, 91
- Plane frames
 - transverse deformation, 612
- Plane trusses
 - 2-D, 118
 - definition, 47
 - node, 56
 - statical determinacy, 142
- plastic fracture model, 1018
- plastic hinges, 1023, 1025
- Platforms, 4, 13
 - Portal frames
 - anti-symmetrical loading, displacement method
 - chord rotation, 690
 - frame with no sideway, 692–694
 - frame with sideway, 694–697
 - moments and shear, 692
 - slope-deflection equations, 690
 - bending moment distribution, 621–622
 - expression, displacement, 614
 - gravity-loading
 - anti-symmetrical model, 618
 - bending moment distributions, 619
 - compatibility equation, 618
 - decomposition, loading, 617
 - horizontal reaction, 619
 - net bending moment distribution, 620
 - peak moments, 620
 - symmetrical model, 618, 619
 - two-hinged, 618
 - lateral loading symmetrical
 - two-hinged, 616
 - overhang, 321–323
 - reaction, gravity loading, 613, 614
 - simply supported, 316–318
 - structure, 613, 614
 - symmetrical
 - anti-symmetrical loading, 622
 - bending moment distribution, two-hinged frame, 623, 624
 - displacement, 622
 - hinged and fixed supports, bending moment distribution, 624, 625
 - structures, 622
 - symmetrical loading, displacement method
 - description, 689–690
 - moment equilibrium, 690
 - Portal method
 - axial and shear forces, 773, 775, 776, 778
 - bending moment distribution
 - beams, 773, 775, 776, 778
 - columns, 773, 776, 777
 - description, 772, 796
 - moments, joints, 772, 773, 777
 - reactions, shear forces and moment distribution, 773, 775, 776, 778
 - rigid frame, 771–772, 776
 - steel frame, 799
- Positive sense, bending, 310
- Primary structure
 - description, 562
 - displacement, 564, 577
 - fixed end moments, 590
 - flexibility
 - coefficients, 564
 - matrix, 613
 - force redundants, 566, 568
 - geometric compatibility equation, 563
 - multi-span beam, 568
 - pitched roof frames, 625–629
 - redundant moment, 568
 - vertical restraints, 564
- Principle of virtual forces
 - axial and shear forces, 345
 - deflections, computation
 - cantilever-type structure, 345–347
 - horizontal displacements and rotation, 348–350
 - non-prismatic member, 352–355
 - steel structure, 350–353
 - low-rise frames, 345
 - planar frame structure, 344–345
- Prismatic beams
 - combined bending and torsion, 164, 166
 - cross-sections and bending mode, 163, 164, 166
 - geometrical parameters and notation, 163
 - Mechanics Theory, 164
 - planar bending, 164, 286

Q

- Qualitative reasoning, deflected shapes
 - beam and moment release, 217–218
 - cantilever beam, 216
 - moments, positive and negative, 213, 215
 - overhang and beam, 216
 - positive and negative curvature, 213
 - shape transition at inflection point, 214
 - supports-displacement measures, types, 213, 214
 - uniformly loaded and simply supported beam, 215

R

- Rankine theory
 - defined, magnitude per unit wide strip, 531
 - distribution, soil pressure, 530
 - horizontal forces, 531
 - soil pressure, surcharge, 532
- Reactions
 - planar loading
 - beam and two overhangs, 174–175
 - beam free body diagram, construction, 175
 - horizontal beam supports, vertical sign, 180–182
 - simply supported beam, 175–176
 - statically determinate and indeterminate structure, 173
 - three-span beam and two moment releases, 179–180
 - two-span beam and moment release, 176–179
 - structural engineering
 - forces, 30
 - statically indeterminate beam, 41–42
 - supports, planar structures, 7, 10

Rectangular footing, loading, 483, 496

Redundant

- cable force, 582
- displacements, primary structure, 586
- external loading, 586
- force
 - expression, primary structure, 567
 - reaction, 563, 567
 - steps, 562
- internal force, 567
- matrix equations, 613
- tension, tie, 610
- three-span beam, 576

Refined mesh, 1026

Relative stiffness

- bending moment distribution, 597
- clamped/hinged model, 770
- end moments estimation, 771
- flexibility coefficients, 625
- hinged and clamped end model, 770
- internal force distribution, 631
- multi-span beam, 768, 769
- qualitative reason, 797
- two-span beam, 597

Resultant

- centroid, 480
- force, 479
- pressure distributions, 505

Resultant

- combined footings, 493
- factored loads, 494
- line of action, 481, 493

Rigid body motion

- prevent
 - arranged, 58
 - insufficient, 59
 - order, 114
 - reactions, 87
 - required, 57
 - respect, 114
 - supported, 48

Rigid frame

- displacement method
 - anti-symmetrical loading, portal frames, 690–697
 - description, 685
 - free body diagrams, members and nodes, 686, 688
 - moment equilibrium, 686, 690
 - sideway, 686
 - slope-deflection equations, 658
 - symmetrical loading, portal frames, 689–690
- five story symmetrical rigid frame building, 986
- lateral loading, 330, 332
- multistory, 306
- pitched roof frames, 326
- simply supported gable, 330–335
- triangular, 380

Roller support, 169–170

Rotation, 309, 345–346, 348, 350, 358, 359, 375, 376

Rupture strain, 1014

S**Sag**

- arc length, 403–406
- concentrated loads, horizontal cables
 - angle of inclination, relationship, 388
 - downward vertical, 391
 - expression, 387, 389
 - profile, 392
- distributed loading, 395–397
- equivalent axial stiffness, 409
- inclined cables and concentrated loading, 393–397

Sandy soil

- allowable pressures, 477, 479
- pressure distributions, 477, 478

Sections

- cantilever walls design, 549–552

Service loads, 26, 483, 486, 498, 500, 501, 516

Shallow curved members

- non-shallow curved member, 445–446
- trigonometric measures, 436
- vs. deep, 436

Shallow foundations

- allowable soil pressure, 516
- combined footing, 520
- dimensions, square/rectangular, 517
- pad footing, 522
- service loads, 516
- square columns, 517

- strap footing, 521
- types
 - combined footing, 477
 - footings, 476
 - single footing, 476
 - strap footing, 476
 - structure, 475, 476
 - superstructure, 475
- Shear force, 184, 246, 262–266
 - influence line
 - construction, 262–266
 - maximum bending moment, 184
 - transverse, 246
 - maximum moment occurs at mid-span, 442
- Shear stiffness method
 - approximate analysis, 783–784, 794–796
 - bottom story-fixed support, transverse shear model, 782
 - description, 796–797
 - elements, 950
 - exterior and interior element—upper story, 781
 - factors, 949
 - low-rise frame, 780
 - parameter, 785
 - ratios
 - lowest story, 783
 - upper stories, 781
 - slope-deflection equations, 781
 - steel frame, 799
 - sub-elements, base story
 - fixed support, 782
 - hinged support, 783
 - total transverse shear, 779
- Shear walls, concrete frame, 916
- Shell, 4, 7
- Sideway
 - with sideway, frame's moment distribution, 694–697
 - computer-based analysis, frame with inclined legs, 726–729
 - fixed end moments, 718
 - frame with inclined legs, 722–726
 - “holding” forces, 718
 - portal bent, 719–722
 - without sideway, frame's moment distribution
 - end actions, 723–726
 - support settlement, two-bay portal frame, 713–715
 - symmetrical loading, two-bay portal frame, 711–713
 - temperature increase, two-bay portal frame, 715–718
- Sign convention
 - matrix formulation, beam bending problem, 183
 - positive directions, 183
- Simple planar truss, 48, 49
- Simple space truss, 48
- Single footings
 - column position, 483
 - dowels use, 485
 - effective soil pressure, 483
 - procedure, 484
 - service loads, 486–489
 - shear and moment, 484, 485
 - shear, location, 484, 485
 - square/rectangular, 488–493
 - steel reinforcement, 485
- Slender beams
 - centroidal axis, strain, 211
 - cross section rotation angle, 212
 - curvature relationship, moment, 212–213
 - differential elements, 211, 212
 - express and curvature, extensional strain, 212
 - homogeneous beam, 211, 213
 - Kirchoff's hypothesis, 211
 - moment area theorems, 218–230
 - non prismatic members, 241–244
 - qualitative reasoning, deflected shapes *see* Qualitative reasoning, deflected shapes
 - virtual forces method, 231–232
- Sliding
 - defined, 532, 536
 - stability, 553
 - vs. safety, 533
- Snow load
 - drift profiles, 24
 - flat and sloped roof, 23, 24
- Soil friction angle, 553
- Soil pressure distributions
 - allowable pressures, 477, 479
 - analytical method
 - equilibrium, 480
 - line of action, 481
 - peak pressure, 480, 481
 - plan, rectangular area, 482
 - single footing, 479
 - trapezoidal, 481
 - concentric load, 477, 478
 - description, 477
 - determination, 515
 - dimensions, footing, 477–479
 - footing/wall base, 539
 - Rankine theory, 531–532
- Spectral acceleration, 922, 923
- Stability
 - 3-D trusses, equilibrium analysis
 - Cramer's rule, 135
 - requirement, 135
 - and determinacy, beams
 - concurrent displacement constraints, 166, 167
 - fixed and hinged support, 168
 - 3-D fixed support, 170
 - 3-D hinged support, 170
 - moment release, 172–173
 - multiple supports, 171, 172
 - planar rigid body motions, 165, 167
 - 3-D roller support, 170
 - roller support, 169
 - static determinacy, 171

- Stability (*cont.*)
- unstable support arrangements, 171
 - X–Y plane, 165
 - planar truss
 - complex truss, 61
 - compound truss, 60, 61
 - equilibrium equations, 58
 - plane truss, 57, 58
 - simple and compound trusses, 61
 - simple trusses, 58
 - suitably restrain, 58
 - unstable, motion restraints, 58
 - structural engineering
 - initial, 7–11
 - loss and material failure, 11–12
 - priorities, 12
- Stabilizing effect, 527
- Static determinacy
- 2-D plane trusses, 118
 - stable determinate structure, 118
 - structure, 118
 - unstable structure, 119–120
- Statically determinate beams
- engineering process, 258–259
 - force envelopes, 259–262
 - influence lines, 259–262
- Statically determinate curved members
- arch-type structures, 423–428
 - factors and concepts, 463–464
 - internal forces, 431–435
 - models, arch structures, 429–431
 - objectives, 463
 - parabolic geometry, 435–436, 439, 443, 451, 454
 - problems, parabolic member, 464–473
 - three-hinged arches, analysis, 450–463
 - virtual forces
 - circular, 447–450
 - displacements, 442
 - non-shallow slender, 443
 - shallow slender, 443–447
- Statically determinate plane frames
- axial forces and end moments, 380
 - beams and columns, 305
 - bending moment distributions, 369
 - computer-based analysis, 358
 - displacement determination, 381
 - planar loading
 - adequate support schemes, 307
 - indeterminate portal and A-frames, 309
 - indeterminate support schemes, 307
 - nodal forces and rigid plane frames, 309
 - three-hinge plane frames, 306–310
 - reactions, shear and moment distributions, 363
 - rigid plane frames, 305, 309
 - steel material, 380
 - virtual force
 - method, 374–378
- Steel base plate, 485
- Stiffness
- definition, 34
 - material, 27
 - method, 40
- Stiffness factor, 39
- Straight members
- “equivalent”, 409
 - slender, 442
- Strain hardening, 1013, 1015
- Strands, 384, 409
- Strap footings
- description, 504
 - design approach, 505, 511
 - equilibrium, 503
 - notation and pressure distribution, 504, 505
 - reinforcing patterns, 507
 - soil pressure profile, 509
 - summing moments, 505
- Stress-strain, 11, 213, 651, 738, 1013–1015, 1017
- Structural components, 4, 11, 12, 30, 42
- Structural engineering
- components and types, 4, 5
 - design
 - loading, 4, 7
 - philosophy, 26–27
 - reactions, 7, 11
 - stability
 - initial, 7–11
 - loss and material failure, 11–12
 - priorities, 12
- Structural idealization, 48, 50
- Structural steels, 1013–1015
- Structural types
- function, 4, 5
 - makeup, 4, 7
- Superposition, 655, 656
- Support constraints, 806
- Support settlement
- moments, 891
 - resulting moments, 891
 - three-span beam, 890
- Surcharge, soil pressure, 532, 553
- Surface elements, 4, 7
- Symmetrical buildings
- earthquake floor loads, 956
 - flexible floors, 955
 - floor load distribution, 956
 - frame load-rigid, 957
 - idealized building model, 945
 - maximum column moments-rigid and flexible floors, 955
 - one story frame, 960
 - rigid frame building, 954
 - rigid frame structure, 951
 - segmental areas, 953
 - shear stiffness factors, 952
 - structure, 949
 - total story stiffness, 952

- typical floor, 952
- typical frame, 949
- Symmetry and anti-symmetry
 - deflected shapes, 254–258
 - shear and moment diagrams, 250–252
- T**
- Tall building
 - lateral deflections, 791, 792
 - quantities, M_i+ and VT_i+ , 1, 792
 - segment, 792
- Tandem, 17
- “Tangent” stiffness matrix, 1028
- Temperature change
 - effect, 103
 - total extension, 91
- Tension
 - cable-stayed structures, 384
 - concentrated loads
 - horizontal cables, 386, 389
 - determination
 - catenary equations, 414
 - maximum tension, 418
 - peak values, 421
 - segment, cable, 413, 414, 416
 - distributed loading
 - horizontal cables, 398, 408
 - inclined cable, 399, 401
 - equivalent axial stiffness, 407–409
- Terrorist loads, 14
- Terzaghi, K., 479, 530
- Thermal loading, 13
- Three-dimensional (D) formulation, 3
 - displacement measures, 850–851
 - notation, 850
- Three-dimensional (D) trusses, 3
 - equilibrium analysis, 114
 - joints, 120–131
 - restraining rigid body motion, 114–117
 - restraints, rigid object, 115
 - space truss structures, 114
 - static determinacy, 118–120
 - tetrahedron units, -D trusses, 3, 114
- Three-hinged arches
 - and geometry and reactions, 450
 - 1° indeterminate, 429
 - optimal shape, statically determinate arch, 462, 463
 - parabolic arch
 - concentrated load, mid-span, 456–459
 - force equilibrium, 451
 - horizontal and vertical loads, 460, 461
 - uniform vertical loading, 452–456
- Three-Hinge frames
 - deflection profiles, 356–358
 - description, 309
 - gable
 - lateral loading, 335–337
 - gravity loading, 330, 331
 - lateral loading, 330, 332
- portal
 - shear and moment distributions, 363
 - shear and moment, 339–341
- 3-D Hinged support, 170
- Three-span arch study
 - discrete force envelopes, 895, 897
 - idealized model, 902, 904
- Three-span continuous girder bridge
 - axle loading, 888
 - cross-section, 895
 - loading patterns, 894, 895
 - support settlement, 899
 - truck loading, 896, 897
 - uniform load patterns, 895
- Three-span parabolic arch response, 902–903
- Thrust, 610, 611
- Tied arches, 610
- Torsional response
 - floor rotation, 929
 - shearing, 945
- Toughness, 1014
- Tower, 4, 14
- Transverse distribution, truck loading
 - axle distribution factor, 888
 - loading, 888
 - slab-stringer bridge deck cross-sections, 887, 888
 - vehicle wheel loads, 887
- Trapezoidal rule, 299
- Truck load, 17
- Truss
 - defined, 7
 - formulation
 - fixed end actions—members and joints, 838
 - force and displacement, 834
 - load vectors, 838
 - local and global frames, 835
 - stiffness matrix and displacement vector, 837
 - topological and geometric information, 823
 - unknown displacements, 838
- Truss structures
 - facts and concepts, 142
 - matrix formulation
 - displacements, computation, 135–141
 - force equilibrium equations, 133–135
 - manual techniques, 131
 - member–node incidence, 133
 - notation, 131–133
 - stability, 135
 - objectives, 141
 - planar trusses, analysis
 - 3-D space structures, 55
 - complex trusses, 86–89
 - equilibrium considerations, 56
 - joints, method, 61–77
 - sections, method, 77–86
 - stability criterion, 58–61
 - statically determinate planar trusses, 57–58
 - problems
 - plane trusses, classification, 142, 161

Truss structures (*cont.*)

types

- complex planar, 49
- compound planar, 49
- compression elements, 52
- covered wood bridges, 51
- Egyptian boat built, 50
- flourishing industry, New England, 52
- force parallelogram, 50
- high-strength bolts and welding, 54
- iron trusses, 52, 53
- pin joint connections, 54
- plane and joints, 47
- simple planar and space, construction, 48
- single span truss bridge system, 50
- steel, 52
- structural systems, 49
- three-dimensional truss roof system, 55
- wooden bridge truss structures, 52

Two-hinged arch

- and 1° indeterminate, 429
- structure, 429

Two-hinged parabolic arch response

- discrete force envelopes—truck loading, 890, 894, 897
- idealized model, 902, 904

3-D Hinged support, 170

Type of foundations

footings

- description, 475
- single, 476
- strap, 476, 477
- structure, 475, 476
- superstructure, 475

U

Unstable

- initially, 59
- structure, 119

V

Vertical retaining wall structures

- cantilever, 527, 544
- concrete piles, 547
- design, cantilever walls, 549–551
- gravity, 526–527
- gravity wall, 533, 534
- peak pressure, 534
- stability analysis
 - cantilever and gravity, 533
 - concrete gravity wall and soil backfill, 535
 - defined, safety for sliding, 533
 - equilibrium, 532
 - force summation, 533

gravity wall, 532

overturning, 533

types, 525

with footing, 539, 544

Virtual forces method

and actual force, 101

application, 141

curved members

circular, 447–450

displacements, 442

non-shallow slender, 443

shallow slender, 443–447

definition, 93

deflection, computation, 95–97

diagonal pattern reversed, 102

matrix equations, 137

procedure, 93

truss applications, 103

W

Whitman, R.V., 530

Wind load

pressure

distribution, 17–19

profiles, 19–22

vortex shedding, 22

velocity distribution, 19, 20

Wind pressure

distribution, 17–19

profiles

Bernoulli's equation, 19

stagnation and design pressure, 20

vortex shedding, 22

Wind speed, 19, 20

Wind velocity, 19

Y

Yielding

bending envelopes, 901

concrete, 1013

elastic limit, 1015

factor loads, 516

necking, 1013

steel, 1013, 1014

yield strain, 11, 1013

Yielding support, beam

axial force, 583–584

deflection, 578–579

external concentrated loading, 580

force redundant and displacement profiles, 577, 579

force redundant system, primary structure, 580

linear elastic behavior, 579

supporting members, 577

vertical restraint, 578